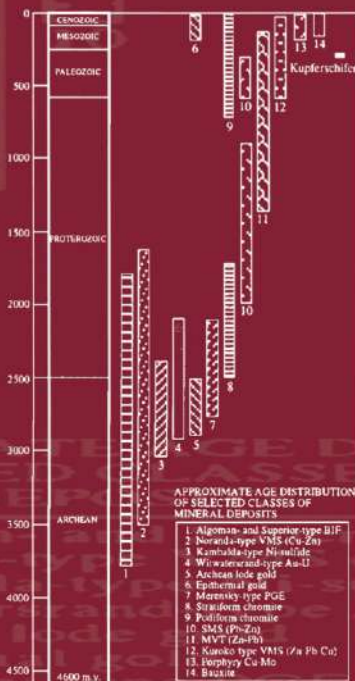


Understanding Mineral Deposits

Kula C. Misra

Volume I



Springer-Science+Business Media, B.V.

UNDERSTANDING MINERAL DEPOSITS

Understanding Mineral Deposits

by

Kula C. Misra

*Department of Geological Sciences,
The University of Tennessee, Knoxville, U.S.A.*



SPRINGER-SCIENCE+BUSINESS MEDIA, B.V.

A C.I.P. Catalogue record for this book is available from the Library of Congress.

ISBN 978-94-010-5752-3 ISBN 978-94-011-3925-0 (eBook)
DOI 10.1007/978-94-011-3925-0

Printed on acid-free paper

All Rights Reserved

© 2000 K.C. Misra

Softcover reprint of the hardcover 1st edition 2000

No part of the material protected by this copyright notice may be reproduced or utilized in any form or by any means, electronic or mechanical, including photocopying, recording or by any information storage and retrieval system, without written permission from the copyright owner.

*To my wife, Geeta,
for her patience
during the years of preoccupation with the book
and the clutter it generated all around our home*

TABLE OF CONTENTS

PREFACE	xiii
CHAPTER 1. INTRODUCTION	1
1.1. Mineral Deposit versus Orebody	1
1.2. Styles of Mineralization and Morphology of Mineral Deposits	2
1.3. Distribution of Mineral Deposits	3
1.3. Understanding Mineral Deposits	4
CHAPTER 2. FORMATION OF MINERAL DEPOSITS	5
2.1. Ore-forming Processes	5
2.2. Orthomagmatic Processes	6
2.3. Examples of Orthomagmatic Deposits	18
2.4. Sedimentary Processes	33
2.5. Metamorphic Processes	49
2.6. Examples of Metamorphic Deposits	54
2.7. Hydrothermal Processes	56
2.8. Examples of Hydrothermal Deposits	73
2.9. Summary	89
2.10. Recommended Reading	92
CHAPTER 3. INTERPRETATION OF MINERAL DEPOSITS - I	93
3.1. Introduction	93
3.2. Geologic Setting	94
3.3. Ore Minerals	94
3.4. Ore-Gangue Textures	95
3.5. Stability Relations of Ore Minerals and Assemblages	107
3.6. Hydrothermal Alteration	116
3.7. Zoning	124
3.8. Fluid Inclusions	131
3.9. Trace Element Distribution	142
3.10. Recommended Reading	147
CHAPTER 4. INTERPRETATION OF MINERAL DEPOSITS - II	148
4.1. Stable Isotopes	148
4.2. Sulfur Isotopes	153

4.3. Carbon Isotopes	164
4.4. Oxygen and Hydrogen Isotopes	168
4.5. Lead Isotopes	177
4.6. Strontium Isotopes	186
4.7. Geothermometry and Geobarometry	193
4.8. Metamorphism of Ore Assemblages	219
4.9. Age of Mineralization	228
4.10. A Comprehensive Example: The Creede District, Colorado, USA	231
4.11. Summary	235
4.12. Recommended Reading	237
CHAPTER 5. CHROMITE DEPOSITS	238
5.1. Introduction	238
5.2. Types of Deposits	238
5.3. Distribution	239
5.4. Stratiform Deposits	240
5.5. Podiform Deposits	244
5.6. Examples	248
5.7. Chromite Composition	256
5.8. Origin	261
5.9. Metallogensis	267
5.10. Summary	270
5.11. Recommended Reading	272
CHAPTER 6. NICKEL (-COPPER) SULFIDE DEPOSITS	273
6.1. Introduction	273
6.2. Distribution	273
6.3. Types of Deposits	275
6.4. Examples	281
6.5. Ore Composition	292
6.6. Hydrothermal Alteration and Metamorphism	298
6.7. Origin of Kambalda-type Deposits	299
6.8. Metallogensis	308
6.9. Summary	316
6.10. Recommended Reading	318
CHAPTER 7. PLATINUM-GROUP ELEMENT (PGE) DEPOSITS	319
7.1. Introduction	319
7.2. Types of Deposits	321
7.3. Examples	323
7.4. Ore Composition	335
7.5. Origin of Merensky-type PGE Deposits	337

7.6. Origin of PGE-enriched Chromitites in Layered Intrusions	347
7.7. Metallogenesis	350
7.8. Summary	351
7.9. Recommended Reading	352
CHAPTER 8. PORPHYRY DEPOSITS	353
8.1. Introduction	353
8.2. Porphyry Copper Deposits	353
8.3. Porphyry Molybdenum Deposits	397
8.4. Porphyry Tin Deposits	409
8.5. Summary	412
8.6. Recommended Reading	413
CHAPTER 9. SKARN DEPOSITS	414
9.1. Introduction	414
9.2. Skarns and Skarn Deposits	414
9.3. Types of Skarns and Skarn Deposits	417
9.4. Examples	428
9.5. Origin	437
9.6. Metallogenesis	441
9.7. Summary	448
9.8. Recommended Reading	449
CHAPTER 10. VOLCANIC-ASSOCIATED MASSIVE SULFIDE (VMS) DEPOSITS	450
10.1. Introduction	450
10.2. Distinguishing Features	451
10.3. Distribution	452
10.4. Types of Deposits	455
10.5. Examples	464
10.6. Ore Composition	470
10.7. Hydrothermal Alteration	473
10.8. Metamorphism and Deformation	477
10.9. Origin	478
10.10. Metallogenesis	487
10.11. Summary	495
10.12. Recommended Reading	496
CHAPTER 11. SEDIMENT-HOSTED MASSIVE ZINC-LEAD SULFIDE (SMS) DEPOSITS	497
11.1. Introduction	497
11.2. Distinguishing Features	498

11.3. Distribution	500
11.4. Types of Deposits	504
11.5. Examples	504
11.6. Ore Composition	521
11.7. Hydrothermal Alteration	523
11.8. Origin	524
11.9. Metallogensis	530
11.10. Summary	538
11.11. Recommended Reading	538
CHAPTER 12. SEDIMENT-HOSTED STRATIFORM COPPER (SSC) DEPOSITS	539
12.1. Introduction	539
12.2. Distinguishing Features	540
12.3. Distribution	541
12.4. Types of Deposits	544
12.5. Examples	545
12.6. Ore Composition	559
12.7. Origin	561
12.8. Metallogensis	567
12.9. Summary	571
12.10. Recommended Reading	572
CHAPTER 13. MISSISSIPPI VALLEY-TYPE (MVT) ZINC-LEAD DEPOSITS	573
13.1. Introduction	573
13.2. Distinguishing Features	573
13.3. Distribution	575
13.4. Examples	578
13.5. Ore Composition	588
13.6. Alteration	590
13.7. Brecciation	591
13.8. Origin	593
13.9. Metallogensis	602
13.10. Summary	607
13.11. Comparison of VMS, SMS, SSC, and MVT Deposits	608
13.12. Recommended Reading	612
CHAPTER 14. URANIUM DEPOSITS	613
14.1. Introduction	613
14.2. Types of Deposits and Distribution	613
14.3. Examples	627

14.4. Mineralogy and Textures	635
14.5. Origin	636
14.6. Metallogenesis	647
14.7. Summary	658
14.8. Recommended Reading	659
CHAPTER 15. PRECAMBRIAN IRON-FORMATIONS	660
15.1. Introduction	660
15.2. Iron-formation	660
15.3. Distribution	661
15.4. Iron-formation Facies	662
15.5. Types of Iron-formations	667
15.6. Examples	669
15.7. Ore Composition	675
15.8. Metamorphism	678
15.9. Secondary Enrichment	680
15.10. Origin	680
15.11. Time-bound Distribution of Iron-formations	694
15.12. Summary	696
15.13. Recommended Reading	697
CHAPTER 16. GOLD DEPOSITS	698
16.1. Introduction	698
16.2. Distribution	699
16.3. Types of Gold Deposits	699
16.4. Examples	725
16.5. Origin of Hydrothermal Gold Deposits	731
16.6. Metallogenesis	749
16.7. Summary	756
16.8. Recommended Reading	759
REFERENCES	761
INDEX	839

PREFACE

Mineral deposits have supplied useful or valuable material for human consumption long before they became objects of scientific curiosity or commercial exploitation. In fact, the earliest human interest in rocks was probably because of the easily accessible, useful (e.g., red pigment in the form of earthy hematite) or valuable (e.g., native gold and gemstones) materials they contained at places. In modern times, the study of mineral deposits has evolved into an applied science employing detailed field observations, sophisticated laboratory techniques for additional information, and computer modeling to build complex hypotheses. Understanding concepts that would someday help geologists to find new mineral deposits or exploit the known ones more efficiently have always been, and will continue to be, at the core of any course on mineral deposits, but it is a fascinating subject in its own right, even for students who do not intend to be professional economic geologists. I believe that a course on mineral deposits should be designed as a “capstone course” that illustrates a comprehensive application of concepts from many other disciplines in geology (mineralogy, stratigraphy and sedimentation, structure and tectonics, petrology, geochemistry, paleontology, geomorphology, etc.).

This book is intended as a text for such an introductory course in economic geology, primarily for senior undergraduate and graduate students in colleges and universities. It should also serve as a useful information resource for professional economic geologists. The overall objective of the book is to provide the reader with a critical *understanding* of selected classes mineral deposits: how are they distributed in space and geologic time, what are their distinguishing and general characteristics, and what can be inferred about their genesis from the available data. The expectation is that the information and discussions in this text will provide students with an insight into the formulation of appropriate exploration strategies for various classes of mineral deposits and kindle their interest in further research on aspects of mineral deposits that are poorly understood or that remain unresolved.

As an applied discipline, the study of economic geology requires a background in other disciplines of geology (particularly mineralogy, petrology, structural geology, and stratigraphy and sedimentation) as well as in allied sciences, such as physics and chemistry. It is assumed that the student has had one or more courses in these subjects and is in a position to appreciate the applications of various principles taught in those courses to issues related to mineral deposits. There is an emphasis on geochemistry throughout the book; this is necessary because the formation of almost all mineral

deposits ultimately involves the chemical precipitation of minerals from fluids of appropriate characteristics.

Considering the vast spectrum of mineral deposits that are either of potential economic interest or are actually being exploited for our use, it is practically impossible to include a comprehensive treatment of mineral deposits in an introductory text of this kind constrained by page limitations. The selection included here is based on what I perceive as the more interesting (and usually controversial) classes of deposits, especially from the points of view of origin and crustal evolution in space and time. This does not imply that the classes of deposits excluded from consideration here are not interesting or that their origins are devoid of controversy, but I had to draw the line somewhere.

A recurring problem I have had to deal with in writing this book is to keep it updated with the latest information, which is being produced at an ever increasing rate. In addition, space limitation has compelled me to a selection of the references I have used, a judgement, which I am afraid, is probably not totally devoid of personal bias.

Kula C. Misra
Knoxville, Tennessee
August, 1999

ACKNOWLEDGMENTS

The information contained in this book has come from a variety of sources: thousands of journal articles, scores of books, visits to many mines around the world, and a lifetime of endeavor to understand mineral deposits. I am thankful to all those authors who have shared their knowledge, the publishers who have been instrumental in disseminating the information, the mine geologists and mine managers who have made the mine visits a rewarding experience, and the teachers, such as Samar Sarkar, Asoke Mookherjee, Sisir Sen, and Michael Fleet, who taught me to think critically.

A book of this length and effort does not happen without the sustained cooperation and help of a substantial number of individuals. In addition to the anonymous reviewers selected by the publisher, I am grateful to my colleagues Harry Y. McSween, Jr., Otto C. Kopp, Robert D. Hatcher, and Marvin Bennett for critically reviewing several of the chapters. I am particularly indebted to Hap McSween for his continued support throughout the writing of this book.

I thank Marvin Bennett for all the help with the computer softwares I have used for this book, especially for graphics. The Office of Research, The University of Tennessee, Knoxville, is gratefully acknowledged for a generous grant toward the completion of this project.

This book would not have been completed without the encouragement of my wife, Geeta, our children, Lolly and Anand, and our son-in law, Tom, or published without the patience of the publishers.

CHAPTER 1

INTRODUCTION

1.1. Mineral Deposit versus Orebody

A *mineral deposit* (or an *ore deposit*) may be defined as a rock body that contains one or more elements (or minerals) sufficiently above the average crustal abundance to have potential economic value. It has been a common practice to classify mineral deposits into two broad categories: (a) *metallic* mineral deposits (e.g., deposits of copper, lead, zinc, iron, gold, etc.), from which one or more metals can be extracted; and (b) *nonmetallic* (or *industrial*) mineral deposits (e.g., deposits of clay, mica, fluorite, asbestos, garnet, etc.), which contain minerals useful on account of their specific physical or chemical properties. The minerals of economic interest in a deposit are referred to as *ore minerals* and the waste material as *gangue*. Accessory sulfide-group and oxide-group minerals (e.g., pyrite, arsenopyrite, magnetite, ilmenite), especially in metallic mineral deposits, however, are sometimes described as ore minerals, although they actually constitute part of the gangue.

An *orebody* refers to a specific volume of material in a mineral deposit that can be mined and marketed at a reasonable profit under the prevailing conditions of commodity prices, costs, and technology. Thus, many mineral deposits are not mined because they fail to pass the test of profitability. *Grade* (or *tenor*) is the average concentration of a valuable substance in a mineral deposit, and *cut-off grade* the minimum concentration required to achieve the break-even point for a mine in terms of revenue and costs. Any detailed exploration program is designed to collect an adequate amount of data that would enable the determination of cut-off grade, so that the *reserves* (tonnage of material) and *average grade* of an orebody can be calculated. The determination of the cut-off grade is a critical step in the evaluation of a mineral deposit because the size of the reserves increases progressively, often exponentially, with decreasing cut-off grade. Depending on the degree of geologic certainty of existence (as estimated from the results of drilling and other methods of exploration), the reserves of an orebody are commonly classified as *measured*, *indicated*, or *inferred*. (Fig. 1.1). Identified, subeconomic materials in a mineral deposit constitute *potential resources* (materials that may be profitably mined in the future), which may be further subdivided into *paramarginal* and *submarginal* categories on the basis of economic feasibility. Strictly speaking, *ore* refers to the material in an orebody, although the term is also used to denote ore-like material (in terms of mineral assemblage) that cannot be mined because of lower grade or other reasons.

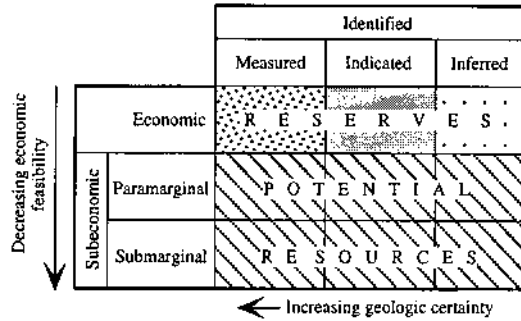


Figure 1.1. Classification of ore reserves based on degrees of geologic certainty and economic feasibility

1.2. Styles of Mineralization and Morphology of Mineral Deposits

The style of mineralization refers to the pattern of distribution of ore minerals in a host rock, and it varies from being very subtle (even invisible to the naked eye as in some precious metal deposits) to quite pronounced (as in the case of massive sulfide deposits). The shapes of mineral deposits are also highly variable, from concordant tabular and stratiform to discordant veins and breccia bodies. Some commonly used terms in the literature are summarized in Table 1.1.

TABLE 1.1. Some commonly used terms for style of mineralization and morphology of mineral deposits

	Mode of occurrence	Typical examples
<i>Disseminated</i>	Ore minerals dispersed through the host rock	Diamond in kimberlite pipes
<i>Stockwork</i>	An interlacing network of small and narrow (commonly measured in centimeters), close-spaced ore-bearing veinlets traversing the host rock	Footwall alteration zone of volcanic-hosted massive sulfide deposits (see Figs. 10.1, 10.4)
<i>Massive</i>	Mineralization comprising >50% of the host rock	Volcanic-hosted massive sulfide lenses (see Fig. 10.4)
<i>Tabular</i>	An ore zone that is extensive in two dimensions, but has a restricted development in its third dimension	Sandstone-type uranium deposits (see Figs. 14.3, 14.7)
<i>Vein-type</i>	Mineralization in veins, commonly discordant to the host rock layering (depositional)	Base- and precious metal veins (see Figs. 2.28, 2.29)
<i>Stratiform</i>	Mineralization confined to a specific bed and, thus, broadly conformable to the host rock layering (depositional)	Kupferschiefer-type stratiform copper deposits (see Fig. 12.4)
<i>Strata-bound</i>	Mineralization discordant to host rock layering (depositional), but restricted to a particular stratigraphic interval	Mineralized breccia bodies in Mississippi Valley-type deposits (see Fig. 13.9)

1.3. Distribution of Mineral Deposits

Mineral deposits have formed throughout the Earth's geologic history and in a wide spectrum of geologic environments. The space-time distribution of mineral deposits, however, is not uniform. As will be discussed in later chapters, certain types of mineral deposits tend to be concentrated in specific parts of the Earth's crust, often in clusters or arranged in linear belts, and/or particularly well represented within restricted intervals of geologic time. The recognition of this preferential distribution, which has enormous exploration and scientific significance, has given rise to the concepts of metallogenic provinces and metallogenic epochs. Following Turneure (1955), a *metallogenic province* may be defined as a mineralized area or region containing mineral deposits of a specific type or a group of deposits that possess features (e.g., morphology, style of mineralization, composition, etc.) suggesting a genetic relationship, and a *metallogenic epoch* as a geologic time interval of pronounced formation of one or more kinds of mineral deposits. The size of a metallogenic province can be as large as the Superior Province (Canadian Shield) or as small as the Upper Michigan Peninsula native copper province. Similarly, a metallogenic epoch can be as broad as the entire Proterozoic or as restricted as the Permian (Zechstein stratiform copper deposits).

A first-order control on the localization of mineral deposits is tectonic setting that, in turn, controls other factors favorable for the formation of mineral deposits. These factors include, for example, the form and composition of the associated igneous bodies, the formation of sedimentary basins and the characteristics of sediments that fill the basins, the development of faults and shear zones that provide conduits for mineralizing fluids or places for ore localization. It is not surprising, therefore, that many authors have attempted to relate the distribution of mineral deposits to plate tectonics (e.g., Guild 1972, Sillitoe, 1972a, 1972b, Garson & Mitchell 1973, Mitchell & Garson 1976, Hutchinson 1980, Guilbert & Park 1986, Sawkins 1972, 1976a, 1976b, 1990b). The exercise has been particularly successful for some kinds of deposits, such as porphyry copper deposits, volcanic-hosted massive sulfide deposits, and podiform chromite deposits, but many kinds of deposits (e.g., Precambrian massive sulfide and Ni-sulfide deposits, sediment-hosted uranium deposits, Kupferschiefer copper deposits) cannot yet be readily assigned to specific plate tectonic regimes or processes (see discussion by Sangster 1979). Moreover, plate-tectonic settings of many crustal segments, especially during the Precambrian, are highly controversial. Thus, inferred paleotectonic settings have not been adopted as the framework for this book.

1.4. Understanding Mineral Deposits

The discipline of *economic geology* encompasses three broad aspects: (a) *scientific study* — an understanding of known mineral deposits in terms of their distribution, characteristics, and genesis ; (b) *exploration* — application of the knowledge so

gathered and various techniques (geologic, geophysical, and geochemical) to the discovery and evaluation of new mineral deposits; and (c) *exploitation* — continued investigation of a deposit being mined for maintaining adequate reserves and optimum grade. This book focuses on the first and the most fundamental of these tasks. The discovery of new mineable deposits is becoming increasingly more difficult as we continue to look in virgin territories of uncertain potential, for lower and lower grades of ore at greater and greater depths, resulting in higher and higher costs of exploration and exploitation. This challenge has to be met, in addition to improved techniques of exploration, mining, extraction, and management, by a better understanding of the geologic setting and genesis of the various classes of deposits. The latter aspect, for any class of deposit, involves the unraveling of answers to some rather complex questions. How variable are the characteristics of this class of deposits? Were some geologic environments particularly favorable for the emplacement of these deposits? What were the controls of mineralization? What ore-forming processes were involved? Do we understand the deposits well enough to formulate a generalized genetic model that would account for the observed characteristics, be compatible with the crustal evolution in space and time, and serve as a discriminating exploration guide for this class of deposits?

The book may be perceived as consisting of two parts. The first part, comprising the next three chapters, emphasizes *principles* that provide the foundation for discussion of specific classes of mineral deposits covered in later chapters. Chapter 2 outlines the various ore-forming processes that formed mineral deposits of different kinds through geologic time and includes some typical examples. Chapters 3 and 4 discuss the principles and application of various kinds of field and laboratory data that can be used to interpret the genesis of a given mineral deposit, culminating with the Creede vein-type deposit (Colorado, USA) as a comprehensive example.

The second part of the book, comprising 12 chapters (Ch. 5 to Ch. 16), elaborates on the characteristics and genesis of selected classes of deposits. The overall format for these chapters is similar, with minor modifications to accommodate the special features of each class. It is true that each mineral deposit is unique at least in some respects (or no two deposits are exactly the same), but it is impracticable to learn about the thousands of known mineral deposits individually. On the other hand, many similar (not identical) deposits, irrespective of geographic and, in some cases, temporal distribution, share enough unifying characteristics that permit them to be treated as a group sharing a broadly common genetic model. Exceptions to this theme are the chapter on uranium deposits, which explores the implications for atmospheric evolution, and the chapter on gold deposits, which emphasizes the diversity of ore-forming processes that are capable of concentrating the same element in the Earth's crust. It is unlikely that a single deposit of a given class or subclass would fit the generalized genetic model in all aspects, but the formulation of conceptual genetic models not only provides the basis for exploration strategies, but also helps to identify gaps that need to be addressed with better data or alternative interpretations.

CHAPTER 2

FORMATION OF MINERAL DEPOSITS

2.1. Ore-forming Processes

All the common ore-forming elements are present in magmas and ordinary rocks, in amounts ranging from a few parts per billion to several thousands of parts per million (Table 2.1). The formation of a mineral deposit represents the convergence of a set of favorable circumstances leading to a significantly higher concentration of one or more elements in a limited portion of the Earth's crust. The required *concentration factor*, which is defined as the ratio of the average concentration of an element in a mineable mineral deposit to its average crustal abundance, is highly variable and depends not only on the particular element but also on the type of deposit. The concentration factors range from about 5-10 for geochemically abundant elements (e.g., aluminum and iron) to about 100-1,000 for less abundant elements (e.g., copper, zinc, and uranium). It is indeed remarkable that geologic processes, which normally result in further dispersal of trace elements, have been able to produce mineable deposits of geochemically scarce elements, such as gold and mercury, involving concentration factors in the thousands.

In general, selective concentration of one or more ore constituents to form a mineral deposit is achieved by some combination of the following: (a) extraction of the constituents from magmas, rocks, and oceans; (b) transport of the constituents in a fluid medium from the source region to the site of deposition; and (c) localization of the constituents at certain favorable sites. The mechanism, duration, and relative importance of these steps vary among the different ore-forming processes, but they all are controlled essentially by a similar set of physico-chemical principles.

For the present purpose, the ore-forming processes may be grouped into the following four broad categories:

- (a) Orthomagmatic processes
- (b) Sedimentary processes
- (c) Metamorphic processes
- (d) Hydrothermal processes

The formation of mineral deposits may also involve a combination of processes, for example, sulfide accumulation as a chemical sediment from metal-bearing hydrothermal fluids discharged on the sea-floor (*exhalative* deposits).

TABLE 2.1. Average abundances of selected ore-forming elements (in ppm) in the earth's continental crust, major rock types, and seawater (simplified from the compilation by Krauskopf and Bird 1995)

Element	Crust (a)	Granite (b)	Diabase (c) (Basalt)	Shale	Seawater (d)
Al	81,300	74,300	79,400	80,000	0.003
Fe	50,000	13,700	76,600	47,200	0.003
Ti	4,400	1,500	9,400	4,600	0.0001
Mn	950	195	1,280	850	0.0002
S	260	58	123	2,240	900
C	200	200	100	1,000	28
V	135	17	264	130	0.0022
Cr	100	20	114	90	0.0003
Ni	75	1	76	68	0.0005
Zn	70	45	86	95	0.0003
Cu	55	13	110	45	0.0002
Co	25	2.4	47	19	1×10^{-6}
Pb	13	48	7.8	20	3×10^{-6}
U	1.8	3.4	0.6	3.7	0.0032
Sn	2	3.5	3.2	6.0	6×10^{-7}
Mo	1.5	6.5	0.6	2.6	0.01
W	1.5	0.4	0.5	1.8	0.0001
Hg	0.08	0.1	0.2	0.4	4×10^{-7}
Ag	0.07	0.05	0.08	0.07	3×10^{-6}

Concentrations of Au and Pt are <0.05 ppm in rocks and <0.00001 ppm in seawater.

(a) "Crust" means the continental crust only, a part of the crust that is assumed to be made up of roughly equal parts of granite and basalt. For the oceanic crust a composition similar to that of average basalt can be assumed.

(b) "Granite" includes silica-rich rocks ranging from alkali granite to granodiorite and their volcanic equivalents.

(c) "Diabase" includes the more common varieties of basaltic lava, diabase, and dolerite.

(d) "Seawater" is an average analysis of deep Atlantic and deep Pacific water.

2.2. Orthomagmatic Processes

Theoretical considerations and field relations suggest that ore-forming processes related to the evolution of magmas emplaced at crustal levels span a continuum. The two end-members of this continuum are: (a) *orthomagmatic* processes — concentration of ore minerals as a direct consequence of magmatic crystallization dominated by silicate melt-crystal equilibria; and (b) (magmatic) hydrothermal processes — concentration of ore

minerals from magmatic hydrothermal fluids by crystallization dominated by crystal-volatile equilibria.

2.2.1. IGNEOUS ASSOCIATION

A strong argument for a genetic relationship between magmas and mineral deposits is the observed consistent association that can be rationalized on the basis of magmatic crystallization. Deposits of iron, copper, nickel, chromium, titanium, and platinum, are restricted to mafic and ultramafic rocks which also show markedly higher concentrations of these elements compared with more siliceous varieties (Table 2.1). In addition, deposits of some of these metals characteristically occur in particular kinds of mafic and ultramafic rocks — e.g., chromium in dunite and peridotite, nickel in peridotite and norite, and titanium in gabbro and anorthosite. Because of the small quantity of dissolved water, crystallization of mafic and ultramafic magmas seldom leads to the generation of large amounts of ore-forming hydrothermal fluids, except perhaps when substantial assimilation of water-bearing crustal rocks is involved.

A genetic relationship between felsic magmas and mineral deposits is much less convincing, because the association of metals with specific felsic rocks is not as clear as with mafic and ultramafic rocks (Krauskopf 1967b). Of the deposits commonly associated with felsic intrusives, only those of tin are restricted to granites and these granites themselves are often anomalously rich in this metal. Other deposits — such as those of copper, silver, gold, lead, zinc, molybdenum, tungsten — are associated with rocks ranging from granite to diorite, although there may be a preferential association with a particular rock type in a given geologic setting. Moreover, the host rocks of these deposits do not appear to be consistently enriched or depleted in the respective elements. On the other hand, the well-established tendency of mineral deposits to cluster near the periphery of felsic intrusives and the many well-documented examples of hydrothermal alteration and metal zoning centered on such intrusives (see Ch. 3) strongly suggest a genetic connection between felsic magmas and the associated hydrothermal deposits.

2.2.2. MAGMAS AS SOURCES OF ORE CONSTITUENTS

Magmas — essentially silicate melts with variable amounts of ore metals and other elements, water, and relatively minor amounts of other volatile constituents (e.g., CO₂, H₂S, SO₂, HCl, HF, H₂) — are generated by *partial melting* of lower crustal or upper mantle material. It is generally accepted that partial melting of the top 100-200 km of the upper mantle by adiabatic decompression (pressure-release melting) produces primary magmas of mafic (basaltic or picritic) or ultramafic (komatiitic) composition in most tectonic settings, and that the wide compositional spectrum of terrestrial igneous rocks is attributable to parental magmas formed by subsequent differentiation and/or assimilation. The generation of significant amounts of water-saturated magmas or hydrous fluids is unlikely in the upper mantle because of its low water content

(Burnham 1967). On the other hand, dioritic and granitic magmas generated by partial melting of lower crustal rocks are likely to be more hydrous and capable of generating an aqueous fluid phase with progressive crystallization.

As some elements are preferentially partitioned into the melt phase, partial melting is a critical step for concentrating ore constituents in a magma. Whereas the major element composition of partial melts is largely insensitive to the mechanism of partial melting process, the trace element composition is not. The two main end-member models of partial melting are: (a) *equilibrium* or *batch* melting that involves continuous reaction and equilibration of the partial melt with the crystalline residue, until mechanical conditions allow the melt to escape (or segregate) as a single 'batch' of magma; and (b) *fractional* or *Rayleigh* melting in which the partial melt is continuously removed from the system as soon as it is formed, thereby preventing further reaction between the melt and the solid residue. Assuming modal melting (i.e., melting of the phases in proportion to their modal abundance in the source), the concentration of a trace element i in the melt ($C_{i(L)}$) is related to that in the source ($C_{i(O)}$) by the following expressions:

$$\text{Batch melting} \quad C_{i(L)} / C_{i(O)} = 1/[D+F(1-D)] \quad (2.1)$$

$$\text{Fractional melting} \quad C_{i(L)} / C_{i(O)} = 1/D [(1-F)^{(1/D)-1}] \quad (2.2)$$

where X_α = the weight fraction of the solid phase α in the source, D_α = the solid-liquid partition coefficient of the element i = (concentration of i in the solid phase) / (concentration of i in the partial melt), D = the bulk distribution coefficient for all the solid phases combined = $\sum X_\alpha D_\alpha$, and F = the weight fraction of partial melt formed. It follows that for small degrees of partial melting, the melt phase would be significantly enriched in incompatible elements ($D < 1$), such as rare-earth elements (REE), relative to compatible elements ($D > 1$), such as Ni, and that high degrees of partial melting would be necessary for significant enrichment of compatible elements in the melt phase. Moreover, because of relatively higher average contents of base and precious metals, mafic and ultramafic source rocks would tend to yield magmas (partial melts) enriched in these elements; felsic rocks, on the other hand, would tend to produce magmas enriched in Sn, Be, Ta, Nb, REE, and alkali metals.

The mantle, with an estimated sulfur concentration in the range of 300-1,000 ppm (Sun 1982), is believed to be the dominant source of sulfur carried in basaltic magmas, because experimental studies (MacLean 1969, Shimazaki & Clark 1973) have shown that during partial melting of the mantle the available iron sulfide would melt well before the beginning of silicate melting. Estimates of the juvenile sulfur concentration in oceanic basalts, which appear to be saturated or nearly saturated with respect to sulfur (Czamanske & Moore 1977, Hamlyn & Keays 1986), range from 600 ± 150 ppm (Moore & Fabbi 1971) to as high as 1,600 ppm (Anderson 1974). It is, however, difficult to predict the sulfur contents of silicate melts, because the solubility of sulfur is controlled by a number of interdependent variables, such as temperature, pressure,

fO_2 , fS_2 and, especially, the activities of FeO and SiO_2 in the melt (Fincham & Richardson 1954, Haughton et al. 1974, Shima & Naldrett 1975, Buchanan & Nolan 1979, Buchanan et al. 1983). In general, the sulfur solubility in silicate melts decreases with (a) decreasing temperature, (b) decreasing activity of FeO or increasing activity of SiO_2 , and (c) decreasing fS_2 or increasing fO_2 . For example, at fO_2 conditions below the NNO buffer (see Fig. 3.7) the maximum sulfur solubility in granitic-granodioritic melts (1 to 8 wt % FeO) is about 100-300 ppm and reduced sulfur species dominate, whereas at fO_2 above the NNO buffer the maximum sulfur solubility is about 100-2,000 ppm with oxidized species dominant over reduced species (Fig. 2.1). Li and Naldrett (1993) have discussed a theoretical quantitative model that relates dissolved sulfide contents of a magma to temperature, fO_2 , fS_2 , and the activity of FeO. The actual amount of juvenile sulfur carried by a basaltic magma might be significantly higher than its saturation limit at the source, if some of the sulfide melt in a given volume of mantle material was incorporated into the partial melt as an immiscible phase. The sulfur content of a sulfur-undersaturated basaltic or granitic magma emplaced in the crust might also be enhanced by assimilation of sulfur from the country rocks. Because of the higher initial temperatures and fO_2 (Fig. 2.2), I-type granitoid magmas (White & Chappell 1977) have a greater potential for bulk-assimilation of country-rock sulfur than S-type magmas.

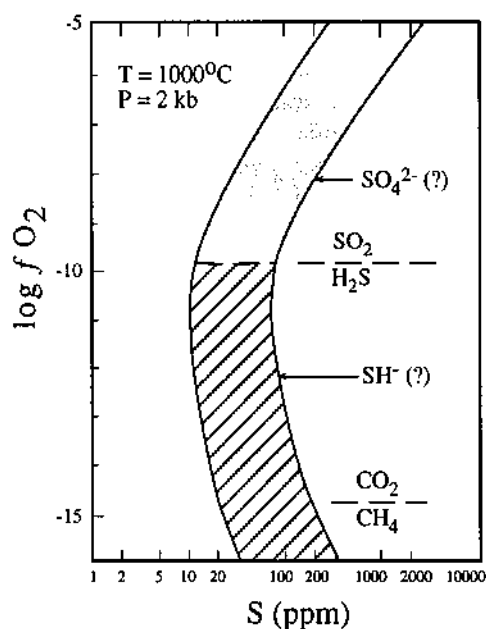


Figure 2.1. Estimated solubility and speciation of sulfur in silicate melts of granodioritic to granitic composition based on experimental data of Bradbury (1983) and Carroll and Rutherford (1985). (After Ohmoto 1986.)

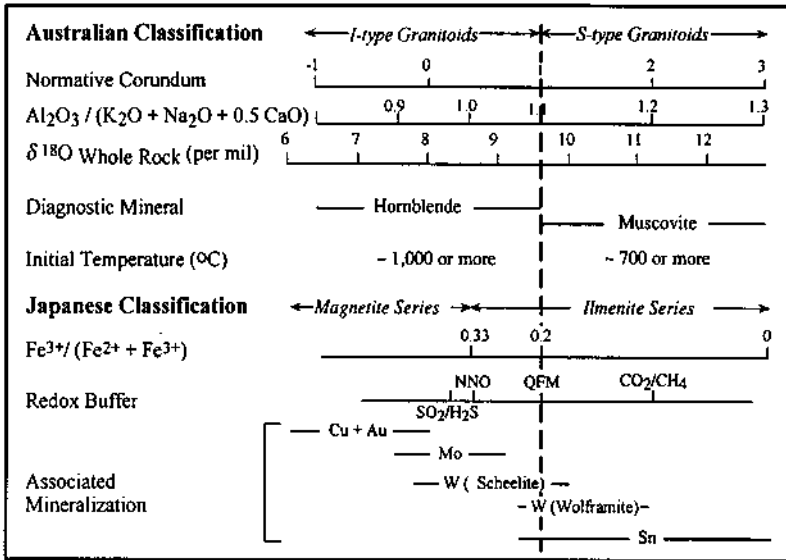


Figure 2.2. Generalized characteristics of I-type and S-type granitoids (after Ohmoto 1986). Note that magnetite-series and ilmenite-series granitoids, as defined by Ishihara (1977) on the basis of modal compositions (relative abundance of magnetite vs. ilmenite) and bulk Fe_2O_3/FeO ratios, correspond only roughly to I-type and S-type granitoids.

2.2.3. MAGMATIC FLUIDS

Experimental results and thermodynamic considerations for the evolution of magmatic fluids have been discussed in considerable detail by Burnham (1967, 1979, 1997). The separation of an aqueous phase (or an aqueous liquid phase and an aqueous vapor phase) from a magma, commonly referred to as *boiling*, is controlled mainly by the solubility of H_2O in the melt, which is very strongly pressure dependent but only weakly temperature dependent (Fig. 2.3). The amount of hydrothermal fluid that will be exsolved from a magma depends on its initial H_2O content, its depth of emplacement, and its crystallization history. The initial H_2O contents of magmas with which extensive hydrothermal activity is associated generally range from ≈ 2.5 to 6.5 wt%, with a median value close to 3.0 wt%. The lower limit is set by pressure-temperature projections of melting relations in hornblende-bearing basaltic amphibolites, typical of rocks melted in subduction zones, and biotite-bearing gneisses and schists, typical of rocks melted in the lower crustal environments. For dioritic and granitic magmas generated by partial melting the initial melt would contain, respectively, in excess of 3.3 wt% H_2O for hornblende and 2.7 wt% H_2O , for biotite to be in stable coexistence at near-liquidus temperatures, regardless of the amount of H_2O initially bound in hydrous minerals. The upper limit of H_2O is the saturation value at approximately 2.1 kb, the

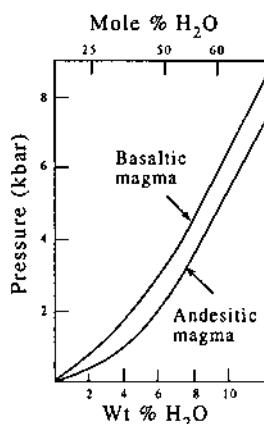


Figure 2.3. Solubility of H_2O in silicate melts of basaltic and andesitic composition at 1100°C as a function of pressure. The mole% water on top axis is approximate, because the actual mole% will vary as a function of melt composition. (After Burnham 1979.)

pressure equivalent to a lithostatic load of about 8 km of crustal rocks, and is probably close to the upper pressure limit of extensive hydrothermal activity.

When an ascending water-bearing magma begins to crystallize, the volume of the residual magma becomes smaller and smaller, and H_2O (with other volatiles) gets concentrated in this decreasing volume. Boiling occurs when an increase in vapor pressure due to confinement of dissolved gases in a smaller and smaller body of melt exceeds the total external pressure (P_{total}). The phenomenon of crystallization-driven volatile exsolution in plutonic environments (represented by the reaction H_2O -saturated melt \Rightarrow crystals + aqueous fluid), commonly referred to as *retrograde boiling* (also as *second boiling*, or *resurgent boiling*), is a natural consequence of the cooling of a melt when it becomes saturated with respect to water and one or more crystalline phases. Any granitic magma that contains more than approximately 0.6 wt% H_2O , which is close to the maximum amount of H_2O that can structurally be bound in hydrous minerals (mostly hornblende and biotite) under magmatic conditions, must undergo the process of retrograde boiling prior to reaching the H_2O -saturated solidus. For felsic magmas with high enough initial H_2O content ($\approx 2\text{--}4$ wt%), second boiling should occur at a depth of 2-6 km, before the magma becomes approximately 75% crystalline (Burnham & Ohmoto 1980). The exsolved aqueous fluid phase can be highly saline, as is predicted from thermodynamic modeling (Cline & Bodnar 1991, Shinohara 1994) and documented by fluid inclusions from many porphyry copper deposits (Roedder 1984).

The development of a magmatic fluid phase may contribute to the formation of mineral deposits in two ways. First, the increase in the volume of the magma body, which results from the fact that the molal volume of H_2O "vapor" at these temperatures

and pressures is much larger than the partial molal volume of H_2O in the melt, leads to an increase in the internal pressure of the magma body and causes hydrofracturing of the wallrocks, creating channelways for migration of magmatic and other ore-forming fluids. Second, the fluid phase becomes enriched in certain elements relative to the residual melt, thus making it a potential ore-forming fluid. The solute composition of this aqueous fluid will vary from one magma to another and is difficult to predict accurately with our current knowledge of partitioning of ore metals between a magmatic melt and its exsolved aqueous fluid. Available experimental data and thermodynamic extrapolations, however, suggest that such aqueous fluids separated from felsic magmas will be enriched in incompatible elements (including chalcophile ore metals) and total chlorides (the major portion of the dissolved solutes, except for silica, occurring commonly as chloride complexes), slightly acidic (one or two pH units below neutral at 700-750°C and 1,000- 2,000 bars), and capable of forming deposits of molybdenum, tungsten, tin, iron, and base metals (Burnham 1967, Holland 1972, Burnham & Ohmoto 1980, Candella & Holland 1984, Urabe 1987, Coetzee & Twist 1989). The sulfur content of the aqueous fluid is determined by its $SO_2:H_2S$ ratio that increases with increasing fO_2 of the parent magma prior to the onset of second boiling. Aqueous fluids derived from I-type (high fO_2) magmas may contain large quantities of SO_2 as well as H_2S , but at lower temperatures on cooling hydrolysis of SO_2 ($4SO_2 + 4H_2O = H_2S + 3H_2SO_4$) or its reaction with Fe^{2+} -bearing minerals of the wallrocks ($SO_2 + 6 "FeO" + H_2O = H_2S + 3 "Fe_2O_3"$) increases the activity of H_2S , causing precipitation of sulfide ore minerals from the metal-chloride complexes in the aqueous solution. In contrast, aqueous fluids derived from S-type (low fO_2) magmas may contain as much H_2S as those derived from I-type magmas, but because of lower fO_2 they contain much smaller amounts of SO_2 and, therefore, total sulfur. Thus, aqueous fluids that separate from I-type magmas tend to produce Cu-Mo-Zn-Fe sulfide deposits, whereas fluids from S-type magmas generally precipitate smaller quantities of sulfides, mainly pyrrhotite, and correspondingly larger quantities of oxides, such as cassiterite (Burnham & Ohmoto 1980). In either case, the precipitation of sulfides from metal-chloride complexes is accompanied by generation of HCl. The HCl and the H_2SO_4 produced by SO_2 hydrolysis are consumed by "acid" alteration of aluminosilicate minerals in the wallrocks. The formation of mineral deposits by contact metamorphic and hydrothermal processes, involving fluids from magmatic sources, will be discussed in later sections.

2.2.4. CONCENTRATION BY MAGMATIC CRYSTALLIZATION

Ore constituents present in a magma may be concentrated further during the course of crystallization. Three *magmatic differentiation* processes have been considered particularly important for the formation of *orthomagmatic* deposits: (a) liquid immiscibility (Vogt 1926); (b) gravitative crystal settling (Bowen 1928); and (c) fitter pressing (Daly 1933).

Liquid Immiscibility

Liquid immiscibility is the phenomenon of separation of a cooling magma into two or more liquid phases of different composition in equilibrium with each other. Experiments have demonstrated three cases of liquid immiscibility under geologically reasonable conditions: (a) separation of Fe-rich tholeiitic magmas into two liquids, one felsic (rich in SiO_2) and the other mafic (rich in Fe); (b) splitting of CO_2 -rich alkali magmas into one melt rich in CO_2 and the other rich in alkalis and silica, which may account for the origin of carbonatite magmas; and (c) segregation of sulfide melts (or oxysulfide melts containing a few percent dissolved oxygen) from sulfide-saturated mafic or ultramafic magmas.

Conditions or processes that are likely to promote sulfide immiscibility in a mafic or ultramafic magma are: (a) cooling of the magma, which not only decreases its sulfur solubility, but also causes crystallization of silicate minerals, thereby increasing the sulfur concentration in the residual magma; (b) silica enrichment of the magma by reaction with felsic country rocks (Irvine 1975, Naldrett & Macdonald 1980); (c) mixing of a more fractionated magma with a less fractionated magma, both of which were nearly saturated with sulfur (Irvine 1977, Campbell et al. 1983); and (d) assimilation of sulfur from country rocks (Godlevsky & Grinenko 1963, Mainwaring & Naldrett 1977, Ripley 1981, Buchanan & Rouse 1984). Other processes which can, in theory, cause sulfide saturation are oxidation (MacLean 1969) and an increase in pressure (Wendlandt 1982).

Criteria for the existence of immiscibility in natural systems are based on textural, mineralogical, and chemical data. A small amount of sulfide melt segregating from a silicate magma is likely to be dispersed as minute droplets in the magma. Thus, the globular texture of sulfide(-oxide) disseminations in the Skaergaard and Sudbury intrusions have been considered a diagnostic evidence of sulfide immiscibility (Wager et al. 1957, Hawley 1962). Analogous textures ascribed to liquid immiscibility have also been described in modern basaltic lavas (Skinner & Peck 1969, Czamanske & Moore 1977). Another useful criterion for recognizing sulfide immiscibility in silicate magmas is the depletion of chalcophile elements (e.g., Ni, Cu) in the resulting igneous rocks, because chalcophile elements are strongly partitioned into the sulfide phase. The magnitude of the depletion of an element i depends on the *Nernst partition coefficient* $D_i^{\text{sul-sil}}$ [defined as $D_i^{\text{sul-sil}} = \text{concentration of } i \text{ in the sulfide melt (sul)} / \text{concentration of } i \text{ in the silicate melt (sil)}$] as well as on the sulfide segregation process.

Similar to partial melting, immiscible sulfide segregation may be viewed in terms of two end-member processes (Figs. 2.4 and 2.5): (a) *batch segregation (equilibrium crystallization)* that involves the segregation of a significant amount of sulfide in a single stage and its equilibration with the entire body of residual magma before the sulfide is removed from the system; and (b) *fractional segregation (Rayleigh fractionation)* in which case very small amounts of sulfide become continuously immiscible, equilibrate with the silicate magma, and then are removed from the system by settling or by some other mechanism, thereby preventing further interaction with the residual magma. Fractional segregation typically occurs during the crystallization

of a sulfide-saturated silicate magma, because the crystallization of even a small amount of olivine (or other sulfur-free minerals) leads to sulfide immiscibility (Fig. 2.4). Sulfide immiscibility induced by a sudden change in intensive parameters (e.g., due to sulfur or silica assimilation from country rocks) should produce batch segregation (Fig. 2.5). Such sulfide segregation may or may not be accompanied by silicate crystallization, but sulfide segregation before the onset of significant silicate crystallization would provide a more favorable situation for the formation of *magma segregation* deposits.

Consider an element i whose initial concentration in the magma is C_{im} . For fractional segregation (Rayleigh fractionation), the concentration of i in the residual magma, C_{rm} , is given by:

$$C_{rm} = C_{im} F^{(D-1)} \quad (2.3)$$

where F = the weight fraction of silicate melt remaining in the system undergoing crystallization, and D = the bulk partition coefficient of phases being removed from the magma. If olivine (ol) is the only phase being removed from the silicate melt (sil), $D = D_i^{ol-sil}$; if the magma is sulfide-saturated so that both olivine and sulfide (sul) are being removed, D is the sum of D_i^{ol-sil} and $D_i^{sul-sil}$ weighted according to the relative proportions of olivine and sulfide. For an ultramafic (komatiitic) magma, which initially contained 32 wt % MgO and 1,750 ppm Ni, the calculated Ni-depletion trends

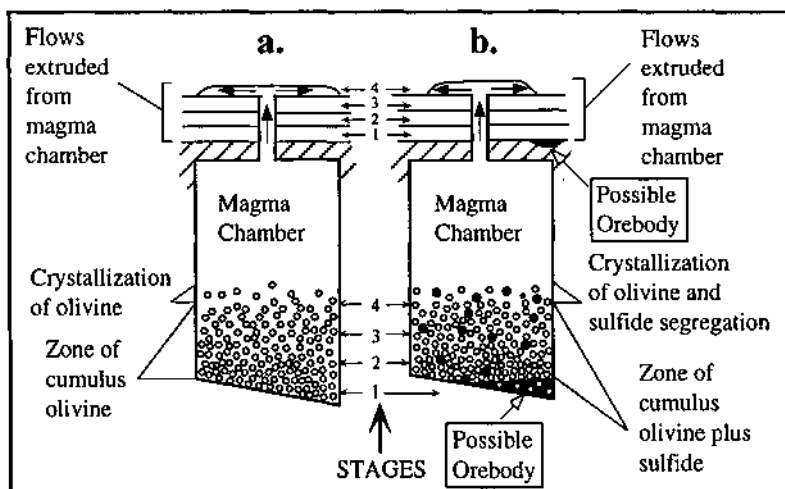


Figure 2.4. Fractional crystallization of olivine and fractional segregation of sulfide from a cooling magma: a. Sulfide-undersaturated; b. Sulfide-saturated. The fractionated magma is assumed to erupt periodically to give rise to a series of flows (1, 2, 3, 4) of successively lower MgO content. (After Naldrett et al. 1984.)

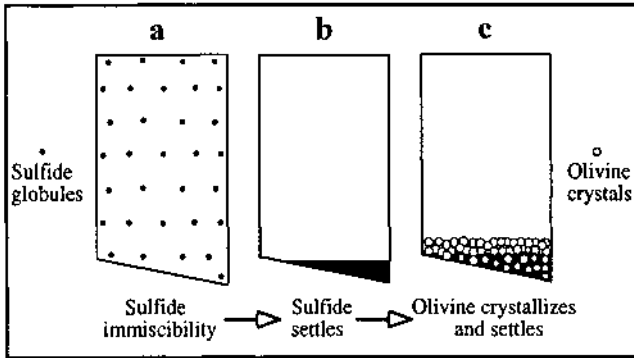


Figure 2.5. Batch segregation of sulfide phase from a cooling magma: a. Sulfide immiscibility due to sulfur saturation in the magma; b. Settling of the sulfide, preventing further interaction with the magma; and c. Beginning or resumption of silicate (e.g., olivine) crystallization. (After Naldrett et al. 1984.)

due to olivine fractionation under sulfide-unsaturated and a series of sulfide-saturated conditions are shown in Figure 2.6a. As $D_{Ni}^{sul-sil}$ is significantly higher than D_{Ni}^{ol-sil} , the difference between fractional and batch segregation processes becomes more pronounced with decreasing olivine:sulfide ratio.

For batch segregation of an immiscible sulfide melt, the concentration of i in the remaining silicate magma is given by (Campbell & Naldrett 1979):

$$C_{rm} = C_{im} [(R+1)/(R+D_i)] \tag{2.4}$$

where R = mass ratio of the silicate magma to the sulfide melt, and $D_i^{sul-sil}$ is denoted, for the sake of convenience, by D_i . As an example, the trend of Ni depletion in a basaltic magma, which initially contained 400 ppm Ni but has undergone batch equilibration with an immiscible sulfide melt at varying values of R , is shown in Figure 2.6b. Note that Ni depletion in both the magma and the olivine becomes significant only for R values below about 1,000.

What about the concentration of i in the immiscible sulfide melt? For a small amount of segregated sulfide melt in equilibrium with the remaining silicate magma, the concentration of i in the sulfide melt (Y_i) is given by:

$$Y_i = C_{rm} D_i \tag{2.5}$$

Equation 2.5 also gives satisfactory approximation for Y_i if C_{rm} is substituted by C_{im} , the initial concentration of i in the silicate magma, provided R is very large. For batch segregation of a large volume of sulfide melt, D_i should be calculated from (Campbell & Naldrett 1979):

$$Y_i = C_{im} D_i [(R+1)/(R+D_i)] \quad (2.6)$$

The effects of R and D_i on Y_i are shown schematically in Figure 2.7a. Equation 2.6 may be simplified for special cases. For example, if $R \ll D_i$, then

$$Y_i \approx C_{im} (R+1) \quad (2.7)$$

so that Y_i becomes virtually independent of D_i and a function of R (Fig. 2.7b). On the other hand, if $R \gg D_i$, equation 2.6 reduces to equation 2.5, so that for a given value of D_i , variations in R have relatively little effect on Y_i . Thus, for small amounts of immiscible sulfide liquid relative to the silicate magma, the concentrations of various elements in the sulfide liquid are determined largely by their partition coefficients, but when a large volume of sulfide liquid is segregated, a necessary condition for the formation of sulfide deposits, its bulk composition is also influenced by the value of R . For practical purposes, Y_i may be computed by using equation 2.6 when $R > 10D_i$ (as further increases in R have little effect on Y_i) and equation 2.7 when $R < D_i/10$ (Campbell & Naldrett 1979). The significance of D_i and R in modeling the values of D_i and R , will be discussed later (Ch. 6 and Ch. 7).

Gravitational Settling

The formation of massive deposits of magmatic crystallization products, such as chromite and sulfides, requires that they be concentrated by some mechanism in a restricted part of the magma chamber. The lack of efficient segregation from the silicate minerals, for example, because of the solidification of a large portion of the magma before the onset of chromite crystallization or sulfide immiscibility, would normally result in relatively low-grade, *disseminated* mineralization.

A possible mechanism of crystal-liquid separation in a magma undergoing crystallization is *gravitational settling* (or floating) of crystals by virtue of their density differences relative to the liquid. Assuming Newtonian fluid dynamics (i.e., the viscosity of the fluid is independent of the stress and strain rate), the settling velocity (v) for spherical particles is given by the Stokes' Law equation:

$$v = 2r^2 g \Delta\rho / \eta \quad (2.8)$$

where r = radius of the crystal, $\Delta\rho$ = density contrast between the crystal and melt, η = viscosity of the melt, and g = acceleration due to gravity. Calculated settling velocities using this equation are compatible with effective crystal fractionation on the time scale (10^4 - 10^6 years) envisaged for the cooling of large bodies of magma.

Cumulate layers, including chromite-rich layers, in large differentiated complexes such as the Bushveld and the Stillwater, have generally been regarded as products of gravitational crystal settling. Recent studies, however, have argued against crystal settling being the dominant mechanism for the formation of such cumulate layers. The

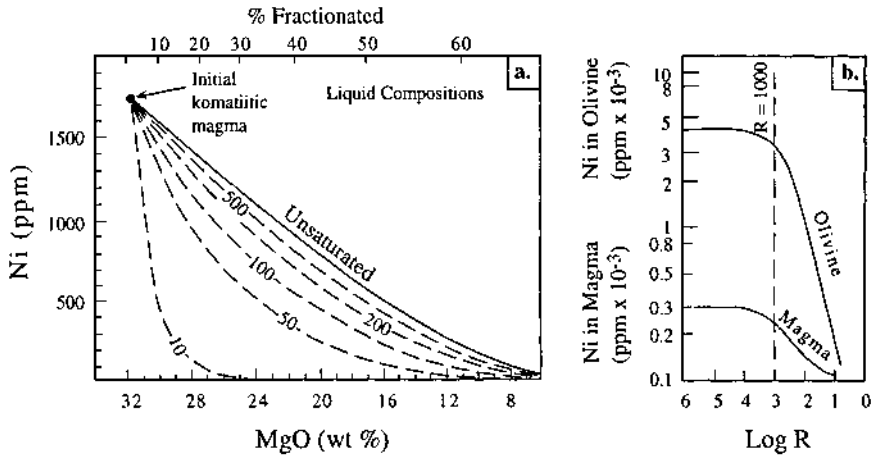


Figure 2.6. a. Calculated trends of Ni depletion by fractional segregation of an ultramafic (komatiitic) magma, initially containing 32 wt % MgO and 1,750 ppm Ni, under sulfide-unsaturated condition (solid line) represented by separation of olivine only, and a series of sulfide-saturated conditions (broken lines) with olivine:sulfide weight ratios of 500, 200, 100, 50, and 10. b. Calculated trends of Ni depletion in a magma, containing initially 400 ppm Ni, and in the olivine in equilibrium with the magma resulting from batch segregation of immiscible sulfide melt as a function of R (mass ratio of silicate magma to immiscible sulfide melt). Values used for D (Nernst partition coefficient) are: $D_{Ni}^{sulfide\ melt / silicate\ magma} = 275$ and $D_{Ni}^{olivine / silicate\ magma} = 7.23$. (After Naldrett et al. 1984.)

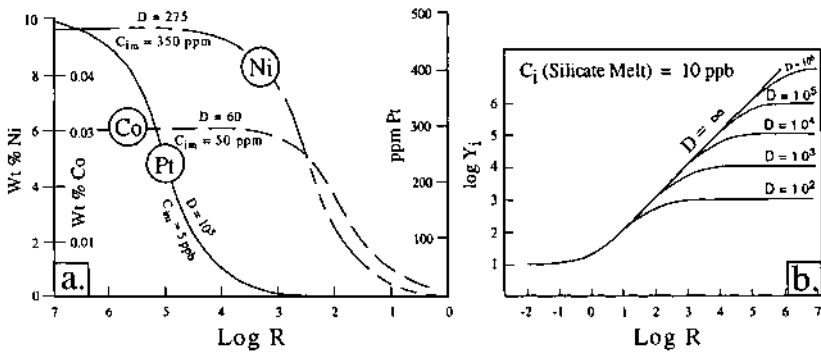


Figure 2.7. a. Variation in the concentration of Ni, Co, and Pt in a batch-segregated sulfide melt (Y_1) as a function of R (mass ratio of silicate magma to immiscible sulfide melt) and D (Nernst partition coefficient). The assumed initial concentrations of the elements in the magma (C_m) are 350 ppm Ni, 50 ppm Co, and 5 ppb Pt (after Naldrett & Barnes 1986). b. The effect of variation in the silicate:sulfide ratio (R) on the precious metal content of an immiscible sulfide melt (Y_1) for different values of partition coefficient D . The initial concentration of the precious metal in the silicate melt (C_1) is assumed to be 10 ppb. Note that if R is less than about $D/10$, Y_1 is virtually independent of D . (After Campbell et al. 1983.)

main arguments against the crystal settling hypothesis include: a lack of *hydraulic equivalence* between olivine and chromite in individual cumulate layers of the Stillwater complex (Jackson 1961); the occurrence of lighter plagioclase-rich cumulates below heavier pyroxene-rich cumulates in some layered intrusions (Campbell 1978); and the likelihood of convective velocities in the magma being orders of magnitude greater than the settling velocities of individual crystals, calculated using the Stokes' Law (Sparks et al. 1984). The available evidence appear to favor *in situ* growth of cumulus minerals along the margins and especially on the floor of the magma chamber (Campbell 1978, Irvine 1980).

Filter Pressing

Magmatic segregation deposits may also form by crystallization of residual magmas. A mafic magma without a high enough fO_2 for early crystallization of Fe-Ti oxide minerals would produce enrichment of iron and titanium in the residual magma. This heavier liquid, then, may drain downward, collect below as a segregation resting on a solid floor of early formed sunken crystals, and crystallize into a layer with significant concentration of Fe-Ti oxide minerals. In some situations, the residual magma may be squeezed out by *filter pressing* and form *magmatic injection* deposits. The Fe-Ti oxide deposits associated with anorthosites and anorthositic gabbros are believed to have formed by gravitative accumulation and injection of residual magmas (see Fig. 2.16).

2.3. Examples of Orthomagmatic Deposits

Orthomagmatic deposits occur in ultramafic and related mafic igneous rocks (Table 2.2), but a close spatial association between a mineral deposit and an igneous body does not guarantee an orthomagmatic origin for the deposit. To prove an orthomagmatic origin for the deposit, it is necessary to establish that the distribution, mineralogy, and textures of the deposit are compatible with a magma composition and crystallization process that would also account for the features of the host igneous body. This is not an easy task, because ore mineral assemblages tend to lose some of their igneous imprints through re-equilibration during cooling, and because superimposed deformation and metamorphism may complicate matters even further. Nevertheless, there are many deposits for which the available data strongly suggest an orthomagmatic origin. Some important examples of deposits which are commonly ascribed to orthomagmatic process are listed in Table 2.3.

2.3.1. MAFIC-ULTRAMAFIC COMPLEXES: CHROMIUM, NICKEL-COPPER, AND PLATINUM-GROUP ELEMENTS (PGE)

Deposits of chromite, nickel (-copper) sulfides, and platinum-group elements (PGE) occur exclusively in mafic-ultramafic complexes and commonly are regarded as products of orthomagmatic processes. The best examples are the 'stratiform' chromite deposits

TABLE 2.2. Simplified classification of ultramafic and mafic bodies (modified from Naldrett & Cabri 1976, Naldrett 1981a)

Class of body	Examples	Associated mineral deposits
<i>A. Synvolcanic bodies (excluding those related to intracratonic volcanism)</i>		
1. Komatiitic suites		
(a) Lava flows	Eastern Goldfields, Western Australia	Ni-sulfide (Kambalda)
(b) Layered sills	Barberton, South Africa	
(c) Dunitic-peridotite lenses	Eastern Goldfields, Western Australia	Ni-sulfide (Preservance)
(d) Uncertain type	Manitoba, Canada	Ni-sulfide (Thompson)
2. Tholeiitic suites		
(a) Layered picritic intrusions	Eastern Goldfields, Western Australia	Ni-sulfide (Carr Boyd)
(b) Anorthositic bodies	Doré Lake Complex, Canada	
<i>B. Intrusions in cratonic areas</i>		
1. Intrusions related to flood basalts	Duluth Complex, USA Noril'sk-Tanakh, Siberia	Ni-sulfide Ni-Cu sulfide
2. Large layered complexes	Bushveld Complex, South Africa Stillwater Complex, USA Great Dyke, Zimbabwe Sudbury Complex, Canada	Chromite, Ni-Cu sulfide, Pt-Pd ore Pt-Pd ore Chromite, Pt-Pd ore Ni-Cu sulfide
3. Medium and small layered intrusions	Skaergaard, Greenland	
4. Kimberlites	Kimberly, South Africa	Diamond
<i>C. Bodies emplaced during orogenesis</i>		
1. Synorogenic intrusions	Rona, Norway	Ni-sulfide
2. Tectonically emplaced alpine-type bodies		
(a) Ophiolite complexes	Troodos Complex, Cyprus Theftford Complex, Canada	Chromite, Cu-sulfide Asbestos
(b) Mantle diapirs (?)	Mt. Albert, Canada	
3. Alaskan-type zoned complexes	Union Bay, Alaska, USA Duke Island, Alaska, USA	

hosted in the ultramafic zone of layered (differentiated) complexes such as the Bushveld and Stillwater; the so called 'podiform' chromite deposits, which occur as discontinuous pods and lenses in alpine-type ultramafic intrusions, are also believed to be orthomagmatic cumulates, but formed in tectonically active settings. The origin of nickel (-copper) sulfide deposits associated with layered intrusions and tholeiitic-komatiitic suites have been ascribed to orthomagmatic processes by most authors, although some aspects of fundamental importance remain controversial. The origin of the platinum-palladium deposits is not well understood. These three types of deposits

TABLE 2.3. Examples of deposits formed predominantly by orthomagmatic processes

Host rock association	Ore type	Important examples
Mafic-ultramafic complexes		
Layered intrusions	Chromite	Bushveld, South Africa Great Dyke, Zimbabwe
	Ni(-Cu) sulfide	Sudbury, Canada Bushveld, South Africa
	Pt-Pd	Bushveld, South Africa Stillwater, USA
Ophiolites	Chromite	Kempirsai, Ural Mountains Kavak, Turkey
Tholeiitic-komatiitic suites	Ni-sulfide	Kambalda district, W. Australia Pechanga, Russia
Kimberlites	Diamond	Kimberly, South Africa Yakutia, Russia
Carbonatite complexes	Nb	Oka, Canada
	Rare earth elements	Sulfide Queen, USA
	Cu	Palabora, South Africa
Anorthosite complexes	Ilmenite	Allard Lake, Canada Sanford Lake, USA
Alkali igneous complexes	Fe-Ti oxide - Apatite	Kiruna district, Sweden Roseland district, USA
Granitic pegmatites*	Sheet mica, beryl/emerald, spodumene (Li), niobite-tantalite (Nb-Ta), cassiterite (Sn)	Kings Mountain district, USA Petaca district, USA Nellore district, India

* Some pegmatites, such as those of the Petaca district, appear to have formed in two stages: an early magmatic stage involving crystallization of a water-rich residual melt derived from a granitic magma; and a later hydrothermal stage involving precipitation from related magmatic-hydrothermal fluids (Jahns 1946).

are discussed in detail in later chapters (Ch. 5, 6, and 7). Ultramafic-mafic complexes, especially the alpine-type intrusions, are also well known for their asbestos and magnesite deposits, which form by later hydrothermal alteration and metamorphism of ultramafic rocks.

2.3.2. CARBONATITES: NIOBIUM, RARE-EARTH ELEMENTS (REE), COPPER

Carbonatites are carbonate-rich rocks (>50 modal% carbonate minerals) of apparent magmatic derivation or descent (Heinrich 1966). They occur as both intrusive and

extrusive bodies — the former as plutonic and hypabyssal dikes, sills, sheets, pipes, stocks, and more irregular bodies; the latter as flows and pyroclastics. About 330 carbonatites are now known worldwide; approximately one-half of these occur in Africa, with the majority concentrated in or close to the East African Rift (Fig. 2.8). They are typically associated with nephelinitic and phonolitic magmatism, in well-defined petrographic provinces, although the carbonatite invariably forms a very small component of the associated alkali igneous complex. Carbonatites are located predominantly in tectonically stable continental, cratonic, or peripheral-cratonic areas, with close relationships to zones of major faulting (rifting?) in many cases (Heinrich 1966). Some carbonatites, however, do occur close to plate margins and their distribution appears to be related to plate movements (Garson 1984) and many can be linked with orogenic activity (Woolley 1989). Carbonatites range in age from late Archean to Recent, with an apparent trend of increasing carbonatite production with time and a maximum peak starting at 200 Ma that may be associated with the breakup of Pangea (Woolley 1989).

Carbonates are the most diagnostic minerals of carbonatites, which may be further subdivided into calcite-carbonatite (sövite, coarse-grained; alvikite, medium- to fine-

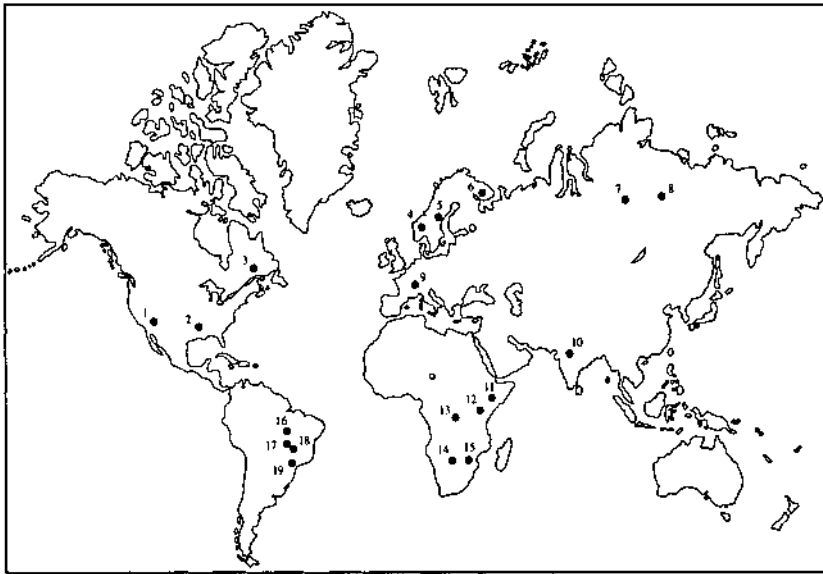


Figure 2.8. Important carbonatite complexes of the world. The numbered locations are (with available ages in parenthesis): 1. Mountain Pass, California, USA (1523 Ma); 2. Magnet Cove, Arkansas, USA (99 Ma); 3. Oka, Quebec, Canada; 4. Fen, Norway (565 Ma); 5. Alnö, Sweden (537 Ma); 6. Kola, Russia; 7. Maimiecha-Kotui, Russia (220-245 Ma); 8. Olenek, Russia; 9. Kaiserstuhl, Germany; 10. Amba Dongar, India (68 Ma); 11. Oldoinyo Lengai, Tanzania (active volcano); 12. Panda Hill, Tanzania; 13. Kaluwe, Zambia; 14. Glenover, South Africa; 15. Palabora, South Africa (2047 Ma); 16. Catalão, Brazil (114 Ma); 17. Araxá, Brazil (87 Ma); 18. Tapira, Brazil (70 Ma); 19. Jacupiranga, Brazil (131 Ma). Source of age data: compilation by Woolley (1989).

grained), dolomite-carbonatite (beforsite), ferrocarnatite (essentially composed of iron-rich carbonates such as ankerite), and natrocarbonatite (essentially composed of Na-K-Ca carbonates). Sövite is the most common variety of carbonatite and natrocarbonatite is known only as the extrusive product of Oldoinyo Lengai volcano in Tanzania (Dawson et al. 1994). The accessory minerals vary widely in kind and proportion and include apatite, pyroxene, olivine, K-feldspar, albite, phlogopite, wollastonite, riebeckite, pyrochlore, barite, fluorite, strontianite, sulfides, and Fe-Ti oxides. Alkali metasomatism (fentization) of wallrocks is a characteristic feature of carbonatites.

The close similarity between the Nd and Sr initial isotopic compositions of most carbonatites and some oceanic islands suggests that the parental magmas of carbonatites are generated within the mantle (Bell & Blenkinsop 1989). This conclusion is also corroborated by carbon isotope ratios of calcites from carbonatites indicating a juvenile source of CO₂ in the parent magmas (Heinrich 1966, Deines 1989). Experimental phase equilibria investigations in appropriate systems, as summarized by Wyllie (1989) and Kjarsgaard and Hamilton (1989), are consistent with three possible models for the generation of carbonatitic magmas: (a) direct partial melting of the upper mantle peridotite induced by addition of CO₂ and probably also by reduced gases in the system C-H-O at depths greater than about 75 km; (b) fractional crystallization of a nepheline-normative, silica-undersaturated, relatively alkali-rich silicate magma containing dissolved CO₂ and probably also H₂O; and (c) separation of an immiscible carbonatite melt from an alkali-rich or Ca-rich silicate magma. The large volumes of igneous silicate rocks in carbonatite complexes argue against the generation of primary carbonatite magmas directly by partial melting. Field relations do not support the fractional crystallization model either, because carbonatites are not found associated with a differentiated series of silicate rocks. The liquid immiscibility model, on the other hand, is supported by several lines of field and chemical evidence (Le Bas 1989, Kjarsgaard and Hamilton 1989, Dawson et al. 1994). These include: (a) the occurrence of syenites and ijolites as discrete intrusions in carbonatite complexes, without any gradational relationship with associated carbonatite intrusions; (b) examples of extrusive carbonatite interbedded with nephelinite and phonolite lavas (e.g., at Shombole and Tinderet, Kenya, and Oldoinyo Lengai, Tanzania); and (c) the similarity in chemical composition of apatite in carbonatite and nephelinitic rocks in western Kenyan alkaline complexes. The chemical diversity of carbonatites is also quite compatible with a liquid immiscibility origin. Factors that contribute to the diversity are: (a) chemical composition of the parental magma; (b) pressure and temperature at which liquid immiscibility may take place; (c) crystal fractionation of carbonate minerals (calcite and/or dolomite) and the early precipitation of a range of minerals such as apatite, magnetite, bastnäsite, baddeleyite, and pyrochlore; (d) loss of alkalis by fentization; and (e) contamination by adjacent country rocks.

As a group, the carbonatites are relatively enriched in a characteristic set of minor elements: Nb, REE (especially light REE), P, F, Th, Ti, Ba, Sr, and Zr. The most important mineral products of carbonatites probably are calcite for cement and apatite for phosphatic fertilizer. Many carbonatites contain traces of Th-bearing monazite,

pyrochlore, and uranothorianite, which are useful for outlining carbonatite bodies by radiometric surveys. The principal metals for which the carbonatites are considered a major resource are niobium and REE; some carbonatites also contain significant concentrations of Fe (magnetite, hematite), Ti (rutile, brookite, ilmenite, perovskite), Cu-sulfides, barite, fluorite, and strontianite, which may be recoverable as byproducts (Deans 1966).

Pyrochlore ($\text{CaNaNb}_2\text{O}_6\text{F}$) is by far the most abundant primary niobium mineral in carbonatite associations and it is found in nearly all rock types of carbonatite complexes in accessory amounts. Concentrations of potential economic significance are much less widespread and occur mainly in the carbonatites themselves, often in rather well-defined zones or shoots. One of the well-explored deposits is the Panda Hill carbonatite of Tanzania, which contained 125 million tons of proved reserves averaging 0.3% Nb_2O_5 . The ore is largely apatite-bearing sövite (carbonatite composed almost entirely of calcite) and dolomitic sövite, but among the small, richer ore zones is an area of biotitic contact rock rich in pyrochlore and pandaite (hydrated Ba-pyrochlore) of which 3.8 million tons were proved averaging 0.79% Nb_2O_5 . A large pilot mill operated at Panda Hill from 1957 to 1960 producing concentrates containing 10 to 25% Nb_2O_5 , but operations have since been suspended (Deans 1966). The Araxá deposit, Minas Gerais, Brazil, with 2,800 million tons of ore grading 2.81% Nb_2O_5 , is the world's largest niobium deposit (Verwoerd 1989). Other important deposits include those of Tapira, Minas Gerais, Brazil (126 million tonnes of ore with 1.2 wt% Nb_2O_5), Oka, Quebec, Canada (25.4 million tonnes of ore with 0.44 wt% Nb_2O_5), and Honoré, Quebec, Canada (12.2 million tonnes of ore with 0.66 wt% Nb_2O_5) (Mariano 1989). Most pyrochlore-rich bodies in carbonatite complexes appear to have formed during the late magmatic-early deuteric stage of carbonatite crystallization. This is evidenced by a lack of correlation between the pyrochlore-rich bodies with the shape of the host carbonatite, an association or parallelism of the mineralization with fracture zones, and the association of pyrochlore with deuteric minerals (Heinrich 1966).

Many carbonatites contain significant concentrations of REE as solid solution components of carbonates, phosphates, perovskite, and pyrochlore. REE minerals in most carbonatites appear to have been precipitated from hydrothermal solutions. Several of the African carbonatite complexes include rocks, predominantly dolomitic or ankeritic, containing 1-20% rare-earth oxides (RE_2O_3). The greatest concentration of REE known in the world occurs in the carbonatites of the Mountain Pass district, California (USA), a rare case where REE minerals are primary phases. According to Olsen et al. (1954), the inferred reserves for the district is more than 25 million tons of carbonatite with 5-10% RE_2O_3 ; the potential reserve may exceed 100 million tons of ore containing more than 10 billion pounds of RE_2O_3 . The most important deposit of the district, the Sulfide Queen, consists of 40-75% calcite, 15-50% barite, and 5-15% Ce-enriched bastnäsite $\{(\text{REE})(\text{CO}_3)_2\text{F}_2\}$, with RE_2O_3 contents ranging from less than 1% to 38.92% and averaging 6.89%. The bulk of the REE occurs in bastnäsite and about 85% of the REE content is accounted for by Ce and La (Shaw 1959). The Araxá deposit, Minas Gerais, Brazil contains 800,000 tonnes of ore averaging 13.5% REE-

oxides, but the REE enrichment in this case is in carbonatite-derived laterites.

Most carbonatites contain minor amounts of disseminated sulfides, predominantly as pyrite and pyrrhotite, but much below ore-grade concentration. A notable exception is the carbonatite of the Palabora ultramafic-alkaline igneous complex located in northeast Transvaal, South Africa (Palabora Mining Company Limited Mine Geological and Mineralogical Staff 1976). The complex intrudes Archean gneisses and is believed to be older than 2060 Ma. It is estimated to contain about 700 million tons of copper ore averaging 0.68% Cu (Guilbert & Park 1986, p. 361) and has been in production since 1966. The principal copper sulfides are chalcopyrite and bornite. Ti-bearing magnetite (0.6-2.8% TiO₂) is a major constituent of the ore and is recovered as a byproduct.

2.3.3. KIMBERLITES: DIAMOND

Kimberlites constitute a complex suite of igneous rocks and it is difficult to formulate a simple definition that will accommodate their petrologic variations. In essence, kimberlites are volatile-rich (dominantly CO₂), potassic (up to about 5% K₂O, K₂O:Na₂O ratio typically 2-5), ultramafic (<35% SiO₂) rocks with a distinctive inequigranular texture resulting from the presence of relatively large (0.5-10 mm), rounded to anhedral crystals set in a fine-grained matrix. The larger crystals include olivine (the dominant phase), phlogopite, magnesian ilmenite, Ti-poor chrome spinel, pyrope-rich garnet, Cr-poor clinopyroxene, and enstatite. The matrix assemblage consists of second-generation euhedral olivine, phlogopite, serpentine, pyroxene (Al- and Ti-poor), perovskite, Ti-Mg-Al chrome spinel, Fe-Ti spinel, monticellite, carbonate (usually calcite), and apatite (Dawson 1980, Clement et al. 1984, Mitchell 1986).

Kimberlites occur as narrow dikes, locally enlarged into pipelike diatremes, as sills, and only occasionally as extrusives. They are virtually restricted to ancient (>2.4 Ga) cratons and the younger (>1.0 Ga) accreted belts of cratonized regions that are underlain by cratons, a feature well illustrated by the distribution of kimberlites in southern Africa (Fig. 2.9). The intrusions tend to occur in clusters, and commonly are associated with major lineaments and fault zones, which appear to have acted as foci of repeated cycles of kimberlite magmatism. The initiation of magmatism might have been associated with the rise of sublithospheric mantle plumes or with intralithospheric metasomatic processes, but no simple relationships to tectonic events occurring at plate margins are evident (Mitchell 1986). The Cretaceous was a major period of kimberlite magmatism, particularly in Africa, but the ages of kimberlites range from Proterozoic to Tertiary. It is important to note that some southern African kimberlites dated at about 90 Ma contain diamonds older than 2.0 Ga (Kramers 1979).

The crystals in kimberlites are of three types: (a) mantle-derived xenoliths, mainly of peridotite (hercynite and harzburgite) and eclogite, which occur as rounded-to-subangular blocks or as xenocrysts derived by fragmentation of such blocks during their transport in the kimberlite magma; (b) megacrysts (Dawson 1980) and macrocrysts

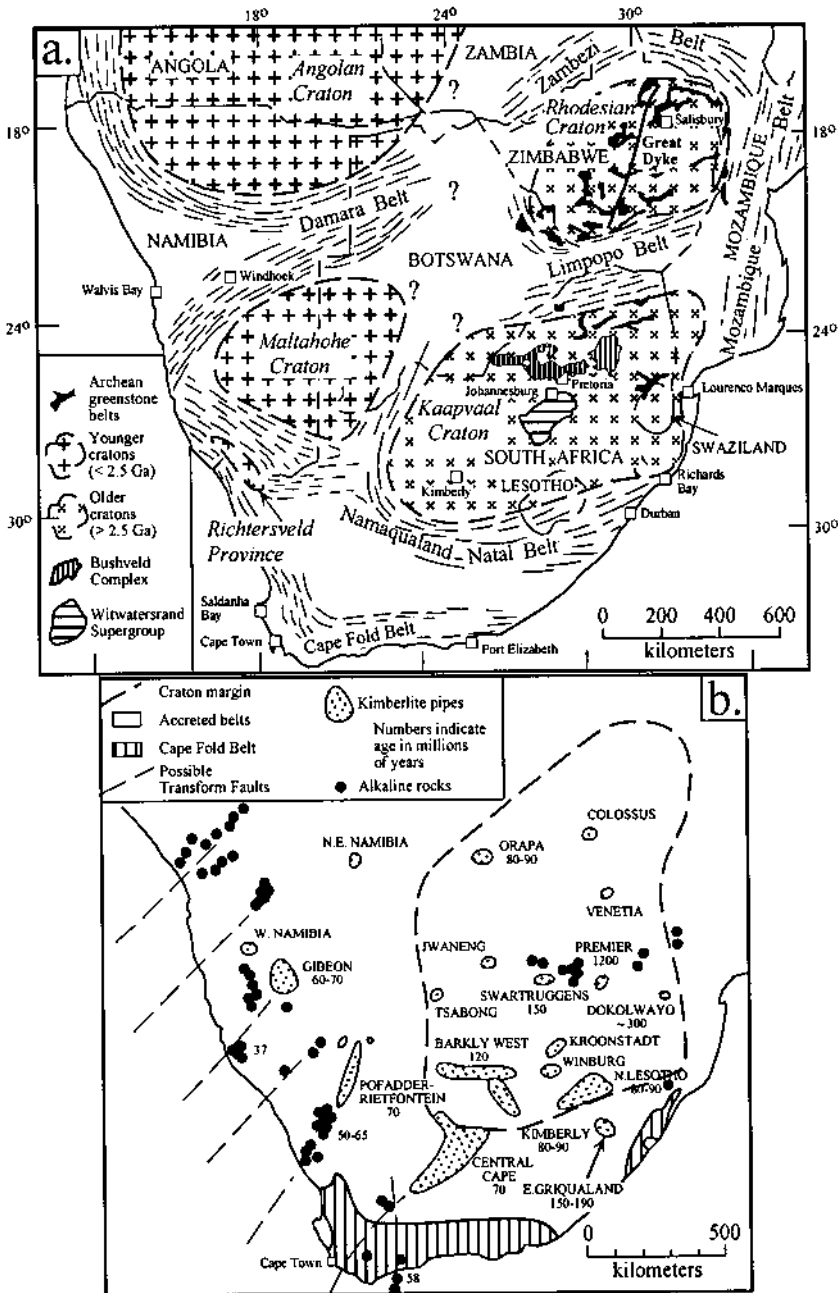


Figure 2.9. a. The main crustal provinces of southern Africa and the locations of some important geological formations (after Pretorius & Maske 1976); b. Distribution of kimberlite fields in the southern African kimberlite province (after Mitchell 1986).

(Clement et al. 1984) of controversial origin; and (c) phenocrysts formed by crystallization of the kimberlitic magma. Pressure-temperature estimates from mantle xenoliths in kimberlites indicate a depth of about 100-250 km for the generation of kimberlite magmas, whereas crystallization of the groundmass is considered to have taken place at shallow depths and at temperatures as low as 600°C (Mitchell 1973, Shervais et al. 1987). The compositional variations and relationships exhibited by the coexisting members of the megacryst-macrocryst suite suggest that they are products of crystallization differentiation, but opinions differ as to the nature of the magma. Some authors have argued that the megacrysts-macrocrysts are xenocrysts unrelated to kimberlite, but were derived from "crystal-mush" magmas sampled by kimberlites during their ascent (Nixon & Boyd 1973, Pasteris 1983). Others believe that they are phenocrysts of cognate origin, products of high-pressure crystallization of kimberlite magmas (Gurney & Harte 1980, Mitchell 1986). From a critical appraisal of the available data, Mitchell (1986) attributed the mineralogy, geochemistry, and petrology of kimberlites to a combination of the following processes: (a) metasomatism of the upper mantle source; (b) partial melting of the upper mantle source; (c) high-pressure crystallization, magma mixing, and assimilation; (d) crystallization and contamination during transit from the source to the upper crust; and (e) low-pressure crystallization, hybridization, and contamination.

The economic potential of kimberlites lies in the fact that many contain extractable natural diamond (crystals and cleavage fragments) as a highly dispersed accessory mineral. For example, the Mir pipe in Yakutia (Russia), perhaps the most diamond-bearing kimberlite pipe in the world, contains only one part of diamond per every one and half million parts of kimberlite. Economically important kimberlites appear to be localized in regions underlain by portions of the cratons which are older than 2.4 Ga. These include the diamond-bearing kimberlites of Africa (Angola, Botswana, Lesotho, Sierra Leone, South Africa, Swaziland, Tanzania), Russia (Yakutia), Australia (Western Australia), and the recently discovered kimberlite pipes in Canada (NWT). Kimberlites are also believed to be the ultimate source of diamonds found in placer deposits, which have supplied about 90% of the world's diamond output. It should be pointed out that diamond crystals have been found occasionally in other igneous rocks such as dunite, basalt, and particularly lamproites (ultrapotassic ultramafic rocks with large olivine phenocrysts set in a fine-grained to glassy matrix); thus, all placer diamonds may not have been derived from kimberlite sources.

The origin of diamonds in kimberlites is controversial and has been reviewed in several publications (Robinson 1978, Meyer 1985, Mitchell 1986); some of the salient conclusions are summarized below. There is little dispute that the kimberlite diamonds must have formed under upper mantle conditions. A comparison between anticipated geothermal gradients and the graphite-diamond stability curve suggests that diamond formation is likely only at depths greater than about 140 km (Fig. 2.10). Also, equilibrium temperatures and pressures estimated from inclusions in diamonds are in the range of 900°-1,300°C and 45-65 kbar, corresponding to 140-200 km depth. The consistent association of diamonds with kimberlites, as well as the general agreement

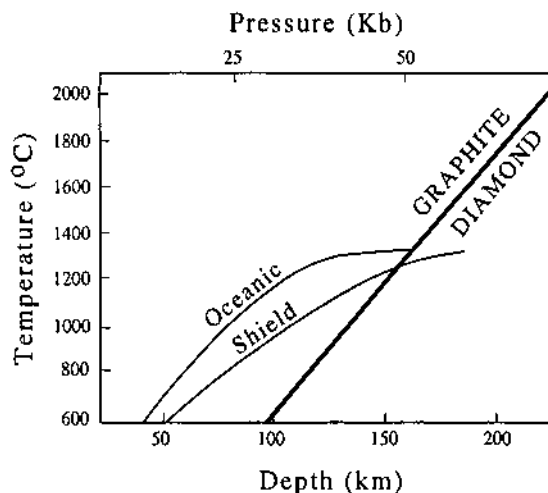


Figure 2.10. Diamond-graphite inversion curve (Berman 1965) and its relationship to calculated shield and oceanic geothermal gradients (Harte 1978). The intersection of the two curves indicates a minimum depth of about 150 km for the formation of diamond in shield areas.

between the temperature-pressure estimates for diamonds and those obtained for xenoliths and megacrysts (including diamond-bearing ones), have led many authors to support a "phenocrystal model" of origin for the diamonds — i.e., the diamonds are genetically related to the early crystallization products of kimberlite magmas within the upper mantle. The current opinion, however, appears to favor a "xenocrystal model" — that the diamonds are xenocrysts, which were picked up from fragmented diamond-bearing eclogite and peridotite in the upper mantle and transported by the kimberlite magma. The xenocrystal model is based on the following lines of evidence: (a) the presence of diamonds, with similar suite of inclusions in both kimberlites and lamproites; (b) the chemical differences between these inclusions and cognate minerals in the host kimberlites and lamproites; (c) the much older age of diamonds, as obtained from peridotitic suite inclusions (e.g., olivine, enstatite, pyrope) in diamonds, compared with their host kimberlites (Kramers 1979, Richardson et al. 1984); (d) the similarity in chemical composition of mineral inclusions in diamonds to those of upper mantle eclogite and lherzolite xenoliths in kimberlites; and (e) the common occurrence of diamonds in eclogite xenoliths, which apparently crystallized earlier from melts unrelated to kimberlite magmas. However, eclogitic suite inclusions (e.g., almandine-pyrope garnet, omphacitic pyroxene) in diamonds generally yield younger ages, sometimes approaching the age of kimberlite emplacement (Phillips et al. 1989). Two other problems of diamond genesis that still remain unresolved are the mechanism of diamond growth and the source of carbon in the mantle. The available data, according

to Meyer (1985), favor the formation of diamonds either directly from an igneous melt or from some type of metasomatising fluid, with dissolved CO_2 or CH_4 , that has pervaded various types of mantle rocks, perhaps at different times.

Why some kimberlites contain diamond whereas others do not is a difficult question to answer. It follows from the xenocrystal model that the virtual restriction of primary diamonds to kimberlites is related not to any unique chemistry of kimberlite magmas but to the generation of such magmas at sufficient depths with the opportunity to sample potentially diamond-bearing horizons in the mantle. Further, as the minimum depth of diamond formation is a function of the prevailing geothermal gradient, the apparently greater diamond-bearing potential of kimberlites in the shield regions may be a consequence of less steep geothermal gradients beneath the shields (Robinson 1978). Some kimberlites are non-diamondiferous either because the magma was generated outside the P - T stability field of diamond or because the magma never picked up any diamond xenocryst due to the non-uniform distribution of diamonds in the upper mantle. Boyd (1982) has shown that nodules (mantle xenoliths) in kimberlites from diamond-producing areas plot within the P - T stability field of diamond, whereas those of barren kimberlites plot outside the diamond stability field (Fig. 2.11), an observation of considerable significance in the evaluation of diamond-bearing potential kimberlite pipes. Alternatively, a kimberlite may appear to be non-diamondiferous if its diamond xenocrysts were lost by resorption during transportation or left behind.

2.3.4. ANORTHOSITES: TITANIUM

Many rocks contain small amounts of titanium locked in silicate minerals (e.g., biotite, amphibole), but the economically useful minerals at present are the Ti-rich oxide minerals (see Fig. 4.33): Fe-Ti oxides (members of the ulvöspinel-magnetite and ilmenite-hematite solid solution series) and Ti-oxides (mainly rutile). Significant concentrations of Fe-Ti oxides occur in anorthosite suites (anorthosites, anorthositic gabbros, and gabbroic anorthosites), alkali igneous complexes (e.g., Magnet Cove, USA; Kola Peninsula, Russia; and Tapira, Brazil; Herz 1976a) and in high-grade metamorphic rocks of Barrovian and high-pressure facies. The Ti-enriched metamorphic rocks of upper amphibolite and granulite facies are believed to be the source of many placer deposits of titanium, and titanium ore has been mined from eclogite and glaucophane-eclogite rocks in the former USSR (Blake & Morgan 1976), but the anorthositic association has been and continues to be the dominant source of primary titanium ores (Herz 1976b).

Anorthosites occur in two different settings: (a) as layered units in mafic-ultramafic differentiated intrusions, such as the Bushveld Complex (see Fig. 5.5); and (b) as large bodies or massifs in Precambrian high-grade gneissic terranes. A characteristic difference between the two lies in the plagioclase composition — highly calcic (bytownite-anorthite) in the former and less calcic (andesine-labradorite) in the latter. The Upper Zone of the Bushveld Complex contains at least 30 discrete vanadium-bearing Ti-magnetite layers that vary between 0.1 and 10.0 m in thickness and are

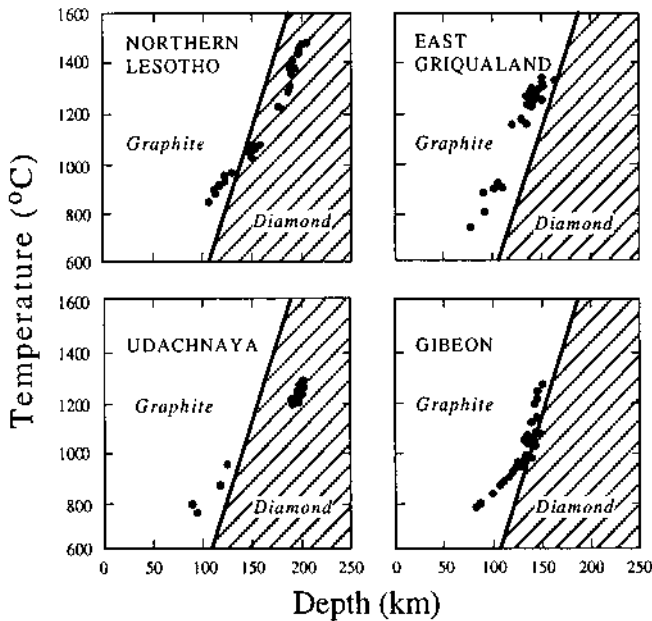


Figure 2.11. Estimates of the temperatures and depths of origin of peridotite nodules in kimberlite samples from four areas. The diamond and graphite fields have been determined by experimental studies. The Northern Lesotho and Udachnaya kimberlites are diamondiferous, whereas the kimberlites from East Griqualand and the Gibeon area do not contain commercial quantities of diamond. (After Boyd 1982.)

concordant with the igneous layering. The economically important Main Magnetite Layer (MML), located close to the base of the Upper Zone, varies between 1.0 and 2.5 m in thickness and has been traced over a strike length of approximately 200 km in the western Bushveld Complex and 120 km in the eastern Bushveld Complex (Willemsse 1969b). The magnetite layers show an overall antipathetic relationship between the TiO_2 and V_2O_5 contents, ranging from about 2% V_2O_5 and 12-14% TiO_2 in the lowermost horizon to about 0.2-0.3% V_2O_5 and 18-20% TiO_2 in the uppermost horizon (Willemsse 1969b, Molyneux 1970, Klemm et al 1985). The overall increase in the titanium content of magnetite upward in the Upper Zone has been attributed to a progressive decrease in oxygen fugacity in the magma chamber (Willemsse 1969b) and the formation of the magnetite layers to *in situ* bottom growth of Ti-magnetite crystals caused by episodic increases in oxygen fugacity (Reynolds 1985). However, a comprehensive genetic model that would also account for an overall upward trend of Cr depletion in the layered magnetite, the many reversals in the geochemical trends, and the episodic oxidation events that must have been operative more or less simultaneously over the entire extent of the magma chamber to allow for the lateral continuity of the magnetite layers is yet to be formulated (see Cawthorn & Lee 1998).

It is now well established that massif anorthosite complexes are Precambrian plutonic igneous bodies, but the nature and source of the parental magmas and the tectonic setting of their emplacement remain controversial (Carmichael et al. 1974). According to Emslie (1978), the North American anorthosite massifs (Fig. 2.12) are products of Paleohelikian (about 1400-1500 Ma) anorogenic magmatism in a cratonic setting, involving plagioclase accumulation from parental aluminous gabbro magmas, which, in turn, were derived by fractionation of olivine tholeiite magmas at or near the base of a stable continental crust. He postulated that the anorogenic magmatism probably represented the initiation of mantle upwelling that eventually matured into continental rifting in late Proterozoic.

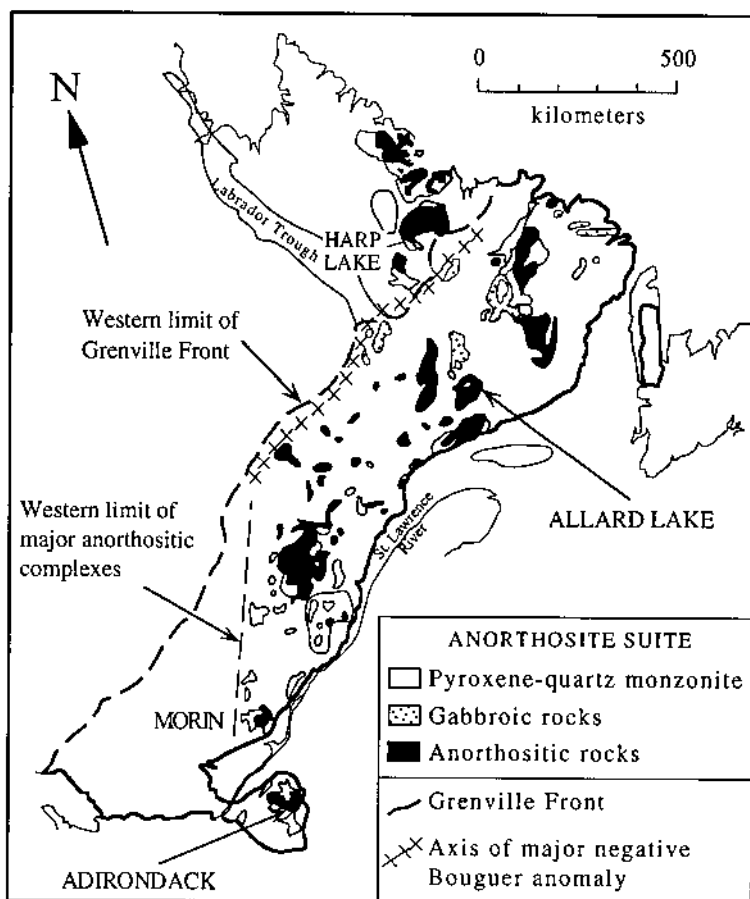


Figure 2.12. Distribution of anorthosite complexes in the eastern Canadian Shield (after Emslie 1979). The two producing Fe-Ti oxide deposits, Sanford Lake (New York, USA) and Lac Tio (Quebec, Canada), are located in the Adirondack and Allard Lake anorthosite massifs, respectively.

Anorthosite massifs may be divided into two types based on their plagioclase and oxide compositions (Anderson & Morin 1968): (a) labradorite-anorthosite massifs, characterized by plagioclase of An_{45-68} composition and titanomagnetite (or its oxidized equivalent, magnetite + ilmenite); and (b) andesine-anorthosite massifs, characterized by plagioclase of An_{25-48} composition and hemo-ilmenite. The genetic relationship, if any, between the two types is not clear. Many anorthosite massifs are composed of only one type of anorthosite, but others contain subunits of both (Emslie 1975) and their trace element geochemistry is not suggestive of a genetic link through fractional crystallization of a common parental magma (Duchesne & Demaiffe 1978). The distinction between the two types, however, is important from an exploration perspective, because the principal ilmenite deposits of the world are associated with the andesine-type (the "Adirondack-type" of Buddington 1931) anorthosites.

The most well-known anorthosite massif for titanium deposits is located at Allard Lake, Quebec, Canada. The Allard Lake deposits are of three types (Hammond 1952): concordant tabular bodies of large aerial extent (Lac Tio deposit and satellites); steeply dipping dike-like bodies (Puyjalon deposit); and lenticular masses of irregular shape (Mills deposit). The Lac Tio deposit, the largest anorthosite-hosted titanium deposit in the world, was estimated to contain more than 125 million short tons of ilmenite ore averaging about 32% TiO_2 and 36% Fe (Hammond 1952). The ore is made up of a thick (more than 90 m) section of massive hemo-ilmenite capped by a thinner (less than 60 m) section of banded hemo-ilmenite and anorthosite with disseminated hemo-ilmenite; individual layers vary from a few centimeters to a few meters in thickness. Inclusions of anorthosite in the ilmenite ore is a common feature. Typical high-grade ore consists of hemo-ilmenite with 20-22% Ti-bearing hematite, 3% Fe-spinel and 0.5% pyrite, and has the following chemical composition (wt%): TiO_2 - 34.3, FeO - 27.5, Fe_2O_3 - 25.2, SiO_2 - 4.3, Al_2O_3 - 3.5, CaO - 0.9, MgO - 3.1, Cr_2O_3 - 0.10, V_2O_5 - 0.27, MnO - 0.16, S - 0.3, $N_2O + K_2O$ - 0.35, and P_2O_5 - 0.15 (Bergeron 1972).

The Sanford Lake mining district in the state of New York (USA) is the most important titanium deposit of the Adirondack anorthosite massif (Fig. 2.12). It has produced more titanium ore than any anorthosite deposit in the world. The ores of the district are of two types (Fig. 2.13): (a) anorthositic ore ($Fe:TiO_2 > 2:1$); and (b) gabbroic ore ($Fe:TiO_2 < 2:1$). The anorthositic ore occurs as massive lenses with irregular dimensions in contact with anorthosite waste rock, is coarse grained, shows little or no flow structure, and has sharp though irregular contacts with the anorthosite. The gabbroic ore occurs as oxide-enriched bands of varying thickness (a few millimeters to several meters) within the gabbro, is fine to medium grained, contains well-defined flow structure similar to that of the gabbro, and shows sharp to gradational contacts with the gabbro. The cut-off grade at Sanford is 9.5% TiO_2 , but the high-grade ore contains >17.5% TiO_2 . The main ore mineral is hemo-ilmenite, which is invariably accompanied by titanomagnetite containing ilmenite and ulvöspinel intergrowths.

A hydrothermal replacement origin for the titanium deposits of anorthositic association is clearly untenable in view of the lack of alteration of the feldspar and ferromagnesian minerals in the anorthositic and gabbroic host rocks. Concentration

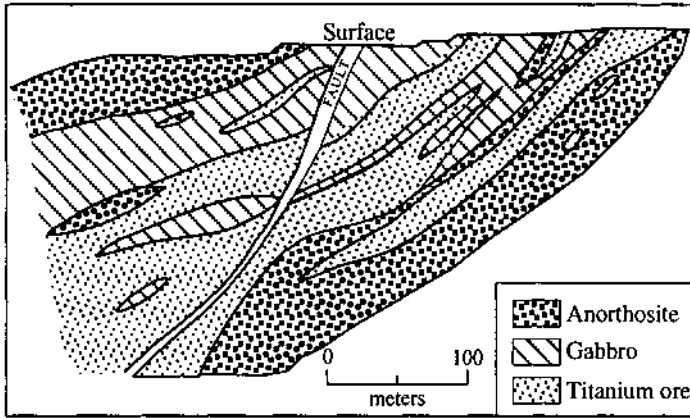


Figure 2.13. Typical geologic section of the Sanford Hill pit, Sanford Lake district, showing the distribution of titanium ore (after Gross 1968).

of the Fe-Ti oxide minerals by gravitative settling of early-formed minerals is not consistent with the observed textures, which indicate that the Fe-Ti oxide minerals crystallized contemporaneously or later than the silicate minerals. Most of the observed features of these deposits are best explained by a combination of two magmatic processes (Fig. 2.14), *residual liquid segregation* and *residual liquid injection* (Bateman

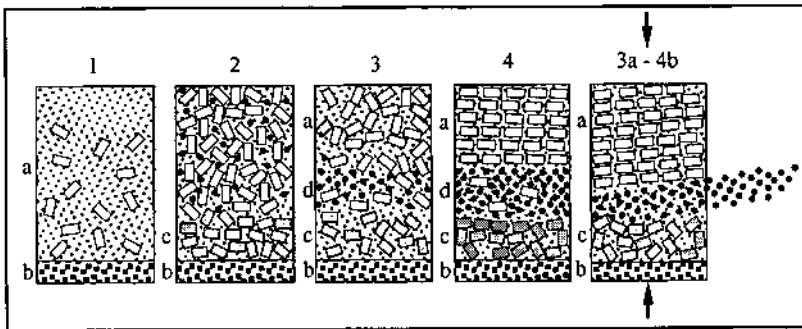


Figure 2.14. Diagrammatic representation of the formation of Fe-Ti oxide deposits by residual liquid segregation and residual liquid injection as postulated by Bateman (1951). 1. Early stage of crystallization of a basic magma (a) after formation of chill zone (b); 2. Layer of sunken early-formed ferromagnesian crystals (c), resting on chill zone (b), with mesh of later crystals above, whose interstices are occupied by residual magma enriched in ore oxides; 3. Mobile, oxide-rich, residual liquid draining down to layer (d) and floating up later silicate crystals; 4. Formation of a concordant oxide orebody in which a few late silicate crystals are trapped; 3a-4a. Mobile, enriched gravitative accumulation (d) squeezed out or decanted to form late magmatic injections. (After Bateman 1951.)

(1951). The concordant deposits, such as those of the Allard Lake Complex, appear to have formed by crystallization of a segregated residual liquid that accumulated on a solid floor of early-formed sunken crystals. Such an origin is supported by the fact that minor element compositions of oxide minerals in the concordant deposits follow the general trends in minor element compositions of their host rocks (Lister 1966). The ores of the anorthosite massifs appear to have experienced variable and sometimes quite substantial deformation, suggesting that their formation involved injection of a residual crystal-liquid mush. Such a mechanism would easily account for the discordant oxide-rich bodies in massif anorthosites; the concordant bodies may simply represent injection along the layering of the already solidified parent intrusive.

2.4. Sedimentary Processes

Under favorable conditions, sediments and sedimentary rocks formed by normal sedimentary processes become selectively enriched in certain elements to be of potential economic value. The two main processes which may produce such enrichment are: (a) chemical weathering; and (b) sedimentation. Weathering may lead to *residual concentration* of weathering-resistant minerals of the parent rock or of relatively insoluble elements reconstituted into stable minerals. A special case of weathering is the so-called *supergene enrichment* process, which involves the leaching of ore-forming elements, such as copper, from surficial parts of a low-grade sulfide deposit and reprecipitation below the water table. Sedimentation may also lead to the formation of mineral deposits through either *clastic accumulation* (placer deposits) or *chemical/biochemical precipitation* of economically important constituents. The various types of deposits formed by these sedimentary processes, along with some important examples, are listed in Table 2.4. The formation of exhalative deposits, which involves chemical precipitation from fluids discharged onto the ocean floor, is considered a hydrothermal process rather than a sedimentary process.

2.4.1. RESIDUAL CONCENTRATION

Chemical weathering includes processes by which rocks at or near the Earth's surface tend to achieve equilibrium with the surface environment. Water is by far the most important agent of chemical weathering; other substances which may take part in weathering reactions include free oxygen, and inorganic and organic acids. The simplest of the weathering reactions is the dissolution of soluble minerals either by ionization (e.g., dissolution of evaporite minerals) or by formation of acids (e.g., H_4SiO_4 by dissolution of quartz). More complex reactions include hydration, hydrolysis, carbonation, oxidation, and sulfidation (see Ch. 3, Hydrothermal Alteration); the most important weathering reactions involve hydrolysis of rock-forming silicates. The parameters most commonly used for evaluating stability of minerals under weathering conditions are Eh and pH; other parameters, which can be used in appropriate cases, are

TABLE 2.4. Examples of mineral deposits formed predominantly by sedimentary processes

Process	Deposit types	Important examples
Weathering		
Residual concentration	Lateritic nickel	New Caledonia; South Pacific islands; Brazil
	Bauxite	Jamaica; Darling Range, Western Australia; Weipa, Queensland, Australia; Guyana; Surinam
	Manganese	Precambrian schist belts, India; Morro da Mina, Minas Gerais, Brazil
	Clay (kaolin)	Gabbin, Western Australia; western Georgia, USA
Oxidation and supergene enrichment	Enriched 'cap' on disseminated and vein-type sulfide deposits	Porphyry copper deposits (Morenci and Ray, Arizona, USA; El Salvador, Chile; Sonora, Mexico); epithermal silver deposits (Chañarcillo, Chile)
	Iron	Precambrian banded iron-formations
	Manganese	Groote Eylandt, Northern Territory, Australia
Sedimentary accumulation		
Clastic sedimentation	Placers	Gold-uranium (Witwatersrand, South Africa); uranium (Elliot Lake, Canada); gold (California and Alaska, USA); ilmenite-rutile (Trail Ridge, Florida, USA); diamond (South Africa, Zaire, Angola); tin (Kinta Valley, Malaysia); monazite (Kerala, India)
Chemical and/or biochemical precipitation	Evaporites	Gulf Coast, USA (salt domes); Saskatchewan, Canada; Strassfurt, Germany
	Iron-formations	Clinton-type iron-formations (e.g., Clinton Formation, eastern USA); banded iron-formations (Ch. 15)
	Bedded manganese	Nikopol, Ukraine; Chiatara, Georgia; Groote Eylandt, Northern Territory, Australia
	Phosphorite	Florida, USA; Central Tennessee, USA
	Metalliferous black shale	Zunyi (Guizhou Province) and Dayong (Hunan Province), China
	Manganese nodules	Sea-floor (Pacific Ocean)

the partial pressures of oxygen, sulfur, and CO_2 (see Ch 3, Stability of Minerals). In essence, weathering provides mechanisms for leaching of more mobile constituents from the parent rock, thus resulting in residual concentration of the less mobile ones in the soil profile. The most important controls of pedogenesis (formation of soil profiles) are climate and drainage which, in turn, control the release of elements by the breakdown of primary minerals and their entrapment in secondary minerals depending on Eh-pH conditions (Lelong et al. 1976). Arid regions produce neutral to alkaline soils, which selectively concentrate alkaline and alkaline-earth elements (*pedocal* soil); humid climates give rise to acidic soils where the alkaline and alkaline-earth elements, and to a lesser extent silica, are leached out and relatively immobile elements (e.g., iron, aluminum, and manganese) are concentrated mostly as hydroxides (*pedalfer* soil). In well-drained locations under the hot and humid conditions of tropical climate, the leaching of silica becomes very efficient, and the resulting soil with very high residual concentrations of iron and/or aluminum is commonly called *laterite*. Depending on the Al:Fe ratio, laterites are subdivided into (lateritic) bauxites, aluminoferruginous laterites or impure (lateritic) bauxites, and ferruginous laterites (also referred to simply as laterites). The ore-grade bauxite generally contains $>50\%$ Al_2O_3 ($>80\%$ Al_2O_3 , water-free basis). Laterites are not enriched enough in iron to be commercially exploitable as iron ores at present, but laterites developed on ultramafic rocks constitute important resources of nickel and cobalt. Other important residual concentration deposits include those of manganese and clays derived from manganese- and feldspar-rich parent rocks, respectively. A lateritic gold deposit is under development in the Carajas region of Brazil (Zang and Fyfe 1993).

The requirements for the formation of a residual concentration deposit by weathering processes are: (a) parent rock of appropriate composition, (b) leaching of the undesirable constituents by intense chemical weathering and adequate drainage, and (c) low relief and crustal stability so that the residual accumulation is not eroded away as soon as it is formed.

Bauxite Deposits

Bauxite is by far the most important ore material of aluminum metal. Bauxite deposits are of three types (Fig. 2.15): (a) lateritic bauxites, which commonly occur in the upper parts of lateritic blankets capping hills and plateaus; (b) karst bauxites that lie, directly or indirectly, on a carbonate and more or less karstified bed rock; and (c) sedimentary bauxites, which are stratiform aluminous accumulations, probably of both detrital and chemical origin, intercalated in sedimentary rocks.

Although bauxite deposits as old as late Proterozoic to Cambrian are known, the most intense period of bauxite formation was from Cretaceous to Recent. The large, lateritic bauxite deposits, which account for more than 80% of the world's supply of bauxite, were formed during this time interval on stable continental platforms. The most important deposits of this type occur in Guinea, Brazil, Australia, India, Guyana, and West Africa. These deposits, referred to as 'high-level' laterites because of their common occurrence at high elevations, are considered by most workers as remnants of

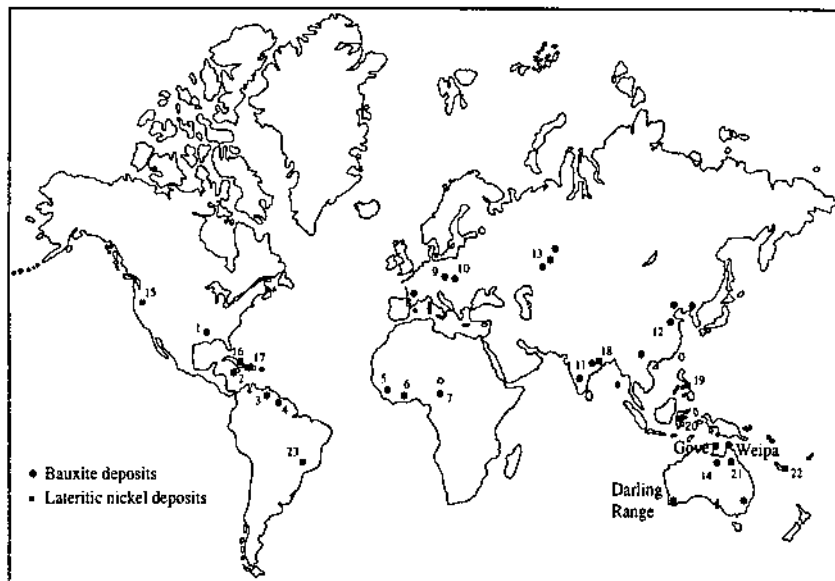


Figure 2.15. World distribution of major bauxite and lateritic nickel deposits. Bauxite deposits: 1. Arkansas, USA (lateritic and sedimentary); 2. Jamaica (karst); 3. British Guyana (lateritic and sedimentary); 4. Surinam (lateritic and sedimentary); 5. French Guyana (lateritic); 6. Ghana (lateritic); 7. Cameroon (lateritic); 8. France (karst); 9. former Yugoslavia (karst); 10. Hungary (karst); 11. India (lateritic); 12. China (karst); 13. former USSR (karst); 14. Australia (lateritic and sedimentary). Lateritic nickel deposits: 15. Oregon, USA; 16. Moa Bay, Cuba; 17. Falcondo, Dominican Republic; 18. Sukinda, India; 19. Nonoc Islands, Philippines; 20. Pomalaa and Soroake, Indonesia; 21. Greenvale, Australia; 22. New Caledonia; 23. Minas Gerais, Brazil.

ancient peneplains, but Valeton (1983) argued that many actually formed in coastal plains and were subsequently uplifted to their present altitude. Karst bauxites tend to be older in age (e.g., Cretaceous in the Mediterranean zone, and Jurassic or even Paleozoic in the Urals). The Cenozoic deposits are restricted to latitudes from 30°N to 30°S, indicating a strong climatic control on bauxite formation. It is possible that karst bauxites, which are now located in temperate and subtropical zones, were derived by erosion and redeposition of vast ancient lateritic blankets formed in tropical latitudes (Lelong et al. 1976).

Bauxite is composed dominantly of three Al-hydroxide minerals: gibbsite [γ -Al(OH)₃], boehmite [γ -AlOOH], and diasporite [α -AlOOH]. In general, lateritic bauxites, which are predominantly of Tertiary age, tend to be composed of microcrystalline gibbsite with minor boehmite (mostly replacing gibbsite). Some karst bauxites, especially the relatively younger deposits as in Jamaica (Eocene to Lower Miocene), are composed chiefly of gibbsite, but boehmite or diasporite is the predominant Al-mineral of most older karst bauxites. This variation may be related to

greater degree of diagenesis in the older bauxites (Lelong et al. 1976). Common impurities in bauxites include kaolinite, quartz, and goethite, as well as minor to trace amounts of many other minerals. Bauxite ores are classified into various commercial grades by end-use (metallurgical, chemical, cement, refractory, and abrasive) based on the content of Al_2O_3 as well as of SiO_2 , Fe_2O_3 , and TiO_2 . Bauxite grades into a laterite with increasing iron content and into an aluminous clay with increasing ratio of aluminosilicates (such as kaolinite) to aluminum hydroxides.

Bauxite deposits may form on any type of parent rock containing a significant concentration of aluminum, but most have been derived from rocks that are low in quartz, such as syenites, basalts, and limestones. The formation of bauxite by weathering of silico-aluminous rocks involves two essential chemical changes: removal of silica, and separation of Al from Fe. These processes are largely controlled by the initial oxidation potential (Eh) and acidity (pH) of the groundwater and the modifications resulting from water-rock reactions. From appropriately constructed Eh-pH diagrams (see Ch. 3), Norton (1973) concluded that: (a) under a wide range of Eh-pH conditions (oxidizing and $\text{pH} > 4.0$), both Al and Fe are much less mobile than Si and the soil formed would reflect the Al:Fe ratio of the parent rock; (b) the separation of Al and Fe would take place either by selective mobilization of Al if the pH was less than about 4.0 under oxidizing conditions (leading to residual enrichment of Fe) or by selective mobilization of Fe with a pH above about 4.0 under more reducing conditions (leading to residual enrichment of Al); and (c) subsequent changes in Eh and particularly increases in pH would result in the precipitation of Fe or Al, the amounts depending upon the initial groundwater composition. The behavior of Mn, Co, and Ni is similar to that of Fe (although they are somewhat more mobile than Fe and Al for any given Eh-pH) so that these elements tend to be relatively enriched in laterites but depleted in bauxites. The conversion of aluminosilicate minerals into aluminum hydroxides probably occurs through an intermediate step of kaolinite formation and, if so, the solubility of kaolinite should play a role in the bauxitization process (Lelong et al. 1976). For example, if the groundwater contains less than 1 ppm of dissolved SiO_2 , kaolinite will dissolve incongruently with the precipitation of gibbsite; at higher concentrations of dissolved SiO_2 , the dissolution of kaolinite becomes congruent (i.e., the precipitation of gibbsite does not occur) and both Si and Al will be removed by soil solutions at similar rates, leaving an Fe-rich residuum. This may explain why quartz-rich rocks normally produce iron-rich laterites and not bauxite (Meillon 1978).

Lateritic Nickel Deposits

Lateritic nickel deposits, which account for about 65% of the known land-based nickel resources in Western countries (hypogene nickel sulfide deposits account for the rest; see Ch. 6), are restricted to laterites derived from ultramafic rocks (especially peridotites and serpentinites) which contain up to about 0.4 % Ni. The relatively high Ni content is attributable mainly to the substitution of Ni^{2+} for Mg^{2+} in olivine or its altered product, serpentine. The requirement of lateritic weathering and a nickel-rich parent rock makes commercial deposits of this type relatively uncommon. The first

commercial nickel laterite deposit was discovered in 1865 by Garnier in the South Pacific island of New Caledonia and it has been mined sporadically since 1876. Other important lateritic nickel deposits, as shown in Figure 2.15, are located in Australia (Greenvale, Queensland), Indonesia (Pomalaa and Soroake), the Philippines (Nonoc Island), Guatemala (Exmibal), Greece (Island of Euboea), Brazil (Niquelandia, Goias; Morrodo Niquel, Minas Gerais), and Colombia (Cerro Matoso); smaller deposits occur in the United States (Nickel Mountain, Oregon), Cuba (Moa Bay), the Dominican Republic (Falcondo), and India (Sukinda, Orissa). The grade of most deposits being mined is from 1.5 to 2.0% Ni, but may range up to about 3% Ni or even higher. The grade of the New Caledonian ore mined in the 1900's was as high as 10% Ni. From data on 64 districts around the world, Foose et al. (1980) estimated the average size of nickel laterite deposits as 40 million tons of ore with an average grade of 1.41% Ni. Although supergene enrichment does occur in Ni-sulfide ores (Nickel et al. 1974), it does not produce significant new orebodies.

High-temperature rocks like peridotites are particularly susceptible to extreme leaching and redistribution of elements under humid climates. The Fe-Si separation is effective only in well-drained zones and under very humid climate. The Fe-Cr-Al separation is always negligible and that of Fe-Ni remains incomplete (Lelong et al. 1976). The relative nickel enrichment in the weathered rock is mostly due to the almost complete removal of Mg in solution except for the small amounts retained in the altered silicate minerals such as talc, serpentine, chlorite, and sepiolite. The Si is also leached, but only partially and more slowly. The iron, which occurs as Fe^{2+} in the peridotite minerals, becomes readily oxidized to insoluble Fe^{3+} , and is retained as Fe-hydroxides (mainly goethite). The most important residual accumulation of Mn and Co, which are oxidized to relatively insoluble Mn^{4+} and Co^{3+} , respectively, takes place in the middle part of the profile, reaching concentrations up to 1% CoO and 3% MnO_2 . Ni is retained in the laterite by substituting for Fe^{2+} in goethite or in association with discrete cryptocrystalline masses of Mn-Co oxide (called *absolite*) in the zone of oxidation, and for Mg^{2+} in the silicate minerals mentioned above in the underlying saprolite zone. This distribution of Ni enrichment matches the pH increase in typical Ni-laterites from about 5 at the top of the oxide zone to about 8.5 at the base of the saprolite zone (Golightly 1981) and may be ascribed to slow leaching of Ni from the oxide zone and reprecipitation in the saprolite zone. In the saprolite zone, the Ni is held in solid solution in Mg-silicates, but it is not known if the introduction of Ni takes place by simple ionic substitution or involves dissolution-reprecipitation of the silicates (Maynard 1983). Ni-rich variants of serpentine, talc, chlorite, and sepiolite have been referred to in the literature as garnierite, willemsite, nimite, and falcondite, respectively.

The details of a Ni-laterite profile varies with the degree of serpentinization of the ultramafic bedrock and the climatic environment (Golightly 1981). A generalized, uneroded nickeliferous laterite profile consists of four zones above fresh peridotite containing about 0.2 % Ni and 0.02 % Co (Fig. 2.16):

- (a) An Fe-rich cuirasse (hard crust with the richest concentration of iron and/or aluminum hydroxides) grading downward into a dull-red concretionary layer.
- (b) A ferrallitic (Fe-rich), Co -enriched (up to 0.3% Co) brownish red clay zone becoming yellow at depth. Nickel enrichment in this zone is in the oxides and hydroxides of iron and manganese, and nickel ore begins in the lower half of this horizon.
- (c) A Ni-enriched, saprolite zone with colors varying from brownish yellow to greenish brown and the original texture discernible as vaguely concentric lines surrounding less weathered gray or dark green peridotite remnants. Nickel enrichment in this zone (and in the zone below) is in the form of Ni-silicates.
- (d) A boulder saprolite zone consisting of spheroids of nickeliferous weathered material surrounding nearly barren peridotite cores.

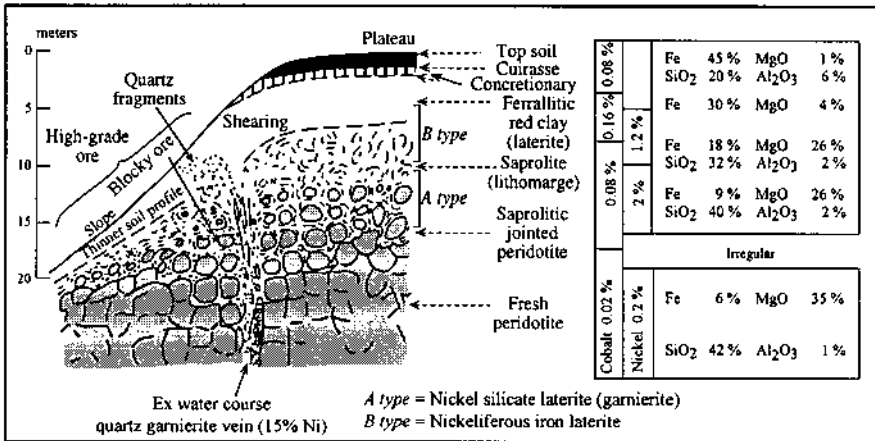


Figure 2.16. Schematic cross section through a generalized nickel laterite deposit (after Meillon 1978). Type A and Type B ores refer to the concentration of nickel in silicates (silicate ore) and oxides (oxide ore), respectively. Note the position of high-grade ores on the topographic slope where weathering is more efficient.

As shown in Figure 2.16, there are two potential horizons of nickel enrichment in the laterite profile — near the base of the saprolite zone, and below the zone of maximum iron and cobalt enrichment— which have been designated as Type A ore and Type B ore, respectively, by Zeissink (1969). Type A ore, the so called *silicate ore* or *garnierite ore*, is dominated by Ni-silicates. Nickel enrichment in this zone, generally with a grade of more than 1.5% Ni, is partly residual through depletion in MgO and SiO₂ and partly by downward migration from the leached upper parts of the profile. Type B ore, the so called *oxide ore*, is dominated by Ni-enriched goethite and is

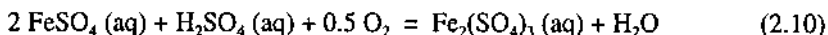
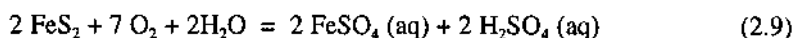
characterized by lower MgO, SiO₂, and Ni (<1.5 %), but higher Fe. In mature profiles, where residual concentration as well as downward leaching of nickel have taken place, both types may be found within the same deposit (e.g., New Caledonia), but most commercial deposits are dominated by one type or the other.

2.4.2. SUPERGENE SULFIDE ENRICHMENT

The second type of process which causes metal enrichment during weathering of a pre-existing hypogene sulfide body is called supergene enrichment. The process involves the release of ore metals from unstable sulfide minerals to downward percolating meteoric water and precipitation of more stable secondary oxide and sulfide mineral assemblages in the subsurface environment. The end-product varies depending on the factors that govern chemical weathering and on the physical and chemical nature of the sulfide assemblages and host rocks (Blain & Andrew 1977), but tends to be enriched in one or more metals. The process has been responsible for rendering the top parts of many low-grade, disseminated, otherwise uneconomic deposits, especially of copper, mineable.

A typical profile through a mineral deposit, which has undergone supergene enrichment, consists of three zones (Fig. 2.17): (a) hypogene or protore zone; (b) supergene enrichment zone; and (c) oxidized zone, which may be capped by an Fe-enriched zone commonly referred to as *gossan*. Much of the dissolution and precipitation processes that lead to the development of this zonation can be written as oxidation-reduction reaction couples involving exchange of electrons and, therefore, may be explained in terms of Eh-pH variations (Garrels 1954, Blain & Andrew 1977, Anderson 1982), subject to limitations due to departures from equilibrium (Nickel & Thornber 1977).

Chemical reactions involved in the development of the oxidized zone, which is generally lies above the groundwater table, include oxidation of sulfide minerals that are unstable under oxidizing conditions, leaching of metals from hypogene sulfide minerals as soluble sulfate solutions, and precipitation of some of the metals as insoluble oxide, hydroxide, carbonate, and sulfide minerals that are stable under oxidizing conditions. The process starts with the oxidation of pyrite, the most common hypogene sulfide mineral, to strong oxidizing solvents such as H₂SO₄ and Fe₂(SO₄)₃:



In the absence of pyrite, only minor amounts of solvents are produced; the sulfides tend to be converted *in situ* into oxidized compounds and hypogene sulfides are not significantly enriched.

A characteristic product in all oxidized zones is *limonite*, a field term for amorphous, colloidal iron oxides or finely crystalline goethite [α -FeOOH] with

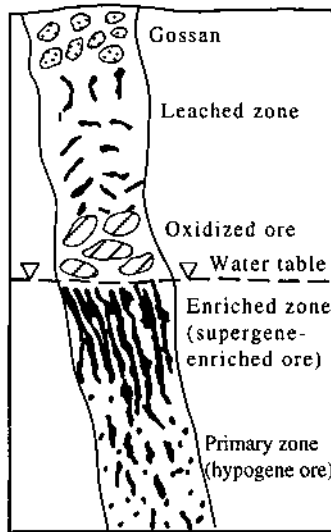
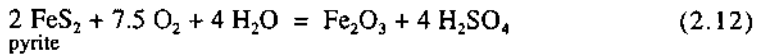
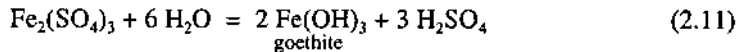


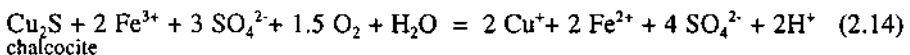
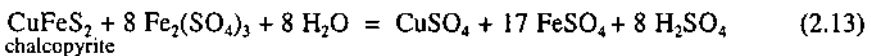
Figure 2.17. Schematic cross section of a sulfide-bearing vein illustrating the relationship among the zones of oxidation, supergene enrichment, and hypogene (protore) sulfide (after Jensen & Bateman 1979).

subordinate admixed silica, hematite, jarosite, lepidocrocite [β -FeOOH], or manganese oxides in various proportions and states of hydration. The formation of limonite, either by hydrolyzation of ferric sulfate or by the direct oxidation of pyrite (and other sulfide minerals), may be represented by reactions such as:



As in the lateritization process discussed earlier, the aluminum-silicate minerals are leached of silica and converted into clay minerals. A portion of the leached silica may be redeposited as jasper, the iron-bearing cryptocrystalline variety of quartz.

Possible reactions for dissolution of hypogene sulfides producing soluble sulfates can be written in various ways, but the end result may be represented by reactions of the type:



The process is particularly important for Cu and Ag (Garrels 1954). Lead sulfate is insoluble and so is left behind in the oxidized zone as dispersed anglesite. Zinc is relatively soluble under all conditions and tends to be lost from the system altogether, except in carbonate-hosted lead-zinc deposits where it may be redeposited lower in the profile as smithsonite. In the presence of carbonates providing a source of CO_2 , copper may also be precipitated as malachite or azurite. Covellite is a common mineral in the oxidized zone just above the water table, and is believed to be formed by the oxidation of chalcopyrite, digenite ($\text{Cu}_{1.69}\text{S}$), and blaubleinder covellite ($\text{Cu}_{1.26}\text{S}$) (Andrew 1980). The combination of limonitization and dissolution produces the diagnostic replica textures, called *boxworks*, in gossans. In the initial stages of oxidation, thin septa of goethite or hematite precipitate along mineral cleavages or twin planes and around grain boundaries. Continued oxidation dissolves the rest of the sulfide grain, leaving a cellular boxwork texture that is characteristic of the particular sulfide species (Fig. 2.18). Such boxworks provide a useful tool for interpreting the original sulfide assemblage in a leached outcrop. The mineralogy of most gossans is dominated by limonite and silica in mutually antipathetic abundance. They also contain distinctive accessory minerals indicative of the hypogene sulfide assemblages — for example, emerald-green minerals moreosite (fibrous) and annabergite (earthy) in nickel-copper sulfide gossans, malachite and azurite in copper-zinc sulfide gossans, and cerussite and smithsonite in lead-zinc sulfide gossans. The identification and interpretation of gossans are valuable exploration guides in weathered terrains.

Sulfate solutions from the oxidized zone eventually percolate downward to the water table, and under the prevailing reducing conditions the dissolved metal species are consumed in a series of enrichment reactions involving hypogene sulfides, such as pyrite, chalcopyrite, and bornite. A characteristic supergene enrichment mineral in copper systems is chalcocite. This chalcocite, referred to as 'sooty' chalcocite, is commonly, but not necessarily, soft and powdery in contrast to the massive gray crystalline 'steely' chalcocite of hypogene ores. The analogous silver mineral is acanthite (monoclinic Ag_2S). As has been pointed out by Guilbert and Park (1986), the cubic polymorph argentite, which is stable above 180°C , indicates a hypogene origin, but acanthite may be either of hypogene or of supergene origin.

2.4.3. PLACER DEPOSITS

The term *placer* was used by the early Spanish miners in North and South America for gold deposits found in the sands and gravels of streams. The term has since been used in a more general way to describe deposits formed by mechanical accumulation of economically important detrital, resistate minerals — minerals that are stable or metastable in the weathering environment — released by weathering from appropriate source rocks. Minerals that are commonly concentrated in modern placer and paleoplacer deposits are relatively inert and heavy. Notable examples are diamond, some native metals (especially gold and platinum-group elements), oxides (uraninite, chromite, magnetite, ilmenite, rutile, cassiterite, wolframite, and columbite-tantalite),

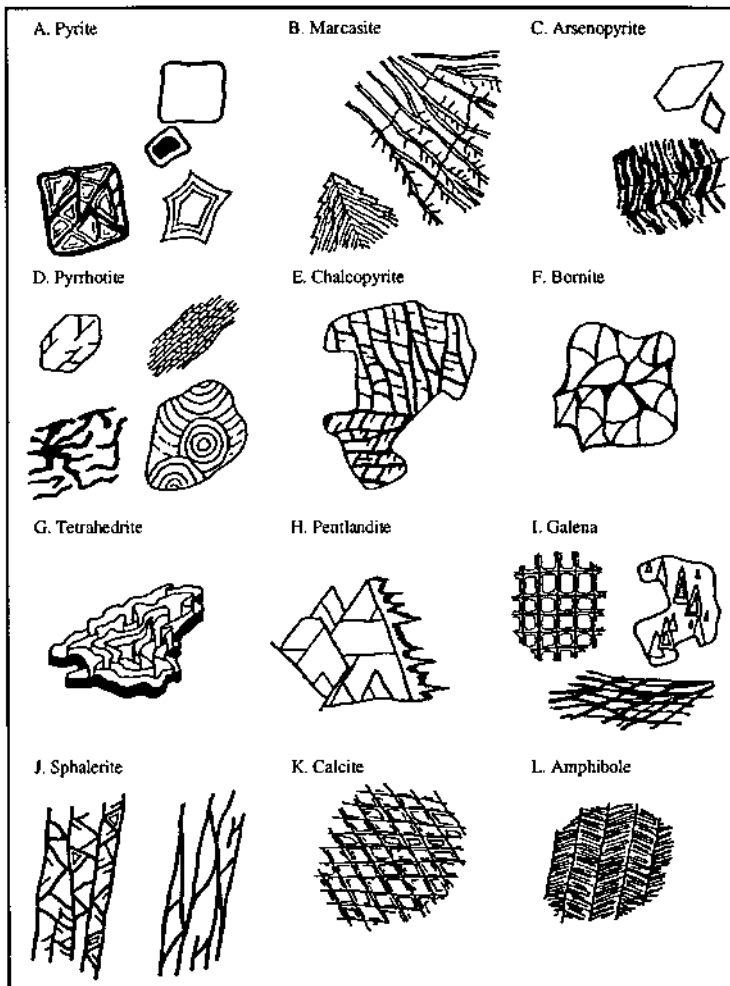


Figure 2.18. Diagnostic boxwork textures of selected minerals (after Andrew 1980).

silicates (zircon, garnet, gemstones), and phosphates (monazite, apatite). Because of susceptibility to decomposition by oxygenated meteoric waters, sulfides rarely form placer deposits.

Being products of normal surficial processes, modern placer deposits have a widegeographic distribution, although most of these deposits are small and uneconomic. Placer deposits have formed throughout geologic time, but the bulk of the world's placer deposits, including most of the modern gold placers, are Tertiary or Quaternary in age. The paucity of older deposits is ascribed primarily to removal by

erosion before they could be preserved by burial. It is also possible that placer formation was favored in the Tertiary because of rapid uplift during the orogenies at the Mesozoic-Cenozoic transition and because of sea-level changes in the Quaternary. Nevertheless, some of the most productive paleoplacer deposits, such as of gold and uranium in South Africa and of uranium in Canada, are Precambrian in age (see Ch. 14 and Ch. 16).

Based on the geologic environment of accumulation, placer deposits may be classified into eluvial (sometimes referred to as residual), colluvial, fluvial (or alluvial), eolian, lacustrine, beach, and marine. The most important are the fluvial and beach placers. Alluvial placers are composed of loose, unconsolidated sands and gravels that are commonly quite clean. The heavy mineral suite in alluvial placers varies with the source rock, but the most common heavy minerals are magnetite and ilmenite. Economic alluvial placer deposits are almost restricted to gold, uranium, diamond, platinum, and tin. Beach placers are formed by the winnowing action of waves and currents along shorelines where a source of heavy minerals has been available. Important beach placer deposits are those of ilmenite, rutile, zircon, monazite, garnet, and gemstones.

The process common to all placer deposits (except the eluvial and colluvial placers, the formation of which is controlled by gravity) is mechanical concentration controlled by the differences in specific gravity, size, and shape of particles in a moving fluid. Thus, an important line of evidence in support of placer origin of a deposit is the hydraulic equivalence of the constituent particles. Considering that the detritus in a fluid medium is sorted as a function of size, shape, and density of the constituent particles, there are three types of hydraulic equivalence to be considered (Singerland & Smith 1986; Force 1991): (a) settling equivalence, deposition from suspension resulting in accumulation together of particles of the same settling velocity (described by Stokes' Law and its variants); (b) entrainment equivalence, largely a function of grain size; and (c) transport equivalence, the combined effect of settling and entrainment equivalence on the transport of particles.

2.4.4. CHEMICAL AND BIOCHEMICAL PRECIPITATION

Depending on the Eh-pH conditions of the depositional environment, sediments deposited by normal chemical and biochemical processes in surface waters may be enriched in certain ore constituents (Krumbein & Garrels 1952, Vaughan 1976). In most cases, however, such syngenetic mineralization does not attain ore-grade concentrations, but there are many notable exceptions. Principal types of mineral deposits formed by syngenetic chemical/biochemical precipitation include evaporite deposits, iron-formations, sedimentary manganese deposits, phosphorite deposits, and metalliferous black shales (Table 2.4).

Sedimentary Phosphorite Deposits

There are three types of phosphatic rock of economic potential: sedimentary

phosphorites of marine origin; apatite-bearing alkaline igneous complexes (e.g., Khibina deposit of the Kola peninsula, which averages 27% P_2O_5 ; McKelvey 1973); and phosphorites of guano origin. More than 80% of the world's production of phosphate rock, mainly to meet the demand for fertilizers, is supplied by marine phosphorite deposits. The largest producers are USA, former USSR, and Morocco. The most important deposits in the United States, the leading producer in the world, occur in Florida (the Miocene Hawthorn Formation and the Pliocene-to-Holocene Bone Valley Formation) and North Carolina (the Miocene Pungo River Formation), and are part of an extensive belt of phosphatic sediments of Miocene age (Fig. 2.21). Other important deposits occur in Tennessee (probably of Ordovician age and unrelated to the Atlantic Coastal Plain deposits) and in the Rocky Mountain states of Montana, Idaho, Utah, and Wyoming (the Permian Phosphoria Formation).



Figure 2.19. Major phosphorite deposits of the southeastern United States (after Gurr 1979).

Phosphorite beds, often extensively interbedded with a more normal sequence of marine and terrigenous sediments, occur in long, narrow belts (sometimes in the order of more than 1,000 km in length and about 100-200 km in width) and generally range in thickness from less than a meter to 3-6 m. The phosphate grains, which normally amount to 10-30% by volume, are composed of various very fine-grained mineralogical and biological components (Riggs 1979a). The primary component is the carbonate-fluoroapatite matrix with various types and amounts of coloring matter (organic matter, iron oxides, sulfides). The rest represents materials that were present in the environment at the time of the precipitation of the phosphorite mud. These consist mainly of bacteria-like rods and aggregates, microorganism fossil hash, dolomite

rhombs, Mg-rich clay minerals, terrigenous sand and mud, and other clastic phosphate grains.

Phosphorites range in age from Lower Proterozoic to Recent, but the temporal distribution is uneven. The majority formed at low-latitude locations, within 40° north or south of the paleoequator, and the apparent paucity of Silurian-to-Carboniferous and Triassic phosphorite deposits may be attributed to the lack of extensive coastal areas at low-latitude locations during particular phases of plate-tectonic separation of continents and ocean formation (Cook & McElhinny 1979). Based largely on the Florida deposits, Riggs (1979b) has suggested that the two essential variables controlling the formation of potentially economic phosphorite deposits are the overall tectonic setting and the regional structural framework. The optimum tectonic setting lies somewhere between total quiescence favoring the development of carbonate banks and extreme mountain-building activity producing a deluge of terrigenous and volcanic sediments. A favorable structural framework within the essential shallow-water coastal and shelf marine environments comprises (a) one or more structural arches or topographic highs, which are the sites of optimum phosphate formation, and (b) adjacent topographic lows or entrapment basins in which major concentrations of phosphorite can accumulate.

The warm surface waters of the present-day oceans contain 0.0033 ppm P or less, whereas deep cold waters contain nearly 0.1 ppm P (McKelvey 1973). This distribution results from the uptake of phosphorous by organisms in the shallow waters and the dissolution of phosphorous contained in the accumulated organic debris at depth. Other possible sources of phosphorous in the oceans include volcanic and hydrothermal exhalations. Oceanic upwellings are believed to be the major mechanism of recycling the deep-water phosphorous for phosphorite deposition in shallow waters. The phosphate is precipitated as a loose colloidal microcrystalline mud suspension (microsphorite) and also as other biologically produced phosphate material (such as teeth and bones, shells, etc.). The microspherite mud and other marine and terrigenous components residing in the system are reworked and distributed according to the local energy conditions and biological processes within the environment (Riggs 1979b).

Sedimentary Manganese Deposits

Primary manganese deposits may be classified into two broad genetic groups (Roy 1992): (a) strata-bound and vein deposits of hydrothermal origin; and (b) bedded (stratiform) deposits of sedimentary origin. An earlier classification (Roy 1976) of the sedimentary deposits into volcanogenic and nonvolcanogenic (terrigenous) types, based on the presence or absence of volcanic rocks in the sequence, is considered unsatisfactory, because such a spatial association does not necessarily establish a volcanic or terrigenous source for the manganese. Besides, bedded manganese deposits formed in large open basins, such as oceans, probably had metal contribution from multiple sources. Both modern and ancient hydrothermal manganese deposits have been documented in continental and oceanic settings, especially at or around the axial regions of spreading centers, but they are mostly small and uneconomic. Most of the world's manganese production comes from a few giant sedimentary deposits (Fig. 2.20). Two

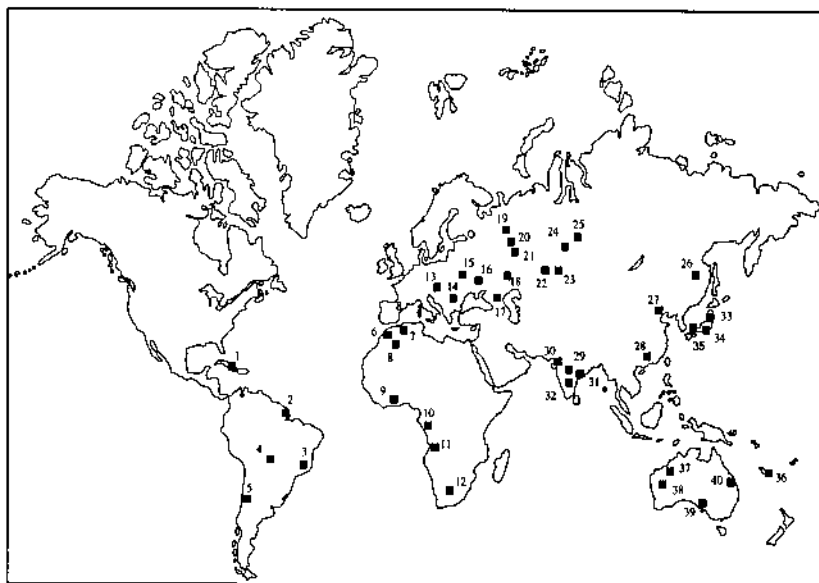


Figure 2.20. World distribution of major sedimentary manganese deposits: Cuba - Chario Redondo (1); Brazil - Serro do Navio (2), Morro da Mina (3), Morro do Urucum (4); Chile - Ovalle and La Serena (5); Morocco - Imni (6), Bou Arfa (7); Algeria - Guettara (8); Ghana - Nsuta (9); Gabon - Moanda (10); Angola - E. Coquendo Angola (11); South Africa - Postmasburg and Kalahari (12); Hungary - Urkut (13); Bulgaria - Varna (14); Ukraine - Nikopol (15), Laba (16), Chiatura (17), Mangyshalk (18), Polunochnoe (19), Ulu-Telyak (20), Kusa (21), Dzhezda (22), Karadzhal (23), Usinsk (24), East Sayan (25), Khirgansk (26); China - Wafantsu (27), Wu Hsuan (28); India - Madhya Pradesh-Maharashtra belt (29), Panch Mahals (30), Srikakulam (31), Sandur (32); Japan - Noda Tamagawa (33), Kaso (34), Kiuragi (35); New Caledonia - Raymond (36); Australia - Woody-Woody (37), Peak Hill (38), Iron Baron (39), Gladstone (40).

such deposits, Chiatura in Georgia and Nikopol in Ukraine, contain 75-80% of the world's present onshore reserves of manganese. The iron-formation associated early Proterozoic Kalahari field in Cape Province, South Africa, is estimated to contain over three-quarters of the world's in-place manganese resources.

The mineralogy of manganese deposits is generally quite complex because of the presence of a large number of manganese minerals, their small grain size and poor crystallinity, and intimate intergrowth textures. The oxides — pyrolusite, psilomelane, and cryptomelane — are the most common ore minerals of sedimentary manganese deposits. Many deposits contain Mn-carbonates, usually described as rhodochrosite, and manganite. Mn-minerals diagnostic of metamorphosed deposits include a variety of oxide and hydroxides (e.g., braunite, bixbyite, hollandite, hausmannite, vredenbergitte, jacobsonite) and silicates (e.g., rhodonite, spessartine garnet).

Sedimentary manganese deposits range in age from Archean (e.g., Iron Ore Group deposits in India) to Recent (e.g., deep-sea ferromanganese nodules) and are hosted by a

variety of sedimentary rocks such as sandstones-claystones, black shales, iron-formations, and carbonates, or their metamorphic equivalents. Although manganese deposition of an economic scale was initiated about 3000 m.y. ago, the formation of large- to moderate-size deposits began only in the early Proterozoic, coincident with the Superior-type iron-formations (see Ch. 15), probably corresponding to substantial oxygenation of the atmosphere-hydrosphere system. Schissel and Aro (1992) attributed the worldwide abundance of sedimentary iron and manganese deposits in the early Proterozoic to the development of large sedimentary basins during the amalgamation of a Proterozoic supercontinent (2000 to 1800 Ma), a suggestion consistent with a shallow-water, continental margin setting of these deposits. Important sedimentary manganese deposits are known from the entire span of the Phanerozoic, with a major concentration in the Oligocene. This concentration is due almost entirely to the deposits in the Black Sea region, particularly Chiatura and Nikopol, which are believed to have formed within the Paratethys seaway. Frakes and Bolton (1992) argued that the localization of Phanerozoic deposits could be broadly correlated with changes in ocean chemistry, sea level, and climate. The separation of manganese from iron and the transport and deposition of manganese in the sedimentary environments are governed by the stability fields of the various species in Eh-pH space (Krauskopf 1957, Hem 1972). Iron gets fixed as an oxide or hydroxide under moderately reducing conditions, which might prevail a few centimeters below the sediment-water interface, whereas manganese remains in solution and might be precipitated later as an oxide or a carbonate depending on changed Eh-pH conditions. The precipitation of manganese might also involve direct or indirect biotic mediation. An excellent discussion of the various environments and processes of manganese deposition has been presented by Roy (1992).

All Precambrian and most Phanerozoic bedded manganese deposits are sediment-hosted and appear to have formed near the margins of stratified basins, in the zone of mixing between shallow oxygenated water and deep anoxic water. Based on modern analogs, such as the Black Sea and the Baltic Sea, a transgression-regression model (Fig. 2.21) proposed by Frakes and Bolton (1984, 1992) offers a reasonable explanation for the formation of the ancient shallow-water manganese deposits. An essential component of the model is a high concentration of dissolved manganese in the anoxic parts of a stratified basin margin, as would be the case due to increased rates of supply of organic matter from surface waters during a marine transgression. The requirement of anoxic water arises from the fact that it can contain three orders of magnitude more dissolved manganese (about 1 ppm) than normal seawater (Maynard 1983). The other essential component of the model is the precipitation of manganese in the near-shore oxygenated water during a marine regression. The model is independent of the source of the manganese — chemical weathering of terrestrial rocks, basinal volcanism, mobilization from basinal sediments — but the precise mechanisms that result in oxygen depletion during transgression and oxygenation of basins during regression remain unidentified.

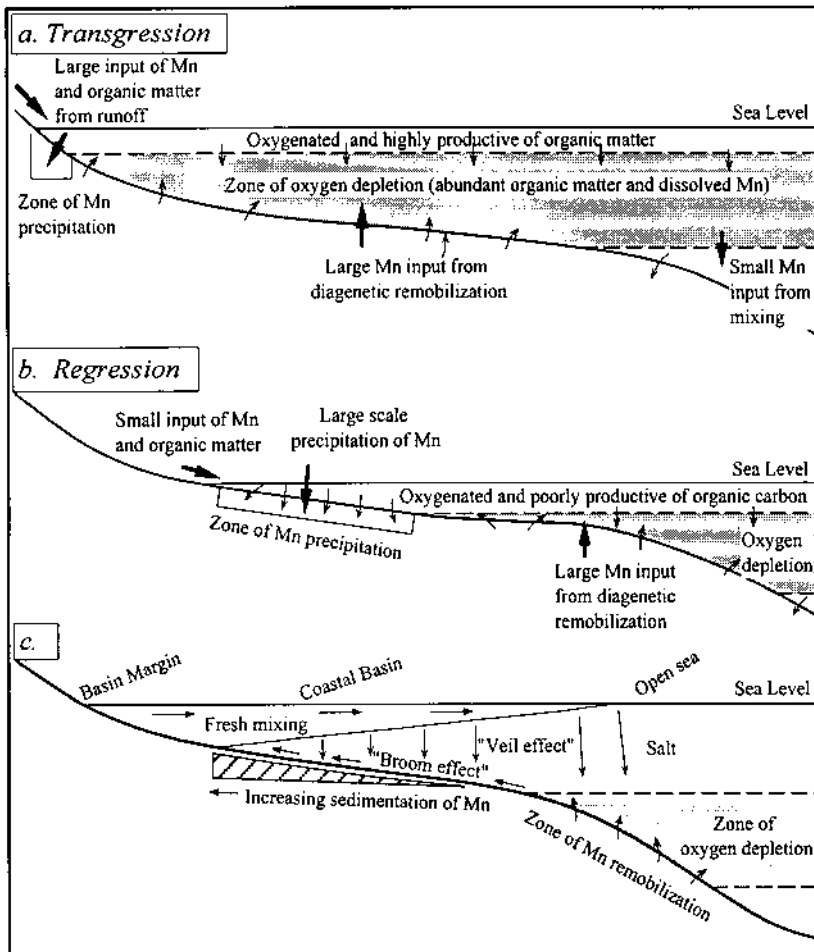


Figure 2.21. A marine transgression-regression model for the formation of sedimentary manganese deposits at the margin of a stratified basin (after Frakes & Bolton 1984, 1992): a. Relationships at the basin margin during marine transgression, showing zone of oxygen depletion, dissolved Mn enrichment in the water column impinging on the bottom, inferred movements of Mn, and a narrow zone of manganese accumulation; b. Relationships during marine regression, with abundant diagenetic remobilization and a wide zone of manganese precipitation in reducing and oxidizing zones, respectively; c. Manganese sedimentation in coastal zone of intracratonic basin, showing "veil effect" (floculant fallout) from saline mixing and "broom effect" (bottom transport and concentration) from tidal activity.

2.5. Metamorphic Processes

Metamorphic processes may lead to the formation of new mineral deposits or they may modify pre-existing deposits. In this section we will restrict our attention to

metamorphic deposits that owe their origin to contact or regional metamorphism and involve recrystallization, commonly accompanied by mobilization of disseminated ore constituents by metamorphic fluids. We will concentrate here particularly on the role of metamorphic fluids, assuming that the reader is already familiar with the principles governing metamorphic recrystallization. *Metamorphosed* deposits that record the imprint of post-mineralization metamorphism, including remobilization of ore constituents, will be discussed in the next chapter (Ch. 3).

2.5.1. METAMORPHIC FLUIDS

Several lines of evidence suggest the existence of a volatile-rich fluid phase in rocks during metamorphism (Ferry & Burt 1982). These include: (a) synmetamorphic fluid inclusions in metamorphic minerals; (b) depletion of volatile components (such as H₂O and CO₂) in high-grade metamorphic rocks relative to their low-grade equivalents, presumably due to the loss of these components as a fluid phase; (c) prevalence of devolatilization mineral reactions during prograde metamorphism; and (d) presence of hydrates, carbonates, and sulfides in metamorphic rocks requiring non-zero values for the partial pressure of H₂O, CO₂, and S₂ during metamorphism.

Fluid Composition

The techniques commonly used to characterize the composition of metamorphic fluids are: (a) microthermometric analysis of fluid inclusions (see Ch. 3), which may be reasonably inferred to have been trapped in minerals during metamorphism; and (b) analysis of equilibria involving minerals which contain those elements that constitute the fluid phase (Ferry & Burt 1982, Ferry 1986).

Fluid inclusion studies have documented that the fluids in low- to medium-grade metamorphic rocks are dominated by H₂O, CO₂, and CH₄, generally in that order of abundance, whereas most fluid inclusions in high-grade rocks contain high concentrations of CO₂ or are of almost pure CO₂ (Roedder 1984). The concentration of sulfur-bearing species (mainly H₂S or SO₂) in the fluid is usually less than 1 mole percent. The nature and relative amounts of C-O-H species in fluid inclusions appear to depend strongly on metamorphic grade and the variations in fluid composition are in general agreement with thermodynamic predictions (Crawford 1981, Holloway 1981, Touret 1981). It is difficult to predict the compositions of aqueous fluid inclusions from a consideration of mineral-fluid equilibria, because the fluid phase contains species, such as Cl and Br, that do not occur in major quantities in the associated mineral phases. The aqueous fluids, in general, are Na-K-Mg-Ca-Cl brines with highly variable solute ratios; the salinities range from about 2-6 wt% NaCl equivalent in pelitic schists and gneisses to 20-25 wt% NaCl equivalent in calcareous rocks, and reach even higher values where dissolution of evaporites is involved (Crawford & Hollister 1986). In some cases, the high salinities may be the result of unmixing of CO₂-H₂O-chloride fluids of low to moderate original salinity either before or after entrapment as inclusions, because fluid phase separation causes a strong partitioning of

the dissolved salts into the aqueous phase (Bowers & Helgeson 1983). In any case, fluids with such high salinity and low dissolved sulfur suggest the possibility of dissolution and transport of significant quantities of metals in metamorphic terrains.

Prograde metamorphism of sedimentary rocks (and to a lesser degree of igneous and metamorphic rocks) leads to the evolution of a volatile-rich fluid phase through devolatilization reactions. Dehydration is most common; decarbonation occurs in carbonate-bearing rocks and desulfidation can be locally important. In some cases, the composition and volume of the fluid in equilibrium with the metamorphic rock can be accounted for by devolatilization reactions in a closed system, particularly at low fluid:rock ratios (Labotka et al. 1984); in others, externally derived fluids appear to have made a contribution. Ferry (1986) cited several studies of metamorphic terrains which show that fluid compositions computed from observed mineral assemblages are quite different from those that would evolve from devolatilization reactions alone. For example, the inferred prograde dehydration-decarbonation reactions that accompanied the metamorphism of impure carbonate rocks of the Vassalboro Formation in south-central Maine evolved a CO_2 -rich fluid ($X_{\text{CO}_2} > 0.5$), yet various mineral equilibria record that the carbonate rocks were in equilibrium with a H_2O -rich fluid ($X_{\text{CO}_2} < 0.3$) during the metamorphic event. Such discrepancies in the fluid composition are attributed to chemical interaction of the rock with externally derived fluids, because oxygen and carbon isotopic data do not support preferential loss of CO_2 from the fluid evolved during metamorphism (Valley 1986, Ferry 1986). In contact metamorphic terrains, the infiltrating fluid may be a consequence of crystallization of the intruding magma or fluid convection in the surrounding country rocks. In regional metamorphic terrains, the source of external fluids may be linked to dehydration of sediments being subducted below the metamorphic pile or advection of hydrous magmas from the underlying slab of mantle wedge.

Fluid Flow

Devolatilization reactions during progressive metamorphism produce about 2 moles of fluid per kilogram of pelite and this amount of fluid would occupy about 12 volume percent of the rock at 500°C and 5 kb (Walther & Orville 1982). In contrast, the total porosity of pelitic schists seldom exceeds a few tenths of a percent by volume. Although the present porosity of the rocks is not necessarily a proper estimate of the porosity that existed during metamorphism, the relatively small amount of retrograde hydration and carbonation observed in most high-grade metamorphic rocks suggests that nearly all volatiles produced during prograde metamorphism were expelled from the rock before the waning of metamorphic temperatures. The fluid escapes primarily by mass flow along discrete fractures, not by grain boundary diffusion; the 'segregation' veins of quartz commonly observed in metamorphic terrains probably represent the major channelways for the fluid transport (Walther & Orville 1982, Newton 1989). The transport of metamorphic fluids may occur as single-pass flow or as convective flow (Fig. 2.22). A hot fluid, because of its lower density relative to the surrounding rock,

must flow upward, but as it gets denser due to cooling at upper levels it may convect downward if the rock is permeable enough for such movement (Fig. 2.22a). The fluid circulation will continue until the temperature gradient declines to a point at which the deeper fluids are no longer buoyant. Since rocks are nearly three times as dense as H_2O-CO_2 fluids, a necessary condition for fluid convection is that the rock is strong enough to allow a hydrostatic pressure gradient to be maintained through a system of interconnected pores and fractures. If the rock is of insufficient strength to support the difference between the lower hydrostatic pressure of the fluid within its pores and the high lithostatic pressure exerted on it by the overlying column of rock ($P_{lithostatic} \approx 3 P_{hydrostatic}$), the pores will collapse until the fluid becomes pressurized to lithostatic pressure. As the pressure on the fluid approaches lithostatic pressure, convection must give way to single-pass flow (Fig. 2.22b).

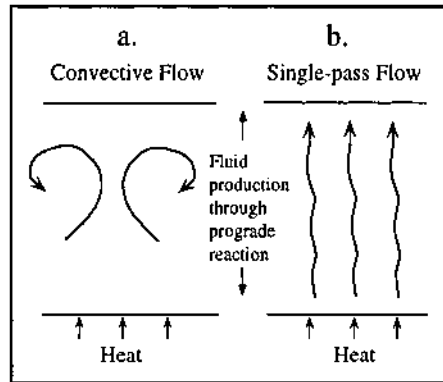


Figure 2.22. Two scenarios for fluid flow during metamorphism: a. Convective flow if the rocks are strong enough to hold an interconnected pore and fracture system open for fluid circulation; b. Single-pass flow if the pores collapse so that fluid pressure equals or exceeds lithostatic pressure. (After Wood & Walther 1986.)

The transition from lithostatic to hydrostatic pressure, which is related to brittle/ductile transition for rock deformation and is time-dependent, does not occur at a fixed depth. The downward limit of fluid convection varies considerably from one sedimentary basin to another, but is generally less than 6 km (Rubey & Hubbert 1959) and probably in the range of 3-6 km (Wood & Walther 1986). Thus, fluid flow by convection should be prevalent only at the upper levels of the crust, especially around shallow-level igneous intrusions (Norton & Knight 1977) where it is aided by high thermal gradients and hydrofracturing, although in some contact aureoles the fluid flow appears to have been channeled along the more permeable interbeds (Nabalek et al. 1984). On the other hand, as regional metamorphism almost invariably takes place at depths >6 km, the flow of the fluid released by dehydration reactions during regional

metamorphism is likely to be of the single-pass type, focused along shear zones (see Fig. 2.25f). An argument in favor of convective flow of metamorphic fluids at depths greater than 10 km in the crust is the petrologic and isotopic evidence for the chemical interaction of rock with at least 1-5 rock volumes of fluid at depths of 13-22 km in the crust during metamorphism (Ferry 1986). Calculations by Wood and Walther (1986), however, show that similar fluid:rock ratios may accompany metamorphism of carbonate and pelitic rocks in the case of single-pass fluid flow. At present, there are no convincing examples of large-scale, pervasive, lithostatically-pressured convection cells in regional metamorphic terrains (Valley 1986). The channeled flow of metamorphic fluids in the deeper crust, as the current evidence seems to indicate (Newton 1989), is particularly important for the ore-forming potential of such fluids.

The large-scale fluid transport in the crust presents an apparent paradox. Fluid-rock interaction involving extensive exchange of solutions should plug much of the pore spaces with secondary minerals, yet there is convincing evidence that fluid flow has somehow been maintained over time scales of millions and billions of years. The answer may lie in a time-dependent cycling of rocks between hydrostatic and lithostatic pore pressures (Nur & Walder 1988). Pores are open at hydrostatic pressure, but as the pores begin to be filled with minerals the pressure builds up to lithostatic pressure. When the pressure of the isolated pore space reaches the level of the least compressive stress, natural hydrofracturing leads to a pressure drop and fluid movement is resumed at hydrostatic pressure. Repetition of this cycle may maintain fluid flow through fractures for a long time and explain the episodic nature of mineralization in some deposits.

2.5.2. METAMORPHIC MOBILIZATION

Metamorphic *mobilization* refers to the movement and increased concentrations, as a consequence of metamorphism, of ore constituents originally dispersed or disseminated in ordinary rocks (Mookherjee 1970). The mechanism of mobilization (and *remobilization*) may be classified as (Marshall & Gilligan 1987): (a) chemical — fluid-state transport including wet diffusion, solution, and melting; and (b) mechanical — solid-state transport including plastic and cataclastic flow, diffusive mass transfer, and grain-boundary sliding. In reality, the mobilization process involves both chemical and mechanical mass transfer. However, considering the limited distances over which solid-state migration of constituents is effective, a mobilization process of ore-forming potential must involve mass transfer by a fluid phase, the fluid generated by metamorphic reactions (Hobbs 1987).

Deformation during metamorphism plays a crucial role in mobilization of constituents, because mobilization occurs by a combination of pressure-induced dissolution, solution transfer, and precipitation processes during foliation development (Cox et al. 1987). The preferred sites of mass loss are discrete, subparallel arrays of dissolution surfaces or zones, typically oriented at high angles to the maximum principal shortening direction (Engelder & Marshak 1985). The evidence for dissolution and mass loss from specific microstructural sites is clear in low- to

medium-grade metamorphic rocks and includes partly dissolved fossils and detrital grains as well as widespread development of axial-plane solution cleavages. Further evidence for substantial fluid migration and large-scale mass transfer during metamorphic and deformation events is provided by mass-balance calculations based on prograde metamorphic reactions (Ferry 1981, Rumble et al. 1982) and the extent of isotopic exchange in a number of metamorphic environments (Rumble & Spear 1983, Kerrich et al. 1984). From an analysis of aluminous metapelites of the Damara orogen in Namibia, Haack et al. (1984) concluded that substantial loss of ore-forming constituents occurred between the biotite isograd and anatexis: 61% Cu, 20% Tl, 34% Ba, 59% Pb, 86% Bi, 46% Hg, 30% Sr, 25% Zn, and 31% Cd. Glasson and Keays (1978) showed that about 10% S and 10% Au of their original concentrations in the sedimentary rocks of the auriferous Slate Belt in central Victoria, Australia, were mobilized during cleavage development.

The transport of the dissolved material is controlled by several factors such as fluid composition, fluid:rock ratio, temperature and pressure, redox conditions, and permeability (Hobbs 1987, Cox et al., 1987). For long-distance transport, a critical factor is the enhancement of permeability by hydraulic fracturing and the development of grain-scale dilatancy. The low solubilities of most minerals in metamorphic fluids requires effective fluid:rock ratios of 10^3 or greater in order to accomplish a mass loss of about 10% (Fyfe et al. 1978). Thus, another essential requirement of significant metamorphic mobilization is the circulation of large volumes of fluids.

Precipitation of material removed by dissolution occurs in a variety of 'sinks' (e.g., pore surfaces, grain-scale microcracks, and veins) at various distances from the source. A requirement of the formation of ore deposits by metamorphic mobilization is focused fluid flow (e.g., along fault and shear zones) so that the precipitation of mobilized species occurs in a limited volume of rock. Vein-type gold deposits in the Precambrian greenstone belts are now interpreted to have originated by such a process (see Ch. 16). The involvement of metamorphic fluids has also been suggested for some shallow-level vein-type silver-base metal deposits, such as those of the Coeur d'Alene mining district, Idaho-Montana, USA (Leach et al. 1988, Constantopoulos & Larson 1991).

2.6. Examples of Metamorphic Deposits

With the exception of local concentrations of anhydrous alumino-silicate minerals (e.g., garnet, andalusite), metamorphic recrystallization alone within contact aureoles around igneous intrusions seldom leads to the formation of economic mineral deposits. Mineral deposits in contact aureoles (e.g., skarn deposits, see Ch. 9) are essentially formed from fluids derived from the magma, and are regarded as hydrothermal.

Fluids generated during regional metamorphism appear to have contributed to the formation of some vein-type hydrothermal deposits (Table 2.7). According to the scheme adopted in this book, metamorphic deposits include only those that not only involved metamorphic fluids but also were formed by recrystallization, reconstitution,

and mobilization during, and as a direct consequence of, metamorphism (and deformation). The most common examples of deposits formed by regional metamorphism are those of graphite, garnet, asbestos, talc, corundum, kyanite-sillimanite, and gemstones (e.g., ruby, sapphire, emerald).

2.6.1. GRAPHITE DEPOSITS, SRI LANKA

The graphite deposits of Sri Lanka, well known for their economic importance, occur as veins, pockets, and lenses occupying fissures and cracks in early Precambrian metasediments of pyroxene-granulite and almandine-amphibolite facies (Erdosh 1970). The veins commonly dip steeply, and are both concordant and discordant to the foliation of the country rocks. The distribution of the veins appear to have been controlled by two major lineaments.

According to Katz (1987), the graphite deposits formed as a direct consequence of granulite facies metamorphism in the presence of a CO₂-rich fluid phase under low fO_2 conditions. From carbon isotope ratios of the graphite, the CO₂ is interpreted to be of deep crustal origin. The migrating front of CO₂ flushed H₂O out of the system, caused hydraulic fracturing where pore fluid pressures exceeded the tensile strength of the invaded rocks, and precipitated graphite in the fractures. This model is consistent with the high temperature of graphite formation ($\approx 700^\circ\text{C}$), as indicated by the fully ordered structure and cell parameters of the graphite.

2.6.2. RÖSSING URANIUM DEPOSIT, NAMIBIA

Uranium is mobilized during high-grade metamorphism involving partial melting of siliceous rocks because it partitions strongly into silicate melts. Examples of deposits in which the uranium is believed to have been scavenged from uraniferous sedimentary sections or basement rocks and concentrated in anatectic granites and pegmatites include the Bancroft district in Canada (Robinson 1960) and the Rössing district in Namibia (Berning et al. 1976, von Backstrom & Jacob 1979).

The Rössing deposit, the largest known metamorphic uranium deposit, is located in the central zone of the late Precambrian Damaran orogenic belt that occupies much of the northern Namibia (see Fig. 2.11a). The rocks of the area have experienced two pulses of regional metamorphism, an earlier pulse of Barrovian type ($\approx 700^\circ\text{C}$ and 6-8 kb) and a later pulse of Abukuma type ($675^\circ\text{-}750^\circ\text{C}$ and 3-5 kb). Disseminated uranium mineralization, with uraninite as the dominant primary radioactive mineral, is associated with concordant and discordant alaskitic granite/pegmatite bodies that were emplaced preferentially in the migmatized calcareous rocks of the Khan and Rössing Formations (≈ 1000 Ma) during and after the Damaran orogeny some 510 m.y. ago. The Rössing deposit, with reserves of 390 million tonnes of ore averaging only about 0.035 % U₃O₈ (Bray et al. 1987), occurs along the southern flank of a domal structure (Fig. 2.23). Primary uranium minerals are uraninite and betafite, but approximately 40% of the uranium and most of the economic ore occur as secondary U⁶⁺-minerals

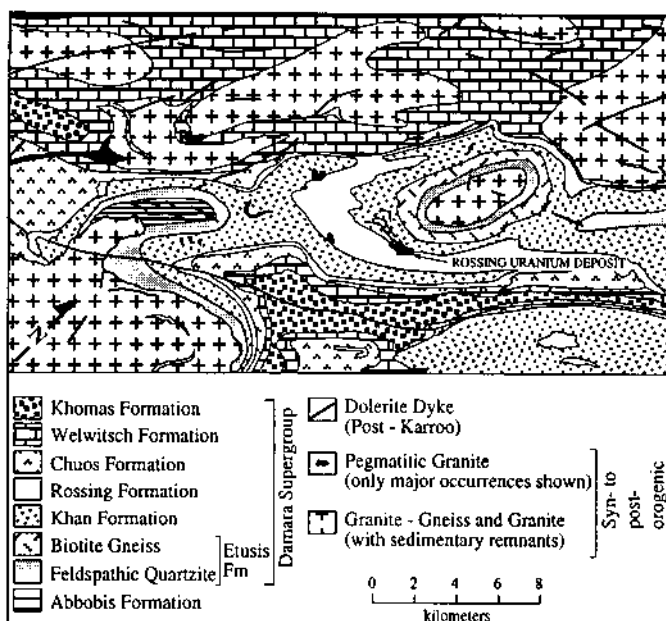


Figure 2.23. Geologic setting of the Rössing uranium deposit in the central portion of the Damaran orogenic belt (after Berning et al. 1976).

formed by oxidation and supergene enrichment.

Completely barren or very sparsely mineralized "alaskite" is widespread beyond the limits of the orebody. The alaskite has a fairly uniform mineralogy and K-rich composition irrespective of its uranium tenor, the nature of the host rock, or the elevation of the intrusion. This, according to Berning et al. (1976), suggests that the alaskitic melt was generated by partial melting of the granitic basement rocks which are highly radioactive regionally. The variable tenor of uranium in the alaskite bodies is probably a reflection of the nonuniform uranium content of the basement rocks, which were subjected to partial melting. Another possible source of uranium is the arkosic rocks of the underlying Etusis Formation. Precipitation of uranium from the anatectic melt may have been caused as a result of (a) reduction by iron in mafic xenoliths and wallrocks (Backstrom & Jacob 1979) or (b) a decrease in Eh and an increase in pH by assimilation of mafic country rock (Berning et al. 1976).

2.7. Hydrothermal Processes

Precipitation from aqueous fluids has been one of the most important mechanisms of ore formation. Evidence for this conclusion includes localization of ores along

permeable zones in deformed and undeformed rocks, zoning in mineral deposits, compositions and temperatures obtained from fluid inclusions trapped in ore and gangue minerals, wallrock alteration mineralogy dominated by hydrous minerals, common replacement textures in ore-gangue assemblages, the common association of certain types of base metal deposits with felsic intrusions related to hydrous parental magmas, and the potential of active geothermal systems for forming mineral deposits.

The formation of mineral deposits by hydrothermal processes involves precipitation of ore constituents from 'hot, watery' fluids of variable composition and source in a variety of geologic environments. Based on the concept of a fluid continuum from high, magmatic temperatures at depth to lower temperatures near the surface, Lindgren (1933) classified hydrothermal mineral deposits in terms of the depth of emplacement into three groups: (a) *hypothermal*, formed at great depths (300°-500°C, very high pressure); (b) *mesothermal*, formed at intermediate depths (200°-300°C, high pressure); and (c) *epithermal*, formed at shallow depths (50°-200°C, moderate pressure). Subsequently, Graton (1933) proposed the term *telethermal* for deposits formed at the low temperature-pressure end of the spectrum, and Buddington (1935) introduced the term *xenothermal* for deposits formed at shallow depths but at relatively high temperatures. However, available data on the formation of mineral deposits, especially from fluid inclusion studies, do not fall into such discrete *P-T* regimes. In modern literature, these terms are used only in a qualitative sense and without any connotation of a magmatic source of ore-forming fluids.

Fluid inclusion studies and thermodynamic calculations based on the stabilities of observed mineral assemblages (see Ch. 3) indicate that ore-forming *hydrothermal fluids* are moderately hot (generally 50°-500°C), aqueous solutions with an assortment of dissolved constituents including gaseous species. The salinity of the fluids (total dissolved solid constituents in wt%) varies widely (<5% to >40%), but the major dissolved components invariably are chlorine, sodium, calcium, magnesium, and potassium (Table 2.6). Other important components include heavy metals (Fe, Mn, Cu, Zn, Pb), sulfur (as either SO_4^{2-} or S^{2-} or both), carbon (as HCO_3^- and CO_2), and nitrogen (as NH_4^+), some of which may be present in excess of 1,000 ppm. The pH of the fluid is an important parameter because of its effect on the solubility of the ore metals, but commonly it is not well constrained. On general principles, one would expect the pH of ore-forming fluids to be pretty close to neutral, because strongly acidic solutions should be quickly neutralized by reactions with silicate and carbonate minerals, and strongly alkaline solutions should be neutralized by silica. Wallrock alteration mineralogy (see Ch. 3) suggest that ore-forming fluids normally are weakly alkaline to somewhat acidic.

The formation of a hydrothermal deposit requires a favorable combination of: (a) source(s) of water; (b) source(s) of ore constituents; (c) dissolution of ore constituents in sufficient concentrations in the fluids to render them potentially ore-forming; (d) migration of the enriched fluids to sites of deposition; and (e) focused discharge of a large volume of fluids into an appropriate environment, leading to precipitation of ore

constituents in large quantities in a relatively limited volume of rock.

2.7.1. SOURCES OF WATER

The most useful kinds of data in deducing the source(s) of water are obtained from: (a) fluid inclusion studies of ore and gangue minerals for information about the temperature and chemical composition of the fluids (see Ch. 3); (b) analysis of stable isotope ratios (D/H, $^{18}\text{O}/^{16}\text{O}$) of inclusion fluids and associated minerals (see Ch. 4); and (c) Br/Cl ratios of inclusion fluids and of rocks with which the fluids interacted (Rittenhouse 1967, Carpenter et al. 1974, Panno et al. 1983, McKibben et al. 1988); and (d) studies of natural waters and active geothermal systems.

The waters of hydrothermal fluids may be classified into four end-member categories (White 1974, Skinner 1979):

- (a) meteoric - water recently involved in atmospheric circulation (including rain water, lake water, ocean water, river water, and groundwater);
- (b) connate - formational water trapped in the pores of sediments deposited in an aqueous medium (the term 'evolved connate' is used sometimes to emphasize that the connate water may have changed in chemical and isotopic composition by reactions with the host sediment);
- (c) metamorphic - water produced by metamorphic dehydration reactions or water that equilibrated with metamorphic rocks at temperatures above about 300°C; and
- (d) magmatic - water derived from a magma, regardless of its ultimate origin.

Any of the above categories of water can evolve into a potential ore-forming fluid if other critical requirements are satisfied. However, from studies of modern geothermal systems and their ancient analogs (White 1974, 1981), it is now well established that many deposits formed from waters of at least two, possibly more, sources and that similar deposits could have formed from quite different kinds of water. The latter observation suggests that the actual source of water is apparently not the controlling factor in the formation of hydrothermal mineral deposits.

2.7.2. SOURCES OF ORE CONSTITUENTS

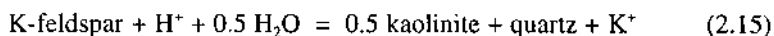
The ultimate source of all ore constituents is the mantle. The immediate sources of the dissolved constituents of hydrothermal fluids are: (a) magmas, which tend to concentrate certain constituents in the fluids that separate as a consequence of magmatic crystallization (magmatic hydrothermal fluids, discussed earlier); and (b) crustal rocks, including subducted oceanic crust, with which the hydrothermal fluids interact at their source or during their subsequent migration.

The potential of crustal rocks as sources of ore constituents depends on many

variables that are not easily quantified. These include the initial concentrations of different ore-forming elements in the rock (although the tendency of a metal to form hydrothermal deposits bears little relation to its average crustal abundance), the volume of rock affected by hydrothermal circulation, the extent of chemical interaction between the rock and the hydrothermal fluids, and the fluid:rock ratio (the mass of a given aliquot of fluid divided by the mass of rock with which it has chemically interacted). It can be shown by simple calculations that the metal contents of even large deposits can be accounted for by assuming the extraction of a small fraction of the metals from fairly modest volumes of rocks (Krauskopf 1967a). For example, the average concentration of copper in granites is about 10-20 ppm, and to concentrate a million tonnes of copper in an orebody requires that the copper content in 100 km³ of granite be diminished by only about 3 ppm or by even a smaller amount for a correspondingly larger volume of granite. Thus, for elements with crustal abundances in the range of 10-100 ppm (e.g., copper, lead, zinc), the potential source rocks need not be unusually rich in these elements; the limiting factor usually is the efficiency with which elements can be extracted from the rocks by the hydrothermal fluid. On the other hand, for the geochemically very scarce elements with crustal abundances below 10 ppm (e.g., tin, silver, mercury), enrichment of the source rocks prior to solution extraction, by some process of recycling, may be a prerequisite (Krauskopf 1971; Skinner, 1979).

With a few notable exceptions (e.g., Fe, Al), crustal rocks contain ore metals only at trace levels (see Table 2.1), predominantly as solid solution components of silicate minerals — for example, lead in potassium feldspars, copper and zinc in micas, chromium and nickel in olivines and pyroxenes, titanium in amphiboles, etc. Adsorption on the surfaces of mineral and organic particles may be important in some rocks, but in most rocks the bulk of the trace elements occur as bound components in the crystal structure of the minerals. As has been discussed in detail by Lydon (1983, 1986), solution leaching of metals held in solid solution can take place only during destruction of the host minerals by dissolution (“mineral-solution disequilibrium”) or during conversion of the host mineral into an alteration assemblage (“mineral-mineral disequilibrium”). Circumstances favorable to both types of reactions are hydrothermal alteration and metamorphism.

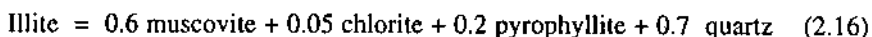
Mineral-solution reactions such as



usually do not result in greater than 1 ppm concentrations of trace metals in a hydrothermal solution, because the solution reaches chemical equilibrium with the rock before it can destroy sufficient quantities of primary minerals. This is a major reason why most hydrothermal fluids do not attain significant concentrations of dissolved trace metals. A special case where mineral-solution disequilibrium can produce high concentrations of trace metals in solution is the destruction of primary mineral assemblages of basaltic and ultramafic rocks by hydration reactions. The essential reactant in this case is the water itself, so that in reactions of this type the solution

does not lose its reactive capacity. Calculations show that a basalt can be completely converted into a greenschist facies assemblage of albite - chlorite - epidote - actinolite by hydration reactions at a water:rock ratio of only 1:30, and with 50 ppm leachable metals and 20% porosity the water could achieve concentrations of over 1,500 ppm trace metals (Lydon, 1986).

Reactions due to mineral-mineral disequilibrium in the presence of an aqueous solution do not depend on the supply of any components from the solution. These reactions can proceed at very low water:rock ratios and produce high concentrations of metals in solution. An important reaction of this type



occurs during the burial diagenesis of marine shales (Burst, 1969). At 200°C and 10% porosity, and with 50 ppm leachable trace metals in the illite, this reaction would release theoretically 1,638 ppm of trace metals into the pore solutions. The proportion of different ore metals extracted by a hydrothermal solution will obviously depend on the composition of the rocks it reacts with and the concentration of each metal carried in the solution will be limited by its solubility. As we will discuss later, the availability of complexing agents such as Cl^- , HS^- or S^{2-} is a prerequisite for maintaining high concentrations of ore metals in a hydrothermal fluid.

Experimental studies, although rather limited, attest to the viability of crustal igneous and sedimentary rocks as potential sources of ore constituents for hydrothermal fluids. Studies conducted over a range of conditions (70°-500°C, 1-1,000 bar, and water:rock mass ratios of 0.5 to 125) have shown that, over the conditions likely to be encountered within the oceanic crust at mid-ocean ridges, the seawater:rock ratio and the temperature are the most important parameters in determining the alteration mineralogy and the resulting solution chemistry (Bischoff & Dickson 1975, Hajash 1975, Seyfried & Bischoff, 1979, 1981, Mottl & Holland 1978, Mottl et. al. 1979, Seyfried & Mottl, 1982, Seyfried & Janecky 1985). As a generalization, in reactions of seawater with basalt, Mg is lost from the solution into smectite-type phyllosilicates, producing an acidic environment which leads to significant leaching of Na, K, Ca, Mn, Fe, Cu, Zn and Ni, and calcium sulfate is precipitated from the solution. The efficiency of leaching generally increases with increasing temperature. At low water:rock ratios (<10), after initial removal of Mg from solution, the pH rises slowly in response to H^+ -metasomatism of aluminosilicates; at higher water:rock ratios (>50), the fluid is depleted in Mg, but the pH remains low permitting strong leaching of Ca, K, Ba, and heavy metals. The reacting solution is enriched in sulfide sulfur due to extraction from the basalt as well as due to reduction of seawater sulfate, although part of the sulfur may be reprecipitated in the basalt as pyrite or pyrrhotite replacing silicates.

Hydrothermal experiments have also been performed to evaluate the leachability and alteration of greywacke (rock:fluid ratio of 1:10) by reaction with seawater, saturated NaCl brine containing Ca, Mg and K (approximating a typical sedimentary brine of the Mississippi Valley, as described by Carpenter et al. 1974), and 4 molal pure NaCl

(Bischoff et al. 1981, Rosenbauer et al. 1983). The degree of reaction was minimal at 200°C but was found to be significant at 350°C. The most effective leaching of heavy metals from the greywacke was observed in experiments with the Na-Ca-Mg-K brine, suggesting the importance of acidity (as in the case with basalt-seawater reactions) and chloride complexing for this process. An experimental study of brine-arkose interaction at 200°C and 500 bars (Lentini & Shanks 1983) showed that iron-rich arkose sandstone could be an excellent source rock for generation of Fe-Zn-Pb-Mn-Ba-rich brines, even at relatively low temperatures, through acid-producing reactions. It should be noted that the compositional changes in the reacted greywacke and arkose in the above experiments were too small to be detectable in the field. Several laboratory studies have shown that metals can also be leached from clays and shales by a variety of solutions. For example, Long and Angino (1982) found that NaCl brines at 90°C and with ionic strengths of 4 were effective in leaching Pb and Zn from various shales, as were CaCl₂ brines. However, their results are somewhat ambiguous because no attempt was made to prevent oxidation and, hence, acid production during the experiments.

Most ore fluids contain chloride as the dominant anion, and its relative dominance generally increases with increasing salinity. The source of the chloride cannot be determined directly, but may be inferred from the geologic environment and from the likely origin of the water. For example, the source of chloride is likely to be magmatic if a magmatic origin of the water is indicated, or seawater if the water appears to be oceanic or evolved-connate. In some cases, the chloride concentration and salinity of the fluid seem to be anomalously high compared with the inferred source of the water. Suggested explanations for such anomalies include: (a) infiltration and burial of brines produced by subaerial evaporation of surface waters; (b) evaporite dissolution; (c) membrane filtration; and (d) boiling. Evaporites are potential source rocks for many elements (e.g., Cl, K, Na, Mg, S, Pb, Cu, Zn) in hydrothermal fluids (Carpenter et al. 1974, Thide & Cameron 1978). In fact, many Phanerozoic sediment-hosted Pb-Zn and Cu deposits either are associated with evaporites (Davidson 1966, Renfro 1974, Bogashova 1987) or preserve evidence of the former presence of evaporites (Beales & Hardy 1977, Hersch & Misra 1979), suggesting a possible genetic link between certain types of ore deposits and evaporites. The commonly observed increase in salinity with depth in sedimentary basins could also be explained if fine-grained argillaceous sediments behaved as semi-permeable membranes, which would allow water molecules to pass through during compaction but retard or prevent the migration of dissolved species (DeSitter 1947, Berry 1969), thus increasing the concentration of solutes (e.g., Mg²⁺, Ca²⁺, Cl⁻) in the fluid left behind the membrane. The process is of special importance in apparently evaporite-free basins, but should also be expected to operate in evaporite-bearing sequences (Graf, 1982). However, no unambiguous, large-scale example of salinity enhancement by membrane filtration has yet been identified in the field (Hanor 1983, 1995). Boiling of a hydrothermal fluid occurs when the vapor pressure exceeds the lithostatic or hydrostatic pressure, and it results in the separation of a lower-salinity vapor phase, thereby increasing the salinity of the residual fluid. For

example, experimental observations indicate that decompression of a $\text{H}_2\text{O-NaCl}$ liquid containing 10 wt% NaCl at 500°C to 400 bars would boil to give a vapor phase containing about 0.1 wt% NaCl and a co-existing liquid phase of correspondingly higher NaCl. Evidently, boiling cannot account for high salinities of deep basinal brines, but it is a possible mechanism for producing anomalous salinities in some shallow-level hydrothermal systems.

The sources of sulfur for hydrothermal fluids are either magmas from which the fluids are derived (discussed earlier), or rocks with which the fluids interact, or both. The average sulfur content of crustal rocks is $<1,000$ ppm. In igneous and metamorphic rocks the sulfur occurs primarily in sulfide and sulfate minerals. In sedimentary rocks, the sulfur is essentially recycled seawater sulfur, which occurs in the form of evaporite minerals (mostly as gypsum and anhydrite), diagenetic sulfides (mostly as pyrite and marcasite), and sulfur-bearing organic compounds. Buried marine sediments may contain up to 10 wt% S or more (Dinur et al. 1980). The inferred source of sulfur in a deposit must be consistent with its geological environment, and it may be quite different from the sources of the water and other constituents. As will be discussed later, how much sulfur can be carried in a hydrothermal fluid and in what form (oxidized versus reduced) are constrained by several parameters (T , pH, $f\text{O}_2$, $f\text{S}_2$). It appears that, at least in some cases, the precipitation of a large quantity of hydrothermal sulfides would require the addition of reduced sulfur at the site of deposition (White 1968, 1974).

Sulfur isotope ratios are useful in determining the source of sulfur in a sulfide or a sulfate deposit (see Ch. 4). On the other hand, it is usually very difficult to establish with any certainty the specific source rocks from which the ore metals of a deposit were derived, although some rocks may be eliminated from consideration either because they are younger than the deposit or because they occur outside the inferred flow paths of the mineralizing fluids. A possible clue to the identification of source rocks may lie in the geographic association and in some cases a local source appears to have been adequate. For example, it is now generally accepted that the base metals of the Cu-Zn sulfide deposits associated with ophiolites were leached by circulating ocean water from the underlying ocean-floor basalts. This model is compatible with the concentrations of base metals in ocean-floor basalts, experimental studies on the leachability of metals by brines (discussed earlier), and oxygen isotope ratios of fluid inclusions indicating a seawater-dominated mineralizing fluid (see Ch. 10). In other cases, such as the breccia-fill Zn-Pb sulfide deposits hosted in carbonate rocks, the hydrothermal fluids as well as their dissolved ore metals seem to have been derived from regions well beyond the immediate host rocks (Sverjensky 1984, Leach & Rowan 1986). Present-day ore metal concentrations of suspected host rocks seldom provide an unequivocal answer. Suppose, the field relationship, age of mineralization, and hydrologic relationship of a hydrothermal zinc deposit are compatible with a shale formation as the source of the zinc. The question is: should the shale be expected to show a high concentration of zinc reflecting an even higher original concentration, or a relatively low zinc concentration because of depletion by leaching? Moreover, the low analytical precision

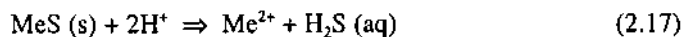
for trace elements becomes a limiting factor in ascertaining the depletion of a rock mass by a few ppm or ppb of an ore metal.

A potentially promising approach to determining the source of lead, and by implication of associated ore metals, in a deposit is through the use of lead isotope ratios (see Ch. 4). For some deposits, such as the Pb-Zn deposits of central Ireland (LeHuray et al. 1987) and the Creede deposit in Colorado (Doe & Stacey 1974), the lead isotope ratios appear to indicate a Precambrian basement source. On the other hand, the lead in the high-temperature copper ores of Utah appears to have been derived from associated igneous rocks (Stacey et al. 1968) and that in the Ducktown mining district of Tennessee from U/Pb-enriched clastic sediments (LeHuray 1984). Doe and Delavaux (1972) proposed that the source of lead in the Old Lead Belt, southeast Missouri, was probably the feldspars in the Cambrian Lamotte sandstone, the main aquifer for hydrothermal fluids in the district, but the correlation between lead and sulfur isotope ratios in ore galena in the New Lead Belt, Missouri, is not consistent with a single lead source (Sverjensky et al. 1979).

2.7.3. TRANSPORT OF ORE CONSTITUENTS

Sublimates deposited from volcanic gases around fumaroles (small gas vents) are mostly composed of chlorides and sulfates of Na, K, Ca, Mg, Al, and Fe, oxides of Si and Fe, ammonium chloride, and native sulfur, but they contain in minor or trace amounts all the metals commonly found in sulfide ores. This raises the possibility that ore metals contained in some hydrothermal deposits might have been transported in a gaseous phase. Thermodynamic calculations by Krauskopf (1964, 1967b) showed that much of the concentration of the common ore metals in volcanic sublimates could be accounted for by the volatility of their most stable chloride compounds at magmatic temperatures, but the volatilities drop sharply with decreasing temperature and are too small for most ore metals below about 400°-500°C. Moreover, Barnes (1962) has shown that the observed zoning sequences in hydrothermal deposits (see Ch. 3) are quite different from what would be expected from the relative volatilities of the metals or of the sulfides. Thus, it is unlikely that the transport of ore metals for hydrothermal deposits is controlled by their volatility.

Most of the common ore metals — such as lead, zinc, copper, silver, molybdenum, mercury — occur chiefly as sulfide and sulfosalt minerals, and these were precipitated from aqueous solutions at moderate temperatures. This raises a serious problem about hydrothermal ore deposits, because sulfide and sulfosalt minerals are extremely insoluble in aqueous solutions at such temperatures and realistic pH values. This can be demonstrated for metallic sulfides (MeS) by considering dissolution in neutral to acidic solutions (where the dominant aqueous sulfide species is H₂S, not S²⁻), which can be represented by the reaction



The calculated activity products of Me^{2+} and aqueous H_2S for several common sulfides (with values of a_{H_2S} roughly in the range of 0.1-0.001), listed in Table 2.5, show that they have negligible solubilities even at 200°C and a pH value two units below neutrality (pH_{n-2}). In theory, it is possible to compensate for the low solubilities by proportionately larger amounts of solution and longer periods of sulfide deposition, but rough estimates of these parameters for deposits of known size suggest some realistic lower limits of solubility in potentially ore-forming solutions — at least 1-10 ppm of metal, preferably 100 ppm or more (Roedder 1960, Anderson 1983). Also, the relative solubilities of metal sulfides do not agree with the zoning sequences observed in mineral deposits (Barnes 1962). Thus, simple ionic solubility of sulfides is clearly inadequate for the required concentrations of metals in ore-forming fluids.

TABLE 2.5. Activities of metal ions in equilibrium with sulfides (Barnes 1979)

Sulfide	$\text{Log}(a_{Me^{2+}} \cdot a_{H_2S})$					
	25°C		100°C		200°C	
	pH_n	pH_{n-2}	pH_n	pH_{n-2}	pH_n	pH_{n-2}
FeS	-10.58	- 6.58	- 9.47	- 5.47	- 9.2	- 5.2
NiS	-15.14	-11.14	-13.56	- 9.56	-12.60	- 8.6
ZnS	-19.03	-15.03	-16.48	-12.48	-14.61	-10.6
CdS	-21.30	-17.30	-18.03	-14.03	-15.7	-11.7
PbS	-22.17	-18.17	-18.19	-14.19	-15.40	-11.4
CuS	-29.96	-25.96	-25.15	-21.15	-21.43	-17.4
HgS	-46.8	-42.8	-38.2	-34.2	-31.4	-27.4

pH_n represents the neutral pH at a given temperature (e.g., 7.00 at 25°C, 6.12 at 100°C, and 5.69 at 200°C) and pH_{n-2} is two pH units acidic.

The solubility problem is less severe if ore metals are transported as aqueous complexes, which generally have a much greater stability (i.e., capacity for remaining in the ionized state) than simple ions. The increase in solubility due to complexation can be illustrated by thermodynamic calculations using galena as an example. At 200°C, saturated water vapor pressure, $H_2S = 10^{-3}$ molal, $pH = 3.0$, and assuming activities of aqueous species to be equal to their molal concentrations, the solubility of galena due to chloride complexation (in the presence of 1.0 molal Cl^-) works out to be 1,038 mg/L, which is nearly 4.5 orders of magnitude higher compared with its solubility (47.4 $\mu\text{g/L}$) as simple Pb^{2+} ion (Wood & Samson 1998).

Three kinds of aqueous complexes have been considered as likely candidates for many ore metals: (a) chloride complexes (Helgeson 1964); (b) sulfide complexes (Barnes & Czamanske 1967, Barnes 1979); and (c) organometallic complexes (Giordano & Barnes 1981, Giordano 1985, Hennet et al. 1988). Apparently, above about 300°C, organic complexes are dissociated and are unlikely to be important in high-temperature ore fluids; their importance at lower temperatures is probably limited by the low concentrations of organic acids in hydrothermal fluids (Kharaka et al. 1986, Gize Gize & Barnes 1987, Shock & Sverjensky 1989). The recent study of Hennet et al. (1988) has shown that acetate complexes (and other soluble carboxylates) with Pb^{2+} and Zn^{2+} can dominate over chloro-complexes in neutral to slightly acidic Na-Ca-Cl brines containing in excess of 10^{-5} molal acetate and other carboxylic acids. The efficiency of acetate complexing in typical hydrothermal fluids is inversely proportional to the concentrations of Ca and Cl (and other competing cations) as well as temperature. Basinal brines containing such high organic ligand concentrations are rather rare, but some transport of ore metals (especially zinc and lead) as metal-rich organic complexes in oxidized and slightly acidic basinal brines is likely (Giordano 1990).

For the temperature-pH range appropriate for ore-forming fluids, the dominant complexing ligand among sulfur species is more likely to be HS^- or H_2S rather than S^{2-} or SO_4^{2-} (Fig. 2.24). Stronger complexing is caused by the bisulfide ionic field than by the dipole field of molecular H_2S , so that it is in or close to the stability field of HS^- that sulfide complexing is more likely to result in higher solubilities of the sulfides (Barnes 1979). The HS^- stability field deviates by as much as 3 pH units from neutrality toward higher pH (Fig. 2.24), indicating that very alkaline solutions are required above about 300°C for HS^- to become a dominant species. Thus, bisulfide complexes — such as $Zn(HS)_3^-$, $Cu(HS)_2^-$, $HgS(HS)^-$, $Au(HS)_2^-$ — may be important to ore metal transport at temperatures below about 300°C and in moderately alkaline solutions. The major limitation is the high concentration of reduced sulfur (HS^- or H_2S) required to keep them stable, a concentration much higher than what is usually found in fluid inclusions or in the fluids of modern hydrothermal systems. Moreover, the recent experimental study of Barrett et al. (1988) has shown that the H_2S solubility in NaCl solutions decreases with increasing temperature (in the range 0–95°C) and is about 0.1 *m* H_2S for 0.5 *m* NaCl solutions at 95°C.

The high Cl^- contents of fluid inclusions and modern hydrothermal fluids point to the high probability of ore metal transport as chloride complexes (e.g., $PbCl^+$, $ZnCl_2^{2-}$). The case for the dominance of chloride complexes is also supported by experimental studies and thermodynamic calculations (Crerar & Barnes 1976, Barrett & Anderson 1982 & 1988, Ruaya & Seward 1986, Bourcier & Barnes 1987, Ruaya 1988, Hemley et al. 1992), the observed increase in the solubility of lead and zinc with increasing chloride concentration in basinal fluids (Hanor 1995), and the general agreement between the order of stability of chloride complexes at 25°C ($Cu < Zn < Pb < Ag$; Helgeson 1964) with the zoning sequence in some mineral deposits. The requirements for chloride complexing, in addition to an abundance of Cl^- , are a slightly

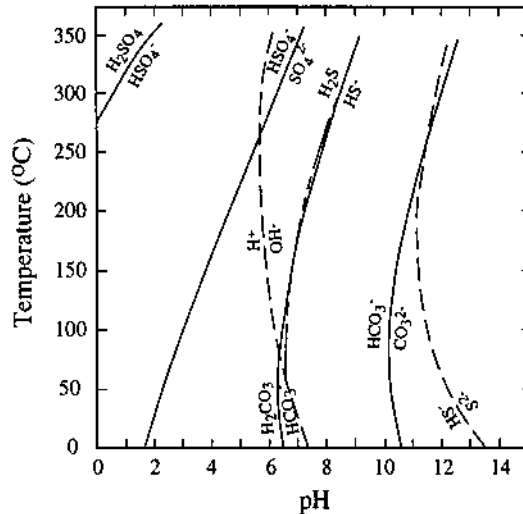


Figure 2.24. The ionization of some aqueous acids and bases. The curves represent equal activities of aqueous species and separate their regions of predominance. (After Barnes 1979.)

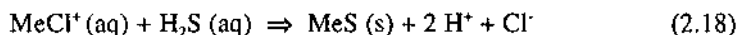
acidic pH, moderately elevated temperatures, and low concentrations of reduced sulfur species (H_2S , HS^- , or S^{2-}) in the solution. Experimental studies by Hemley et al. (1986, 1992) conducted in the temperature and pressure ranges of 300°-700°C and 0.5-2 kb have shown that Fe, Pb, Zn, and Cu sulfide solubilities in chloride solutions increase with increasing temperature and total chloride, but decrease with increasing pressure.

The relative importance of chloride and sulfide complexes for transport of ore metals in hydrothermal fluids is still a matter of controversy. Chloride complexes appear to have been more important for most hydrothermal sulfide deposits, although bisulfide complexing may have dominated in some cases such as the volcanic-hosted Cu-Zn deposits (see Ch. 10). Sulfide complexes are particularly important for hydrothermal gold deposits (see Ch. 16). For example, the $\text{Au}(\text{HS})_2^-$ complex is believed to be responsible for gold transport in some epithermal ore-depositing environments in which the solutions are at low salinity, near neutral to weakly alkaline pH, and temperatures between 200°C and 300°C. The roles of other ligands such as fluoride, phosphate, carbonate, and hydroxide, have not been adequately evaluated, but they are known to be important for transport of some metals such as uranium (Langmuir 1978). No single complex or species probably predominates for any metal over the entire range of reasonable solution composition and temperature; different metals are likely to be transported by quite different mechanisms, and mixed ligands and perhaps also polynuclear species may be involved.

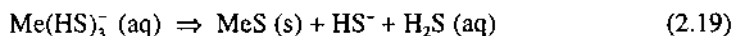
The transport of ore metals mostly as chloride complexes imposes certain restrictions on the transport of reduced sulfur in the same fluid. In fact, the metal-rich brines of the active geothermal systems (e.g., Salton Sea, Red Sea) normally appear to be sulfide-deficient, in the sense that an average volume of fluid contains higher molar concentrations of sulfophile metals than that of total dissolved sulfide species (White 1974). Thermodynamic and experimental data suggest that at temperatures higher than about 200°C (Crerar & Barnes 1976, Barrett & Anderson 1982, 1988) or in NaCl-rich solutions (Sverjensky 1986), sufficient amounts of metals, such as zinc and lead, can be transported as chloride complexes in the presence of reduced sulfur (H_2S or HS^-). At temperatures lower than about 150°C this will be possible only at pH values one to two units lower than the neutral (Barrett & Anderson 1982). Thus, precipitation of sulfides from non-acidic ore fluids will require the addition of reduced sulfur at the site of deposition by one or more of the following mechanisms: (a) reduction of the sulfate in the fluid (Barton 1967); (b) bacterial or inorganic reduction of the sulfate in the environment (e.g., in the ocean-floor environment); (c) inorganic decomposition of sulfur-containing organic compounds (Skinner 1967); (d) interaction of the fluid with the sulfides of the invaded rocks (Lovering 1961); and (e) mixing with a H_2S -rich fluid (Jackson & Beales 1967).

2.7.4. PRECIPITATION MECHANISMS

Conditions favorable for sulfide precipitation from hydrothermal solutions depend on specific reactions, but the principles may be illustrated by considering representative reactions involving the two major types of aqueous metal complexes (Barnes 1979). A reaction for chloride complexes in weakly acidic solutions can be written as



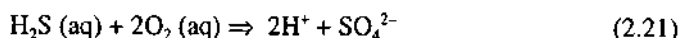
The reaction is written in terms of H_2S , not HS^- or S^{2-} , because it is the predominant sulfur species at pHs below neutrality at low temperatures as well as in mildly alkaline solutions at temperatures above about 300°C (Fig. 2.24). For sulfide (MeS) deposition, the reaction must proceed to the right and this will be favored by increased $a_{\text{H}_2\text{S}}$, decreased a_{Cl^-} , and decreased a_{H^+} (i.e., increased pH). Acid neutralization is a common mechanism of ore precipitation from weakly acidic chloride solutions, especially in carbonate rocks. For sulfide complexes in moderately alkaline solutions, a representative reaction such as



indicates that sulfide precipitation will be favored by any process that reduces the activity product $a_{\text{H}_2\text{S}} \cdot a_{\text{HS}^-}$, for example, by a decrease in pH through the reaction



The effect of oxygen fugacity on reactions 2.18 and 2.19 can be evaluated from the reaction



Addition of oxygen simultaneously decreases the H_2S concentration and pH (unless well buffered by the host rocks) and so should cause sulfide precipitation from sulfide complexes; the effect on chloride complexes will be in the opposite direction. Thus, oxidation is unlikely to be the dominant cause of precipitation of most base and ferrous metal sulfides because these metals are more commonly transported as chloride complexes, especially above about 250°C (Seward & Barnes 1997).

The common absence of ore sulfides along presumed flow channels suggests that ore-forming fluids are generally undersaturated before arrival at depositional sites. This is a favorable condition for concentrating ore minerals in a limited volume of rock. Precipitation of sulfides at the depositional sites may be caused by one or more of the following that cause the aqueous metal concentration to exceed saturation (Anderson 1975, Skinner 1979, Barnes 1979, Sverjensky 1986): (a) change in temperature; (b) boiling; (c) interaction with wallrock; and (d) fluid mixing. It is usually difficult to isolate the dominant cause of sulfide precipitation in a given deposit.

Temperature changes may cause precipitation in three ways (Skinner 1979): (a) by affecting the solubility products of sulfide and oxide minerals; (b) by affecting the formation and stability of the complex ions transporting the metals; and (c) by affecting the hydrolysis constants of ligands, such as Cl^- and HS^- , involved in the formation of metal complexes. Temperature gradients could induce deposition of the sulfides of base and ferrous metals if these metals are carried as chloride complexes, but they are less effective in the case of bisulfide complexes whose stabilities change relatively little with temperature. A significant temperature drop, probably in the order of 20°C or more, in a localized area is required to remove a lot of material from solution. The three likely mechanisms of localized cooling of hydrothermal fluids, in decreasing order of effectiveness, are mixing with cooler meteoric or ocean water, adiabatic decompression (throttling) when the pressure on the fluid approaching the surface changes over a short distance from lithostatic to hydrostatic, and conductive heat loss to wallrocks. Only large changes in pressure, in the order of 1,000 bars, can cause significant changes in solubility, so it is seldom a factor in sulfide precipitation except when a pressure decrease leads to boiling. In fact, contrary to the general expectation of decreasing metal solubility with decreasing pressure, Hemley et al. (1986, 1992) have shown experimentally that the solubilities of iron, zinc, and lead sulfides in chloride solutions increase with decreasing pressure, so that these metals may be carried over long distances along a decreasing pressure gradient so long as the temperature drop is not large enough to offset the pressure effect. Boiling produces a vapor phase enriched in volatile constituents; the residual aqueous phase becomes cooler (due to enthalpy

changes), more saline (due to partitioning of NaCl into the liquid phase), more alkaline (due to partitioning of H₂S and CO₂ into the vapor phase), and more oxidized (due to loss of H₂ and H₂S to the vapor phase). The situation in real rock systems, however, is much more complex because of the simultaneous fluid-rock reactions that affect the pH and composition of the fluid (Bowers 1991).

Three types of wallrock interactions may cause sulfide precipitation from hydrothermal fluids (Skinner 1979): (a) hydrogen exchange reactions that modify the pH of the fluid, especially the H⁺-consuming reactions such as dissolution of carbonates and hydrolysis of feldspars and mafic minerals that lead to an increase in pH; (b) addition of components from wallrock, especially of reduced sulfur species (H₂S or S²⁻) from pyrite; and (c) reactions such as sulfate reduction that change the oxygen fugacity of the fluid. The reduction of dissolved SO₄²⁻ to H₂S, which is equivalent to addition of H₂S from an external source, may be prompted by the organic matter in wallrock. The process may be aided by bacterial reduction of sulfate (Dexter-Dyer et al. 1984, Trudinger et al. 1985), but bacterial action is very slow and effective only at temperatures less than about 80-90°C. Mixing of fluids of different temperature and/or composition must be considered an effective mechanism of sulfide precipitation, although the thermal and chemical effects of mixing are usually indistinguishable without a detailed isotopic study (see Ch. 4). Depending on the chemistry of the fluids, the chemical effects leading to sulfide precipitation may include dilution, change in pH and *f*O₂, and addition of metals or reduced sulfur.

2.7.5. FLUID CIRCULATION

Recognition of ore-fluid migration paths through crustal rocks is obviously important for exploration of concealed hydrothermal deposits, but a very difficult task in most ore-forming systems. Fluid channelways within or in the vicinity of hydrothermal deposits may be decipherable in some cases from wallrock alteration and mineral or element zoning, localization of mineralization along faults or shear zones, or restriction of mineralization to certain aquifers (e.g., sandstone-hosted, peneconcordant uranium deposits of the Colorado Plateau, USA; Fischer 1970), but detailed reconstruction of the paleohydrology of a single ore-forming system still remains a largely unanswered challenge. Some notable exceptions include the models for the shale-hosted copper deposits of White Pine district, Michigan (White 1971), the uranium deposits of the Catahoula Formation, Texas (Galloway 1978), and the ophiolite-hosted exhalative massive sulfide deposits of Cyprus (Spooner 1977).

Generalized models of hydrothermal fluid circulation relevant to ore formation may be grouped under six broad categories (Fig. 2.25): (a) convection at submarine rift environments (spreading centers); (b) flow systems driven by the heat of igneous intrusions; (c) compaction-driven or gravity-driven flow of (sedimentary) basinal fluids; (d) deep crustal convection of seawater; (e) focused flow of metamorphic water along shear zones (discussed earlier); and (f) fluid flow caused by tectonic squeezing.

The measured values of conductive heat flow at spreading centers fall far short of

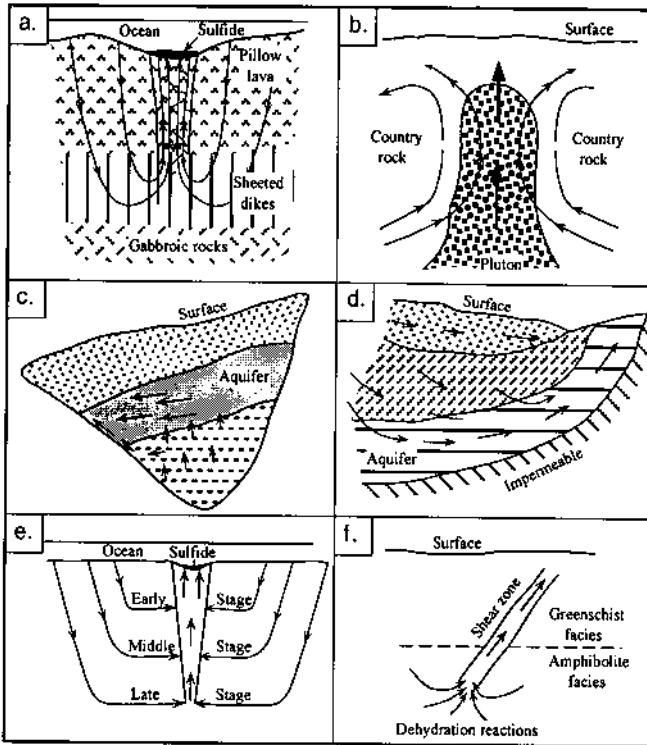


Figure 2.25. Schematic illustration of hydrothermal fluid flow systems. **a.** Convection of ocean water through oceanic crust at a spreading center; **b.** Fluid motion associated with a cooling felsic igneous intrusion (magmatic fluids and thermally driven convective circulation of groundwater); **c.** Compaction-driven fluid flow in a sedimentary basin; **d.** Gravity-driven fluid flow in a sedimentary basin, controlled by the slope of water table (assumed to be a subdued replica of the topography) and the permeability of the formations; **e.** Convection of seawater extending to progressively deeper levels of the crust in an extensional setting; **f.** Focused flow of metamorphic water, generated by dehydration reactions, along shear zones.

those appropriate for thermal contraction models and the discrepancy is attributed to heat loss due to appreciable hydrothermal circulation. The convection of seawater is effective enough to cool the upper 5 km of an oceanic plate rapidly to less than 500°C everywhere except in the axial zone, so that the strongest hydrothermal circulation occurs right at the spreading axis (Fig. 2.25a). The total bulk fluid:rock ratio in the upper 5 km of the oceanic plate is less than about 10, and perhaps about 40% of the total seawater that could ultimately circulate through a particular portion of the plate circulates through in the first million years of its existence (Cathles 1981). This initial, vigorous circulation is probably episodic, occurring during and after pulses of local sea-floor spreading. Sulfide (and amorphous silica) deposits may form at this stage by focused discharge of fluids, probably at temperatures around 300°C, on to the

sea-floor. The sulfide deposition may be followed by the deposition of Fe-oxide-rich muds and still later by Mn-oxide-rich muds (umbers) during the waning stages of the hydrothermal circulation, when oxidizing conditions may prevail due to better mixing of the upwelling hydrothermal fluids with the near-surface seawater. The ubiquitous low-intensity hydrothermal circulation at slow-spreading centers is unlikely to form any significant sulfide mineralization, but may produce Fe-oxide and Mn-oxide deposits. Faster spreading ridges may be associated with more vigorous hydrothermal systems and less widely spaced fractures, and thus be more conducive to ore deposit formation. According to Lowell and Rona (1985), the crustal heat source at a spreading center is not sufficient to drive a hydrothermal system large enough to generate ore deposits of 3 million tons or greater; heat extraction from the underlying convecting magma chamber is necessary.

The concentration of active hydrothermal systems in volcanic belts and the association of hydrothermal mineral deposits (including porphyry, vein, and skarn types) with igneous intrusions constitute evidence for the involvement of magmatic heat in driving certain hydrothermal systems (Fig. 2.25b). As discussed by Cathles (1981), the magmatic heat to drive hydrothermal circulation can be provided by thermal conduction from the intrusion (initially to the cooler intruded rocks and later directly to fluids circulating through the intrusion), by magmatic volatiles venting from the cooling intrusion, or by radioactive decay. The cooling times anticipated for intrusive bodies of reasonable size (<10 km width), particularly when aided by the convective circulation of pore water, are relatively short, perhaps in the order of 10,000 years. For a hydrothermal system to remain active for a much longer duration necessary for the formation of a sizable mineral deposit, either the heat source must be reactivated periodically by fresh intrusions or the fluid circulation must be restricted by an impermeable cap. Forced venting of metal-enriched magmatic hydrothermal fluids plays a significant role in the transport and deposition of ore constituents (Henley & McNabb 1978), but its impact on driving fluid circulation is limited by the fact that the volatiles vented by an igneous source are much less than the mass of meteoric water likely to circulate in response to that source. Thus, much of the hydrothermal alteration and mineralization within and around the intrusion is probably controlled by the thermally driven convective circulation of groundwater in the country rock (Cathles 1977, Norton 1978). Hydrothermal circulation driven by heat from radioactive decay can persist for hundreds of millions of years, driving fluid flow every time the pluton or its environment is fractured sufficiently to allow meteoric water convection to take place (Cathles 1981). An igneous intrusion may also be affected by hydrothermal fluids of deep crustal origin. For example, oxygen and hydrogen isotopic systematics suggest that hydrothermal veins crosscutting the Bushveld Complex are related to a large-scale fluid flow system that occurred at crustal depths of up to at least 15 km and temperatures up to at least 700°C, and was dominated by metamorphic water derived from external fluid reservoirs (Schiffries & Rye 1990).

The formation of many strata-bound, sediment-hosted, epigenetic deposits (e.g., Pb-Zn±Cu, U) is ascribed to brines derived from adjacent sedimentary basins. The

conceptual models proposed for the fluid flow through sedimentary basins fall under two main categories: (a) compaction-driven fluid flow (Fig 2.25c), induced by the weight of the overlying sediments (Noble 1963, Jackson & Beales 1967, Cathles and Smith 1983); and (b) gravity-driven flow (Fig. 2.25d), caused by hydraulic gradients (Garven & Freeze 1984a, 1984b, Garven 1985, Bethke 1986). Fluid flow due to compaction is an inevitable consequence of basin evolution. As the porosity decreases due to compaction, to burial depths of at least 6 km (Hanor 1979), pore fluid may percolate uniformly upward or, more likely, migrate into more permeable strata and then laterally to an easier escape route such as a fault or an unconformity. Two attractive features of the compaction-driven (or *stratal aquifer*) flow are (Lydon 1986): (a) the expulsion of very large quantities of fluids within a short time; and (b) the low water:rock ratio of the stratal aquifer system that allows the fluids to attain high concentrations of metal by leaching of the aquifer rocks. Such fluids, termed *stratafugic* by Jackson and Beales (1967), are believed by many to have been the ore fluids for Mississippi Valley-type Pb-Zn deposits (see Ch. 13).

The critical requirement of the compaction-driven model is the periodic development of geopressure, and this may not happen in the mature stage of basin evolution when the basin has been uplifted and most of the strata indurated. In this situation, the basinal fluid flow is likely to be primarily of gravity-driven groundwater from areas of high elevation to areas of low elevation along the slope of the water-table, which is commonly a subdued replica of the basin topography. As depicted in Figure 2.25d, large volumes of low-permeability basinal shales would constitute potential source rocks for ore constituents and serve to focus fluid flow down into basal aquifers. Water-rock interactions, membrane filtration, and evaporite dissolution could transform fresh waters into brines as they flow through deeper parts of the basin. The main requirement of the model is a paleotopographic gradient. The viability of gravity-driven flow system for forming large sediment-hosted deposits has been advocated by Garven and Freeze (1984b) and Bethke (1986). Graven and Raffensperger (1997) have discussed hydrogeologic and mathematical models for the formation of lead-zinc, copper, and uranium deposits in sedimentary basins.

Another model of hydrothermal fluid flow, which could account for the episodic nature of the mineralizing process in vein-type and massive sulfide deposits and their association with contemporaneous faulting, is seismic pumping (Sibson et al. 1975). The essence of the model is that seismic faulting acts as a pumping mechanism whereby individual earthquakes are capable of moving significant quantities of mineralizing fluid rapidly from one crustal environment to another, provided that the fault intersects a suitable source region such as a pile of volcanic rocks, sediments undergoing lithification or metamorphism, or a hydrous igneous intrusion. The resulting hydrothermal deposits may be localized on the fault itself in both sheared and unsheared regions, and in connected extension fractures including those created by hydraulic fracturing. The process works best for wrench faults, because differential stresses associated with normal faulting are relatively low. Seismic pumping has been suggested as an important mechanism for the genesis of some major sediment-hosted

Pb-Zn sulfide deposits such as the McArthur River, Australia (Muir 1983) and Tynagh, Ireland (Boast et al. 1981).

Russell (1983, 1986) proposed a deep crustal convection model for the formation of sediment-hosted exhalative Pb-Zn deposits, especially for the Silvermines and Tynagh deposits of Ireland (Fig. 2.25e). The model envisages a one-pass convection of seawater and meteoric water in fractures generated by crustal extension (incipient rifting), driven by the regional geothermal gradient. The hydrothermal convection cell, according to Russell, would extend to the brittle-ductile transition zone that is advanced to progressively greater depths by the concomitant cooling, permitting scavenging of metals by hydrothermal fluids from increasingly deeper levels of the crust. Mathematical modeling by Sterns et al. (1987) suggests that such a convection system is capable of forming large Pb-Zn deposits, provided that the relevant metals are available within the hydrothermal circulation system. According to their computation, nearly 20 million metric tons of sulfide can be generated in 50,000 years either by circulation penetrating to a 10-km depth in rocks with a geothermal gradient of 30°C/km or by circulation to a 6 km depth if the geothermal gradient is 60°C/km. However, based on the characteristics of modern hydrothermal systems, Lydon (1986) argued against the development of such deep convection cells and their ability to leach significant amounts of zinc or lead from the metamorphosed sediments or crystalline rocks of the basement.

Large-scale fluid flow might have been controlled also by tectonic processes. Oliver (1986) proposed a "speculative hypothesis" that fluids contained in the continental margin sediments in convergent zones may be squeezed out by an overriding thrust sheet. These fluids, then, would travel ahead of the thrust sheet and may mix with compaction- or gravity-driven basinal fluids, thereby modifying their thermal and chemical characteristics. Such fluids may play a key role not only in the transport of ore constituents and hydrocarbons but also in faulting and metamorphism (Oliver 1986). Stable isotope ratios of quartz veins in the Canadian Cordillera have been interpreted to indicate convection of evolved meteoric water to depths of at least 15 km in regions of strike-slip and extensional faulting (Nesbitt et al. 1989b).

2.8. Examples of Hydrothermal Deposits

2.8.1. ACTIVE HYDROTHERMAL SYSTEMS

Most of the active hydrothermal systems occur in the Earth's mobile belts, in areas of recent volcanism, high heat flow, and tectonic activity (Fig. 2.26); they are dominated by meteoric or seawater and are driven by magmatic heat sources. A few systems have also been recognized in the sedimentary terranes of the continental interiors; these are dominated by connate water and are driven primarily by the regional geothermal gradient. Although only a few of these systems have deposited mineable ores (mainly of mercury and sulfur), they are believed to represent modern analogs of some ancient

ore-forming hydrothermal systems that were operative for long periods of time. This correlation is supported by the similarities between ore fluids and modern hydrothermal fluids (Table 2.6) in terms of temperature, salinity and chemistry, and by the fact that chemical precipitates formed from modern geothermal fluids are often considerably enriched in ore metals, occasionally approaching ore-grade concentrations. It is conceivable that many of the active systems, if allowed to continue for geologically reasonable durations, would produce deposits of mineable size and grade.

The characteristics of active hydrothermal systems and their relationships to analogous fossil hydrothermal systems (ancient mineral deposits) have been reviewed by many authors (e.g., Ellis 1969, Tooms 1970, Weissburg et al. 1979, White 1974, 1981, and Henley & Ellis 1983, Scott 1997). The discussion presented here is largely based on White (1981) who classified them into three main types: (a) mercury-depositing systems; (b) epithermal systems depositing precious metals (Au-Ag); and (c) systems dominated by base metals (Fe-Cu-Zn-Pb-Mn).

Mercury-depositing Systems

Reported mercury contents of geothermal fluids are uniformly low, generally from a few parts per billion to less than the limits of detection (≈ 0.01 to 0.1 ppb). Such fluids, however, are apparently capable of forming mercury deposits. For example, about 5 million kg of mercury has already been recovered from the Sulfur Bank deposit, California (USA), the world's most productive mercury deposit that is clearly related to hot springs. Mercury is now being deposited there at significant but unknown rates from CO_2 -rich vapor and associated liquid at temperatures in the range of 80°-150°C. A generalized scenario for the mercury-depositing hydrothermal systems may be as follows (White 1981): scavenging of the mercury from Hg-rich sedimentary rocks and organic matter by meteoric water at temperatures above 200°C; transport of mercury in a neutral to slightly acidic solution as Hg^0 , which is quite soluble in hot water (ranging from 0.5 ppm at 100°C to about 16 ppm at 200°C and about 400 ppm at 300°C), mostly in the vapor phase; condensation of Hg^0 at temperatures below 100°C at the site of deposition and reaction with H_2S or S^0 to precipitate HgS . The precipitation of cinnabar must have involved boiling of the ore fluid, because the associated mineral assemblage indicates an equilibration temperature of 155°C compared with less than 50°C required for cinnabar supersaturation in the fluid without boiling (Reed & Sphycher 1984). A detailed discussion of the geochemistry of mercury transport and deposition in geothermal systems has been presented by Barnes and Seward (1997).

Epithermal Precious Metal Systems

Some active hydrothermal systems such as Steamboat Springs, USA (White 1981) and Broadlands, New Zealand (Weissburg et al. 1979) are considered the modern equivalents of long-lived systems that generated epithermal gold-silver deposits in volcanic terrains. These meteoric water-dominated systems are characterized by chemical precipitates (sinters, muds, sulfides) with relatively high contents of gold and silver as well as other ore-forming elements (As, Sb, B, Hg, Tl, Cu, Zn, Pb). The deep fluids of the

TABLE 2.6. Analyses (in ppm) of selected modern and ancient hydrothermal fluids

	Modern hydrothermal systems					Inclusion fluids		
	SB	BD	SS	RS	CMISS	CR	OH	BC
	1	1	1	1	2	3	3	3
Na	1190	635	50400	92600	76200	40400	19700	152000
Ca	20	1.5	28000	5150	36500	8600	7500	4400
K	23	142	17500	1870	979	3500	3700	67000
Mg	55	L	54	764	2400	5600	570	n.d.
Fe	n.d.	0.4	2290	81	294	n.d.	n.d.	8000
Mn	0.2	L	1400	82	102	450	690	n.d.
Zn	n.d.	L	540	5.4	342	10900	1330	n.d.
Pb	n.d.	L	102	0.6	96	n.d.	n.d.	n.d.
Cu	L	L	8	0.3	n.d.	9100	140	n.d.
Ag	L	L	1.4	n.d.	n.d.	n.d.	n.d.	n.d.
Cl	644	1181	155000	156030	193000	87000	46500	295000
Br	n.d.	3.9	120	n.d.	1510	n.d.	n.d.	n.d.
H ₂ S	12	107	16	n.d.	n.d.	n.d.	n.d.	n.d.
SO ₄ ²⁻	598	5.4	5.4	840	3	1200	1600	11000
SCO ₂	3290	121	150	n.d.	n.d.	n.d.	n.d.	n.d.
NH ₄	464	1.4	409	n.d.	n.d.	n.d.	n.d.	n.d.
T°C	69	261	340	56	n.d.	n.d.	n.d.	n.d.
pH	6.8	6.2	5.2	5.3	n.d.	n.d.	n.d.	n.d.

(1) Data compiled by White (1981), Table 1, p. 396-397; (2) Carpenter et al. (1974), Table 5, p. 1199, Sample no. 66; (3) Data compiled by Skinner (1979), Table 1-1, p. 12.

L = values less than 0.01; n.d. = values not determined.

Abbreviations: SB = Sulfur Bank, California, USA; BR = Broadlands, New Zealand; SS = Salton Sea, California, USA; RS = Red Sea, Atlantis II; BC = Bingham Canyon deposit (core zone), Colorado, USA; CMISS = Central Mississippi, USA; CR = Cave-in-Rock district, Illinois, USA; OH = OH Vein, Creede deposit, Colorado, USA.

Rotokawa geothermal system in New Zealand, with a maximum temperature of 320°C, are dilute chloride (0.022 mole/kg) waters containing appreciable concentrations of reduced sulfur (H₂S = 7 x 10⁻³ mole/kg), higher than any other active geothermal system (Krupp & Seward 1987). Another characteristic feature is the metal zoning with depth — As, Sb, Hg, Ti, B, and Au in near-surface parts; and Ag, base metals,

and some Au at greater depths. Similar zoning observed in the epithermal precious metal deposits associated with the Cenozoic volcanic environments of the southwest USA is ascribed by Buchanan (1981) to boiling of the hydrothermal fluids (see Ch. 16).

Base Metal Sulfide Systems

Modern hydrothermal systems relevant to the formation of base metal sulfide deposits include: (a) the geothermal brine pools of Salton Sea (Skinner et al. 1969, Younker et al. 1982, McKibben & Elders 1985), Red Sea (Bischoff 1969, Hackett & Bischoff 1973, Schoell et al. 1976, Shanks & Bischoff 1980, Pottorf & Barnes 1983), and Cheleken Peninsula (Lebedev 1973); (b) the sea-floor hot springs at spreading centers (Haymon & Kastner 1981, Rona 1984, Scott 1985, Haymon & Macdonald 1985, von Damm 1990, Scott, 1997); (c) the oil-field brines of central Mississippi (Carpenter et al. 1974, Lydon 1986) and Alberta (Billings et al. 1969). Excellent reviews of these systems have been presented by White (1981) and Cathles (1981).

Salton Sea. The rift-related Salton Sea convection system (temperatures up to 360°C), located in the Imperial Valley of southern California, is considered an excellent modern example of ancient ore-forming systems that produced strata-bound sediment-hosted massive sulfide deposits. The Salton Sea brine is highly saline (Table 2.6), containing up to 25-30% dissolved salts, and has an estimated volume of 11.6 km³ to a depth of 3 km with ore metal contents (in tonnes) as follows: Zn - 5 x 10⁶, Pb - 9x10⁵, As - 1.2 x 10⁵, Cu - 6x10⁴, Cd - 2x10⁴, and Ag - 1x10⁴ (White 1981). Analyses of sulfide-rich portions of siliceous scales deposited on the brine-discharge well-pipes (Skinner et al. 1967) showed several ore minerals (digenite, bornite, chalcocite, stromeyerite, arsenopyrite, tetrahedrite, chalcopyrite, pyrite, and native silver) and high concentrations of copper (up to 20 wt%) and silver (up to 8 wt%). Base metal ore mineralization in the host sediments, however, is limited to sparsely distributed strata-bound diagenetic Fe-sulfides and epigenetic vertical veinlets containing Fe-Zn-Cu-Pb sulfides and Fe-oxides (McKibben & Elders 1985). Diapiric rise of hypersaline brines from deeper levels has generated a domal fluid interface at 1-3 km depth within the system and vein sulfide deposition is localized within fracture zones transecting the interface (McKibben et al. 1989).

Oxygen and hydrogen isotope geochemistry of the Salton Sea geothermal system indicates the water of the brines to be dominantly meteoric in origin (Craig 1966, 1969), most likely evaporated Colorado river water (McKibben et al. 1988). The high salinity of the brines is attributed to a combination of evaporation of fossil lakewaters, groundwater dissolution of shallow lacustrine evaporites, and subsurface hydrothermal metamorphism of buried halite-bearing lacustrine evaporites (McKibben et al. 1988). Lead and strontium isotopic compositions of the brines provide strong evidence for derivation of the metals from the host sediments by interaction with brines, although some of the metals may have been derived from a magmatic source (Doe et al. 1966). Calculated metal chloride solubilities agree well with vein assemblages and brine analyses, suggesting that chloride complexing, mostly as monochloro and dichloro

complexes, can adequately account for base metal transport in this metal-rich hydrothermal system (McKibben & Elders 1985, McKibben & Williams 1989). Sulfur isotope ratios of the brine and epigenetic sulfides indicate that the sulfur for the vein mineralization was derived not from the diagenetic sulfides but from the evaporite anhydrite in the host sediments (McKibben et al. 1989). Ore-grade vein sulfide deposition is limited by the low amounts (<30 ppm) of H_2S in the metal-rich hypersaline brines. It is reasonable to speculate that such a hydrothermal system would be capable of producing a major ore deposit in an environment where additional reduced sulfur could be provided at the site of deposition.

Red Sea. The Red Sea hydrothermal system, also a convective system related to rifting and driven by magmatic heat, is the best known present-day example of syngenetic sulfide accumulation which locally reaches ore-grade concentrations of base metals. At least 13 brine pools are known in the Red Sea. The largest of these pools and the one with most significant hydrothermal activity is the Atlantis II Deep, which contains approximately 5 km^3 of brine with a salinity of about 26% and appreciable amounts of dissolved base metals (Table 2.6). Maximum temperature of the brine pool was about 60°C in 1972 (compared with about 56°C in 1964 when it was discovered), but mineral assemblages in bottom sediments indicate precipitation from a fluid above 200°C . It is generally accepted that the brine has been derived from normal Red Sea water that acquires high salinity by subsurface interaction with thick Miocene evaporite-bearing sequences (Craig 1969). The metalliferous sediments of the Atlantis II Deep, averaging 20 m in thickness, occur as fine-grained (mostly $<2 \mu\text{m}$ in grain size), thin-bedded oxides, silicates, sulfides, sulfates and carbonates over a depositional area of approximately 50 km^2 , and have an interstitial fluid content of up to 95%. The metal contents of individual metal-rich samples range up to about 21% ZnO, 4% CuO, 0.8% Pb, 8.5% Fe_2O_3 , and 5.7% Mn_3O_4 , but in general they are much lower (Bischoff 1969). The metals were probably derived from both the mafic volcanics underlying the sediments and the Miocene evaporite-shale sequences and transported as chloride complexes (Pottorf & Barnes 1983). The sulfur isotope data on the sulfides have been interpreted to indicate inorganic reduction of sulfate-sulfur carried by the hydrothermal fluids as the source of reduced sulfur for sulfide precipitation (Shank & Bischoff 1980). Pottorf and Barnes (1983) proposed that a temperature decrease due to mixing of two circulating hydrothermal fluids — one of shallow level with $\text{SO}_4^{2-} > H_2S$ at $<250^\circ\text{C}$, and the other a deeper, hotter fluid with $H_2S \gg \text{SO}_4^{2-}$ — was the main cause of sulfide precipitation. According to these authors, the Atlantis II sulfide-rich sediments resemble volcanogenic massive sulfide deposits in most characteristics, including associated volcanism, tectonic setting, pyrrhotite - chalcopyrite - sphalerite zoning, metal grade, sedimentary textures, and most fluid properties.

Modern Sea-floor. The most spectacular modern hydrothermal systems depositing polymetallic sulfides and Fe-Mn-rich sediments occur along the globe-encircling system

of oceanic ridges and rifts that extend through all the major ocean basins as sea-floor spreading centers (Fig. 2.26); a few have also been identified at intermediate- to fast-spreading centers in back-arc basins (Rona 1984) and on seamounts. Starting with the discovery in 1976 of buoyant but relatively low-temperature fluids (<13°C) venting from the Galapagos spreading center, more than 100 such hydrothermal discharge sites are now known, some with fluid temperatures as high as 405°C. In the present economic context, none of the well-documented sea-floor deposits, can be exploited profitably, but their study over the last two decades has provided valuable insights into the formation of ancient polymetallic (Fe-Cu-Zn±Pb±Ag) sulfide deposits in volcanic, sedimentary, and mixed volcanic-sedimentary environments.

The sea-floor spreading centers constitute an ideal setting for development of ore-forming systems because they satisfy all essential requirements for formation and preservation of massive sulfide deposits (Cathles et al. 1983; Scott 1985, 1997). These requirements include: (a) a fluid (dominantly seawater, possibly with some magmatic fluid) which can evolve into an ore-forming brine containing several ppm of dissolved metals by interaction with the thick pile of submarine basaltic rocks; (b) a heat source (a magma or its recently crystallized product) of sufficient size to cause large-scale convective circulation of this fluid through several kilometers of sea-floor rocks; (c) a fracture system that permits fluid circulation through the oceanic crust and focuses discharge onto the sea-floor; (d) a mechanism for precipitating sulfides from the fluid, such as boiling of the hydrothermal fluid or its mixing with cold ambient seawater; and (e) a sufficient influx of new volcanic or sedimentary material to bury the deposit and thus protect it from oxidation and erosion. The presence of a cap rock to act as both a thermal blanket and a physical barrier to diffuse upward flow should favor the formation of large deposits (Scott 1985), but probably is not a requirement (Cathles 1993).

Although the fundamental ore-forming process is similar in all sea-floor hot spring deposits, their metal concentrations, morphology, and size vary according to local conditions. One major factor is the lithology of material filling the rift axis because of its control in determining the characteristics of the circulating fluid. For example, the estimated composition of the fluid at the East Pacific Rise 21°N site (sediment-starved ridge crest) is quite different from that at the Guaymas Basin (sediment-filled ridge crest) (Fig 2.27). In a 'leaky' convection system, the sulfide deposition may be disseminated in subsea-floor rocks, whereas focused discharge of fluids onto the sea-floor is more likely to produce massive sulfide deposits. The mechanism of sulfide precipitation may also influence the distribution of the sulfides. Rapid precipitation due to fluid mixing on the sea-floor will result in *proximal* deposits near the discharge vents; boiling of the hydrothermal fluid in shallow marine environments may result in the discharge of a dense, bottom-seeking fluid and the formation of *distal* deposits at some distance from the hydrothermal vent. Available data suggest that the occurrence of hydrothermal sulfide deposits is more frequent at fast than at slow (half-rate <2 cm/year) spreading centers, but the potential for the accumulation of large hydrothermal deposits is greater at slow-spreading centers (Rona 1984). An excellent review of the geochemistry of the modern sea-floor hydrothermal deposits has been presented by Scott (1997).

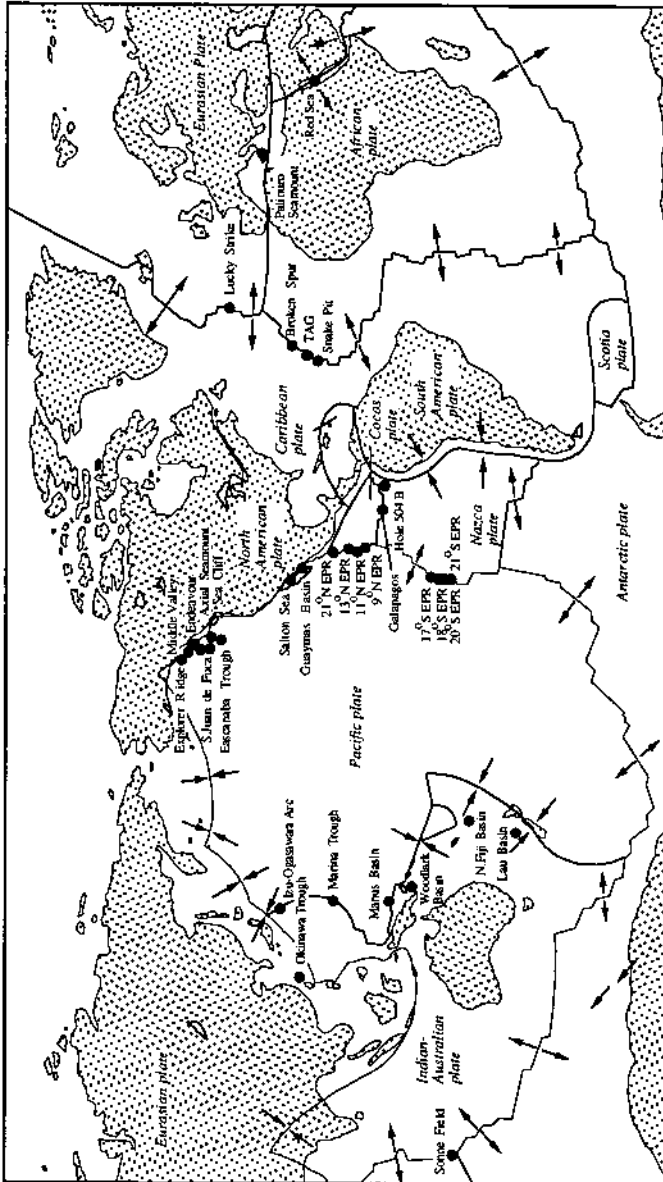


Figure 2.26. World map showing boundaries of lithospheric plates and locations of known sulfide-generating hydrothermal systems at the modern seafloor (data from Hertzog & Hannington 1995).

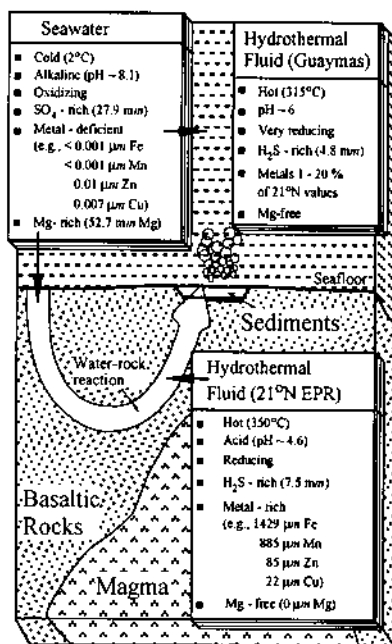


Figure 2.27. A comparison of fluid compositions at 21°N East Pacific Rise (sediment-starved ridge crest) and Guaymas Basin (heavily sedimented ridge crest) sulfide-forming hydrothermal systems (after Scott 1992). The hydrothermal fluid circulation model is the same in both cases, except that in the Guaymas Basin the upwelling fluid passes through 400 m of sediments, in addition to hot basaltic rocks, before discharge onto the sea-floor.

Oil-field Brines. Two illustrative examples of modern hydrothermal fluids in sedimentary terrains are the oil-field brines of central Mississippi, Gulf Coast, USA (Carpenter et al. 1974) and Alberta, Canada (Billings et al. 1969). The central Mississippi brines are exceptionally high in Pb (generally 10-80 mg/l) and Zn (average about 180 mg/l); they occur in Cretaceous marine sediments at depths of 2.4-4 km, where present temperatures are in the range of 100°-150°C. The Cl:Br and K:Br ratios of the brines suggest an origin from the evaporation of seawater past the point of halite deposition. According to Carpenter et al. (1974), the brines originated as connate water in the underlying Jurassic evaporites (the Lunon Formation), were expelled upward by compaction as the overlying sediments were deposited, and extracted Pb and Zn from Upper Jurassic shales during migration.

In northern Alberta, brine samples from the Devonian Presqu'île carbonate reef, which hosts the famous Pine Point Pb-Zn sulfide deposit (see Ch. 13), show present temperatures of 27°-119°C (average ≈76°C), comparable to fluid inclusion homogenization temperatures in the ore sphalerite, and contain fairly high concentrations of base metals— on the average (in mg/l), Zn - 19, Cu - 0.1, Fe - 0.5,

Mn - 5.9, and detectable (but not quantitatively determined) Pb. It appears that the source rocks for the brine were the shales of the Mackenzie Basin and that the Presqu'île reef was the conduit through which the fluid moved toward Pine Point, a scenario compatible with the formation of the Pine Point deposit from this fluid. The brines of the Western Canada Basin show a much lower concentration of zinc (≈ 1.0 mg/l), but it is estimated that the total amount of dissolved zinc in the brines is adequate to form several large zinc deposits (Billings et al. 1969). Modeling based on experimental data suggests that such oil field brines may evolve into ore-forming fluids appropriate for sediment-hosted Pb-Zn deposits by water-rock interactions in sandstone and carbonate aquifers (Sverjensky 1984), or for sediment-hosted Cu-rich deposits during migration through evaporite and red-bed sequences (Bartholomé et al. 1972, Sverjensky 1987).

2.8.2. ANCIENT HYDROTHERMAL DEPOSITS

Ancient mineral deposits formed by hydrothermal processes comprise a wide spectrum in terms of metal associations, host rocks, geologic settings, forms, sources of ore fluids, precipitation mechanisms, and controls of ore emplacement. Most hydrothermal deposits fall into one of the following broad groups (Table 2.7): (1) stratiform and strata-bound base metal sulfide deposits; (2) porphyry-type deposits associated with felsic intrusions; (3) skarn deposits, including carbonate-replacement deposits; (4) sediment-hosted disseminated deposits; and (5) vein deposits. The stratiform to strata-bound sulfide group is a mixed bag of stratigraphically controlled deposits. It includes: strata-bound, syngenetic-exhalative massive sulfide deposits hosted in volcanic rocks (VMS) and clastic sediments (SMS); stratiform, diagenetic Cu-rich deposits in redbed sequences (SSC); and carbonate- and sandstone-hosted, strata-bound, epigenetic Zn-Pb deposits commonly referred to as Mississippi Valley-type (MVT) deposits. Porphyry-type deposits refer to disseminated and stockwork mineralization spatially associated with and genetically related to felsic intrusions. The most important porphyry-type deposits are of copper, molybdenum, and tin, but similar low-grade deposits of other metals, such as uranium and gold, related to granitic intrusions may also be included in this group. Skarn deposits are also related to igneous intrusions, but their genesis involves contact metasomatism of favorable host rocks, most commonly limestones. High-temperature, carbonate-replacement deposits (Tittley 1993) without an obvious igneous connection probably are distal representatives of this group. These four classes of hydrothermal deposits are discussed in detail in later chapters.

The most convincing examples of hydrothermal deposits are epigenetic vein systems that are discordant to stratification or lithologic boundaries in host rocks and represent dominantly open-space filling of structurally controlled fractures and faults. Vein-type deposits comprise a highly variable group. Some vein-type deposits, such as tin and tungsten deposits with or without base metal sulfides, are believed to be genetically related to exposed or buried igneous, especially felsic, intrusions, because fluid inclusion and isotopic data provide evidence for a major contribution of magmatic water in the ore-forming fluids (e.g., vein-type tungsten deposits in China; Liu &

TABLE 2.7. Examples of mineral deposits formed by hydrothermal processes

Deposit type	Important examples	Source(s) of water
<i>1. Stratiform and strata-bound base metal sulfide deposits</i>		
(a) Volcanic-associated Cu-Zn±Pb massive sulfide (VMS) deposits (Ch. 10)	Noranda district, Canada; Bathurst district, Canada; Kuroko district, Japan; Sulfjelma district, Norway (see Table 10.1)	Ocean (± magmatic)
(b) Sediment-hosted Zn-Pb massive sulfide (SMS) deposits (Ch. 11)	Mt. Isa, Australia; Howard's Pass, Canada; Sullivan, Canada; Red Dog, USA; Aggeneys, South Africa; Rajpura-Dariba, India (see Table 11.1)	Connate (basinal brine)
(c) Sediment-hosted stratiform Cu (SSC) deposits (Ch. 12)	Zambian copper belt; Kupferschiefer, Germany-Poland; White Pine, USA (see Table 12.1)	Connate (basinal brine)
(d) Mississippi Valley-type Zn-Pb (MVT) deposits (Ch. 13)	Pine Point, Canada; Viburnum Trend, Missouri, USA; East and Central Tennessee districts, USA	Connate (basinal brine)
<i>2. Porphyry deposits associated with felsic intrusions</i>		
(a) Porphyry copper deposits (Ch. 8)	Valley Copper, Canada; Bingham, USA; Morenci, USA; Panguna, Papua New Guinea; Atlas, Philippines; El Salvador, Chile; Chuquibambilla, Chile (see Table 8.1)	Magmatic + meteoric
(b) Porphyry molybdenum deposits (Ch. 8)	Climax, USA; Questa, USA; Endako, Canada; El Creston, Mexico; Jin Dui Cheng, China (see Table 8.3)	Magmatic ± meteoric
(c) Porphyry tin deposits (Ch. 8)	Llallagua, Bolivia tin belt	Magmatic
<i>3. Contact metasomatic deposits associated with felsic intrusions</i>		
Skarn deposits (including carbonate-replacement deposits) (Ch. 9)	Carr Fork, Utah, USA (Cu); King Island, Tasmania, Australia (W); Moina, Tasmania, Australia (Sn); Little Boulder Creek, Montana, USA (Mo); Fortitude, Nevada, USA (Au); Blue Bell, British Columbia, Canada (Zn-Pb); Nalca, Chihuahua, Mexico (Zn-Pb); Darwin, California, USA (Ag-Pb-Zn); Providence, Zacatecas, Mexico (Ag-Pb-Zn-Cu); Tintic, Utah, USA (Ag-Pb-Zn-Au); Cerro de Pasco, Peru (Cu-Zn-Pb-Ag)	Magmatic ± meteoric
<i>4. Sediment-hosted disseminated deposits</i>		
(a) Carlin-type gold deposits (Ch. 16)	Carlin, Getchell, and Cortez trends, Nevada, USA	Multiple sources
(b) Sandstone-type uranium deposits (Ch. 14)	Colorado Plateau, Wyoming-South Dakota, and Texas Coastal Plain regions, USA	Meteoric

TABLE 2.7 (continued)

Deposit type	Important examples	Source(s) of water
<i>5. Vein deposits</i>		
(a) Epithermal Au-Ag deposits (Ch. 16)	Guanajuato, Mexico; Pachuca-Real Del Monte, Mexico; Tayolita, Durango, Mexico; Tonopah, Nevada, USA; Ladolam, Papua New Guinea (see Table 16.1)	Meteoric ± magmatic
(b) Archean lode gold deposits (Ch. 16)	Timmins district, Canada; Kalgoorlie district, Western Australia; Kolar district, India (see Table 16.5)	Various fluids at different crustal levels
(c) Granitoid-associated Sn, W, and Sb deposits	Cornwall, UK (Sn); Panasqueira, Portugal (W-Sn); Pasto Bueno, Peru (W-Cu-Pb-Ag), China (W, Sb)	Magmatic, meteoric
(d) Granitoid-associated Ag-base metal sulfide deposits	Cour d'Alene, USA (Ag-Pb-Zn); Creede, USA (Ag-Pb-Zn); Casapalca, Peru (Ag-Pb-Zn-Cu); Fresnillo, Zacatecas, Mexico (Ag-Zn-Pb-Cu-Au)	Magmatic, meteoric
(e) Granitoid-associated uranium deposits (Ch. 14)	Bois Noirs Limouza and Limousin, Massif Central, France	Meteoric
(f) Unconformity-type uranium deposits (Ch. 14)	Rabbit Lake and Key Lake, Saskatchewan, Canada; Alligator Rivers-Rum Jungle region, northern Australia	Connate ± meteoric
(g) Ag-sulfarsenide deposits	Cobalt-Gowganda, Ontario, Canada (Ag-Co-Ni); Great Bear Lake area, NWT, Canada (Ag-Co-Ni-Bi-U); Erzebirge district, Germany (Ag-Co-Ni-U)	Connate ± meteoric? magmatic?

Ma 1993). Ore fluids for other types of vein deposits may have been dominated by magmatic water (e.g., base metal vein deposits such as Casapalca, Peru), meteoric water (e.g., epithermal Au-Ag veins), or basinal brines (e.g., silver-sulfarsenide veins of the Cobalt-Gowganda district, Canada). Some vein-type deposits are discussed in later chapters; a few examples are briefly described below.

Casapalca Ag-Pb-Zn-Cu Vein Deposit, Peru

The Casapalca vein deposit (Rye & Sawkins 1974, Wu & Peterson 1977), located on the west flank of the Central Andes of Peru, is hosted by early Tertiary volcanic rocks and redbeds, which are unconformably underlain by Cretaceous limestone. Guilbert and Park (1986) cited this deposit as a typical example of "Cordilleran vein type deposits" formed by ascending hydrothermal fluids of magmatic or meteoric origin, but which they considered to be related to adjacent igneous activity. Dioritic or syenitic intrusions

are present in the Casapalca area and at least one of the major intrusions is cut by the Casapalca vein system, but none of the intrusions is apparently related directly to the Casapalca mineralization (Wu & Petersen 1977). The igneous connection for this deposit, as discussed below, is inferred largely from isotopic data.

The Casapalca vein system corresponds to a group of steeply dipping, pre-mineralization, tectonic fractures with a general northeast strike (Fig. 2.28). The fracture system is mineralized over a horizontal distance of 5 km and a known vertical interval of 2,000 m. Individual veins are mostly narrow and only in a few instances exceed 1 m in width. Most veins are tightly filled, but some are quite vuggy, locally. The average grade of the mined ore is about 2% Pb, 3% Zn, 0.3% Cu, and 0.03% Ag, but much higher values are common in single assays (Guilbert & Park 1986).

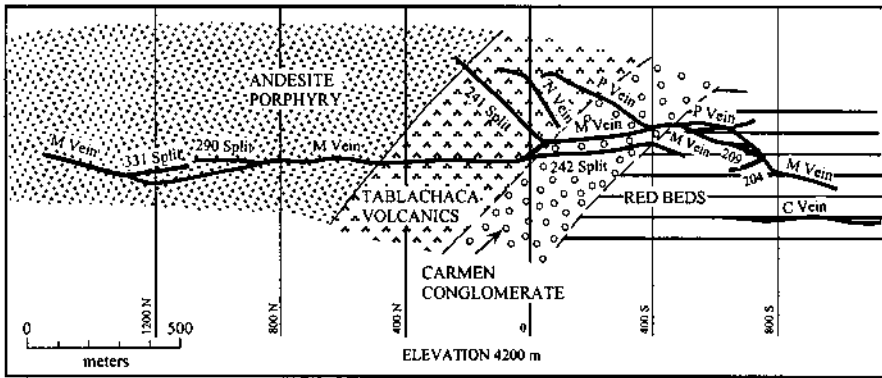


Figure 2.28. 1,700-level plan of the Casapalca vein system, central Andes, Peru (after Rye & Sawkins 1974).

Wu and Peterson (1977) identified four stages of mineralization which, from the oldest to the youngest, are characterized by the following assemblages: Stage I, sphalerite-galena-pyrite; Stage II, chalcopryrite-pyrite-sphalerite; Stage III, tetrahedrite; and Stage IV, quartz-carbonates (essentially barren of ore minerals). Fluid inclusion studies (Rye & Sawkins 1974) have established that the temperature decreased progressively from $\approx 370^\circ$ to $\approx 280^\circ\text{C}$ and the fluid salinity ranged erratically between 4 and 40 wt% NaCl equivalent during the ore deposition. The fact that mineral assemblages of different major veins can be correlated suggests a single episode of sulfide-sulfosalt mineralization over the entire vein system. Moreover, Wu and Petersen (1977) have shown that tetrahedrite, the main source of silver, varies from an Ag-poor, As-rich composition in the central part of the vein system, which is probably close to the center of the hydrothermal system at Casapalca, to an Ag-rich, Sb-rich composition in the outer part. This zoning pattern is compatible with the observed decrease in the extent of wallrock alteration from the central part outward.

Fluid inclusion data and stable isotope ratios (sulfur, oxygen, hydrogen) discussed by Rye and Sawkins (1974) indicate that hydrothermal fluids for the sulfide-sulfosalt stage of mineralization were derived from a deep-seated felsic intrusion (of Tertiary age), but the post-ore calcite deposition was dominated by the incursion of meteoric waters and components derived from upper crustal sources.

Panasqueira W-Sn Vein Deposit, Portugal

The Panasqueira W-Sn deposit, located in the Beira Baxia province of central Portugal, is the largest quartz-vein type deposit of the Iberian peninsula and one of the world's largest wolframite producers. The salient features of the deposit summarized below have been extracted largely from Kelly and Rye (1979) and Poyla (1989).

The deposit is hosted by the Cambrian to late Precambrian Beira Schist, a complexly deformed series of marine pelitic and semi-pelitic sediments, which have been metamorphosed to low greenschist facies assemblages during early compressive stages of the Hercynian orogeny. The ore zone, about 100 to 200 m thick, consists of more than a thousand, predominantly subhorizontal, wolframite-bearing quartz veins that cut across the steep bedding and foliation of the host rocks. Individual veins range from a few millimeters to more than a meter in thickness and extend laterally for tens of meters; thicker veins tend to be more persistent and some of them can be traced laterally for up to 100 m or more with a fairly uniform thickness. The ore zone intersects a greisenized granite cupola (Fig. 2.29), which is exposed only in the underground workings. The cupola is believed to be underlain by a multiply-intrusive, Hercynian (≈ 300 Ma) granitoid body, referred to as the Panasqueira Granite, a porphyritic muscovite-biotite granite with microcline phenocrysts. An unusual lensoid mass of quartz, called the "silica cap", occurs at the apex of the cupola (Fig. 2.29). Kelly and Rye (1979) interpreted the silica cap as a hydrothermal filling of an open chamber formed by slight contraction or withdrawal of the granite melt. Around the Panasqueira deposit, the Beira Schist is intensely contact metamorphosed to cordierite-bearing hornfels. The orebody has not been affected significantly by post-Permian deformation and metamorphism.

Quartz comprises more than 90% of the vein material and the rest is composed of variable amounts of a variety of ore and gangue minerals. The main ore minerals of the veins, in decreasing order of abundance, are wolframite, cassiterite, and chalcocopyrite. Textures of vein material, including unusually large-size crystals, indicate mineralization by open-space filling. According to Kelly and Rye (1979), the open space was the result of dilation of pre-ore joints due to hydraulic pressures exerted by the earliest pulses of ore fluids. The mineralization history is complex, but four distinct depositional stages, indicating changing ore-fluid characteristics, were recognized by Kelly and Rye (1979): (a) oxide-silicate stage, marked by the precipitation of all of the wolframite, cassiterite, and almost all of the quartz, silicate gangue (muscovite, tourmaline), and arsenopyrite; (b) main sulfide stage, characterized by time-overlapping deposition of pyrite, pyrrhotite, chalcocopyrite, sphalerite, minor stannite, and rare galena; (c) pyrrhotite alteration stage, identified by fine-grained

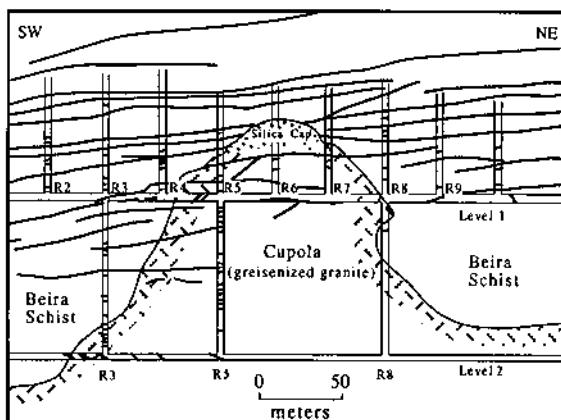


Figure 2.29. Cross section of the Panasqueira cupola showing the silica cap, subhorizontal vein system, and flat stopes (after Kelly & Rye 1979).

intergrowth of pyrite and marcasite, and coarse-grained siderite; and (d) later carbonate stage, dominated by calcite, dolomite, and chlorite that form crusts on minerals of the preceding stages.

Despite a vast amount of fluid inclusion and isotopic data (Kelly and Rye 1979), the genesis of the Panasqueira mineralization is not fully resolved. Fluids for the oxide-silicate, main sulfide, and pyrrhotite alteration stages were NaCl-dominated brines, with salinities in the range of 5 to 10 wt% NaCl equivalent and temperatures in the range of 230° to 360°C. Oxygen and hydrogen isotope ratios indicate extensive equilibration with the Beira Schist and/or granitic host rocks. Sulfur isotope ratios of sulfides from these earlier depositional stages are compatible with a magmatic source of sulfur. However, the fluid inclusion data and the open space-filling type of deposition in large subhorizontal veins indicate very shallow depths of mineralization (600 to 1,300 m below the groundwater table existing during mineralization) and, thus, the likely involvement of meteoric water. If the mixing of magmatic and meteoric waters was involved in the Panasqueira mineralization, a lack of inverse correlation between fluid salinity and temperature and the uniformity of oxygen isotope ratios would suggest that the mixing occurred outside the vein system, probably at depth, and therefore could not have been the cause of W-Sn deposition in the veins. Higgins (1985) attributed wolframite deposition in the Grey River prospect, Newfoundland (Canada) to progressive CO₂ loss from the hydrothermal fluid by immiscibility and retrograde boiling; a similar mechanism might have been responsible for W-Sn deposition at Panasqueira. The relatively low-salinity (<5 wt% NaCl equivalent) and low-temperature (120°C or less) fluids for the late carbonate stage was dominated by meteoric waters, which derived sulfur and carbon from a shallow heterogeneous source, probably the Beira Schist (Kelly and Rye 1979). A significant meteoric input to the

hydrothermal fluids has also been identified in some other tungsten vein deposits in Peru, such as Pasto Bueno (Landis & Rye 1974) and San Cristobal (Campbell et al. 1984). On the other hand, Poyla (1989) proposed that the water in the Panasqueira ore fluids was dominantly meteoric, although the major source of the metals (W, Sn, Cu, Zn, As) was probably the subjacent granite bodies. For estimated concentrations of W and Sn around 0.2 ppm and 5 ppm, respectively, in a typical Panasqueira ore fluid, the total mass of hydrothermally induced tungsten and tin in and around the deposit would require an ore-forming fluid flux of at least several hundred km³. Such large fluid fluxes, he argued, would be difficult to achieve through the single-pass release of magmatic or metamorphic fluids. At the other extreme, ore fluids for the Chicote tungsten vein deposit of the Bolivian tin belt appears to have been entirely of magmatic source (Thorn 1988).

Native Silver-Sulfarsenide Vein Deposits, Cobalt-Gowganda District, Canada

Vein deposits of native silver, characteristically associated with an array of arsenides and sulfarsenides of Co, Ni, Sb, and Fe, and carbonate-dominated gangue (mainly calcite and dolomite, less commonly siderite and ankerite), are not very common, but they are scattered throughout the world and exhibit a remarkable consistency of mineralogy and textures despite considerable variation in host lithology (Badham 1976, Kissin 1992). The most famous and thoroughly studied examples of this deposit type, sometimes referred to as the five-element (Ni-Co-As-Ag-Bi) ore type, occur in the Precambrian Cobalt-Gowganda district of northeastern Ontario, Canada (Berry 1971, Andrews et al. 1986, Kerrich et al. 1986, Marshall et al. 1993), which by 1984 had yielded nearly one-half billion ounces of silver. Other important examples of this deposit type include: Thunder Bay Island Group and the Great Bear Lake area (Echo Bay and Camsell River districts), Canada; Erzebirge district, Germany; Jachymov (Joachimsthal), Czechoslovakia; and the Paleozoic deposits of Kongsberg-Modum district, Norway. Some of these deposits (Echo Bay, Jachymov, Erzebirge) contain significant amounts of uranium as pitchblende, but others (Cobalt, Thunder Bay, Kongsberg-Modum) have very little or no uranium. A succinct review of this deposit type has been presented by Kissin (1992).

The vein deposits of the Cobalt-Gowganda area occur along the north and northeastern margin of the Cobalt Embayment (Fig. 2.30). The embayment comprises mainly clastic sediments of the Huronian Supergroup (Aphebian age) that unconformably overlies the basement composed of Keewatin volcanic rocks of Archean age. The basement and all formations of the Huronian sequence are intruded by a complex of mafic dikes and sills of olivine tholeiite composition, known collectively as the Nipissing Diabase. Mineralization occurs in vertical to steeply dipping veins and nested vein systems hosted by Archean volcanic basement rocks, in Huronian sediments (Coleman Member of the Lower Gowganda Formation) below the Nipissing Diabase and in Nipissing Diabase sills. No deposits are known to occur in the Huronian sediments above the Nipissing Diabase. All the economically productive deposits occur in close proximity to the Archean-Huronian unconformity (Fig. 2.30).

U-Pb ages of the Nipissing Diabase and the vein mineralization are very similar, 2217.5 ± 1.6 Ma for the Diabase based on primary baddeleyite and 2217.0 ± 6 Ma for the mineralization based on secondary rutile.

The ore veins may be over 300 m long and 100 m deep, with widths varying from a few millimeters to more than 30 cm, but the mineralization is typically discontinuous along any given vein structure and occurs in the form of massive pods, bands, zoned rosettes, dendrites, plates, and leaves. The mineralization is characteristically of the cavity-filling type and the veins are commonly completely filled with hydrothermally deposited minerals of the Fe-Co-Ni-Ag-As-S system. Some 40 opaque minerals have been identified in the district (Petruk 1971). These include, apart from the common sulfides (e.g., pyrite, chalcopyrite, galena), a host of native metals (silver, bismuth, silver alloys with Sb and Hg), arsenides and sulfarsenides (arsenopyrite, cobaltite, gersdorffite, loellingite, maucherite, niccolite, rammelsbergite, parammelsbergite, safflorite, skutterudite), antimonides and sulfantimonies (breithauptite, dyscrasite, ullmanite), and sulfosalts (polybasite, proustite-pyrargyrite, tetrahedrite). Details of the ore and gangue mineralogy and textures have been discussed by Petruk (1971) and Jambor (1971a). High-grade pockets commonly are localized in the vicinity of vein intersections, lithological contacts, and abrupt changes in the configuration of the

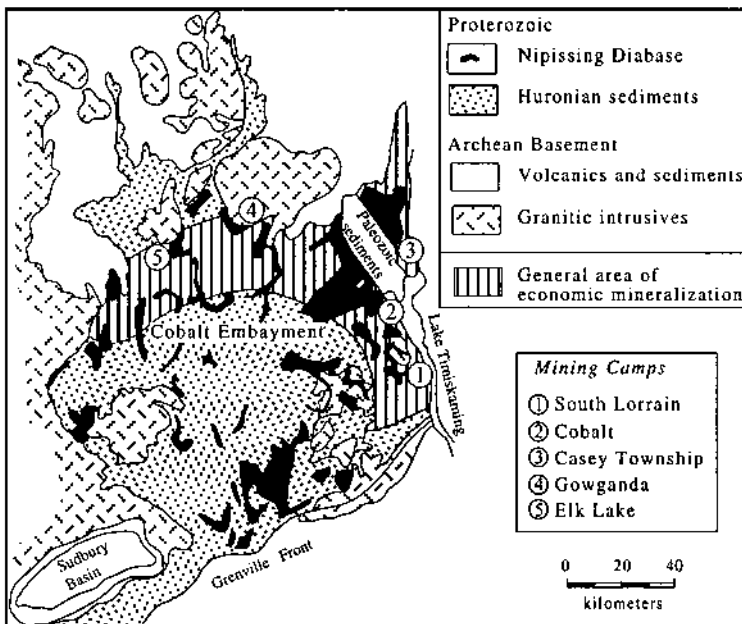


Figure 2.30. Simplified geology of the Cobalt Embayment, Ontario, Canada, illustrating the general area of economic silver-sulfarsenide vein deposits and the mining camps (after Andrews et al. 1986).

Archean basement topography. The district also contains a set of subhorizontal veins, but these generally lack silver and sulfarsenide mineralization, except in the immediate vicinity of intersections with steeply-dipping ore-bearing structures, and are dominated by silicate minerals (in contrast to the carbonate gangue of the ore-bearing veins). Both types of veins are directly or indirectly associated with faults or shear zones.

The limited extent of wallrock alteration coupled with the results of the mass-balance calculations indicate that the process of mineralization involved the introduction of hydrothermal fluids from a source external to the immediate environment of ore deposition (Andrews et al. 1986). Noting a coincidence among ore veins, vein-bearing faults, and structures containing remobilized and replacement sulfides, Smyk and Watkinson (1990) proposed that sulfides were remobilized from Archean basement rocks into Proterozoic vein-bearing structures, presumably during a tectonic event that predated or accompanied the development of the veins. Fluid inclusion studies, however, indicate that the hydrothermal fluids were highly saline NaCl-CaCl₂ brines, with up to 54 wt% NaCl equivalent and highly variable Na:Ca ratios. Oxygen and hydrogen isotope ratios of silicate gangue minerals are compatible with the derivation of the fluids from Huronian aquifers and Proterozoic meteoric water recharge of the sedimentary basin (Kerrick et al. 1986). Kerrich et al. (1986) suggested CO₂ effervescence and aqueous boiling as the cause of ore and gangue precipitation, but according to Marshall et al. (1993), ore precipitation occurred because of the mixing of a highly saline, Ag-bearing fluid with a genetically unrelated, weakly saline fluid.

The role of the Nipissing Diabase in the formation of the silver-sulfarsenide deposits is not clear. There is no evidence that the diabase magma served as a significant fluid source, but it may have provided the heat source and structural permeability for the circulation of formation brines which, in turn, extracted the metals from the volcanic and sedimentary rocks of the region (Andrews et al. 1986, Kerrich et al. 1986). If this interpretation is correct, then the Cobalt-Gowganda district may be anomalous in the sense that most deposits of the silver-sulfarsenide association appear to be related to magmatic activity in continental-margin orogens (Badham 1976).

2.9. Summary

A mineral deposit is a rock body containing significantly higher concentration of one or more elements (or minerals) of economic interest compared with average crustal abundances. The required concentration factor, which may be defined as the ratio of the average concentration of an element in a mineable mineral deposit to its average crustal abundance, is highly variable and depends not only on the particular element but also on the type of deposit. The various geologic processes that may create a set of favorable conditions to produce this enrichment may be grouped into four end-member categories: orthomagmatic, sedimentary, metamorphic, and hydrothermal (Table 2.8).

Orthomagmatic deposits are direct products of magmatic crystallization, which is

TABLE 2.8. Formation of mineral deposits — a summary

	Orthomagmatic	Sedimentary	Metamorphic	Hydrothermal
<i>Process</i>	Magmatic crystallization	Weathering and sedimentary accumulation	Metamorphic reactions and remobilization	Precipitation from ascending or convecting hot, aqueous solutions from various sources
<i>Source(s) of ore constituents</i>	Magma (\pm country rocks)	Surface rocks and water	Rocks being metamorphosed	Magmas and subsurface rocks
<i>Transport of ore constituents</i>	Dissolved ionic species	Dissolved ionic species, detrital particles	Diffusion, flow	Dissolved ionic species
<i>Deposition mechanism</i>	Crystallization	Mechanical accumulation and chemical precipitation	Metamorphic and metasomatic recrystallization	Chemical precipitation -- cavity filling and replacement
<i>Concentration mechanism</i>	Liquid immiscibility, crystal settling, filter pressing	Leaching, supergene enrichment, sedimentation	Metamorphic reconstitution, partial melting	Focused discharge of metal-enriched fluids
<i>Ore localization</i>	Igneous bodies	Sedimentary beds	Favorable host rocks, structures	Volcanic centers, contact aureoles, seafloor, favorable host rocks, structures, breccias
<i>Examples of deposit types</i>	Chromite, Ni-sulfide, carbonatite	Iron-formations, bedded manganese, placers, phosphorite, Ni-laterite	Graphite, sillimanite	Vein deposits, porphyry Cu-Mo, ore skarns, volcanic- or sediment-associated massive sulfides, sediment-hosted disseminated deposits

dominated by silicate melt-crystal equilibria. The magmas provide practically all of the ore constituents; in some cases part or most of the sulfur appears to have been assimilated from the country rocks. Ore constituents are concentrated in some of the crystallization products through sulfide liquid immiscibility and segregation, gravitative settling of early formed crystals, or filter pressing of the residual liquid (+ crystals) after partial crystallization. Essential evidence for an orthomagmatic origin of a deposit type is a consistent spatial and temporal association with a particular suite of igneous rocks that can be rationalized on the basis of magmatic crystallization. Typical examples of this group of deposits are chromite deposits in layered intrusions and ophiolites, carbonatites, and titanium deposits hosted by anorthosites. Diamonds are

consistently associated with kimberlites, but are interpreted to have been picked up from the mantle rather than crystallized from parental kimberlite magmas.

Chemical weathering and sedimentation are the main sedimentary processes capable of generating mineral deposits. Chemical weathering may lead to residual concentration of relatively less mobile elements (e.g., bauxite, lateritic nickel, and clay deposits) or to supergene enrichment of sulfide deposits (especially of copper). Clastic sedimentation of weathering-resistant minerals (e.g., uraninite, cassiterite, diamond, gold) produce placer deposits. Sedimentary deposits, such as those of manganese, iron, phosphorite, and silica, involve chemical-biochemical precipitation of ore constituents from aqueous solutions.

The most common examples of metamorphic deposits — deposits formed by recrystallization, reconstitution, and mobilization during and as a direct consequence of metamorphism (and deformation) — are those of graphite, garnet, asbestos, talc, corundum, Al_2SiO_5 polymorphs (andalusite, kyanite, sillimanite), and gemstones. Mineralization related to fluids evolved by devolatilization reactions during metamorphism is considered hydrothermal.

Hydrothermal deposits encompass a large spectrum of deposit types that form by precipitation of ore constituents from hot, aqueous fluids of variable composition and source in a variety of subsurface geologic environments. The water of hydrothermal fluids may be meteoric, connate, metamorphic, or magmatic, but often is a mixture from more than one source. The potential sources of ore constituents include magmas (in the case of magmatic fluids) and crustal rocks along the flow paths of the mineralizing fluids. In many cases, it is possible to infer the source(s) of sulfur from sulfur isotopic ratios of sulfide and sulfate minerals, but it is usually very difficult to determine the exact source(s) of the metals. Ore metals are transported in hydrothermal fluids mostly as chloride or bisulfide complexes, depending on temperature, pH, $f\text{O}_2$, and activities of chloride and sulfur in the fluids; the role of organic complexes is limited by the low concentrations of organic acids in hydrothermal fluids. The precipitation of ore constituents at depositional sites are caused by changes in temperature, boiling, interaction with wallrock, and fluid mixing. The actual patterns of fluid circulation through the rocks are too complex in detail, but generalized models may be grouped under six broad categories: convection at submarine rift environments; flow systems driven by the heat of igneous intrusions; compaction-driven or gravity-driven flow of (sedimentary) basinal fluids; deep crustal convection of seawater; focused flow of metamorphic water along shear zones; and fluid flow caused by tectonic squeezing. In recent years, much has been learned about the formation of several types of mineral deposits from extensive studies of active continental and submarine hydrothermal systems, which are believed to represent modern analogs of ancient ore-producing hydrothermal systems. Structurally controlled, discordant vein deposits provide the most convincing examples of epigenetic hydrothermal deposits. Other examples of hydrothermal deposits include stratiform and strata-bound base metal sulfide deposits, porphyry-type deposits associated with felsic intrusions, skarn deposits, and sediment-hosted disseminated deposits (see Table 2.7).

2.10. Recommended Reading

Orthomagmatic: Krauskopf (1967a), Burnham and Ohmoto (1980), Mitchell (1986).

Sedimentary: Meillon (1978), Blain and Andrew (1977), Roy (1992), Frakes and Bolton (1992).

Metamorphic: Walther and Orville (1982), Skinner and Johnson (1987).

Hydrothermal: Skinner (1979), White (1981), McKibben et al. (1988), Scott (1997)

CHAPTER 3

INTERPRETATION OF MINERAL DEPOSITS - I

3.1. Introduction

A comprehensive study of a mineral deposit comprises three essential steps:

- (a) Data Collection
 - (i) Field relations
 - Local and regional geology
 - Nature and distribution of mineralization
 - Sampling appropriate to the objective(s) of the study
 - (ii) Laboratory analyses
 - Petrography (mineralogy and textures)
 - Bulk and phase chemistry (major and trace elements)
 - Isotope ratios
 - Fluid inclusions
- (b) Data reduction and presentation
 - Maps and sections
 - Plots of laboratory data
 - Statistical analysis
- (c) Interpretation
 - Controls of ore mineralization
 - Mode of formation (magmatic crystallization, precipitation, etc.)
 - Conditions of formation (pressure, temperature, fO_2 , fS_2 , etc.)
 - Post-emplacement history (metamorphism, deformation, alteration)
 - Spatial and temporal relationship to similar deposits
 - Relationship to crustal evolution (metallogenesis)

A mineral deposit can be studied with one or more of the following objectives: evaluation of its resource potential and possible exploitation, characterization, and understanding of its genesis. The genesis of a deposit, however, is not merely an academic exercise; it may result in data and concepts applicable to exploration for similar deposits in adjacent and other areas. In fact, most exploration strategies in operation are based on some conceptual model of ore genesis, ideally tied to regional crustal evolution through geologic time.

The basic considerations in the interpretation of a mineral deposit are summarized in Table 3.1. The choice of techniques in a given study is dictated by the type of deposit, the aspects being stressed, and the resources available. However, the need for a multi-directional approach in all cases cannot be over-emphasized.

TABLE 3.1. Basic considerations for interpretation of mineral deposits

Geologic setting
Ore-gangue minerals
Ore-gangue textures
Stability of ore-gangue assemblages
Hydrothermal alteration
Zoning
Fluid inclusions
Trace element distribution
Stable isotope ratios
Radiogenic isotope ratios
Geothermometry and geobarometry
Metamorphism
Age of mineralization

3.2. Geologic Setting

The interpretation of a mineral deposit obviously requires a detailed study of the deposit and its host rocks in terms of petrology, geochemistry, distribution of mineralization in relation to stratigraphy, rock types and structural elements, alteration and metamorphism, and the timing of mineralization. It is also important to realize that a mineral deposit is merely a manifestation of special conditions that existed in the course of the overall geologic evolution of the area. Moreover, mineral deposits tend to occur in clusters or along discernible trends controlled by the regional and local geologic framework. Thus, a thorough understanding of the regional and local geologic setting is a pre-requisite to the proper interpretation of a mineral deposit. This includes, in broad terms, the stratigraphy and structure of the rocks, their age and environments of deposition, the distribution of igneous activity in time and space, and the tectonic evolution of the formations of interest.

3.3. Ore Minerals

One of the first steps in the study of a mineral deposit is the identification of its ore and gangue minerals. Many of the common minerals can be identified in hand specimens, but it is a good practice to check their identification by more sophisticated methods in the laboratory. The laboratory methods for identification and characterization of ore minerals are similar to those employed for rock-forming minerals and are based on an

appropriate combination of (a) physical properties (color, hardness, etc.), (b) optical properties, (c) crystal structure (as revealed in powder or single-crystal diffraction patterns), and (d) chemical composition. Reflected-light microscopy is by far the most widely used technique for a detailed petrographic study of ore minerals, and there are many excellent textbooks that may be used for this purpose (e.g., Cameron 1961, Uytendogardt & Burke 1971, Ramdohr 1980, Craig & Vaughan 1994).

A classification scheme for ore minerals, comparable to the structural classification of silicate minerals, is yet to be established. Some workers (e.g., Ross 1957, Zoltai 1974) have tried to systematize sulfide structures on the basis of close-packed sheets of spheres, but many common sulfide minerals cannot be accommodated in such schemes. Most of the important ore minerals, however, can be ordered into a relatively small number of groups (Stanton 1972), as presented in Table 3.2, although this table is not intended to provide a comprehensive listing of the important ore minerals. The chemical compositions of minerals seldom match their ideal chemical formulae given in Table 3.2. Most sulfide, sulfosalt, and oxide minerals are solid solutions, a property that is potentially useful in geothermometry and geobarometry (see Ch. 4). Unfortunately, the optical properties of opaque minerals are not yet adequately calibrated for the determination of their chemical compositions. Chemical compositions of individual opaque minerals are commonly determined by electron microprobe analysis; line spacings in X-ray powder diffraction patterns also provide satisfactory results in some cases.

3.4. Ore-Gangue Textures

The *texture* (or microstructure, according to some authors) of a mineral assemblage includes three important geometric aspects of the minerals — their sizes, shapes, and mutual arrangement. The term ore texture is used here in a broad sense to include the textures of ore and gangue minerals in the ore material as well as in the poorly mineralized and barren rocks associated with a mineral deposit. The focus here, of course, is on ore minerals, especially sulfides, which constitute the bulk of the ore minerals of interest. Ore-microscopic study of a mineral deposit routinely includes the identification of opaque minerals as well as the characterization of their textures. Examination of doubly polished thin sections with both reflected and transmitted light is recommended. A complementary technique for studying textures of ore-gangue assemblages is cathodoluminescent petrography using a luminoscope. This technique is particularly useful for observing zoning in minerals, grain boundary relationships, and relict fabrics (Kopp 1981). The information obtained from a systematic study of ore textures is valuable not only for the interpretation of ore genesis but also for ore beneficiation (Hagni 1978, Ramdohr 1980, Craig & Vaughan 1994).

TABLE 3.2. Important ore minerals (after Ross 1957 and Stanton 1972)

NATIVE METALS AND ALLOYS					
<i>Gold Group</i>		<i>Platinum Group</i>		<i>Arsenic Group</i>	
Gold	Au	Platinum	Pt	Arsenic	As
Silver	Ag	Palladium	Pd	Antimony	Sb
Copper	Cu	Osmium	Os	Bismuth	Bi
				Alieumontite	AsSb
SULFIDES AND ARSENIDES (INCLUDING SULFOSALTS, SULFARSENIDES, ETC.)					
A. M_2X type					
<i>Argentite Group</i>		<i>Chalcocite Group</i>			
Argentite	Ag_2S	Chalcocite	Cu_2S		
Hessite	Ag_2Te	Stromeyerite	$CuAgS$		
Digenite	$Cu_{2-x}S$	Rickardite	Cu_2Te		
Petzite	Ag_3AuTe_2				
B. MX type					
<i>Galena Group</i>		<i>Sphalerite Group</i>		<i>Wurtzite Group</i>	
Galena	PbS	Sphalerite	ZnS	Wurtzite	ZnS
Altaite	PbTe	Metacinnabar	HgS	Greenockite	CdS
Albandite	MnS	Coloradoite	HgTe	Cubanite	$CuFe_2S_3$
Oldhamite	CaS	Chalcopyrite	$CuFeS_2$	Sternbergite	$AgFe_2S_3$
Clausthalite	PbSe	Stannite	Cu_2FeSnS_4	Emplectite	$CuBiS_2$
Matildite	$AgBiS_2$	Tetrahedrite	$Cu_{12}Sb_4S_{13}$	Chalcostibite	$CuSbS_2$
		Tennantite	$Cu_{12}As_4S_{13}$		
		Famatinite	Cu_3SbS_4		
		Enargite	Cu_3AsS_4		
<i>Niccolite Group</i>				<i>Covellite Group</i>	
Niccolite	NiAs			Covellite	CuS
Breithauptite	NiSb			Klockmanite	CuSe
Pyrrhotite	$Fe_{1-x}S$				
C. M_3X_4 (Spinel) type					
Linnaeite	Co_3S_4	Carrolite	Co_2CuS_4	Pentlandite	$(Fe,Ni)_9S_8$
Siegenite	$(Co,Ni)_3S_4$	Violarite	Ni_2FeS_4	Livingstonite	$HgS \cdot 2Sb_2S_3$
Greigite	Fe_3S_4	Polydymite	Ni_3S_4		
D. M_2X_3 type (Tetradymite Group)					
Tetradymite	Bi_2Te_2S	Tellurobismutite	Bi_2Te_3	Joseite	$Bi_{4-x}(Se,Te,S)_{3-x}$
Stibnite	Sb_2S_3	Bismuthinite	Bi_2S_3	Berthierite	$FeS \cdot Sb_2S_3$
E. MX_2 type					
<i>Pyrite Group</i>		<i>Marcasite Group</i>		<i>Krennerite Group</i>	
Pyrite	FeS_2	Marcasite	FeS_2	Krennerite	$(Ag,Au)Te_2$
Cattierite	CoS_2	Loellingite	$FeAs_2$	Calaverite	$AuTe_2$
Vaesite	NiS_2	Safflorite	$CoAs_2$	Sylvanite	$(Au,Ag)Te_2$
Sperryllite	$PtAs_2$	Rammelsbergite	$NiAs_2$		
Hauerite	MnS_2	Arsenopyrite	$FeAsS$	<i>Molybdenite Group</i>	
Bravoite	$(Ni,Fe)S_2$	Glaucodot	$(Fe,Co)AsS$	Molybdenite	MoS_2
Cobalite	$CoAsS$	Gudmundite	$FeSbS$	Tungstenite	WS_2
Gersdorffite	$NiAsS$				
Ullmanite	$NiSbS$				
Costibite	$CoSbS$				
Willyamite	$(Ni,Co)SbS$				

TABLE 3.2 (continued)

F. MX₃ type (Skutterudite Group)

Skutterudite (Fe,Co,Ni)As_{3-x}

OXIDES

A. MO type (Zincite Group)

Zincite	ZnO	Tenorite	CuO	Montroydite	HgO
Litharge	PbO				

B. MM₂O₄ type (Spinel Group)

	<i>Spinel Series</i>		<i>Magnetite Series</i>		<i>Chromite Series</i>
Hercynite	FeO.Al ₂ O ₃	Magnetite	FeO.Fe ₂ O ₃	Chromite	FeO.Cr ₂ O ₃
Spinel	MgO.Al ₂ O ₃	Magnesioferrite	MgO.Fe ₂ O ₃	Magnesiochromite	MgO.Cr ₂ O ₃
Gahnite	ZnO.Al ₂ O ₃	Franklinite	ZnO.Fe ₂ O ₃		
Galaxite	MnO.Al ₂ O ₃	Jacobsite	MnO.Fe ₂ O ₃		

C. M₂O₃ type (Hematite Group)

Hematite	Fe ₂ O ₃
Ilmenite	FeTiO ₃
Corrundum	Al ₂ O ₃
Pyrophanite	MnTiO ₃
Geikielite	MgTiO ₃

D. MO₂ type

	<i>Rutile Group</i>		<i>Uraninite Group</i>
Rutile	TiO ₂	Uraninite	UO ₂
Pyrolusite	MnO ₂	Thorianite	ThO ₂
Cassiterite	SnO ₂	Cerianite	CeO ₂

3.4.1. PRINCIPLES

The formation of a mineral assemblage, either by precipitation from a fluid or magma or by solid-state transformation, is an attempt to minimize the free energy of the system under prevailing conditions of temperature and pressure. The texture of the assemblage during its growth and subsequent evolution is largely governed by processes that tend to minimize the total free energy of the system by minimizing the *surface or interfacial free energy* (γ) associated with the crystal surfaces or interfaces in the system. (The other important constraint is the available space to be filled by the minerals.) For a liquid (liquid-vapor interface), the surface free energy (γ), defined as the free energy per unit area of surface, is numerically equal to the surface tension (σ) but the two have different dimensions (ergs/cm² for γ , dynes/cm for σ). In the case of solids (solid-fluid interfaces), the surface energy is not numerically equal to the surface tension (although it is often assumed to be so, as an approximation), and an added complexity is often introduced by the anisotropy of crystals. The analog of surface free energy in polycrystalline aggregates is called the interfacial free energy, which is the

free energy per unit area associated with a solid-solid interface. The interfacial energy (γ) depends not only on the anisotropy of the two crystals but also on the degree of crystallographic coherence at the interface.

The reduction of surface or interfacial energy can be achieved by (a) decreasing the total surface or interface area for a given volume, and (b) substituting parts of the surface or interface characterized by higher free energy by a corresponding area of surface or interface characterized by lower free energy. The former may be accomplished, for example, by forming larger grains at the expense of smaller ones, and the latter by forming lower energy contacts (such as boundaries of high degree coherency, low-energy contact and penetrative twins, and intergrowths) and segregation of impurities to the contact zones. From the point of view of thermodynamics, some or all of these processes should continue to operate until the surface or interfacial energy of a system is reduced to the minimum possible; the kinetics of the processes, however, are controlled by atomic mobility and, hence, to a large extent by the temperature of equilibration.

Consider the simplest case, the growth of an isotropic crystal in a fluid medium. If change of area is the only factor influencing surface free energy, to achieve minimum surface energy the crystal should assume a spherical shape, because a sphere has the lowest surface area per unit volume. The 'grape shot' chromite ore, consisting of rounded single crystals of chromite as disseminations in ultramafic rocks, is an example of such a texture (Stanton 1972). The development of a curved surface, however, may yield a large number of atoms in corner or edge positions, in which case a planar surface of larger area may be energetically more favorable. In reality, the textures of minerals formed in a 'free growth' or 'open space' environment are controlled by many factors such as mechanisms of nucleation and crystal growth, anisotropy of crystals, presence of impurities, and concentration gradients (Stanton 1972).

The importance of interfacial energy in controlling the grain boundary relationships in polycrystalline aggregates has long been recognized by physical metallurgists and applied successfully to the interpretation of textures in annealed metal alloys (Smith 1964). The same principles have also been applied to the interpretation of textures in annealed silicate assemblages (Kretz 1966, Vernon 1968) and sulfide assemblages (Stanton 1964). From a textural point of view, the most useful feature of such polycrystalline aggregates is that the majority of the grains meet in threes along lines (meeting of four or more grains at a point is possible but infrequent), called *triple junctions*, and the junction lines appear as points, called *triple-junction points*, on a petrographic section prepared for microscopic study. For a single-phase aggregate in textural equilibrium the relationship between interfacial energies (γ_i) and corresponding interfacial angles (θ_i) is given by (Fig. 3.1a):

$$\frac{\gamma_1}{\sin \theta_1} = \frac{\gamma_2}{\sin \theta_2} = \frac{\gamma_3}{\sin \theta_3} \quad (3.1)$$

Assuming no anisotropic effects, as is likely to be the case for most metals and the sulfides with close-packed structures, in a section normal to the triple junction line:

$$\gamma_1 = \gamma_2 = \gamma_3$$

so that

$$\theta_1 = \theta_2 = \theta_3 = 120^\circ$$

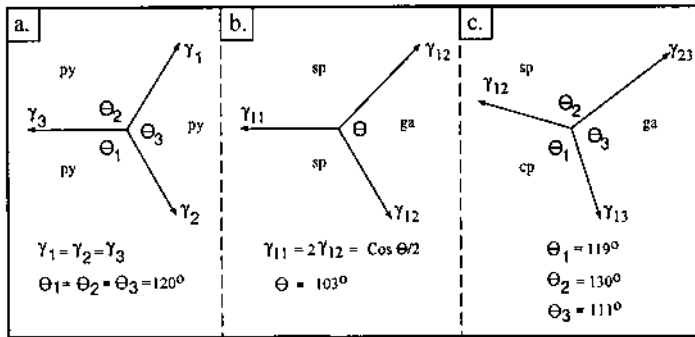


Figure 3.1. Triple junction points: a. single-phase assemblage; b. two-phase assemblage; c. three-phase assemblage. γ 's represent interfacial free energies and θ 's are interfacial angles. The values of the interfacial angles are from Stanton (1964). In each case, the assemblage is in surface tension equilibrium and the junction line is normal to the plane of the paper. Abbreviations: py = pyrite; cp = chalcopyrite; sp = sphalerite; ga = galena.

Such a configuration of grain boundaries, often referred to as *foam structure* by analogy to the shape of bubbles in a foam, has been well documented in annealed single-phase metals (Smith 1964). Close statistical approximation to such an interfacial relationship is also quite common among single-phase aggregates of isotropic sulfides (e.g., pyrite, sphalerite) in metamorphosed deposits.

For a two-phase aggregate (Fig. 3.1b), the analogous relationship is (Smith 1964):

$$\gamma_{11} = 2 \gamma_{12} \cos (\theta / 2) \tag{3.2}$$

so that the value of θ , called *dihedral angle*, controls the shape of the minor phase (Fig. 3.2). In fact, textural relations of many two-phase sulfide assemblages can be explained in terms of their characteristic dihedral angles estimated statistically from a large number of measurements (Stanton 1964). Examples include the rounded form of sphalerite as a minor phase in galena (high dihedral angle, $\theta \approx 130^\circ$), the intergranular habit of galena as a minor phase in sphalerite (low dihedral angle, $\theta \approx 103^\circ$), and the commonly observed inconclusive mutual boundaries between sphalerite and chalcopyrite or pyrrhotite (similar dihedral angles, $\theta \approx 106^\circ$ to 108°). Stanton (1964)

has shown that the measured interfacial angles in a three-phase assemblage, such as galena - sphalerite - chalcopyrite (Fig. 3.1c), are consistent with the dihedral angles measured in corresponding two-phase assemblages. The textures of natural ore assemblages, of course, can be much more complicated because of several variables not considered here: nucleation, crystal growth, impurities, concentration gradients, atomic mobility, and strain energy.

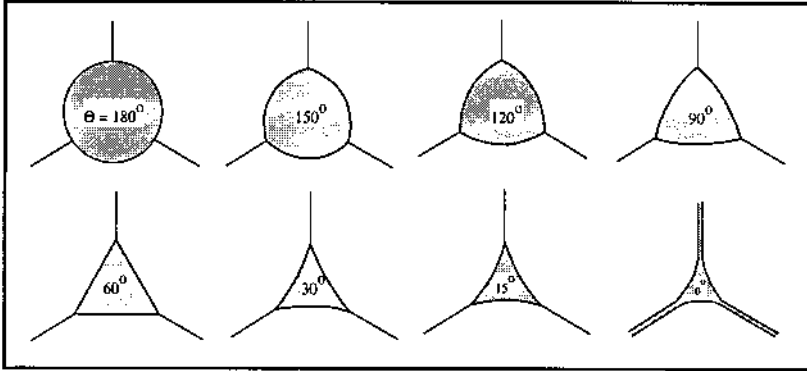


Figure 3.2. Schematic diagram showing the control of dihedral angle (θ) on shapes of a minor phase in a two-phase crystalline aggregate if the minor phase appears at the junction of three grains of the major phase (after Smith 1948).

3.4.2. CLASSIFICATION

Two schemes of classification are normally employed for treatment of ore textures: descriptive and genetic. A descriptive classification, based on fabric properties considered from a purely geometric point of view, provides a convenient way of describing ore textures using, as far as possible, a set of standard terms entrenched in the literature (e.g., Bastin 1950, Schwartz 1951, Schneiderhöhn 1952, Ramdohr 1980). Such a scheme is particularly useful in the early stages of an investigation when the data base may be inadequate for genetic interpretation. For example, a vermicular intergrowth between two minerals may arise from eutectic crystallization, exsolution, or replacement; such a texture is best described by the non-genetic term 'myrmekitic' until such time that its origin can be ascertained, if at all, from additional information.

In the present context, however, it is the genetic aspects of ore textures that need to be emphasized. There is no universally accepted genetic classification of ore textures. A simplified genetic classification, largely based on treatments by Stanton (1972) and Ramdohr (1980), is given below:

- A. Textures formed by free growth of crystals
 - a. Magmatic crystallization
 - b. Sedimentation
 - c. Open-space (or cavity) filling
- B. Textures of polycrystalline aggregates
 - a. Exsolution
 - b. Replacement
 - c. Crystalline transformation
 - d. Deformation
 - e. Annealing

Ore textures resulting from magmatic crystallization and sedimentation are essentially the same as in igneous and sedimentary rocks, respectively, and are discussed in standard textbooks on these subjects. Textures formed during diagenesis are governed by the same principles as for polycrystalline aggregates. *Open-space filling* textures, formed during precipitation of ore and gangue minerals from hydrothermal fluids in pre-existing cavities (e.g., vesicles in a lava flow, open spaces in a breccia, dissolution cavities in carbonate rocks, tension fractures, etc.), are characterized by relatively large crystals with well developed faces and compositional zoning (both in terms of growth zoning in single crystals and compositional layering) which record the changes in fluid chemistry. These textures include free growth of crystals in a fluid medium as well as impingement among crystals growing in close proximity.

Exsolution is the process by which a new phase unmixes from a solid solution when it is cooled to a temperature below its solvus. Exsolution involves nucleation of the exsolved phase resulting from compositional fluctuation in the host and its subsequent growth by diffusion of constituents from the host. The potential sites of nucleation are the surfaces of high interfacial energy (such as twin boundaries, grain boundaries, crystal imperfections, etc.) or the surfaces where nucleation can be achieved with minimal addition of interfacial energy (such as certain crystallographic planes). Crystallographic planes are preferred where there are compatible crystallographic planes between the two phases (*coherent* exsolution); imperfections and grain boundaries are preferred where there are no atomic planes within the exsolved phase that can fit well with those of the host (*noncoherent* exsolution). Examples of coherent exsolution, which commonly results in oriented intergrowths of bladed or lamellar forms, are common in ore minerals: exsolution of cubanite, tetrahedrite, and bornite along (111) of host chalcopyrite; of pentlandite parallel to (0001) and (1010) planes of pyrrhotite; of hematite parallel to (0001) of ilmenite, and of ulvöspinel parallel to (111) of magnetite. (The very common occurrence of ilmenite lamellae in magnetite is a result of oxidation of exsolved ulvöspinel.) Noncoherent exsolution usually produces unoriented (myrmekitic) intergrowths, but coherent exsolution may also produce random orientation of exsolved blebs if the cooling is rapid (Francis et al. 1976). Pyrite exsolved from pyrrhotite on cooling (see the pyrite-pyrrhotite solvus, Fig. 4.26), an example of noncoherent exsolution, usually appears as individual grains because of its

strong tendency to form idiomorphic crystals. The kinetics of exsolution are influenced by many factors that control nucleation and diffusion in a given system. These include the kinds and amounts of impurities, types and distribution of crystal imperfections, degree of supersaturation, and pressure (Yund & McAllister 1970).

Although textures formed by exsolution often resemble those formed by *replacement*, the two processes are very different. The former is an isochemical process whereas the latter is an allochemical (metasomatic) process. Replacement may involve cations, anions, or both, and it may be highly selective. The process is commonly regarded as one involving dissolution of one or more minerals and simultaneous precipitation of others. Simultaneous dissolution and deposition, when considered on a submicroscopic scale, involve diffusion of the replacing ions from the replacing medium (generally an aqueous fluid) towards the interface and diffusion of the replaced ions in the opposite direction. Thus, the progress of replacement in a given system is governed not only by the relative stabilities of the pre-existing and possible new phases, but also by factors that influence the efficiency of diffusion. Fractures, cleavages, grain boundaries, and certain crystallographic planes are often the preferred sites of replacement because diffusion occurs more readily along such surfaces. High temperatures facilitate diffusion, whereas high pressures may inhibit diffusion by the healing of fractures. In general, the process of replacement appears to be volume-for-volume rather than atom-for-atom (because there is usually no evidence for change in porosity), but this creates problems for writing balanced equations to represent replacement reactions. If volume changes in a replacement reaction are known or can be assumed (including the case of no volume change), a balanced equation can be written by making use of actual chemical compositions of rocks and minerals (Gresens 1967). Consideration of such volume-composition relationships in metasomatic reactions allows a quantitative evaluation of released trace elements which may be mobilized and concentrated to form mineral deposits.

Deformation textures in a mineral assemblage owe their origin to the application of differential stress in excess of the elastic limit of the assemblage. Additional variables which influence the extent and type of deformation include temperature, confining pressure, fluid pressure, chemically active medium, and strain rate (McDonald 1967). The deformation may occur by plastic flow (ductile failure) involving introduction and migration of crystal defects (point defects, and line defects or dislocations) under the influence of thermal energy and stress, or by brittle failure involving fracturing and cataclasis. In single crystals, plastic deformation may occur by slip (translation gliding), twinning, lattice bending, kinking, and creep (slow deformation under low stress over a long period of time). Additional mechanisms that operate in polycrystalline aggregates include flattening and preferred orientation of grains and adjustment of interfacial boundaries.

Annealing is the process by which the accumulated strain energy in a polycrystalline aggregate is reduced, thereby reducing the free energy of the system. Annealing includes a combination of (a) recovery and (b) recrystallization (Cahn 1971). *Recovery* refers to internal crystallographic changes that result in crystal defects being

arranged into lower energy configurations, such as subgrain boundaries. *Recrystallization* is achieved by migration of high-angle grain boundaries; it is driven by strain and surface energy, but its rate is temperature dependent and controlled by diffusion. Recrystallization involves nucleation and growth of unstrained grains (primary recrystallization) and further enlargement or coarsening of some recrystallized grains at the expense of others (secondary recrystallization) for minimization of surface free energy. Some amount of recrystallization may accompany deformation; this is called *syntectonic recrystallization*. Annealing may partially or totally obliterate the effects of earlier deformation. It should be pointed out that a polycrystalline sulfide aggregate is not necessarily the product of annealing of previously deformed material. It might be produced also by simple grain growth from microcrystalline aggregates, leading to coarsening, segregation of different minerals into discrete grains, and acquisition of crystal habits in accordance with prevailing surface energy requirements, and there is no obvious method of distinguishing between the two (Stanton 1964).

3.4.3. APPLICATIONS

The obvious application of ore-gangue textures in ore genesis lies in their potential for providing information on the process of ore deposition (e.g., open-space filling versus replacement) and postdepositional history (e.g., oxidation, hydrothermal alteration, metamorphism). For example, interpretation of textures have played a major role in determining that the Mississippi Valley-type lead-zinc sulfide deposits were formed predominantly by open-space filling, that the grain boundary relationships in many stratiform copper-lead zinc sulfide deposits are a result of metamorphism rather than replacement, and that the conglomerate-type uranium deposits are actually paleoplacers. A summary of the important criteria useful in the recognition of origin of ore textures in mineral deposits is listed in Table 3.3.

Another important application of textural studies in ore genesis is the determination of the time sequence of mineral deposition, or *paragenesis*, in unmetamorphosed deposits. The paragenesis of a mineral deposit provides a record of the local changes in geochemical parameters (*T*, *P*, fluid composition, etc.) in the course of mineralization. In European literature, the term paragenesis has been used to refer to characteristic ore mineral assemblages, but its prevalent use in the modern economic geology literature is in the sense of 'paragenetic sequence' and this usage is adopted here.

The paragenesis for a mineral deposit or a genetically related group of deposits is inferred from the mutual relationships among the minerals and assemblages. Normally, it involves the study of a large number of specimens in the laboratory, but some features, such as open-space filling and veining, are often seen more readily in large exposures in a mine or an outcrop. Useful criteria for determining the relative age sequence of minerals are: (a) banded textures, (b) exsolution, (c) crosscutting relationship (veining), (d) replacement, (e) inclusions, and (f) twinning.

Banded textures such as crustification banding and comb structure resulting from open-space filling are among the most reliable for determining paragenesis, because

TABLE 3.3. Criteria for recognition of the origin of ore textures in mineral deposits

Process	Criteria for recognition
<i>Magmatic crystallization</i>	Spheroidal disseminations of early formed crystals (e.g., chromite) or of sulfide + oxide aggregates Cumulus texture Interstitial sulfides in silicate aggregates (without replacement textures) Skeletal crystals
<i>Sedimentation</i>	Sedimentary layering or laminations Crossbedding Graded bedding Framboids (usually recrystallized) Oolites Detrital constituents Penecontemporaneous deformation (slump folds, growth faults, etc.) Geopetal fabric
<i>Open-space (or Cavity) filling</i>	Comb structure Crustification banding (often symmetrical or rhythmic, more complex patterns due to dissolution and redeposition) "Colloform" textures Matching of vein walls
<i>Exsolution</i>	Consistent intergrowth relationship between a mineral pair Solid solution relationship between the host and the exsolved phase(s) at high temperatures Orientation of exsolved bodies along crystallographic directions of host mineral, accompanied by depletion of the relevant constituents from the immediate surroundings of the exsolved bodies
<i>Replacement</i>	Pseudomorphs Unsupported residual island of the unreplaced material, especially with a preferred orientation or with structures conformable to those of the unreplaced material Gradational boundary between the replaced and unreplaced material Strong correlation of replacing material with permeable zones (e.g., fractures) in the replaced material, with enlargement of replacement at intersection of such zones Embayed margins with reaction rims
<i>Crystallographic transformation</i>	Inversion twins
<i>Deformation</i>	Slip lines and slip bands Kink bands Deformation twins Lattice bending (bent cleavages, twins, etc.) Preferred orientation Brecciation (cataclasis) Mesoscopic and microscopic folds defined by layers of ore or gangue minerals Sulfide veinlets (especially of galena, chalcopyrite, and pyrrhotite) transgressing lithological layering and schistosity
<i>Annealing</i>	Subgrain development Recrystallization Foam structure Porphyroblasts

open spaces are filled from the walls inward. Sphalerite bands and growth zones in sphalerite and dolomite crystals have been correlated within or even across mineralized districts, suggestive of a depositional microstratigraphy (Ebers & Kopp 1979, McLimans et al. 1980, Voss & Hagni 1985, Rowan 1986). Pairs of minerals showing exsolution relationship (e.g., sphalerite-chalcopyrite, pyrrhotite-pentlandite) must have formed essentially contemporaneously from a high-temperature solid solution, whereas minerals of a crosscutting veinlet are younger than the minerals the veinlet cuts. If a mineral *A* replaces another mineral *B*, *A* is obviously the younger mineral; if *A* occurs as inclusions in *B*, *A* is the older mineral unless it was formed by exsolution or selective replacement. Twinning may form during initial growth (*growth twins*), through phase inversion (*inversion twins*), or as a result of deformation (*deformation* or *pressure twins*) (Ramdohr 1980). Growth twins occur as lamellae of irregular width and uneven distribution, and may be absent from other grains in the same section. Inversion twins are commonly spindle-shaped, form intergrowth networks, and are not accompanied by deformation features. Deformation twins, in contrast, are characterized by uniformly thick lamellae, which often extend into adjacent grains and are associated with deformation fabric. The type of twinning present in only some grains of a specific mineral may be useful in distinguishing different generations of that mineral. For example, Taylor et al. (1983b) distinguished three generations of sphalerite in the Mascot-Jefferson City zinc district of eastern Tennessee (USA) partly on the basis of the prevalence of deformation twins in sphalerite. However, one must recognize the limitation of this approach, because deformation of crystals depends not only on the magnitude of the applied stress but also on the composition of crystals and their surroundings (Churnet 1985).

The degrees of idiomorphism of minerals and their mutual grain boundary relationships have also been used as criteria of paragenesis. Early formed minerals in open spaces often tend to be idiomorphic in the directions of unobstructed growth, but, as discussed earlier, morphology and grain boundary relationships of minerals in a polycrystalline aggregate are controlled to a large extent by interfacial energies. In fact, on the basis of relative tendencies to idiomorphism and the size of characteristic dihedral angles, Stanton (1964) proposed a generalized silicate-oxide-sulfide crystalloblastic series: magnetite-arsenopyrite, pyrite, dolomite, tremolite, muscovite, chlorite, pyrrhotite, sphalerite, chalcopyrite, galena. Thus, in a pyrite - pyrrhotite - chalcopyrite - sphalerite - galena assemblage, typical of strata-bound Cu-Zn-Pb massive sulfide deposits, the common idiomorphism of pyrite may have little paragenetic significance.

The *paragenesis* is commonly depicted by means of a bar diagram, an example of which is illustrated in Figure 3.3 for the ores of the Magmont mine in southeast Missouri (USA). The paragenesis was worked out by Hagni and Trancynger (1977) from a careful study of 262 polished sections and a few thin sections prepared from 175 hand specimens. The minerals of this carbonate-hosted (Mississippi Valley-type) lead-zinc deposit, classified according to texture as (a) disseminated, (b) colloform, and (c) vug-filling crystalline, have been interpreted to correspond to three successive stages of deposition. Among the ore minerals, the disseminated iron and iron-nickel sulfide

minerals (pyrite, bravoite, marcasite) are the earliest and probably represent sedimentary or early diagenetic sulfide formation. Siegenite commonly coats and replaces the margins of chalcopyrite grains, both chalcopyrite and sphalerite replace pyrite, and galena contains inclusions of irregularly shaped replacement remnants of the earlier disseminated sulfides (pyrite, marcasite, chalcopyrite, and sphalerite). The colloform ores, developed primarily in the open spaces of breccias and fractures, are inferred to be younger than disseminated ores on the basis of the following textural relationships: (a) disseminated sulfide minerals (pyrite, bravoite, sphalerite, and galena) are enclosed and partially replaced by colloform pyrite and marcasite; (b) colloform pyrite and marcasite masses that locally enclose disseminated bravoite are surrounded by repetitively deposited bravoite; (c) disseminated sphalerite is enclosed, partly replaced, and veined by colloform chalcopyrite; (d) colloform chalcopyrite and pyrite, deposited on disseminated sphalerite, are surrounded by colloform sphalerite; and (e) colloform masses are not replaced by disseminated sulfide grains. The vug-filling minerals occur as well-formed crystals in small vugs distributed throughout the Magmont orebodies. Evidence cited for their later age relative to the colloform ores are as follows: (a) cubic galena and crystalline quartz and calcite commonly line vugs and fractures; (b) brecciated pyrite and marcasite masses of the colloform stage are usually coated, cemented, and partly replaced by cubic galena, quartz and calcite; (c) replacement remnants of disseminated and colloform sulfides occur as inclusions in cubic galena; (d) siegenite, quartz, and cubic galena fill cavities formed by leaching of colloform pyrite-marcasite bodies; and (e) octahedral galena belonging to the earlier stages of deposition is partly to completely leached, whereas cubic galena is not.

It is important to bear in mind the limitations of textural interpretations. Primary depositional textures, especially of relatively high-temperature sulfide assemblages, are often obliterated by re-equilibration to lower temperatures or by metamorphism. Also, the precise origin of many textures is not well understood, because morphologically similar textures can be produced by entirely different processes and these cannot be distinguished without adequate theoretical or experimental foundation. For example, the intergrowth texture resulting from oriented and unoriented inclusions of chalcopyrite in sphalerite (the so-called "chalcopyrite disease"; Barton 1978) has been variously ascribed to (a) exsolution of chalcopyrite from a high-temperature sphalerite-chalcopyrite solid solution (Ramdohr 1980), (b) replacement of sphalerite by interaction with Cu-bearing hydrothermal solutions (Eldridge et al. 1988, Barton & Bethke 1987, Sugaki et al. 1987, Bortnikov et al. 1991), and (c) coprecipitation of sphalerite and chalcopyrite (Kojima 1990). However, experimental investigations in the Cu-Fe-Zn-S system (Wiggins & Craig 1980, Hutchinson & Scott 1981, Kojima & Sugaki 1985, Kojima 1990) have demonstrated that the solubility of copper in sphalerite at 300° to 700°C is extremely limited, indicating that exsolution cannot account for much of the chalcopyrite disease in natural assemblages, especially those formed at low temperatures. A replacement origin, on the other hand, is strongly supported by hydrothermal experiments by Eldridge et al. (1988) in which the chalcopyrite disease was produced by reacting iron-bearing sphalerites with copper-bearing chloride fluids.

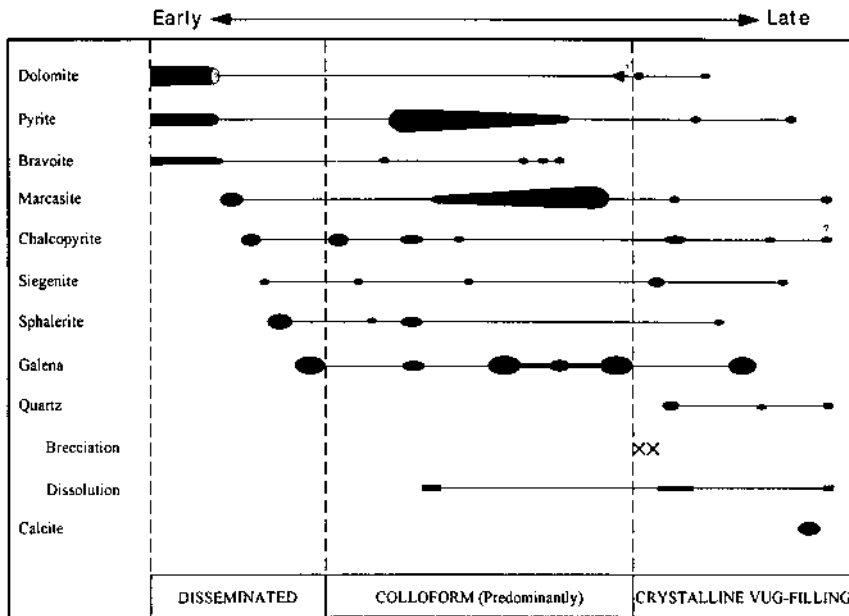


Figure 3.3. Paragenesis of ore-gangue assemblage in the Magmont lead-zinc mine, Viburnum Trend, southeast Missouri (USA). Relative time decreases from left (early) to right (late), and relative amounts of the phases precipitated are indicated by line thickness (after Hagni and Trancyger 1977).

3.5. Stability Relations of Ore Minerals and Assemblages

Mineral deposits in crustal rocks form under a wide range of temperature and pressure conditions. The upper limit of temperature is on the order of 1,200°C, the temperature of basaltic melts, and that of pressure is about 12 kbar, the estimated pressure at the base of the crust in continental regions. The fluids involved are also highly variable, from silicate melts to dilute meteoric water. A meaningful interpretation of the environment (temperature, pressure, activities of components, etc.) in which a mineral deposit formed or subsequently evolved requires a detailed knowledge of the likely response of mineral phases to changes in geochemical parameters. Two basic approaches are employed in the evaluation of stability relations: thermodynamic calculation and experimental investigation. Actually, the two are interrelated in the sense that designs and interpretations of experimental studies make use of thermodynamic principles, and experimental results are essential for verification, refinement, and extrapolation of thermodynamic parameters.

The thermodynamic approach is a powerful one if appropriate data exist. Thermodynamic data for many of the common ore and gangue minerals are available (e.g., Kubaschewski et al. 1967, Robie & Waldbaum 1968, Robie et al. 1978, Stull & Prophet 1971, Chase et al. 1974, 1975a, 1975b, 1975c, Mills 1974), but a general lack

of data on solid solutions limit their application to natural assemblages. Moreover, reactions and assemblages predicted from thermodynamics may not actually occur in nature because of kinetic factors. The main limitations of experimental investigations arise from the fact that only a few variables can be controlled simultaneously in an experiment and equilibrium may not be attained, particularly in systems at low temperatures. Often, the best interpretation of natural assemblages is obtained through a combination of experimental and thermodynamic data.

3.5.1. EXPERIMENTAL INVESTIGATIONS

As expected, most laboratory investigations on stability relations of ore minerals have been devoted to sulfides, although some systems involving arsenides, tellurides, selenides, and sulfosalts have been investigated. The term sulfide-type systems is used here in a broad sense to include all these systems. A discussion, or even a listing, of the published data on the various experimentally investigated systems pertinent to ore minerals is beyond the scope of this book, but excellent compilations on the subject, including the principles and techniques used in such investigations, are available (e.g., Kullerud 1964, Ribbe 1974, Moh 1975, Rumble 1976, Barton & Skinner 1979, Vaughan & Craig 1997). Liquidus relations in a few sulfide-silicate systems have also been investigated (e.g., MacLean 1969, Naldrett 1969, Shimazaki & Clark 1973).

Laboratory experiments on synthetic sulfide-type systems are normally designed to record the interrelationship between two variables at a time, most commonly between temperature and composition. In practice, this amounts to determining the phases and their compositions corresponding to a series of known bulk compositions (prepared by mixing appropriate starting materials in various proportions) annealed at discrete temperatures, ensuring that the products have attained equilibrium at each temperature. Evacuated silica tube experiments (Kullerud 1971), the most commonly used technique for synthesizing sulfides, are invariably polybaric because a vapor phase is always present and the equilibrium vapor pressure, although usually not measured, varies with the equilibrium assemblage. This vapor pressure, however, has little effect on phase relations because most solids and liquids are incompressible under small magnitudes of pressure. Phase relations in such *condensed* systems (so called because the system loses a degree of freedom due to the presence of a vapor phase with all assemblages) are most conveniently represented by temperature-composition (T - X) diagrams for binary systems such as the Cu-S system (Fig. 3.4). For a ternary condensed system (e.g., the Fe-Ni-S), the easiest two-dimensional representation of phase relations is by isothermal sections (Fig. 3.5) of the temperature-composition prism. For a quaternary condensed system (e.g. the Cu-Fe-Ni-S system), only a portion of the compositional field can be represented in a two-dimensional isothermal section. With appropriate experimental data for total pressure (P_T) as a variable, phase relations in binary systems can be shown by T - X (isobaric), P_T - X (isothermal), or P_T - T diagrams (see Barton & Skinner 1979, Figs. 7.3 and 7.4), and by isothermal-isobaric sections for ternary systems.

However, there is a general lack of experimental data on the effect of total pressure

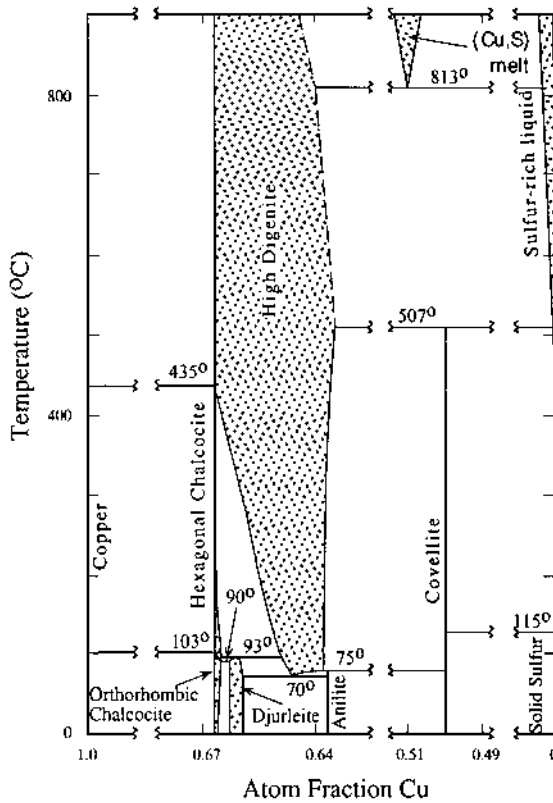


Figure 3.4. Temperature-composition (T - X) diagram showing stability of phases in the condensed binary Cu-S system, compiled from experimental data of various investigations (after Barton and Skinner (1979)).

on sulfide-type systems, because phase equilibria in these systems are not particularly sensitive to small variations in total pressure. On the other hand, partial pressure of a volatile species such as sulfur or arsenic (or its corresponding thermodynamic function, activity or fugacity) is important for phase equilibria in sulfide-type systems, and it is possible to design experiments in which this variable can be controlled or measured.

3.5.2. THERMODYNAMIC APPROACH

Because of constraints of time, technique, and reaction kinetics, reliable experimental data are limited to simple sulfide-type systems equilibrated at relatively high temperatures (usually above 200°-300°C). The thermodynamic approach allows extrapolation to complex systems and lower temperatures.

Of the three important variables of state (T , P_T , X), total pressure (P_T) is of

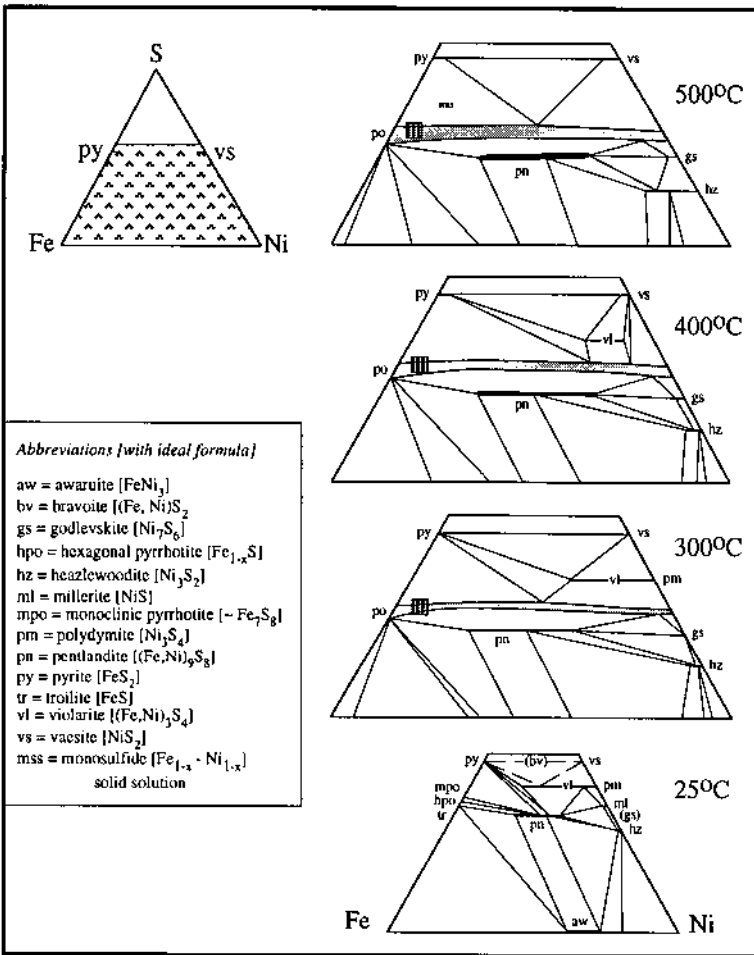


Figure 3.5. Isothermal sections showing phase relations in the central part of the condensed ternary Fe-Ni-S system, compiled from experimental data of various investigations (Misra & Fleet 1973, Craig 1973, Barker 1983). Compositions of the phases are in atomic%. The likely phase relations at 25°C are based on extrapolation of experimental data and natural assemblages (Misra & Fleet 1974). The shaded rectangular box in the isotherms represents the approximate range of bulk compositions for the nickel-sulfide ores of the Sudbury district, Canada.

relatively minor significance in sulfide-type systems. Volume changes for reactions between sulfide phases are usually so small that phase relations of sulfides are relatively insensitive to pressures of the magnitude found in the upper crust (<5 kb) where most of the sulfide deposits seem to have formed. Neglecting the effect of pressure in such deposits results in most cases in an uncertainty of no greater than ≈ 100 calories in the molal free energy change for a reaction of significance in sulfide petrogenesis, compared with hundreds of calories uncertainty in standard free energies (Barton 1970). Of course, total pressure cannot be ignored for sulfides formed in the lower crust or mantle.

For thermodynamic manipulations, the compositional parameters to be considered are the activities of the various components of a system. Because sulfur is a common component of all sulfide phases, a particularly useful compositional parameter is the activity of sulfur (a_{S_2}), which serves as a unifying variable for comparison of phase assemblages corresponding to different bulk compositions. The convenient standard state of sulfur for this purpose is the ideal diatomic gas, S_2 , at a fugacity of 1 atm and at the temperature of interest; for the standard state of sulfur defined this way, activity of sulfur (a_{S_2}) is numerically equal to fugacity of sulfur (f_{S_2}). If a univariant sulfidation reaction is written in such a way that all the reactants and products except S_2 are in their standard states (i.e., activity of each component is unity, except a_{S_2}), then the equilibrium constant (K) for the reaction is given by

$$K = 1 / a_{S_2} = 1 / f_{S_2} \quad (3.3)$$

and its variation with temperature at constant pressure is given by the van't Hoff expression

$$\frac{d(\log K)}{d(1/T)} = \frac{-\Delta H^0}{2.303R} = \frac{-d(\log a_{S_2})}{d(1/T)} \quad (3.4)$$

where ΔH^0 = standard enthalpy of the reaction, T = temperature (Kelvin), and R = the gas constant. Thus, $(\log K)$ is a linear function of $(1/T)$, i.e., the plot of $(\log a_{S_2})$ against $(1/T)$ will be a straight line with a slope of $(\Delta H^0/2.303R)$ as long as the solid reactants and products are in their standard states. If they are not in their standard states, then their activities have to be taken into account for solving Equation 3.4. Figure 3.6 shows a series of such curves for sulfidation reactions; many others have been compiled by Barton and Skinner (1979).

From considerations similar to those presented above, it can be shown that for an oxidation reaction the equilibrium constant (K) varies with temperature (at constant pressure) as

$$\frac{d(\log K)}{d(1/T)} = \frac{-\Delta H^0}{2.303R} = \frac{-d(\log a_{O_2})}{d(1/T)} \quad (3.5)$$

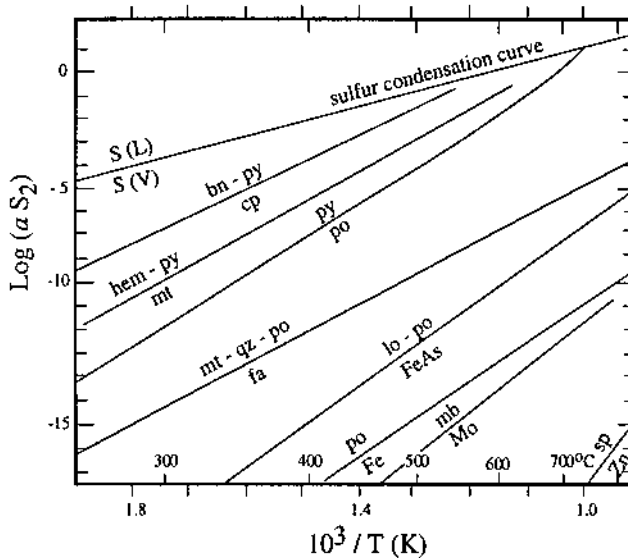


Figure 3.6. Activity of sulfur (a_{S_2})-temperature (in Kelvin) diagram for selected sulfidation reactions (a_{S_2} buffers) at 1 atmosphere total pressure (compiled from data in Barton & Skinner 1979). Abbreviations: bn = bornite; cp = chalcopyrite; hem = hematite; lo = löellingite; mb = molybdenite; mt = magnetite; po = pyrrhotite; py = pyrite; qz = quartz; fa = faylite; sp = sphalerite.

so that univariant curves defining the stabilities of oxide phases and assemblages can be represented conveniently in a ($\log a_{O_2}$) vs. ($1/T$) diagram (Fig. 3.7).

An activity-temperature diagram is clearly inadequate for depicting phase relations in systems involving more than one compositional variable. For such systems, activity-activity diagrams are often the best choice. The most commonly used are a_{S_2} - a_{O_2} diagrams, which are particularly suitable for showing the equilibria among sulfides and oxides (Fig. 3.8). The details of construction of activity-activity diagrams and a number of examples applicable to a variety of ore-forming phases at different temperatures are discussed by Holland (1959, 1965).

At a given temperature, stabilities of aqueous species are controlled largely by pH (acidity) and Eh (redox potential) of the environment. Thus, equilibria involving aqueous species are represented commonly by isothermal Eh-pH diagrams (with additional constraints on activities of the components). The thermodynamic principles and techniques used in constructing Eh-pH diagrams are discussed by Garrels and Christ (1965), who also include many examples of such diagrams related to ore-forming hydrothermal systems. An Eh-pH diagram delineating the stability fields of common iron minerals and aqueous ionic species is presented in Figure 15.2. The activity of oxygen (a_{O_2}) is related to Eh by the reaction

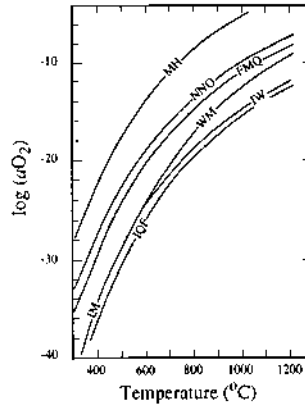


Figure 3.7. Activity of oxygen (a_{O_2})-temperature (in $^{\circ}C$) diagram for selected oxidation reactions (a_{O_2} buffers) at 1 atmosphere total pressure (after Lindsley 1976). Abbreviations: MH = magnetite-hematite; NNO = nickel-nickel oxide; FMQ = faylite-magnetite-quartz; WM = wüstite-magnetite; IM = iron-magnetite; IW = iron-wüstite; IQF = iron-quartz-faylite. The buffer curves would be straight lines if plotted against $1/T$ (Kelvin).

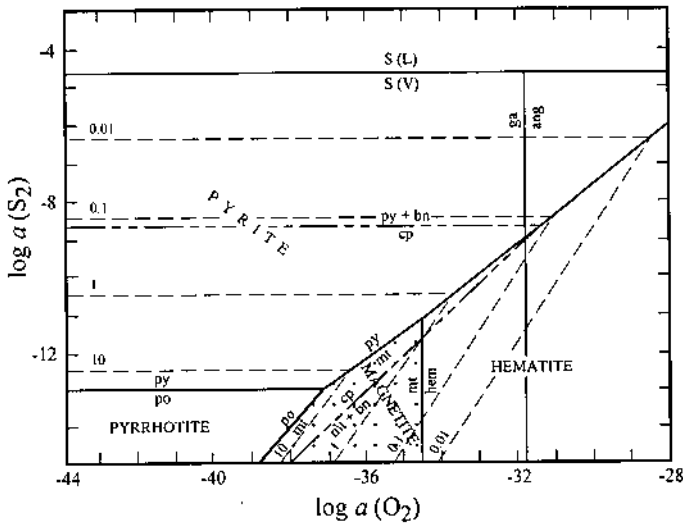
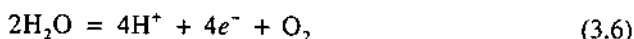


Figure 3.8. An activity-activity diagram for representing multicomponent phase equilibria at $T = 250^{\circ}C$ and $P_{H_2O} = 50$ bars (after Barton & Skinner 1979). Abbreviations: py = pyrite; ga = galena; ang = anglesite; cp = chalcopyrite; bn = bornite; mt = magnetite; po = pyrrhotite. Single-dashed lines represent contours of mole% FeS in sphalerite in equilibrium with other phases; the 20 mole% FeS contour coincides with the pyrrhotite field boundary.



which gives the following relationship between Eh and $a\text{O}_2$:

$$\text{Eh} = -1.229 - 0.0015 \log a\text{O}_2 + 0.059 \text{pH} \quad (3.7)$$

Thus, $a\text{O}_2$ -pH diagrams, such as Figure 3.9, can be constructed from the same data used for constructing Eh-pH diagrams. An $a\text{O}_2$ -pH diagram is topologically identical to the corresponding Eh-pH diagram but easier to read.

3.5.3. APPLICATIONS

Consideration of phase equilibria is an integral part of ore petrology. Reference to relevant phase diagrams can help in (Craig & Vaughan 1994): (a) anticipation and recognition of phases; (b) recognition of equilibrium or disequilibrium assemblages; (c) understanding of textural features; (d) interpretation of the chemistry of the ore-forming fluid and its variation in time and space; and (e) estimation of temperature and pressure during mineralization and subsequent metamorphism (discussed later).

The application of phase equilibria in the Fe-Ni-S system (Fig. 3.5) to the nickel-copper sulfide ores of the Sudbury district (Canada) is an example of how phase relations in the synthetic sulfide-type systems have contributed to our understanding of ore assemblages. The Sudbury ores consist mainly of pyrrhotite (hexagonal and monoclinic), pentlandite, pyrite, chalcopyrite, and magnetite, with minor amounts of cubanite and violarite. However, the ore material is interpreted to have been emplaced at a temperature above 1,000°C as an immiscible sulfide-oxide melt, which subsequently crystallized as a magnetite-*mss* (*monosulfide solid solution*) assemblage (Naldrett & Kullerud 1967). Phase equilibria in the Cu-Fe-Ni-S system (Craig & Kullerud 1969) reveal that the *mss* contained a significant amount of copper in solid solution, which formed a high-temperature chalcopyrite-like phase (*intermediate solid solution, iss*) and recrystallized as chalcopyrite at lower temperatures, much of it between 500° and 600°C. Pentlandite, the predominant Fe-Ni sulfide of the Sudbury ores, formed not by direct crystallization of the immiscible melt but from the *mss* by exsolution (Kullerud 1963). The pentlandite exsolution is inferred have started at a temperature of about 400°C or less when the lower-sulfur compositional limit of the *mss* had shifted sufficiently to a higher-sulfur position, leaving the sulfur-poor bulk compositions in the *mss*-pentlandite divariant field. The spectacular 'flames' of pentlandite, which occur as crystallographically oriented lamellae in pyrrhotite (Francis et al. 1976), represent the lower temperature product of this exsolution process. For sulfur-rich bulk compositions (containing >39 wt% S) pyrite may have exsolved from

the *mss* even before pentlandite (Naldrett & Kullerud 1967), but for sulfur-poor bulk compositions (containing <38 wt% S) pyrite could not have formed from the *mss* until the *mss* field became discontinuous (around 200°C), permitting tie-lines to be established between pentlandite and pyrite. The Sudbury pyrrhotite is a mixture of hexagonal and monoclinic forms and represents the low-temperature remnant of the *mss*. The monoclinic pyrrhotite, which is stable below $\approx 300^\circ\text{C}$ (see Fig. 4.26), could have formed as a consequence of any one of the following: reaction of low-temperature hexagonal pyrrhotite with pyrite; exsolution of pentlandite; or oxidation by solutions percolating through the ore (Naldrett & Kullerud 1967). Phase relations in the Fe-Ni-S system have not been determined at temperatures below 200°C. The likely phase relations at lower temperatures (Fig. 3.5e), inferred from extrapolation of higher temperature experimental data and naturally occurring assemblages, suggest that the assemblage hexagonal pyrrhotite + monoclinic pyrrhotite + pentlandite + pyrite, common to many Sudbury-type deposits, is a disequilibrium assemblage, probably because of metastable persistence of hexagonal pyrrhotite or pyrite. The violarite in these ores is clearly a later alteration product of pentlandite (Misra & Fleet 1974).

Interpretation of hydrothermal mineral deposits can be constrained also from the stability relations of their ore and gangue minerals (Barnes 1979, Holland & Malinin 1979). For example, Crerar and Barnes (1976) inferred the depositional environment of porphyry copper ores from an $a\text{O}_2$ -pH diagram (Fig. 3.9), which was constructed with appropriate boundary conditions obtained from other lines of evidence. The preferred conditions of ore deposition as shown in this figure were deduced in the following manner. The conditions must have been close to the bornite + pyrite/chalcopyrite line, because the ore assemblage is characterized by the presence of these minerals and the absence of pyrrhotite and hematite. The pH is fixed generally in the muscovite (sericite) stability field near the feldspar limit. The $a\text{O}_2$ must be higher than that for the graphite field because graphite is absent in the assemblage. Barite and anhydrite are present either in trace or in major amounts, suggesting that the hydrothermal solution must have been close to the 'Barite and Anhydrite Insoluble' curve. The presence of calcite veins in the ores indicates that the solution must have become saturated in calcite and been close to the 'CaCO₃ Insoluble' curve. From further thermodynamic calculations the authors showed that the copper and iron in these ores were deposited mainly from chloride complexes, rather than sulfide complexes, at temperatures above 250°C but below 350°C as indicated by the fluid inclusion data (Nash 1976).

An obvious limitation of applying phase relations determined experimentally in synthetic systems or derived from thermodynamics to naturally occurring mineral assemblages is the non-ideal chemical composition of the minerals. Two other complicating factors are the recognition of equilibrium in natural assemblages and the intervention of post-depositional process (Barton 1970). A mineralization event usually occurs over a period of time with fluctuations in the chemistry of the mineralizing fluid and temperature. As a result, the number of mineral species in a deposit may be much greater than would be permitted by the phase rule. However, sorting out the paragenesis of such a deposit commonly reveals that for any single

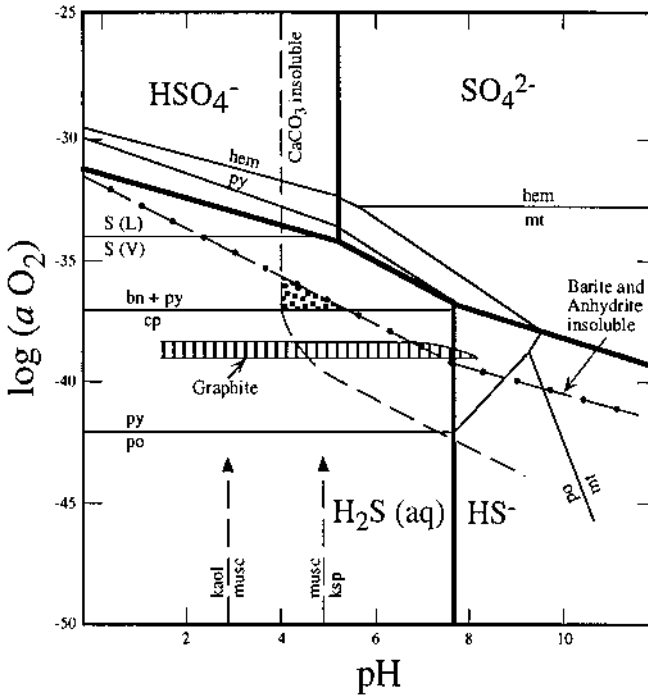


Figure 3.9. The a_{O_2} -pH stabilities of Cu-Fe-S-O minerals, calcite, barite, anhydrite, graphite, sericite (muscovite), and aqueous sulfur species at 250°C (after Crerar & Barnes 1976). Activities used for construction of the stability fields: $\Sigma S = 0.1$; $Ba^{2+} = 10^{-3}$; $\Sigma C = 0.1$; $K^+ = 0.5$; $Ca^{2+} = 0.1$. Abbreviations: py = pyrite; bn = bornite; cp = chalcopyrite; hem = hematite; mt = magnetite; po = pyrrhotite; kaol = kaolinite; musc = muscovite; ksp = potassium feldspar. The stippled area outlines the preferred conditions of deposition of porphyry copper ores. Thick lines denote stability fields of aqueous sulfur species.

stage of mineralization (representing an interval of deposition during which there was no discernible chemical or physical change) there are too few, rather than too many, phases for the number of components. In other words, the system was open with respect to some components. Post-depositional re-equilibration is much more rapid for sulfides than for silicates or oxides, but it is possible in many cases to unravel the evolution of sulfide ore assemblages from a consideration of phase equilibria in appropriate systems.

3.6. Hydrothermal Alteration

Mineral deposits formed from hydrothermal fluids are often accompanied by alteration of the surrounding rocks by the same fluids. In essence, the process of hydrothermal

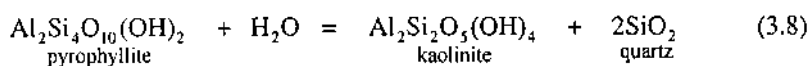
alteration is the response of a rock to new conditions of temperature, pressure, and composition imposed by the introduced fluid; the result is an altered rock with changed mineralogy and texture that may provide an interpretable signature of the characteristics of hydrothermal fluid. The hydrothermal fluid can be any one from the list discussed in Ch. 2, and the temperatures can range from less than 100°C for meteoric water circulated to shallow depths to about 600°C for magmatic fluids. The extent and products of alteration are determined by: (a) the temperature gradient between the fluid and the invaded rocks; (b) the composition gradient; (c) the types of alteration reactions; and (d) the ratio of fluid to rock (commonly referred to as water:rock ratio) in the reaction that produced the alteration. The lithostatic pressure gradient is usually small and relatively unimportant in controlling the alteration assemblages.

3.6.1. PRINCIPLES

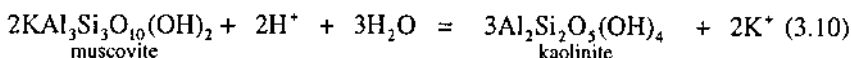
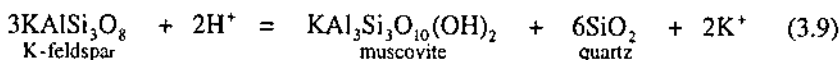
Hydrothermal alteration is a type of allochemical metamorphism (metasomatism). Its distinctive features include the role of fluids in transferring heat and chemical constituents, the relatively large volumes of fluid involved in reactions, and fluctuations in the chemical properties of the fluid over relatively short periods of time, probably a result of changes in the plumbing system (Rose & Burt 1979). The high physical-chemical gradients and the generally short time spans available for alteration reactions often result in incomplete reactions and assemblages with metastable phases. However, thermodynamic relationships developed for treatment of metasomatic processes (Korzhinskii 1959, Thompson 1959) can still be used in cases where attainment of local equilibrium can be inferred, for example, by the absence of incompatible phases in contact (Burt 1974). The theory of metasomatic processes in hydrothermal alteration and the methods used in calculation of alteration equilibria are summarized in Rose and Burt (1979).

The actual reactions that occur between the minerals in a rock and hydrothermal fluids are very complex. For the purpose of experimental studies and thermodynamic calculations, they can be viewed as a combination of many simpler types of reactions. Another simplification commonly employed for reactions involving solid solutions is to represent a reaction in terms of end-member components rather than by their actual chemical compositions. For example, biotite in a reaction may be represented by its annite component ($\text{KFe}_3\text{AlSi}_3\text{O}_{10}(\text{OH})_2$), plagioclase by its albite ($\text{NaAlSi}_3\text{O}_8$) or anorthite ($\text{CaAl}_2\text{Si}_2\text{O}_8$) component, pyrrhotite by its troilite (FeS) component, etc. Types of reactions that are particularly important in hydrothermal processes are listed below, with illustrative examples.

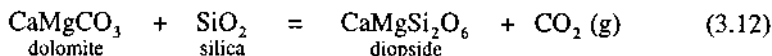
- (a) Hydration-Dehydration: reactions involving removal of water from, or its addition to, the fluid without any change in the $\text{H}^+:\text{OH}^-$ ratio of the fluid.



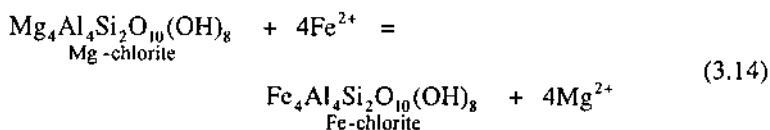
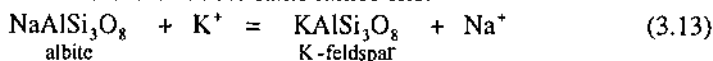
- (b) Hydrolysis: reactions in which either H^+ or OH^- is selectively consumed, resulting in a change in the $H^+ : OH^-$ ratio of the fluid and release of cations equivalent to the H^+ consumed by the solution (Hemley & Jones 1964).



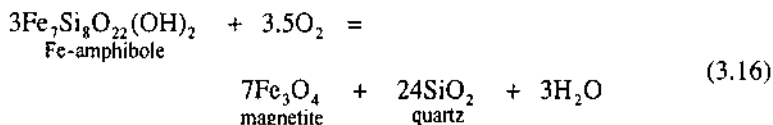
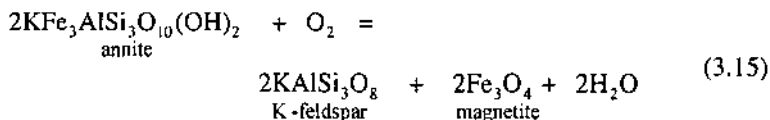
- (c) Carbonation-Decarbonation: reactions involving CO_2 , typical of skarn formation.



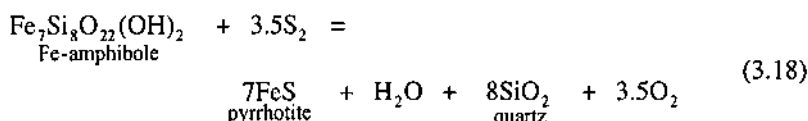
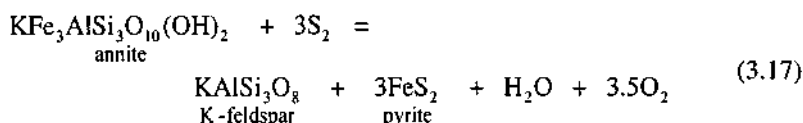
- (d) Cation-exchange: reactions involving solid solutions in which two or more components can be substituted in the same lattice site.



- (e) Oxidation-Reduction: reactions involving elements with different valence states (e.g., Fe^{2+} - Fe^{3+} , Mn^{2+} - Mn^{4+} , U^{4+} - U^{6+}).



- (f) Sulfidation-Desulfidation: reactions involving sulfur, particularly important for precipitation of sulfides.



A wide variety of variables (pressure, temperature, mole fraction, molality, Eh, pH, activity, fugacity, chemical potential) can be used to depict equilibria of alteration assemblages, all of them conforming to the constraints imposed by the phase rule and stabilities of individual minerals, and thus resulting in equivalent topologies (Rose & Burt 1979). The choice of representation in a given case is dictated by the variables inherent in the reactions being considered and available experimental and thermodynamic data. For example, equilibria involving oxidation and sulfidation reactions may be represented by calculated activity (of sulfur or oxygen) vs. temperature diagrams (Fig. 3.6), or by isothermal sections in $a\text{S}_2$ - $a\text{O}_2$ space (Fig. 3.8); silica-dependent mineral equilibria may be presented in terms of a plot with experimentally determined $m\text{SiO}_2$ and temperature as coordinates (Fig. 3.10).

Equilibria involving hydrolysis reactions, by far the most important in hydrothermal alteration, are often represented in terms of activities of the ionic species involved in the reactions (Fig. 3.11). For an illustration of the underlying principle,

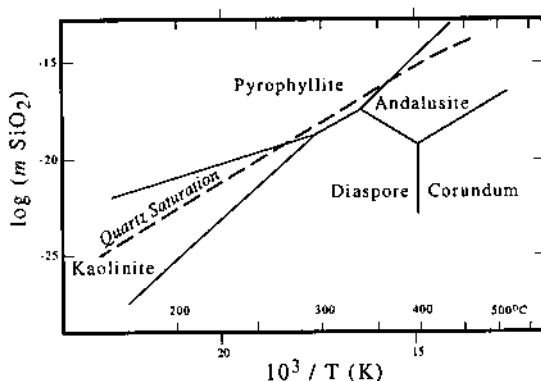
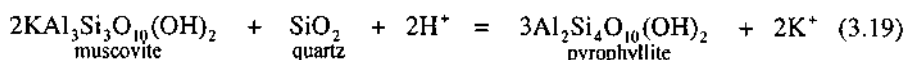


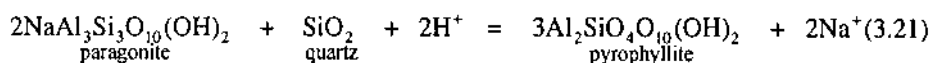
Figure 3.10. Mineral stability relations in the system Al_2O_3 - SiO_2 - H_2O as a function of molality of SiO_2 [$m\text{SiO}_2$] and temperature at $P_{\text{H}_2\text{O}} = 1$ kb (after Hemley et al. 1980).

consider the stability relations among pyrophyllite, K-mica, and Na-mica in the K_2O - Na_2O - Al_2O_3 - SiO_2 - H_2O system. For the pyrophyllite-muscovite and pyrophyllite-paragonite equilibria:



$$K = \frac{a_{\text{pyroph}}^3 \cdot a_{K^+}^2}{a_{\text{musc}}^2 \cdot a_{SiO_2} \cdot a_{H^+}^2} \quad (3.20)$$

and



$$K' = \frac{a_{\text{pyroph}}^3 \cdot a_{Na^+}^2}{a_{\text{parag}}^2 \cdot a_{SiO_2} \cdot a_{H^+}^2} \quad (3.22)$$

If the solid phases pyrophyllite, muscovite, paragonite, and quartz are all present as essentially pure end members (unit activities), then

$$K = \left(\frac{a_{K^+}}{a_{H^+}} \right)^2 \quad \text{and} \quad K' = \left(\frac{a_{Na^+}}{a_{H^+}} \right)^2 \quad (3.23)$$

The ratios a_{K^+} / a_{H^+} and a_{Na^+} / a_{H^+} can be evaluated from available experimental and thermodynamic data (Montoya & Hemley 1974, Helgeson 1974) and the pyrophyllite-muscovite and pyrophyllite-paragonite stability boundaries drawn in a diagram with these ratios as coordinates. Because of solid solution of Na in muscovite, $a_{\text{musc}}^{KAl_3Si_3O_{10}(OH)_2}$ is less than unity at relatively high a_{Na^+} / a_{H^+} ratios, and the boundary between pyrophyllite and K-mica (muscovite with Na solid solution) curves to lower values of a_{K^+} / a_{H^+} with increasing a_{Na^+} / a_{H^+} . Other phase boundaries shown in Figure 3.11 can be drawn by following the procedure outlined above. Also, using the simplification of pure end-member phases (unit activities), the equilibrium constant of a hydrolysis reaction becomes a function only of temperature so that alteration equilibria in the appropriate system can be represented by a_{K^+} / a_{H^+} vs. temperature (Fig. 3.12) or a_{Na^+} / a_{H^+} vs. temperature diagrams.

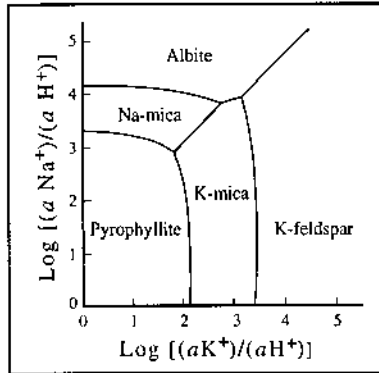


Figure 3.11. Schematic stability of silicate minerals in the system $K_2O - Na_2O - Al_2O_3 - SiO_2$ at $400^\circ C$ and 1 kb total pressure as a function of the activity ratios $a(K^+)/a(H^+)$ and $a(Na^+)/a(H^+)$ of a fluid in equilibrium with the phases (after Rose & Burt 1979).

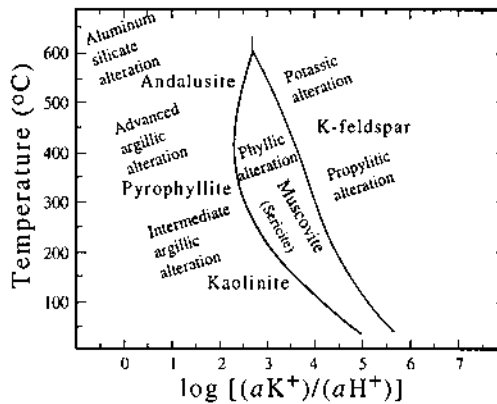


Figure 3.12. Stability of silicate minerals as a function of temperature and calculated $a(K^+)/a(H^+)$ ratio, based on experimental data in the system $K_2O - Al_2O_3 - SiO_2 - H_2O - HCl$ at 1 kb total pressure and saturated water vapor pressure above $100^\circ C$ (Montoya & Hemley 1975), and approximate correlation with alteration types in aluminosilicate rocks (see Table 3.4).

3.6.2. ALTERATION TYPES IN ALUMINOSILICATE ROCKS

A systematic classification of the alteration types, although desirable, is hindered by the great diversity of alteration processes and products. A simple classification scheme is to designate an alteration type by the most abundant or most obvious mineral in the altered rock: for example, sericitization, dolomitization, chloritization, silicification,

etc. Another is to use special names for altered rocks with characteristic mineral associations, such as greisen, skarn, and propylite. A third approach is to recognize the dominant chemical change during alteration, such as sodium metasomatism.

The modern approach to classifying alteration types in terms of mineral assemblages, first devised by Creasey (1959), has been developed to a large extent from many studies on porphyry copper deposits. One of the most widely used classification schemes based on mineral assemblages distinguishes five major types of alteration in aluminosilicate rocks (Meyer & Hemley 1967): *potassic*, *propylitic*, *phyllic* (sericitic), *intermediate argillic*, and *advanced argillic*. Typical mineral assemblages of these alteration types are shown in Figure 3.13 and their essential features are summarized in Table 3.4. It should be emphasized that these terms should be used on the basis of mineral assemblages, not abundance of minerals.

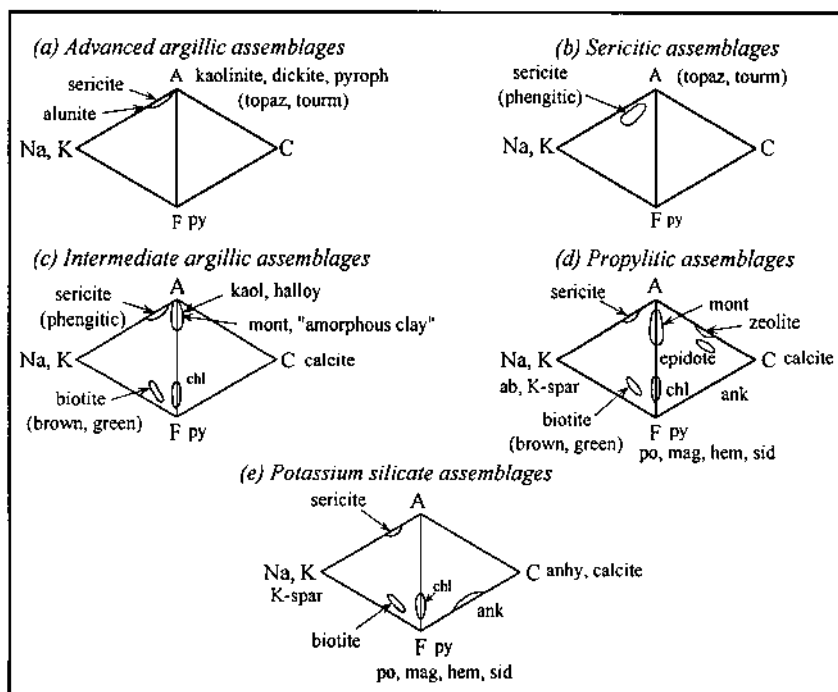


Figure 3.13. Mineral assemblages characteristic of major types of hydrothermal alteration in aluminosilicate rocks shown on ACF and AKF diagrams (after Meyer & Hemley 1967). Quartz is usually present. The minerals named on each diagram are the common phases of each type of alteration. Except for the zeolites, and to a lesser extent kaolinite, these have wide P - T ranges of formation. High-temperature equivalents of the aluminous argillic assemblages would be andalusite-bearing assemblages (Fig. 3.12). Abbreviations for mineral phases: ab = albite; anhy = anhydrite; ank = ankerite; chl = chlorite; dick = dickite; halloy = halloysite; hem = hematite; K-spar = K-feldspar; kaol = kaolinite; mag = magnetite; mont = montmorillonite; po = pyrrhotite; py = pyrite; pyroph = pyrophyllite; sid = siderite; tourm = tourmaline.

TABLE 3.4. Hydrothermal alteration characteristics of aluminosilicate rocks (after Meyer & Hemley 1967, Rose & Burt 1979)

Alteration type	Characteristics	Typical assemblages
Potassic	High K^+/H^+ , high temperature. Replacement of plagioclase by K-feldspar (felsic rocks). Biotization of mafic minerals (mafic rocks).	Quartz - K-feldspar - biotite \pm sericite \pm chlorite
Propylitic	High K^+/H^+ , low temperature. Lack of appreciable leaching or addition of alkali and alkaline earth elements. Replacement of plagioclase and mafic minerals by epidote, chlorite, and carbonates.	Chlorite - epidote \pm calcite (ankerite)
Phyllic (Sericitic)	Intermediate to high K^+/H^+ , high temperature. Plagioclase, K-feldspar, and mafic minerals converted to sericite (phengitic) and quartz. Veinlets of sericitic-quartz-pyrite very common.	Quartz - sericite - pyrite \pm chlorite \pm kaolinite
Intermediate Argillic	Low K^+/H^+ , low temperature. Unaltered K-feldspar (metastable). Significant alteration of plagioclase and mafic minerals to clay minerals (kaolinite, montmorillonite). Appreciable leaching of Ca, Na, and Mg.	Quartz - clay minerals (kaolinite, montmorillonite) sericite \pm chlorite \pm biotite
Advanced Argillic	Low K^+/H^+ , intermediate to high temperature. Complete alteration of feldspars and mafic minerals to clay minerals and Al-rich minerals (pyrophyllite, andalusite). Strong leaching of alkali and alkaline earth elements.	Quartz kaolinite - sericite \pm Al-rich silicate minerals

3.6.3. APPLICATIONS

Hydrothermal alteration patterns constitute an excellent guide for exploration of mineral deposits because of two main reasons. First, as will be discussed in more detail in later chapters, many types of deposits are associated with characteristic alteration patterns. Some examples are: a crudely concentric pattern of alteration types (potassic \Rightarrow phyllic \Rightarrow propylitic) in porphyry copper deposits (Lowell & Guilbert 1970); a pipelike chlorite-sericite alteration envelope in the footwall rocks of many volcanic-hosted massive sulfide deposits (Franklin et al. 1981); an alteration zone rich in Al-rich minerals (sericite, pyrophyllite, kyanite, topaz, kaolinite) adjacent to and stratigraphically below siliceous strata with gold mineralization (Worthington et al. 1980); and zoning of high-temperature calcium-rich silicates (garnet - clinopyroxene - wollastonite) in skarn deposits (Burt 1974). Second, in most cases the alteration is far more extensive and obvious than the associated ore mineralization. The occurrence of hydrothermal alteration does not guarantee a mineral deposit, but it certainly is an encouraging signal for a careful examination of the area. For example, in the Bergslagen area of Sweden, a regional potassium enrichment in felsic volcanic rocks,

presumably the result of seawater-rock interaction in a subsea-floor hydrothermal environment, is generally not associated with sulfide mineralization, but the occurrence of localized phyllic-potassic alteration systems superimposed on the regional potassium metasomatism may prove useful as exploration guides for base metal sulfide deposits in the area (Hellingwerf 1986).

The relationship between alteration and ore mineralization may be complex, requiring detailed mapping and laboratory studies for proper interpretation. In a classic study of the vein deposits of Butte, Montana (USA), Sales and Meyer (1948) demonstrated that all 'main-stage' ore-bearing veins are associated with the same sequence of alteration zones (sericitic - argillic - propylitic) in the host monzonite, a convincing evidence for their interpretation that the alteration zones formed contemporaneously with the ore and from the same fluid. A very different interpretation emerged from a detailed study of the lead-zinc-silver replacement vein deposits of the East Tintic district, Utah (USA), by Lovering (1949). He described five successive stages of hydrothermal alteration of the host rocks, with only the last two stages ("early productive" and "productive") being associated with sulfide mineralization.

Experimental and thermodynamic data on stability of alteration silicate minerals are extremely useful for determining the geochemistry of hydrothermal fluids. A few such relationships have been mentioned here, and a lot more is available in the published literature (e.g., Hemley et. al. 1969, Hemley et. al. 1971, Hemley et. al. 1980, Hemley et. al. 1984, Barton 1982, Reed 1997). A correlation between alteration and genetically related sulfide-oxide assemblages provides information about oxygen fugacity, sulfur fugacity, and pH of the hydrothermal fluid.

3.7. Zoning

Zoning refers to an orderly pattern of mineral or element distribution in space associated with an individual deposit or a group of deposits in a contiguous terrain. Mineral and compositional zoning are extremely common. In fact, most mineral deposits and mining districts show some form of zoning, although the pattern may be quite complicated owing to various reasons. The order of mineral zoning does not necessarily reflect the time sequence of mineral deposition (paragenesis).

3.7.1. SCALES AND PATTERNS OF ZONING

In terms of recognition and description, the two basic aspects of zoning are scale and pattern. Based on scale, zoning in mineral deposits may be divided into three intergradational categories (Guilbert & Park 1986):

- (a) Regional (or metallogenic) zoning, discernible from distribution of mineral deposits over a large tract of the crust;

- (b) District zoning, shown by a related group of deposits in a particular mineral or mining district;
- (c) Orebody (or deposit) zoning, localized in or around individual deposits.

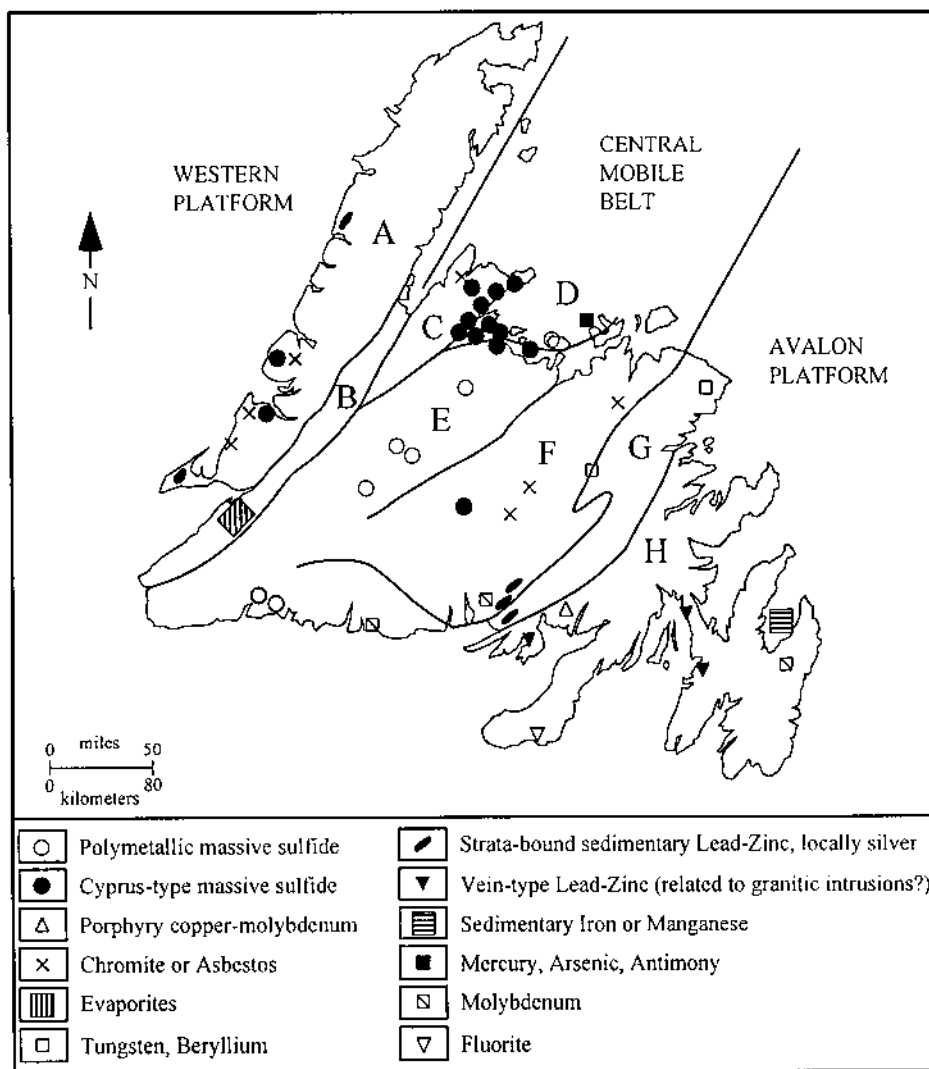


Figure 3.14. Distribution of important types of mineral deposits in relation to the tectonostratigraphic belts of Newfoundland, Canada (after Swinden & Strong 1976). Tectonostratigraphic belts (William et al. 1974): A = Lomond; B = Hampden; C = Fleur de Lys; D = Notre Dame; E = Exploits; F = Botwood; G = Gander; and H = Avalon.

Figure 3.14 shows an example of regional zoning, apparently related to the development of the tectonostratigraphic belts of Newfoundland, Canada (Swinden & Strong 1976). Similar examples have been described from other tectonic belts, such as the southern Appalachians of USA (Pardee & Park 1948, Swinden & Strong 1976), the North American Cordillera (Wolfhard & Ney 1976, Damon et al. 1981), the Andes (Sillitoe 1976), and the Tasman Geosyncline in Australia (Solomon et al. 1972). District zoning is common among porphyry-type (Cu-Mo) and granophile (Sn-W-Mo-U) deposits (Strong 1981) associated with granitic intrusions. A classic example of district zoning occurs in the Cornwall area of England (Hosking 1964, Jackson 1979), a simplified version of which, compiled from different veins in the district, is shown in Figure 3.15. The type of zoning in the Bingham district, USA (Fig. 3.16), is quite typical of porphyry copper systems. Orebody zoning is extremely variable; the zoning observed in the Rosebery sulfide deposit, Tasmania (Fig. 3.17), is typical of the volcanic-hosted Cu-Zn-Pb massive sulfide deposits.

<i>Veinstones or gangue minerals</i>	MINERAL ZONES	Thickness (feet)	Approximate temperatures of formation (°C)
	Zone of carbonates (Fe, Mn, etc)	400	up to 150
		200	
	Zone of sulfides of Pb and Ag, giving place at depth to Zn	1800	400
	Zone of sulfides of Cu intermixed with W and Sn for 700 feet	2500	500
	Zone of oxide of Sn with W in the upper parts	2500	550 to 575

Figure 3.15. Generalized scheme of vertical zoning in tin (-tungsten) deposits of the Cornwall district, southwestern England (after Park 1955). More elaborate zoning schemes are given in Hosking 1964, Jackson 1979, and Guilbert and Park 1986.

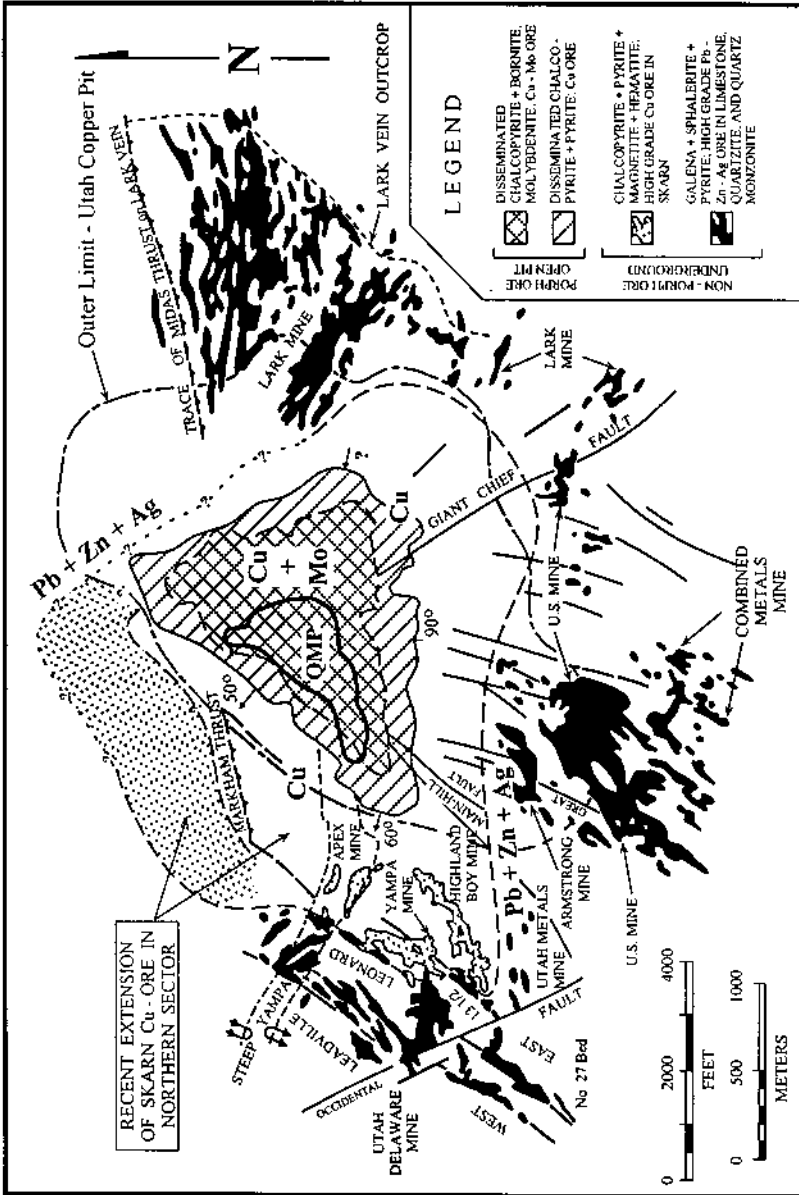


Figure 3.16. District zoning in the porphyry copper and associated skarn mineralization, Bingham district, Utah, USA (after Atkinson & Einaudi 1978). QMP = quartz monzonite porphyry.

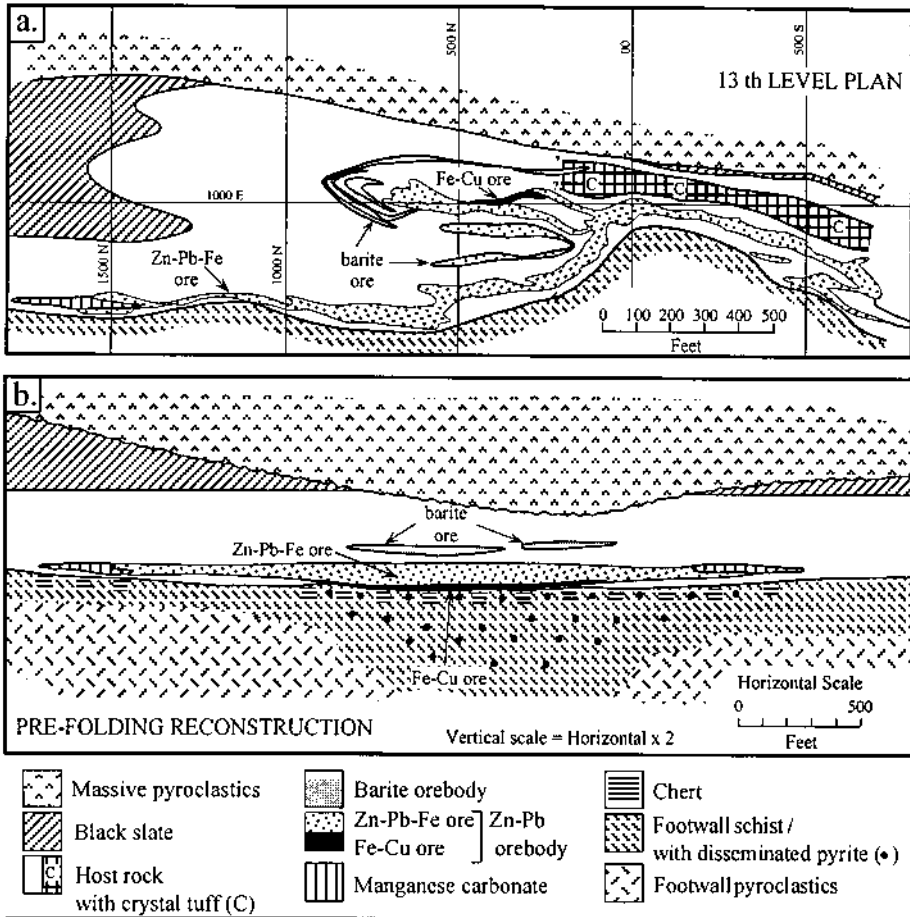


Figure 3.17. Zoning in the Rosebery Cu-Zn-Pb massive sulfide orebody, Tasmania, Australia (after Brathwaite 1974.): a. Geological plan of the Rosebery mine (13th level); b. Pre-folding reconstruction of the deposit (vertical section).

Mineral deposits formed by magmatic crystallization (e.g., Ni-Cu sulfide deposits in mafic-ultramafic complexes) may show zoning due to differentiation or post-crystallization equilibration. Sedimentary deposits, such as those of iron and manganese, are often zoned due to variations in the environment of deposition (Eh, pH, organic content, etc.). The most conspicuous zoning, however, is found in mineral deposits formed from hydrothermal fluids. The general patterns of zoning in some of the important types of hydrothermal deposit are summarized in Table 3.5, although significant variations exist within each type, as will be discussed in later chapters.

3.7.2. CAUSES OF ZONING IN HYDROTHERMAL DEPOSITS

A unifying model of zoning in hydrothermal deposits is yet to be developed. The earliest discussions attributed zoning in hydrothermal mineral deposits to cooling of ascending ore fluids and successive precipitation of increasingly soluble mineral phases (Spurr 1907, Emmons 1936). An assortment of variables and processes have since been invoked to explain zoning in different types of hydrothermal deposits. These include temperature and pressure (Blanchard 1947), heat of formation of the minerals (White 1945), relative volatility of the minerals (Brown 1948), free energies of formation of solute ions and complexes (Likhachev 1975), changes in the solvent composition (Spence & de Rosen-Spence 1975), electrode potential (Butler & Burbank 1929, Govett & Whitehead 1974), stabilities of metal-chloride complexes (Garrels 1941, White 1974) and metal-sulfide complexes (Barnes & Czamanske 1967), relative metal ion concentrations in the fluid (Taylor 1963), multiple pulses of fluids (Watanabe 1943, Derbikov & Nurav'yeva 1967), and fluid mixing (Sato 1973, Urabe 1974, Large 1977). The consistency of zoning patterns in the various types of mineral deposits (Table 3.5), however, has encouraged some workers to look for some simple and uniform chemical controls for zoning (Taylor 1963, Barnes 1975, Susak & Crerar 1982).

It is generally believed that zoning develops in response to the changing solubilities of ore constituents within a hydrothermal system. Taylor (1963) proposed that the mass-action effect (relative abundances of ore metals in the hydrothermal solution) is a major factor in fixing the order of sulfide mineral deposition, i.e., the metal sulfides precipitate in decreasing order of abundance of metals in the solution. From a review of the literature, Barnes (1975) concluded that the zoning in hydrothermal ore deposits are of two distinct types: $Fe \Rightarrow Ni \Rightarrow Sn \Rightarrow Cu \Rightarrow Zn \Rightarrow Pb \Rightarrow Ag \Rightarrow Au \Rightarrow Sb \Rightarrow Hg$ in syngenetic and epigenetic hydrothermal deposits; and $Cu \Rightarrow Ag \Rightarrow Pb \Rightarrow Zn$ in sedimentary (syngenetic) deposits. According to him, the relative stabilities of bisulfide-metal ion complexes predicted from thermodynamic calculations and experimental data, when corrected for the mass-action effect, precisely match the generalized zoning sequence of hydrothermal deposits, whereas zoning in sedimentary deposits is compatible with transport of metals as chloride-metal ion complexes. The problem with this explanation is that the current evidence is strongly in favor of transport of most metals in ore-forming fluids as chloride complexes (see Ch. 3).

A generalized treatment of mineral zoning in hydrothermal deposits is discussed by Susak and Crerar (1982). The approach emphasizes the role of different "zoning classes" of sulfides based on mineral stoichiometries and charge of the aqueous metal ion. In this formulation, the saturation concentration of a metal (Σm^o) in an aqueous fluid at a given temperature and pressure is a function of three terms — an environmental term (Q_E), a mineral term (Q_{min}), and a dissolved ion term (Q_{ion}) — which may be expressed by the relation:

$$\Sigma m^o = Q_E \cdot Q_{min} \cdot Q_{ion} \quad (3.24)$$

TABLE 3.5. Generalized pattern of metal zoning in selected types of hydrothermal mineral deposits

Type of deposit	Pattern of vertical (V) and lateral (L) zoning	References
Shale-hosted Cu-sulfide deposits	(L) Cu \Rightarrow Zn \Rightarrow Pb \Rightarrow Fe	Renfro (1974), Gustafson and Williams (1981)
Sediment-hosted Pb - Zn massive sulfide deposits	(L) Cu \Rightarrow Pb \Rightarrow Zn \Rightarrow (Ba) (V) Cu \Rightarrow Zn \Rightarrow Pb \Rightarrow (Ba)	Gustafson and Williams (1981), Large (1983)
Volcanic-hosted Cu - Zn \pm Pb massive sulfide deposits	(V) Fe + Cu \Rightarrow Zn + Pb \Rightarrow Ba	Stanton (1972), Large (1977)
Porphyry Cu - Mo systems	(L) Fe + Cu + Mo (porphyry) \Rightarrow Fe + Cu + Pb + Zn + Ag (skarn)	Einaudi (1982a)
Granophile deposits	(L) Sn + W + As + U \Rightarrow U + Ni Co \Rightarrow Pb + Zn + Ag \Rightarrow Fe + Sb	Strong (1981)

Deposition of a mineral would occur when the actual concentration of the corresponding metal (Σm) exceeds Σm^o . The higher the initial Σm and the closer it is to Σm^o , the earlier in the zoning sequence would that particular mineral occur; this is simply another way of expressing the mass-action effect discussed by Taylor (1963).

Large (1977) argued that the mass-action effect cannot explain the sequence of mineral precipitation in the volcanogenic massive sulfide deposits. Instead, he suggested that the zoning in this group of deposits can be best accounted for by the effects of temperature, pH, fO_2 , and ΣS on the solubility and stability of ore constituents in NaCl-rich ore-forming fluids. For example, he demonstrated that the zoning sequence in the Archean Cu-Zn massive sulfide ores can be rationalized from changes in temperature and fO_2 due to mixing of the exhalative hydrothermal fluid with seawater (Fig. 3.18).

3.7.3. APPLICATIONS

Recognition of mineral or element zoning is important for exploration and mining. Regional zoning helps to define broad exploration targets, district and orebody zoning aid in planning and evaluating exploratory drilling programs, and orebody zoning helps to plan grade control during mining.

Interpretation of the zoning associated with a mineral deposit is an integral part of its genetic interpretation, because the zoning sequences provide information on the changing composition of the ore-forming fluid as well on the fluctuating conditions of the depositional environment. As was pointed out Barnes (1975), no matter how attractive a theory of ore formation may be for other reasons, it is untenable unless the inferred ore fluid is capable of depositing the ore minerals in the observed zoning

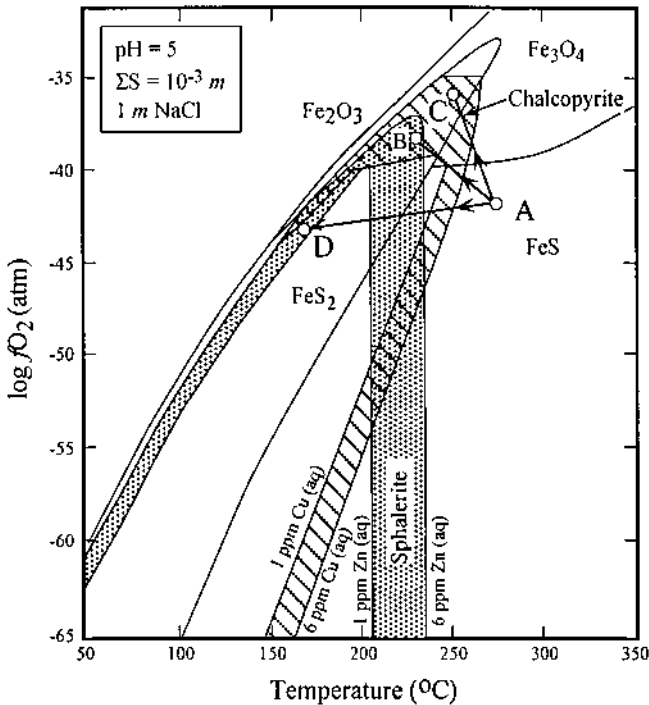


Figure 3.18. Family of mixing paths in fO_2 - T space to represent the observed sequential deposition and zoning in Archean volcanic-hosted Cu-Zn massive sulfides from a 1 m NaCl solution at $pH = 5$ with $\Sigma S = 10^{-3} m$ (after Large 1977). The mixing is with Archean seawater. The diagonally shaded area represents chalcopyrite deposition between 6 ppm and 1 ppm contours of soluble copper; the stippled area represents sphalerite deposition between 6 ppm and 1 ppm contours of soluble zinc. The expected zoning sequences for the various empirical mixing paths are: $A \Rightarrow B$ = pyrrhotite + chalcopyrite + magnetite (initial stage of mixing) \rightarrow sphalerite + pyrite (late stage of mixing); $A \Rightarrow C$ = chalcopyrite + pyrrhotite or magnetite \rightarrow chalcopyrite + pyrite (no sphalerite); $A \Rightarrow D$ = pyrrhotite + chalcopyrite \rightarrow sphalerite + pyrite. For the paths $A \Rightarrow B$ and $A \Rightarrow C$, no chalcopyrite will be precipitated in the pyrite field as the trends are toward increasing copper solubility. It appears that the Archean seawater was reducing enough to prevent the precipitation of sulfate gangue minerals.

sequences. The fact that the problem remains unresolved for many types of hydrothermal mineral deposits simply attests to our inadequate understanding of ore-forming fluids.

3.8. Fluid Inclusions

A fluid inclusion is a minute aliquot of fluid that was trapped inside a crystal at some stage of its history. On the basis of their origin, fluid inclusions may be classified as *primary*, *secondary*, or *pseudosecondary*. Primary inclusions result from fluids trapped

in growth irregularities during the growth of the surrounding host crystal. A crystal may be fractured one or more times after its formation and the fractures healed in the presence of fluids; fluids trapped in these fractures yield secondary inclusions. A crystal may contain secondary inclusions of several generations, each representing a different fluid. Pseudosecondary inclusions originate from trapping of fluid in a fracture that formed during the growth of the crystal; such inclusions show a distribution similar to that of secondary inclusions but are primary in terms of their age relative to the host crystal, although not necessarily of the same composition as the primary inclusions. Distinction among the three genetic types of fluid inclusions (and different generations of secondary inclusions) in a given sample is of fundamental importance in correlating the fluid inclusion data to geologic processes. The guidelines of Roedder (1984, p. 43-45) for genetic categorization of fluid inclusions are very useful, but the task is usually difficult and sometimes impossible.

Subsequent to its trapping, commonly as a homogeneous fluid at some elevated temperature, a fluid inclusion may undergo various physical changes (e.g., necking down to form several small inclusions, leakage) and phase transformations (e.g., separation into immiscible gas and liquid phases, crystallization of daughter minerals). The essence of most fluid inclusion studies is to interpret the characteristics of the original fluid from a set of cogenetic inclusions, mainly by retracing its path in P - T - X space. Evidently, this requires not only various measurements on the inclusions, such as temperatures of different phase transitions and volume ratios of the different phases, but also experimentally determined P - T - X data for the appropriate system. Most of the physical changes are irreversible, but they must be carefully considered in the evaluation of the P - T - X data obtained. The interpretation of fluid inclusion data is seldom an easy task, sometimes impossible due to various limitations, and always involves some reasonable assumptions. Nevertheless, it is a worthwhile effort considering that fluid inclusions, except for a few special situations, provide the only direct samples of fluids from which the host crystals grew or with which they have subsequently interacted. The minerals most suitable for fluid inclusion studies are sphalerite, fluorite, calcite, quartz, and barite; other minerals such as dolomite, scheelite, rhodochrosite, topaz, spodumene, and garnet may also contain measurable fluid inclusions.

3.8.1. PRINCIPLES

All fluid inclusion studies are based on five major assumptions (Roedder 1979b):

- (a) the inclusion fluid was trapped and sealed as a single, homogeneous phase;
- (b) the cavity in which the fluid is trapped has not changed in volume after sealing, either in nature or during heating-freezing experiments in the laboratory;
- (c) nothing has been added to or lost from the inclusion after sealing;
- (d) the origin of the inclusion (i.e., primary, pseudosecondary, or secondary) is

known; and

(e) the effects of pressure are either insignificant or known.

The appropriateness of these assumptions in a given study can usually be evaluated from the physical characteristics of the fluid inclusions and their behavior during freezing and heating experiments. Cases in which one or more of the above assumptions are not satisfied may yield misleading results, unless the deviations are known (or can be estimated) and their effects given appropriate consideration.

A set of fluid inclusions represents only a minuscule fraction of the fluid that was present in the system, yet a careful study of the inclusions can provide a wealth of information about the system (Roedder 1984):

(a) Temperature. A fluid inclusion at surface temperature usually consists of some combination of gaseous, liquid, and solid phases (Fig. 3.19). If the fluid trapped was homogeneous, heating of the inclusion results in filling the cavity with a single homogeneous fluid at some temperature, called the *homogenization temperature* (T_h). The homogenization temperature, the basis of fluid inclusion geothermometry, is normally a minimum value for the *trapping temperature* (T_t), the temperature at the time of trapping of the inclusion. Obtaining the temperature of trapping generally involves a correction based on some independent evidence (e.g. depth of cover) for the pressure of the environment at the time of trapping. This so-called pressure correction is small ($<25^\circ\text{C}$) for low-temperature deposits formed from dense,

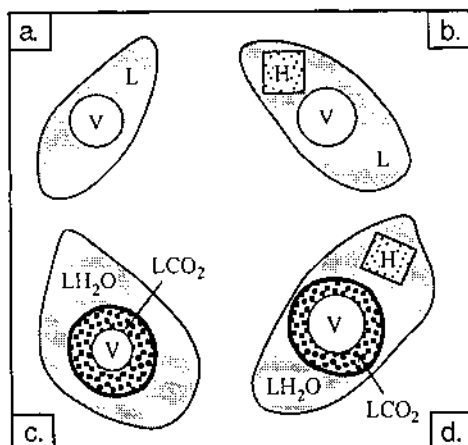


Figure 3.19. Sketches of some common types of fluid inclusions at room temperatures: a. two-phase (L + V) aqueous inclusion; b. three-phase (L + V + H) aqueous inclusion; c. CO_2 -bearing inclusion ($\text{LCO}_2 + \text{V} + \text{LH}_2\text{O}$); d. CO_2 -bearing inclusion with salt crystals ($\text{LCO}_2 + \text{V} + \text{LH}_2\text{O} + \text{H}$). Abbreviations: L = liquid; V = vapor; H = halite.

strongly saline brines at shallow depths but can be considerable ($>300^{\circ}\text{C}$) for high-temperature deposits formed from low-salinity fluids at depths greater than 10 km. Silicate melts are relatively incompressible, so there is little need for a pressure correction to be applied to homogenization temperatures of silicate melt inclusions in minerals.

- (b) Pressure. Some fluid inclusions are suitable for determining the *trapping pressure* (P_t), the pressure of the environment at the time of fluid entrapment (Roedder & Bodnar 1980). Procedures for pressure estimation require data on the composition of the fluid phase (or phases) trapped, and the phase behavior and P - V - T - X properties of that composition in the range involved. In most cases, only the minimum or maximum pressure can be estimated.
- (c) Density. The density of the fluid can be calculated from the composition (salinity), volume, and density of each phase (liquid, gas, and crystals) now present in a set of cogenetic fluid inclusions. A useful method for determining fluid inclusion volumes is discussed by Bodnar (1983). Estimated ore fluid densities range from $<0.2 \text{ g/cm}^3$ (essentially high-pressure, high-density steam) to 1.5 g/cm^3 for highly saline brines, but mostly lie close to 1.0 g/cm^3 , similar to that of the surrounding groundwater. The relative density of a hydrothermal fluid is a factor in controlling its rate and direction of flow.
- (d) Composition. The extremely small sizes of fluid inclusions (usually $<30 \mu\text{m}$ in diameter), their tiny masses (typically only about 10^{-11} grams), and the very low concentration levels of most of the solutes in the fluids (in the ppm and ppb range) are major problems in obtaining accurate chemical analyses of fluid inclusions. Often, only semiquantitative or qualitative analysis is possible. Fluid extracted from a sample of the host mineral (bulk extraction) can be analyzed by standard techniques (atomic absorption, gas chromatography, gas mass spectrometry, neutron activation, etc.), but the results may not be meaningful if the sample contains inclusions of different generations. A crushing stage can be very useful in the detection of even small amounts of gases in inclusions. Quantitative to semiquantitative analyses of volatile species of individual inclusions are possible with laser Raman microprobe (e.g., Pasteris et al. 1986), or with mass spectrometer after thermal decrepitation (Barker & Smith 1986, Leach et al. 1987). A method consisting of thermal decrepitation and energy-dispersive analysis of the precipitate (Haynes et al. 1987) appears promising for quantitative determination of the dissolved salts in individual inclusions of different generations. Other methods potentially applicable to the analysis of individual inclusions include Fourier transform infrared spectroscopy (FTIR), UV fluorescence spectroscopy (UVFS), laser ablation inductively coupled plasma mass spectrometry (ICP-MS), scanning electron microprobe (SEM), proton-induced X-ray emission (PIXE) and proton-

induced gamma-ray emission (PIGE), synchrotron X-ray fluorescence (SXRF), micro-laser Raman spectroscopy, secondary ion mass spectrometry (SIMS), and super-high-resolution ion microprobe (SHRIMP). A recent article by Shepherd and Rankin (1998) presents an informative discussion of the advantages and limitations of various techniques available for analysis of fluid inclusions. Most commonly, however, the composition of a set of cogenetic fluid inclusions is evaluated from microthermometric measurements, which permit an estimation of the salinity (total dissolved salts) of the fluid.

- (e) Isotope Ratios. More commonly fluid inclusion waters have been analyzed either for oxygen isotope ratios (e.g., Rye & O'Neil 1968) or for hydrogen isotope ratios (e.g., Ohmoto & Rye 1974), but it is also possible to measure both ratios simultaneously in the same sample (Knauth & Beeunas 1986, Gray et al. 1987). Fluid inclusion waters can also be analyzed for strontium isotope ratios (Shepherd & Darbyshire 1981, Norman & Landis 1983, Medford et al. 1983, Changkakoti et al. 1988).

The practical and interpretative aspects of fluid inclusion study are quite involved, as discussed in Hollister and Crawford (1981) and more recently by Roedder (1984). The basic principles, however, can be illustrated by considering NaCl-containing aqueous inclusions, which are one of the most common kinds of fluid inclusions encountered in mineral deposits. First, consider the heating-cooling behavior of inclusions of pure water (Fig. 3.20). Suppose homogeneous liquid water (LH_2O) was trapped in a crystal at 250°C and 620 bars (point *A*). Assuming no change in the mass or volume of such an inclusion during cooling, it would cool along the 0.85 isochore (line of constant density) as a homogeneous liquid phase until point *B* on the liquid-vapor univariant curve. At point *B* it would become a two-phase (liquid + vapor) inclusion with separation of a vapor bubble. Further cooling along the liquid-vapor curve to the temperature of observation results in a gradual increase in the size of the vapor bubble. When the inclusion is heated on a heating-cooling stage, the inclusion would reverse its path and homogenize to a liquid phase at point *B* giving a homogenization temperature (T_h) of about 212°C, the minimum estimate of its trapping temperature (T_t). Further heating would drive the liquid along the 0.85 isochore toward point *A*. The actual trapping temperature can be determined only if the trapping pressure is known from another source, for example, the depth of overburden. Conversely, the trapping pressure can be estimated if an independent estimate of trapping temperature is available from some other technique of geothermometry. In the special case where the inclusions were trapped from a boiling fluid (point *B* in Fig. 3.20 for a fluid of density 0.85), the homogenization temperature is the same as the trapping temperature and the corresponding pressure (P_h) is the trapping pressure. The same principles apply to a NaCl-containing aqueous fluid, but the liquid-vapor curve and isochores are different for each specific fluid composition (Fig. 3.21).

The use of microthermometry in estimating the composition of NaCl-containing

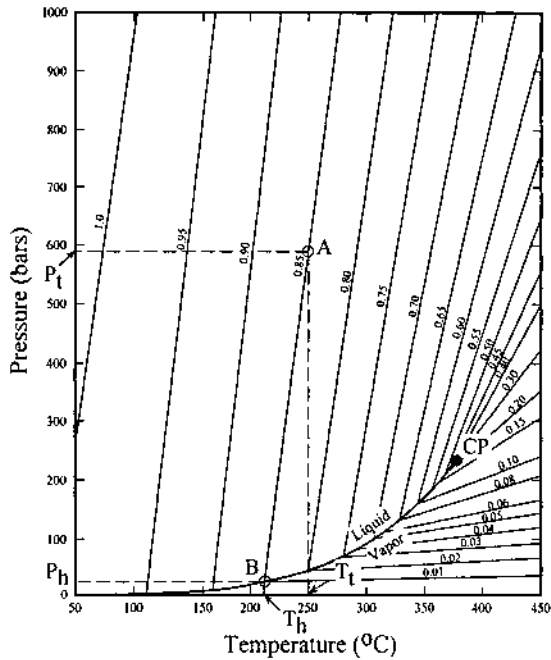


Figure 3.20. Pressure-temperature diagram for a portion of the H_2O system with isochores (in g/cm^3) (after Crawford 1981). Abbreviations: CP = critical point of water; T_h = homogenization temperature; T_t = trapping temperature; P_h = internal pressure at homogenization; P_t = trapping pressure. An inclusion A of density $0.85 \text{ g}/\text{cm}^3$ trapped at temperature T_t and pressure P_t would homogenize at B (T_h, P_h) provided there was no change in the mass or volume of the inclusion subsequent to its trapping.

aqueous inclusions is illustrated with the help of a T - X diagram for the NaCl - H_2O system (Fig. 3.22). If a 10 wt% NaCl solution is cooled from room temperature (point C), it would follow the path $C \Rightarrow D$ (first appearance of ice crystals) $\Rightarrow E$ (crystallization of an eutectic mixture of ice and hydrohalite, $\text{NaCl} \cdot 2\text{H}_2\text{O}$), and the temperature of phase transition at point D should give the NaCl content of the fluid. However, as nucleation of phases often requires considerable undercooling, phase transition temperatures are recorded more accurately during heating rather than cooling runs. In actual practice, the inclusion is cooled to a frozen state and the phase transition temperatures corresponding to the points E , first melting of ice crystals (T_c), and D , final melting of ice crystals (T_m), are recorded during the heating. The salinity of the fluid (wt% NaCl), then, is determined either graphically from the NaCl - H_2O phase diagram (Fig. 3.22) or, more conveniently, calculated from the freezing point depression of ice (θ) using the following equation (Bodnar 1993):

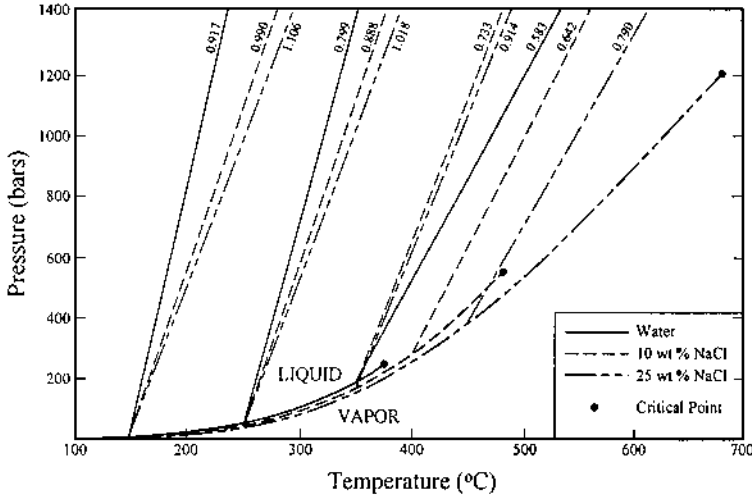


Figure 3.21. Liquid-vapor curves and several isochores for H₂O and 10 and 25 wt% NaCl solutions compiled from various sources (after Roedder & Bodnar 1980).

$$\text{Salinity (wt \% NaCl)} = - 1.78 T_m - 0.0442 T_m^2 - 0.000557 T_m^3 \quad (3.25)$$

Equation (3.25) is applicable to fluids containing less than 23.2 wt% NaCl. For fluid bulk compositions between 23.2 and 26.3 wt% NaCl, the final phase to melt is hydrohalite rather than ice and the equation for calculating salinity from final melting temperature (T_m) is (Bodnar 1993):

$$\text{Salinity (wt \% NaCl)} = 26.271 + 0.181 T_m + 0.002 T_m^2 \quad (3.26)$$

If the fluid inclusion contains a daughter crystal of halite at room temperature, the bulk salinity of the inclusion fluid should be more than 26.3 wt% NaCl. The bulk salinity of such an inclusion fluid may be determined by noting the dissolution temperature (in °C), the temperature at which the last bit of halite daughter crystal finally dissolves, and applying the equation (Sterner et al. 1988):

$$\begin{aligned} \text{Salinity (wt \% NaCl)} = & 26.242 + 0.4928 T_d + 1.42 T_d^2 - 0.223 T_d^3 \\ & + 0.04129 T_d^4 + 0.006295 T_d^5 - 0.001967 T_d^6 + 0.00011112 T_d^7 \end{aligned} \quad (3.27)$$

where T_d = halite dissolution temperature / 100

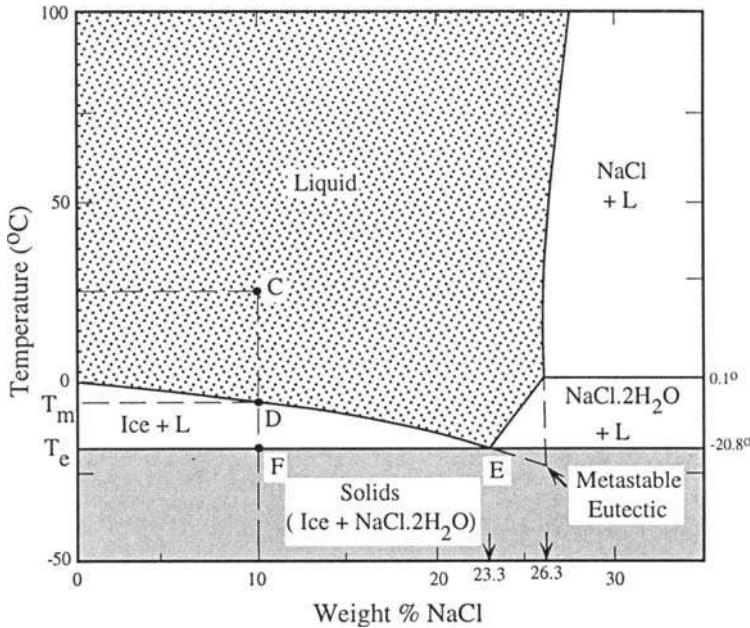


Figure 3.22. Temperature-composition diagram for a portion of the NaCl-H₂O system at 1 bar total pressure (after Crawford 1981). All phases coexist with vapor. *E* = eutectic (binary), *T_e* = eutectic temperature, *T_m* = temperature of final ice melting. See text for explanation.

A departure of the eutectic temperature (*T_e*) from its ideal value of -20.8°C for the NaCl-H₂O system would suggest the presence of other components (such as KCl, CaCl₂, MgCl₂) in the inclusion fluid (Crawford 1981), as commonly is the case. In such cases, the salinity of the fluid corresponding to the temperature *T_m* is expressed as 'wt% NaCl equivalent'. The final melting point of ice (*T_m*) is also affected by the amount of dissolved CO₂ in the aqueous solution (Collins 1979, Hedenquist & Henley 1985a).

3.8.2. APPLICATIONS

Study of fluid inclusions can provide valuable information on various aspects of the genesis of hydrothermal mineral deposits: characteristics of the hydrothermal fluids (salinity, solute composition, isotopic ratios) and their likely sources, directions of fluid migration, *P-T* environments of ore-gangue assemblages, and mechanisms of ore-gangue precipitation (mixing or boiling of fluids, cooling). Some generalized conclusions highlighting major contributions of fluid inclusion research to the understanding of hydrothermal mineral deposits are listed below.

- (a) Ore-forming fluids for all studied deposits are predominantly aqueous Na-K-Ca-Mg-Cl solutions (Table 3.6). CO₂ contents of the fluid inclusions are highly variable; significant concentrations have been found in some porphyry copper deposits and a variety of molybdenum, tin, tungsten, and uranium deposits. Available data on trace element concentrations in fluid inclusions are too sparse for generalization.
- (b) The ore-forming fluids are very diverse in terms of their salinity and formation temperature (Fig. 3.23). Salinity ranges from less than that of seawater for some epithermal vein deposits to more than 60 wt% NaCl equivalent for cores of some porphyry copper deposits characterized by boiling of the fluid. Formation temperatures range from less than 100°C for some carbonate-hosted lead-zinc deposits to about 700°C for some porphyry copper deposits. Many deposits show a decrease in fluid salinity and temperature for the late-stage minerals in the paragenetic sequence, probably reflecting a decay in the heat or fluid source, or mixing with meteoric water (Richardson & Pinckney 1984, Gratz & Misra 1987).
- (c) Mineral deposits have formed from a variety of fluids, the dominant component being magmatic water, seawater, meteoric water, or formation water (Table 3.6).
- (d) Boiling of ore fluids may have played a role in the genesis of some deposits, but it is not a necessary condition for ore deposition. In some cases, ore deposition was probably caused by mixing of fluids (Taylor et al. 1983a, Zimmermann & Kesler 1981). The lack of evidence for boiling may be useful in obtaining a minimum pressure estimate for ore deposition.

Fluid inclusion data are also useful for mineral exploration (Spooner 1981, Roedder & Bodnar 1997). Potential applications range from using vertical and lateral temperature gradients to predict likely localization of ores in a known district or identification of promising hydrothermal systems for a particular type of deposit to formulation of exploration strategies based on conceptual models constrained by the fluid inclusion data. High salinity and boiling are characteristic of inclusions in cores of porphyry copper deposits; fortunately, these inclusions are in quartz, which remains unaffected in gossans, leached outcrops, and soils (Nash 1976). Moore and Nash (1974) showed that the limits of occurrence of halite-bearing inclusions in the Bingham Canyon, Utah, porphyry copper deposit closely matched the limits of bornite mineralization in the deposit. Bodnar (1981) suggested that the presence of halite and, particularly, chalcopyrite daughter crystals in fluid inclusions and homogenization to vapor phase might constitute favorable criteria for porphyry copper mineralization and that the position within a porphyry copper system could be determined from the temporal relations of the various inclusion types. In epithermal gold-silver vein deposits with evidence for boiling of the ore fluid, the ore horizons are characterized by inclusions trapped from immiscible fluids that generally contain CO₂ and are quite different from the

TABLE 3.6. Nature of ore-forming fluids for selected types of hydrothermal mineral deposits as interpreted from fluid inclusion characteristics (after Spooner 1981, Roedder 1984)

Deposit type	Fluid inclusion characteristics*	Inferred nature of ore-forming fluids
Porphyry copper deposits	Very high T_h ($\approx 400^\circ\text{--}700^\circ\text{C}$) and salinities ($\approx 40\text{--}60$) for the cores (potassic alteration and strongest mineralization). Moderate T_h ($\approx 200^\circ\text{--}400^\circ\text{C}$) and salinities (typically <12) for the peripheral parts (vein-type mineralization and phyllic-argillic alteration). Evidence of boiling of fluids.	Predominantly magmatic fluid in the deeper parts of the system, diluted and cooled by mixing with other fluids in upper parts of the system. (Oxygen and hydrogen isotopic studies indicate the non-magmatic fluid to be meteoric water in some cases and seawater in others.) Pressure estimates from boiling suggest 1,800-3,000 m as depths of mineralization.
Ophiolite-hosted stockwork Cu-sulfide mineralization (Cyprus type)	Moderate T_h ($\approx 300^\circ\text{--}370^\circ\text{C}$) but low salinities (≈ 3) close to that of seawater. Evidence of boiling in some cases.	Convecting seawater, mixing with overlying seawater below the original ocean floor. Boiling at about 250 bars pressure corresponding to an original water depth of $\approx 2,500$ m.
Volcanic-associated Pb-Zn sulfide deposits of Japan (Kuroko-type)	Moderate T_h ($\approx 260^\circ\text{--}330^\circ\text{C}$) but low salinities for stockwork mineralization; somewhat lower T_h (typically $\approx 200^\circ\text{--}310^\circ\text{C}$, but may be as low as 130°C) and lower salinities ($\approx 2\text{--}8$) for overlying stratiform ore. No evidence of boiling.	Convecting seawater, probably with a magmatic component; mixing with seawater near the ocean floor. Lack of boiling suggests pressures corresponding to an original water depth of greater than $\approx 1,000\text{--}1,500$ m.
Carbonate-hosted Zn-Pb \pm barite \pm fluorite deposits (Mississippi Valley-type)	Low T_h ($\approx 80^\circ\text{--}150^\circ\text{C}$), in a few cases $> 200^\circ\text{C}$, but high salinities ($\approx 15\text{--}25$) for strata-bound mineralization. Rare occurrence of daughter crystals (despite high salinity). Ubiquitous presence of inclusions containing hydrocarbon liquid and gas. No evidence of boiling.	Highly saline (Cl $>$ Na $>$ Ca $>$ K $>$ Mg $>$ B), dense (density $> 1\text{ g/cm}^3$) formational waters (similar to oil-field brines). Evidence of mixing of two or more fluids in some deposits.
Epithermal vein-type deposits of Au \pm Ag \pm Cu \pm Pb \pm Zn	Moderate T_h ($\approx 200^\circ\text{--}330^\circ\text{C}$) and highly variable salinities (<1 to 12), some values being lower than the salinity of seawater and even approaching that of pure water. $T_h < 200^\circ\text{C}$ for late-stage carbonate-sulfate precipitation. Evidence of boiling in many, but not all, deposits.	Dominantly meteoric water similar to waters of active geothermal systems. (Isotopic evidence for significant to large component of magmatic fluids in some systems.) Depths of mineralization estimated at 500-1,500 m below the prevailing local water table.
Some W-Sn-base metal vein deposits associated with felsic igneous intrusions	Moderate T_h ($\approx 200^\circ\text{--}400^\circ\text{C}$) and salinities ($\approx 5\text{--}10$) for earlier stages of mineralization; lower T_h (usually $<200^\circ\text{C}$) and salinities (often <5) for later stages of mineralization. High temperature ($\approx 400^\circ\text{--}500^\circ\text{C}$) boiling and high salinity in some deposits.	Early fluids probably dominantly magmatic, later mixed with cooler and more dilute fluids (probably meteoric water as indicated by isotopic data in a few cases).
W-Mo skarn deposits	High T_h ($\approx 400^\circ\text{--}650^\circ\text{C}$) and variable salinities ($\approx 10\text{--}45$) for ore stages. Relatively low CO_2 content ($X_{\text{CO}_2} < 0.01$). Boiling only in the upper parts of the system.	Various mixtures of highly saline, originally magmatic fluids and later circulating groundwaters (corroborated by isotopic data in a few cases).

* Salinities expressed as wt% NaCl equivalent.

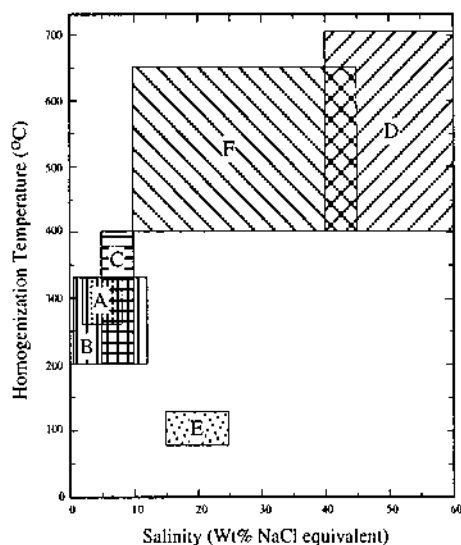


Figure 3.23. Typical ranges of homogenization temperature and salinity of ore-stage fluid inclusions from selected types of mineral deposits (after compilations by Spooner 1981 and Roedder 1984). The various fields: A = Stockworks of volcanogenic (Kuroko-type) Cu-Zn-Pb massive sulfide deposits; B = Epithermal An-Ag-Cu-Pb-Zn vein and replacement deposits; C = W-Sn-base metal vein deposits associated with igneous intrusions; D = Cores of porphyry copper deposits (potassic alteration and strongest mineralization); E = Mississippi Valley-type (carbonate-hosted) Zn-Pb-fluorite-barite deposits; F = W-Mo skarn deposits.

below the ore horizons (Buchanan 1979). Some other examples where fluid-inclusion characteristics have been successfully correlated with ore distribution include: lower CO_2 contents of fluid inclusions in the ore zone of the Pueblo Viejo gold-silver deposit, Dominican Republic, compared with peripheral barren jasperoids (Kesler et al. 1986); CH_4 - and N_2 -enriched fluid inclusions in shale-hosted auriferous quartz, compared with barren quartz veins, in the Dolgellau gold belt, North Wales, UK (Shepherd et al. 1991); and CO_2 -rich inclusions in ore veins of the Archean Hollinger-McIntyre gold deposit, Timmins, Canada, relative to inclusions in non-ore veins (Smith & Kesler 1985). Fluid inclusion data have played a major role in formulation of the hypothesis that ore fluids for carbonate-hosted lead-zinc deposits are connate brines, a hypothesis that largely governs the current exploration strategy for these deposits in North America, although fluid inclusions within the mineralized zones show almost no distinguishing characteristics that would aid the prediction of actual ore localization. Future exploration of unconformity-related uranium deposits may be significantly

influenced by the conclusion from fluid inclusion studies on the Rabbit Lake deposit (Canada) that the deposit is related to evolution of a sedimentary basin rather than to weathering associated with the overlying unconformity (Pagel 1977).

With additional *P-T-V-X* data on relevant synthetic systems and improvement in techniques for quantitative analysis of composition, fluid inclusion research is bound to assume even greater importance in the interpretation and exploration of mineral deposits.

3.9. Trace Element Distribution

Trace elements in mineral deposits occur mainly as: (a) mineral phases, forming discrete grains or intergrowth textures (inclusions, exsolved lamellae, etc.); (b) solid solution (substitutional or interstitial) components of minerals; and (c) adsorbed impurities on surfaces of the other minerals. A variety of analytical techniques (e.g., atomic absorption and emission, X-ray fluorescence, neutron activation, wet chemistry) are capable of yielding reliable analysis of trace elements in bulk samples, but trace element analysis of mineral phases remains a problem. Mineral separates can be handled by bulk chemical techniques, but the contamination due to unclean separation of a mineral from its matrix and intergrown phases may produce appreciable errors. The electron microprobe can be used for reliable analysis of trace elements only at higher concentration levels (generally above 100 ppm); other versions of the microprobe (laser, ion, proton) at various stages of development and operation in a few laboratories may alleviate this problem in the near future.

The trace element distributions in rocks are useful in determining their petrogenesis, discriminating between ore-associated barren rocks, and recognizing ancient hydrothermal systems. Determination of the environment in which the host and country rocks were formed is a critical aspect of ore genesis, especially for syngenetic deposits. Trace element data, considered in conjunction with other geologic information, may aid in such interpretation. Some examples include the use of immobile (e.g., Ti, Zr, Y, Nb) and rare-earth elements in basalt genesis (e.g., Schilling 1971, Pearce & Cann 1973, Floyd & Winchester 1975, Pearce & Gale 1977, Garcia 1978, Hanson 1980); of platinum group elements for discriminating ophiolites from other mafic-ultramafic complexes (e.g., Page et al. 1982); of elements such as Na, Sr, and Mn for reconstruction of paleoenvironments of carbonate rocks (e.g., Veizer et al. 1977, Brand & Veizer 1980, Pingitore 1978, Churnet & Misra 1981).

A variety of trace elements (Ba, Rb, Sr, Li, Th, Zr, Nb, Y, Ti, etc.), along with major elements, help to distinguish between calc-alkaline granites, with which porphyry copper and porphyry molybdenum deposits are associated, and alkaline to subalkaline granites, which host tin-uranium mineralization (Saunders et al. 1980, Beus & Grigorian 1977, Plant 1986). A useful geochemical indicator of hydrothermal mineralization associated with granites is the increased standard deviation of trace (and major) element contents (Bus & Grigorian 1977, Simpson et al. 1979). Indications of

hydrothermal activity due to mineralizing fluids may also be recognized in variation diagrams (e.g., Rb-Sr, Rb-Ba, K-Rb, Sr-Ba, and U-Th) involving large-ion lithophile (LIL) elements. These plots show relatively simple trends in rocks formed mainly by magmatic processes reflecting diadochic substitution, but they are dispersed and scattered in mineralized intrusions (Plant 1986).

Graf (1977) suggested that, because of their coherent and somewhat predictable geochemical properties, REE can serve as tracers of the alteration reactions in hydrothermal systems. He found that the REE patterns of massive sulfide deposits and associated rocks from the Bathurst-Newcastle district, New Brunswick (Canada), are consistent with the formation of the sulfides by precipitation from solutions that derived metals from host volcanic rocks by water-rock interactions. Leshner et al. (1985) proposed that, with certain limitations, the trace element (including REE) geochemistry of felsic metavolcanic rocks might aid in the selection of targets for base metal exploration in the Superior Province (Canada).

Many Phanerozoic strata-bound base metal sulfide deposits are characterized by primary manganese haloes (Russell 1974, Gray & Russell 1984, Gwosdz & Krebs 1977), and in Precambrian deposits such haloes appear to have survived metamorphism up to granulite facies with the manganese preferentially concentrated in garnet, pyroxene, and biotite (Stanton 1976a, Plimer 1977, Stumpfl 1979). Also, the association of manganese-rich sediments with modern spreading-center hydrothermal systems (Rona 1984) suggests that manganese distribution in sediments may aid in recognition of fossil hydrothermal systems and areas of potential sulfide mineralization. Thallium enrichment in modern ocean-ridge basalts and associated manganese crusts suggests that Tl-enriched country rock may occur around sulfide deposits in which seawater has acted as the ore fluid (McGoldrick et al. 1979). A regional survey of the element distribution may enable one to determine the source directions of the mineralizing fluids in a district (Baird & Dennen 1985).

A knowledge of the distribution of trace elements in a mineral deposit or orebody is obviously important for considerations of grade distribution, beneficiation, and metal extraction. As an interpretative tool, studies of trace elements in sulfides have pursued one or more of the following objectives (Loftus-Hills & Solomon 1967): (a) determination of temperature of deposition, (b) identification of metallogenic provinces, and (c) determination of environment of deposition. The geothermometric aspect of trace element partitioning between coexisting sulfide phases is discussed in Chapter 4. A metallogenic province, a particular region containing mineralization of a specific type or genetically related types, sometimes contains sulfides enriched in the same elements that have been concentrated to form mineral deposits in the province (Warren & Thompson 1945, Burnham 1959). Trace element distribution patterns may also help to distinguish mineral deposits formed in different metallogenic epochs.

Application of trace element studies to the interpretation of ore genesis is based on the premise that the trace element contents of sulfides reflect the composition of the fluids from which the sulfides crystallized. Thus, mineral deposits that formed from different fluids are likely to record corresponding differences in their trace element

composition. For example, Both (1973) documented significant differences in the trace element compositions of sphalerite (Fe, Mn, Cd, Co, and Cu) and galena (Ag, Sb, Sn, Bi, and Se) among the various Pb-Zn-Ag ore lenses of the Broken Hill Lode (N.S.W., Australia), and considered this observation as an evidence for origin of the sulfides by syngenetic accumulation rather than by hydrothermal replacement. Nickel sulfide deposits of different origin may be discriminated by their Pd and Ir contents, especially by Ir, which is not easily transported by hydrothermal fluids. According to Keays et al. (1982), Pd and Ir contents of deposits of magmatic origin tend to be relatively high and bear a consistent relationship with the Pd and Ir contents of the host rocks; deposits of hydrothermal origin are characterized by lower Pd and much lower Ir.

3.9.1. SULFUR:SELENIUM RATIO

Sulfur and selenium, being neighbors in the periodic table of elements, are closely related in chemistry and crystal chemistry. The selenium content of rocks is generally less than 1 ppm, much lower than that of sulfur (Table 3.7). With sufficient local concentration, selenium may form selenides such as clausthalite (PbSe) and tiemannite (HgSe); more commonly, however, the small amount of available selenium enters the sulfide minerals substituting for sulfur. The selenium content of a hydrothermal sulfide minerals is controlled by the ΣSe , ΣS , temperature, pH, and $f\text{O}_2$ of the hydrothermal fluid (Yamamoto 1976).

Because of their geochemical coherence, selenium follows sulfur in the magmatic cycle, but sedimentary processes cause a differentiation between the two elements because of the lesser mobility of selenium (Stanton 1972). Compared with the selenides, sulfides oxidize more readily under weathering conditions and are removed as sulfates in solution. Much of the selenate that is formed during weathering and transported in solution is precipitated out as selenides when the transporting medium encounters a slightly less oxidizing environment. The small amount of selenium that ultimately reaches the ocean is mostly precipitated in organic sediments (reduced environment). Thus, the S:Se ratio of seawater is very high (about 232,000:1 by weight) compared with an average 6,000:1 for igneous rocks and about 4,000:1 for shales, the richest in Se among sedimentary rocks (Goldschmidt 1954).

The marked difference in the S:Se ratios of igneous and sedimentary environments suggests that this ratio in sulfides should be useful for discriminating between certain environments of ore deposition. The results of such studies, however, have not been too encouraging because the S:Se ratios of sulfides depend also on the S:Se ratios of the source rocks. For example, Edwards and Carlos (1954) found that although the S:Se ratios of magmatic-hydrothermal pyrites in some Australian sulfide deposits were generally lower (<15,000) compared with pyrites of sedimentary origin (>30,000), high ratios did not necessarily prove a sedimentary origin, because some pyrites of high S:Se ratios were of magmatic origin. Also, pyrite precipitated from non-igneous hydrothermal solutions, such as the pyrite in the uranium ores of the Colorado Plateau (USA), can be quite high in selenium (up to 3 wt% Se; Coleman & Delevaux 1957).

TABLE 3.7. Average contents (in ppm) of cobalt, nickel, sulfur, and selenium in selected crustal rocks (Turekian & Wedepohl 1961)

	Co	Ni	Co:Ni	S	Se	S:Se
Igneous rocks						
Ultramafic	150	2000	0.075	300	0.05	6000
Basaltic	48	130	0.369	300	0.05	6000
Granitic (high Ca)	7	15	0.467	300	0.05	6000
Granitic (low Ca)	1	4.5	0.222	300	0.05	6000
Syenite	1	4	0.250	300	0.05	6000
Sedimentary rocks						
Shale	19	68	0.279	2400	0.60	4000
Sandstone	0.3	2	0.150	240	0.05	4800
Carbonate	0.1	20	0.005	1200	0.08	15000
Deep-sea sediments						
Carbonate	7	30	0.233	1300	0.17	7647
Clay	74	225	0.329	1300	0.17	7647

From a survey of available data, Stanton (1972) concluded that most sulfides of undoubted igneous affiliation have S:Se ratios of less than 20,000, whereas most sulfides deposited as marine sediments usually have S:Se ratios of more than 100,000, but there are too many exceptions to this generalization for the S:Se ratios to be considered a reliable discriminator of sulfide origin.

3.9.2. COBALT:NICKEL RATIO

Cobalt has a lower abundance than nickel in most natural environments. The Co:Ni ratio is about 0.07 in ultramafic rocks (Table 3.7) but may be as high as about 2.0 in silica-rich differentiates (Davidson 1962). The trend of increase in the Co:Ni ratio by magmatic differentiation is due to the fact that nickel is incorporated in the ferromagnesian minerals more readily than cobalt. The cobalt and nickel contents of magmatic and magmatic-hydrothermal sulfides are determined by their crystal structure, temperature, and availability of the elements at the time of sulfide crystallization. For example, the trace element data presented by Hawley & Nichol (1959) suggest that the Co:Ni ratios of pyrite are lower in the Sudbury nickel sulfide ores (about 10) compared with those in the base metal sulfide ores (12-40) of the Noranda district (Canada); pyrrhotite and chalcopyrite in these two groups of deposits show a similar trend, although the concentration levels of nickel and cobalt in them are different. The cobalt and nickel contents of sediments and sedimentary sulfides are also controlled by many variables (ΣCo , ΣNi , ΣFe , pH, Eh, organic content, etc.). Nevertheless, the Co:Ni ratio in sedimentary pyrite is usually low (Keith & Degens 1959), often less than 1, and in some areas containing both magmatic and magmatic-hydrothermal pyrites, the latter show much lower ratios (Roscoe 1965).

Analysis of pyrites from several mineral deposits in the Tasman Geosyncline (Australia) enabled Loftus-Hills and Solomon (1967) to distinguish three groups of pyrite: (a) those of sedimentary or diagenetic origin in shales (high Co and Ni, Co:Ni < 1); (b) those of probable volcanic origin without accompanying lead and zinc minerals (Co:Ni > 1); and (c) those of probable volcanic origin associated with lead and zinc minerals, and those with cassiterite or argentiferous galena related to granitic intrusions (low Co and Ni, Co:Ni < 1). From a detailed survey of the published literature, Price (1972) was able to establish a statistically significant difference among sedimentary (diagenetic and sedimentary exhalative), hydrothermal (replacement veins), and massive sulfide (volcanic exhalative) pyrites (Table 3.8). According to this study, the massive sulfide pyrites are characterized by a Co:Ni ratio between 5 and 50, and usually greater than 100 ppm Co and less than 100 ppm Ni; hydrothermal pyrites by a variable Co:Ni ratio (often less than 5), greater than 100 ppm Co and Ni; and sedimentary pyrites by a much lower Co:Ni ratio (typically <1). Bralía et al. (1979) confirmed this basis of distinction between massive sulfide and hydrothermal pyrites using additional data from the literature and from their own investigation of pyritic deposits in southern Tuscany (Italy). More recent studies employing Co:Ni ratios of pyrites for the interpretation of ore genesis include those of Xuexin (1984) and Bajwah et al. (1987). Approximate compositional fields (in terms of Co:Ni ratios) of pyrites from different types of deposits are presented in Figure 3.24.

TABLE 3.8. Geometric means (with logarithmic standard deviations in parenthesis) of cobalt and nickel contents (in ppm) and Co:Ni ratios of sedimentary, hydrothermal, and massive sulfide pyrites (Price, 1972)*

Type of pyrite	Co	Ni	Co:Ni
Syngenetic	41 (0.813)	65 (0.672)	0.63
Hydrothermal	141 (0.996)	121 (0.954)	1.17
Massive sulfide	486 (0.366)	56 (0.600)	8.70

* The differences between syngenetic and hydrothermal as well as between syngenetic and massive sulfide pyrites are statistically significant at 95% confidence level.

This empirical approach to ore genesis must be applied with extreme caution and never without regard to local and regional geology. Co:Ni ratios of sedimentary pyrites show a strong correlation ($r = 0.93$) with those of the host rocks; thus, cobalt and nickel concentrations in sedimentary pyrites are at least partly controlled by their concentration in adjacent sediments (Price 1972). Metamorphism may significantly alter the Co:Ni ratios of pyrites (Cambel & Jarkovsky 1968, Itoh 1971a & 1971b, Allison & Misra 1984) and lead to misinterpretation of their primary genesis.

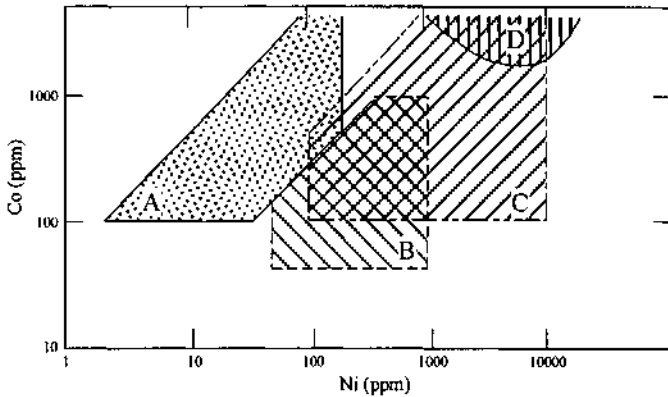


Figure 3.24. Approximate compositional fields (in terms of Co:Ni ratios) of pyrites from different types of deposits: A. Massive (volcanic exhalative) sulfide deposits; B. Hydrothermal gold-vein deposits; C. Hydrothermal tin-molybdenum-tungsten vein deposits; and D. Magmatic segregation deposits. Co:Ni ratios of sedimentary pyrites are highly variable, but typically less than unity. Sources of data: Campbell & Ethier (1984) for magmatic segregation deposits; Price (1972) for others.

Moreover, the Co:Ni ratios of pyrites from some apparently unmetamorphosed deposits are either inconsistent with their origin inferred from other lines of evidence or inconclusive (Mercer 1976, Campbell & Ethier 1984).

3.10. Recommended Reading

Ore Mineralogy: Stanton (1972, p.61-93).

Textures: Bastin (1950), Schwartz (1951), Ramdohr (1980, p.82-182).

Stability Relations: Barton and Skinner (1979), Holland and Malinin (1979).

Hydrothermal Alteration: Meyer and Hemley (1967), Rose and Burt (1979).

Zoning: Susak and Crear (1982), Guilbert and Park (1985, p. 217-245).

Fluid Inclusions: Crawford (1981), Spooner (1981), Shepherd and Rankin (1998).

Trace Element Distribution: Loftus-Hills and Solomon (1967), Bralía et al. (1979).

CHAPTER 4

INTERPRETATION OF MINERAL DEPOSITS - II

4.1. Stable Isotopes

The application of stable isotope ratios ($^{18}\text{O}/^{16}\text{O}$, D/H, $^{34}\text{S}/^{32}\text{S}$ and $^{13}\text{C}/^{12}\text{C}$) to the characterization, interpretation, and exploration of hydrothermal mineral deposits is one of the major recent advances in the field of economic geology. As has been emphasized by Ohmoto (1986), isotopic data by themselves do not provide unique answers to any geological problem, because similar isotopic characteristics in a mineral deposit may be produced by different processes and the same general process may produce dissimilar isotopic characteristics under different conditions. However, isotopic data, complemented by relevant geologic, mineralogic, and geochemical studies, can provide information on several aspects of ore genesis:

- (a) temperatures of formation of ore and gangue minerals (stable isotope geothermometry);
- (b) origin and evolution of ore-forming fluids;
- (c) characteristics of ore-forming fluids, such as $f\text{O}_2$, pH, sulfate:sulfide ratio, $\text{CO}_2:\text{CH}_4$ ratio, etc.;
- (d) sources of ore constituents, especially sulfur and carbon; and
- (e) mechanisms of ore precipitation.

Some isotopes are more suitable than others for the interpretation of one or more aspects of ore genesis listed above. For example, oxygen and hydrogen isotopes are particularly suitable for providing information on the source of hydrothermal fluids and their subsequent interaction with the rocks, sulfur isotopes for geothermometry, and sulfur and carbon isotopes for characteristics of ore-forming fluids and mechanisms of ore precipitation. A comprehensive study of a mineral deposit should, therefore, include as many kinds of stable isotope data as applicable.

4.1.1. THE δ NOTATION

The variations in stable isotope ratios in natural materials are caused by the slightly different chemical behavior of isotopes of the same element because of difference in the atomic mass (e.g., ^{18}O vs. ^{16}O). Because isotope ratios can be measured more precisely

and more easily than absolute abundances, the stable isotope abundances and variations are expressed in per mil (‰), relative to an appropriate calibration standard by a relative difference value, δ , which is defined as:

$$\delta = \frac{R_{\text{sample}} - R_{\text{standard}}}{R_{\text{standard}}} \times 10^3 \quad (4.1)$$

where R is the ratio of the heavy to the light isotope (e.g., $^{18}\text{O}/^{16}\text{O}$, D/H , $^{34}\text{S}/^{32}\text{S}$, or $^{13}\text{C}/^{12}\text{C}$) (Table 4.1). A positive value of δ means enrichment of the heavier isotope in the sample relative to the standard, a negative value relative depletion of the heavier isotope in the sample. For example, a sample with a $\delta^{18}\text{O}$ value of -10 is depleted in $^{18}\text{O}/^{16}\text{O}$ ratio by 10.0% (or 1%) relative to the standard.

Various working standards are used by different laboratories for the measurement of δ values, but to facilitate interlaboratory comparisons, the δ values are scaled to internationally accepted standards (Table 4.1). Troilite (FeS) from the Cañon Diablo iron meteorite is the standard used for reporting $\delta^{34}\text{S}$ values. The standard commonly used for reporting $\delta^{18}\text{O}$ and δD values is SMOW (Standard Mean Ocean Water), which was defined by Craig (1961) in terms of a National Bureau of Standards (USA) reference water, NBS-1, as follows:

$$(^{18}\text{O}/^{16}\text{O})_{\text{SMOW}} = 1.008 (^{18}\text{O}/^{16}\text{O})_{\text{NBS-1}} \quad (4.2)$$

$$(\text{D}/\text{H})_{\text{SMOW}} = 1.050 (\text{D}/\text{H})_{\text{NBS-1}} \quad (4.3)$$

A commonly employed silicate standard at present is NBS-28 quartz, which has $\delta^{18}\text{O} = +9.60\%$ on the SMOW scale. The universally employed reference standard for $\delta^{13}\text{C}$ values is the Chicago PDB standard (Belemnite from the Cretaceous Peedee Formation, South Carolina), which was the laboratory working standard used at the University of Chicago during the time that the oxygen isotope paleotemperature scale was developed. The original supply of this standard has been exhausted for a long time. The current working standard for carbon isotopes is a new carbonate reference standard, NBS-19, which is scaled as:

$$\delta^{13}\text{C}_{\text{NBS-19}} / \delta^{13}\text{C}_{\text{PDB}} = 1.95 \quad (4.4)$$

4.1.2. ISOTOPIC FRACTIONATION

The partitioning of isotopes of an element between two coexisting substances resulting in different isotopic ratios in the two substances is called *isotopic fractionation*. Isotopic fractionation occurs because certain thermodynamic and kinetic properties of molecules depend on the masses of the atoms of which they are composed. It can be shown from statistical mechanics that between coexisting molecules the heavier isotope

TABLE 4.1. Some definitions used in the study of stable isotope ratios (Rye & Ohmoto 1974, Taylor 1974, Faure 1986, Hoefs 1987)

(a) *Oxygen Isotopes*

Natural abundance (in air oxygen): $^{18}\text{O} : ^{17}\text{O} : ^{16}\text{O} = 0.1995 : 0.0375 : 99.763$

$$\delta^{18}\text{O}_i \text{ (per mil)} = \frac{(^{18}\text{O}/^{16}\text{O})_i - (^{18}\text{O}/^{16}\text{O})_{\text{standard}}}{(^{18}\text{O}/^{16}\text{O})_{\text{standard}}} \times 1,000$$

Standard: Standard Mean Ocean Water (SMOW):

$$(^{18}\text{O}/^{16}\text{O})_{\text{SMOW}} = 1.008 \times (^{18}\text{O}/^{16}\text{O})_{\text{NBS-1 Standard}}$$

(b) *Hydrogen Isotopes*

Natural abundance: $^2\text{D} : ^1\text{H} = 0.0156 : 99.9844$

$$\delta\text{D}_i \text{ (per mil)} = \frac{(\text{D}/\text{H})_i - (\text{D}/\text{H})_{\text{standard}}}{(\text{D}/\text{H})_{\text{standard}}} \times 1,000$$

Standard: Standard Mean Ocean Water (SMOW)

$$(\text{D}/\text{H})_{\text{SMOW}} = 1.050 \times (\text{D}/\text{H})_{\text{NBS-1 Standard}}$$

(c) *Sulfur Isotopes*

Natural terrestrial abundance: $^{36}\text{S} : ^{34}\text{S} : ^{33}\text{S} : ^{32}\text{S} = 0.02 : 4.21 : 0.75 : 95.02$

$$\delta^{34}\text{S}_i \text{ (per mil)} = \frac{(^{34}\text{S}/^{32}\text{S})_i - (^{34}\text{S}/^{32}\text{S})_{\text{standard}}}{(^{34}\text{S}/^{32}\text{S})_{\text{standard}}} \times 1,000$$

Standard: Troilite (FeS) of the Cañon Diablo meteorite:

$$(^{34}\text{S}/^{32}\text{S})_{\text{CDM}} = 0.0450045$$

(d) *Carbon Isotopes*

Natural terrestrial abundance: $^{13}\text{C} : ^{12}\text{C} = 1.11 : 98.89$

$$\delta^{13}\text{C}_i \text{ (per mil)} = \frac{(^{13}\text{C}/^{12}\text{C})_i - (^{13}\text{C}/^{12}\text{C})_{\text{standard}}}{(^{13}\text{C}/^{12}\text{C})_{\text{standard}}} \times 1,000$$

Standard: Chicago Standard (PDB):

$$(^{13}\text{C}/^{12}\text{C})_{\text{PDB}} = 0.0112372$$

(e) *Isotopic Fractionation Factor (α_{A-B}) for fractionation between phases A and B*

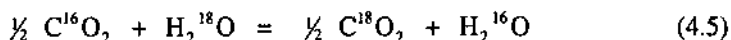
$$\alpha_{A-B} = R_A/R_B \quad [R = ^{18}\text{O}/^{16}\text{O} \text{ or } \text{D}/\text{H} \text{ or } ^{34}\text{S}/^{32}\text{S} \text{ or } ^{13}\text{C}/^{12}\text{C}]$$

$$1,000 \ln \alpha_{A-B} \equiv \delta_A - \delta_B = \Delta_{A-B}$$

is preferentially partitioned into the one in which it can form stronger bonds. For example, minerals such as quartz and calcite, in which oxygen is bound to small Si^{4+} or C^{4+} ions by covalent bonds, tend to incorporate a greater proportion of ^{18}O and thus characteristically have large positive values of $\delta^{18}\text{O}$. The main mechanisms for fractionation of stable isotopes are:

- (a) isotopic exchange reactions, which involve the redistribution of isotopes of an element among different molecules containing that element without any change in the chemical make-up of the reactants or products;
- (b) bacteriogenic reactions (e.g., bacterially mediated reduction of sulfate species to sulfide species); and
- (c) physical-chemical processes such as evaporation and condensation, melting and crystallization, adsorption and desorption, and diffusion of ions or molecules due to concentration or temperature gradients, in which mass differences come into play.

Effects of isotopic fractionation are generally evaluated as: (a) equilibrium isotopic effects, produced by equilibrium isotope exchange reactions, which are independent of the pathways or mechanisms involved in the achievement of equilibrium; and (b) kinetic isotopic effects, produced by unidirectional reactions (e.g., bacteriogenic generation of methane from organic matter, evaporation, etc.), which depend on reaction mechanisms and possible intermediate products. For ease of mathematical manipulations, isotope exchange reactions are usually written in such a way that only one atom is exchanged. For example, the oxygen isotope exchange between CO_2 and H_2O may be represented as

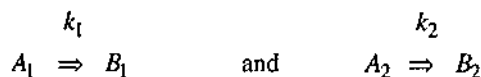


although such molecules actually do not exist in nature. The equilibrium constant (K) for this exchange reaction is written in terms of concentrations as

$$K = \frac{[\text{C}^{18}\text{O}_2]^{1/2} [\text{H}_2^{16}\text{O}]}{[\text{C}^{16}\text{O}_2]^{1/2} [\text{H}_2^{18}\text{O}]} \quad (4.6)$$

and calculated using methods of statistical mechanics. Concentrations are used rather than activities or fugacities because ratios of activity coefficients for isotopically substituted molecules are equal to unity (O'Neil 1986).

The instantaneous isotopic fractionation accompanying a unidirectional chemical reaction, where the rate of backward reaction is much slower than that of the forward reaction, can be considered in terms of rate constants for the reactions. For two competing isotopic reactions



the ratio of the rate constants, k_1/k_2 , is the *kinetic isotopic effect*. The isotopic fractionation in this case occurs because one isotopic species reacts more rapidly than the other. In general, the molecules containing the lighter isotope have the faster reaction rate because of the smaller bonding energy, so that the product tends to be enriched in the lighter isotope. The magnitude of kinetic isotopic fractionation is generally smaller than that of equilibrium fractionation and kinetic fractionation effects become smaller with increasing rates of overall reaction. The kinetic effect can also be calculated from statistical mechanics, although the calculations are usually not as precise because of a lack of detailed knowledge of the transition state. As will be elaborated later, the kinetic isotopic effect is particularly important for bacteria-mediated sulfur isotopic fractionation.

4.1.3. ISOTOPIC FRACTIONATION FACTOR

The isotopic fractionation between two coexisting species (*A* and *B*) in equilibrium is expressed as the *isotopic fractionation factor* (α_{A-B}), which is defined as

$$\alpha_{A-B} = R_A / R_B \quad (4.7)$$

where R_A is the ratio of heavy to light isotope in species *A* and R_B is the corresponding ratio in species *B*. Isotopic fractionation factor is analogous to distribution coefficient and is the most important quantity used in evaluating stable isotope variations observed in nature. If the isotopes are randomly distributed over all possible sites or positions in the species *A* and *B*, the fractionation factor (α) is related to the equilibrium constant (K) for the isotope exchange reaction by the relation

$$\alpha = K^{1/n} \quad (4.8)$$

where n is the number of atoms exchanged. Thus for the exchange reaction between CO_2 and H_2O (Eqn. 4.5), $K = \alpha$ (since $n = 1$), so that

$$K = \alpha = \frac{[^{18}\text{O}/^{16}\text{O}]_{\text{CO}_2}}{[^{18}\text{O}/^{16}\text{O}]_{\text{H}_2\text{O}}} \quad (4.9)$$

Values of α are normally very close to unity, typically of the form 1.00*X*. Commonly, isotopic fractions are discussed in terms of the value of *X*, in per mil. For example, the statement " $\text{CO}_2\text{-H}_2\text{O}$ fractionation is 0.0412 at 25°C" means that the

fractionation factor is 1.0412 and that CO_2 is enriched in ^{18}O by 41.2‰ relative to H_2O at 25°C. The fractionation factor may be less than unity in which case X will have a negative value.

The isotopic fractionation factor, like the equilibrium constant, is a function of temperature and generally approaches unity at increasing temperatures. The temperature dependence of α_{A-B} can usually be described by the relation $\ln \alpha_{A-B} \approx A + B/T^2$ at high T and by $\ln \alpha_{A-B} \approx A + B/T$ at low T , where A and B are constants and T is in Kelvin. As will be discussed later, the temperature dependence of isotopic fractionation factors is the basis of stable isotope geothermometry.

The experimental determination of the isotopic fractionation factor (α_{A-B}) is facilitated by the fact that it can be expressed conveniently in terms of δ_A and δ_B as shown below. From Equation 4.1,

$$\delta = \left(\frac{R_{\text{sample}}}{R_{\text{standard}}} - 1 \right) \times 10^3 \quad (4.10)$$

Substituting for R_A and R_B in Equation 4.7,

$$\ln \alpha_{A-B} = \ln \left(1 + \frac{\delta_A}{10^3} \right) - \ln \left(1 + \frac{\delta_B}{10^3} \right) \quad (4.11)$$

Using the approximation $10^3 \ln(1.00X) \approx X$, if $X \ll 1$, Equation 4.11 reduces to

$$10^3 \ln \alpha_{A-B} \approx \delta_A - \delta_B = \Delta_{A-B} \quad (4.12)$$

This approximation works very well for Δ_{A-B} values up to $\pm 10\%$ and reasonably well for values up to $\pm 40\%$, which cover almost all oxygen Δ values observed in geologic systems. For larger fractionations, as often is the case in the hydrogen system, the fractionation factors should be calculated using Equation 4.11. Experimentally determined fractionation factors between mineral pairs or mineral-fluid pairs yield smooth and often linear curves in a $1,000 \ln \alpha$ versus $1/T^2$ plot, commonly above 150°C. The recent review article by Campbell and Larson (1998) includes a useful compilation of oxygen, hydrogen, carbon, and sulfur isotope fractionation factors for some of the minerals and phases commonly used for ore deposit studies.

4.2. Sulfur Isotopes

4.2.1. PRINCIPLES

Typical ranges of sulfur isotopic composition in geologic systems are summarized in Figure 4.1. In general, sulfides in igneous rocks are isotopically similar to those in

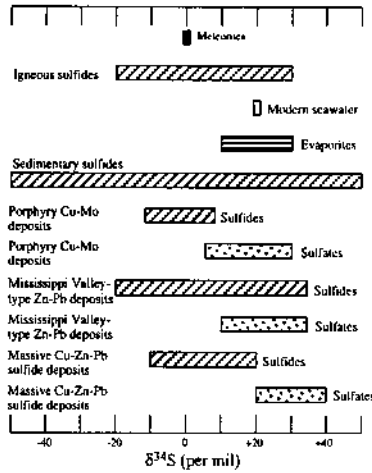


Figure 4.1. Typical ranges of $\delta^{34}\text{S}$ values (per mil) in geologic systems. (Sources of data: Thode 1970, Hoefs 1987, Ohmoto and Rye 1979, Field and Fife 1985.)

meteorites, with average $\delta^{34}\text{S}$ close to 0‰; sedimentary sulfates are enriched in ^{34}S ($\delta^{34}\text{S} = +10$ to $+30\%$); and sedimentary sulfides show a wide spread of $\delta^{34}\text{S}$ values (mostly in the range of $+50$ to -50%) but are typically depleted in ^{34}S . Considering that the mantle sulfur ($\delta^{34}\text{S} \approx 0\%$) is the ultimate source of all sulfur, the variation of $\delta^{34}\text{S}$ values in natural systems is a result of isotopic fractionation of recycled sulfur under different conditions.

It is unlikely that any significant isotopic fractionation takes place between sulfur in the mantle and lower crustal parental rocks and sulfur in the magma generated by partial melting, or between sulfur in such a magma and primary sulfide minerals that crystallize from it; i.e., $\delta^{34}\text{S}$ (magmatic sulfide) $\approx \delta^{34}\text{S}$ (magma) $\approx \delta^{34}\text{S}$ (parental rock) $\approx 0\%$ (Ohmoto & Rye 1979). Significant deviations in $\delta^{34}\text{S}$ values of magmatic sulfides are attributed to the assimilation of crustal sulfur by magmas. The $\delta^{34}\text{S}$ values in such cases depend on the isotopic composition of the assimilated sulfur and the process of assimilation (i.e., bulk assimilation or selective assimilation).

Sulfur in sedimentary and hydrothermal mineral deposits, which is commonly fixed as sulfide \pm sulfate minerals, has originated ultimately from (a) an igneous source (magmatic fluids and magmatic sulfur-bearing minerals), commonly with $\delta^{34}\text{S} \approx 0\%$, or (b) seawater sulfate (in connate water trapped in marine sediments and in meteoric water as sulfate dissolved from marine evaporites, which practically have the same $\delta^{34}\text{S}$ as the parent seawater) with an average $\delta^{34}\text{S} \approx 20\%$. In some early literature, interpretation of sulfur isotope ratios in mineral deposits was largely based on the distribution pattern of $\delta^{34}\text{S}$. Mineral deposits in which the sulfides showed a narrow range of $\delta^{34}\text{S}$ values with a mean close to 0‰, diagnostic of mantle-derived sulfur, were interpreted to have formed from magmatic fluids; mineral deposits in which the

sulfides showed a wide range but mostly negative $\delta^{34}\text{S}$ values were interpreted as being sedimentary and usually of biogenic origin, because at low temperatures bacterial reduction of sulfate is the most effective mechanism of ^{34}S depletion in the sulfides. An underlying assumption of this simplistic interpretation, that the minerals from a hydrothermal fluid accurately reflect the isotopic composition of the fluid, is not valid in all cases (Sakai 1968, Thode 1970, Kajiwara 1971, Ohmoto 1972). As was pointed out by Rye and Ohmoto (1974), sulfides precipitated from fluids with magmatic sulfur can exhibit a wide range of $\delta^{34}\text{S}$ values (e.g., Mogul base metal deposit, Ireland) whereas sulfides precipitated from fluids with nonmagmatic sulfur can have a modest range of $\delta^{34}\text{S}$ values near 0‰ (e.g., Kuroko massive sulfide deposits, Japan). The $\delta^{34}\text{S}$ value of magmatic fluids can be quite different from that of the magma depending on the temperature, $\text{SO}_2\text{:H}_2\text{S}$ ratio in the fluid (a function of the oxidation state of the fluid), and the relative masses of fluid and magma at the time of separation. The $\delta^{34}\text{S}$ value of fluids containing sulfur leached from magmatic minerals depends on the source of the sulfur (mantle or crustal). The $\delta^{34}\text{S}$ values of sulfide and sulfate minerals precipitated from such fluids vary according to the T - $f\text{O}_2$ conditions of precipitation as determined by the cooling path of the fluids (Ohmoto & Rye 1979).

Sulfur isotopic variations in hydrothermal systems are produced by two kinds of reactions: (a) various chemical exchange reactions, for example, between sulfate and sulfides and between sulfides; and (b) bacterial reduction of sulfate (SO_4^{2-}) to sulfide (H_2S). In the former case, isotopic fractionation may proceed while maintaining isotopic equilibrium among various sulfur-bearing species in fluids, melts, and minerals, or may proceed in a nonequilibrium manner; in the latter case, the fractionation is always unidirectional. Moreover, in either case fractionation may take place in closed or open system. Thus, a proper interpretation of the observed sulfur isotopic ratios in hydrothermal minerals requires a thorough understanding of the interrelationship among the various parameters that govern sulfur isotopic fractionation (Ohmoto 1972, Rye & Ohmoto 1974, Ohmoto & Rye 1979, Ohmoto 1986).

Equilibrium Systems

The $\delta^{34}\text{S}$ values of hydrothermal sulfide and sulfate minerals are controlled by many factors (Ohmoto, 1972, Rye & Ohmoto 1974): (a) temperature, the dominating factor in determining fractionation among given sulfur-bearing species in a closed system (Fig. 4.2); (b) the isotopic composition of sulfur in the ore fluid ($\delta^{34}\text{S}_{\text{ES}}$), which varies with the source of the fluid (Fig. 4.1); and (c) the ratio of oxidized (SO_4^{2-}) to reduced (H_2S) sulfur species in the solution which, in turn, is controlled by the temperature, pH, and $f\text{O}_2$ of the hydrothermal fluid. For hydrothermal mineral deposits involving equilibrium sulfur isotopic fractionation, the $\delta^{34}\text{S}$ values of minerals can be used to determine the $\delta^{34}\text{S}_{\text{ES}}$ value of the fluid and the source of sulfur only when the geochemical parameters (T , pH, $f\text{O}_2$) of the ore fluid are known. Conversely, if the value of the $\delta^{34}\text{S}_{\text{ES}}$ of the ore fluid is known, the sulfur isotopic composition of the minerals can be used to estimate other parameters (T , pH, $f\text{O}_2$) of the ore fluid.

Methods for estimating the $\delta^{34}\text{S}_{\Sigma\text{S}}$ of an ore-forming fluid are discussed by Ohmoto and Rye (1979), Ohmoto (1986), and Ohmoto and Goldhaber (1997). In most cases, the $\delta^{34}\text{S}_{\text{H}_2\text{S}}$ and $\delta^{34}\text{S}_{\Sigma\text{SO}_4}$ values of hydrothermal fluids responsible for the formation of sulfide-bearing and sulfate-bearing ore deposits, respectively, can be estimated by using the following approximations:

$$\delta^{34}\text{S}_{\text{H}_2\text{S}} \approx \delta^{34}\text{S}_{\text{sulfide minerals}} \quad \text{and} \quad \delta^{34}\text{S}_{\Sigma\text{SO}_4} \approx \delta^{34}\text{S}_{\text{sulfate minerals}}$$

At low temperatures (below $\approx 150^\circ\text{C}$), the H_2S and ΣSO_4 in the hydrothermal fluids can

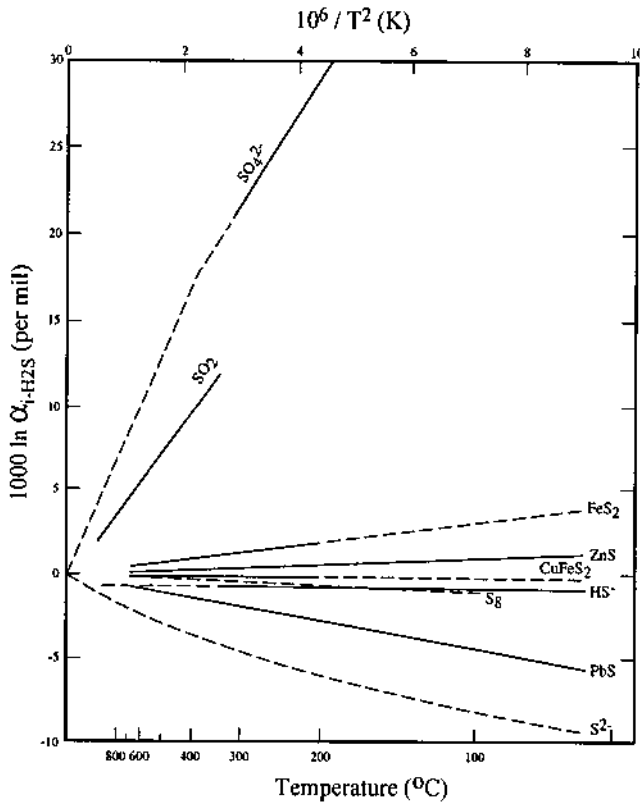


Figure 4.2 Experimentally determined (solid lines) and extrapolated or theoretically calculated (dashed lines) equilibrium sulfur isotopic fractionation factors (α) for various sulfur minerals and fluid species relative to H_2S as a function of temperature (after Ohmoto & Rye 1979). For small values of α , $1,000 \ln \alpha_{i-\text{H}_2\text{S}} \approx \delta^{34}\text{S}_i - \delta^{34}\text{S}_{\text{H}_2\text{S}}$.

be treated as nonreactive independent components, so that the $\delta^{34}\text{S}_{\text{H}_2\text{S}}$ value may directly indicate the source of the H_2S and the $\delta^{34}\text{S}_{\Sigma\text{SO}_4}$ value the source of ΣSO_4 .

However, this may not be the case in higher temperature fluids (greater than $\approx 200^\circ\text{C}$), where all sulfur species may be expected to be in equilibrium before arriving at depositional sites. In such cases, under certain simplifying assumptions, the $\delta^{34}\text{S}_{\Sigma\text{S}}$ of a fluid in an equilibrium system at a given temperature can be calculated from

$$\delta^{34}\text{S}_{\Sigma\text{S}} = \delta^{34}\text{S}_{\text{H}_2\text{S}} + \Delta_{\text{SO}_4\text{-H}_2\text{S}} [R / (1 + R)] \quad (4.13)$$

where $\Delta_{\text{SO}_4\text{-H}_2\text{S}} = 1,000 \ln \alpha_{\text{SO}_4\text{-H}_2\text{S}}$ and $R =$ the mole ratio $m_{\text{SO}_4}/m_{\text{H}_2\text{S}}$ in the fluid. At temperatures above about 350°C , where SO_2 rather than SO_4^{2-} becomes the dominant oxidized species, $\Delta_{\text{SO}_4\text{-H}_2\text{S}}$ in Equation 4.13 is substituted by $\Delta_{\text{SO}_2\text{-H}_2\text{S}}$ and R in Equation 4.15 by $m_{\text{SO}_2}/m_{\text{H}_2\text{S}}$ ratio. As a general rule, when $T < 500^\circ\text{C}$, $\text{pH} < 6$, and pyrrhotite occurs as a stable mineral, H_2S is the dominant sulfur species in the fluid (i.e., $R < 0.01$), and

$$\delta^{34}\text{S}_{\Sigma\text{S}} \approx \delta^{34}\text{S}_{\text{H}_2\text{S}} \quad (4.14)$$

On the other hand, when magnetite or hematite is a stable mineral, $R < 1$ (i.e., H_2S is not the dominant sulfur species in the fluid), and

$$\delta^{34}\text{S}_{\Sigma\text{S}} \approx \delta^{34}\text{S}_{\text{H}_2\text{S}} + \Delta_{\text{SO}_4\text{-H}_2\text{S}} \quad (4.15)$$

Nonequilibrium Systems

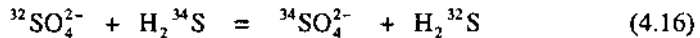
The $\delta^{34}\text{S}$ variation of hydrothermal sulfides in several mineral deposits that formed at temperatures in the range $350^\circ\text{-}200^\circ\text{C}$ can be explained in terms of the variation in the $\text{SO}_4^{2-}:\text{H}_2\text{S}$ ratio of the mineralizing fluid together with the assumption of isotopic equilibrium between the oxidized and reduced sulfur species in the fluid. In some other hydrothermal deposits formed under similar temperature conditions, the $\delta^{34}\text{S}$ values of sulfides appear to reflect nonequilibrium isotopic fractionation (Rye & Ohmoto 1974). Nonequilibrium isotopic fractionation between aqueous sulfates and sulfides may be the consequence of a variety of reasons, but a common one (particularly at temperatures $< 200^\circ\text{C}$) is the kinetic isotopic effect that occurs when one of the sulfur species is produced by oxidation or reduction, or when both species are produced from another compound, for example, by dissolution of pyrite (Ohmoto & Rye 1979).

An important source of H_2S for the precipitation of sulfides is seawater sulfate. The sulfate may be reduced to H_2S by thermochemical reduction, especially in the presence of organic reductants, or by organic reduction through the catalyzing action of sulfate-reducing bacteria. Available experimental data suggest that non-bacterial reduction of sulfates takes place at sufficiently high rates in laboratory at temperatures above about

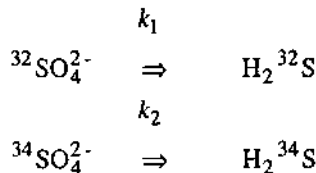
175°C, although it may occur at much lower temperatures ($\approx 80^\circ\text{C}$) (Powell & Macqueen 1984). Kinetic isotopic effect may produce H_2S (and, thus, sulfides) with a range of $\delta^{34}\text{S}$ values, but in a system closed to sulfide and sulfate complete thermochemical reduction will yield $\delta^{34}\text{S}_{\text{H}_2\text{S}}$ essentially identical to $\delta^{34}\text{S}_{\Sigma\text{SO}_4}$ (Ohmoto 1986). For example, the very positive $\delta^{34}\text{S}$ values of H_2S in many natural gas fields (about 20‰; Thode & Monster 1965) probably reflect the complete reduction of evaporite sulfate by organic matter at less than 200°C.

Fractionation of sulfur isotopes because of bacterial reduction of sulfate to sulfide species, perhaps the only effective mechanism of sulfate reduction at low temperatures ($< 50^\circ\text{C}$), is a nonequilibrium (unidirectional) process. Anaerobic bacteria such as *Desulfovibrio desulfuricans*, which live in oceanic and lake sediments, split oxygen from sulfate ions and excrete H_2S that is enriched in ^{32}S relative to the sulfate. In most marine sediments, H_2S (or HS^- , depending on pH) reacts with iron to form pyrite during early diagenesis when the sediments are still within about a meter of the seawater-sediment interface. Typically, only 15 to 45% of the total organic carbon in marine sediments is consumed in this sulfate reduction process (Berner 1985), which leads to a positive correlation between the amount of sulfide-sulfur and the residual organic carbon in marine sediments. If the observed S:C mass ratio in a sediment-hosted mineral deposit is much greater than 1, diagenetic sulfide precipitation may not be the only or even the dominant source of sulfur in the deposit.

The $\delta^{34}\text{S}$ distribution of biogenic H_2S and related sedimentary sulfides is controlled by (a) sulfur isotopic composition of the source (seawater), (b) the kinetics of the reduction process, and (c) whether the reduction occurs in a closed or open system with respect to SO_4^{2-} and H_2S . The sulfur isotopic exchange between sulfate and sulfide can be represented by the exchange reaction



The calculated theoretical value of the equilibrium constant (K) for this reaction is 1.075 at 25°C (Tudge & Thode 1950). Thus, if this exchange takes place, although no mechanism is yet known, it should lead to sulfides being depleted in ^{34}S by amounts up to 75‰ relative to sulfates (and sulfates being enriched in ^{34}S by amounts up to 75‰ relative to sulfides). For bacterial reduction process, however, the sulfate-sulfide exchange reaction should be represented by two separate reactions with different rate constants:



where k_1 and k_2 are the isotope rate constants so that the ratio k_1/k_2 (kinetic isotope effect) determines the extent of isotopic fractionation. A value of 1.024 for this ratio, as was determined by Harrison and Thode (1957), means that the H_2S produced at any instant should be enriched in ^{32}S , or depleted in ^{34}S , by 24‰ relative to the remaining SO_4^{2-} . Factors influencing the degree of bacterial fractionation are mainly those that affect the metabolic activity of the sulfate-reducing bacteria (e.g., temperature, light, availability of nutrients such as phosphate and nitrate) and sulfate concentration. A detailed discussion of the rate-controlling mechanisms of bacterial sulfate reduction is provided by Rees (1973). The ratio k_1/k_2 increases from 1.015-1.025 at relatively high rates of sulfate reduction to more than 1.065 at low rates of sulfate reduction (Goldhaber & Kaplan 1975). The latter value is close to the equilibrium value of 1.075 at 25°C. Thus, the kinetic isotope effects are small in sedimentary environments of slow rate of sulfate reduction.

The magnitude of bacterial sulfur isotope fractionation also depends on whether the sulfate-sulfide reduction occurs in an open system or in a closed system with respect to SO_4^{2-} and H_2S (Ohmoto & Rye 1979, Ohmoto & Goldhaber 1997). Most sedimentary systems can be considered as open to H_2S , because the H_2S produced by bacterial reduction escapes to the overlying oxygenated sediments and water column or is fixed as iron sulfides and organic sulfur that, as a first order approximation, may be considered nonreactive to SO_4^{2-} (Ohmoto & Goldhaber 1997). In a system open to SO_4^{2-} (e.g., an open marine basin), the rate of SO_4^{2-} reduction is much slower than the rate of SO_4^{2-} supply so that the sulfate content and isotopic composition ($\delta^{34}S_{H_2S}$, $\delta^{34}S_{\Sigma SO_4}$) of the basin water remain essentially constant, with a shift of the $\delta^{34}S_{H_2S}$ value from the $\delta^{34}S_{\Sigma SO_4}$ value by $\Delta_{SO_4-H_2S}$ (Eqn. 4.15). For example, assuming an average k_1/k_2 ratio of 1.025 and a $\delta^{34}S_{\Sigma SO_4}$ value of 20‰ for the basin water, bacterial isotopic fractionation will result in H_2S and precipitated pyrite of $\delta^{34}S = -5‰$. In a system closed to SO_4^{2-} (e.g., a barred shallow-marine basin), the rate of sulfate reduction exceeds that of sulfate supply, so the isotopic composition of the basin water cannot be maintained at a constant value, and all sulfate is eventually consumed within the system. Continued fractionation under closed condition would produce sulfates and sulfides of progressively higher $\delta^{34}S$, according to Rayleigh fractionation (as discussed in detail by Ohmoto and Goldhaber 1997), although the $\delta^{34}S$ of the total sulfide mass (i.e., bulk-rock sulfide) would tend to be identical to the $\delta^{34}S$ of the initial SO_4^{2-} . Thus, sulfides precipitated by such a batch process in a restricted basin by bacterial reduction of sulfate tend to be characterized by (a) a wide spread of $\delta^{34}S$ values that is skewed toward positive values and (b) a progressive increase in $\delta^{34}S$ values toward the stratigraphic top in a sedimentary sequence.

Evaluation of the sulfur isotope data from ancient bacteriogenic sulfide deposits requires a knowledge of the isotopic composition of the coeval seawater. As chemical precipitation by itself does not result in significant isotopic fractionation, the isotopic

composition of ancient evaporite (gypsum and anhydrite) deposits has been used to estimate the $\delta^{34}\text{S}$ values of coeval seawater sulfate through geologic time (Claypool et al. 1980). The $\delta^{34}\text{S}$ value of ancient seawater sulfate is estimated to have fluctuated between approximately +10 and +35‰ and averaged around 17‰ over the last 1.9 billion years (Fig. 4.3). The secular variation has been attributed to changes in the rate of accumulation of ^{32}S in sedimentary sulfides and to the consequent depletion of this sulfur isotope from the marine reservoir during periods of increased burial rates. A combination of this variation with the likely range of k_1/k_2 ratios (1.015-1.065) for sedimentary environments could produce bacteriogenic sulfides with mean $\delta^{34}\text{S}$ values in the range of -50 to +10‰. It is not surprising, therefore, that the Phanerozoic sedimentary sulfides show a large variation in $\delta^{34}\text{S}$ values (from about -60 to +30‰). The extremely narrow range of $\delta^{34}\text{S}$ in Archean sulfides ($0 \pm 5\%$) and the scarcity of sulfates in Archean sediments have been interpreted as evidence for sulfate-deficient seawater and precipitation of sedimentary sulfides without the involvement of sulfate-reducing bacteria during the Archean (Monster et al. 1979a, b). However, the distribution pattern could also mean that sulfate-reducing bacteria were able to convert sulfate ($\delta^{34}\text{S} \approx 0\%$) to reduced sulfur more efficiently in the Archean, resulting in limited isotopic fractionation between sulfide and sulfate (Ohmoto 1986).

4.2.2. APPLICATIONS

Sangster (1976a) compared average $\delta^{34}\text{S}$ (sulfide) values of 110 massive strata-bound sulfide deposits hosted by Phanerozoic marine sedimentary or volcanic rocks with coeval seawater $\delta^{34}\text{S}$ (sulfate) values. The "fractionation factors" [$\Delta(\delta^{34}\text{S})$] for the deposits, calculated for each deposit as

$$\Delta(\delta^{34}\text{S}) = [\delta^{34}\text{S}(\text{coeval seawater sulfate}) - \delta^{34}\text{S}(\text{mean of sulfides for the deposit})] \quad (4.17)$$

are summarized in the histograms of Figure 4.4, which also show for comparison the experimentally determined range and average $\Delta(\delta^{34}\text{S})$ values of sulfide produced by bacterial reduction of sulfate (about 15‰). The sediment-hosted strata-bound ores give an average $\Delta(\delta^{34}\text{S})$ value of 13.9‰ and the volcanic-hosted ores an average of 17.4‰, both values in close agreement with the average bacterial fractionation factor of 15‰. From this correlation, Sangster (1976a) concluded that the sulfides in both types of ores were derived mainly by bacterial reduction of coeval seawater sulfate at the site of deposition of the ores; the slightly greater fractionation in the volcanic-hosted deposits was probably caused by the relatively lower metabolic rate of sulfur-reducing bacteria living in a volcanic environment. From a similar study, but restricted to a few selected deposits associated with clastic sediments, Schwarcz and Burnie (1973) concluded that distributions of sulfide $\delta^{34}\text{S}$ values in ancient strata-bound sulfide deposits associated with marine clastic sediments fall between two end-member types: (a) a broad

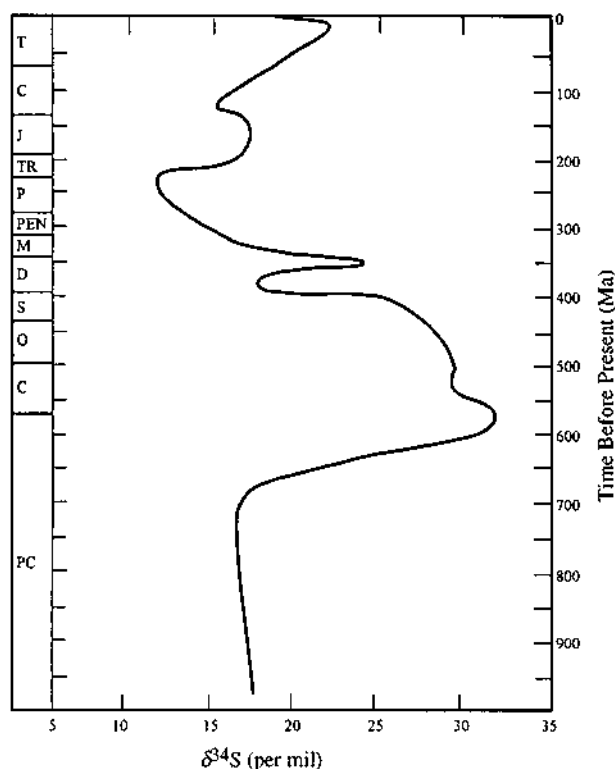


Figure 4.3. Variation (best estimate) in the sulfur isotopic composition of seawater through geologic time as estimated from marine evaporite (sulfate) deposits (after Claypool et al. 1980).

distribution centered around $\delta^{34}\text{S} = 0\text{‰}$ and ranging from $\delta^{34}\text{S}$ of coeval seawater sulfate to about 25‰ lower ("type 1"), characteristic of deposits formed in shallow marine or brackish water environments; and (b) a narrow distribution around a mode of 45 to 60‰ lighter than the $\delta^{34}\text{S}$ of coeval seawater sulfate ("type 2"), characteristic of deposits formed in deep, euxinic basins.

An obvious limitation of the approach used by Sangster (1976) and Schwarcz and Burnie (1973) is that it cannot be applied with any confidence to the Precambrian sulfide deposits because of insufficient data regarding $\delta^{34}\text{S}$ of Precambrian, especially Archean, seawater sulfate. A large number of the important strata-bound base metal sulfide deposits are hosted by volcanic or clastic sedimentary rocks of Precambrian age. Even for the Phanerozoic deposits, a common bacterial origin for all volcanic-hosted and sediment-hosted strata-bound sulfide ores, as interpreted by Sangster (1976), is questionable. As will be elaborated later (Ch. 10), many lines of evidence, including

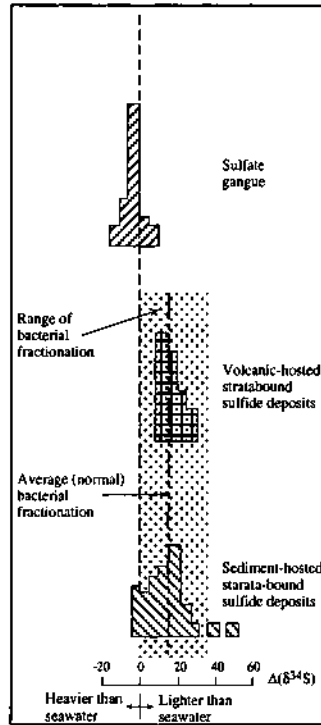


Figure 4.4. Frequency diagrams of $\Delta(\delta^{34}\text{S})$ values (per mil) in strata-bound sulfide deposits in marine sedimentary and volcanic rocks (after Sangster 1976). The heavy vertical line represents coeval marine sulfate. $\Delta(\delta^{34}\text{S})$, defined by Equation 4.17, is a measure of the sulfur isotopic fractionation relative to the coeval seawater sulfate.

the improbability of bacterial reduction at the estimated temperatures ($>200^\circ\text{C}$) of ore deposition and the narrow range of $\delta^{34}\text{S}$ within individual deposits, suggest that the reduction process was inorganic (Kajiwara 1971, Ohmoto & Rye 1979). For the sediment-hosted deposits (Ch. 11), the correlation between $\delta^{34}\text{S}$ (sulfides) and $\delta^{34}\text{S}$ (seawater sulfate) is not as good as was claimed by Sangster (Gustafson & Williams 1981), and the source of the sulfur and the mechanism of sulfide precipitation in many of these deposits continue to be largely unresolved questions, mainly because of a lack of knowledge of the $\delta^{34}\text{S}_{\text{ES}}$ values of the ore fluids.

It should be clear from the discussion presented here that the origin of sulfur in a hydrothermal mineral deposit cannot be interpreted merely from the variation in the $\delta^{34}\text{S}$ values of its sulfides; such interpretation must be based on the estimated isotopic composition of the total sulfur in solution ($\delta^{34}\text{S}_{\text{ES}}$), in addition to the time and space

distribution of $\delta^{34}\text{S}$ values in the deposit and its geologic setting. Figure 4.5 summarizes $\delta^{34}\text{S}$ (sulfide), $\delta^{34}\text{S}$ (sulfate), and estimated $\delta^{34}\text{S}_{\text{ES}}$ values of 15 hydrothermal deposits of various affiliations. The $\delta^{34}\text{S}_{\text{ES}}$ values fall into three groups corresponding to the three major sources of sulfur in hydrothermal mineral deposits: igneous, sedimentary, and seawater. One group is characterized by $\delta^{34}\text{S}_{\text{ES}}$ values close to 0‰ (Providencia, Casapalca, Pasto Bueno, Panasqueira, Darwin, and Mogul deposits), suggesting that the sulfur was derived probably from igneous sources such as magmatic fluids or sulfides in igneous rocks. Another group has $\delta^{34}\text{S}_{\text{ES}}$ values

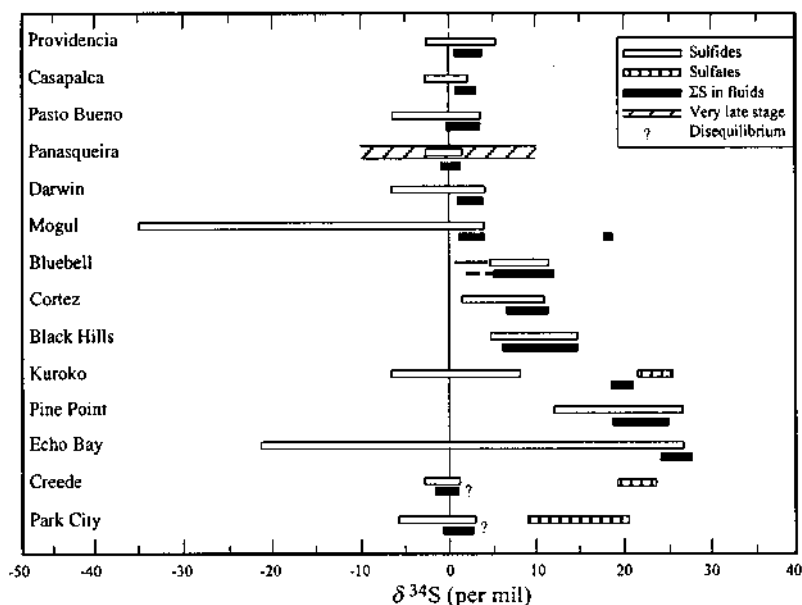


Figure 4.5. $\delta^{34}\text{S}$ values (per mil) of sulfides and sulfates, and estimated $\delta^{34}\text{S}_{\text{ES}}$ of fluids for selected hydrothermal ore deposits (after Rye & Ohmoto 1974).

close to the $\delta^{34}\text{S}$ for seawater sulfates, a reasonable case for derivation of the sulfur from seawater (Kuroko and Echo Bay deposits) or marine evaporites (Pine Point deposit). The source of sulfur for the third group with intermediate $\delta^{34}\text{S}_{\text{ES}}$ values was probably local sedimentary formations, although this is a more difficult case to interpret. The $\delta^{34}\text{S}_{\text{ES}}$ values for the Creede and Park City deposits suggest an igneous sulfur source. A consideration of the mineral equilibria, however, shows that the $\delta^{34}\text{S}_{\text{ES}}$ values represent sulfur isotopic disequilibrium (Rye & Ohmoto 1974), a possibility which must be taken into account for interpretations of sulfur isotope data.

4.3. Carbon Isotopes

4.3.1. PRINCIPLES

Applications of carbon isotopic composition of carbon-bearing minerals to the study of hydrothermal deposits are similar in principle to those for sulfur (Ohmoto 1972, Ohmoto & Rye 1979, Ohmoto 1986, Ohmoto & Goldhaber 1997). However, the usefulness of carbon isotopes in the evaluation of ore genesis is limited because the carbon-bearing minerals commonly postdate the main-stage sulfide minerals and may have formed from fluids that were quite different from those responsible for the sulfide ore deposition. Of the two common carbon-bearing mineral constituents, graphite and carbonates, graphite is seldom, if ever, a primary mineral in hydrothermal deposits. Carbonates, however, are quite abundant in many hydrothermal deposits and constitute the main target for carbon isotope studies related to mineral deposits. In addition, fluid inclusions may be analyzed to determine the carbon isotopic composition of the hydrothermal fluid ($\delta^{13}\text{C}_{\Sigma\text{C}}$) at a particular stage of its evolution.

Typical ranges of carbon isotopic compositions in geologic systems are summarized in Figure 4.6. Carbon isotope fractionation occurs in nature by both inorganic and organic processes. In low-temperature environments, where bacteriogenic sulfides are produced, anaerobic bacteria also produce CO_2 and CH_4 from the associated organic matter. Because of large isotopic fractionation of carbon between oxidized and reduced species, biogenic carbonates can show a wide spread of $\delta^{13}\text{C}$ values and, depending on the $\text{CO}_2:\text{CH}_4$ ratio, some very negative $\delta^{13}\text{C}$ values. A similar range of $\delta^{13}\text{C}$ values can also result from inorganic precipitation of carbonates because of variations in fluid and depositional conditions. Thus, as is the case with sulfur isotopes, a proper evaluation of the carbon isotopic composition of a mineral deposit requires a consideration of many variables (T , $m_{\Sigma\text{C}}$, $\delta^{13}\text{C}_{\Sigma\text{C}}$, pH , $f\text{O}_2$) as well as of its geologic setting.

Inorganic precipitation of carbonates from hydrothermal fluids involves reactions with oxidized species of carbon (CO_2 , HCO_3^- , H_2CO_3 , and CO_3^{2-}) in the fluid. Oxidized carbon species in hydrothermal fluids may originate from (a) a magmatic source, (b) oxidation of reduced carbon species in rocks (organic compounds in sedimentary rocks, graphite in igneous and metamorphic rocks), and (c) leaching of sedimentary carbonates (Ohmoto & Rye 1979). Analogous to the situation with sulfur isotopes, the $\delta^{13}\text{C}$ values of precipitated carbonate minerals depend on: (a) temperature; (b) $\delta^{13}\text{C}_{\Sigma\text{C}}$, which varies with the source of the fluid and can have very negative values; (c) the proportion of the different carbon species because of large isotopic fractionations between oxidized and reduced species (Fig. 4.7), especially between CO_2 and CH_4 , which are the dominant oxidized and reduced species in hydrothermal fluids; and (d) other geochemical parameters, such as temperature, pH , and $f\text{O}_2$, which determine the proportion of the different carbon species in the fluid of a given $\delta^{13}\text{C}$ (Ohmoto 1972). The effects of temperature, pH , $f\text{O}_2$, and $\delta^{13}\text{C}_{\Sigma\text{C}}$ on the $\delta^{13}\text{C}$ values of carbon-bearing

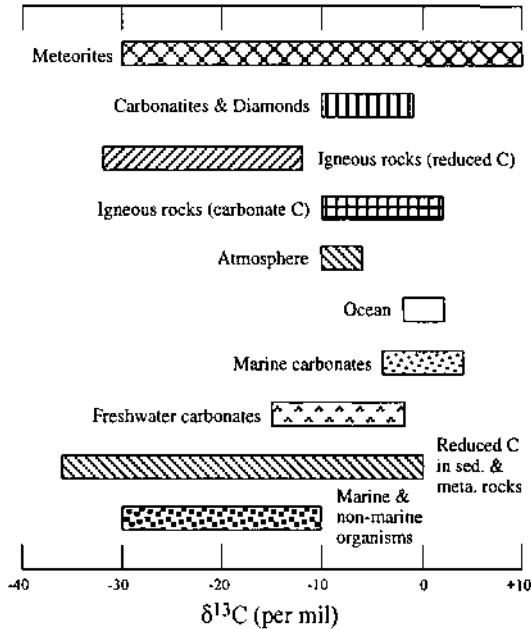


Figure 4.6. Approximate range of $\delta^{13}\text{C}$ (PDB) values in geologic systems. (Sources of data: Hoefs 1987, Ohmoto and Rye 1979, Field and Fifarek 1985.)

minerals have been discussed by Ohmoto (1972) and Ohmoto and Rye (1979). They have shown that a wide range of $\delta^{13}\text{C}$ values does not necessarily indicate bacteriogenic carbon; it can be produced by variations in $f\text{O}_2$ and pH of hydrothermal fluids during ore deposition. Also, carbonates with very negative $\delta^{13}\text{C}$ values, a common consequence of biogenic precipitation, can be formed from fluids of very negative $\delta^{13}\text{C}_{\text{FC}}$ values, as would be the case, for example, when graphite dissolution is a major contributor to the carbon content of the fluid.

Data from modern geothermal systems suggest that carbon isotope equilibrium between CO_2 and CH_4 is not attained in geothermal fluids. Thus $\delta^{13}\text{C}$ variation of fluid and mineral species in low temperature deposits ($T < 250^\circ\text{C}$?) is probably a reflection of variation in the carbon source (Ohmoto 1986). At higher temperatures, especially in systems in which the carbon species experience a long period of residence, equilibrium between CO_2 and CH_4 is likely to be achieved. The methods for estimating the $\delta^{13}\text{C}_{\text{FC}}$ value and the source of carbon in hydrothermal fluids are basically the same as those for sulfur (Ohmoto & Rye 1979, Ohmoto & Goldhaber 1997). First, the value of $\delta^{13}\text{C}_{\text{CO}_2}$ is calculated from the $\delta^{13}\text{C}$ value of a carbonate mineral believed to have been precipitated from the fluid:

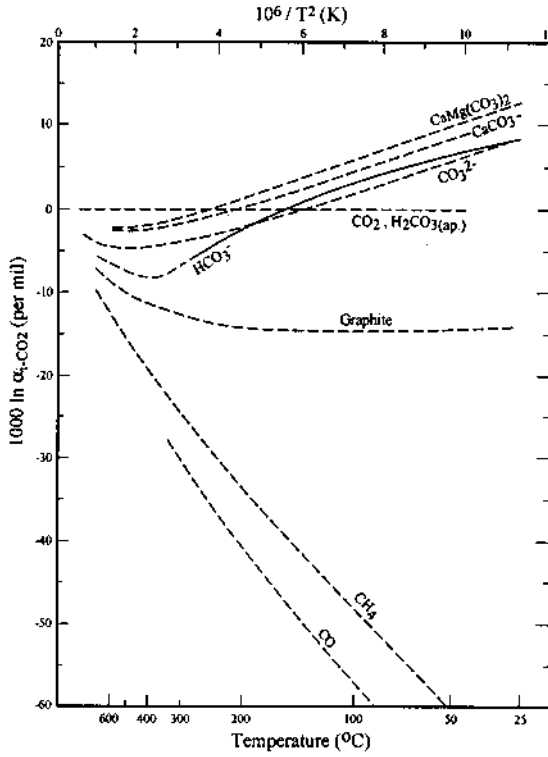


Figure 4.7. Calculated equilibrium isotopic fractionation factors (α) for CaCO_3 , $\text{CaMg}(\text{CO}_3)_2$, and important carbon species in hydrothermal systems relative to CO_2 . $\text{H}_2\text{CO}_3(\text{ap}) = \text{H}_2\text{CO}_3 + \text{CO}_2(\text{aq})$ and $\delta^{13}\text{C}_{\text{H}_2\text{CO}_3(\text{ap})} = \delta^{13}\text{C}_{\text{CO}_2(\text{aq})}$ (after Ohmoto & Rye 1979).

$$\delta^{13}\text{C}_{\text{CO}_2} = \delta^{13}\text{C}_{\text{carb. mineral}} - \Delta_{\text{carb. mineral-CO}_2} \quad (4.18)$$

where $\Delta_{\text{carb. mineral-CO}_2}$ is the equilibrium isotopic fraction factor between the carbonate mineral and CO_2 (Fig. 4.7). The $\delta^{13}\text{C}_{\Sigma\text{C}}$ value can, then, be calculated from the following equation:

$$\delta^{13}\text{C}_{\Sigma\text{C}} = \delta^{13}\text{C}_{\Sigma\text{CO}_2} + \Delta_{\text{CH}_4\text{-CO}_2} [1 / (1 + R')] \quad (4.19)$$

where $\Delta_{\text{CH}_4\text{-CO}_2} = 1,000 \ln \alpha_{\text{CH}_4\text{-CO}_2}$, and R' is the mole ratio $m_{\text{CO}_2} / m_{\text{CH}_4}$ in the fluid. The R' value can be calculated from the $f\text{O}_2$ value of the fluid which, in turn,

can be estimated from the stability relationships of coexisting ore minerals (Fig. 4.8). As the amount of the HCO_3^- is negligible compared with the amount of $\text{H}_2\text{CO}_{3(\text{ap})}$ in most geologic fluids at temperatures above about 100°C , the $\delta^{13}\text{C}_{\Sigma\text{C}}$ can be calculated from the $\delta^{13}\text{C}$ value of a carbon-bearing mineral (i) and the fractionation factor between the mineral and $\text{H}_2\text{CO}_{3(\text{ap})}$ (Fig. 4.7) by using the approximate relationship

$$\delta^{13}\text{C}_{\Sigma\text{CO}_2} = \delta^{13}\text{C}_i - \Delta_{i-\text{H}_2\text{CO}_{3(\text{ap})}} \quad (4.20)$$

If there is evidence to conclude that the temperature or the residence time of the carbon species in the fluid was not adequate to establish isotopic equilibrium between CO_2 and CH_4 , the $\delta^{13}\text{C}_{\text{CO}_2}$ value itself may be regarded as a reasonable estimate of the $\delta^{13}\text{C}_{\Sigma\text{C}}$ (Ohmoto 1986).

4.3.2. APPLICATIONS

Published data on carbon isotope compositions of mineral deposits are quite limited, because in many such deposits the carbonates were precipitated later than the sulfides and probably from different fluids. However, the $\delta^{13}\text{C}$ for the few deposits discussed by Ohmoto and Rye (1979) will suffice to illustrate the complexity of interpretation. As shown in Figure 4.9, many hydrothermal deposits contain different generations of hydrothermal carbonate minerals and in most cases with a trend of increasing $\delta^{13}\text{C}$ for later stage carbonates. This trend is real, because $\delta^{13}\text{C}$ values of hydrothermal carbonate minerals are "frozen in" as they crystallize and are not altered by exchange with later hydrothermal fluids (Rye & Ohmoto 1974). The source of carbon for the earlier generations of carbonates in these deposits is difficult to assess because observed $\delta^{13}\text{C}$ values (mostly between -5 and -10‰) can be produced by fluids from different sources. If the pH and $f\text{O}_2$ values of the fluids were such that $\delta^{13}\text{C} = \delta^{13}\text{C}_{\Sigma\text{C}}$, then a deep-seated source for the carbon is a likely, but not the only, possibility (Rye & Ohmoto 1974). The very negative $\delta^{13}\text{C}$ values of the Panasqueira carbonates (average about -14‰) are probably due to a graphite source of the carbon. The increase in $\delta^{13}\text{C}$ values upwards in the paragenetic sequence is often too large (e.g., $>15\text{‰}$ for Pine Point deposit) to be accounted for solely by a decrease in temperature. Other factors that have been invoked to explain the $\delta^{13}\text{C}$ increase include: (a) increasing $\text{CH}_4:\text{CO}_2$ ratios in the fluid, as evidenced by abundance of organic matter (e.g., Pine Point); and (b) increasing $\delta^{13}\text{C}_{\Sigma\text{C}}$ of the fluid resulting from CO_2 contributed by dissolution or decarbonation of limestones traversed by the fluids (e.g., Providencia, Casapalca, and Sunnyside).

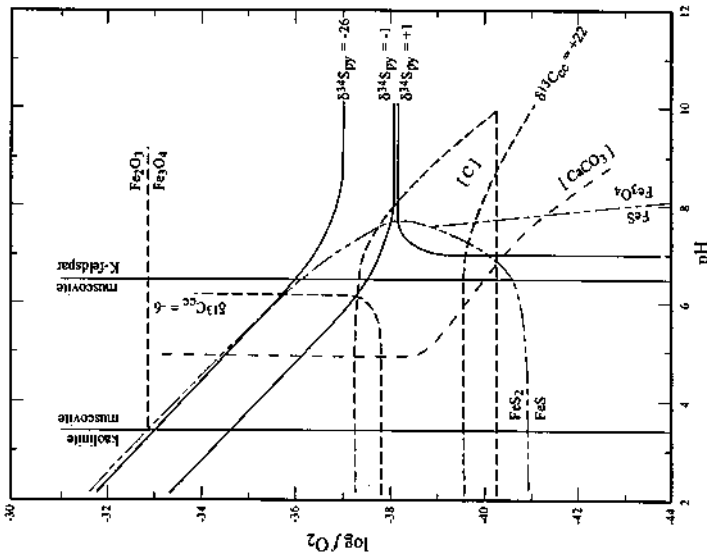


Figure 4.8. Composite diagram ($T = 250^\circ C$, ionic strength = 1.0) showing the fO_2 - pH relationships among the $\delta^{34}S$ contours for pyrite (py) at $\delta^{34}S_{FS} = 0\%$, the $\delta^{13}C$ contours for calcite (cc) at $\delta^{13}C_{cc} = -5\%$, and the stability fields of Fe - S - O minerals ($\Sigma S = 0.01$ mole/kg H_2O), calcite, and graphite ($\Sigma C = 1$ mole/kg H_2O). The muscovite - K-feldspar boundary is at $K^+ = 0.001$ mole/kg H_2O and the kaolinite - muscovite boundary is at $K^+ = 0.1$ mole/kg H_2O . The field for muscovite (sericite) in the diagram is the maximum stability field, since the molality of K^+ in ore-forming fluids seldom lies outside of 0.001 to 1 m range. (After Ohmoto 1972.)

4.4. Oxygen and Hydrogen Isotopes

4.4.1. PRINCIPLES

Because water is the predominant constituent of all hydrothermal fluids and the isotopic fractionation of both oxygen and hydrogen is appreciable in many systems of geologic interest (Fig. 4.10), it is only logical that the $^{18}O/^{16}O$ and D/H ratios be considered together. This combined approach is particularly useful in tracing the origin and evolution of hydrothermal fluids, because $^{18}O/^{16}O$ and D/H ratios are affected somewhat differently in water-rock systems. Because of the extremely small amount of hydrogen in rocks (usually <2,000 ppm), the D/H ratio of a fluid undergoes negligible change by

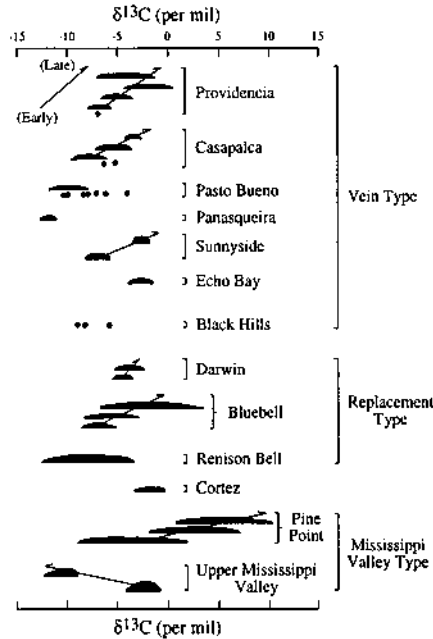


Figure 4.9. Carbon isotopic data for gangue minerals and fluid inclusions (solid circles) in selected hydrothermal ore deposits (after Ohmoto & Rye 1979).

mineral-water exchange reactions. In contrast, the $^{18}\text{O}/^{16}\text{O}$ ratio of the fluid may be modified significantly unless water:rock ratios are very high or the isotopic exchange reactions are ineffective for kinetic or other reasons. The magnitude of the shift, which is generally to higher $\delta^{18}\text{O}$ values as a result of the water trying to attain oxygen isotopic equilibrium with the ^{18}O -rich silicates and carbonates, is determined by (Sheppard 1986): (a) the ratio of the amount of oxygen in the exchangeable minerals to that in the fluid; (b) the magnitude of mineral- H_2O fractionation factors (which takes into account the temperature of isotopic exchange); and (c) the initial isotopic composition of the mineral phases. Thus the D/H ratio of a hydrothermal fluid is a better indicator of the source of the fluid, whereas its $^{18}\text{O}/^{16}\text{O}$ ratio may provide information about its subsequent evolution. Excellent reviews on the subject have been presented by Taylor (1974, 1979, 1997).

Two methods are used to determine D/H and $^{18}\text{O}/^{16}\text{O}$ ratios of hydrothermal fluids related to mineral deposits. The direct method can be used only in cases where the fluids can be sampled directly, such as connate brines, geothermal waters, and fluid inclusions. Isotopic compositions of fluids that are not amenable to direct sampling, as in the case of igneous and metamorphic rocks, are determined indirectly from mineral

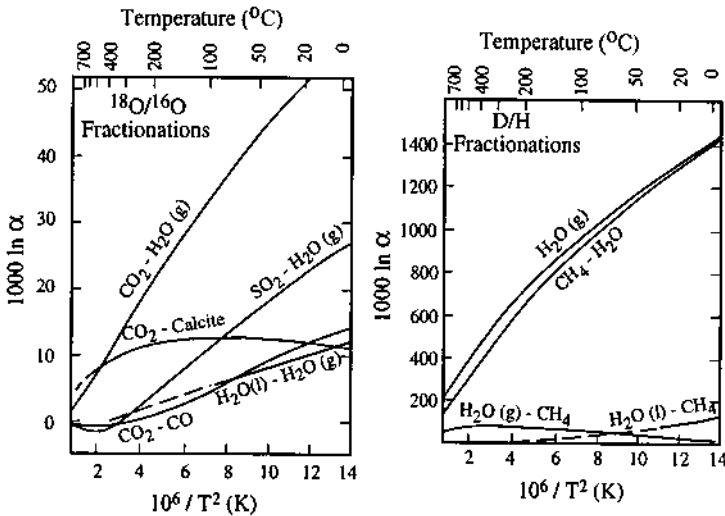


Figure 4.10. Oxygen and hydrogen isotope fractionation factors (α) in selected systems as a function of temperature. The liquid water - vapor water curves are experimental, the rest are calculated. (After Taylor 1974.)

assemblages presumed to have been in equilibrium with the fluid. In essence, the indirect method involves the following steps: isotopic analysis of mineral assemblages, estimation of temperature of formation utilizing appropriate geothermometers, and calculation of D/H and $^{18}O/^{16}O$ ratios of fluids in equilibrium with assemblages at their temperatures of formation using appropriate mineral- H_2O fractionation factors. The uncertainty in the δD and $\delta^{18}O$ values of fluids estimated by the indirect method arises largely from uncertainties in the temperatures of mineral deposition and in the values of isotopic fractionation factors. The indirect method is more commonly used, especially for $^{18}O/^{16}O$ ratios, because it is technically much easier. Because of paucity of hydrogen-bearing minerals in many ore deposits, fluid inclusion analysis usually is the only method for obtaining information on the δD values of ore-forming fluids. The accuracy of determination of δD is typically an order of magnitude worse than for $\delta^{18}O$ ($\pm 1.0\%$ versus $\pm 0.1\%$). However, the natural variations in D/H are also much larger than for $\delta^{18}O$; so a 10‰ variation generally represents a very large $\delta^{18}O$ change but only a small δD change.

The basic strategy in the application of oxygen and hydrogen isotope ratios to the interpretation of mineral deposits is to compare the $^{18}O/^{16}O$ and D/H ratios (a) of ore-forming fluids with those of the natural waters and (b) of minerals and rocks associated with ore deposits with those of normal rocks. The isotopic compositions of different kinds of natural waters, discussed in detail by Taylor (1974, 1979) and Sheppard (1986), are summarized in Figure 4.11. As expected, the most well established are the isotopic

compositions of present-day meteoric water and ocean water. The oxygen and hydrogen isotopic composition of present-day ocean water is relatively uniform ($\delta D = +5$ to -7‰ , $\delta^{18}\text{O} = +0.5$ to -1.0‰) with mean values very close to the defined values of the SMOW standard ($\delta D = 0\text{‰}$, $\delta^{18}\text{O} = 0\text{‰}$). Larger variations exist, but only in special situations, such as seas in arid regions with restricted access to the open ocean. The result of isotopic fractionations during evaporation of water from the oceans and subsequent condensation of vapor in clouds is that fresh water is generally depleted in ^{18}O and D (i.e., enriched in ^{16}O and H) compared with seawater. Because of temperature dependence of oxygen and hydrogen isotope fractionation between the liquid and vapor phases of water, the δD and $\delta^{18}\text{O}$ values of meteoric water vary with latitude and elevation (the higher the latitude or elevation, the more depleted is the water in ^{18}O and D), but the D/H fractionation is proportional to the $^{18}\text{O}/^{16}\text{O}$ fractionation because condensation of H_2O from the Earth's atmosphere is essentially an equilibrium process. Thus in a $\delta^{18}\text{O}$ vs. δD plot, all meteoric waters fall close to a straight line, called the *meteoritic water line* (MWL), defined by the equation (Craig 1961):

$$\delta D = 8 \delta^{18}\text{O} + 10 \quad (\text{in per mil}) \quad (4.21)$$

Surface waters that have been affected by evaporation may deviate from the meteoric water line, because evaporation is usually accompanied by kinetic isotopic effects. If the oxygen and hydrogen isotopic compositions and temperature of ancient ocean waters were comparable to present-day values, then ancient meteoric waters would be expected to follow a relation similar to MWL. The variation of ocean water isotopic composition through geologic time is not known with any certainty, but indications are that the composition has been essentially the same at least during the Cenozoic and the Mesozoic ($\pm 1\text{‰}$ for $^{18}\text{O}/^{16}\text{O}$ and $\pm 10\text{‰}$ for D/H), and possibly as far back as the Lower Paleozoic (Knauth & Roberts 1991, Kolodny & Luz 1991). $^{18}\text{O}/^{16}\text{O}$ values of ancient cherts suggest that Precambrian seawater was depleted in ^{18}O by up to 20‰ (Perry 1967), but other studies have concluded that the $\delta^{18}\text{O}$ values of the ocean waters have remained relatively constant throughout much of the Precambrian (Knauth & Epstein 1971, Holmden & Muehlenbachs 1993), and even during the Archean (Beaty & Taylor 1982). Discussing the various approaches that have been used to resolve this question, Sheppard (1986) proposed that the isotopic compositions of ancient ocean waters, at least since about 2500 Ma, have stayed within narrow limits of about 0 and -3‰ for $\delta^{18}\text{O}$ and about 0 and -25‰ for δD , not radically different from their present-day values. Thus the present-day MWL is commonly used as a reference line for evaluating fossil hydrothermal systems. The *kaolinite line* in Figure 4.11 represents the locus of isotopic data points in pure kaolinites from weathering zones formed in equilibrium with meteoric water at surface temperatures (Savin & Epstein 1970). It is potentially useful for discriminating clay minerals formed by supergene alteration from those formed by hypogene alteration. Most volcanic and plutonic igneous rocks have very uniform $\delta^{18}\text{O}$ values ($+5.5$ to $+10.0\text{‰}$) and δD values (-50 to -85‰); the field

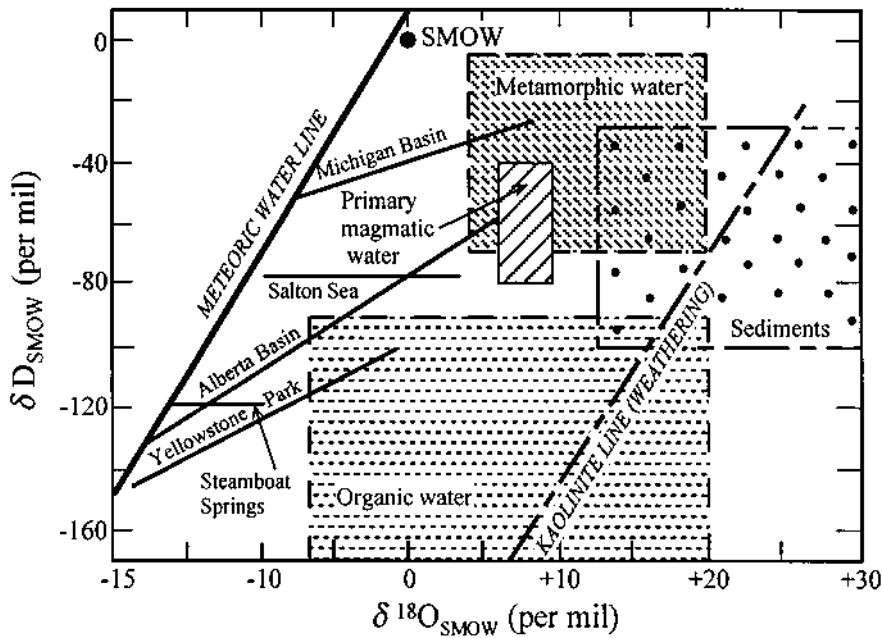


Figure 4.11. Oxygen and hydrogen isotopic compositions of various hydrothermal waters relative to SMOW standard. The meteoric water line (MWL) defines the compositions of meteoric water; the kaolinite line represents the compositions of kaolinites formed by supergene alteration. The field of primary magmatic water is calculated for water in equilibrium with "normal" igneous rocks ($\delta D = -50$ to -85‰ , $\delta^{18}O = +5.5$ to $+10.0\text{‰}$) at $T \geq 700^\circ\text{C}$; the field of metamorphic water is calculated for water in equilibrium with metamorphic silicate minerals at $T = 300^\circ$ to 600°C . Also shown are trends for the Michigan Basin and the Alberta Basin geothermal brines, and the $\delta^{18}O$ shifts of the geothermal waters of Steamboat Springs (Nevada) and Yellowstone Park (Wyoming) relative to the isotopic composition of present-day meteoric water in these areas. (Sources of data: Taylor 1974; White 1974; Sheppard 1986.)

shown as "primary magmatic water" in Figure 4.11 corresponds to the calculated isotopic composition of water in equilibrium with such normal igneous rocks at $T \geq 700^\circ\text{C}$. The field of metamorphic water shown in Figure 4.11 also represents calculated values for waters in equilibrium with metamorphic minerals at $T = 300^\circ$ to 600°C . Evidently, the fields for magmatic and metamorphic waters shown in Figure 4.11 are approximate.

4.4.2. APPLICATIONS

Analyses of waters from active geothermal systems around the world have shown that these waters essentially are of local meteoric derivation. Some examples are shown in Figure 4.11. In almost all cases, the hot water or steam shows a characteristic shift to

higher $\delta^{18}\text{O}$ values as a result of isotopic exchange with silicate and carbonate minerals of the country rocks. In contrast, because of the extremely small initial hydrogen content of the rocks relative to the amounts of water involved, the δD values remain almost identical to the local meteoric waters (e.g., Steamboat Springs, Nevada, USA); in some cases (e.g., Yellowstone Park, Wyoming, USA), the δD values show a linear increase compared with the local meteoric waters because of evaporation. Meteoric water is considered to be the main, if not the only, source of recharge for the Salton Sea geothermal brines, California (Craig 1966, Clayton et al. 1968). The 1.5 to 2‰ higher $\delta^{18}\text{O}$ in these waters relative to the meteoric water line is probably because of evaporation of the meteoric waters in the desert environment prior to infiltration (White 1974). On the other hand, the isotopic data for the Red Sea brine pools clearly show that the Red Sea, with waters enriched in the heavy isotopes relative to the average ocean water because of evaporation, is the major source of the hot-brine water (White 1974). On the basis of δD vs. $\delta^{18}\text{O}$ trends, the oil-field brines (formation waters), once thought to represent connate waters (seawater trapped in sediments), are now believed to contain a major component of circulating meteoric groundwater. Similar to surface meteoric waters, the oil-field brines show a general increase in δD and, to a lesser extent, in $\delta^{18}\text{O}$ toward lower latitudes (e.g., the Michigan Basin brines versus the Alberta Basin brines, Fig. 4.11). Within a given sedimentary basin, however, the δD values generally increase with $\delta^{18}\text{O}$ (and salinity). According to Taylor (1974), this trend is a result of one or more of the following processes: mixing of meteoric waters with waters of connate or other origin; isotopic exchange with clay minerals in the rocks; fractionation effects by processes such as membrane-filtration; and reactions involving petroleum hydrocarbons.

Isotopic data for hydrothermal fluids in various mineral deposits and their interpretation have been reviewed by several authors (Taylor 1974, 1979, 1997; White 1968, 1974; Ohmoto 1986). For the purpose of illustration of the principles, a few selected examples are shown in Figure 4.12 and discussed below; data for specific types of mineral deposits, as available, are discussed in later chapters. The simplest of the cases are those where ocean water or meteoric water, both of which have well defined δD - $\delta^{18}\text{O}$ ranges, constitute the sole or major component of the fluid. Isotopic studies have now shown that the water in the ore- and alteration-forming fluids for many epithermal (low-temperature, near surface) Au-Ag deposits hosted in volcanic rocks was dominantly, and in some cases probably exclusively, meteoric in origin (O'Neil & Silberman 1974). For example, the proximity of the isotopic composition of fluid inclusions in the 8 Ma-old Bodie deposit (California, USA) to the meteoritic water line leaves little doubt about the predominance of meteoritic water in this ore fluid. The δD difference between the meteoric waters of the former Bodie system and the present meteoric waters of the area ($\delta\text{D} \approx -130\text{‰}$) is best explained by changes in climate over the 8 m.y. interval (O'Neil et al. 1973). The nearly constant δD of the Blue Bell sphalerite - galena deposit (British Columbia, Canada) indicates a dominantly meteoric origin of the water, whereas the $\delta^{18}\text{O}$ variation reflects the mixing of two meteoric waters, one of which had previously exchanged ^{18}O with ^{18}O -enriched rocks at high

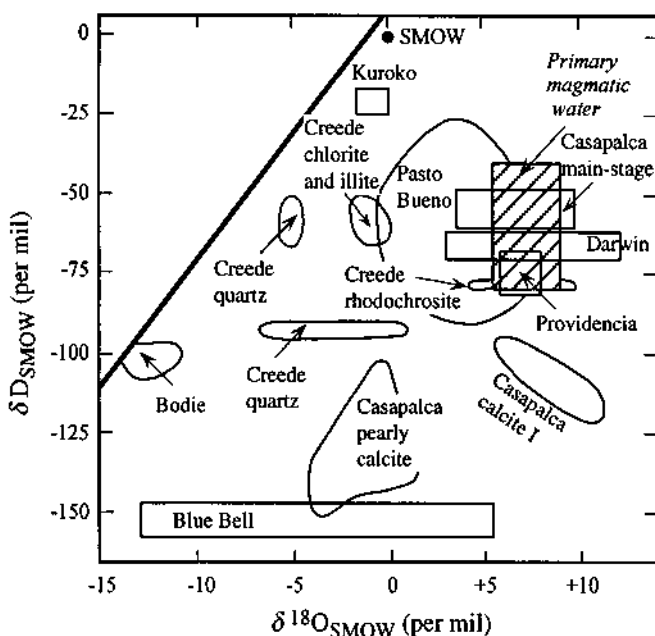


Figure 4.12. $\delta D - \delta^{18}O$ ranges of hydrothermal fluids for a variety of mineral deposits relative to SMOW standard. (After compilation by Taylor 1979.)

temperatures (Ohmoto & Rye 1970). An example where the isotopic ratios are compatible with a magmatic origin of the ore fluid is provided by the Darwin (California, USA) lead-zinc sulfide deposit (Rye et al. 1974). Despite the similarity of the δD values of the ore fluids and the present-day meteoric waters in the area, the ore fluids for the pipelike zinc-lead ore deposits of Providencia (Mexico) are interpreted to be dominantly magmatic, because it is difficult to explain the tight clustering of δD and $\delta^{18}O$ values in this deposit by any model involving ^{18}O shifts in a saline formation water or meteoric ground water. The isotopic data for the base metal-silver deposits of Casapalca (Peru) indicates the involvement of more than one type of hydrothermal fluid: a dominantly magmatic fluid for the main-stage mineralization, and meteoric hydrothermal fluids for the post-ore calcite I and pearly calcite precipitation (Rye & Sawkins 1974). The Pasto Bueno tungsten - copper - lead - silver vein-type deposit (Peru) presents an even more complex evolution of the hydrothermal fluids. Landis and Rye (1974) proposed the following interpretation of the isotopic (and fluid inclusion) data: (a) the greisenization and early-stage vein mineralization occurred from a very saline (>40 wt% NaCl equivalent), high temperature (400°-500°C) fluid of magmatic derivation; (b) this fluid mixed with meteoric water, and possibly a "connate-metamorphic water" (later termed "evolved water"; Norman & Landis 1983), resulting in a fluid of lower salinity (2 to 17 wt% NaCl equivalent) and lower temperature (175°

to 290°C) for the main-stage vein mineralization; and (c) sulfide deposition was associated with the magmatic fluid (supported by $\delta^{34}\text{S}$ values of pyrite), wolframite deposition with episodes of meteoric water influx.

Evidently, the interpretation of δD and $\delta^{18}\text{O}$ values of hydrothermal fluids and hydrothermally altered rocks requires an evaluation of the isotopic exchange between the fluid and rocks. The quantitative evaluation of isotopic exchanges between water and rock is treated in detail in several recent publications (Taylor 1979, 1997; Gregory & Criss 1986; Criss & Taylor 1986). For the purpose of illustration, consider a simple case where the change in $\delta^{18}\text{O}$ or δD due to water-rock interaction can be evaluated from the following material-balance equation (Taylor 1979):

$$w \delta_{\text{H}_2\text{O}}^i + r \delta_{\text{rock}}^i = w \delta_{\text{H}_2\text{O}}^f + r \delta_{\text{rock}}^f \quad (4.22)$$

The superscripts *i* and *f* refer, respectively, to the initial state (i.e., before water-rock interaction) and the final state (i.e., after interaction), *w* is the atom percent of water oxygen in the rock + water system, and *r* is the atom percent of exchangeable rock oxygen in the rock + water system. When the water and rock reach isotopic equilibrium at a given temperature, the final isotopic composition of water, $\delta_{\text{H}_2\text{O}}^f$, and rock, δ_{rock}^f , assuming a closed system, can be expressed by the following relations:

$$\delta_{\text{H}_2\text{O}}^f = \frac{\delta_{\text{rock}}^i - \Delta + \delta_{\text{H}_2\text{O}}^i (w/r)}{1 + (w/r)} \quad (4.23)$$

$$\delta_{\text{rock}}^f = \frac{\delta_{\text{rock}}^i + [\delta_{\text{H}_2\text{O}}^i + \Delta] (w/r)}{1 + (w/r)} \quad (4.24)$$

where $\Delta = [\delta_{\text{rock}}^f - \delta_{\text{H}_2\text{O}}^f]$ at the given temperature. Note that for a given set of initial conditions and constant *w/r* ratio, δ_{rock}^f or $\delta_{\text{H}_2\text{O}}^f$ is determined solely by Δ , which is a function of temperature only. Conversely, for a given set of initial values and constant temperature, δ_{rock}^f or $\delta_{\text{H}_2\text{O}}^f$ is determined only by the *w/r* ratio. Also, for very small values of *w/r* (i.e., a rock-dominated system), δ_{rock}^f will tend to be close to δ_{rock}^i and $\delta_{\text{H}_2\text{O}}^f$ will tend to attain the same value [= $\delta_{\text{rock}}^i - \Delta$] regardless of its origin (i.e., its $\delta_{\text{H}_2\text{O}}^i$ value). Only when the *w/r* ratio is much greater than 1 (i.e., a water-dominated system) can the $\delta_{\text{H}_2\text{O}}^i$ value estimated from the $\delta_{\text{H}_2\text{O}}^f$ value be used to identify the origin of the fluid. Conversely, if the origin of the fluid is known, then the $\delta^{18}\text{O}$ or δD shift in a rock-water system can be used to estimate the *w/r* ratio. For this purpose, $\delta^{18}\text{O}$ is more useful than δD , because D/H fractionation is relatively much smaller in most rock-water systems. Similar considerations apply to open rock-water systems, but the corresponding equations are slightly different (see Taylor 1979).

There are, however, several limitations to this approach of computing water:rock ratios in hydrothermal systems (Ohmoto 1986, Bowman et al. 1994, Campbell & Larson 1998). The most fundamental of these is that a specific site of hydrothermal alteration or ore deposition under investigation constitutes only one part of a hydrothermal flow system, commonly a small part near the end or discharge portion of the flow system. A more realistic approach may be the model discussed by Bowman et al. (1994) that uses one-dimensional transport equations to evaluate the time-space evolution of oxygen isotopic compositions of rock and infiltrating fluid.

In spite of the uncertainties involved in a quantitative evaluation of isotopic ratios in a hydrothermal system, whole-rock oxygen and hydrogen isotopic ratios, particularly the former, may be used to identify contemporaneous alteration zones associated with hydrothermal mineral deposits. For example, Beatty and Taylor (1982) showed that many massive sulfide deposits, ranging in age from Archean to Cenozoic, were characterized by pronounced depletion or enrichment of $\delta^{18}\text{O}$ relative to the country rocks (Fig. 4.13). Such a pattern, if observed in the course of reconnaissance study of an area, can be useful in delineating exploration targets. Green et al. (1983) established that the areal extent of the $\delta^{18}\text{O}$ anomaly for the Fukazawa area of the Hokuroku district (Japan) was much larger than that of other geochemical anomalies, and that the variability of $\delta^{18}\text{O}$ values within a site was much less than that of the elemental compositions. As pointed out by Beatty and Taylor (1982), oxygen isotopes may also be valuable in rock types that do not show diagnostic alteration mineral assemblages,

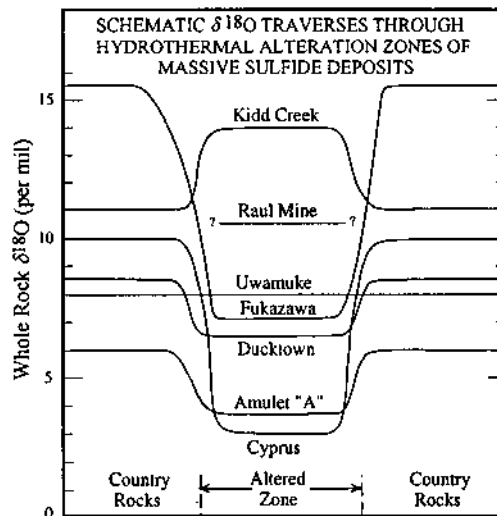


Figure 4.13. Patterns of $\delta^{18}\text{O}$ (whole-rock) variation in the hydrothermal alteration zones associated with selected massive sulfide deposits. The widths of the alteration zones have been adjusted to the same value for comparison. (After Beatty & Taylor 1982.)

as well as in those situations in which the alteration assemblages have been obliterated by subsequent metamorphism. At least in the case of the Amulet deposit in the Archean Abitibi greenstone belt (Canada) studied by those authors, the zones of ^{18}O depletion seems to have survived relatively high-grade metamorphism. Beatty and Taylor (1982) also raised the possibility that the high $\delta^{18}\text{O}$ of ore fluids (6 to 9‰) calculated for the Kid Creek deposit (Canada) might be a characteristic of very large deposits and thus serve as an exploration guide. Several other illustrative examples, covering a variety of scales and a range of isotopic signatures, have been discussed by Taylor (1997). It is a cost-effective exploration technique as maps of the isotopic anomalies associated with various ore bodies may be constructed simply by analyzing whole-rock $\delta^{18}\text{O}$ values and plotting the data.

Recrystallization of carbonate minerals in the presence of carbon-bearing fluids tends to alter their $^{18}\text{O}/^{16}\text{O}$ and $^{13}\text{C}/^{12}\text{C}$ ratios by isotopic exchange with the fluids. This has led to isotopic studies on the carbonate rocks hosting hydrothermal mineral deposits with the hope that $\delta^{18}\text{O}$ and $\delta^{13}\text{C}$ variations in the host rocks might be useful as ore guides. The results, however, have not been encouraging. Many such deposits show a consistent decrease in $\delta^{18}\text{O}$ by a few per mil in the zone of transition from the unaltered host rocks to ore (Hall & Friedman 1969, Pinckney & Rye 1972), but the $\delta^{18}\text{O}$ halo is too small to be useful for delineation of orebodies. Ideally, $\delta^{13}\text{C}$ values should show a systematic relationship with $\delta^{18}\text{O}$ values, but they often do not, suggesting that the factors controlling $\delta^{13}\text{C}$ values of recrystallized carbonates are more variable in space and time in comparison with those controlling $\delta^{18}\text{O}$ values. This limits the usefulness of carbon isotopes as an exploration guide for carbonate-hosted hydrothermal deposits (Fritz 1976).

4.5. Lead Isotopes

Radiogenic isotopes are produced by radioactive decay of unstable elements. The present discussion is limited to lead and strontium isotopes, the two radiogenic isotopes that are being used increasingly in the study of mineral deposits. As in the case of stable isotopes, attention here is focused primarily on the principles governing their applications to interpretation of mineral deposits; the isotopic data and their implications for specific types of mineral deposits will be dealt in later chapters.

4.5.1. PRINCIPLES

Potential applications of lead isotope ratios in the study of mineral deposits include: (a) estimation of the age and subsequent history of the deposit; (b) evaluation of the source of lead (Stanton & Russell 1959, Russell & Slawson 1967, Richards 1971, Sangster 1976, Koppel & Saager 1976, Doe & Stacey 1974, Doe & Zartman 1979); (c) providing information on geochemistry of uranium, thorium, and lead in the crust and mantle (Doe & Zartman 1979); and (d) exploration of mineral deposits (Cannon et al.

1961, Doe & Stacey 1974).

There are four main isotopes of lead: ^{204}Pb , ^{206}Pb , ^{207}Pb , and ^{208}Pb . One of these isotopes, ^{204}Pb , has no long-lived radioactive parent, so that the terrestrial abundance of ^{204}Pb may be presumed to have been constant through geologic time. The other three isotopes are radiogenic and their terrestrial abundances have steadily increased throughout the geologic time by radioactive decay of parent uranium and thorium into ^{206}Pb , ^{207}Pb , and ^{208}Pb (Table 4.2). Thus, lead isotope measurements are commonly reported as ratios normalized to the index isotope ^{204}Pb : $^{206}\text{Pb}/^{204}\text{Pb}$, $^{207}\text{Pb}/^{204}\text{Pb}$, $^{208}\text{Pb}/^{204}\text{Pb}$.

Lead that occurs in minerals with very low U/Pb and Th/Pb ratios is called *common lead*, because its isotopic composition does not change appreciably with time. The recommended common-lead mineral for lead-isotope analysis is galena. When galena is not available, samples with at least 500 ppm lead in sulfide are preferable. Samples of silicate rock (or mineral) or sulfide with very low lead content and uncertain sulfide mineralogy carry the risk that decay of included uranium and thorium has increased the radiogenic content, so that the measured lead-isotope ratios will not be representative of the sulfide occurrence. In addition, because of the very low isotopic abundance of ^{204}Pb (only 1.4% of the total lead), analytical error becomes increasingly a factor in samples with very low total lead content (Young 1995).

The simplest formulation of the lead isotope evolution is the Holmes-Houtermans *single-stage model*, which involves the following assumptions (Cannon et al. 1961):

- (a) The primordial lead, the lead at the birth of the Earth (time T), had a unique and uniform isotopic composition ($^{206}\text{Pb}/^{204}\text{Pb}$, $^{207}\text{Pb}/^{204}\text{Pb}$, $^{208}\text{Pb}/^{204}\text{Pb}$); this composition is assumed to be the values in the troilite phase of meteorites, the least radiogenic leads ever found (Table 4.2).
- (b) The changes in the ratios of the radioactive parent isotopes to the nonradiogenic isotope ^{204}Pb ($^{238}\text{U}/^{204}\text{Pb}$, $^{235}\text{U}/^{204}\text{Pb}$, $^{232}\text{Th}/^{204}\text{Pb}$) in any given region were entirely due to radioactive decay within one or more closed systems, with constant proportion of lead to uranium and thorium maintained in each system.
- (c) The formation of galena or other Pb-bearing sulfide minerals during a mineralization event represents the separation of lead from a mantle or crustal source and the lead-isotope ratios of the source are frozen in the mineral.
- (d) The lead source is an 'infinite reservoir', i.e., withdrawal of some lead, uranium, and thorium from the source by magmas, ore fluids, or other mechanisms has not significantly disturbed the ratios involving the radioactive parent isotopes ^{238}U , ^{235}U , or ^{232}Th .

The *single-stage lead evolution curve* is commonly represented either on a $^{206}\text{Pb}/^{204}\text{Pb}$ vs. $^{208}\text{Pb}/^{204}\text{Pb}$ diagram or, more commonly, on a $^{206}\text{Pb}/^{204}\text{Pb}$ vs. $^{207}\text{Pb}/^{204}\text{Pb}$ diagram by solving Equations 4.25, 4.26, and 4.27 given in Table 4.2. Each point on

TABLE 4.2. Some parameters and equations relevant to lead isotope studies

(a) Decay constants (Jaffey et al. 1971)

Parent Isotope	Daughter Isotope	Decay Constant
^{238}U	^{206}Pb	$\lambda = 0.155125 \times 10^{-9} / \text{year}$
^{235}U	^{207}Pb	$\lambda' = 0.98485 \times 10^{-9} / \text{year}$
^{232}Th	^{208}Pb	$\lambda'' = 0.049475 \times 10^{-9} / \text{year}$

(b) Age of the Earth (T), as defined by meteoritic isochron = 4.57 b.y.

(c) Primordial ratios (at time T), from troilite of the Cañon Diablo meteorite (Tatsumoto et al. 1973)

$$a_o = {}^{206}\text{Pb} / {}^{204}\text{Pb} = 9.307$$

$$b_o = {}^{207}\text{Pb} / {}^{204}\text{Pb} = 10.294$$

$$c_o = {}^{208}\text{Pb} / {}^{204}\text{Pb} = 29.476$$

(d) Present-day ratios (normalized for radioactive decay) of the lead reservoir

$${}^{238}\text{U} / {}^{235}\text{U} = 137.88 \quad {}^{238}\text{U} / {}^{204}\text{Pb} = \mu$$

$${}^{232}\text{Th} / {}^{238}\text{U} = k \quad {}^{235}\text{U} / {}^{204}\text{Pb} = \mu / 137.8$$

$${}^{232}\text{Th} / {}^{204}\text{Pb} = \mu k$$

(e) General equation for radioactive decay in a closed system

$$\frac{dN}{dt} = -\lambda N \quad \lambda = \text{Decay constant} = 0.693 / \text{half-life}$$

$$D = N_o - N \quad N_o = \text{Original number of parent isotope atoms}$$

$$D / N = e^{\lambda t} - 1 \quad N = \text{Remaining number of parent isotope atoms}$$

$$D = \text{Number of radiogenic daughter isotope atoms}$$

$$t = \text{duration of radioactive decay}$$

(f) Equations for single-stage evolution of lead isotope ratios at geologic time t (counted backward from the present, as per standard convention), with abundances of uranium and thorium isotopes expressed in terms of their equivalent present-day ratios

$$({}^{206}\text{Pb} / {}^{204}\text{Pb})_t = a_o + \mu (e^{\lambda T} - e^{\lambda t}) \tag{4.25}$$

$$({}^{207}\text{Pb} / {}^{204}\text{Pb})_t = b_o + (\mu / 137.8) (e^{\lambda' T} - e^{\lambda' t}) \tag{4.26}$$

$$({}^{208}\text{Pb} / {}^{204}\text{Pb})_t = c_o + \mu k (e^{\lambda'' T} - e^{\lambda'' t}) \tag{4.27}$$

where t = geologic time at which single-stage evolution stopped (*model lead age*), i.e., when the sample became isolated from U-Th system
 T = geologic time at which single-stage evolution started (age of the Earth)

TABLE 4.2 (continued)

(g) Equation for (single-stage) primary isochron ($^{207}\text{Pb}/^{204}\text{Pb}$ vs. $^{206}\text{Pb}/^{204}\text{Pb}$ plot)

$$\frac{(^{207}\text{Pb}/^{204}\text{Pb})_t - b_0}{(^{206}\text{Pb}/^{204}\text{Pb})_t - a_0} = \frac{1}{137.8} \frac{(e^{\lambda T} - e^{\lambda t})}{(e^{\lambda T} - e^{\lambda t})} \quad (4.28)$$

with origin (x, y) at $x = a_0$, $y = b_0$ and

$$\text{slope } (m) = \frac{1}{137.8} \frac{(e^{\lambda T} - e^{\lambda t})}{(e^{\lambda T} - e^{\lambda t})} = \frac{(^{207}\text{Pb}/^{204}\text{Pb})_t - b_0}{(^{206}\text{Pb}/^{204}\text{Pb})_t - a_0} \quad (4.29)$$

The intersection of the isochron, for a particular value of t , with the single-stage evolution curve defines the corresponding single-stage lead isotope ratios.

the single-stage growth curve marks the theoretical lead isotope ratios corresponding to a discrete geologic time (t). The *primary isochron* corresponding to a particular value of t can be drawn by using Equation 4.28 (Table 4.2). The age (t) of a lead sample determined using the single-stage model is called the *model (lead-lead) age*.

Evidently, many single-stage evolution curves can be constructed, each corresponding to a set of chosen values for the basic parameters (a_0 , b_0 , c_0 , m , and T); the currently accepted values of these parameters are listed in Table 4.2. For the purpose of illustration, a set of single-stage growth curves with different assumed values of μ and corresponding primary isochrons for a few selected values of t are shown in Figure 4.14. Note that the slope of the primary isochron is independent of the value of μ so that all single-stage leads that were removed from sources with different μ but at the same time (t) must lie on the isochron corresponding to time t . The isochron representing leads having $t = 0$ is called the *geochron*, because all modern single-stage leads in the Earth (and in meteorites) lie on it.

If the isotopic composition of the lead contained in a rock or in an ore can be accounted for by the single-stage evolution model, it is called *ordinary lead*, and its model age gives the time of its formation within experimental error; if not, it is called *anomalous lead*, and its model age may be appreciably different from its actual time of formation. Typical examples of anomalous leads are the J-type leads (Russell & Farquhar 1960), so named after their type occurrence in the galena - sphalerite ores of Joplin (Missouri, USA), which contain excess radiogenic lead and yield model ages that are younger than the age of the ore deposit. In special cases, the anomalous leads appear to have been produced by the mixing of two ordinary leads of different ages, (Fig. 4.15). More commonly, anomalous leads represent multi-stage evolution in two or more source regions having different values of μ and require more sophisticated techniques of interpretation (e.g., Koppel & Saager 1976, Faure 1986).

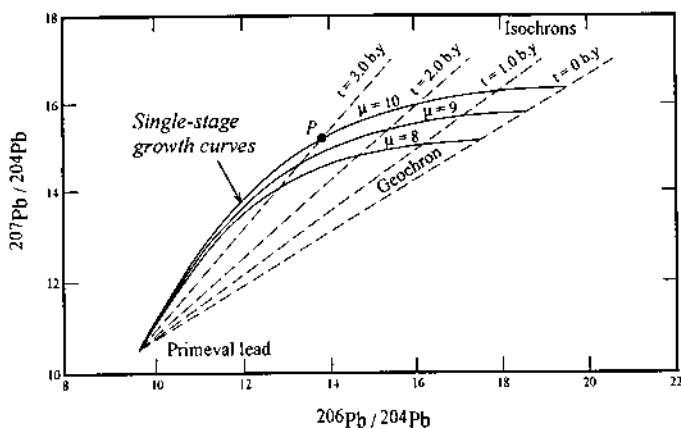


Figure 4.14. Single-stage lead evolution curves for U-Pb systems with different present-day μ ($=^{238}\text{U}/^{204}\text{Pb}$) values. The straight lines are primary isochrons for selected values of t ; the isochron for $t = 0$ is called the geochron. Equations and values of a_0 , b_0 , T , λ , λ' and present-day $^{238}\text{U}/^{235}\text{U}$ ratio used for construction of the evolution curves and primary isochrons are as given in Table 4.2. The coordinates of point P represent the $^{207}\text{Pb}/^{204}\text{Pb}$ and $^{206}\text{Pb}/^{204}\text{Pb}$ of a galena lead that was withdrawn 3.0 b.y. ago from a source region of $\mu = 10.0$; the model lead age of this galena is 3.0 b.y. This diagram was constructed by solving Equations 4.25 and 4.26, assuming that the age of the Earth (T) = 4.55 b.y. (After Faure 1986.)

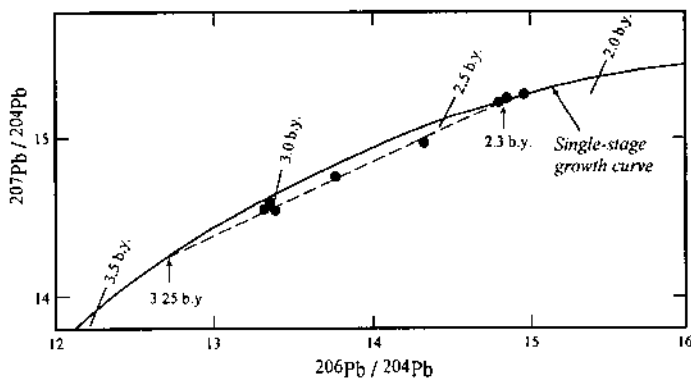


Figure 4.15. Lead isotope ratios in galena samples from the Cobalt-Noranda area, Ontario (Canada) in relation to the single-stage growth curve having $\mu = 8.99 \pm 0.07$. The constants are: $\lambda = 1.537 \times 10^{-10}/\text{year}$, $\lambda' = 9.722 \times 10^{-10}/\text{year}$, $a_0 = 9.56$, $b_0 = 10.42$, $T = 4.55 \times 10^9$ years. The anomalous leads are interpreted to represent mixing of two ordinary leads, one 3250 ± 150 m.y. old and the other 2300 ± 150 m.y. old (Kanasewich & Farquhar 1965). More recent lead isotope data from the area (Thorpe 1974) suggest that this simple interpretation of the anomalous leads may not be valid.

4.5.2. APPLICATIONS

In addition to the common usage as a technique for age determination, lead isotope ratios are used as tracers of the source of metals in mineral deposits. The basic premise for the latter is that, irrespective of the specific mode of ore deposition, the lead isotopic composition of any ore is characteristic of the source or sources from which the lead was derived, (Cooper & Richards 1969, Richards 1971, LeHuray 1984). The most convincing example of this premise is provided by the recently active mid-ocean ridge hydrothermal vents, where lead-isotope ratios of the hydrothermal sulfides can clearly be correlated with a basaltic, sedimentary, or mixed source of lead, consistent with the geologic setting of the vents (LeHuray et al. 1988). As discussed below, the interpretation of lead isotope ratios in ancient deposits is generally more complicated.

In earlier literature, the single-stage ore lead was interpreted to have been derived from the mantle, an interpretation supported by the uniformity in lead isotopic composition of many conformable sulfide deposits (Stanton & Russell 1959). But more recent studies (e.g., Cooper & Richards 1969) have revealed that many young oceanic volcanic rocks, which are least likely to have been contaminated during passage from the mantle, have lead isotopic ratios markedly different from what would be predicted from the single-stage model. Thus many ore leads which were earlier believed to be single-stage do not fit the model perfectly and those that closely approach evolution under single-stage conditions (Fig. 4.16) seem to have no more than a

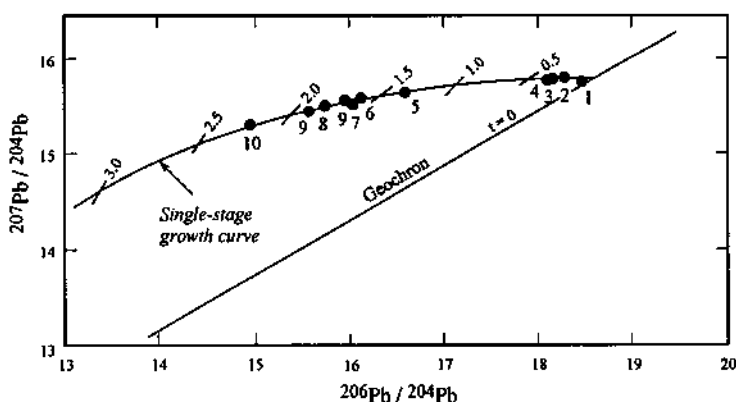


Figure 4.16. Isotope ratios of lead from conformable ore deposits that appear to fit a single-stage growth curve (the same as in Fig. 4.14). The data are from a compilation by Kanasewich (1968) and include samples from the following deposits: (1) Hall's Peak, NSW, Australia; (2) Bathurst, NB, Canada; (3) Cobar, NSW, Australia (five mines); (4) Captain's Flat, NSW, Australia; (5) Sullivan Mine, BC, Canada; (6) Mt. Isa, Queensland, Australia (two mines); (7) Broken Hill, NSW, Australia (five mines); (8) Finland (five mines including Orijarvi); (9) Errington Mine, Sudbury, Canada (two sets of values); (10) Cobalt, Ontario, Canada. The isochrons (3.0, 2.5, 2.0, 1.5, 1.0, and 0.5) are in billion years before present. (After Faure 1986.)

component of mantle lead in them. The close approach to single-stage conditions, rather than implying horizons inside the Earth with constant $^{238}\text{U}/^{204}\text{Pb}$ and $^{232}\text{Th}/^{204}\text{Pb}$ ratios, is probably best explained by the gathering of lead from very large volumes of rock and multiple-reworked sediments, homogenization of heterogeneous source materials throughout geologic time, and continuous diffusion of uranium, thorium, and lead throughout the crust and upper mantle during geologic time (Doe & Stacey 1974).

Lead isotope data on different types of mineral deposits have been reviewed in several publications (e.g., Koppel & Saager 1976, Sangster 1976, Doe & Zartman 1979, Farquhar & Fletcher 1980, Gulson 1986). As a generalization, ore leads from most mineral deposits, especially those younger in age than the Archean (Stacey & Kramers 1975, Cumming & Richards 1975), are anomalous in varying degrees. Thus, obtaining useful information from lead isotope data on mineral deposits depends largely on meaningful interpretation of anomalous leads.

Many leads are anomalous in the context of the Holmes-Houtermans model, because their lead isotope ratios are being evaluated with reference to an evolution model that assumes that the $^{238}\text{U}/^{204}\text{Pb}$ ratio of the lead reservoir has changed with time only by radioactive decay and not by other processes such as differentiation and homogenization. Such an assumption is unrealistic in view of the dynamic evolution of the Earth involving repeated interaction between the mantle and the crust. This realization has led to several recently proposed lead evolution models that allow for variation in the $^{238}\text{U}/^{204}\text{Pb}$ ratio of the lead reservoir by mixing of leads of different isotopic compositions. For example, Stacey and Kramers (1975) constructed an "average" lead growth curve incorporating a two-stage process that involved a change in $^{238}\text{U}/^{204}\text{Pb}$ and $^{232}\text{Th}/^{204}\text{Pb}$ ratios of the reservoir (by geochemical differentiation) at 3.7 b.y. ago and found this to yield good model ages for lead samples of different ages (Fig. 4.17). The model postulates a first stage of lead evolution from a primordial composition assumed to be that of meteoritic troilite lead ($^{238}\text{U}/^{204}\text{Pb} = 7.19$, $^{232}\text{Th}/^{204}\text{Pb} = 32.19$) beginning at 4.57 b.y. ago, and a second stage evolution with $^{238}\text{U}/^{204}\text{Pb} \approx 9.74$ and $^{232}\text{Th}/^{204}\text{Pb} \approx 37.19$ in those portions of the Earth that took part in the mixing events, giving rise to "average" lead. Doe and Zartman (1979) discussed the lead isotope data from several geologic environments in relation to four growth curves generated by a dynamic lead evolution model: (a) a curve for the mantle lead ($\mu = 8.92$), (b) a curve for the "orogene", representing a balance of lead input from the mantle, upper crust, and lower crust sources ($\mu = 10.87$), corresponding to the "average" curve of Stacey and Kramers (1975); (c) a curve reflecting lead contribution from only the upper crust to the orogene ($\mu = 12.24$); and (d) a curve reflecting lead contribution from the lower crust only to the orogene ($\mu = 5.89$).

When combined with regional and local geologic data, such dynamic models offer significant improvements in the interpretation of anomalous leads, although they often do not lead to unequivocal identification of the lead source. A few of the examples discussed by Farquhar and Fletcher (1980) will suffice to illustrate the point. The data shown in Figure 4.18 all fall between the mantle and orogene growth curves and into two distinct patterns of distribution: one typical of the Central Metasedimentary Belt of

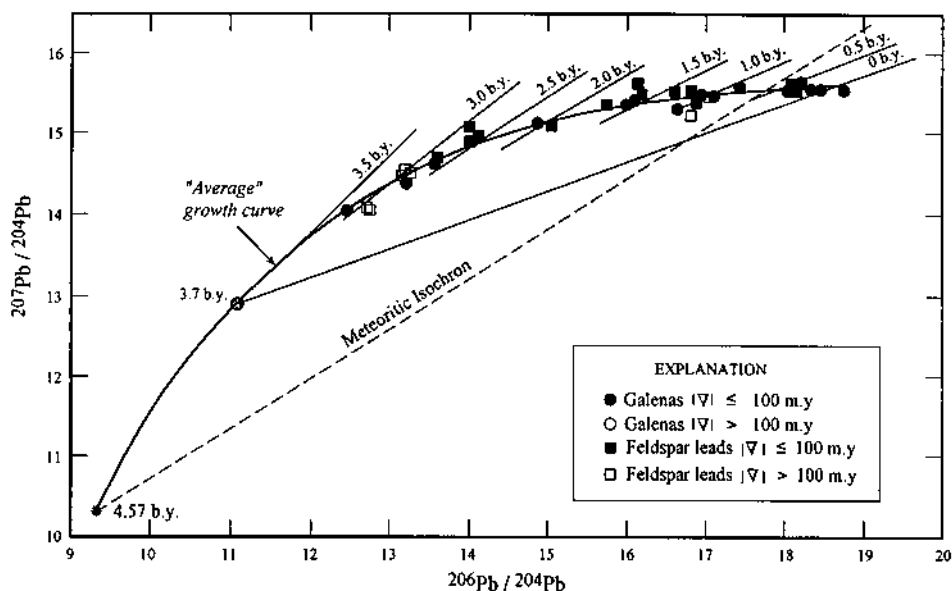


Figure 4.17. Lead isotopic ratios of 13 galena samples from conformable deposits and 23 least radiogenic feldspar leads in relation to the two-stage lead evolution curve of Stacey and Kramers (1975). For the first-stage evolution $\mu = 7.19$ and for the second stage $\mu = 9.74$; the first stage began at $T = 4.57$ b.y. and the second stage began at $t = 3.7$ b.y. The ∇ value for a sample represents the difference between its accepted age and the model age obtained from the two-stage lead evolution curve. The ∇ values of all galena samples lie within ± 100 m.y. (actually within ± 50 m.y. for all except the two youngest samples) and the values of 17 out of 23 feldspar samples lie within ± 100 m.y. (After Stacey & Kramers 1975.)

the North American Grenville Province (the "CMsB type"), characterized by a low-angle and broadly linear distribution close to the mantle curve (low μ values), and the other typical of the Balmat-Edwards (New York, USA) massive sulfide deposit (the "Balmat-Edwards type"), characterized by a steep-angle linear distribution and variable μ values. The distribution of the isotope ratios in the Besshi deposit (Japan), which is associated with rift-zone mafic volcanic rocks, is similar to that of the mid-oceanic ridge basalts (MORB) and probably reflects the heterogeneities of the lead isotopes in the oceanic mantle beneath the Japanese Paleozoic arc. Some of the CMsB sulfides are hosted by island-arc volcanics and the lead was probably derived also from a heterogeneous mantle. The Coeur d'Alene-type deposits (hosted by the Belt Supergroup rocks of Idaho-Montana, USA) are believed to be of the same age as the host sediments, but there is no evidence that the sulfides are volcanogenic. According to the model proposed by Doe and Zartman (1979), the apparent μ values of these leads lying between the growth curves for the mantle and the orogene suggest a combination of mantle and crustal sources for the lead. However, in view of the unlikely preservation of original mantle isotopic distribution through substantial mixing, the lead might

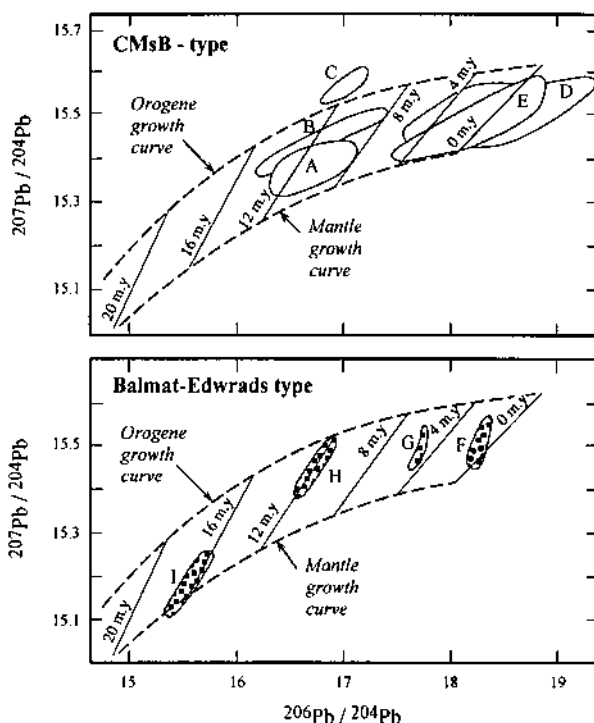


Figure 4.18 Data-field outlines for isotope ratios of selected CMsB (Central Metasedimentary Belt) type and Balmat-Edwards type leads in relation to the mantle and orogenic growth curves of Doe and Zartman (1979). Lines joining points of equal time on the two growth curves are equivalent to isochrons. Fields: A = CMsB, B = Coeur d'Alene, C = Namaqualand, D = Oceanic volcanics, E = Besshi, F = Kuroko, G = Buchans, H = Balmat-Edwards, I = Flin Flon-Snow Lake. (After Farquhar & Fletcher 1980.)

have been entirely crustal.

Fletcher and Farquhar (1982) confirmed that the trend for Balmat data represents a mixing line, not an isochron; the same is likely to be the case with other trends in this group. The mixing of two lead components of the same age, a low- μ mantle component and a high- μ component from older continental crust, might explain the Balmat-Edwards lead isotope distribution. The Balmat area, however, lacks extensive local occurrence of metavolcanic rocks and the lead-isotopic composition of older continental crust is not known. The steep-angled trend of the ore leads from the volcanogenic Kuroko sulfide deposits (Japan) associated with Tertiary calc-alkaline volcanic rocks is probably not the result of a second stage of lead isotopic generation, because this would require a much older source for the leads compared with the age of the rocks found in or around Japan. The interpretation favored by Doe and Zartman

(1979) is the mixing of lead from pelagic sediments with lead of continental crustal or mantle isotopic composition in varying proportions.

Lead-isotope geochemistry is a potentially useful tool in mineral exploration (Doe & Stacey 1974, Gulson 1986, Young 1995), although at present it lacks the level of sophistication achieved by other methods of geochemical prospecting. Applicable techniques discussed by Doe and Stacey (1974) may be summarized as follows:

- (a) the ordinary lead method (Cannon et al. 1961) — there is a greater probability of finding an economic deposit when the $^{208}\text{Pb}/^{204}\text{Pb}$ model age is in agreement with the primary Pb-Pb isochron age;
- (b) the fingerprint method (Delevaux et al. 1967) — a mineral prospect that has the same lead isotopic composition as a producing orebody in the district may be economic itself, a technique that may be particularly useful for exploration of Mississippi Valley-type lead-zinc deposits characterized by highly radiogenic, anomalous leads (J-type leads);
- (c) the magmatic source method (Stacey et al. 1968) — the closer the lead isotopic composition of galena in a prospect to the initial lead isotopic composition in the suspected igneous source, the larger is its ore potential; and
- (d) the zoning relations (Doe et al. 1968) — if leads similar in lead isotopic composition to igneous rocks are indicative of high-temperature, near-source deposits, such as copper, then more radiogenic leads in the ores within an igneous rock sequence may be indicative of lower-temperature, distal deposits, such as the Pb-Zn-Ag deposits at Creede, Colorado.

Young (1995) has espoused the promise of lead-isotope ratios in identifying large volcanic-associated and sediment-hosted massive sulfide deposits in a metallogenic province.

4.6. Strontium Isotopes

4.6.1. PRINCIPLES

The two most common applications of strontium isotopes are radiometric dating of rocks and determination of the source regions of magmatic rocks. Such information about the host rocks is obviously valuable for the interpretation of the mineral deposits they contain. In addition, strontium isotope ratios are potentially useful for determining the source of strontium (and possibly of associated metals) in mineral deposits and the source of ore-forming fluids.

Depending on the purpose of the study, strontium isotopes are measured either in whole-rock samples or in Sr-bearing minerals separated from the rocks of interest. Strontium forms its own minerals, strontianite (SrCO_3) and celestite (SrSO_4), both of

which occur in certain hydrothermal deposits and in carbonate rocks. The predominant mode of occurrence of strontium in rocks, however, is by substitution for calcium, potassium, and barium in other minerals (feldspars, micas, calcite, aragonite, fluorite, barite, etc.). Even base metal sulfides, such as galena, may contain measurable amounts of strontium isotopes (Lange et al. 1983, Nakai et al. 1990, Nakai et al. 1993). It is also possible to measure strontium isotope ratios in fluid inclusions (Norman 1978, Norman & Landis 1983).

Strontium has four naturally occurring isotopes (^{88}Sr , ^{87}Sr , ^{86}Sr , and ^{84}Sr), all of which are stable. Only one of these isotopes, ^{87}Sr , is radiogenic and is produced by radioactive decay of ^{87}Rb . Thus the ^{87}Sr content of a Rb-bearing mineral or rock in a closed system with respect to rubidium and strontium depends not only on its initial ^{87}Sr value ($^{87}\text{Sr}_0$) but also on the addition of radiogenic ^{87}Sr . From the general equation for radioactive decay (see Table 4.2), the ^{87}Sr content of a closed Rb-Sr system can be expressed as

$$^{87}\text{Sr} = ^{87}\text{Sr}_0 + ^{87}\text{Rb} (e^{\lambda t} - 1) \quad (4.30)$$

where λ ($= 1.39 \times 10^{11}/\text{y}$) is the decay constant for the ^{87}Rb to ^{87}Sr decay and t is the geologic age of the mineral or rock (counted backward from the present time, as per standard convention). Normalizing the above equation to ^{86}Sr , a non-radiogenic isotope of strontium, Equation 4.30 reduces to

$$^{87}\text{Sr} / ^{86}\text{Sr} = (^{87}\text{Sr} / ^{86}\text{Sr})_0 + (^{87}\text{Rb} / ^{86}\text{Sr}) (e^{\lambda t} - 1) \quad (4.31)$$

This equation is the basis for age determination by the Rb-Sr radiometric method. With the $^{87}\text{Sr}/^{86}\text{Sr}$ and $^{87}\text{Rb}/^{86}\text{Sr}$ values obtained from analysis of the sample, the equation can be solved for t if the *initial ratio*, $(^{87}\text{Sr}/^{86}\text{Sr})_0$, is known. Without a knowledge of the $(^{87}\text{Sr}/^{86}\text{Sr})_0$, as commonly is the case, the method is applied by selecting a suite of samples that spans a wide range of Rb/Sr ratios and is likely to satisfy the assumptions that the samples were formed at the same time, had the same initial $^{87}\text{Sr}/^{86}\text{Sr}$ ratio, and have remained in closed systems since their formation (Faure 1986). Such a suite of samples define a straight line, an *isochron*, on a $^{87}\text{Rb}/^{86}\text{Sr}$ versus $^{87}\text{Sr}/^{86}\text{Sr}$ plot. The y-intercept of the isochron gives the $(^{87}\text{Sr}/^{86}\text{Sr})_0$ value and the geologic age of the samples (t) is determined from the slope of the isochron ($= e^{\lambda t} - 1$) or by solving Equation 4.31 for t . For example, strontium isotope ratios of norite and granophyre samples from the Sudbury Complex (Ontario, Canada) define an isochron that gives an initial ratio of 0.7073 ± 0.0004 and an age of 1722 ± 22 Ma for the Complex (Fig. 4.19).

Strontium isotope ratios can be used to determine the source or origin of rocks associated with mineral deposits. For magmatic rocks, such determinations are based on their present-day $^{87}\text{Sr}/^{86}\text{Sr}$ ratios as well as their $(^{87}\text{Sr}/^{86}\text{Sr})_0$ ratios extrapolated from isochrons. From analysis of basaltic achondrites, which are believed to provide the best

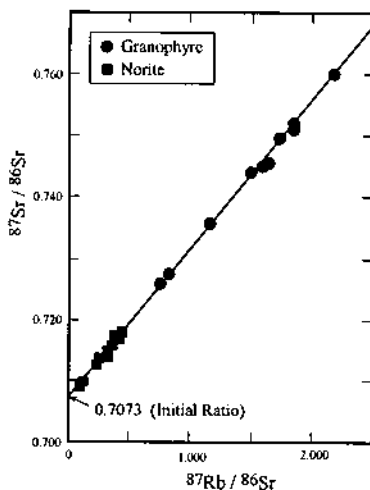


Figure 4.19. Rb-Sr Isochron for the Sudbury Complex (Ontario, Canada) based on strontium isotope data for granophyre and norite discussed by Gibbins and McNutt (1975). The slope of the isochron gives an age of 1722 ± 22 Ma and its y-axis intercept gives an initial ($^{87}\text{Sr}/^{86}\text{Sr}$) ratio of 0.7073 ± 0.0004 . (After Naldrett & Hewins 1984.)

samples for estimating the $^{87}\text{Sr}/^{86}\text{Sr}$ ratio in the solar nebula at the time of formation of planetary bodies, an initial ratio of 0.698990 ± 0.000047 , known as BABI (basaltic achondrite best initial), is widely accepted as the best estimate of the primordial $^{87}\text{Sr}/^{86}\text{Sr}$ ratio of the Earth. The modern oceanic basalts show a discernible scatter in their $^{87}\text{Sr}/^{86}\text{Sr}$ ratios (Fig. 4.20), and this may be due to heterogeneity in the upper mantle as well as to more local factors related to fractionation and assimilation processes (Faure 1986). However, analyses of young basalts and large gabbroic intrusives that are presumed to represent upper mantle material without significant crustal strontium contamination suggest that the present-day $^{87}\text{Sr}/^{86}\text{Sr}$ ratios of the upper mantle lie within a narrow range of 0.704 ± 0.002 (with a corresponding Rb/Sr ratio of about 0.025). In contrast, enrichment of crustal material in rubidium by geochemical differentiation very early in the Earth's history has resulted in a much larger increase in the $^{87}\text{Sr}/^{86}\text{Sr}$ ratios of the crustal rocks. Values as high as 0.712 to 0.726 have been estimated for the Precambrian gneisses of the Canadian Shield (Faure et al. 1963) and higher values should be expected for younger granitic rocks of crustal derivation. Several factors, including the initial Rb/Sr ratios of the source materials and the age and geological history, determine the $^{87}\text{Sr}/^{86}\text{Sr}$ ratio of a crustal rock, but the ratio, in general, should be significantly greater than that of a rock formed from upper mantle material. A modern igneous rock with $(^{87}\text{Sr}/^{86}\text{Sr})_0$ close to 0.704 indicates an upper mantle origin, whereas one with an elevated initial ratio indicates

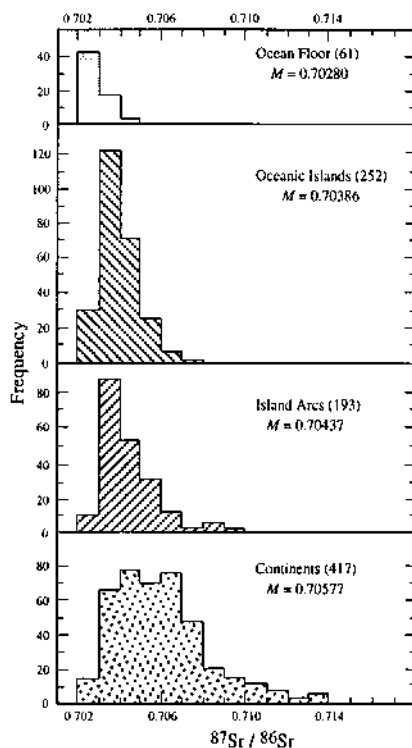


Figure 4.20. Histograms of $^{87}\text{Sr}/^{86}\text{Sr}$ ratios of young volcanic rocks of basaltic and intermediate composition in different geological environments. The number in brackets indicates the number of samples and M is the arithmetic mean. All the histograms are skewed toward higher values of $^{87}\text{Sr}/^{86}\text{Sr}$, which in some cases may have resulted from contamination of the magma with radiogenic ^{87}Sr derived from old sialic rocks or their derivatives. (After Faure 1986.)

incorporation of crustal strontium and implies formation, at least partly, from crustal material. The general validity of this principle is well corroborated by field data. For example, $(^{87}\text{Sr}/^{86}\text{Sr})_0$ ratios of felsic intrusions related to porphyry copper mineralization (see Ch. 8) are significantly higher in the continental settings (mostly 0.706-0.709) than in the island-arc settings (mostly <0.705) (Titley & Beane 1981).

Strontium isotope ratios may also be useful for distinguishing between carbonate minerals and rocks of marine and nonmarine origin. Available data compiled by Veizer (1989) suggest that the strontium isotopic composition of the oceans has fluctuated during the Phanerozoic, from a low of less than 0.707 in the Jurassic and Permian to a high of 0.709 in the late Cambrian and at present (Fig. 4.21). Thus Phanerozoic marine carbonates should have $^{87}\text{Sr}/^{86}\text{Sr}$ ratios in the approximate range of 0.707 to 0.709. Evaluation of $^{87}\text{Sr}/^{86}\text{Sr}$ ratios in clastic sediments is usually more involved

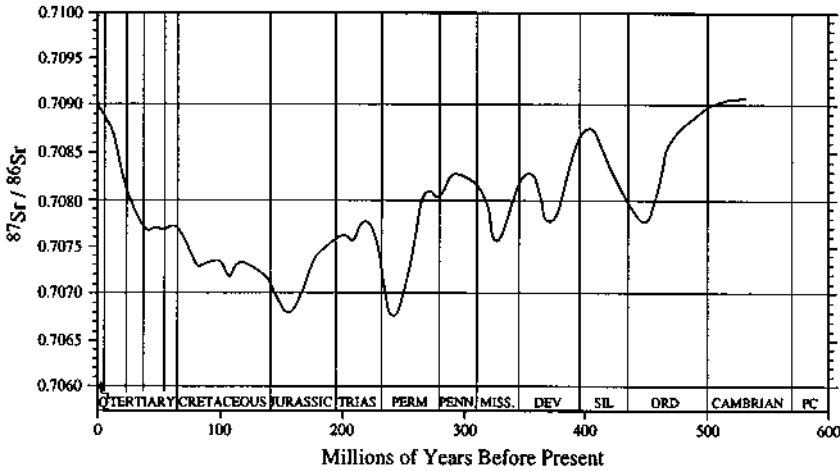


Figure 4.21. $^{87}\text{Sr}/^{86}\text{Sr}$ ratio of the oceans during the Phanerozoic time as indicated by Sr-isotope ratios of marine carbonate, evaporite, and phosphate samples of known age (after Veizer 1989).

because of mixing of materials from multiple sources.

Because ore-forming fluids commonly are mixtures of fluids from different sources, the measured strontium isotopic ratios may actually represent mixing of materials having different strontium contents and $^{87}\text{Sr}/^{86}\text{Sr}$ ratios. At least in a two-component system, the simplest case of mixing, it is usually possible to estimate the strontium concentration and $^{87}\text{Sr}/^{86}\text{Sr}$ ratios of the two end-members. Consider a mixture (M) of two components A and B with different concentrations of Sr and $^{87}\text{Sr}/^{86}\text{Sr}$ ratios. Assuming no modifications of the Sr concentrations or ratios after mixing, the $^{87}\text{Sr}/^{86}\text{Sr}$ ratio of the mixture is given by (Faure 1986) as:

$$\begin{aligned}
 (^{87}\text{Sr}/^{86}\text{Sr})_M &= \frac{\text{Sr}_A \text{Sr}_B [(^{87}\text{Sr}/^{86}\text{Sr})_B - (^{87}\text{Sr}/^{86}\text{Sr})_A]}{\text{Sr}_M (\text{Sr}_A - \text{Sr}_B)} \\
 &+ \frac{\text{Sr}_A (^{87}\text{Sr}/^{86}\text{Sr})_A - \text{Sr}_B (^{87}\text{Sr}/^{86}\text{Sr})_B}{\text{Sr}_A - \text{Sr}_B}
 \end{aligned}
 \quad (4.32)$$

where the suffixes A , B , and M refer, respectively, to component A , component B , and the mixture. This is the equation of a hyperbola, in a Sr_M vs. $(^{87}\text{Sr}/^{86}\text{Sr})_M$ plot (Fig. 4.22a), of the form

$$(^{87}\text{Sr}/^{86}\text{Sr})_M = (a/\text{Sr}_M) + b \quad (4.33)$$

where a and b are constants for a given proportion of A and B in the mixture. The

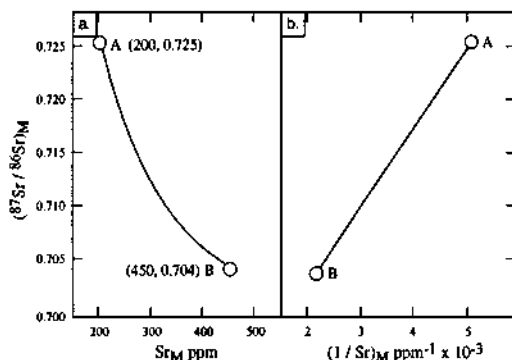


Figure 4.22. Calculated $^{87}\text{Sr}/^{86}\text{Sr}$ ratios of mixtures of two components (A and B) with different Sr contents and Sr isotope ratios: a, form of the mixing hyperbola (Equation 4.32); b, transformation of the hyperbola to a mixing line by plotting the reciprocal of the strontium concentration. (After Faure 1986.)

mixing parabola can be transformed to a more readily usable form, a straight line, by plotting $(^{87}\text{Sr}/^{86}\text{Sr})_M$ vs. $1/\text{Sr}_M$ (Fig. 4.22b). Thus, a plot of $(^{87}\text{Sr}/^{86}\text{Sr})_M$ versus $1/\text{Sr}_M$ values of a suite of samples representing mixtures of two components in varying proportions produces a straight line (within acceptable statistical error) if the mixing hypothesis is correct. The strontium concentrations of the end-members A and B can then be obtained by solving Equation 4.32, assuming reasonable values for $(^{87}\text{Sr}/^{86}\text{Sr})_A$ and $(^{87}\text{Sr}/^{86}\text{Sr})_B$; conversely, the strontium isotope ratios for the end-members A and B can be estimated by assuming reasonable values for Sr_A and Sr_B . The evaluation of mixtures containing three or more components is too complex to be treated here.

4.6.2. APPLICATIONS

The application of the Rb-Sr technique to dating of mineral deposits directly is limited by the difficulty of obtaining a suite of samples suitable for defining an isochron. A suite of samples involving variable mixtures of two components having different Rb/Sr and ^{87}Sr and ^{86}Sr ratios can yield a straight line in a $^{87}\text{Rb}/^{86}\text{Sr}$ versus $^{87}\text{Sr}/^{86}\text{Sr}$ plot, but this is a mixing line, not an isochron. Mineral deposits that contain strontium-bearing minerals precipitated from fluids of varying chemical and isotopic composition are particularly prone to such misinterpretation. For example, Lange et al. (1983) used the Rb-Sr method on a set of galena samples to determine the age of lead-zinc mineralization in the Viburnum Trend (southeast Missouri, USA). But, if the galenas did not precipitate from a mineralizing fluid of homogenous Rb-Sr isotopic composition, as has been argued by Ruiz et al. (1985), then the "isochron" of Lange et al. (1983) would represent a mixing line with no real age significance.

An obvious application of strontium isotope ratios is to determine the source of strontium in hydrothermal mineral deposits, mainly by comparison of their $^{87}\text{Sr}/^{86}\text{Sr}$ ratios with those of the likely sources, taking into account the possibility of mixing. In one of the earliest detailed studies of this kind, Reesman (1968) found that the strontium in the gangue minerals in several vein-type hydrothermal deposits ranging in age from Precambrian to Tertiary was derived, at least to a very large extent, from the rocks of the immediate host environment. From a similar study of fluorite deposits in Coahuila (Mexico), Kesler et al. (1983) concluded that those limestone-replacement deposits were formed by solutions that obtained almost all (about 98%) of their strontium from limestone at the site of deposition, whereas about 20% of the strontium in the vein and manto deposits was contributed by the Tertiary igneous rocks of the district. Barbieri et al. (1984) used strontium isotope ratios to distinguish different sources of strontium for the different types of barite deposits in Sardinia (Italy): contemporaneous seawater for the Cambrian stratiform barite, Cambrian wallrocks for the karst barite, and Lower Paleozoic marine shales for the epigenetic hydrothermal barite. It should be emphasized, however, that the source of other metals, particularly base metals, in a hydrothermal mineral deposit may be quite different from that of strontium.

Perhaps the most promising application of strontium isotopes is as a tracer of hydrothermal fluids. The use of strontium isotopes has some advantages over hydrogen and oxygen isotopes: there are no serious fractionation effects in the strontium isotope system; the strontium isotope ratio may better indicate the source of dissolved solids (solute) in hydrothermal fluids; and in some cases the source $^{87}\text{Sr}/^{86}\text{Sr}$ ratio can be determined precisely (e.g., magmatic fluids should have the same $^{87}\text{Sr}/^{86}\text{Sr}$ ratio as the source magma). From $^{87}\text{Sr}/^{86}\text{Sr}$ ratio measurements in gangue minerals (calcite, dolomite, fluorite, barite) of the Elmwood zinc deposit (Central Tennessee zinc district, USA), Grant and Bliss (1983) found that the pre-sulfide minerals formed from a fluid in isotopic equilibrium with the host carbonates, whereas the post-sulfide minerals precipitated from a fluid containing more radiogenic strontium. This variation, they concluded, was consistent with the idea that the sulfide ore was precipitated by the mixing of two fluids.

Strontium isotope ratios, which basically monitor the events that affect dissolved constituents (or solutes), can be even more useful when combined with oxygen and hydrogen isotope ratios, which measure the changes in the fluid (or solvent). Oxygen and hydrogen isotope data (see Fig. 4.12) suggest that mineralization in the Pasto Bueno (Peru) sulfide - wolframite deposit associated with a quartz monzonite stock was caused by the mixing of magmatic and meteoric waters, and possibly an "evolved water" of uncertain origin. Strontium isotope data do not identify the origin of the evolved water, but a δD vs. $^{87}\text{Sr}/^{86}\text{Sr}$ plot (Fig. 4.23) clearly delineates the fields of magmatic, meteoric, and evolved waters and mixtures of these waters. In particular, the fields of magmatic water and evolved water are quite distinct, whereas this distinction is not clear from the δD and $\delta^{18}\text{O}$ data. The combined data enabled Norman and Landis (1983) to conclude the following: (a) the tungsten-bearing solution had a magmatic

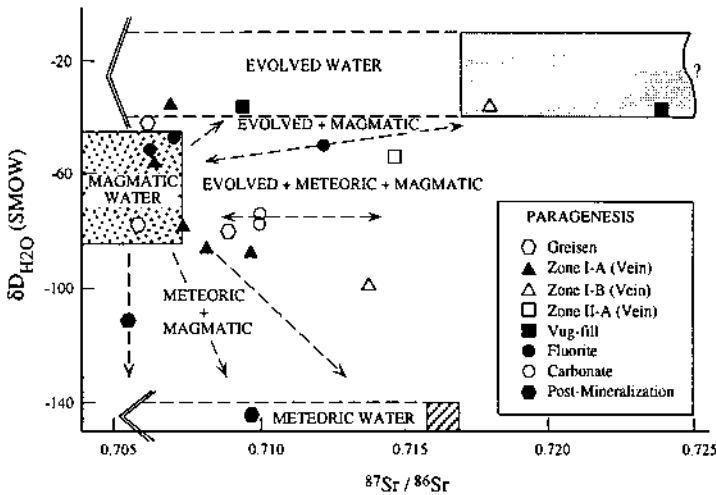


Figure 4.23. Plot of the independent variables δD and $^{87}Sr/^{86}Sr$ ratio illustrating the three-component mixture of hydrothermal fluids for the Pasto Bueno (Peru) sulfide - wolframite vein deposit associated with a quartz monzonite stock. Magmatic strontium is defined by the measured values of the host igneous rocks. Both meteoric and evolved waters have a possible range in isotopes as indicated by the dashed extensions. The mixtures are not restricted to the ternary space defined by the three end-member compositions. (After Norman & Landis 1983.)

source, but wolframite deposition was caused by a large (30-50%) meteoric water influx; (b) the source of sulfur (and possibly of metals) was magmatic (on the basis of sulfur isotope data), but the sulfide precipitation was from ore fluids of mixed derivation; and (c) the host igneous stock provided both the fluids and the solutes for the vug-fill fluorites in the deposit.

4.7. Geothermometry and Geobarometry

The temperature and pressure of formation of a mineral deposit, if they can be determined, provide valuable clues to the origin of the deposit. A *geothermometer* is a mineral or a mineral assemblage that yields information about its temperature of formation; a *geobarometer* is one that yields information about its pressure of formation. Three types of potential geothermometers and geobarometers are discussed here: (a) those based on stable isotope ratios; (b) those based on phase equilibria; and (c) those based on fluid inclusions. All these have one limitation in common. The temperature or pressure determined by any of the above methods relates to the last event of equilibration, which may or may not be the main-stage mineralization, especially if the deposit has been subsequently subjected to hydrothermal alteration or

metamorphism. The interpretation of geothermometric and geobarometric data, therefore, must be considered in conjunction with other geologic features of the deposit. The uncertainty in the estimated temperature or pressure varies with the method but is usually appreciable, either because of assumptions involved or errors in the calibration curves used. It is desirable to use more than one technique for the estimation of temperature or pressure. A concordance of temperature and pressure estimated by different geothermometers and geobarometers increases the reliability of the numbers.

4.7.1. STABLE ISOTOPE FRACTIONATION

The temperature dependence of equilibrium isotope fractionation is the basis of stable isotope geothermometry. As discussed earlier, the isotopic fractionation factor (α_{A-B}) between two species (*A* and *B*) coexisting in equilibrium is related to δ_A and δ_B by the relation

$$10^3 \ln \alpha_{A-B} \approx \delta_A - \delta_B = \Delta_{A-B} \quad (4.12)$$

The principle of isotope geothermometry, in essence, involves direct measurement of δ_A and δ_B and estimation of the temperature of isotopic equilibration corresponding to the particular value of $(\delta_A - \delta_B)$ from an appropriate $(\delta_A - \delta_B)$ versus temperature calibration curve. Calibration curves for some pairs of species have been calculated (e.g., see Figs. 4.2, 4.7, 4.10), but experimentally determined calibration curves are usually more reliable. The unique advantage of isotope geothermometry is that the effect of pressure on isotopic fractionation is negligible in most systems, especially at pressures less than 10 kb. This is so because the volumes of isotopically substituted molecules and crystals are not sensitive to pressure changes.

The essential requirements of isotope geothermometry are: (a) measurable and regular variation of the equilibrium fractionation factor with temperature; and (b) availability of a reliable, calculated, or experimentally determined calibration curve for the mineral pair under consideration. Other conditions that must be satisfied for successful application of isotope geothermometry depend on the suitability of the samples. These conditions include (Taylor 1967, Rye & Ohmoto 1974): (a) contemporaneous crystallization of the mineral phases from essentially the same fluid and in equilibrium with each other; (b) attainment of isotopic equilibrium between the minerals under consideration (which is not guaranteed by chemical or textural equilibrium); (c) preservation of their isotopic compositions (i.e., no isotopic exchange between the minerals or between a mineral and a fluid phase subsequent to the formation of the minerals); and (d) purity of mineral concentrates separated for isotopic analyses. A general limitation of isotopic geothermometry is its insensitivity at temperatures above a few hundreds of degrees Celsius and the difficulty of attaining isotopic equilibrium in laboratory determination of calibration curves at low temperatures.

In principle, fractionation of any of the four stable isotopes (oxygen, hydrogen, sulfur, and carbon) discussed earlier should have potential application in geothermometry. In practice, however, isotope geothermometry of mineral deposits is restricted to sulfur and oxygen isotopes. Hydrogen isotope fractionations are usually large, but their relatively small temperature dependence in mineral - H₂O systems, especially below 400°C, and the ease of isotope exchange between fluids and minerals even at low temperatures preclude their use in geothermometry (Taylor, 1974). Similarly, carbon isotopic fractionation among carbonate minerals is too insensitive to temperature variations to be useful in geothermometry (Ohmoto & Rye 1979). The potential carbon isotope geothermometers for mineral deposits are calcite - graphite, calcite - CO₂, and dolomite - CO₂ (see Fig. 4.7). The calcite - graphite geothermometer is not applicable to hydrothermal deposits because they rarely contain primary graphite. It may be possible to determine temperatures to within ±20°C from calcite - CO₂ and dolomite - CO₂ pairs if δ¹³C values of CO₂ can be obtained from primary inclusion fluids in contemporaneous carbon-free host minerals, such as quartz and sulfides.

An assemblage of *N* oxygen-bearing or sulfur-bearing minerals in equilibrium for which calibration curves are available should give *N*-1 oxygen or sulfur isotopic temperatures. A close agreement of temperatures determined from different pairs of minerals increases the reliability of the estimated temperature and provides evidence for isotopic equilibrium among the minerals in the assemblage, indicating their formation from the same fluid or fluids of fairly uniform temperature. A lack of agreement among the temperatures usually implies non-attainment of equilibrium at the time of crystallization or non-contemporaneity of one or more minerals in the assemblage.

Sulfur Isotopes

Equilibrium sulfur isotope fractionation among coexisting sulfide minerals is a function of temperature as well as of relative metal-sulfide bond strengths (Sakai 1968, Bachinski 1969). At a given temperature, under equilibrium conditions, the heavier isotope is enriched in minerals with stronger sulfur bonds. The order of ³⁴S enrichment in the important sulfide minerals of the Cu-Zn-Pb-Fe system, predicted from theoretical consideration, is (Bachinski 1969): pyrite > sphalerite > chalcopyrite > galena. The experimentally determined fractionation factors are in general agreement with this order, but there are significant discrepancies among calibration curves determined by various workers (e.g., see Czamanske & Rye 1974). Figure 4.24 shows the sulfur isotopic fractionation of important sulfur-bearing minerals and hydrothermal species relative to pyrite. Evidently, the larger the separation of the curves for any two minerals, the more sensitive will the mineral pair be as an isotopic geothermometer. Note that the calibration curves are straight lines, each of which may be described by an equation of the form $\Delta_{A-B} = (A \times 10^6)/T^2$, where *T* is the temperature in Kelvin and *A* is a constant equal to the slope of the line through the origin. Equations for the commonly used sulfur isotopic geothermometers, derived on the basis of a critical evaluation of the available theoretical and experimental data (Ohmoto & Rye 1979), are given in Table 4.3. The pyrite - galena pair is the most sensitive sulfide geothermometer, but

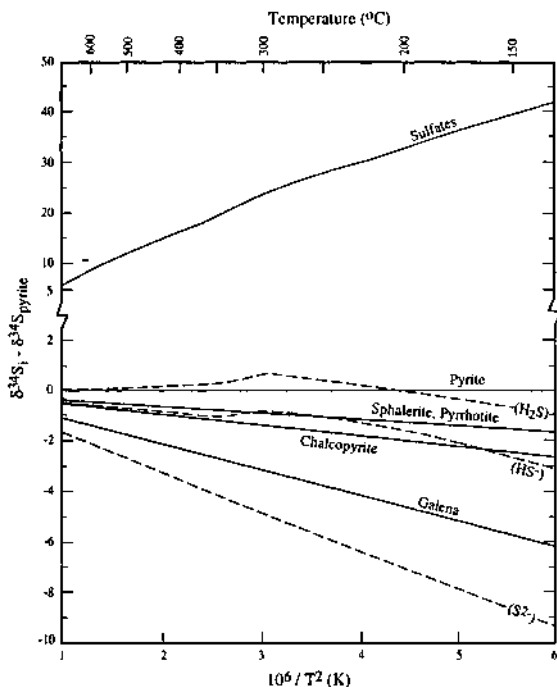


Figure 4.24. Sulfur isotopic fractionation among sulfur species (dashed lines) and hydrothermal minerals (solid lines) relative to pyrite. $1,000 \ln \alpha_{i,pyrite} = \delta^{34}S_i - \delta^{34}S_{py} = \Delta_{i,py}$ (After Rye & Ohmoto 1974.)

temperatures obtained involving pyrite may show an appreciable spread because of the common occurrence of several stages of pyrite crystallization. Sphalerite - galena is the most commonly used pair and in many cases it yields temperatures consistent with those obtained from fluid inclusion data, even when they are not strictly contemporaneous, suggesting that sphalerite and galena in many hydrothermal deposits are precipitated by similar mechanisms and under similar conditions. Inconsistent temperatures obtained from this geothermometer in some studies has been attributed to isotopic disequilibrium (Yamamoto et al. 1984, Botnikov et al. 1995).

It is evident from Figure 4.24 that sulfide-sulfate pairs should be more sensitive for sulfur isotopic geothermometry than sulfide-sulfide pairs. All sulfate minerals have approximately the same fractionation with respect to H_2S , so any of the common sulfate minerals (such as barite, anhydrite, gypsum) should be suitable for geothermometry. In reality, sulfate-sulfide pairs should be used with caution because they are often not contemporaneous in hydrothermal ore deposits and they are sluggish to equilibrate at temperatures below about 300°C (Ohmoto & Rye 1979).

TABLE 4.3. Sulfur isotopic geothermometers (Ohmoto & Rye 1979)

Mineral Pair (A - B)	Equation (T in Kelvin; $\Delta = \delta^{34}S_A - \delta^{34}S_B$)		Uncertainties #	
			1	2
Sulfates - chalcopyrite	$T = \frac{2.85 \times 10^3}{\sqrt{(\Delta \pm 1)}}$	($T > 400^\circ\text{C}$)	$\pm 25^*$	$\pm 5^*$
	$T = \frac{2.30 \times 10^3}{\sqrt{(\Delta - 6 \pm 0.5)}}$	($T < 350^\circ\text{C}$)	± 10	± 5
Sulfates - pyrite	$T = \frac{2.76 \times 10^3}{\sqrt{(\Delta \pm 1)}}$	($T > 400^\circ\text{C}$)	$\pm 25^*$	$\pm 5^*$
	$T = \frac{2.16 \times 10^3}{\sqrt{(\Delta - 6 \pm 0.5)}}$	($T < 350^\circ\text{C}$)	± 10	± 5
Pyrite - galena	$T = \frac{(1.01 \pm 0.04) \times 10^3}{\sqrt{\Delta}}$		± 25	± 20
Sphalerite (pyrrhotite) - galena	$T = \frac{(0.85 \pm 0.03) \times 10^3}{\sqrt{\Delta}}$		± 20	± 25
Pyrite - chalcopyrite	$T = \frac{(0.67 \pm 0.04) \times 10^3}{\sqrt{\Delta}}$		± 35	± 40
Pyrite - pyrrhotite (sphalerite)	$T = \frac{(0.55 \pm 0.04) \times 10^3}{\sqrt{\Delta}}$		± 40	± 55

1 = uncertainty in the calculated temperature from uncertainty in the equation (at $T = 300^\circ\text{C}$);
 2 = uncertainty in the calculated temperature from the analytical uncertainty of $\pm 0.2\%$ for Δ values
 (at $T = 300^\circ\text{C}$).

* Uncertainties in the calculated temperature at $T = 450^\circ\text{C}$.

Commonly, the sulfide-sulfate disequilibrium does not affect the equilibrium between sulfide mineral pairs, because the kinetics of $\text{H}_2\text{S}(\text{aq})$ - sulfide exchange is much more rapid than $\text{H}_2\text{S}(\text{aq})$ - $\text{SO}_4^{2-}(\text{aq})$ exchange, probably because the isotopic exchange between oxidized and reduced sulfur species occurs through thiosulfate as an intermediary reaction step (Ohmoto & Lasaga 1983).

Oxygen Isotopes

Equilibrium oxygen isotopic fractionation curves for various silicate and oxide minerals relative to quartz are presented in Figure 4.25. A widely used pair is quartz - magnetite, which is common in a variety of mineral deposits (e.g., porphyry copper, volcanogenic massive sulfide, skarn, and vein deposits). Other mineral pairs that yield good temperature estimates include calcite - magnetite, plagioclase - magnetite, and quartz - scheelite (Ohmoto 1986). In some cases, the calibration curves in Figure 4.25 may also be used to calculate the $\delta^{18}\text{O}$ values of H_2O in equilibrium with a particular mineral, if the temperature of equilibration can be estimated by some other technique, for example, from fluid inclusions (Taylor 1997).

4.7.2. PHASE EQUILIBRIA

An ideal equilibrium assemblage for geothermometry and geobarometry is one that simultaneously defines the temperature and pressure — for example, the assemblage andalusite + kyanite + sillimanite, which defines a true invariant point ($T = 501^\circ\text{C}$, $P = 3.76$ kb; Holdaway 1971). In the absence of such assemblages in the realm of ore

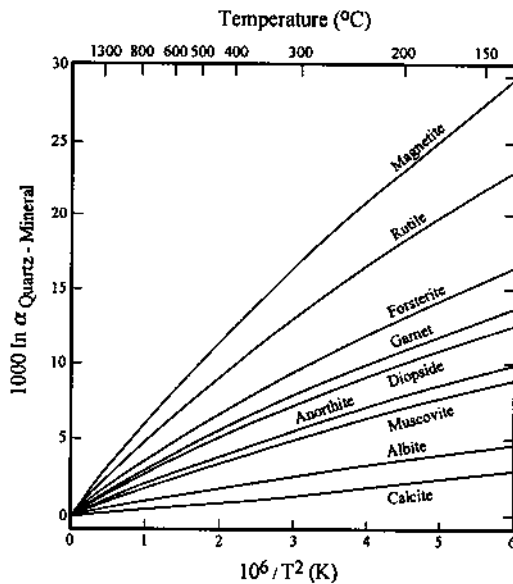
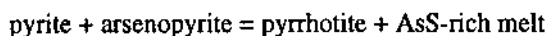


Figure 4.25. Equilibrium geothermometric calibration curves for $^{18}\text{O}/^{16}\text{O}$ fractionations between quartz and various silicate and oxide minerals. The fractionations are all positive, because at equilibrium quartz concentrates ^{18}O relative to all other minerals (the Si-O covalent bonds are extremely strong in quartz, resulting in very high vibrational frequencies for the oxygen atoms). (After compilation by Taylor 1997.)

mineral systems, the best that can be hoped for are minerals or mineral assemblages that can be used either as geothermometers or as geobarometers.

Geothermometers and geobarometers based on sulfide (and oxide) phase equilibria are either of *fixed-point* type, defined by a reaction at a fixed temperature or pressure, or of *sliding-scale* type, defined by a univariant reaction that may occur over a range of temperature or pressure. Fixed-point geobarometers are not known among sulfide systems; an extensive list of potential fixed-point geothermometers, invariant points in the experimentally investigated condensed sulfide systems, is given in Barton and Skinner (1979). Such geothermometers only set upper or lower limits of temperature of equilibration. For example, in the Fe-As-S condensed system, the invariant point (with the restriction that an additional phase, a vapor, is present) corresponding to the equilibrium assemblage



is $491 \pm 12^\circ\text{C}$ (Clark 1960a). Re-equilibration of this assemblage to a lower temperature may yield a pyrite + arsenopyrite or a pyrite + pyrrhotite + arsenopyrite assemblage. All that can be said about the temperature from the presence of either of these assemblages in a mineral deposit is that it has equilibrated to below 491°C . Further uncertainty arises from the fact that the invariant point in the condensed system is not a true invariant point; it increases with pressure at the rate of $1.8^\circ\text{C}/\text{kb}$ (Clark 1960b).

The thermodynamic basis for evaluating the potential of any univariant reaction as a sliding-scale type geothermometer or geobarometer is the relationship

$$\ln K = -\Delta G_r^\circ / RT \quad (4.34)$$

where ΔG_r° = the standard Gibbs free-energy change of the reaction, K = equilibrium constant of the reaction (at temperature T Kelvin and pressure P bars), and R = gas constant. The variation of K with temperature (at constant pressure) and with pressure (at constant temperature) can be expressed as

$$\left(\frac{\partial \ln K}{\partial T} \right)_P = \frac{\Delta H_r^\circ}{RT^2} \quad (4.35)$$

[van't Hoff equation]

and

$$\left(\frac{\partial \ln K}{\partial P} \right)_T = -\frac{\Delta V_r^\circ}{RT} \quad (4.36)$$

where ΔH_r° = the standard enthalpy change of the reaction and ΔV_r° = volume change produced by the reaction. If the right-hand side of Equation 4.35 is much larger than the right-hand side of Equation 4.36, K varies much more with temperature than with

pressure and the reaction is a potential geothermometer. The opposite condition applies for a potential geobarometer. In general, ΔV_r° for reactions involving solid phases is small except at very high pressures, so that sulfide minerals and assemblages are not likely to provide good geobarometers for deposits formed under upper crustal conditions. A few potential sliding-scale type geothermometers-geobarometers are discussed below.

Pyrrhotite Composition

Phase relations in the Fe-S system are fairly well established from many experimental studies (Fig. 4.26). Of particular interest in the present context is the solvus along which high-temperature pyrrhotite solid solution (Fe_{1-x}S) coexists with pyrite (FeS_2). The thermodynamic basis of the pyrrhotite-pyrite geothermometer is the stability relationship between pyrrhotite (po) and pyrite (py), which can be represented by the sulfidation reaction

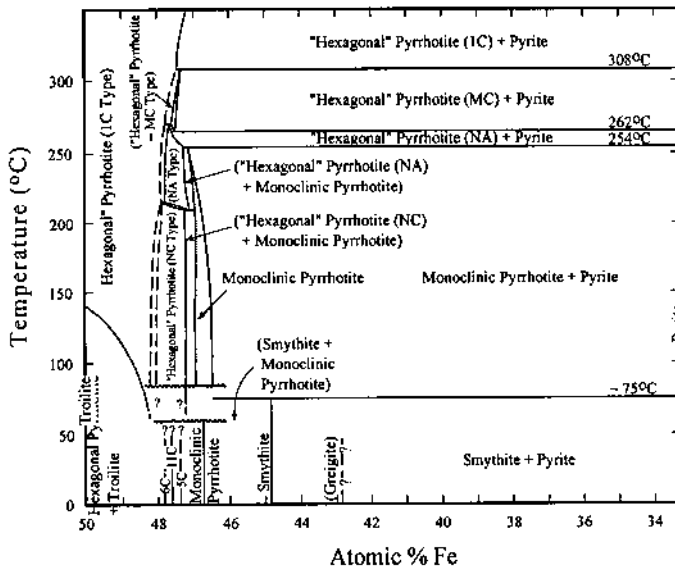


Figure 4.26. Experimentally determined phase relations in the central part of the condensed Fe-S system below 350°C (after Kissin & Scott 1982). The numbers within the pyrrhotite fields (1C, 5C, 6C, 11C, NA, NC, MC) are designations for superstructure types of pyrrhotite. Phase boundaries marked by dashed lines are inferred and those with question marks are hypothetical. All assemblages coexist with a vapor phase. According to the recent experimental study of Lusk et al. (1993), hexagonal pyrrhotite continues to be a stable phase down to about 150°C below which it may stably invert to monoclinic pyrrhotite.

The equilibrium constant (K) for the reaction at (P, T) is given by

$$K_{P,T} = \frac{a_{\text{FeS}_2}^{\text{py}}}{a_{\text{FeS}}^{\text{po}} (f\text{S}_2)^{1/2}} \tag{4.38}$$

where $a_{\text{FeS}}^{\text{po}}$ is the activity of FeS component in pyrrhotite solid solution relative to its standard state (pure FeS at the same P, T). Pyrite does not depart measurably from stoichiometric FeS_2 , so that $a_{\text{FeS}_2}^{\text{py}} = 1$. But $a_{\text{FeS}}^{\text{po}}$ in Equation 4.38 is never equal to 1, because at no temperature does troilite (FeS) coexist in equilibrium with pyrite (see Fig. 3.5). Ignoring the negligible effect of total pressure on this equilibrium, it follows from Equation 4.38 that $a_{\text{FeS}}^{\text{po}}$ is a unique function of temperature and sulfur fugacity ($f\text{S}_2$). In other words, it should be possible to use the composition (FeS content) of pyrrhotite (which is related to $a_{\text{FeS}}^{\text{po}}$; see Toulmin & Barton 1964) coexisting in equilibrium with pyrite and determine simultaneously both temperature and $f\text{S}_2$.

From an experimental study of FeS- FeS_2 portion of the Fe-S system, using the electrom-tarnish method for measurement of sulfur fugacities, Toulmin and Barton (1964) established that the composition of hexagonal pyrrhotite, fugacity of sulfur, and temperature are related by the equation

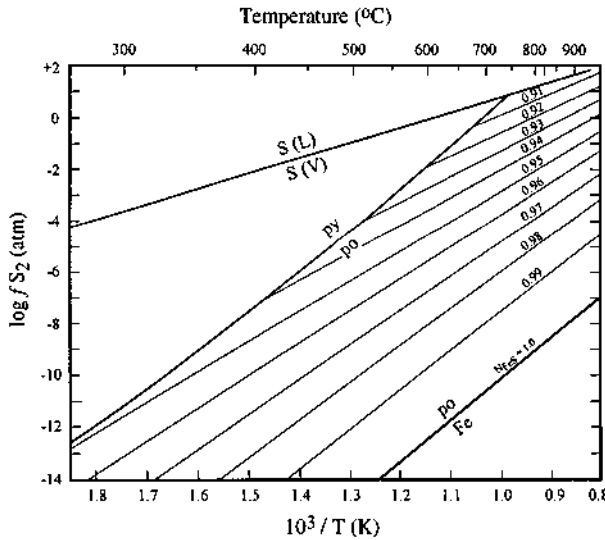


Figure 4.27. Composition of pyrrhotite in the Fe-S system at 1 bar pressure as a function of temperature and sulfur fugacity. N_{FeS} is the mole fraction of FeS in pyrrhotite in the system FeS-S_2 . The magnetic transition in pyrrhotite in the vicinity of 320°C and the phase relations below this temperature have been ignored in this figure. Abbreviations: S(L) = sulfur liquid; S(V) = sulfur vapor; po = pyrrhotite; py = pyrite (After Barton & Toulmin 1966.)

$$\log_{10} fS_2 = (70.03 - 85.83N_{\text{FeS}}) (1000 / T - 1) + 39.30 \sqrt{(1 - 0.9981N_{\text{FeS}})} - 11.91 \quad (4.39)$$

where fS_2 is the fugacity of sulfur relative to the ideal diatomic gas at 1 atm, N_{FeS} is the mole fraction of FeS in pyrrhotite, and T is the temperature in Kelvin. This expression, in the form of isopleths of N_{FeS} on a plot of $\log fS_2$ versus $1000/T$, is presented graphically in Figure 4.27.

The composition of pyrrhotite (N_{FeS}) in a natural assemblage can be measured either by an X-ray spacing method (Arnold & Reichen 1962, Yund & Hall 1969) or by electron microprobe analysis, and then its temperature of equilibration can be estimated from Equation 4.39 if the value of fS_2 is known from some other source. Conversely, if the temperature is known from another appropriate geothermometer, Equation 4.39 can be used to calculate the relevant fS_2 . Of greater practical use are assemblages in which pyrrhotite coexists in equilibrium with pyrite. As is evident from Figure 4.27, the fS_2 is fixed in such an assemblage, so that the pyrrhotite composition becomes a function of temperature only.

In principle, the application of the pyrrhotite - pyrite geothermometer is restricted to the temperature range from 742°C (the upper stability of pyrite in condensed Fe-S system) to about 300°C (the lower stability of hexagonal 1C pyrrhotite) below which the phase relations of pyrrhotite are quite complicated (Fig. 4.26). In practice, the use of this geothermometer is severely limited by (a) the low-angle intersection of the N_{FeS} isopleths with the pyrite - pyrrhotite solvus (Fig. 4.27), which produces relatively large errors in temperature for small errors in N_{FeS} , and (b) the relatively rapid re-equilibration of the pyrrhotite composition to lower temperatures after its formation. However, the principle discussed above does illustrate one important point — the role of pyrite + pyrrhotite as a sulfur fugacity buffer in natural sulfide assemblages.

Sphalerite Composition

Sphalerite is one of the most useful indicators of the environment of ore deposition because of its refractory nature, wide distribution in natural environments, and wide range of composition resulting from substitution of Zn by Fe. The potential of sphalerite as a geothermometer was first recognized by Kullerud (1953). Subsequent investigations have shown that although the FeS content of sphalerite in equilibrium with hexagonal pyrrhotite and pyrite can be used as a geothermometer over a small range of temperature, sphalerite + hexagonal pyrrhotite ± pyrite assemblages are more promising as geobarometers, because the sphalerite composition is more sensitive to variations in pressure than temperature.

It is well established from experimental studies on the synthetic Fe-Zn-S system that sphalerite has a large solid solution field in terms of Zn:Fe ratio and that its composition (FeS content) varies both with temperature and the composition (or the corresponding thermodynamic parameter, $a_{\text{FeS}}^{\text{po}}$) of the coexisting pyrrhotite solid solution. The maximum FeS content of sphalerite occurs when the coexisting

pyrrhotite is stoichiometric FeS (troilite), i.e., where activity of FeS is maximum ($a_{\text{FeS}}^{\text{po}} = 1$). Because the compositions of sphalerite (and of its high temperature polymorph, würtzite) fall on the FeS-ZnS join (i.e., the metal:sulfur ratio of sphalerite is 1:1 for all practical purposes), the ternary phase relations involving sphalerite can be conveniently represented by a T - X projection from the sulfur corner onto the FeS-ZnS join (Fig. 4.28).

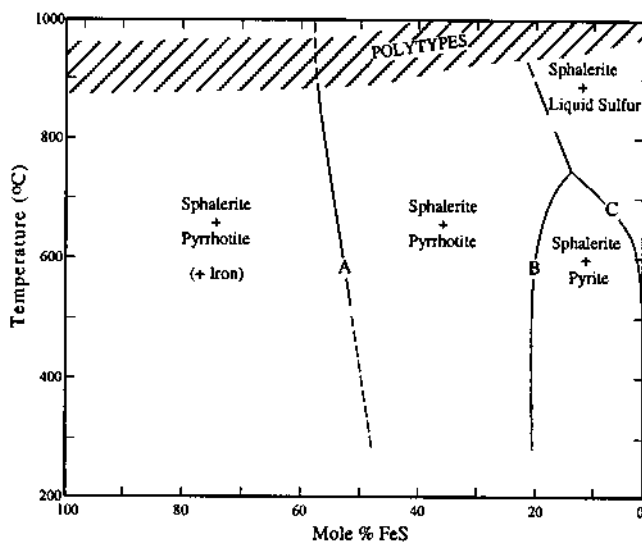


Figure 4.28. Composition of sphalerite in Fe-Zn-S system projected onto the FeS-ZnS plane (after Barton & Skinner 1979). Experimental data and calculations (Barton & Toulmin 1966, Scott and Barnes 1971, Scott 1973, Schwarcz et al. 1975, Lusk & Ford 1978, Hutchinson & Scott 1981) indicate that the curves *A* and *B* shift progressively to more Fe-rich sphalerite compositions at higher pressures. Low-temperature (< 350°C) phase relations involving sphalerite, pyrrhotite, and pyrite (Scott & Kissin, Kissin & Scott 1982, Lusk et al. 1993) are excluded for clarity.

The curves *C* and *D* in Figure 4.28, involving liquid sulfur in the sphalerite-bearing assemblages, are obviously of little use in geothermometry. The univariant curve *A*, which defines the temperature dependence of sphalerite composition in equilibrium with native iron and pyrrhotite of FeS composition (i.e., troilite with $a_{\text{FeS}}^{\text{po}} = 1$), is too steep to be useful in geothermometry; moreover, this assemblage is rare in terrestrial environments. The effect of pressure on this assemblage has been utilized in the cosmobarometry of iron meteorites (Schwarcz et al. 1975, Kissin et al. 1986). This cosmobarometer was experimentally calibrated by Hutchinson and Scott (1983).

The sphalerite + hexagonal pyrrhotite assemblage is of interest in that it covers the entire fS_2 -temperature range encountered in mineral deposits. Isoleths of sphalerite composition shown in Figure 4.29 are based on experimental data (Barton & Toulmin

1966, Scott & Barnes 1971). The regression equation for the isopleths is (Scott & Barnes 1971)

$$X_{\text{FeS}}^{\text{sp}} = 72.26695 - 15900.5 / T + 0.01448 \log fS_2 - 0.38918 (10^8 / T^2) - (7205.5 / T) \log fS_2 - 0.34486 (\log fS_2)^2 \pm 1.7 \quad (4.40)$$

where $X_{\text{FeS}}^{\text{sp}}$ is the mole% FeS in sphalerite in equilibrium with pyrrhotite, T is the temperature in Kelvin, and fS_2 is the sulfur fugacity. However, this relationship (or the calculated isopleths shown in Fig. 4.29) cannot be used for geothermometry without additional information on fS_2 during deposition. The coexisting pyrrhotite usually undergoes post-depositional changes, which prohibits a reliable determination of fS_2 .

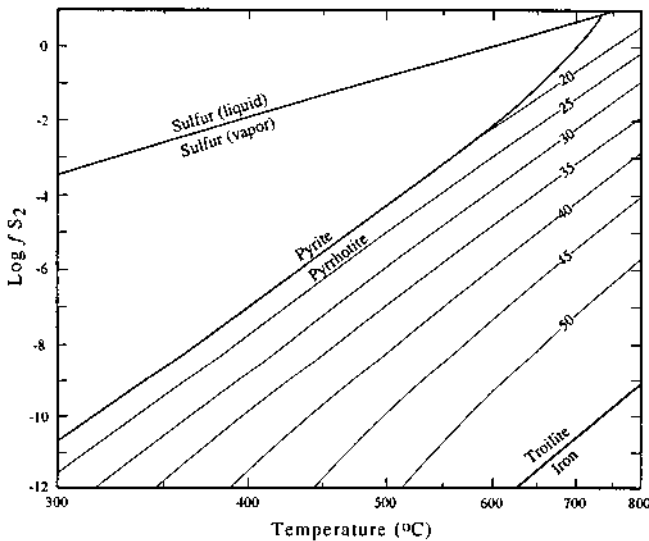


Figure 4.29. Sphalerite composition in equilibrium with pyrrhotite or pyrrhotite + pyrite as a function of sulfur fugacity and temperature at 1 bar (after Scott & Barnes 1971). The sphalerite composition isopleths (light contours in mole% FeS) in equilibrium with pyrrhotite have been calculated using Equation 4.40.

The assemblage pyrite + sphalerite + hexagonal pyrrhotite, in which the fS_2 is buffered by the reaction 4.37, offers the best promise of a geothermometer. In this assemblage fS_2 is defined by the coexisting pyrite and pyrrhotite of a specific composition (see Fig. 4.27) so that the temperature can be obtained from the FeS content of sphalerite (Fig. 4.29). However, the geothermometer is useful only over a very limited range of temperature, because the corresponding solvus (Curve B, Fig.

4.28) remains vertical below about 550°C at a sphalerite composition of 20.7 ± 0.6 mole% FeS (Boorman 1967, Boorman et al. 1971, Scott & Barnes 1971) and the phase relations become very complicated below about 300°C (Scott & Kissin 1973, Kissin & Scott 1982, Lusk et al. 1993). It is not an ideal geothermometer even above 550°C because of the strong pressure dependence of sphalerite composition.

The use of sphalerite-bearing assemblages of the Fe-Zn-S system in geobarometry is based on the variation of the activity of FeS in sphalerite ($a_{\text{FeS}}^{\text{sp}}$) with pressure. The relationship expressed in terms of the mole fraction FeS content of sphalerite ($N_{\text{FeS}}^{\text{sp}}$) is (Barton & Toulmin 1966)

$$\left(\frac{dN_{\text{FeS}}^{\text{sp}}}{dP} \right)_T = \frac{1}{\gamma_{\text{FeS}}^{\text{sp}}} \left(\frac{da_{\text{FeS}}^{\text{po}}}{dP} \right)_T - a_{\text{FeS}}^{\text{po}} \left(\frac{d \ln \gamma_{\text{FeS}}^{\text{sp}}}{dP} \right)_T \quad (4.41)$$

where $\gamma_{\text{FeS}}^{\text{sp}}$ is the activity coefficient = $a_{\text{FeS}}^{\text{sp}} / N_{\text{FeS}}^{\text{sp}}$. From calculations based on this equation, Scott and Barnes (1971) showed that the sphalerite composition in a pyrite + pyrrhotite + sphalerite equilibrium assemblage is practically independent of temperature below 550°C (with a value of 20.7 ± 0.6 mole% FeS at 1 bar) but is strongly dependent on pressure. The geobarometer has since been calibrated experimentally up to 10 kb pressure (Scott 1973, Lusk & Ford 1978, Hutchinson & Scott 1981), confirming its temperature independence below about 500°-600°C (Fig. 4.30), an encouraging situation for geobarometric applications (although the temperature independence in this region has been disputed by Toulmin et al. 1991 on thermodynamic grounds). The equation for the pressure dependence of sphalerite composition for the temperature- independent portion of the geobarometer is (Hutchinson & Scott 1981)

$$P \text{ (kbars)} = 42.30 - 32.10 \log X_{\text{FeS}}^{\text{sp}} \pm 0.30 \quad (4.42)$$

where P is the pressure in kilobars and $X_{\text{FeS}}^{\text{sp}}$ is the mole% FeS in sphalerite.

The sphalerite + hexagonal pyrrhotite assemblage (without pyrite) may also be used as a geobarometer. From experimental studies at 450°-750°C and 1-6 kbars, Bryndzia et al. (1988) found $\gamma_{\text{FeS}}^{\text{sp}}$, defined as $a_{\text{FeS}}^{\text{sp}} / X_{\text{FeS}}^{\text{sp}}$, to be practically independent of temperature, and Bryndzia et al. (1990) derived the following relation for the sphalerite + hexagonal pyrrhotite geobarometer:

$$P \text{ (kbars)} = 27.982 \log \gamma_{\text{FeS}}^{\text{sp}} - 8.549 \pm 0.5 \quad (4.43)$$

The determination of P from this equation involves the measurement of sphalerite and pyrrhotite compositions and estimation of $\gamma_{\text{FeS}}^{\text{sp}}$ as discussed in Bryndzia et al. (1988). Ideally, a plot of $a_{\text{FeS}}^{\text{sp}}$ vs. $X_{\text{FeS}}^{\text{sp}}$ for sphalerite + pyrrhotite pairs from an equilibrium

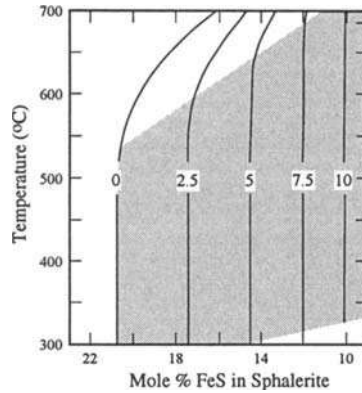


Figure 4.30. T - X projection on the FeS-ZnS join of the sphalerite + pyrite + pyrrhotite solvus isobars (in kilobars). Temperature-independent portions of the isobars are from Equation 4.42, incorporating the data of various investigations (Boorman 1967, Scott & Barnes 1971, Scott & Kissin 1973, Scott 1973, Lusk & Ford 1978, Hutchinson & Scott 1981); curved portions are from Scott (1973). The sphalerite + pyrrhotite assemblage is stable to the left of each isobar and the sphalerite + pyrite assemblage to the right. The stippled portion represents the useful portion of the diagram for geobarometry. (After Hutchinson & Scott 1980.)

assemblage should give a linear array, defining $\gamma_{\text{FeS}}^{\text{sp}}$ as the slope of the array.

The sphalerite geobarometer has been used by many workers to estimate pressures for metamorphosed strata-bound ore deposits and regionally metamorphosed terrains, but with varying degrees of success (Scott 1976, Scott et al. 1977, Brown et al. 1978, Bristol 1979, Hutchinson & Scott 1980, Willan & Hall 1980, Scott 1983, Bryndzia et al. 1990). In many cases, the sphalerites either have a wide range of FeS contents, giving a range of pressure estimates, or are notably iron-poor, resulting in anomalously high estimates of metamorphic pressure (Groves et al. 1975, Lusk et al. 1975, Ethier et al. 1976, Scott 1976, Brown et al. 1978, Ringler 1979, Stumpfl 1979, Plimer 1980). Situations that would not give satisfactory pressure estimates are: (a) preservation of primary compositional variations, as has been suggested to be the case with some metamorphosed strata-bound deposits (Stumpfl 1979, Plimer 1980); (b) retrograde recrystallization (Groves et al. 1975, Plimer 1980, Toulmin et al. 1991), probably aided by a fluid phase; and (c) equilibration below about 300°C, which may lower the FeS content of sphalerite and thus indicate a higher pressure. In other cases, the problem may lie in the inhomogeneous distribution of FeS in the sphalerite. Scott et al. (1977) attributed the compositional variations in sphalerites of the Broken Hill region (Australia) to the very small size (less than the diameter of a polished section) of equilibrium domains of a_{FeS} and $f\text{S}_2$. Such small distances of equilibration are consistent with the diffusion rates of Fe and Zn in sphalerite (Goble et al. 1979) and the

refractory character of sphalerite in solid state reactions (Barton 1970). Hutchinson and Scott (1980) observed that in many metamorphosed ores the sphalerites, which were poikiloblastically encapsulated within metablastic pyrite, appeared to have been isolated from subsequent re-equilibration. In any case, sphalerites with inhomogeneous distribution of FeS should be avoided. Impurities (such as Co, Ni, Cd, Mn) at concentration levels normally found in sphalerite and pyrrhotite are unlikely to affect the sphalerite geobarometer (Hutchinson & Scott 1981), but Cu is problematical. Because of the low solubility of copper in sphalerite in the four-phase assemblage pyrite + pyrrhotite + sphalerite + chalcopyrite, the presence of chalcopyrite in natural ores should not affect sphalerite geobarometry over its temperature-independent region. However, a common feature of many sulfide ores is the presence of sphalerite with an abundance of chalcopyrite blebs (the so called "chalcopyrite disease") in excess of the amount that can be reasonably accounted for by an equilibrium process of solubility and subsequent exsolution. Because the chalcopyrite - sphalerite intergrowth texture may be produced by several mechanisms, it is best not to use chalcopyrite-bearing sphalerite at all for geobarometric exercises (Hutchinson & Scott 1981). In summary, the sphalerite geobarometer is attractive from considerations of precision and potential wide application, but it must be ensured that the sphalerite analyzed was in equilibrium with pyrite and pyrrhotite and that its composition has not been modified by post-equilibration events.

Arsenopyrite Composition

Arsenopyrite, a widely distributed but commonly a minor constituent of mineral deposits, is the most refractory of the common sulfide minerals and has a large solid solution field in terms of As:S ratio. The promise of arsenopyrite solid solution ($\text{FeAs}_{1-x}\text{S}_{1+x}$) as a geothermometer lies in the systematic variation of its composition as a function of assemblage and temperature (Figs. 4.31, 4.32) in the synthetic Fe-As-S system (Clark 1960a, Barton 1969, Kretschmar & Scott 1976). A knowledge of the activity of sulfur (a_{S_2}) in the mineral assemblage is essential for proper application of the arsenopyrite geothermometer because the composition of arsenopyrite within its solid solution field is a function of both temperature and sulfur activity (the arsenic activity is not an independent variable at fixed temperature and a_{S_2}). In some cases other Fe-As-S phases may provide this information and Figure 4.31 can be used directly; in others this information may be obtained from other coexisting a_{S_2} -buffering assemblages (e.g., pyrite - pyrrhotite, bismuth - bismuthinite, which lie within the stability field of arsenopyrite) and the temperature estimated from Figure 4.31.

A more favorable geothermometer is provided by the compositions of coexisting arsenopyrite and sphalerite with pyrite and/or pyrrhotite (Fig. 4.32). As each sphalerite and arsenopyrite isopleth in this assemblage is univariant at fixed pressure, their intersections are invariant and define a unique a_{S_2} as well as temperature. Moreover, the isopleths for sphalerite and arsenopyrite intersect at sufficiently high angles to constitute a useful geothermometer.

For several reasons, arsenopyrite composition should be a good indicator of

temperature and sulfur activity during ore formation (Kretschmar & Scott 1976). Despite frequently observed compositional zoning, the compositions of naturally occurring arsenopyrites, including those from highly metamorphosed ores, are consistent with experimental studies, attesting to the refractory nature of arsenopyrite during post-depositional re-equilibration of mineral deposits. Because it is usually a minor constituent of mineral deposits, arsenopyrite is unlikely to have buffered the ore-forming environment. Also, the T - a_{S_2} stability field of arsenopyrite effectively straddles the range of temperatures and sulfur activities of the common ore-forming environments (Barton 1970). A major problem in the application of this method lies in the evaluation of the effect of confining pressure on arsenopyrite composition.

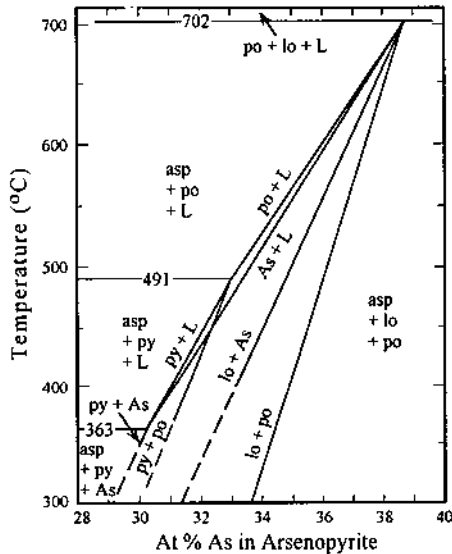


Figure 4.31. Pseudobinary T - X section along the FeS_2 - $FeAs_2$ join of the condensed Fe - As - S system showing the arsenopyrite composition as a function of temperature and equilibrium mineral assemblage. All assemblages include a vapor phase. Abbreviations: asp = arsenopyrite; po = pyrrhotite; py = pyrite; lo = löellingite; As = arsenic; L = liquid. (After Kretschmar & Scott 1976.)

Clark (1960b) investigated the effect of pressure on the Fe - As - S system up to 2.07 kb. The potential of arsenopyrite composition as a geobarometer stems from his observation that confining pressure apparently produced a more S -rich arsenopyrite for each assemblage and temperature, and raised the arsenopyrite + pyrite + pyrrhotite + liquid + vapor invariant point (491°C) by 1.8°C/kb. In a later study, Kretschmar and Scott (1976) questioned the usefulness of arsenopyrite as a geobarometer because they suspected the effect of confining pressure to be much smaller than reported earlier.

Based on thermodynamic calculations, Sharp et al. (1985) argued that (a) increasing pressure would decrease the As content of arsenopyrite coexisting with löellingite (FeAs_2), and would increase the upper stability of arsenopyrite coexisting with pyrite by approximately $14^\circ\text{C}/\text{kb}$; and (b) pressure would have a negligible effect on the composition of arsenopyrite coexisting with pyrite, but sulfidation buffer curves would be shifted to higher a_{S_2} values (by about 0.1 log unit/kbar than predicted by Fig. 4.32), introducing significant errors in geothermometry. From a study of many natural arsenopyrite-bearing assemblages for which independent temperature estimates were available, they found the arsenopyrite geothermometer to be valid for assemblages metamorphosed to greenschist and lower amphibolite facies, but to yield relatively lower temperatures for assemblages metamorphosed to upper amphibolite and granulite

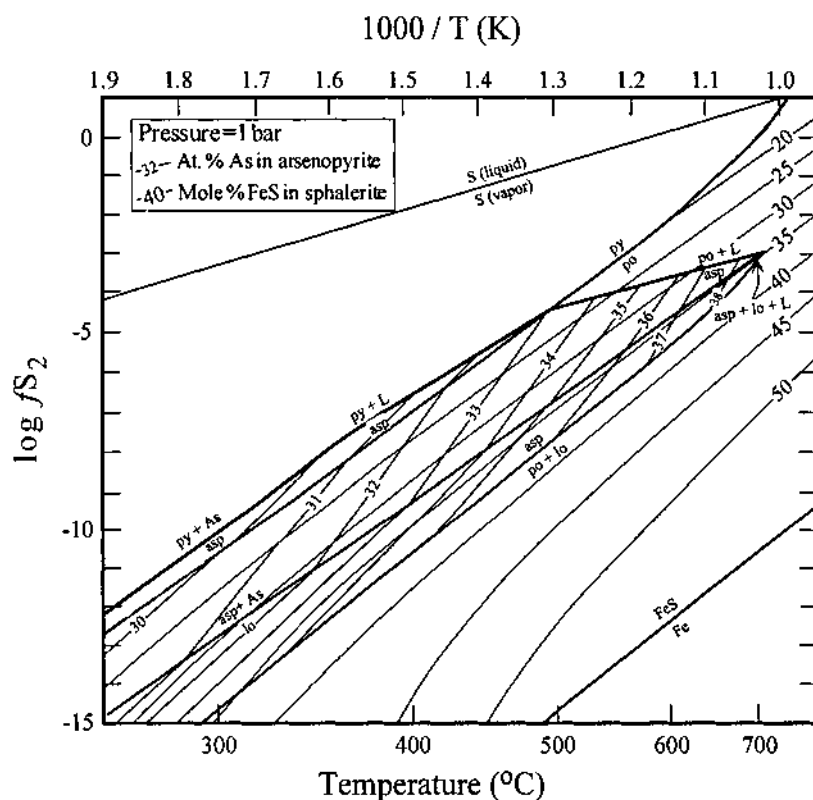


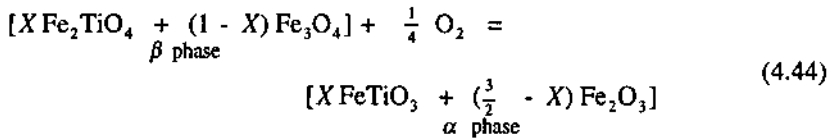
Figure 4.32. Compositions of coexisting sphalerite and arsenopyrite in the Fe-Zn-As-S system at low pressure. Isopleths are in mole% FeS for sphalerite (Scott & Barnes 1971) and in atomic% As for arsenopyrite (Kretschmar & Scott 1976). The intersections of the sphalerite and arsenopyrite isopleths provide unique values of both a_{S_2} and temperature. Abbreviations for phases as in Figure 4.31. (After Scott 1983.)

facies and inconsistent temperatures for low-temperature hydrothermal deposits (probably because of non-attainment of equilibrium).

Compositions of Iron-titanium Oxides

The two common iron-titanium-oxide phases in rocks and mineral deposits are the cubic magnetite - ulvöspinel solid solution (β phase) and the rhombohedral hematite - ilmenite solid solution (α phase) (Fig. 4.33). The compositions of these two solid solution phases coexisting in equilibrium are a function of both temperature and oxygen fugacity. Thus, this geothermometer is capable of yielding information on temperature of equilibration as well as on the corresponding oxygen fugacity.

The conversion of the β phase to the α phase is an oxidation reaction, which can be represented as (Carmichael et al. 1974)



The equilibrium constant (K) for the reaction is given by

$$K = \frac{(a_{\text{FeTiO}_3}^\alpha)^X \cdot (a_{\text{Fe}_2\text{O}_3}^\alpha)^{3/2-X}}{(a_{\text{Fe}_2\text{TiO}_4}^\beta)^X \cdot (a_{\text{Fe}_3\text{O}_4}^\beta)^{1-X} \cdot (f_{\text{O}_2})^{1/4}} \quad (4.45)$$

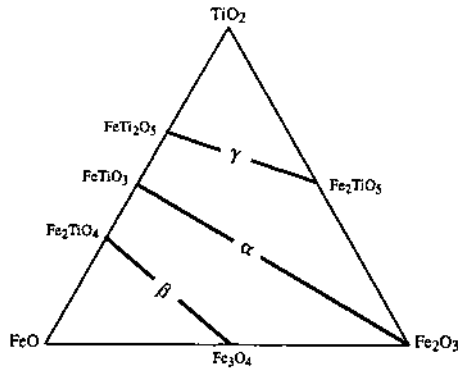


Figure 4.33. The major solid solution series of the FeO-Fe₂O₃-TiO₂ system: ilmenite (FeTiO₃) - hematite (Fe₂O₃) solid solution [α phase, rhombohedral]; magnetite (Fe₃O₄) - ulvöspinel (Fe₂TiO₄) solid solution [β phase, cubic]; and ferropseudobrookite (FeTi₂O₅) - pseudobrookite (Fe₂TiO₅) solid solution [γ phase, orthorhombic]. Compositions are in mole%.

Because the effect of total pressure on this equilibrium is negligible (Lindsley 1963), K is essentially a function of temperature and fO_2 . At a given temperature, the oxygen fugacity is defined if the activities of all the solids are fixed, and the compositions of the two coexisting solid solutions are uniquely defined by both temperature and fO_2 . Experimental studies on the $FeO-Fe_2O_3-TiO_2$ system (Buddington & Lindsley 1964) and thermodynamic modeling (Spencer & Lindsley 1981) have resulted in the construction of a surface in fO_2-T-X space for magnetite - ulvöspinel solid solution and another such surface for the coexisting hematite - ilmenite solid solution. Portions of these two surfaces, expressed by appropriate contours, are projected on to the fO_2-T plane in Figure 4.34. These contours are effectively univariant curves, if the experimentally

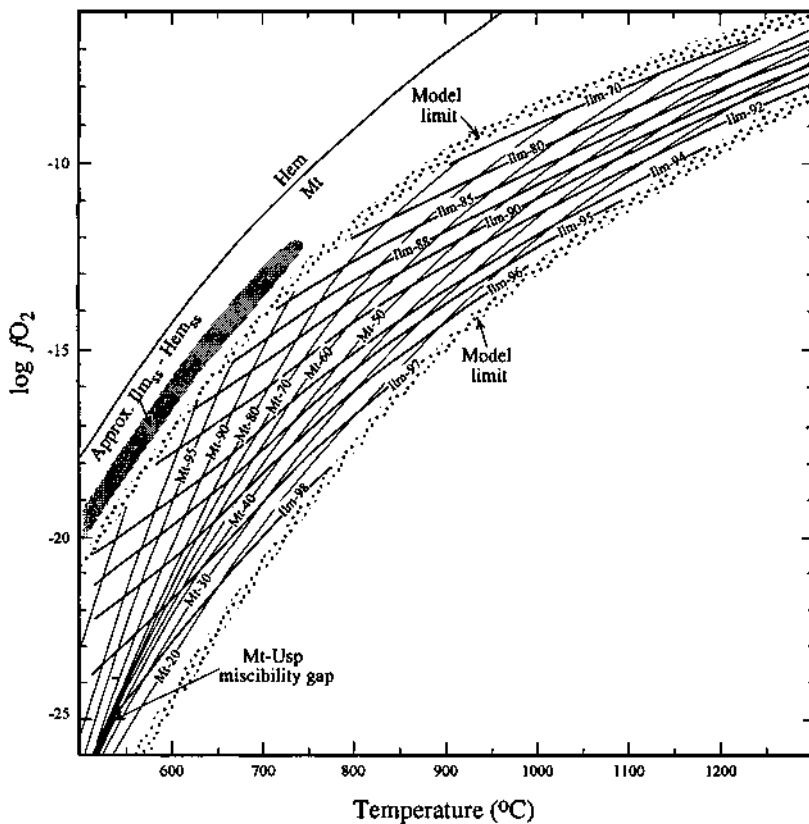


Figure 4.34. Temperature ($^{\circ}C$) - fO_2 grid for compositions, in mole percent, of coexisting magnetite (Mt) - ulvöspinel (Usp) solid solution (Mt_{100}) and ilmenite (Ilm) - hematite (Hem) solid solution (Ilm_{100}) pairs based on experimental data (Buddington & Lindsley 1964) and a solution model (Spencer & Lindsley 1981). The intersection of contours for the compositions of these two phases provide a measure of both temperature and oxygen fugacity. The stippled fields are estimates of the limits of the model. The Mt - Usp miscibility gap is calculated for the three-phase assemblage $Mt_{100} + Usp_{100} + Ilm_{100}$. The Ilm - Hem miscibility gap (labeled "Approx. Ilm_{100} - Hem_{100} ") is the best guess from experimental data (it is not calculated). The Mt_{100} and Ilm_{100} are assumed to be pure binary Fe-Ti oxides; no minor constituents are considered. (After Spencer and Lindsley 1981.)

undetectable effect of total pressure is ignored, and can be used as calibration curves to estimate temperature and oxygen fugacity of equilibration of naturally occurring samples, if the compositions of the coexisting magnetite - ulvöspinel and hematite - ilmenite solid solutions are known, for example, by electron microprobe analysis.

According to Buddington and Lindsley (1964), the errors of the method due to uncertainties in the experimental results are $\pm 30^\circ\text{C}$ for temperature and ± 1 log unit for oxygen fugacity. Additional errors may arise because of the presence of other components as solid solutions in the naturally occurring iron-titanium oxide minerals. From experiments on the $\text{MgO-FeO-Fe}_2\text{O}_3\text{-TiO}_2$ system, Speidel (1970) showed that the amount of β phase dissolved in the α phase decreases with increasing MgO content and that the oxygen fugacities predicated from the Fe-Ti contents of coexisting oxides, using the data of Buddington and Lindsley (1964), are an order of magnitude too low with Mg present in the oxides. The effects of other components in solid solution in α and β phases have not been evaluated.

Inherent to the application of this method to natural assemblages is the assumption that the compositions of the two coexisting solid solution phases have remained unchanged after their formation. The method is best suited to extrusive and hypabyssal igneous rocks that were subjected to rapid cooling and are unmetamorphosed (Hammond & Taylor 1982). Its application to plutonic igneous rocks (several examples are discussed by Buddington & Lindsley 1964 and Elsdon 1975) must be viewed with caution because of possible re-equilibration during or after magmatic crystallization (Anderson 1966, Czamanske & Mihalik 1972). Similarly, the temperature and oxygen fugacity obtained from iron-titanium oxide assemblages associated with a mineral deposit may actually represent conditions of re-equilibration rather than of formation.

4.7.3. PARTITIONING OF TRACE COMPONENTS BETWEEN SULFIDE PAIRS

Concentration levels of trace elements in sulfide phases often vary with temperature. It has been suggested, for example, that a low temperature of formation may be indicated by low In and high Ge contents in sphalerite, low Ag, Sb, and Bi in galena, and low Co in pyrite (Fleischer 1955, Bjorlykke & Jarp 1950). However, the concentration of a particular trace element in one phase only is not thermodynamically constrained to be useful in quantitative geothermometry. The distribution of a trace element between two coexisting phases in equilibrium reduces the degrees of freedom of the system and, in appropriate cases, becomes a unique function of temperature. Incorporation of such an 'impurity' in a mineral may occur in several ways (e.g., substitutional solid solution, coupled substitution, absorption), but the one that is amenable to simple quantitative interpretation is substitutional solid solution.

The distribution (or partitioning) of a common trace element component (i) between two immiscible phases (A and B) in equilibrium (at T Kelvin and P bars) is measured by its *distribution coefficient*, $K_{D(i)}^{A-B}$, which is defined as

$$K_{D(0)}^{A-B} = N_i^A / N_i^B \quad (4.46)$$

where N_i is the mole fraction of the component i in a given phase. Expressing N_i in terms of its corresponding activity (a_i) and activity coefficient (γ_i),

$$K_{D(0)}^{A-B} = \frac{N_i^A}{N_i^B} = \frac{a_i^A / \gamma_i^A}{a_i^B / \gamma_i^B} = \frac{a_i^A}{a_i^B} \cdot \frac{\gamma_i^B}{\gamma_i^A} \quad (4.47)$$

At equilibrium,

$$\Delta G_{r,T}^{\circ} = - RT \ln K = - RT \ln (a_i^A / a_i^B) \quad (4.48)$$

where $\Delta G_{r,T}^{\circ}$ is the standard Gibbs free energy change for the distribution reaction $i(B) \rightleftharpoons i(A)$ at temperature T (in Kelvin), R the gas constant, and K the equilibrium constant for the distribution reaction. Substituting, Equation. 4.47 reduces to

$$\ln K_{D(0)}^{A-B} = - (\Delta G_{r,T}^{\circ} / RT) - \ln (\gamma_i^A / \gamma_i^B) \quad (4.49)$$

For example, the equilibrium partitioning of Mn between sphalerite (sp) and galena (gn) for the distribution reaction $MnS^{gn} \rightleftharpoons MnS^{sp}$ is given by

$$\ln K_{D(MnS)}^{sp-gn} = - (\Delta G_{r,T}^{\circ} / RT) - \ln (\gamma_{MnS}^{sp} / \gamma_{MnS}^{gn}) \quad (4.50)$$

In general, the activity coefficient (γ_i) is a function of temperature, pressure, composition of the host phase(s), and the concentration of the component. The variation of γ_i with pressure is relatively insignificant in systems involving solid phases only, and minor amounts of other components in solid solution usually do not influence appreciably the activity coefficients of components present in small amounts. Thus the distribution coefficient becomes a sole function of temperature, provided the concentration level of the component i is sufficiently low for γ_i to remain a constant (Henry's Law behavior for very dilute solutions). Under these conditions, the distribution coefficient (K_D) may be used as a geothermometer if it can be calibrated at various temperatures. The effect of temperature on K_D (at constant pressure) is given by

$$\left(\frac{\partial \log K_D}{\partial (1/T)} \right)_p = - \frac{\Delta \bar{H}_i^{\circ}}{2.303R} \quad (4.51)$$

where $\Delta \bar{H}_i^{\circ}$ is the change in partial molar enthalpy for the distribution reaction. Thus all the assumptions stated above are satisfied, the calibration of $\log K_D$ vs. $1/T$ should plot as a straight line. The analogous expression for the pressure dependence of K_D

may be expressed as

$$\left(\frac{\partial \log K_D}{\partial P} \right)_T = - \frac{\Delta \bar{V}_r^0}{2.303RT} \quad (4.52)$$

where $\Delta \bar{V}_r^0$ is the change in partial molar volume for the distribution reaction.

Available thermodynamic data do not permit theoretical evaluation of K_D at different temperatures and pressures using Equations 4.51 and 4.52. However, some experimentally determined calibration curves are available. Bethke and Barton (1971) studied experimentally the distribution of Cd, Mn, and Se between coexisting sphalerite and galena and of Cd and Mn between wurtzite and galena over the temperature range 600°-800°C, as well as the distribution of Se between galena and chalcopyrite in the temperature range 390°-595°C. The resulting calibration curves for some of the investigated systems (Fig. 4.35) appear quite sensitive to qualify as potential geothermometers, although the accuracy of these calibration curves remains to be established. Regression equations derived by Bethke and Barton (1971) to describe the

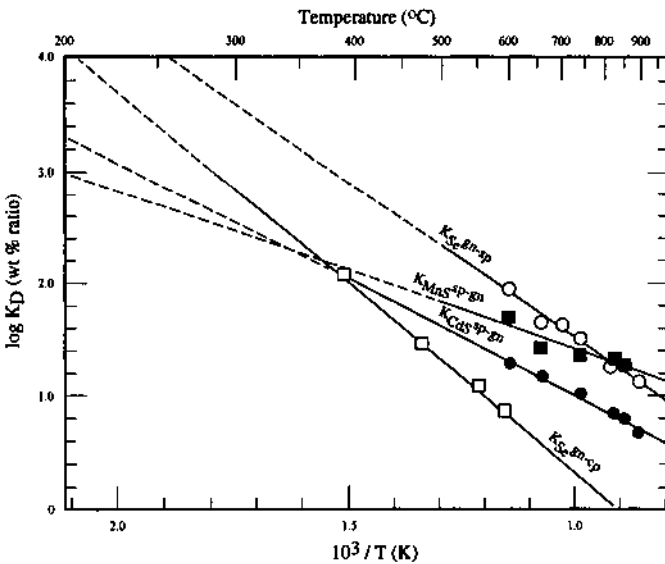


Figure 4.35. Variation of distribution coefficients (K_D) for trace-element partitioning between coexisting sulfide phases as a function of temperature. Solid lines represent portions determined experimentally, dashed lines their likely extensions to lower temperatures. The graph for K^{Mn-sp} involves some reduction of the experimental data. Equations for the calibration curves are given in Bethke and Barton (1971). For this diagram, concentrations of the components were converted from mole fraction to weight percent values for calculation of K_D . Abbreviations: cp = chalcopyrite, gn = galena, sp = sphalerite. (After Bethke & Barton 1971.)

temperature and pressure dependence of the distribution of Cd and Mn between coexisting sphalerite and galena, for example, are

$$\log K_{D(\text{CdS})}^{\text{sp-gn}} = [(2,080 - 0.02642P)/T] - 1.08 \quad (4.53)$$

$$\log K_{D(\text{MnS})}^{\text{sp-gn}} = [(1,410 - 0.0261P)/T] - 0.01 \quad (4.54)$$

where T is in Kelvin and P in kb.

Limited studies (e.g., Mishra & Mookherjee 1988, Bortnikov et al. 1995) on the distribution of Cd and Mn between coexisting sphalerite and galena indicate that only the distribution of Cd is likely to give reasonable temperatures, especially when the assemblages have equilibrated at relatively high temperatures. The application of the selenium and manganese geothermometers to galena - sphalerite pairs from the Darwin mine (California, USA) yielded significantly higher temperatures than those obtained by sulfur isotope geothermometry (Hall et al. 1971), and recent experimental work by Yamamoto et al. (1984) has produced a calibration curve for $K_{D(\text{Se})}^{\text{sp-gn}}$ which is quite different from that of Bethke & Barton (1971). Clearly, more experimental studies, particularly at low temperatures, are needed to establish reliable calibration curves. Some workers have used distribution coefficients based on ratios of components for this technique of geothermometry. Using an experimentally determined calibration for distribution of Fe:Zn ratio between coexisting stannite and sphalerite (Nakamura & Shima 1982), Shimizu and Shikazono (1985) obtained temperatures for several Japanese deposits that correlated well with temperatures obtained from fluid inclusion and sulfur isotope geothermometry. Another set of geothermometers that appears to hold promise is based on the distribution of the Ni:Fe and Co:Fe ratios between pyrite and pyrrhotite. According to Bezman et al. (1975), the partition coefficients for these elemental ratios are linear functions of temperatures (for Co and Ni concentrations up to 1.5 wt%) and yield good results for various types of mineral deposits.

A critical assumption in the application of the K_D -based geothermometry to natural assemblages is that the K_D is a sole function of temperature; that is, the activity coefficients remain constant over the observed concentration ranges of the minor elements (see Equation 4.49). The investigation of Ghosh-Dastidar et al. (1970) demonstrated that this might not be the case, probably because of point defects in the crystal structures of the minerals induced by element substitution. Other constraints for the successful application of this method include (Bethke & Barton 1971, Mishra & Mookherjee 1988, Bortnikov et al. 1995): (a) the necessity of obtaining samples of utmost purity for analysis (except when the analysis is done by electron, ion, or laser microprobe); (b) the difficulty of high-precision chemical analysis of elements at trace-level concentrations; (c) nonuniformity of geochemical conditions during precipitation of a sulfide mineral as is evidenced by the common presence of growth zoning; (d) the requirement of contemporaneity and equilibrium between sulfide phases of interest,

which is always difficult to establish; and (e) likely post-depositional re-equilibration of sulfide phases. Concordant temperature estimates based on the partitioning of two or more elements, however, should provide a check on the reliability of this technique of geothermometry.

4.7.4. FLUID INCLUSIONS

The use of fluid inclusions for geothermometry and geobarometry requires three kinds of data: (a) homogenization temperatures (T_h); (b) the composition of the trapped fluid phase (or phases) from microthermometric measurements and other methods mentioned in Chapter 2; and (c) P - V - T - X properties of the inclusion fluid in the range of interest (see Roedder 1984 for a review of the available data on various systems).

Thermometry

As mentioned earlier, the homogenization temperature gives the minimum *trapping temperature* (T_i). The 'pressure correction' (actually, a temperature correction because of pressure difference; Roedder 1984) to obtain the trapping temperature (T_i) requires a knowledge of the trapping pressure (P_i). The pressure correction for aqueous inclusions containing NaCl solution is discussed by Potter (1977) and Roedder (1984). In many cases, this pressure cannot be determined from the inclusions and has to be estimated from an independent source (e.g., sphalerite geobarometer or the depth of cover at the time of trapping).

Barometry

The total pressure determined from fluid inclusions may be *hydrostatic*, resulting from the weight of the column of overlying fluid, or *lithostatic*, resulting from the weight of the overlying rock, or some intermediate value (Fig. 4.36). Case *A* in Figure 4.36 represents the simplest possibility, in which the hot fluid moves up in a fracture open to the ground surface, and the pressure at the inclusion is that from a column of fluid of appropriate composition and temperature. Case *B* is similar except for the variation in fluid density caused by the introduction of cooler and dilute groundwater at a shallow level. Cases *C*, *D*, and *F* involve boiling of the fluid. If the fluid in the vein above the inclusion is at the point of boiling throughout its length (case *C*) and its salinity is known, the pressure can be calculated (Haas 1971). More commonly, however, a progressive decrease in pressure causes the fluid to boil at some shallow depth (case *D*) and, because of the vapor column, the pressure at the inclusion is considerably less than simple hydrostatic. In a vein not open to the ground surface, the total pressure at the inclusion may be close to the hydrostatic pressure of the fluid column (h) as in case *E*, or the sum of the pressures of the fluid column (h_1) and the rock column (l_1) as in case *G*, or simply lithostatic corresponding to the rock column (l) as in case *H*. Case *F* represents an extreme condition, in which boiling occurs at some depth by a sudden reduction in pressure, for example, because of tensional enlargement of the vein aperture.

The techniques of fluid inclusion barometry have been discussed by Roedder and Bodnar (1980) and Roedder (1984). Two-phase, liquid and vapor aqueous inclusions are the most common type of fluid inclusions encountered in mineral deposits. Without any evidence of boiling, the only pressure constraint that can be inferred from such inclusions is that the hydrostatic pressure at trapping was greater than the vapor pressure of that particular fluid at the trapping temperature. A minimum trapping pressure, equal to the internal pressure at homogenization (P_h), can also be calculated (under certain simplifying assumptions) for aqueous inclusions containing daughter minerals (Roedder & Bodnar 1980).

Two special situations, both involving immiscibility of pure phases, are of particular interest, because both allow simultaneous determination of trapping pressure and trapping temperature. Where two immiscible fluids with known P - V - T properties were trapped at the same time as separate inclusions, the trapping temperature (T) and

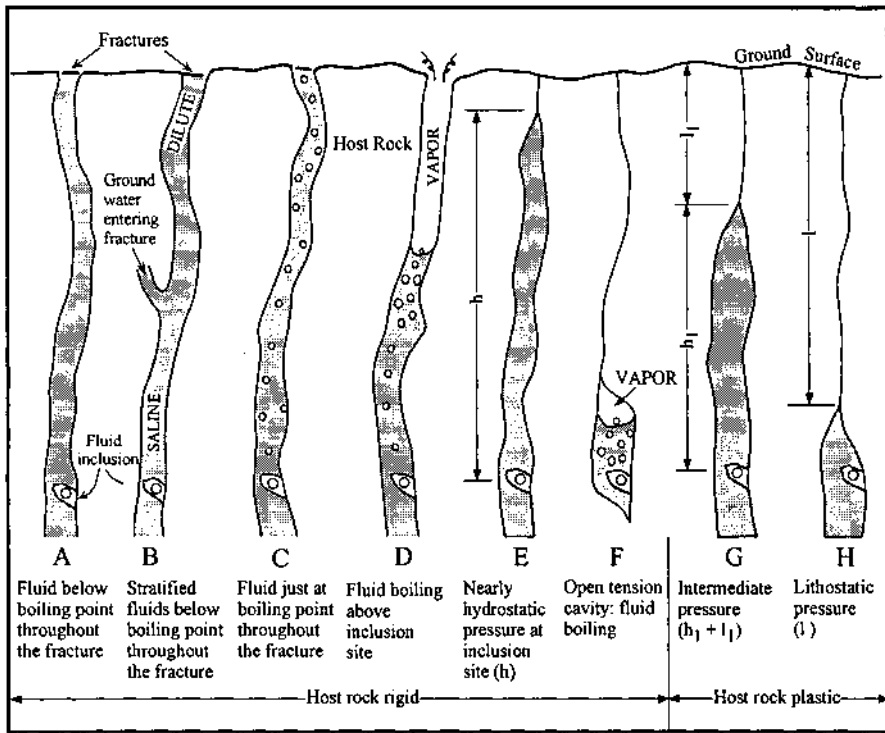


Figure 4.36. Range of possible pressure conditions on a fluid inclusion trapped in a crystal growing freely into a fluid in a vein that may be open or closed to the ground surface. Case A represents the situation where the total pressure at the inclusion is hydrostatic, and Case H the other extreme where the total pressure is almost entirely lithostatic. Case C is a special situation which permits unambiguous determination of the pressure if the salinity of the fluid is known (Haas 1971). See text for further details. (After Roedder & Bodnar 1980.)

trapping pressure (P_t) would be uniquely defined by the intersection of the isochores. The only pair of fluids that are potentially capable of providing good geobarometric data by this method are the oil and brine inclusions found in some Mississippi Valley-type deposits, but the P - V - T data on the oil phase are not known. The other situation is the immiscibility related to a boiling fluid. If the liquid and vapor phase from such a fluid were trapped separately as a pair of inclusions, the two would homogenize in the liquid and in the vapor phase, respectively, at the same temperature. If the boiling curve is known for this fluid, the trapping pressure can be determined from the homogenization temperature (which, in this case, is the trapping temperature).

CO_2 -bearing inclusions occur in rocks from a variety of geologic environments, and many methods have been suggested for determining T_t and P_t from these inclusions (Roedder 1984). The technique is rather simple if essentially pure CO_2 and essentially pure H_2O coexist as separate inclusions. If it is reasonable to assume that the two inclusions were trapped at the same P - T conditions (either at the same location at different times or at the same time but at different locations), then the P_t and T_t are defined by the intersection of the isochore corresponding to the CO_2 inclusion with that corresponding to the H_2O inclusion (Fig. 4.37). Pressure determinations from mixed H_2O - CO_2 inclusions are much more complex. At ambient temperatures, such an inclusion commonly contains three essentially pure phases (relative to each other) — liquid CO_2 , gaseous CO_2 , and liquid H_2O — so that the mole% CO_2 in the inclusion

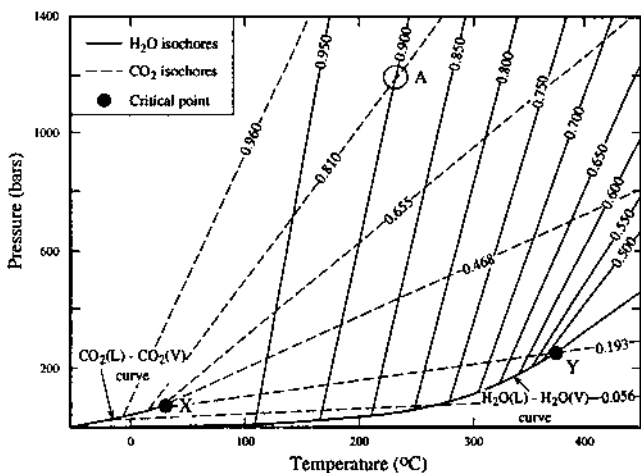


Figure 4.37. Determination of the trapping temperature (T_t) and trapping pressure (P_t) from homogenization temperatures (T_h) of separate CO_2 and H_2O inclusions trapped at the same time. The 0.810 isochore corresponds to the homogenization of the CO_2 inclusion in the liquid phase at 11°C , the 0.900 isochore to the homogenization of the H_2O inclusion in the liquid phase at 167°C . Point A, the intersection of the two isochores, defines the trapping temperature (237°C) and trapping pressure (1180 bars) of the two inclusions. X represents the critical point of CO_2 and Y that of H_2O (After Roedder & Bodnar 1980.)

can be calculated from measured volumes of the three phases at a known temperature and the density data for CO₂ and H₂O (Bodnar 1983). Knowing the mole% CO₂ in the inclusion and its homogenization temperature, one can determine the internal pressure at homogenization or the minimum pressure at trapping. In most fluid inclusion work, the CO₂ content of the fluid is either unknown or known only imprecisely from volume measurements. In this situation, the only reliable pressure estimate may be the maximum trapping pressure defined by the critical pressure of the isotherm corresponding to the homogenization temperature. The usefulness of this geobarometer is further restricted by the fact that most CO₂-bearing inclusions contain an aqueous salt solution rather than pure H₂O and this results in considerable widening of the miscibility gap. The mole% CO₂ in a NaCl - H₂O - CO₂ inclusion can be estimated (Parry 1986), but the errors in pressure determinations are likely to be large because of the relatively steep slopes of the isotherms.

4.8. Metamorphism of Ore Assemblages

An unmetamorphosed mineral deposit hosted by metamorphic rocks is clearly epigenetic and post-metamorphic, whereas a mineral deposit metamorphosed along with its enclosing rocks is at least pre-metamorphic and may even be syngenetic. Also, features in ore-gangue assemblages resembling those commonly attributed to epigenesis or even magmatic processes might have been actually produced by metamorphism. The recognition of superimposed metamorphic features, therefore, are crucial to the genetic interpretation of a metamorphosed mineral deposit. The reconstruction of the metamorphic history of a deposit, however, can be quite difficult because of complications due to deformational structures, polymetamorphism (Schreyer et al. 1964, Lawrence 1973), and retrograde metamorphism (Richards 1966).

The effects of metamorphism are particularly well documented for two groups of mineral deposits: the sedimentary iron and manganese oxide deposits (James 1955, Roy 1966, Klein 1973, French 1973, Stanton 1976a), and massive sulfide deposits hosted by metamorphosed volcanic and sedimentary rocks (Kanehira 1959, Banno & Kanehira 1961, Schreyer et al. 1964, Kalliokoski 1965, Kinkel 1967, McDonald 197, Lawrence 1973, Bachinski 1976, Vokes 1976, McClay 1983). Also available in the published literature are several review articles on the subject (McDonald 1967, Vokes 1969, Sen et al. 1973, Mookherjee 1976, Gilligan & Marshall 1987, Plimer 1987).

Metamorphic effects important for the interpretation of ore genesis include: (a) textural changes; (b) mineralogic changes; (c) remobilization of sulfide constituents; and (d) modification of isotope ratios. In general, the oxide deposits are more susceptible to mineralogic changes because the oxide minerals react readily with associated silicates and carbonates, whereas the sulfides show more pronounced textural changes because of their vulnerability to deformation and high capacity for annealing and grain growth (Stanton 1972). The effects of contact metamorphism increase toward the heat source (e.g., a post-ore dike); the effects of regional metamorphism are most

obvious at higher grades and are best appreciated by comparison of similar deposits occurring in different zones of progressive metamorphism (see Mookherjee 1976, Table II, p. 216-217). A summary of metamorphic effects on massive sulfide deposits, as exemplified by the Norwegian Caledonide deposits, is presented in Table 4.4.

TABLE 4.4. Summary of metamorphic effects on massive sulfide deposits of the Norwegian Caledonides (after Vokes 1976)

Textural changes

General increase in grain size with increasing metamorphic grade.
 Development of porphyroblasts (pyrite, arsenopyrite, magnetite, garnet, staurolite).
 Polygonization with foam texture (pyrrhotite, sphalerite, chalcopyrite, galena, quartz).
 Cataclasis prior to or subsequent to recrystallization.
 Preferred orientation of minerals.
 Deformation twinning in sulfide minerals.
 Ductile deformation (microfolding, disruption of banded textures, "durchbewegung," etc.).

Mineralogic changes

Increase in pyrrhotite content due to breakdown of pyrite.
 Increase in Fe content of sphalerite.
 Sulfide-silicate (-oxide, -carbonate) reactions.
 Sulfurization of Fe-bearing minerals.
 Formation of gahnite (Sunbald 1982).

Remobilization of sulfide constituents

Thickening of sulfides in fold hinges and concomitant thinning of limbs.
 Development of elongated sulfide bodies parallel to regional foliation or lineation.
 Selective mobilization of ore forming components (up to some tens of meters) by creep, fluid phase transport, or as melts at very high grade metamorphism. Most mobile: galena, sulfosalts, chalcopyrite; mobile: pyrrhotite, sphalerite; least mobile: pyrite, magnetite.

4.8.1. TEXTURAL CHANGES

Metamorphism and deformation are commonly broadly coeval, and textural changes produced by metamorphism are essentially a combination of deformation and annealing textures in polycrystalline aggregates. Metamorphic textures common to both contact and regionally metamorphosed assemblages include coarsening of grains, development of porphyroblasts (often with poikilitic inclusions), polygonization ('foam texture') (Lawrence 1972), and formation of inversion and annealing twins. In addition, regional metamorphism may produce in sulfide assemblages, especially in high-grade zones, dimensional and crystallographic preferred orientation (Kanehira 1959, Davis 1972), segregation banding, and flowage migration of the softer sulfides, resulting in boudins, folding of sulfide layers with attenuated limbs and thickened noses, and localized piercement structures (Gilligan & Marshall 1987). Very high temperatures (around

500°C or more, depending on the assemblage) may lead to partial melting of sulfides (Brett & Kullerud 1966, Lawrence 1967, Mookherjee & Dutta 1970, Vokes 1971) and the resulting melt may be segregated into veins and offshoots. The effects of cataclastic (or dislocation) metamorphism are localized along shear and fault zones and essentially consist of plastic deformation and cataclasis without significant annealing.

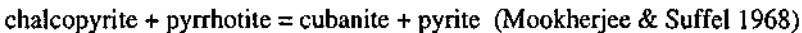
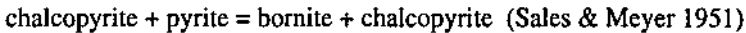
As expected, textural studies have shown that different minerals respond differently to metamorphism (McClay 1983, Gilligan & Marshall 1987, Cox 1987), and this is also borne out by several experimental studies (e. g., Stanton & Gorman 1968, Clark & Kelly 1973, Atkinson 1974, Salmon et al. 1974, Atkinson 1975, Roscoe 1975, Clark et al. 1977). The experimental results are specific to the ranges of conditions (temperature, differential stress, confining pressure, and strain rate) employed in the experimental studies, and caution should be exercised in extrapolating these results to natural assemblages. However, certain qualitative generalizations are in order: (a) sphalerite deforms more easily than pyrrhotite at lower temperatures, but the reverse is true at higher temperatures (greater than about 200°C); (b) chalcopyrite deforms more easily by plastic flow even under conditions of low-grade metamorphism; (c) pyrite deforms by brittle failure, although plastic flow may occur at high temperatures (> 400°C) and high sulfur fugacities; (d) galena is one of the most easily deformed and annealed sulfide minerals at all grades of metamorphism; and (e) it is not possible to devise a universally applicable ranking of these sulfide minerals in terms of their vulnerability to metamorphism, because they undergo pronounced changes and even reversals in strength at least as a function of temperature (Kelly & Clark 1975). That different sulfide minerals respond differently to metamorphism is an important consideration for the interpretation of paragenesis. For example, in a metamorphosed sphalerite - galena assemblage the sphalerite might appear more deformed than the galena, not because of their different positions in the paragenetic sequence but because galena is much more amenable to annealing recrystallization (Stanton & Wiley 1970).

4.8.2. MINERALOGIC CHANGES

Mineralogic changes during metamorphism occur primarily in response to higher temperatures although other variables such as the activities of oxygen, sulfur, CO₂, and H₂O are important in determining the metamorphic assemblages. As mentioned earlier, manganese and iron oxide deposits often provide a good record of mineralogic changes by metamorphism. In a classic study of the Precambrian banded iron-formations of the Lake Superior region (USA), James (1955) showed that mineral assemblages of the iron-formations varied systematically with the grade of regional metamorphism established on the basis of the associated argillaceous rocks. Another well documented example is the contact metamorphism (pyroxene hornfels facies) of the Precambrian Gunflint Iron Formation of Minnesota (USA)-Ontario (Canada) in the contact aureole of the Duluth Complex. Floran and Papike (1976) delineated three metamorphic zones based on mineralogic changes in the contact aureole and a fourth zone corresponding to essentially unmetamorphosed iron-formation. Each zone was recognized by the

dominant iron silicate present: zone 1 - greenalite zone (unmetamorphosed), zone 2 - minnesotaite zone (slightly metamorphosed), zone 3 - grunerite zone (moderately metamorphosed), and zone 4 - ferroporphyrine zone (highly metamorphosed). Mineralogic changes accompanying metamorphism of sedimentary manganese deposits are also well documented in the literature (e.g., Dorr et al. 1956, Roy 1966).

Iron sulfides formed in sedimentary environments include hydrotroilite, melnikovite, mackinawite, gregite, and pyrite (Berner 1964). The dominance of pyrite at low metamorphic grades points to substantial mineralogic changes during metamorphism. The large stability fields of the common sulfide minerals and their relatively simple chemical compositions, however, do not lend sulfide assemblages to be sensitive indicators of progressive metamorphism. Moreover, the subsolidus mineralogic changes that do occur at higher temperatures, as predicted from experimental studies on sulfide systems, seldom survive the post-metamorphic equilibration to lower temperatures. Mineral transformations such as



have been recognized at the contact zones of post-ore dikes traversing sulfide deposits, and the increasingly complex ore mineralogy of deposits in areas of increased regional metamorphism may be attributed to a greater degree of recrystallization (McDonald 1967). The most commonly cited effect of metamorphism on sulfide mineralogy is the conversion of pyrite to pyrrhotite (\pm magnetite), well documented for both contact metamorphism (Mookherjee & Suffel 1968, Mookherjee 1970) and regional metamorphism (Gammon 1966, Thompson & Norton 1968, Carpenter 1974). In some regional metamorphic terrains it has been possible to establish a correlation between an increase in pyrrhotite:(pyrite + pyrrhotite) ratio and increasing metamorphic grade (Ferry 1981, Runyon & Misra 1985). The transformation of pyrite is accompanied by release of a significant amount of sulfur which, in turn, may affect the ore-gangue mineralogy by modifying assemblages whose equilibrium is controlled by sulfur fugacity. An increase in sulfur fugacity may result in a variety of mineralogic changes: transformation of chalcopyrite to bornite + pyrite, a decrease in the iron content of sphalerite or pyrrhotite (Barton & Toulmin 1966), development of pyrrhotite rims around gangue inclusions, and a new generation of pyrite porphyroblasts from pyrrhotite and ferromagnesian silicates (Mookherjee & Suffel 1968).

4.8.3. METAMORPHIC REMOBILIZATION

Metamorphic remobilization — redistribution and modified concentrations of constituents of pre-existing massive and semi-massive mineralization during metamorphism — is governed by the same principles as discussed earlier for

metamorphic mobilization (Ch. 2). Remobilization occurs mainly in response to regional metamorphism and tectonism and involves both solid-state (mechanical) and fluid-phase (chemical) transport of constituents. In general, evidence for modifications by low and medium grades of metamorphism is often clear and convincing, because primary genetic features of mineral deposits can usually still be discerned for comparison. The effects are likely to be more pronounced at high grade metamorphism, but also more difficult to decipher.

The effects of remobilization may range from localized migration of sulfide species into secondary structures to major changes in the external dimensions of a deposit, and may even include sulfide accumulation removed from the metamorphosed source. The effects may be summarized under three broad categories (Skinner & Johnson 1987): (a) redistribution of material within a deposit without concomitant change in the overall composition of the ore mass; (b) movement of material into, or out of, a deposit; and (c) physical displacement of a deposit.

Differential remobilization of the "soft" sulfide minerals (such as galena, chalcopyrite, and pyrrhotite) on millimeter and centimeter scales is a common result of regional metamorphism, especially at high grades, and may be ascribed mainly to plastic flow. Evidence of such remobilization includes (Vokes 1969, Gilligan & Marshall 1987, Plimer 1987): (a) healing of cataclastically deformed pyrite and arsenopyrite by the inflowing of chalcopyrite and other sulfides; (b) migration of galena, chalcopyrite, and pyrrhotite into the pressure-shadow tails of deformed pyrite grains or silicate fragments; (c) transgressive veinlets of schistose galena, pyrrhotite, or chalcopyrite adjacent to metamorphosed massive sulfides; (d) sulfide-filled tension fractures (gash veins); and (e) the flow of sulfide mass around detached silicate fragments ("durchbewegung" texture). Plastic flow of sulfides, perhaps aided by pressure-induced solution transfer, may also take place during folding, even at relatively low temperatures, in response to a variable stress field acting over a considerable period of time, producing thickened hinge zones with concurrent limb attenuation. A good example, described by Hewlett and Solomon (1964), is the concentration of massive sulfide in the fold hinges and cross-fractures in the banded and highly folded Mt. Isa Pb-Zn deposit (Queensland, Australia). Other examples have been described by Plimer (1987) and Cook et al. (1990). Concentration of galena along the crests of folds and its depletion along the limbs is a common feature in many deformed and metamorphosed orebodies (McDonald 1970, Juve 1977, Pederson 1980), although deformation textures in the galena might be obliterated by subsequent recrystallization. Variations in metal ratios, such as enhanced Ag:Pb ratio in deformed "steely" galena in the Coeur d'Alene district (Idaho, USA) and lower Zn:Cu ratios at the center of the Broken Hill No. 3 orebody (Australia), have also been cited as examples of selective remobilization within individual deposits (McDonald 1967, Vokes 1971).

Metamorphism of sulfide deposits may also produce variations in oxide, carbonate, and silicate mineralogy in and around such deposits (Nesbitt 1986a, 1986b), and these variations may be useful as exploration guides. For example, the amphibolite facies regional metamorphism ($T = 540^\circ \pm 40^\circ\text{C}$, $P = 6 \pm 1 \text{ kb}$; Nesbitt & Essene 1982) of

the Ducktown massive sulfide deposits (Tennessee, USA) resulted not only in a sulfide - oxide - graphite zonation around the ore zone (Fig. 4.38a), but also in a systematic decrease in the mole fraction of iron in the ferromagnesian silicates from the wallrocks to the ore zone (Nesbitt & Kelly 1980, Nesbitt 1982). This zonation can be correlated to a decrease in fO_2 and fS_2 toward the country rocks (Fig. 4.38b). The fS_2 for the metamorphic reactions was controlled by either diffusion of sulfur outward from the ore zone or sulfur enrichment in the wallrocks during the pre-metamorphic emplacement of the ore; the inferred increase in fO_2 values was probably an artifact of the increasing fS_2 values and the resultant sulfur-silicate reactions (Nesbitt 1982). A feature common to many metamorphosed Cu-Zn-Pb massive sulfide deposits is the occurrence of the zinc spinel gahnite $[(Zn,Fe,Mg)Al_2O_4]$, which is considered a potential exploration guide for such deposits (Sunbald 1982, Sheridan & Raymond 1984, Spry 1987b). The gahnite is interpreted to have formed predominantly by desulfurization reactions involving a member of the Fe-S-O system and either sphalerite and garnet or sphalerite and aluminosilicate (Spry & Scott 1986, Spry 1987b). Some of the gahnite-bearing deposits are also associated with high-zinc staurolite (>6 wt% ZnO) that probably formed also by desulfurization reactions (Spry & Scott 1986).

The unusual composition of some deposits may have resulted from selective removal of material during metamorphism. For example, the Zn-rich ores (mixtures of willemite, zincite, franklinite, and a range of Mn-pyroxenes and Mn-garnets) of Franklin Furnace and Sterling Hill deposits (New Jersey, USA) might represent metamorphosed stratiform Zn-Pb deposits of sedimentary origin (Fronde! & Baum 1974). As a general rule, however, massive sulfide deposits, whether metamorphosed or unmetamorphosed, are mixtures of pyrite \pm pyrrhotite, galena, sphalerite, and chalcopyrite. Such consistency of composition is not compatible with metamorphic remobilization (Skinner & Johnson 1987). According to Gilligan and Marshall (1987), dissolution is inhibited by the low permeability of homogeneous, low-silicate, massive sulfides, whereas remobilization of disseminated mineralization peripheral to the massive ore seems more probable. Although metamorphic fluids have properties suitable for transport of heavy metals and sulfur, there are no well documented examples of deposits formed entirely by the remobilizing action of metamorphic fluids. One possible example is the vein-type mineralization in the Broken Hill district, Australia (Barnes 1987), but the main evidence for a genetic link between the vein-type and the highly metamorphosed, massive sulfide mineralization in the district — the similarity of lead isotope ratios — is not convincing.

In the extreme case, metamorphic remobilization may occur through partial melting of sulfides, at least on a local scale. Lawrence (1967) attributed the transgressive sulfide pegmatoid and sulfide-silicate pegmatites in the Broken Hill ores to partial melting at the peak of granulite-facies regional metamorphism. Mookherjee and Dutta (1970) presented evidence of sulfide melting adjacent to diabase dikes by contact metamorphism. Experimental studies, however, do not support the metamorphic generation of partial melts (sulfide neomagmas) of appropriate composition to form the commonly Fe-rich massive sulfide deposits (Skinner & Johnson 1987). In the Fe-Cu-

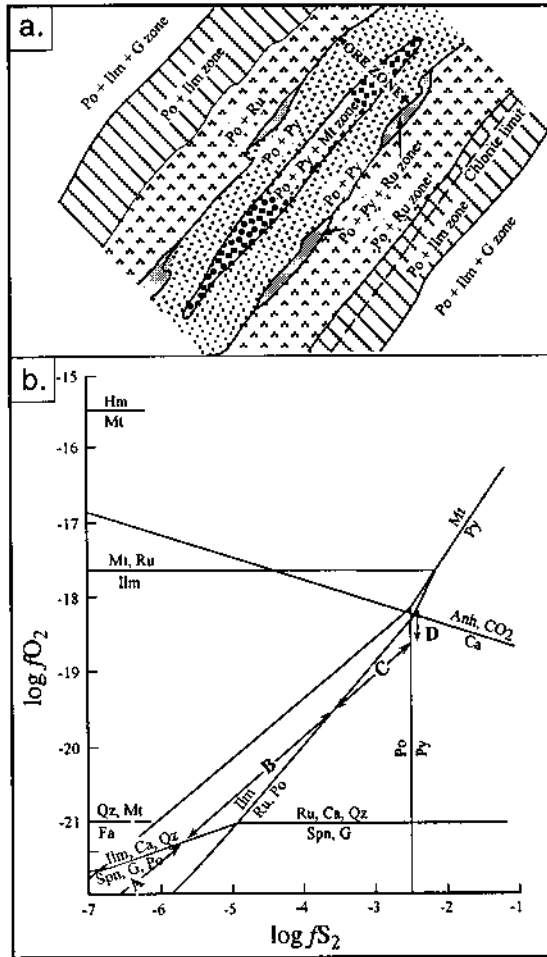


Figure 4.38. Mineralogical changes produced by regional metamorphism of massive sulfide deposits of the Ducktown district, Tennessee, USA. a. Schematic diagram showing the distribution of sulfide - oxide - graphite zones around the ore zone (approximately 40 to 60 m). Dashed lines represent the outer extent of primary metamorphic chlorite. Staurolite does not persist into the Po + Py + Ru zone and is also absent from muscovite-bearing units in the Po + Ru zone. b. The probable fS_2 - fO_2 ranges of the sulfide - oxide - graphite zone assemblages in relation to stabilities of phases in the system C-O-S-Ti-Fe at 550°C and 6 kb. Stability of the reaction $Anh + CO_2 = Ca + 0.5 S_2 + 2O_2$ was calculated assuming $X_{CO_2} = 0.15 \pm 0.05$ and $P_{fluid} = P_{total}$. Zones A through D representing the ranges in the fS_2 and fO_2 stabilities of the various oxide - sulfide - graphite assemblages are as follows: Zone A, pyrrhotite + ilmenite + graphite; zone B, pyrrhotite + ilmenite; zone C, pyrrhotite + rutile; zone D, pyrrhotite + pyrite + rutile and ore zone. Abbreviations: Po = pyrrhotite; Py = pyrite; Ilm = ilmenite; Ru = rutile; G = graphite; Hm = hematite; Mt = magnetite; Qz = quartz; Fa = fayalite; Anh = anhydrite; Ca = calcite; Spn = sphene. (After Nesbitt & Kelly 1980.)

Pb-S condensed system (Craig & Kullerud 1969), a sulfide-rich liquid forms at 508°C, but this melt contains practically no Fe. As the liquid field expands at higher temperatures, it becomes increasingly enriched in Fe, but at no stage below about 900°C does it come anywhere close to the Fe-rich composition of a typical massive sulfide deposit. The presence of ZnS would raise rather than lower the temperature of the sulfide liquidus. There is no significant solubility of water in sulfide melts and no detectable depression of the liquidus. An Fe₃O₄ component (or any other iron oxide) would lower the liquidus, but most massive sulfide ores do not contain much magnetite. Thus, generation of Fe-Cu-Zn-Pb sulfide melts during metamorphism, if it occurs at all, must be an uncommon process (Skinner & Johnson 1987).

Many examples of sulfide-bearing bodies of likely remobilization origin at distances up to about 5 m from metamorphosed sulfide deposits have been cited in the literature (Mookherjee 1970, Vokes 1971), but the formation of new mineral deposits by remobilization at distances in the order of kilometers, or even tens of meters, from the source is rather unlikely. This is because the rates of ductile deformation are generally too slow to permit transport of materials over long distances in a reasonable time. Possible exceptions to this generalization are transport along major shear zones and gravitational sinking due to density contrast between the massive ores and country rocks in high-grade metamorphic environments (Skinner & Johnson 1987), but neither is well documented. Some Precambrian massive sulfide deposits are believed to have been displaced from their root (such as footwall alteration zones and hypabyssal intrusives), but such displacements probably were caused by tectonic transport, not metamorphic remobilization (Jenks 1971). Distant remobilization is likely to be achieved only by advective transfer via an aqueous or magmatic fluid (Marshall & Gilligan 1993).

Mobilization and remobilization are not mutually exclusive processes. Both are capable of yielding the same or similar geometric relationships, fluid inclusion data, fluid chemistry, and metal and sulfur sources. How, then, can we distinguish between mobilization leading to syntectonic mineralization and remobilization of pre-tectonic mineral deposits? Marshall and Gilligan (1993) have discussed several guidelines, the application of which "require a thorough geometric and kinematic analysis on all scales," and the task is a difficult one. That is one of the reasons why the origin of many strata-bound massive sulfide deposits, which are discordant to host stratigraphy (e.g., Cobar and Mt. Isa, NSW, Australia; Roseberry, Tasmania, Australia; Heath Steele, New Brunswick, Canada) remain controversial.

4.8.4. EFFECTS ON SULFUR ISOTOPE RATIOS

On the basis of several studies of metamorphosed strata-bound deposits reported in the literature, Rye and Ohmoto (1974) concluded that large-scale, pre-metamorphic $\delta^{34}\text{S}$ variations are generally preserved despite superposition of small-scale sulfur isotope changes during metamorphism.

The average $\delta^{34}\text{S}$ values for sulfides in major lithologic units, such as formations,

are generally unchanged, presumably because of little migration of sulfur across formational boundaries. For example, the $\delta^{34}\text{S}$ values of pyrrhotite and arsenopyrite in the Homestake gold mine (South Dakota, USA) range from 5.6 to 9.8‰ in the highly deformed and gold-bearing Precambrian Homestake Formation, from 2.7 to 5.1‰ in the underlying Poorman Formation, and from 4.1 to 29.8‰ in the overlying Ellison Formation. This formational dependence of $\delta^{34}\text{S}$ values, according to Rye and Rye (1974), indicates a sedimentary origin of the sulfur in the Homestake deposit. In the Homestake Formation, the lowest $\delta^{34}\text{S}$ values are in the large dilatant cross-folded zones where sulfide concentration is high (8 wt%), and the highest $\delta^{34}\text{S}$ values are in the stretched limbs where sulfide concentrations are low (≈ 1 wt%). The interpretation offered by Rye and Rye (1974) is that the sulfur released by conversion of pyrite to pyrrhotite during greenschist to lower amphibolite facies regional metamorphism was transported by metamorphic fluids into the dilatant zones where sulfur reacted with the wallrocks to produce iron-rich sulfides; the present $\delta^{34}\text{S}$ distribution resulted from the fractional distillation of sulfides in the limbs as the sulfides broke down and as excess sulfur was removed by the metamorphic fluids.

A correlation between $\delta^{34}\text{S}$ values of sulfides and stratigraphy has been noted in many metamorphosed strata-bound sulfide deposits such as at Broken Hill and Mt. Isa in Australia (Stanton & Rafter 1966), Rammelsberg in Germany (Anger et al. 1966), Ducktown in USA (Mauger 1972), and Heath Steele in Canada (Lusk 1972). The isotopic patterns in these deposits, although somewhat modified within stratigraphic units by attainment of isotopic equilibrium between sulfide minerals, are believed to reflect variations related to syngenetic sulfide mineralization.

The small-scale sulfur isotope changes in a mineral deposit during metamorphism include (Rye & Ohmoto 1974): (a) redistribution of sulfur isotopes among coexisting sulfide minerals that define the temperature of metamorphism; and (b) local $\delta^{34}\text{S}$ variations which reflect the structural or chemical aspect of the metamorphic history. For the metamorphosed Broken Hill Pb-Zn deposit (NSW, Australia), Both and Smith (1975) obtained mean sulfur isotopic fractionation factors of 0.88‰ for the sphalerite - galena pair and 0.72‰ for the pyrrhotite - galena pair, which gave equilibration temperatures in good agreement with the earlier estimates of Binns (1964) for the temperatures of metamorphism (700°-800°C) of the enclosing rocks. From a recent study of several metamorphosed volcanic-hosted sulfide deposits, spanning the range from lower greenschist to upper amphibolite facies, Crowe (1994) found that the original sulfur isotopic compositions were preserved in discrete monomineralic sulfide grains encapsulated by quartz matrix, but not by sulfide pairs in direct contact with each other. Apparently, minerals in mutual contact are prone to isotopic re-equilibration during metamorphism, whereas isolated sulfide grains shielded by a non-sulfide matrix are not.

4.9. Age of Mineralization

The age of mineralization is a critical piece of information required for understanding the genesis of any mineral deposit, because the age provides constraints on potential controls of ore emplacement, such as igneous activity, tectonic setting, metamorphic remobilization, sources of ore fluids and ore constituents, etc. For some types of deposits, the multiplicity of genetic models, to a large extent, is the result of a lack of knowledge about the timing of mineralization. For example, the understanding of the volcanogenic massive sulfides has evolved rapidly in recent years, only after it was realized that ore emplacement in these deposits was a syngenetic rather than a post-lithification event. In contrast, the continued lack of a generally acceptable genetic model for the epigenetic Mississippi Valley-type deposits stems largely from a lack of knowledge regarding the age of mineralization for most deposits of this type. Thus any comprehensive study of a mineral deposit must include efforts to determine the timing of mineralization as precisely as possible.

4.9.1. RELATIVE AGE

The relative age of mineralization is determined from constraints revealed by stratigraphic relations, such as crosscutting veins or dikes and restriction of mineralization to a certain stratigraphic interval, metamorphism, and deformation. Mineral deposits, especially those hosted by sediments, are often described as (a) *syngenetic*, formed contemporaneously with (and essentially by the same process as) the host rocks or (b) *epigenetic*, formed later than the host rocks. The timing of mineralization of some sediment-hosted deposits has been described as *syndiagenetic* (or *diagenetic*) but not in the same sense by all authors (see, for example, Brown 1989).

Considering the lack of a clear boundary between diagenesis and epigenesis, in terms of either process or time, it may be prudent to include all modifications to a sediment between deposition and metamorphism as diagenesis. This approach, however, does not help to relate the mineralization event (or events) in a sedimentary basin to its evolution. Tourtelot and Vine (1976) proposed that post-depositional mineralization might be distinguished as diagenetic if the mineralizing fluids evolved from within the host sequence and epigenetic if the fluids were derived from an external source. This distinction is not objective as the limits of the host rock sequence may be chosen arbitrarily. Moreover, it does not help to constrain the relative timing of mineralization because the influx of hydrothermal fluids may occur in several stages in the course of the evolution of a sedimentary basin. For sediment-hosted deposits, we will use syngenetic in the sense of synsedimentary, syndiagenetic in the sense of early diagenesis (i.e., before or during the stage of lithification of unconsolidated sediments into consolidated rocks), epigenetic in the sense of late diagenesis (i.e., post-lithification stage), and post-depositional or post-sedimentary where the stage of diagenesis is unclear. Some useful criteria for distinguishing among syngenetic, syndiagenetic, and epigenetic mineralization in sediments are listed in Table 4.5.

TABLE 4.5. Criteria for syngenetic, syndiagenetic, and epigenetic mineral deposits hosted by sediments (after Snyder 1967)

Evidence for	Evidence against
<i>Syngenetic</i> (mineralization contemporaneous with sedimentation)	
Stratiform mineralization at a given stratigraphic position or within a restricted stratigraphic interval.	Similar mineralization in a variety of rock types.
Close correspondence between mineralization (mineralogy and textures) and sedimentary features (stratification, rock types, structures, facies).	Transgressive relationships of mineralization unrelated to facies changes; mineralization in post-depositional structures.
Lateral uniformity in thickness, width, tenor, and metal ratios, with variations controlled by sedimentary features.	Marked lateral changes in thickness, width, tenor, and metal ratios of ore, unrelated to sedimentation.
<i>Syndiagenetic</i> (mineralization after sedimentation but before complete lithification)	
Stratiform to strata-bound mineralization within a restricted stratigraphic interval.	Similar mineralization in a variety of rock types.
Close correspondence between mineralization (mineralogy and textures) and sedimentary features (stratification, rock types, structures, facies).	Extensive transgressive mineralization unrelated to depositional or diagenetic features
Mineralization related to diagenetic features and structures.	Mineralization in post-lithification structures; extensive cavity-filling type mineralization.
<i>Epigenetic</i> (mineralization after sedimentation and lithification)	
Discordant (may be strata-bound) mineralization without apparent stratigraphic control.	Evidence for syngenetic or diagenetic mineralization.
Mineralization correlated with post-lithification (including tectonic) structures and minerals.	
Marked lateral variations in thickness, width, tenor, and metal ratios that cannot be related to sedimentary or diagenetic features or environments.	
Extensive cavity-filling type mineralization.	

4.9.2. ABSOLUTE AGE

The absolute age of mineralization in a deposit is determined, where possible, by radiometric dating of ore minerals or contemporaneous gangue minerals. Ore assemblages containing galena may be dated by the Pb-Pb method, but, as discussed earlier, many ore leads are anomalous and often do not yield unique ages. Deposits containing micas and feldspars may be dated by $^{40}\text{K} - ^{40}\text{Ar}$ and $^{87}\text{Rb} - ^{86}\text{Sr}$ methods, but only if such minerals can be shown to be contemporaneous with mineralization. A

basic assumption of the conventional $^{40}\text{K} - ^{40}\text{Ar}$ method is that the sample contained no argon at the time of its formation and has not lost any argon subsequently by diffusion. The $^{39}\text{Ar} - ^{40}\text{Ar}$ age-spectrum method (Dalrymple and Lanphere 1974, Dallmeyer 1979), which is a high-precision variant of the $^{40}\text{K} - ^{40}\text{Ar}$ method, can overcome some of the limitations of the $^{40}\text{K} - ^{40}\text{Ar}$ method. The $^{39}\text{Ar} - ^{40}\text{Ar}$ age-spectra of K-bearing minerals, such as muscovite, biotite, and adularia, have been found useful for dating episodes of mineralization and alteration in hydrothermal systems (Lanphere 1988). York et al (1982) even obtained a $^{40}\text{Ar}/^{36}\text{Ar}$ vs. $^{39}\text{Ar}/^{36}\text{Ar}$ isochron (2500 ± 120 Ma) for pyrite samples from a volcanic-hosted massive sulfide deposit and the date is similar to that obtained from the $^{39}\text{Ar} - ^{40}\text{Ar}$ age-spectra of two biotites from the same deposit. In some cases it has been possible to date ore-stage calcite by $^{238}\text{U} - ^{206}\text{Pb}$ and $^{232}\text{Th} - ^{208}\text{Pb}$ methods (Brannon et al. 1993, 1995), sphalerite by $^{87}\text{Rb} - ^{86}\text{Sr}$ method (Nakai et al. 1993, Christensen et al. 1993, 1994, 1997), fluorite by $^{147}\text{Sm} - ^{143}\text{Nd}$ method (Chesley et al. 1994), and molybdenite by $^{187}\text{Re} - ^{187}\text{Os}$ method (Stein et al. 1998). Shepherd and Darbyshire (1981) obtained Rb-Sr isochrons from measurements on fluid inclusions; although promising, the general applicability of the method is yet to be tested.

Fission-track dating is now used for dating a variety of minerals and natural glass. For all practical purposes, the fission tracks in a terrestrial mineral can be assumed to have resulted from alpha emission by spontaneous fission of ^{238}U atoms incorporated in the mineral at the time of its formation. When charged alpha particles travel through a solid medium, they leave a trail of damage resulting from the transfer of energy to the atoms of the medium. Thus, in principle, the observed fission track density (number of tracks per unit area) in a given specimen is related to the original uranium concentration of the specimen and the length of time over which the tracks have accumulated. The track density is determined by counting the number of tracks on polished and etched surfaces of the specimen. The uranium concentration is determined by a procedure that involves counting fission tracks produced by induced fission of ^{238}U due to irradiation of the specimen with thermal neutrons in a nuclear reactor. The measurement techniques and age calculation procedure are discussed in Fleischer et al. (1975), Naeser (1977), and Faure (1986). Minerals such as zircon, apatite, and sphene are considered the most suitable for fission-track investigations, but recent studies suggest that fluorite may also be suitable for fission-track dating (Harder 1986). This is encouraging in view of the fact that fluorite occurs in a wide variety of hydrothermal mineral deposits. Another application of fission-track analysis arises because the tracks tend to fade at elevated temperatures as the damage done by the charged particles is healed, but at different rates for different minerals. Thus, two different but cogenetic minerals subjected to the same elevated temperature for the same length of time may yield discordant fission-track dates and provide information about the thermal history of the specimen (Arne et al. 1989).

As a result of the development of cryogenic magnetometers, in which the total noise level has been reduced to 10^{-7} emu, it is now possible to measure natural remanent magnetization (NRM) intensities of 10^{-8} to 10^{-9} emu/g using large volume samples. This has opened up the possibility of using paleomagnetism for a variety of geological interpretations, including dating of mineral deposits containing magnetic

minerals such as pyrrhotite, magnetite, or hematite (Park 1983). In principle, the method is based on relating magnetic poles inferred from samples of interest to calibrated apparent polar wandering paths; the details of measurements and data reduction are too complicated to be discussed here. The method has been applied to date a number of Mississippi Valley-type lead-zinc deposits (see Ch. 13).

4.10. A Comprehensive Example: the Creede District, Colorado, USA

The Creede mining district, an example of volcanic-hosted epithermal base and precious metal deposits of the adularia-sericite type (see Ch. 14), is located along the western edge of the Central San Juan caldera complex. The complex comprises a series of seven nested calderas from which quartz-latic to rhyolitic ash-flow sheets erupted over the brief interval of 27.6 to 26.2 Ma. The Ag-Pb-Zn-Cu (-Au) mineralization in the district is hosted mainly by the intracaldera ash-flows of the Bachelor caldera. The ores are contained in a set of fractures defining a graben that lies between the Creede caldera, the youngest of the calderas, and the slightly older San Luis caldera (Fig. 4.39). The district is divisible into three parts: the Ag-rich (Ag: Au » 1,000) southern part, which historically has been the most productive; the central part, which contains a few small mines and prospects; and the northern part (Northern Amethyst veins) with Ag-Au-rich mineralization (not found in central and southern parts) that predates the more extensive Ag-base metal mineralization. Nearly all the production in the district has come from ores filling the Amethyst, OH, and P veins, and the Bulldog Mountain faults or fault systems in the southern part of the district. The ore zone, which occupies a narrow vertical range from 250 to 400 m, has been mined continuously for approximately 3 km along strike on the Amethyst-OH vein system, and for over 2 km on the Bulldog Mountain vein system. Nearly a century of mining in the district ended in 1987 with the closure of operations at Homestake's Bulldog Mountain mine. During its lifetime, the Creede district produced 4.88 million tons of ore yielding 85 million ounces of silver, 314 million pounds of lead, 90 million pounds of zinc, 6 million pounds of copper, and 150,000 ounces of gold as a byproduct (Campbell 1993).

The Creede district has been the focus of many investigations, particularly by the geologists of the US Geological Survey, over the last two decades. An excellent summary of the district, including pertinent references, is given by Hayba et al. (1985), and some additional data and interpretation are included in Foley and Ayuso (1994), Plumlee (1994), and Plumlee et al. (1994). Table 4.6 summarizes the various kinds of data that have been used for formulating a comprehensive genetic model, as outlined below, for the Creede deposits.

Briefly stated, the unmetamorphosed epithermal, vein-type deposits of the Creede district were emplaced contemporaneously in caldera-related fault systems, at the interface of a deeply circulating, hot (as high as 285°C), saline (up to 13 wt% NaCl equivalent) fluid, and overlying, steam-heated, dilute ground waters. The saline fluids responsible for ore deposition probably originated as pore-waters in the Creede

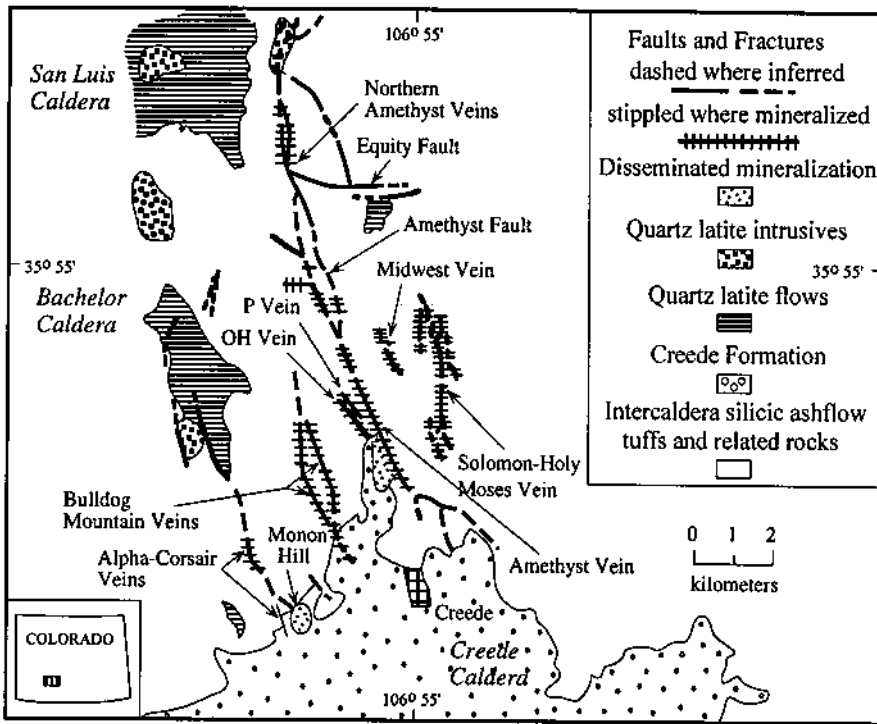


Figure 4.39. Generalized geologic map of the Creede mining district and vicinity, Central San Juan caldera complex, Colorado (USA), showing the various ore veins. Faults are dashed where uncertain or inferred, and stippled where mineralized. Formations: Tc = Creede Formation; Tf = Fisher quartz latite flow. The rest of the area is covered with undifferentiated ash flow tuffs. (After Foley & Ayuso 1994.)

Formation which accumulated in the evaporative, playa lake in the moat of the Creede Formation from a magmatic source, but the bulk of the lead came from the Precambrian basement lying at a depth of about 2.5-3.0 km below the ore zone. (Isotopic data indicate that the lead in the North Amethyst vein system was derived in part from the volcanic rocks of the area; Foley & Ayuso 1994.) Fluid mixing was the dominant cause of ore precipitation, although fluid boiling probably played a subordinate role. The essence of this genetic model has subsequently been confirmed by speciation and reaction path calculations (Plumlee 1994), using the computer programs SOLVEQ and CHILLER (Reed 1982, Reed & Spycher 1985, Spycher & Reed 1989). These calculations show that the high-salinity brines were relatively acidic (pH near 5.5) and transported significant quantities of base metals (i.e., up to $10^{-2} m \Sigma Zn$) as chloride complexes, and that the strong zoning of the main-stage mineralization can be accounted for by variable boiling of the brines along the flow path, followed by lateral mixing of the brines with overlying, steam-heated ground waters (Fig. 4.40).

TABLE 4.6. Summary of salient data and interpretations pertaining to the Ag-Pb-Zn-Cu (-Au) epithermal vein deposits of the central and southern parts of Creede mining district, Colorado, USA

	Data	Interpretation
Geologic setting	Ores localized in a set of fractures defining a graben between two calderas.	Ground preparation for the epigenetic mineralization was controlled by tectonics. Pore-waters of the playa-lake sediments (the Creede Formation) were probably the main component of the ore-fluids.
Age of mineralization	Ore veins cut the Fisher Quartz Latite and Creede Formation (26.4 ± 0.6 Ma); mean K-Ar age of vein adularia and sericite = 24.6 ± 0.3 Ma.	Epigenetic mineralization, which post-dated the youngest volcanic event in the district by more than 1 m.y.
Ore-gangue mineralogy	Ag-Cu sulfides and sulfosalts, native silver, galena, sphalerite, pyrite, chalcopyrite, native gold, quartz, rhodochrosite, barite, fluorite, siderite, hematite, chlorite, K-feldspar (adularia), sericite, illite/smectite.	Ag-Pb-Zn-Cu (-Au) deposits of the "adularia-sericite type"; combined base metals - 5% , Ag:Au = 400. Low FeS content of sphalerite closely matches the value predicted from the aS_2 - aO_2 regime of the ore-forming system.
Ore textures	Crustification banding, growth zoning in sphalerite; no metamorphic or deformation textures.	Cavity-filling type mineralization in tension fractures; unmetamorphosed and undeformed.
Zoning	Strongly zoned from base metal-rich ores in the central part of the district (OH assemblage) to barite- and Ag-rich ores in the southern part of the district (Bulldog Mountain assemblage) with Ag mineralization toward the south, but the P and Amethyst vein systems contain both the assemblages.	The two assemblages represent different facies of one mineralization event, formed by the chemical evolution of the ore-forming fluids as they flowed up and to the south through the central and southern ore zones. Interpretation compatible with the fluid inclusion data.
Paragenesis	Five stages of mineralization, based on mineralogy and texture, correlatable between the two facies.	The different mineralized vein systems, representing parts of a single hydrothermal system, were filled during the same mineralization event.
Wallrock alteration	Argillic and phyllic alteration contemporaneous with mineralization; hydrothermal K-metasomatism earlier and unrelated to ore mineralization.	pH of the ore fluid was buffered by the reaction $3K\text{-feldspar} + 2H^+ = K\text{-mica} + 6\text{quartz} + 2K^+$; calculated pH = 5.4 (nearly neutral pH at 250°C).
Stability of ore-gangue assemblages	aS_2 - aO_2 and aO_2 -pH diagrams constructed for boundary conditions inferred as follows: $T = 250^\circ\text{C}$, $P = 50$ bars, $XS = 0.02$ molal, salinity = 1 molal with $Na^+:K^+ = 9$.	aS_2 buffered by the reaction 3 daphnite (Fe-chlorite) + 3 K-feldspar + $5S_2 = 5$ hematite + 5 pyrite + 3 K-mica + 9 quartz + 9 H_2O ; at 250°C, $\log aS_2 \approx 11.0$ and $\log aO_2 \approx 34.2$ as defined by Fe-chlorite + pyrite + hematite triple point (see Fig. 3.8; Fe-chlorite would preempt the field occupied by magnetite).

TABLE 4.6 (continued)

	Data	Interpretation
Fluid inclusions	<p>Primary inclusions in sphalerite, fluorite and quartz (earlier studies): $T_h = 190^\circ - 285^\circ\text{C}$; salinity = 5-13 wt% NaCl equivalent; Cl = 0.92-1.86 molal; $\Sigma S = 0.018-0.30$ molal; Na:K = 7.4-9.9; Na:K:Ca = 9:1:2. A trend from higher T_h in the north (OH vein) to lower T_h in south (A methyst vein). Evidence of boiling of the ore-fluid at the top of OH vein (40-50 bars pressure).</p> <p>Quartz (Foley et al. 1989): T_h and salinity data consistent with those stated above; pseudosecondary inclusions have similar T_h range but much lower salinity (0-1 wt% NaCl equivalent).</p>	<p>Mixing of at least two fluids of similar temperature but markedly different salinities — a saline brine carrying base metals probably as chloride complexes, and a dilute fluid. Ore-gangue deposition was caused by lateral fluid mixing and several stages of boiling, mainly the former. Sudden changes in the mixing ratio, presumably from changes in the plumbing, punctuated long periods of uniform conditions of fluid flow and slow rates of deposition. Interpretation compatible with stable isotope data.</p>
Light stable isotope ratios (δD from fluid inclusions and $\delta^{18}\text{O}$ calculated from mineral analyses)	<p>Bethke and Rye (1979): For fluid inclusion waters in sphalerite, $\delta D = -50$ to -81‰, $\delta^{18}\text{O} = -5.8$ to -4.5‰; in quartz, $\delta D = -86$ to -97‰, $\delta^{18}\text{O} = -5.9\text{‰}$.</p> <p>Foley et al. (1989): δD of water from primary inclusions in quartz = -69‰, but from pseudosecondary inclusions in quartz = -102‰.</p> <p>For fluid inclusion CO_2 in rhodochrosite and siderite, $\delta^{13}\text{C} = -2.7$ to -6.9‰.</p>	<p>The ore-fluids involved at least two components. The main component was a deep-circulating, saline fluid (probably originated as pore-waters in the Creede Formation); the other component was steam-heated ground water. One or more episodes of abrupt incursions of overlying groundwater may have resulted from either collapse of a transient vapor-dominated region of the ore zone, or catastrophic venting of the system through hydrothermal eruption(s). Periodic influx of C-bearing magmatic fluids is a possibility.</p>
Sulfur isotope ratios	<p>$\delta^{34}\text{S}$ (sphalerite, galena, pyrite) = $+1.7$ to -4.1‰; $\delta^{34}\text{S}$ (barite) = $+3$ to $+47\text{‰}$ (mostly between $+19.8$ and $+31.3\text{‰}$). Isotopic and chemical disequilibrium between oxidized and reduced sulfur species in solution.</p>	<p>Not fully understood. The reduced sulfur came with the brine from a deep-seated, igneous sulfide reservoir with $\delta^{34}\text{S} = 0\text{‰}$. The oxidized sulfur may have been carried also by the brine or derived from the moat sediment pore fluids, but the isotopically heavy sulfur originated ultimately from bacterial sulfate reduction in Creede caldera moat sediments.</p>
Lead isotope ratios	<p>Ore leads from veins are remarkably uniform in composition, but more radiogenic than any Mesozoic or Cenozoic rock from the Rocky Mountain region.</p>	<p>Bulk of the lead (and presumably other metals) was derived by leaching of the 1.4-1.7 b.y.-old Precambrian basement (suggesting circulation of fluids to a minimum depth of 2.5 - 3.0 km below the ore zone), and the lead was thoroughly mixed during transport of the mineralizing fluids.</p>

Sources of data: Barton et al. (1977), Bethke and Rye (1979), Hayba et al. (1985), Foley et al. (1989), Plumlee (1994), Foley and Ayuso (1994), Plumlee and Whitehouse-Veaux (1994).

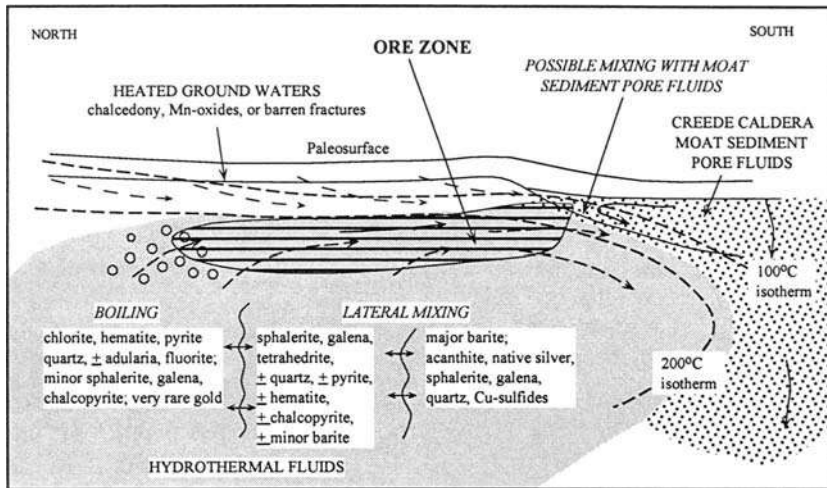


Figure 4.40 Schematic north-south cross section depicting a genetic model for the main-stage mineralization in the central (OH, P, central Amethyst, northern exposed Bulldog Mountain) and southern (southern Bulldog Mountain, southern Amethyst) vein systems of the Creede mining district, Colorado, USA. The model integrates results of reaction path modeling with observed field relations, mineral zoning patterns, and fluid inclusion and stable isotope data. The positions of the different mineralization facies shown in the diagram shifted considerably over time during mineralization because of changes in local hydrology. (After Plumlee 1994.)

Several aspects of the genesis of the Creede epithermal deposits, such as their relations to possible deeper mineralization and associated igneous heat sources, remain controversial. In 1991, as part of the US Continental Scientific Drilling Program, two vertical boreholes were drilled through the lacustrine sedimentary rocks (Creede Formation) filling the moat of the Creede caldera (Campbell 1993). It is anticipated that the data collected from these cored boreholes will provide answers to some of the unresolved questions.

4.11. Summary

The ultimate goal of a comprehensive study of any mineral deposit is to understand the genesis of the deposit so that the knowledge may be utilized in the exploration for similar deposits. Generally, the task involves three basic steps: (a) characterization of the deposit in terms of field relations, stratigraphy, tectonic setting, style of mineralization, mineralogy and textures, wallrock alteration, temperature and pressure of mineralization, fluid inclusion characteristics, radiogenic and stable isotopic systematics, age of mineralization, etc.; (b) distinguishing the features related to original mineralization from those superimposed by later tectonic activity,

hydrothermal alteration, and metamorphism, and (c) construction of a genetic model that is consistent with the characteristics of the deposit as well as with the physical and chemical principles that govern the derivation, transport, and deposition of ore constituents.

A generalized summary of various techniques commonly used for the collection and interpretation of data pertaining to mineral deposits is presented in Table 4.7. Specific questions to be answered would vary from one deposit to another in some respects, and so would the data collection. For example, for a strata-bound sulfide deposit hosted by a volcanic sequence and interpreted to be of orthomagmatic origin, the data should show that the distribution of mineralization as well as the composition and textures of the primary sulfides can be explained by the crystallization of a parental magma of appropriate composition derived from a reasonable source. On the other hand, for a strata-bound sulfide deposit hosted by a sedimentary sequence and interpreted to be epigenetic-hydrothermal in origin, the data should be consistent with a post-sedimentation mineralization event caused by hydrothermal fluids of appropriate geochemical characteristics. In reality, however, the genesis of most mineral deposits tends to be controversial, either because the available data are amenable to alternate interpretations, or because no single genetic model appears to accommodate all the

TABLE 4.7. Techniques commonly employed for data collection and interpretation of mineral deposits

Data to be collected	Techniques for data collection and interpretation
Tectonic setting	Mapping, regional synthesis
Field relations (stratigraphy, relationship to igneous bodies and structures, style of mineralization, relative ages of host rocks and mineralization)	Mapping on appropriate scales, stratigraphic correlation, structural analysis
Host rocks, alteration, ore-gangue mineralogy and textures, paragenesis, metamorphism	Petrography, major and trace element chemistry, phase equilibria analysis, radiogenic and stable isotope systematics
Temperature and pressure of mineralization	Oxygen and sulfur isotope ratios, fluid inclusion microthermometry, compositions of selected phases in equilibrium, phase equilibria analysis
Geochemistry of hydrothermal fluids	Fluid inclusion studies, alteration assemblages, phase equilibria analysis, stable isotope systematics
Absolute ages (host rocks, igneous intrusions, alteration, metamorphism, and mineralization)	Radiogenic isotope systematics, paleomagnetism, fission track dating
Parental magma	Petrography, phase equilibria analysis
Sources of ore constituents	Radiogenic isotope systematics, chemistry of suspected source rocks

available pieces of information. Nevertheless, the formulation of genetic models and the continual revision of such models as more data become available are essential for improving our understanding of mineral deposits.

4.12. Recommended Reading

Stable Isotopes: Ohmoto (1972, 1986), Ohmoto and Rye (1979), Taylor (1979), Sheppard (1986).

Radiogenic Isotopes: Doe and Stacey (1974), Doe and Zartman (1979), Norman and Landis (1983).

Geothermometry and Geobarometry: Bethke and Barton (1971), Elsdon (1975), Ohmoto and Rye (1979), Taylor (1979), Hutchinson and Scott (1980), Roedder (1984, p.221-289).

Metamorphism: Vokes (1969), Plimer (1987), Skinner and Johnson (1987), Gilligan and Marshall (1987).

Age of Mineralization: Naeser (1977), Dallmeyer (1979), Symons et al. (1997), Christensen et al. (1997).

Creede District: Hayba et al. (1985), Plumlee (1994).

CHAPTER 5

CHROMITE DEPOSITS

5.1. Introduction

Chromite deposits constitute the only primary source of chromium metal; in addition they record a remarkable phenomenon in the overall process of concentration by magmatic crystallization. Extensive literature exists on both aspects of chromite deposits. The readers are particularly referred to the review articles by Duke (1983) and Stowe (1994), and a book edited by Stowe (1987a).

Chromite is the only ore mineral of chromium, a metal in demand for its alloying and refractory properties. It is normally marketed, according to usage, under three categories (Stow 1987a): (a) metallurgical ore (commonly $\text{Cr}_2\text{O}_3 > 40\%$ and Cr:Fe ratio > 2.2), which is smelted to produce ferrochrome or ferro-silicochrome for addition to the furnace charge for the manufacture of special steels, including stainless steel (commonly containing 18% Cr, 8% Ni, and 74% Fe); (b) Chemical ore ($\text{Cr}_2\text{O}_3 > 42\%$), the raw material for the production of Cr-chemicals used in a variety of applications such as paints and electroplating; and (c) refractory ore ($\text{SiO}_2 < 10\%$, $\text{Al}_2\text{O}_3 > 20\%$, $\text{Cr}_2\text{O}_3 + \text{Al}_2\text{O}_3 > 60\%$), used for foundry molding sands and furnace-lining briquettes.

5.2. Types of Deposits

Almost all producing and potential chromite deposits occur as massive to heavily disseminated segregations in ultramafic igneous rocks of layered complexes and alpine-type complexes (see Table 2.2). Known resources of alluvial and eluvial placer deposits derived by erosion of such rocks are low in grade and of very minor importance. Extensive nickel-chromium laterites occur in Cuba and Papua New Guinea, but so far there has been no significant production from these deposits.

Following Thayer (1960), chromite deposits associated with ultramafic-mafic igneous rocks are commonly classified according to their forms and textures as: (a) *stratiform* deposits; and (b) *podiform* deposits. The two classes are also quite distinct in terms of geologic setting. The stratiform deposits occur as conformable layers, usually of great lateral extent, in Precambrian layered intrusions emplaced within continental crust and are characterized by cumulus textures. The podiform deposits comprise a more heterogeneous group. Typically, they occur as irregular (mostly lenticular),

concordant to discordant chromite-rich bodies in tectonically-emplaced alpine-type peridotite complexes (ophiolites) that formed originally in oceanic settings. Some podiform deposits show deformation as well as relict cumulus textures, suggesting that they may represent disrupted stratiform-type chromite layers (Thayer 1969, Jackson & Thayer 1972). Considering that the ophiolite-hosted podiform class of deposits also contain segregated layers of chromite within crustal cumulates, Stowe (1994) designated the stratiform and podiform types as *Bushveld-type* and *ophiolite-hosted*, respectively, but we retain here Thayer's terminology which is entrenched in the literature (e.g., Leblanc et al. 1980, Cassard et al. 1981, Lago et al., 1982, Duke 1983, Arai & Yurimoto 1994, Zhou et al., 1994).

5.3. Distribution

The distribution of important chromite deposits is shown in Figure 5.1. Layered intrusions occur sporadically in stable cratonic regions and only a few of them contain chromite deposits in production or of commercial potential (Table 5.1). The most important of these are the Bushveld Complex (South Africa), the Great Dyke (Zimbabwe), the Stillwater Complex (USA), the Kemi Complex (Finland), and the Campo Formoso district (Brazil). The alpine-type complexes are ubiquitous in Phanerozoic orogenic belts (although a few have also been reported from Proterozoic mobile belts) and practically every one of them contains some noteworthy podiform chromite deposits. The most important podiform deposits are located in the Urals (Perm and Kempirsai mining districts), Albania, Turkey, Philippines, New Caledonia, Cuba (Moa district) and India (Sukinda and Nausahi districts). About 45% of the current world chromite production comes from stratiform deposits, but they account for about 70% of the world's chromite reserves and 90% of the world's chromite resources. The layered complexes of South Africa and Zimbabwe account for the bulk of the reserves and resources (Table 5.1).

Two types of chromite deposits, both of relatively minor economic importance, occur in the early Archean (3700-3200 Ma) sequences. One type is hosted by layered gneissic and anorthositic complexes and resembles stratiform deposits in form and composition. Examples include those of Fiskenaesset and Akilia (western Greenland), the Limpopo gneissic belt (South Africa), and the Sitampundi anorthositic complex (India). The other type, such as the Bird River sill (Canada), is associated with sill-like ultramafic complexes in some greenstone belts. In terms of past production (some 12 million tonnes of ore mined since 1906), current production (0.2 million tonnes per year) and known reserves (approximately 3 million tonnes of ore), the most important deposits of this type are located in the early Archean (3340 ± 60 Ma) Shurugwi (Selukwe) greenstone belt, Zimbabwe (Prendergast 1984). More than 100 orebodies are known in the Selukwe Ultramafic Complex, ranging in thickness from 2 to 25 m and in length from 5 to 1,000 m. These deposits show characteristics of both stratiform and podiform deposits (Cotterill 1969, Stowe 1994). The morphology of the deposits

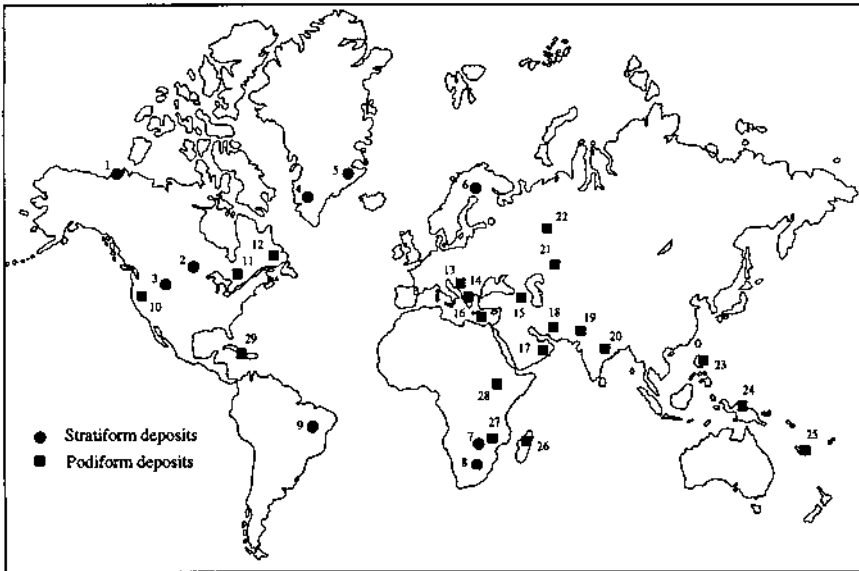


Figure 5.1. World map showing locations of important chromite deposits and ore-fields (including some subeconomic ones). Stratiform deposits: 1. Muskox Intrusion, Canada; 2. Bird River Sill, Canada; 3. Stillwater Complex, USA; 4. Fiskenaasset Complex, Greenland; 5. Skaergaard Intrusion, Greenland; 6. Kemi Complex, Finland; 7. Great Dyke, Zimbabwe; 8. Bushveld Complex, South Africa; 9. Campo Formoso, Brazil. Podiform deposits: 10. Oregon, USA; 11. Thetford Complex, Canada; 12. Bay of Island, Canada; 13. Albania; 14. Greece; 15. Pontids and Taurids Mountains, Turkey; 16. Troodos, Cyprus; 17. Semail, Oman; 18. Faryah, Iran; 19. Zhob Valley, Pakistan; 20. Sukinda and Nausahi, Orissa, India; 21. Kempirsai, former USSR; 22. Perm, former USSR; 23. Zambales, Philippines; 24. New Guinea; 25. New Caledonia; 26. Tsaratanana, Madagascar; 27. Selukwe (Shurugwi) Complex, Zimbabwe; 28. Ingessana Hills, Sudan; 29. Cuba.

and the chromite textures are similar to those of podiform deposits, but the host rocks, despite intense alteration to serpentinite and talc-chlorite-carbonate schist, show cumulate layering and geochemical trends suggestive of a layered complex. The ultramafic bodies that host the Inyala chromite deposit located in the Belingwe greenstone belt, Zimbabwe, have also been interpreted as fragments of a layered intrusion.

5.4. Stratiform Deposits

5.4.1. HOST ROCKS

Layered intrusions, the hosts of stratiform chromite deposits, are large, sill-like or funnel-shaped ultramafic-mafic complexes of bulk gabbroic composition that owe their layering to differentiation by fractional crystallization. The layers are composed of a framework of cumulus crystals (crystals which nucleate and grow in equilibrium with

TABLE 5.1. Layered ultramafic-mafic complexes with significant chromite

Layered complex	Surface area (km ²)	Age (Ma)	Reserves (Mt)	Estimated sub-economic resources (Mt)
Skaergaard, Greenland	104	52	--	Very thin layers
Muskox, Canada	350	1160	--	20
Bushveld, South Africa	67,340	2095 ± 24	431	3,910
Kemi, Finland	30 (?)	2200 - 2100	33	15
Great Dyke, Zimbabwe	3,265	2461 ± 16	64	353
Campo Formoso, Brazil	?	2000 (?)	4	16
Stillwater, USA	194	2700	--	4
Mashaba, Zimbabwe	?	2900	--	4
Bird River Sill, Canada	25	Archean	--	Negligible
Fiskanaeset, Greenland	3,000	Early Archean	--	38

Sources of data: Willems (1969), Stowe (1987a).

the main magma) with the interstices filled by postcumulus crystals (crystals which precipitate from intercumulus liquid during and/or after accumulation of cumulus crystals). Most earlier models on the origin of cumulate layers were based on the concept that the cumulus crystals nucleated in some part of the magma chamber and settled to the floor of the chamber under the influence of gravity. The current opinion appears to be in favor of *in situ* crystallization of cumulus crystals at the temporary floor and walls of the magma chamber (Jackson 1961, Campbell 1978, McBirney & Noyes 1979). In this case, fractional crystallization of the chamber magma would be possible only if the depleted melt was removed from contact with the growing cumulus crystals by a combination of diffusive and convective processes (Sparks et al. 1984).

As a generalization, layered intrusions may be viewed as consisting of two broad zones (Fig 5.2): a lower ultramafic zone of olivine ± clinopyroxene cumulates; and an upper mafic zone of plagioclase ± olivine ± pyroxene cumulates (Raedeke 1981). A special feature of many layered intrusions is the presence of *cyclic units* — repetition of specific sequences of cumulate layers — on a scale of meters to tens of meters. Each cyclic unit is believed to have recorded the influx of a new pulse of primitive magma into the magma chamber and its mixing with the more differentiated, residual chamber magma (Campbell 1977, Irvine 1980). The spatial variations in ultramafic to felsic rocks within individual cyclic units is attributed to the variable proportions in which the two magmas mixed. As will be discussed later, magma mixing is also regarded as a viable model for the origin of stratiform chromite deposits.

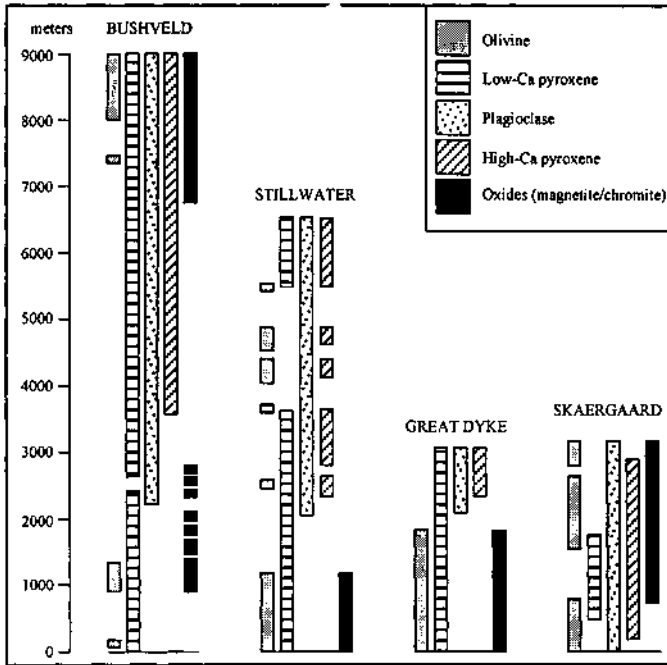


Figure 5.2. Simplified representation of the distribution of cumulus minerals with stratigraphic height in selected layered intrusions (after Raedeke 1981).

5.4.2. CHROMITE MINERALIZATION

Stratiform chromite deposits typically consist of thin but laterally continuous, generally conformable layers of *chromitite*, a term used for massive chromite containing 50% to more than 95% cumulus chromite. The chromitite layers are invariably located in the lower ultramafic zone, often in association with cyclic units, and are an integral part of igneous layering, but the crystallization sequence varies from one layered intrusion to another and even for different chromitite layers in the same intrusion. For example, of the 14 cyclic units recognized in the Great Dyke, 11 contain a chromitite layer at the base. The ideal sequence within each cyclic unit is, from the base upward, chromitite, dunite, harzburgite, olivine bronzitite, and bronzitite, but chromitite and dunite are missing from some of the upper units (Wilson 1982). The Peridotite Member of the Ultramafic Zone in the Stillwater Complex is composed of 15 cyclic units characterized by the following upward sequence: poikilitic harzburgite (olivine cumulate), granular harzburgite (olivine-bronzite cumulate), and bronzitite (bronzite cumulate); 13 of these units contain chromitite zones in the poikilitic harzburgite members (Jackson 1968). Chromitite layers in the Bushveld Complex are

principally associated with orthopyroxenite and anorthosite in sections with more complicated stratigraphy (see Fig. 5.5).

The characteristics of chromitites in major stratiform deposits are summarized in Table 5.2. The thickness of chromitite layers ranges from less than 2 cm to more than 1 m, but the lateral extent may be traced or correlated over distances measured in kilometers or even tens of kilometers. Individual chromitite layers have been traced for almost 20 km in the Stillwater Complex (Jackson 1968), for more than 30 km in the Bushveld Complex (Cameron and Desborough 1969), and for at least 185 km in the Great Dyke (Stowe 1987a).

TABLE 5.2. Characteristics of chromitite layers in the major stratiform chromite deposits

Layered complex	Stratigraphic position	Lithologic association*	Number of layers	Thickness of layers	Grade
Bushveld (South Africa)	Critical Zone	Fluctuating rhythmic layers, mainly of H-P-A	15	15 cm - 2.3 m	Cr ₂ O ₃ = 43-48 % Cr:Fe = 1.1-2.5
Great Dyke (Zimbabwe)	Ultramafic Sequence (lower part)	Cyclic units of D-H-OB-B	11	5 cm - 1 m	Cr ₂ O ₃ = 36-54 % Cr:Fe = 2.0-3.9
Stillwater (USA)	Ultramafic Zone (lower part)	Cyclic units of H-OB-B	13	< 2 cm - 4 m	Cr ₂ O ₃ = 20-23 % Cr:Fe = 0.9-2.3
Kemi (Finland)	Ultramafic Zone (lower part)	D-P-Pe	2	Commonly 3 cm - 4.5 m; 30 - 90 cm over a strike length of 4.5 km	Cr ₂ O ₃ = 26 % Cr:Fe = 1.6
Campo Formoso (Brazil)	Lower part of the ultramafic sequence	SD	5 (?)	10 cm - 6 m	Cr ₂ O ₃ = 38-46 % Cr:Fe = 1.5-2.2

* Rock types: anorthosite (A), bronzitite (B), dunite (D), harzburgite (H), olivine bronzitite (OB), peridotite (Pe), pyroxenite (P), serpentinized dunite (SD).

Sources of data: Duke (1983), Stowe (1987a), Hatton & Von Gruenewaldt (1987), Prendergast (1987).

The chromite of stratiform deposits is a cumulus phase and is typically euhedral to subhedral. Smooth faces and sharp edges of the chromite crystals indicate equilibrium with the magmatic liquid during crystal growth, although evidence of minor postcumulus dissolution is sometimes present. In single-phase chromite aggregates, the texture is polygonal (foam texture), but in polyphase aggregates the texture depends on the relative proportion of chromite (Jackson 1969). With increasing proportion of

silicates, the texture grades from *occluded silicate texture*, characterized by silicate minerals isolated (occluded) in chromite, to *net texture* comprised of a network of fine chromite grains in the intergranular spaces between large silicate crystals. The occluded silicates often consist of clear cores and selvages with poikilitically included fine-grained chromite of likely postcumulus origin.

5.5. Podiform Deposits

5.5.1. HOST ROCKS

Except for minor occurrences in Archean greenstone belts, podiform chromite deposits are associated with alpine-type ultramafic-mafic complexes. Compared with layered complexes, alpine-type complexes are relatively small in size, are highly serpentinized, occur in orogenic belts, often show evidence of tectonic emplacement, and overwhelmingly are Phanerozoic in age. Alpine-type complexes may be subdivided into two classes (see Table 2.2): (a) ophiolites; and (b) mantle diapirs. By analogy with modern oceanic lithosphere at mid-oceanic ridges, ophiolites are believed to have been generated initially at spreading centers and subsequently obducted onto continental margins during plate convergence (Coleman 1977, Moores 1982). The allochthonous nature of the ophiolites is evidenced by their basal tectonic contact, but the mechanism of emplacement is quite controversial (Dewey 1976). Mantle diapirs occur as small and lenticular isolated bodies of ultramafic (peridotitic) composition, and are believed to represent diapiric emplacement of mantle material in a solid state. Chromite concentrations in these bodies are limited to a few small pods and lenses of little economic potential.

Ophiolite refers to a distinctive assemblage of mainly ultramafic to mafic rocks with an ideal succession as shown in Figure 5.3. The essential components of this succession, in descending order, are: (a) a thin layer (a few centimeters to a few meters thick) of marine sediments, usually Fe-Mn rich and cherty; (b) basaltic pillow lavas (up to about 2 km thick); (c) a zone (1-5 km thick) dominated by nearly vertical sheets of diabase, believed to be feeder dikes for the overlying pillow lavas; (d) gabbroic rocks (2-3 km thick), commonly with recognizable cumulate layering; (e) ultramafic cumulates (generally <500 m thick), mainly of olivine \pm pyroxene; and (f) ultramafic tectonite (the residual mantle), composed mainly of tectonized harzburgite or lherzolite, but usually with lenses of serpentinized dunite in the intensely deformed upper parts. The boundary between the ultramafic cumulates and the ultramafic tectonite is the *petrologic Moho*. This boundary is usually marked by a zone of "transitional dunite", which is interpreted by most workers as the topmost part of the mantle tectonite. Most ophiolites, however, lack the ideal succession described above, presumably because of dismemberment during or after emplacement (Misra & Keller 1978).

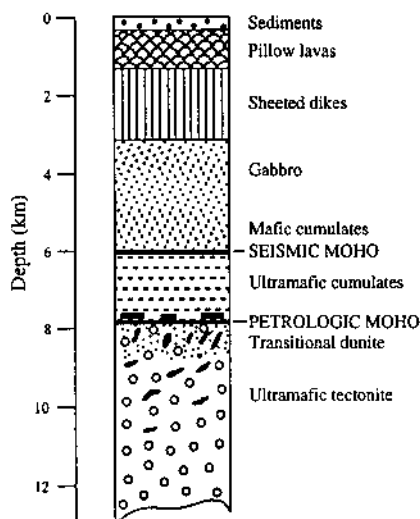


Figure 5.3. Ideal ophiolite succession with likely locations of sulfide and chromite deposits. Podiform chromite bodies (solid black blobs and rectangles) tend to be most abundant in the uppermost part of the tectonite unit but also occur in deeper parts and in the ultramafic cumulate unit. Volcanogenic massive sulfide (VMS) mineralization of the Cu-pyrite type may be present in the pillow lava unit.

5.5.2. CHROMITE MINERALIZATION

Jackson and Thayer (1972) divided alpine peridotite complexes into harzburgite and lherzolite subtypes depending on whether the residual mantle is composed predominantly of harzburgite or lherzolite. Podiform chromite deposits, with a few exceptions, occur only in the harzburgite subtype, in which clinopyroxene is at best a minor constituent. In peridotites of the lherzolite subtype, the chromium and aluminum are generally combined in chrome-diopside or chrome-garnet. The preferential association of podiform chromite deposits with the harzburgite subtype is probably related to higher degrees of partial melting in this system compared with the lherzolite subtype.

Chromite deposits are restricted to ultramafic rocks of the ophiolite succession and concentrated predominantly in the transition zone between the lower crustal ultramafic cumulates and the residual mantle peridotite. The chromite bodies commonly occur as (Stowe 1987a): (a) small pods, lenses and pipes, invariably with a thin envelope of dunite depleted in incompatible elements, within the upper section of the tectonite; (b) isolated pods within the serpentinized tectonite zone; (c) bands and layers near the base of the transitional dunite; and (d) bands, layers, and lenses within the lowermost dunitic cumulates. Important chromite deposits may occur in any or all of the above settings

(Turkey), in the cumulates (Pakistan), in the transition zone (Cyprus, Northern Appalachians), or in the residual mantle (New Caledonia, Cyprus).

A characteristic feature of podiform deposits, in addition to irregular and varied form reflecting the unstable tectonic setting, is their small size. Most are only a few meters thick and a few meters to a few hundred meters in lateral extent; individual pods containing more than 1 million tonnes of ore are rare. Probably the largest podiform deposit, 1500 m x 200-300 m x 145 m (thickness), occurs in the Melodezhnoe Mine, southern Urals (Smirnov 1977). The economic viability of most podiform chromite mines depends on access to a number of ore-grade pods in a limited area. The chromite pods in a given district often show wide variations in composition, suggesting that they probably are not disrupted blocks of a single continuous body (Thayer 1969).

The chromite bodies in the crustal cumulate sequence display vestiges of cumulate textures and tend to be banded and tabular, similar to stratiform chromite except for continuity; they are often folded with an axial-planar flow fabric and are elongated parallel to the lineations. The tectonite-hosted deposits show a wide variety of orientations relative to the host rocks, perhaps reflecting varying degrees of plastic deformation due to mantle flow. Based on the relationship between the attitude of the chromite body and structures (foliations, lineations, and banding) in the host tectonite peridotites, Cassard et al. (1981) divided the podiform chromite bodies of New Caledonia into discordant, subconcordant, and concordant types and correlated them with the degree of deformation as evidenced by the chromite textures. Where less intensely deformed, both chromite bodies, presumably filling magma conduits within the upper mantle (Lago et al. 1982, Leblanc & Ceulener 1992), and their dunite selvages are discordant to the flow fabric in the mantle tectonite, but with increasing deformation they become sheared into varying degrees of concordance. Similar is the case with most other podiform deposits (Nicolas 1989): discordant chromite pods are relatively "primary" in terms of deformation than the more deformed concordant ones. This hypothesis is consistent with a lack of discernible geochemical differences between the concordant and discordant chromite pods in New Caledonia and elsewhere.

Disseminated chromite in the ultramafic cumulates is very similar in grain size and shape to that observed in layered intrusions. In the tectonite peridotite, the accessory chromite occurs as large, elongate anhedral grains defining a weak lineation in the plane of the tectonite foliation. Chromite with a "prophyroclastic" texture, considered to be residual in origin, probably formed as a result of incongruent melting of chromian diopside during partial melting of a spinel lherzolite mantle source, whereas other chromites were exsolved from orthopyroxenes. In both cases, the chromite is believed to have formed by *in situ* crystallization under directive stress (Malpas & Robinson 1987). Heavily disseminated chromite in both ultramafic cumulates and tectonites often displays typical cumulate textures, rhythmic layering, and graded layers (Duke 1983). Cumulate textures, such as occluded silicate texture and net texture, are common in massive chromites, but compared with stratiform deposits the chromite grains tend to be anhedral and coarser grained; granular aggregates with 1-10 mm grains are typical of larger podiform orebodies and probably resulted from recrystallization.

Two characteristic, perhaps exclusive, features of podiform deposits are the nodular and orbicular textures of chromite (Thayer 1969). Most nodules, set in an olivine (serpentinized) \pm plagioclase matrix, are rounded to flattened ellipsoids 5-25 mm in longest dimension and composed of granular aggregates of interlocking chromite anhedral 1-3 mm in diameter. Some nodules in the Troodos Ophiolite Complex (Cyprus) consist of a core of chromite dendrites intergrown with secondary silicate minerals (Greenbaum 1977, Malpas & Robinson 1987). The interstices between the dendrites are filled with serpentinized olivine, subordinate clinopyroxene, and minor saussuritized plagioclase. Closely associated with these "cored" nodules are large, isolated dendrites and skeletal crystals of chromite within the dunitic matrix between the nodules. There is no systematic compositional difference between coexisting nodules and skeletal chromite crystals, or between cored and solid nodules, suggesting a common origin. Whether zoned or unzoned, elliptical or round, chromite nodules show little evidence of compaction or deformation, and are believed to be largely a magmatic feature, although the actual mechanism is not understood. Proposed mechanisms for the formation of chromite nodules include the aggregation of free-formed chromite grains prior to settling (Thayer 1969), "snowballing" within a turbulent zone of magma segregation (Dickey 1975), and crystallization of a magma that was significantly undercooled and/or supersaturated with respect to chromium (Greenbaum 1977).

Orbicular textures are much less common. Thayer (1969) described the orbicules as zoned ellipsoidal masses (nodules) consisting of chromite cores and rims of either olivine set in a matrix of chromite or of several alternating thin shells of chromite and olivine, and ascribed them to alternate crystallization of chromite and olivine. He considered the orbicular texture to be related to the nodular texture, but reflecting a different crystallization sequence. In the Troodos Complex, the sporadic orbicules consist of an ellipsoidal nucleus of serpentinized dunite enclosed by one or more shells of chromite alternating with olivine. According to Greenbaum (1977), these orbicules were probably produced by "accretion of previously settled chromite and olivine around a nucleus of dunite as a result of their being rolled, either under gravity down slumps in the crystal mush or by oscillatory bottom currents in the magma."

Plastic deformation textures (e.g., foliation and lineation) are common in ophiolites, but the chromite appears to have yielded mostly by granulation rather than by plastic flow, with little apparent recrystallization. It appears that the stresses were mostly absorbed by the weaker olivine, shielding the chromite from intense deformation (Thayer 1964). A common deformation texture in coarse-grained chromites is the pull-apart texture that consists of tensional cracks normal to the direction of maximum stretching. These cracks are commonly filled with serpentine. Other deformation textures include elongation of nodules and occluded silicates by moderate to strong deformation and gneissic structures by extreme flowage. The schlieren structures (laterally discontinuous planar and linear structures) that characterize many podiform deposits appear to have formed in two ways: by shearing of low-grade net-textured olivine chromitite, and by admixture of olivine and chromite during granulation of massive chromitite (Thayer 1964).

5.6. Examples

5.6.1. BUSHVELD COMPLEX, SOUTH AFRICA

The Bushveld Complex (Fig. 5.4) is not only the largest and most extensively studied of the known layered intrusions, it is also the richest in terms of mineral deposits. In addition to deposits of chromite, platinum-group minerals, Ni-Cu sulfide, and titaniferous and vanadiferous magnetite associated with the mafic and ultramafic layered rocks, the granitic rocks of the complex are associated with endogenetic and exogenetic deposits of tin and fluorite. Asbestos is mined from serpentinized parts of ultramafic layers in the Complex and exploitation of andalusite in hornfels adjacent to the complex accounts for nearly one-half of the global production of aluminosilicates. The emplacement of the complex may also be responsible for the sparse lead-zinc-fluorite and gold mineralization in the surrounding rocks of the Transvaal Supergroup. The vast amount of published literature on Bushveld includes several review articles (e.g., Willemse 1969a, von Gruenewaldt 1979, von Gruenewaldt et al. 1985, Hatton & von Gruenewaldt 1987, Cawthorn & Lee 1998), which discuss the complexity of its geology and the diversity of ideas regarding its evolution.

The Bushveld Complex, with an exposed area of 65,000 km² in the Kaapvaal craton of southern Africa (see Fig. 2.10), was emplaced about 2100 m.y. ago (Hamilton 1977). The country rocks belong to the early Proterozoic Transvaal Supergroup, an 11 km-thick succession of sediments with four intercalated volcanic horizons. Ages of the Transvaal Supergroup rocks are uncertain, but the basal rocks may be as old as 2.5 Ga (Walraven et al. 1990). The Complex includes three major rock groups: the andesitic to rhyolitic Rooiberg Felsite and Dullstroom Volcanics; the ultramafic to mafic Rustenburg Layered Suite; and the Bushveld Granites. The most precise and reliable ages on these rock suites cluster round 2.06 Ga (Walraven et al. 1990). It has been suggested (e.g., Hamilton 1970, Rhodes 1975) that the emplacement of the Complex was the result of a major meteorite impact, which also gave rise to the Vredefort Dome to the south of the Complex, but shock metamorphic features, such as shatter cones, present around the Vredefort Dome have not been found in the rocks associated with the Bushveld Complex. The Complex is located at the intersection of several structural trends, suggesting that its emplacement was largely controlled by the structural framework of the Kaapvaal craton.

The mafic-ultramafic rocks of the Complex, the Rustenburg Layered Suite, occur in three major compartments (Fig. 5.4): (a) the western Bushveld, including the Nietverdiend area in the far west; (b) the eastern Bushveld, which contains the best exposure of the Layered Suite; and (c) the Potgietersrus lobe or northern Bushveld. The succession of rock types within the three compartments is broadly similar, indicating that the bulk composition of magmas and the conditions of fractional crystallization were comparable. It appears that the magmas for the three compartments were derived from a centrally located master magma chamber and emplaced simultaneously through a system of feeders (von Gruenewaldt et al. 1985).

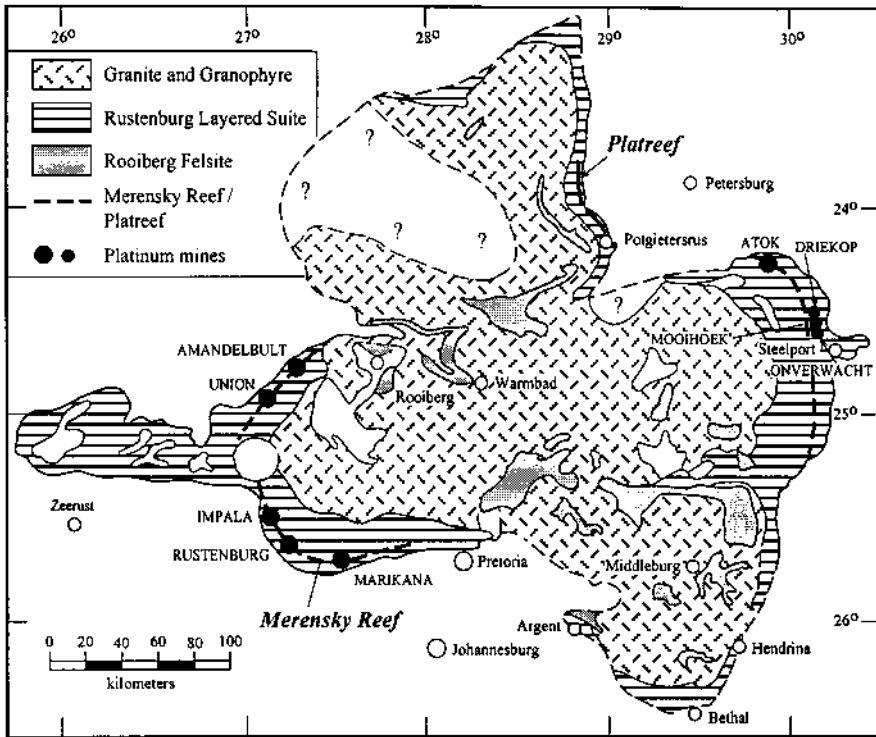


Figure 5.4. Simplified geologic map of the Bushveld Complex, South Africa, showing the Merensky Reef, the Platreef, and the location of important platinum mines hosted by the Merensky Reef (larger solid circles) and dunite pipes (smaller solid circles). (After von Gruenewaldt 1977, McLaren & De Villiers 1982.)

The Rustenburg Layered Suite, which ranges in thickness from about 7.5 km in the western compartment to about 9 km in the eastern compartment, has been subdivided into five informal zones (Fig. 5.5): Marginal (Basal) Zone, Lower Zone, Critical Zone, Main Zone, and Upper Zone. The Lower Zone is composed of alternating layers of bronzitite and harzburgite, with a few layers of dunite. The Critical Zone consists of two subzones: a lower pyroxenitic subzone, composed essentially of pyroxenites; and an upper anorthositic subzone dominated by norites and anorthosites, marking the incoming of cumulus plagioclase. Norites, anorthosites, and gabbronorites constitute the main rock types of the Main Zone. The Upper Zone is distinctly Fe-rich and contains at least 30 vanadiferous magnetite seams interlayered with ferrogabbros and ferrodiorites. Variation in the Mg-number [$Mg/(Mg + Fe)$ atomic ratio] of bronzite and olivine indicates an overall upward Fe-enrichment in the Complex, consistent with fractional crystallization, although in detail there are numerous reversals and large

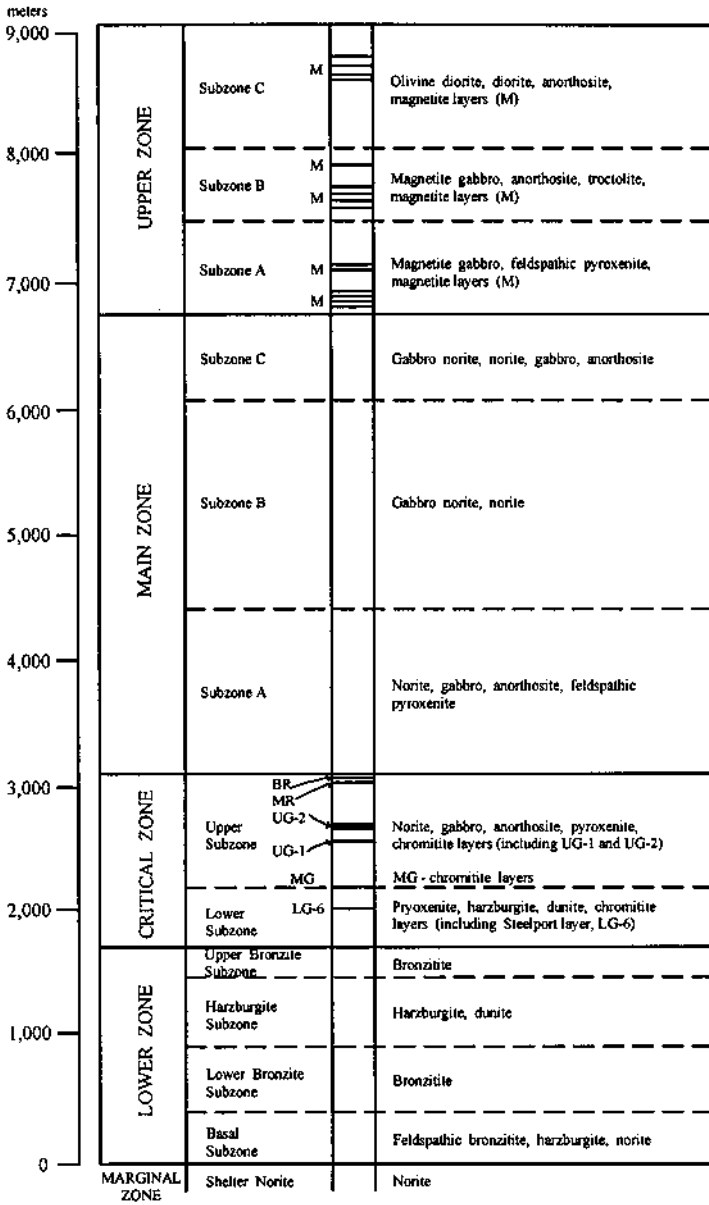


Figure 5.5. Simplified lithostratigraphic column of the Rustenburg Layered Suite, eastern Bushveld Complex, showing the locations of important chromitite and magnetite layers. Note that the chromitite layers are restricted to the Critical Zone and the magnetite layers to the Upper Zone. Chromitite layers: LG-6 (the Steelport Seam) of the Lower Group, MG (Middle Group), and UG-1 and UG-2 of the Upper Group. BR = Bastard Reef, MR = Merensky Reef. (Source of data: von Gruenewaldt et al. 1985.)

intervals over which no systematic compositional variation can be discerned (Naldrett et al. 1987). The different zones and subzones vary greatly in thickness throughout the Complex, and are absent in some areas. The Marginal Zone marks the contact between the cumulate sequence of the Complex (the four zones mentioned above) and the floor rocks (Transvaal Supergroup). In eastern Bushveld, the Marginal Zone rocks show a broad correspondence with the overlying cumulate rocks: a predominantly pyroxenitic group borders the Lower Zone and the lower part of the Critical Zone; a predominantly gabbroic group borders the feldspathic upper portion of the Complex. Many samples of marginal rocks represent quenched liquid compositions and such liquids may have been parental to certain parts of the layered cumulate pile (Harmer & Sharpe 1985). The recent field excursion guidebook compiled by Cawthorn and Lee (1998) includes an excellent summary of the petrologic and isotopic characteristics of the Layered Suite.

The Critical Zone is by far the most important interval for chromite, sulfide, and platinum-group-element (PGE) concentrations in the Complex. Except in the Potgietersrus area (northern Bushveld), the chromitite layers are restricted to the Critical Zone. Correlation between the western and eastern Bushveld has established the presence of three groups of chromitite layers of varying thickness and composition (Table 5.3): the Lower Group (LG), the Middle Group (MG), and the Upper Group (UG). The Lower Group comprises a maximum of seven chromitite layers (LG-1 to LG-7) that occur essentially within the lower pyroxenite subzone of the Critical Zone. The Middle Group chromitite layers (MG-1 to MG-4) straddle the boundary between the lower pyroxenite and the upper norite-anorthosite subzones of the Critical Zone. The Upper Group chromitite layers (UG-1 to UG-3) occur near the top part of the Critical Zone. The Merensky Reef could be denoted UG-4 as its sulfides typically accompany two very thin (1-5 cm) chromite-rich layers, which bound a roughly 1-m-thick pegmatitic feldspathic pyroxenite and/or harzburgite unit (see Fig. 7.2). The most important chromitite layer for the purpose of mining is the LG-6 layer of the Lower Group. It has a strike length of about 70 km in the western Bushveld (where it is also called the Main Seam) and about 90 km in the eastern Bushveld (where it is often referred to as the Steelpoort Seam), a thickness of 3 cm to 2.5 m, and an estimated reserve of 752 million tonnes to a depth of 300 m (Buchanan 1979). The other chromitite layers are commonly 5-30 cm thick, and LG-1, 2, 3, 4 and MG-1 have been mined locally. All the chromitite layers have anomalous PGE values and UG-2 contains sulfides and ore-grade concentrations of PGE (Lee & Tredoux 1986). The Critical Zone hosts the PGE-bearing Merensky Reef, which also contains significant Cu-Ni sulfides, and platinumiferous pipelike bodies of dunite (see Ch. 7).

The Lower Zone in eastern and western Bushveld is characterized by the absence of chromitite layers and low chromium content of the rocks. In contrast, the Lower Zone in the Potgietersrus area contains several well-developed chromitite layers associated with very magnesian (olivine-rich) rocks. Two of these layers, locally known as the lower and upper layers, are being mined at the Grasvalley Chrome Mine. The thickness of the layers is less than 50 cm, but the Cr_2O_3 contents (54-55%) and Cr:Fe ratios (2.5-3) are much higher than any of the chromitite layers in western or eastern Bushveld and

TABLE 5.3. Thickness (in meters) and composition (in wt %) of chromitite layers in the Critical Zone of eastern and western Bushveld Complex

Chromitic interval	Upper Group	Middle Group	Lower Group
Number of layers	4 (UG-1 to 3a)	4 (MG-1 to 4)	7 (LG-1 to 7)
Thickness	0.50 - 1.62	0.35 - 2.23	0.15 - 2.25
FeO	27 - 35	26 - 33	19 - 28
MgO	0 - 10	6 - 11	8 - 14
Al ₂ O ₃	0 - 18	14 - 20	11 - 17
Cr ₂ O ₃	38 - 46	42 - 49	45 - 53
Cr:Fe ratio	1.1 - 1.4	1.2 - 1.6	1.4 - 2.5

Source of data: compilation by Hatton & Von Gruenewaldt (1987).

resemble more closely the Great Dyke chromitite (Hatton & von Gruenewaldt 1987).

It has been argued that the evolution of the Layered Suite, including the generation of cyclic units, involved the mixing of derivatives of two parental magma types in varying proportions at different levels (Cawthorn et al. 1981, Irvine & Sharpe 1982, 1986, Todd et al. 1982, Irvine et al. 1983, Harmer & Sharpe 1985, Cawthorn & McCarthy 1985, von Gruenewaldt et al. 1985). The two-magma concept is dictated by the observation that the Layered Suite contains substantial units of both ultramafic and anorthositic one-mineral cumulates. There is simply no straightforward way by fractional crystallization alone that a single magma crystallizing mafic minerals can switch to crystallizing only plagioclase. Moreover, Sharpe (1981) has distinguished two suites of syn-Bushveld sills that appear to have formed from different magmas: an earlier suite of orthopyroxene-rich sills, representing offshoots of magma that was introduced during the formation of bronzite-rich cumulates; and a later suite of gabbroic sills (with practically no orthopyroxene) associated with the formation of anorthositic and gabbroic cumulates in the Layered Suite. The two-magma concept has also been applied to the Stillwater Complex, although based on a different line of argument (Todd et al. 1982, Irvine et al. 1983). These two types of magmas have been termed 'U' (Ultramafic) and 'A' (Anorthositic) by Todd et al. (1982) to emphasize their olivine \pm pyroxene-rich and plagioclase-rich early differentiates, respectively. The magma mixing hypothesis is consistent with variations of $^{87}\text{Sr}/^{86}\text{Sr}$ ratio in the Bushveld Complex cumulate zones, but there is some controversy as to whether the 'A' magma was a distinct magma (e.g., Sharpe 1985) or a residual magma that evolved in the magma chamber (e.g., Eales et al., 1990).

Primitive compositions of these magmas, designated as U_0 and A_0 , are not known precisely, but have been estimated from the syn-Bushveld sills representing variously

fractionated derivatives (designated as U_1 , U_2 , ... and A_1 , A_2 , ...). The estimated Bushveld A_0 melt is a silica-undersaturated, high-alumina basalt, not unlike common mid-oceanic ridge tholeiites but somewhat richer in normative plagioclase; the estimated U_0 parent has no volcanic equivalent, but the chilled U_1 derivatives are compositionally similar to olivine boninites (Irvine & Sharpe 1982, Irvine et al. 1983, Sharpe & Hulbert 1985). Judged from the products, the U liquids were rich in SiO_2 (52-56%), MgO (12-16%), compatible elements (e.g., Cr 800-2,000 ppm), and incompatible elements (e.g., Rb 20-50 ppm, Zr 150-400 ppm), and had an initial $^{87}\text{Sr}/^{86}\text{Sr}$ ratio of 0.703-0.705. In contrast, the A liquids had lower concentrations of SiO_2 (48-50%) and MgO (8-10%), lower concentrations of compatible and incompatible elements, and a higher initial $^{87}\text{Sr}/^{86}\text{Sr}$ ratio of 0.707-0.708 (von Gruenewald et al. 1985). As will be discussed later, the mixing of U and A magmas, as they underwent crystallization differentiation, is the most widely accepted explanation for the origin of chromitite layers in layered intrusions.

Melting experiments (Sharpe & Irvine 1983) on Bushveld chilled margin compositions (U_1 and A_1) have shown that under conditions of fractional crystallization, the crystallization order for the U_1 melt (olivine + minor chromite \Rightarrow orthopyroxene \Rightarrow plagioclase) is appropriate to yield dunitic, harzburgitic, and noritic cumulates of the Bushveld Lower and Critical zones and that for the A_1 melt (plagioclase + chromite \Rightarrow olivine \Rightarrow Ca-rich pyroxene \Rightarrow Ca-poor pyroxene) should produce cumulate units of anorthosite, troctolite, olivine gabbro, and two-pyroxene gabbro, of which the first and the last are well represented in the upper (anorthositic) subzone of the Critical Zone and in the Main Zone. It follows that anorthosite layers in the Layered Suite record major influxes of A magma and chromitite layers, if they are formed by the mixing of A and U magmas, should be associated with anorthosites. This happens to be the case generally in the Bushveld Complex.

The chronology of magma addition during the evolution of the Layered Suite is yet to be worked out. In general terms, the Lower Zone rocks containing abundant ultramafic cumulate layers appear to have crystallized from melts in which the U component was dominant. The upward increase in the abundance of plagioclase, in the initial $^{87}\text{Sr}/^{86}\text{Sr}$ ratio, and in the thickness of chromitite layers indicate an increasing influx of A liquids during the lower part of the Critical Zone. Crystallization of the Upper Critical Zone was marked by frequent reversals of mineral compositions and initial $^{87}\text{Sr}/^{86}\text{Sr}$ ratio, representing multiple inputs of A magmas. The marked increase in the initial $^{87}\text{Sr}/^{86}\text{Sr}$ ratio at the Merensky Reef level at the top of the Critical Zone (as well as the Cu-Ni and PGE mineralization associated with the Merensky Reef) is believed to be related to a major influx of A liquids (Kruger & Marsh 1985). The Main Zone and Upper Zone crystallization was dominantly from A liquids, and at least the uppermost 500 m of the Layered Suite has trace element geochemistry consistent with its derivation from a single homogeneous magma (Cawthorn & McCarthy 1985). The final major A magma input probably occurred at the level of the "pyroxenite marker" of the Main Zone (Cawthorn et al. 1981, von Gruenewaldt et al. 1985, Kruger 1994).

5.6.2. TROODOS MASSIF, CYPRUS

The ophiolite complex in the island of Cyprus, known as the Troodos Massif, lies in the Tethyan ophiolite zone. It is one of the least deformed and most extensively studied ophiolites. The complex has an annular outcrop pattern, with the basal part exposed at the central region (Fig. 5.6). The pattern indicates an overall domal structure, which is believed to be the result of late Tertiary differential uplift and subsequent erosion (Gass 1980). The complex has an aggregate thickness of about 6-7 km consisting of a typical ophiolite sequence (Fig. 5.7) that includes both mantle tectonite (harzburgite) and crustal layered cumulates, separated by a transitional dunite zone. The lower part of the sequence comprises two crosscutting plutonic suites, which are believed to have been derived from different magma sources. The older suite, which includes tectonized harzburgite and dunite with chromite, probably formed as a large solid-state mantle diapir; the younger suite is less deformed, consists of ultramafic and mafic rocks, and displays cumulate layering. Based on the age of the overlying sediments and sparse K-Ar dates, the age of the Troodos ophiolite is considered to be Upper Cretaceous (pre-Maestrichtian, most likely Campanian) (Malpas & Robinson 1987).

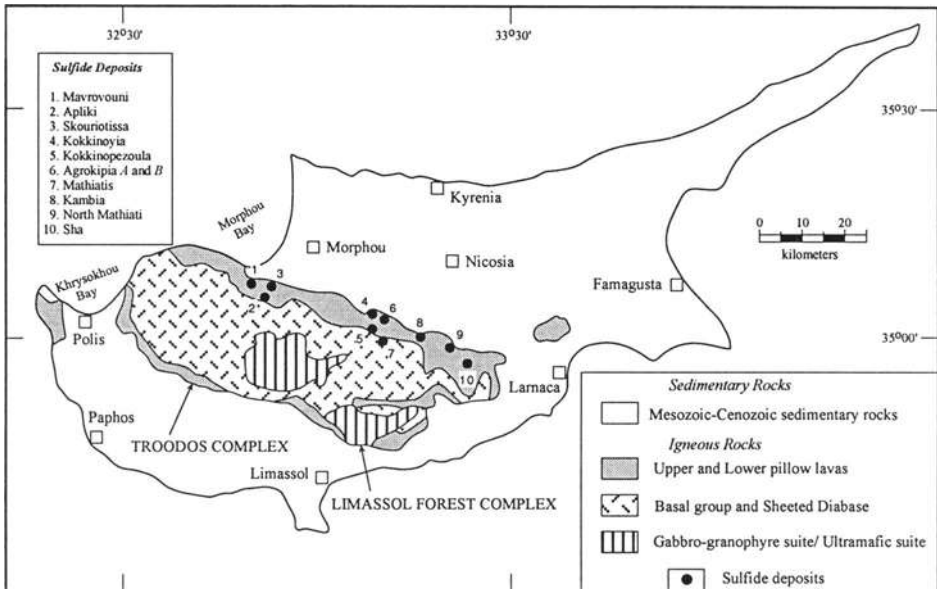


Figure 5.6. Generalized geologic map of the Troodos ophiolite complex and the Limassol Forest ophiolite complex, Cyprus. Chromite deposits occur in the metamorphic peridotite (mantle tectonite) and in the cumulate ultramafic rocks (dunite) close to the contact with metamorphic peridotite. Also shown are some of the massive sulfide (pyrite-chalcopyrite) deposits hosted by the pillow lavas of the Troodos complex. (Sources of data: Constantinou & Govett 1973, Constantinou 1980, Malpas & Robinson 1987.)

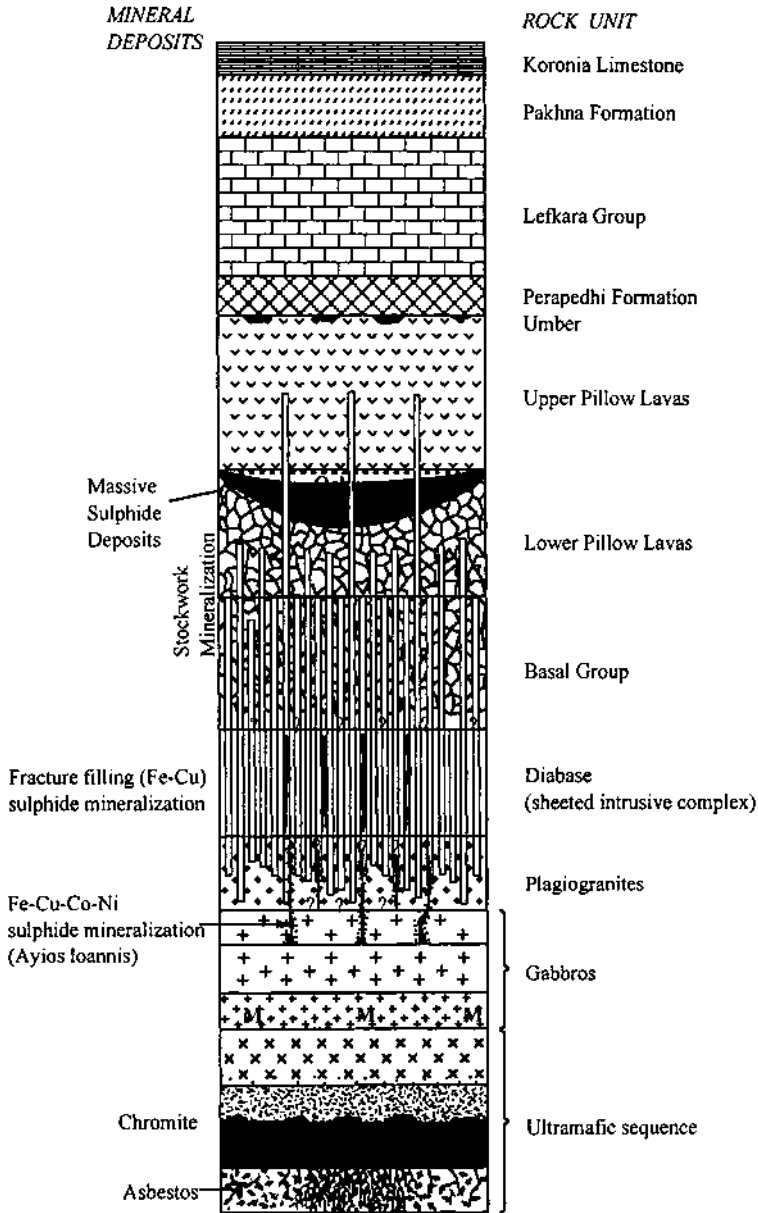


Figure 5.7. Composite vertical section of the Troodos ophiolite complex, Cyprus, showing generalized distribution of various types of mineral deposits associated with the complex (after Constantinou 1980).

The tectonic environment of the Troodos ophiolite has been discussed extensively in the literature. The sheeted dike complex strongly suggests a spreading center and for a long time a mid-ocean ridge setting was the generally accepted model (Coleman 1977). Such a setting, however, cannot be reconciled with the fact that the Troodos ophiolite contains two distinct magma suites: an early, relatively high-TiO₂ basaltic suite encompassing the upper gabbros, the sheeted dike complex, and the andesitic to rhyodacitic lower pillow lavas (LPL); and a late, low-TiO₂ basaltic andesite suite constituting the lower ultramafic to gabbroic cumulates and the upper pillow lavas (UPL). Studies of isotope and trace-element geochemistry of the rock package suggest a subduction-related spreading-center setting for the ophiolite emplacement (Pearce 1975, 1980, Gass 1980, McCulloch & Cameron 1983, Moores et al. 1984, Thy & Moores 1988). Synthesizing the available data, Thy & Moores (1988) proposed that the Troodos ophiolite probably developed in a short-lived spreading basin tectonically and petrologically in an arc position above a subducting oceanic crust but without the development of a mature arc, a setting analogous to the present-day plate-tectonic configuration in the Andaman Sea of the eastern Indian Ocean as suggested by Moores et al. (1984). Other Mideast ophiolite complexes may also have formed in a similar manner along short spreading segments separated by transform faults above a subduction zone.

Chromite mineralization in the complex ranges from accessory chromite as disseminations (<5% chromite) to pods of massive chromitite (>90% chromite), all believed to be of magmatic origin and subjected to variable degrees of deformation. Accessory chromite is ubiquitous in all rocks of ultramafic composition, but most chromite segregations occur either in the dunite close to the harzburgite contact (64% of deposits) or in the tectonite harzburgite, within 1 km beneath the lowermost cumulates, as pods and lenses enclosed in dunite (33% of deposits); the dunite cumulates contain only a small fraction (3%) of the chromite deposits (Greenbaum 1977, Malpas & Robinson 1987). The chromite bodies show all gradations between cumulate textures (polygonal, net, occluded silicate, nodular and orbicular textures) and deformation textures (schlieren and pull-apart textures).

Chromite has been mined in the Troodos area from a number of prospects since 1924, but no mines are currently in production. Most of the production in recent years came from the Chrome Mine situated near the summit of Mt. Olympus, where massive podiform ore occurs in dunite, close to the harzburgite-dunite contact. More than 0.5 million tonnes of ore was mined from this deposit; typical production-grade ore after concentration contained 47% Cr₂O₃ with a Cr:Fe ratio of about 2.7 (Greenbaum 1977).

5.7. Chromite Composition

Chromite (FeCr₂O₄) belongs to the spinel group of minerals. Natural chromite (chrome spinel) is a solid solution having the general formula (Mg,Fe²⁺)(Cr,Al,Fe³⁺)₂O₄ and its composition may be represented adequately within a six-component triangular

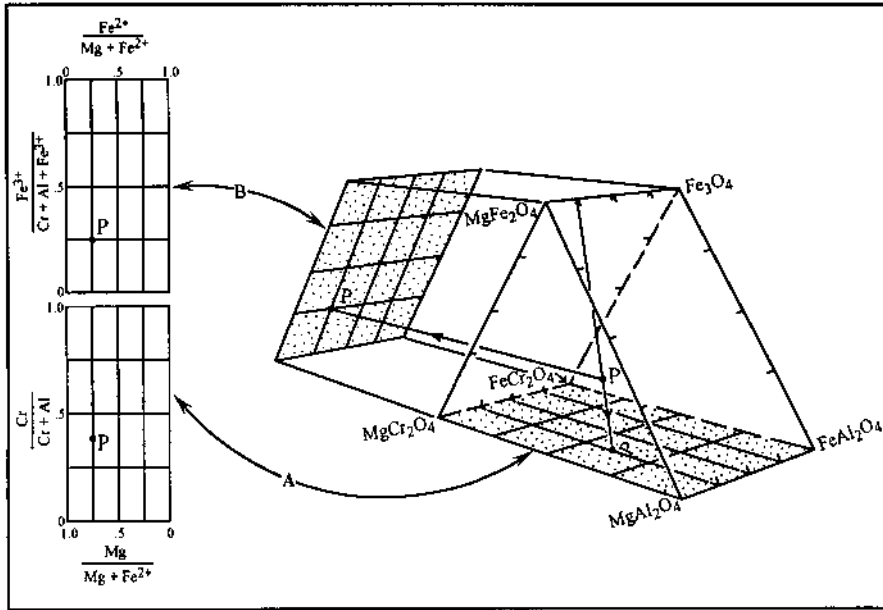


Figure 5.8. The compositional prism for representing chrome spinel solid solutions (e.g., composition *P*) in terms of six principal end-members and the two binary projections commonly used for illustrating chromite compositional variations (after Irvine 1965).

prism and three of its faces as shown in Figure 5.8. The face corresponding to $Mg/(Mg+Fe^{2+})$ versus $Cr/(Cr+Al)$ is particularly important because most chromian spinel compositions plot close to that face. The $Mg:(Mg+Fe^{2+})$ ratio of chromite (referred to as *magnesium ratio*) is largely temperature dependent and, considered in conjunction with the $Mg:(Mg+Fe^{2+})$ ratio of coexisting olivine or pyroxene, is useful for estimating the temperature of magmatic crystallization or metamorphic re-equilibration (Irvine 1967, Jackson 1969, Evans & Frost 1975, Henry & Medaris 1980). The variation in the $Cr:(Cr+Al)$ ratio of chromites (referred to as *chrome ratio*) is due to Cr-Al substitution and it is controlled partly by variation in total pressure of crystallization. The chrome ratio is also affected by partitioning of Al^{3+} into cumulus Al-silicate phases, which causes a relative increase of Cr in the residual melt. The other binary graph, $Fe^{3+}/(Cr+Al+Fe^{3+})$ versus $Mg/(Mg+Fe^{2+})$, incorporates the variation in $Fe^{3+}:Fe^{2+}$ ratio of chromian spinels and provides an approximate indication of the oxygen fugacity (Irvine 1965, 1967), a controlling parameter for magmatic crystallization of chromite (Osborn 1959, Hill & Roeder 1974, Ulmer 1969). Available experimental data and thermodynamic formulations bearing on compositional variations in natural chromites have been discussed by Irvine (1965, 1967) and Haggerty (1991).

As has been discussed by many authors (Thayer 1964, Irvine 1967, Duke 1983, Dickey 1975, Leblanc et al. 1980, Stowe 1994), despite some overlap, the compositional trends of stratiform chromites are quite distinct from those of the podiform chromites (see Table 5.4). Stratiform deposits are characterized by a large variation in the magnesium ratio ($\approx 0.2-0.70$) relative to the chrome ratio ($\approx 0.6-0.8$) (Fig. 5.9), low Cr:Fe(total) ratio (< 2.5), generally high $\text{Fe}^{3+}:\text{Fe}^{2+}$ ratio (up to about 1), and Ti content that may reach up to 1%. Stratigraphic variations generally follow fractionation trends, but may be complicated because of fluctuations in temperature, total pressure, $f\text{O}_2$, or co-crystallization of Fe-Mg-Al silicate minerals. The general upward decrease in the magnesium ratio and a slight upward decrease in the chrome ratio are usually attributed to decreasing Mg^{2+} and Cr in the residual melt during fractional crystallization. The Cr:Fe(total) ratio also generally decreases upward because of Cr depletion and Fe increase in the residual melt. For example, in the Bushveld Complex, the Upper Group chromites have a distinctly lower Cr:Fe(total) ratio compared with the Lower Group chromites (Table 5.3, Fig. 5.10). An overall upward decrease in the Cr:Fe(total) ratio of chromite seams (up to 3.9; Prendergast 1987) is also present in the Great Dyke, but in the Stillwater Complex the Cr:Fe(total) ratio of chromitite layers first increases upward and then decreases toward the top (Jackson 1968).

The composition of chromites in the ultramafic cumulate section of ophiolites is broadly similar to that of stratiform chromites. The contrasting compositional features of podiform chromites in the mantle tectonite include a larger range of chrome ratio ($\approx 0.2-0.9$) for a relatively smaller variation in the magnesium ratio ($\approx 0.4-0.7$) (Fig. 5.9), higher Cr:Fe(total) ratio ($\approx 2.4-4.6$), lower $\text{Fe}^{3+}:\text{Fe}^{2+}$ ratio (commonly < 0.5), and

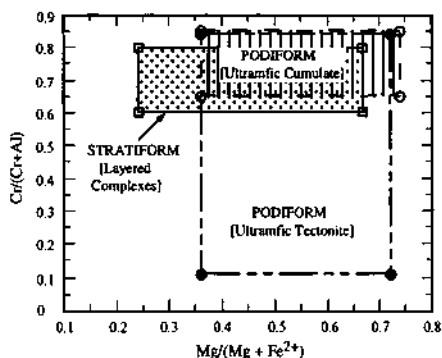


Figure 5.9. Compositional fields of stratiform and podiform chromites on the $\text{Mg}/(\text{Mg}+\text{Fe}^{2+})$ versus $\text{Cr}/(\text{Cr}+\text{Al})$ projection of the spinel compositional prism. Stratiform deposits (layered complexes): Bushveld, Great Dyke, and Stillwater. Podiform deposits (ophiolites): Cyprus (Troodos), Oman (Semail), New Caledonia (Tiébaghi and Massif du Sud), Canada (Thetford), and Pakistan (Zhob Valley). Data for chromites in Archean layered complexes and Archean greenstone belts are excluded for the sake of clarity. (Source of data: compilation by Stowe 1994.)

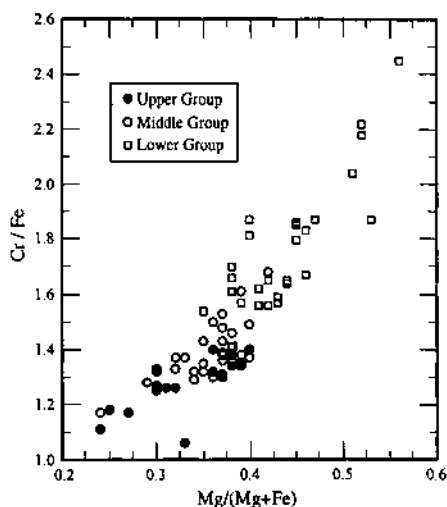


Figure 5.10. Comparison of the Lower Group, Middle Group, and Upper Group chromite compositions, Critical Zone, Bushveld Complex (data from Hatton & von Gruenewaldt 1987). $Mg/(Mg+Fe)$ is cation ratio and Cr/Fe is weight ratio; $Fe = Fe^{2+} + Fe^{3+}$ in both cases.

and lower Ti (<0.1%). There is a distinct inverse relationship between Cr and Al, but in contrast to the stratiform deposits the relationship is independent of the fractionation trend and so cannot be ascribed to Cr depletion in the residual melt fraction. Two additional features of podiform chromite composition deserve mention. One is the wide variation of the chrome and Cr:Fe(total) ratios even in individual deposits. For example, the chrome and Cr:Fe(total) ratios in podiform chromites hosted by mantle tectonite range from 0.1 to 0.8 and from 0.8 to 3.9, respectively, in the Semail (Oman) ophiolite (Brown 1980, Auge 1987) and from 0.2 to 0.8 and from 1.4 to 4.6, respectively, in the New Caledonia ophiolite (Leblanc et al. 1980, Leblanc 1987). The other is an apparent bimodal distribution of the chrome ratio in the tectonite-hosted chromites (Leblanc & Violette 1983), with Al-rich chromite pods (chrome ratio typically between 0.4 and 0.6) distributed along the harzburgite-dunite transition zone not far from the base of the ultramafic cumulates and the Cr-rich pods (chrome ratio typically >0.6) located in deeper peridotites. As will be discussed later, the compositional variation provides important clues to the origin of podiform chromites.

Investigations of the geochemistry of platinum-group elements in chromites have shown that podiform deposits hosted in Paleozoic and Mesozoic ophiolite complexes have distinctly different chondrite-normalized PGE profiles compared with those hosted by layered complexes (Fig. 5.11). A reason for the marked enrichment of stratiform

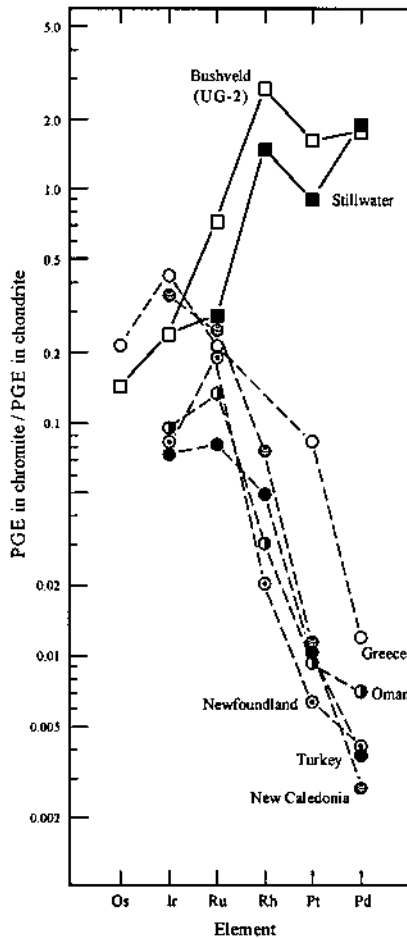


Figure 5.11. Chondrite-normalized plots of average concentration of platinum-group elements (PGE) in stratiform chromites from layered complexes (Bushveld and Stillwater) and podiform chromites from ophiolites (Oman, Turkey, Greece, New Caledonia, and Newfoundland). (After Page et al. 1985.)

chromitites in Pt and Pd is the higher original abundance of PGE-enriched sulfides in these chromitites (Naldrett & von Gruenewaldt 1989); a contributing factor may be the difference in relative proportions of PGE in the source magmas for layered intrusions and ophiolites. Chromitites of the Sukinda and Nausahi districts in Orissa (India), interpreted earlier as stratiform deposits on the basis of chemical composition and texture (Chakraborty & Chakraborty 1984), have been reinterpreted as ophiolite-hosted podiform deposits based on their PGE profiles (Page et al. 1985).

5.8. Origin

5.8.1. STRATIFORM DEPOSITS

From the textures of stratiform chromite deposits and their association with ultramafic cumulates, it is quite clear that the chromite-rich layers represent segregation of chromite crystals that crystallized from a basaltic magma. It is also evident that, because of the very low solubility of chromium in basaltic magmas (e.g., a maximum of $\approx 1,000$ ppm Cr in a magma containing 13% MgO; Barnes 1986), the accumulation of Bushveld-type chromitite layers must have involved the processing of tremendous volumes of magma. The features which have remained controversial and need to be addressed are: (a) the formation of chromitite layers (in which chromite is the only cumulus phase); (b) the great lateral extent of chromitite layers in some deposits; and (c) the presence of many such layers in a given layered intrusion. A good summary of the various hypotheses has been presented by Duke (1983).

The liquidus phase relations in the $(\text{Mg,Fe})_2\text{SiO}_4\text{-SiO}_2\text{-(Mg,Fe)Cr}_2\text{O}_4$ system (Fig. 5.12a) provide a reasonable representation of chromite crystallization from basaltic magmas at low pressures. The abundance of olivine cumulates at the lowermost parts of layered intrusions suggests that the parent magma compositions should plot in the olivine liquidus field, such as point *a* in Figure 5.12a. Fractional crystallization of olivine from such a magma drives the liquid composition away from the olivine corner toward the olivine-chromite cotectic line. Crystallization of chromite begins at point *b* and co-precipitation of olivine and chromite continues as the liquid composition moves along the cotectic. Crystallization of both olivine and chromite terminates at point *c*, a reaction or distribution point, and orthopyroxene becomes the sole crystalline phase as the liquid composition moves along *cd*. The sequence of cumulus minerals for this crystallization path ($a \Rightarrow b \Rightarrow c \Rightarrow d$) is: olivine, olivine + chromite, orthopyroxene. Note that chromite becomes an early-crystallizing phase despite the very small amount of dissolved chromite in the parent magma, but only a small proportion of chromite (about 2 modal%) co-precipitates with olivine (Irvine 1965). The olivine:chromite ratio crystallizing at any point on the cotectic line is given by the intersection of the tangent to the cotectic line with the olivine-chromite join.

The crystallization sequence described above explains the commonly observed chromite disseminations in ultramafic cumulates, but not the formation of chromitite layers. Settling of chromite crystals may be possible when chromite crystallizes alone from a magma supersaturated in chromium, but effective gravitative separation of the very small amount of chromite from a cotectic chromite-silicate mixture is considered unlikely. To obtain monomineralic chromite layers, some perturbation in the system must lead to an interval when chromite is the sole crystallizing phase. Postulated mechanisms by which chromite-silicate cotectic crystallization may be supplanted by crystallization of chromite unaccompanied by silicate minerals include: (a) change in magma composition by silica assimilation or mixing of magmas, (b) increase in the oxygen fugacity, and (c) increase in the total pressure of crystallization.

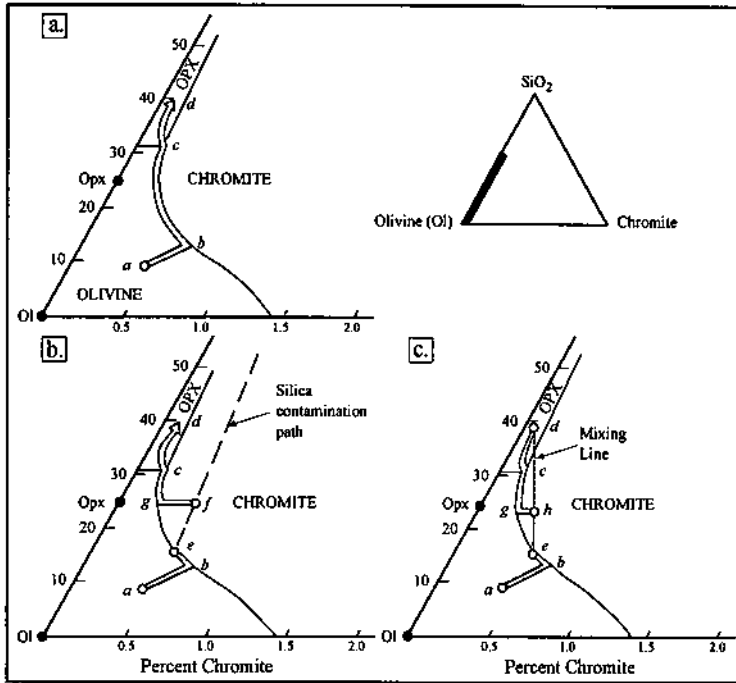


Figure 5.12. Schematic phase relations in a portion of the $(\text{Mg,Fe})_2\text{SiO}_4\text{-(Fe,Mg)Cr}_2\text{O}_4\text{-SiO}_2$ system illustrating the normal crystallization path of a basaltic magma (a), and the change in crystallization path due to either silica contamination (b) or magma mixing (c). Only the latter two cases are conducive to the formation of chromitite layers. Details of the diagram are explained in the text. (After Irvine 1975, 1977.)

Ulmer (1969) and Cameron and Desborough (1969) proposed that the “chromitic intervals” in the Critical Zone of the Bushveld Layered Series formed due to periodic increase in the oxygen fugacity of the magma. Experimental investigations (Ulmer, 1969, Hill & Roeder 1974) do suggest a significant expansion of the liquidus chromite field with increasing oxygen fugacity. However, because of the internal buffering capacity of a large body of magma, it is difficult to visualize the rapid but spatially uniform fluctuations in oxygen fugacity implied by the repetition of chromitite layers of great continuity. Subsequently, Cameron (1980) abandoned this hypothesis in favor of chromitite formation in response to tectonically induced changes in total pressure in the magma chamber. An expansion of chromite stability field with increasing pressure should be expected, as has been demonstrated by Osborn (1978) for Mg-Fe-Al spinel in a simplified basaltic system, and a pressure increase also increases the stability of pyroxene relative to plagioclase (Lipin 1993). Moreover, variations in total pressure due to, for example, tectonic activity or addition or withdrawal of large batches of

magma, are likely to be laterally uniform. However, the magnitude of pressure change required to shift the spinel-silicates cotectic surface sufficiently so as to form a 1 m-thick chromitite layer can be qualitatively estimated to be unrealistically large, and the direct effect of pressure change on mineralogy, in general, has been shown to be trivial (Hatton and von Gruenewaldt 1987). In a chamber as large as the Bushveld Complex the roof could not have been rigid, but merely floating on the magma. Hence, mechanisms which would increase the pressure at the base of the chamber are difficult to envisage (Cawthorn & Lee 1998).

Irvine (1975) proposed that chromitite layers in the layered intrusions were formed on occasions when the mafic parental magma of the intrusion was extremely contaminated with granitic material derived from sialic roof rocks. The principle of this hypothesis is illustrated in Figure 5.12b. The curvature of the olivine-chromite cotectic is such that addition of SiO_2 to a liquid on the cotectic, such as at point *e*, drives the liquid composition to some point *f* inside the liquidus chromite field, resulting in the crystallization of chromite alone. Chromite continues to be the only crystallizing phase until the liquid composition reaches the cotectic at point *g*, at which point the normal crystallization path is resumed. Variations of this model with different amounts or episodes of silica assimilation could account for the formation of the more common stratigraphic sequences involving chromitite layers in the Muskox, Stillwater, Great Dyke, and Bushveld complexes (see Irvine 1975, Figs. 10 and 11). Alapieti et al. (1989) have concluded that the silica contamination hypothesis offers the best explanation for the main chromitite layers in the Kemi Complex, where evidence for silica contamination is found in the form of small silicate inclusions in chromite grains. The inclusions are rich in alkalis and apparently represent trapped droplets of the contaminant sialic melt. As the sulfur solubility in a mafic magma decreases with an increase in its silica activity, the silica contamination hypothesis offers a possible explanation also for the occurrence of sulfide deposits in some mafic-ultramafic complexes (see Ch. 6).

Although sound in principle, the above mechanism would require geologically improbable amounts of silica contamination to account for the Bushveld chromitites. Moreover, the marked Fe-enrichment trend of differentiation in the Bushveld Complex suggests a tholeiitic melt relatively uncontaminated by alkali-rich granitic melt. The alternative hypothesis proposed by Irvine (1977) is based on the same phase relations, but calls for influxes of a more primitive magma at different stages of fractionation, actually an extension of the scheme believed to have been responsible for the formation of cyclic units. For example, as illustrated in Figure 5.12c, the mixture of a more evolved magma of composition *d* with a less evolved magma of composition *c* would result in a magma composition represented by a point such as *h* in the liquidus field of chromite (provided that points on the mixing line lie above the liquidus surface), inducing the crystallization of chromite alone. Murck and Campbell (1986) have shown that the solubility of Cr in a basalt magma in equilibrium with chromite decreases more rapidly per unit fall in temperature at higher temperatures ($\approx 1,400^\circ\text{C}$) than at lower temperatures ($\approx 1,200^\circ\text{C}$). Because of the resulting concave-upward

curvature of the Cr solubility curve, the mixing of two magmas, both saturated (or nearly saturated) in chromite but at different temperatures, would place the hybrid above the saturation curve, suggesting that point *h* in Figure 5.12c would likely lie above the liquidus. In the case of the Bushveld Complex, such mixing adequately explains the chromitite layers (LG-1 to LG-4) associated with olivine cumulates, but the thicker layers associated with orthopyroxene only (LG-5 to LG-7) or with orthopyroxene and plagioclase (MG-2 to MG-4 and UG-1, UG-2) are better explained by mixing of two quite distinct magmas (Hatton & von Gruenewaldt 1987).

As mentioned earlier, the crystallization of the Rustenburg Layered Suite involved the mixing of derivatives of an ultramafic (*U*) magma and an anorthositic (*A*) magma. The *U* liquid is believed to have been the main carrier of Cr, the Cr content decreasing rapidly with decreasing normative olivine content of the liquid. From melting experiments on Bushveld chilled margin rocks, Sharpe and Irvine (1983) showed that each of these melts at its liquidus would be saturated in chromite and a silicate mineral — olivine in the case of *U* melt and plagioclase in the case of *A* melt — and yield cumulates containing only accessory amounts of chromite, but hybrids of the two would have the capability to form chromitite by virtue of being saturated only in the oxide mineral. Chromite would remain the sole liquidus phase over almost the entire region of intermediate composition, even for relatively low fO_2 conditions under which the *U* melt has only olivine on the liquidus and the *A* melt only plagioclase (Irvine & Sharpe 1986).

A problem with the magma-mixing hypothesis discussed above is that the temperature interval over which chromite is the sole crystallizing phase is small ($\approx 20^\circ\text{C}$), after which a silicate mineral begins to crystallize; this should dilute the chromite to accessory concentrations or even terminate its crystallization through a liquidus reaction relationship. Experiments with U_1 and A_1 melt compositions by Sharpe and Irvine (1983) indicated that the hybrid melts would yield 0.02–0.04 wt% chromite by this process, or a little more (≈ 0.05 wt%) with a more primitive *U* liquid — certainly not enough to produce a Bushveld-type chromitite layer. For example, to form a 1 m-thick chromitite layer like LG-6 by this process would require a layer of parent liquid of equivalent lateral extent and at least 1 km thick! To circumvent this geologically unrealistic situation, Todd et al. (1982) and Irvine et al. (1983) proposed a “double-diffusive convection magma mixing model” for the solidification of large layered intrusions such as the Bushveld and the Stillwater. The essence of this model is that the *U* and *A* liquids differ sufficiently in density to form separate layers in the magma chamber and their crystallization and mixing are controlled by double-diffusive convection. Whole sequences of cumulates form concurrently by down-dip accretion from a column of density-stratified liquid layers that are separated primarily by diffusive interfaces. Each cumulate layer accumulates from one or more liquid layers and the lower cumulates, because of their higher crystallization temperatures, grow in advance of the upper cumulates. Thus, chromitite layers grow (prograde) continuously by the down-dip accretion process, a little bit at a time and at particular levels on the basin-form intrusion floor, while silicate cumulate layers are prograding concurrently from

liquid layers of appropriate compositions at other levels (Irvine & Sharpe 1986).

Campbell et al (1983) have discussed the application of hydrodynamic theory for modeling the mixing process when a fresh primitive silicate magma is introduced into a magma chamber that is stratified by composition and density. The form and efficiency of mixing depends on the density contrast between the two magmas and on the velocity and volume of the input magma. If the input magma is more dense than the lowest magma layer in the chamber, the initial momentum of the input magma may carry it in the form a turbulent fountain, mixing and entraining with the resident magma, but eventually it will fall back forming a dense layer at the top of the cumulate pile. If the resident magma is denser, then the input magma is likely to rise as a turbulent plume, entraining and mixing with a high proportion of the resident magma on the way, and the hybrid, when it reaches its own density level, will spread out as a turbulently convecting layer. Barnes and Naldrett (1985) have estimated that the density of a mafic magma should decrease by the fractional crystallization of olivine, remain about the same by the crystallization of orthopyroxene, but tend to increase once plagioclase becomes a liquidus phase. Thus, a turbulent plume is most likely to develop if the influx of primitive magma is preceded by significant plagioclase crystallization in the magma chamber. The Bushveld Upper Group chromitites probably formed in such an environment that was conducive to efficient mixing; the Lower Group chromitites of the Bushveld Complex and those of the Stillwater Complex appear to have formed before the onset of plagioclase crystallization and, therefore, in an environment of less efficient mixing (Naldrett & von Gruenewaldt 1989). Other problems with the magma mixing model include the systematic vertical variation in chromite composition, the lateral uniformity of the chromitite layers, and the absence of cryptic variations.

Despite uncertainties in the details of the mechanism, mixing of magmas of different composition and density is currently the favored model for explaining the igneous stratigraphy of large layered complexes as well as for the formation of stratiform chromitite layers hosted by them. Magma mixing is also a popular model for the PGE-enriched sulfide mineralization in layered complexes (see Ch. 7).

5.8.2. PODIFORM DEPOSITS

The common occurrence of cumulate textures and chromitite layers in podiform deposits points to a significant role for fractional crystallization in their formation, subject to the same phase equilibria constraints as discussed earlier for stratiform deposits. This analogy is particularly appropriate for podiform deposits hosted by the ultramafic cumulate sequence of ophiolites, although it is unlikely that they ever attained the lateral continuity so characteristic of stratiform deposits. Other features of podiform deposits — small size, irregular form, random distribution with wide compositional variation among neighboring deposits, and deformation textures — are believed to be the consequence of disruption of originally larger bodies and tectonic mixing of the disrupted parts in the unstable environment (spreading centers) in which ophiolites form and during subsequent tectonic emplacement (Thayer 1969, 1980).

Various models have been proposed for the origin of podiform deposits hosted by the mantle tectonite section of ophiolites, but none of them satisfactorily accounts for all the essential features of these chromite deposits: the cumulate and deformation textures, the concordant to discordant disposition of the pods, the dunite envelope around the pods, and the variation of chromite composition with depth or host lithology. The cumulate textures indicate the chromite to be a product of fractional crystallization of a melt, not a residue of partial melting of the mantle harzburgite as has been suggested by Cassard et al. (1981). One possibility is that the chromite pods actually formed in the ultramafic cumulate sequence but were subsequently emplaced in the underlying tectonite either as autoliths by gravitative sinking (Dickey 1975) or by infolding of the lowermost cumulate layers (Greenbaum 1977). Such an origin, however, does not explain the variation of Cr:Fe ratio in chromite with depth observed in many ophiolites (Brown 1980, Leblanc 1987, Leblanc & Violette 1983). Also, Dickey's hypothesis does not account for the dunite envelope around chromite pods.

Most authors consider the podiform chromite deposits to be indigenous to mantle peridotites where they crystallized at different times and at different places by fractional crystallization of ascending basaltic melts. Brown (1980) suggested that in the Semail (Oman) ophiolite chromite crystallization occurred in periodically replenished "mini chambers" beneath the main cumulate magma chamber, but within the tectonized mantle harzburgite. A variation of this model, proposed by Lago et al (1982), envisages the precipitation and accumulation of chromite (from melts invading the harzburgite) in cavities that formed by local widening of magma conduits. Leblanc (1987) advocated a similar origin by crystallization of chromite in magma conduits for the chromite deposits in the New Caledonia ophiolite and ascribed the dunitic wallrock of the chromite pods to partial melting of surrounding peridotites by the high-temperature magma. However, textures and cryptic variations suggest the accumulation of chromite in horizontal layers in many occurrences (Duke 1983).

In the mantle tectonite section of ophiolites, high-Cr podiform chromite is generally associated with highly depleted peridotites and high-Al podiform chromite with less-depleted peridotites. This difference may be attributed to the difference in magma composition resulting from different degrees of partial melting: highly magnesian (boninitic type) magmas formed by high degrees of partial melting for Cr-rich chromite and tholeiitic magmas by lower degrees of partial melting for Al-rich chromite (Dick & Bullen 1984, Arai 1992, Zhou et al. 1994).

The precipitation of chromite without silicate phases for the formation of podiform chromite deposits, as in the case of stratiform chromite deposits described earlier (see Fig. 5.12), requires some mechanism to drive the melt composition into the liquidus field of chromite. In addition, this mechanism should be consistent with the occurrence of depleted dunite envelopes around podiform chromite bodies. A model proposed by Arai and Yurimoto (1994) calls for the injection of an exotic melt into the harzburgite that reacts with the wallrock to form depleted dunite and a secondary Si-rich melt. This melt, in turn, mixes with a successively supplied, relatively primitive melt to precipitate chromite. A somewhat different model proposed by Zhou et al. (1994)

attributes the compositional modification of an ascending basaltic magma (formed by partial melting of the upper mantle) to reaction with the host peridotites rather than magma mixing. The melt-rock interaction model relies on the incongruent dissolution of pyroxenes in the host peridotites to produce a melt relatively enriched in SiO_2 (Keleman et al. 1992) and thus drive the melt composition into the stability field of chromite. A byproduct of this process is a residue of olivine that appears as the depleted dunite envelope around the podiform chromitite body. According to this model, the main controlling factor for the formation of podiform chromitites is the degree of melt-rock interaction.

Recently, Ballhaus (1998a) has proposed a magma mixing model based on experiments designed to study the fractionation of chromite between conjugate siliceous and fayalitic melts. In his model, podiform chromite bodies outline conduits in the shallow lithosphere where an olivine-normative, high-pressure, low-viscosity melt (picritic) mixed with a siliceous, low-pressure, more viscous melt (boninitic). The viscosity contrast would inhibit instant mixing of the melts and, according to his experiments, cumulus chromite would nucleate and grow only in the mafic melt where the crystal (chromite)/melt interfacial energy was the lowest, the siliceous melt serving merely as a diffusive chromium reservoir. The richest chromite ores would form when the volume ratio of the melt nucleating chromite was small relative to the ambient melt. The experiments simulated two characteristic features of podiform chromite deposits: the nodular texture of chromite and the dunitic envelope of chromite pods.

5.9. Metallogenesis

5.9.1. PALEOTECTONIC SETTINGS

Layered complexes do not seem to have formed in one particular tectonic setting. Some layered intrusions, such as the Duluth Complex (Minnesota, USA), are clearly related to a continental rift system (Basalt Volcanism Study Project, 1981), but the settings of others, such as the Bushveld and Stillwater, are controversial. For example, Irvine and Sharp (1982) suggested that the U_o and A_o melts involved in the formation of the Bushveld Complex came, respectively, from deep in the upper mantle (perhaps from a depth of 180-200 km) and from the bottom of thick (40-50 km) segments of continental crust. Hatton (1989), on the other hand, favored a supra-subduction setting for the Complex. In his model, the U_o magma was derived from a depleted-mantle source that had been metasomatized by fluids from subducted sediments and the A_o magma from subducted oceanic lithosphere in a region of retro-arc spreading when the Kaapvaal and Zimbabwe cratons collided around 2700 Ma. Stowe (1989) proposed that the Complex was intruded in a region of crustal extension, and von Gruenewaldt and Harmer (1992) discussed evidence favoring the emplacement of the Complex into an intracratonic environment in which rifting had occurred during deposition of the sediments of the Transvaal Sequence. An extensional setting has also been proposed

for the Great Dyke (Bichan 1969, Prendergast 1987) and the Skaergaard (Brooks & Nielsen 1982). The intrusion of the Stillwater Complex is believed to be related to strike-slip faulting in a continental environment (Page & Zientek 1985). A continental environment for the Stillwater magmas is supported by Rh-Os and Sm-Nd systematics. Lambert et al. (1989) determined that *U*-type magmas for the Stillwater Complex had initial ϵ_{Nd} of -0.8 to -3.2 and a chondritic initial $^{187}Os/^{186}Os$ ratio of ≈ 0.88 , whereas *A*-type magmas had ϵ_{Nd} of -0.7 to $+1.7$ and initial $^{187}Os/^{186}Os$ ratio of ≈ 1.13 . These data suggest that *U*-type magmas were derived from a lithospheric mantle source containing recycled crustal materials, whereas *A*-type magmas originated either by crustal contamination of basaltic magmas or by partial melting of basalt in the lower crust. Despite some lingering uncertainties, it is reasonable to conclude that layered complexes were emplaced into already stabilized continental crust. This conclusion is consistent with the pervasive cumulate layering, including stratiform chromitites, in the complexes.

Because of the remarkable similarity with oceanic crust formed at modern oceanic spreading centers, ophiolites are believed to have formed originally in a similar setting (Coleman 1977). However, there is a growing body of geochemical evidence in favor of a subduction-related model for many ophiolites, probably a back-arc basin rift environment that can account for both the sheeted diabase dike complex, requiring sea-floor spreading, and the geochemistry of the pillow basalts, requiring magma generation above a subduction zone (Pearce 1980, McCulloch & Cameron 1983, Coleman 1984). As an extension of the melt-rock interaction model for the origin of podiform chromite deposits (Zhou et al. 1994), Zhou and Robinson (1997) suggested that the occurrence of podiform chromitites and their chemical compositions could be correlated with formation in two environments: in island arcs, and in nascent spreading centers, such as back-arc basins. The island-arc environment, characterized by high degrees of partial melting because of high input of volatiles from the subducting slab into the overlying mantle wedge, is conducive to the formation of high-Cr chromite (e.g., Troodos ophiolite). Back-arc basins, on the other hand, should favor the crystallization of high-Al chromite because of smaller degrees of partial melting due to a lower influx of volatiles in this environment. Mature spreading centers, such as mid-ocean ridges, do not provide a favorable environment for the formation of podiform chromite deposits. The composition of mid-ocean ridge basaltic magmas remain remarkably uniform through time, providing little drive for melt-rock interaction once the magmas have equilibrated with the wallrocks through which they pass.

Stowe (1994) proposed that the chemical composition of chromite ores might be used as an indicator of their tectonic setting. It is well established that the principal control on chromite chemistry is the composition of the melt from which it crystallizes (Dick & Bullen 1984, Roeder & Reynolds 1991) and that the melt (magma) composition varies from one tectonic setting to another because of differences in the parent material and conditions of partial melting. There is a good correlation between liquidus chromite composition — e.g., Cr:(Cr+Al) ratio versus Mg:(Mg+Fe²⁺) ratio — and magma type, but the extrapolated correlation between magma type and tectonic

setting can be equivocal (Rollinson 1995). Moreover, the composition of chromites subjected to subsolidus re-equilibration during serpentinization and regional metamorphism may be significantly different from the original liquidus compositions. An evidence for subsolidus re-equilibration is the development of Fe- and Ti-enriched "ferrit-chromite" rims on serpentine-hosted chromite grains.

5.9.2. AGE DISTRIBUTION

The known chromite deposits range in age from early Archean to Miocene (Table 5.1, Fig. 5.13). The overwhelming majority of the deposits, however, fall into two age groups: stratiform deposits hosted by layered mafic complexes ≈ 2900 -2000 Ma (late Archean to early Proterozoic) in age; and podiform deposits hosted by ophiolitic complexes of Mesozoic-Tertiary age. This distribution can be broadly correlated with crustal evolution through geologic time (Stowe, 1994).

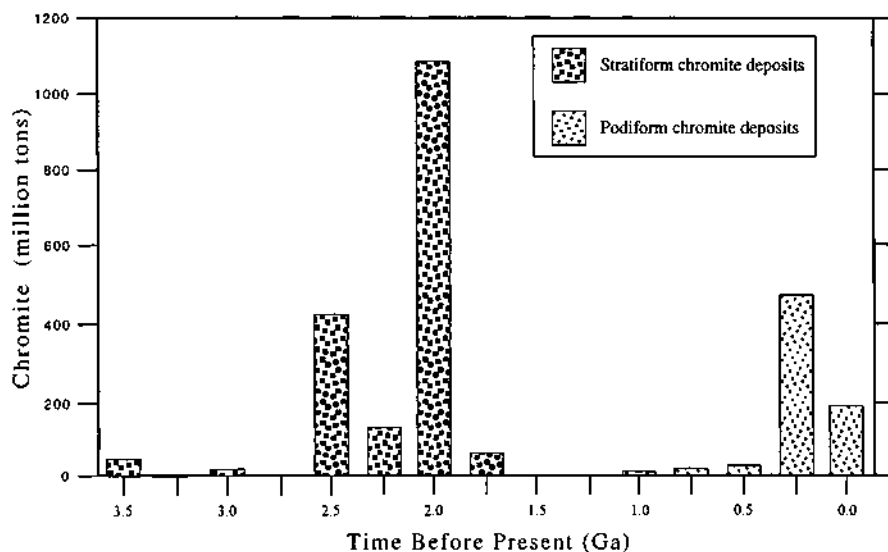


Figure 5.13. Age distribution of stratiform and podiform chromite deposits. The x-axis age class interval is 0.25 b.y. and the y-axis indicates the total chromite (past production + R1 E/M resources) for the various age intervals. R1 category = resource *in situ*, a known deposit, reliable resource estimate; E = economically exploitable grade; M = marginal grade ore. (After Stowe 1994.)

The layered intrusions with appreciable chromite concentrations (e.g., Bushveld, Great Dyke, Mashaba, Stillwater, and Kemi) were emplaced into already stable continental-type crust during the Archean to Proterozoic transition following cratonization of the Archean continental nuclei. The chromium enrichment in these magmas was probably a result of high degrees of partial melting in the mantle due to relatively high geothermal gradients. The younger layered complexes (e.g., Muskox

and Skaergaard) carry only thin, subeconomic layers of chromite with low Cr:Fe ratios, possibly reflecting decreased continental thermal gradients. The intensely deformed Fiskenaasset complex of Greenland may represent an early Archean analog of stratiform chromite, emplaced prior to continental cratonization (Stowe 1994).

The evolution of most ophiolite-hosted podiform deposits are clearly related to both spreading and plate convergence processes during the Mesozoic and Tertiary. The lack of economic-grade chromite deposits in the middle Proterozoic (2000-800 Ma), the so-called "Proterozoic gap", is an enigma. The oldest known ophiolite sequences with podiform ores occur in orogenic belts of late Proterozoic age in Sudan, Saudi Arabia, and Morocco, implying that plate tectonics was operative at least by about 800 Ma. If plate tectonic processes operated before this time, the oceanic crust might have been too thick for obduction (Moores 1986, Stowe 1994). The tectonic setting of Archean greenstone belts, some of which contain podiform chromite deposits (e.g., the Shurugwi greenstone belt, Zimbabwe), remains poorly understood (see Ch. 6).

5.10. Summary

Primary chromite deposits represent syngenetic segregations of chromite in ultramafic igneous rocks and are believed to be products of fractional crystallization of basaltic magmas. Based on forms and textures, massive chromite (chromitite) deposits are divided into two descriptive types: (a) stratiform deposits, which occur as multiple, conformable chromitite layers of considerable lateral extent in the lower ultramafic zone of a few of the continental layered intrusions (e.g., the Bushveld Complex, the Great Dyke); and (b) podiform deposits, which occur as small and discontinuous, concordant to discordant bodies of variable morphology in the ultramafic cumulate and mantle peridotite (tectonite) sections of obducted ophiolites (e.g., the Troodos Massif), especially in the "transitional dunite". The distinctive characteristics of the two types of deposits (Table 5.4) appear to be related mainly to the differences in their tectonic setting and parent magma composition. Both types contribute almost equally to the current world production of chromite, but stratiform deposits, largely because of the Bushveld Complex, far outweigh podiform deposits in terms of reserves and resources.

The textures and composition of podiform chromites in ultramafic cumulates are similar to those of stratiform chromites, but podiform chromites hosted by mantle peridotites have distinctive composition and they commonly show deformation textures and structures. Compared with stratiform chromites, tectonite-hosted chromites are characterized by a much wider range of Cr:(Cr+Al) ratio relative to a smaller range of Mg:(Mg+Fe²⁺) ratio, higher Cr:Fe(total) ratio, lower Fe³⁺:Fe²⁺ ratio, lower Ti, and lower Pt and Pd concentrations.

The common occurrence of disseminated, accessory chromite in ultramafic rocks is easily explained by cotectic crystallization of chromite as an early cumulus phase (with olivine or orthopyroxene) from most basaltic magmas. The formation of essentially silicate-free chromitite requires special conditions that would drive the liquid

TABLE 5.4. Comparison between stratiform chromite deposits hosted by layered intrusions and podiform chromite deposits hosted by ophiolites

	Stratiform deposits	Podiform deposits
<i>Geologic setting</i>	Layered intrusions.	Ophiolites (harzburgite subtype).
<i>Host rocks</i>	Lower ultramafic zone.	Ultramafic cumulate (oceanic crust) and ultramafic tectonite (depleted mantle).
<i>Chromite mineralization</i>	Conformable, multiple chromitite layers of considerable lateral continuity.	Thin, discontinuous layers in ultramafic cumulate; small, concordant to discordant bodies of irregular form (pods, lenses, pipes) in mantle tectonite.
<i>Textures</i>	Cumulate; euhedral to subhedral chromite.	Cumulate (anhedral chromite) and deformed; nodular and orbicular textures are diagnostic. In the mantle tectonite, concordant bodies generally are more deformed than discordant ones.
<i>Chromite composition</i>	Large range of Mg:(Mg+Fe ²⁺) ratio ($\approx 0.2-0.7$) relative to Cr:(Cr+Al) ratio. Low Cr:Fe(total) ratio ($\approx 1.4-2.6$). High Fe ³⁺ :Fe ²⁺ (up to ≈ 1). Marked enrichment in Pt and Pd.	Chromites in ultramafic cumulate similar to that of stratiform chromites. Chromites in mantle tectonite are characterized by: Large range of Cr:(Cr+Al) ratio ($\approx 0.2-0.9$) relative to Mg:(Mg+Fe ²⁺) ratio ($\approx 0.4-0.7$). High Cr:Fe(total) ratio ($\approx 2.4-4.6$). Low Fe ³⁺ :Fe ²⁺ ratio (commonly < 0.5). Marked depletion in Pt and Pd. TiO ₂ $< 0.3\%$.
<i>Age of host complexes</i>	Predominantly late Archean to early Proterozoic (2500-2100 Ma).	Predominantly Mesozoic-Tertiary.
<i>Paleotectonic setting (original)</i>	Stable continental areas.	Spreading centers above subduction zones.
<i>Typical examples</i>	Bushveld Complex (South Africa) Stillwater Complex (USA)	Troodos Massif (Cyprus) New Caledonia

composition into the liquidus chromite field. The mixing of two compositionally distinct melts offers a viable mechanism for the origin chromitite layers (as well as of cyclic units) in layered intrusions. For the Bushveld Complex, the two parental magmas have been estimated to be boninitic ultramafic (*U*) and anorthositic (*A*) in composition. The magma-mixing model is also believed to be applicable to the Stillwater Complex and possibly other layered intrusions. Mixing of magmas of different silica activity has also been suggested for the origin of podiform chromite deposits located in the mantle tectonite of ophiolite complexes. A variation of the

mixing model that may account for tectonite-hosted podiform chromitites involves the mixing of an exotic melt with a Si-enriched melt produced by its reaction with the harzburgitic wallrock. An ascending basaltic magma may also attain Si enrichment, without magma mixing, by incongruent dissolution of pyroxenes when it reacts with the host peridotite. The olivine residue produced as a byproduct of the latter process would represent the depleted dunite envelope commonly observed around the tectonite-hosted podiform chromitite bodies

The age distribution of chromite deposits is strongly bimodal and is related to crustal evolution. Most layered intrusions appear to have been emplaced in extensional, continental regimes during late Archean to early Proterozoic, following cratonization of the Archean nuclei, and stratiform chromite deposits hosted by them formed in relatively stable tectonic settings. Ophiolite-hosted podiform chromite deposits, on the other hand, are predominantly Mesozoic to Tertiary in age. The ophiolite hosts and their chromite deposits were originally emplaced at back-arc basin spreading centers and have been preserved by obduction onto continental margins. The lack of economic chromite deposits during the 200-800 Ma interval remains a puzzle.

5.11. Recommended Reading

Thayer (1969), Greenbaum (1977), Duke (1983), Hatton & von Gruenewaldt (1987), Leblanc (1987), Zhou et al. (1994), Stowe (1994), Ballhaus (1998).

CHAPTER 6

NICKEL (-COPPER) SULFIDE DEPOSITS

6.1. Introduction

Nickel is one of the most important ferro-alloy metals and its major use today, accounting for about half of the world's total production, is for making nickel steels and nickel cast irons. It is also used for many other alloys, especially with copper (Monel metal) and chromium (stainless steel). Nickel imparts to its alloys toughness, strength, and anti-corrosion qualities; nickel steels and alloys are preferred for moving and wearing parts of many types of machinery. Other important uses of nickel include electroplating and coinage.

Nickel is one of the metals which is depleted in the crust but enriched in the mantle. Thus, ultramafic and mafic rocks formed from mantle-derived magmas tend to have relatively high nickel contents. The nickel in these rocks resides in olivines and pyroxenes, substituting for Mg^{2+} and Fe^{2+} , and may amount to as high as 0.3% in some dunites and peridotites. Mineable orebodies of nickel commonly contain in excess of 1% Ni, requiring a concentration of more than 4 times that of typical mantle material.

The nickel resources of the world are of three types: (a) deep-sea Fe-Mn nodules (typically with >1% Ni), related to ocean-floor volcanic activity; (b) lateritic deposits (<0.8 to 3% Ni), representing residual concentrations of nickel resulting from the weathering of ultramafic rocks (see Ch. 2); and (c) Ni (-Cu) sulfide deposits (<0.8 to >6% Ni and variable amounts of Cu) resulting from concentration of Ni-sulfide minerals (pentlandite, millerite, hazlewoodite) by orthomagmatic or magmatic-hydrothermal processes. Commercial-scale mining of Fe-Mn nodules, which constitute about 17% of world's nickel resources, is yet to be tested. This chapter deals only with the sulfide ores, which account for about one-third of the resources but about two-thirds of the current world production of nickel (Naldrett 1989).

6.2. Distribution

The world distribution of nickel sulfide deposits (Fig. 6.1) is restricted essentially to (a) ultramafic lavas and intrusions in Precambrian greenstone belts, predominantly of Archean age, and (b) differentiated intrusions of an overall gabbroic composition, spanning both the Precambrian and the Phanerozoic. In terms of nickel sulfide

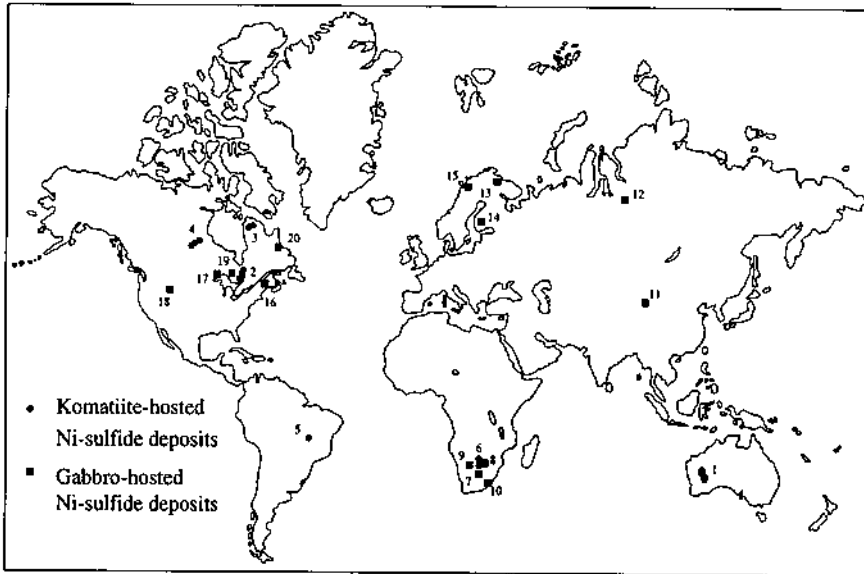


Figure 6.1. World map showing the important nickel sulfide deposits and belts. (a) Deposits hosted in extrusive or intrusive komatiitic rocks in Precambrian greenstone belts: 1. Norseman-Wiluna belt, Yilgarn Block, Western Australian Shield (see Fig. 6.5); 2. Abitibi belt, Superior Province, Canadian Shield (Langmuir, Alexo, Dundonald, Texmont); 3. Ungava (Cape Smith) nickel belt, Canada; 4. Thompson nickel belt, Manitoba, Canada (see Fig. 6.7); 5. Paramirim craton, Brazil (O'Toole); 6. Rhodesian Craton, Zimbabwe (Empress, Trojan, Damba, Shangani). (b) Deposits hosted in gabbroic intrusives: 7. Bushveld Complex, South Africa (see Fig. 5.4); 8. Great Dyke, Zimbabwe; 9. Phikwe-Selebi, Botswana; 10. Insizwa, Transkei; 11. Jinchuan, PRC; 12. Noril'sk-Talnakh, Russia; 13. Pechanga (Petsamo), Kola Peninsula, Russia; 14. Kotlahti, Finland; 15. Rona, Norway; 16. Moxie and Katahdin, Maine, USA; 17. Duluth Complex, Minnesota, USA; 18. Stillwater Complex, Montana, USA (see Fig. 7.5); 19. Sudbury Complex, Canada (see Fig. 6.9); 20. Voisey's Bay Complex, Canada.

deposits, important examples of Precambrian greenstone belts include those of the Western Australian shield (Yilgarn Block), the Rhodesian craton (Zimbabwe Province), and the Canadian shield (Abitibi belt, Ungava nickel belt, and Thompson nickel belt). Only minor occurrences are known in the Kaapvaal craton in southern Africa (Hammerbeck 1984), the Pilbara Block of the Western Australian shield (Mathison & Marshall 1981), and the Paramirim craton of central Brazil (Brenner et al. 1990). The most important gabbroic intrusions for nickel sulfide deposits are located in Canada (Sudbury Complex), the Siberian Platform (Noril'sk-Talnakh), Kola Peninsula (Pechanga), and PRC (Jinchuan). The large layered intrusions, such as the Bushveld Complex (South Africa), Great Dyke (Zimbabwe), Stillwater Complex (USA), and Duluth Complex (USA), contain enormous low-grade (<0.8% Ni) resources, but only very limited quantities of mineable reserves. The Bushveld Complex alone is estimated to contain about 23 million tonnes of Ni in low-grade resources averaging only 0.35% Ni (von Gruenewaldt 1979), and the estimated resources of the Duluth Complex are in

the order of 12 million tonnes of Ni in mineralized rocks averaging 0.2% Ni (Ross & Travis 1981). The Sudbury Complex is estimated to contain in excess of 1,548 million tonnes of ore (past production + reserves) grading ≈ 1.2 wt% Ni (with Ni:Cu ≈ 1.1), ≈ 0.4 g/t Pt, and ≈ 0.4 g/t Pd (Lightfoot et al. 1997). Other world-class nickel sulfide deposits are those of Noril'sk (900 million tonnes of ore grading 2.7 wt% Ni), Jinchuan (more than 500 million tonnes of ore grading 1.2% Ni and 0.7% Cu), and the recently discovered Voisey's Bay (124 million tonnes of ore grading 1.66 wt% Ni) (Naldrett et al. 1992, Chai & Naldrett 1992, Naldrett 1999).

6.3. Types of Deposits

Insufficient geologic information does not allow classification of many nickel sulfide deposits into the elaborate scheme presented in Table 2.1. According to the simplified scheme adopted here (Table 6.1), nickel sulfide deposits are classified into two principal classes based on the petrology of the host rocks and several subclasses based on the form or geologic environment of the hosting bodies:

- (a) Peridotite-dunite class (komatiitic association)
 - (i) komatiitic peridotite association
 - (ii) komatiitic dunite association
- (b) Gabbroid class (tholeiitic association)
 - (i) intrusive mafic-ultramafic complexes
 - (ii) large layered complexes
 - (iii) the Sudbury Complex

Minor nickel sulfide deposits occur in sulfidic metasediments and quartz-carbonate veins associated with ultramafic bodies (Bavinton 1981, Marston et al. 1981), but they constitute less than 1% of the world's nickel resources. The relative importance of the various subclasses of deposits in terms of original resources of nickel is depicted in Figure 6.2. The gabbroid class deposits contain more than 80% of the nickel resources of both $\geq 0.8\%$ Ni and $< 0.8\%$ Ni categories, and they account for about 75% of the current world nickel production. The Sudbury Complex, considered a subclass by itself because of its unique characteristics, such as a meteorite-impact origin and an unusual abundance of sulfides, has been the leading producer of nickel in the world for a long time and contains about 40% of the original nickel resources with $\geq 0.8\%$ Ni. The large layered complexes account for a mere 0.1% of the $\geq 0.8\%$ Ni resources and contribute $< 5\%$ to the world's annual nickel production, but they contain more than 75% of the low-grade ($< 0.8\%$ Ni) resources of the world. From a long-term perspective, deposits in the gabbroid class constitute the most important resource of Ni, even when the Sudbury Complex is excluded (Ross & Travis 1981).

TABLE 6.1. Types of nickel (-copper) sulfide deposits based on the characteristics of the host rocks

Type of deposit	Nature of mineralization	Ni:Cu	Paleoecctonic setting	Important examples
<i>Peridotite-dunite class (Komatiitic association)</i>				
Komatiitic peridotite association	Thin layers of massive and disseminated sulfide at the base of olivine peridotite flows that are commonly <100 m thick and occur at or near the base of volcanic ultramafic sequences	3 - 27 (typically 10 - 15)	Precambrian (mostly Archean) greenstone belts	Western Australia: Kambalda Scotia Nepean
Komatiitic dunite association	Sulfides as internal low-grade disseminations or as near-contact higher grade concentrations (locally massive) in large bodies of serpentinized dunite	15 - 30 (typically >20)	Precambrian (mostly Archean) greenstone belts	Western Australia: Agnew Mt. Keith Forrestania Canada: Dumont
			Precambrian mobile belts	Canada: Thompson belt Ungava belt
<i>Gabbroid class (Tholeiitic association)</i>				
Intrusive mafic-ultramafic complexes	Sulfides as disseminated or matrix accumulations in the ultramafic rocks, and commonly in breccia zones and pipes in the mafic rocks	<1 - 7 (typically <3)	Precambrian greenstone belts	Western Australia: Carr Boyd Canada: Montcalm
			Precambrian mobile belts	Russia: Pechanga Canada: Lynn Lake PRC: Jinchuan
			Phanerozoic fold belts	Russia: Noril'sk-Talnakh USA: Moxie Norway: Rona
Large layered complexes	Extensive, low-grade, stratiform sulfide mineralization that may include high-grade concentrations of PGE	<1 - 3 (typically <2)	Stable continental platform	South Africa: Bushveld USA: Stillwater Duluth Zimbabwe: Great Dyke
Sudbury complex (Canada)	An unusually large number of deposits of high sulfide concentration in noritic rocks	1 - 3	Stable continental platform	Murray, Levack, Frood (see Fig. 6. 10)

Source of data: Ross & Travis (1981).

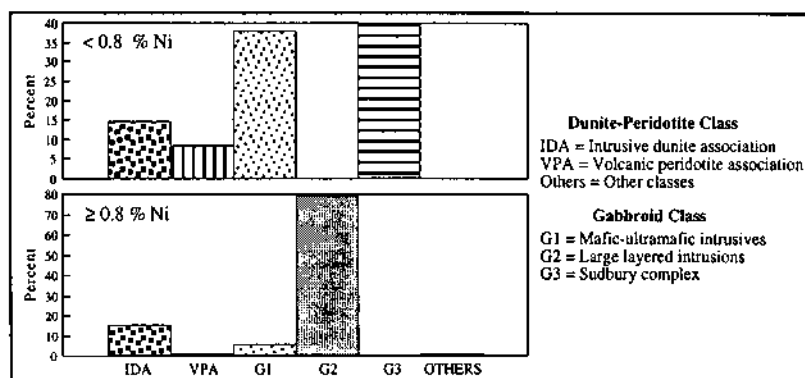


Figure 6.2. The world distribution of original resources of sulfide Ni by deposit type in ores containing $\geq 0.8\%$ Ni and $< 0.8\%$ Ni (source of data: Ross & Travis 1981). The world total of original resources of the two categories are estimated to be 31.74 and 53.04 million tonnes, respectively. The 'volcanic peridotite' and 'intrusive dunite' subclasses are equivalent to the 'komatiitic peridotite' and 'komatiitic dunite' subclasses of the classification scheme adopted here (see Table 6.1).

6.3.1. PERIDOTITE-DUNITE CLASS

Deposits included in the peridotite-dunite class are hosted by synvolcanic komatiite suites of Precambrian, dominantly Archean, greenstone belts. A typical Archean greenstone belt is linear to cusped in form, contains a variety of volcanic and plutonic rocks, volcanoclastic and chemical sedimentary rocks, and is commonly set in a granite-gneiss terrain. The igneous rocks comprise mostly pillow lavas and flows of tholeiitic and komatiitic basalts, with a komatiite sequence at the base of the volcanic pile.

The term *komatiite* was introduced by Viljoen and Viljoen (1969) to describe a new suite of extrusive rocks from greenstone belts of the Barberton Mountain Land in South Africa, ranging from ultramafic (peridotitic) to mafic (basaltic) in composition and characterized by unusually high $\text{CaO}:\text{Al}_2\text{O}_3$ ratios and low abundances of incompatible elements. Arndt and Nisbet (1982) proposed that the term komatiite be used for ultramafic volcanic rocks characterized in part by distinctive spinifex textures of skeletal or platy olivine and MgO contents in excess of 18% (anhydrous basis) corresponding to about 20-35% modal olivine. Donaldson et al. (1986) extended the arbitrary lower limit of 18% MgO to include pyroxenitic komatiites (pyroxene-rich *in situ* differentiates with 15-18% MgO) within some komatiite flows (Fig. 6.3). *Komatiitic basalts* refer to the basaltic rocks of the komatiite suite and represent mafic differentiates of parental ultramafic melts. The basalts often contain pyroxenes or, less commonly, olivines showing spinifex textures, and their chemical characteristics include $<18\%$ MgO, $\text{CaO}:\text{Al}_2\text{O}_3$ ratios greater than 0.8-1.0, low abundances of Ti, Nb, Y, Zr, and depleted light-REE patterns. There is some overlap, however, between low-Mg ($<10\%$

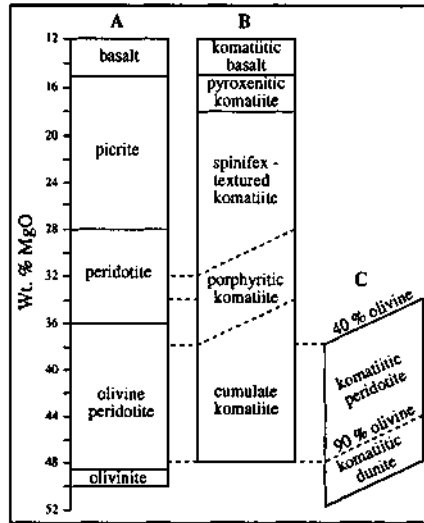


Figure 6.3. Nomenclature of komatiitic rocks in Western Australia: A. Previous nomenclature (Ross & Hopkins 1975, Marston et al. 1981, Gresham and Loftus-Hills 1981); B. and C. Nomenclature proposed by Donaldson et al. (1986). The distinction between B and C is the nature of mesostasis, skeletal in B and poikilitic in C. (After Donaldson et al. 1986.)

12% MgO) komatiitic basalts and high-Mg tholeiitic basalts (Fig. 6.3); the criteria to be used for their geochemical discrimination are still being debated. For the present, the term komatiitic basalt should be restricted to the basaltic rocks that can be shown to be genetically linked to komatiitic ultramafic lavas (Arndt & Nisbet 1982).

Komatiitic host rocks of nickel sulfide deposits have been subjected to varying degrees of deformation, metamorphism, and hydrothermal alteration. It is possible, however, to describe the altered rocks using igneous terminology, because textural preservation is commonly excellent and chemical compositions have not been greatly affected by alteration, except for addition of volatile components and loss of CaO and alkalis in some cases (Marston et al. 1981, Donaldson et al. 1986).

Ross and Travis (1981) recognized two subtypes of the peridotite-dunite class: the volcanic peridotite association and the intrusive dunite association. The two subtypes are designated here as komatiitic peridotite association and komatiitic dunite association, respectively, because the dunite bodies hosting nickel sulfide deposits are not necessarily intrusives. Donaldson et al. (1986) have argued that close similarities in compositions of relict olivine, pyroxene, and chromite from dunitic and peridotitic host rocks, and the compositional and textural similarities between their chilled margins in some cases, indicate origins from similar komatiitic liquids which contained 20-32% MgO. According to their interpretation, the dunites probably represent slowly

cooled lateral stratigraphic equivalents of spinifex-textured komatiites. In fact, many of the dunite bodies in Western Australia, such as that at Agnew (also called the Preservance deposit), previously considered to be intrusives, have been reinterpreted as being integral parts of the extrusive komatiite sequence (Barnes et al. 1988a). Another such example is the mineralized Katiniq "sill", a roughly concordant lenticular body of olivine cumulates in the Cape Smith fold belt of Canada (Barnes & Barnes 1990). The terms peridotite and dunite are used here to denote mineralogic-chemical composition of rocks without any implication regarding their intrusive or extrusive origin.

Nickel sulfide deposits of both subtypes are quite abundant in the greenstone belts (Archean) of the Yilgarn Block, Western Australia (see Fig. 6.5). The important nickel sulfide deposits located in the Archean Abitibi greenstone belt of Canada (Alexo, Dundonald, Langmuir, Texmont) and Zimbabwe Province (Damba district, Shangani, Trojan, Empress) are also of the peridotite-association subtype. Examples of the dunite-association subtype in Canada include the Dumont deposit (Abitibi belt), and deposits of the Thompson nickel belt (see Fig. 6.8) and the Proterozoic Ungava nickel belt located in the Thompson-Wabowden and Cape Smith-Wakeham Bay fold belts, respectively. The general characteristics of the two subtypes summarized below are based largely on the extensively described deposits of Western Australia (Marston et al. 1981, Gresham & Loftus-Hills 1981, Groves & Hudson 1981, Lesher 1989).

Komatiitic Peridotite Association

Nickel sulfide deposits of komatiitic peridotite association (commonly referred to as *Kambalda-type* deposits after their most important occurrence, the Kambalda district in Western Australia) are invariably located within a komatiitic volcanic sequence that is commonly overlain and underlain by komatiitic and tholeiitic metabasalts. The ultramafic sequence is commonly 100 to 600 m thick and is composed of several flow units that can be recognized by chilled contacts, the distribution of spinifex textures, marked mineralogical or compositional changes at unit boundaries, and the presence of flow-top breccia or sulfidic interflow metasediment at unit contacts. Sulfide mineralization is practically restricted to olivine peridotite ($MgO \approx 40\%$) lenses of komatiitic affinity that occur at the base of the komatiitic sequence and represent the most magnesian differentiates of the komatiitic volcanic suites. The host units have been interpreted variously as phenocryst-enriched lava flows (Gresham & Loftus-Hills, 1981), overflowing lava ponds (Naldrett 1973), ponded lava flows (Ussleman et al. 1979), or dynamic lava channels (Lesher et al. 1984, Lesher & Groves 1986, Barnes & Naldrett 1987). As will be discussed later, the interflow sulfidic sediments may have played a major role in the localization of the sulfide ores.

Most of the sulfide mineralization occurs as "contact ore" at or near the base of the lowermost peridotite unit in the ultramafic pile, typically within local depressions ("embayments") in the ultramafic-footwall metabasalt contact. Individual ore shoots are generally less than 5 m in thickness and contain less than 5 million tonnes of ore, with most containing between 0.5 and 2 million tonnes. Characteristic features of these deposits include a consistent vertical zonation with progressively higher concentration

of sulfides toward the base, high grade (commonly 2-4 wt% Ni), and a bulk sulfide Ni:Cu ratio typically in the range of 10 to 15. The deposits of the Ungava nickel belt, hosted by Proterozoic greenstones, have lower Ni:Cu ratios (3.4-4.2) that overlap with some deposits of the gabbroid class, but their geologic environment closely resembles that of komatiitic peridotite-associated deposits (Ross & Travis 1981).

Komatiitic Dunite Association

Nickel sulfide deposits of the komatiitic dunite association occur within discontinuous dunitic (MgO > 45%) lenses or pods along major lineaments up to 200 km in extent. Individual lenses, which may be more than 1,000 m in thickness, appear to be mostly concordant with the country rocks (greenstones). In Western Australia, the dunitic bodies have been interpreted as subconcordant bodies emplaced along major fracture zones, presumably following initial deformation of the greenstone sequences (Binns et al. 1977), or as tectonic slices of original sill-like feeder chambers for the overlying komatiitic volcanics (Naldrett & Turner 1977). However, their similarities with komatiitic peridotites and stratigraphic relationships, such as general conformability with the overlying komatiites and basalts and along-strike gradation into komatiites and komatiitic peridotites, suggest that many komatiitic dunite bodies represent dynamic lava channels (Donaldson et al. 1986, Barnes et al. 1988a, Leshner 1989).

The dunite bodies range from olivinite to olivine peridotite in composition and some appear to be zoned with an olivinite core and olivine peridotite margin. Nickel mineralization typically occurs as disseminated sulfides, mainly in the olivinite cores (e.g., Mt. Keith and Yakabindie deposits), forming interstitial films or lobate to round aggregates, although marginal and more massive sulfides occur in high-grade metamorphic environments. Generally, the larger zones of mineralization are associated with the thickest portions of the largest ultramafic lenses. Compared with peridotite-associated deposits, individual ore lenses are much larger, although commonly of lower grade (mostly 0.4-1% Ni). Bulk sulfide Ni:Cu ratios are also higher, typically >20. Examples include Mt. Keith (\approx 290 million tonnes of ore, average grade 0.6% Ni) and Agnew (\approx 45 million tonnes of ore, average grade 2.05% Ni). The Dumont deposit (Canada) is comparable to the Mt. Keith deposit in terms of nickel resources, but is of much lower grade (0.3% Ni).

6.3.2. GABBROID CLASS

The gabbroid class deposits occur in mafic-ultramafic intrusive complexes, and, compared with the peridotite-dunite class deposits, they are characterized by much lower Ni:Cu ratios (usually <3, rarely >5), lower Ni:Co ratios, and much higher PGE contents (Ross & Travis 1981). These differences are largely the consequence of the lower MgO contents of the tholeiitic parental magmas (Naldrett 1981a), although the influence of other factors (e.g., fS_2 and fO_2) may have been significant and responsible for the overlap in Ni:Cu ratios between the two classes of deposits.

The Sudbury deposits, hosted in noritic rocks of a gabbroic complex, constitute a

distinctive subtype and are described in a later section. The PGE-enriched Ni-sulfide deposits hosted by large layered intrusions will be discussed in Ch. 7.

6.4. Examples

6.4.1. KAMBALDA DISTRICT, WESTERN AUSTRALIA

The greenstone-granitoid terrane of the Yilgarn Block (Western Australia) is subdivided into the Eastern Goldfields, Southern Cross, and Murchison provinces (Fig. 6.4), mainly on the basis of differing structural trends and lithostratigraphic associations. The Kambalda district lies in the Norseman-Wiluna Belt, which forms the western part of the Eastern Goldfields Province. The district contains a high concentration of nickel sulfide deposits of both komatiitic peridotite and komatiitic dunite associations, almost all of them localized in greenstones (Fig. 6.5). With 26 ore shoots (1-4% Ni) and some poorly defined additional bodies of mineralization, the Kambalda district is by far the best known example of komatiitic peridotite-associated nickel sulfide deposits in the world. The district was discovered in 1966, following the recognition of a nickeliferous limonitic gossan. By 1980, the district had produced about 13 million tonnes of ore of 3.15 % Ni and had ore reserves of about 22 million tonnes averaging 3.28 % Ni (Gresham & Loftus-Hills 1981). Virtually all of the subsequent discoveries of nickel sulfide deposits in Western Australia resulted from the correct identification and characterization of gossans.

The geology and genesis of the Kambalda nickel deposits have been discussed in numerous publications. The summary presented here is taken mostly from the published articles by Gresham and Loftus-Hills (1981), Groves and Hudson (1981), Groves et al. (1984), Leshner et al. (1984), and Leshner (1989).

The Kambalda area, complexly folded and faulted by four deformational events, contains two sequences of ultramafic-mafic rocks, which have been metamorphosed to lower amphibolite facies and subjected to varying degrees of hydration (alteration of pyroxenes to tremolite and chlorite, olivine to serpentine), carbonation (talc-dolomite and talc-magnesite assemblages in ultramafic rocks), and late-stage K-metasomatism (replacement of chlorite by biotite). Almost all of the nickel ores are associated with the lower Kambalda sequence. The upper Bluebush sequence contains rocks very similar in chemical and textural characteristics to those of the Kambalda sequence, but contains no significant mineralization.

Nickel ores of the Kambalda district are classified into three broad categories: (a) contact ore; (b) hanging-wall ore; and (c) offset ore. Contact ores, the dominant type of ore in the district, generally occur as ribbonlike bodies (1-5 m in thickness) at or close to the contact between the footwall basalt and the overlying ultramafic sequence, commonly within embayments ('trough structures') at the top of the footwall basalt (Fig. 6.6), but also occasionally on or within a sedimentary layer at this contact or in the lower portion of the ultramafic sequence. The major footwall troughs are from

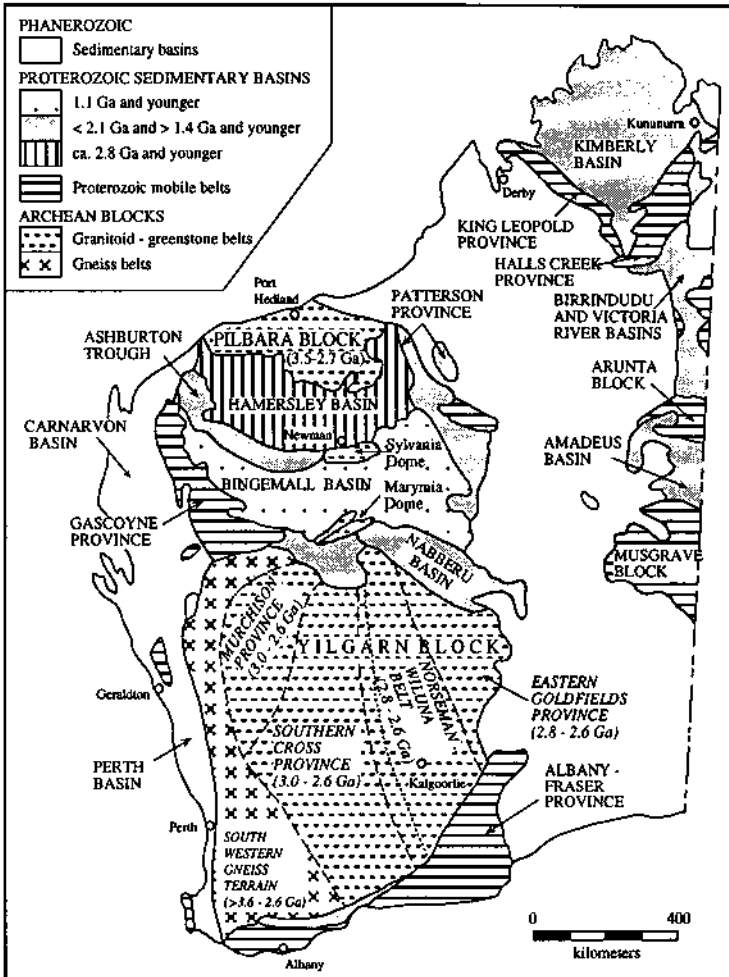


Figure 6.4. Major tectonic units of Western Australia (after Groves et al. 1984, adapted from 1:1,000,000 map of Geological Survey of Western Australia, 1979). Except for very minor occurrences of komatiitic peridotite-associated and gabbroid-associated deposits in the Pilbara Block (Ruthwell, Mt. Sholl), Halls Creek Province (Sally Malay, Keller Creek, Corkwood), and Musgrave Block (Giles complex), the Ni-sulfide deposits of Western Australia are located in the Yilgarn Block, predominantly in the Norseman-Wiluna Belt (see Fig. 6.5).

1,000 to more than 2,300 m in length and generally 150 to 250 m in width. There is an antipathetic relationship between the contact ore and the sulfidic interflow sediments — it is extremely rare to find sediments within the troughs. The embayments probably represent a combination of volcanic topography (Gresham & Loftus-Hills 1981), syn-volcanic faulting (Ross & Hopkins 1975), thermal erosion beneath linear lava channels

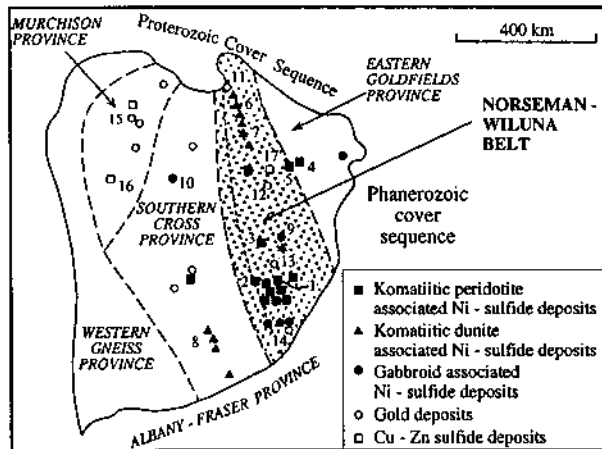


Figure 6.5. Major komatiite-associated Ni (-Cu) sulfide, volcanic-associated Cu-Zn sulfide, and volcanic-hosted gold deposits in the Archean granitoid-greenstone Yilgarn Block, Western Australia. Deposits referred to in the text are numbered. Nickel deposits of (a) komatiitic peridotite association: 1. Kambalda, 2. Nepean, 3. Scotia, 4. Windarra, 5. South Windarra; (b) komatiitic dunite association: 6. Mt. Keith, 7. Agnew, 8. Forrestania; and (c) gabbroid association: 9. Carr Boyd, 10. Youangarra. Gold deposits of mafic-ultramafic association: 11. Wiluna, 12. Sons of Gwalia (Lenora), 13. Kalgoorlie and Golden Mile; 14. Norseman, 15. Silver Bell. Cu-Zn sulfide deposits: 16. Golden Grove, 17. Teutonic Bore.

(Huppert & Sparks 1985), and post-volcanic structural deformation (Cowden 1988). Whatever their origin, the embayments appear to have played a significant role in the localization of the contact ore. Other distinguishing features of the ore environment compared with the non-ore environment in the Kambalda district include: anomalously thick and highly magnesian (36-45 % MgO) basal host units; a relatively "disordered" internal stratigraphy of the ultramafic sequence; and better textural and compositional differentiation in the komatiites. These stratigraphic variations define elongate prisms of rock parallel to and overlying ore shoots, indicating a strong volcanic control on ore localization. The distinctiveness of the ore environment volcanic sequence has been attributed to ponding of lavas adjacent to proximal feeding fissures (Gresham & Loftus-Hills 1981, Gresham 1986) or channelization of lava flows from a distant eruptive site (Leshner et al. 1981, 1984; Cowden 1988, Leshner 1989).

Hanging-wall ores generally occur within 100 m of the footwall basalt-ultramafic contact, are usually stratiform, and in some ore shoots account for significant sulfide concentrations. Offset ores are small bodies of originally contact or hanging-wall ores that have been displaced by faulting or remobilized into fault planes. Although such displaced sulfides are generally minor in amount, they may be rich in pentlandite.

The interflow sedimentary layers contain abundant Fe-sulfides (pyrrhotite and pyrite) and generally less than 0.1% Ni, but nickeliferous equivalents with 0.3% to more than

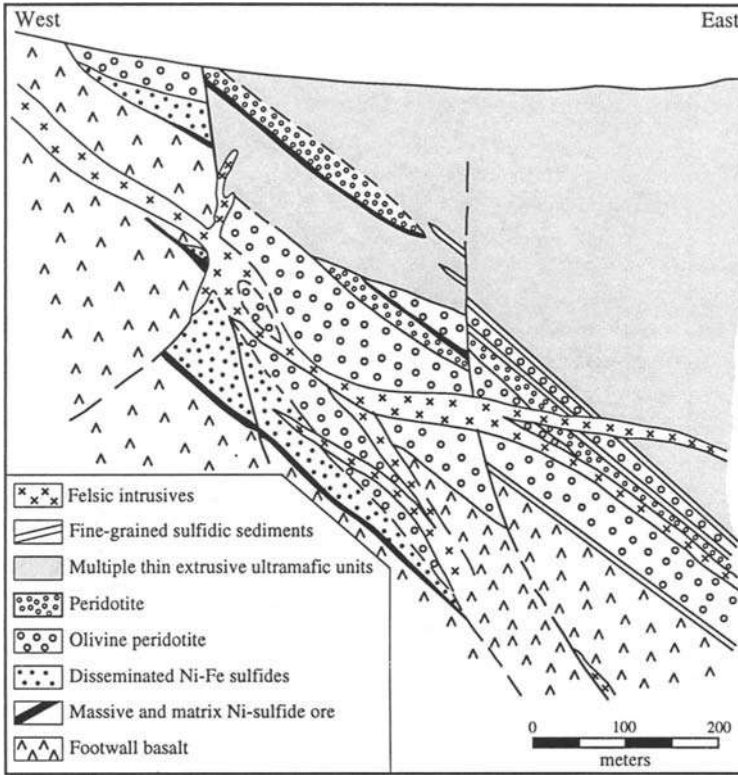


Figure 6.6. Generalized east-west section of the Lunnon Shoot, Kambalda district, showing the distribution of contact (massive and matrix) and hanging-wall (disseminated) nickel sulfide ores in the Kambalda sequence (after Ross & Hopkins 1975). Note the localization of contact ore in a "trough structure" and its antipathetic relationship to sulfidic metasediment.

6% Ni occur locally and ore-grade (>1% Ni) sediments occur only adjacent to massive Fe-Ni-Cu sulfide ore. Nickeliferous sediments have been mined at several locations in the Kambalda district, but collectively they constitute <2% the total Kambalda nickel reserves (Paterson et al. 1984).

Ore zones in Kambalda are generally 1 to 3 m thick and seldom exceed 10 m. In terms of textures, the ores are classified, depending on the sulfide:silicate ratio, as: (a) massive ore (80% or more sulfides); (b) matrix or net-textured ore (40-80% sulfides); and (c) disseminated ore (10-40% sulfides). The average thickness of massive ores, common in contact orebodies, seldom exceeds 1 m, but the thickness may vary from a few centimeters to about 5 m within short distances along contacts, presumably due to deformation and remobilization. The massive ore is often banded, commonly with alternating pyrrhotite-rich and pentlandite-rich bands, and the banding is believed to

have been caused by recrystallization under directed stress (Ewers & Hudson 1972).

Matrix and disseminated ores occur in both contact and hanging-wall orebodies; they commonly lack planar or linear fabrics. Triangular-textured matrix ore, consisting of an interlocking three-dimensional framework of metamorphic olivine (subsequently retrograded to serpentine) in sulfide matrix, occurs in some highly metamorphosed deposits (e.g. Nepean).

Sequential layering of massive, matrix, and disseminated ores, as observed in the Lunnon Shoot (Fig. 6.6), is quite rare (Ewers & Hudson, 1972). Whereas massive sulfides often underlie more disseminated sulfides, there is considerable variation in ore sequences within and among deposits in the district.

6.4.2. THOMPSON NICKEL BELT, MANITOBA, CANADA

The Thompson belt is a linear, fault-bounded, NE-trending tectonic feature located at the juncture of the Superior Province (last regional metamorphism 2.5 Ga.) and the Churchill Province (last regional metamorphism 1.8 Ga.) in north-central Manitoba (Fig. 6.7). The rocks of the belt are Archean in age (2.8 Ga; Cranstone & Turek 1976) and have experienced the Hudsonian tectonic event (1.8 Ga).

The belt is comprised largely of migmatitic gneisses, metasedimentary, metavolcanic, and ultramafic rocks, and felsic plutons (Peredery 1979, Peredery & Geological Staff 1982). The metavolcanic pile, which appears to be coeval with the metasediments and to overlie the gneisses, consists mostly of pillowed and massive metabasaltic flows of komatiitic affinity (up to 11% MgO and <1% TiO₂). Closely associated with these metabasalts are more magnesian, komatiitic metabasalts (12-15% MgO, <1% TiO₂) with relict quench textures and minor ultramafic flows (about 19% MgO, <1% TiO₂). The ultramafic rocks are divided into two groups: serpentinites, and ultramafic amphibolites (metapicrites). The serpentinites range in composition from dunite through peridotite to pyroxenite, the ultramafic amphibolites from picrite to pyroxenite and include minor peridotitic components. Most of the ultramafic rocks are located in a zone about 6 km wide along the western margin of the belt and they occur as tabular or lenticular concordant bodies in the gneisses, and metasedimentary and metavolcanic rocks. The largest bodies of ultramafic rocks, mostly serpentinites, are found within the metasedimentary rocks. Most of the ultramafic bodies were probably emplaced originally as sills and were involved, along with the metasedimentary and metavolcanic host rocks, in the Hudsonian folding event.

The ultramafic and mafic rocks of the belt show chemical trends similar to those shown by most komatiite suites and, therefore, are interpreted as komatiites and komatiitic basalts (Peredery 1979, Paktunc 1984). According to Paktunc (1984), the petrogenesis of the ultramafic-mafic suite can be explained by a combination of (a) high degrees of partial melting of mantle material with chondritic abundances of CaO, Al₂O₃, and TiO₂, producing a komatiitic melt and (b) low-pressure olivine and pyroxene fractionation after emplacement of the melt.

Nickel sulfide deposits of the belt are genetically related to the serpentinites (the



Figure 6.7. Regional geology of the Thompson nickel belt with locations of important komatiite-hosted Ni-sulfide deposits (after Paktunc 1984, simplified from the Geological Map of Manitoba, Manitoba Mineral Resources Division, 1979).

ultramafic amphibolites do not carry significant sulfide mineralization), but their present spatial distribution is largely the result of remobilization during the long and complex tectonic history of the Thompson belt (Peredery & Geological Staff 1982). About 75% of all known nickel (predominantly as nickel sulfides) in the belt is directly associated with serpentinites; the remaining 25% occurs in metasedimentary rocks and gneisses. For example, the mineralization in the Moak Lake deposit is entirely confined to serpentinites, whereas the Thompson deposit is believed to represent the extreme case where extensive remobilization (perhaps in the order of several kilometers) has localized much of the ore along pelitic members of the metasedimentary sequence (Fig. 6.8). Some deposits (e.g., Pipe 2) contain both kinds of sulfide mineralization.

Sulfides directly associated with the serpentinite bodies may be classified into 6 types (Peredery & Geological Staff 1982): (a) primary interstitial sulfides; (b) sulfide veins, which range from a few millimeters to a meter in thickness and locally constitute the ore (e.g., Pipe 2 mine); (c) sulfide breccia, consisting of serpentinite and/or other host rocks in a sulfide matrix (the bulk of the ore at Pipe 2 open-pit mine);

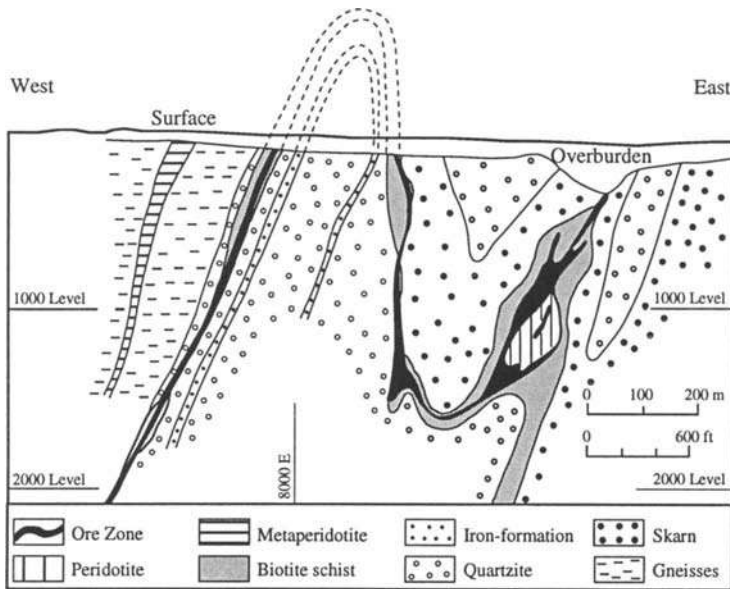


Figure 6.8. Vertical section of the Thompson nickel sulfide deposit, Thompson nickel belt, Manitoba (after Zurbriggen 1963). Note the localization of ore, which contains numerous blocks of serpentinite (up to tens of meters in diameter) within the biotite schist and at the schist-peridotite contact, and the small amount of ultramafic rock relative to the sulfide ore.

(d) massive sulfides, which occur at variable positions within serpentinite bodies due to varying degree of deformation but, in the extreme case, may be completely detached from serpentinite bodies; (e) dust-like disseminated sulfides, probably a byproduct of serpentinitization of Ni-bearing silicates; and (f) interstitial spinifexoid sulfides, which refers to a particular type of mineralization characterized by sulfides interstitial to very coarse-grained, lath-like to lozenge-shaped crystals of olivine. Much of the ore in the pelitic rocks belongs to the categories of massive sulfides and sulfide breccia (locally called "inclusion-bearing sulfides") described above; a small proportion occurs as sulfide stringers commonly oriented parallel to the schistosity.

The sulfides are composed of hexagonal and monoclinic pyrrhotite, pentlandite, minor chalcopyrite and cubanite, traces of sphalerite, small amounts of niccolite and other Ni-Co-Fe arsenide minerals, and alteration products such as violarite. The sulfides were metamorphosed and deformed during the Hudsonian orogeny. The effects attributed to this tectonic event include metamorphic banding between pentlandite-rich and pyrrhotite-rich layers, folding of sulfide-rich layers, mobilization of pentlandite-rich sulfides to the noses of fold structures with concomitant enrichment in nickel, and large-scale mobilization of sulfides.

6.4.3. SUDBURY COMPLEX, ONTARIO, CANADA

Since the construction of the Canadian Pacific Railway led to the discovery of Ni-Cu mineralization near the present city of Sudbury in 1833, the Sudbury Complex has remained a focal point of geologic studies in Canada, primarily because of its abundant Ni-Cu ores but also because of the likely meteorite-impact origin of the Sudbury structure. Much of the available information on the Sudbury structure and its mineral deposits has been reviewed in a treatise edited by Pye et al. (1984); the reader is referred particularly to the excellent synthesis by Naldrett (1984a) which is the main source of the summary presented below.

The Sudbury Complex (1.85 Ga) is a large, differentiated intrusive body that straddles the erosional boundary between the Archean Levack Gneiss Complex (2.71 Ga) to the north and the early Proterozoic Huronian Supergroup (clastic and minor chemical sediments, mafic and felsic volcanics) to the south (Fig. 6.9). A notable feature of the footwall rocks is the Sudbury Breccia that occurs as dikes and irregular bodies cutting all rocks older than the Complex up to a distance of 25 km from its outer contact. The Breccia has been interpreted as a product of the meteorite impact that initiated the Sudbury structure. The Complex is overlain by the Whitewater Group comprising the Onaping, Onwatin, and Chelmsford Formations. The Onaping Formation, the lowest formation of this Group, consists of 1,800 m of breccias which have been interpreted as a series of pyroclastic and ash flows, or the result of fall-back after meteorite impact. Correlatives of the Whitewater Group have not been found outside the Sudbury basin. The Whitewater Group contains some minor, uneconomic mineralization — disseminated sulfides in the Onaping Formation and base metals (\pm Au, Ag) in the Onwatin Formation — which is unrelated to the Ni-Cu mineralization in the Sudbury Complex and will not be discussed further.

The Main Mass of the Complex, also referred to as the Sudbury Igneous Complex (SIC), is attributed to multiple magma injections and fractional crystallization. It consists of three zones (Fig. 6.9): a lower zone, predominantly of norites (mafic norite, felsic norite, quartz-rich norite); a middle zone composed of quartz-rich gabbro; and an upper zone composed of granophyre. The Ni-Cu ores occur around the margin of the Complex, associated with a group of norites, gabbros and quartz diorites collectively known as the *sublayer*. Variants of this discontinuous unit include the *contact sublayer* that occurs close to the outer contact of the Main Mass of the Complex and *offsets* that occur as dikes of quartz diorite composition radiating outward from the Complex. Whether the sublayer is younger or older than the Main Mass is not clear from field relations, but REE profiles and olivine compositions suggest that the sublayer and the Main Mass norites are genetically related.

Following the suggestion of Dietz (1964), there is widespread, although not unanimous, support in favor of the hypothesis that the Sudbury Structure resulted from a hypervelocity meteorite impact that also triggered the Sudbury magmatism by pressure-release partial melting of the underlying material. The main arguments for an impact origin rest primarily on the recognition of shock features in the Sudbury area:

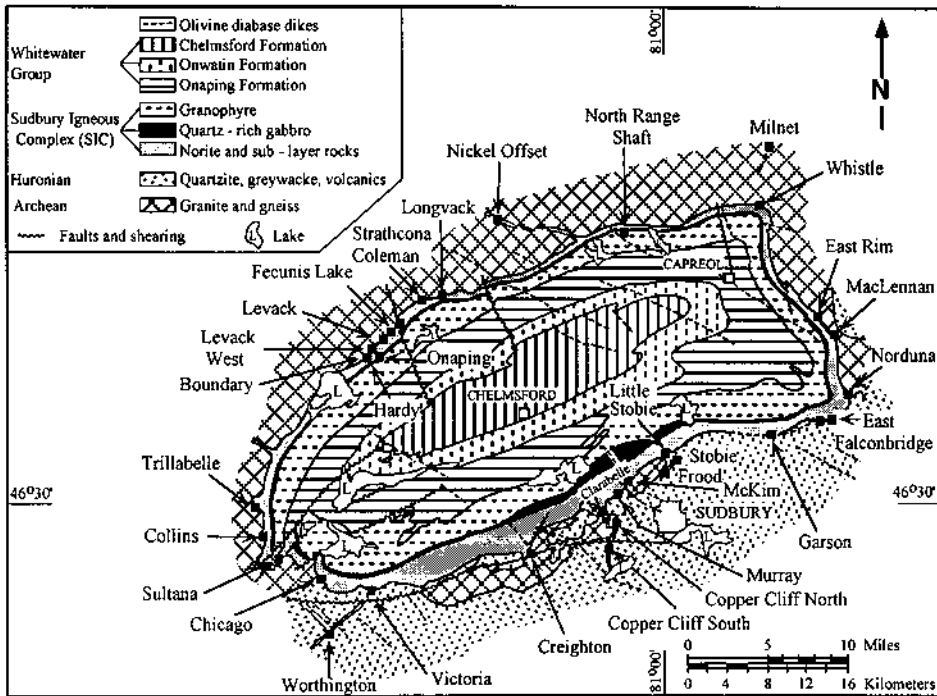


Figure 6.9. Geologic map of the Sudbury district, Canada. All the Ni-Cu ore deposits are located in the sublayer of the Sudbury Complex. (Sources of data: Cabri & Laflamme 1976, Innes & Colvine 1984, and Naldrett 1989.)

shatter cones in the country rocks, melt bodies in the basal member of the Onaping Formation, and shock-deformed quartz and plagioclase in the Sudbury Breccia. Also, Nd-Sm isotopic data on whole rocks and minerals of the Sudbury Complex and REE patterns of Sudbury rocks suggest that the Complex formed from melts generated in the upper crust and are consistent with a meteorite impact origin (Faggart et al. 1985). Lightfoot et al. (1997) have shown that the rocks of the SIC have similar ratios of the highly incompatible trace elements (e.g., La/Sm = 4.5-7, La/Nb = 2.8-4.2, Th/Zr = 0.04-0.05) and that these values are consistent with the crystallization and differentiation of magma types largely (>80%) derived from the upper crust, with a small contribution of mantle-derived picritic magma emplaced along crustal fractures produced by the impact event. A mantle contribution is required to account for the abundant Ni, Cu, and PGE in the Sudbury deposits, as well as the magnesian compositions of the mafic norite and the sublayer, and a maximum of 20% mantle contribution of primitive picritic magma can be accommodated without changing the ratios of the incompatible trace elements. Features inconsistent with an impact origin and favoring an endogenic origin include the following: (a) available structural and

paleomagnetic data suggest that the Sudbury Structure was never circular in shape; (b) the location of the Sudbury structure at the junction of three major tectonic provinces (Grenville, Superior, and Southern) and its spatial relationship to other tectonic features such as the Onaping Fault System and the Ottawa-Bonnechere graben suggest that it may be a crustal feature; and (c) the shock features found at Sudbury are also associated with the Vredefort structure in the Witwatersrand basin of South Africa which may not be of meteorite-impact origin. Fleet and Barnett (1978) have argued that the so called shatter cones are actually conical fractures formed by metamorphism and deformation after the emplacement of the Sudbury igneous body.

Ni-Cu ore deposits of the Complex are of two main types: (a) marginal (or contact) deposits that occur near the contact of the Sublayer with the footwall; and (b) offset deposits that occur as dike-like offsets of the sublayer extending several kilometers away from the Complex into the footwall. The marginal deposits of the South Range, of which the Murray mine is a typical example (Fig. 6.10A), are generally zoned from inclusion-rich massive ore at the footwall contact to disseminated sulfide ore toward the hanging-wall. In the marginal deposits of the North Range, massive and disseminated mineralization occurs mainly within brecciated footwall rocks (Footwall Breccia), often in trough-like structures (embayments), and as fracture-controlled massive stringers in country rocks underlying the breccias. The Levack deposit (Fig. 6.10B) is a good example of the control of embayments on mineralization. The embayments, filled with sublayer rocks, occur at irregular intervals along the norite contact and may represent slump terraces along the crater wall (Morrison 1984). In offset deposits, the sulfides generally form steeply plunging, lenslike pods of massive and interstitial ore containing a high proportion of inclusions. The Frood deposit (Fig. 6.10C), the largest of the offset deposits, is unusual in that it lies parallel to the southern contact of the Complex (Fig. 6.9).

In addition to its likely meteorite-impact origin and the presence of a large number of occurrences of very concentrated sulfide mineralization, the Sudbury Complex differs from other layered complexes in a number of significant ways. These include the absence of stratiform chromite and PGE deposits, the absence of cyclic units, and the lack of ultramafic rocks, although recent gravity and magnetic studies (Gupta et al. 1984) suggest that the Sudbury Structure is underlain at a depth of 5-8 km by partly serpentinized mafic-ultramafic rocks 3-4 km in maximum thickness. Another notable feature of the Sudbury Complex is the unusually siliceous composition of the source magma for its state of fractionation, as evidenced by the Mg:(Mg+Fe) ratios of the pyroxenes in the differentiates. The silica enrichment is believed to be a consequence of assimilation of more siliceous rocks by the magma, probably by mixing with a felsic crustal melt resulting from meteorite impact, and the cause of its sulfur saturation that led to segregation of immiscible sulfides (Naldrett & MacDonald 1980). The crustal contamination hypothesis is supported by: (a) the high percentage of normative quartz, coexisting with pyroxenes and plagioclase whose compositions are relatively primitive, reflecting little differentiation; (b) numerous, partially digested inclusions in the host rocks; (c) the relatively high initial $^{87}\text{Sr}/^{86}\text{Sr}$ ratio (0.706) of the noritic host rock

(Gibbins & McNutt 1975); (d) the Sm-Nd isotopic ratios and REE concentration patterns of Sudbury rocks (Naldrett 1984, Faggart et al. 1985); and (e) Re-Os isotope ratios of Sudbury sulfide ore samples (Walker et al. 1991).

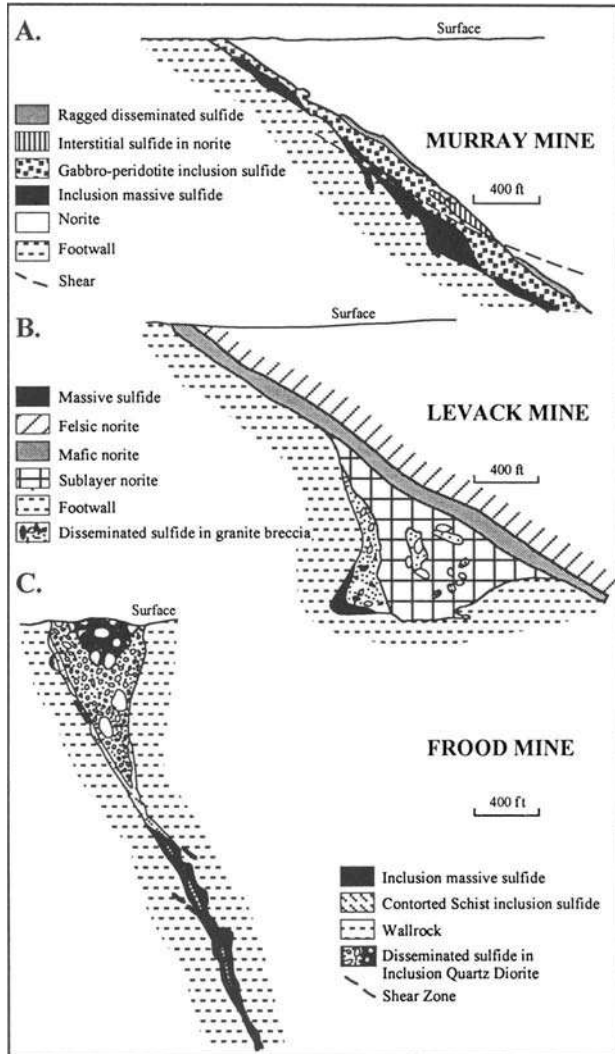


Figure 6.10. Generalized sections of selected Ni-Cu sulfide deposits of the Sudbury Complex: a. Murray mine, South Range (looking west); b. Levack mine, North Range (looking east); and c. Frood mine, Frood-Stobie offset (looking southwest). (After Souch et al. 1969.)

6.5. Ore Composition

6.5.1. MINERALOGY

A large number of sulfide, oxide, telluride, and sulfosalt minerals and native elements have been identified in nickel sulfide ores (Hawley 1962, Groves & Hudson 1981). Most ores are dominated by some combination of pyrrhotite, pentlandite, chalcopyrite, pyrite, and magnetite, all with compositions typical of low-temperature equilibration (see Fig. 3.5). Pentlandite is by far the most important nickel mineral of all sulfide ores; other nickel sulfide minerals, some of which may occur in significant amounts locally, include millerite, hazlewoodite, godlevskite, polydymite, and violarite.

Pyrrhotites of nickel sulfide ores typically contain <1% (Ni+Co). Monoclinic pyrrhotite (Fe_7S_8) is generally dominant in pyrite-rich ores, although the disequilibrium assemblage containing both monoclinic pyrrhotite and hexagonal pyrrhotite (Fe_9S_{10}) along with pyrite and pentlandite is not uncommon. The Fe:Ni ratio of pentlandites varies widely depending on the Fe-Ni sulfide equilibrium assemblage (Misra & Fleet 1973), the latter being a function of the bulk sulfide composition and the temperature of equilibration (see Fig. 3.5). Despite the relatively low Co contents of most pentlandites (<1% Co), they contain the bulk of the Co in the sulfide ores.

Chalcopyrite is a common constituent of nickel sulfide ores, especially of the gabbroid class. As the solid solution of Cu affects the thermal stability of pentlandite and $\text{Fe}_{1-x}\text{S}-\text{Ni}_{1-x}\text{S}$ solid solution (*mss*), a rigorous treatment of the sulfide mineralogy of nickel deposits should be based on phase equilibria in the quaternary Fe-Ni-Cu-S system. The estimated primary chalcopyrite-free bulk compositions of most nickel sulfide ores, however, lie within the *mss* field at 600°C in the Fe-Ni-S system (Naldrett & Kullerud 1967, Groves & Hudson 1981, Naldrett 1989) and the sulfide mineralogy of the nickel sulfide ores can be adequately explained in terms of lower temperature phase relations in the Fe-Ni-S system (see Fig. 3.5). The *mss* at 600°C may contain significant amount of Cu in solid solution, resulting in the crystallization of chalcopyrite at lower temperatures (Craig & Kullerud 1969). For example, chalcopyrite would start crystallizing at about 450°C from *mss* containing 1.5 wt.% Cu, a situation applicable to many nickel sulfide ores.

Ferrochromites, usually with magnetite rims, occur in most Western Australian komatiite-associated ores (Groves et al. 1977) and have also been reported from gabbroid class deposits such as LaPerouse, Alaska (Czamanske et al. 1976) and Insizwa, southern Africa (Groves & Hudson 1981). The experimental demonstration of the solubility of Cr in sulfide melts and the crystallization of chromite euhedra with magnetite rims similar to those of natural ores (Ewers et al. 1976), combined with the restriction of ferrochromite to the sulfide fraction of nickel ores in many deposits, are considered to be strong evidence for ferrochromite crystallization from oxy-sulfide liquids during the formation of nickel ores. Woolrich et al. (1981) proposed that the ferrochromite crystallized at the magmatic stage on interfaces between layers of different sulfide content in response to gradients in $f\text{O}_2$.

Ni- and Fe-sulfide minerals are unstable in the presence of oxygen or oxygenated groundwater, and rapidly oxidize to secondary or supergene sulfide minerals and finally to iron oxides and hydroxides. A common sulfide mineral of the supergene zone is violarite which readily, and often pseudomorphically, replaces pentlandite; alteration of millerite and pyrrhotite to violarite has also been reported (Nickel et al. 1974, Misra & Fleet 1974).

6.5.2. BULK COMPOSITION

Naldrett (1981a, 1989) has presented an elaborate discussion of the bulk compositional characteristics of nickel sulfide ores of various associations. Some generalized conclusions for unaltered ores are summarized below:

- (a) Average ore compositions of most deposits plot within or close to the *mss* field at 600°C in the Fe-Ni-S system consistent with a magmatic origin, although individual samples show appreciable scatter owing to variable degrees of magmatic fractionation and metamorphic modification. The narrow range of metal:sulfur ratio and the small proportion of magnetite (mostly <10 modal%; Doyle & Naldrett 1987) in the magmatic ores are attributable to the limited variation in the FeO content of most mafic and ultramafic magmas and the low oxygen content (<5 wt%) of the immiscible sulfide liquid segregating from such magmas.
- (b) Deposits hosted in ultramafic (komatiitic) rocks generally have higher Ni:Cu ratios than those hosted in gabbroic rocks, a reflection of the higher Ni:Cu ratios of ultramafic magmas (Fig. 6.11a). For example, estimated metal concentrations typical of Archean komatiitic magmas containing 27 wt% MgO are 1,500 ppm Ni, 50 ppm Cu, 75 ppm Co, 5 ppb Pt, and 7.5 ppb Pd; those for the Sudbury source magma are 240 ppm Ni, 169 ppm Cu, 22 ppm Co, and 2.5 ppb Pd. The relatively higher Cu contents of deposits in gabbroic intrusions associated with flood basalts may be attributed to generation of the host magmas by partial melting of pristine (previously unmelted), subcontinental mantle, complete removal of the sulfide present in the source, and fractional crystallization of host magmas (Naldrett & Barnes 1986).
- (c) There is a negative correlation between Pt:(Pt+Pd) and Cu:(Cu+Ni) ratios in the sulfide ores associated with tholeiitic magmas (Fig. 6.11b). The trend of increasing Cu:(Cu+Ni) ratios with decreasing Pt:(Pt+Pd) ratios is believed to reflect progressive differentiation of the host silicate magma. Ores associated with komatiitic magmas are the exception to this trend.
- (d) Some redistribution of metals in ores is attributable to diffusion in response to a thermal gradient (Naldrett & Kullerud 1967, Hoffman et al. 1979). Much of the variations in Ni, Cu, Co, Pt, and Pd contents of unaltered nickel sulfide ores of various associations, however, may be modeled in

terms of the initial concentrations of metals in the parent magmas of basaltic or komatiitic compositions controlled by partial melting processes, progressive fractional crystallization of parent magmas of basaltic or komatiitic compositions, and fluid dynamics of the system, coupled with equilibration with immiscible sulfide melts at different ratios of silicate magma to sulfide melt (R factor) and appropriate sulfide-silicate partition coefficients (see Eqn. 2.6). The precise values of the partition coefficients would depend on a number of factors, such as temperature, pressure, bulk composition, and perhaps fO_2 : fS_2 ; the values preferred by Naldrett (1989) are listed in Table 6.2. The apparent success of such modeling is considered a strong evidence in favor of the origin of komatiitic and gabbroic nickel sulfide deposits due to sulfide immiscibility in mafic magmas (Naldrett 1979, 1981a, Naldrett & Duke 1980, Lesher et al. 1981, Naldrett et al. 1984, Lesher & Campbell 1993). Large variations in the Ni tenors of orebodies in the Kambalda district, hosted by komatiites of similar composition and occurring in identical tectonic and metamorphic settings, have been attributed to fO_2 variations in the silicate-sulfide system, either prior to eruption (Cowden & Woolrich 1987) or during emplacement by assimilation of hydrous sediments (Lesher 1989).

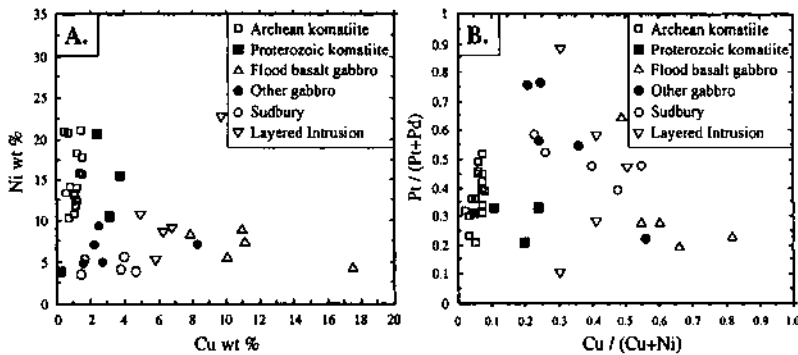


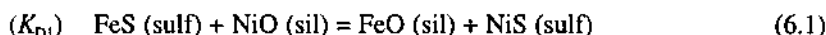
Figure 6.11. Compositions of Ni-sulfide ores (normalized to 100% sulfide) of different associations (simplified from Naldrett 1981): a. Ni vs. Cu; b. Pt/(Pt + Pd) vs. Cu/(Cu + Ni). Compositional fields: Archean komatiites (Western Australia, Canada, Zimbabwe), excluding altered, Ni-enriched deposits; Proterozoic komatiites (Ungava and Thompson belts, Canada); Gabbroic bodies related to flood basalts (Talnakh, Noril'sk, Duluth Complex, Insizwa, Great Lakes); Other gabbroic bodies (Montcalm, Espedalen, Kanichee, Pechanga, Kenbridge); Sudbury Complex (Levack West, Little Stobie 1 and 2, Strathcona, Falconbridge); Layered Intrusions (Merensky Reef, Platereef, J-M Reef - see Ch. 7). (Sources of data: Naldrett and Barnes 1986, Naldrett 1989.)

TABLE 6.2. Sulfide melt-silicate melt partition coefficients preferred by Naldrett (1989)

	Ni	Cu	Co	Pt	Pd
Komatitic magma					
27 wt % MgO	100	250	40	10 ⁵	10 ⁵
19 wt % MgO	175	250	58	10 ⁵	10 ⁵
Basaltic magma	275	250	80	10 ⁵	10 ⁵

6.5.3. NICKEL CONTENT OF THE ASSOCIATED OLIVINE

For a mafic silicate magma saturated with sulfur and crystallizing olivine as a liquidus phase, the equilibrium partitioning of Ni among the three coexisting phases — silicate liquid (sil), olivine (ol), and immiscible Fe_{1-x}-Ni_{1-x} monosulfide liquid (sulf) — is best represented by Ni-Fe exchange reactions between pairs of phases, resulting in three interrelated equilibrium constants: K_{D1} (sulf-sil), K_{D2} (ol-sil), and K_{D3} (ol-sulf):



Owing to the complex chemistry of natural silicate liquids and the reactivity of sulfide and many silicate phases at subsolidus temperatures, only K_{D3} (ol-sulf) may provide a suitable test for the existence of early magmatic immiscible sulfide liquids in mafic magmas (Fleet et al. 1977, 1981).

Assuming ideal solutions, so that concentrations can be expressed as mole fractions (X_i) instead of activities, K_{D3} can be written as:

$$K_{D3} = \frac{(X_{\text{NiS}}^{\text{sulf}})(X_{\text{FeSi}_{0.5}\text{O}_2}^{\text{ol}})}{(X_{\text{FeS}}^{\text{sulf}})(X_{\text{NiSi}_{0.5}\text{O}_2}^{\text{ol}})} = \frac{K_{D1}}{K_{D2}} \quad (6.4)$$

which can be further simplified to

$$K_{D3} = \frac{(\text{Ni/Fe})_{\text{sulfide}}}{(\text{Ni/Fe})_{\text{olivine}}} \quad (6.5)$$

The bulk Ni:Fe ratio of a sulfide ore can be estimated under certain assumptions (Naldrett 1981a, Thompson et al. 1984), and the Ni:Fe ratio of the associated olivine

can be obtained from electron microprobe analysis. Thus, the above relationship should provide, in principle, a thermodynamic test for sulfide immiscibility. The Ni:Fe ratio of olivine formed in equilibrium with a sulfide ore of immiscibility origin should be close to that calculated from the above relationship, provided the value of K_{D3} corresponding to the temperature (and other conditions) of equilibration is known.

There is, however, considerable controversy regarding the 'correct' value of K_{D3} . Values of K_{D3} determined from direct olivine-sulfide equilibration experiments at 900°-1,400°C range from 8 to 38 and values deduced from natural assemblages range from 5 to 63 (Table 6.3). The 'correct' value of K_{D3} has become one of the key arguments both in favor of and against the validity of the magmatic segregation hypothesis for the origin of Ni-Cu-PGE sulfide ores (e.g., Fleet 1979, 1986, Naldrett 1979, 1981a, Fleet & MacRae 1983, 1987, Naldrett et al. 1984, Barnes & Naldrett 1986a, Naldrett 1989). Boctor (1981, 1982) investigated the partitioning of Ni between Mg-rich olivine (Fo 82-87) and Fe-Ni monosulfide liquid under controlled fO_2 and fS_2 conditions and concluded that K_{D3} was essentially independent of fS_2 , but varied inversely with temperature and fO_2 (Table 6.3). Although K_{D3} , as defined by equation 6.3, is independent of fO_2 and fS_2 , Doyle and Naldrett (1987) suggested that K_{D3} would be sensitive to the $fO_2:fS_2$ ratio, or the O:(O+S) ratio, of the sulfide liquid, because the ideality of the sulfide liquid is strongly affected by its dissolved oxygen content. They noted that a sulfide melt with a molar O:(O+S) ratio of 0.67 would reduce K_{D3} from 30 for the oxide-free liquid to 8 and thus offer a possible explanation for Boctor's (1982) K_D value of 8.2 for 1,400°C, $fO_2 = 10^{-8}$, $fS_2 = 10^{-2.9}$. Fleet and MacRae (1987) pointed out that molar O:(O+S) ratio of 0.67 is equivalent to the presence of about 60 modal% magnetite in the quenched sulfide-oxide liquid and Boctor (1982) would not have failed to notice such a large quantity of magnetite in his quenched products. Combining their earlier data with additional experiments, Fleet and MacRae (1987) have concluded that K_{D3} is essentially constant at about 30 to 35 in the temperature range 900° to 1,400°C for olivine composition FO_{97} to FO_{91} , monosulfide solid solution composition containing up to 70 mole% NiS, and a wide range of fO_2 and fS_2 . On the other hand, numerical modeling of the observed compositional variations in the West Australian komatiite-hosted ores appears to be consistent with a decrease in D_{Ni} with increasing $fO_2:fS_2$ ratio (Leshar & Campbell 1993), which is in accord with the thermodynamic prediction of Peach and Mathez (1993) that D_{Ni} would decrease nearly an order of magnitude per two orders of magnitude increase in $fO_2:fS_2$ ratio.

Values of K_{D3} determined from natural assemblages have not helped to resolve the controversy. Pederson (1979) calculated a K_{D3} value of 63 for a natural sulfide assemblage, equilibrated at 1,200°C and extremely reducing condition ($fO_2 = 10^{-12}$ to 10^{-13}), from a chilled dike in Greenland, and attributed the unusually high K_{D3} to the excess metal component in the quenched immiscible sulfide melt. The corrected value, corresponding to stoichiometric monosulfide solution, is given by Fleet (1986) as 35. Excluding this and the highly variable values for the Babbitt deposit (Duluth Complex), the calculated and K_{D3} values for natural assemblages range from about 5 to 25 (Table 6.3). The values seem to fall into two groups: one with values in the range

TABLE 6.3. K_{D3} (olivine-sulfide) values for Ni partitioning between sulfide melt (*mss*) and olivine*Experimental Data*

Reference	Temperature (°C)	Olivine mole % Fo	<i>mss</i> mole % NiS	log f_{O_2}	K_{D3}
Clark and Naldrett (1972)	900	0	-4 - 28	QFM	33.2 ± 3.4
Fleet et al. (1977)	1,160	84	20 - 48	≈QFM	35 ± 3
	1,050	83	28	≈QFM	29
Boctor (1981)	1,400	82 - 87		-9.0	13.4 ± 1.4
Boctor (1982)	1,400	82 - 87		-8.0	8.2 ± 0.6
	1,300	82 - 87		-9.0	18.7 ± 0.8
	1,300	82 - 87		-9.0	18.8 ± 1.4
Fleet and MacRae (1983)		96 - 97		≈F, W	27.7 ± 3.5
Fleet and MacRae (1987)	1,200	94 - 96	29 - 59	?	25 - 27
	1,300	94 - 98	29 - 70	?	25 - 30
	1,385	92 - 96	16 - 70	-8.8	30 - 38
	1,390	94 - 96	49 - 51	-8.9	32 - 34

Natural Samples

Reference	Deposit	Olivine mole % Fo	Olivine wt % NiO	K_{D3} Mean (std. dev.)
Thompson et al. (1984)	Moxie	72 - 85	0.02 - 0.09	8.3 (3.1)
	Katabhdin	74 - 80	0.01 - 0.02	5.0 (1.7)
	Stillwater	71 - 79	0.34 - 0.56	11.4 (4.8)
	Dumont	89 - 93	0.16 - 0.53	10.8 (2.3)
Ripley and Alawi (1986)	Duluth (Babbitt)	23 - 57	0.04 - 0.20	2.6 - 39.6
Fleet and MacRae (1983)	Great Lakes	-65	0.18	8.2
	Duluth (Water Hen)	-65	0.25	5.9
	Renzy Lake	-85	0.10	21.6 (3.4)
Binns and Groves (1976)	Agnew	89 - 93	0.07 - 0.34	23.9 (1.0)

QFM = Silica phase - fayalite - magnetite buffer; F, W = fayalite or wüstite field; *mss* = monosulfide ($Fe_{1-x}Ni_x$) solid solution.

20-25 for deposits metamorphosed to upper amphibolite or granulite facies (Agnew and Renzy Lake), the other with values in the range 5-12 for deposits at low to moderate grade of metamorphism (Dumont, Stillwater, Great Lakes, and Water Hen). If the experimental data of Boctor (1981, 1982) are correct and K_{D3} varies inversely with

temperature, K_{D3} values at the lower end of the spectrum may represent sulfide-olivine equilibration essentially under igneous conditions, and high K_{D3} values equilibration at metamorphic rather than magmatic temperatures (Thompson et al. 1984, Barnes and Naldrett 1986, Naldrett 1989). On the other hand, if K_{D3} values are in the order of 30, the discrepancies shown by the low-grade natural assemblages may be attributed to a lack of chemical equilibration of olivine with sulfides, suggesting that the nickel sulfide ores were not concentrated by magmatic crystallization but were introduced into the host rocks at subsolidus temperatures (Fleet & MacRae 1983, 1987).

6.6. Hydrothermal Alteration and Metamorphism

The ultramafic host rocks of Ni-sulfide deposits are almost always partly or completely altered to serpentine, talc, amphibole, chlorite and/or carbonate minerals. Kilburn et al (1969) have illustrated that the sulfide-silicate textural relationships in disseminated sulfides undergo progressive modification with increased serpentinization, from a primary matrix texture in which the primary silicate minerals (olivine, pyroxene) are embedded in an almost continuous sulfide matrix to a sulfide-serpentine intergrowth texture controlled by the crystallographic directions of the intergrown minerals. Serpentinizing fluids may contain small amounts of sulfur, producing some sulfides in previously barren ultramafic rocks (Groves et al. 1974, Donaldson 1981). Even without the introduction of sulfur, serpentinization may significantly modify the mineralogy and tenor of the pre-existing sulfides, although the process may be essentially isochemical except on a very small scale. Serpentinization of olivine is accompanied by the formation of magnetite and release of the Ni contained in olivine. Incorporation of the oxygen in magnetite results in a reducing environment and may lead to the formation of awaruite (Ni_3Fe) (Eckstrand 1975). If a small amount of disseminated sulfide is present in the rock, the released Ni may be added to or substituted for Fe in the sulfide phases, producing Ni-rich minerals, such as millerite, godlevskite, violarite, or bravoite. Talc-carbonate alteration may also result in Ni enrichment in talc and, at high sulfur activity, the formation of Ni- and Fe-sulfides (Donaldson 1981). Such Ni-upgrading during serpentinization and talc-carbonate alteration may spell the difference between a marginal and an economic deposit.

The effects of regional metamorphism and deformation on Ni-sulfide ores have been particularly well documented for the komatiite-associated ores in Western Australia (Barrett et al. 1976, 1977, Groves & Hudson 1981, Marston et al. 1981, Leshner & Keays 1984, Cowden & Archibald 1987). During metamorphism, which ranges from lower amphibolite facies (e.g., Kambalda) to upper amphibolite facies (e.g., Nepean, Agnew), much of the sulfides must have reverted to Fe-rich and/or Ni-rich *ms*s and Cu-Fe intermediate solid solution (*iss*), accompanied by obliteration of primary textures and compositional inhomogeneities, sulfide remobilization, and redistribution of elements. The present sulfide assemblages are the result of subsequent equilibration of this metamorphic *ms*s. Observed features of the Ni-sulfide ores attributable to

metamorphism and deformation include the following: (a) offset mineralization, thickened ore sections, stringer mineralization, breccia ores, and sulfides in metasomatic reaction zones; (b) mineralogic layering due to segregation of low-strength (pyrrhotite, chalcopyrite) versus high-strength (pentlandite, pyrite) minerals; (c) changes in metal ratios (Ni:Cu, Ni:Fe, Ni:Pd) in some parts of an orebody and diffusion of Ni into barren sulfidic sediments; (d) sulfide-silicate intergrowth textures (e.g., triangular-textured ore), annealing textures in sulfides, and porphyroblastic pyrite and pentlandite; and (e) increase in modal pyrite and magnetite due to oxidation of *mss* or pyrrhotite. Barrett et al. (1977) suggested that some massive sulfide ores resulted from plastic flow of original magmatic net-textured and disseminated sulfides to zones of low pressure during metamorphism, but Keays et al. (1982) argued that such a model would not be consistent with the appreciably higher concentration of Ir, a highly immobile element, in the massive ore layers compared with the associated matrix ore layers at Kambalda. There is no conclusive evidence in favor of metamorphism being a major process of massive ore formation in Western Australia or anywhere else (Groves & Hudson 1981, Godlevsky & Likhachev 1986).

6.7. Origin of Kambalda-type Deposits

Genetic models proposed for the Kambalda-type nickel sulfide deposits may be grouped under two broad categories: (a) magmatic segregation — segregation of immiscible sulfide melts from ultramafic-mafic magmas and accumulation within the igneous pile (Ewers & Hudson 1972, Naldrett 1973, 1979, 1989, Groves et al. 1979, Marston et al. 1981, Groves & Hudson 1981, Leshner et al. 1984, Naldrett et al. 1984, Leshner & Groves 1986, etc.); and (b) hydrothermal emplacement — precipitation of sulfides from hydrothermal fluids, either as syngenetic chemical sediments on the ocean-floor from volcanic exhalations (Lusk 1976, Hutchinson et al. 1980, Robinson & Hutchinson 1982) or as epigenetic replacement of pre-existing minerals (Fleet 1977, 1979).

6.7.1. HYDROTHERMAL MODELS

The volcanic-hosted pyritic Cu-Zn massive sulfide deposits of the Abitibi greenstone belt in Canada are associated with exhalites (chemical sediments of predominantly volcanic exhalative origin) and are generally accepted to have formed from submarine volcanic exhalations (see Ch. 10). Lusk (1976) considered the association between volcanic-hosted Ni-Cu massive sulfide deposits and sulfidic metasediments in Western Australia to be similar and proposed a volcanic-exhalative origin for the massive nickel sulfide deposits. According to his model, massive sulfides precipitated as lenticular accumulations in banded chemical sediments around sea-floor fumaroles, from hydrothermal fluids that obtained the metals and sulfur from a deeper source or the wallrocks; the disseminated and matrix ores formed by melting of part of the massive ores by subsequent ultramafic flows and segregation of the sulfide liquid. Although a

volcanic-exhalative origin of the ores cannot be discounted entirely in a few cases (e.g., Redstone massive nickel sulfide deposit, Canada; Robinson and Hutchinson 1982), its general applicability to volcanic-hosted nickel sulfide deposits of Western Australia has been questioned on many grounds (Groves et al. 1979, Groves & Hudson 1981, Marston et al. 1981). These include: (a) a lack of widespread wallrock alteration beneath ore zones so characteristic of volcanic-associated exhalative sulfide deposits (see Ch. 10); (b) the formation of ores at the beginning of a komatiitic volcanic cycle, as indicated by the association of the ores with MgO-rich komatiitic units, rather than during the waning stages of komatiitic volcanism; (c) absence of a specific association of the sulfidic metasediments with ultramafic volcanism, and the younger position of the metasediments in some cases; (d) an antipathetic spatial relationship between massive ores and metasediments, and sharp contacts between them in most cases where they are juxtaposed; and (e) compositional dissimilarity between the metasediments believed to be of exhalative origin and the ores (e.g., the higher Pd/Ir ratios of the metasediments — Keays et al. 1982, Paterson et al. 1984). The deposits contain very little Zn, a major constituent of nearly all Precambrian exhalative sulfide deposits but, with a K_{D1} (sulf-sil) of about 1, Zn would not be expected to be concentrated in magmatic sulfide deposits (Naldrett 1979).

Fleet (1977) suggested an epigenetic hydrothermal replacement process for the disseminated nickel sulfide mineralization in the Froid mine of the Sudbury Complex, based on the wide range in pentlandite composition and inclusion of host rock (quartz diorite) minerals in the sulfide blebs. Later, Fleet (1979) proposed a hydrothermal origin for other Ni-Cu sulfide deposits hosted in gabbroic intrusions and komatiites, mainly on the basis of, as discussed earlier, higher than expected Ni contents of olivines from these deposits. Arguments cited against an hydrothermal origin for most Ni-sulfide deposits, in addition to the evidence cited in favor of a magmatic segregation origin (discussed later), include the virtual absence of Zn in the Ni-Cu ores (Naldrett 1979) and the high Ir contents of the Ni-Cu ores relative to normal crustal rocks (Keays & Davidson 1976). Hydrothermal alteration of the host rocks is a common feature of most deposits, but it is not restricted to zones of nickel sulfide mineralization.

Keays et al. (1982) suggested that Ir might be a useful discriminant of sulfide mineralization from hydrothermal fluids because of its immobility. Some minor Ni-sulfide mineralization in Western Australia considered to be of hydrothermal origin (Groves et al. 1978, Nickel et al. 1979) are characterized by significantly lower Ir contents and highly variable Ir:Ni ratios. In contrast, komatiite-associated Ni-sulfide deposits have Pd:Ni and Ir:Ni ratios that are consistent with segregation of immiscible sulfides from komatiitic magmas (Keays et al. 1982). It should be pointed out, however, that many authors now favor a hydrothermal origin for the PGE enrichment of Ni-Cu sulfide horizons in large layered intrusions (see Ch. 7).

6.7.2. MAGMATIC MODELS

For the vast majority of Ni-sulfide deposits, most authors favor a genetic model that

involves the segregation of an immiscible sulfide liquid from a sulfur-saturated mafic or ultramafic magma at some stage of its crystallization history. The evidence cited in favor of a magmatic segregation origin (Duke & Naldrett 1978, Naldrett 1979, Groves et al. 1979, Groves et al. 1981, Naldrett 1981a, Campbell & Barnes 1984, Naldrett et al. 1984, Leshner & Campbell 1993, Naldrett 1998) is summarized below:

- (a) As a rule, the ores in relatively undeformed sequences are localized toward the base of the mafic or ultramafic unit with which they are associated, often in embayments (troughs) in the footwall rocks. Exceptions to the generalization are ores displaced by metamorphism and deformation (e.g., Thompson nickel belt, Canada) and examples of inclusion-bearing sulfides concentrated in fractures (Pechanga) or irregular pipes (Lynn Lake), or associated with mafic pegmatoids (Bushveld Complex).
- (b) The high concentration of chalcophile elements (Ni, Cu, PGE) (and a corresponding depletion of these elements in the host rock — a possible exploration tool) and the low concentration of elements such as Zn in the ores, as well as the element ratios (Ni:Cu, Ni:Ir, Pd:Ir, Cu:Rh) in the ores, are consistent with known and inferred metal partitioning behavior in mafic-ultramafic magmatic systems. The komatiitic ores contain ferrochromites, similar to those crystallized experimentally from sulfide-oxide liquids and apparently unrelated to the metamorphic grade of host rocks.
- (c) The common occurrence of sulfides interstitial to the silicates of relatively undeformed magmatic rocks (net texture) in both komatiitic and gabbroid class deposits supports a magmatic origin. A hydrothermal origin for such ores would require an unrealistic selective replacement of certain minerals. The gradation between massive and net-textured ores in komatiites can be accounted for by magmatic segregation involving gravitational settling of early-formed sulfides.

Leshner et al. (1981) have shown that the spinifex-textured peridotites from the entire Kambalda succession are depleted in Ni, and that the pattern of Ni depletion, despite some scatter in the data, is consistent with differentiation of a parental magma (initially containing about 32% MgO and 1,750 ppm Ni) by fractional segregation of olivine and sulfide in a 200:1 ratio (Fig. 6.12). Although such a model is compatible with the observed silicate and sulfide compositions, it does not account for the occurrence of the Kambalda orebodies at the base of the ultramafic sequence in association with the most magnesian komatiites. One would expect the ores to occur at the top of the ultramafic sequence, in association with less magnesian flows, if they had formed by the accumulation of fractionally segregated sulfides (Duke 1990).

Field relations at Kambalda are more consistent with batch segregation of immiscible sulfide melt as a result of some sudden change in the intensive parameters (e.g., increase in the activity of SiO_2 or $f\text{S}_2$), although the pattern of Ni-depletion in the overlying ultramafic succession does indicate protracted fractional segregation of

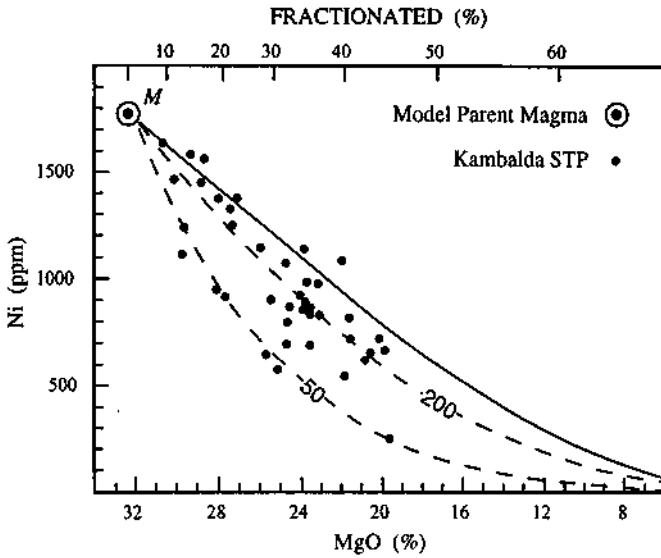


Figure 6.12. Computed depletion in the Ni concentration of a model komatiite magma (M) due to fractional crystallization of olivine (indicated by decreasing MgO content) under sulfide-saturated (solid line) and sulfide-unsaturated (dashed lines, with numbers representing olivine:sulfide weight ratios) conditions. The compositions of Kambalda spinifex-textured peridotites (STP) are consistent with fractional segregation of olivine and sulfide in a 200:1 ratio. (Sources of data: model curves, Naldrett et al. 1984; compositional data, Lesher et al. 1981).

olivine and sulfide. The R factor suggested for modeling batch segregation (Eqn. 2.6) ranges from a high of 2,500 based on the composition of Kambalda sulfide ores (Naldrett et al. 1979) to a low of 500 (Naldrett 1981), or even 300 (Campbell & Barnes 1984), based on the low concentrations of PGE in the ores. A much higher value of the R factor, about 6,500, has been estimated by Duke (1990) for the Kambalda sulfide ores. This estimate, which is based on the observed proportion of sulfide ores relative to their host rocks, is in apparent agreement with the Ni and Cu concentrations in the average Kambalda millhead ore, recalculated to 100% sulfide, if the sulfides resulted from batch equilibration with komatiite liquids containing 28-32% MgO (Fig. 6.13). Assuming a Pd concentration of 9.2 ppb in the Kambalda parental magma, the average of 42 spinifex-textured peridotite samples reported by Keays (1982), and an R factor of 6,500, a reasonable match with the Pd content of the average millhead ore (1,586 ppb) requires a D_{Pd} of 250 (Duke 1990), the same as used for Cu, but well below the D_{Pd} values (in the range of 10^4 to 10^5) proposed by Campbell and Barnes (1984) and preferred by Naldrett (1989). Batch equilibration with an R factor of 300 and a D_{Pd} value of 30,000 yields a reasonable match for the PGE concentrations in the Kambalda

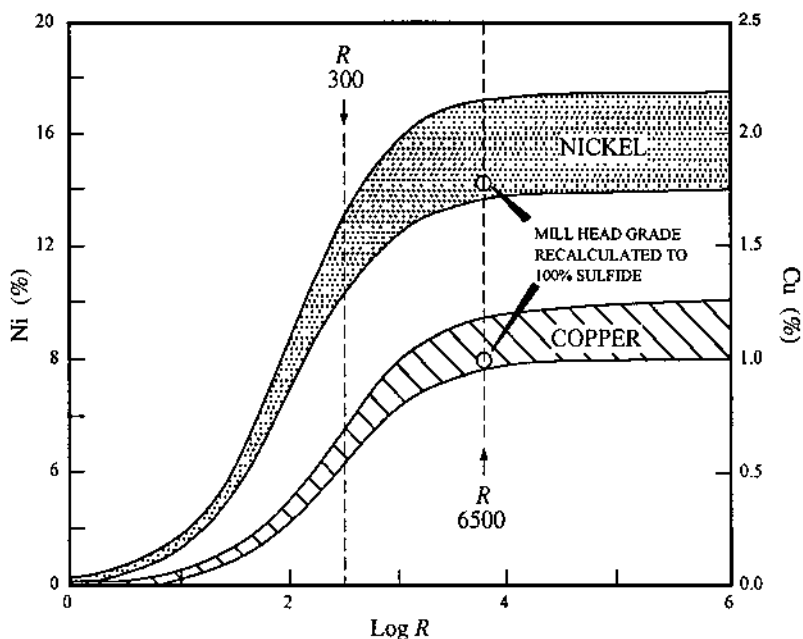


Figure 6.13. Concentration of Ni and Cu in sulfides resulting from batch equilibration with komatiite liquids containing from 28 to 32% MgO as a function of R (the silicate:sulfide mass ratio). The concentrations in the Kambalda millhead ore, recalculated to 100% sulfide are plotted for $R = 6,500$ as estimated by Duke (1990). (After Duke 1990.)

sulfide, but does not account for the lack of a strong Pd depletion in the associated spinifex-textured rocks. For example, overlying komatiite flows at Kambalda contain an average of 8.9 ppb Pd (Keays 1982), whereas a very high D_{Pd} should have almost completely stripped the silicate liquid of its Pd (Duke 1990). More recently, Leshner and Campbell (1993) have been able to model the observed compositional range of the komatiite-associated nickel sulfide deposits of Western Australia using R factors of 100 for low-tenor ores to 500 for high-tenor ores and D_{Ni} values of 100 to 200 (which are significantly lower than the 500-900 range for D_{Ni} given by Peach et al. 1990 based on analyses of coexisting MORB sulfide and glass).

Sulfur Saturation and Sulfide Segregation

Sulfur saturation of the magma is a prerequisite for magmatic sulfide segregation. To explain the disproportionately high sulfide content in the Strathcona mine (Sudbury Complex) relative to the limited sulfur solubility in silicate magmas, Naldrett and Kullerud (1967) suggested that the bulk of the sulfides was brought in from an undefined deeper source as immiscible sulfide-oxide droplets suspended in the noritic

magmas. Naldrett (1973) and Naldrett and Cabri (1976) envisaged a similar situation for the ore-forming Archean komatiitic magmas. According to the model presented by Naldrett and Cabri (1976), sulfides in the mantle would melt below about 100 km depth, the point of intersection of the sulfide melting curve with the Archean geotherm postulated by Green (1975), percolate downward and accumulate at a depth of about 200 km corresponding to the source region of komatiitic magmas (discussed later), and eventually be incorporated as immiscible sulfide blebs in the komatiitic magma. The sulfur concentration in the mantle has been estimated by Sun (1982) to be in the order of 300-1,000 ppm, i.e., between 0.1 and 0.3% sulfide. Assuming the maximum sulfur solubility of basaltic melts as 0.26% (Wendlandt 1982), between 13% and 18% partial melting would be required to dissolve all the sulfide (Barnes et al. 1985). Arndt (1977) argued that even with less than 20% partial melting of the mantle, solids and liquids would separate, but whether the sulfide liquid would be left behind or carried in the silicate liquid as a dispersed phase was another issue.

An important constraint in this context is the viscosity of the source magmas. That the Kambalda komatiite sequences are differentiated, with the most primitive lavas (with the highest MgO contents) at the base, suggests that the magmas probably underwent fractional crystallization during their ascent. Intratelluric olivine in a komatiite magma would certainly increase its viscosity, and this led Marston et al. (1981) to question the feasibility of transporting sulfide blebs in such magmas. However, olivine phenocrysts in the chilled margins of most komatiite lava flows and the composition of relict olivines in the flows suggest that the precursor komatiitic magmas did not contain much intratelluric olivine (Leshner & Groves 1986).

Computations by Leshner and Groves (1986), using a value of 1 poise for the viscosity of a 32% MgO liquid, indicate that at least fine sulfide droplets could be supported and transported in an ascending magma, but they presented two main lines of argument against the eruption of sulfide-bearing komatiites. First, if the magma was sulfur-saturated, the entire host unit should contain ubiquitous disseminated sulfide, but the upper and adjacent portions of the host units, as well as the overlying komatiite units, are barren of mineralization. Even the olivine-enriched units, where olivine crystallization should be accompanied by sulfide exsolution and enrichment, are also devoid of mineralization. Second, komatiite magmas with low viscosity, as evidenced by their lack of significant intratelluric phenocryst contents, should ascend rapidly along steep P - T trajectories close to the adiabatic gradient (decrease in temperature with decrease in pressure, but without loss of heat from the magma). Experimental studies have shown that there is a strong negative pressure-dependence on sulfur solubility in basaltic melts and that sulfur saturation isopleths are parallel to silicate liquidus. A komatiite magma, which was sulfur-saturated at depth, would remain sulfur-saturated during its ascent along the liquidus path, but should arrive at the surface superheated but undersaturated along an adiabatic P - T trajectory (Fig. 6.14).

For the komatiite-hosted ores of Western Australia, assimilation of sulfur and silica from sulfidic interflow sediments along lava channels may have been the dominant process for sulfur saturation (Leshner et al. 1984, Leshner & Groves 1986, Groves et al.

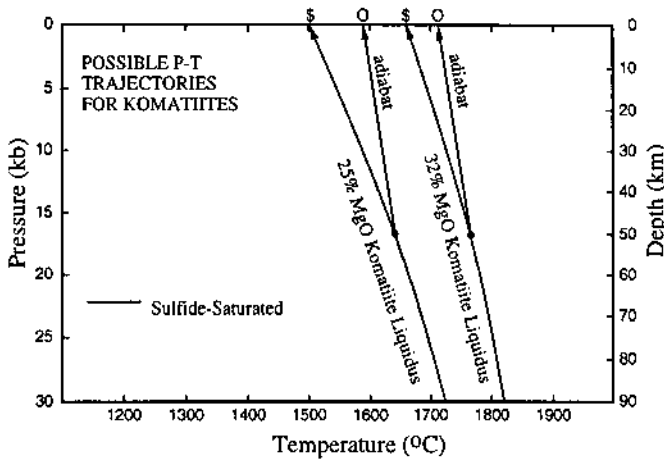


Figure 6.14. Possible pressure-temperature trajectories for ascending komatiite magmas (after Lesher & Groves 1986). The dashed curves are liquidus ascent paths and the solid curves are adiabatic ascent paths ($dT/dP = 3^{\circ}\text{C}/\text{kb}$). Sulfide saturation isopleths are assumed to be parallel to the silicate liquidii. \$ = sulfide-saturated komatiite magmas, O = sulfur-undersaturated komatiite magmas.

1986, Lesher 1989). Evidence cited for this conclusion includes a considerable variation in the composition of the sulfide fraction in different ore shoots despite a limited range of parental liquid compositions (generally 28-32% MgO), thermal erosion of associated sediments, and an antipathetic relationship between sulfidic sediments and contact ores. Flows that assimilated relatively large amounts of footwall rocks, especially sulfidic sediments, achieved sulfide saturation early in their crystallization history, and gravitative settling of the immiscible sulfide blebs gave rise to massive-matrix-disseminated sulfide ores; flows that assimilated proportionately small amounts of material achieved sulfide saturation later in their crystallization history and formed only disseminated sulfide ores.

The assimilation of significant amounts of country rocks by komatiite flows, both during their ascent through underlying crust and while flowing across the surface, is supported by the Sm-Nd and REE characteristics of the komatiites (Arndt & Jenner 1986), but it is not certain that local assimilation of sulfidic sediments was the most important factor in the generation of nickel ores in Western Australia. Gresham (1986) argued against such a conclusion on the following grounds: (a) in some deposits, extensive zones of magmatic sulfide are associated with sulfidic sediments with no evidence of assimilation; (b) in the Kambalda district, the amount of sulfur in the sediments (about 4%) would not be enough to account for the amount of observed Ni-sulfide ores; and (c) in the ore shoots intimately associated with sediments and where some local assimilation of sediments is probable, the ores have a significantly higher

Zn content (160 ppm) than normal massive ores (40 ppm). Moreover, a large-scale crustal or selective sulfidic contamination of komatiitic magma is not compatible with the typically high Os concentrations, low Re:Os ratios, and near-chondritic initial Os-isotope compositions of komatiite-associated Ni-sulfide ore systems, which are interpreted to have experienced low R factors (<500) (Lambert et al. 1998). It is possible that the crystallization of magma was a significant factor for some komatiite-associated deposits (Naldrett et al. 1984, Barnes & Naldrett 1987), especially in the case of disseminated mineralization in komatiitic dunites.

Compared with the Kambalda system, Cu-Ni sulfide ore systems at Duluth, Sudbury, and Stillwater have low Os concentrations, high Re:Os ratios, and high initial Os-isotope compositions, indicating significant interactions between their parental basaltic magmas and crustal material (Lambert et al. 1998). Also, there is evidence from sulfur isotopic ratios (discussed later) that many gabbroid class deposits, such as those of Noril'sk-Talnakh district and Duluth Complex, are related to assimilation of sulfur from country rocks. Sulfur saturation in the case of the Sudbury Complex, as mentioned earlier, was most likely achieved by silica assimilation from more siliceous crustal sources, probably by mixing with a felsic crustal melt resulting from meteorite impact. Crustal contamination of a picritic, Ti-poor magma has been suggested as the reason for sulfur saturation and sulfide immiscibility in the Noril'sk region (Naldrett et al. 1992). A variety of mechanisms have been proposed for the segregation of PGE-rich Ni-Cu sulfides in the Stillwater, Duluth, and Bushveld complexes: fractional crystallization (Vermaak 1976), assimilation of sulfur from country rocks (Ripley 1981, Buchanan & Rouse 1984, Zientek & Ripley 1990), magma mixing (Irvine et al. 1983, Campbell et al. 1983), and the action of volatile-rich hydrothermal fluids (Elliot et al. 1982, Ballhaus & Stumpfl 1986). The possible role of hydrothermal fluids in the formation of PGE deposits will be elaborated further in Ch. 7.

Emplacement of Komatiite-hosted Ores

The formation of nickel-sulfide ore, especially massive ore, requires some mechanism by which the immiscible sulfide blebs exsolved from a sulfur-saturated magma could get concentrated. The general occurrence of massive ores at the basal parts of host units is a strong indication that gravitative settling of the sulfide-blebs played a major role in this concentration process. The net-textured and disseminated ores represent sulfides trapped in the interstices of early-formed silicate minerals.

Naldrett (1973) proposed a "billiard ball model" (Fig. 6.15) to explain the upward sequence of massive ore to net-textured ore to low-grade sulfide disseminations found in some komatiite-hosted deposits. Barrett et al. (1977) raised several objections to this model of static segregation of sulfides from ponded lava flows, the most important of which are as follows: (a) much of the net-textured ore at Kambalda contains more than 60% sulfide interstitial to olivine, whereas the billiard-model should result in a fabric containing no more than 40% porosity; and (b) the overlying mass of cumulus olivine should have forced olivine crystals all the way to the base of the zone of sulfide liquid, increasing the thickness of the net-textured ore and eliminating the massive ore.

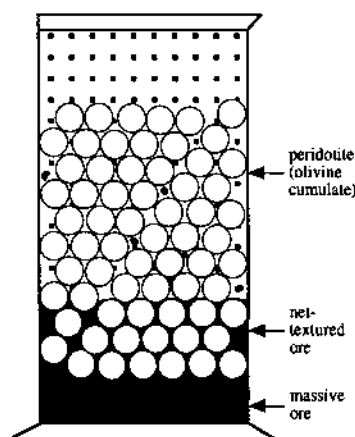


Figure 6.15. The "billiard ball model" — an analogy with billiard balls in a cylinder of mercury and water — proposed by Naldrett (1973) to explain the sequence of massive to net-textured to low-grade disseminated ore (or barren peridotite) formed by gravitative settling of a magmatic immiscible sulfide liquid. The open circles are billiard balls representing olivine crystals, the stippled area is water, and the black areas are mercury representing denser sulfide liquid. Some of the balls are forced down by the weight of the overlying balls and become enclosed in a continuous network of mercury, analogous to the net-textured sulfide ore. (After Naldrett & Campbell 1982.)

Presenting a thermal model of the cooling of a flow, Usselman et al. (1979) suggested that the sulfide liquid that accumulated at the base of the flow solidified before a large amount of olivine could crystallize from the overlying magma. They also pointed out that the porosity would not be a problem as long as the magma contained a restricted proportion of phenocrysts, less than 11% in the case of a 60-m flow and less than 23% in the case of a 30-m flow.

Accepting that the mineralized komatiitic units represent dynamic lava channels, the observed massive-matrix-disseminated ore profile observed in some deposits may be attributed to a combination of flow differentiation along the lava channels between silicate magma, or silicate magma with olivine crystals, and sulfide liquid due to viscosity contrast, and gravitative settling of the sulfide liquid due to density contrast (Marston et al. 1981, Leshner et al. 1984). Depending on the degree of assimilation of footwall rocks, the magma could become sulfur-saturated close to the eruption center forming proximal deposits or, at some distance from the eruption center, forming distal deposits (Leshner & Groves 1986). Most komatiite-hosted deposits are distal deposits (Leshner 1989). Once the magma was sulfur saturated, sulfide precipitation would occur rather quickly. Leshner and Campbell (1993) proposed that low-tenor sulfides (R factor ≈ 100) were not entrained into the komatiite lava but remained as a segregated layer at the base of the flow, whereas high-tenor sulfides (R factor ≈ 500) were not transported long distances in suspension but settled rapidly to the base of the flow.

6.8. Metallogenesis

6.8.1. AGES OF HOST ROCKS

The age distribution of sulfide nickel resources is presented in Figure 6.16. The host rocks of the gabbroid class deposits are predominantly Proterozoic in age; exceptions are the Noril'sk-Talnakh deposits (Triassic), the Insizwa Complex (Jurassic), and the relatively less important tholeiitic intrusions (e.g., Rona, Moxie, Katahdin) of Paleozoic age. With the exception of the Proterozoic Ungava nickel belt, all komatiite-hosted Ni-sulfide deposits are restricted to greenstone belts of Archean age.

Excluding the essentially unmineralized pre-3.5 Ga Isua sequences (Greenland), the Archean greenstone-granite terrains may be broadly subdivided into two major temporal groups (Windley 1977, Groves & Blatt 1984): "older terrains" with supracrustal rocks of ≈ 3.0 -3.3 Ga in age; and "younger terrains" with supracrustal rocks of ≈ 3.0 -2.7 Ga in age. The relation between the "older" and "younger" terrains is not clear, but the older Archean rocks juxtaposed with late Archean greenstones probably represent accreted terrains rather than underlying basement (Lowe & Ernst 1992). Most Ni-sulfide deposits occur in Archean terrains dominated by "younger greenstones": the Yilgarn Block (Eastern Goldfields Province), Western Australia; the Abitibi greenstone belt (Superior Province), Canada; and the Bulawayan sequence in the Rhodesian Craton (the Zimbabwe Province), southern Africa. No significant deposits have been reported in Archean terrains dominated by "older greenstones" (e.g., Barberton Mountain Land,

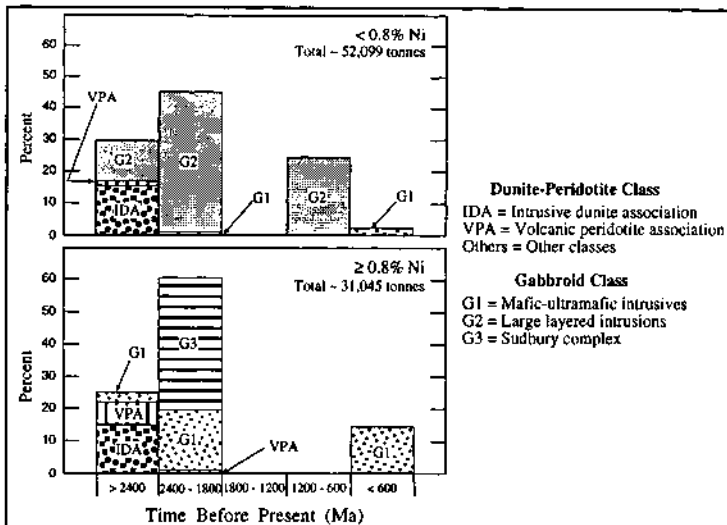


Figure 6.16. Age distribution of sulfide nickel resources by deposit type containing $\geq 0.8\%$ Ni and $< 0.8\%$ Ni. (Source of data: Ross and Travis 1981.)

South Africa; Pilbara Block, Western Australia; the Sebakwian sequence, Zimbabwe), although the thickest komatiite sequences seem to occur in some of the "older" belts.

6.8.2. KOMATIITIC MAGMAS

It is generally believed that basaltic magmas are generated in the upper mantle by partial melting of mantle diapirs above the solidus during their ascent along adiabatic gradients. Tholeiitic magmas, such as the parents for the gabbroid-class deposits, may be produced by moderate amount (<20%) of partial melting of a lherzolite mantle, or by differentiation of picritic magmas produced by higher degrees of partial melting.

The generation and ascent of komatiitic magmas is a more complex and contentious issue. Whole-rock analysis of olivine phenocryst-impoverished glassy margins of komatiite flows and spinifex-textured portions of such flows, compositions of relict olivines ($Fe_{92} - Fe_{94}$) from spinifex-textured or cumulate zones, and Fe-Mg variation in suites of komatiite samples indicate that Archean komatiite lavas were highly magnesian, with 24-32% MgO (Bickle 1982); the Proterozoic analogs were somewhat less magnesian, with MgO contents of about 19% (Barnes et al. 1982).

Experimental studies (e.g., Green et al. 1975, Bickle et al. 1977, Arndt 1977) have shown that liquidus temperatures of high-Mg liquids are very high — about 1,600°C and 1,820°C for a 30% MgO liquid at 1 bar and 30 kb, respectively, and about 1,500°C and 1,725°C for a 25% MgO liquid at similar pressures. Thus very high temperatures must have existed, at least locally, in the Archean upper mantle (Nisbet & Walker 1982). The extrusion temperature of about 1,600°C for Archean peridotitic komatiite magma implies diapirism of upper mantle peridotite from a depth of at least 200 km if the Archean geothermal gradient was similar to the modern geothermal gradient, or from a lesser depth if steeper geothermal gradients prevailed during the Archean. A hydrous mantle (Allègre 1982, Grove et al. 1997) would lower the liquidus temperatures to more "normal" values, but the geochemistry and Sm-Nd systematics of well-preserved komatiites from different parts of the world support the interpretation that most komatiite magmas were generated in unusually hot, and essentially dry, parts of the mantle (Arndt et al. 1998). Cawthorn (1975) suggested that high degrees of partial melting could have been caused by local hot spots during the Archean and that elimination of these hot spots through magma generation might account for the decrease in komatiitic magmatism with decreasing geologic time. Alternatively, the paucity of komatiites in the Proterozoic greenstone belts and their absence in the Phanerozoic might be a consequence of the thickened crust or lower mantle temperature that prevented the dense magnesian liquids from reaching the surface (Nisbet 1982).

The estimated MgO content of the upper mantle is in the order of 37% for a pyrolitic model, a synthetic mantle composition with non-volatile major components matching those in chondritic meteorites (Green 1975), and 42% for a garnet lherzolite model (O'Hara et al. 1975). Generating a komatiitic magma with 32% MgO from such a mantle diapir would require a high degree of partial melting, about 70% for a pyrolite mantle and about 44% for a garnet lherzolite mantle. Alternative models proposed for

the generation of komatiitic magmas include: low degree of partial melting under high pressure (Takahashi & Scarfe 1985); sequential (multi-stage) melting (Arth et al. 1977, Nesbitt et al. 1979); two-stage melting-mixing (Smith & Erlank 1982); polybaric assimilation in which a magnesian liquid separates from a dunitic or harzburgite residue and in course of its upward movement assimilates a crystalline fraction of garnet lherzolite composition (Bickle et al. 1977); extraction from a globally extensive molten layer of ultramafic composition in the upper mantle (Nisbet & Walker 1982); and melting of a degassed, dry Archean mantle that would account for the high liquidus temperatures of komatiitic melts (Warren 1984). According to Naldrett and Barnes (1986), Ni, Co, and Cu contents of komatiitic to basaltic magmas can be modeled satisfactorily as the consequence of about 15 to 60% single-stage partial melting of a spinel lherzolite mantle (2,056 ppm Ni, 106 ppm Co, and 40 ppm Cu), using the partition coefficients available in the literature and assuming that they vary with magma composition as discussed by Naldrett and Duke (1980).

Nesbitt et al. (1979) distinguished two distinct types of peridotitic komatiites in the Archean greenstone belts: (a) an Al-depleted type (*ADPK*), characterized by high CaO:Al₂O₃ ratios (≈ 1.5), low Al₂O₃:TiO₂ ratios (≈ 11), and depleted heavy rare-earth elements (HREE), and (b) an Al-undepleted type (*AUPK*), with CaO:Al₂O₃ ratios close to 1, high Al₂O₃:TiO₂ ratios (≈ 20), and depleted light rare-earth elements (LREE). The *ADPK* magma was depleted in Al (as evidenced by their depleted HREE) due to removal of garnet either by desegregation of the upwelling source or by crystallization from the ascending komatiite magma; the *AUPK* magma was generated by a process of sequential melting, with Al remaining in the source as aluminous orthopyroxene. Alternatively, the differences between komatiite types might reflect significant lateral mantle heterogeneity. Their observation that peridotitic komatiites from the Barberton and Pilbara greenstone belts are dominantly of the *ADPK* type, whereas those from the Abitibi and Yilgarn greenstone belts are dominantly of the *AUPK* type, suggests some fundamental difference between the two types of komatiite magmas for Ni-sulfide mineralization. Perhaps, the *ADPK*-type magma was sulfur saturated, whereas the *AUPK*-type magma was not (Arndt et al. 1997). A sulfur saturated magma would start to segregate sulfide as soon it entered cooler overlying levels of the mantle and crust; the magma would be rapidly depleted in sulfur and chalcophile elements and rendered incapable of forming significant sulfide deposits when emplaced at or near the surface. A magma undersaturated in sulfur, on the other hand, would likely reach crustal levels with its full load of sulfur and chalcophile elements and thus have the potential to segregate enough sulfide to form an economic deposit.

6.8.3. SOURCES OF METALS AND SULFUR

The metals in Ni-sulfide deposits are believed to have been derived predominantly, if not entirely, from the magmas, because much of the compositional variations in the ores may be accounted for by models of magmatic crystallization (Naldrett 1981a, 1989; Lesher & Campbell 1993, Li & Naldrett 1994). The source of sulfur, as

interpreted from sulfur isotopic data (Table 6.4), appears to be varied. For the Sudbury ores, the narrow range of $\delta^{34}\text{S}$ values close to 0‰ suggests an entirely magmatic source of the sulfur (Naldrett 1984b). On the other hand, the spread of $\delta^{34}\text{S}$ values and their correspondence with the $\delta^{34}\text{S}$ values of the associated country rocks have been considered as evidence for a significant contribution of crustal sulfur for gabbroid-class deposits associated with flood basalts — sulfate-bearing evaporites in the case of the Noril'sk-Talnakh deposits (Godlevsky & Grinenko 1963, Grinenko 1985) and sulfide-bearing sediments (the Virginia Formation) in the case of Duluth deposits (Mainwaring & Naldrett 1977, Ripley 1986a, Lee & Ripley 1995). The $\delta^{34}\text{S}$ values of the komatiite-hosted nickel sulfide ores fall within the magmatic range, but so do the $\delta^{34}\text{S}$

TABLE 6.4. Sulfide sulfur isotope ratios of nickel sulfide deposits and associated country rocks

Deposit	Material analyzed	$\delta^{34}\text{S}$ values (per mil)		Reference
		Range	Average	
Sudbury Complex	Ore sulfides		0.5 - 2.7	Naldrett (1984b)
Duluth Complex				
Dunka Road	Ore sulfides	0.2 - 15.3	7.5	Ripley (1981)
	Sediments	0.2 - 25.8	11.6	
Babbitt	Ore sulfides	0.7 - 19.7	8.6	Ripley & Al-Jassar (1987)
	Sediments	1.5 - 21.4	6.9	
Water-Hen	Ore sulfides	11.0 - 14.8	13.5	Mainwaring & Naldrett (1977)
	Sediments	17.2 - 18.2	17.9	
Noril'sk-Talnakh	Unmineralized intrusions	-2 - 16	0.1 - 4.6	Grinenko (1985)
	Mineralized, uneconomic	-2 - 16	5.5 - 8.4	
	Economic intrusions	5 - 16	8.9 - 11.4	
Abitibi greenstone belt				
Alexo	Ore sulfides	4.5 - 6.5	5.0	Naldrett (1966)
	Country rock	3.5 - 5.0	4.5	
Langmuir No. 2	Ore sulfides	-2.0 - 2.0	0	Green & Naldrett (1981)
	Country rock	-2.5 - -8.0	-5.5	
Western Australia				
Kambalda	Ore sulfides	-1.4 - 3.6	2.3	Donnelly et al. (1977)
	Sediments	-7.6 - 5.2	1.6	
Mt. Windarra	Ore sulfides	-2.5 - 1.0	-0.5	Secombe et al. (1977)
	Sediments	-4.5 - 1.5	-1.5	

values of the associated sediments. Thus, the sulfur isotopic data, while being consistent with extraction of sulfur from the sediments, do not necessarily prove such a source (Groves et al. 1979, Green & Naldrett 1981). However, as discussed earlier, there are other lines of evidence which point to the footwall rocks as the source of sulfur for the komatiite-associated deposits in Western Australia.

6.8.4. PALEOTECTONIC SETTINGS

Nickel sulfide deposits occur in four major tectonic settings (Table 6.1): Precambrian greenstone belts (overwhelmingly Archean), Precambrian mobile belts, stable continental platforms (essentially Precambrian), and Phanerozoic fold belts. Archean greenstone belts constitute the predominant terranes for the peridotite-dunite class deposits; tholeiitic intrusions in Precambrian greenstone belts, with the exception of the Pechanga district, are of much less importance. Deposits of the gabbroid class mafic-ultramafic intrusives constitute the most important type in Precambrian mobile belts, largely accounted for by the Jinchuan deposit, and the sole contributor to Phanerozoic fold belts (Ross & Travis 1981). Most nickel resources occur in the stable platform environment, even when the Sudbury Complex is excluded. The 1.1-Ga Duluth Complex is an intrusive part of the intracontinental rift-related Keewawanawan flood basalt province of the Lake Superior region. The Noril'sk-Talnakh deposits in the Siberian platform are also associated with intrusions related to flood basalts (Naldrett and Macdonald 1980, Naldrett et al. 1992). The tectonic setting of the other layered complexes has been discussed in Ch. 5.

The tectonic framework of Archean (and Proterozoic) greenstone belts is largely speculative and controversial. Depending on the nature of lithospheric plate movements, most proposed models for the evolution of Archean granitoid-greenstone terranes may be viewed as either "fixist" or "mobilist". Fixist models, in essence, postulate the deposition of supracrustal volcanic-sedimentary sequences in rifts along fundamental fractures in pre-existing sialic crust. The development of Archean cratons in these models is ascribed to continued downwarping (sagduction), partial melting, diapiric plutonism, deformation, metamorphism, thickening, and uplift — all products of vertical tectonics. Mobilist models, in contrast, envisage the development of Archean cratons by subduction-related horizontal accretion of mobile continental and oceanic plates, involving production and destruction of oceanic crust, partial melting, and magmatism, mainly in convergent plate boundary settings. The tholeiitic to calc-alkaline composition of the volcanic rocks of greenstone sequences, especially within the upper parts, similar to that of modern island-arc complexes appear to favor a mobilist model (Goodwin 1977, Sylvester et al. 1987, Barley et al. 1989, Card 1990, Poulsen et al. 1992). For the late Archean greenstone belts, an evolution along convergent plate margins is further supported by widespread evidence for compressional, nappe-forming events during their deformation (Lowe & Ernst 1992).

An ensialic or intracontinental rift setting would be more likely if the greenstone belt volcanics were emplaced on a sialic crust. There is conclusive evidence in the form

of a basal unconformity in the Belingwe greenstone belt, Zimbabwe (Bickle et al 1975), basal orthoquartzites in Southern Cross Province, Yilgarn Block (Gee et al. 1981), crustally derived xenocrystic zircons in komatiitic basalts in the Kambalda area (Compston et al. 1986), and strong inference from other areas (e.g., the Abitibi belt of Canada and the Pilbara Block of Western Australia) that at least some komatiites were erupted onto pre-existing continental crust (Baragar & McGlynn 1976, Nisbet 1984, Thurston & Chivers 1990). Moreover, the geochemistry of late Archean (≈ 2.7 Ga) volcanic rocks in some greenstone belts, such as the Norseman-Wiluna belt of Western Australia, provides indirect evidence for the presence of older sialic crust, because their incompatible element distribution patterns (Barley 1986, Jolly & Hallberg 1990) and isotopic ratios (Chauvel et al. 1985, Arndt & Jenner 1986) strongly suggest contamination by continental crust. On the other hand, Krogstad et al. (1989) have cited Nd-Sm isotopic data to argue against discernible crustal contamination of the komatiitic magmas in the Dharwar craton (Indian shield). The lack of any significant Ni-sulfide deposits in the komatiite, dated at 2.7 Ga, in the Dharwar craton makes one wonder about a possible genetic relationship between crustal contamination and Ni-sulfide mineralization!

The available field and isotopic evidence indicates that most of the supracrustal volcanic-sedimentary sequences of the Superior Province in Canada, ranging in age from about 3.1 to 2.6 Ga, were not deposited on older sialic crust nor were rocks older than about 3.1 Ga involved in their production. The supracrustal sequences are composed of several distinct lithostratigraphic associations (Thurston & Chivers 1990, Poulsen et al. 1992): (a) platform-type quartz arenite-stromatolitic carbonate sequences with some komatiite or tholeiite (mostly older than 2.8 Ga), found only in the northern greenstone belts; (b) mafic-ultramafic submarine sequences (mostly 2.8 to 2.7 Ga in age), consisting of laterally extensive pillowed and massive tholeiitic flows with komatiites, mafic-ultramafic sills, sulfide facies iron-formation, chert, and argillite; (c) mafic to felsic volcanic cycles (mostly 2.75 to 2.70 Ga in age, but a few are 2.8 Ga or older) that form the more areally restricted central complexes (volcanic centers) and are composed of both tholeiitic and calc-alkaline suites with deep-water interflow argillites; and (d) 'Timiskaming-type' sequences (younger than 2.7 Ga in age) of fluvial sediments largely of locally derived debris and calc-alkaline to alkaline volcanics, which occur in or at the margins of greenstone terranes throughout Superior Province. These areally restricted sequences commonly unconformably overlie older volcanic rocks and subvolcanic plutons, and many of the sequences are spatially related to, and partly bounded by, major subprovince boundaries.

The platform sequences represent mafic volcanism and shallow-water sedimentation in rift-related basins undergoing minor subsidence. However, it is not certain if these sequences record only ensialic rifting, as has been argued for other Archean cratons (e.g., Groves & Blatt 1984), or represent the transition from passive platformal margins to oceanic crust. In any case, these sequences represent only an early history in the Superior Province and are not representative of the mineral-rich late Archean sequences that characterize most granitoid-greenstone terranes of the rest of the Superior

Province. These sequences may contain komatiite-associated Ni-sulfide and PGE mineralization, but the known deposits are associated with the ≈ 2.7 -Ga mafic-ultramafic sequences, which have been variously interpreted as the lower parts of oceanic arcs or islands, or as oceanic lava plain and Hawaiian-type shield volcanic accumulations. Poulsen et al. (1992) argued that the komatiitic rocks of the sequence formed in a rifted arc or in a marginal basin behind an arc, not in abyssal oceanic or shallow continental environments. They also suggested that the paucity of komatiite-hosted nickel sulfide deposits in the Superior Province relative to the abundance of komatiites was because of insufficient sulfur in the primary melts. Only the lower parts of the sequences are productive because they overlie felsic arc sequences containing abundant sulfide facies iron-formation as a possible source of external sulfur.

The mafic-to-felsic volcanic complexes are the most significant sites of Archean mineral deposits in the Superior Province, especially of volcanic-associated massive sulfide deposits (see Ch. 10) and banded iron-formations (see Ch. 15). Zircons from the complexes indicate a general absence of sialic basement, except in the northern part. These complexes appear to have been emplaced in island-arc or, possibly, continental-arc environments. Some layered complexes contain significant proportions of ultramafic rocks and are hosts to Ni-sulfide deposits that are similar to those hosted by ultramafic-mafic sequences (Barrie & Naldrett 1990), but these are of minor importance. The Timiskaming-type sequences of immature sedimentary rocks, interpreted to represent accumulations in pull-apart basins developed by strike-slip movement on major subprovince boundary faults, are the hosts to lode gold deposits (see Ch. 16). According to Card (1990), a model that best accounts for the characteristics of the plutonic-volcanic-sedimentary assemblages of Superior Province involves subduction-related accretion, during the late Archean Kenoran orogeny (≈ 2.7 Ga), of crustal elements formed in a variety of tectonic environments.

An accretionary tectonic model, involving the 2.7 Ga-old tholeiitic-komatiitic magmatism at spreading centers and the subsequent accretion of these volcanic terranes, has also been suggested for the Kolar Schist Belt of the Indian Shield (Krogstad et al. 1989). De Ronde and Witt (1994) interpreted the 3.55-3.22 Ga Barberton greenstone belt as an accretionary belt composed of two major units, both containing early basaltic and komatiitic units resembling mid-ocean ridge rocks and later felsic volcanic units formed along one or more convergent margins. Lowe (1994) presented a model for the evolution of the belt as a complex of diachronous tectonostratigraphic blocks formed during multiple periods of extension and magmatic and tectonic accretion.

The developmental sequence of greenstone lithostratigraphic associations in the Yilgarn Block of the Western Australian Shield is broadly analogous to that of the Superior Province (Thurston & Chivers 1990). As described by Barley et al. (1989) and Barley & Groves (1990), available geochronologic data provide evidence for two major lithostratigraphic packages in the Yilgarn Block (Fig. 6.17): (a) an older (>2.9 Ga) package represented by tholeiites, komatiitic basalts, minor komatiites, intermediate to silicic volcanic rocks, and banded iron-formations (BIF), overlain by dominantly terrigenous sedimentary successions; and (b) a younger (≈ 2.7 Ga) package

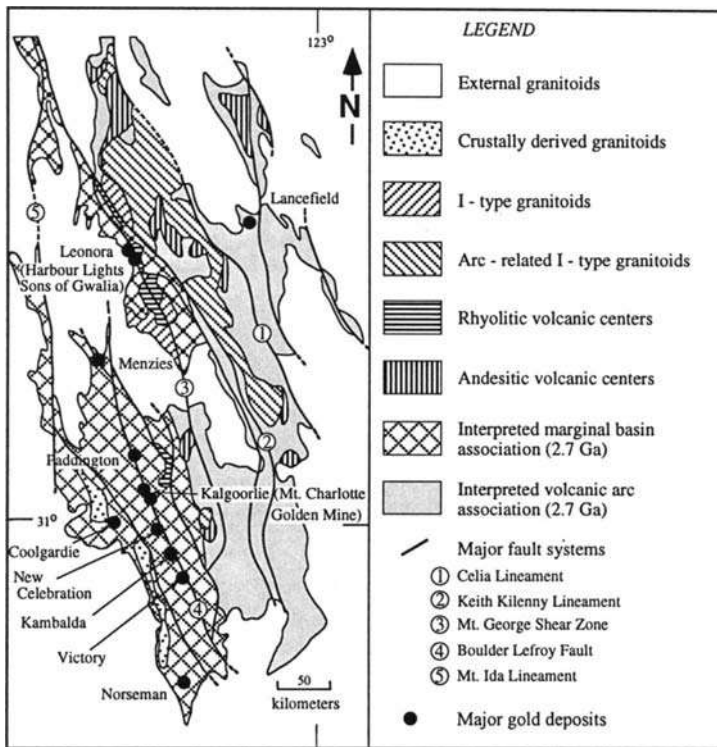


Figure 6.17. Simplified geological map of the Norseman-Wiluna greenstone belt, Western Australia, showing major faults and lineaments, and major gold deposits, as well as the interpreted distribution of ≈ 2.7 Ga tectonostratigraphic associations, granitoids, and minor intrusive suites. The komatiite-associated Ni-sulfide deposits are located in the marginal (back-arc) basin association. Note that the gold deposits occur either along or close to major faults or shear zones. (After Barley et al. 1989.)

of tholeiitic and calc-alkaline volcanic rocks with abundant komatiites. The older greenstone successions are abundant in the Murchison and Southern Cross provinces, but they also crop out along the western and eastern margins of the Norseman-Wiluna belt and locally form part of the basement to the 2.7-Ga greenstones within the belt. The original tectonic framework of the older successions is yet to be defined, but analogies with similar, but less deformed, ≈ 2.8 -2.5 Ga successions in the Pilbara Block suggest quiet shelf or intraoceanic platform settings during BIF deposition. The Norseman-Wiluna belt, dominated by ≈ 2.7 Ga-old volcanic-sedimentary successions, is divisible into two broad associations. The eastern part of the belt contains tholeiitic basalts interlayered with partly subaerial sequences of calc-alkaline volcanics as well as epiclastic sediments and I-type granitoids, and the assemblage is typical of modern

ensialic volcanic arcs. To the west of this association, and separated from it by major faults, is an association comprised of tholeiites, komatiites, and sulfidic shales overlain by silicic pyroclastics and associated sediments. This association is comparable to crust in younger submarine basins in back-arc settings and probably developed behind a volcanic arc. Thus, the Norseman-Wiluna belt probably represents a volcanic arc and back-arc basin complex developed in response to westward-dipping subduction at an obliquely convergent Archean craton or proto-craton margin (Barley & Groves 1990). This model is similar to the generalized model for greenstone belt development proposed by Tarney et al. (1976), which was based on an analogy to the southern Andean Cordillera.

Some komatiite-associated Ni-Cu sulfide mineralization occurs in the >2.9 Ga-old tholeiite-komatiite-BIF successions where they contain significant amounts of komatiites (and volcanic-associated Cu-Zn sulfide deposits where they contain significant amounts of deep-water felsic volcanics). However, Ni-Cu sulfide mineralization is most abundant in 2.7 Ga-old tholeiite-komatiite-sulfidic shale association in the Norseman-Wiluna belt. The concentration of Ni-sulfide deposits in this belt may be attributed to a favorable combination of abundant komatiites, the source of metals, and sulfidic shales, the likely major source of external sulfur. Incidentally, this belt also contains numerous epigenetic gold deposits (see Ch. 16), and the gold mineralization is believed to be an integral part of the orogeny that followed within about 50 m.y. of the major period of volcanism and resulted in the stabilization of the Yilgarn Craton (Barley & Groves 1990). The Abitibi greenstone belt in Canada may also represent a late Archean convergent margin orogen with a tectonic history similar to that of the Norseman-Wiluna belt (Ludden et al. 1986).

The spatial separation of volcanic peridotite-associated and intrusive dunite-associated deposits in the Norseman-Wiluna belt (Fig. 6.5) is an unresolved issue. Groves et al. (1984) suggested that the volcanic peridotite-associated deposits formed during the initial stretching phase of rifting, the most important mineralization being concentrated in the axial zone, and the dunite-associated deposits were emplaced at a higher stratigraphic level during the subsequent thermal subsidence phase of the basin. According to O'Driscoll (1989), both the clusters of Ni-sulfide deposits in the belt are related to transcurrent gravity lineaments of regional magnitude.

6.9. Summary

Of the various types of Ni (-Cu) sulfide deposits (Table 6.1), all hosted by ultramafic to mafic igneous rocks, the most productive at present are: (a) the extrusive komatiite-associated deposits of Archean greenstone belts, especially those of the Yilgarn Block of the Western Australian shield; (b) deposits of the Sudbury Complex, a gabbroic intrusion, believed by many to be of meteorite-impact origin, with an unusual concentration of high-grade ores in mafic (noritic) differentiates; and (c) a few ultramafic-mafic intrusives of tholeiitic association (e.g., the Noril'sk-Talnakh). The

large layered complexes (Bushveld, Stillwater, Duluth, Great Dyke) contain very large quantities of low-grade (<0.8% Ni) resources (Fig. 6.2), but commercial exploitation in these complexes is currently limited to the PGE-rich sulfide horizons.

Pentlandite is by far the most important Ni-bearing mineral of Ni-sulfide deposits and pyrrhotite - pentlandite - chalcopyrite, with or without pyrite, is the typical sulfide assemblage. More Ni-rich minerals, such as millerite, hazlewoodite and violarite, are products of serpentinization and alteration. Deposits of the gabbroid class, especially those related to flood basalts, tend to have lower Ni:Cu ratios compared with the komatiite-associated deposits.

Most geologists consider Ni-Cu sulfide deposits as typical examples of magmatic segregation, involving sulfide liquid immiscibility in a komatiitic or tholeiitic silicate magma soon after its emplacement and concentration of the sulfide in basal parts of the host unit by gravitative settling. Proposed mechanisms for sulfur saturation of the parent magma range from assimilation of country rocks to mixing of magmas and interaction with volatile-rich fluids. A strong argument cited in favor of the magmatic genetic model is the success in modeling the composition of Ni-sulfide ores using Equation 2.6 with appropriate D and R values. There is some controversy, however, about the validity of the liquid immiscibility model. This is related primarily to the Ni content of olivines in these deposits and is based on the discrepancy in the Ni (olivine)-Ni (silicate magma) distribution coefficient obtained by various workers.

Nickel sulfide deposits occur in four major tectonic settings (Table 6.1): Precambrian greenstone belts (essentially Archean), Precambrian mobile belts, stable continental platforms, and Phanerozoic fold belts. The most important in terms of total resources is the stable continental platform because of the low-grade mineralization in large layered complexes. If Sudbury is excluded from consideration, Precambrian mobile belts are the most important environment for Ni-sulfide deposits with $\geq 0.8\%$ Ni, followed by Archean greenstone belts and Phanerozoic fold belts. The latter two contain the highest grade deposits, accounted for by deposits of the komatiitic peridotite association and the high-grade gabbroid class deposits of the Noril'sk region.

Komatiite-associated nickel sulfide deposits tend to be concentrated in greenstone-granitoid belts dominated by 'younger' greenstone successions (<2.9 Ga), as in the Norseman-Wiluna belt (Western Australia) and the Abitibi belt (Canada), compared with belts dominated by 'older' greenstone successions (>2.9 Ga), although the older successions may contain thick komatiitic sequences. The ≈ 2.7 -Ga Norseman-Wiluna belt has been interpreted as a back-arc basin-ensialic arc complex. The localization of Ni-sulfide deposits mainly in the back-arc basin assemblage may be attributed to a favorable combination of abundant komatiites (metal source) and an external source of sulfur in the associated sulfidic sediments. The tectonic setting of the Abitibi belt was probably broadly similar, but the controls of mineralization are not known. The paucity of komatiites in the Proterozoic greenstone belts and their absence in the Phanerozoic may be a consequence of thickened crust or lower mantle temperature that did not permit the dense magnesian liquids to reach the surface.

6.10. Recommended Reading

Naldrett (1979), Marston et al. (1981), Naldrett (1984b), Fleet and MacRae (1987), Naldrett (1989, Ch. 6), Leshner (1989), Barley & Groves (1990), Card (1990), Naldrett (1999).

CHAPTER 7

PLATINUM-GROUP ELEMENT (PGE) DEPOSITS

7.1. Introduction

The platinum-group elements (PGE) comprise a geochemically coherent group of siderophile to chalcophile metals that includes osmium (Os), iridium (Ir), ruthenium (Ru), rhodium (Rh), platinum (Pt), and palladium (Pd). Based on association, the PGE may be divided into two subgroups: the Ir-subgroup (IPGE) consisting of Os, Ir, and Ru and the Pd-subgroup (PPGE) consisting of Rh, Pt, and Pd.

The demand for platinum, the most important metal of the group, in many key industrial processes is due to its unique combination of physical, chemical, and mechanical properties: high melting point (1,769°C), very high density, resistance to chemical attack, high catalytic activity, mechanical strength, and malleability. The global demand for platinum in 1997, estimated at 161.7 tonnes, was shared by four major market segments: jewelry (41%), autocatalyst systems (28%), industrial (25%), and investment (6%) (Emmett 1998). Japan accounted for about 65% of the jewelry market, with China running a distant second (although the demand in China increased from 20,000 oz in 1990 to 360,000 oz in 1997). United States is the largest user of platinum (and palladium as a substitute in some cases) in autocatalyst systems to convert harmful automobile emissions (carbon monoxide, nitrogen oxides, and hydrocarbons) to water, carbon dioxide, and nitrogen. The future growth of demand for this usage is expected to occur in developing markets. The industrial use of platinum covers a wide variety of processes and products such as alloys used in magnetic hard disks, fuel cells, glass fiber, optical glass, TV tubes, and petroleum refining. The total demand for platinum is expected to grow at a modest rate of 2% per annum to the year 2010 (Emmett 1998).

The concentration of PGE in terrestrial environments ranges from sub-ppb level in rocks of felsic and intermediate composition to generally 1-100 ppb in mafic and ultramafic rocks. Economic deposits typically contain 5-10 ppm PGE and involve concentration factors in the order of one thousand, similar to those for gold deposits. Recent advances in analytical techniques — e.g., radiochemical neutron activation analysis (RNAA), instrumental neutron activation analysis (INAA), secondary ion mass spectrometer (SIMS), proton-induced X-ray emission (PIXE) — that permit reliable determination of such low level PGE concentrations in rocks and ores have considerably facilitated the detailed study of PGE deposits. In addition, electron microprobe analysis

has played a major role in the characterization of platinum-group minerals (PGM). Cabri (1976) published a glossary of 74 platinum-group minerals and mentioned the reported occurrence of 65 or more unnamed minerals awaiting further characterization. The most common platinum-group minerals are listed in Table 7.1.

TABLE 7.1. Common platinum-group minerals in PGE deposits (after Cabri 1976)

Mineral	End-member	Composition
Atokite	Pd_3Sn	$(\text{Pd},\text{Pt})_3\text{Sn}$
Braggite	$(\text{Pt},\text{Ni})_{6-x}\text{Pd}_{2+x}\text{S}_8?$	$(\text{Pt},\text{Pd},\text{Ni})\text{S}$
Cooperite	PtS	$(\text{Pt},\text{Pd},\text{Ni})\text{S}$
Froodite	PdBi_2	$(\text{Pd},\text{Pt})(\text{Bi},\text{Te})_2$
Hollingworthite	RhAsS	$(\text{Rh},\text{Ru},\text{Pt},\text{Pd},\text{Co},\text{Ni})\text{AsS}$
Insizwaite	PtBi_2	$(\text{Pt},\text{Pd},\text{Ni})(\text{Bi},\text{Te},\text{Sb},\text{Sn})_2$
Irarsite	IrAsS	$(\text{Ir},\text{Ru},\text{Rh},\text{Pt},\text{Pd},\text{Os},\text{Ni},\text{Co})\text{AsS}$
Isoferroplatinum	$\sim\text{Pt}_3\text{Fe}$	$\sim(\text{Pt},\text{Ir},\text{Os},\text{Ru},\text{Rh})_3(\text{Fe},\text{Ni},\text{Cu},\text{Sb})$
Konulskite	PdTe	$(\text{Pd},\text{Ni})(\text{Te},\text{Bi},\text{Sb},\text{Pb})$
Laurite	RuS_2	$(\text{Ru},\text{Ir},\text{Os})\text{S}_2$
Merenskyite	PdTe_2	$(\text{Pd},\text{Pt},\text{Ni})(\text{Te},\text{Bi},\text{Sb})_2$
Michenerite	PdBiTe	$(\text{Pd},\text{Pt},\text{Ni})(\text{Bi},\text{Sb})\text{Te}$
Moncheite	PtTe_2	$(\text{Pt},\text{Pd},\text{Ni})(\text{Te},\text{Bi},\text{Sb})_2$
Niggliite	PtSn	$(\text{Pt},\text{Pd})(\text{Sn},\text{Bi},\text{Te})$
Potarite	PdHg	PdHg
Rustenburgite	Pt_3Sn	$(\text{Pt},\text{Pd})_3\text{Sn}$
Sperryite	PtAs_2	$(\text{Pt},\text{Rh},\text{Ir})(\text{As},\text{Sb},\text{S})_2$
Stillwaterite	Pd_8As_3	$\text{Pd}_8(\text{As},\text{Sb},\text{Te},\text{Sn},\text{Bi})_3$
Sudburyite	PdSb	$(\text{Pd},\text{Ni})(\text{Sb},\text{Bi},\text{Te},\text{As})$
Vysotskite	PdS	$(\text{Pd},\text{Ni},\text{Pt})\text{S}$

The increased demand for PGE and improved analytical techniques have resulted in a recent surge of publications related to the distribution, mineralogy, geochemistry, and genesis of PGE mineralization. Notable among these are the special issues of *Economic Geology* (v. 71, No. 7, 1976; v. 77, No. 6, 1982; v. 81, No. 5, 1986), *Canadian Mineralogist* (v. 17, Pt. 2, 1979), and *Canadian Institute of Mining and Metallurgy* (Spec. Volume 23, 1981) dedicated to PGE deposits. Mention should also be made of excellent discussions on the subject by Macdonald (1987) and Naldrett (1989, Ch. 5), and in the Abstracts, Proceedings Volumes, and Field Excursion Guides pertaining to the eight International Platinum Symposia held so far at various places around the world.

7.2. Types of Deposits

Anomalous concentrations of PGE are known from high-temperature magmatic to low-temperature hydrothermal and sedimentary environments (Kucha 1982, Macdonald 1987, Lechler 1998), but significant concentrations of PGE are virtually restricted to ultramafic rocks. Two types of deposits, both intimately associated with Ni-Cu sulfides, account for about 98% of the world's identified PGE resources: (a) stratiform (or, more correctly, strata-bound) deposits in large, layered complexes (e.g., Bushveld, Stillwater, and Great Dyke), mined primarily for PGE; and (b) Ni-Cu sulfide deposits mined primarily for Ni-Cu sulfides, but containing recoverable amounts of PGE as byproducts (e.g., the Sudbury, Noril'sk-Talnakh, Jinchuan, and Kambalda deposits). The distinctive characteristics of stratiform PGE deposits, the focus in this chapter, include (Naldrett 1989): (a) their occurrence as relatively weak disseminations of sulfides in silicate rocks, rather than as massive concentrations, at specific horizons or "reefs" (mineralized rock layers with a distinctive texture and/or mineralogy) within layered intrusions; and (b) their association with chromite, either within layers of massive chromitite or within strata that also contain small amounts of chromite, in contrast with chromite-free strata above and below the mineralized horizons.

The large layered intrusions contain about 90% of the world's PGE resources, with the Bushveld Complex accounting for about 80% (Table 7.2). About two-thirds of total world production of PGE comes from the Bushveld Complex, a situation that is likely to continue for a long time. Other notable producers are Noril'sk-Talnakh deposits (Siberian Platform), the Great Dyke (Zimbabwe), and the Stillwater Complex (USA). Compared with the Bushveld and Great Dyke deposits, the Stillwater deposit is much smaller in size, but carries a much higher PGE grade (Table 7.2) over a mining width twice as great (2 m compared with typically about 1 m or less for the Bushveld and the Great Dyke). The rest of the world, including the Sudbury Complex (Canada), provides less than 5% of the world's PGE production.

About 2% of the world's identified PGE resources occur in other mafic and ultramafic bodies (e.g., the Fiskenaesset Complex, Greenland; the Jinchuan Complex, China; the Kambalda district, Western Australia) and as alluvial placer deposits (e.g., the Choco district, Columbia; the Goodnews Bay district, Alaska) commonly associated with 'Alaskan-type' zoned ultramafic complexes. The placer deposits of the Ural Mountains, related to 'Alaskan type' and 'Alpine type' complexes, constituted virtually the sole world source of platinum in the 19th century. The auriferous conglomerates of Witwatersrand (South Africa) contain less than 10 ppb PGE, which are collected as a bonus during extraction of gold from crushed ore (Reimer 1979).

The cumulus gabbroic and ultramafic rocks in ophiolites, particularly the units associated with chromitite and high sulfide concentrations, may contain PGE values of economic interest (Crocket 1981, Page & Talkington 1984, Pedersen et al. 1993). In fact, platinum has been extracted as a byproduct from the mining of Ni-Cu sulfide ores located within strongly serpentinized "black dunites" of the Zambales ophiolite. Concentrations of PGE in ophiolitic chromite ores are generally low, ranging from

TABLE 7.2. Identified resources (tonnes) and grade (g/tonne) of PGE in major deposits and their most important platinum-group minerals

	Bushveld		Great Dyke	Stillwater	Sudbury*	Norilsk-Talnakh	Reference
	Merensky Reef	UG-2 Chromitite					
Grade ΣPGE + Au (g/tonne)	8.1	8.71	4.7	22.3	0.9	3.8	1
Pt (tonnes)	10,323	13,547	4,130	217	105	1,550	2
Pd (tonnes)	4,371	11,315	2,936	713	112	4,402	2
ΣPGE Resources (tonnes)	16,957	32,054	7,892	1,057	217	6,200	2
ΣPGE Resources (% of total)	22.4	42.3	10.4	1.4	0.3	8.2	
Important Pt-group minerals (References)	braggite Pt-Fe alloy cooperite laurite moncheite (3)	laurite cooperite braggite Pt-Fe alloy Cu-sulfide (4)	Pt-Fe alloy cooperite sperrylite moncheite (3)	braggite vysotskite Pt-Fe alloy moncheite cooperite (5, 6)	michenerite moncheite sperrylite froidite koutskite (7)	Pt-Fe alloy cooperite sperrylite rustenburgite native Pt (8)	

* Ni-Cu sulfide deposits with recoverable amounts of PGE as byproducts. References: (1) Macdonald 1987, (2) Naldrett 1989, (3) Kinloch 1982, (4) McLaren & DeVilliers 1982, (5) Bow et al. 1982, (6) Volbroth et al 1986, (7) Cabri and Laflamme 1976, (8) Genkin and Evstigneveva 1986.

<100 ppb to a few hundred ppb, but samples from several ophiolite complexes have been found to contain up to tens of ppm PGE. Such enrichment appears to be related to chromitites hosted in supra-Moho dunites and dunites in the uppermost stratigraphic levels of the mantle sequence, and independent of the chromitite major element composition and the chromite potential of the ophiolite complexes (Economou-Eliopoulos 1996). Ophiolites should not be overlooked as potential resources of PGE.

7.3. Examples

7.3.1. BUSHVELD COMPLEX, SOUTH AFRICA

PGE mineralization occurs in four distinct settings in the Bushveld Complex (Macdonald 1987): (a) the Merensky Reef; (b) the UG-2 chromitite layer; (c) the Platreef of the Potgietersrus limb (northern sector of the Bushveld Complex); and (d) the platiniferous ultramafic pipes of the eastern sector (Fig. 5.5). UG-2 is probably the world's largest PGE resource and deposits in the Merensky Reef and UG-2 chromitite currently produce more than 50% of the world's PGE.

Merensky Reef

The Merensky Reef, with an exposed strike length of more than 250 km, is the most important PGE-enriched horizon of the Complex, and it is being extensively mined at present (Fig. 5.5). The Reef was discovered to be platiniferous by a prospector on the farm Maandagshock in 1924 and was later named in honor of Dr. Hans Merensky, who was in charge of the prospecting operation (Cousins 1969).

The Merensky Reef occurs near the top of the Critical Zone (Fig. 5.6) and constitutes the base of the Merensky cyclic unit, one of the several well-documented cyclic units in the Upper Critical Zone (Fig. 7.1). The thickness of the Reef ranges from 4 cm to 4 m (typically ≈ 1 m) and its dip from 9° to 27° (Cawthorn & Lee 1998). Seismic surveys show reflectors correlated with the position of the Merensky Reef that can be traced as far as 50 km down-dip of outcrop and as deep as 6 km below the surface (du Plessis & Kleywecht 1987). Typically, the Reef is composed of a layer of coarse-grained to pegmatoidal, feldspathic pyroxenite (with some olivine at places) that overlies an anorthosite-leuconorite unit and underlies a finer-grained pyroxenite (bronzitite) unit (Fig. 7.2). The Reef rock is an orthocumulate composed of very coarse-grained subhedral to euhedral orthopyroxene (70-90%) and up to 30% plagioclase as an intercumulus phase. Clinopyroxene oikocrysts (up to 3 cm long) occur throughout the rock and mica is a common accessory mineral. The PGE ore zone, generally in the order of 1 m in thickness, includes the pegmatoidal unit, but the maximum PGE concentrations are localized in the vicinity of the two associated chromitite layers, which generally occur at the top and bottom of the pegmatoidal unit. In the western Bushveld, the bottom chromitite layer ranges in thickness from 3 mm to 3 cm and is quite persistent, but the top chromitite layer is only a few

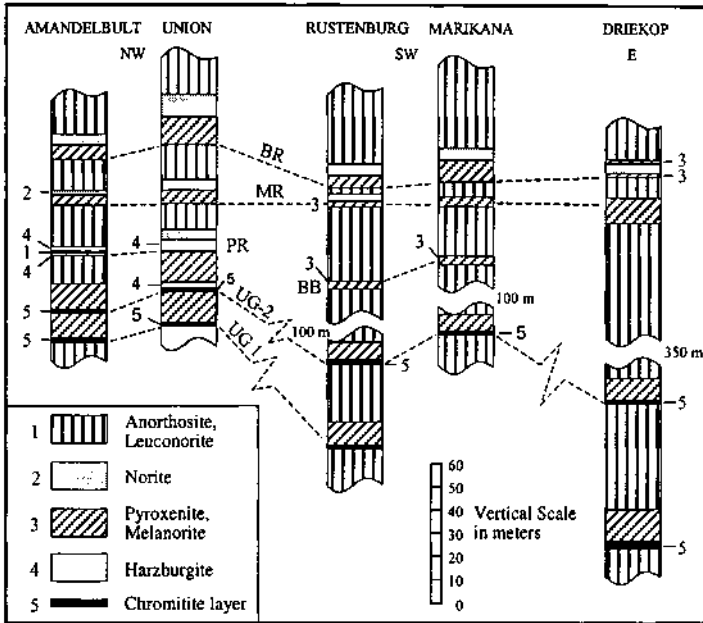


Figure 7.1. The Bastard, Merensky, Pseudoreef, UG-2, and UG-1 cyclic units near the top of the Upper Critical Zone, the Bushveld Complex, with their bases marked, respectively, by the Bastard Reef (BR), Merensky Reef (MR), Pseudoreef (PR), UG-2 chromitite, and UG-1 chromitite. The Boulder bed (BB) is a layered unit containing ellipsoidal masses of pyroxenite embedded in anorthosite. The top of the Critical Zone is defined as the top of the anorthosite of the Bastard cyclic unit. (After Naldrett 1981b.)

millimeters thick and much less continuous. The most important metal values are associated with the upper chromitite. The PGM are dominated by Pt-Pd sulfides, and lesser and approximately equal amounts of PGE-arsenides, tellurides, and other semi-metal phases. Ru-sulfides, dominated by laurite, are associated with the chromitite layers of the Reef.

The PGE grade of the Merensky Reef is clearly related to its higher sulfide concentration (about 2-3 wt%) relative to the rest of the Merensky cyclic unit (Vermaak & Hendriks 1976, Lee 1983, Naldrett et al. 1986). The sulfide assemblage of the Reef is typical of Ni-Cu sulfide deposits, and is dominated by pyrrhotite, chalcopyrite, and pentlandite, with subordinate amounts of either pyrite or cubanite and mackinawite, and rare sulfarsenides, sphalerite, and galena. The main mass of the sulfide mineralization is found chiefly as irregular blebs and interstitial grains. The sulfides are extremely enriched in Ni and Pt (Table 7.3) compared with the sulfides in the rest of the Merensky unit. For example, sulfides in the Reef contain about 600 ppm Pt compared with about 20 ppm in the sulfides of the Merensky unit, and the Pt:Cu ratios are higher in

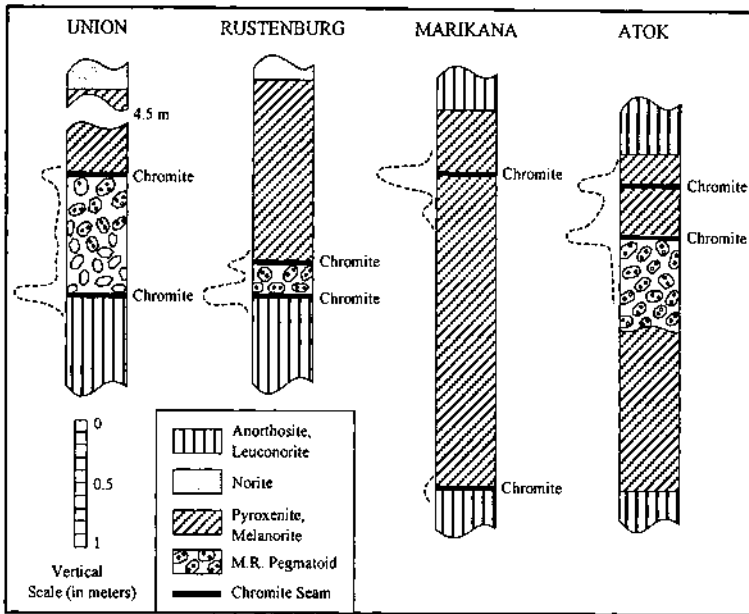


Figure 7.2. Generalized disposition of the Merensky Reef pegmatoid (olivine shown as 6-sided symbols, bronzite as 8-sided symbols that contain 2 circles) in different areas of the Bushveld Complex. Variation of the PGE tenor in the Merensky Reef and its vicinity is shown schematically by dashed lines to the left of each column. (After Naldrett 1981b.)

TABLE 7.3. Comparison of compositions of sulfide ores (normalized to 100% sulfide) of the J-M and Merensky reefs with major classes of Ni-Cu deposits

	Archean komatiites	Flood basalts	Sudbury deposits	Noril'sk-Talnakh	J-M Reef	Merensky Reef	UG-2 chromitite
Ni (5)	10.7-30.2	3.9 - 8.3	3.6-5.7	5.5- 9.0	9.3	10.8	22.5
Cu (%)	0.4- 1.4	7.6-17.4	1.2-4.4	8.7-10.9	6.9	4.6	9.7
Pd (ppm)	0.9- 6.4	2.3-22.4	0.4-6.0	36.0-47.0	5440	120	1112
Pt (ppm)	0.4- 4.2	2.6- 5.6	0.4-2.1	13.7-18.0	1560	279	1235
Rh (ppm)	0.2- 1.4	0.1- 0.6	0.1-0.3	1.4- 2.2	48	19	198
Ru (ppm)	0.6- 4.9	0.1- 0.7	<0.1-0.2	1.5	16	35	371
Ir (ppm)	0.1- 0.6	<0.1- 0.2	<0.1-0.2	1.5	6	7.8	99
Os (ppm)	0.1- 1.0	<0.1- 0.2	<0.1	1.5	7	5.2	37

the Reef sulfides by a factor of about 10 to 40 (Naldrett et al. 1986). A sharp break in the metal tenors occurs just above the upper chromitite layer, but PGE and base metal mineralization commonly extends into the immediate hanging-wall and footwall rocks of the Reef and tends to be of economic grade in thinner reef facies. The sulfide content of the hanging-wall rocks is usually greater than that of the footwall rocks. The Merensky Reef package is unique in that it has a high Pt:Pd ratio (≈ 3) and a constant total metal content, so that thinner mineralized horizons are of relatively higher grades compared with thicker ones. A suggested explanation is that in thinner facies the volume of the sulfide melt exceeded the interstitial volume of the silicates, causing sulfide migration from the Reef into adjacent rocks (Cawthorn & Lee 1998).

The regularity of the Bushveld magmatic stratigraphy is punctuated at certain stratigraphic levels by the so-called "potholes", which are circular to elliptical transgressive depressions with gently to steeply dipping walls extending into the footwall stratigraphy (Fig. 7.3). They are up to several hundred meters in length and their depths, defined by the thickness of the missing cumulate package, typically range from a few to several tens of meters. Potholes are particularly abundant at the level of the Merensky Reef, where they were first recognized, but they also occur at other stratigraphic levels, such as the Bastard Reef and the chromitite layers (Cousins 1969). Similar features have also been described from the Stillwater Complex (Turner et al. 1985), but not in much detail because of limited underground development.

The Merensky Reef changes strike and dip as it wraps over the pothole edge, and the footwall cumulates pinch out. The pothole bottom generally coincides with one of the marker horizons of the footwall stratigraphy and is conformable with layering.

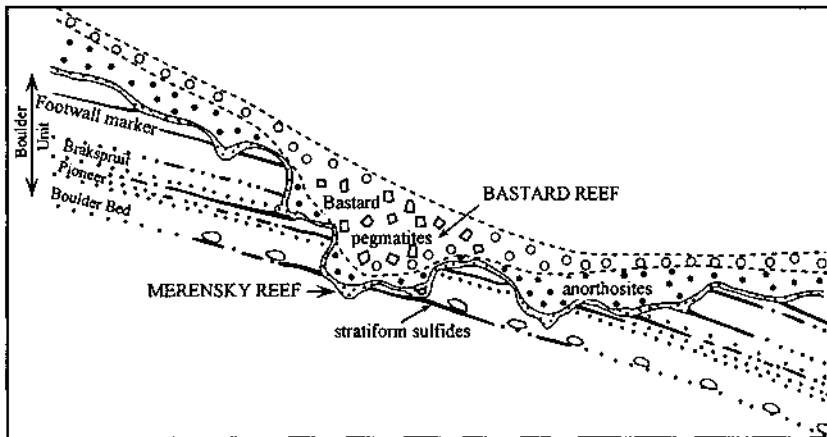


Figure 7.3. Schematic section of a typical pothole at the level of the Merensky Reef. The marker sequence to the Merensky Reef is denoted by dotted lines and the stratiform sulfide horizons by thick solid lines along marker contacts. Note that the Merensky Reef crosscuts the marker sequence and that the Bastard Reef grades into thick Bastard pegmatites within the pothole. (After Ballhaus 1988.)

Along the pothole flanks, the Merensky Reef and its hanging-wall units crosscut the footwall rocks at a steep to locally overturned angle. Some notable features of the Merensky potholes are the abundance of pegmatoidal pyroxenite, the presence of significant amounts of graphite, the occasional occurrence of iron-rich replacement pegmatite, and predominance of PGE alloys and semi-metallic compounds over PGE sulfides (Ballhaus 1988).

The Merensky potholes have been interpreted variously as (a) representing localized depressions due to resorption of footwall cumulates by influx of a fresh hot magma (Irvine et al. 1983, Campbell 1986), (b) discharge zones of volatile-enriched intercumulus liquid during compaction of the lower stratigraphic pile (Buntin et al. 1985), (c) sites of nondeposition where locally high concentrations of dissolved volatiles (C-H-O-S) lowered the liquidus temperature of the magma and suppressed the crystallization of cumulus plagioclase (Ballhaus 1988), or (d) zones of synmagmatic deformation resulting from the loading of the Bushveld magma chamber by a voluminous magma pulse in a regional extensional setting (Carr et al. 1994). A major argument for the interpretation of Ballhaus (1988) is that the stratiform sulfide horizons in footwall units are continuous with and appear to be genetically related to the Merensky Reef (Fig. 7.3). The apparent contemporaneity of the sulfide horizons with both the footwall units and the Merensky Reef suggests that potholes developed gradually during the crystallization of the footwall cumulates. The abundance of pegmatoidal rocks, graphite, and Pt-group alloys in the potholes has been attributed to the influence of high volatile activity during their development. On the other hand, Sr-isotopic data, as discussed by Carr et al. (1999), do not support significant interaction of footwall material with the overlying magma during, or after, the formation of Merensky Reef potholes, but are consistent with the footwall extension model presented by Carr et al. (1994).

Platreef

The Platreef occurs in the Potgietersrus limb, which has a strike length of about 60 km and a thickness of up to 200 m. The mafic rocks of the limb are considered to be part of the Critical Zone of the western and eastern Bushveld Complex and located at the same general stratigraphic level as the Merensky Reef (Van der Merwe 1976). The Platreef strikes northwest and dips 40° southwest. The sequence varies in thickness and has an irregular footwall contact and undulating hanging-wall contact. The hanging-wall of the Platreef consists of fairly homogeneous gabbro-norite typical of the Main Zone elsewhere in the Complex. The floor of the Platreef is occupied by contact-metamorphosed sedimentary rocks (dolostone, shale, ironstone) of the Transvaal Supergroup in the southern portion of the limb and by Archean granitic rocks in the northern part. The Platreef itself is composed of a series of cumulus pyroxenite units. Generally, average PGE grades are highest in the middle part (*B* reef), which is a medium- to coarse-grained pyroxenite (+ norite + melanorite + serpentinite) with minor chromite, and the PGE content does not vary with the thickness of the mineralized pyroxenite. Estimated reserves for the present operations are 23.5 million tonnes of ore

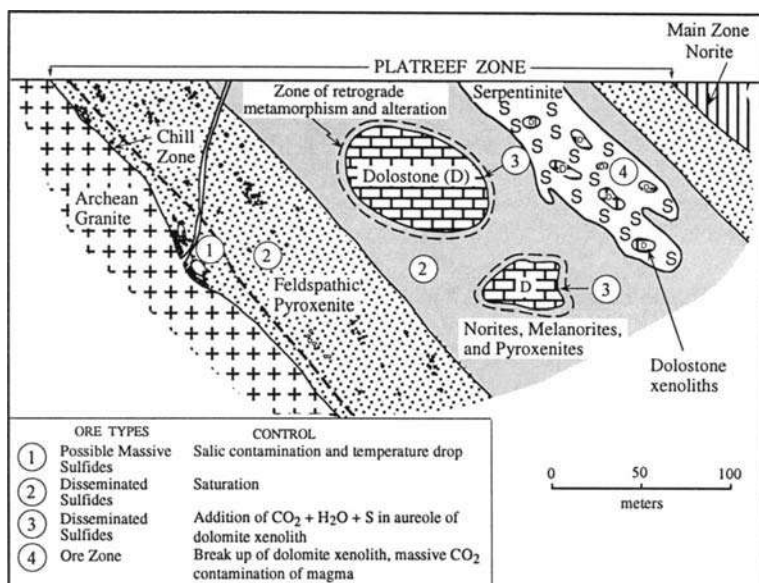


Figure 7.4. Cross section through the Platreef, northern limb of the Bushveld Complex, showing the main lithologic units and the generalized distribution pattern of Ni-Cu sulfide and PGE mineralization (after Gain & Mostert 1982). Metasediments of the Transvaal Supergroup form the footwall of the Platreef in the southern part of the limb.

with an average grade of 5.73 ppm Pt+Pd+Rh+Au; additional ore reserves along strike and to a depth of 250 m are estimated to be 151 million tonnes at 4.98 ppm (Cawthorn & Lee 1998). Xenoliths of metadolostone and calc-silicate rock (1-100 m across) derived from the floor are quite common in the Platreef (Fig. 7.4) and these often contain or are rimmed by concentrations of sulfide, sometimes with high Cu, Ni, and PGE values. Some PGE mineralization occurs in metamorphosed floor rocks.

The PGE mineralogy of the Platreef is highly variable and comprises Pt-Pd sulfides (e.g., cooperite), tellurides, arsenides (e.g., sperrylite), Pt-Fe alloys, and electrum. The PGE mineralization is associated with sulfides, typically a pyrrhotite - pentlandite - chalcopyrite assemblage, but an increase in the PGE concentration is not necessarily accompanied by a corresponding increase in the modal percentage of sulfides, suggesting likely redistribution of the PGE by some post-consolidation process such as serpentinization. Sulfide-PGE mineralization is distributed heterogeneously as disseminations and blebs along the floor, as uneconomic disseminations in the unaltered igneous rocks, as enrichments in the reaction aureoles of dolostone xenoliths, and as relatively high concentrations in the serpentinized zones (Gain & Mostert 1982). The initial PGE-scavenging sulfide mineralization is believed to have occurred by the segregation of an immiscible PGE-enriched sulfide melt from a silicate magma.

Suggested mechanisms for inducing sulfur saturation in the magma include: introduction of additional sulfur into the magma through reaction with anhydrite-bearing floor rocks (Buchanan & Rouse 1984) and dolostone xenoliths (Gain & Mostert 1982); contamination by a partial melt or, more likely, a fluid phase generated by rheomorphism from granites in the Archean basement (Cawthorn et al. 1985); and the influx of a new pulse of more primitive magma (Barton et al. 1986). The high initial $^{87}\text{Sr}/^{86}\text{Sr}$ ratio (0.7104-0.7227, compared with 0.7079 for the overlying gabbro-norite) and the anomalously high Rb/Sr (0.05-0.26) and Ba/Zr (16-44) ratios of the Platreef cumulate-textured pyroxenites indicate substantial assimilation of siliceous material, but the pattern of $^{87}\text{Sr}/^{86}\text{Sr}$ variation indicates that the contamination was a post-emplacement event and an unlikely mechanism for liquating sulfides (Cawthorn et al. 1985, Barton et al. 1986). The model preferred by Barton et al. (1986) is one of magma addition, analogous to that for the normal Merensky Reef. The high PGE tenors of the sulfide fraction, relative to its Cu and Ni contents, probably reflects the combined contribution from PGM precipitated from a sulfide liquid and PGE held in sulfide solid solution (Cawthorn and Lee 1998).

UG-2 Chromitite

All the chromitite layers of the Bushveld Complex (see Table 5.3) are enriched in PGE (mostly greater than 1 ppm Pt and 0.2 ppm Pd) relative to the surrounding cumulate rocks (von Gruenewaldt et al. 1986, Lee & Parry 1988). The UG-2 is the most continuous and the richest chromitite layer; values as high as 10.7 ppm Pt and 8.5 ppm Pd have been reported from individual samples. (Hiemstra 1985). It contains just over 50% of the PGE resources of the Complex (von Gruenewaldt 1977) and has been a significant producer since 1986. The UG-2 occurs 15 to 400 m below the Merensky Reef, the vertical separation being the smallest in the western Bushveld and the largest in the eastern Bushveld. Circular potholes, ranging from less than 10 m to more than 50-100 m in diameter, are a common feature of the UG-2 chromitite. Potholes associated with the UG-2 share many common features with those associated with the Merensky Reef, but they are not spatially correlated. However, large scale disruptions to the layering often affect both sequences, particularly at Union mine where the stratigraphic separation between them is only about 15 m (Cawthorn & Lee 1998).

The UG-2 chromitite layer, about 0.5 to 2.5 m (mostly 0.5-1.0 m) in thickness, occurs within a bronzite cumulate at the base of the UG-2 cyclic unit (upper Critical Zone). The layer is underlain in most cases by a zone of pegmatoidal feldspathic pyroxenite (composed of coarse bronzite and interstitial plagioclase) containing irregular layers of harzburgite and chromitite. The chromitite consists of 60-90% chromite, 5-25% bronzite, and 5-15% plagioclase, with accessory clinopyroxene, base metal sulfides, PGM, ilmenite, magnetite, rutile, and biotite. The average Cr:Fe ratio ranges between 1.26 and 1.4 with 43.5% Cr_2O_3 (Cawthorn & Lee 1998). Average ΣPGE grades for the UG-2 chromitite range from 4.3-4.9 ppm at the Western Platinum mine to 9.3 ppm in the northwestern sector and 8.2 ppm at Maandagshoek in the eastern Bushveld (McLaren and de Villiers 1982). Average Pt:Pd ratio is 2.5 in the western

Bushveld and ≈ 1 in the eastern Bushveld (Gain 1985). The Σ PGE+Au grade of the UG-2 is higher in thinner facies than in thicker facies (Vermaak 1985), so that the precious metal content of the UG-2 is fairly uniform, as is the case with the Merensky Reef.

Regionally, the PGM assemblage in the UG-2 is dominated by Pt-Pd sulfides and laurite (RuS_2), which occur as minute, discrete grains interstitial to the chromite grains. The only PGM commonly enclosed by chromite is laurite. Cu and Ni contents of the UG-2 are low, generally $<0.05\%$; the amount of base metal sulfides is also extremely low, but these are present throughout the layer. Locally, sulfides can be more abundant without affecting the overall PGE tenor (Cawthorn & Lee 1998). Most PGM are attached to base metal sulfide minerals (pentlandite, chalcopyrite, pyrrhotite, millerite, and pyrite), although some occur within the orthopyroxene gangue. Thus, there is a strong association between base metal sulfides and PGE mineralization, as is the case with the Merensky Reef, but the PGE tenor (calculated PGE content in 100% sulfides, assuming that all the PGE are concentrated in the sulfides) in the UG-2, ranging from 2,000 ppm to just under 12,000 ppm and averaging about 3,300 ppm (McLaren & de Villiers 1982, Gain 1985), is about 5 to 10 times as high as that of the Merensky Reef. Apparently, all the UG and MG chromitite layers have very high PGE:S and high Cu:S and Ni:S ratios.

The much higher PGE content of the UG-2 compared with that of the Merensky Reef may simply be a reflection of the difference in their sulfide contents, as judged from their Ni+Cu grades (see Table 7.3), dictated by different conditions of magmatic crystallization. Removal of FeO from the magma as a consequence of chromite crystallization would lower its sulfur-carrying capacity and lead to the separation of an immiscible sulfide melt. If such a melt acted as the collector of PGE, as the correlation of PGE with sulfides seems to suggest, then the silicate magma:sulfide melt ratio (the R factor in Equation 2.6) must have been very high (Campbell et al. 1983). This situation is compatible with the mixing of host magma with an influx of fresh magma at the level of UG-2 crystallization, but the modeling of the PGE concentration on the basis of high D and R values runs into a serious problem. The estimated tenors of Ni and Cu in the sulfides (22.5 and 9.75 wt%, respectively; Gain 1985) are much higher than the values calculated using the compositions of parental liquids corresponding to marginal samples analyzed by Harmer and Sharpe (1985) and Davies and Tredoux (1985). For example, taking Davies and Tredoux's average Ni content of 274 ppm and a partition coefficient of 275 for Ni (Rajamani and Naldrett 1978), the resulting sulfide would be expected to contain 7.5 wt% Ni (Naldrett 1989). Thus, either the PGE concentration in the UG-2 is not directly related to sulfide immiscibility or the UG-2 ore has been modified to some extent subsequent to its segregation as an immiscible sulfide melt. A mechanism proposed by von Gruenewaldt et al. (1986) for upgrading the Cu, Ni, and PGE tenor of the UG-2 ore involves the selective loss of Fe and S from sulfides in the chromitite horizon, transfer of the Fe to fill vacancies in the chromite lattice, and diffusion of S into the surrounding rocks. Such a process could be accomplished by a subsolidus reaction involving pyrrhotite and chromite to produce more Fe-rich chromite, thereby releasing sulfur (Naldrett and Lehmann 1987).

An alternative explanation may be deuteric or hydrothermal modifications similar to that proposed for Merensky-type ores (discussed later). Gain (1985) proposed that PGE enrichment in the UG-2 involved collection of PGE by pre-existing sulfides in the chromitite layer from upward-migrating, highly fractionated, volatile- and PGE-rich intercumulus fluids under highly reducing conditions during early stages of formation of the layer. At a later stage, the volume of sulfides was reduced by oxygen-enriched volatiles passing through the layer, resorbing the sulfides and blowing off SO_2 . This model does not require abnormally high values of PGE partition coefficients.

Ultramafic Pipes

Many distinct, but possibly genetically related, groups of transgressive, post-cumulus bodies of ultramafic rocks have been recognized in the Bushveld Complex (Wagner 1929, Willemse 1969a, Viljoen & Scoon 1985, Scoon & Mitchell 1994). The most well known of these are the four occurrences (Driekop, Mroihoek, Onverwacht, and Maandagschoek) of platiniferous ultramafic (or dunitic) pipes, which (except Maandagschoek) were mined earlier for platinum. Average grades were in the order of 10 ppm PGE or less, with irregular patches up to 80-100 ppm; Wagner (1929) cited grades reaching locally up to 2,050 ppm total PGE.

The pipes cut both the lower and upper Critical Zone cumulates and are aligned almost at right angles to the cumulate layering; close to the pipes the igneous layering of the country rocks dips steeply downward toward the pipe. The pipes are composed of downward-tapering, cylindrical bodies of magnesian dunite, which enclose core zones of pegmatoidal iron-rich dunite (composed of hortonolite, olivine with 50-70% fayalite) and wehrlite; some pipes have an outer shell of pegmatoidal wehrlite or clinopyroxenite (Viljoen & Scoon 1985). PGE mineralization (up to 31 ppm Pt in the Onverwacht pipe) with high Pt:Pd ratios and minor base metal sulfides are essentially restricted to the core zone, which represents only a small proportion of the overall pipe. The PGM suite is composed of Pt-Fe alloy, sperrylite, hollingworthite, irasite, and a variety of rare minerals.

Most workers have attributed the origin of the pipes and their PGE mineralization to post-cumulus infiltration metasomatism by magmatic hydrothermal fluids rather than to the intrusion of an olivine-rich magma (Cameron & Desborough 1964, Stumpfl & Rucklidge 1982, Schiffries 1982). A key evidence for this interpretation is the presence of disrupted slabs of chromitite within the Onverwacht pipe, more or less at the projected stratigraphic level at which the pipe transects the LG-6 chromitite layer (Steelport seam). The genetic model presented by Schiffries (1982) envisages channeled flow of high-temperature ($600 \pm 150^\circ\text{C}$) chloride-rich solutions and replacement of bronzitites involving desilication of orthopyroxene to produce olivine, dissolution of plagioclase, and Fe enrichment of some olivine to fayalitic compositions. Aqueous chloride complexes are believed to have played an important role in the transport and precipitation of PGE, base metals, and other cations. The fluids, which apparently contained large amounts of CO_2 and other volatiles, probably affected the mineralogy of the UG-2 chromitite and the Merensky Reef in the vicinity of the pipes.

7.3.2. STILLWATER COMPLEX, MONTANA, USA

The Stillwater Complex in south-central Montana (USA) is an early Precambrian (≈ 2.7 Ga; De Paolo & Wasserburg 1979) layered intrusion with an exposed strike length of about 48 km and a visible thickness of almost 6 km (Fig. 7.5). The Complex intrudes older (3.14 Ga) sedimentary rocks, which have been contact-metamorphosed, and is overlain by Phanerozoic sedimentary rocks. Many schemes of stratigraphic nomenclature have been proposed for the Complex (see Zientek et al. 1985); the one followed here is by Todd et al. (1982). They divided the Complex into three series (Fig. 7.6): (a) the Basal Series (up to 400 m thick), consisting dominantly of sulfide-bearing orthopyroxene cumulates (norite and bronzitite); (b) the Ultramafic Series (up to 2,000 m thick), composed of cumulate dunite, harzburgite, bronzitite, and thin chromitite seams; and (c) the Banded Series (up to 4,500 m thick), comprising both layered and massive gabbro, norite, anorthosite, and minor troctolite. The boundary between the Ultramafic Series and the Banded Series is marked by the first appearance of cumulus plagioclase. The Banded Series is subdivided into six megacyclic units (I to VI), each of which may locally contain smaller cyclic units. Each megacyclic unit is further subdivided into several zones, and each zone into several subzones, based on the abundance of cumulus minerals and the order in which they crystallized. In the megacyclic units III, IV, and V, the cumulus minerals appear generally in the order plagioclase \Rightarrow olivine \Rightarrow augite \Rightarrow bronzite (or hypersthene). In the norite and gabbro zones of megacyclic units I and II and in the underlying Ultramafic Series, the general order of cumulus minerals is olivine \Rightarrow bronzite \Rightarrow plagioclase \Rightarrow augite. Of

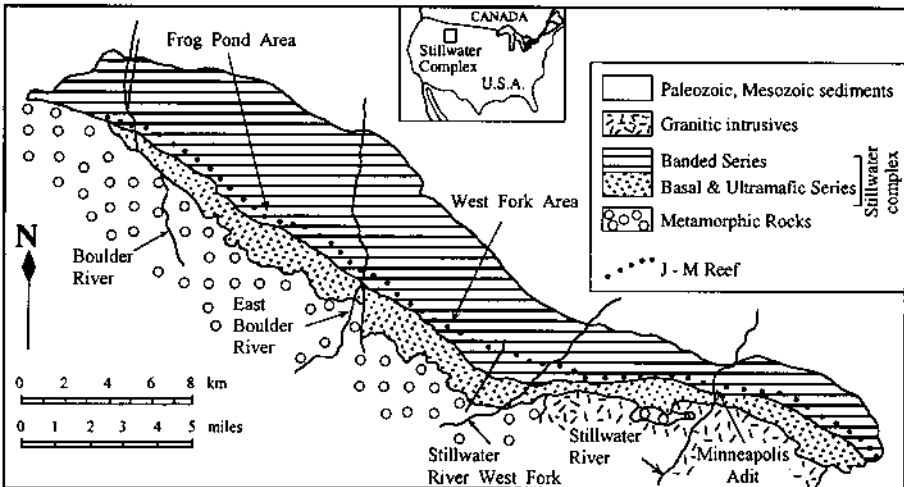


Figure 7.5. Generalized geologic map of the Stillwater Complex showing the J-M Reef, the main PGE-enriched horizon of the Complex. The J-M Reef occurs within the Troctolite-Anorthosite Zone I (TAZ₁) of the Banded Series (see Fig. 7.6). (Simplified from Todd et al. 1982.)

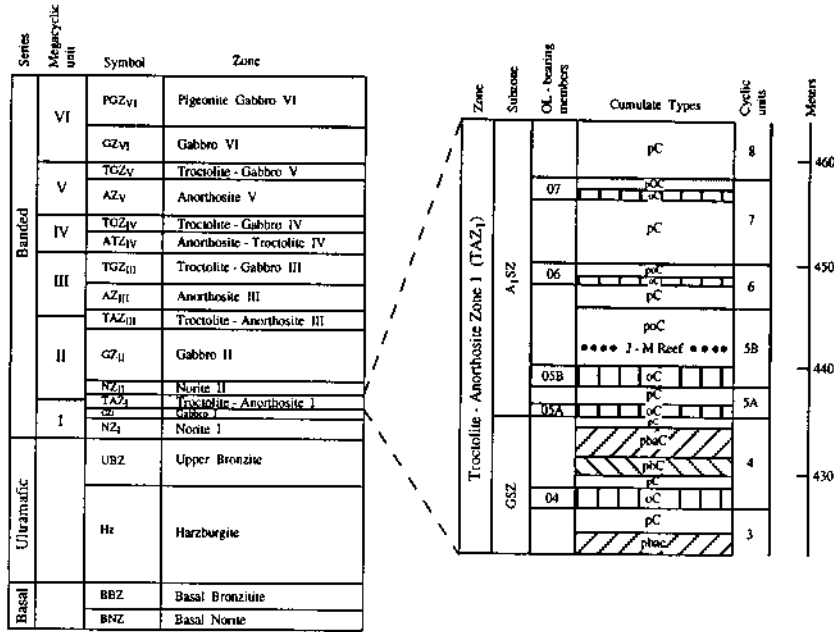


Figure 7.6. Simplified stratigraphic section of the Stillwater Complex as proposed by Todd et al. (1982), with a more detailed section of the Troctolite-Anorthosite Zone I (TAZ₁) showing the locations of five olivine-bearing members (O4, O5A, O5B, O6, and O7) and the position of the J-M Reef. GSZ = Gabbro subzone and A₁SZ = Anorthosite subzone. Stratigraphic height is measured above the Ultramafic Series-Banded Series contact. Cumulate assemblages (C) in the detailed section are described by acronyms of abbreviations of minerals listed in decreasing order of abundance: a = augite (clinopyroxene), b = bronzite (orthopyroxene), o = olivine, and p = plagioclase. (Compiled from Todd et al. 1982, Lambert & Simmons 1988.)

particular importance for the evolution of the Complex are the five troctolite-anorthosite zones (olivine-bearing subzones of McCallum et al. 1980) each of which marks the reappearance of Mg-rich olivine as a cumulus phase.

Sulfide-associated PGE mineralization occurs at several stratigraphic levels of the Complex. The most important PGE horizon has been named the J-M Reef by Todd et al. (1982) in recognition of its discovery and delineation by the Johns-Manville Corporation through an exploration program that was initiated in 1967. The J-M Reef (also known as the Howland Reef) is located in the basal part of the Anorthosite I subzone within the Troctolite-Anorthosite zone I (Fig. 7.6), the olivine-bearing zone I (OB-I) of McCallum et al. (1980), which is the lowest unit with cumulus Mg-rich olivine in the Banded Series. The Reef is a sulfide-bearing stratigraphic horizon, generally 1 to 3 m thick (maximum thickness about 5 m), that has been traced on surface and by drill hole intersections over almost the entire strike length of the Complex (Fig. 7.5). It contains only a fraction of the resources in the Merensky Reef,

but the PGE grade and Pd:Pt ratio are significantly higher (Table 7.3). Other PGE-rich horizons exist stratigraphically higher in the complex — e.g., the Picket Pin zone in the upper part of Anorthosite V zone (Boudreau & McCallum 1986) — but they lack the lateral continuity and grade of the J-M Reef.

The J-M Reef is distinguished by small concentrations (0.5-2 wt%) of sulfides consisting principally of pentlandite, pyrrhotite, chalcopyrite, and pyrite. The sulfides generally occur as blebs or as an interstitial network in the lower part of the Reef, and as fine disseminations toward the top. Textures, such as spherical bodies of sulfide within olivine grains and cusped masses of sulfide molded about olivine, indicate that the sulfides were present at the magmatic crystallization stage. In some cases, cusped sulfides are entirely enclosed in oikocrystic bronzite, which also contains remnants of resorbed olivine, indicating that the resorption occurred after the sulfide liquid had solidified. Tiny grains of various platinum-group minerals occur with the sulfides. A strong statistical correlation among the PGE, Ni, Cu, and S indicates that all these elements are held dominantly in the sulfide fraction of the Reef and that the PGE grade of the Reef is controlled primarily by the sulfide abundance (Barnes & Naldrett 1985).

Raedeke and Vian (1986) described PGE-sulfide mineralization at four stratigraphic levels ("zones") within the J-M Reef in the Minneapolis adit area, where the Stillwater Mining Company's active mine is located. These zones, relative to the base of olivine-bearing zone I (OB-I), are (Fig. 7.7): (a) the Footwall zone, characterized by relatively continuous but thin sulfide layers within about 10 m below the base of OB-I; (b) the Basal zone that straddles the base of OB-I; (c) the Main zone within OB-I but close to its base; and (d) the Upper zone well above the basal contact. Generally, only one mineralization zone is present over any significant strike length, but stacking of up to three zones has been observed. The basal and main zones contain much of the higher grade PGE mineralization. In general agreement with many previous workers (e.g.,

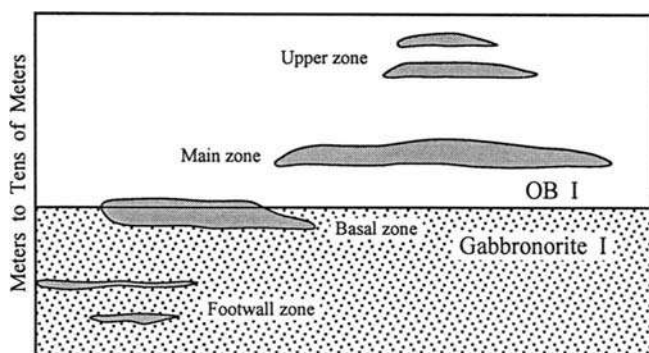


Figure 7.7. Schematic cross section showing four zones of sulfide-PGE mineralization relative to the basal contact of the olivine-bearing zone I (OB-I) in the Minneapolis Adit area, the Stillwater Complex (after Raedeke & Vian 1986). The OB-I and Gabbro-norite I zones shown here are equivalents of Troctolite-Anorthosite Zone I (TAZ₁) and Gabbro Zone I (GZ₁), respectively, in Figure 7.6.

Todd et al. 1982, Campbell et al. 1983, Barnes & Naldrett 1985), Raedeke and Vian (1986) proposed a model involving mixing of magmas of two distinct compositions for the formation of the OB-I cumulate layer and its sulfide-PGE zones.

7.4. Ore Composition

7.4.1. MINERALOGY AND TEXTURES

The most obvious geochemical characteristic of platinum-group elements is their siderophile nature, as evidenced by strong partitioning of the PGE into the Fe-Ni metal phase of iron meteorites and chondrites (Crocket 1981). Metal alloys are common in PGE deposits and many platinum-group minerals have metallic-type bonding. However, in the range of oxygen and sulfur fugacities prevalent in the crust and upper mantle, the PGE commonly exhibit chalcophile behavior (Naldrett & Duke 1980).

A small proportion of the total PGE in ores occurs as solid solution components of other minerals. In general terms, sulpharsenides, arsenides, sulfides, oxides, and silicates represent a sequence of decreasing PGE content, ranging from tens to thousands of ppm in sulpharsenides and arsenides to concentrations probably as low as 0.001 ppb in silicates (Crocket 1981). Experimental data show that $Ni_{11}As_8$ can accommodate up to 8.6 wt% Pd at 450°C and up to 2.4 wt% Pd at 790°C; NiAs can accommodate 3.4 wt% Pd at 450°C and 5.8 wt% Pd at 790°C (Gervilla et al. 1994). A similar behavior should also be expected for Pt. Natural sulpharsenide and arsenide minerals (e.g., cobaltite, niccolite, maucherite, löellingite, and gersdorffite) are also relatively enriched in PGE (up to 1.95 wt% Pd, 0.25 wt% Pt, and 1.53 wt% Rh have been reported by Cabri and Laflamme 1976), but owing to their limited abundance they do not contribute much to the PGE grade of ore deposits. Chromites from many ophiolites show elevated concentrations of PGE (Page & Talkington 1984, Pedersen et al. 1993), especially of IPGE, but it is not certain if the high PGE values result from solid solution or inclusions of platinum-group and/or sulfide minerals in the chromite.

It is now well established that the pyrrhotite - pentlandite - chalcopyrite assemblage of Ni-Cu sulfide accumulations are relatively enriched in PGE, but the pattern of PGE enrichment in individual sulfide minerals is less clear, except for the strong preferential concentration of Pd (commonly in the order of 100-400 ppm) and, to a lesser extent, of Rh (commonly in the order of 25-70 ppm) in pentlandite (Chyi & Crocket 1976, Brynard et al. 1976, Vermaak & Hendriks 1976, Cabri & Laflamme 1976, Cabri 1981, Kinloch 1982, Cowden et al. 1986). From a consideration of size, charge, and electronegativity, the divalent PGE are capable of substituting for base metals in sulfide structures, and Skinner et al. (1976) have reported up to 1.5 atomic% Pd, but less than 0.5 atomic% Pt, in synthetic pyrrhotite at 1,000°C. The relative contribution of solid solution and submicroscopic inclusions of discrete platinum-group minerals to the PGE values of natural sulfide minerals is difficult to assess.

The bulk of the PGE values in ores, however, is accounted for by discrete platinum-

group minerals (PGM). The mode of occurrence of the PGM, which is of importance not only from a genetic viewpoint but also for the recovery of PGE values, may be classified into three categories (Vermaak & Hendriks 1976, Kinloch 1982): (a) PGM enclosed in or attached to base metal sulfides (BMS); (b) PGM enclosed in silicates; and (c) PGM enclosed in or attached to chromite. In most ores, a large proportion of the PGM is preferentially concentrated at the sulfide-gangue contacts. For example, in the Merensky Reef, on the average 71% (by volume) of the PGM occur at the BMS-gangue contact, 16% within BMS, and 13% within gangue minerals (Vermaak & Hendriks 1976). The distribution of PGE minerals in the UG-2 chromitite is similar (McLaren & De Villiers 1982).

The most common PGM in ore deposits are Pt-Fe alloys (commonly intergrown with BMS), arsenides (sperrylite, irarsite), Pt-Pd sulfides (braggite, cooperite), and Pt-Pd tellurides (moncheite, merenskyite, kotulskite). The list of important PGM in various deposits as presented in Table 7.2 is a generalization; all of them contain a wide variety of PGM including a number of unnamed minerals, with considerable spatial variation in mineralogy (Cabri & Laflamme 1976, Vermaak & Hendriks 1976, Page et al. 1976, McLaren & De Villiers 1982, Kinloch 1982, Genkin & Evstigneeva 1986, Volborth et al. 1986). In the Bushveld Complex, the mineralogy of the UG-2 and the Merensky Reef are broadly similar and vary together along the strike. Also, the proportions of Pt-Fe alloy in both units are much higher than normal in certain localized areas (for example, Union mine, northwestern Bushveld), which are thought to have been close to postulated centers of increased volatile activity or perhaps regional feeder zones. Kinloch (1982) proposed that both the regional and local variations developed in response to the introduction of relatively oxidized fluids. The fluids caused the breakdown of sulfide minerals, loss of sulfur, and reaction of platinum with the released iron to form Pt-Fe alloy.

A platinum-group mineral that is predominantly associated with chromitites of layered intrusions (and also of ophiolite complexes) is laurite (RuS_2). Inclusions of laurite in chromite have been attributed by some authors to exsolution of PGE from the host chromite during subsolidus equilibration (Gijbels et al. 1974, Oshin & Crockett 1982). Others have favored magmatic crystallization of both laurite, probably from an immiscible sulfide liquid, and chromite (McLaren & De Villiers 1982, Stockman & Hlava 1984, Talkington & Lipin 1986). Experimental studies by Amossé et al. (1990) have shown that, in a silicate melt, increasing $f\text{O}_2$ results in much sharper decrease in Ir solubility compared with that of Pt, whereas increasing $f\text{S}_2$ results in a pronounced increase in Pt solubility without affecting Ir solubility. Assuming that IPGE's behave as Ir and PPGE's as Pt, they have proposed that laurite inclusions in chromite represent preferential early precipitation of IPGE's in the form of alloys or sulfides (depending on $f\text{S}_2$) due to an increase in $f\text{O}_2$ at the stage of copious chromite precipitation.

7.4.2. BULK COMPOSITION

Bulk compositional data presented in Table 7.3 and Figure 7.8 have been extracted

primarily from Naldrett (1989), which includes a comprehensive compilation of PGE concentrations in Ni-Cu sulfide accumulations of various magmatic associations, recalculated to concentrations expected in 100% sulfides. Some generalizations about PGE distribution in Ni-Cu sulfides and chromitites are summarized below (Naldrett, 1989, Naldrett & von Gruenewaldt 1989, Peach & Mathez 1996):

- (a) Typical ophiolitic chromitites are characterized by IPGE in the range of 0.1 to 1.0 times chondritic abundance, and PPGE abundances about 0.01 times chondritic or less (see Fig. 5.11), probably because of preferential partitioning of IPGE into the spinel phases (Capobianco & Drake 1990). In contrast, the Bushveld Upper and Middle Group chromitites have IPGE and PPGE abundances in the order of 0.5-1.0 and 0.5-4 times chondritic, respectively. The Stillwater chromitites fall in between these two extremes. This contrast in the PGE profiles between the ophiolitic and layered intrusion chromitites has been ascribed to differences in the relative proportions of PGE in the source magmas and original abundance of PGE-enriched sulfides (Naldrett & von Gruenewaldt 1989).
- (b) The correlation between sulfide (approximated by wt% Ni+Cu recalculated to 100% sulfide) and PGE is strong for individual deposits, but the overall correlation is poor, except for the komatiite-hosted Ni-sulfide deposits.
- (c) Although the PGE content of parent magmas for the Bushveld and Stillwater complexes is similar to that of other types of continental basaltic magmas, the sulfide-associated stratiform ores of layered complexes (e.g., the Merensky Reef, the J-M Reef) are remarkably enriched in PGE compared with almost all other kinds of magmatic sulfides.
- (d) Relative to mantle abundances, fractionation of IPGE from PPGE is ubiquitous in sulfide accumulations in terrestrial rocks. The fractionation appears to be related in part to the igneous host rocks in the sense that PPGE/IPGE ratios vary from ≤ 3 in sulfides associated with komatiitic peridotites, which crystallized from magmas containing >20 wt% MgO, to ≥ 12 in sulfides associated with gabbroic rocks that crystallized from magmas containing <12 wt% MgO.

7.5. Origin of Merensky-type PGE Deposits

The Merensky Reef and J-M Reef PGE deposits have many similar features, suggesting a common origin (Campbell et al. 1983, Naldrett 1989). The most important of these are summarized below:

- (a) Both reefs occur about 500 m above the first appearance of cumulus plagioclase in their respective host intrusions, i.e., above the level at which the magmatic stratigraphy is first dominated by gabbroic, rather than

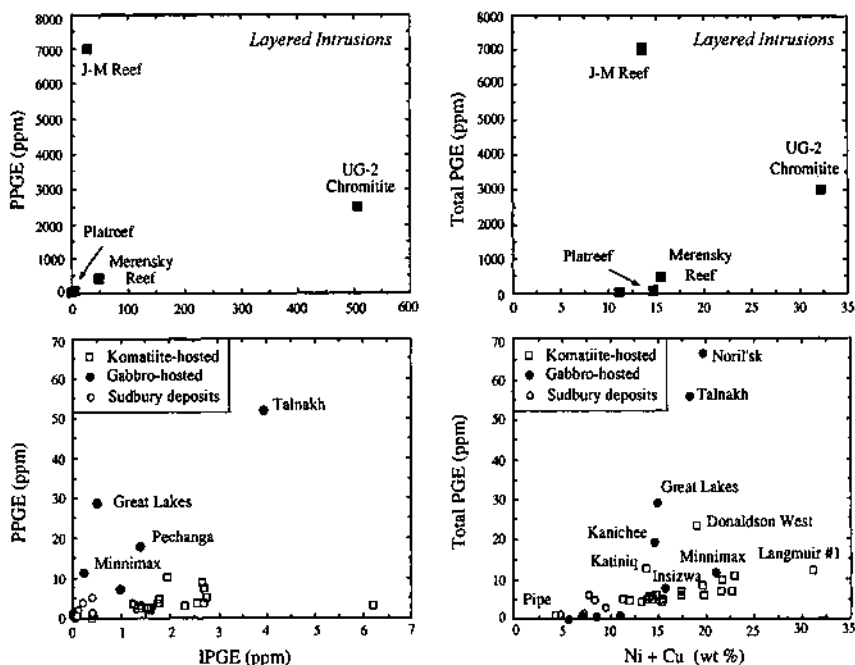


Figure 7.8. Comparison of PGE concentrations in PGE-rich Ni-sulfide and chromitite accumulations hosted by layered intrusions with those in Cu-Ni dominant sulfide ores hosted by komatiites (Western Australia, Canada, Zimbabwe), gabbroic intrusions (Talnakh, Noril'sk, Duluth, Insizwa, Great Lakes, Montcalm, Espedalen, Kanichee, Pechanga, Kenbridge), and the Sudbury Complex (Levack West, Little Stobie 1 and 2, Strathcona, Falconbridge). Element concentrations have been recalculated to 100% sulfide. PPGE = Pt+Pd+Rh; IPGE = Ru+Ir+Os. (Sources of data: Gain 1985, Naldrett and Barnes 1986, Naldrett 1989.)

ultramafic, rocks. (The Main Sulfide Zone (MSZ) of the Great Dyke is an exception to this generalization.) In general, chromitite layers that occur at horizons below the appearance of cumulus plagioclase are much lower in PGE than those that occur above. (The PGE-enriched A chromitite of the Stillwater Complex is an exception.)

- (b) PGE mineralization in both reefs is associated with interstitial Ni-Cu sulfides, which are concentrated at or near the base of cyclic units marked by reappearance of high-temperature cumulus phases (olivine and chromite in the Stillwater Complex; bronzite and chromite, and locally olivine, in the Bushveld Complex) and reversals in fractionation trends.
- (c) A striking feature of the PGE-rich horizons of both reefs is the relatively high Pt:S and Pd:S ratios. For example, the Merensky Reef ore contains ≈ 2 wt% sulfide, only about one-fifteenth of that typical of the Sudbury ore, but its PGE tenors are about ten times those of the Sudbury ore and two to

- three orders of magnitude higher than typical values for Ni-Cu sulfide deposits, without any parallel marked differences in Ni, Cu, and Co values.
- (d) Both reefs are characterized by the occurrence of coarse-grained, pegmatoidal gabbroic rocks and "potholes".
 - (e) The sulfides in both reefs are associated with Cl-rich hydrous silicates.

The various genetic models proposed for the Merensky-type deposits may be grouped into two categories: (a) orthomagmatic models, which consider the sulfide-PGE mineralization as an integral part of magmatic crystallization, with some modification by post-cumulus processes; and (b) hydrothermal models, which ascribe the sulfide-PGE mineralization to volatile-rich fluids derived from pre-existing cumulate sequences.

7.5.1. ORTHOMAGMATIC MODELS

The essence of orthomagmatic models lies in the separation of a PGE-enriched sulfide liquid from the silicate magma and its accumulation on or close to the floor of the magma chamber. Evidence in favor of such an origin includes (Naldrett & Duke 1980, Naldrett 1981b, Campbell et al. 1983, Irvine et al. 1983, Barnes & Naldrett 1985, Naldrett et al. 1986, Barnes & Campbell 1988, Naldrett 1989, Wilson et al. 1989):

- (a) the close association of PGE reefs with specific features of magma evolution, such as cyclic units and chromitite layers;
- (b) the lateral persistence and relative uniformity of PGE grade of the reefs;
- (c) systematic stratigraphic controls on PGE tenors of sulfides, for example, within the Upper Critical Zone of the Bushveld Complex; and
- (d) a strong correlation of PGE ores with Ni-Cu sulfide accumulations, which themselves are believed to be of orthomagmatic origin (sulfide liquid immiscibility).

Of the possible mechanisms by which a magma may achieve sulfur saturation and, hence, sulfide immiscibility (see Ch. 6), magma mixing appears to offer the best choice for the Merensky-type deposits. The Pt-Pd-rich sulfide horizons in layered intrusions are closely linked with the base of cyclic units, and the development of each cyclic unit is generally attributed to the influx of a new pulse of primitive magma into the chamber (Campbell 1977, Irvine 1980, Todd et al. 1982, Sharpe 1982, Irvine et al. 1983, Lambert & Simmons 1988). The magma-mixing model discussed earlier in connection with the formation of chromitite layers in layered intrusions (see Ch. 5) may also be invoked as a likely explanation for the formation of PGE-rich sulfide horizons in these intrusions (Irvine et al. 1983, Campbell et al. 1983, Barnes & Naldrett 1985, Naldrett & von Gruenewaldt 1989, Naldrett et al. 1990), although opinions differ about magma compositions and the mixing process.

Refining the magma mixing-models proposed earlier for the J-M Reef sulfides (Todd et al. 1982) and for the host rocks of the UG-2 and the Merensky Reef (Sharpe 1982),

Irvine et al. (1983) proposed that for the Bushveld and Stillwater complexes, double-diffusive convective mixing of an ultramafic (*U*) magma of olivine-boninitic affinity, exceptionally rich in PGE (up to 100 ppb Σ PGE + Au) but low in S content, and an anorthositic (*A*) magma, similar to mid-ocean ridge tholeiites, would yield not only chromitite (see Ch. 5) but also sulfide-associated PGE deposits. The critical difference between the two cases is that the *U* and *A* liquids were saturated with chromite from the start, whereas they apparently did not become saturated with sulfide until after they had been extensively fractionated, either within the magma chamber or during filter-pressing of the trapped liquid. The late segregation of sulfide, which scavenges PGE because of the high partition coefficients of PGE in favor of sulfides relative to silicates, is an important requirement for the concentration of PGE at the observed levels. Barnes and Naldrett (1985), however, have argued against the derivation of all the PGE from a strongly PGE-enriched resident melt, because this should have produced a strong enrichment of Cu over Ni instead of the observed relatively high Ni:Cu ratio of the Reef sulfides (Table 7.3).

Arguments in favor of a liquid immiscibility origin for the Ni-Cu dominant sulfide ores have been discussed in Ch. 6. Naldrett (1981b) showed that the PGE values associated with these deposits could be modeled as a consequence of the same magmatic fractional crystallization process (Equation 2.6) with appropriate values of *R* (mostly in the order of 300 to 3,000) and *D* (in the order of 1,000 to 1,500 for Pt and Pd). Successful application of the model to Pt-Pd dominant Merensky-type sulfides requires much higher values of *D* and *R*, in the order of 10^4 to 10^6 (Campbell et al. 1983). Experimentally determined *D* values are in the order of 10^4 (Table 7.4) and, for high *D* values to have a significant impact on Y_i (Equation 2.6), *R* values must also be high, in the order of 10^4 or higher (see Fig. 2.7). For example, Naldrett et al. (1986) have argued that if the partition coefficients for PGE are in the order of 10^5 , and for Ni and Cu are similar to the experimentally determined values of Rajamani and Naldrett (1978) as listed in Table 6.2, raising log *R* from 2.5 to 5.3 would account for the differences in the concentrations of PGE between the sulfides of the Merensky-type and those of the Ni-Cu dominant deposits as well as for their comparable Ni and Cu contents. Calculations with *R* and *D* values chosen to fit the field data, however, are not constrained by the geochemistry of the deposits and, as stated by Peach and Mathez (1996), "such a large latitude exists in estimating these parameters that virtually any set of observations can be accounted for."

A major problem with the orthomagmatic model, as discussed elegantly by Peach and Mathez (1996), is the high Pd (representing PPGE):Ir (representing IPGE) ratios of sulfide fractions in Merensky-type deposits (see Table 7.3) compared with a Pd:Ir ratio of only about 1.3 estimated for the mantle. This implies a major fractionation between Pd and Ir either during the source magma generation by partial melting of the mantle or during fractional crystallization of the magma. A possible mechanism for Pd-Ir fractionation is compatibility of Ir in olivine. Ross and Keays (1979) reported Ir and Pd concentrations of 5.7 and 0.21 ppb, respectively, in cumulate olivines from Western Australian komatiites, compared with 1.4 ppb Ir and 10 ppb Pd in rocks representing

TABLE 7.4. Partition coefficients for iridium (D_{Ir}) and palladium (D_{Pd}) as determined from experimental studies, modern MORB, and natural assemblages (source of data: compilation by Peach et al. 1994)

Study	T (°C)	P	Fluid	Silicate / sulfide equilibrium	Relative fO_2	$\log fS_2$	D_{Ir}	D_{Pd}
Peach et al. (1990)	~1,200	>1 bar	COS	Natural MORB / po+cp+pn	- QFM - 2	-2.0	1.4×10^4	$>2.3 \times 10^4$
Peach et al. (1994)	1,450	8 kb	COS	MORB / natural po	- CCO (8 kb)	-1.6	3.5×10^4	4.3×10^4
Peach et al. (1994)	1,450	8 kb	COS(Cl)	synthetic basalt / natural po	- CCO (8 kb)	-2.0 to -0.5	4.5×10^5	3.3×10^4
Stone et al. (1990)	1,200	1 bar	COS	AOB / synthetic FeS+NiS	- WM	-0.9	1.3×10^5	8.8×10^4
Fleet et al. (1991) low PGE	1,300	>1 bar	SC(C)	AOB / synthetic FeS+NiS	CCO-magnetite (?)	low	3.0×10^3	2.0×10^3
Fleet et al. (1991) high PGE	1,300	>1 bar	SO(C)	AOB / synthetic FeS+NiS	CCO-magnetite (?)	low	2.8×10^4	1.5×10^4
Crocket et al. (1992)	1,300	>1 bar	SO	AOB / synthetic FeS+NiS	IQF (?)	low	3.2×10^3	5.0×10^3
Fleet et al. (1996)*	1,250	>1 bar		AOB / synthetic FeS+NiS	$\log fO_2 = -8.5$	-1.0	2.6×10^3	1.7×10^4
Bezmen et al. (1994)	1,200 - 1,300	1-4 kb	HCOS (Cl)	synthetic basalt / synthetic po+cp+pn	- IQF-IW	-4 to -0.3	3.1×10^5	5.5×10^4

Data represent averages of values reported in the literature.

*For 37 mol % NiS, 100-1,000 ppm PGE in sulfide; 48 hours run time.

Abbreviations: po = pyrrhotite; cp = chalcopyrite; pn = pentlandite; AOB = alkaline olivine basalt; MORB = mid-ocean ridge basalt. D_1 = (wt % concentration of *i* in sulfide liquid / wt % concentration of *i* in silicate melt).

the parent liquid composition. These and other data (e.g., Crocket 1981, Peck & Keays 1990) have led to the suggestion that Ir partitions into olivine in preference to silicate liquid, but that Pd concentrates in the silicate liquid relative to olivine. It follows that at low degrees of partial melting the Pd:Ir ratio in a single-stage partial melt would be higher than that of the mantle sulfide, depending on the proportion of mantle sulfide being dissolved in the melt, approach the mantle sulfide ratio when the mantle sulfide is just exhausted (between 20-25% partial melting, Peach et al., 1990), and decrease at higher degrees of partial melting as the melts incorporate more Ir due to the melting of olivine. Thus, the lower Pd:Ir ratios of the komatiite-associated sulfides, compared with sulfide accumulations in gabbroic intrusions, may be accounted for by the greater degree of partial melting required for the generation of komatiitic magmas. Other data, however, are inconsistent with Ir compatibility in olivine (and, by extension, in other silicate phases). For example, Mitchell and Keays (1981) found that in mineral separates from mantle peridotites olivine had the lowest Ir concentration (≈ 0.2 ppb) of all major mantle phases, and in the Lower Zone of the Bushveld Complex Lee and Tredoux (1986) found generally lower Ir concentration in olivine-rich rocks than in pyroxene-rich assemblages. Assuming that all S in the primitive mantle resides in a bulk sulfide assemblage containing 35 wt% S (typical S content of MORB sulfide globules), Peach et al. (1994) showed that the maximum Pd:Ir ratio of a mantle-derived partial melt (at about 20% single-stage partial melting at which point the mantle sulfide would be just exhausted) would not be comparable to the observed ratios.

Another possibility is that Ir prefers chromite, resulting in an Ir-depleted residual magma and an Ir-enriched chromite cumulate (Barnes et al. 1985). The compatibility of Ir in chromite is supported by analytical data on komatiites (e.g., Stone et al. 1993), podiform chromitites in ophiolites (Oshin & Crocket 1982, Page et al. 1982, Stockmann & Hlava 1984, Talkington & Watkinson 1986), and the Bushveld chromitites (Lee & Fesq 1986, Teigler & Eales 1993), as well as by experimental studies (e.g., Capobianco & Drake 1990). However, chromite may not be present in all differentiated rock sequences in which Pd:Ir ratios vary (e.g., Keays 1982). The case is much weaker for Pd-Ir fractionation by sulfide liquid immiscibility. It is clear from experimental studies (Table 7.4) that the sulfide liquid-silicate melt partition coefficients are very high (in the 10^3 - 10^4 range) for both Ir and Pd, attesting to their strongly incompatible character, but too similar to account for the high Pd:Ir ratios in immiscible sulfide liquids. It follows that either the observed Pd-Ir fractionation was not controlled entirely by the sulfide phase or it reflects redistribution of PGE metals subsequent to their initial concentration. In fact, the high PGE concentration in the Merensky and J-M reefs are probably related to deuteric or hydrothermal activity.

Recently, Ballhaus (1998b) has proposed an interesting orthomagmatic model that does not rely on the partitioning of PGE into an immiscible sulfide melt and, therefore, is not constrained by the high D and R values required by the sulfide immiscibility model. His model envisages the following steps: (a) oversaturation of an early, relatively pre-Merensky silicate melt with PGE, causing exsolution of the dissolved PGE in the form of polymetallic micronuggets; (b) sulfur saturation of the silicate

melt, possibly as a result of magma mixing, leading to exsolution of monosulfide liquid; and (c) the capture of the PGE by droplets of monosulfide liquid. The premise for the model is the occurrence of microinclusions ($<0.1 \mu\text{m}$ in diameter) of Os-Ir-Pt alloys, identified by laser probe analysis, in the Merensky sulfide minerals. However, it is yet to be demonstrated experimentally that a basaltic melt in equilibrium with PGE-rich sulfide liquid of the Merensky sulfide concentrate composition (500 ppm of total PGE) is oversaturated with some PGE.

7.5.2. HYDROTHERMAL MODELS

A leaning toward hydrothermal models of PGE mineralization in recent years is based on four considerations: the inadequacy of orthomagmatic models (discussed above), the occurrence of unquestionably hydrothermal PGE mineralization, the experimental determination of PGE solubility in hydrothermal fluids, and the presence of features in the Merensky-type deposits that are better explained by hydrothermal processes.

The notion that the PGE are chemically inert and immobile under most geologic conditions is now known to be erroneous. There is ample evidence of the mobility of Pt and Pd in the weathering environment (Fuchs & Rose 1974, Bowles 1986, Wood & Vlassopoulos 1990) as well as in other hydrothermal systems. The metal-rich Salton Sea geothermal brines carry up to ≈ 1 ppb each of dissolved Pt and Pd at about 300°C and near-neutral pH (McKibben et al. 1990) and as high ≈ 50 ppb Pt in some samples (Harrar & Raber 1984). Up to 1 wt% Pt has been reported from exhalative massive sulfide deposits on the East Pacific Rise (Hekinian et al. 1980) and the Pt contents of komatiites associated with Ni-Cu sulfide deposits appear to have been modified by talc-carbonate alteration (Barnes et al. 1985). PGE enrichment in a wide variety of mineral deposits has been ascribed to hydrothermal fluids. Notable examples include: the Kupferschifer copper deposit in Poland, with reported maximum values of >200 ppm Pt over 50 m strike lengths (Kucha 1982); the Messina copper deposit in Transvaal (Mihalik et al. 1974); the Allard Stock porphyry copper mineralization in Colorado, typically with 100-170 ppb PGE (Werle et al. 1984); and several Cu \pm Ni sulfide deposits such as New Rambler in Wyoming, which contains an average of 75 ppm Pd and 4 ppm Pt in copper ores (McCallum et al. 1976), Rathburn Lake in northwestern Ontario (Rowell & Edgar 1986), and Donaldson West in Quebec (Dillon-Leitch et al. 1986). Fluid inclusion and isotopic studies indicate the involvement of Cl-rich hydrothermal fluids with a strong crustal signature in the formation of vein-type Ni-Cu-PGE mineralization in footwall rocks of the Sudbury Igneous Complex (Farrow et al. 1994, Molnár et al. 1997). Many other examples of hydrothermal PGE mineralization are listed by Lechler (1998).

Quantitative data on the PGE solubility in hydrothermal fluids are limited, but quite revealing. Calculations by Mountain and Wood (1988) and Wood et al. (1989), based on limited thermodynamic data for solubility and complexation reactions, predicted that: (a) Pt^{2+} and Pd^{2+} complexes with CO_3^{2-} , HCO_3^- , SO_4^{2-} , PO_4^{3-} , and F^- should be very weak; (b) hydroxyl complexes are unlikely to be important, except in certain surficial,

highly oxidized environments; (c) up to 10 ppb or more of either Pt or Pd can be transported in hydrothermal fluids as chloride complexes under extremely oxidizing (hematite stability field) and acidic conditions; and (d) the solubility of Pt and Pd bisulfide complexes may be as high as 1,000 ppb even at relatively low concentrations of dissolved ΣS (0.005 *m*). Calculations by Sassani and Shock (1990) also indicated that under conditions appropriate to the late-stage magmatic-hydrothermal regime of mafic intrusions, Pd solubility as chloride complexes could reach 0.1 ppm. The solubility issue has also been addressed recently in some experimental investigations. Chloride complexes ($PtCl_3^-$, $PdCl_4^{2-}$) may contribute significant solubilities (>1 ppb) at low to moderate temperatures under highly oxidizing (hematite stable), highly saline (>3 *m* NaCl equivalent), and/or unusually acidic (pH <4) conditions, but PGE solubilities are extremely low in the presence of aqueous sulfide (Gammons et al. 1992). The much higher solubility of Pd in chloride-rich solutions reported by Hsu et al. (1991) was probably an overestimation, resulting either from their experimental technique (Wood & Mountain 1991) or from the lack of fO_2 control in their experiments (Gammons et al. 1992). Subsequent experimental studies by Gammons and Bloom (1993), Wood et al. (1994), and Pan and Wood (1994) have clearly established that bisulfide complexes, such as $Pt(HS)_2^0$ and $Pd(HS)_2^0$, are far more important under mildly reducing, near neutral-pH conditions. For example, under the experimental conditions selected by Pan and Wood (1994) — 200°-350°C, pH = 5.91-9.43, $\Sigma S = 0.3$ -2.2 *m*, and oxidation state buffered by $H_2S/HS^-/SO_4^{2-}$ — the solubilities were found to be 4-800 ppb for Pt, 1-400 ppb for Pd, and 2-300 ppm for Au. (The much higher solubility of Au, they suggested, might explain why hydrothermal epigenetic deposits of gold are so much more abundant than those of PGE.) Thus, as summarized by Wood (1998), bisulfide complexes are likely to have been important for Pt-Pd enrichments in sea-floor accumulations and ophiolites that involved lower temperature hydrothermal solutions buffered to relatively reducing conditions (pyrite/pyrrhotite stability field) and slightly acidic to neutral pH (by the presence of feldspar, chlorite, epidote, amphibole, etc.). Pt-Pd enrichment in porphyry copper, Kuperschifer-type copper, and unconformity-type uranium deposits probably involved chloride complexes under a favorable combination of high temperature, high fO_2 (hematite stability field), high salinity, and low pH (muscovite stability field). Chloride complexes might also have played a role in hydrothermal PGE enrichment of layered intrusions, but only if these fluids had temperatures significantly above 300°C.

As discussed earlier, the dunitic pipes of the Bushveld Complex and their PGE mineralization appear to be related to late magmatic hydrothermal fluids. The sulfide-associated Picket Pin Pt-Pd deposit of the Stillwater Complex, which occurs in the upper 150 m of Anorthosite Zone V (see Fig. 7.6), has also been attributed to upward percolation of mineralizing fluids during solidification of the anorthosite (Boudreau & McCallum 1986). Several recent studies have concluded that volatile-rich late-magmatic fluids exsolved from intercumulus melt were also involved in the localization of PGE and base metal sulfide mineralization in Merensky-type deposits (Kinloch

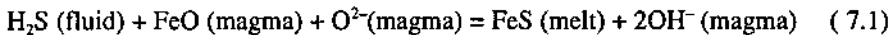
1982, Schiffries 1982, Boudreau et al. 1986, Stumpfl & Ballhaus 1986, Ballhaus & Stumpfl 1986, Volborth et al. 1986, Ballhaus et al. 1988, Boudreau 1988, Kinloch & Peyerl 1990, Mogessie et al. 1991, Boudreau & McCallum 1992, Mathez et al. 1994, Mathez 1995). Evidence cited in favor of this conclusion includes the following:

- (a) The reefs are typically very coarse grained (pegmatoidal) compared with surrounding rocks and contain abundant volatile-rich phases such as phlogopite and hornblende (Todd et al. 1982, Ballhaus & Stumpfl 1985).
- (b) The PGE grade of the J-M Reef is extremely patchy on a scale of tens of meters (Bow et al. 1982, Raedeke & Vian 1986) and the variation in PGE mineralogy of the Merensky Reef may be related to kinds and periods of volatile activity (Kinloch 1982, Kinloch & Peyerl 1990).
- (c) Base metal sulfides, closely associated with PGM, are commonly intergrown with high-temperature, intercumulus hydrous minerals (such as phlogopite, amphiboles, and apatite) and associated with late deuteric alteration of the cumulates (Volborth et al. 1985, Fleet 1986, Ballhaus & Stumpfl 1986, Boudreau et al. 1986, Kinloch & Peyerl 1990).
- (d) The reef sulfides are predominantly intercumulus and the PGM, including the largest grains, are mostly concentrated at the contact between sulfides and silicate gangue (Vermaak & Hendriks 1976, Volborth et al. 1985, Ballhaus & Stumpfl 1986, Ballhaus et al. 1988).
- (e) Apatite and phlogopite from PGE reefs have unusually high Cl:F ratios. As Cl is less soluble in silicate melts than F and melts with extremely high Cl:F ratios are unknown, it is argued that the Cl-rich phases equilibrated with Cl-rich hydrothermal fluids that exsolved during solidification of the cumulate sequence (Boudreau et al. 1986). The presence of a late-magmatic Cl-rich fluid phase in the system is also indicated by the high-temperature fluid inclusions of the system $H_2O-NaCl-CO_2$ hosted by postcumulus quartz (Ballhaus & Stumpfl 1986).
- (f) Significant amounts of graphite, in some cases with high Cl content, are associated with sulfides and late hydrous phases in the Merensky Reef potholes (Ballhaus & Stumpfl 1985, Buntin et al. 1985), within platiniferous pegmatitic pyroxenite in the Stillwater Complex (Volborth & Housley 1984), and as fracture fillings in altered silicates in the Duluth Complex (Mogessie et al. 1991).
- (g) The narrow range of the D/H ratio of all the rocks ($\delta D_{SMOW} = -55\text{‰}$ to -93‰) in the Upper Critical Zone (Atok Section, eastern Bushveld) is consistent with a model involving addition of hydrous vapor to the Merensky Reef protoreef horizon (Mathez et al. 1994).

Detailed discussions of hydrothermal models for PGE mineralization in the Merensky and J-M reefs have been presented by Kinloch and Peyerl (1990) and Bourdeau and McCallum (1992). The central theme of the hydrothermal models for the

formation of a Merensky-type strata-bound ore zone comprises two components: (a) regeneration of Cl-rich hydrothermal fluids (vapor-rich), capable of carrying base metals, PGE, and S in solution, late in the solidification history of the magma; and (b) precipitation of sulfides and platinum-group minerals from the fluids where their upward migration is prevented by a physical-compositional discontinuity, such as the Merensky Reef or J-M Reef, within the cumulate sequence (Ballhaus & Stumpfl 1986, Boudreau et al. 1986, Boudreau 1988, Boudreau & McCallum 1992). The loss of Cl to an exsolving fluid phase due to crystallization is countered by an enrichment of Cl in the interstitial melt, which eventually exsolves an extremely Cl-rich, high-temperature, vapor-rich fluid capable of dissolving and transporting ore metals as it migrates upward through the largely solidified cumulate pile. A critical requirement of this interpretation is that the PGE are preconcentrated in footwall cumulates by the precipitation of sulfide. The lithologic discontinuity, acting as a barrier to fluid migration, could be provided by vapor-undersaturated, hotter intercumulus melt at a higher stratigraphic level (Boudreau 1988, Boudreau & McCallum 1992). The upward-percolating fluid is redissolved in the intercumulus melt, adding both S and PGE to the silicate melt, and PGE-enriched sulfide precipitation occurs because of the limited solubility of sulfide and PGE in silicate melt. An earlier magma mixing event may also provide a stratigraphic discontinuity for trapping the upward-percolating fluids and thus control ore localization, but the magma-mixing event is not a prerequisite as it is in the case of the magmatic model proposed by Naldrett and von Gruenewaldt (1989).

A reaction considered to be of fundamental importance by Ballhaus and Stumpfl (1986) for the segregation of an immiscible PGE-bearing sulfide melt involves the dissolution of H_2S from the volatile-fluid phase into the silicate magma:



The liberation of OH^- by this reaction eventually causes the magma to be saturated in water. Further progress of the reaction leads to the unmixing of an aqueous fluid phase coexisting with magma and sulfide melt. Such a situation explains in part the association of sulfides with hydrous minerals.

The hydrothermal model described above has its problems too. The low OH contents of apatites and micas in the J-M and Merensky reefs (Boudreau et al. 1986) indicate that fH_2O of the fluids must have been very low. As fH_2S varies linearly with fH_2O , the sulfur content of the Cl-rich fluids would be too low to account for the observed amount of reef sulfides (Barnes & Campbell 1988). However, Boudreau and McCallum (1992) have presented calculations to argue that Cl-rich fluids at high temperatures should be capable of carrying enough dissolved S and PGE to account for the PGE-enriched reef sulfides. A similar mass-balance problem has also been raised with respect to the adequacy of the footwall cumulates as the source of PGE. For example, Naldrett and von Gruenewaldt (1988) argued that for reasonable estimates of the Pt content of the initial Bushveld magma (15 ppb) and the volume of liquid trapped in the cumulates (20%), the total amount of Pt contained in the Merensky Reef, the

Middle and Upper Group chromitite layers, and the cumulates below Merensky Reef would require about 6 km of underlying cumulates. This happens to be three times the known thickness of cumulates beneath the Merensky Reef throughout most of the Bushveld Complex. According to others, there is more than enough PGE-enriched footwall cumulates beneath the J-M Reef (Boudreau & McCallum 1992) and the Merensky Reef (Ballhaus et al. 1988) to account for the PGE enrichment of the reefs. However, a systematic positive correlation between the PGE grade and thickness of footwall cumulate units, as would be expected according to the hydrothermal model discussed above, has not been documented for either reef.

It is difficult to imagine how the Bushveld or Stillwater magma could have solidified without generating a significant amount of volatile-rich fluids. The much higher and more variable concentrations of rare-earth elements in the Merensky Reef pyroxenes compared with their cumulus counterparts several meters below the reef is a good evidence for what Mathez (1995) has called "magmatic metasomatism". Whether the hydrothermal fluids were the primary factor for the sulfide-PGE mineralization in the Merensky and J-M reefs, or they merely caused some redistribution of magmatic sulfides and their associated PGE, remains an unresolved question, although at the present time the hydrothermal models seem to be gaining favor.

7.6. Origin of PGE-enriched Chromitites in Layered Intrusions

As discussed earlier (Ch. 5), the mixing of two magmas, one more fractionated than the other, could inhibit the fractional crystallization of silicate minerals, such as olivine and orthopyroxene, and permit the crystallization of chromite as the sole liquidus phase. As the PGE in chromitite layers of the Bushveld Complex appear to be correlated with sulfides, we need a mechanism for broadly contemporaneous crystallization of chromite and sulfide to account for PGE-enriched chromitite.

Naldrett and von Gruenewaldt (1989) have proposed an orthomagmatic model (Fig. 7.9) to explain qualitatively, under certain assumptions, the precipitation of both PGE-rich sulfides and chromite in layered intrusions. The model is based on the variation in sulfide solubility and density of the residual melt with progressive fractional crystallization of a Bushveld-type primitive picritic magma. An important observation in this context is the positions of the PGE-enriched layers of the Bushveld and Stillwater complexes relative to the first appearance of cumulus plagioclase (Campbell et al. 1983). For example, in the Bushveld Complex PGE concentrations decrease from 3-7 ppm in the Upper Group chromitites (including the UG-2) which occur well above this level, to 2-3 ppm in the Middle Group chromitites which occur within 20 m above or below this level, to generally less than 1 ppm in chromitites which occur below this level. Also, the Merensky and J-M reefs occur about 500 m above the first appearance of cumulus plagioclase. This relationship is significant, because with crystallization of plagioclase the density of the resident magma tends to increase above that of the primitive magma, so that an influx of a fresh pulse of primitive magma is likely to

rise as a turbulent plume, the most conducive situation for efficient mixing and a large R value (silicate magma:sulfide melt ratio). The other important observation is the covariation of PGE and sulfide concentrations, which brings us to a consideration of the variation in sulfide solubility with magma crystallization (Fig. 7.9).

The numerical values attached to the sulfide solubility curve in Figure 7.9 are based on limited experimental data. The most important feature of the model, however, is the shape of the curve. The shape is constrained by the fact that, at constant pressure, the sulfide solubility of a silicate melt is controlled mainly by temperature and FeO content — a decrease in either lowers the sulfide solubility. Sulfide solubility of a magma decreases sharply during olivine crystallization due to the combined effect of decreases both in temperature and FeO content (although the FeO:MgO ratio of the magma increases). With the onset of orthopyroxene crystallization, the FeO content of the magma becomes relatively constant and then increases as the increase in FeO:MgO ratio becomes more pronounced, but the sulfide solubility continues to decrease because of continued sharp decline in temperature. When plagioclase becomes a liquidus phase, a significant increase in the FeO content of the magma results in a flattening of the sulfide solubility curve; continued crystallization (plagioclase \pm orthopyroxene \pm clinopyroxene) may even increase the sulfide solubility of the magma.

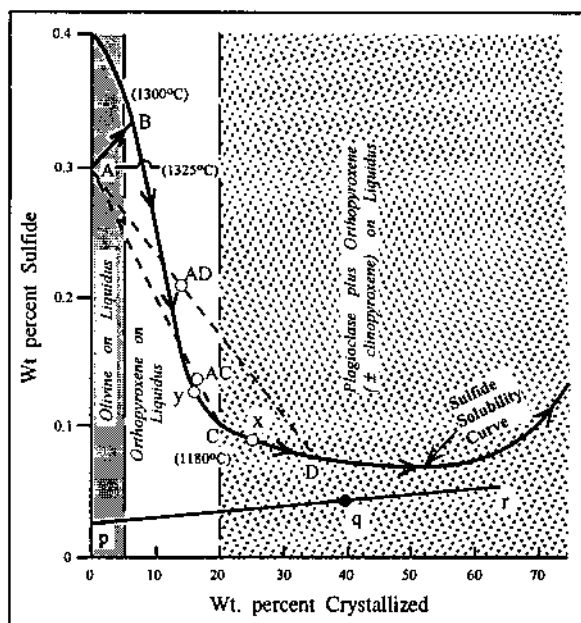


Figure 7.9. Schematic diagram illustrating the variation in the solubility of iron sulfide with the fractionation of what Cawthorn and Davies (1983) considered the best representative (a sample of chilled margin material) for the magma responsible for the Lower Zone of the Bushveld Complex (after Naldrett & von Gruenewaldt 1989). See text for explanation.

Consider an initial magma input of composition *A* as shown in Figure 7.9. As a consequence of olivine crystallization, the sulfide concentration of the magma will increase along the path $A \Rightarrow B$, reaching saturation at *B* after about 8% crystallization. Continued crystallization will cause sulfide segregation and the sulfide still dissolved in the magma will decrease along the solubility curve. The magma will also be depleted in PGE because of strong partitioning of PGE into the sulfide phase.

Suppose that the magma in the chamber immediately overlying the cumulates has reached point *D* when a new pulse of picritic magma enters the chamber. The hybrid such as *AD* will be saturated in sulfide and enriched in PGE compared with the composition *D*. Also, having crystallized plagioclase for some time, the magma of composition *D* is likely to be denser than the fresh input of *A* so that the mixing of the two magmas of different densities will likely be turbulent. Sulfide melt segregated from the hybrid in this situation will have the opportunity of equilibrating with a large volume of silicate magma (i.e., with a high value of *R*) and, therefore, of being considerably enriched in PGE. If the two liquids are saturated or nearly saturated in chromite, the hybrid will probably fall in the liquidus field of chromite (see Fig. 5. 12) and have the potential of producing sulfide-bearing, PGE-enriched chromitite such as the Bushveld Upper Group chromitites (including the UG-2); if not, the hybrid may produce a PGE-rich sulfide horizon such as the Merensky or the J-M reef.

If the mixing occurs when the initial magma has crystallized nearly to the point of appearance of plagioclase (point *C* in Fig. 7.9), the low *A:C* ratio implies a lesser PGE-enrichment of the sulfides relative to the mixing of *A* and *D*, a situation that corresponds to the modest PGE concentrations in the Bushveld Middle Group chromitites. If the magma overlying the cumulates has not fractionated beyond point *Y*, mixing with a fresh input of melt *A* will not produce sulfide saturation. Such a hybrid may, however, be saturated in chromite and produce chromitite associated with orthopyroxene or olivine cumulates, but without sulfides this chromitite will not be enriched in PGE. Such a scenario may explain the very low PGE concentrations in the Bushveld Lower Group chromitites. A possible alternate scenario for producing PGE-rich chromitite or sulfide consists of evolution of a primitive magma along the path $p \Rightarrow r$ (without ever reaching sulfide saturation) and mixing of *A* with an intermediate composition such as *q*, but Naldrett and von Gruenewaldt (1989) consider this less likely as it involves two magmas with widely varying initial sulfide concentration.

To satisfy the condition for density inversion, a critical assumption in the model discussed above is that the new magma added at point *D* is picritic, similar to the primitive parental magma *A*, whereas most workers have argued for the influx of an anorthositic new magma at the level of PGE reefs (see Lambert & Simmons 1988b). Another critical assumption of the model — that the magma was not sulfur-saturated prior to the level of the PGE reef — is also questionable, at least for the J-M Reef. Boudreau and McCallum (1992) have argued that the Stillwater magma was sulfur-saturated throughout much of its crystallization history, as is evidenced by the much stronger Pt-Pd enrichment of the cumulate rocks than would be expected from trapped liquid concentrations alone, and that the present low sulfur abundance of the cumulate

rocks is due to preferential loss of sulfur to a sulfur-bearing fluid phase during solidification of the intercumulus liquid. The occurrence of discordant, PGE-enriched sulfide-bearing bodies scattered throughout the cumulate sequence below the J-M Reef is consistent with this interpretation. The present PGE tenors of the Bushveld chromitite layers also reflect the superimposed effects of subsolidus equilibration (von Gruenewaldt et al. 1986) and magmatic hydrothermal fluids (Gain 1985). It is quite likely that PGE enrichment in the UG-2 chromitite involved a hydrothermal process similar to that advocated for the Merensky Reef.

7.7. Metallogensis

The age distribution and tectonic setting of layered intrusions have been discussed in Ch. 5. Here we address the problem of generating magmas that could produce Merensky-type PGE deposits with such high Pt:S and Pd:S ratios.

The absolute and relative abundances of the PGE in a silicate magma is controlled by the PGE content of the mantle source, the degree of partial melting, and the partial melting process. A model proposed by Hamlyn and Keays (1986) calls for the involvement of PGE-enriched, but S-deficient, second-stage melts in the formation of Merensky-type PGE-sulfide ores. First-stage melts, such as the magmas for mid-ocean ridge basalts (MORB), produced by low to moderate degrees of partial melting of an undepleted or mildly depleted mantle source, would incorporate much of the mantle sulfide and be close to sulfur saturation at the point of generation. Such a magma would likely become rapidly depleted in PGE due to the segregation of accessory sulfides over much of its crystallization history, especially during its ascent when the *R* factor (silicate magma:sulfide melt ratio) might be very high, and be incapable of forming a Merensky-type sulfide-associated PGE deposit. Such a magma, however, should be capable of producing Fe-Ni-Cu sulfide mineralization as is found in the Basal Series of the Stillwater Complex. Second-stage melts generated by melting of the residual mantle, after the extraction of first-stage melts, present a more favorable situation. The high Pd abundances of mantle-derived peridotites residual from mid-ocean ridge basalt genesis imply that a small amount of PGE-enriched sulfide component is retained in the residuum. Partial melting of this residual mantle would result in the complete dissolution of the sulfide component, as the available sulfur would be considerably less than that required to saturate the second-stage melt. This melt, undersaturated in sulfur but enriched in PGE and chalcophile elements, would be capable of forming a Merensky-type PGE deposit if sulfide liquid immiscibility occurred under conditions of high *R* factor. Hamlyn and Keays (1986) have proposed that the first-stage and second-stage melts may correspond, respectively, to the *A*-type and *U*-type magmas of Sharpe and Irvine (1983) discussed earlier.

Dynamic partial melting (Langmuir et al. 1977) involving incomplete melt extraction from the mantle would also result in the generation of sulfur-saturated early partial melts and sulfur-undersaturated, but PGE-enriched, later partial melts. An

advantage of this process over the two-stage batch-melting process proposed by Hamlyn and Keays (1986) is that the small amount of melt in the mantle would act as a flux and permit greater degrees of partial melting (Lambert & Simmons 1988b).

Naldrett and Barnes (1986) have argued that it is not necessary to invoke a two-stage melting of the mantle to generate a magma capable of forming Merensky-type PGE deposits. According to their model, using partition coefficients derived for fractional crystallization, estimated Pd and Ir contents of the Bushveld and Stillwater magmas (Page et al. 1976, Sharpe 1982) can be reproduced as the result of about 8 to 20% single-stage melting of a typical spinel-lherzolite mantle (4.4 ppb Pd, 4.1 ppb Ir, 2,056 ppm Ni, 106 ppm Co, and 40 ppm Cu), provided that all sulfide present in the mantle source enters the partial melt. As discussed earlier, the formation of a Merensky-type ore would require that the immiscible sulfide melt that eventually segregated from the silicate magma equilibrate with a very large volume of magma.

Thus, for an orthomagmatic origin of Merensky-type deposits, a potentially favorable magma must be undersaturated in sulfur as it leaves the source, so that sulfur saturation may be delayed until appreciable fractional crystallization has taken place. The PGE extracted from the mantle source during partial melting, then, would be retained in the magma and concentrated in the igneous body itself, possibly as PGE-rich sulfide accumulations under favorable circumstances. The requirement of hydrothermal models of origin, which rely on remobilization of preconcentrated PGE and S, is quite different. In this case, the source magma should be close to sulfide saturation so that enough PGE-enriched sulfide precipitates within the footwall cumulate sequence.

7.8. Summary

Ore-grade concentrations of PGE, generally in the range of 10-20 ppm, are virtually restricted to igneous ultramafic-mafic complexes and involve concentration factors in the order of one thousand. Strata-bound PGE-rich horizons in large layered intrusions, such as the Bushveld, Stillwater, and Great Dyke complexes, contain about 90% of the world's PGE resources. With about 80% of the world's PGE resources, the Bushveld Complex is by far the most important PGE producer today, a position it is likely to retain for a long time. Significant PGE production also comes from the Stillwater Complex and the Great Dyke. PGE are also recovered as a byproduct from Ni-Cu sulfide ores of the Noril'sk-Talnakh, Sudbury, Jinchuan, and Kambalda deposits.

The most important PGE-rich horizons in the Bushveld Complex are the UG-2 chromitite layer and a distinctive, laterally continuous, pegmatoidal ultramafic unit near the top of the Critical Zone called the Merensky Reef. In both cases, the PGE values, mostly in the form of discrete minerals, are clearly correlated with the concentration of Ni-Cu sulfides. The J-M Reef, the most important PGE-rich horizon in the Precambrian Stillwater layered complex, contains only a fraction of the resources in the Merensky Reef, but the PGE grade is significantly higher. The two reefs, however, share many common characteristics, suggesting a similar origin. These include the

presence of pegmatoidal gabbroic rocks and “potholes”, the stratigraphic position of the reefs relative to the first appearance of cumulate plagioclase, the lateral continuity of the reefs, the close connection between PGE values and Ni-Cu sulfides, the high PGE:S and Pd:Ir ratios of the reef sulfides, and the association of Cl-rich hydrous silicates with reef sulfides.

The unresolved debate over the origin of Merensky-type PGE deposits involves the choice between two alternate models: orthomagmatic and (magmatic-) hydrothermal. The essence of the orthomagmatic models is that the PGE were concentrated by immiscible Fe-Ni-Cu sulfide liquids that segregated at the reef level under favorable circumstances, such as mixing of magmas of appropriate compositions and very high R values (silicate magma:sulfide melt ratios). The logic of this view is based largely on the position of the PGE-rich horizons relative to magma evolution, such as cyclic units and chromitite layers, the widely accepted liquid immiscibility origin of Ni-Cu sulfides in mafic-ultramafic complexes, and the strong chalcophile character (i.e., very high D values) of the PGE. However, several features of the PGE reefs — such as the relatively high PGE tenors and their unsystematic relationship with Ni+Cu tenors, the very high PPGE:IPGE ratios (or Pd:Ir ratios) of the sulfides, and the evidence of volatile activity in the PGE-enriched sulfide horizons — are not compatible with the control of absolute and relative PGE abundances by sulfide accumulation solely through liquid immiscibility. The hydrothermal view of origin, on the other hand, holds that the PGE were preconcentrated in footwall cumulates by the precipitation of sulfides, and that the accumulation of PGE-enriched sulfides in the reefs involved transport of metals and sulfur by post-cumulus, upward-percolating, volatile-rich fluids. In addition to the experimental and field data in support of adequate solubility of PGE in hydrothermal systems, the main evidence for this interpretation consists of the pegmatoidal texture of the reef rocks, the intergrowth of reef sulfides with intercumulus hydrous minerals, the high Cl:F ratios of apatite and phlogopite from PGE reefs, and the presence of a late-magmatic Cl-rich fluid phase in the system as indicated by fluid inclusions. The problems raised with respect to hydrothermal models include mass balance for the PGE-enriched reef sulfides and the apparent lack of systematic positive correlation between the PGE grade and thickness of footwall cumulate units

Chromitites and associated sulfides in layered intrusions are believed to have formed by mixing of U -type (ultramafic) and A -type (anorthositic) magmas, but how such mixing produces varying degrees of sulfide-associated PGE enrichment in different chromitite layers is not quite clear. At least some of the variations appear to be related to subsolidus re-equilibration and/or interaction with magmatic volatiles.

7.9. Recommended Reading

Ballhaus et al. (1988), Barnes and Campbell (1988), Boudreau (1988), Boudreau et al. (1986), Irvine et al. (1983), Kinloch (1982), Naldrett (1989, Ch. 5 & 6), Naldrett and von Gruenewaldt (1988), von Gruenewaldt et al. (1986), Peach and Mathez (1996).

CHAPTER 8

PORPHYRY DEPOSITS

8.1. Introduction

The most well known among the *porphyry-type deposits* are the porphyry copper deposits. Originally, the term *porphyry copper* was applied to stockwork copper mineralization in felsic, porphyritic igneous intrusions. With the development of large-scale open-pit mining methods and froth flotation techniques for efficient beneficiation of low-grade ores, the meaning of the term has been expanded to include economic considerations as well as engineering characteristics. It now refers to large (many with hundreds of million tonnes of ore), relatively low-grade (commonly <1 wt% Cu), epigenetic, intrusion-related, disseminated (stockwork), hypogene copper deposits that can be exploited by bulk-mining techniques. Similar large-tonnage and low-grade disseminated deposits related to igneous intrusions are also important for molybdenum (*porphyry molybdenum*) and tin (*porphyry tin*), and constitute part of the potential resources of uranium (*porphyry uranium*) and gold (*porphyry gold*). Association with porphyritic rocks is not considered an essential component of the definition of porphyry deposits, but the related intrusions almost always contain one or more porphyritic members, implying an epizonal environment (less than 5 km depth) of emplacement of partly crystallized magmas. Other common characteristics of the porphyry-type deposits include a large hydrothermal system dominated by magmatic ± meteoric fluids, pervasive hydrothermal alteration of host rocks, fracture-controlled ore mineralization, and association with breccias of diverse origins and variable degrees of mineralization. In this chapter we will focus on porphyry copper and porphyry molybdenum deposits.

8.2. Porphyry Copper Deposits

Porphyry copper deposits contain approximately one-half of the world's copper reserves and currently account for more than 50% of the world's annual copper production. They are the best studied of all porphyry-type deposits and their salient features have been discussed in a number of review articles (e.g., Lowell & Guilbert 1970, Sillitoe 1988, Lowell 1974; Laznicka 1976; Nielsen 1976; Hollister 1975, 1978; McMillan & Panteleyev 1980; Titley & Beane 1981, Beane & Titley 1981; Titley 1993).

8.2.1. DISTINGUISHING FEATURES

As a group, porphyry copper deposits exhibit many distinctive characteristics:

- (a) close spatial and genetic relationship with apical parts of epizonal, felsic, multiple igneous intrusions, which invariably include porphyritic members containing primary phenocrystic hornblende or biotite (commonly both);
- (b) occurrence at continental margins and island-arc settings, with evidence at places for fault-controlled emplacement of related intrusions;
- (c) fracture-controlled disseminated hypogene Fe-Cu-sulfide mineralization and hydrothermal alteration with characteristic patterns of lateral zoning, all centered on one or more of the intrusions;
- (d) association with molybdenum or gold or both with potential for byproduct recovery;
- (e) association with genetically related breccia bodies (pipes and dikes), which are generally rooted in marginal parts of the host porphyries and, in some cases, carry ore-grade mineralization; and
- (f) pronounced supergene alteration, which in some deposits may be critical to the economics of mining.

8.2.2. SIZE AND GRADE

Large tonnage and low grade are characteristic features of porphyry copper deposits. According to Lowell (1974), a deposit should have at least 20 million tonnes of ore containing a minimum average grade of 0.1% Cu to qualify as a porphyry copper deposit. Reserve and production data compiled by Gilmour (1982) show that all producing deposits had initial reserves in excess of 40-50 million tonnes with an average grade of more than 0.4% Cu. The initial reserves of most 'giant' deposits exceeded 500 million tonnes, with average grades ranging from 0.4 to about 1%, and some contained >1 billion tonnes of ore with average grades exceeding 0.7-0.8% Cu. The largest known porphyry copper deposit is located at Chuquicamata (Chile) with total reserves (proved + probable + possible) of about 10 billion tonnes averaging 0.56% Cu. Other notable giant deposits are: Valley Copper and Staff Creek (Canada); Bingham, Morenci, San Manuel-Kalamazoo, and Safford (USA); La Caridad (Mexico); Cerro Colorado (Panama); Santa Rosa (Peru); El Abra, Andiana, and El Teniente (Chile); Sipalay and Atlas (Philippines); Freda River and Panguna (Papua New Guinea); and Kalmakyr, Almalyk district, Uzbekistan (Table 8.1).

8.2.3. DISTRIBUTION

The overwhelming majority of the porphyry copper deposits are related to Mesozoic-Cenozoic orogenic belts and currently active lithospheric plate boundaries. In orogenic belts, the deposits occur in two broad tectonic settings: island arcs, and continental

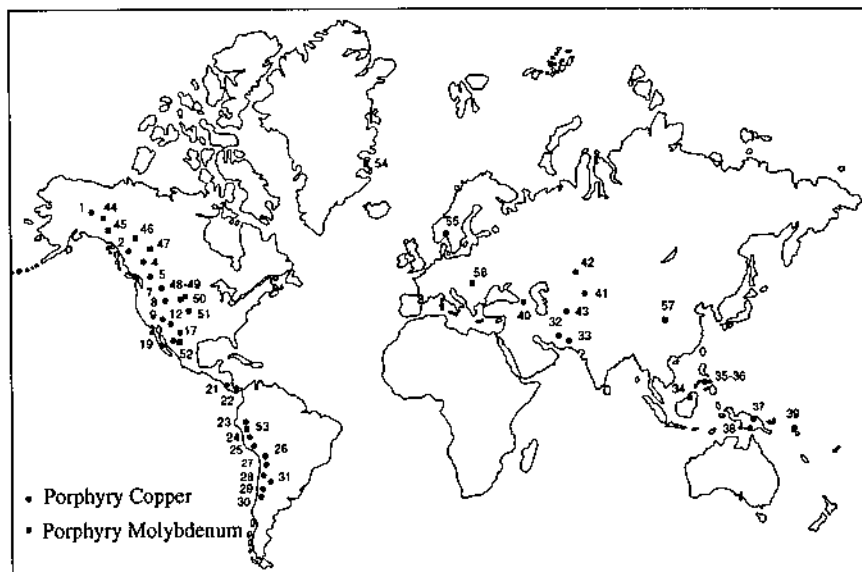


Figure 8.1. World distribution of major porphyry copper and porphyry molybdenum deposits and districts. Numbers are cross-listed in Tables 8.1 and 8.3.

margins. Four post-Paleozoic orogenic belts contain most of the deposits (Fig. 8.1): (a) the western American belt, which has the greatest concentration of known porphyry copper deposits including the important porphyry copper provinces of the Andes (Chile, Peru, Argentina), the southwestern USA (Arizona, New Mexico, Nevada) and the Canadian Cordillera (British Columbia); (b) the southwest Pacific belt (Taiwan, Fiji, Philippines, Borneo, Papua New Guinea, and Solomon Island region); (c) the Caribbean belt (Dominican Republic, Puerto Rico, Haiti); and (d) the Alpine belt (Romania, Yugoslavia, Bulgaria, Armenia, Iran, and Pakistan).

The only well authenticated occurrences of economic porphyry copper deposits outside of the post-Paleozoic orogenic belts are the Paleozoic deposits in the Uzbekistan-Kazakhstan region of the former USSR. Other Paleozoic deposits have been reported from the Appalachian orogen (Hollister et al. 1974, Kirkham & Soregaroli 1975), the Argentinean Andes (Sillitoe 1977), and Queensland, Australia (Horton 1978). Sikka and Nehru (1997) listed some 40 Precambrian deposits (ranging in age from 3314 ± 6 to 561 ± 9 Ma) which they believed to be of the porphyry copper type. The most important of these, all of Proterozoic age, are: Malanjkhanda, India (788 million tonnes, 0.83% Cu, 0.004% Mo, 0.2 g/t Au, 6 g/t Ag); Tongkuangyu, PRC (380 million tonnes, 0.67% Cu); Troilus Lake, Quebec, Canada (42.9 million tonnes, 0.12% Cu, 1.4 g/t Au, 1.4 g/t Ag); and Haib River, Namibia (600 million tonnes, 0.3% Cu). The Malanjkhanda and Tongkuangyu deposits are

TABLE 8.1. Tonnage and grade of major Phanerozoic porphyry copper deposits/districts

Deposit/District @	Tonnage (million tonnes)	Grade				Age (Ma)
		Cu (%)	Mo (%)	Au (g/t)	Ag (g/t)	
Western Canada						
Casino, Yukon (1)	162	0.37	0.023	-	-	72
Berg, British Columbia (2)	308	0.63	0.023	-	-	51-48
Lornex, British Columbia (3)	455	0.41	0.015	-	-	
Valley Copper, British Columbia (4)	855	0.48	-	-	-	
Brenda, British Columbia (5)	227	0.16	0.039	-	-	150
Shaft Creek, British Columbia (6)	907	0.30	0.020	-	-	186
Southwestern United States						
Butte, Montana (7)	500+	0.08	-	-	-	
Bingham, Utah (8)	2,869	0.81	0.044	-	-	40-39
Bagdad, Arizona (9)	640	0.42	0.021	-	-	72
Globe-Miami, Arizona (11)	690	0.69	0.001	0.01	0.42	67-63
Morenci, Arizona (12)	660	0.82	0.009	0.02	1.20	67
Sierreta-Esperanza, Arizona (13)	719	0.30	0.028	-	-	67-58
San Manuel-Kalamazoo, Arizona (14)	350	0.58	0.009	0.02	1.20	67
Twin Buttes, Arizona (15)	413	0.63	0.023	-	-	60-59
Safford-Kennecott (Lone Star), Arizona (16)	970	0.41	-	-	-	
Bisbee, Arizona	150	2.35	-	0.58	20.90	178-163
Santa Rita, New Mexico (17)	500+	0.97	-	-	-	Laramide
Tyrone, New Mexico (18)	400+	0.70	-	-	-	56
Mexico						
El Arco, Baja California (19)	550	0.60	-	-	-	
La Caridad, Sonora (20)	680	0.67	0.020	-	-	54
Central America						
Cerro Colorado, Panama (21)	1,800±	0.60	0.015	0.06	4.60	
Petaquilla, Panama (22)	450	0.40	-	-	-	
South America						
Santa Rosa, Peru (23)	1,060	0.55	-	-	-	59
Michiquillay, Peru (24)	575	0.72	0.022	-	-	21-29
Cuajone, Peru (25)	426	0.70	0.025	-	-	52
Mohococha, Peru	325	0.76	0.020	-	-	7
Toquepala, Peru	430	0.99	0.020	-	-	59
El Abra, Chile (26)	1,200+	0.60	-	-	-	33
Andacollo, Chile	320	0.69	0.015	-	-	?
Chuquicamata, Chile (27)	9,450	0.56	0.024	-	-	29
El Salvador, Chile (28)	535	1.10	0.025	-	-	42
Andina (Rio Blanco), Chile (29)	3,000	1.24	0.025	-	-	8-5
El Teniente (Braden), Chile (30)	8,350	0.68	-	-	-	4.3
El Pachon, Argentina (31)	770	0.59	0.016	-	-	Tertiary

already in production and the other two are being considered for exploitation. However, some of the deposits listed by Sikka and Nehru (1997), such as Malanjhand (Sarkar et al. 1996, Panigrahi & Mookherjee 1997), may not actually be porphyry deposits. In this chapter we will discuss only the Mesozoic-Cenozoic deposits, mostly those of the circum-Pacific rim.

TABLE 8.1 (continued)

Deposit/District @	Tonnage (million tonnes)	Grade				Age (Ma)
		Cu (%)	Mo (%)	Au (g/t)	Ag (g/t)	
Southern Asia						
Sar Cheshmeh, Iran (32)	450	1.13	0.030	-	-	
Saindak South, Pakistan (33)	75	0.43	0.006	0.51	-	20-19
Southwestern Pacific						
Mamut, Sabah (34)	69	0.61	-	0.65	3.98	9-5
Sipalay, Philippines (35)	805	0.50	0.015	0.35	1.55	Up. Cret- Pliocene
Atlas, Philippines (36)	1,000+	0.46	-0.01	0.25	?	
Frieda River, Papua New Guinea (37)	800	0.46	0.005	0.20	-	
Ok Tedi, Papua New Guinea (38)	300	0.75	0.010	0.62	-	1.2
Panguna, Papua New Guinea (39)	900±	0.47	0.005	0.5-	-	3.4
				0.62		

@ Numbers in parentheses refer to locations shown in Figure 8.1.

Important deposits not included in the table because of lack of adequate tonnage-grade data are (with estimated economic copper content in 10³ tons; Laznicka 1976): (40) Agark, Armenia (700); (41) Kounrad, Kazakhstan (10,000); (42) Boshchekul, Kazakhstan (2,160); and (43) Kalmakkyr, Almalyk, Uzbekistan (3,500).

Sources of data: compilations by Hollister (1973), Gilmour (1982), Titley (1993), Sillitoe (1993), Carten et al. (1993), Hutchinson (1996).

8.2.4. GEOLOGIC SETTINGS

The geologic settings of the circum-Pacific porphyry copper deposits are broadly similar (Titley & Beane 1981). In general, the deposits in South America and in the Canadian Cordillera lie within a thick sequence of deformed Mesozoic to Tertiary volcanic-sedimentary succession sandwiched between a linear zone of Mesozoic batholiths to the west and older cratonic elements to the east. In southwestern United States and adjoining Mexico, the deposits are also situated landward of the Mesozoic batholiths of the west coast, but on the North American craton are flanked on the northeast by uplifted Precambrian basement. The separation of batholithic terrane, craton, and deformed volcanic-sedimentary belt is less distinct in southwestern Pacific islands containing cratonic elements (e.g., Papua New Guinea), but is recognizable in the overprint of successive stages of orogenesis and intrusion. The major exception to this pattern of geologic setting in the circum-Pacific rim occurs in the volcanic islands of the Pacific (e.g., Bougainville and Fiji) where continental edges are not involved and porphyry deposits are parts of very young island-arc volcanic systems.

A control of pre-existing faults or fault systems on the emplacement of porphyry intrusions has been suggested for the Canadian Cordillera (Hollister 1978), southwestern United States (Schmitt 1966, Lowell 1974), and the Chilean Andes

(Hollister 1973). The correlation is based primarily on the permissive evidence of close proximity of porphyries to major faults, but the faults generally record a history of multiple, including post-mineralization, movements (Sillitoe 1981) and their importance in controlling the localization of porphyries is still unresolved except in a few cases (e.g., Bagdad and Sierrita deposits, southwestern USA; Tittley 1993).

8.2.5. HOST ROCKS

Igneous Intrusions

Porphyry copper deposits are intrusion-related mineralized hydrothermal systems. Large deposits (>100 million tonnes of ore) are commonly related to relatively large (≈ 5 km in diameter) intrusions or intrusive complexes and relatively small deposits to smaller (<1 km in diameter) plutons (Tittley & Beane 1981). Chemical analyses representative of unaltered or only weakly altered igneous rocks show that the intrusions are quite diverse in composition, but generally represent intermediate to felsic differentiated members of the calc-alkaline magma series (quartz diorite - quartz monzonite - granodiorite) (Fig. 8.2). The most common in the continental margin areas of southwestern United States, northern Mexico, and western South America are granodiorites and quartz monzonites. In contrast, porphyry copper deposits in island arcs, such as the southwestern Pacific islands, Philippines, and the Caribbean, are typically associated with lower-potassium quartz diorite intrusions. Island-arc intrusions also include granodiorites, quartz monzonites, and syenites, but compared with their cratonic equivalents, the potassic island-arc intrusions lack K-feldspar phenocrysts (Kesler et al. 1975a). A small number of deposits are associated with quartz-deficient diorite-monzonite-syenite intrusions of alkalic igneous suite. In some complexes, intrusions represent single discrete magma bodies, but multiple intrusions are more common. When different rock types are present in a district, as in the Papua New Guinea-Solomon islands region, the porphyry copper deposits tend to be associated with relatively late, low-K intrusions (Mason & McDonald 1978).

The textures commonly range from strongly porphyritic with aphanitic groundmass in the upper parts of intrusions to more equigranular textures at greater depths, but porphyritic members are commonly the most important for mineralization. In southwest United States, for example, copper-molybdenum ores have not been observed directly associated with rocks exhibiting phaneritic textures. Interpretations from rock textures, estimates of pre-ore geologic cover, and stability relations of mineral assemblages suggest that porphyry copper-related plutons were emplaced at shallow crustal levels, their tops lying at 1 to 4.5 km depth, mostly at less than 2 km (Sillitoe 1973, Tittley 1982a). There is compelling evidence in some regions (e.g., El Salvador, Chile; Red Mountain, Arizona) that the intrusions represent subvolcanic plutons of volcanic-plutonic complexes, as was proposed by Sillitoe (1973), but all shallow-level porphyry copper plutons are not accompanied by coeval volcanic rocks. There is no evidence for a 'volcanogenic' association of porphyry copper deposits in the sense of a common genesis of volcanic rocks, metals, and plutons, not even in the

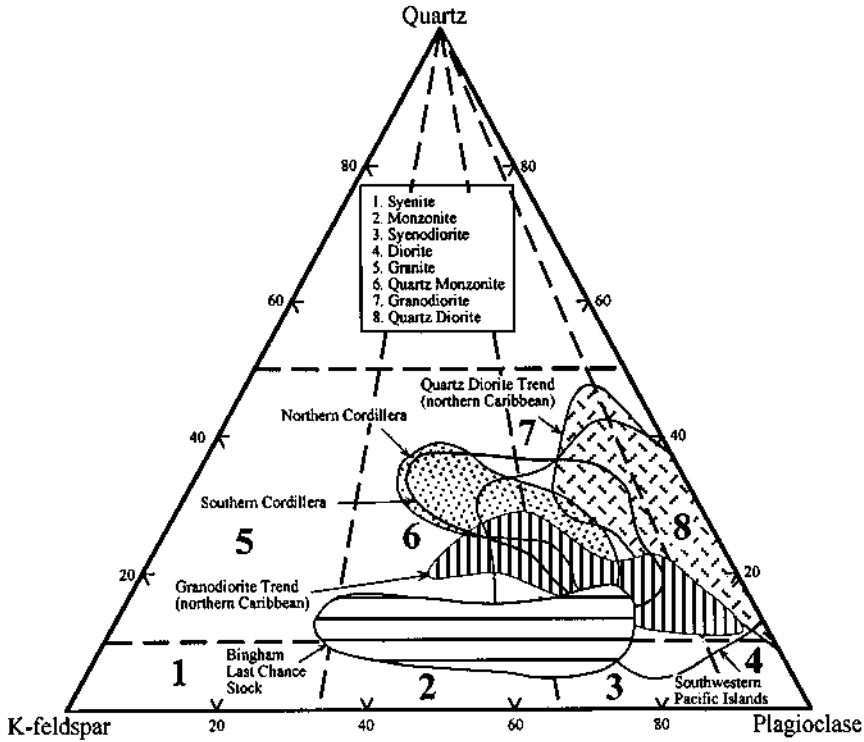


Figure 8.2. Modal composition of igneous intrusives related to porphyry copper deposits. Sources of data: Kesler et al. (1975a) for northern Caribbean and Bingham, Titley (1975) for southwestern Pacific islands, and Hollister (1978) for northern and southern Cordillera.

the very young (≈ 1 Ma) deposits of the southwestern Pacific Islands (Titley & Beane 1981).

Within every porphyry copper province there are barren intrusions that are generally indistinguishable from productive plutons in terms of age, overall composition, hydrothermal alteration, or fluid inclusion characteristics. A petrologic criterion of distinction may be the relative abundance of ferromagnesian minerals — pyroxene is rare or virtually absent in copper porphyries, whereas hornblende and, particularly, biotite are conspicuous (Titley & Beane 1981). An earlier suggestion that anomalously high Cu, Zn, and Pb contents of magmatic biotite are characteristic of ore-related intrusions (Putman & Burnham 1963, Parry & Nackowski 1963) is now known to be invalid (Banks 1974). In fact, according to Kesler et al. (1975a) and Feiss (1978), early-formed ferromagnesian minerals from mineralized intrusives may actually be Cu-deficient compared with barren systems.

The halogen abundance in biotite does not appear to be a useful discriminant (Parry & Jacobs 1975, Kesler et al. 1975b). Biotites from mineralized intrusions are, on the average, slightly enriched in Cl and F, but the difference is slight and the populations overlap extensively. Moreover, whether mineralized or barren, biotites of more potassic intrusions such as granodiorites and syenites contain more Cl and F than those of K-poor variants such as quartz diorite. Geochemical criteria that may be useful for distinguishing potentially productive plutons from barren ones, especially in specific districts or tectonic belts, include the following: (a) high $Al_2O_3:(K_2O+Na_2O+CaO)$ whole-rock ratio, perhaps because of its correlation with increased number of octahedral sites in the melt phase, a situation conducive to retention of copper in the melt for later partitioning into a magmatic aqueous phase (Mason & Feiss 1979); (b) low whole-rock contents of both Y and Mn (Baldwin & Pearce 1982); (c) and the pattern of compositional zoning in amphiboles (an increase in $Mg:(Mg+\Sigma Fe)$ ratio toward the rims) and biotites (an increase in $Mg:(Mg+\Sigma Fe)$ ratio and a decrease in TiO_2 toward the rims), perhaps reflecting a high initial fO_2 that became increasingly higher during crystallization (Mason 1978). The most useful guide to mineralized plutons is a high fracture density (fracture length per unit area or fracture area per unit volume of rock) in and around the pluton (Heidrich & Titley 1982). This is to be expected, because crystallization of a water-bearing magma eventually produces an aqueous fluid (a 'vapor' phase) by second boiling and the resulting internal pressures are generally sufficient to induce brittle failure of the enclosing rocks (Burnham 1979), and fracture-related permeability exerts a fundamental control on the alteration and mineralization in any porphyry copper system.

Country Rocks

Country rocks at the level of porphyry copper emplacement vary a great deal in composition and age. For example, in southwestern United States the country rocks range from Proterozoic basement to Paleozoic marine strata to Mesozoic volcanic and clastic sequences (Titley 1993). In Chile and Argentina, they range from Precambrian basement to Paleozoic and Tertiary volcanic-sedimentary sequences, although there appears to be a predominance of volcanic wallrocks of Cretaceous to early Tertiary age (Sillitoe 1981). Volcanic rocks of Tertiary age also predominate as wallrocks of porphyry systems in southwestern Pacific islands (Titley 1975). Thus, the development of porphyry copper deposits appears to be controlled overwhelmingly by magmatic systems, without preferential association with country rocks of any particular lithology or age.

Breccias

Most porphyry copper systems (as well as other porphyry systems) contain one or more varieties of breccias, which range from being minor adjuncts to typical stockwork-type mineralization in most cases to the economically dominant part in some systems (e.g., Copper Flat deposit, Arizona; Dunn 1982). Following Sillitoe's (1985) genetic classification scheme for ore-related breccias in volcanoplutonic arcs,

breccias associated with porphyry deposits fall, in decreasing order of importance, to three categories: (a) magmatic-hydrothermal breccias, attributed to the violent release of hydrothermal fluids from magma chambers (irrespective of the original source of fluids — magmatic, meteoric, or connate), which also cause stockwork fractures in porphyry systems; (b) hydromagmatic breccias, generated by the interaction of magma and an external source of water; and (c) magmatic (including volcanic) breccias, which represent products of fragmentation and eruption of magma from subsurface chambers. Relative to the associated porphyry deposit, the breccias may be premineral (with no evidence of an earlier stage of mineralization), early mineral (with minor evidence of prebrecciation alteration and mineralization), or intermineral (with evidence of breccia emplacement being later than one or more main stages of alteration and mineralization). Gilmour (1977) has suggested that mineralized intrusive breccias containing copper and other metallic minerals, or 'limonite' from the oxidation of copper and/or iron sulfides, probably indicate the existence of a concealed or buried porphyry copper system, even if the country rocks are not exposed or, if exposed, are weakly mineralized or barren.

All copper-bearing, intrusion-related breccia bodies are not integral parts of porphyry copper deposits, although they often show close space-time association with porphyry copper emplacement in a given tectonic unit. Such breccia bodies, often referred to as breccia pipes or 'chimneys' because of their cylindrical morphology, are of minor importance compared to porphyry copper deposits, but they are attractive targets of exploration as they tend to carry higher grades and require less capital investment to develop. Breccia pipe deposits typically occur in plutons of granodioritic composition and exhibit hydrothermal mineral assemblages similar to those in porphyry copper systems. Quartz is ubiquitous as a gangue mineral and tourmaline is an important constituent of many pipes, especially in the Andes (Sillitoe & Sawkins 1971). Generally, they contain significant amounts of molybdenite and scheelite (up to 0.7% WO_3), and tungsten and gold are recovered as byproducts from some tourmaline-bearing breccia pipes in the Andean belt (Sillitoe 1981). Notable examples of copper-bearing breccia pipes include those of Ilkwang mine in Korea (Fletcher 1977), Redbank in Australia (Knutson et al. 1979), Tumulina in Peru (Carlson & Sawkins 1980), Cumobabi in Mexico (Scherkenback et al. 1985), and Los Bronces-Rio Blanco in Chile (Warnaars et al. 1985).

8.2.6. MINERALIZATION AND ALTERATION

Metal Association

Molybdenum, gold, and silver are recovered as byproducts from a number of porphyry copper deposits. Most North American porphyry copper deposits contain between 0.01 and 0.05 wt% MoS_2 ; the average is $\approx 0.02\%$. South American porphyry copper deposits, especially those in Chile, have moderately high molybdenum contents averaging $\approx 0.05\%$ MoS_2 (White et al. 1981). The concentrations of other metals, such as zinc and lead, are too low for economic recovery.

All porphyry copper deposits contain some gold (ranging from <0.05 ppm to as high as 2 ppm, with an average around 0.05 ppm; Lowell 1989, Sillitoe 1993b), and many carry high enough concentrations for recovery as a coproduct or byproduct, especially after the surge in gold price during the 1970s. Recent compilations of compositional data (Tittley 1978, Sillitoe 1979, 1993b, Lowell 1989) have confirmed that, depending on whether they carry byproduct molybdenum or byproduct gold, porphyry copper deposits are divisible, as originally proposed by Kesler (1973), into two subclasses: (a) porphyry copper-molybdenum deposits (containing up to about 0.2% Mo); and (b) porphyry copper-gold \pm molybdenum deposits (generally with low Mo). It is difficult to define a minimum gold concentration for copper-gold deposits; Sillitoe (1979) set an arbitrary lower limit of 0.4 ppm Au for gold-rich porphyry deposits. Some recent discoveries (e.g., Grassberg, Indonesia; Lepanto Far Southeast, Philippines; and Marte and Lobo, Chile) are estimated to contain 700-900 tonnes of gold (average grade at least 1.5 ppm Au); the latter two should be considered as porphyry gold deposits on account of their low copper contents.

Gold in gold-rich porphyry deposits occurs mainly as very fine-grained (generally $<60 \mu\text{m}$, commonly $<20 \mu\text{m}$, in size) native metal of high purity in zones of veinlet stockwork and as disseminations within or immediately contiguous to porphyry stocks. The overall correlation between copper and gold contents of gold-rich porphyry deposits is rather poor (Fig. 8.3). As a general rule, however, the grades of gold and copper vary sympathetically in individual deposits, suggesting that the bulk of the two metals was introduced together during the K-silicate alteration stage, although locally sericitic and advanced argillic alteration zones carry appreciable gold and copper values. Except for the obvious enrichment in gold and general (but not universal) impoverishment in molybdenum, gold-rich deposits possess all essential geological features (such as composition of the host intrusive, nature of the wallrocks, size of orebody, pattern of hydrothermal alteration, age of mineralization, erosion level) of their gold-poor counterparts, and both apparently were generated in volcanic-plutonic arcs over the same time interval around the world. Many gold-rich deposits, however, are appreciably richer in hydrothermal magnetite \pm hematite (e.g., 3-10 volume percent in the Panguna deposit), suggesting that the gold enrichment may be related to abnormally high $f\text{O}_2$: $f\text{S}_2$ ratios in the hydrothermal system (Sillitoe 1979).

The reason why some porphyry copper systems are enriched in gold and others are not, even in a given province, is not understood. Solomon (1990) pointed out that many gold-rich deposits in the southwestern Pacific region were emplaced immediately after a reversal in subduction polarity, which resulted in remelting of a previously melted, relatively gold-enriched mantle material, but this is not a valid explanation for all gold-rich porphyry deposits. Generally, porphyry copper deposits in the continental margin orogens (subduction zones underlain by continental crust), such as the Cordilleran-Andean belt, tend to be richer in molybdenum and poorer in gold than those in the island-arc settings (constructed on a foundation of oceanic lithosphere), but there are many exceptions. The Bingham deposit, a giant gold-rich porphyry

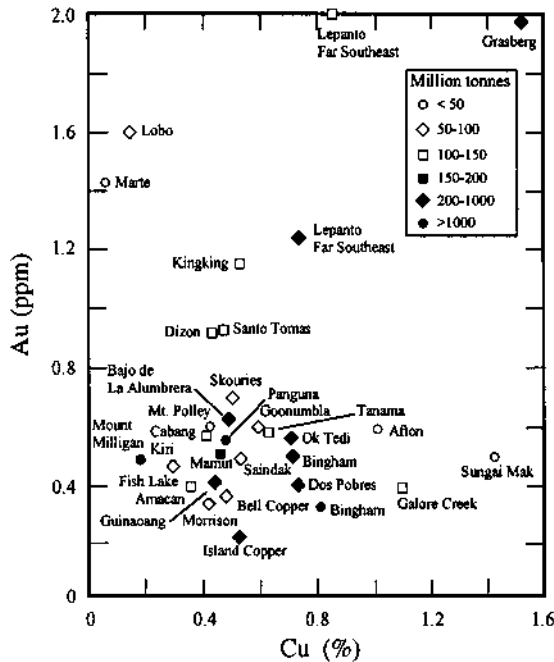


Figure 8.3. Gold and copper contents and approximate production plus reserve tonnages of gold in principal gold-rich porphyry copper deposits: Australia (Goonumbia); Papua New Guinea (Panguna, Ok Tedi); Indonesia (Grasberg, Cabang Kiri, Sungai Mak); Philippines (Kingking, Amacan, Dizon, Santo Tomas, Guinaoang, Lepanto Far Southeast); Malaysia (Mamut); British Columbia, Canada (Galore Creek, Morrison, Bell Copper, Mount Milligan, Mt. Polley, Fish Lake, Island Copper, Afton); Utah, USA (Bingham); Arizona, USA (Dos Pobres); Puerto Rico (Tanama); Argentina (Bajo de La Alumbraera); Chile (Marte, Lobo); Greece (Skouries); Pakistan (Saindak). Copper grades are hypogene except for Ok Tedi and Sungai Mak, where the grades have been enhanced by supergene enrichment. Included in the diagram are deposits which contain large tonnages of >0.4 ppm Au, although the average grade <0.4 ppm (e.g., Bingham). Not included is the very high grade in the leached capping at Oak Tedi (0.5 to 5 ppm Au with an average grade of 2.4 ppm Au; Lowell 1989) that facilitated the development of this deposit. (After Sillitoe 1993b.)

deposit, with an annual production target of about 515,000 ounces of gold (and 4.4 million ounces of silver) along with 310,000 tons of copper, is also Mo-rich and belongs to a continental margin setting. The Ok Tedi and Grassberg gold-rich (but Mo-poor) systems were emplaced at the leading edge of the Australian craton in an active foreland thrust belt produced as a result of collision with an island-arc terrane to the north (Rogerson & McKee 1990). Gold-rich porphyry deposits (e.g., Saindak, Pakistan) also occur in the Alpine-Himalayan orogenic belt. Thus, geodynamic setting does not appear to have been the critical factor in controlling the Au:Cu and Mo:Cu ratios in porphyry copper deposits. The controlling factors probably are

related to the geochemical conditions of gold transport and deposition in the upper continental crust rather than at deeper levels during magma generation and ascent (Sillitoe 1979).

Hypogene Hydrothermal Alteration

Porphyry copper mineralization involves hydrothermal systems that encompass far greater volumes of rock compared with the associated intrusion complex. The evidence for this is the spatial distribution of alteration-mineralization zones centered on porphyry intrusions or their contacts and comparable K-Ar ages of intrusions and hydrothermal minerals in the alteration aureole. A variety of factors influence the degree, extent, and type of hypogene hydrothermal alteration: temperature and pressure, mineralogy and fracture-permeability of the rocks, and the chemistry and flow patterns of the hydrothermal fluids. The result is a complex phenomenon in time and space.

In terms of its mode of occurrence, the hydrothermal alteration may be described as selectively pervasive, pervasive, or localized along veins and veinlets (Titley 1982b). *Selectively pervasive alteration*, commonly the earliest manifestation of hydrothermal alteration, is restricted to specific minerals and results either in the recrystallization of these minerals or in their conversion to new ones without the destruction of original rock texture. Examples include: the conversion of igneous hornblende or igneous biotite to secondary, recrystallized biotite (characterized by atomic Mg:Fe ratios >1.5 , compared with ratios <1.0 for igneous biotite; Beane 1974); alteration of feldspar phenocrysts to kaolinite, chlorite, or epidote; and, in later stages of hydrothermal alteration or at a distance from the intrusion, conversion of hornblende or biotite to chlorite. In most cases, this type of alteration is controlled by the mineralogy of the host rocks, rather than by the composition of hydrothermal solutions. *Pervasive alteration* is non-selective and occurs when a large volume of intensely fractured host rock becomes overwhelmed by the effects of large shifts in the chemical composition of hydrothermal fluids. The result is complete destruction of the original minerals and textures, and the formation of a new minerals (e.g., orthoclase, biotite, quartz + sericite, calc-silicates, etc.). In contrast to wide aureoles of selectively pervasive alteration, pervasive alteration is most commonly present in intensely fractured rocks within or near the mineralized centers. The most conspicuous type of pervasive alteration is the quartz - sericite - (pyrite) alteration, which also contributes to the sulfide mineralization, although to a much lesser extent than the earlier biotite alteration. *Vein-veinlet alteration* develops in fractures and is the most obvious kind of alteration present in a porphyry copper system. Sets of intersecting cracks filled with different alteration mineral assemblages indicate that fracture development and vein-veinlet alteration occur over the entire cooling history of the pluton. Most of the sulfide mineralization is localized along the vein-veinlet centers. A typical sequence of K-silicate veins from a granitic host rock is shown in Fig. 8.4a. A common example of vein-veinlet alteration is that of quartz - pyrite veins flanked by relatively wide vein selvages in which original silicates have been converted to quartz + sericite (Fig. 8.4b). With close fracture spacing, alteration selvages of adjacent

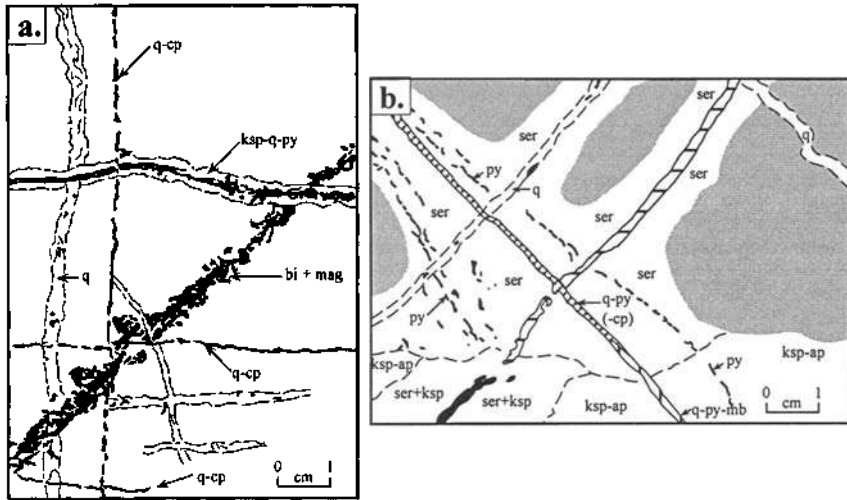


Figure 8.4. Sketches illustrating examples of vein-veinlet alteration associated with porphyry copper deposits. **a.** Typical sequence of K-silicate veins in a quartz monzonite host at Sierrita, Arizona (after Titley 1982b). The veining sequence inferred from crosscutting relationship is: biotite (bi) - magnetite (mt) veins, quartz (q) veins, K-feldspar (ksp) - quartz - pyrite (py) veins, and latest quartz - chalcopyrite (cp) veins representing the principal stage of copper mineralization. The alteration assemblage is designated as potassic because of the presence of biotite in some veins and of orthoclase selvages in others and because of the stability of interstitial biotite in the rock. **b.** Quartz - sericite (phyllic) alteration of schist at Ithaca Peak, Arizona. Note the wide alteration selvages of quartz (q) - sericite (ser) veins, and the change in mineralogy of the sulfide veins on crossing from schist to aplite (ksp-ap): from q-py-cp to q-py-mb (molybdenite) (northwest to southeast) and from q-py to py (northeast to southwest). (After Titley 1982b.)

veins overlap and the vein-veinlet alteration progresses to pervasive alteration.

Based on resulting mineral assemblages, hydrothermal alteration of aluminosilicate rocks are classified into four main types: *potassic* (K-silicate), *phyllic* (sericitic), *argillic*, and *propylitic* (see Table 3.4, Fig. 3.14). Details of these alteration types as applicable to porphyry copper systems, with emphasis on those of the southwestern United States, have been discussed by Beane and Titley (1981) and Beane (1982). Characteristic minerals of the potassic alteration are K-feldspar (orthoclase), biotite, and quartz. K-feldspar and quartz are stable as original rock-forming minerals and as vein-filling constituents, but K-feldspar also forms as an alteration product after plagioclase. Magmatic biotite is altered to a more magnesian variety and the iron released from the alteration of biotite or other mafic minerals goes to form a small amount of one or more of the minerals magnetite, pyrite, and chalcopyrite. Potassic alteration is most prominent in or near 'porphyry centers', although a broad aureole of biotite alteration commonly pervades igneous wallrocks (see Figs. 8.8 and 8.11). Phyllic alteration involves extensive leaching of sodium, calcium, and magnesium, and may lead to complete replacement of the aluminosilicate minerals by sericite and

quartz, with potassium obtained from the fluids or original feldspar. Iron from pre-existing mafic minerals, including early hydrothermal biotite, supplemented by introduced iron and sulfur, may produce as much as 10 volume percent pyrite (and <0.5 volume percent chalcopyrite). The diagnostic assemblage of phyllic alteration is sericite - quartz - pyrite. Argillic alteration, when present, is characterized by assemblages containing clay minerals (or minerals such as diaspore, andalusite, or alunite in the case of *advanced argillic* alteration); pyrite is the major sulfide mineral and it may be accompanied by minor amounts of chalcopyrite, bornite, enargite, and tennantite. The argillic alteration in porphyry copper systems is either late, supergene, and pervasive, or is shallow-hypogene and the result of selective attack on feldspars and sericite; in a few instances, the alteration is restricted to veinlets. Propylitic alteration produces the assemblage chlorite - epidote - calcite at the expense of ferromagnesian minerals and plagioclase of the igneous protolith. Generally, very few sulfide minerals form during this alteration. Beane and Titley (1981) described a silicic alteration, which appears in the form of quartz veins and replacement of both silicate and carbonate rocks, or as jasper or chalcedony; pyrite and, less commonly, chalcopyrite or bornite accompany this alteration and locally attain ore grade.

In older terranes, metamorphism may mask original alteration types and zoning due to superimposed changes in mineralogy and textures. Propylitic, phyllic, and argillic alteration assemblages are quite resistant to low-grade metamorphism, but only phyllic alteration assemblages are likely to survive medium- to high-grade metamorphism.

Hypogene Mineralization

Hypogene mineralization in porphyry copper systems is localized in the intrusions as well as in the wallrocks. In fact, the presence of a large component of total reserves and mine production in host rocks other than the porphyry stock is quite common. The nature of hypogene mineralization is commonly described as *disseminated* in the sense that large volumes of rock contain relatively uniformly distributed values of metal. On a finer scale, much of the disseminated mineralization occurs in the form of fracture-controlled stockworks, and is the product of alteration along vein-veinlet walls, with concurrent deposition of sulfide minerals in the vein or within the vein-veinlet alteration selvage (Titley 1982b).

Textural relations demonstrate that the hypogene sulfide mineralization constitutes an integral part of the overall alteration process and spans a range of time. Pyrite is by far the most abundant and widespread sulfide mineral in porphyry copper deposits. The main copper mineral is chalcopyrite and it is accompanied by minor amounts of bornite, commonly as exsolution intergrowths with the chalcopyrite. Hypogene chalcocite and covellite may be present, but they are typically products of supergene alteration. Other ore minerals, which occur in varying proportions, include tennantite-tetrahedrite, molybdenite, enargite, and magnetite \pm hematite. Copper mineralization is normally present over the entire potassic alteration zone (Fig. 8.5), but much of the chalcopyrite deposition occurs late in the evolution of potassic alteration or during a transitional stage between potassic and phyllic alteration. The latter represents a

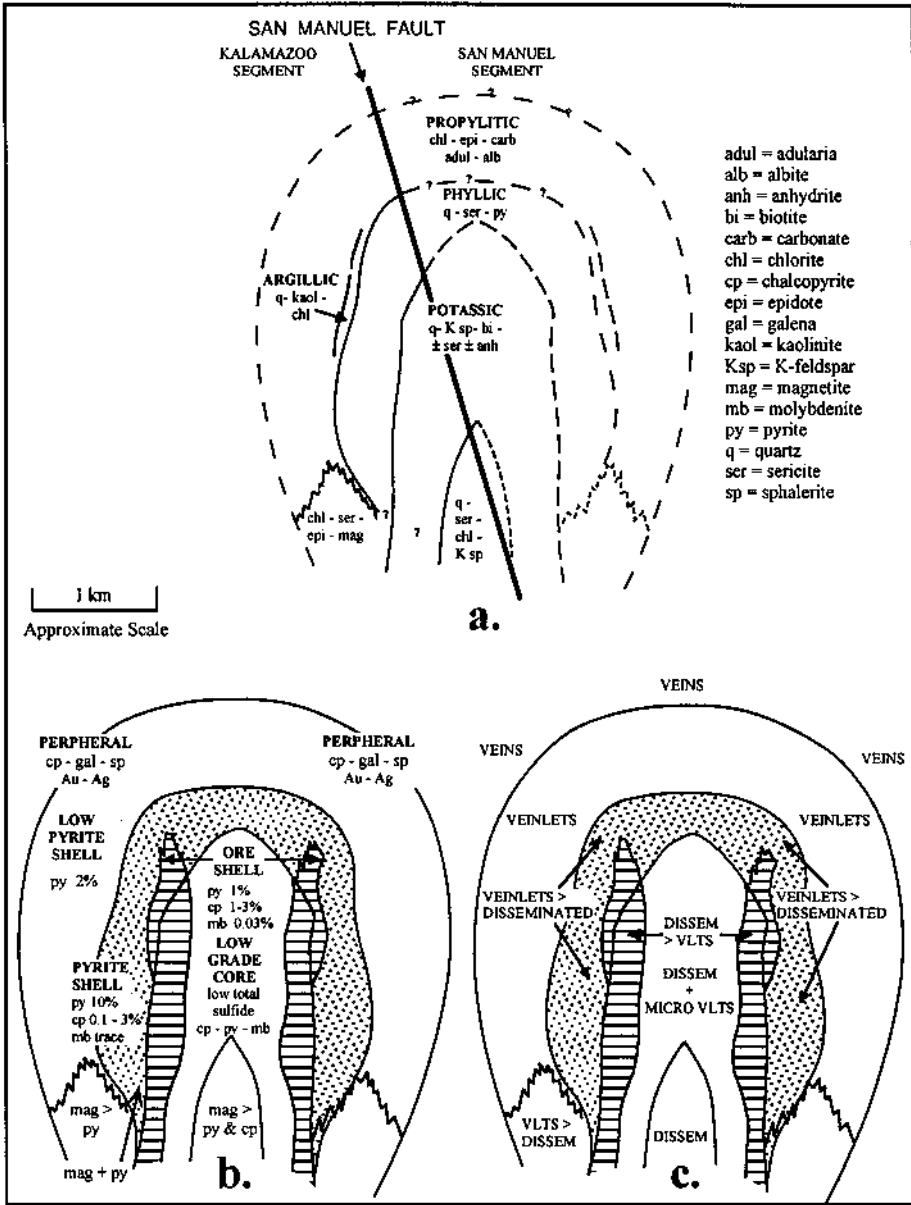


Figure 8.5. Schematic of concentric alteration-mineralization zones in porphyry copper systems, based on San Manuel-Kalamazoo deposits, Arizona, USA (after Lowell & Guilbert 1970): a. Alteration zones (broken lines indicate uncertainty regarding continuity or location); b. Mineralization zones; c. Style of sulfide mineralization.

transition to pervasive alteration in which evolving alteration mineralogy begins to be controlled by the hydrothermal fluids rather than by the host rock.

Several porphyry copper systems have a peripheral zone of vein-type copper (chalcopyrite) - zinc (sphalerite) - lead (galena) - gold - silver mineralization. Some noteworthy examples in USA are: Bingham Canyon, Utah (see Fig. 3.19); the Pima district, Arizona (Tittley 1982c); Mineral Park, Arizona (Eidel et al. 1968, Wilkinson et al. 1982, Lang & Eastoe 1988); and Butte, Montana (Meyer et al. 1968). However, base and precious metal veins spatially associated with porphyry-style mineralization may represent a separate mineralization event in some cases. For example, petrographic and fluid inclusion data indicate that the peripheral base metal-precious metal veins at Mineral Park (Arizona) formed from fluids of 1-7 wt% NaCl equivalent salinity and about 400-200°C temperature, and that the event probably was related to a much larger intrusion at depth (Lang & Eastoe 1988). Skarn-type copper and lead-zinc mineralization in carbonate rocks associated with porphyry copper systems will be discussed in the next chapter (Ch. 9).

Zoning and Paragenesis

Zoning of hydrothermal alteration and hypogene ore mineral assemblages in porphyry copper deposits has been recognized since a long time and discussed by many authors (e.g., Lowell & Guilbert 1970, Rose 1970b, James 1971, DeGeoffroy & Wignall 1972, Tittley 1982b, Beane 1982). A generalized pattern of coaxial alteration-mineralization zoning compiled by Lowell and Guilbert (1970) was based on porphyry copper systems in southwestern USA (Figure 8.5). The "typical" porphyry copper system in the Lowell-Guilbert model is centered on a Laramide (65 Ma) quartz monzonite stock emplaced in Cretaceous aluminous sediments and contains 140 million tons of ore (0.45% hypogene Cu, 0.15% hypogene Mo, and 0.35% supergene Cu), 70% of which occurs in the igneous host rocks and the rest in the surrounding pre-ore rocks. The ideal sequence of concentric alteration zones from the core outward is: potassic (quartz - orthoclase - biotite) \Rightarrow phyllic (quartz - sericite - pyrite) \Rightarrow argillic (quartz - kaolinite - montmorillonite) \Rightarrow propylitic (epidote - calcite - chlorite). The argillic zone is not well developed in many systems and its distribution may lack the symmetry of alteration zoning. Discernible alteration commonly extends several hundreds of meters beyond the copper ore zone, which is best developed at or near the interface between the potassic and phyllic zones (Fig. 8.5a). Variations in the ore mineral assemblage (Fig. 8.5b) and in the style of mineralization (Fig. 8.5c) bear a systematic relationship to the alteration zoning.

The generalized pattern of vertical and lateral zoning depicted in the Lowell-Guilbert model has proved very useful in exploration and as a generalized framework for porphyry copper genesis, especially for the silica-saturated, high-molybdenum, low-gold deposits at continental margins, but it does not, and was never intended to, apply to every porphyry copper deposit. In many deposits (e.g., El Salvador, Chile), phyllic alteration overprints earlier alteration types, rather than form an intermediate zone between potassic and propylitic zones. In addition to apparent variations due to

the level of exposure, structural and compositional inhomogeneity, and post-ore faulting or intrusive activity or metamorphism, real deviations from the idealized pattern may occur due to one or more of the following factors (Guilbert & Lowell 1974, Hollister 1978, Beane & Titley 1981): composition and size of the central intrusion, mineralogy of pre-ore wallrocks, composition and flow paths of the hydrothermal fluids, permeability of the rocks, and the extent of supergene alteration. Moreover, with the exception of alteration types, which are pervasive and texturally destructive, most rocks within porphyry systems preserve a sequence of overprinted vein-alteration types; in such cases, the designation of alteration zones becomes uncertain.

The most obvious departure from the Lowell-Guilbert model occurs when the ore-related intrusions are quartz-dioritic or dioritic-syenitic, and not granodioritic-quartz monzonitic, in composition. The alteration-mineralization pattern associated with dioritic intrusions, described as the "diorite model" by Hollister (1975), are significantly influenced by the low $\text{SiO}_2:(\text{Na}_2\text{O}+\text{K}_2\text{O})$ ratio in the host pluton. The alteration zoning may be indistinct; K-feldspar may not be a prominent phase in the biotite-rich potassic zone, reflecting the more mafic character of the intrusion; phyllic alteration is commonly only poorly developed or absent, and is substituted by a chlorite-rich hydrothermal mineral assemblage (propylitic) because of the incomplete removal of iron as pyrite; sulfide mineralization accompanies either or both potassic and propylitic assemblages, and occurs more frequently as disseminations rather than in veinlets; and chalcopyrite:pyrite ratios often approach unity, so that hypogene copper contents are commonly high enough ($\geq 0.4\%$) to make ore grade without the benefit of supergene enrichment. The alteration-mineralization features associated with alkalic intrusions are very similar to those found in quartz diorite intrusions.

The extent of hydrothermal alteration in the wallrocks depends on the size of the central intrusion and rock permeabilities. Where wallrocks and intrusions have similar bulk compositions, as envisaged in the Lowell-Guilbert model, alteration assemblages in the wallrocks differ merely as a function of lower temperature and modified fluid chemistry. A marked difference in the wallrock composition is likely to produce substantially different alteration assemblages. The most striking example of the latter situation is the formation of skarns and skarn deposits in carbonate wallrocks (see Ch. 9). Dioritic intrusions in volcanic terrains develop Ca-Mg-rich alteration assemblages in the wallrocks (e.g., Panguna deposit), and recognition of different alteration types becomes very difficult where the basaltic wallrocks were subjected to prior lower greenschist facies metamorphism (e.g., the Caribbean deposits).

The spatial distribution of alteration assemblages (zoning) does not provide much information about their interrelationship with respect to time (paragenesis). Time is an important variable in this context, because cooling of the central intrusion causes changes in fracture density and each fracturing event is followed by the development of discrete stable alteration assemblages, resulting in superposition of alteration types in some fractures. Thus, a proper understanding of the alteration zones requires a knowledge of the alteration paragenesis. A generalized alteration paragenesis for the

southwestern USA porphyry copper province, as deduced from crosscutting veinlet relationships and an assessment of relative stability of hypogene alteration assemblages in the veinlets, is shown in Figure 8.6. The progress of hypogene alteration according to this interpretation may be summarized as follows (Beane 1982):

- (a) Sinuous quartz veins develop during the early history of cooling of the pluton and commonly are restricted to the intrusion.
- (b) With cooling, selectively pervasive biotite alteration develops over a wide area around the intrusion. Simultaneously, propylitic alteration (interpreted as metamorphism) moves away with outward dissipation of heat.
- (c) Following an early fracturing event, biotite is precipitated in microfractures as veins and veinlets. The selective biotite alteration and veinlet biotite compose the biotite aureole within which most deposits lie. As temperatures in the wallrock fall, propylitic alteration (mainly chloritization of secondary biotite) encroaches inward, overlapping earlier alteration types.
- (d) Subsequent fracturing events, at apparently successively lower temperatures, retreat toward the pluton. Each fracturing event is followed by the development of discrete alteration assemblages, and precipitation of metal sulfides occurs at specific stages of alteration. Propylitic alteration continues to encroach toward the pluton.
- (e) Phyllic alteration (quartz - sericite - pyrite) follows the last major fracturing event, which produces a much higher fracture density compared with earlier fracturing episodes, and its destructive effect obliterates most earlier types of alteration.

Supergene Effects

Nearly all porphyry copper deposits, particularly those emplaced in continental margin environments, possess a capping of supergene alteration and enrichment (see Ch. 2) overlying the hypogene sulfide mineralization. In a few cases, most or all of the commercially exploitable ore (average grade 1.0-1.5% Cu) occurs in the supergene zone. Leaching of metals from the oxidation zone (above the water table) is controlled by the amount of H_2SO_4 acid produced by the oxidation of sulfides and, thus, depends on the total sulfide content, especially on the proportion of pyrite, in the hypogene ore. Metals left behind in the oxidation zone are precipitated as oxides, hydroxides, carbonates, sulfates, or silicates. Characteristic iron and copper minerals of the oxidation zone include hematite, goethite, borgstromite, jarosite, cuprite, antlerite, brochantite, chalcantite, malachite, azurite, nectocite, and chrysocolla (Anderson 1982). Metal ions, particularly copper, that migrate to reducing environments (mostly below the water table) form a zone of supergene sulfide enrichment. Characteristic copper minerals of this zone are chalcocite and covellite. Repeated cycles of oxidation, leaching, and enrichment in porphyry copper deposits, in response to repeated

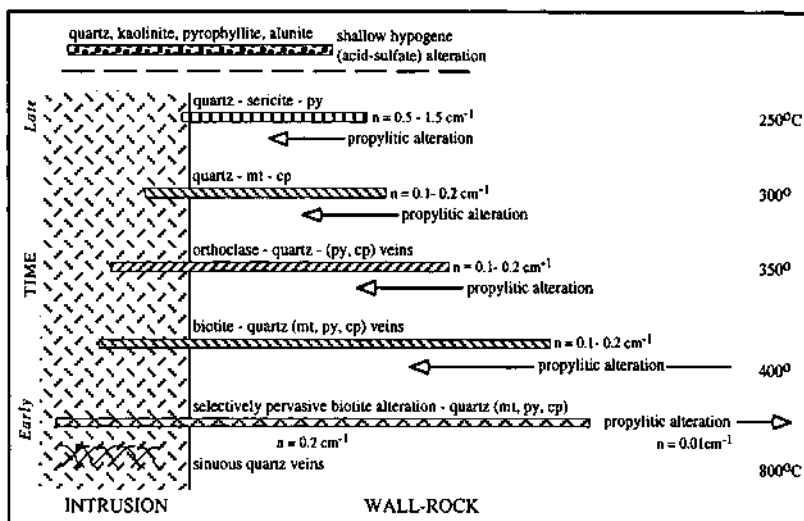


Figure 8.6. Time-space development of hydrothermal alteration in a porphyry copper system formed in plutons and wallrocks of potassium silicate mineralogy, modeled after deposits in the southwestern United States. Temperature ranges shown are approximate, intended only to indicate general cooling. Early, high-temperature potassic alteration (biotitization), which may have developed during prograding thermal effects, as well as successive overprinting alteration stages are, in turn, overprinted in a collapsing thermal environment by the effects of low-temperature fluids normally associated with propylitic alteration. The end result of the individual events is a composite formed by overprinting of alteration types: phyllic (quartz-sericite) alteration superimposed on most earlier types and flanked by potassic alteration in the intrusion and by potassic and then propylitic alteration away from it. Note that the argillic alteration (quartz, kaolinite, pyrophyllite, alunite) is interpreted as a later, shallow-hypogene event. n = fracture density, which is measured as the length of fractures per unit area and has the dimension cm^{-1} . py = pyrite, cp = chalcopyrite, mt = magnetite. (After Titley 1993.)

fluctuations of the water table, produce increases in the copper content of successive enrichment zones, culminating in almost complete replacement of hypogene sulfides by chalcocite. Subsequent oxidation of this chalcocitic blanket generates *in situ* oxide ore that commonly overlies zones of leaching and enrichment formed by oxidation of deeper primary sulfide ores. An excellent discussion of the subject is provided by Anderson (1982), who also pointed out how the grade of the hypogene sulfide mineralization might be predicted from the characteristics of the leached capping, a technique of great importance in exploration.

Supergene enrichment also occurs in parts of porphyry copper systems containing skarn-type mineralization, but the dissolution of primary sulfides in this case results in the precipitation of the metals as oxides and silicates near the surface.

8.2.7. EXAMPLES

Southwestern North American Province: Christmas Deposit, Arizona, USA

The southwestern United States and the adjacent area of Mexico contain the largest concentration of productive porphyry copper deposits in the world (Fig. 8.7). The deposits occur in belts aligned parallel to the inferred Laramide continental margin. The host intrusions were emplaced in a narrow time interval (≈ 55 to 72 Ma) within the Laramide orogeny. The Bisbee deposit (178-163 Ma) is an exception. The widely scattered remnants of Laramide dacitic and andesitic volcanic rocks in the province suggest that the porphyry plutons are subvolcanic intrusions of now-eroded andesitic stratavolcanoes. Many of the deposits occur in areas where the pre-ore Phanerozoic column was comparatively thin (4-5 km). The emplacement of the plutons may have been controlled by an ENE-trending grain within the Precambrian basement as well as by a pronounced NW-trending structural grain characterized by faults. The faults, which may be as old as Precambrian, were certainly active during the upper Paleozoic and throughout the Mesozoic, but no fundamental crustal structure has been recognized or shown to be a regional control (Titley 1993). Although there are variations on a regional scale, the deposits are characterized by: association with calc-alkaline

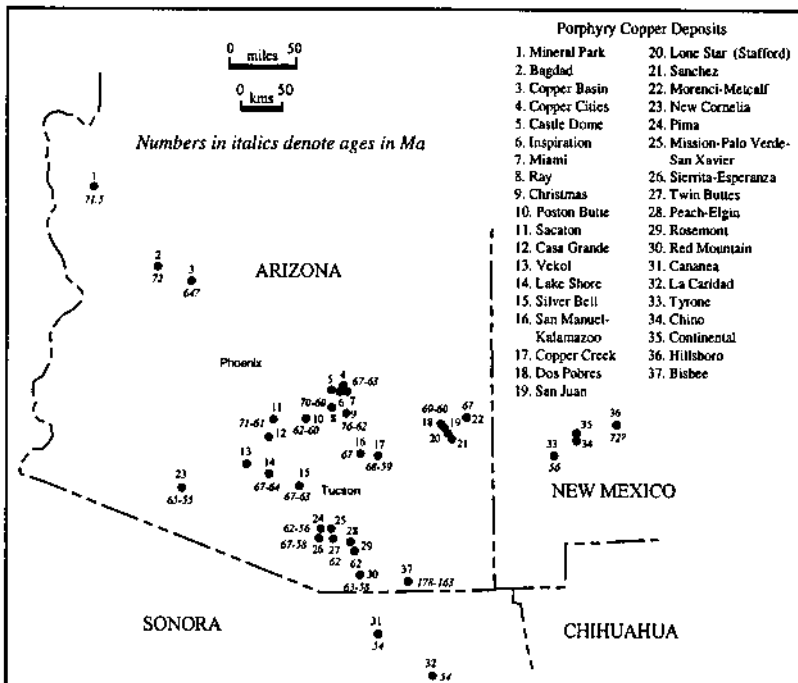


Figure 8.7. Ages of the principal porphyry copper intrusions of Arizona and contiguous regions of New Mexico and Mexico (after Titley 1993).

porphyritic intrusions of intermediate to felsic composition emplaced at shallow crustal levels, well-developed hydrothermal alteration and mineralization zones, significant mineralization in wallrocks of the intrusions, recoverable amounts of molybdenite, coeval breccia bodies, and pronounced supergene alteration.

Ore-grade mineralization in southwestern USA deposits are localized in the potassic alteration zone or in skarns (calc-silicate alteration) or in both. The Christmas deposit (Koski & Cook 1982) in southeastern Arizona is a relatively small but well-documented example of hypogene porphyry copper alteration-mineralization, where much of the copper production has come from the associated skarn-type mineralization in the carbonate wallrocks, mainly the Pennsylvanian Naco Limestone (Eastlick 1968, Perry 1969). The center of the porphyry system is a composite, porphyritic quartz diorite - granodiorite - dacite stock (the Christmas intrusive complex) of early Paleocene age (≈ 62 Ma) that intruded a thick Precambrian-Paleozoic sequence topped by the Upper Cretaceous Williamson Canyon Volcanics (Fig. 8.8). The mineralization is centered on the Christmas stock, but the core of the stock is poorly mineralized (generally $<1\%$ sulfide by volume and only 0.05- 0.1% Cu) with chalcopyrite and bornite as sparse disseminations and minor chalcopyrite deposited

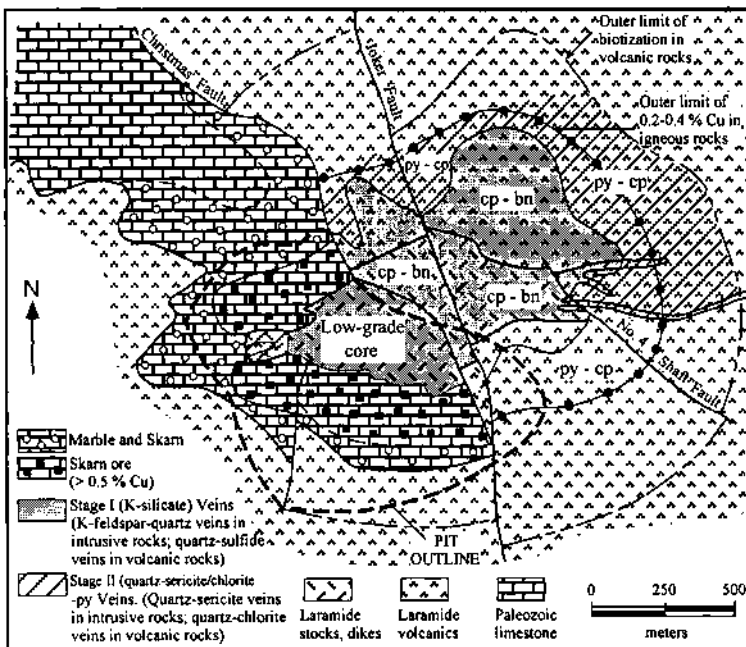


Figure 8.8. Hydrothermal alteration-mineralization zoning in relation to lithologic units, Christmas porphyry copper deposit, Arizona, USA. Note that ores from this deposit has been mined mostly from the mineralized skarn at the contact of the Laramide Christmas stock (simplified from Koski & Cook 1982).

along quartz - K-feldspar alteration veins. Progressively stronger chalcopyrite - bornite mineralization (0.2-0.6% Cu) as veins, fracture fillings, and disseminations in both the Christmas stock and the adjacent volcanic rocks occur at higher levels in the porphyry system east of the Christmas fault, perhaps in response to a steeper temperature gradient. Bornite is typically subordinate to chalcopyrite, and magnetite is a common constituent of quartz - sulfide veins of this stage of mineralization associated with potassic alteration. The outer limit of the chalcopyrite - bornite zone corresponds generally with the outer margin of the strong secondary biotite subzone in volcanic rocks. The biotite alteration zone extends beyond the zone of superimposed phyllic alteration, which is characterized by quartz with sericite or chlorite (in volcanic rock). This alteration is accompanied by significant amounts (1-10 volume percent) of pyrite and chalcopyrite in composite veins, each vein consisting of a filled central fracture and a wider, more diffuse wallrock envelope. Total sulfide content and the chalcopyrite:pyrite ratio decrease rapidly toward background values in the surrounding propylitic alteration zone characterized by epidote - chlorite - sphene assemblages. The propylitic zone extends well beyond the outermost limit of biotite alteration into the Cretaceous wallrocks, but it is difficult to establish its extent and paragenetic position because of widespread regional epidotization of the Williamson Canyon Volcanics prior to the intrusion of the Christmas stock. An argillic alteration zone has not been identified in the Christmas porphyry copper system.

The zoned pattern of hypogene alteration-mineralization (Fig. 8.8) is interpreted to have evolved in two stages (Koski & Cook 1982): (a) an early-stage (Stage I) of K-silicate (potassic) alteration, dominated by K-feldspar-rich and quartz-rich veinlets and biotitization of the stock and volcanic wallrocks, and contemporaneous chalcopyrite - bornite - molybdenite mineralization; and (b) a late-stage (Stage II) quartz - sericite - chlorite (phyllic) alteration, accompanied by pyrite and chalcopyrite mineralization. Field observations supplemented by fluid inclusion data suggest that Stage I fluids were magmatic, which evolved over a period of repeated surges of magma, particularly within the core of the Christmas stock. The presence of both primary and secondary gas-rich inclusions in Stage I quartz veins indicates that boiling was a recurring event. Propylitic alteration in the volcanic rocks may have been a contemporaneous process. The transition to Stage II alteration, largely a function of decreasing K:H ratio and/or cooling of the hydrothermal fluids, probably commenced with significant incursion of meteoric water into the system following an episode of intense fracturing, particularly near the stock. The mixing of cool, meteoric water and magmatic hydrothermal fluids decreased sulfide solubilities and led to the precipitation of pyrite and chalcopyrite along irregular fractures.

The Andean Belt: El Salvador Deposit, Chile

Most of the porphyry copper deposits of the Andean belt are associated with calc-alkaline intrusions, predominantly of felsic to intermediate composition (from tonalite through granodiorite to adamellite), emplaced over a wide range of geologic time extending from late Carboniferous to late Miocene (281-5 Ma). The wallrocks are

dominantly andesitic volcanics, and at least in some centers the volcanics are coeval and probably comagmatic with porphyry copper-bearing stocks. The general geologic characteristics of the Andean deposits are similar to those of the southwestern USA. Many major deposits exhibit well-developed concentric zoning of hypogene, fracture-controlled alteration and mineralization. Highest-grade hypogene ore is commonly associated with K-silicate alteration, but phyllic, advanced argillic, and propylitic zones also are locally ore-bearing. Hypogene Cu:Mo ratios range from about 20:1 to 50:1 (skewed toward the higher end) and, with minor exceptions (e.g., Andacollo), the gold contents are low (<0.2 ppm) (Sillitoe 1981). Some special features of the Andean belt include mineralized tourmaline-bearing breccia pipes (e.g., El Pachon, Argentina; El Tiente, Chile; Toquepala and Cuajone, Peru), common association of stockwork-type deposits with major faults and lineaments (which may or may not have influenced the emplacement of porphyry stocks), and the occurrence of enargite in ore assemblages (e.g., Chuquicamata, Chile; Morococha, Peru) (Hollister 1973).

The mineralization ages, which are estimated to be within 2 million years of the age of their progenitor stocks, define a series of longitudinal metallogenic sub-belts that are roughly parallel to the continental margin and the Peru-Chile trench (Fig. 8.9). About 90% of the Andean copper resources lie within three well-defined Cenozoic sub-belts: (a) Paleocene - early Eocene (66-52 Ma); (b) late Eocene - early Oligocene (42-31 Ma); and (c) middle Miocene - early Pliocene (16-5 Ma). The progressive eastward younging of the porphyry copper sub-belts in the central Andes has been attributed to eastward subduction of oceanic lithosphere (Sillitoe 1981). The reason for the geographic separation of the Andean porphyry copper belt from the Bolivian tin-tungsten province of similar age (Clark & Farrar 1973), at a similar distance from the paleo-trench and in the same orogen, is not understood. A possible explanation may lie in the thicker sialic crust under the tin-tungsten belt (Hollister 1978).

The El Salvador deposit is one of the most intensively studied deposits in the Andean belt (Gustafson & Hunt 1975, Field & Gustafson 1976, Sheppard & Gustafson 1976). The country rocks are Cretaceous andesitic flows and sedimentary rocks, which are overlain unconformably by early Tertiary volcanics. Minor copper - molybdenum mineralization is associated with 46-Ma, irregularly shaped subvolcanic intrusions of quartz rhyolite and quartz porphyry, but the main center of mineralization is related to a 41-Ma granodioritic porphyry complex (Fig. 8.10). The commercial orebody is relatively small, roughly 300 million tonnes of 1.6% Cu, and was formed by supergene enrichment, but the underlying lower-grade porphyry type mineralization is much more extensive.

The pattern of hypogene hydrothermal alteration and sulfide mineralization is quite complex because of the overlapping effects of multiple intrusions (Gustafson & Hunt 1975). Much of the copper was emplaced during an "early stage" hydrothermal alteration-mineralization event that followed the first two major intrusions ("X" and "K" porphyry stocks) due to metasomatic introduction of metals and sulfur from the solidifying melt into both the porphyries and the country rock. The result was a central zone of K-silicate alteration with veins of quartz - perthitic feldspar - anhydrite -

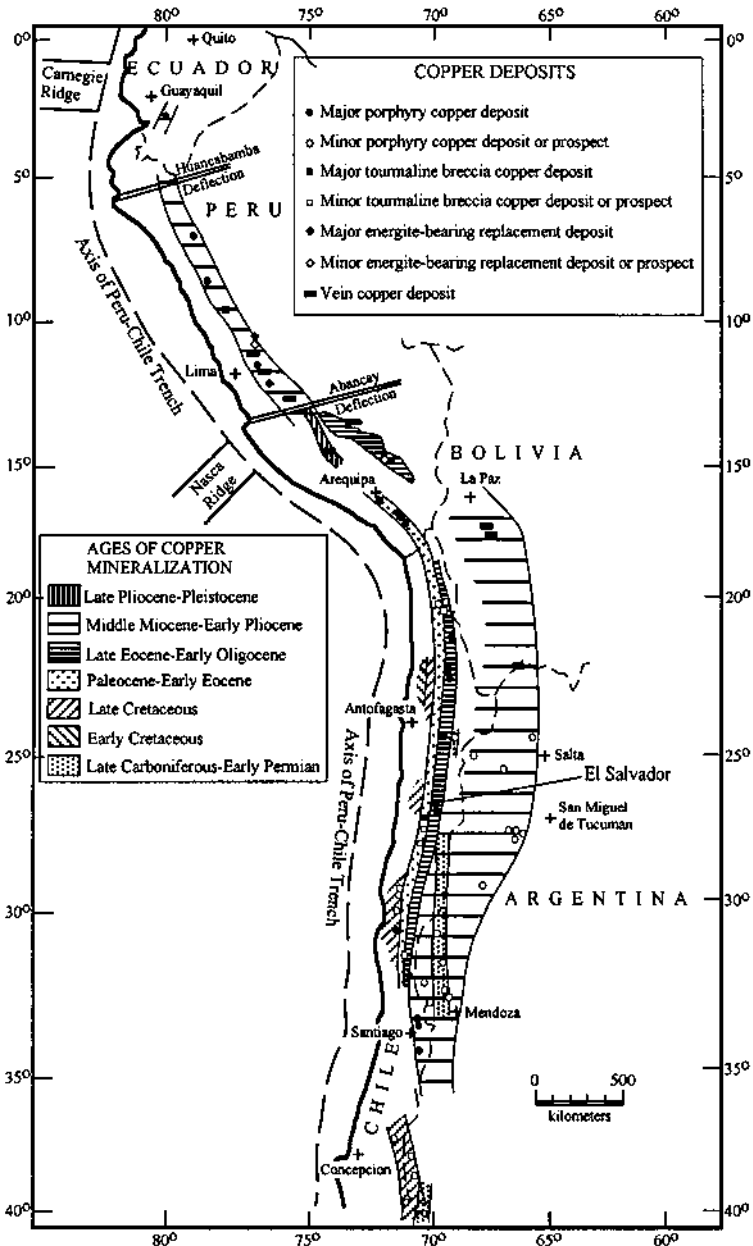


Figure 8.9. Ages of copper mineralization in the Andes of Ecuador, Peru, Bolivia, Argentina, and Chile. Note that bulk of the porphyry copper deposits lie within three well-defined, eastward-younging Cenozoic sub-belts: (a) Paleocene - early Eocene (66-52 Ma); (b) Late Eocene - early Oligocene (42-31 Ma); and (c) middle Miocene - early Pliocene (16-5 Ma). (Simplified from Sillitoe 1988.)

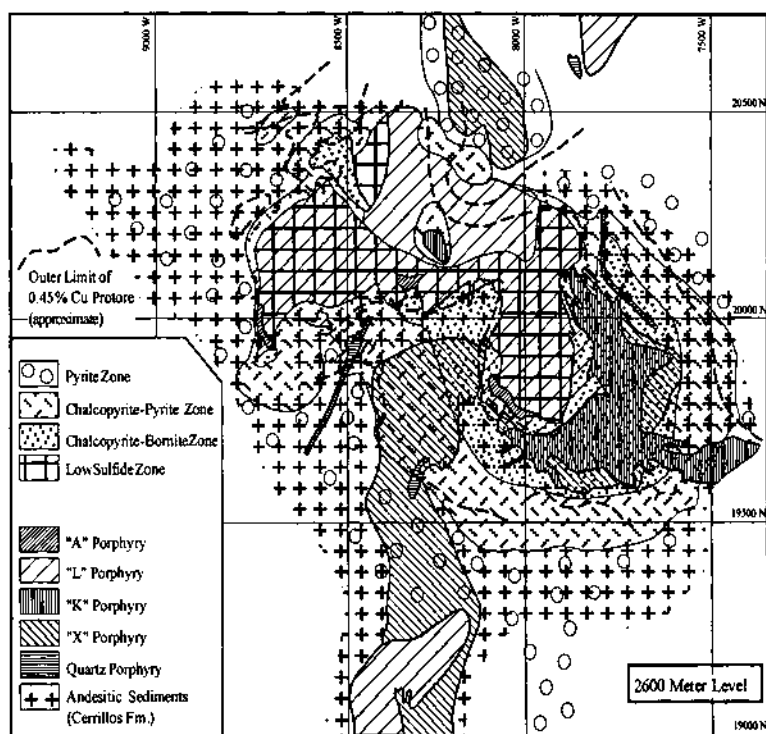


Figure 8.10. Simplified geological map of the 2600-meter level, El Salvador mine, Chile, with superimposed sulfide zones (modified from Gustafson & Hunt 1975).

chalcopyrite - bornite (called "A" veins), which was surrounded by a broad zone of propylitic alteration (epidote - chlorite - calcite) with decreasing abundance of sulfides and proportion of bornite. Pyrite is closely associated with sericite or sericite - chlorite, and pyrite - sericite - chlorite veining, which clearly postdated both K-silicate and propylitic assemblages. The "early-stage" hydrothermal solutions were dominantly primary magmatic waters as indicated by the $\delta^{18}\text{O}$ - δD values of biotites in K-silicate alteration assemblages (see Fig. 8.13). Oxygen isotope geothermometry has yielded a minimum temperature of 525°C for K-silicate alteration assemblages (Sheppard & Gustafson 1976).

Intrusion and cooling of the last major ("L") porphyry complex, which is relatively unaltered and unmineralized, destroyed part of the early-stage alteration and contributed minor chalcopyrite - pyrite mineralization, abundant molybdenite, and some tourmaline. These veins (called "B" veins), which lack alteration halos, cut A veins and K-silicate alteration assemblages. They mark a transition in the pressure-temperature regime and chemical character of the mineralizing fluids. A "late stage"

mineralization-alteration occurred in response to invasion of the hydrothermal system by meteoric water, after the intrusive complex had cooled to below $\approx 350^{\circ}\text{C}$. This resulted in the superposition of K-feldspar- and biotite-destructive alteration in parts of the K-silicate zone and the formation of pyrite - sericite assemblages and pyrite-rich "D" veins with sericitic alteration halos. A very late-stage hot spring system produced advanced argillic alteration near the surface and over the mineralized center. The dominance of meteoric water during the "late" and argillic stages is consistent with the oxygen-hydrogen isotopic compositions of the fluids (Sheppard & Gustafson 1976).

Sulfur isotopic data on hypogene sulfides ($\delta^{34}\text{S} = -10.1$ to -0.3‰ ; average -3.0‰) and hypogene sulfates ($\delta^{34}\text{S} = +7.3$ to $+17.0\text{‰}$; average $+10.7\text{‰}$) do not provide any unique interpretation for the source of sulfur (Field & Gustafson 1976). One permissible interpretation is that the early-stage sulfur was magmatic, whereas the late-stage sulfur was derived either by remobilization of early-stage assemblages below the deepest level of exposure or from volcanic wallrocks surrounding the deposit. Alternatively, the underlying magma chamber (estimated $\delta^{34}\text{S}_{\text{ES}} \approx +2\text{‰}$) continued to be the predominant source of sulfur throughout the entire sequence of alteration-mineralization.

Southwest Pacific Islands: Panguna Deposit, Bougainville Island

More than 25 porphyry copper systems have been discovered in the southwest Pacific islands (West Irian-Papua New Guinea, Manus, New Britain, New Ireland, Bougainville, New Georgia, British Solomon islands, Guadalcanal). Many of these deposits have been described in a special issue of *Economic Geology* (v. 73, no. 5, 1978). As summarized by Titley (1978), some of these porphyry systems are clearly related to island arcs, whereas others, such as in New Guinea, are related to more complex interactions involving continental and oceanic plates. All the deposits lie on islands or parts of islands that are either above present-day subduction zones or are considered to be parts of dormant arc systems. In all cases, the porphyry copper mineralization is related to Miocene and younger intrusions, commonly in contact with andesitic to dacitic volcanic rocks and very minor sedimentary components. Older, presumably pre-Miocene, intrusions are present, but are not known to carry economic mineralization. The intrusive rocks belong to the calc-alkaline series, ranging from diorite to quartz monzonite and granodiorite, but quartz diorite dominates in mineralization-related complexes. Mineralized alkalic intrusives similar to those associated with some porphyry copper deposits in the Canadian Cordillera have not been recognized in this province. The deposits exhibit mineralization and hydrothermal alteration patterns similar to those of the southwestern United States, but generally have higher contents of precious metals and a greater proportion of the copper mineralization in the wallrocks rather than within the intrusions.

The Panguna deposit, located in the central Bougainville Island, is one of the largest porphyry copper deposits in the region. It was discovered in 1964 and brought into commercial production in 1972. Reserves at Panguna, as reported by Titley (1978), were estimated as 840 million tonnes of ore averaging 0.46% Cu, 50 ppm

Mo, 0.51 ppm Au, and 2.08 ppm Ag.

The geology of central Bougainville Island is dominated by the Oligocene(?)–Lower Miocene Kieta Volcanics, a thick sequence of andesitic and basaltic lavas and pyroclastics. The Panguna deposit is situated at the southern margin of a Pliocene-age calc-alkaline plutonic complex (Fig. 8.11). The earliest and largest part of the complex, the Kaverong Quartz Diorite stock, intruded the Panguna Andesite Member of the Kieta Volcanics 4 to 5 m.y. ago (Page & McDougall 1972). Along its southern margin, the Kaverong Quartz Diorite consists of a biotite-bearing assemblage and is known as Biotite Diorite. The Panguna orebody is centered on three smaller porphyry stocks — the Biotite Granodiorite (with minor intrusive breccia and quartz-feldspar porphyry phases), the Leucocratic Quartz Diorite, and the Biuro Granodiorite. These stocks were emplaced at or near the southern margin, probably in the order given, about 3.4 ± 0.3 m.y. ago, which is also interpreted as the age of hydrothermal alteration and mineralization at Panguna (Page & McDougall 1972).

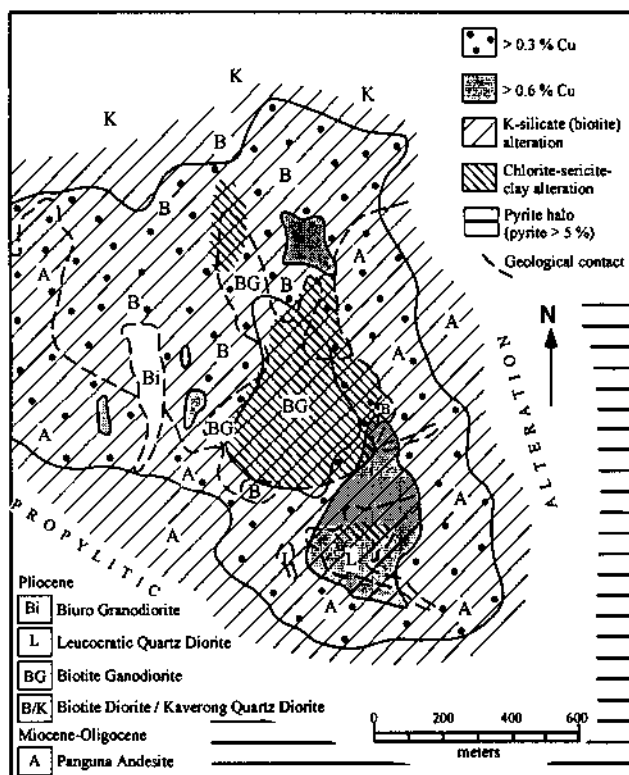


Figure 8.11. Simplified geological map of the Panguna mine, Bougainville Island, Papua New Guinea, showing distribution of copper grades and mineralization-alteration pattern. (Sources of data: Baldwin et al. 1978, Ford 1978, Eastoe 1978.)

The alteration-mineralization zoning at Panguna (Fig. 8.11) is the result of three broad alteration types represented by amphibole - magnetite (early), K-silicate (main-stage), and feldspar-destructive (late, retrogressive) assemblages (Fountain 1972, Ford 1978). Owing to a lack of evidence for recrystallization, the higher-temperature amphibole-magnetite alteration is regarded as a product of hydrothermal alteration rather than of hornfels facies metamorphism. This alteration is essentially confined to the Panguna Andesite, and its distribution is generally coincident with the later K-silicate (potassic) alteration. The K-silicate alteration, represented mainly by secondary biotite, affected all the intrusions except the Biuro Granodiorite, and is most intense in and adjacent to the Leucocratic Quartz Diorite. Much of the feldspar-destructive (argillic) alteration, consisting of a silica - sericite - kaolinite - chlorite assemblage, is largely confined to the Biotite Granodiorite; it clearly postdated biotite alteration and formed at lower temperatures. Propylitic alteration, characterized by chlorite - epidote - quartz - calcite - pyrite - chalcopyrite (minor), is regionally extensive and includes a pyrite halo within the inner margins of Panguna Andesite. Propylitic alteration apparently proceeded simultaneously with, but peripheral to, both amphibole-magnetite and K-silicate alterations. There is no well-defined phyllic zone as late-stage quartz - sericite - pyrite alteration in most Panguna rocks is minor and irregularly distributed. The development of hydrothermal alteration and veining in relation to the sequence of intrusions is yet to be established.

Copper sulfide mineralization was coeval with the K-silicate alteration, as is evidenced by the spatial coincidence of higher grade (>0.3% Cu) mineralization with this alteration zone. Total sulfides in the Panguna system vary between 1 and 4 wt%. Within the orebody, about 60% of the copper sulfides occurs in the andesite and the rest in the intrusives. The highest grade ore (>0.6% Cu) is localized in and around the Leucocratic Quartz Diorite (Fig. 8.11). Quartz veining and sulfide veins are prerequisites for high grade ore, and the grade falls rapidly where the frequency of quartz veins decreases and the mineralization is localized mainly in fractures. The Biotite Granodiorite is the most intensely altered of the stocks, but it hosts only subeconomic mineralization (average grade 0.23% Cu), except near the contacts with the Biotite Granite and in the central part of the intrusion where it attains ore grade (>0.3% Cu). The mineralization, however, appears to be centered on this intrusion, which led Fountain (1972) to consider it a likely progenitor of the main mineralization, but Eastoe (1978) did not find any pattern of fluid inclusion temperature-salinity data centered on the intrusion. The average grade of Biuro Granodiorite is only 0.05% Cu; it is weakly altered to argillic assemblages and does not appear to be the progenitor of or host to any copper mineralization. The average concentrations of molybdenum are 72 ppm in the Leucocratic Quartz Diorite, 80 ppm in the Biotite Granite, and 33 ppm in the Panguna Andesite (Ford 1978).

Chalcopyrite is the dominant copper mineral and it varies inversely with the pyrite content. Bornite is significant locally and is associated with minor free gold. Mineral analyses indicate that gold is spotty in chalcopyrite, anomalously high in bornite (300-400 ppm), and negligible in pyrite (Baldwin et al. 1978). The highest grade ores

usually have high contents of magnetite, up to 10 wt%, compared with an average of 2.7 wt% for the whole orebody (Ford 1978).

Studies emphasizing field relations (Baldwin et al. 1978), geochemistry of hydrothermal alteration (Ford 1978), and fluid inclusion characteristics (Eastoe 1978, Eastoe & Eadington 1986) indicate that the distribution and sequence of alteration-mineralization in the Panguna deposit is consistent with a genetic model in which an inner magmatic-hydrothermal system became surrounded by a cooler meteoric-hydrothermal system, the latter collapsing inward as the former waned. Based largely on fluid inclusion data, Eastoe (1978) proposed that the mineralization occurred in three phases. The first phase ("phase A") was associated with the emplacement of the Kaverong Quartz Diorite and dominated by very high-salinity (46-76 wt% NaCl+KCl), magmatic hydrothermal fluids at >700°C temperatures. The system cooled to less than 400°C and was inundated with low-salinity (<10 wt% salts) groundwater before renewed mineralization ("phase B") at temperatures above 400°C that accompanied the emplacement of the Leucocratic Quartz Diorite. The third phase of mineralization ("phase C") was centered on an area close to the western margin of the Biotite Granodiorite and postdated the Biuro Granodiorite. Phase A preceded the emplacement of the Biotite Granodiorite, and phases B and C, which may have been concurrent, succeeded that event. Eastoe (1982) argued that the copper was deposited mainly from high-salinity fluids, expelled directly from the magma or condensed from a vapor plume. Apparently, copper-bearing, magmatic fluids (high-salinity liquids + vapor) coexisted with silicate melt during the crystallization of Biotite Granodiorite, but did not produce significant mineralization (Eastoe & Eadington 1986).

8.2.8. ORIGIN

Source of Ore-forming Fluids

One of the controversial aspects of porphyry copper genesis pertains to the source of the hydrothermal fluids. Field and petrologic relations strongly point to the associated intrusions as the major, if not the only, source of fluids. This conclusion is in accord with experimental and theoretical considerations, which indicate (see Ch. 2) that the crystallization of water-bearing calc-alkaline magmas emplaced at shallow depths can produce metal- and sulfur-enriched hydrothermal fluids as a normal byproduct of their crystallization (Burnham 1967, 1979, 1997). Based on experimental data and heat-flow calculations under simplifying assumptions, Whitney (1975) has shown that, in a cooling, crystallizing stock of quartz monzonitic magma with an initial water content of 4 wt% (appropriate for the typical 3-4 km depth of porphyry copper mineralization), an aqueous vapor phase can exist in domal cupolas over the stock center; for a higher temperature magma of tonalitic (quartz diorite) composition, the vapor-saturated cap may extend to even deeper levels, perhaps down to 7 km or so (Whitney 1977). Burnham (1979) has also presented an elegant discussion of how a water-saturated carapace in a stock-like granodiorite magma, initially containing approximately 3 wt% H₂O and emplaced in a subvolcanic environment, could

theoretically expand about 30% upon complete crystallization at a depth of 3 km. Interaction of the vapor phase with the magma results in strong partitioning of chlorine, ore-forming metals (such as Cu, Mo, Sn), and sulfur into the vapor phase (Holland 1972, Burnham 1979, Candela & Holland 1984, 1986). Furthermore, the volume change associated with the vapor-forming reaction (melt \Rightarrow crystal + vapor) may promote the rise of the residual melt and/or induce fracturing of the solidified intrusion, producing crackle breccias, breccia pipes, and stockworks (Phillips 1973, Burnham 1979).

Some authors (e.g., Rose 1970b, Henley & McNaab 1978, Norton 1982), on the other hand, have made a case for the involvement of groundwaters from the wallrocks in the genesis of porphyry copper systems. In fact, numerical solutions of fluid flow in porphyry copper environments (Cathles 1981, Norton 1982) suggest that, whereas magmatic fluids may be present at an early stage of evolution, wallrocks adjacent to the intrusive are the source of much of the fluids circulating through a fractured hypabyssal pluton during its cooling history. The close association of porphyry mineralization with specific intrusive bodies within an igneous complex, however, is difficult to explain without the involvement of the intrusive in the hydrothermal convection system. Fluid inclusion and stable isotope data provide some constraints on these issues.

Fluid Inclusion Data

Very high homogenization temperatures ($>600^{\circ}\text{C}$) and salinities ($>40\text{wt}\%$ NaCl equivalent), with evidence of boiling in many cases, are distinctive features of fluid inclusions from porphyry copper deposits, although the reported temperatures and salinities span much broader ranges ($\approx 200\text{-}860^{\circ}\text{C}$ and $\approx 30\text{-}80\text{ wt}\%$ NaCl equivalent, respectively) (Nash 1976, Roedder 1984). Aqueous fluid inclusions from southwestern USA deposits, which account for bulk of the reliable microthermometric measurements reported in the literature, fall into three groups (Fig. 8.12): (a) hypersaline fluids with salinities generally $>30\text{ wt}\%$ NaCl equivalent, which homogenize at temperatures $>650^{\circ}\text{C}$ (type I); (b) high-salinity fluids, which homogenize in the range of $350^{\circ}\text{-}550^{\circ}\text{C}$, commonly by halite dissolution (type II); and (c) lower-salinity ("dilute") fluids with salinities $<20\text{ wt}\%$ NaCl equivalent, which homogenize by disappearance of vapor bubble at temperatures $<450^{\circ}\text{C}$ (type III). A similar range of homogenization temperatures ($\approx 150^{\circ}$ to $>600^{\circ}\text{C}$) and salinities (<5 to $76\text{ wt}\%$ NaCl equivalent) have also been reported for the Panguna deposit (Eastoe 1978). Type I fluids, where recognized, are the earliest in the paragenesis and in some porphyry copper deposits are associated with magmatic features (Moore & Nash 1974, Eastoe 1978, Reynolds & Beane 1985, Eastoe & Eadington 1986). The hypersalinity of inclusion fluids has generally been attributed to boiling (see Roedder 1984), but Cline and Bodnar (1991) have argued that the salinity of fluids exsolved from calc-alkaline magmas can be very high (up to $84\text{ wt}\%$ NaCl at 700°C) even without boiling. Type II fluids, most abundant in the early-stage hydrothermal assemblages, appear to have been at or near boiling conditions and were either approximately

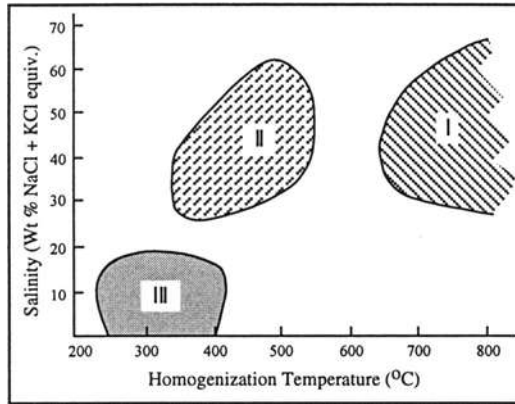


Figure 8.12. Types of fluid inclusions observed in porphyry copper deposits of southwestern USA, based on homogenization temperatures and salinities as compiled by Titley (1993).

saturated with halite or accompanied by halite when trapped (Cunningham 1978). Additional fluid inclusion data (e.g., Reynolds & Beane 1985) suggest that the gap in homogenization temperatures between type I and type II fluids may not be real and that type II fluids may have been derived from type I fluids by declining temperature and pressure accompanied by moderate dilution by meteoric water. Type III fluids are usually associated with hydrothermal assemblages formed late in the paragenesis (Preece & Beane 1982, Reynolds & Beane 1985). Such fluids may have evolved from higher salinity fluids by precipitation and separation of halite (Cloke & Kesler 1979), or by mixing with substantial amounts of more dilute meteoric and connate waters. Thus, the fluid inclusion data are compatible with the transport of copper as dissolved chloride complexes (most probably as CuCl^0 ; Candela & Holland 1984) in the magmatic hydrothermal fluids and with a scenario involving progressive dilution of the fluids by meteoric water as the porphyry system cooled. Candela and Holland (1984) experimentally determined the aqueous vapor-silicate melt partition coefficient of copper ($D_{\text{Cu}}^{\text{v-l}}$) to be strongly dependent on the concentration of chlorine in the vapor phase [$D_{\text{Cu}}^{\text{v-l}} = (9.1 \pm 2.5)m_{\text{Cl}}^{\text{v}}$ to at least 4.5 moles of chlorine per kg of solution] at 750°C, 1.4 kb, and nickel-nickel oxide (NNO) $f\text{O}_2$ buffer. The relatively smaller partition coefficient of molybdenum ($D_{\text{Mo}}^{\text{v-l}} = 2.5 \pm 1.6$ at the stated experimental conditions), which was also found to be independent of chlorine concentration up to at least 4.5 moles of chlorine per kg of solution, may account for the much lower concentration of molybdenum in porphyry copper deposits.

Daughter crystals which have been reported from fluid inclusions include hematite, magnetite, pyrite, chalcopyrite, and other minerals (Roedder 1984). The actual copper contents of the fluid inclusions are not known, but estimates based on the size of the chalcopyrite daughter crystals range from about 250 ppm to 5,000 ppm Cu at

magmatic and submagmatic temperatures. Thermodynamic calculations by Beane (1974) also suggest that high-salinity hydrothermal solutions in equilibrium with the mineral assemblage characteristic of the potassic alteration zone should contain on the order of 1,000 ppm dissolved copper and sulfur at temperatures of 350°C.

Oxygen and Hydrogen Isotope Ratios

Interpretation of the available oxygen-hydrogen isotopic data for discriminating between possible magmatic and non-magmatic components of porphyry copper hydrothermal fluids has two limitations (Taylor 1979): (a) most common meteoric waters on Earth have δD values that are similar to primary magmatic waters; and (b) the $\delta^{18}O$ changes due to interactions with meteoric water may be very small, relative to natural isotopic variations in igneous rocks, because of low water:rock ratios. An approach that circumvents these limitations is to consider deposits from different geographic areas (Sheppard et al. 1971), because the isotopic composition of meteoric water (and connate water) varies with latitude whereas that of magmatic water does not (see Fig. 4.14). A δD - $\delta^{18}O$ plot of most of the presently available analyses of OH-bearing minerals from porphyry copper (and porphyry molybdenum) deposits is presented in Figure 8.13. With minor exceptions (e.g., Butte deposit, Montana, USA), either because of lower temperature of the magmatic fluid or some mixing with meteoric water, hydrothermal biotites (potassic alteration) formed at relatively high temperatures (≈ 400 - 600°C) define a very tight group similar to 'normal' igneous biotites and show no relationship to latitude. The calculated isotopic composition of water in equilibrium with these biotites fall within or close to the hypothetical field of primary magmatic waters. In contrast, the δD values of hypogene clay minerals and sericites from deposits become lower at higher latitudes, suggesting the involvement of meteoric waters in their formation. This by itself does not answer the question whether they represent the original δD values of the sericites and clays or are a result of later exchange with groundwaters. However, the uniformity of the δD values in a given deposit such as Santa Rita, the very low $\delta^{18}O$ values of sericites and clays from some of the northerly deposits (e.g., Butte), and the similarity in δD values of sericites of vastly different grain size from the Climax porphyry molybdenum deposit (Sheppard et al. 1971) require pervasive exchange with heated meteoric waters rather than partial low-temperature exchange with groundwaters (Taylor 1979). The Panguna sericites are anomalous in the sense that they appear to have formed from magmatic-dominated fluids of similar isotopic composition as the hydrothermal biotites. The isotopic ratios of the supergene clays are quite distinct from those of hypogene clays. The supergene clays plot either on the *kaolinite line*, defined by pure kaolinites from weathering zones, or slightly to the left of it because of higher temperatures (50 - 60°C) of formation compared with surface weathering (Sheppard et al. 1971). Thus, the δD - $\delta^{18}O$ data indicate the evolution of mineralizing fluids in porphyry copper systems from being dominantly magmatic at the potassic alteration stage to being dominantly nonmagmatic (meteoric \pm connate water) at the phyllic (sericitic) alteration stage.

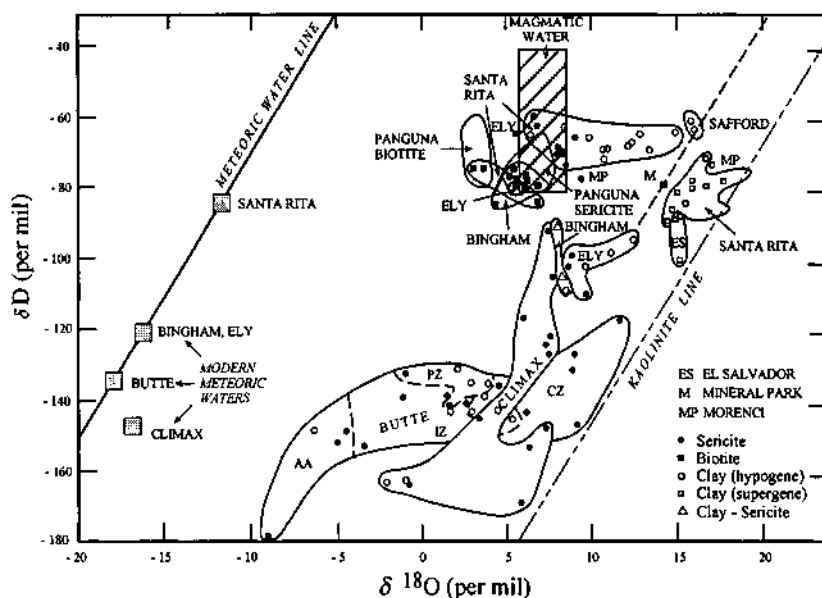


Figure 8.13. Plot of δD vs. $\delta^{18}O$ for hydrous minerals from porphyry copper and porphyry molybdenum deposits in relation to the "meteoric water line" (Craig 1961), "kaolinite line" (Savin & Epstein 1970) and the field of primary magmatic water (Taylor 1974). The dotted line near the 'kaolinite line' is drawn merely to emphasize the separation of supergene and hypogene clays. Biotites from the El Salvador deposit (Sheppard & Gustafson 1976) plot within the cluster for biotites from other porphyry copper deposits. For the Butte deposit: AA = advanced argillic alteration, PZ = peripheral zone, IZ = intermediate zone, CZ = central zone. Approximate values for modern meteoric waters are from White (1974). Sources of data for porphyry deposits: Ford and Green (1977); compilation by Taylor (1979).

Genetic Model

Considering that the stable isotope and fluid inclusion data discussed above require the presence of both magmatic and nonmagmatic (meteoric \pm connate) waters in the porphyry copper hydrothermal fluids (Sheppard et al. 1971, Taylor 1974, 1979, 1997), the hydrothermal system for porphyry copper deposits may be conceptualized as some combination of two end-member models (McMillan & Panteleyev 1980): a *magmatic-hydrothermal model* (the 'orthomagmatic' model of McMillan and Panteleyev 1980), and a *convective model* (Fig. 8.14). The fundamental difference between the two lies in the source and flowpath of the hydrothermal fluids. In the magmatic-hydrothermal model, the hydrothermal fluid, dominated by magmatic water, ascends as a vapor-dominated plume through the stock and produces potassic and propylitic alteration, with narrow zones of phyllic alteration in the area of interaction between magmatic

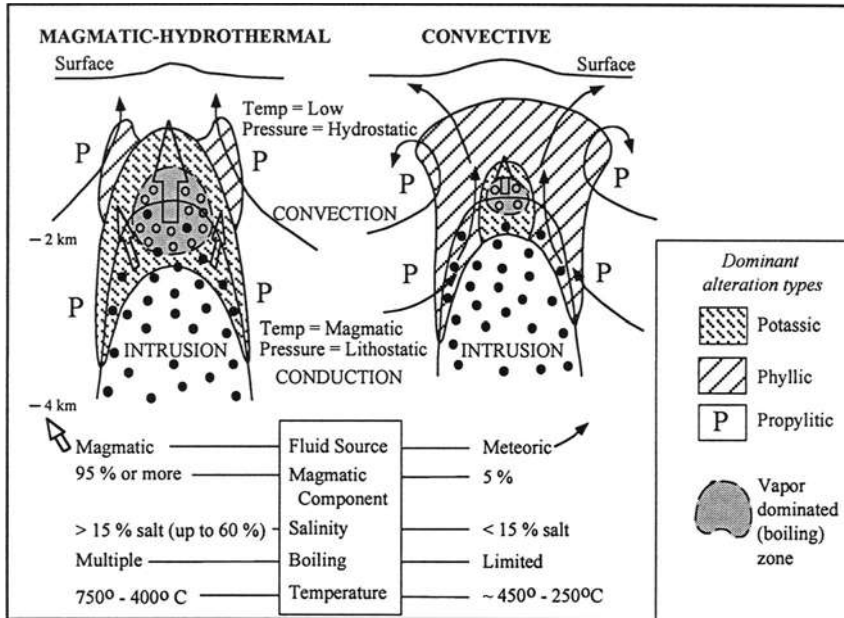


Figure 8.14. The two end-member genetic models, magmatic-hydrothermal and convective, for porphyry copper systems (after McMillan & Panteleyev 1980). The fundamental difference between the two models lies in the source and flow-path of the hydrothermal fluids.

and meteoric fluids. In the convective model, the hydrothermal fluid, dominated by groundwater (meteoric and connate waters) from the country rocks, is set in thermally driven convective motion by the emplacement of the magma, and produces phyllic alteration, with peripheral propylitic alteration around potassic core zones. Sulfide distribution patterns can be identical in the two systems, but the source of metals and sulfur are mainly from the magma in the magmatic-hydrothermal model and from the country rocks in the convective model. Most porphyry copper systems contain elements of both models, commonly with evidence for evolution from an early, dominantly magmatic-hydrothermal system to a later groundwater convective system, as has been interpreted for a number of deposits, such as El Salvador (Gustafson & Hunt 1975), Panguna (Eastoe 1978), Santa Rita (Ahmad & Rose 1980, Reynolds & Beane 1985), and Mineral Park (Lang & Eastoe 1988). Both hydrothermal systems are simultaneously present early in the history of the porphyry stock, but the expanding envelope of magmatic H_2O and the higher lithostatic H_2O pressures of the internal system prevent the external hydrothermal system from invading the stock (Fig. 8.15). However, the external system persists even after the magmatic-hydrothermal system fades away and eventually collapses onto the hydrothermally altered rocks formed by

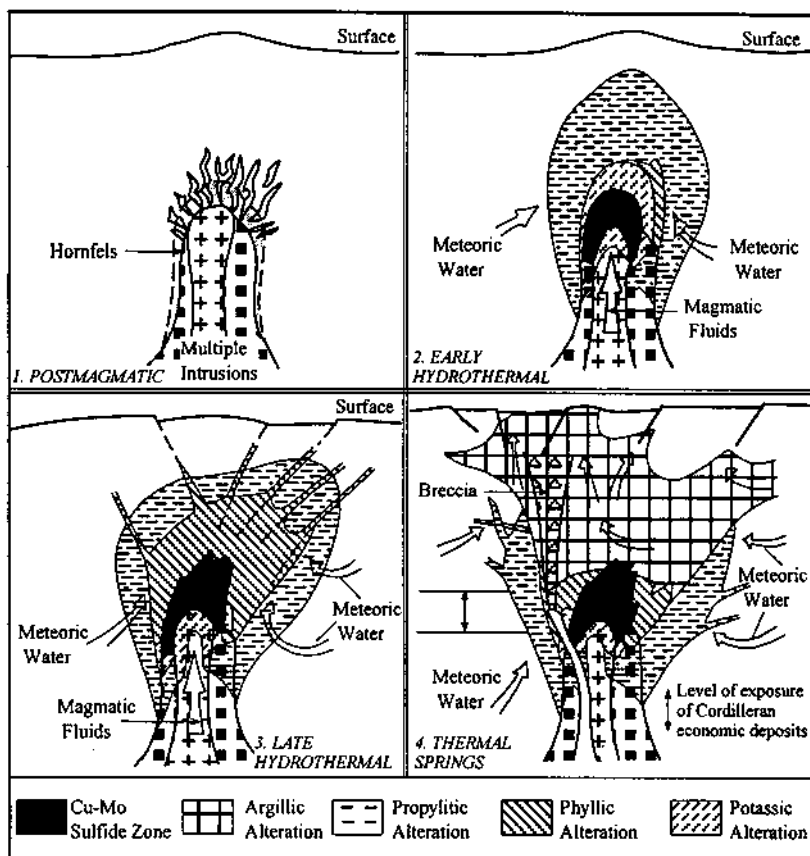


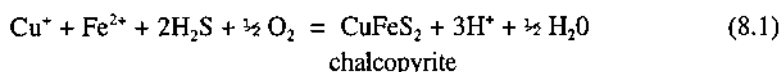
Figure 8.15. Model of the sequential development of alteration-mineralization in a porphyry copper system patterned after Gustafson and Hunt's (1975) interpretation of the El Salvador deposit in Chile (after McMillan & Panteleyev 1980).

the internal system. This results in the superposition of the sericite - pyrite and argillic alteration zones upon the potassic alteration zone or upon the unaltered intrusive. The preferential localization of porphyry copper ore along the boundary between the two different types of hydrothermal systems suggests that the mixing interface may have been important in ore deposition. Owing to variable water contents and permeabilities of country rocks, the size of the external hydrothermal system varies considerably in known porphyry copper deposits, from "wet" types (e.g., Butte, Bingham, Morenci) having high pyrite:chalcopyrite ratios and surrounded by enormous halos of pyrite-sericite-quartz to "dry" deposits (e.g., Bethlehem) with relatively minor sericite-pyrite zones (Taylor 1997). In some cases, the primary ores may be dissolved and redeposited by the late-stage meteoric-hydrothermal fluids. The

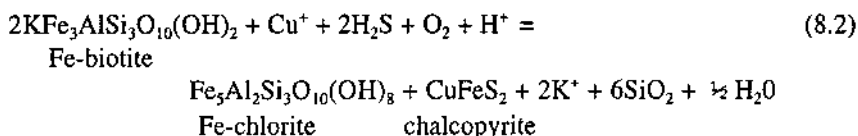
very rich main-stage Cu-Zn-Pb veins at Butte (Montana, USA), with low- $\delta^{18}\text{O}$ and low- δ^{D} sericite alteration envelopes, may have originated this way, the whole hydrothermal system being driven by a largely hidden porphyry copper intrusion at depth (Sheppard and Taylor 1974).

Correlation of Mineralization with Alteration

Deposition of chalcopyrite (and bornite) in the porphyry copper environment occurs by open space (or vein-veinlet) filling through reactions such as (Beane 1982)



and by replacement (or alteration) of pre-existing minerals through reactions such as



As indicated by the adjoining alteration selvages, vein-veinlet mineralization involves interaction between wallrocks and hydrothermal fluids, including contribution of iron from the wallrocks. Replacement mineralization involves diffusion of copper and sulfur from the hydrothermal fluids. It generally occurs at the sites of pre-existing ferromagnesian minerals in close proximity to fluid channelways and gives rise to disseminated mineralization.

It follows from the stability relations shown in Figure 3.14 that the alteration mineralogy of porphyry copper deposits can be explained in terms of variations in temperature or $\alpha_{\text{H}^+}:\alpha_{\text{K}^+}$ ratio. The transition from potassic to phyllic alteration may be attributed to decreasing temperature of the hydrothermal fluid, but fluid inclusion data do not support a decrease in temperature as the cause of the observed ore minerals paragenesis. As discussed earlier, the spatial distribution of ore mineralization relative to hydrothermal alteration zones indicates that much of the chalcopyrite deposition occurs late in the evolution of potassic alteration, or during a transitional stage between potassic and phyllic (sericitic) alteration when early hydrothermal biotite is converted to chlorite while K-feldspar remains stable. This association provides the link in terms of $a_{\text{Fe}^{2+}}:a_{\text{H}^+}^2$ ratio between silicate minerals (Fig. 8.16a) and sulfide/oxide minerals (Fig. 8.16b) in porphyry copper deposits (Beane 1982). The arrows in Figure 8.16 show the evolution of reaction-controlled assemblages as the hydrothermal alteration proceeds from potassic to phyllic, producing the generalized paragenetic sequence (with ubiquitous quartz): K-feldspar + biotite + magnetite \Rightarrow K-feldspar + chlorite + chalcopyrite \Rightarrow muscovite (sericite) + pyrite. The precipitation of magnetite, chalcopyrite, and pyrite are acid-producing reactions, which result in a progressive decrease in the pH of the fluid in such a system and constitute the

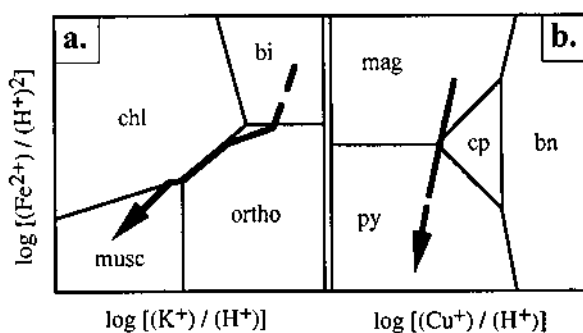


Figure 8.16. Schematic stability relations among (a) silicate minerals and (b) sulfides and oxides of copper and iron in the presence of an aqueous solution. Chlorite and biotite represent the Fe component of solid solutions. Relative positions of the two diagrams in terms of the Fe^{2+} compositional variable are based on common mineral assemblages in porphyry copper deposits in the southwestern United States. Arrows indicate changing assemblages from early to late. Abbreviations: bi = biotite, bn = bornite, chl = chlorite, cp = chalcocopyrite, mag = magnetite, musc = muscovite, ortho = orthoclase, py = pyrite. (After Beane 1982.)

principal source of acid for phyllic alteration. That is why phyllic alteration tends to be most abundantly associated with maximum total sulfide (mainly pyrite) deposition in porphyry systems. Paragenetic studies of hydrothermal minerals in southwestern USA deposits generally indicate that, if mineralization had not developed prior to the point at which the ferromagnesian silicates began to undergo quartz - sericite - pyrite alteration, it was not likely to develop with further evolution of the hydrothermal system (Beane 1982).

8.2.9. METALLOGENESIS

Age Distribution of Porphyry Copper Intrusions

In the Pacific Basin rim, igneous intrusions related to porphyry copper deposits were emplaced episodically over a considerable span of time (from ≈ 200 Ma to 1 Ma). Three main intervals of porphyry copper intrusions can be recognized in this region: (a) 140-75 Ma in North America, mostly in Canada (batholiths of comparable ages are common in the Andes, but the porphyry copper deposits are much younger and are superimposed on the older system; Titley & Beane 1981); (b) 75-50 Ma, a Pacific-wide episode (excluding the southwestern Pacific island arcs) that took place during the Laramide orogeny; and (c) <40 Ma, which is important throughout the circum-Pacific belt, except southwestern North America, especially during the last 10 m.y. Another characteristic of intrusive activity within some of the Pacific Rim regions is a landward migration of magmatism with time that includes a migration of porphyry copper evolution in some terranes such as the Andes (Sillitoe 1981), southwestern USA (Titley 1993), and New Guinea (Titley & Heidrick 1978).

The relative scarcity of extensive ore-grade mineralization in porphyry systems

older than about 200 Ma has been attributed to removal of the upper parts, the loci of mineralization, by deep erosion in older terranes (Sillitoe 1972, Hollister et al. 1974). This is not an entirely satisfactory explanation considering the worldwide preservation of numerous Paleozoic and older massive sulfide deposits associated with calc-alkaline and tholeiitic suites. Perhaps the highly fractured rocks of a porphyry system were more susceptible to rapid erosion than the volcanic suites associated with massive sulfide deposits. Nielson (1976) suggested that the abundance of post-Paleozoic porphyry copper deposits might be a function of the close link between plate convergence and the generation of magmas conducive to porphyry copper mineralization.

Sources of Porphyry Copper Magmas

The $^{87}\text{Sr}/^{86}\text{Sr}$ initial ratios of porphyry copper-related intrusions are strongly correlated with their tectonic settings (Kesler et al. 1975a, Titley & Beane 1981): ratios less than 0.705 for island-arc deposits, close to values measured for oceanic basalts of mantle origin; and ratios in the range of 0.704-0.710 for continental margin deposits, distinctly higher than the ratios for oceanic basalts (but lower than the ratios of 0.720-0.750 typical of Precambrian crustal rocks). Thus, island-arc intrusions are believed to have been derived from upper mantle material or recycled oceanic crust, presumably along a subduction zone, with very limited contamination from continental crust. The strontium isotope ratios of porphyry magmas at continental margins, on the other hand, are compatible with an upper mantle source with a different isotopic composition beneath the continents than ocean basins, or contamination by continental crust or subducted oceanic sediments (Hedge 1974, Thorpe et al. 1981, Hawkesworth 1982). Based on additional information, such as REE patterns and neodymium isotope ratios, Anthony and Titley (1988a, b) have attributed the source of Laramide porphyry magmas in Arizona (southwestern USA) to melting in the lower crust, probably of amphibolite.

For a better understanding of the relationship between source rocks and parent porphyry magmas, we should consider the physicochemical constraints they impose on such magmas. These constraints for porphyry magmas, as discussed by Burnham (1981), are: (a) an H_2O content in the range of 2-5 wt% so that the magmas can reach depths of ≈ 2 to 6 km without much crystallization; (b) high initial temperatures ($\approx 800^\circ\text{C}$), which are inversely related to the H_2O contents, to carry the magmas to depths of 4 km or less in a largely liquid state; (c) sufficient enrichment in appropriate metals; (d) sufficient chlorine content so that magmatic aqueous fluids exsolved during second boiling will have adequate salinity to transport metals as chloride complexes (at least 0.05 wt% Cl for Cu-Au and Cu-Mo porphyry systems, but lower for Mo, Sn, and W porphyry systems for which chloride complexes are not important); (e) adequate sulfur content (≥ 0.2 wt% S) for sulfide-rich porphyry copper systems (unimportant for sulfide-poor tin and tungsten porphyry systems); and (f) high enough $f\text{O}_2$ so that hydrothermal fluids exsolved from the magma can carry large quantities of sulfur, together with metal chloride complexes (not critical for tin and tungsten porphyry

systems). At depths shallower than ≈ 2 km, neither hornblende nor hydroxyl-rich biotite, which occur as phenocrysts in mineralized porphyry stocks, are stable at magmatic temperatures. At depths greater than ≈ 2 km, neither of these minerals crystallize as phenocrystal phases unless the H_2O content of the magma is generally greater than ≈ 2 wt%. Felsic magmas with more than 5 wt% H_2O are likely to become water-saturated at depths greater than about 6 km and, owing to their low liquidus temperatures, completely crystallize before reaching shallow depths. Second boiling in magmas containing less than 2 wt% H_2O , hence at more advanced stages of crystallization, generally does not release sufficient mechanical energy to produce the extensive fracturing necessary for the circulation of large quantities of mineralizing fluids from depths greater than approximately 2 km (Burnham & Ohmoto 1980).

According to Burnham (1981), source rocks capable of producing magmas that would satisfy the constraints stated above for the different porphyry systems are: (a) hornblende-bearing mafic rocks of igneous origin for Cu-Au; (b) biotite-bearing continental crust rocks of intermediate composition for Cu-Mo and Mo, and (c) muscovite-bearing (pelitic) metasedimentary rocks for Sn-W. The relationships are summarized in Figure 8.17. Some molybdenum porphyries appear to represent partial melts formed from mixed biotite- and muscovite-bearing source rocks (mixed I- and S-types). Felsic magmas derived by partial melting of hornblende-bearing rocks and of biotite-bearing rocks, in which the melt phases contain 2.7 and 3.3 wt% H_2O , become H_2O -saturated at depths of approximately 2 and 3 km, respectively, without becoming completely crystalline (Burnham & Ohmoto 1980). The too high initial H_2O contents and, therefore, too low temperatures of S-type magmas formed by partial melting of muscovite-bearing sedimentary rocks generally do not permit these magmas to reach the epizonal environment before complete crystallization.

Sources of Sulfur and Ore Metals

Based on available sulfur isotopic data (Ohmoto & Rye 1979, Eastoe 1983), the source of sulfur in porphyry copper deposits is believed to be upper mantle or homogenized crustal material. The majority of the $\delta^{34}S$ values of the sulfides and sulfates in these deposits (excluding those associated with host rocks containing sedimentary anhydrite-bearing units) fall between -3 and $+1\%$ and between $+8$ and $+15\%$, respectively (Fig. 8.18). Although $\delta^{34}S_{SS}$ values of the mineralizing fluids at each deposit cannot be determined precisely due to a lack of corresponding fO_2 information, they have been estimated to lie between -3 and $+9\%$ for most deposits, suggesting the derivation of sulfur largely from igneous sources, either through magmatic fluids or by dissolution of igneous sulfides in country rocks (Ohmoto & Rye 1979). Sedimentary sulfides may have contributed sulfur in the case of a few deposits, such as Galore Creek, exhibiting low $\delta^{34}S$ values for sulfides. An evaporitic source of sulfur is a possibility for deposits, such as Morocochoa, that have high $\delta^{34}S$ values for both sulfides and sulfates.

A dominantly magmatic source of sulfur in porphyry deposits is consistent with the source rocks for porphyry magmas discussed earlier (see Fig. 8.17). Owing to

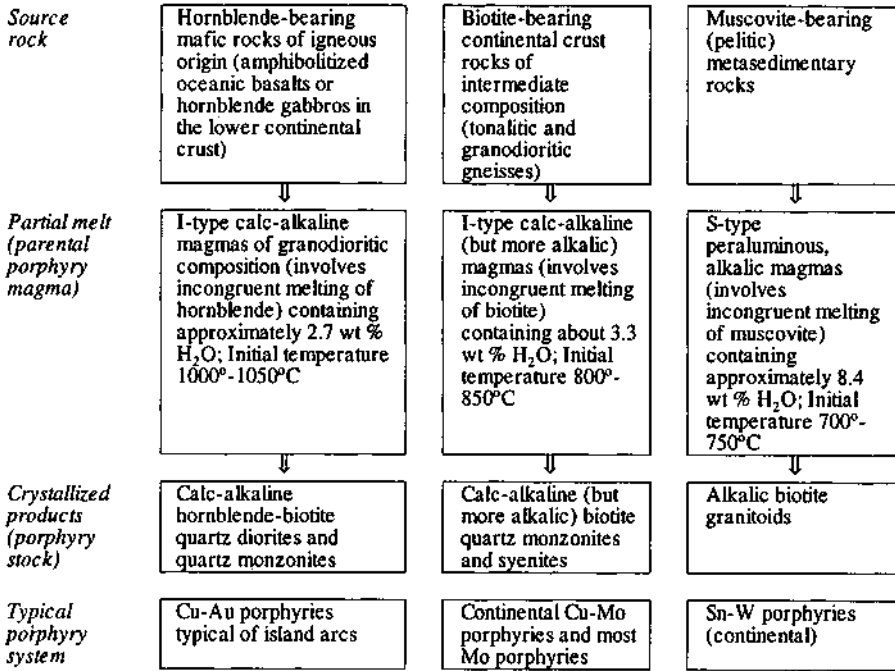


Figure 8.17. Potential source rocks for magmas appropriate for the different porphyry systems, as proposed by Burnham (1981). Some molybdenum porphyries possess chemical and mineralogical characteristics that suggest derivation from mixtures of biotite- and muscovite-bearing rocks (mixed I- and S-type magmas). Because of their high H₂O content and, therefore, low temperatures, S-type magmas do not reach the epizonal environment without becoming completely crystalline.

higher sulfur solubilities — predominantly as SH⁻ — in more oxidized, I-type hydrous magmas (Burnham & Ohmoto 1980), the degree of partial melting is generally sufficient to extract all of the sulfur from the source rocks, and such magmas may commonly contain in excess of 0.2 wt% S (compared with perhaps an order of magnitude less sulfur in low-*f*O₂, S-type magmas). Hydrothermal fluids exsolved from I-type magmas by second boiling can contain enough sulfur to account for the sulfides even in giant porphyry deposits. The sulfur is released from the magma as SO₂ (because of high *f*O₂), which on cooling is converted to H₂S either through redox reactions with Fe²⁺-bearing minerals in the wallrocks or by hydrolysis in the fluid. Eastoe (1983) calculated that less than 2% of the sulfur released by the magma was fixed in the Panguna porphyry copper deposits, the remainder being available for mineralization higher in the hydrothermal system. Noting that the chlorites contain

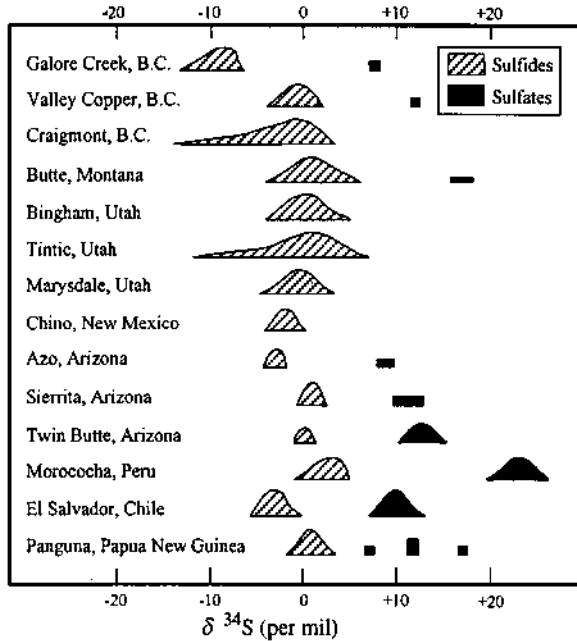


Figure 8.18. Sulfur isotopic data for selected porphyry copper deposits (modified from Ohmoto & Rye 1979). The data for the Panguna deposit are from Eastoe (1983).

much less sulfur than precursor biotites in porphyry systems, Banks (1973) raised the possibility that part of the sulfur could have come from biotite via propylitizing fluids of meteoric origin. Such a connection may also account for the preferential association of porphyry copper deposits with biotite-rich plutons.

The source of the base metals in porphyry copper deposits is another controversial issue. One possibility is that the metals were scavenged from country rocks by convecting groundwater driven by the magmatic heat, but this is rather unlikely in view of the close spatial association between sulfide mineralization and potassic alteration. Also, the Cu:Mo ratios of the deposits show no correlation with their spatial distribution as well as with crustal thickness or the lithology or age of the basement rocks. The more likely possibility, supported by the correlation between copper mineralization and intrusions of specific compositions in a given igneous complex, is a magmatic source of the metals, ultimately derived from the source region of magma generation. Except for lead, which can be accommodated diadochically in feldspars, the valuable metal content of an I-type porphyry magma increases with increasing metal content and decreasing partial melting of the source

rock (the latter related to the hydrous mineral content of the source rock). From theoretical considerations, Cline and Bodnar (1991) have argued that "typical" calc-alkaline magmas contain sufficient copper, chlorine, and water to produce economic porphyry copper mineralization. Moreover, a study of the Nd and Sr isotopic composition of the late Cretaceous monzogranite stock and its mineralized alteration aureole at San Manuel, Arizona, has shown that the material flow was primarily from the stock into the wallrock (Farmer & DePaolo 1987).

An intrinsic component of the plate-tectonic model of Sillitoe (1972b) is the extraction of metals from the oceanic crust of the subducted slab. Ocean-floor basalts are a particularly attractive source of metals because they are already somewhat enriched (87 ppm Cu, 1.5 ppm Mo, and 4 ppb Au; Turekian & Wedepohl 1961) compared with average crust. Such a source may be viable for the Andean belt porphyry copper belt which appears to have involved subduction of oceanic crust (Sillitoe 1988), but there is no clear-cut evidence of oceanic crust subduction for the Cordilleran porphyry copper provinces. It is difficult to specify a minimum copper content that a magma must possess to yield economic mineralization, because the copper that ultimately ends up in a deposit depends on various additional factors such as the mass of the magma, the extent of crystallization before the magma becomes water-saturated, the efficiency of copper extraction by the exsolved aqueous fluid phase, and the configuration of the hydrothermal plumbing system. In any case, considering that the copper contained in a 100-million-tonne orebody averaging 0.5% Cu could be obtained from just about one cubic kilometer of magma containing only 200 ppm of Cu, partial melting of amphibolitized average oceanic basalt or of many biotite-bearing granodioritic source rocks is quite capable of providing sufficient copper for economic mineralization (Burnham 1981).

Paleotectonic Settings

As mentioned earlier, porphyry copper deposits occur in two tectonic settings: cratonic continental margin and island-arc. A comparison of deposits in the two settings, with southwestern USA and Philippines as representative examples, is presented in Table 8.2. The most conspicuous difference between the two types lies in the typical composition of the cogenetic intrusion — quartz diorite to diorite for island-arc deposits, and quartz monzonite for continental margin deposits. Also, the island-arc deposits are relatively younger in age, have lower initial $^{87}\text{Sr}/^{86}\text{Sr}$ ratios (<0.705), are Mo-impoverished but enriched in Au, and show less distinct alteration zoning. These differences are attributable largely to differences in the source region of magma generation and the crystallization history of the magma.

Porphyry copper deposits in both island-arc and continental margin settings have commonly been interpreted to have formed along destructive plate margins above zones of oceanic crust subduction (Sillitoe 1972b, Sawkins 1972, Mitchell & Garson 1972, Garson & Mitchell 1973). The main lines of evidence for this interpretation are: (a) the association of porphyry copper deposits with predominantly calc-alkaline magmatism which is characteristic of subduction zones (Dickinson 1968, Hamilton

TABLE 8.2. Comparison of porphyry copper deposits of island-arc (Philippine) and cratonic continental margin (southwestern United States) settings

Characteristic	Island-arc (Philippine)	Cratonic continental margin (Southwestern USA)
Country rocks	Cretaceous to Mid-Tertiary metavolcanic-metasedimentary rocks and keratophyres	Precambrian to Cretaceous sediments and metasediments ± volcanics
Mineralization- related intrusions	Quartz diorite to diorite $^{87}\text{Sr}/^{86}\text{Sr}$ initial ratio <0.705	Quartz monzonite $^{87}\text{Sr}/^{86}\text{Sr}$ initial ratio >0.705
Age (pluton and mineralization)	Paleocene to Late Miocene	Predominantly Laramide (Late Cretaceous to Early Eocene)
Average ore tonnage and hypogene ore grade	133 million tonnes of ore; Cu - 0.46%, Mo - 0.007%, Au - 0.3 g/t	136 million tonnes of ore; Cu - 0.45%, Mo - 0.015%, very minor gold
Ore and gangue minerals	2-6% sulfides in ore zones (average 3%); major chalcopyrite and minor bornite; abundant pyrite; abundant magnetite (average 3%); anhydrite or gypsum common in moderate amounts (often post-mineralization)	3-10% sulfides in ore zones; major chalcopyrite and minor bornite; abundant pyrite; sparse magnetite; anhydrite or gypsum common in minor amounts
Style of mineralization	Tabular orebodies; about 50% of the ore in pluton; quartz-sulfide veinlets, with minor sulfide disseminations	Orebodies as vertical cylinders; about 70% of the ore in pluton; sulfides as fracture-filling veinlets and disseminations
Hydrothermal alteration	Potassic (biotite, chlorite, epidote, sericite, alkali feldspar) in ore zones; propylitic (chlorite, epidote, calcite, sericite, clay minerals) in fringe areas	Potassic to phyllic in ore zones; phyllic, argillic, and propylitic in fringe areas
Alteration zoning	Overlapping, indistinct	Distinct
Supergene enrichment	Negligible	Common
Post-mineralization structures	Abundant shatter fractures	Major fault displacements

Sources of data: Sillitoe (1972a, 1986), Hollister (1975), Titley and Beane (1981), and Hutchinson (1983).

1969); (b) linear disposition of deposits in a given province suggestive of a tectonic control in the emplacement of the related intrusives; and (c) presence of active subduction zones beneath porphyry copper districts in the Andes and Central America and in the Philippines and Solomon Island arcs (Mitchell & Garson 1972). The details of plate convergence in the various circum-Pacific provinces and the time-space relationships of plate convergence to the evolution of porphyry copper systems, however, are not all that clear.

Perhaps the best case for subduction-dominated tectonics for the emplacement of

porphyry copper intrusions has been made in the central Andean orogen (James 1971, Sillitoe 1975, 1976, 1981, 1988). In this orogen, successive longitudinal sub-belts of different ore-types, including porphyry Cu-Mo deposits and their associated magmatism, can be rationalized with an overall plate-tectonic model involving a shallow-dipping subduction of the Nazca plate under the South American plate from the Triassic to the late Tertiary. These sub-belts terminate, or their characteristics change, at transverse tectonic boundaries, which are believed to represent divisions between discrete segments of the underlying subduction zone. Each segment was characterized by a different subduction history and, consequently, by a different space-time pattern of intrusion and copper mineralization. The two most important first-order boundaries for intrusion-related copper mineralization appear to be in the general vicinities of the Huancabamba and Abancay Deflections (see Fig. 8.9). Several second-order boundaries appear to have caused more subtle changes along individual copper sub-belts.

Our present knowledge of the plate-tectonic setting of the southwestern Pacific islands does not permit a detailed correlation of the porphyry copper deposits with specific subduction zones, although some of the younger deposits, such as the 1.1-1.2 Ma Ok Tedi (Papua New Guinea), are believed to be located above active subduction zones (Bamford 1972). Titley (1975) suggested a strong correlation of dated events in the geologic history of the Pacific Basin, including changes in the rates and directions of plate convergence, with the times of porphyry copper evolution in the region.

Porphyry copper deposits in the North American cordillera apparently do not lie in linear belts and are not associated with obvious paleosubduction zones. They tend to occur in clusters and are located far inland from inferred trenches. Emplacement of the related plutons have been variously ascribed to structures formed by tensional stresses without the involvement of subduction (Hodder & Hollister 1972, Lowell 1974), northwesterly motion of the North American Plate over a mantle hot spot and a clockwise rotation of the plate (Livingston 1973), and plate convergence (Sillitoe 1972a, 1975, Griffiths & Godwin 1983). The limited data available at present appear to support a plate convergence scenario.

In southwestern United States, analysis of fracture and dike patterns associated with Laramide plutons suggests a ENE to WSW compressive stress for the tectonism during the Laramide orogeny (80-40 Ma), most probably due to plate convergence (Heidrick & Titley 1982). According to Coney (1976), the eastward convergence between the oceanic Farallon Plate and the continental North American Plate due to the opening of the North Atlantic Ocean changed at about 80 m.y. ago to ENE convergence, with a marked increase in the relative motion from 8 cm/year to 14 cm/year. A low-dipping subduction of the Farallon Plate, a result of relatively rapid rate of convergence (Luyendyk 1970), may account for the magmatism considerably inland from the continental margin, although within this regional compressive stress field plutons might have been emplaced along local tensional structures (Nielsen 1976).

8.3. Porphyry Molybdenum Deposits

Economic deposits of molybdenum occur in various metal associations (such as Mo-Cu, Mo-W, Mo-Sn-W, and Mo-Bi) and are almost always related to granitic plutons. The two most important sources of recoverable molybdenum, from molybdenite as the ore mineral, are porphyry molybdenum deposits (typical Mo:Cu > 1), which characteristically do not contain recoverable copper, and porphyry copper deposits (typical Mo:Cu < 0.1), many of which contain enough molybdenum to be recovered as a coproduct or as a byproduct. The ore tonnages of porphyry molybdenum deposits are comparable to those of porphyry copper deposits, and the average grades range from about 0.05 to 0.3 wt% Mo (Table 8.3).

8.3.1. DISTRIBUTION

The greatest concentration of porphyry molybdenum deposits, both in terms of number and production, occurs in the western Cordillera of North America that extends from British Columbia (Canada) and adjacent parts of southeastern Alaska southward through the western United States to Mexico (Fig. 8.1, Table 8.3). A few important deposits have also been found in Peru, Greenland, former Yugoslavia, former USSR, and PRC. The relatively restricted global distribution of porphyry molybdenum deposits compared to porphyry copper deposits suggests that the formation of the latter requires somewhat more stringent conditions. It is also noteworthy that the two classes of porphyry deposits seldom occur in close proximity. For example, porphyry molybdenum deposits are quite scarce in the Basin and Range Province of western United States, a region with abundant porphyry copper deposits. On the other hand, the Colorado mineral belt, which contains three of the largest porphyry molybdenum deposits of the world (Climax, Urad-Henderson, and Mt. Emmons) and many smaller ones, is notably impoverished in porphyry copper deposits.

Ages of porphyry molybdenum deposits range from about 340 Ma (Mt. Pleasant, New Brunswick, Canada) to about 5 Ma (Silver Creek, Colorado mineral belt, USA), but almost all economic deposits are Cretaceous to Tertiary, dominantly Tertiary, in age. Thus, the age distribution of porphyry molybdenum and porphyry copper deposits are very similar. As is the case with porphyry copper deposits, this age distribution cannot be explained entirely by preferential erosion of older subvolcanic porphyry deposits, although erosion certainly has reduced the number of occurrences. As alkali basalts appear to be a critical component in the formation of high-grade porphyry molybdenum deposits (discussed later), the age distribution may be correlated with the appearance of significant volumes of alkali basalts in the Mesozoic and Cenozoic (Carten et al. 1993), possibly as a result of recycling processes in the lower mantle related to subduction (Ringwood & Irifune 1988).

TABLE 8.3. Tonnage and grade of selected major porphyry molybdenum deposits

Deposit #	Type	Tonnage* (10 ⁶ tonnes)	Grade		Age (Ma)
			Mo (%)	Cu (%)	
Canada					
Red Mountain, Yukon (44)	QM	187 (G)	0.100	-	87
Logtung, Yukon	QM	162 (G)	0.031	-	118-109
Adanac, British Columbia (45)	QM	270 (G)	0.094	-	75-71
Bell Molly, British Columbia	QM	32 (M)	0.066	-	54-53
Endako, British Columbia (46)	QM	336 (M)	0.087	-	146-141
Boss Mtn., British Columbia (47)	QM	63 (G)	0.074	-	107-99
Kitsault, British Columbia	QM	108 (G)	0.115	-	55-49
Yorke-Hardy, British Columbia	QM	125 (G)	0.151	-	72-70
United States					
Quartz Hill, Alaska	QM	1,216 (G)	0.077	-	30-27
Mt. Tolman, Washington	QM ?	2,177 (G)	0.054	0.090	60-50
Big Ben, Montana	C**	376 (G)	0.098	-	51-50
Cannivan, Montana	QM	185 (G)	0.096	-	64-61
Cumo, Idaho	QM ?	1,258 (G)	0.059	0.074	52-45
Pine Grove, Utah	C**	125 (G)	0.170	-	23-22
Henderson, Colorado (48)	C	727 (G)	0.171	-	28
Urad, Colorado (49)	C	12 (Mined)	0.209	-	29.5
Climax, Colorado (50)	C	770 (M)	0.216	-	33-24
Mt. Emmons, Colorado	C	141 (M)	0.264	-	18
Buckingham, Nevada	QM ?	1,297 (G)	0.058	0.034	86
Hall, Nevada	QM ?	181 (M)	0.091	0.045	70-66
Mt. Hope, Nevada	C**	510 (G)	0.100	-	38-36
Pine Nut, Nevada	QM	181 (G)	0.060	-	Late Creta.
Questa, New Mexico (51)	C**	277 (M)	0.144	-	25-24
Others					
Cumobabi, Mexico	QM ?	67 (G)	0.099	0.266	57
El Creston, Mexico (52)	QM ?	181 (G)	0.074	0.060	Tertiary
Compaccha, Peru (53)	QM	100 (G)	0.072	-	9.5-12
Copaquire, Chile	QM ?	50 (G)	0.070	0.300	30
Malmberg, Greenland (54)	A	136 (G)	0.138	-	28-32
Nordli, Norway (55)	A	181 (G)	0.084	-	247-280
Mackatica, Yugoslavia (56)	QM	181 (G)	0.078	-	36-40
Jin Dui Cheng, PRC (57)	QM ?	907 (G)	0.100	0.030	70

Source of tonnage, grade, and age data: compilation by Carten et al. (1993); *G = Geologic, M = Mineable.

Deposit type classification after White et al (1981): C = Climax-type, QM = Quartz monzonite-type.

** C = Sub-Climax-type according to Wallace (1995).

A = Alkalic sub-type of high-silica rhyolite-alkalic suite of Carten et al. (1993); not included in White et al. (1981).

Numbers in parentheses refer to locations shown on Figure 8.1.

8.3.2. HOST INTRUSIONS AND TYPES OF DEPOSITS

Porphyry molybdenum deposits are spatially, temporally, and genetically associated with porphyritic intrusions ranging in composition from quartz monzonite to high-

silica (75-77 wt% SiO₂), alkali-rich (up to 10 wt% Na₂O+K₂O) granite. Thus, based mainly on the composition of cogenetic intrusions (which, of course is related to the magma chemistry and the tectonic environment of magma generation), porphyry molybdenum deposits are divisible into two major types, both with broadly similar silicate alteration assemblages: one associated with arc-related, relatively less differentiated, calc-alkaline magmas, and characterized by low fluorine contents and low Mo-grades; and the other associated with rift-related, highly evolved, rhyolitic-alkalic magmas, and characterized by high fluorine contents and high Mo-grades. Broadly equivalent classifications described in the literature include (a) rift-related (back-arc setting) and subduction-related (continental margin setting) porphyry molybdenum deposits (Sillitoe 1980); (b) granodiorite and granite molybdenum systems (Mutschler et al. 1981); (c) calc-alkaline ($K_{57.5} = 1.5-2.5$) and alkali-calcic to alkalic ($K_{57.5} = 2.5-6.0$) molybdenum stockwork deposits (where $K_{57.5}$ is defined as the K₂O value of the magma series at 57.5 wt% SiO₂) (Westra & Keith 1981); (d) quartz monzonite-type and Climax-type (so named after the Climax mine, Colorado) molybdenum deposits (White et al. 1981); and (e) Climax-type low-fluorine and Climax-type high-fluorine porphyry molybdenum deposits (Ludington 1986, Theodore 1986); and (e) differentiated monzogranite and high-silica rhyolite-alkalic suite (>75 wt% SiO₂ on an anhydrous basis) porphyry molybdenum deposits, the latter consisting of Climax, transitional, and alkalic subtypes (Carten et al. 1993). We will follow here the classification of White et al. (1981), which is summarized in Table 8.4. Judging from the examples listed, the "Climax-type" of White et al. (1981) is roughly equivalent to the entire 'rhyolite-alkali suite' of Carten et al. (1993) who reserve the term "Climax-type" for two specific deposits, Climax and Henderson (Colorado, USA). Our emphasis will be on the *Climax-type* deposits, which account for nearly 50% of the world's molybdenum production.

8.3.3. QUARTZ MONZONITE-TYPE DEPOSITS

The general characteristics of the quartz monzonite-type deposits, by far the most common type of porphyry molybdenum deposits, are very similar to those of porphyry copper deposits. Deposits of this type are associated with small composite or single-phase stocks, or with late phases of batholiths. The composition of cogenetic intrusions range from quartz diorite or diorite to granodiorite to quartz monzonite, but the most common is quartz monzonite porphyry. The hydrothermal alteration zoning in most deposits consists of a potassic core, a quartz - sericite - pyrite - (pyrrhotite) envelope (phyllitic alteration), an outer (upper?) argillic zone, and a propylitic halo. The mineralization style is dominated by stockwork veinlets, and the highest molybdenite molybdenite concentrations are generally found at the outer edge of the potassic alteration zone and within the inner quartz - sericite - pyrite zone. The average grade of ores ranges from 0.10 to 0.20% MoS₂, significantly lower than that for Climax-type deposits. With the exception of a small number of deposits, which appear to have formed in island arcs (e.g., Canicanian, Polillo Island, Philippines, and

TABLE 8.4. Comparison of Climax-type and quartz monzonite-type porphyry molybdenum deposits (after White et al. 1981)

Characteristics	Climax-type	Quartz monzonite-type
Type of intrusion	Stock	Stock or batholith
Age of intrusive activity	Middle to late Tertiary	Mesozoic and Tertiary
Intrusive phases	Multiple intrusions of granites	Composite intrusions of diorite to quartz monzonite
Cogenetic rock type	Granite porphyry	Quartz monzonite porphyry
Style of mineralization	Stockwork veinlets; very minor disseminations	Stockwork veinlets; very minor disseminations
Orebody shape	Inverted cup	Inverted cup, tabular
Average ore grade (% MoS ₂)	0.30 to 0.45	0.10 to 0.20
Orebody tonnage (million tonnes)	50 to 1,000	50 to 1,000
Ore-associated minerals	pyrite wolframite (huebnerite) cassiterite, stannite fluorite, topaz bismuth sulfosalts chalcopyrite (rare)	pyrite scheelite tin minerals (rare) fluorite bismuth sulfosalts chalcopyrite (minor)
Cu:Mo ratio in ore zone	1:100 to 1:50	1:30 to 1:1
Distinctive hydrothermal alteration	High-silica core Greisen common	No high-silica zone No greisen
Typical examples	Climax, CO, USA Henderson, CO, USA Mt. Emmons, CO, USA	Endako, BC, Canada Red Mtn., Yukon, Canada Quartz Hill, Alaska, USA

possibly Quartz Hill, Alaska and Endako, Canada), deposits of this type occur within continental magmatic arcs in convergent plate margin settings.

There are, however, some noteworthy differences between quartz monzonite-type porphyry molybdenum deposits and porphyry copper deposits associated with intrusions of similar composition and age. The former are characterized by much higher W:Mo ratios (and by the common occurrence of scheelite as an accessory mineral), much lower Re:Mo ratios, and the common presence of accessory fluorite. Also, most porphyry molybdenum deposits do not occur within the extrusive phases of their related magma systems, suggesting a greater depth of porphyry magma emplacement (Hollister 1978).

Some deposits (e.g., Mount Tolman, Cumo, and Buckingham; see Table 8.3) included under the quartz monzonite-type appear to be hybrid systems intermediate between true porphyry molybdenum deposits and porphyry copper deposits. Such hybrid systems are generally characterized by central molybdenite zones with significant overlapping or peripheral copper sulfide zones. Mo:Cu ratios in such

deposits range from 1:1 to 10:1. (White et al. 1981).

Why do intrusives of similar composition emplaced in similar tectonic environments generate porphyry copper (-molybdenum) deposits in some cases and porphyry molybdenum deposits in others? The answer probably lies in (a) the markedly different behavior of the two elements during magmatic evolution and (b) the different $C_w^{i,0}:C_w^{i,s}$ ratio in the two systems ($C_w^{i,0}$ = the initial water content of the melt; $C_w^{i,s}$ = the water content of the melt at saturation) (Candela & Holland 1986, Candela 1989). Data on the concentration of copper in igneous rock suites suggest that copper behaves as a compatible element during magmatic crystallization prior to water saturation, but as an incompatible element after vapor saturation; molybdenum, on the other hand, behaves as an incompatible element throughout. Generally, a low $C_w^{i,0}:C_w^{i,s}$ ratio indicates a large amount of crystallization before water saturation and results in a high Mo:Cu ratio in the magmatic aqueous phase. Conversely, a high $C_w^{i,0}:C_w^{i,s}$ ratio indicates a small amount of crystallization before water saturation and allows copper enrichment in the magmatic aqueous phase by inducing the early evolution of vapor in the magmatic system. The initial water content of a magma is a source region-dependent parameter and, therefore, is likely to be similar for quartz monzonite-type porphyry copper and porphyry molybdenum deposits. Thus, it is the water content at saturation that controls the Mo:Cu ratio of the magmatic aqueous fluids. According to this model, then, early vapor evolution (low $C_w^{i,s}$), which allows the vapor to compete effectively with the crystallizing phases for copper, is essential for efficient extraction of copper from the porphyry intrusion. A late evolution of the vapor phase (high $C_w^{i,s}$), on the other hand, is conducive to the formation of molybdenum deposits as much of the copper would be lost to the crystallized material under this scenario. As the solubility of water in silicate melts is much less sensitive to temperature than pressure (see Fig. 2.3), the parameter $C_w^{i,s}$ can be correlated with the depth at which the magma exsolves an aqueous phase given a particular geobaric gradient. So, the formation of porphyry copper deposits should be favored by vapor evolution at a shallow depth and of porphyry molybdenum deposits at a deeper level.

8.3.4. CLIMAX-TYPE DEPOSITS

Typical examples of this deposit type are Climax (Wallace et al. 1968, White et al. 1981), Urad-Henderson (Wallace et al. 1978, Sedorff 1988), and Mt. Emmons-Redwell located in the Colorado mineral belt (western USA), which is defined by a northeast-southwest trend of Laramide-Tertiary intrusions (Fig. 8.19). These deposits are associated with Oligocene-Miocene composite stocks of silicic granite and rhyolite porphyry. The belt also contains late Cretaceous to middle Tertiary intrusions of more intermediate to alkalic composition, which have locally produced lead \pm zinc \pm copper \pm silver \pm gold \pm fluorite \pm subeconomic molybdenum mineralization and are believed to have resulted from subduction-dominated tectonics related to the Laramide orogeny (Dickinson & Snyder 1978). The emplacement of the Climax-type granites, on the

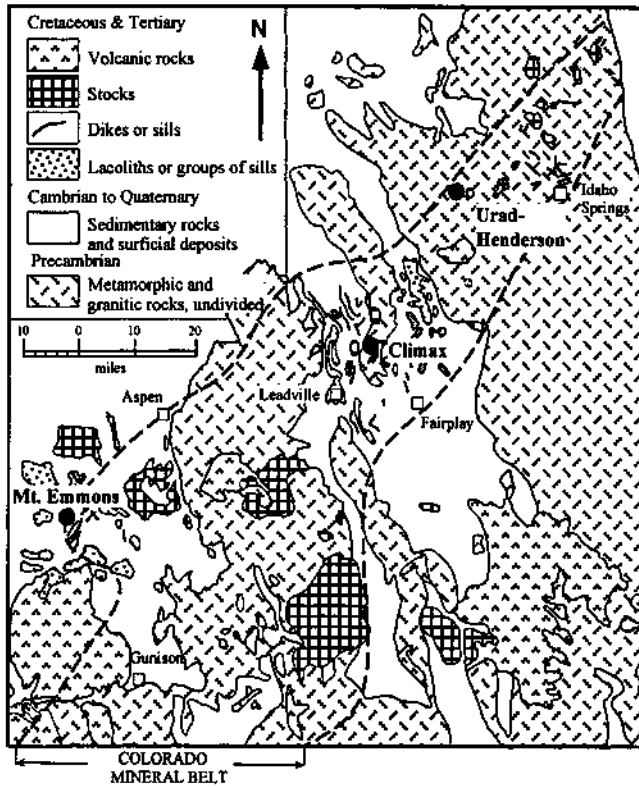


Figure 8.19. Simplified geologic map of a portion of central Colorado (USA) showing locations of the Urad-Henderson, Climax, and Mt. Emmons porphyry molybdenum deposits, all of which lie within the Colorado mineral belt. Silver Creek, another Climax-type deposit within the Colorado mineral belt, lies on the southwestern extension of the belt. (After Wallace et al. 1978.)

other hand, began with the development of the Rio Grande system about 25 to 30 Ma, marking the transition from subduction-dominated tectonics to rift-dominated tectonics (Tweto 1979). A number of other porphyry molybdenum deposits exhibit some features of both Climax and quartz monzonite types, but seem closer to the Climax-type on account of their anomalous fluorine content. Included in this group, termed "sub-Climax-type" by Wallace (1995), are the deposits of Questa (New Mexico), Mount Hope (Nevada), Pine Grove (Utah), and Big Ben (Montana).

Characteristics

Characteristics of typical Climax-type deposits, based on those of the Colorado mineral belt, may be summarized as follows (Mutschler et al. 1981, White et al. 1981, Westra & Keith 1981, Wallace 1995):

- (a) Each Climax-type orebody occurs in a complex intrusive suite that is composed of composite stocks of many separate but compositionally similar intrusions (high-silica, alkali-rich granite and rhyolite porphyries), radial and concentric dikes, and volumetrically subordinate breccia units. Molybdenum mineralization and associated hydrothermal alteration are clearly related to some of these intrusions. The individual porphyry bodies within the composite stocks are generally cylindrical and nearly vertical, and granite porphyries volumetrically dominate these systems. The ore-related stocks are highly differentiated and interpreted as high cupolas of leucogranitic batholiths, but rarely, if ever, have their parent intrusion been recognized. The multiple intrusive-mineralization events have commonly resulted in superimposed patterns of metal and alteration zoning.
- (b) Molybdenite forms a discrete ore shell, generally centered on the apex of a plug-shaped intrusion. Typically, the orebodies are elliptical in plan and arcuate, concave downward in section. Average ore-grades, with a 0.20% cutoff, are 0.35-0.45% MoS₂. Molybdenite gradients tend to be very sharp and the grades rapidly decrease to less than 0.1% MoS₂ toward the margins of a mineralized zone. Several ore shells may be present in a deposit. They may be stacked, each shell associated with a separate phase of magma crystallization (e. g., Climax, Urad-Henderson), or they may occur in close proximity, each related to a separate apophysis (e. g., Mt. Emmons).
- (c) The predominant style of mineralization is in the form of stockwork consisting of thin (<3 mm thick), moderately to steeply dipping, quartz - molybdenite ± fluorite veinlets. Much of the molybdenite is concentrated along veinlet walls, but it also occurs in discontinuous streaks within quartz veins, or as disseminations throughout the vein quartz. Molybdenite disseminations outside the stockwork veinlets are minor. A molybdenite orebody is generally capped by a pyrite-rich zone, locally with topaz, and is underlain by a zone of pervasively silicified rock.
- (d) Other vein types present within the deposit include: early, barren quartz veins; quartz - pyrite veins with local topaz and huebnerite; and late-stage open veins containing varying amounts of fluorite, rhodochrosite, sphalerite, galena, and chalcopyrite. The late-stage veins are best developed in areas peripheral to an orebody.
- (e) The main hydrothermal alteration zones are similar to those described earlier for porphyry copper deposits: potassic zone, distinguished by the total replacement by plagioclase by K-feldspar (but with very little hydrothermal biotite); phyllic (quartz - sericite - pyrite) zone, characterized by the sericitization of K-feldspar and plagioclase; argillic zone, characterized by selective alteration of plagioclase to clay minerals; and propylitic zone, defined by the presence of chlorite, epidote, calcite, clay minerals, and sericite. Five other types of alteration zones — vein silica (40-70% quartz), pervasive silica (>90% quartz), magnetite-topaz, greisen

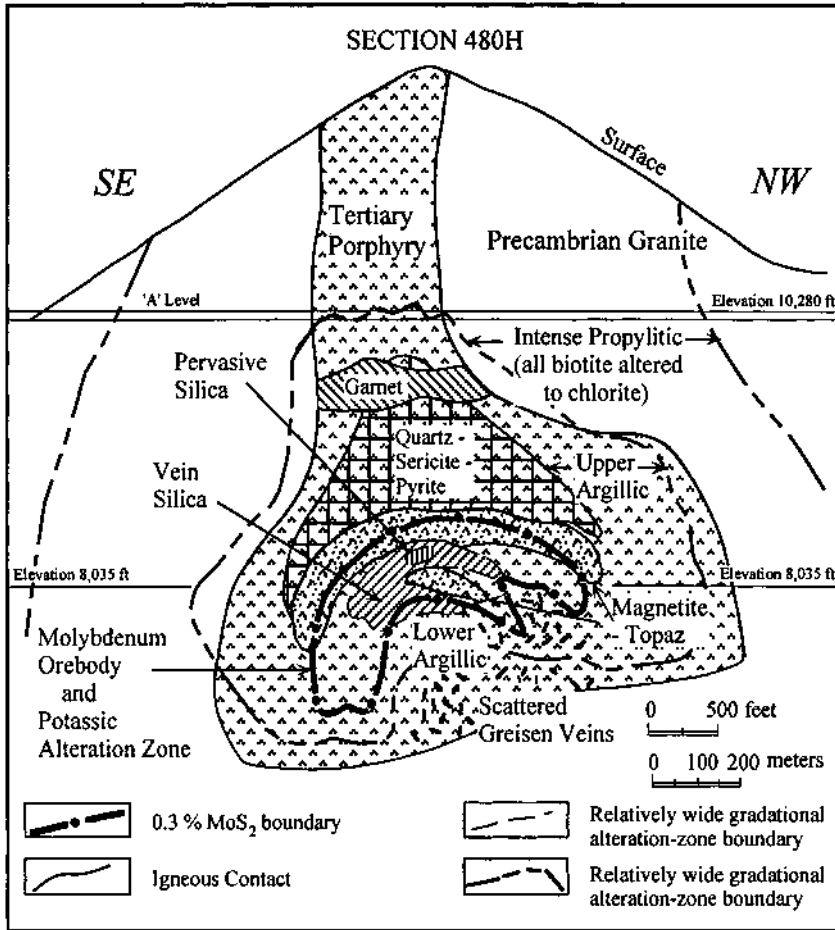


Figure 8.20. A cross section (Section 480H) of the Henderson porphyry molybdenum deposit, Colorado, showing the distribution of hydrothermal alteration zones. (After White et al. 1981.)

(quartz - muscovite - topaz), and garnet — are particularly well developed in the Henderson deposit (Fig. 8.20). These alteration zones are of limited areal extent, but can be recognized by the presence of discrete alteration minerals that are distinct from the major alteration assemblages in which they occur.

- (f) The deposits are underlain by thick Precambrian continental crust.
- (g) The deposits are mid- to late-Tertiary in age and were emplaced in a tectonic environment of incipient crustal extension.

Example: Climax Deposit, Colorado, USA

The Climax deposit, which contains mineable reserves in excess of 760 million tonnes of ore averaging 0.216% Mo (Carten et al. 1993), is the largest known porphyry molybdenum deposit and is also the largest single producer of molybdenum. As described by Wallace et al. (1968) and White et al. (1981), the molybdenum mineralization is spatially and genetically related to the Climax Stock, a composite stock of Oligocene age comprised of successive intrusions of very similar composition (Fig. 8.21). The major intrusive bodies (or phases) of the stock, each with its own suite of hydrothermal products, are (from oldest to youngest): (a) the Southwest Mass, a biotite-poor, fine-grained granite to aplite porphyry; (b) the Central Mass, a coarse-grained, biotite-poor, commonly foliated granite porphyry; (c) the Lower Intrusive Series, which includes biotite-bearing, fine-grained granite to aplite porphyry and intermineral porphyry dikes; and (d) the Postore Intrusive Series, composed of Late Rhyolite Porphyry and Seriate Granite (so named because of the serial range in grain size of more than one order of magnitude).

The Climax deposit consists of three distinct but overlapping orebodies, each related spatially, temporally, and genetically to one of the first three phases of the composite stock. The Southwest Mass was the source of the Cresco orebody, the Central Mass of the Upper orebody, and the Lower Intrusive Series of the Lower orebody. The Cresco orebody is the uppermost of the three and has been largely removed by erosion. The Upper orebody is the largest, contains the highest grade ore, exhibits the most intense hydrothermal alteration, and has produced almost all of the mined ore. The Postore Intrusive Series contains only minor amounts of molybdenite.

Quartz - molybdenite veinlets, formed by open-space filling and replacement, represent by far the most common style of mineralization and account for 95-97% of all the molybdenum in the Upper orebody. Other minerals found in variable amounts within these veinlets include orthoclase, sericite, pyrite, and topaz. Pyrite and topaz are generally concentrated near intersections of quartz - molybdenite veinlets with quartz - sericite - topaz - pyrite veinlets. Tungsten mineralization forms a well defined zone, about 1,200 m in diameter and 90-150 m in thickness, on the hanging-wall of the Upper orebody. The tungsten zone associated with the Lower orebody is about 200 m thick on the average, and it extends well down into the orebody and even into the footwall at several points. Much of the byproduct tungsten recovery has come from this zone. Tin is present in trace amounts in the Climax ore and is also recovered as a byproduct, but very little is known about its distribution.

Origin

Porphyry molybdenum deposits, like porphyry copper deposits, are formed from metal-enriched hydrothermal fluids released from porphyry magmas at some stage in the course of their crystallization. Fluid inclusion homogenization temperatures from Henderson, Questa, Hudson Bay Mountain, and Endako deposits (Kamilli 1978, Bloom 1981, White et al. 1981, Cline & Bodnar 1994) range from about 200° to

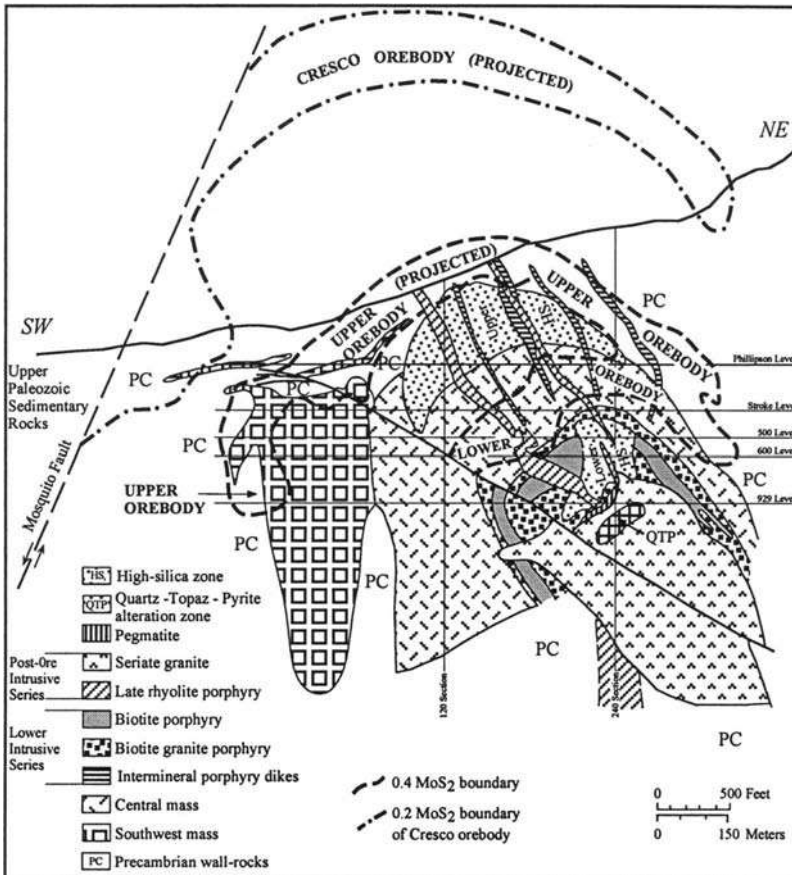


Figure 8.21. Cross section (Section 16) of the Climax porphyry molybdenum deposit, Colorado, showing generalized geology and ore zones (after White et al. 1981).

>600°C and salinities from <5 to >60 wt% NaCl equivalent. Fluids corresponding to molybdenite mineralization fall in much smaller ranges, 300°-400°C and >30 wt% NaCl equivalent, although trapping temperatures (corrected for pressure) may be higher by about 100°C (White et al 1981). In the absence of evidence for boiling, the high-salinity fluids appear to have been generated directly by the crystallizing magma (Bloom 1981, Cline & Bodnar 1994). Oxygen and hydrogen isotope data on hydrothermal minerals (Hall et al. 1974, Stein & Hannah 1985) also support the dominance of magmatic fluids during potassic alteration that was broadly coincident with molybdenum mineralization; the very low δD values (about -120 to -140‰) recorded from the Climax deposit (see Fig. 8.13) probably reflect the effect of a late-

stage introduction of meteoric water. Whole-rock δD values from the Mount Emmons deposit (-127 to -146‰) also indicate post-mineralization alteration by meteoric water at very low (<0.1) water:rock ratios (Taylor et al. 1984).

Molybdenum in porphyry magmas is probably derived from both upper mantle and lower crustal sources, but the immediate source of molybdenum and sulfur in Climax-type deposits are believed to be the cogenetic stocks. Stein and Hannah (1985) have shown that lead isotope ratios in the Henderson and Mount Emmons complexes form tight clusters, without any indication of lead contribution from country rocks, suggesting an upward and outward movement of magmatic material from the stock. Furthermore, the narrow range of $\delta^{34}S$ values for molybdenites from Climax (+2.5 to +3.6‰), Henderson (+4.7 to +5.3‰), and Mount Emmons-Redwell (+3.7 to +4.6‰) deposits, despite highly variable host rock types and molybdenite occurrences (e.g., vein versus disseminated), also indicate an essentially magmatic origin of the sulfur (Stein & Huebner 1984, Stein & Hannah 1985). Assuming equilibrium isotopic fractionation, oxidizing conditions, and an initial $\delta^{34}S_{ES}$ value of 0‰ in the melt, the maximum possible heavy sulfur isotope enrichment in the ore fluid at magmatic-hydrothermal temperatures is only +2 to +3‰ (Ohmoto & Rye 1979). Thus, the positive $\delta^{34}S$ values indicate the addition of isotopically heavy sulfur, most likely at or near the site of magma generation (Stein 1988).

The relatively high Mo-grade of Climax-type deposits may be attributed partly to the high molybdenum solubility in alkalic silica-rich rhyolite magmas and partly to the incompatible behavior of molybdenum that permits its strong enrichment in the differentiates as well as in the aqueous phase exsolved from such magmas. Experimental studies by Isuk and Carman (1981) have shown that molybdenite solubilities in hydrous potassium and sodium disilicate melts are very high, up to 12.5 wt% MoS_2 in vapor-saturated K-disilicate liquids and 10 wt% MoS_2 in vapor-saturated Na-disilicate liquids at 650°C and 680 bars. Mo-silicate and/or Mo-hydroxylated silicate complexes, such as $MoSi_2O_5^{2+}$, $MoSi_2O_6^0$, and $MoSi_2O_4(OH)^{3+}$, are probably the most important species for the observed molybdenum solubility. Apparently, these complexes are destabilized by HCl, which may account for the very low molybdenite solubility in magmas with high chloride concentration. According to Carten et al. (1988), primitive leucogranitic magmas for Urad-Henderson system contained 2-5 ppm Mo, progressively differentiated magmas 5-10 ppm Mo, and the apical portion of the ore-related Sreiate stock of the Urad porphyry as high as 1,300 ppm Mo. The aqueous fluid-melt partition coefficient of molybdenum is not that high — Candela and Holland (1984) obtained a value of about 2.5 under the conditions of their experiments — but the efficiency of molybdenum removal into the aqueous fluid phase is (Candela & Holland 1986). This is because solidus mineral assemblages formed from Climax-type magmas contain few sites in which molybdenum is apt to be accommodated.

Unlike copper, which is concentrated as chloride or other halide complexes in a chloride-rich brine, molybdenum is probably concentrated as molybdic acid (H_2MoO_4) in the H_2O -rich "steam phase" (Burnham 1981). Precipitation of molybdenite

presumably occurs in response to one or, more likely, a combination, of the following: (a) a decrease in $f_{\text{H}_2\text{O}}$ as hydrothermal fluids escape into the fracture system from the H_2O -saturated carapace; (b) a decrease in temperature; or (c) a relative increase in $f_{\text{H}_2\text{S}}$ fugacity that accompanies hydrolysis of SO_2 with decreasing temperature. The first two factors are also primarily responsible for precipitation of silica, which explains the close association of molybdenum mineralization with silica rather than with maximum sulfide deposition.

As high fluorine concentration (as fluorite and topaz) is a characteristic feature of Climax-type deposits, it is reasonable to suspect that fluorine may be involved in the formation of these deposits, but its role is not clear. Candela and Holland (1984) have shown that the aqueous fluid-melt partition coefficient of molybdenum is independent of the fluorine concentration in the melt up to 1.7 wt% fluorine. Moreover, quartz monzonite-type porphyry molybdenum deposits contain no more fluorine than do porphyry copper systems. Magmas generated by the partial melting of a source region with a high F: H_2O ratio would be relatively impoverished in water and, therefore, attain water saturation (and vapor evolution) only after a protracted history of crystallization, a scenario that should favor the formation of Climax-type deposits because of the incompatible behavior of molybdenum (Candela 1989). If fluorine was introduced into the magma chamber from an external source (Carten et al. 1993), however, its high concentration in Climax-type of deposits might simply be an artifact of their continental rift setting. This aspect is elaborated in the next section.

Source of Magmas and Ore Constituents

Westra and Keith (1981) suggested a subduction-related mantle source for Climax-type magmas, but a lower crustal source seems to be most compatible with the geologic setting of these deposits as well as with the strontium and lead isotope ratios of the host intrusives. Various rock types in the Colorado Rocky Mountain region, ranging in age from more than 1.7 Ga to less than 17 Ma, contain anomalous concentrations of Mo, W, and F (White et al. 1981, Bookstrom 1981). This suggests a relatively stationary long-term source for these elements, most likely the continental lithosphere beneath the region. Subducted slabs or convecting asthenosphere, by contrast, would not have remained stationary through the episodes of plate tectonic movements in the region over the last 1.7 billion years. Initial $^{87}\text{Sr}/^{86}\text{Sr}$ ratios of Climax-type granites, calculated from Rb-Sr isotopic data on plagioclase separates, are all greater than 0.710 (close to 0.7105 for Climax and Mount Emmons, and 0.730-0.740 for Urad-Henderson) and have been interpreted as being indicative of a Precambrian lower crustal source for the magmas (Stein 1988, Bookstrom et al. 1988). A lower crustal source, possibly a biotite-bearing felsic granulite, is also in accord with the lead isotope ratios of the Climax-type intrusives (Stein & Hannah 1985, Stein 1988). Potassium feldspars from the Climax, Urad-Henderson, and Mount Emmons-Redwell deposits have average $^{206}\text{Pb}/^{204}\text{Pb}$: $^{208}\text{Pb}/^{204}\text{Pb}$ ratios of 17.62:38.22, 17.70:39.60, and 17.30:38.00, respectively, and the average $^{206}\text{Pb}/^{204}\text{Pb}$: $^{208}\text{Pb}/^{204}\text{Pb}$ ratio for galena samples from Henderson is 17.70:39.49. The very low radiogenic $^{206}\text{Pb}/^{204}\text{Pb}$ and

average to high $^{208}\text{Pb}/^{204}\text{Pb}$ ratios of the Climax-type granites are consistent with "lower crustal sources which were particularly depleted in uranium relative to lead (low U/Pb or μ), but which maintained fairly average Th/Pb ratios throughout their history."

An entirely crustal source of magmas, however, does not account for the high concentrations of trace elements such as U, Zn, Pb, Mn, Ti, Sc, Mo, Sn, W, Nb, Ta, Zr, Y, Ce, and La in Climax-type systems. Carten et al. (1993) have proposed that an influx of alkalic mafic magma from a deeper level into the lower crustal magma chamber was responsible for the enrichment of Climax-type magmas in these elements as well as in Na, K, F, Cl, S, and Mo. The generation of alkalic mafic magma is commonly associated with continental rifts, the inferred tectonic environment of Climax-type deposits, and the common presence of cogenetic alkali-rich mafic rocks (such as biotite-plagioclase lamprophyre, trachybasalt or trachyandesite) in Climax-type systems provide evidence for the mixing of mafic and felsic magmas. Perhaps, it was the underplating by mafic magmas that provided the heat for the generation of parental leucogranitic magmas by small degrees of partial melting of lower crustal metasedimentary rocks (Bookstrom et al. 1988). Carten et al. (1993) have argued that a critical factor in the formation of Climax-type deposits was the upward percolation of a volatile-rich alkalic mafic magma from the asthenosphere and the transport of the volatiles from the base of the magma chamber to the cupola. The accumulation of mineralizing fluids at the top of the magma column is consistent with the localization of mineralization and high-temperature alteration near the top of the cogenetic intrusion in Climax-type systems. A likely mechanism of upward volatile transport was the convection of the magma itself within a sub-deposit conduit under appropriate rates of magma flux, the process involving separation of vapor bubbles near the top of the magma column and downward descent of degassed magma (Shinohara et al. 1995).

8.4. Porphyry Tin Deposits

The Bolivian tin province of the central Andes, which extends for about 900 km from southern Peru through Bolivia to northwest Argentina (Fig. 8.22), is one of the world's most productive tin belts. The belt is divisible into three subprovinces (Grant et al. 1977): a northern tin-tungsten subprovince (Cordillera Real) associated with a series of small batholiths of Triassic to early Jurassic age; a central tin \pm silver subprovince associated with lower Miocene high-level stocks, which includes almost all the major tin producers in Bolivia; and a southern tin - silver - base metal subprovince, extending southward from Potosi, associated with upper Miocene high-level stocks. The Llallagua deposit of the central subprovince is considered to be the largest hard-rock tin deposit in the world; it has produced more than 0.5 million tonnes of tin metal since production started at the beginning of the 20th century. The intrusion-related tin deposits are linked in some way to the subduction process, and the different metal ratios displayed by these subprovinces may be related to the depth of

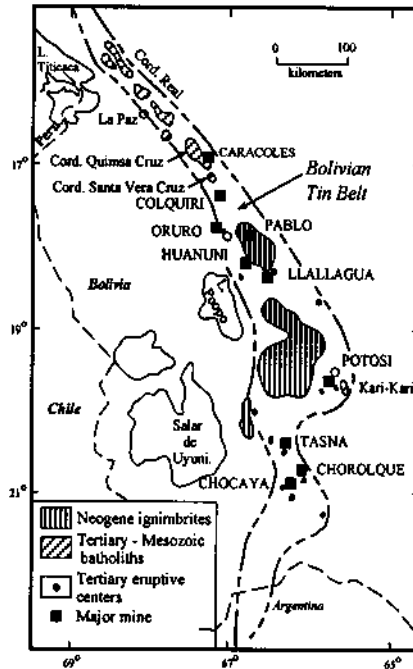


Figure 8.22. Locations of major tin and tin-silver deposits of the Bolivian tin belt, central Andes (compiled from Turneaure 1971, Sillitoe et al. 1975, and Grant et al. 1977).

erosion rather than a change in chemistry of the parent magma with time.

Tin (cassiterite) and silver from the central and southern subprovinces has been produced largely from late-stage through-going veins (lodes) within or peripheral to the high-level stocks. The deposits also contain lower-grade mineralization in the form of disseminations, stockwork veinlets, and breccia-fillings, very similar to the style of mineralization in porphyry copper deposits. Although through-going metal-rich veins are present only in a few porphyry deposits (e.g., Butte and Endako), Sillitoe et al. (1975) designated the Bolivian tin-silver deposits as *porphyry tin* deposits, because they possess many features considered to be diagnostic of porphyry deposits, as exemplified by the porphyry coppers. The most important of these features are: (a) small (1-2 km²), substratovolcanic, calc-alkaline porphyry stocks of intermediate composition (quartz latite porphyry) as cogenetic intrusions; (b) widespread occurrence of hydrothermal intrusion breccias, many of which are cassiterite-cemented and thus intermineral in character; (c) pervasive hydrothermal alteration which is unrelated to the major tungsten-silver veins and commonly zoned, the zoning pattern being centered on the host stocks; (d) the association of dispersed cassiterite mineralization with pervasive sericitic alteration (quartz - sericite - pyrite); (e) occurrences of lead-

zinc-, silver-, and barium-bearing veins peripheral to the stockwork and disseminated mineralization; and (f) fluid inclusion data indicating hydrothermal fluids ranging from high-salinity Na-Ca-Cl brines of a dominantly magmatic source during the early stage of pervasive quartz-tourmaline alteration (barren) in the stock to progressively more dilute fluids, most likely due to the influx of meteoric water, during the later stages of pervasive sericitic alteration with vein-type cassiterite and sulfide mineralization (Fig. 8.23). A reconstruction of an ideal Bolivian porphyry tin system is shown in Figure 8.24. The evolution of porphyry tin deposits, as conceptualized by Grant et al. (1980), is remarkably similar to that depicted in Figure 8.15 for porphyry copper deposits.

There are, however, some noticeable differences between porphyry copper and the Bolivian porphyry tin deposits (Sillitoe et al. 1975). Potassium silicate alteration has not been identified in the Bolivian tin deposits, although it may be present in the deeper parts of the deposits which have not yet been penetrated. The host stocks commonly have the form of inverted cones. The upward flaring of the stocks during intrusion was probably due to an abrupt reduction in confining pressure in the vicinity of the contact between Paleozoic basement and the overlying volcanic piles. In contrast, the majority of porphyry copper stocks have a dominantly cylindrical form and appear to have been emplaced below the contact of the basement and the overlying volcanic sequence (Sillitoe 1973). The Bolivian deposits lack supergene enrichment, but this is to be expected as cassiterite remains essentially insoluble in the zone of oxidation, which is also the reason why, unlike copper, tin may be concentrated in placers.

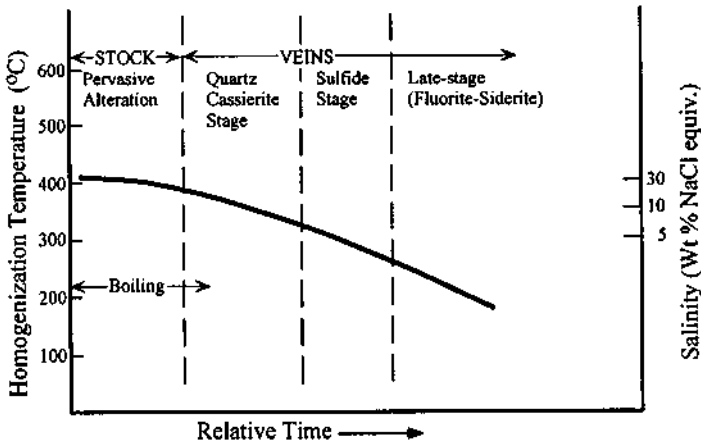


Figure 8.23. Summary diagram of fluid inclusion data for the Llallagua hydrothermal system, Bolivian tin belt (after Grant et al. 1977).

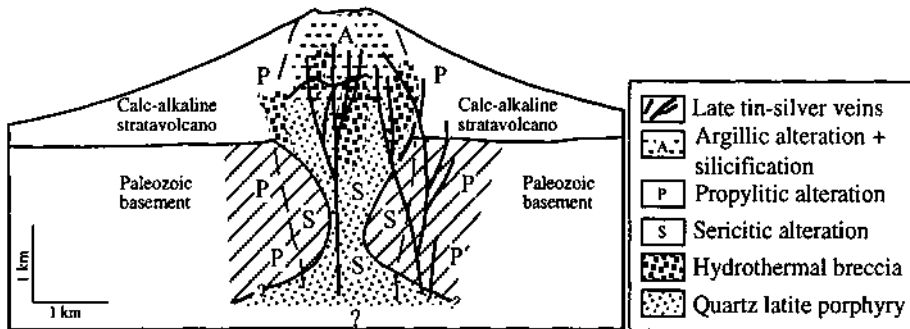


Figure 8.24. Idealized reconstruction of a porphyry tin deposit based on deposits in the Bolivian tin belt (after Sillitoe et al. 1975).

8.5. Summary

Porphyry deposits are large-tonnage, low-grade, largely magmatic hydrothermal deposits spatially associated with and genetically related to felsic stocks (commonly composite) emplaced in epizonal environments, most likely beneath stratavolcanoes. Mineralized porphyry systems may be divided into three broad compositional groups (Burnham 1981): (a) calc-alkaline hornblende-biotite quartz diorites and granodiorites that are typical of island-arc copper-gold porphyries; (b) more alkalic biotite quartz monzonites and granites that are typical of most molybdenum and many continental copper-molybdenum porphyries; and (c) markedly peraluminous, generally biotite-bearing granitoids that are typical of the tin and tungsten porphyries. The most important, in terms of resources and production, are the porphyry copper (mostly chalcopyrite) deposits, many with recoverable molybdenum or gold as a coproduct or byproduct, and porphyry molybdenum (molybdenite) deposits, a few of which contain recoverable tungsten \pm tin. Deposits of the Bolivian tin province are considered here as examples of porphyry tin deposits because of many similarities with porphyry copper deposits, although the tin - silver production in this province has come largely from late-stage, through-going veins rather than from stockwork veinlets.

In addition to cogenetic felsic intrusions, which almost always include one or more porphyritic members, deposits of this class share many other characteristics. These are: extensive, fracture-controlled hydrothermal alteration which, depending on the mineralogy, are designated as potassic (K-feldspar - biotite), phyllic (sericite - quartz - pyrite), argillic (clay minerals), and propylitic (chlorite - epidote); disseminated mineralization dominated by stockwork veinlets; a strong correlation between alteration and mineralization zoning; association with cogenetic breccia bodies; a predominantly magmatic source of metals and sulfur; and a remarkable paucity of Precambrian examples.

The overwhelming majority of porphyry copper deposits are related to Mesozoic-Cenozoic orogenic belts and most of these are located in the circum-Pacific rim. Cogenetic intrusions are intermediate to felsic members of the calc-alkaline magma series (quartz diorite - quartz monzonite - granodiorite); a small number of deposits are associated with diorite - monzonite - syenite intrusions of alkalic affinity. The deposits were emplaced in cratonic continental margin or oceanic island-arc settings, and the two types differ significantly in terms of age, the composition of cogenetic intrusions, Cu:Mo and Cu:Au ratios, and alteration zoning.

Porphyry molybdenum deposits may be subdivided into quartz monzonite-type and Climax-type. The quartz monzonite-type deposits are similar in many respects to continental margin porphyry copper deposits. The Climax-type deposits are associated with highly differentiated, alkalic, silica- and fluorine-rich, multiple intrusions of granitic composition. Much of the molybdenum production comes from the higher-grade Climax-type deposits, the typical examples of which are located in the Colorado mineral belt. The Climax-type deposits are believed to have formed in continental rift environments and to have involved an influx of volatile-rich mafic magma into a lower crustal magma chamber.

The basic process of formation of all porphyry-type deposits involves the following essential steps: (a) generation of parental magma from appropriate source material with adequate concentration of ore constituents and water; (b) saturation of the magma with respect to water at some stage in its crystallization history, determined by the pressure (depth) of crystallization and the initial water content of the melt; (c) exsolution of an aqueous fluid from the magma, which becomes enriched in ore elements preferentially partitioned into the aqueous phase; (d) hydrofracturing of the rocks providing ground preparation for hydrothermal alteration-mineralization; and (e) precipitation of hydrothermal minerals from magmatic fluids, with or without the involvement of meteoric water, resulting in alteration and mineralization. The differences between porphyry copper and porphyry molybdenum deposits, and among the subclasses of these, are attributable mainly to differences in the source regions of magma generation, which control the initial concentrations of ore constituents and water in the magma, compatible versus incompatible behavior of the ore elements, depth at which the magma becomes water saturated, and the melt-aqueous fluid partition coefficients of ore elements. These considerations can account for the relatively shallow depth of emplacement of quartz monzonite-type porphyry copper deposits compared with quartz monzonite-type porphyry molybdenum deposits and the special characteristics of Climax-type porphyry molybdenum deposits.

8.6. Recommended Reading

Lowell & Guilbert (1970), Nielsen (1976), McMillan & Panteleyev (1980), Grant et al. (1980), White et al. (1981), Burnham (1981), Beane (1982), Sillitoe (1988), Candela and Holland (1986), Tittley (1993), Carten et al. (1993), Wallace (1995).

CHAPTER 9

SKARN DEPOSITS

9.1. Introduction

Skarn deposits represent a very diverse class in terms of geologic setting and ore metals. They constitute the world's premier sources of tungsten (more than 70% world's tungsten production); major sources of copper; important sources of iron, molybdenum and zinc; and minor sources of cobalt, gold, silver, lead, bismuth, tin, beryllium, rare earth elements, fluorine, and boron (Einaudi et al. 1981, Meinert 1993). The deposits occur in a broad spectrum of geologic environments and range from Precambrian to late Tertiary in age. Most deposits of economic importance are relatively young, however, and are related to magmatic-hydrothermal activity associated with dioritic to granitic plutonism in orogenic belts. Owing to their economic importance and wide geographic distribution (Fig. 9.1), a wealth of literature is available on the descriptive and genetic aspects of skarn deposits, including some excellent review articles (e.g., Burt 1977, Shimazaki 1980, Einaudi et al. 1981, Einaudi 1982a and b, Meinert 1983, 1992, 1993, Kwak 1987, Ray & Webster 1991) and a special issue of *Economic Geology* (v. 77, no. 4, 1982). A continuum exists between the porphyry-type (Ch. 8) and skarn-type ore deposits, and at least some skarn deposits appear to be mineralization in carbonate wallrocks within porphyry systems. Nevertheless, skarn deposits do possess enough special characteristics to be treated as a distinct class.

9.2. Skarns and Skarn Deposits

The term *skarn* was originally used for the relatively coarse-grained, calc-silicate gangue (garnet + pyroxene + epidote) associated with Swedish magnetite and chalcopyrite deposits (Geijer & Magnusson 1952). In modern usage, the term encompasses a wide variety of generally coarse-grained calc-silicate rocks that are rich in calcium, iron, magnesium, aluminum, and manganese, regardless of their association with minerals of potential economic value, and were formed by replacement of originally carbonate-rich rocks by metasomatic processes (Einaudi et al. 1981). Carbonate rocks (limestones and dolostones) are by far the most common protoliths of skarns, although occurrences of skarns in shales (Shimazaki 1982), quartzites (Atkinson & Einaudi 1978), and igneous

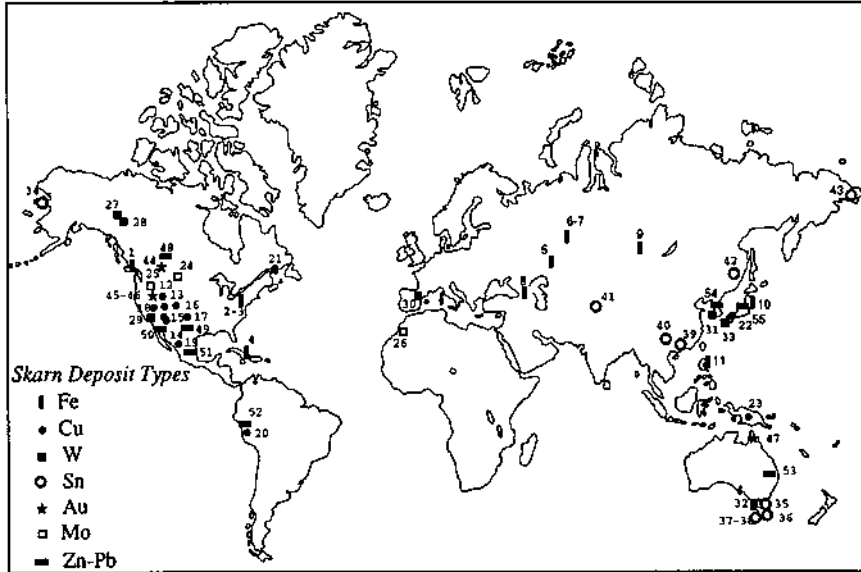


Figure 9.1. World distribution of important skarn districts and deposits. Iron skarns: 1. Empire, BC, Canada; 2. Cornwall, PA, USA; 3. Grace, PA, USA; 4. Daiquiri, Cuba; 5. Sarbai, West Siberia; 6. Peschansk, Urals; 7. Goroblagodat, Urals; 8. Dashkesan, Azerbaidzhan; 9. Teya, Russia; 10. Kamaishi, Japan; 11. Larap, Philippines. Copper skarns: 12. Bingham, Utah, USA; 13. Christmas, AZ, USA; 14. Twin Buttes, AZ, USA; 15. Mission, AZ, USA; 16. Continental, NM, USA; 17. Santa Rita, NM, USA; 18. Ely, Nevada, USA; 19. Cananea, Mexico; 20. Morococha, Peru; 21. Mines Gaspé, Quebec, Canada; 22. Yoshoka, Japan; 23. Ok Tedi (Mt. Fubilan), Papua New Guinea. Molybdenum skarns: 24. Cannivan Gulch, MT, USA; 25. Little Boulder Creek, ID, USA; 26. Azegour, Morocco. Tungsten skarns: 27. MacMillan Pass (MacTung), Yukon-N.W.T., Canada; 28. Canada Tungsten (CanTung), N.W.T., Canada; 29. Pine Creek, CA, USA; 30. Salau, France; 31. Sangdong, South Korea; 32. King Island, Tasmania, Australia; 33. Fujigantani, Japan. Tin skarns: 34. Lost River, Alaska, USA; 35. Mt. Bischoff, Tasmania, Australia; 36. Moina, Tasmania, Australia; 37. Renison Bell, Tasmania, Australia; 38. Cleveland, Tasmania, Australia; 39. Xinlu, China; 40. Dachang, China; 41. Uchkoshkon, Russia; 42. Yaroslavsk, Russia; 43. Itenyurginsk, Russia. Gold skarns: 44. Nickel Plate, BC, Canada; 45. Fortitude, Nevada, USA; 46. McCoy, Nevada, USA; 47. Red Dome, Australia. Zinc-Lead skarns: 48. Bluebell, BC, Canada; 49. Linchburg, NM, USA; 50. Darwin, CA, USA; 51. Providencia, Mexico; 52. Uchucchacau, Peru; 53. Ban Ban, Queensland, Australia; 54. Ulchin, South Korea; 55. Nakatatsu, Japan.

rocks (Einaudi et al. 1981, Harris & Einaudi 1982, Vidal et al. 1990) have also been reported. *Calc-silicate hornfels* is a descriptive term commonly used for the relatively fine-grained calc-silicate rocks that result from isochemical (except for devolatilization, especially of H_2O and CO_2) metamorphic recrystallization of impure carbonate units, such as silty limestone or calcareous shale. The bulk composition and texture of calc-silicate hornfels are controlled primarily by the protolith. Generally, calc-silicate hornfels and skarn can be distinguished on the basis of geologic setting, morphology, grain size, and composition, and by the fact that skarns display abrupt discontinuities in bulk composition across monomineralic or bimineralic zonal boundaries whereas

hornfels do not (Einaudi & Burt 1982). *Skarnoid* is a descriptive term for fine-grained, iron-poor, calc-silicate rocks of uncertain origin; it probably is intermediate between a metamorphic (isochemical) hornfels and a metasomatic (allochemical) skarn.

A diagnostic feature of typical skarns is their mineral assemblages. The 'primary' assemblage varies with the compositions of the skarn-forming fluids and the invaded rocks, but is characterized, in general, by anhydrous Ca-Fe-Mg silicates. Of special importance are pyroxenes (including pyroxenoids) and garnets: wollastonite, salite (members of the diopside-hedenbergite series), and grandite (members of the grossularite-andradite series with varying amounts of spessartine and almandine components). Experimental studies (e.g., Gamble 1982, Burton et al. 1982), however, have shown that the pyroxenes and garnets are not necessarily high-temperature phases as they can be stable also at relative low temperatures (350°-450°C), particularly at low values of total pressure, oxygen and sulfur fugacities, and X_{CO_2} . Hydrous minerals such as tremolite, talc, epidote, and serpentine in skarns are generally attributed to retrograde hydrothermal alteration, although such minerals may also form during the prograde stage of skarn formation. Unusual minerals in skarn assemblages include idocrase (vesuvianite) $[\text{Ca}_{10}(\text{Mg}, \text{Fe}, \text{Mn})_2 \text{Al}_4 \text{Si}_9 \text{O}_{34}(\text{OH}, \text{Cl}, \text{F})_4]$, johannsenite $[\text{CaMnSi}_2\text{O}_6]$, bustamite $[(\text{Mn}, \text{Ca}, \text{Fe})_2 \text{Si}_2\text{O}_6]$, and ilvaite $[\text{CaFe}_3^{2+}\text{Fe}^{3+}\text{OSi}_2\text{O}_7(\text{OH})]$. Skarn assemblages are commonly zoned, the zoning manifested by a sequence of monomineralic or bimineralic layers relative to sedimentary or igneous contacts and fissures or fractures. The generalized zoning pattern is marked by an increase in the pyroxene:garnet ratio away from the igneous contact and the occurrence of idocrase (or a pyroxenoid such as wollastonite, bustamite, or rhodonite) at the contact between skarn and marble. In addition, individual skarn minerals may display systematic color or compositional variations within the larger zonal pattern. For example, garnet is commonly dark red brown in proximal zones, becomes lighter brown in more distal locations, and is pale green near the marble front (Atkinson & Einaudi 1978). Pyroxene does not show such pronounced color change, but typically has a progressive increase in iron and/or manganese content toward the marble front (Harris & Einaudi 1982). The zoning pattern, however, may be quite complex because of superimposed events of mineral deposition during prograde and retrograde stages of skarn formation. Nevertheless, mineralogic zoning is a potential exploration guide for skarn systems, just as alteration zoning is for porphyry systems.

Skarns (metasomatic) are of two general types (Einaudi et al. 1981): (a) *reaction skarns* involving bimetasomatic diffusion of components on a local scale (millimeters to a few meters) in a possibly stagnant, intergranular hydrothermal fluid — for example, between interlayered shale and carbonate units — and controlled by the lithology (chemical reactivity) of the contact rocks which provide the metasomes; and (b) *igneous metasomatic skarns* formed by reaction with the infiltrating magmatic hydrothermal fluids on a larger scale (meters to hundreds of meters) and controlled by the properties of the hydrothermal fluids. It is the latter variety of skarns (also referred to as *infiltration skarns*) that may be accompanied by some kind of ore deposition (*ore*

skarns). Mineral deposits associated with (or related to) skarns are called *skarn deposits*.

Skarns and skarn deposits may be formed by either contact or regional metasomatic processes. Kwak (1987) has discussed many examples of tungsten deposits, including the stratiform and strata-bound deposits in the Broken Hill area, Australia (Barnes 1983), which have mineral assemblages typical of ore skarns formed near contacts with granitic plutons, but are found instead in moderate- to high-grade regional metamorphic terranes. Such "regional" skarns unrelated to igneous plutons are not included in this chapter. The focus here is on the vast majority of the world's important skarn deposits that occur in the contact zones of small- to medium-sized discordant igneous intrusions and are believed to be related largely or entirely to magmatic-hydrothermal fluids released from the intrusions. In older literature, such deposits have been described variously as 'igneous metamorphic', 'contact metamorphic', 'pyrometasomatic', 'hydrothermal metamorphic', or 'tactite'. None of these terms is entirely appropriate, because igneous contacts are not always apparent and because calc-silicate rocks associated with skarns span the entire range from being dominantly metamorphic to dominantly metasomatic. The non-genetic term 'skarn deposits' is preferable (Burt 1977, Rose & Burt 1979, Einaudi et al. 1981) as it emphasizes the most fundamental feature of these deposits, the association with skarn. In modern literature, however, the term skarn deposit is used in a broader sense to include deposits that may lack typical skarn-type gangue but may be inferred from other lines of evidence (such as regional geologic setting, fluid inclusion data, stable isotope ratios, etc.) to be genetically related to skarn-forming processes. This flexibility is reasonable, because in both *proximal* (close to the pluton) and *distal* (away from the pluton) deposits the earlier formed skarn silicates are commonly destroyed to varying degrees by superimposed retrograde alteration, and in some distal deposits skarn minerals may never have formed. Admittedly, whether a particular carbonate-replacement distal deposit belongs to the class of skarn deposits or is a hydrothermal vein deposit unrelated to skarn formation may be difficult to determine in some cases.

The distinctive features of proximal skarn deposits are:

- (a) spatial association with igneous intrusions;
- (b) calc-silicate gangue mineralogy;
- (c) ore formation by replacement of carbonate rocks;
- (d) irregular form of orebodies, controlled by local variations in permeability;
- (e) disseminated and vein-type mineralization, depending on the permeability pattern in the host rocks; and
- (f) alteration and mineralization zoning centered on the intrusion.

9.3. Types of Skarns and Skarn Deposits

Skarns are classified in various ways. A commonly used classification scheme — endoskarns and exoskarns (Perry 1969) — is based on the position of the skarn relative

to the coeval pluton. *Endoskarn* refers to partial replacement of the intrusive body, *exoskarn* to selective replacement of country rocks in the contact zone. The two may not be clearly separable, however, where the wallrocks contain abundant pelitic or volcanic interbeds that may closely approximate an igneous bulk composition. Endoskarns form in those areas where fluid flow is dominantly into the pluton (presumably at depth) or upward along its contacts with carbonates, rather than where metasomatic fluid flow is dominantly up and out of the pluton; the dominant metasomatic process involved is infiltration, not diffusive exchange (Einaudi & Burt 1982). Generally, endoskarn would be absent if skarn development occurred near or over the tops of plutonic cupolas, as in tin skarns and most skarns related to porphyry copper plutons. Where an endoskarn-exoskarn couplet is developed, skarn-ore is usually restricted to the exoskarn, except when limestone is absent in the contact zone.

Exoskarns are further classified as *calcic skarns* or *magnesian skarns* on the basis of the dominant mineral assemblage, which in most cases reflects the composition of the carbonate rock replaced. Calcic skarns are characterized by high Ca:Mg ratios and Ca- or Ca-Fe silicates (e.g., ferrosalite, andraditic garnet, wollastonite, idocrase), magnesian skarns by low Ca:Mg ratios and Mg-silicates (e.g., forsterite, talc, tremolite, serpentine). Generally, calcic skarns are formed by the replacement of non-magnesian limestones and the magnesian skarns by the replacement of dolomitic rocks, but this is not always the case (Einaudi & Burt 1982). The distinction between the two becomes more difficult and less useful where limestone and dolostone units are interbedded. The bulk of the world's economic skarn deposits occurs in calcic exoskarns.

The bulk compositions of skarn deposits bear no simple relation to the protolith as their formation invariably involves large-scale metasomatism by hydrothermal fluids. Skarn deposits are best classified on the basis of the dominant economic metal(s) — iron, copper, molybdenum, gold, tungsten, tin, and zinc-lead (Table 9.1). The main ore minerals of these skarn types are, respectively, magnetite, chalcopyrite ± bornite, molybdenite, electrum, scheelite, cassiterite, and sphalerite - galena. In addition to distinctive metal associations, the skarn deposits exhibit a systematic variation in skarn mineralogy, especially in terms of pyroxene and garnet compositions (Fig. 9.2). For example, Einaudi and Burt (1982) noted an increase in hedenbergite and johannesenite components and a decrease in diopside component of pyroxenes through the sequence $\text{Cu} \Rightarrow \text{Fe} \Rightarrow \text{W} \Rightarrow \text{Zn-Pb}$ skarn deposits, and an increase in grossular and spessartine + almandine components and a decrease in andradite component of garnets through the sequence $\text{Cu} \Rightarrow \text{Fe} \Rightarrow \text{Zn-Pb} \Rightarrow \text{W}$ skarn deposits. Amphiboles from the skarn types vary both in composition (Fe, Mg, Mn, Ca, Al, Na, and K contents) and crystal structure. Amphiboles in gold, tungsten, and tin skarns are progressively more aluminous (actinolite - hastingsite - hornblende); those in copper, molybdenum, and iron skarns are progressively more iron rich in the tremolite-actinolite series; and those in zinc skarns are both Mn-rich and Ca-deficient, ranging from actinolite to dannemorite $[\text{Mn}_2(\text{Fe,Mg})_3\text{Si}_8\text{O}_{22}(\text{OH})_2]$ (Meinert 1983, 1992). Skarn types cannot be uniquely characterized by the composition of one of these three minerals (except perhaps zinc skarns by the presence of Mn-rich pyroxene); a consideration of the compositions of all

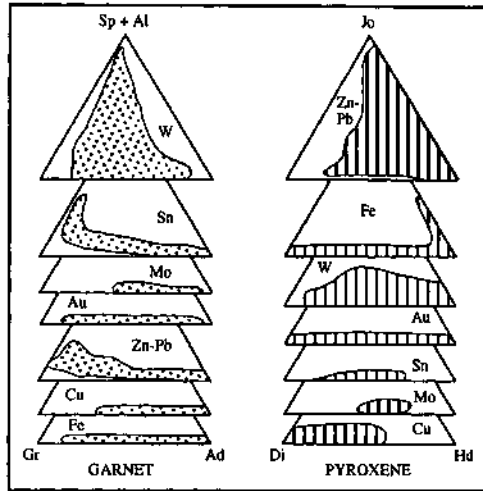


Figure 9.2. Ternary plots of garnet and pyroxene compositions (electron microprobe analyses) from major skarn deposits classified by dominant metal (after compilation by Meinert 1992). End-members are: Ad = andradite $[\text{Ca}_3\text{Fe}_2(\text{SiO}_4)_3]$; Gr = grossularite $[\text{Ca}_3\text{Al}_2(\text{SiO}_4)_3]$; Al = almandine $[\text{Fe}_3\text{Al}_2(\text{SiO}_4)_3]$; Sp = spessartine $[\text{Mn}_3\text{Al}_2(\text{SiO}_4)_3]$; Hd = hedenbergite $[\text{CaFeSi}_2\text{O}_6]$; Di = $[\text{CaFeSi}_2\text{O}_6]$; Jo = johannsenite $[\text{CaMnSi}_2\text{O}_6]$.

the three minerals provides a better constraint for classification.

Important characteristics of the major types of skarn deposits are described below briefly and summarized in Table 9.1.

9.3.1. IRON SKARNS

Magnetite is a common oxide mineral of most skarn deposits. The calcic iron skarns, virtually the only skarn-type found in oceanic island-arc terranes (see Fig. 9.11), are distinguished from other magnetite-rich skarns by the following features (Einaudi et al. 1981): (a) association with epizonal gabbroic to dioritic stocks emplaced in a cogenetic basalt-andesite sequence; (b) Fe-rich calc-silicate gangue consisting of epidote, grandite, and ferrosalite; (c) extensive development of endoskarn (epidote - pyroxene or albite - scapolite), involving sodium metasomatism, in the associated igneous rocks; (d) low sulfide content; (e) a minor metal suite of Cu, Zn, Co, Au, and sometimes Ni; and (f) a lack of W, Sn, and Pb. Zoning of skarn minerals is poorly developed or difficult to recognize because of the wide spectrum of protoliths involved. Magnetite orebodies typically occur close to garnet zones or in limestone beyond the skarn zone. Most deposits are irregular and small (5-20 million tonnes of ore) as in North America and Japan, but some in Russia and Philippines are large (many with >500 million tonnes of ore containing >300 million tonnes of Fe) and tend to be stratiform. Magnesian

TABLE 9.1. General characteristics of major skarn types

Skarn type	Iron (calcic)	Iron (magnesian)	Copper (calcic)
<i>Size</i>			
Largest known (Ore tonnage, grade)	Sarabai, Siberia (725 m.t., 47% Fe)	Sherogesh, USSR (234 m.t., 35% Fe)	Twin Buttes, AZ, USA (500 m.t., 0.8% Cu)
Typical size, grade	5-200 m.t., 40% Fe	5-100 m.t., 40% Fe	1-100 m.t., 1-2% Cu
<i>Metal Association</i>	Fe (Cu, Co, Au)	Fe (Cu, Zn)	Cu (Mo, W, Zn)
<i>Associated Igneous Rocks</i>			
Intrusives	Gabbro to syenite, mostly diorite	Granodiorite to quartz monzonite, rarely granite	Granodiorite to quartz monzonite (-monzonite)
Cogenetic volcanics in ore zone	Common; basalt, andesite	Absent	Rare; andesite, quartz latite
Intrusive morphology	Large to small stocks and dikes	Small stocks, dikes, sills, breccia pipes	Small stocks; dikes
Endoskarn	Extensive endoskarn; Na-silicates	Minor endoskarn; propylitic	Local endoskarn; K-silicate, sericitic
<i>Mineralogy</i>			
Prograde (Early)	Ferrosalite (Hd ₂₀₋₈₀), salite, magnetite, grandite (Ad ₂₀₋₉₅), epidote	Olivine (Fo ₈₅₋₁₀₀), diopside (Hd ₃₋₁₅), spinel	Andradite (Ad ₆₀₋₁₀₀), diopside (Hd ₃₋₅₀), wollastonite
Retrograde (Late)	Amphibole, chlorite, ilvaite	Amphibole, humite, serpentine, phlogopite	Actinolite, chlorite, montmorillonoids
Ore minerals	Magnetite, (chalcopyrite, pyrrhotite, cobaltite)	Magnetite (chalcopyrite, pyrite, sphalerite, pyrrhotite)	Chalcopyrite, pyrite, hematite, magnetite (bornite, molybdenite)
<i>Tectonic setting</i>	Oceanic island arc; rifted continental margins	Continental margin; synorogenic	Continental margin; syn- to late-orogenic
<i>Examples</i> (* discussed in text)	Peschank, Urals Empire, BC, Canada Cornwall, PA, USA Larap, Philippines Daiquiri, Cuba	Teya, Russia Eagle Mtn., CA, USA	Bingham, Utah, USA * Santa Rita, NM, USA Cananea, Mexico Gaspé, Quebec, Canada Ok Tedi, Papua New Guinea

TABLE 9.1 (continued)

Molybdenum (calcic)	Tungsten (calcic)	Tin (calcic)	Zinc-Lead (calcic)
Little Boulder Creek, Idaho, USA (167 m.t., 0.15% MoS ₂)	MacMillan Pass (MacTung), Yukon-NWT, Canada (63 m.t., 0.95% WO ₃)	Moina, Tasmania (30 m.t., 0.15 % Sn, 0.05-0.10% W)	Naica, Mexico (10 m.t., 10% Zn, 13% Pb, 13 oz/ton Ag)
0.1-2 m.t. ?	0.1-2 m.t., 0.7% WO ₃	0.1-3 m.t., 0.1-0.7% Sn	0.2-3 m.t., 9% Zn, 6% Pb, 5 oz/ton Ag
Mo, W (F, Bi, Zn)	W, Mo, Cu (Zn, Bi)	Sn, F (Be, W, B, Li)	Zn, Pb, Ag (Cu, W)
Quartz monzonite to granite	Quartz diorite to quartz monzonite	Granite	Granodiorite to granite, diorite to syenite; plutons commonly absent
Absent	Absent (eroded?)	Absent	Absent
Stocks	Large plutons, batholiths, dikes	Stocks, batholiths	Stocks, dikes (if present)
Quartz veins; K-silicate	Local endoskarn; mica, calcite, pyrite	Greisen	Local but intense endoskarn; epidote-pyroxene-garnet
Hedenbergitic pyroxene, grandite garnet, quartz	Mn-hedenbergite (Hd ₆₀₋₉₀ Jo ₅₋₂₀), grandite (Ad ₁₀₋₅₀), idocrase, wollastonite	Spessartine-rich grandite, Sn-bearing andradite, malayaite, idocrase, danburite, datolite	Mn-hedenbergite (Hd ₃₀₋₉₀ Jo ₁₀₋₄₀), andradite-spessartine garnet, bustamite
Amphibole, chlorite	Spessartine-almadine-grandite garnet, hornblende, biotite	Amphibole, chlorite, tourmaline, fluorite	Mn-actinolite, ilvaite, chlorite, danneborite, rhodochrosite
Molybdenite, scheelite, pyrite, chalcopyrite, bismuthinite	Scheelite, molybdenite, chalcopyrite (sphalerite), pyrite, pyrrhotite, magnetite	Cassiterite (scheelite, sphalerite, pyrrhotite, arsenopyrite, magnetite)	Sphalerite, galena, pyrrhotite, pyrite, magnetite (chalcopyrite, arsenopyrite)
Continental margin: late orogenic	Continental margin; syn- to late-orogenic	Continental; late- to post-orogenic or anorogenic	Continental margin; syn- to late-orogenic
Yongchiachangtze, PRC Azegour, Morocco Mt. Tennyson, Australia	Sangdong, Korea CanTung, NWT, Canada King Island, Tasmania * Fujigantani, Japan	Renison Bell, Tasmania, Australia * Lost River, Alaska, US Dachang, PRC Iteynyurginsk, Russia	Linchburg, NM, USA Darwin, CA, USA Ulchin, Korea Providencia, Mexico * Ban Ban, Australia

m.t. = million tons

Sources of data: Einaudi et al. (1981), Meinert (1983, 1992), Kwak (1987).

iron skarns, in contrast to calcic iron skarns, are associated with silicic and Fe-poor felsic intrusions in continental margins, Cordilleran-type orogenic belts, and dolomitic wallrocks. The magnetite formation in this case is a consequence of the replacement of dolomitic host rocks by Mg-rich skarn silicates (forsterite, diopside, talc, serpentine), which do not take up much iron in solid solution. These skarns lack well developed endoskarn and may contain noticeable amounts of sulfides. Magnesian iron skarns are found in most base metal sulfide skarn districts where dolostone is present and they commonly display transitions to more typical copper skarns.

9.3.2. COPPER SKARNS

The vast majority of skarn-type copper deposits occur in calcic skarns associated with calc-alkaline granodiorite to quartz monzonite stocks emplaced at shallow depths in continental margin orogenic belts (see Fig. 9.11). As a group, calcic copper skarns are characterized by the following features (Einaudi et al. 1981, Meinert 1992): (a) close spatial (proximal) association with felsic, porphyry-textured stocks, many of which have cogenetic volcanic rocks, stockwork veining, and hydrothermal alteration, indicative of a relatively shallow environment of emplacement; (b) relatively oxidized skarn assemblages (andraditic garnet, diopsidic pyroxene, magnetite + hematite); (c) high garnet:pyroxene ratios; and (d) moderate to high sulfide contents. The skarn is commonly zoned, with massive garnetite near the pluton, idocrase and/or wollastonite near the marble contact, and increasing amounts of pyroxene away from the contact. The sulfides and oxides occur as disseminations, massive streaks, and veins in skarn and as massive replacement of marble at the skarn front. The sulfide zoning pattern is from pyrite + chalcopyrite + magnetite near the pluton (with chalcopyrite:pyrite ratio increasing away from the pluton) to chalcopyrite + bornite (with lesser amounts of sphalerite and tennantite, often accompanied by andradite) in idocrase/wollastonite zones near the marble contacts, reflecting an outward decrease in total iron. According to Burt (1977), the change from andradite - chalcopyrite to bornite - wollastonite is caused by a decrease in the Fe:Cu ratio in the iron-rich oxidizing fluids that alter wollastonite to andradite, resulting in the precipitation of bornite rather than chalcopyrite.

The stocks themselves may be barren or may contain porphyry-type copper mineralization. In fact, almost all porphyry copper plutons emplaced in a carbonate-rich supracrustal environment have generated some copper skarn mineralization (Fig. 9.3). The largest cluster of such copper skarn deposits occur in the Laramide porphyry copper province of southwestern USA. The skarn deposits tend to be large (50 to 500 million tonnes of open-pit copper ore with 0.5 to 5 million tonnes of Cu in skarn and calc-silicate hornfels), indicating the involvement of long-lived hydrothermal systems operating in a highly fractured environment. The porphyry stocks exhibit the characteristic evolutionary alteration trend from early potassic to late phyllic (see Ch. 8), which can be correlated, respectively, with prograde garnet - pyroxene and retrograde epidote - actinolite assemblages in the skarn. In some deposits (e.g., Ely, Nevada, USA; James 1976), however, much of the prograde garnet and pyroxene appears to have

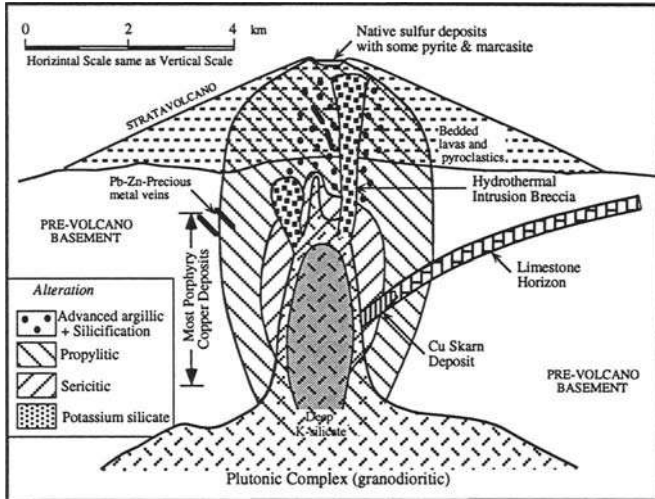


Figure 9.3. Idealized cross section of a typical, simple porphyry copper system showing the position of skarn-type copper deposit. The horizontal and vertical dimensions are meant to be only approximate. (After Sillitoe 1973a.)

been destroyed by intense retrograde alteration. Endoskarn alteration of mineralized stocks is rare. In contrast, barren stocks associated with copper skarns contain abundant epidote - actinolite - chlorite endoskarn and less intense retrograde alteration of the skarn (Meinert 1992). The relatively finer-grained texture of porphyry-associated copper exoskarns arises from rapid deposition at numerous nucleation sites, because a high fracture density in such systems leads to relatively rapid rates of fluid flow. Fluid inclusion microthermometry and mineral equilibria suggest that early skarn formation in porphyry copper systems occurs at temperatures of 500°-350°C, which probably are too low for large-scale scheelite deposition and too high for sphalerite deposition. Some copper skarns, however, contain less oxidized mineral assemblages (e.g., grandite with ferrosalite) and a more complex metal suite (W, Mo, Bi, Zn, Au); these deposits may represent transition either to oxidized tungsten skarns or to Mo-bearing skarns.

All copper skarns are not associated with porphyry copper systems. Copper skarns not related to porphyry systems, generally, are smaller (1-50 million tonnes of ore with an average grade of more than 1% Cu). They are characterized by coarser-grained calc-silicates, lesser vein densities, a lack of quartz-sulfide veinlets or sulfide-filled fractures with actinolite alteration envelopes, and only minor retrograde alteration. These differences from porphyry-related skarns may be attributed to less dynamic magmatic-hydrothermal environments in protoliths of lower fracture density (Einaudi 1982b).

9.3.3. MOLYBDENUM SKARNS

Molybdenum skarns commonly occur in silty carbonate or calcareous clastic rocks, and are typically associated with highly differentiated, silicic intrusives (with only 2-5% mafic minerals), similar in composition to intrusions associated with porphyry molybdenum deposits (Meinert 1983). In contrast to the common association of copper skarns with porphyry copper deposits, molybdenum skarns are not particularly well developed in porphyry molybdenum systems, probably because of relatively smaller amounts of the magmatic fluid phase that separate in porphyry molybdenum systems. Molybdenum skarns range from high-grade ($>1\%$ MoS₂), relatively small (1-7 million tonnes of ore) deposits (e.g., Azegour, Morocco) to low-grade (0.1-0.2% MoS₂), large (≈ 100 million tonnes of ore) deposits amenable to bulk mining methods (e.g., Little Boulder Creek, Idaho). Most molybdenum-bearing skarns contain a variety of metals and the recovery of several metals may be crucial to the economic viability of many of these deposits. Mo (molybdenite) - W (scheelite) - Cu (chalcopyrite) - Bi (bismuthinite) is the most common association; Pb (galena), Zn (sphalerite), Sn, or U may be important locally. Hedenbergitic pyroxene, grandite garnet, wollastonite, amphibole, and fluorite are the main skarn minerals.

9.3.4. GOLD SKARNS

Most skarns, especially copper skarns, contain detectable gold ranging from trace amounts to more than 100 g/t. Gold-bearing skarn deposits, defined as skarns containing an average grade of at least 1 g/t Au (Theodore et al. 1991), comprise two subtypes: gold skarns, which can be mined primarily for their gold content; and byproduct gold skarns, from which gold can be recovered only as a byproduct. According to the compilation of Theodore et al. (1991), median grades and tonnage for 40 gold-skarn deposits are 8.6 g/t Au, 5.0 g/t Ag, and 213,000 tonnes; median grades and tonnage for 50 byproduct gold-skarn deposits are 3.7 g/t Au, 37 g/t Ag, and 330,000 tonnes. The skarns may contain economic concentrations of other metals, such as Cu, Fe, Pb, Zn, As, Bi, W, Sb, and Co. Important examples of gold-skarn deposits include: Nickel Plate (Hedley district), British Columbia, Canada (Ettlinger et al. 1992); Fortitude (Battle Mountain) and McCoy, Nevada, USA (Myers & Meinert 1991, Brooks et al. 1991); and Red Dome, Australia (Ewers & Sun 1988). The Bingham district copper skarn (discussed later) is an example of byproduct gold skarn.

Most gold-bearing skarns are calcic exoskarns. The vast majority of the deposits are found in Paleozoic and Cenozoic orogenic belts and island-arc settings, associated with I-type felsic and intermediate intrusions (which may or may not be porphyritic). In a number of mining districts containing gold skarn deposits (e.g., Battle Mountain, Nevada), ore deposits are zoned from a core area of Cu \pm Au+Ag mineralization (not necessarily of porphyry-type), to an intermediate zone of gold skarn or other types of gold mineralization, to an outermost area of dominantly Zn+Pb+Ag \pm Au mineralization. Andradite-grossularite garnet is the characteristic prograde skarn mineral

(the skarn rock is commonly a massive garnetite), and the skarn pyroxene is typically a low-Mn, diopside-hedenbergite solid solution (Fig. 9.2). Typical ore minerals include native gold, electrum, sulfides and sulfosalts (chalcopyrite, pyrite, pyrrotite, arsenopyrite, sphalerite, galena, bismuthinite, molybdenite, etc.), and hematite (or magnetite). Gold mineralization is associated with intensive retrograde hydrothermal alteration. As is the case with gold-rich porphyry copper deposits, gold-bearing skarns appear to be correlated with high fO_2 in the hydrothermal system (Shimazaki 1980).

9.3.5. TUNGSTEN SKARNS

Tungsten skarns occur in every continent (except Antarctica), but are particularly concentrated in the western Cordillera of North America (Newberry & Swanson 1986). The bulk of world's tungsten production and reserves from skarns is accounted for by a small number of deposits, each of which contains greater than 10 million tonnes of ore. The mineable grade ranges from $\approx 0.35\%$ to $\geq 1\%$ WO_3 , depending on accessibility, mining method, scheelite grain size, and byproduct recovery. Scheelite [$Ca(W,Mo)O_4$] is by far the most important tungsten mineral in skarns, comprising at least 95% of all skarn tungsten minerals present. Powellite [$CaMoO_4$] has not been reported from skarns, but scheelite can contain up to about 40 mole% powellite component in solid solution. Wolframite [$(Fe,Mn)WO_4$] is the dominant tungsten mineral in veins and greisens, but it is rare in skarns, perhaps because of high Ca^{2+} activities in skarn systems. Cu and Mo are the common associated metals; significant concentrations of Au, Ag, Sn, Pb, Zn, Co, or Ni are rare. Tungsten skarn deposits tend to be stratiform; in some cases (e.g., Shangdong, South Korea; Pine Creek, California, USA), the skarn is continuous for hundreds of meters along lithologic contacts, but < 15 m thick.

Tungsten skarn deposits are associated with porphyritic calc-alkaline intrusions, similar in composition and tectonic setting to those associated with large copper skarns, but emplaced at greater crustal depths. The latter is suggested by a lack of indicators (such as breccia pipes and abundant fractures) for forceful emplacement of magma and rapid release of aqueous fluids, the essentially unaltered nature of the intrusions, and the presence of large, high-temperature metamorphic aureoles containing abundant calc-silicate hornfels and skarnoid formed from mixed carbonate-pelite sequences. Tungsten skarns commonly occur in argillaceous carbonate rocks and intercalated carbonate-pelite or carbonate-volcanic sequences. The presence of dolostone in the country rocks has an adverse effect on tungsten grade because of the importance of Ca^{2+} activity in the precipitation of scheelite. Although all rock types in a typical tungsten skarn are affected by metasomatism, ore-grade concentrations of scheelite are generally restricted to metasomatized marble. Skarns related to impure and calc-silicate marbles tend to be coarse-grained, vuggy, and of uneven tungsten grades; skarns related to pure marble, on the other hand, tend to be medium-grained, compact, and of more uniform tungsten grades (Newberry & Einaudi 1981). The very high-grade ores are invariably associated with retrograde assemblages that contain abundant sphene and apatite; perhaps the calcium released by the breakdown of pyroxenes and garnets

facilitates the precipitation of scheelite from hydrothermal fluids.

Two subtypes of calcic tungsten skarns have been recognized on the basis of mineralogy (Newberry & Einaudi 1981): (a) "reduced" skarns, such as the CanTung and MacTung deposits (Canada), formed in carbonaceous host rocks or at great depths; and (b) "oxidized" skarns, such as the King Island deposit (Tasmania), formed in noncarbonaceous or hematitic host rocks, or at lesser depths. Reduced skarns are characterized by abundant Fe^{2+} -bearing assemblages (hedenbergitic pyroxene, almandine-rich garnet, biotite, hornblende), Mo-rich scheelite, and pyrrhotite, and oxidized skarns by Fe^{3+} -bearing assemblages (andraditic garnet, epidote), Mo-poor scheelite, and pyrite.

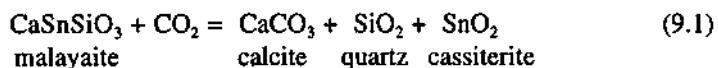
9.3.6. TIN SKARNS

In general, tin skarn deposits are of minor economic interest because of their small size and low grade. The Moina deposit (Tasmania, Australia), with about 30 million tonnes of ore, is probably the largest, but most are much smaller. The average grades range from 0.1 to 0.7 wt% Sn, but much of the tin occurs in silicates and cannot be recovered economically. Cassiterite [SnO_2] is the dominant tin mineral in most tin skarns. Stannite [$\text{Cu}_2\text{FeSnS}_4$], usually with some kesterite [$\text{Cu}_2\text{ZnSnS}_4$] component in solid solution, is also a common constituent of tin skarns, especially in zones of extensive retrograde hydrothermal alteration.

Tin skarns are almost exclusively associated with high-silica, highly differentiated, ilmenite-series granitoids (Ishihara 1977). Several stable isotope studies (e.g., Bowman et al. 1985, Layne et al. 1991, Fu et al. 1991) point to the predominant role played by magmatic hydrothermal fluids in the development of skarn assemblages and mineralization in tin skarns. Chi et al. (1993) have proposed that in the Xinlu tin polymetallic ore field of southern China, proximal deposits are related to high-level intrusions and distal deposits to intrusions emplaced at deeper levels.

In addition to their relatively reduced nature (as evidenced by a lack of magnetite and the presence of ilmenite and Fe^{2+} -rich biotite), 'tin granites' are enriched in a characteristic suite of trace elements (F, Rb, Li, Sn, Be, W, and Mo). This suite also distinguishes tin skarns from all other skarn types. Another distinctive feature of many tin skarns is a greisen alteration stage that is superimposed on the intrusion, early skarn, and unaltered carbonate, and may result in the complete destruction of earlier alteration assemblages (Kwak 1987). Greisen alteration is characterized by high fluorine activity and is recognized by the presence of fluorite, topaz, tourmaline, muscovite, grunerite, and ilmenite, in addition to abundant quartz. Tin skarns may be sulfide-rich or oxide-rich, reduced or oxidized, proximal or distal, and calcic or magnesian (Kwak 1987), and these categories are not mutually exclusive. Magnesian tin skarns generally are lower in sulfur and higher in boron, and they often show an overprinting of calcic skarn at lower temperatures. In both calcic and magnesian tin skarns, cassiterite deposition occurs only when the system evolves to relatively low temperature and acidic condition. Thus, the amount of cassiterite deposited is directly related to the degree of retrograde or greisen alteration of early tin-bearing skarn

minerals. For example, the early stages in calcic tin skarn growth commonly involve the development of Sn-bearing andradite, wollastonite, and malayaite [CaSnSiO_3] or idocrase - magnetite - fluorite, hedenbergitic pyroxene, and spessartine-bearing grandite. Tin resides as a solid solution component of other minerals (up to about 0.6% SnO_2 in garnet and idocrase; Dobson 1982), and very little cassiterite is deposited in the early stages. Subsequently, tin is released by alteration of the tin-bearing silicates (e.g., andradite and malayaite) to form cassiterite, by reactions such as (Burt 1978)



This stage is accompanied by the introduction of low-sulfur sulfides, such as pyrrhotite and arsenopyrite, and less commonly of sphalerite, bornite, and löellingite. In zones characterized by idocrase - garnet - magnetite, the late stages are characterized by fluorite, amphibole, phlogopite, and magnetite in veins and fractures, commonly accompanied by cassiterite and minor pyrrhotite and sphalerite. The most promising deposits occur in distal portions of large, zoned skarn districts (e.g., Renison Bell area, Tasmania), where tin-bearing calc-silicate minerals, such as garnet, are extensively replaced by sulfides and oxides. Close to the intrusive contact, only minor amounts of cassiterite are disseminated in a sulfide-poor garnet - pyroxene gangue (Kwak 1987).

9.3.7. ZINC-LEAD SKARNS

Zinc-lead skarn deposits occur throughout the world in a variety of geologic settings, typically as replacement bodies in limestones at some distance from intrusive contacts (distal deposits), although proximal deposits are known (e.g., Darwin, California, USA; Rye & Ohmoto 1974). Typical grades of ores mined using underground methods are 6-12% Zn, lesser Pb (10-20% Zn+Pb), negligible Cu, and 30-300 g/t Ag. In deposits mined for silver alone, most of the ore comes from replacement deposits in limestone beyond the skarn. Related intrusives include batholiths, stocks, and dikes that range in composition from dioritic to granitic. For some deposits of this group, a magmatic connection is not obvious, because igneous plutons occur at distances of several kilometers (e.g., Linchburg, New Mexico, USA) or no igneous rocks are exposed in the vicinity (e.g., Aravaipa, Arizona, USA).

The distinctive features of this skarn type include (Burt 1977, Einaudi et al. 1981): (a) occurrence along structural or lithologic contacts; (b) absence of significant metamorphic aureoles centered on the skarn; (c) relatively high pyroxene:garnet ratios, (d) distinctive Mn- and Fe-rich minerals (e.g., early johannesenitic pyroxene and minor andraditic garnet, and late bustamite, rhodonite, dannemorite, and ilvaite); and (e) an abundance of sulfides (e.g., sphalerite, galena, pyrite, pyrrhotite) associated with pyroxene rather than with garnet or other silicate minerals. The deposits are commonly localized in fissures related to faults, which appear to have provided the channelways for fluid movement.

Some carbonate-replacement, distal zinc-lead deposits (e.g., Blue Bell, Canada) are not skarn deposits in the strict sense, because they lack calc-silicate gangue. They do contain, however, minor to trace amounts of Mn-silicate minerals commonly found in typical zinc-lead skarns and may represent the distal end-members of zinc-lead skarn deposits (Einaudi et al. 1981). The Blue Bell deposit contains knebelite (Mn-olivine) as a gangue mineral and its massive ores were deposited at temperatures higher than 450°C, but the temperature - salinity - $\delta^{18}\text{O}$ - δD relationships are compatible with a meteoric rather than a magmatic source for the ore fluids (Ohmoto & Rye 1970).

9.4. Examples

9.4.1. BINGHAM DISTRICT, UTAH, USA

The Bingham district (see Fig. 3.19) is unique among the porphyry copper districts of USA because of its importance for both porphyry and non-porphyry ores (Rubright & Hart 1968). The district contains not only the largest known porphyry copper deposit in North America (produced 1.3 billion tons of 0.85% Cu ore between 1904 and 1976), but also the world's largest known copper skarn deposit (reserves of more than 60 million tons of approximately 2% Cu plus a lower-grade resource of 150 million tons of 1.3% Cu). Moreover, it is the only porphyry copper system that has produced major lead - zinc - silver ores (40 million tons during 1870-1971) (Einaudi 1982a). The discussion presented below pertains to the skarn-type mineralization in the Carr Fork area (Fig. 9.4) and is largely extracted from Atkinson and Einaudi (1978).

At the core of the porphyry copper system is the mid-Tertiary Bingham stock, composed of a multiple intrusive sequence of early monzonite, followed by quartz monzonite porphyry and quartz latite porphyry. The intrusive activity appears to have been controlled to a large degree by a zone of northeast-trending Mesozoic faults that later served as major conduits for hydrothermal fluids. The stock itself carries relatively high-grade (about 0.65% Cu) porphyry-type Cu (-Mo) mineralization consisting of chalcopyrite - bornite and chalcopyrite - pyrite assemblages associated with biotite - orthoclase (potassic) alteration. The patterns of alteration (Fig. 9.4a) and mineralization (Fig. 9.4b) are clearly centered on the quartz monzonite porphyry phase, indicating that the causative hydrothermal activity was synchronous with the emplacement and cooling of the porphyry.

Sedimentary rocks of the contact aureole are Pennsylvanian in age and consist of quartzite with lesser amounts of calcareous-carbonaceous siltstone and limestone. The skarn-type ore mineralization occurs in the carbonate-rich rocks. The relatively small volume of such rocks in the Pennsylvanian section at Bingham was probably a key factor in the development of high-grade skarn mineralization. Three metal zones are recognized in the non-porphyry ores surrounding the Bingham stock: (a) copper ore (Pb:Cu \approx 0.02 or less) in the garnet skarn, up to 450 m; (b) lead-copper northeast fissure ore (Pb:Cu = 0.2 to 5) in nonsilicated limestone, up to 900 m, and (c) lead-zinc-

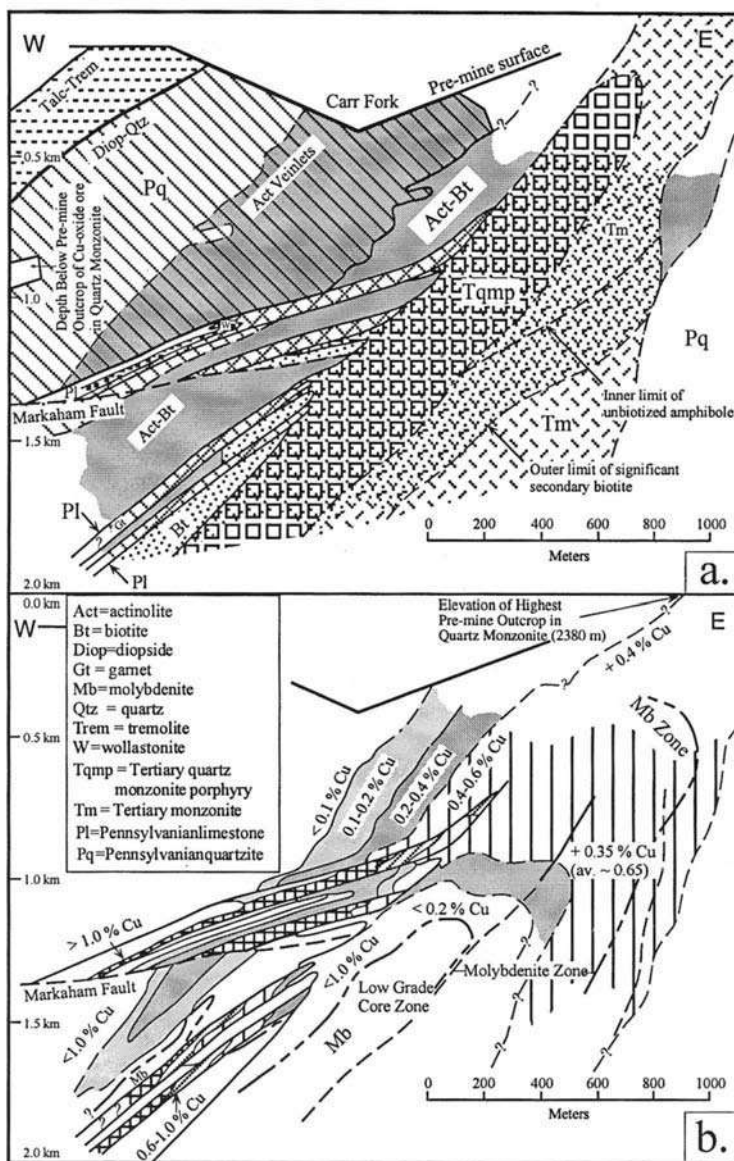


Figure 9.4. Cross section (looking north) of part of the Bingham mining district, Utah, showing skarn-type copper mineralization in the western contact zone (Carr Fork area) of the Bingham stock. a. Zoning of skarn assemblages; b. Zoning of copper mineralization (given as Cu grade). (After Einaudi 1982a.)

silver northeast fissure ore (Pb:Cu = 10 to 30) in non-silicated limestone, up to 1,200 m. The zoning pattern, however, is quite complex (Fig. 9.4b), reflecting multiple stages of hydrothermal activity involving expansion and regression of the zones.

The skarn formation in the Carr Fork area may be separated into three stages on the basis of age relations and distribution of characteristic mineral assemblages (Atkinson & Einaudi 1978): (a) an Early Stage of contact metamorphism and Mg-Si metasomatism; (b) a Main Stage of copper ore deposition; and (c) a Late Stage of retrograde hydrothermal alteration. The Early Stage contact effects produced wollastonite, with minor idocrase and garnet, in thick, cherty limestone up to 600 m from the stock, and diopside in quartzite and silty limestone beds up to 1,500 m from the stock. Only a trace amount of sulfides was deposited at this stage. The sulfide deposition started with the emplacement of the quartz monzonite and continued during the emplacement of the quartz monzonite porphyry. Actinolite alteration of diopside along sulfide-bearing fractures in quartzite and garnetization of wollastonite-bearing marble represent the beginning of Main Stage mineralization, which was contemporaneous with potassic (biotite - orthoclase) alteration of the intrusive rocks by dominantly magmatic fluids (Bowman et al. 1987). Two garnetized cherty limestone beds, 15 to 60 m thick and separated by 100 m of quartzite, contain the major copper-bearing skarns in the district. The assemblages in the ore zones are dominated by andraditic garnet, diopside, and quartz with lesser amounts of Fe-oxide minerals (magnetite and hematite), Cu-Fe sulfides (chalcopyrite and bornite), and pyrite. Near the intrusion, disseminated sulfides consist primarily of chalcopyrite with local bornite. Pyrite:chalcopyrite ratio increases away from the intrusion, and bornite reappears with chalcopyrite and sphalerite in the outer wollastonite zone. The Main Stage of ore deposition culminated in partial destruction of garnet and diopside to variable mixtures of calcite, quartz, hematite, magnetite, siderite, and sulfides.

The Late Stage alteration produced pyrite and hydrous minerals (chlorite, montmorillonite, sericite, talc) from earlier calc-silicates and redistributed sulfides near the intrusive contact. A zone up to 60 m wide in the sedimentary rocks along the porphyry contact contains less than 0.1% sulfides, principally pyrite. This retrograde alteration, triggered by an influx of meteoric waters, is believed to have been synchronous with the sericite - pyrite (phyllic) alteration of early K-feldspar + biotite assemblages in the intrusive rocks (Moore & Nash 1974, Bowman et al. 1987). Gold mineralization, which generally averages about 0.05 oz/ton Au in garnetized limestone containing ore-grade copper mineralization and may range up to 2.3 oz/ton Au locally in silicified and pyritized skarn, is also believed to have occurred during this stage.

In contrast to skarn copper ores, which are restricted to garnetized limestone beds near the intrusion, lead - zinc - silver ores occur mainly in limestone outside the zone of skarn minerals as fissure-replacement deposits. These probably represent distal deposits formed from the late-stage fluids (Atkinson & Einaudi 1978), but their relationship to the proximal copper skarn is not clear.

9.4.2. KING ISLAND TUNGSTEN DEPOSIT, TASMANIA, AUSTRALIA

The King Island tungsten (-molybdenum) deposit represents the largest occurrence of an economic, calcic, oxidized tungsten skarn (>14 million tonnes of ore averaging 0.8 wt% WO_3 and 0.02 to 0.04 wt% MoO_3) and one of the best studied (Edwards et al. 1956, Large 1972, Danielson 1975, Wesolowski 1984, Davis 1986, Kwak 1987). The skarns were produced by the replacement of carbonate and pelitic units in the Cambrian Grassy Group, at the contact zone of the Grassy stock, a granodiorite-adamellite intrusion of Devonian age. The stock is a typical calcic, I-type, magnetite-series pluton and shows only minor development of endoskarn, but the host sequence has been extensively metamorphosed to hornblende-hornfels facies. The three known orebodies of the district — Open Cut (or No. 1 deposit), Dolphin, and Bold Head — are stratiform in nature and the ore horizons vary from 5 to 40 m in thickness.

In the Dolphin mine area (Fig. 9.5), the Grassy Group consists of: (a) lower biotite hornfels; (b) lower metavolcanics; (c) finely banded hornfels and limestone showing extensive bimetasomatism ("Banded Footwall Beds"); (d) the main tungsten skarn unit (C lens), which in many places is separated into an upper part and a lower part by a barren marble unit; (e) pyroxene-garnet (-biotite) hornfels, which is ore-bearing near the Northern Boundary Fault; (f) upper biotite hornfels, with some

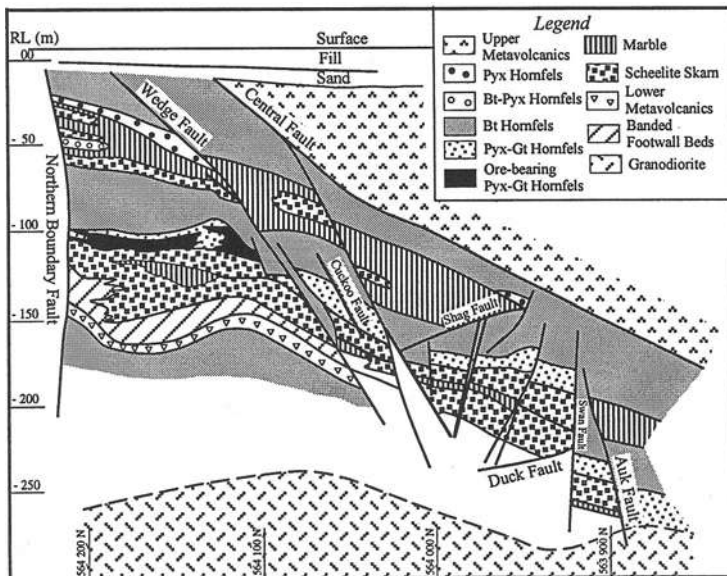


Figure 9.5. Cross section (220 200 E) through the King Island (Dolphin) scheelite mine, Tasmania, Australia. Abbreviations: Bt = biotite, Gt = garnet, Pyx = pyroxene. (After Kwak 1987.)

tungsten skarn (*B* lens); and (g) an upper metavolcanic unit. Nearly all of the marble units present in the Grassy Group have been metasomatically replaced to some extent by ore-skarns, but ore-grade mineralization is much more restricted. The main ore mineral is scheelite, which occurs as disseminated grains (0.05-0.2 mm) in and along the margins of andraditic garnets, in quartz and, sometimes, in calcite; coarser scheelite (up to 50 mm) occurs in joints, tension gashes, and quartz - calcite pods. In some cases (e.g., Bold Head deposit), the main-stage scheelite deposition was accompanied by extensive stockwork-type molybdenite mineralization. Most of the faults in the mine area appear to have predated the intrusive and skarn-forming events and provided conduits for the mineralizing fluids. This conclusion is supported by intense replacement along some of the faults and is consistent with the presence of thick biotite hornfels (without metasomatic calc-silicate alteration) both above and below the skarn horizon. Apparently, the faults in the area played a significant role in the localization of ore-skarns (Kwak 1987).

The compositions of skarn silicates generally reflect decreasing Fe:Mg ratios and fO_2 outward from the source(s) of ore solutions and with time. Fluid inclusion homogenization temperatures and salinities also show a general decrease with the paragenetic sequence as well as with increasing distance from the granitoid contact (Wesolowski 1984). Homogenization temperatures of inclusions in cores of garnet crystals decrease systematically from a maximum of 800°C near the contact to about 300°C at a distance of 500 m, and temperatures for interstitial calcite and quartz are as low as 180°C. Fluid inclusion salinities decrease from ≈ 65 wt% NaCl equivalent for the early-formed minerals (i.e., garnet) nearest the pluton to less than 3 wt% NaCl equivalent for later-formed minerals farthest from the contact (i.e., calcite). These relationships strongly suggest a genetic link between the granitoid and skarn formation. The decrease in temperature and salinity with time and increasing distance from the granitoid contact is attributed to the cooling of the pluton and mixing with cooler, dilute fluids. The interpretation is also supported by the significantly lower $\delta^{18}O$ values of the late-stage calcite and quartz (approximately -1.5 to $+6\text{‰}$) compared with those from skarn minerals of the earlier stages (approximately $+7$ to $+10\text{‰}$), the latter being very similar to $\delta^{18}O$ values estimated for fluids in equilibrium with Devonian granitoids of the area (Wesolowski 1984).

9.4.3. RENISON BELL TIN DEPOSIT, TASMANIA, AUSTRALIA

The Tasman orogenic belt in northwestern Tasmania contains a number of cassiterite-sulfide skarn deposits, the most well known of which are Moina, Renison Bell, Mt. Bischoff, and Cleveland (see Fig. 9.1). The Renison Bell deposit is the largest economic tin deposit in Australia and relatively better studied (e.g., Newnham 1975, Hutchinson 1979, Patterson et al. 1981, Kwak 1987). It is considered to be the best example of a pyrrhotite-dominated distal tin-skarn deposit. The Moina deposit, classified as a proximal tin-skarn deposit, is larger but of lower grade (Kwak 1987).

The cassiterite-sulfide mineralization at Renison Bell is localized mainly as strata-

bound, replacement lenses in three carbonate beds of a late Proterozoic sequence (Fig. 9.6) underlying an early Paleozoic sequence. The carbonate beds represent diagenetically dolomitized marine limestones (Patterson et al. 1981). The No. 2 and No. 3 dolomites (skarns) are economically the most significant.

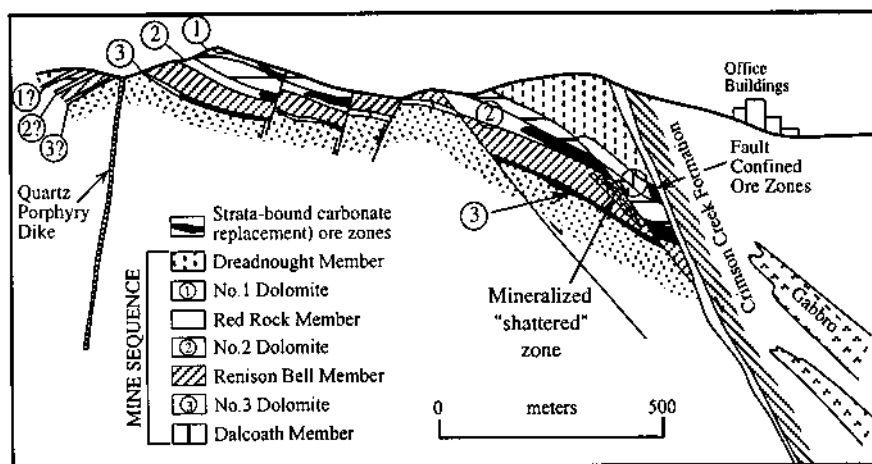


Figure 9.6. A generalized, West-East cross section of the Renison Bell mine, Tasmania, Australia. The mineralized shatter zone is called the "Melba zone" orebody. No granitoid is exposed in the immediate mine area, but granitic rocks have been intersected in several boreholes at depths of 800-1,200 m below the surface. (After compilation by Kwak 1987.)

No granitoids are exposed in the immediate mine area, but granite (which is medium grained at depth but porphyritic near its upper contact) or altered granitoid (sericite \pm fluorite \pm tourmaline) has been intersected in several boreholes at depths of 800-1,200 m below the surface. Also, a number of porphyritic and medium-grained granitic plutons and dikes of Devonian age (the Pine Hill Granite), all greisenised to various degrees, occur in the vicinity, and a large area of albitized granitoid is known to occur at depth near the Pine Hill Granite. The greisenised parts of the Pine Hill Granite carry minor cassiterite and adjacent country rocks have been thermally metamorphosed to hornblende-hornfels facies assemblages. However, the Pine Hill area itself, which is at least 400 m topographically above and about 2 km away from the Renison Bell deposit, was probably not the source of ore fluid. The Pine Hill Granite may represent a mineralized cupola in the same, or in a similar, pluton from which the ore fluids were derived (Kwak 1987).

Several styles of mineralization are present at Renison Bell: magnesian skarn (replacement bodies in carbonate beds), fault and fracture infill, quartz vein stockwork, breccia infill, and poorly defined mineralization in recrystallized non-carbonate rocks adjacent to faults. The skarn-type mineralization is the most important, consisting

principally of massive pyrrhotite with minor cassiterite, arsenopyrite, and other sulfides, along with variable amounts of talc, phlogopite, siderite, and quartz. The generalized paragenetic sequence at the Renison mine has been interpreted to comprise six stages of mineral deposition as given below (Patterson et al. 1981).

Stage I: Cassiterite + Mg-silicates, an early stage of replacement ore formation.

Stage II: Cassiterite + pyrrhotite + arsenopyrite + silicates + minor sulfides and iron oxides, the main stage of mineralization associated with sideritic alteration of dolostones and tourmalinization of clastic sediments.

Stage III: Cassiterite + pyrrhotite + arsenopyrite + silicates, forming veins in major fault zones.

Stage IV: Minor veining by sphalerite + galena + silicates + carbonates \pm fluorite.

Stage V: Minor veining by calcite + quartz \pm chlorite accompanied by extensive replacement of stage II pyrrhotite by pyrite.

Stage VI: Vug-filling sequence of carbonates, quartz, fluorite, and sulfides.

Fluid inclusion studies indicate that the ore-forming fluids (stages I to III) were moderately hot ($\approx 350^\circ\text{C}$) and quite saline (≈ 2 molal total dissolved salts). Oxygen and hydrogen isotope ratios of the fluids, calculated from analysis of gangue minerals and water extracted from fluid inclusions, suggest that the fluids were dominantly of magmatic origin. The ore metals were probably transported as chloride complexes and precipitated as sulfide - cassiterite assemblages due to an increase in pH arising from dolomite replacement. The later fluids were somewhat cooler (300°C for Stage IV to probably less than 200°C - 150°C for Stage VI) and generally less saline, probably because of mixing with meteoric water. Calculated $\delta^{34}\text{S}_{\text{SS}}$ values for stages I to III and Stage IV fluids average $+6.0$ and $+5.3\%$, respectively, and are consistent with a dominantly or solely magmatic source of sulfur for the fluids (Patterson et al. 1981).

Hutchinson (1979) proposed an exhalative origin for the Renison Bell and other similar tin deposits in Tasmania. Exhalative processes have the potential of forming tin-rich exhalites analogous to the better known base metal sulfide examples, and tin does occur in concentrations recoverable as a byproduct in some massive sulfide deposits (e.g., Kid Creek and Sullivan, Canada) that are believed to be of exhalative origin (Badham 1982). The available evidence, however, supports an epigenetic, skarn-type, magmatic hydrothermal origin for the Renison Bell deposit (Solomon 1980, Patterson et al. 1981, Kwak 1987). The most important features in favor of this interpretation are as follows: (a) all the major tin deposits of western Tasmania, including Renison Bell, occur close to granitic bodies; (b) cassiterite - sulfide deposits of similar mineral assemblages are found in a variety of rock types of different ages; (c) the distribution of ore horizons and metal zoning suggest that the faults were the main conduits of fluid transport and there is no evidence that these faults were active during sedimentation; (d) the textures strongly suggest replacement of carbonate units by ore-gangue assemblages; (d) the oxygen and hydrogen isotope ratios indicate that the fluids

for cassiterite deposition were dominantly magmatic, not meteoritic or ocean water as would be expected in an exhalative model; and (e) the available sulfur isotopic and fluid inclusion data are also consistent with a magmatic source of the ore fluids. In fact, some eastern Australian 'stratiform' tin deposits, interpreted earlier as isochemically metamorphosed, calc-silicate-rich, submarine exhalative beds (Stanton 1987) have since been reinterpreted as skarn deposits associated with the emplacement of closely related granitoids (Ashley & Palmer 1989).

9.4.4. PROVIDENCIA ZINC-LEAD-SILVER DEPOSIT, ZACATECAS, MEXICO

The Providencia deposit is one of the few carbonate-hosted zinc-lead sulfide deposits for which the available data (Sawkins 1964, Ohmoto et al. 1966, Rye 1966, Rye & O'Neil 1968, Rye & Haffty 1969) strongly indicate a skarn-type mineralization related to a pluton. The sulfide ores occur as conformable pipelike bodies in steeply-dipping Upper Jurassic and Cretaceous limestone units adjacent to the Providencia stock (Fig. 9.7). The stock is granodioritic in composition, with a K-Ar age of 40 ± 2 Ma and a $^{87}\text{Sr}/^{86}\text{Sr}$ initial ratio of 0.705 ± 0.001 ; gangue minerals in the sulfide ores have given an identical strontium isotope ratio and a K-Ar age of 41 ± 2 Ma. (Ohmoto et al. 1966). The orebodies, some of which lie at distances of more than 1,000 m from the pluton contact, appear to have been structurally controlled by both fractures and bedding. Most of the ore mined at Providencia has come from the "pipes" that occur in the recrystallized Zuloaga Limestone close to the granodiorite contact. It is not known why all the major ore bodies are localized on the southern side of the Providencia stock.

Massive metasomatic replacement of carbonate rocks is the dominant mode of ore mineralization, although vug-fillings with well-formed crystals are quite common. The mineralogy is quite simple: galena, pyrite, and sphalerite are the main sulfide minerals; Mn-calcite and quartz are the main gangue minerals. Other minerals present in varying amounts include chalcopyrite, dolomite, kutnahorite [$\text{CaMn}(\text{CO}_3)_2$], rhodonite, sulfosalts, and fluorite. Calc-silicate gangue minerals, such as grossular garnet, scapolite, and tremolite, are restricted to the lowermost portions of the orebodies. Where present, they are intimately mixed with the sulfide minerals (Sawkins 1964), indicating a genetic relationship between the skarn formation and sulfide mineralization. Analyses of fluid inclusions in sphalerite, quartz, calcite, and fluorite indicate that the ore-gangue assemblages were emplaced at temperatures of $\approx 425^\circ\text{--}200^\circ\text{C}$ from fluids of varying salinity (5 to 40 wt% NaCl equivalent) (Sawkins 1964). The massive ore was emplaced at temperatures above 350°C , but the deposition of very minor amounts of sulfide continued to 200°C ; the precipitation of calcite and quartz occurred generally at temperatures below 300°C . Maximum concentrations of Zn and Pb in inclusion fluids in quartz, a late-stage mineral, were found to be 890 and 530 ppm, respectively. K:Na and Ca:Na ratios of fluid inclusions indicate that the salinity variations in the hydrothermal fluids probably occurred at the source of the fluids and could have resulted from boiling in the magma chamber (Rye & Haffty 1969).

Studies of stable isotope ratios have contributed significantly to the understanding

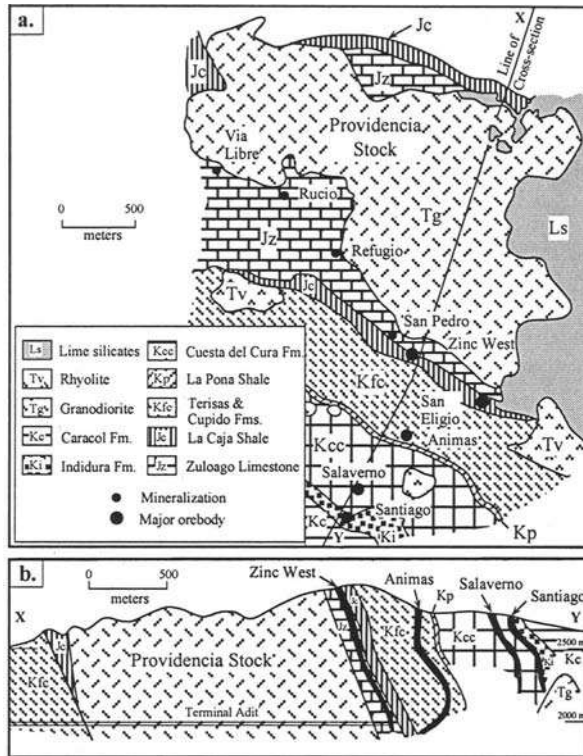


Figure 9.7. Generalized geologic map (a) and cross section (b) of the Providencia mine area, Mexico. In detail, the Pb-Zn-Ag sulfide replacement “pipes” exhibit considerable irregularities in their shapes. (After Sawkins 1964.)

of the Providencia hydrothermal system. Sulfide $\delta^{34}\text{S}$ values fall in the narrow range of -3 to $+6\text{‰}$, suggesting that the sulfur was derived either from the mantle or from a well-homogenized crustal source (Sawkins 1964). The $\delta^{13}\text{C}$ (PDB) values of CO_2 in inclusions in sphalerite (-7.0‰) and calcite (-11.0‰) imply that much of the hydrothermal carbon was most likely obtained from a deep-seated, non-limestone source (Rye 1966, Rye & O’Neil 1968). $\delta^{18}\text{O}$ (SMOW) values of primary fluid inclusions in sphalerite ($+6.2$ to $+6.8\text{‰}$), quartz (-4.5 to -3.7‰), and calcite ($+0.2$ to -0.2‰) (Rye & O’Neil 1968) are lower than the $+7$ to $+9\text{‰}$ range believed to be typical of magmatic waters (see Fig. 4.14), and may be interpreted as a consequence of either the mixing of magmatic hydrothermal fluids with isotopically lighter meteoric waters or the exchange of ^{18}O between the fluids and wallrock. However, mixing is an unlikely explanation in view of the uniformity of estimated $\delta^{13}\text{C}$ and $\delta^{18}\text{O}$ values of the hydrothermal fluids in time and space (Rye & O’Neil 1968, Rye & Haffty 1969). On the other hand, a

predominantly magmatic source of the ore fluids is consistent with the sulfur isotope ratios, the narrow range of Ca:Na and Ca:Cl ratios of fluid inclusions in sphalerite, the δD values (-68 to -83‰) of fluid inclusions (Rye & Haffty 1969), and the similarity in age and strontium isotope initial ratios between the Providencia stock and the ore assemblage (Ohmoto et al. 1966).

9.5. Origin

9.5.1. FLUID INCLUSION AND STABLE ISOTOPE DATA

Systematic fluid inclusion and stable isotope data are available only for a relatively small number of skarn deposits, mostly from tungsten and tin skarns. Particularly limited are data from iron, gold, and molybdenum skarns. Also, most fluid inclusion data are from skarn (gangue) minerals rather than the paragenetically later ore minerals.

A striking feature of skarn fluid inclusions is the low mole fraction of CO_2 , commonly <0.1 . As carbonate replacement is accompanied by the generation of large volumes of CO_2 , skarn-forming systems appear to have been open to CO_2 loss. For skarn deposits as a class, the ranges of fluid inclusion homogenization temperatures and salinities are very large ($\approx 700^\circ\text{--}200^\circ\text{C}$; 10-65 wt% NaCl equivalent). Similar ranges are perhaps applicable to proximal skarns of each type discussed earlier; the temperatures and salinities for distal skarns are generally at the lower ends of these ranges. Many individual skarn deposits, however, exhibit a more systematic pattern of variation, especially of temperature: a progressive decrease in temperature (a) from prograde skarn-forming stage to retrograde alteration stage, both temporally and spatially, and (b) with increasing distance from the pluton during either stage. The temperature decrease is particularly well documented for tin and tungsten skarns (Fig. 9.8). The fluid salinity generally decreases in the direction of decreasing temperature, but less regularly in some cases. The fluid inclusion data provide a strong argument in favor of a predominantly magmatic source of the hydrothermal fluids and possible mixing with variable amounts of meteoric water as the skarn system evolves (e.g., Sawkins 1964, Ahmad & Rose 1980, Patterson et al. 1981, Shelton 1983, Wesolowski 1984, Bowman et al. 1987, Ettlinger et al. 1992). The generalized picture of increasing involvement of meteoric water with increasing distance from the pluton and with time is also corroborated by a progressive decrease in $\delta^{18}\text{O}$ values of skarn minerals and, in a limited number of cases, of inclusion fluids (e.g., Rye 1966, Taylor 1979, 1980, Patterson et al., 1981, Wesolowski 1984, Bowman et al. 1987, Layne et al. 1991).

Some skarn deposits, however, do not conform to the above generalizations. Oxygen and hydrogen isotopic data indicate that there was only a limited and nearly constant influx of meteoritic water into the CanTung (Canada) scheelite skarn system (Bowman et al. 1985). A detailed fluid inclusion study by Gerstner et al. (1989) found no evidence for a significant break in P - T conditions between prograde anhydrous and retrograde hydrous skarns at MacTung (Canada) tungsten deposit. On the basis of stable

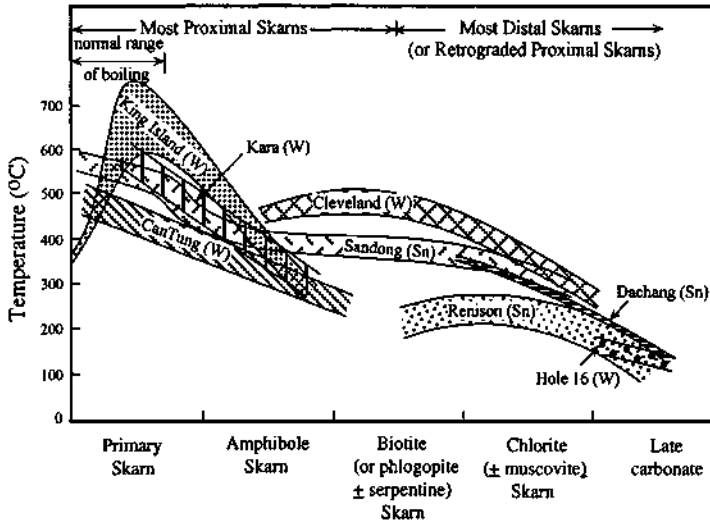


Figure 9.8. Variation of temperature with paragenetic sequence (expressed as “stages” of skarn development) for selected tin and tungsten skarns (after Kwak 1987). The relatively low temperature at the early part of the King Island primary skarn probably represents the mixing of small amounts of hot ore fluids (initially near magmatic temperatures) with cooler country rocks ($\approx 350^{\circ}\text{C}$) (Wesolowski 1984).

isotope systematics, hydrothermal fluids for the Dachang tin skarn deposits appear to have been entirely magmatic (Fu et al. 1991), whereas the ^{18}O - and ^{34}S -enriched ore fluids for the Cornwall and Morgantown (Pennsylvania, USA) magnetite skarn deposits have been interpreted as dominantly nonmagmatic (Rose et al. 1985).

9.5.2. EVOLUTIONARY SEQUENCE

Despite the diversity, skarn deposits seem to share a common evolutionary process related to the emplacement and cooling history of the associated plutons. In most large skarn deposits, skarn and ore minerals result from the same hydrothermal system, although there may be significant differences in the time-space distribution of these minerals on a local scale.

Typically, the development of a skarn deposit comprises a continuum of four successive stages (Fig. 9.9): (a) emplacement of a pluton into a carbonate-bearing supracrustal sequence; (b) essentially isochemical contact metamorphism (700° - 500°C) related to the pluton; (c) multiple stages of metasomatism (650° - 400°C) accompanying crystallization of the magma and the evolution of an ore-forming magmatic hydrothermal fluid; and (d) retrograde hydrothermal alteration (450° - 300°C or lower) during final cooling of the system, which in most cases is accompanied by an influx of

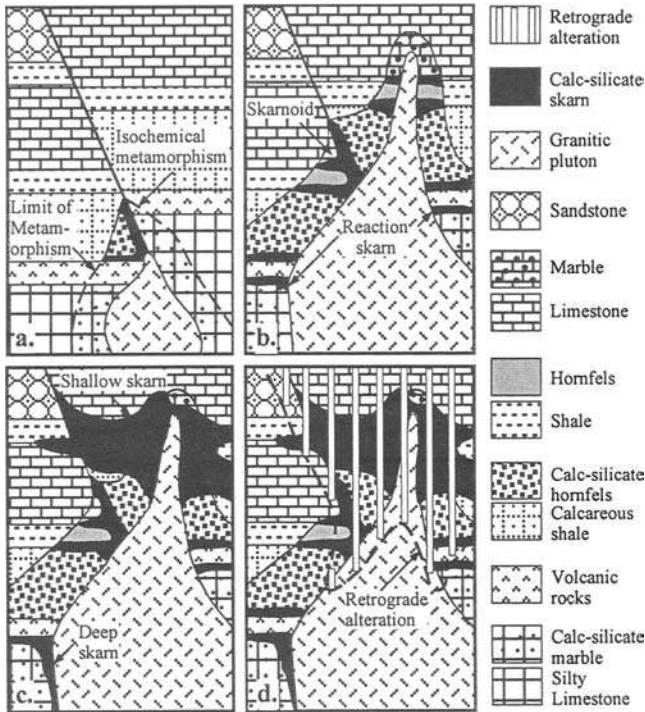
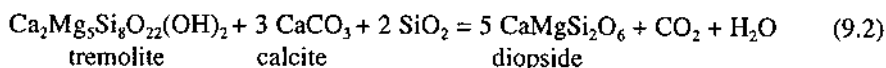


Figure 9.9. Schematic illustration of sequential development of pluton-associated skarns. **a.** Emplacement of intrusion causes metamorphism of surrounding sedimentary rocks and produces calc-silicate hornfels in limestone. **b.** Continued development of hornfels in the wallrocks by metamorphic recrystallization and phase changes, controlled by protolith compositions, with local bimetasomatism and fluid circulation forming reaction skarns and skarnoid in impure lithologies and along fluid boundaries. Note that metamorphism is more extensive and higher in temperature at depth than adjacent to the small cupola near the top of the system. **c.** Crystallization of the magma leads to the release of hydrothermal fluids and the development of fluid-controlled (metasomatic) skarn. The skarn at depth is small relative to the size of the metamorphic aureole; it is also vertically oriented compared with the laterally extensive skarn near the top of the system, with local extensions beyond the metamorphic aureole. **d.** Cooling of the pluton and the possible circulation of cooler, oxygenated meteoric waters cause retrograde alteration of metamorphic and metasomatic calc-silicate assemblages. Note that retrograde alteration is more extensive in shallow zones. (After Meinert 1992.)

meteoric water into the skarn system. Metasomatic minerals commonly occur as overgrowths on, or as veinlets in, metamorphic minerals, and these in turn may break down to polymineralic mixtures during retrograde alteration. Mineral zoning patterns of each successive stage commonly crosscut earlier patterns as a consequence of shifting hydrothermal conduits. Thus, the ultimate zoning pattern is highly variable in skarn deposits as a group and often very complex in a given deposit.

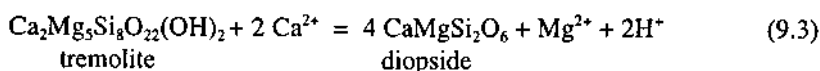
Contact metamorphism produces a zoned thermal aureole of hornfels containing high-temperature, anhydrous silicate assemblages appropriate to the bulk compositions of the country rocks, because reactions at this stage involve only changes in the amount of volatile components (H_2O , CO_2 , O_2 , etc.) in the rock. Such reactions, for example,



are a function not only of the P - T condition but also of the fugacities of the volatile components. Not much sulfides or oxides are formed at the metamorphic stage, but increased porosity due to loss of volatiles and enhanced fracturing of the country rocks result in ground preparation for ore concentration in the subsequent stages.

The metasomatic stage of prograde skarn formation begins with the release of magmatic hydrothermal fluids from the crystallizing plutons. As discussed in connection with porphyry plutons (Ch. 8), the timing and quantity of magmatic fluids exsolved and their dissolved metal contents are controlled by a number of factors, such as the source material for magma generation, the composition of the magma and its crystallization history, and the oxidation state of the magma. The fluids, which may mix with metamorphic waters or at a later stage with meteoric waters, travel along all available permeable zones and produce both endoskarns and exoskarns. Fluid inclusion and petrologic studies indicate that the metasomatic fluids are characterized by low CO_2 content ($X_{\text{CO}_2} < 0.1$), moderate to high salinities (10 to 45 NaCl wt% equivalent), and acidic pH. Most of the ore metals are probably carried as chloride complexes in the aqueous fluid phase; tin may be transported as chloride and/or fluoride complexes, and molybdenum and tungsten probably as molybdic acid [H_2MoO_4] and tungstic acid [H_2WO_4], respectively.

Metasomatic reactions, unlike metamorphic ones, produce changes in the amounts of nonvolatile components (e.g., Ca, Fe, Si, etc.) in the rock by reactions such as



This reaction is dependent on activities of Ca^{2+} , Mg^{2+} , and H^+ in the fluid, in addition to P - T and X_{CO_2} (although CO_2 does not appear as a component in the reaction, X_{CO_2} affects the stability of the two solid phases involved in the reaction). Thus, for thermodynamic evaluations of skarn assemblages — e.g., an assemblage involving diopside — it is necessary to know whether they were produced by contact metamorphic or metasomatic reactions. The distinction, however, is not easy. The following criteria may be useful in some cases (Einaudi et al. 1981): (a) for the same number of components, metamorphic rocks generally contain a large number of phases, whereas metasomatic rocks contain very few phases; and (b) in a given rock type, changes in

bulk composition, except for H₂O or CO₂, is characteristic of metasomatism.

The main period of sulfide and oxide ore deposition generally follows the cessation of skarn growth and is accompanied by the beginning of hydrothermal alteration of earlier skarn assemblages and associated plutons. The retrograde reactions, in response to falling temperature, lead to the replacement of Ca-rich calc-silicates by an assemblage of Ca-depleted silicates, Fe-oxides and/or Fe-sulfides, and carbonates or albitic plagioclase. Calcium thus released to the solution may result in late precipitation of scheelite. Limited retrograde alteration, most likely due to inadequate fluid circulation, may produce only sparse vug-fillings of quartz - carbonate - sulfide, whereas extensive retrograde alteration may convert much of the skarn into a typical low-temperature hydrothermal assemblage (a mixture of quartz, chalcedony, clay minerals, carbonates, sulfides, and Fe-oxides). In the latter case, the only evidence of the former skarn may be preserved in relict minerals and pseudomorphs. Sulfide precipitation is usually restricted to skarns and even specific zones of the earlier skarn pattern, suggesting a control of oxidation-reduction reactions at skarn-carbonate contact (the so-called "marble front") resulting from neutralization of the hydrothermal fluid by the carbonate rocks. Peripheral, carbonate-hosted vein and manto sulfide deposits (distal skarn deposits) may also form at this stage of skarn development. Even massive silica-sulfide replacement deposits in carbonate rocks beyond the limit of skarn, such as at Ely, Nevada (James 1976), may be genetically related to the retrograde stage. A limiting factor in the quantitative interpretation of sulfide deposition in skarns by application of standard thermodynamic techniques (see Ch. 3) is the lack of adequate experimental studies on sulfide solubility in systems buffered by common skarn calc-silicates.

9.6. Metallogensis

The degree to which each stage in the evolutionary sequence of skarn formation is developed in a particular skarn depends on local geological factors, such as stratigraphy (especially, thickness and composition of carbonate units), composition and oxidation state of the magma, depth of magma emplacement and skarn formation, and tectonic setting. Variations in these factors are responsible for the large variations in the size, geometry, mineral assemblages, and metal association of skarn deposits.

9.6.1. HOST ROCKS

The preferential occurrence of skarn deposits in carbonate units is mainly due to the fact that carbonates readily neutralize the acidic, chloride-rich ore solutions, causing precipitation of the ore constituents. Skarns tend to be best developed in the purer carbonate beds of a given sequence but, because of the relatively low permeability of pure limestone, the extent of skarn formation and ore mineralization depends on the fracture permeability or on the presence of permeable sandy or hornfels interbeds

(Einaudi 1982b). For example, the increased fracture permeability of the interbedded pelitic and impure carbonate units during the earlier stage of contact metamorphism appears to have played an important role in the later localization of high-grade skarn orebodies at Carr Fork, Utah (Atkinson & Einaudi 1978), Pine Creek, California (Newberry 1982), and CanTung, Canada (Dick & Hodgson 1982). The presence of minerals, such as graphite, hematite, and pyrite, determine the oxygen buffering capacity of the host rocks and thus exert a strong influence on the skarn mineral assemblage.

Another important factor in the localization of skarns is the geometry of the pluton-host rock contact (Kwak 1987). Where the contact is nearly conformable with the bedding of the carbonate host rocks, skarns tend to form as tabular bodies adjacent and parallel to the contact, with large lateral extents if both the contact and the carbonates are equally extensive. Where the contact transects the bedding, skarns commonly form as lenticular bodies of relatively small dimensions along certain favorable beds, although replacement mineralization may occur at a considerable distance from the contact. Skarns along steeply dipping plutonic contacts are usually thin (<10 m wide) and subeconomic, but larger bodies may be localized in embayments along the contacts, probably controlled by pre- or syn-skarn fracture systems. Some large skarns appear to be related to adjacent faults.

The systematic variations in temperature, mineral compositions, and fluid salinity in most well-studied skarn deposits, as well as the correlation between skarn types and intrusive composition (discussed below), argue against the immediate host rocks being a major contributor of ore-forming elements to skarn formation.

9.6.2. COMPOSITIONS OF SKARN-RELATED PLUTONS

A more fundamental difference among the skarn types appears to lie in the composition and oxidation state of the coeval intrusions. This correlation is perhaps the strongest evidence for a genetic link between magmatic processes and skarn formation (Meinert 1983, 1992, 1993). Some generalized conclusions regarding the compositional variability of intrusions related to the various skarn types are summarized below:

- (a) The SiO_2 contents vary from a low of about 50 wt% to a high of about 78 wt%, the most differentiated rocks being associated with molybdenum and tin skarns, and the least differentiated with iron skarns (Fig. 9.10a). This is corroborated by the $\text{K}_2\text{O}:\text{Na}_2\text{O}$ ratios of these skarn types (approximate average values are 0.4 for iron skarns; close to 1.0 for tungsten, copper, and lead-zinc skarns; and 1.6 for molybdenum and tin skarns). Additional data presented by Kwak (1987) show a wider range of $\text{K}_2\text{O}:\text{Na}_2\text{O}$ ratios for tungsten skarn granitoids (about 0.25 to 5.0), but the largest deposits are related to K_2O -rich plutons. The ratios for tin-skarn granitoids are almost always greater than unity.

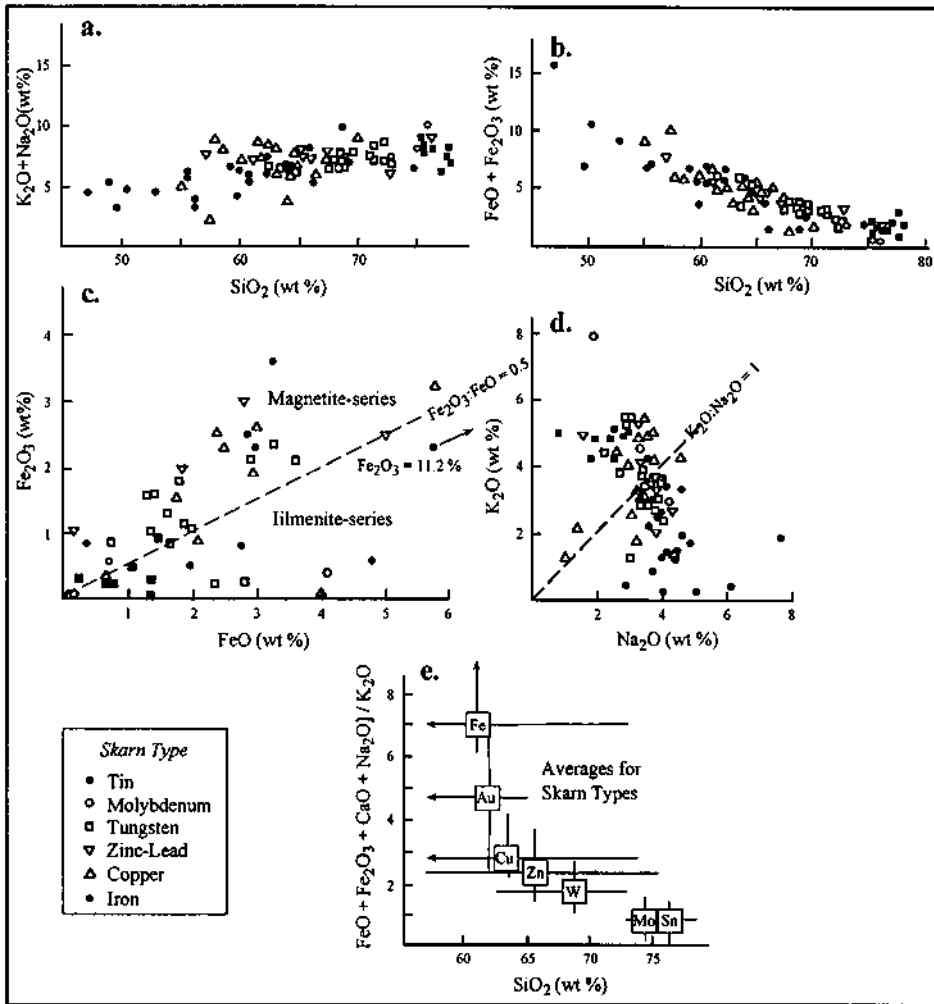


Figure 9.10. Covariation diagrams showing differences in the compositions of igneous intrusives associated with skarn deposits classified by dominant metal (after Meinert 1983, 1992). Bulk Fe_2O_3 :FeO ratios are less than 0.5 for ilmenite-series granitoids and more than 0.5 for magnetite series granitoids (Ishihara 1981). The magnetite-series and ilmenite-series granitoids (Ishihara 1977) are broadly equivalent to, but not synonymous with, I-type and S-type granitoids (White & Chappell 1977), respectively. Note that gold skarns are not included in this figure.

- (b) The total iron content ($\text{Fe}_2\text{O}_3 + \text{FeO}$) is inversely correlated with the silica content (Fig. 9.10b).
- (c) Fe_2O_3 :FeO ratios are mostly close to or less than unity (Fig. 9.10c). Tin skarns are almost always associated with reduced ilmenite-series granitoids

($\text{Fe}_2\text{O}_3:\text{FeO} < 0.5$), whereas tungsten skarns are associated with both magnetite-series ($\text{Fe}_2\text{O}_3:\text{FeO} > 0.5$) and ilmenite-series granitoids, but more typically with the former (Ishihara 1981, Kwak 1987). Plutons associated with copper skarns, particularly those within porphyry copper systems, belong to the magnetite-series. Plutons with the highest average $\text{Fe}_2\text{O}_3:\text{FeO}$ ratios are associated with Zn-Pb skarns, most likely reflecting extensive fluid-rock interaction for these distal deposits. The scatter in Figure 9.10c for iron skarns is probably also due to varying degrees of wallrock assimilation.

The distinction between oxidized magnetite- and reduced ilmenite-series granitoids has two important implications: environment of magma generation, and the oxidation state of the magma. Generally, magnetite-series magmas are generated at great depths (upper mantle to lower crust) from sources enriched in metals such as Fe, Cu, and Au, whereas ilmenite-series magmas are generated from lower crustal materials relatively enriched in metals such as Mo, W and Sn (Ishihara 1981). As discussed earlier (Ch. 2 and Ch. 8), hydrothermal fluids exsolved from oxidized magmas should be richer in sulfur compared with fluids exsolved from reduced magmas. This explains the common association of high-sulfide skarn deposits (Cu, Mo) with magnetite-series granitoids and low-sulfide skarn deposits (W, Sn) with ilmenite-series granitoids.

Skarn-related granitoids do not show a systematic enrichment in the ore metals that are concentrated in the associated skarns. For example, the average tungsten contents of unaltered granitoids associated with scheelite skarns are less than 5 ppm (mostly 1-2 ppm), very similar to the tungsten contents of unaltered host rocks surrounding tungsten skarns (Newberry & Swanson 1986). The only exception appears to be the association of tin skarns with Sn-enriched granitoids, the so called 'tin granites', which are 2 to 20 (and in rare cases up to 100) times enriched in Sn compared with ordinary granites. These granites are characterized by anomalously low Sr, high Rb, and high $^{87}\text{Sr}/^{86}\text{Sr}$ ratios, implying their highly fractionated nature and probable derivation from crustal melts (Groves & McCarthy 1978, Kwak 1987). On a world wide scale, tin deposits are clustered in certain belts (Schuiling 1967), but Lehmann (1982) has argued against the concept of a primary crustal tin anomaly in the "tin belts". Using TiO_2 -Sn and (Rb/Sr)-Sn variation diagrams, he concluded that the controlling factor for generation of tin granites by magmatic differentiation is a special bulk distribution coefficient of Sn, which probably depends on the oxygen fugacity of the melt.

9.6.3. DEPTH OF SKARN FORMATION

The release of a substantial volume of metal-enriched magmatic aqueous fluids is a necessary condition for the formation of skarns. As discussed earlier (Ch. 8), the amount and metal contents of the magmatic hydrothermal fluid depend on the initial water content of the magma, a source region-controlled parameter, and the timing of fluid separation from the magma. If a magma is largely crystallized before water

saturation occurs, the hydrothermal fluid is likely to be depleted in compatible elements (e.g., copper) that can be incorporated into early-formed minerals and enriched in incompatible elements (e.g., molybdenum, tin, and tungsten). The opposite will be the case if the magma attains water saturation after a relatively small degree of crystallization. As the solubility of water in silicate melts is strongly pressure dependent (see Fig. 2.3) and the degree of magma crystallization is essentially a function of cooling, the depth of magma emplacement is a critical factor in determining the amount and composition of the exsolved aqueous fluid. Thus, copper-rich, tungsten-poor skarns are associated with porphyritic (30-50% groundmass) plutons that were emplaced at shallow levels, whereas tungsten-rich, copper-poor skarns are associated with more differentiated, equigranular plutons that were emplaced at deeper levels (Newberry & Swanson 1986). As continued crystallization of a magma results in a loss of water, sulfur, and ore metals to crystallizing phases, the early versus late separation of the hydrothermal fluid may also explain the abundance of large skarn deposits (e.g., copper skarns) in shallow crustal settings and the common occurrence of smaller skarns (e.g., tungsten and tin skarns) in deeper environments (Meinert 1993).

The depth of magma emplacement also has a strong influence on the extent of contact metamorphism and circulation of skarn-forming fluids (Meinert 1983, 1993). Contact metamorphism is likely to be more extensive and of higher grade around an intrusion emplaced at deep crustal level than one formed at relatively shallow depth. Also, the higher temperatures of the country rocks at depth result in a slower cooling rate for the intrusion and thus maintain high contact metamorphic temperatures for a longer period of time. The depth of skarn formation also affects the induced permeability of the country rocks. In deeper environments, rocks tend to deform in a ductile manner, whereas shallow level intrusions greatly enhance the permeability of the wallrocks by hydrofracturing, and facilitate the circulation of not only the intrusion-related fluids but also of possibly cooler meteoric fluids. Thus, skarns formed at relatively deep crustal levels (e.g. many tungsten skarns such as the Pine Creek and Strawberry deposits of California, USA) tend to be small and vertical with extensive metamorphism and limited retrograde alteration, whereas skarns formed at shallower levels (e.g., skarns associated with porphyry copper systems) are generally large and massive with limited metamorphism and extensive retrograde alteration.

9.6.4. AGE DISTRIBUTION

The majority of skarn deposits are Mesozoic or younger in age; copper and zinc-lead skarn deposits, which in most cases represent a relatively shallow environment, are dominantly Tertiary in age. The few important Paleozoic examples are tin and tungsten skarns that probably represent relatively deep environments of formation. Archean skarns are both uncommon and uneconomic, while Proterozoic skarns are rare and found only in shield areas (Kwak 1987). Thus, the temporal distribution of skarn deposits is similar to that of porphyry copper-molybdenum deposits (Ch. 8), which are also rare in the Precambrian. The age distribution of skarn deposits probably reflects differences in

the level of erosion rather than an evolution of skarn-forming conditions with time (Einaudi et al. 1981). A contributing factor may have been the restricted occurrence of suitable carbonate rocks, especially in the early Precambrian. The higher proportion of calcic skarns compared with magnesian skarns in the Phanerozoic fold belts, according to Kwak (1987), may be attributed to an increase in the limestone:dolostone ratio in the post-Proterozoic sedimentary record.

9.6.5. PALEOTECTONIC SETTINGS

As skarn formation is directly related to igneous intrusions, the tectonic settings of skarn deposits are as varied as those for magma generation. On a global scale, skarns having similar compositional, but not necessarily mineralogic, characteristics occur in linear or oval-shaped belts, suggestive of a plate-tectonic control on their distribution. For example, belts containing W-Sn skarns coincide with areas of uplift within continents (e.g., Ural Mountains), continental subduction (e.g., North American Cordillera), and reactivated fold belts in Precambrian shields (e.g. Transbaikalia), and some of these can be rejoined in plate-tectonic reconstructions (Schuiling 1967, Hosking 1979, Kwak 1987). Plate-tectonic settings of the different subclasses of skarn deposits, however, are not well understood; the idealized models proposed by Meinert (1983, 1992) and presented in Figure 9.11 are quite speculative.

The distinctive characteristics of the calcic iron skarns — association with gabbroic and dioritic intrusions, abundant endoskarn, widespread sodium metasomatism, and the absence of Sn and Pb — indicate an affiliation with primitive oceanic crust and magmas. These skarns are interpreted to have formed in early orogenic island-arc terranes associated with steeply dipping subduction zones (Fig. 9.11a). In some cases, as in western North America, these terranes were subsequently accreted to growing continental margins (Meinert 1984). Some economic gold skarns appear to have formed in back-arc basins behind oceanic volcanic arcs, and some calcic and magnesian iron skarns, such as the Cornwall and Grace magnetite deposits in Pennsylvania (USA), are believed to have formed in rifted continental margins. At convergent margins, tin deposits are absent in island arcs but occur in areas underlain by thick clastic sequences in Cordilleran belts (Sillitoe 1981), implying a source for tin, and possibly for other accompanying metals, in continental crust (Hutchinson & Chakraborty 1978). The skarns associated with more felsic intrusions (granite to quartz monzonite, but also diorite) are related to magmatic arcs developed as a consequence of subduction beneath continental crust, as evidenced by the strontium and oxygen isotopic signatures of the plutons, and represent a more evolved orogenic environment. The skarn type formed in this tectonic environment is strongly influenced, in addition to the factors discussed earlier, by the angle of subduction. The angle of subduction may decrease with time (Coney & Reynolds 1977), producing a migration of the magmatic arc inland toward the craton and a change in the magma composition due to increasingly greater interaction with the continental crust.

Moderately-dipping subduction beneath continental crust (Fig. 9.11b), characteristic

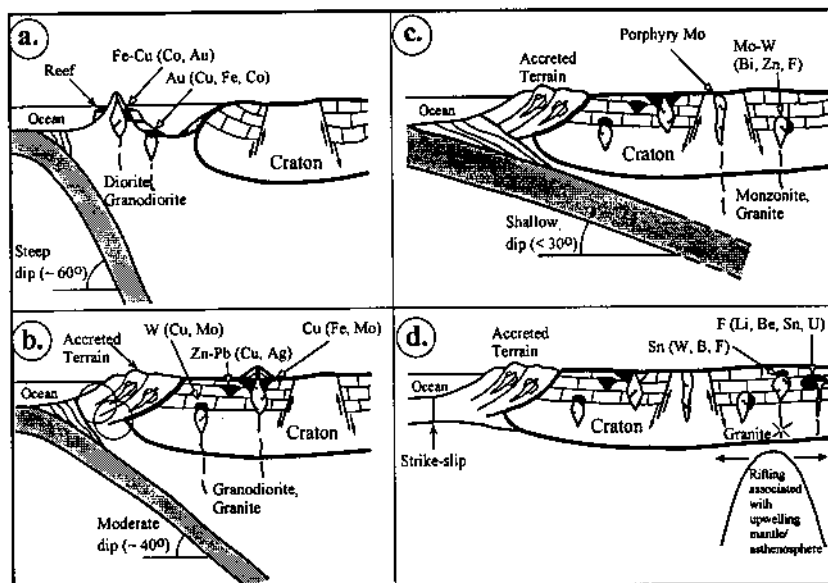


Figure 9.11. Idealized plate-tectonic models for the development of different skarn types: a. Oceanic subduction and back-arc basin environment; b. Continental subduction environment with accreted oceanic terrain; c. Transitional low-angle subduction environment; d. Post-subduction or continental rifting environment. (After Meinert 1992.)

of "middle" orogenic stage, causes the development of a dominantly I-type magmatic arc with plutons commonly of granodioritic to quartz monzonitic composition. Tungsten skarns (with subordinate Cu and Mo) are generally associated with magmas emplaced at relatively great depths (5 to 15 km), whereas copper skarns (with Fe and Mo) are generally associated with magmas emplaced at relatively shallow depths (1 to 6 km). Distal zinc-lead (-Cu-Ag) skarns may form in both settings.

During the transition to post-subduction tectonics, the magmatic arc may widen or migrate farther inland due to low subduction angles (Fig. 9.11c), and the intrusions can be of either I-type or S-type. Plutons are quartz monzonite to granite in composition and the associated skarns are rich in Mo or W-Mo, with appreciable amounts of Cu and Zn and minor amounts of Bi, Pb, Ag, and Au; zinc-lead skarns (with minor amounts of Ag and F) occur distal to the intrusives. Tin skarns (with W, Be, B, F) are associated with ilmenite-series granitoids of both I-type and S-type, more commonly the latter. Emplacement of these plutons is related either to a "late" orogenic stage following a major period of subduction or to incipient continental rifting (Fig. 9.11d).

A plate-tectonic model involving a landward migrating magmatic arc offers a reasonable explanation for the common occurrence of tin and tungsten skarns in the Pacific continental margin (eastern Australia, southern China, western North and South

America) as "paired" belts: W (-Mo-Cu) skarns associated with magnetite- and ilmenite-series granitoids on the oceanward side; and Sn (-W-Be) skarns associated with ilmenite-series granitoids on the landward side. However, it fails to explain the occurrence of paired belts within continents, such as in the former USSR (Kwak 1987).

9.7. Summary

Skarns are coarse-grained calc-silicate rocks formed from carbonate-rich rocks, commonly limestones and dolostones, by hydrothermal-metasomatic processes initiated by the emplacement of small- to medium-sized discordant plutons. A diagnostic feature of typical skarns is the 'primary' mineralogy, which is characterized by anhydrous Ca-Fe-Mg silicates, especially pyroxenes (wollastonite and members of the diopside-hedenbergite series) and garnets (members of the grossularite-andradite series with varying amounts of spessartine and almandine components), and some unusual minerals such as johannsenite, bustamite, ilvaite, and idocrase (vesuvianite). Skarn assemblages are commonly zoned relative to the igneous contact in terms of pyroxene:garnet ratio and the composition of these two minerals. The 'primary', generally high-temperature, skarn assemblages formed during the prograde stage of skarn formation is obliterated to varying degrees by superimposed retrograde alteration as the system cools.

Skarn deposits are mineral deposits of economic potential, which either are associated with skarns or, in the absence of typical skarn-type silicate gangue, can be shown to be genetically related to skarn-forming processes. Deposits of this class occur in a broad spectrum of geologic environments and range from Precambrian to late Tertiary in age; the majority of economic deposits, however, are Mesozoic or younger and occur in orogenic belts. Common general characteristics of skarn deposits include spatial association with igneous intrusions (which may not be apparent in the case of distal deposits) of granitic to dioritic in composition, high-temperature calc-silicate gangue minerals, ore emplacement by replacement of carbonate rocks, disseminated and vein-type mineralization, irregular form of orebodies, and alteration and mineralization zoning centered on the igneous intrusion (although the zoning pattern may be quite complex owing to superimposed events of mineral deposition). The bulk of the world's economic skarn deposits occurs in calcic exoskarns — skarns formed external to the intrusion, by replacement of limestone country rock.

The most important types of skarn deposits, on the basis of dominant economic metal, are those of iron (magnetite), copper (chalcopyrite \pm bornite), molybdenum (molybdenite), tungsten (scheelite), tin (cassiterite), gold (electrum), and zinc-lead (sphalerite - galena). In addition to distinctive metal associations, the different types of skarn deposits show a fairly systematic variation in skarn mineralogy, especially in terms of pyroxene and garnet compositions. The fundamental differences among the various skarn deposit types, however, are related to the composition and oxidation state of the cogenetic intrusion and the depth of magma emplacement, because these parameters determine the timing, amount, and composition of the aqueous fluids

exsolved from a magma.

The skarn assemblage and mineralization in a skarn deposit are products of the same hydrothermal system, the basic components of which are metal-enriched magmatic hydrothermal fluids, as is the case with porphyry deposits, and favorable country rocks in terms of permeability and chemical reactivity. The metasomatic stage of prograde skarn formation begins with the release of magmatic hydrothermal fluids from crystallizing plutons. The main period of sulfide-oxide ore deposition generally follows the cessation of skarn growth, mainly because of falling temperature, and is accompanied by the beginning of retrograde hydrothermal alteration of earlier skarn assemblages and of the associated pluton. Fluid inclusion and stable isotope ratios indicate an increasing involvement meteoric water as the skarn system evolves in time and space, although examples of systems with very little meteoric water mixing or with dominantly nonmagmatic water are known.

The metal contents of skarn-forming magmatic hydrothermal fluids are related to the composition and crystallization history of the associated plutons. The important variables are the source region of magma generation, oxidation state of the magma, depth of magma emplacement, and degree of magma crystallization when it becomes saturated in water. For example, copper skarns are associated with strongly oxidized, magnetite-series magmas emplaced at shallow levels in the Earth's crust, and are interpreted to have formed from hydrothermal fluids that separated before the magma had crystallized to a high degree. Tungsten skarns, on the other hand, are typically associated with more differentiated, reduced, ilmenite-series magmas emplaced at deeper levels, and appear to have formed from fluids that separated after a high degree of magma crystallization.

Compositional differences among the cogenetic intrusions for various types of skarn deposits are related to source regions of magma generation. Inferred plate-tectonic settings of skarn deposits range from oceanic subduction (iron skarns associated with gabbroic and dioritic intrusions), to continental subduction (copper, molybdenum, and tungsten skarns associated with orogenic, calc-alkaline quartz monzonites, granodiorites, and granites), to continental rifting (tin skarns associated with anorogenic granites), but the details are not well understood yet.

9.8. Recommended Reading

Einaudi et al. (1981), Ishihara (1981), Einaudi (1982a, b), Ray and Webster (1991), Meinert (1992, 1993).

CHAPTER 10

VOLCANIC-ASSOCIATED MASSIVE SULFIDE (VMS) DEPOSITS

10.1. Introduction

Massive Cu-Zn-Pb sulfide deposits in predominantly volcanic terranes have been variously termed as 'volcanic-associated', 'volcanic-hosted', and 'volcanogenic'. The term 'volcanic-hosted' is not entirely appropriate, because the deposits included in this class are not consistently hosted by volcanic rocks, nor do the deposits necessarily form as an integral part of the volcanic process as the term 'volcanogenic' implies. The term 'volcanic-associated' is considered more appropriate as it accommodates not only the deposits enclosed entirely within volcanic strata, but also those, such as the Besshi deposits (Japan), hosted by sedimentary rocks formed in a dominantly volcanic regime. The most important requirements of the volcanic-associated class of deposits are that penecontemporaneous volcanism must have accompanied the formation of the deposits, and that volcanic rocks must comprise an essential part of the immediate stratigraphic sequence (Franklin et al., 1981).

Volcanic-associated massive sulfide (VMS) deposits are a major contributor to the world's supply of copper, zinc, lead, silver, and gold, and a variety of byproducts including tin, cadmium, antimony, and bismuth. Individual deposits commonly contain 0.1 to 10 million tonnes of ore with combined Cu+Zn+Pb grades of <10% (Sangster 1971). The collective resources contained in VMS deposits are enormous, conservatively estimated as at least 3.6×10^7 tonnes of Cu, 8.6×10^7 tonnes of Zn, 2.2×10^7 tonnes of Pb, 6.3×10^{10} g of Ag, and 2.2×10^9 g of Au (Franklin et al. 1981).

VMS deposits have become a major focus of scientific studies since the discovery of active high-temperature (>300°C) hydrothermal vents in the ocean-floor ridge-rift systems in the eastern Pacific ocean (see Fig. 2.28). The literature on VMS deposits is very vast. Many articles provide reviews of descriptive and genetic aspects of this class of deposits (e.g., Sangster 1972, Hutchinson 1973, 1980, Lambert & Sato 1974, Solomon 1976, Sangster and Scott 1976, Gilmour 1976, Gale 1977, Klau & Large 1980, Finlow-Bates 1980, Franklin et al. 1981, Ohmoto & Skinner 1983, Stanton 1986, Lydon 1984a, 1988, Franklin 1986, 1993, and Leistel et al. 1998). Particular mention should be made of the excellent summaries by Franklin et al. (1981), Lydon (1984a, 1988), and Franklin (1986, 1993) which have contributed substantially to the discussion presented here.

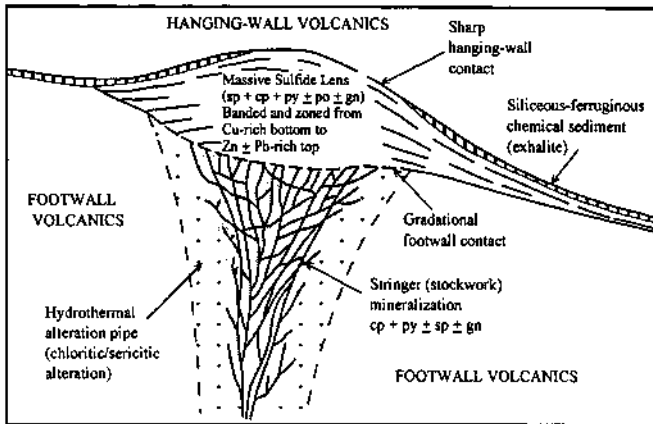


Figure 10.1. Schematic vertical section of an idealized proximal VMS deposit illustrating its essential characteristics (after Lydon 1984a). Mineral abbreviations: py = pyrite, po = pyrrhotite, cp = chalcopyrite, sp = sphalerite, gn = galena.

10.2. Distinguishing Features

The distinguishing features of an ideal VMS deposit may be summarized as follows (Fig. 10.1):

- (a) association with contemporaneous mafic and/or felsic volcanic rocks, including brecciated and pyroclastic variants, commonly localized at breaks in volcanism;
- (b) strata-bound to stratiform Fe-Cu-Zn±Pb sulfide mineralization, comprised of a generally concordant, bulbous lens of massive ore, having sharp contacts with hanging-wall rocks and gradational contacts with footwall rocks, and a discordant body of disseminated and stockwork ore (stringer zone) stratigraphically underlying the massive ore;
- (c) upward and lateral zonation of Cu (chalcopyrite) to Zn (sphalerite) and Pb (galena), with Fe-sulfides (pyrite and/or pyrrhotite) appearing in all zones and often forming a separate facies at the deposit margin;
- (d) common occurrence of Fe-rich, siliceous (and sometimes manganiferous) sediments, thought to represent chemical precipitation on the sea-floor (exhalites) during the waning stages of hydrothermal activity, capping the massive ore or occurring as lateral extensions of the massive ore; and
- (e) chloritic and sericitic alteration of the footwall rocks, commonly in discernible zonal patterns.

Strictly speaking, the above features are diagnostic of proximal VMS deposits that

have experienced little or only mild metamorphism and deformation. In the context of VMS deposits, which are believed to be formed at or near the sea-floor from hydrothermal fluids, proximal deposits refer to sulfide accumulation close to discharge vents. Distal VMS deposits, involving sulfide accumulation at some distance away from the hydrothermal vents, generally occur in a mixed sedimentary-volcanic pile, tend to be Cu-impoverished and pyrite-dominated, lack systematic metal zoning, and are not associated with a footwall alteration zone (Large 1977, Plimer 1978).

10.3. Distribution

VMS deposits occur in volcanic belts of submarine origin, emplaced in a wide spectrum of tectonic settings and ranging in age from Archean to Tertiary (Fig. 10.2, Table 10.1). Of particular importance are the Archean and early Proterozoic greenstone belts of the Canadian Shield, the Lower Paleozoic volcanic belts of the Caledonides in Scandinavia and the northern Appalachians of Newfoundland (Canada), the Upper Paleozoic Iberian pyrite belt extending from southern Portugal to southern Spain, and the Miocene Green Tuff belt of Japan.

Significant occurrences of VMS mineralization are found in greenstone belts of almost all Precambrian shield areas, but those of the Canadian Shield contain the largest concentration of VMS deposits, some 83 economic deposits in the younger

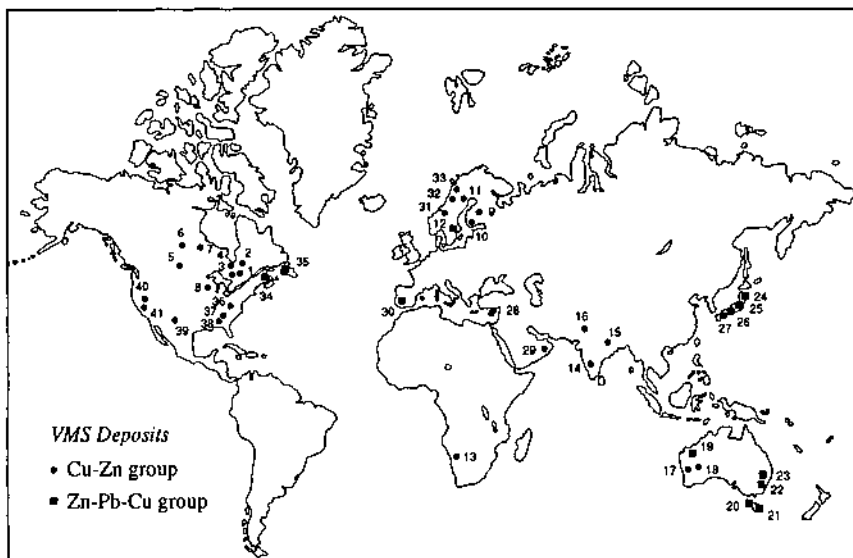


Figure 10.2. World distribution of important VMS districts and deposits. The numbers on the figure are cross-listed in Table 10.1.

TABLE 10.1. Important volcanic-associated massive sulfide deposits

	Age of host sequence	Important districts/deposits	Sulfide mineralization
Canadian Shield			
Abitibi greenstone belt	Archean	Noranda district (1): Corbet, Vauze, Norbec, Amulet, Waite, Millenbach, Horne, Delbridge (Fig. 10.8)	Zn-Cu
		Matagami district (2): Matagami Lake, Norita, Orchan	Zn-Cu
		Timmins district: Kidd Creek (3)	Zn-Cu (-Sn)
Wabigon greenstone belt	Archean	Sturgeon Lake district (4): Mattabi, Sturgeon Lake, Lyon Lake	Zn-Cu ± Pb
Flin Flon-Snow Lake belt	Proterozoic	Flin Flon district (5): Flin Flon, Coronation, Anderson Lake, Sherridon	Zn-Cu
Lynn Lake-Rusty Lake belt	Proterozoic	Fox Lake (6), Ruttan (7)	Zn-Cu
Rhineland-Ladysmith greenstone belt	Proterozoic?	Crandon (8), Flambeau, Pelican River, Thornapple	Zn-Cu
Fennoscandian Shield			
	Proterozoic	Outokumpu-Vihanti districts (9)	Cu-Zn
		Aijala-Orijarvi district (10)	Zn-Cu
		Skellefte district: Boliden (11)	Zn-Cu
		Bergslagen district: Falun (12)	Zn-Pb-Cu
African Shield	Proterozoic	Matchless Belt, Namibia (13)	Cu-Zn
Indian Shield			
Dharwar Supergroup	Archean	Ingladhal (14)	Cu
Singhbhum copper belt	Proterozoic	Singhbhum district (15): Musabani, Rakha	Cu-Zn
Khetri copper belt	Proterozoic	Khetri district (16): Madhan-Kudhan, Kolihan	Cu
Australian Shield			
Yilgarn Block	Archean	Golden Grove (17), Teutonic Bore (18)	Zn-Cu
Pilbara Block	Archean	Mons Cupri (19)	Zn-Pb-Cu
Tasman Geosyncline			
Western Tasmania	Cambrian	Rosebery (20), Mount Lyell (21)	Zn-Pb-Cu
New South Wales	Silurian	Captains Flat (22), Woodlawn (23)	Zn-Pb-Cu

TABLE 10.1 (continued)

	Age of host sequence	Important districts/deposits	Sulfide mineralization
Japan			
Green Tuff belt	Miocene	Hokurouku district (24): Doyashiki, Kosaka, Matsumine, Shaknai, Uchinotai	Zn-Pb-Cu
		Wagaomono district (25)	Zn-Pb-Cu
		Aizu district (26)	Zn-Pb-Cu
Sambagawa Schist belt	Paleozoic	Shikoku district (27): Besshi	Cu-Zn
Mediterranean-Alps Region			
Tethyan ophiolite belt	Mesozoic	Cyprus (28), Oman (29)	Cu-Zn
Spain-Portugal	Carboniferous	Iberian pyrite belt (30): Rio Tinto, Aznalcollar, Aljustrel, Salgadinho, Neves Corvo	Zn-Pb-Cu \pm Sn
Caledonides-Appalachians			
Scandinavia	Lr. Paleozoic	Trondheim district (31): Lokken, Killingdal	Zn-Cu
	Ordovician	Grong-Vasterbotten area (32): Skorovas, Stekenjokk, Joma, Sulitjelma district (33)	Zn-Cu
Newfoundland	Ordovician	Bathurst district (34): Heath Steele, Brunswick No. 12	Zn-Pb-Cu
	Silurian	Buchans district (35): MacLean, Lucky Strike, Rothemere	Zn-Pb-Cu
Southern Appalachians	Proterozoic	Gossan Lead district (36)	Cu-Zn
		Ducktown district (37)	Cu-Zn
		Pyriton district (38)	Cu-Zn
American Cordillera			
Arizona	Proterozoic	Jerome district (39): United Verde, United Verde Extension	Cu-Zn
California	Devonian	West Shasta district (40): Shasta, King, Balaklala, Mammoth, Iron King	Cu-Zn
	Devonian?	East Shasta district (41)	Cu-Zn

Sources of data: Anderson and Nash (1972), Vokes (1976), Klau and Large (1980), Franklin et al. (1981), Patwardhan and Oka (1984), Groves and Blatt (1984), Klemd et al. (1985), Thurston and Chivers (1990), Gaál and Parkkinen (1993), Leistel et al. (1998).

Archean (2.65 to 2.73 Ga) volcanic terrane (Lydon 1984a). The mean (and median) sizes and grades of 92 Canadian deposits are 5.6 million tonnes (1.177 million tonnes) containing 1.23% (1.01%) Cu, 3.60% (2.80%) Zn, 1.46% (0.97%) Pb, 2.0 g/t (0.5 g/t) Au, and 79.0 g/t (57.0 g/t) Ag (Franklin 1993). In contrast, greenstone belts of similar characteristics in other shield areas such as those of Australia, Africa, India, and Brazil, contain very few VMS deposits, although this may, at least in part, be an artifact of inadequate exploration.

Within individual belts, VMS deposits commonly occur in clusters and are probably related to volcanic centers. Most of the deposits in each cluster occur within a restricted stratigraphic interval (the 'favorable horizon'), which occupies only a fraction of the host volcanic sequence, and their localization appears to be controlled by topographical and structural features of the substrate.

10.4. Types of Deposits

Classification schemes proposed for VMS deposits (Table 10.2) are based on one or more of the following variables: ore composition, host-rock lithology, and tectonic setting. Those based solely on the bulk composition of ores are simpler, more reliable, and not subject to uncertainties in the interpretation of tectonic settings. A ternary Cu-Zn-Pb plot of bulk compositions of VMS deposits (Fig. 10.3) suggests a two-fold subdivision: (a) Cu-Zn deposits; and (b) Zn-Pb-Cu deposits. The division between the two groups, according to Franklin (1993), is at $Zn:(Zn+Pb) = 0.9$. This compositional grouping is similar to that proposed earlier by Hutchinson (1973) and Solomon (1976), except that no Cu-type is recognized. Some deposits do plot near the Cu-apex of the ternary plot, but this is probably because the uneconomic concentration of Zn in these deposits are usually ignored in reporting reserves. For example, none of the Cyprus deposits, commonly regarded as typical examples of the Cu-type, are devoid of sphalerite and in some cases their Zn content exceeds that of Cu. Thus, the Cu-rich ores may be considered a variant of the Cu-Zn group (Lydon 1984a). Deposits of the Cu-Zn group occur in two principal geologic settings: (a) Archean and Proterozoic greenstone belts, which are dominated by mafic volcanic rocks; and (b) Phanerozoic arc and back-arc sequences, which contain subequal amounts of mafic volcanic rocks and sedimentary strata. Deposits of the Zn-Pb-Cu group, overwhelmingly Phanerozoic in age, occur mostly in arc-related terranes with bimodal volcanism, where felsic volcanic rocks, with or without associated sedimentary strata, are dominant in the footwall sequences. As will be discussed later, the two-fold subdivision is also justified by a high degree of correlation with other features such as footwall alteration patterns, gangue mineralogy, and Ag:Cu and $^{34}S:^{32}S$ ratios, suggesting significant metallogenetic differences between the two compositional groups (Franklin et al. 1981, Lydon 1988). For the present treatment, VMS deposits are classified into two main groups — the Cu-Zn group, and the Zn-Pb-Cu group — and, for convenience of description, the Cu-Zn group is further subdivided into four types:

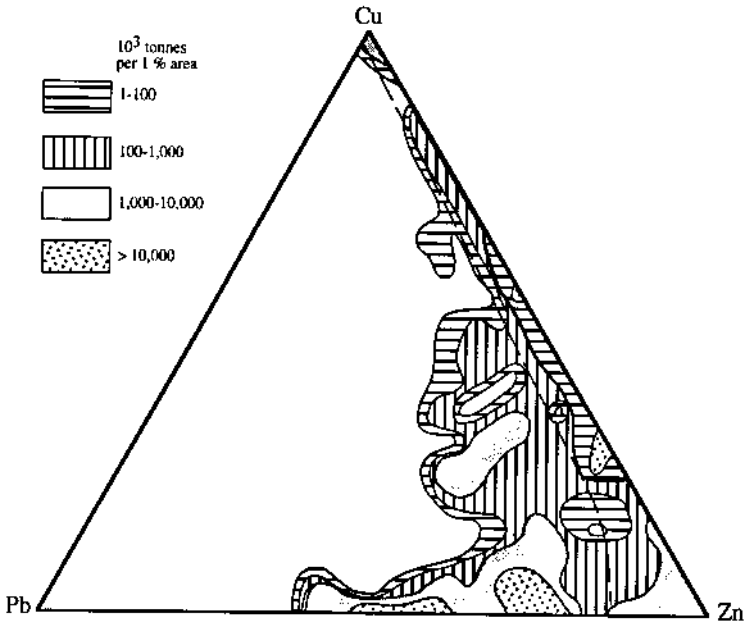


Figure 10.3. Cu-Zn-Pb ternary plot for bulk compositions of approximately 800 VMS deposits as reported in the literature, contoured for thousands of tonnes of contained (Cu+Zn+Pb) per 1% area of the plot (after Franklin 1993). The clustering of compositions suggest a two-fold subdivision of VMS deposits: a Cu-Zn group, and a Zn-Pb-Cu group.

(a) Cu-Zn Group

- (i) Noranda-type, hosted in mafic-felsic volcanic sequences
- (ii) Mattabi-type, similar to the Noranda-type but with significant Pb
- (iii) Cyprus-type, hosted by ophiolites
- (iv) Besshi-type, hosted by sediments in volcanic terranes

(b) Zn-Pb-Cu group (Kuroko-type deposits)

Estimated average grades of selected examples of the various types of VMS deposits are listed in Table 10.3.

10.4.1. NORANDA-TYPE AND MATTABI-TYPE DEPOSITS

The overwhelming majority of VMS deposits occur in the Archean and early Proterozoic greenstone belts. These deposits are hosted by thick volcanic sequences dominated by tholeiitic to calc-alkaline mafic-felsic rocks; the associated sedimentary rocks are immature greywackes and volcanic clastics. Based on volcanic environments, associated volcanic rocks, alteration mineral assemblages in footwall rocks, and metal

TABLE 10.2. Summary of recently proposed classification schemes for volcanic-associated massive sulfide deposits

Author(s)	Basis of classification	Classification scheme	Common host volcanic sequence	Typical examples	Inferred tectonic setting
Solomon (1976)	Ore composition	(a) Cu (-Au) (b) Zn-Cu (-Au-Ag) [Zn > Cu] (c) Zn-Pb-Cu (-Au-Ag) [Zn > Pb > Cu]	Ophiolite, calc-alkaline(?) Calc-alkaline Calc-alkaline	Cyprus, Rio Tinto Noranda, West Shasta Kuroko, Buchans	Tensional fracture systems related to island arcs and mid-ocean ridges
Sawkins (1976a)	Lithologic and inferred tectonic settings	(a) Cyprus-type (Cu-Au-Ag ± Zn) (b) Besshi-type (Cu-Zn-Au-Ag) (c) Kuroko-type (Cu-Zn-Au-Ag ± Pb)	Ophiolite Greywacke-basalt Calc-alkaline	Cyprus, Betts Cove Besshi, Killingdal Noranda, Kuroko, Buchans	Plate divergence Plate convergence (?) Subduction (island arc)
Klau and Large (1980)	Dominant host-rock lithology	(a) Hosted by mafic volcanics Cu (-Zn)-Au Zn-Cu, Cu-Zn (b) Hosted by mafic ± felsic volcanics Zn-Cu-Au (-Pb) (c) Hosted by felsic volcanics Zn-Pb-Cu (-Ag-Sn) Zn-Pb-Cu-Ag-Au (-Ba)	Ophiolite Tholeiitic basalt ± felsic volcanics Greenstone belts Bimodal basalt-rhyolite Calc-alkaline	Cyprus, Betts Cove, Bathurst Lokken, Besshi Noranda, Matagami Bathurst, Rio Tinto Kuroko, Buchans	Spreading center or back-arc basin Immature island arc Archean rift zones Continental rift Mature island arc
Hutchinson (1980) (revised version of Hutchinson 1973)	Ore composition and host-rock lithology	(a) Primitive type (Zn-Cu:Ag-Au) (b) Polymetallic type (Pb-Zn-Cu:Ag-Au) (c) Cupriferous pyrite type (Cu:Au) (d) Kisslager type (Cu-Zn:Au)	Basalt to rhyodacite Tholeiitic basalt, bimodal (?) suite, calc-alkaline Ophiolite, tholeiitic basalt Greywacke-mafic volcanics	Noranda, West Shasta Kuroko, Mt. Isa* Cyprus, Betts Cove Besshi, Ducktown	Subduction (island arc) Back-arc or post-arc spreading Oceanic rifting Fore-arc trough or trench
Franklin et al. (1981), Lydon (1984a), Franklin (1993)	Ore composition [Zn:(Zn+Pb) ratio]	(a) Cu-Zn (b) Zn-Pb-Cu	Mafic, mafic-felsic Felsic	Noranda, Cyprus Kuroko, Bathurst	Compressional and extensional settings

* Most authors consider Mt. Isa an example of sediment-hosted massive sulfide deposit (see Ch. 11)

TABLE 10.3. Average grades of selected volcanic-associated massive sulfide deposits/districts

	Cu wt %	Zn wt %	Pb wt %	Ag g/t	Au g/t	Ref
<i>Cyprus-type</i>						
Kalavassos, Troodos Massif, Cyprus	1.5	0.7	tr	5.7	1.6	1
Mavrovouni, Troodos Massif, Cyprus	4.2	0.5	n.s.	7.1	0.7	2
Ergani Maden, Turkey	10.0	n.s.	n.s.	21.9	1.4	2
Lokken, Norway	2.3	1.8	tr	16.0	n.s.	3
Outokumpu, Finland	3.8	1.1	n.s.	8.9	0.8	4
<i>Noranda-type and Mattabi-type</i>						
Lake Dufault, Noranda district, Canada	4.0	7.2	n.s.	62.4	0.8	2
Millenbach, Noranda district, Canada	3.4	4.2	n.s.	42.5	0.7	5
Vauze, Noranda district, Canada	2.9	0.9	n.s.	19.6	0.5	6
Corbet, Noranda district, Canada	2.9	2.0	n.s.	20.5	0.9	7
Mattagami Lake, Mattagami district, Canada	0.6	8.4	n.s.	29.0	0.5	5
Flin Flon, Flin Flon district, Canada	3.0	4.2	n.s.	35.4	2.5	6
Mattabi, Sturgeon Lake district, Canada	0.9	7.7	0.8	88.7	0.2	2
Kid Creek, Timmins district, Canada	2.5	6.0	0.2	63.0	n.s.	8
Jerome district (5 mines), USA	8.5	?	n.s.	70.9	1.9	2
Balakala, West Shasta district, USA	2.8	1.3	n.s.	28.3	0.8	2
Crandon, Wisconsin, USA	1.1	5.6	0.5	37.0	1.0	9
<i>Besshi-type</i>						
Besshi, Japan	2.5	0.3	n.s.	7.0	0.2	10
Ducktown district, USA	1.0	0.9	n.s.	3.0	0.3	10
Windy Craig, Canada	1.4	0.3	n.s.	4.0	0.2	10
Killingdal, Norway	1.9	5.9	n.s.	23.0	0.9	10
<i>Kuroko-type</i>						
Uchnotai, Kosaka mine, Japan						
Black ore (<i>Kuroko</i>)	1.4	18.3	9.4	646.0	2.1	11
Yellow ore (<i>Oko</i>)	5.4	0.2	0.3	27.0	0.7	
Siliceous ore (<i>Keiko</i>)	2.2	0.2	0.5	18.0	0.4	
Matsumine, Hanaoka mine, Japan						
Black ore (<i>Kuroko</i>)	2.9	11.3	3.0	209.3	1.3	12
Yellow ore (<i>Oko</i>)	3.2	0.7	0.3	27.9	0.5	
Pyrite ore (<i>Ryukako</i>)	0.2	0.2	0.1	9.5	0.3	
Buchans district, Canada	1.3	14.6	7.6	104.6	1.2	13
Heath Steele, Bathurst district, Canada	1.1	7.1	2.9	90.7	0.6	2
Brunswick #12, Bathurst district, Canada	0.3	8.6	3.5	70.0	n.s.	2
Rosebey, Tasmania, Australia	0.7	16.2	5.0	155.0	2.9	14
Hellyer, Tasmania, Australia	0.4	13.0	7.0	160.0	2.3	14
Que River, Tasmania, Australia	0.4	12.9	7.4	204.0	3.5	14
Rio Tinto, Iberian Pyrite Belt, Spain	0.4	0.3	0.1	22.0	0.4	15
Neves Corvo, Iberian Pyrite Belt, Portugal	3.1	4.1	0.7	37.0	n.s.	15

n.s. = not stated; tr = trace

(1) Spooner (1980), (2) Hutchinson (1973), (3) Grenne et al. (1980), (4) Gaál and Parkkinen (1993), (5) Edwards and Atkinson (1986), (6) Sangster and Scott (1976), (7) Knucky and Watkins (1982), (8) Franklin and Thorpe (1982), (9) Lambe and Rowe (1987), (10) Slack (1993), (11) Oshima et al. (1974), (12) Takahashi and Suga (1974), (13) Thurlow and Swanson (1981), (14) Huston and Large (1989), (15) Leistel et al. (1998).

ratios, Morton and Franklin (1987) recognized two types of deposits: the *Noranda-type*, named after the very important Noranda district of Quebec (Canada); and the *Mattabi-type*, named after the Mattabi deposit in the Sturgeon Lake district of Ontario (Canada).

The Noranda-type deposits are characterized by the following (Fig. 10.4): (a) a generally conformable bulbous or conical mound of massive sulfide; (b) a high ratio of mafic to felsic volcanic rocks in the footwall section (although the immediate footwall rocks may be felsic); (c) a general lack of primary, fragmental rocks and vesicular lavas, suggesting a water depth of more than 500 m for most of the footwall volcanic rocks (Gibson et al. 1986); (d) a well-defined and strongly zoned chloritic-sericitic alteration pipe beneath the deposits; and (e) a lower, poorly defined, semiconformable epidote - actinolite - quartz alteration zone. In some cases, the silica-rich footwall rocks actually represent metasomatized mafic flows and flow breccias (Gibson et al., 1983). Noteworthy examples of Noranda-type deposits, in addition to those of the Noranda district, include: Matagami, Quebec, Canada (Roberts 1975, Roberts & Reardon 1978, MacGeehan 1978, Costa et al. 1983); Flin Flon, Saskatchewan-Manitoba, Canada (Byers et al. 1965, Koo & Mossman 1975, Syme & Bailes 1993); Jerome, Arizona, USA (Anderson & Nash 1972), West Shasta, California, USA (Lindberg 1985, Albers & Bain 1985); Crandon, Wisconsin, USA (May & Schmidt 1982, Lambe & Rowe 1987); Khetri, Rajasthan, India (Patwardhan & Oka 1984); and Golden Grove and Teutonic Bore, Western Australia (Frater 1985 a, b, Barley 1992).

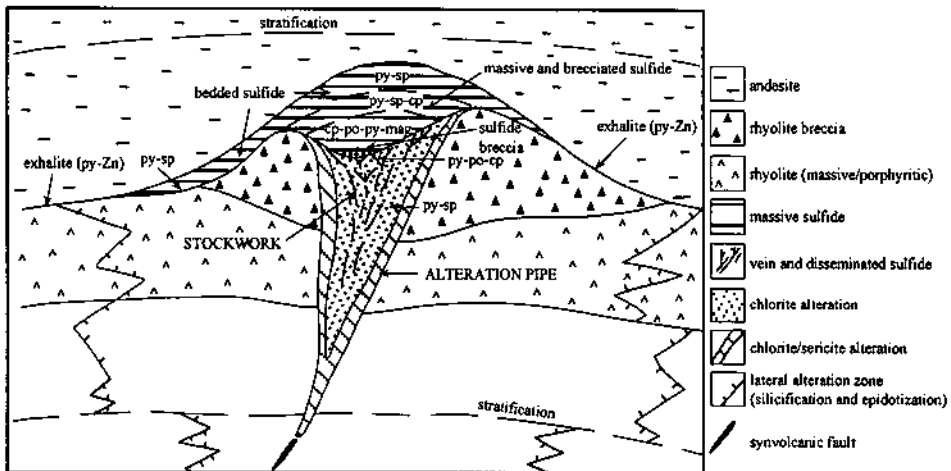


Figure 10.4. Generalized cross section of a typical Noranda-type VMS deposit (after Franklin 1993).

Compared with Noranda-type deposits, Mattabi-type deposits have higher contents of Pb and Ag (Table 10.3) and a much higher proportion of felsic volcanic rocks in the footwall. A semiconformable alteration zone is well developed in the footwall, but the alteration pipe is poorly defined. The footwall rocks contain an abundance of fragmental volcanic rocks that were probably emplaced at water depths of <500 m

(Groves et al. 1984). Only a few examples of this deposit type are known at present. The type example is the Matabi deposit (Franklin et al. 1975); the Kid Creek deposit of Canada may also belong to Matabi type (Franklin 1986).

10.4.2. CYPRUS-TYPE DEPOSITS

Cyprus-type VMS deposits, named after the well-documented deposits in Cyprus (Hutchinson & Searle 1971, Constantinou 1980), occur in the volcanic part of ophiolites and are considered to be the most convincing ancient analogs of sea-floor sulfide deposition at spreading centers (Spooner 1980, Herzig & Hannington 1995). VMS deposits associated with the Troodos ophiolite in Cyprus (see Fig. 5.6) are mostly small in size (<1 million tonne of ore), typically consisting of a strata-bound lens of massive sulfide located within or at the top of the pillow lava sequence and an underlying stringer zone of stockwork mineralization that may extend hundreds of meters below the massive sulfide horizon (Fig. 10.5). The footwall rocks show extensive alteration due to convective circulation of hydrothermal fluids (Parmentier & Spooner 1978). The hanging wall (the Perapadhi Formation) is a Fe-Mn-rich sediment (iron-formation), which may be directly related to hydrothermal activity associated with submarine volcanism (Elderfeld et al. 1972). The sulfide assemblage is composed predominantly of pyrite and chalcopyrite, with variable amounts of sphalerite.

Similar deposits have been described from ophiolites in Newfoundland (Bachinski 1977, Upadhyay & Strong 1980), Oman (Alabaster & Pearce 1975), Turkey (Griffiths et al. 1972), the Norwegian Caledonides (e.g., Løkken, Grenne 1986; Høydal, Grenne & Vokes 1990; Sulitjelma, Cook et al. 1990), and the Ural Mountains. The Løkken deposit (Grenne 1986, 1989), which recently reached the end of its economic life after a production history of 333 years, is probably the largest known ophiolite-hosted sulfide

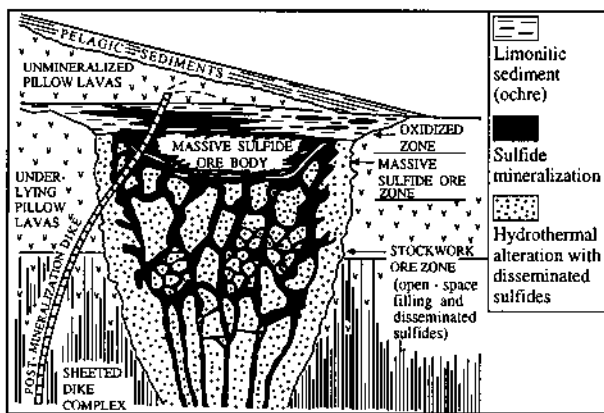


Figure 10.5. Schematic vertical section of an ophiolite-hosted Cyprus-type VMS deposit (after Hutchinson & Searle 1971).

deposit in the world (original ore \approx 25 to 30 million tonnes with an average grade of 2.3% Cu, 1.8% Zn, 0.02% Pb, and 16 ppm Ag; Grenne et al. 1980). It is estimated that the deposit, now folded and tectonically disrupted into one major and several smaller tabular bodies, originally had a skewed lensoid cross-section morphology, with maximum thickness and width of approximately 60 m and 400 m, respectively, and a strike length in excess of 4 km. The Cu-Zn deposits of the Outokumpu district (Fennoscandian Shield), interpreted as Besshi-type by Fox (1984), may represent examples of early Proterozoic Cyprus-type deposits (Gaál & Parkkinen 1993).

10.4.3. BESSHI-TYPE DEPOSITS

The typical example of *Besshi-type* Cu-Zn deposits is the Besshi deposit in Japan. It is the largest of more than a hundred deposits of essentially similar characteristics in the Sanbagawa Schist Belt of Japan, which are hosted by clastic metasedimentary rocks (metapelite and metagreywacke) with variable amounts of associated tholeiitic metabasalt (greenstone, amphibolite) (Hutchinson 1980, Slack & Shanks 1989, Slack 1993). In some cases, such as the Matchless deposit (Namibia), the host chlorite- and biotite-rich schists represent tholeiitic basalt that was extensively altered by submarine hydrothermal fluids during the formation of the massive sulfide mineralization (Klemd et al. 1989). Most Besshi-type deposits contain 3-30 million metric tonnes of ore with grades of 1-3% Cu and practically no lead. Zn contents range from 0.3-0.9% in the Besshi deposit to as high as 5.9% in the Killingdal deposit (Norway), but are usually low. The deposits generally lack a well-defined footwall feeder zone, but the wallrocks commonly include unusual lithologies (e.g., beds or lenses of quartzite or chert, magnetite-bearing iron-formation, quartz-spessartine rock or "coticule", albitite, tourmalinite, and chlorite- and sericite-rich schist), which are believed to have formed by subsea-floor alteration of clastic sediments and/or as exhalative precipitates (Kanehira & Tatsumi 1970, Slack & Shanks 1989). Other characteristics of this deposit type are a broad range of sulfide $\delta^{34}\text{S}$ values (about -2 to $+12\%$), implying both magmatic and seawater sulfur, and a spread of lead isotope ratios, indicating that the lead (and probably other metals) in the ores were derived from both basaltic and sedimentary sources. Sulfide accumulations around submarine hydrothermal discharge centers in the Guaymas basin probably represent modern analogs of Besshi-type deposits (Scott 1985).

Suggested examples of Besshi-type deposits, in addition to those in Japan, include some deposits in the Norwegian Caledonides (e.g., Joma, Killingdal), the Blue Ridge belt of the Southern Appalachians (e.g., Ducktown, Ore Knob, Gossan Lead), British Columbia (e.g., Anyox, Windy Craggy), and the Matchless deposit, Namibia (Fox 1984, Breitkopf & Maiden 1988, Slack & Shanks 1989). The deposits encompass a continuum of geologic settings, ranging from almost entirely clastic metasedimentary rocks (e.g., Ducktown), to metasedimentary sequences with minor felsic metavolcanic rocks (e.g., Anyox), to sequences with abundant metavolcanic rocks (e.g., Matchless). Thus, Besshi-type deposits were emplaced in a variety of tectonic environments.

The massive sulfide deposits of the Kieselager district in the eastern Alps of Austria and Italy are similar to the Besshi deposits in terms of association with metasediments, morphology of ore bodies and ore composition (Klau & Large 1980, Hutchinson 1980). The association of Kieselager deposits with ophiolitic volcanic rocks, however, raises the possibility that they may be a distal variety of Cyprus-type deposits (Franklin et al. 1981).

10.4.4. KUROKO-TYPE DEPOSITS

The type examples of *Kuroko-type* VMS deposits are the practically undeformed and only slightly metamorphosed Kuroko deposits located in the Green Tuff belt of Japan (Fig. 10.6), so named because of the greenish color of the rocks imparted by low-grade hydrothermal alteration or zeolite facies metamorphism. The belt, more than 1,500-km-long, represents a back-arc trough that forms the inner zone of island arcs (the Kurile, Honshu, Izu-Bonin-Mariana, and Ryukyu arcs) and consists of up to 3,000 m of volcanic and sedimentary rocks. The assemblage is a product of the tectonic and igneous activity that accompanied the formation of the Sea of Japan and the Japanese islands during the period from ≈ 65 Ma to the present (Ohmoto 1983). The volcanic and sedimentary accumulations occurred predominantly during the Miocene, in fault-controlled subsidence basins in tensional environments (Sato 1974). Volcanism was most intense and andesitic during the early Miocene, then gradually diminished in intensity and changed from andesitic to bimodal (basaltic and rhyolitic) in composition before becoming very weak and andesitic during the Pleistocene (Ohmoto & Takahashi 1983). The majority of the Kuroko deposits were formed at seawater depths in excess of 2,000 m (Pisutha-Arnond & Ohmoto 1983) during the span of bimodal volcanism in Middle Miocene. In contrast to other types of VMS deposits, the Kuroko deposits are hosted by sequences composed dominantly or entirely of felsic rocks (lavas, breccias, and tuffs). Another characteristic, but not universal, feature of the Kuroko deposits is their association with rhyolitic domes.

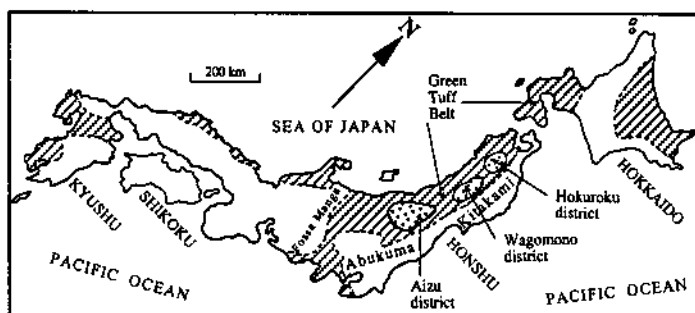


Figure 10.6. The principal districts of Kuroko-type VMS deposits in the Miocene Green Tuff belt of Japan (after Sato 1974).

Due to a lack of intense deformation in the Green Tuff belt, the orebodies maintain their original depositional characteristics. Individual mines commonly consist of a number of closely clustered ore deposits. The size of the orebodies range from less than 1 million tonnes of ore to ≈ 60 million tonnes of ore in the Matsumine mine, the largest orebody in the Green Tuff belt, with a median size of 1.3 million tonnes of ore.

'Kuroko', an old mining term in Japanese for "black ore", refers *sensu stricto* to a massive sulfide ore consisting mostly of sphalerite and galena. The term *Kuroko deposits* is currently used in a broader sense for Miocene-age deposits in the Green Tuff belt that contain not only massive black ore but also other types of ore, commonly in an orderly succession (Fig. 10.7). As discussed by Sato (1974), an idealized Kuroko deposit has seven mineralogic zones which, in ascending order, are listed below.

- (a) Siliceous ore (*Keiko*): pyrite - chalcopyrite - quartz stockwork ore.
- (b) Gypsum ore (*Sekkoko*): gypsum - anhydrite (- pyrite - chalcopyrite - sphalerite - galena - quartz - clay minerals) ore, usually strata-bound but also as veins, occurring on top of or beside siliceous ore, or beside yellow ore.
- (c) Pyrite ore (*Ryukako*): pyrite (- chalcopyrite - quartz) ore, mostly stratiform but occasionally as veins and disseminations.
- (d) Yellow ore (*Okoko*): pyrite - chalcopyrite (- sphalerite - barite - quartz) stratiform ore.
- (e) Black ore (*Kuroko*): sphalerite - galena - pyrite - barite \pm chalcopyrite stratiform ore, with significant amounts of tetrahedrite-tennantite toward the top of the zone and abundant bornite in some deposits.
- (f) Barite ore: thin, well-stratified, bedded ore consisting almost entirely of barite, but sometimes with minor amounts of carbonates (calcite, dolomite, and siderite).
- (g) Ferruginous chert (*tetsusekiei* bed): a thin bed of cryptocrystalline quartz and hematite, with variable amounts of pyrite, clay minerals, magnetite, and braunite.

A few deposits (e.g., Matsumine, Uchinotai, Shakanai No. 4) essentially have all of the above mentioned zones, but most lack one or more of the zones.

Many felsic volcanic-associated massive Zn-Pb-Cu deposits around the world are now interpreted as Kuroko-type deposits. Notable examples are the deposits of the Iberian pyrite belt (Strauss & Gray 1986, Leistel et al 1998), the Tasman geosyncline (Lambert 1979), the Bathurst district of New Brunswick, Canada (Jambor 1979, Davies & McAllister 1980), and the unusually high grade deposits of the Buchans district, Newfoundland, Canada (Thurlow et al. 1975). Every deposit, however, does not show all the diagnostic features of the Japanese Kuroko deposits. For example, the Bathurst and Iberian deposits occur in volcano-sedimentary terranes, are tabular bodies with no association with rhyolite domes, and do not exhibit the pronounced metal zoning of the Kuroko deposits. With more than 80 known deposits and sulfide resources (ore mined + reserves) in excess of 1,700 million tonnes of ore (containing 14.6 Mt Cu, 13.0 Mt

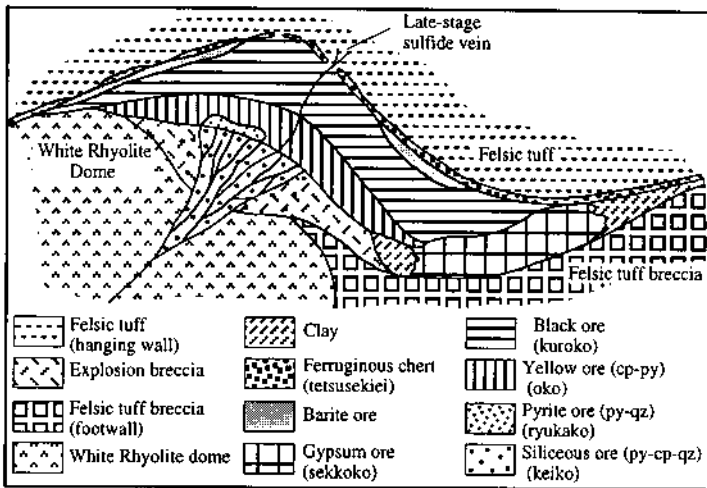


Figure 10.7. Schematic vertical section of an idealized Kuroko deposit (after Sato 1974, Franklin et al. 1981, Eldridge et al. 1983). Mineral abbreviations: sp = sphalerite, gn = galena, cp = chalcopyrite, py = pyrite, ba = barite, qz = quartz.

Pb, 34.9 Mt Zn, 46.1 Kt Ag, and 880 t Au), the Iberian pyrite belt is truly a giant among Kuroko-type deposits. The Neves Corvo deposit alone is comparable to the total of all the deposits in the Canadian and Australian provinces (Leistel et al. 1998).

10.5. Examples

10.5.1. ABITIBI GREENSTONE BELT, CANADIAN SHIELD

The Archean Abitibi greenstone belt (Fig. 10.8) in the Superior Province is the largest single contiguous greenstone belt in the Canadian Shield and one of the world's richest mining areas. It has been a major producer of gold, copper, zinc, silver, and iron ore over the last 100 years. The belt is composed of several major mafic-to-felsic volcanic cycles, coeval intrusions ranging from peridotite to granite, and clastic to chemical sedimentary rocks. The volcanic and sedimentary rocks have been regionally metamorphosed to greenschist facies and deformed by isoclinal folding with easterly axes. The granitic plutons have been emplaced preferentially along anticlinal fold axes.

Volcanic rocks and related intrusions (mostly granitic) constitute about 80% of the Abitibi belt. Of the volcanic sequences, 70% are tholeiitic and 25% are calc-alkaline; komatiitic and alkalic variants make up the rest (Goodwin & Ridler 1970, Card 1990). For the belt as a whole, felsic volcanic rocks are much less abundant than mafic volcanic rocks, but the massive sulfide deposits tend to be localized in the "rhyolites"

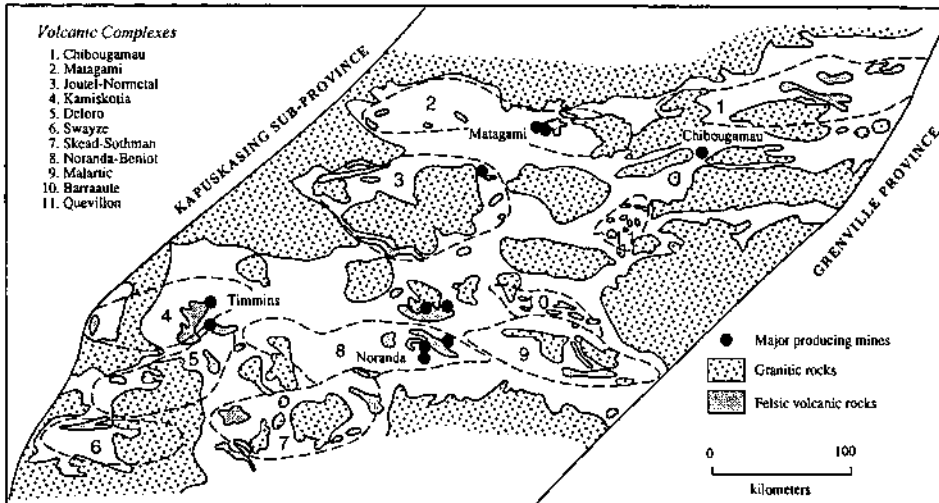


Figure 10.8. Distribution of felsic volcanic complexes and major VMS mining districts in the Abitibi greenstone belt, Superior Province, Canadian Shield (compiled from Goodwin & Ridler 1970, Sangster & Scott 1976, and Franklin et al. 1981).

of presumably calc-alkaline sequences. Significant VMS deposits occur only in four of the eleven volcanic centers delineated by Goodwin and Ridler (1970) (Fig. 10.8).

The most impressive of the VMS deposits in the Abitibi belt is the giant Kidd Creek deposit in the Timmins mining district, described as the world's largest single producer of Zn, Cd, and Ag (Walker et al. 1975). The Timmins district is also well known for its mesothermal gold mineralization (see Ch. 16). The Noranda district in Quebec has the largest cluster of VMS deposits in the Abitibi belt (Fig. 10.9). The deposits occur within a pile of andesites and rhyolites that form the upper part of the Blake River Group, a sequence of submarine volcanic rocks with an apparent stratigraphic thickness of 13.5 km, the base of which is composed of dominantly tholeiitic units (Baragar 1968, Ludden et al. 1986). Two major granitic bodies, the Flavrian Lake Granite and the Lake Dufault Granodiorite, intrude the volcanic sequence. The age (2710 Ma; Krough & Davis 1971) and chemical composition of the Flavrian Lake Granite are very similar to those of the rhyolites.

The andesite-rhyolite sequence of the Noranda district has been subdivided into five zones (Spence & de Rosen-Spence 1975), each represented by a major episode of felsic volcanism (rhyolite with minor dacite) and all separated from one another by periods of andesitic volcanism (with minor basalt). The VMS deposits occur in the upper three zones, most of them within a rather restricted stratigraphic interval enclosed between the top of the Amulet Rhyolite and a couple of hundred meters above the base of the Amulet Andesite (Fig. 10.10). The deposits are hosted by both felsic and mafic

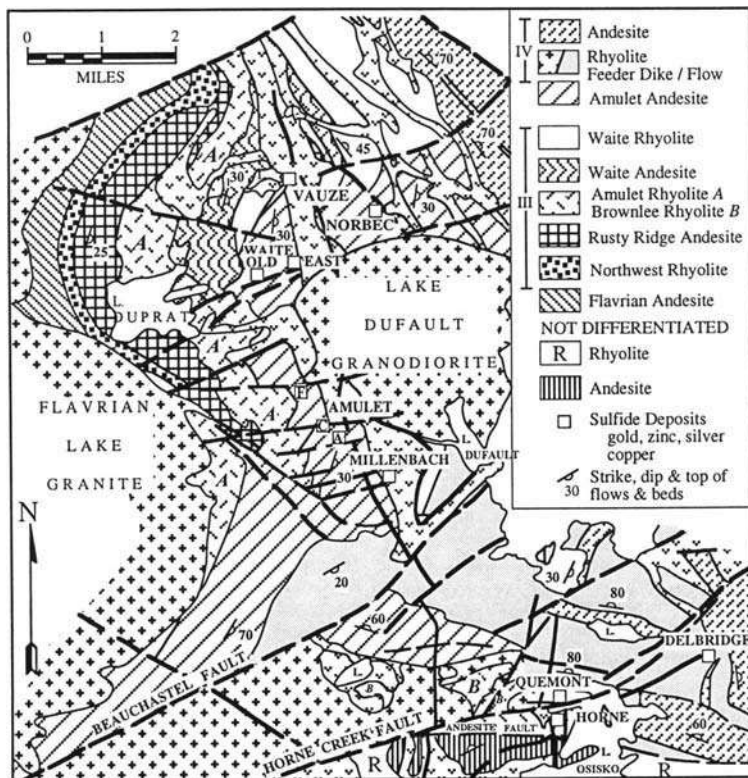


Figure 10.9. Geology of the central part of the Noranda district, Abitibi greenstone belt, with locations of major VMS Cu-Zn deposits (after Spence & de Rosen-Spence 1975). Groups III and IV refer to felsic volcanic cycles in the Noranda district (see Fig. 10.10).

rocks, but andesitic hanging-wall and felsic footwall are more common. According to Gibson et al. (1983), much of the upper part of the Amulet Rhyolite actually represents silicified mafic volcanic rock; thus, many more of the deposits may have a predominantly mafic footwall as well.

The deposits of the district range in size from <1 million tonnes to >10 million tonnes of Cu-Zn ore, often with recoverable amounts of gold and silver. They are typically associated with a felsic assemblage of massive, probably flow, rhyolite (quartz-feldspar porphyry) and explosive rhyolite breccia (Spence & de Rosen-Spence 1975). The strata-bound massive sulfide lenses characteristically overlie well-defined, and often mineralogically zoned, footwall pipes of chloritic-sericitic alteration with stockwork sulfide mineralization. Within the contact aureole of the Lake Dufault Granodiorite, the alteration products have been transformed into spotted hornfels with a

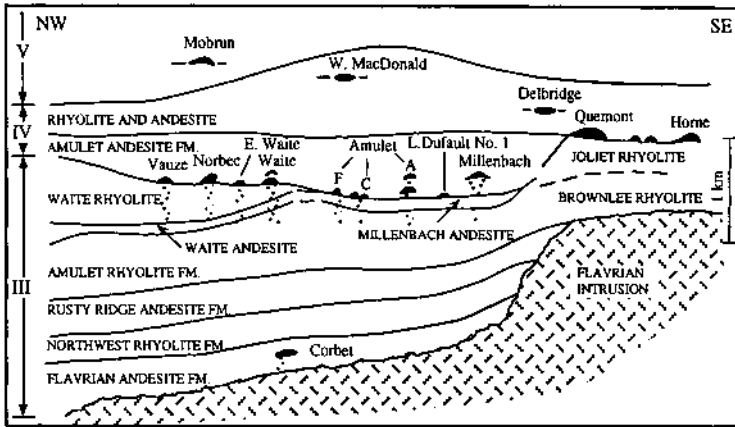


Figure 10.10. A composite stratigraphic section of the Noranda district, Abitibi greenstone belt, showing the preferential localization of VMS deposits (compiled by Franklin et al. 1981). Zones III, IV, and V are the upper three volcanic felsic-mafic volcanic cycles of the Blake River Group as defined by Spence and de Rosen-Spence (1975). Note that most of the deposits lie at or close to the uppermost rhyolite unit of Zone III.

cordierite - andalusite assemblage and spotted texture. In many cases, the massive sulfide lens is associated with a sedimentary layer, locally called "tuffsite" or "tuffaceous exhalite", which is composed of variable amounts of sulfides, tuffs, and chemical sediments, indicating a significant hiatus in volcanism. The persistence of this layer for tens to hundreds of kilometers beyond the sulfide ores is a useful exploration guide in the Noranda district. The Millenbach deposit (Fig. 10.11), described by Simmons (1973) and Riverin and Hodgson (1980), is a representative example of the Noranda-type deposits. It consists of several discrete bodies of massive sulfide, each underlain by a zone of stockwork mineralization. The known reserves are on the order of 3 million tonnes of ore averaging about 3.5% Cu and 4.5% Zn.

10.5.2. HOKUROKU DISTRICT, GREEN TUFF BELT, JAPAN

All major Kuroko-type deposits in Japan are located in the Green Tuff belt, overwhelmingly within the so-called "Kuroko zone", which occupies the central strip of northeastern Honshu island. The zone includes several mining districts (see Fig. 10.6), which appear in many cases to have been topographic depressions at the time of mineralization. About 85% of the known reserves occur within the Hokuroku district, situated primarily within the Middle Miocene Hokuroku basin. The total amount of ore in this district is estimated to be approximately 140 million tons, with an average grade of 1.6% Cu, 3.0% Zn, and 0.8% Pb (Tanimura et al. 1983). The disposition of the orebodies in a broad ring toward the outer edge of the basin (Fig. 10.12) has been

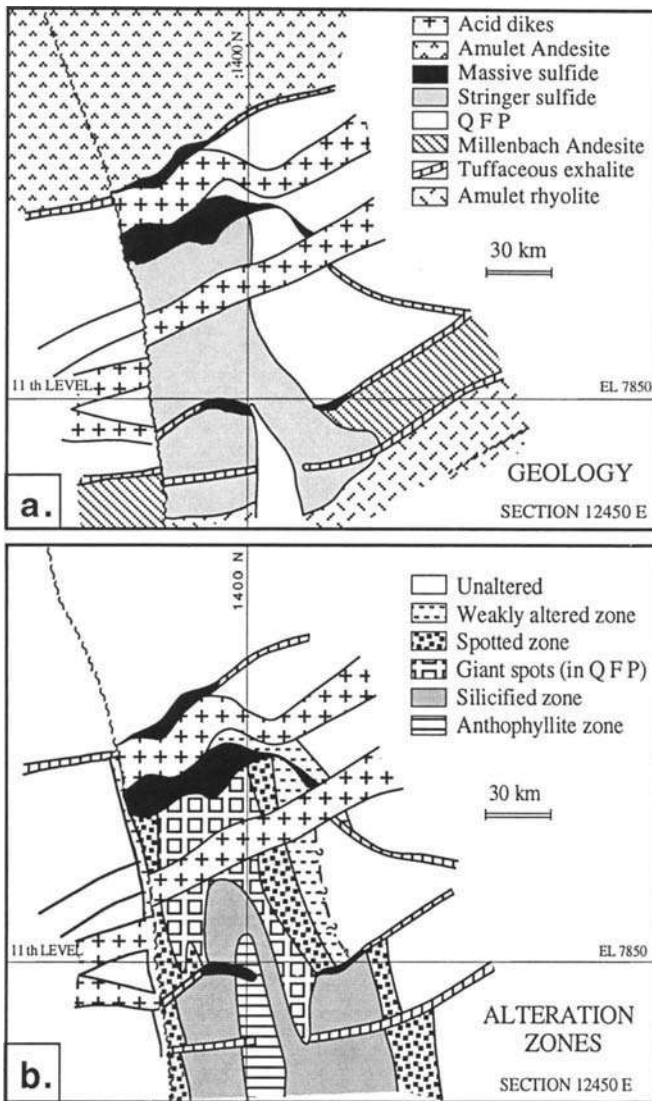


Figure 10.11. Main lens area of the Millenbach deposit, Noranda district, Canada: a. Geological section 12450E; and b. Alteration zones on geological section 12450E (after Riverin & Hodgson 1980). The rocks with spotted texture are contact metamorphic hornfels, locally known as "dalmatianite". Q F P = quartz-feldspar porphyry.

attributed to a conjugate set of basement fractures that controlled the emplacement of the sulfide deposits and their host felsic volcanic rocks (Scott 1978, 1980), or to the development of a resurgent submarine caldera (Ohmoto & Takahashi 1983).

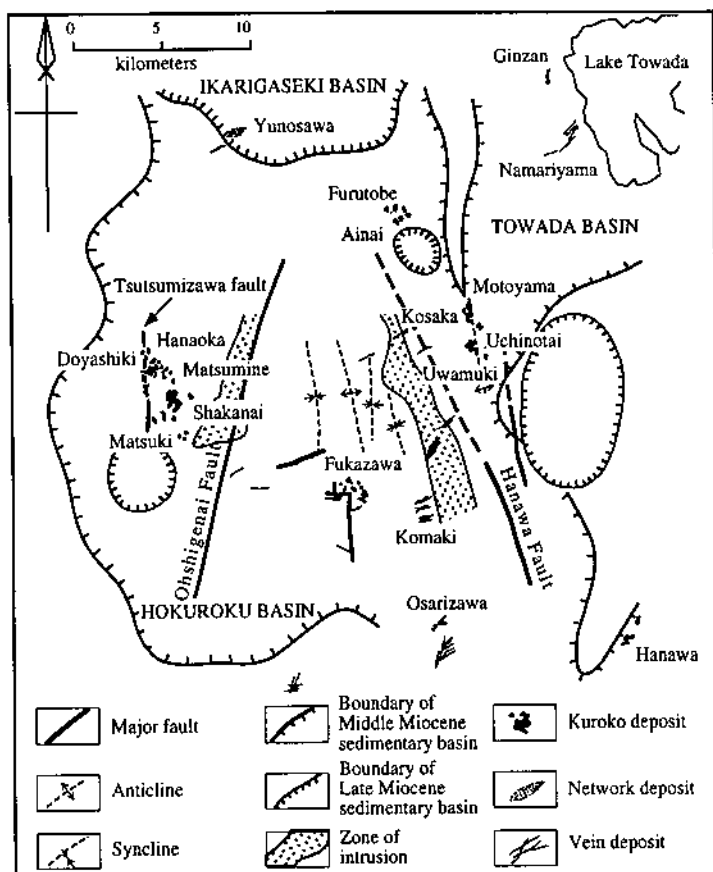


Figure 10.12. Distribution of principal Kuroko-type VMS deposits in the Hokuroku district, Japan, in relation to the Miocene sedimentary basins and major structures (after Sato et al. 1974).

The Miocene Green Tuff strata are divisible into four principal stages: the Monzen stage; the Daijima stage, the Nishikurosawa stage, and the Onnagawa stage. Most of the mineable deposits of the Hokuroku district occur at or near the top of the Nishikurosawa stage, which is represented in the district by a relatively thin (50-600 m) formation of felsic (rhyolitic to dacitic) volcanic rocks and mudstone. The felsic volcanic rocks occur as small domes, but are much more abundant as volcanoclastic products of explosive activity (tuffs, tuff breccias, and volcanic breccias). Most of the orebodies lie above a persistent bed of fragmental rock with "white rhyolite" domes (Fig. 10.7). The Monzen stage contains a thick pile of andesite, and

basalt occurs in significant amounts in the lower Nishikurosawa as well as in the hanging-wall of some of the deposits, but nowhere in the district are mafic rocks found in the immediate footwall sequence. Occasionally (e.g., in the Matsuki mine, which contains about 10 million tonnes of ore), the ore occurs in mudstone and is well removed from felsic Tuff belt spanned a period of about 5 million years (from 16 to 11 Ma), but much of the mineralization probably occurred during a small interval around 13 m.y. ago (Sato 1974, Ohmoto 1983, Cathles et al. 1983) or around 15 m.y. ago (Horikoshi 1990).

Many, but not all, Kuroko deposits occur at the flanks of small-scale "white rhyolite" domes, which commonly are not more than several hundred meters in diameter. "White rhyolite" is a term used by local mining geologists to describe a phenocryst-poor, massive but brecciated, rhyolitic rock now altered to a quartz-sericite rock of white to light-gray color (Matsukuma & Horikoshi 1970). It was previously believed that mineralization occurred after the emplacement of the rhyolite domes, but many geologists in Japan now interpret that the ores accumulated originally in submarine depressions, and that the extrusion of rhyolite domes onto the sea-floor occurred during and after mineralization. The doming was a major cause of deformation and clastic textures of the ores but not of the initial deposition (Ohmoto & Skinner 1983). A characteristic feature of the Hokuroku basin is the pervasive zeolitic and argillic alteration of the rocks, which is most intensely developed within the ore-bearing upper Nishikurosawa stage, particularly in the immediate vicinity of the ore deposits (Iijima 1974). The overall aspect of the basin is a fossil geothermal field with discharge points represented by the ore deposits (Scott 1980).

Ore deposits in the Hokuroku district, as in other parts of the Green Tuff belt, occur in clusters that appear to be related to centers of felsic volcanic activity (Ohmoto & Takahashi 1983). For example, the Kosaka mine encompasses a cluster of six known deposits and the Shakanai mine has at least seven (Lambert & Sato 1974). Orebodies within an ore cluster are contemporaneous, but the different clusters in the Hokuroku district are not, and the same may be the case in other Kuroko districts. The Kosaka mine deposits — Motoyama, Uchinotai Western, Uchinotai Eastern, Uwamuki No. 1, Uwamuki No. 2, and Uwamuki No. 4 — are the most typical of Kuroko deposits in the Green Tuff belt (Oshima et al. 1974). Taken together, they show the characteristic mineralogic-compositional zoning of the Kuroko deposits (see Fig. 10.7), but all the zones are not well developed in each deposit.

10.6. Ore Composition

10.6.1. MINERALOGY AND TEXTURES

A typical proximal VMS deposit is characterized by a zone of massive ore, generally lensoid in cross section and consisting of at least 50% sulfides by volume, underlain by a zone of stringer ore containing less than 25% sulfides by volume. Mineralogic,

textural, and compositional zoning in VMS deposits bear a close correspondence to this morphologic zoning.

The massive ore zone, with invariably sharp contact with stratigraphic hanging-wall rocks and generally diffuse contact with footwall rocks, is essentially composed of discontinuously banded and brecciated ore of Fe-sulfides (pyrite + pyrrhotite) - chalcopyrite - sphalerite \pm galena. A wide variety of accessory ore and silicate minerals have been identified in the massive ores, including magnetite (e.g., Ansil, Quebec), bornite (e.g., Kidd Creek), native silver, native gold, electrum, Ag-sulfides, and Ag-bearing sulfosalts (Matsukuma & Horikoshi 1970, Shimazaki 1974, Vokes 1976, Sangster & Scott 1976). Gahnite is an accessory mineral in virtually all deposits metamorphosed to amphibolite facies.

Fe-sulfides are invariably the most abundant ore minerals in typical massive ores of Cu-Zn deposits, although the pyrite:pyrrhotite ratio varies greatly among deposits and even between different parts of the same deposit. Pyrrhotite in these deposits has been considered to be mainly a product of metamorphism (Vokes 1976, Sangster & Scott 1976), but it may be a primary mineral (Plimer & Finlow-Bates 1978), because deposits in some metamorphic belts do not show a correlation between the pyrite:(pyrrhotite + pyrite) ratio and grade of metamorphism (Rui & Bakke 1975, Misra 1992). Finlow-Bates (1978) has suggested that the primary pyrite:pyrrhotite ratio in submarine exhalative deposits may be a function of the depth of the sea-floor. The FeS content of sphalerite tends to increase with the grade of metamorphism and provides a potential geobarometer for these deposits (see Ch. 3).

The massive sulfide ores of the Kuroko-type deposits (the *Kuroko* or black ore) is characterized by the absence of pyrrhotite, except as a contact metamorphic product near the contacts of post-ore dikes, and an abundance of galena, especially at the top part of the massive ore zone. Other important constituents of the 'black ore' are bornite and tetrahedrite-tennantite, which are rarely more than accessory minerals in the Cu-Zn group of VMS deposits, and barite, which is found in very few Cu-Zn deposits. The barite ore and the bedded anhydrite-gypsum-pyrite ore (*Sekkoko*) of the Kuroko deposits have no equivalents in the Cu-Zn group. Compared with the Cu-Zn group, ores of the Zn-Pb-Cu group are fine-grained and intergrown, which causes recovery problems during processing.

The stringer ore zone is present in most, but not all, VMS deposits. Where present, it is a mappable unit of cylindrical to conical shape, consisting of anastomosing veinlets, veins, and irregular replacement bodies of sulfide and quartz. The sulfide mineralogy is dominated by chalcopyrite and pyrite; the accessory minerals are normally the sulfide and sulfate minerals found in the overlying massive ores. In undeformed deposits, ore-grade material in the stringer zone is almost always in contact with the massive ore, and sulfide mineralization of diminishing intensity may continue downward for several tens of meters before reaching background values of the host rock.

Textures and structures of massive ores believed to be primary depositional features are best preserved in the relatively young deposits and are particularly well documented in the nearly undeformed Kuroko deposits of Japan. These include framboidal and

colloidal pyrite, compositional banding expressed as monomineralic layers of sphalerite and pyrite in the sphalerite-rich portions of the massive ore, soft-sediment slump folding, flame structures and load casts, graded beds and cross-beds, and fragmental or brecciated sulfides considered to have been formed by slumping or sliding of accumulated sulfide masses after or during ore deposition (Kajiwara 1970, Matsukuma & Horikoshi 1970, Eldridge et al. 1983). Such sedimentary features have also been observed, albeit less frequently, in the massive ores of the metamorphosed and deformed Precambrian and Paleozoic VMS deposits (Walker et al. 1975, Sangster & Scott 1976).

Compositional zoning marked by an increase in Zn:Cu ratio or (Zn+Pb):Cu ratio upward and outward from the core of the massive sulfide lens, is one of the diagnostic features of proximal VMS deposits. The compositional zoning parallels the distribution of the three major ore sulfide minerals — sphalerite, chalcopyrite, and galena — and is due more to a decrease in Zn rather than an increase in Cu. Although zoning is best preserved in the Miocene Kuroko deposits, it is quite common even in the metamorphosed Cu-Zn deposits of Precambrian terranes. However, the suggestion that it can be used as a reliable indicator of stratigraphic top (Hutchinson 1973) should be treated with caution in view of the observed concentric zoning in some VMS deposits (Sangster & Scott 1976).

10.6.2. BULK COMPOSITION

The average grades of selected VMS deposits are presented in Table 10.3. In addition to much higher contents of Pb, the Kuroko-type Zn-Pb-Cu deposits generally have significantly higher Ag:Cu ratios with the Cu-Zn group and the Cyprus-type deposits have relatively lower contents of Ag compared with the Noranda-type deposits (Fig. 10.13). The 'black ores' of Kuroko deposits in Japan generally contain 1-2 g/t Au and 150-600 g/t Ag, although in some cases the Ag values may be as high as 6,000 g/t (Shimazaki 1974). The gold occurs mostly as electrum and much of the silver occurs as Ag-bearing sulfosalt and sulfide minerals (e.g., stromeyerite, polybasite, pearcite, tetrahedrite-tennantite, galena, and argentite). Franklin et al. (1981) noted a correlation between Ag and Pb in Phanerozoic VMS deposits.

The mean Au and Ag contents of both Archean and Proterozoic Cu-Zn VMS deposits are quite low — <0.6 g/t Au and <50 g/t Ag — but these deposits account for >15% of the total production and reserves of gold in the Canadian Shield (Franklin et al. 1981). The Mattabi-type Cu-Zn (-Pb) deposits of the Sturgeon Lake district are an exception; they contain ≈0.8-1.2% Pb and several hundred g/t Ag, mainly in tetrahedrite. The concentration and distribution of gold in individual VMS deposits are highly variable and remain poorly understood. Studies of modern sea-floor sulfide deposits, most of which have Ag:Cu ratios comparable to ancient VMS deposits (Fig. 10.13), suggest long-term remobilization of metals by sustained circulation of hydrothermal fluids through massive sulfide bodies (Hannington et al. 1980).

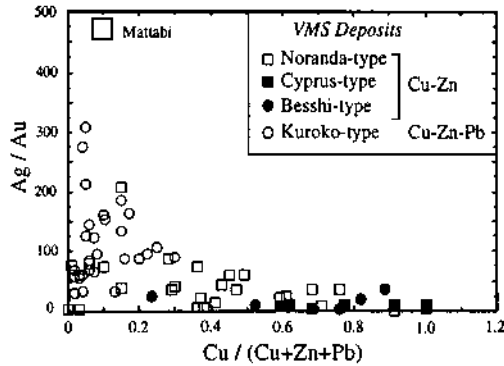


Figure 10.13. Relationship between Cu:(Cu+Zn+Pb) ratio vs. Ag:Au ratio of VMS deposits. (Sources of data: Table 10.3 and references therein.)

10.7. Hydrothermal Alteration

Alteration of the hanging-wall rocks observed in a few deposits have been ascribed to the continued activity of ore-forming hydrothermal solutions, as in the case of some Noranda deposits (Knuckey & Watkins 1982) and Kuroko deposits (Matsukuma & Horikoshi 1970, Shirozo 1974, Iijima 1974), or to the circulation of groundwater during the post-depositional burial history, as in the case of some deposits in Cyprus (Lydon 1984b). In general, however, hanging-wall alteration is subtle and often quite difficult to detect.

Hydrothermal alteration of footwall rocks is a diagnostic feature of VMS deposits (Franklin et al. 1981, Lydon 1984a, 1989, Urabe et al. 1983), although the alteration zone may be removed up to several kilometers from a distal deposit (e.g., the Sherridon deposit, Manitoba, Canada). The footwall alteration is of two types: (a) discordant alteration pipes, comprised of funnel- or carrot-shaped zones associated with copper-bearing stringer mineralization directly below the massive sulfide horizon (Fig. 10. 17); and (b) extensive but patchy semiconformable alteration zones of variable characteristics, which are located several hundred meters or more below the ore horizons. In some cases, the alteration pipe extends stratigraphically downward to meet or intersect this larger alteration zone, but in other cases the alteration pipe is superimposed on the lower zone (Franklin et al. 1981). The alteration pipes are considered to represent in part the zones through which the ore fluids moved to reach the sea-floor. The semiconformable alteration zones present large exploration targets and may have constituted part of the source rock, the "reservoir zone" of Hodgson and Lydon (1977), for metals and sulfur. The alteration features associated with different types of VMS deposits are summarized in Table 10.4.

TABLE 10.4. General characteristics of hydrothermal alteration zones associated with VMS deposits

Deposit Type	Alteration Pipe	Semiconformable Alteration Zone
Cu (-Zn) (Cyprus-type)	Well-defined and zoned; silicified core with Mg- or Fe-chlorite \pm illite or rectorite; outer zones with chlorite and smectite.	Poorly defined.
Cu-Zn (Noranda-type)	Well-defined; vertically extensive (up to several hundred meters); strongly zoned with Mg-chlorite core and sericitic halo; overlies and/or crosscuts the semiconformable alteration zone.	Poorly defined; overlain and/or cut by alteration pipe.
Zn-Cu (-Pb) (Mattabi-type)	Poorly defined and weakly zoned; silicification; sericite zone in immediate footwall, with accessory siderite and chloritoid; may be of limited lateral extent (< 100 m); grades into the semiconformable alteration zone.	Well-defined and well-developed; may extend laterally for several kilometers; grades into alteration pipe. Characterized by silicification, epidotization, carbonates, metal depletion.
Zn-Pb-Cu (Kuroko-type)	Usually well-defined; commonly zoned with a silicic and sericitic core and a broad outer zone of Mg- and Fe-chlorite.	Not identified.

Sources of data: Urabe et al. (1983), Franklin (1986, 1993), Morton and Franklin (1987), Richards et al. (1989), Skirrow and Franklin (1994).

10.7.1. ALTERATION PIPES

The most pronounced development of alteration pipes is associated with the Noranda-type Cu-Zn deposits (Fig. 10.14a), such as those of Millenbach (Riverin & Hodgson 1980, Knuckey et al. 1982), Mattagami (Roberts & Reardon 1978, MacGeehan 1978, Costa et al. 1983), and Corbet (Knuckey & Watkins 1982, Urabe et al. 1983) in the Abitibi greenstone belt. Typically, the alteration pipe is zoned, consisting of a Fe-chlorite-rich core and a sericite-rich envelope. The chloritic core, which commonly has a width similar to that of the massive sulfide lens, is characterized by major addition of Fe and Mg and by depletion of Ca, Na, and Si, reflecting the destruction of feldspar of the original mafic or felsic volcanic rock during the process of chloritization. MgO increases toward the center of most pipes due to an increase in the absolute abundance of chlorite as well as an increase in the Mg:(Mg+Fe) ratio in the same direction. Except for K-enrichment, the metasomatic changes in the sericitic zone, which usually extends beyond the limits of the massive sulfide lens, are less intense gradational continuations of those of the chloritic core. The common occurrence of tourmaline in footwall alteration zones may be useful as a potential exploration guide (Taylor & Slack 1984, Slack & Coad 1989).

Some Noranda-type deposits contain a ferruginous unit immediately below the massive sulfide lens. This may represent oxidized plume fall-out prior to the

establishment of anoxic bottom conditions and stabilization of sulfides (Lydon & Galley 1986). A talcose unit found in some deposits (e.g., Matagami Lake) might also have formed at the sea-floor during the initial discharge of silica-saturated hydrothermal fluids into Mg-bearing seawater (Costa et al. 1983, Aggarwal & Nesbitt 1984).

Alteration zones beneath Mattabi-type deposits (Fig. 10.14b) are less well defined, generally wider, and not as distinctly zoned as those associated with Noranda-type deposits (Franklin et al. 1975, 1985). Alteration minerals consist of variable amounts of Fe-carbonate (siderite and/or ankerite), sericite, quartz, and calcite. Chlorite is subordinate and most abundant on the periphery of the pipes. In areas of greenschist

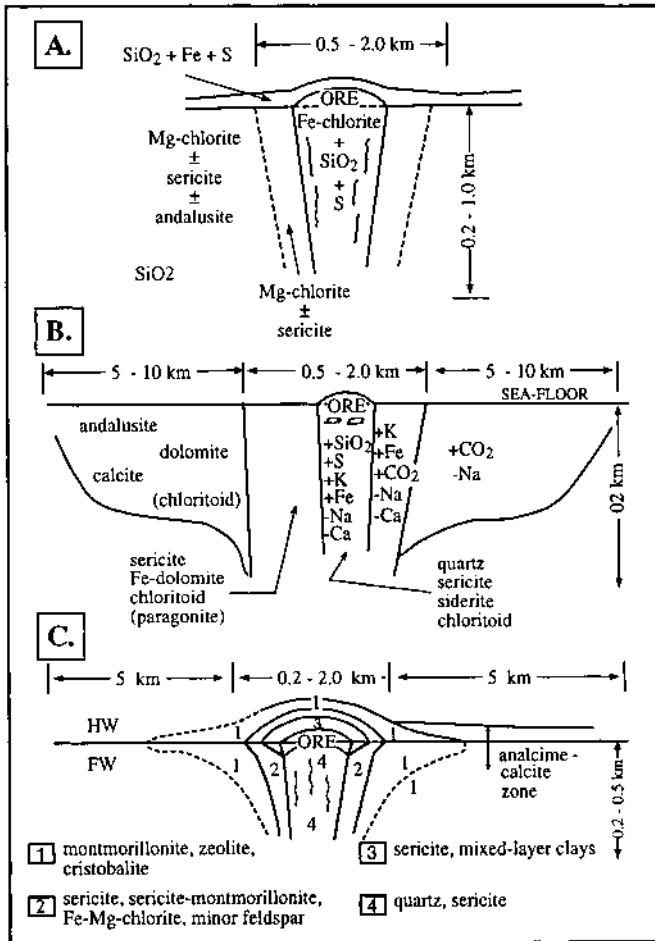


Figure 10.14. Schematic representation of characteristic footwall hydrothermal alteration assemblages and zoning in VMS deposits: a. Noranda-type deposits; b. Mattabi-type deposits; c. Kuroko-type deposits. (After Franklin 1993.)

metamorphism, chloritoid may be an abundant constituent along with andalusite and/or kyanite. The relatively diffused nature of the alteration pipes in Mattabi-type deposits, compared with the focused ones in Noranda-type deposits, may be ascribed to more widespread hydrofracturing of footwall rocks by the ascending fluids due to lower hydrostatic pressure (Morton & Franklin 1987).

Footwall alteration pipes of Cyprus-type deposits are similar to those of Noranda-type deposits, but the K-enrichment is represented by illite-smectite (instead of sericite) and a strong silica metasomatism is characteristic of the upper part of the alteration pipe (Lydon 1984b, Lydon & Galley 1986). Cyprus-type deposits also lack the strongly Mg-enriched axial alteration zone that is so common in the Archean deposits. The alteration pipes underlying Kuroko-type deposits commonly are laterally zoned and characterized by pervasive Si and K metasomatism (Fig. 10.14c). The core of the pipe includes the siliceous ore zone and is essentially a quartz - sericite - pyrite assemblage; the outer zones of alteration are composed of variable amounts of quartz, sericite, chlorite, and clay minerals (Shirozo 1974). For example, in the Uwamuki deposits of the Kosaka mine, the core to margin alteration sequence is as follows: quartz + sericite \Rightarrow sericite + chlorite + quartz \Rightarrow remnant albite + sericite + chlorite + quartz \Rightarrow kaolinite + quartz + sericite + chlorite + albite. Thus, whereas the original ore fluids for Archean deposits were in equilibrium with chlorite, resulting in the cores of alteration pipes being occupied by chlorite and the margins by sericite, the ore fluids for Kuroko deposits appear to have been in equilibrium with sericite, which replaced earlier-formed chlorite. Urabe et al. (1983) attributed this difference to either relatively early sealing of the hydrothermal system for the Kuroko deposits (thereby inhibiting the incursion of seawater, the source of Mg for chlorite), or to more effective removal of Mg from seawater by initially low-Mg felsic rocks beneath the Kuroko deposits.

Despite the difference in the relative distribution of chlorite and sericite, both Noranda-type and Kuroko-type deposits are characterized by a systematic increase in the Fe:(Fe+Mg) ratio of chlorite and in the whole-rock $\delta^{18}\text{O}$ from the core to the margin of alteration pipes (Urabe et al. 1983), as well as by a crude correlation between the alteration intensity and sulfide veining in some deposits (Lydon 1984a). The zonation may represent the product of either essentially contemporaneous processes that occurred during lateral migration of hydrothermal fluids outward from the main ascendant channelways down temperature gradients (Urabe et al. 1983) or interactions during several cycles of hydrothermal activity over several million years (Green et al. 1983).

10.7.2. SEMICONFORMABLE ALTERATION ZONES

Semiconformable alteration zones under Zn-Pb-Cu deposits have not been identified and only a few examples have been documented for the Cu-Zn group of deposits. The alteration zones associated with Noranda-type deposits in the Millenbach-Amulet area near Noranda (Gibson et al. 1983) and at Mattagami Lake (MacGeehan & MacLean 1980a, b) are large with strike lengths up to several kilometers and thicknesses of hundreds to thousands of meters, and are overlain or cut by alteration pipes. The

alteration generally consists of patchy silicification and more extensive spilitization (epidote + quartz + actinolite + quartz \pm albite assemblage), distributed along zones of relatively high permeability. The alteration zone beneath the Mattabi deposit (Zn-Cu-Pb) is similar in size, but better defined (Franklin 1986). A detailed discussion of the alteration and metal leaching associated with the Chisel Lake deposit of the Proterozoic Flin Flon volcanic belt (Canada) has been presented by Skirrow and Franklin (1994).

10.8. Metamorphism and Deformation

A strong correlation exists between the metamorphism of VMS deposits and that of their host rocks. At one end of the spectrum are the VMS deposits of the Precambrian greenstone belts and Paleozoic volcanic belts metamorphosed to greenschist or amphibolite facies; at the other end are the essentially unmetamorphosed Kuroko deposits of Japan, although the Kuroko ores appear to have undergone repeated diagenetic recrystallization (Eldridge et al. 1983).

Generalized aspects of mineralogic and textural changes resulting from metamorphism and deformation of ore-gangue assemblages have been described earlier (see Ch. 3). The commonly observed features in metamorphosed VMS deposits, as summarized by Franklin et al. (1981), include: (a) increase in grain size; (b) 'triple junction' annealing textures; (c) dimensional and crystallographic preferred orientation of ductile minerals along foliation planes; (d) plastic flowage of sulfide minerals; (e) coarsening of chalcopyrite and pyrrhotite intergrowths in sphalerite; and (f) change in pyrrhotite intergrowths from rounded inclusions on grain boundaries to rodlike shapes along sphalerite twin planes.

Except for minor changes in Fe, Zn, and S contents due to interaction between sulfides and silicates (e.g., the formation of gahnite), desulfurization of pyrite to pyrrhotite, and oxidation of pyrrhotite to magnetite, the bulk composition of massive ores have not been significantly affected by metamorphism. In highly metamorphosed ores, as is commonly the case in the Caledonian-Appalachian belt (Vokes 1976, Craig 1983), the inclusion of numerous contorted silicate fragments, which were plucked from the wallrock by plastic flowage of the sulfides and incorporated into the ore mass, may have led to a slight lowering of the ore grade (Sangster & Scott 1976). The sphalerite in such ores may contain 10-20 mole% FeS in solid solution.

Metamorphism may also produce redistribution of elements within an orebody, almost entirely due to the relative mobilities of the ore-forming sulfides, either by solid-state flow or by hydrothermal dissolution and redeposition in dilatant zones (Sangster & Scott 1976). This may modify or even obscure the characteristic Cu-Zn zoning of the massive ores, mobilize galena and sulfosalts into Ag-enriched gash veins in the hanging-wall, and produce chalcopyrite-rich veins that may crosscut the metamorphic foliation and extend into the host rock beyond the limits of the massive ore. If the metamorphism is accompanied by folding, particularly isoclinal folding, differential mobility of the sulfides during plastic flowage may result in a noticeable

increase in ore grade (especially of copper) and thickness toward the nose of the folds, the limbs tending to be thinner and more pyritic. On a larger scale, intense deformation may transpose the entire sulfide mass along shear and foliation planes, causing detachment of the massive ore from the stringer ore.

Metamorphic assemblages in hydrothermal alteration zones beneath metamorphosed massive sulfide ores include varying combinations of biotite, hornblende, Ca-pyroxene, garnet, actinolite-tremolite, anthophyllite, chloritoid, andalusite, sillimanite, kyanite, staurolite, and cordierite (Sangster & Scott 1976, Morton & Franklin 1987). Cordierite (often retrograded to sericite - anthophyllite assemblages) are usually the result of regional metamorphism, but in the Noranda area such assemblages occur in spotted hornfels (locally called "dalmatianite") in the contact aureole of the post-volcanic Lake Dufault granodiorite (see Fig. 10.9).

10.9. Origin

10.9.1. GENETIC MODEL

The overwhelming consensus at the present time, largely influenced by the analogy of sulfide deposition at modern spreading centers (see Ch. 2), is that the VMS deposits were formed at or immediately beneath the sea-floor from ascending hydrothermal fluids. Most VMS deposits consist of two types of broadly contemporaneous mineralization: a stringer-type mineralization, emplaced epigenetically in the brecciated and fractured footwall rocks along the hydrothermal conduits; and an overlying massive sulfide mineralization of submarine exhalative origin (i.e., syngenetic emplacement of sulfides from hydrothermal fluids discharged on to the sea-floor). The evidence for an exhalative origin of the massive sulfide lenses is found in the well-preserved proximal deposits and include the following (Lambert & Sato 1976, Lydon 1988):

- (a) the presence of sedimentary structures (graded bedding, cross-bedding, slump folding, locally transported sulfide breccia, banding) within the massive sulfide lens, as has been described from many Cu-Zn and Kuroko-type deposits (Ishihara 1974, Walker et al. 1975, Sangster & Scott 1976);
- (b) the common lateral continuity of the massive sulfide lens with a horizon of chemical (exhalative) and/or clastic (tuffaceous) sediments, interpreted to have formed during the waning stages of hydrothermal activity (Tsutsumi & Ohmoto 1983);
- (c) the common presence of an alteration pipe beneath the massive sulfide lens, interpreted to represent the uppermost part of the hydrothermal conduit; and
- (d) the sharp and conformable upper contact of the massive sulfide lens with the stratigraphic hanging-wall rocks, indicating that the ore-forming hydrothermal activity was confined to the hiatus between the deposition of the footwall and the hanging-wall rocks.

10.9.2. ORE-FORMING FLUIDS

The two likely ore-forming fluids for VMS deposits are (a) circulating seawater and (b) magmatic water. The suggestion of a dominantly magmatic origin of the ore-forming fluids, especially for the Kuroko-type deposits associated with felsic magmatism, is based largely on the premise (discussed later) that a magmatic derivation offers a more reasonable explanation for the required metal concentrations (especially of Pb) in ore-forming fluids (Urabe & Sato 1978, Sawkins & Kowalik 1981, Stanton 1986, Urabe & Marumo 1991). The present consensus, however, is that the hydrothermal fluids responsible for VMS deposits and associated wallrock alteration were dominantly seawater, possibly containing a component of magmatic water, that was modified to varying extent by interaction with the underlying rocks. The main lines of evidence for this conclusion include: experimental data; oxygen and hydrogen isotopic ratios of the altered volcanic rocks; oxygen, sulfur, and strontium isotopic compositions of the ore-associated sulfate minerals; microthermometric and isotopic analyses of fluid inclusions in ore and gangue minerals, and theoretical modeling.

The hydrothermal fluids emanating from modern sea-floor vents are considered as having been seawater, modified by progressive heating and reactions at higher temperatures during its circulation through the deeper parts of the crust, although a possible magmatic component in some vent fluids is indicated by high CO₂ contents and carbon- and oxygen-isotope ratios of the CO₂ (Sakai et al. 1990) as well as anomalous salinities of the fluids. Experimental studies (see Ch. 2) have established that the reaction between modified seawater and basalt at about 350°-400°C causes sufficient depression of pH to mobilize metals from rocks into the fluid. Reed (1983) performed a series of multicomponent equilibrium calculations involving the reaction of seawater with tholeiitic basalt at 300°C, and the effects of cooling the resultant solution to 25°C and mixing it with seawater. The calculated mineralogy and zoning patterns resemble natural ore assemblages in VMS deposits, attesting to the feasibility of generating VMS deposits by the process modeled. The lack of quartz in the massive ore, a discrepancy from what is predicted from the calculations, could have resulted from a kinetic barrier to quartz precipitation from solutions cooled below 200°C.

For most VMS deposits, oxygen and hydrogen isotopic ratios of mineralizing fluids (Fig. 10.15), estimated from alteration of the volcanic host rocks, either lie near 0‰, typical of normal marine water, or show deviations that may be attributed to mixing with meteoric water or interaction with host rocks with variable water:rock ratios. The unusually high $\delta^{18}\text{O}$ values of the ore fluids for the Raul mine (Ripley & Ohmoto 1977) and the Kidd Creek mine (Beatty et al. 1988) probably reflect evolution of the seawater through rapid evaporation in a closed basin. Of the analyzed deposits, only the presently inactive Blue Hill mine (Maine, USA) shows $\delta^{18}\text{O}$ - δD values strongly suggestive of a significant magmatic component (30 to 60% magmatic water). Although not apparent from the $\delta^{18}\text{O}$ values, the presence of high-salinity (30-40 wt% NaCl equivalent), CaCl₂-dominated hydrothermal fluids for mineralization at the Archean Mattagami Lake mine requires highly evolved solutions, and perhaps a

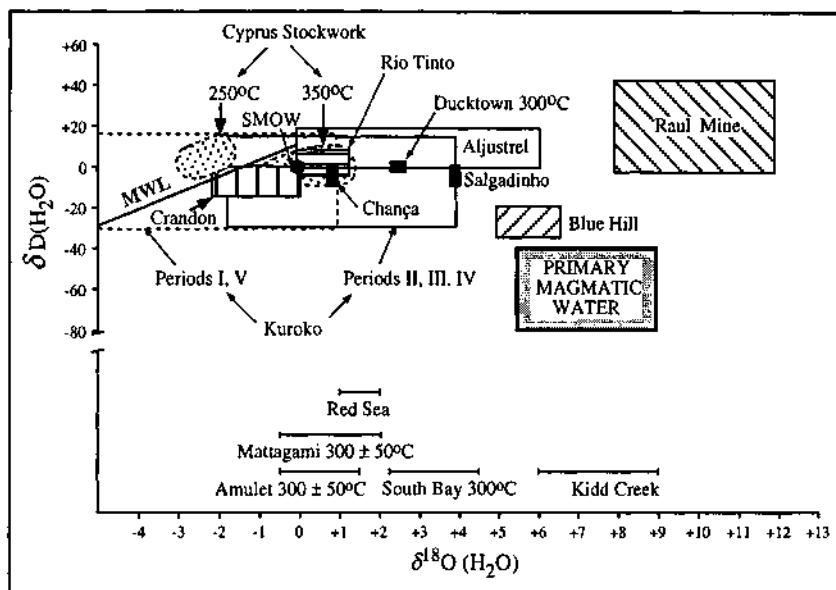


Figure 10.15. Isotopic ratios ($\delta D - \delta^{18}O$) of ore-forming fluids for various VMS deposits (after Munha et al. 1986),

significant magmatic fluid contribution (Costa et al. 1983).

Isotopic data directly related to mineralization, and thus to ore-forming fluids, are also available for some Kuroko-type deposits in Japan. Watanabe and Sakai (1983) attributed the narrow range of $\delta^{18}O$ values (+6.4 to +10.9‰) and $\delta^{34}S$ values (+19.5 to +25.5‰) of the barite, anhydrite, and gypsum in Kuroko deposits to precipitation from Miocene seawater. This conclusion is supported by the narrow range of $^{87}Sr/^{86}Sr$ values (0.7082-0.7087) for the sulfates, the upper limit approaching that estimated for the Miocene seawater (Farrell & Holland 1983). The salinity of primary fluid inclusions in Kuroko ores, however, range from the values of modern seawater (≈ 3.2 to 3.5 wt% NaCl) to about twice that of seawater (Bryndzia et al. 1983, Pisutha-Arnond & Ohmoto 1983). To account for the elevated salinities, Bryndzia et al. (1983) called for the mixing of seawater with a high-salinity fluid, possibly a magmatic fluid from contemporaneous high-level felsic plutons underlying the Kuroko deposits. A contribution of up to 20-33% magmatic water has also been suggested from the estimated $\delta^{18}O$ - δD values of the ore-forming fluids (Ohmoto & Rye 1974, Hattori & Muehlenbachs 1980). On the other hand, Pisutha-Arnond and Ohmoto (1983) argued that the chemical and isotopic compositions of the Kuroko ore fluids ($\delta D = -30$ to +15‰, $\delta^{18}O = -6$ to +4‰), estimated from the analyses of fluids extracted from sulfide minerals and quartz, could be the result of continuous interactions between

volcanic rocks and seawater-derived pore fluids in a rock-dominated system, without significant (>5%) involvement of a magmatic fluid. The high salinity of the Kuroko ore fluids, they suggested, could have resulted from the consumption of H_2O to form hydrous minerals at the early, low-temperature stage of seawater incursion into submarine rocks.

10.9.3. HYDROTHERMAL SYSTEM

The essential requirements of a hydrothermal system capable of producing a reasonable size VMS deposits are (a) a large and sustained heat source that would permit the circulation of vast amounts of seawater at sufficiently high temperatures to account for the quantity of metals and alteration products, (b) an impermeable cap to the hydrothermal reaction zone to prevent unfocused discharge of the buoyant hydrothermal fluids, and (c) a mechanism of focusing the fluid discharge for massive sulfide accumulation. A model hydrothermal system incorporating these elements is presented in Figure 10.16.

Suggested heat sources, depending on the local geologic setting, include rhyolite domes or plugs (Ohmoto & Rye 1974, Cathles, 1981, 1983), subvolcanic intrusions

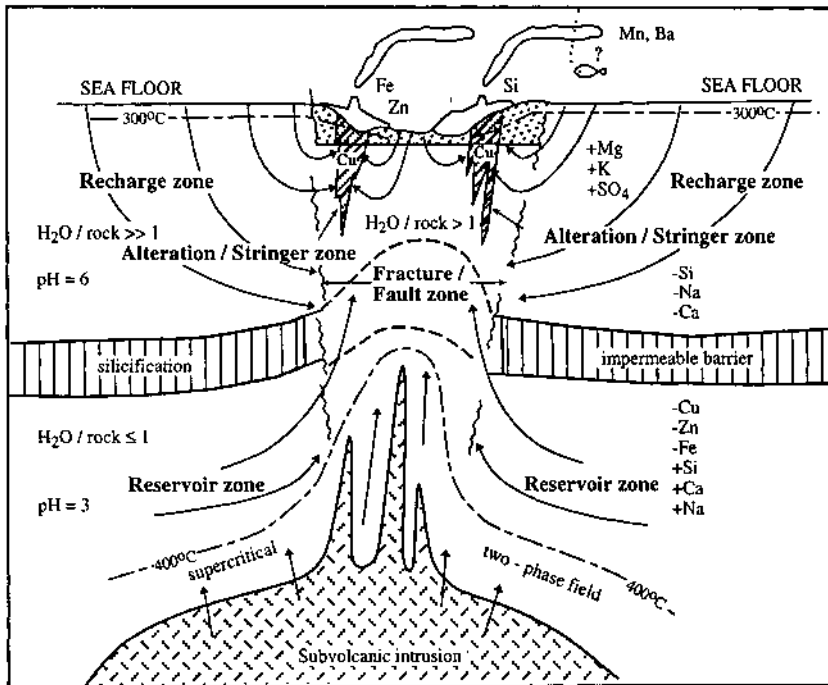


Figure 10.16. Generalized model of VMS-producing hydrothermal system (after Franklin 1993).

(Campbell et al. 1981, Franklin 1986), and magma chambers at a spreading ridge (Spooner 1977, Lowell & Rona 1985, Cann et al. 1985). Calculations indicate that the required magma volumes are quite large — $\geq 169 \text{ km}^3$ of felsic melt for all the deposits in the Hokuroku Basin, $>78 \text{ km}^3$ for the Noranda deposits, and in the order of 300 km^3 for a district of moderate size containing 30 million tonnes of sulfide. Intrusions of an appropriate size are associated with most the Archean and Proterozoic Cu-Zn districts in Canada and in the Hokuroku district of Japan, but the requirement is not easily satisfied in districts where the footwall sequence has a significant component of sedimentary rocks.

The requirement of an impermeable cap may have been satisfied in a variety of ways (Franklin 1993). Some possible examples are pyroclastic ash flows or felsic flows that overlie more mafic flows (e.g., Matagami Lake and Sturgeon Lake deposits in Canada), sediments in the footwall sequence, and silicified semiconformable alteration zones. Conduits for focused discharge of the fluids were most likely provided by tectonically generated faults and fracture zones and, in some cases, by synvolcanic faults.

10.9.4. ORE ACCUMULATION

Sato (1972) suggested that the depositional morphology of VMS deposits was governed by the physical behavior of ore fluids after discharge into a submarine environment. He postulated three types of behavior of a NaCl-rich hydrothermal fluid, depending on its initial temperature and density and subsequent changes due to mixing with seawater (Fig. 10.17):

- (a) Type I or highly saline hydrothermal solution whose density remains greater than the cold seawater at all degrees of mixing. Such a solution would tend to flow down submarine slopes, collect as a stratified brine pool in a topographic depression, and produce a distal massive sulfide deposit of tabular morphology.
- (b) Type II hydrothermal solution with an initial density less than that of seawater, but whose density passes through a maximum, which is greater than that of the cold seawater, at some stage in the mixing process. Such a solution would tend to give rise to proximal massive ores with a conical or mound-like morphology close to the hydrothermal vent. This may be accompanied by distal mineralization from spent brines.
- (c) Type III hydrothermal solution that is initially less dense than the cold seawater and remains so after mixing with seawater. Such a solution would be discharged as a buoyant plume and the sulfides accumulated from plume fall-back would be dispersed as weak mineralization over a large area.

Subsequent experimental and theoretical studies (Turner & Gustafson 1978, Parmentier & Spooner 1978, Solomon & Walshe 1979b, Henley & Thornley 1979, McDougall 1984, Lowell & Rona 1985, Solomon et al. 1987) have shown that,

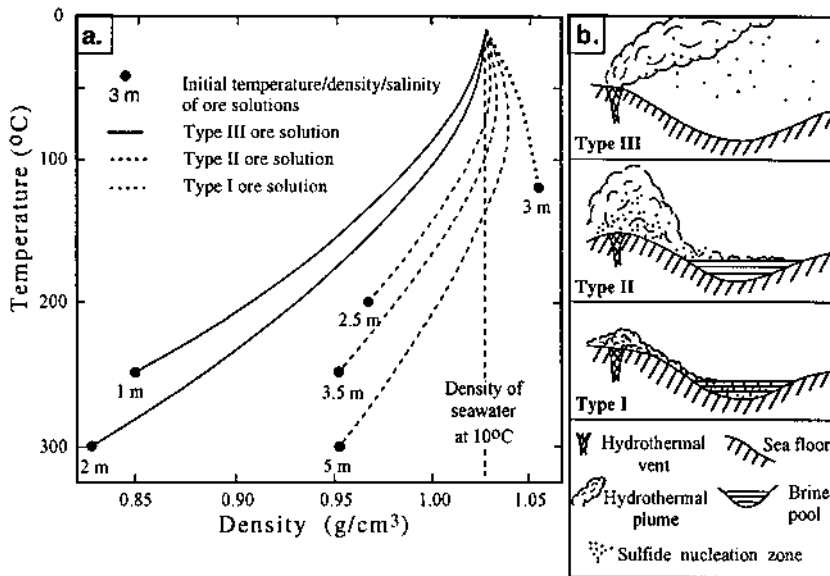


Figure 10.17. a. Density-temperature relationships of hot NaCl solutions mixed with seawater at 20°C illustrating the three types of hydrothermal solutions as defined by Sato (1972); b. Behavior of the three types of hydrothermal solutions when discharged into a submarine environment. (After Sato 1972.)

although Sato's model is correct in principle, the actual processes are much more complex. A conceptual insight into the formation of VMS deposits is provided by numerous studies related to sulfide accumulation at modern spreading centers (Edmund et al. 1979, Haymon & Kastner 1981, Haymon 1983, Goldfarb et al. 1983, Hekinian et al. 1983, Rona, 1984, 1988, Scott 1985, Hekinian & Fouquet 1985, Franklin 1986, Fouquet et al. 1993, Herzig & Hannington 1995). A brief summary, largely based on the review by Lydon (1988), is presented below.

Active sulfide deposition on the ocean floor is restricted to high-temperature (>200°C, but commonly >300°C) hydrothermal vents, often associated with prolific biota (e.g., Rona et al. 1986), and is characterized by sulfide chimneys that rise from a basal mound of sulfides formed through a complex combination of physical and chemical processes. The extreme buoyancy of high-temperature hydrothermal fluids (typically Type III solutions of Sato, 1972) results in the formation of plumes that may rise as much as 200 m above the vent sites. These are the so called *black smokers* (MacDonald et al. 1980), clouds of black smoke with entrained fine particles (commonly 1-3 mm in diameter) of sulfides (pyrrhotite, sphalerite, lesser pyrite, and traces of cubanite) formed due to mixing of the hydrothermal fluid with cold seawater. Much of the particulate matter of a black smoker accumulates as a clastic sulfide layer

that may be traced for at least hundreds of meters away from the plume site or is incorporated into distal marine sediments; only a small proportion (probably 1-10%) goes into the formation of individual chimneys. Growth of a sulfide chimney, estimated to be as much as 30 cm per day (Goldfarb et al. 1983), is initiated by the precipitation of anhydrite (with minor quantities of sulfides) from seawater at the interface between the buoyant hydrothermal plume and surrounding cold seawater (Fig. 10.18a), because the solubility of anhydrite decreases with increasing temperature. The hydrothermal fluid continues to flow upward along the central conduit, but a small portion of it (<1%) flows through the porous anhydrite wall. The porous network of anhydrite crystals is believed to play a critical role in the sulfide accumulation around the hydrothermal vent precipitation process, because the porous barrier defocuses the hydrothermal discharge and thus maximizes its cooling close to the sea-floor. The fluid changes from high temperature (>300°C), acidic (pH ≈3.5), reduced ($\text{H}_2\text{S} \gg \text{SO}_4^{2-}$) conditions on the inside of the anhydrite wall to low temperature (2°C), alkaline (pH ≈7.8), oxidized ($\text{SO}_4^{2-} \gg \text{H}_2\text{S}$) nature of ambient seawater on the outside of the wall. As the chimney grows vertically by the upward extension of its anhydrite collar, the walls of the lower part of the chimney thicken by continued precipitation of Cu-Fe sulfides in the interior portions and of anhydrite in the outer portions (Fig. 10.18b). The latter is a complex process involving oscillation of thermal and chemical profiles, and results in the formation of intermixed mineral assemblages that collectively reflect a wide range of physico-chemical conditions. Mineral zone boundaries migrate outward with time so that lower temperature assemblages are replaced by higher temperature assemblages. Thus, a mature chimney tends to be mineralogically zoned as follows: a higher temperature core zone of chalcopyrite (\pm isocubanite \pm pyrrhotite) \Rightarrow an intermediate zone dominated by pyrite + sphalerite + wurtzite in an anhydrite matrix \Rightarrow a low-temperature outer zone of anhydrite with minor sulfides, amorphous silica, barite, and caminite (a new hydroxysulfate-hydrate mineral) (Figure 10.18c). Eventually, the anhydrite is dissolved by sulfate-free solutions in the interior zones of the chimneys and by cold seawater in the exterior zones as the chimney cools, leaving a sulfide assemblage in which opaline silica is the dominant gangue mineral.

At some stage, the chimney becomes mechanically unstable and collapses to form a mound of chimney talus, covering the original vent orifice and causing diversion of hydrothermal flow to multiple discharge sites on the mound and initiation of new chimneys at these sites. In addition to continual accumulation of talus derived from collapsing chimneys, the mound grows by precipitation of sulfides from the hydrothermal fluids, both as open-space fillings and as replacement of earlier sulfides by higher temperature mineral assemblages. The growth of the mound is governed essentially by the same principles as those described for the chimney growth, the role of the vertical porous anhydrite wall being performed by a horizontal blanket of low-permeability chimney talus composed of anhydrite cemented by sulfides. The creation of new fluid channelways by hydraulic, seismic or tectonic fracturing of the mound, in turn, initiates the growth of new chimneys, and mound growth continues by repetition of this process as long as the flow of high-temperature hydrothermal fluids is sustained.

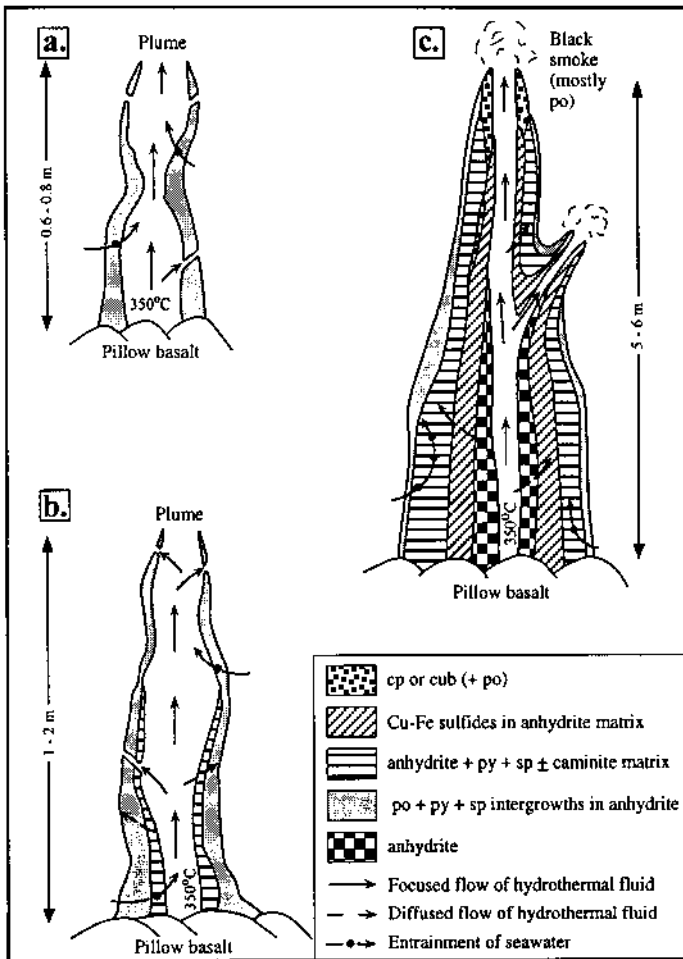


Figure 10.18. Schematic illustration of the growth of a modern sea-floor 'black smoker' sulfide chimney: a. Formation of a chimney; b. Growth of the chimney c. Mineralogical zonation in a mature chimney. Mineral abbreviations: cp = chalcopyrite, cub = cubanite, po = pyrrhotite, sp = sphalerite. Caminite is a new hydroxysulfate-hydrate mineral. (After Goldfarb et al. 1983, Haymon 1983, Lydon 1986.)

Sulfide lenses formed by the mechanism described above tend to be small in size and conical or mound-like in shape, but their morphology may be altered by slumping and gravity sliding. At a few ocean-floor sites, normal faults have exposed the interior of sulfide mounds and the upper parts of the footwall stringer zone with highly altered host rock and abundant stockwork mineralization (Fouquet et al. 1985). The stockwork zone represents a hydrothermal breccia pipe, formed by repeated episodes of hydraulic fracturing and by concomitant precipitation of hydrothermal minerals in fractures and

hydrothermal alteration of the breccia clasts.

It is logical to infer that the ancient proximal VMS deposits were formed at extensional settings in a manner similar to the growth of sulfide mounds at modern hydrothermal vents and preserved due to rapid burial by volcanic flows and/or sediments. The analogy is supported by general similarities between the two in terms of host rocks, mineralogy, mineral and metal zoning, footwall brecciation and alteration, and the recognition of chimney fragments and fossil worm tubes in Cyprus-type VMS deposits (Oudin & Constantinou 1984, Haymon et al. 1984). Also, estimated temperature-salinity relationships of ore-forming fluids for the ancient VMS deposits indicate that they were similar to the highly buoyant Type III fluids of Sato.

A limitation of this analogy at present is the small size of sea-floor accumulations. For example, at 13°N on the East Pacific Rise, more than 80 separate sulfide deposits have been recognized along a 20 km segment of the axial graben, but they contain an estimated total of only 20,000 tonnes of sulfide (Hekinian & Fouquet 1985). The largest volcanic-hosted mound-chimney deposit discovered to date occurs in the TAG field on the Mid-Atlantic Ridge at 26°N and is estimated to contain 4.5 million tonnes of sulfide, which is comparable to an average-sized ancient VMS deposit (about 6 million tonnes sulfide), but most are much smaller, typically containing about 2,000 tonnes of sulfide (Rona 1984, Lowell & Rona 1985, Rona et al. 1986). A major massive sulfide body has recently been discovered in the Middle Valley, a sediment-filled spreading center on the northern Juan de Fuca Ridge (see Fig. 2.28). According to preliminary results (Duckworth et al. 1998), the minimum extent of the conical massive sulfide mound in the Bent Hill area of the Middle Valley, as constrained by drilling, is 100 m (N-S) x 150 m (E-W) x 103 m (thickness). The massive sulfide body is composed mainly of pyrite and pyrrhotite with relatively low base metal concentrations of approximately 1.2% Zn, 0.5% Cu, and 180 ppm Pb. Underlying the massive sulfide is a 100 m-thick feeder zone consisting of subvertical, crosscutting veins filled with Cu-Fe sulfides and pyrrhotite. Continued exploration of the sea-floor may result in the discovery of larger sulfide accumulations, but the formation of very large ancient VMS deposits/districts, such as the Iberian pyrite belt, probably involved ore fluids with considerably more dissolved metal than the ≈100 ppm concentration of the modern sea-floor hydrothermal vents.

The chimney-mound model appears to be most applicable to the proximal Kuroko-type deposits that contain gypsum-anhydrite ore (*Sekkoko*) below and/or adjacent to sulfide ore (Shikazono et al. 1983). VMS deposits lacking anhydrite may also have formed by similar processes, the critical role of the porous anhydrite wall being fulfilled by a layer of fragmental rocks over the hydrothermal vent. For many ancient VMS deposits, there is good evidence that fragmental rocks (and later fragmental sulfides) were the result of recurrent explosive discharge of hydrothermal fluids (Lydon & Galley 1986, Lydon 1988). This scenario is consistent with the interpretation that the stringer zone represents a mineralized hydrothermal breccia pipe. Besshi-type deposits with a sheet-like morphology are more likely to have formed by sulfide accumulation in brine pools from high-density (Sato's Type I) solutions.

10.9.5. METAL ZONING

The Cu-dominant to Zn \pm Pb-dominant lateral and vertical zoning in VMS deposits is not a feature superimposed by metamorphism, because it is generally best displayed by the least metamorphosed deposits. The zoning has been attributed variously to changes in the composition or temperature of the pristine ore fluid with time (Solomon & Walshe 1979b), abrupt variations in pH, fO_2 , ΣS , and temperature over relatively small distances due to mixing of the ore fluid with seawater (Large 1977, Knuckey et al. 1982), and local cooling of acidic and reduced aqueous solutions carrying metals dominantly as chloride complexes (Janecky & Seyfried 1984, Lydon 1988).

Lydon (1988) has proposed that the metal zoning can be explained in terms of the relative solubilities of chalcopyrite and sphalerite (and galena) as a function of temperature if the initial fluid can be assumed to satisfy the following constraints: (a) the concentrations of Fe, Cu and Zn are within one or two orders of magnitude of one another; (b) the metals are in solution dominantly as chloride complexes; (c) molality of dissolved H_2S > molality of dissolved metal; and (d) $a_{H_2S} \gg a_{SO_4^{2-}}$ at chemical equilibrium (i.e., the solution is in a very reduced state). Under these conditions, the solubility of chalcopyrite in equilibrium with an iron sulfide is dominantly a function of temperature, whereas that of sphalerite (and galena) is much less temperature dependent (Fig. 10.19), and the solution will contain significant concentrations of dissolved Zn and Pb at lower temperatures. This model provides a reasonable explanation for the mineral zoning in the modern sea-floor sulfide chimneys (see Fig. 10.18c). The degree of separation of Zn (and Pb) from Cu along the cooling path of a reduced solution depends on the degree of undersaturation of Zn (and Pb) in the initial solution. The relative position of maximum iron sulfide deposition in the cooling sequence is dependent on the concomitant pH and a_{O_2} profile.

The sea-floor sulfide mounds also show a thermal zonation with high-temperature sulfides (e.g., chalcopyrite, isocubanite, pyrite) in the interior and low-temperature precipitates (e.g., sphalerite, anhydrite, amorphous silica) at the margins, which is very similar to the typical zoning in ancient VMS deposits (Hekinian & Fouquet 1985). The core-to-rim thermal and chemical gradients in a sulfide mound are similar to those in sulfide chimneys. The chalcopyrite-rich core may be attributed to deposition mainly in fractures from circulating fluids that are confined by an outer low-permeability crust and to the conversion of earlier sulfides to chalcopyrite, whereas sphalerite and galena continue to be stable in the outer portions of the mound.

10.10. Metallogenesis

10.10.1. HOST ROCKS

With the exception of Besshi-type Cu-Zn deposits, some of which are hosted by metasedimentary rocks, VMS deposits occur in volcanic-dominated sequences of

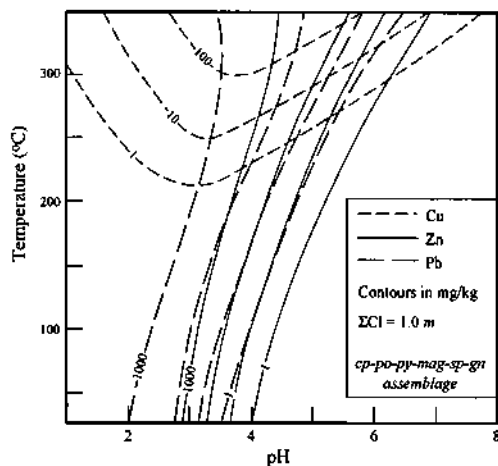


Figure 10.19. Sulfide solubility patterns due to chloride complexing, indicated by calculated total metal concentrations (in mg/kg) in a 1m NaCl solution in equilibrium with a chalcopyrite-pyrite-pyrrhotite-magnetite-sphalerite-galena assemblage. The sulfur content of the solution ranges from $\ll 1$ mg/kg at low pH and low temperature to $> 10,000$ mg/kg at high pH and high temperature. The isothermal decrease in chalcopyrite solubility with decreasing pH at low pH is due to the decrease in a_{Cl^-} as the relative proportion of chloride complexed with metals increases. (After Lydon 1989.)

presumably tholeiitic and calc-alkaline magma series (see Table 10.2). The immediate host rocks of the Zn-Pb-Cu group deposits are dominantly felsic. Only a few smaller districts, such as Buchans (Canada), have a prominent mafic volcanic component in the footwall rocks (Franklin et al. 1981). The overall volcanic succession appears to be bimodal (Munha 1979, Dudás et al. 1983), suggesting a rift environment.

Volcanic rocks associated with the Cu-Zn VMS deposits are more varied. The volcanic stratigraphy is generally dominated by mafic rocks, although the immediate footwall rocks of many deposits in the Archean greenstone belts and Caledonide districts are felsic in composition. There are exceptions to this generalization. For example, the footwall rocks in Skellefte district (Norway) are mostly felsic volcanics; mafic volcanic rocks are present only in the hanging-wall.

In each greenstone belt of the Canadian Shield, the typical volcanic succession has been described as consisting of a laterally extensive sequence of tholeiitic basalt comprising the lower two-thirds of the stratigraphy, overlain by volcanic rocks of calc-alkaline affinity that form thick accumulations at discrete volcanic centers and host the Noranda-type VMS deposits (Sangster 1972, Sangster & Scott 1976). The calc-alkaline affinity of these rocks, however, may be an artifact of widespread hydrothermal alteration that accompanied subsea-floor geothermal activity (MacGeehan 1978, MacGeehan & MacLean 1980a). Although calc-alkaline suites do exist in the Archean

greenstone belts of the Canadian Shield (Descarreaux 1973, Ujike & Goodwin 1987), as well as in other shields, the volcanic successions of the greenstone belts appear to be predominantly bimodal suites of basalt and rhyolite (Thurston et al. 1985), especially those associated with Noranda-type VMS deposits (MacGeehan & MacLean 1980a). In this respect, the Archean greenstone volcanics may be similar to those of the Green Tuff Belt in Japan, emplaced in extensional tectonic settings (Cathless et al. 1983).

10.10.2. SOURCE OF ORE METALS

Considering the very low concentration of base metals in normal seawater and meteoric water, two alternative sources have been suggested for the metals in VMS deposits. One is the footwall volcanic sequence and related basement rocks from which metals were leached by heated seawater convecting above a magmatic intrusion or a volcanic magma chamber (Spooner & Fyfe 1973, Ohmoto & Rye 1974, Solomon 1976, Hutchinson et al. 1980). The other is a magmatic volatile phase from the magmatic system that was responsible for the volcanism (Urabe & Sato 1978, Henley & Thornley 1979, Stanton 1986, Urabe & Marumo 1991).

Two main lines of arguments have been forwarded for the leaching hypothesis. The first relies on a comparison of ore metal abundances or ratios between VMS ores and their associated footwall rocks (Lambert & Sato 1974, Franklin et al. 1981), or mass-balance calculations demonstrating the adequacy of the footwall rocks in supplying the metals contained in the ores (Solomon 1976, MacGeehan 1978, MacGeehan & MacLean 1980a, Sawkins & Kowalik 1981, Ohmoto et al. 1983, Stolz & Large 1992). Such arguments constitute, at best, permissible evidence for the leaching hypothesis (see Ch. 2). Lead isotopic data on VMS deposits are limited and inconclusive. For example, the source of the Pb in the Cyprus deposits has been ascribed variously to a direct or indirect mantle source (Doe & Zartman 1979), a mixture of basaltic and seawater sources (Spooner & Gale 1982), and an oceanic crust of heterogeneous initial isotopic composition or a mixture of basaltic lead with a more radiogenic Pb component from an unidentified source (Hamelin et al. 1988). The similarity of the isotopic composition of ore lead and the lead in oceanic crust basalts at modern spreading ridges is compatible with derivation of the lead (and probably other ore metals in the sulfides) from the basalts, but on ridges covered by sediments, a large portion of the lead in sulfides could also have been leached out of the sediments (Chen et al. 1986, LeHuray et al. 1988).

The other argument for the leaching hypothesis is an indirect one — that the ore-forming fluids evolved dominantly from seawater. The ability of saline aqueous solutions to leach metals from rocks has been amply demonstrated both in the laboratory and by field observations (see Ch. 2). Calculations by Solomon et al. (1987), ignoring possible magmatic input, show that convection cells required for large VMS deposits are in the order of 10^3 km^3 , values consistent with the observed spacings between large deposits, although the volume may be reduced as a result of direct or indirect magmatic contribution where felsic plutons are present. Immiscible magmatic

sulfides in the basaltic rocks may also have contributed to the metal budget of the ore-forming fluids (Keays 1987).

The main objections to the leaching hypothesis are as follows (Urabe et al. 1983, Stanton 1986): (a) the basalt-associated Cyprus-type VMS deposits are relatively smaller and less numerous compared with those associated with dacites, andesites, and rhyolites, although the total volume of marine basalts is several orders of magnitude greater than the rest combined and contain about twice as much Cu+Zn+Pb (≈ 180 ppm) as dacites (≈ 90 ppm); (b) Cyprus-type deposits contain only minor amounts of Zn, but basalts contain at least as much Zn as dacites, andesites, and rhyolites; (c) the Kuroko deposits are remarkably similar in ore mineral assemblages, chemical composition, and vertical zoning despite considerable variation in their footwall rocks; and (d) the deposits in any district are confined to one, or at most two, horizons within the volcanic sequence.

Hydrothermal fluids in equilibrium with granitic magmas may contain a high concentration of base metals (particularly Zn and Pb), especially if such fluids are released from water-saturated magmas at high levels of the crust (see Ch. 2). Stanton (1986) argued that progressive crystallization of a calc-alkaline magma, commonly associated with Zn-Pb-Cu deposits, would result in a substantial loss of Fe, Zn, and Pb to a volatile phase. Earlier, Henley and Thornley (1979) had suggested that part of the ore metals (as well as heat, CO₂, and reduced sulfur) could have been derived from a vapor-dominated plume originating from the interaction of magmatic fluid and the surrounding seawater-derived geothermal fluid. Estimated $\delta^{18}\text{O}$ - δD values of fluids for Kuroko mineralization, wallrock alteration sericite, and kaolinite that formed during the waning stage of mineralization, fall in the range between the fields of magmatic fluids and SMOW.

10.10.3. SOURCE OF SULFUR

The isotopic composition of sulfur in anhydrites from modern hydrothermal vents at spreading centers are close to that of seawater and is consistent with a derivation predominantly from seawater sulfate. The $\delta^{34}\text{S}$ values of the sulfides range from about +1 to +4‰, and the sulfur appears to have been derived from the basaltic substrate as well as from seawater sulfate previously deposited as anhydrite (Styrt et al. 1981, Shanks & Seyfried 1987, Alt 1988). However, based on reaction-path models of seawater-basalt interaction at mid-ocean ridges, Bowers (1989) has argued for an overwhelming influence of basaltic sulfur unless the reduction occurs at high temperature (350°C) or near the venting areas. It is not possible to define precisely the source of sulfur for ancient VMS deposits, but the $\delta^{34}\text{S}$ data are consistent with a dual source of sulfur.

As the massive and stringer ores of ancient VMS deposits are believed to have been precipitated from the same seawater-dominated fluids that caused the footwall hydrothermal alteration, it is logical to expect that the seawater sulfate was the major source of the sulfur in these deposits. Sangster (1971, 1976) emphasized the

correlation between the $\delta^{34}\text{S}$ values of sulfides in Phanerozoic VMS deposits (predominantly Zn-Pb-Cu deposits) and those of coeval seawater sulfate (see Fig. 4.4) and concluded that the sulfides of VMS deposits were derived by the bacterial reduction of seawater sulfate at the site of deposition of the ores. A similar parallel variation of $\delta^{34}\text{S}$ in Phanerozoic VMS deposits and coeval marine sulfate deposits has also been reported by other workers (e.g., Large 1992), implicating seawater sulfate as the major source of sulfur. However, considering the improbability of bacterial reduction at the estimated temperatures of ore deposition ($>150^\circ\text{C}$), most authors have favored an inorganic reduction of seawater sulfate during circulation of seawater through hot volcanic rocks (Sasaki & Kajiwara 1971, Ohmoto & rye 1974, Eastoe et al. 1986). The process probably was more complicated than a direct reduction of seawater SO_4^{2-} as envisaged for the Cyprus-type deposits (Spooner 1977, Bachinski 1977). The $\delta^{34}\text{S}$ values of bulk ore samples from the ophiolite-hosted Løkken and Høydal deposits range from ≈ 0 to $+8\text{‰}$, similar to those of other ophiolite-hosted and modern sea-floor sulfide deposits, and have been interpreted to indicate both reduced seawater sulfate and leached magmatic sulfur in the ore-forming fluids (Grenne 1989, Grenne & Vokes 1990).

In the Kuroko ores of the Hokuroku district, $\delta^{34}\text{S}$ values of H_2S in coexisting fluids at temperatures greater than about 150°C (Ohmoto & Rye 1979) are mostly between $+2$ and $+8\text{‰}$. The $\delta^{34}\text{S}$ values of diagenetic pyrites in sedimentary rocks of the Kuroko ore horizon in the district average around -25‰ and argue against a biogenic origin for the Kuroko ore sulfides. Ohmoto et al. (1983) proposed an "anhydrite buffer model" that attributed the sulfur in the Kuroko ore-forming fluids to H_2S derived through inorganic reduction of seawater sulfate and leaching of country rock sulfides (mostly pyrite). An assumption in this model is that the ore-forming fluids, before mixing with cold seawater or interaction with earlier ore minerals, were saturated only with quartz and pyrite, a reasonable assumption considering that these are two common minerals in all types of country rock in the Hokuroku district. The model postulates an initial fixation of seawater SO_4^{2-} as disseminated gypsum-anhydrite in the country rocks at the low temperatures ($\leq 150^\circ\text{C}$) of diagenetic-early hydrothermal stages, followed by partial reduction of anhydrite and leaching of country rock pyrite at the higher temperatures ($>150^\circ\text{C}$) of later hydrothermal stages. The significantly increased $\text{Fe}^{3+}:\text{Fe}^{2+}$ ratios of volcanic rocks in the strongly altered zones (up to ≈ 50 compared with values around 0.5 in the unaltered rock) suggest that the Fe^{2+} in the volcanic rocks was involved in the reduction of SO_4^{2-} . As the solubility of pyrite increases with temperature, the higher temperature hydrothermal fluids could acquire significant amounts of pyritic sulfur from the country rocks and attain $\delta^{34}\text{S}_{\text{SS}}$ values approaching around $+2$ per‰, the values for the underlying volcanic rocks. At temperatures around 300°C , the fluids may have acquired nearly equal amounts of sulfur from the anhydrite and from the pyrite. A similar model may be applicable to other Phanerozoic Zn-Pb-Cu VMS deposits formed in comparable geologic settings, although the reason for the weak correlation between decreasing $\delta^{34}\text{S}$ values and $\text{Cu}:(\text{Cu}+\text{Zn})$ ratios (Fig. 10.20) is not clear.

Anhydrite probably did not play a major role in the sulfur budget of most Cu-Zn

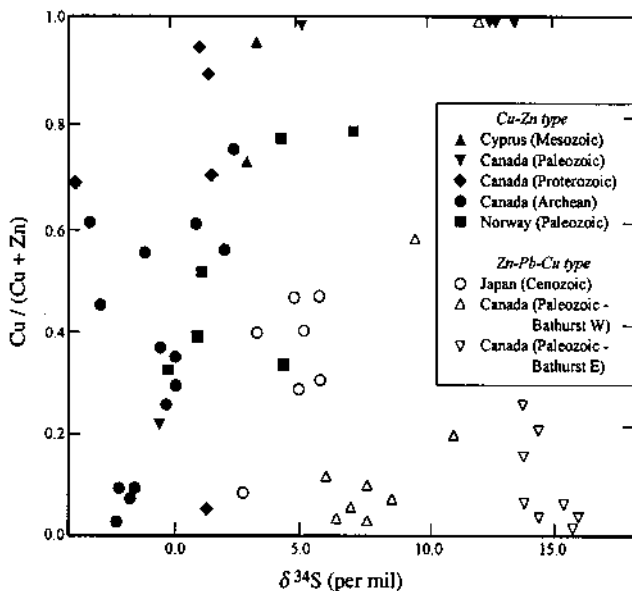


Figure 10.20. Relationship between average sulfur isotope ratio of pyrite from massive sulfide lenses of VMS deposits and bulk Cu:(Cu+Zn) ratio of the deposits (after Lydon 1984a). Note a clear separation between the Cu-Zn and Zn-Pb-Cu groups.

VMS deposits hosted by basaltic rocks and organic-rich sediments, because the higher amounts of reducing agents (Fe and C) in these rocks, compared with felsic rocks, should have led to the consumption of much or all of the early-formed anhydrite during the early stage of hydrothermal activity (Ohmoto et al. 1983). In other cases, such as the Precambrian VMS deposits, the ΣSO_4^{2-} content of seawater was probably too low for the precipitation of sulfates. The $\delta^{34}\text{S}$ values of sulfides in the Precambrian deposits are close to normal igneous values (Franklin et al. 1981) and this supports the idea that the ore fluids acquired H_2S mostly from sulfides in the basaltic host rocks.

10.10.4. PALEOTECTONIC SETTINGS

Massive sulfide accumulations around modern sea-floor hydrothermal vents have now been recognized at mid-ocean ridges and back-arc (intraoceanic and intracontinental) spreading centers. It is, therefore, logical to infer that analogous VMS deposits were emplaced at similar plate-tectonic environments through geologic time.

Plate-tectonic settings proposed for the different types of VMS deposits (Table 10.2) are based primarily on lithologic associations and include both extensional and compressional plate boundaries. The model proposed by Hutchinson (1980) for Phanerozoic volcanic-associated and sediment-hosted exhalative massive sulfide deposits

is interesting in that it emphasizes a space- and time-related evolutionary sequence for VMS deposits. He suggested that Phanerozoic VMS deposits formed at subduction-type convergent margins become progressively younger across a continentward-dipping subduction zone and are accompanied by an increase in Pb and Ag at the expense of Cu and Au. However, it is difficult to establish a consistent correlation between deposit-specific characteristics (e.g., metal ratios, mineral assemblages, morphology, alteration patterns) and tectonic environments, because such characteristics are dominantly controlled by local conditions (Swinden 1991).

An earlier school of thought (e.g., Sato 1974) regarded the Green Tuff belt of Japan, which contains all the Kuroko deposits, as an island-arc phenomenon initiated about 25 m.y. ago when the motion of the subducting Pacific plate changed from a NNW to a WNW direction. On the other hand, Uyeda and Nishiwaki (1980) suggested that the Green Tuff activity was characterized by rift-related bimodal volcanism, which occurred in a back-arc setting of the subducted Pacific plate, and was a part of the same process that resulted in the formation of a marginal sea (i.e., the Sea of Japan), separating the Japan island arc from the Eurasian continent (21-14 Ma). They pointed out that both Kuroko-type VMS and porphyry copper deposits are typical of volcanic-arc complexes, but they seldom occur together because the former forms in a tensional stress environment and the latter in a compressional stress environment. Cathles et al. (1983) have proposed a similar back-arc setting for the Green Tuff-Japan Sea region, but their model also postulates the existence of three centers of rifting and spreading during the late Tertiary time. The first opened the Sea of Japan, and the second, the Yamato Basin. The formation of Kuroko deposits was associated with a third rifting event about 13 m.y. ago that failed to open a marginal basin. A variant of the back-arc model proposed by Horikoshi (1990) envisages the circulation of hydrothermal solutions through extensional crust related to the opening of the Sea of Japan and the formation of Kuroko deposits when the metal-rich solutions were squeezed out due to a change in the tectonic stress field from extensional to compressional.

Other Zn-Cu-Pb as well as Cu-Zn VMS deposits of Phanerozoic age for which detailed geochemical data are available also appear to have formed in subduction-related arc or back-arc settings. Some examples are the deposits of West Shasta district (Albers & Bain 1985), Buchans district (Thurlow & Swanson 1987, Swinden 1991), Bathurst district (Paktunc 1990), Appalachian-Caledonian orogen (Stephens et al. 1984), and the Iberian pyrite belt (Williams et al. 1975). Ophiolites, some of which host VMS deposits, are now also considered to have formed in back-arc basins (Pearce et al. 1984, Thy & Moores 1988). Swinden (1991) has emphasized the importance of rifting for the formation of VMS deposits. Even in areas where the arc signature of volcanic rocks indicate an overall compressional environment, the local depositional environments appear to have been tensional.

The host rocks of VMS deposits in the Archean greenstone belts of the Canadian Shield are 2.7-Ga volcanic sequences comprised of mafic-felsic cycles (Thurston & Chivers 1990) that include both tholeiitic and calc-alkaline compositions, but according to Thurston et al. (1985) are dominantly bimodal basalt-rhyolite suites (Thurston et al.

1985). In the context of the tectonic model of the Canadian Shield discussed earlier (see Ch. 6), the calc-alkaline suites may represent the upper parts of mature island arcs and continental arcs, and the bimodal suites may be products of volcanism in back-arc basins (Card 1990). Thus, the Archean VMS deposits may have formed in subduction-related arc and back-arc settings similar to the Phanerozoic deposits. The relative absence of Cu-Zn VMS deposits in the 2.7 Ga volcanic sequence of the Norseman-Wiluna belt of Western Australia, despite its similarity to the Abitibi greenstone belt of Canada (Thurston et al. 1985, Barley & Groves 1990), is a puzzle. The Teutonic Bore massive sulfide (Cu-Zn-Pb-Ag) deposit, an economically significant VMS deposit within the Norseman-Wiluna rift Zone (see Fig. 6.6) has similarities to both the Noranda-type and Matabi-type deposits of the Canadian Shield; thus, tensional environments may have been important also for the Archean VMS deposits (Hallberg & Thompson 1985). The tectonic setting of the Golden Grove deposit hosted by a ≈ 2.95 -Ga-old bimodal volcanic association in the Murchison Province (see Fig. 6.6), the only other economically significant VMS deposit in the Western Australian Shield, is not well constrained.

The lack of VMS deposits in the older (>3.0 Ga) greenstone belt volcanic sequences, such as those of the Barberton Mountain Land (South Africa) and Pilbara Block (Western Australia), has been ascribed by Lowe (1985) to differences in the environments of volcanism and sedimentation. In contrast to the somewhat deeper depositional settings in the Superior Province of Canada, the older Archean supracrustal sequences were deposited under shallow-water to subaerial conditions. The latter situation was not conducive to the development of ore-forming hydrothermal plumes or preservation of the limited amount of sulfides that may have formed.

10.10.5. NORANDA-TYPE VERSUS KUROKO-TYPE VMS DEPOSITS

VMS deposits have formed throughout the Earth's geologic history, from about 3.5 Ga (Pilbara Block, Western Australia) to the Recent. It is likely that the age-frequency peaks discussed by Hutchinson (1973) and shown in Figure 11.19 would disappear if the number of deposits were normalized to the area of volcanic outcrop of given age ranges (Lydon 1984a). Similarities between the Archean Zn-Cu (e.g., Noranda district) and the Miocene Zn-Pb-Cu (e.g., Hokuroku district) VMS deposits such as the stringer-ore to massive-ore morphological zoning, the Cu to Zn \pm Pb compositional zoning, the chlorite-sericite mineralogy and oxygen isotopic characteristics of the footwall alteration pipes, and the localization of ore bodies at paleo-rift zones suggest that the basic processes of formation of VMS deposits have remained essentially the same throughout the Earth's history. There are, however, notable differences between the two types (Sangster & Scott 1976, Ohmoto 1989). Compared with the Kuroko-type deposits, the Noranda-type deposits are characterized by considerably lower Pb:(Pb+Zn+Cu) and sulfate:sulfide ratios, a generally much higher pyrrhotite:pyrite ratio, typically more Fe-rich chlorite in the alteration pipe, and sulfide $\delta^{34}\text{S}$ values of close to 0‰.

The high Pb content of the Kuroko-type deposits, their most distinguishing feature, may be related to a continuous increase through geologic time in the Pb content of the crust and mantle by radioactive decay of uranium and thorium (Sangster & Scott 1976). However, there is no statistical difference in the Pb contents of Archean and Phanerozoic volcanic rocks (Kanasewich 1968b, Ohmoto 1989). Indeed, some Archean deposits, such as the Mons Cupri deposit in the Pilbara craton of Western Australia (1 million tons of ore containing 3.6% Zn, 2.5% Pb, 1.0% Cu), are of the Kuroko-type (Barley 1992). Moreover, there is an abundance of lead in Proterozoic and Paleozoic base metal deposits (see Ch. 11 and Ch. 13). Thus, it is likely that the lead contents of VMS deposits are a consequence of the availability of a lead source to the mineralizing fluids and the solubility of lead in the fluids rather than the Earth's lead budget through time. The high lead contents of Kuroko-type deposits may be linked to a genetic relationship with calc-alkaline magmatism above a subduction zone, because the critical areas of magma genesis below arc systems are prone to fluid-borne enrichment in elements such as Pb and Ba derived from the subducting slab (Sawkins 1990).

Ohmoto (1989) speculated that the differences between the Archean and Kuroko-type VMS deposits could be explained if the Archean oceans were warmer ($\approx 40^{\circ}\text{C}$ vs. present $\approx 4^{\circ}\text{C}$) and sulfate-rich with $\delta^{34}\text{S}$ values of about +3‰ (compared with +20‰ at present), and if the Archean upper crust had a higher geothermal gradient ($\approx 50^{\circ}\text{C}/\text{km}$? vs. present $25^{\circ}\text{C}/\text{km}$). The consequences of a warmer crust would be slower cooling of subvolcanic plutons and circulation of larger masses of seawater at higher temperatures, causing preferential removal of Pb and Ba relative to Zn and Cu from ore piles by later hydrothermal fluids.

10.11. Summary

Volcanic-associated massive sulfide (VMS) deposits are considered to be ancient analogs of sulfide accumulations near hydrothermal vents at divergent and convergent plate boundary regimes of the modern sea-floor. They tend to occur in clusters, presumably around volcanic centers of the time, so that some mining districts contain large tonnages of VMS ore despite the relatively small size of individual deposits.

A typical proximal VMS deposit consists of a broadly concordant lens of massive sulfide, commonly zoned from Cu to Zn \pm Pb both vertically and laterally, that is stratigraphically underlain by a discordant stringer zone of stockwork and disseminated sulfide mineralization contained in a pipe-like body of hydrothermally altered rock. Commonly, a chemically precipitated sedimentary unit (iron-formation?) caps the massive sulfide lens or occurs as lateral extensions of the lens. A deeper-level, laterally extensive, metal-depleted, semiconformable alteration zone is well-developed in some deposits, but is poorly developed or absent in others. The main sulfide minerals are chalcopyrite, sphalerite, chalcopyrite, and pyrite \pm pyrrhotite; the characteristic hydrothermal alteration products are chlorite and sericite. Both types of sulfide mineralization and the footwall hydrothermal alteration are believed to have been

produced by moderately hot (up to about 350°-400°C) hydrothermal fluids, dominantly heated seawater, but probably with a magmatic component. Leaching of the footwall rocks appear to have provided much of the ore metals and sulfur, but contributions of sulfur from seawater and metals from crystallizing subvolcanic magmas cannot be ruled out. The stringer zone represents the main conduit of hydrothermal flow through the volcanic pile and the massive sulfide lens represents syngenetic (exhalative) accumulation on the sea-floor near the discharge vent. The essential elements of a VMS-producing hydrothermal system are: a sustained and large heat source, such as a subvolcanic pluton or sill, for the circulation of a large amount of relatively hot hydrothermal fluids; an insulating cap over the hydrothermal system for preventing unfocused fluid discharge; a conduit, such as a fracture or shear zone, for focused discharge of hydrothermal fluids; and rapid burial of the sea-floor sulfide accumulation by volcanic flows or sediments, before the sulfide could be destroyed by dissolution or oxidation. One of the least understood aspects of mineralization is the ubiquitous metal and mineral zoning in VMS deposits.

VMS deposits occur in rocks ranging in age from Archean to Recent (see Fig. 11.15), and are divisible into two groups: (a) a Cu-Zn group, hosted by sequences dominated by mafic volcanic rocks and particularly abundant in the Archean and Early Proterozoic greenstone belts of the Canadian Shield; and (b) a Zn-Pb-Cu group, hosted by sequences dominated by Phanerozoic felsic volcanic rocks and best exemplified by Kuroko deposits of the Miocene Green Tuff belt of Japan. Compared with the Cu-Zn group, the Zn-Pb-Cu group is characterized by much higher Pb:(Zn+Pb) ratio, abundant sulfate minerals (gypsum, anhydrite, and barite), lower Au:Ag ratio, sericite-rich footwall alteration pipe, and higher $\delta^{34}\text{S}$ (sulfide) values. The Cu-Zn group may be subdivided further into (a) Noranda-type, (b) Mattabi-type, (c) Cyprus-type, and (d) Besshi-type, based on details such as geologic setting, host rocks, and ore composition.

Deposits of both groups appear to have formed in subduction-type convergent plate boundaries, mostly in back-arc settings. The lack of Archean Zn-Pb-Cu deposits and the abundance of VMS deposits in the Canadian Shield with to other Precambrian shields are unresolved problems.

10.12. Recommended Reading

Lambert and Sato (1974), Spence and de Rosen-Spence (1975), Spooner (1980), Ohmoto et al. (1983), Lydon (1984a, 1988), Stanton (1986), Morton and Franklin (1987), Sawkins (1990), Slack (1993), Franklin (1993), Herzig and Hannington (1995), Leistel et al. (1998).

CHAPTER 11

SEDIMENT-HOSTED MASSIVE ZINC-LEAD SULFIDE (SMS) DEPOSITS

11.1. Introduction

This class of Zn-Pb sulfide (\pm barite \pm Ag \pm Cu) deposits constitutes a major global resource of zinc (>50%) and lead (>60%), and contributes 31% and 25%, respectively, of world's primary production of zinc and lead (Tikkanen 1986). This deposit class has been variously referred to as: Sullivan-type massive sulfide deposits (Sawkins 1976a); subclasses of stratiform sulfides of marine and marine-volcanic association (Stanton 1972); exhalative sedimentary group (Hutchinson 1980); sediment-hosted submarine exhalative deposits (SEDEX) (Large 1980, 1981, Carne and Cathro 1982); sediment-hosted Pb-Zn deposits (Badham 1981); sedimentary-type stratiform ore deposits in flysch basins (Morganti 1981); sediment-hosted stratiform lead-zinc deposits (Lydon 1983); syngenetic and diagenetic lead-zinc deposits in shales and carbonates (Edwards & Atkinson 1986); and shale-hosted deposits of Pb, Zn, and Ba (Maynard 1991b). By analogy with the volcanic-associated massive sulfide (VMS) deposits discussed earlier (Ch. 10), the descriptive term *sediment-hosted massive sulfide (SMS) deposits* is preferred, because it emphasizes the lithologic association of the deposits and excludes any genetic constraint. Most of the deposits included here are dominantly *stratiform* (i.e., the deposits are composed of sulfide layers parallel to the bedding of the host sedimentary rocks), but some are not, particularly those that have been highly deformed (McClay 1983). In addition, many deposits either contain, or are associated with, mineralization that is not stratiform. As has been pointed out by Large (1983), the term *massive sulfide*, which loosely describes mineralization containing more than 50% sulfides, separates this class from other classes of sediment-hosted sulfide deposits, such as the sediment-hosted (stratiform) copper deposits (see Ch. 12) and the Mississippi Valley-type Pb-Zn deposits (see Ch. 13); there are also significant differences in the lithologic association, nature of mineralization, and metal ratios among these three classes of sediment-hosted deposits. Also excluded from the present discussion are sediment-hosted barite deposits without significant base metal enrichment, such as those of the barite districts in Arkansas and Nevada (USA), although both deposit types are regarded as exhalative in origin. In contrast to SMS deposits, which are hosted by basinal clastics in dominantly intracratonic rift settings, barite deposits display geochemical signatures that indicate the influence of oceanic crust and appear to

have formed in compressional continental margin settings (Maynard 1991b), perhaps from cooler and shallower hydrothermal systems.

11.2. Distinguishing Features

The distinguishing features of an idealized, unmetamorphosed or mildly metamorphosed SMS deposit (Fig. 11.1) may be summarized as follows (Large 1981, 1983, Russell et al. 1981, Goodfellow et al. 1993):

- (a) mineralization hosted mostly either by marine, clastic sediments of continental derivation, typically pyritic and carbonaceous shales, or by platform carbonate rocks, with thin (1 to 10 cm thick) tuff horizons in the sedimentary sequence in some cases;
- (b) a zone of stratiform mineralization consisting of (i) stacked lens-like, concordant, tabular bodies of low-Cu massive sulfide ore, commonly composed of thin but remarkably continuous laminations of galena-sphalerite-pyrite that are conformable to the bedding of host rocks and interspersed with barren (meta)sedimentary units (the "bedded ore facies" of Goodfellow et al. 1993), and (ii) an outer margin of bedded hydrothermal products (barite, carbonates, Fe-oxides, chert, minor sulfides) of little economic value ("distal sedimentary facies" of Goodfellow et al. 1993);
- (c) a footwall zone of minor stockwork and vein-type sulfide mineralization associated with hydrothermal alteration (predominantly silicification), similar to the alteration pipe underlying VMS deposits (but termed "feeder pipe" by Goodfellow et al. 1993);
- (d) a distinct $(\text{Cu}) \Rightarrow \text{Pb} \Rightarrow \text{Zn} \Rightarrow (\text{Ba})$ lateral zoning of hydrothermally precipitated minerals and a less systematic $(\text{Cu}) \Rightarrow \text{Zn} \Rightarrow \text{Pb} \Rightarrow (\text{Ba})$ vertical zoning;
- (e) spatial association with a synsedimentary fault system that was active at the time of mineralization and may have been reactivated during later deformation; and
- (f) a general lack of demonstrable magmatic affiliation of the host rocks or of mineralization (although a few districts show a close temporal, and even spatial, relationship with mafic sills, dikes, and related volcanic rocks).

Apparently, SMS deposits have many features in common with VMS deposits (Ch. 10), especially of the Besshi-type, but there are significant distinctions as well (see Table 13.4). Compared with VMS deposits, SMS deposits show no clear evidence of a genetic relationship with volcanism, are characterized by stratiform (rather than strata-bound) mineralization, have higher Pb:Zn and much higher (Pb+Zn):Cu ratios (Fig. 11.2), lack a consistent $\text{Cu} \Rightarrow (\text{Zn}+\text{Pb})$ vertical zoning, and typically contain much

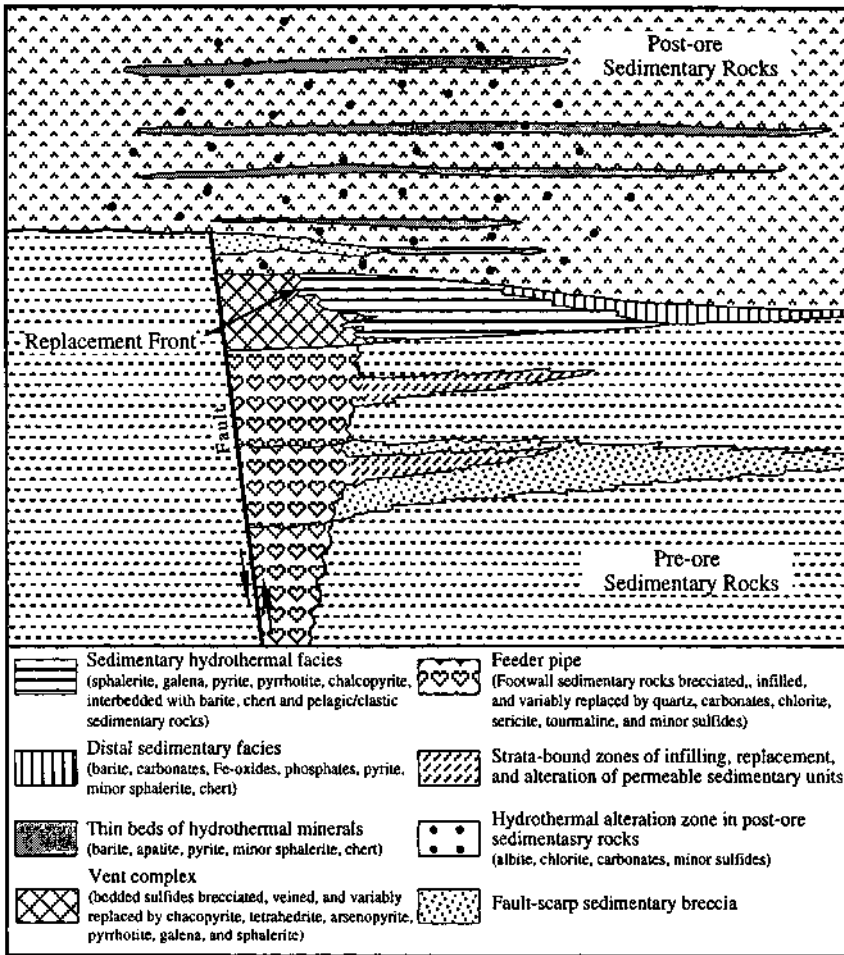


Figure 11.1. Vertical section of an idealized proximal sediment-hosted Pb-Zn-barite (SMS) deposit. Some deposits contain an economically important zone of interaction between upward-flowing hydrothermal fluids and hydrothermal sediments, which has been termed "vent complex" by Goodfellow et al. (1993). (After Goodfellow et al. 1993.)

higher combined (Pb+Zn) grades and tonnages, and higher contents of Ag and Co. The genesis of SMS deposits is more controversial (syndimentary to syndiagenetic to epigenetic) and it is quite possible that they are not bound by a single genetic model. Even for SMS deposits believed to be exhalative in origin, there are notable differences in ore-solution chemistry and depositional environment compared with VMS deposits. Distinguishing between SMS and distal VMS deposits, however, may be quite difficult in some cases, because distal VMS deposits tend to be Zn-Pb-rich, and very few sedimentary basins are completely devoid of volcanic rocks.

11.3. Distribution

As a result of many recent discoveries and re-classification of previously known deposits, it is now realized that SMS deposits have a much wider geographical distribution (Fig.11.3) than previously thought. Some of the largest Pb-Zn deposits in the world, containing between 10 and 50 million tonnes of (Pb+Zn) or more, belong to this class and a few also contain significant amounts of Cu and Ag. The well known examples of SMS deposits (Table 11.1) include those of Australia (Broken Hill, Mount Isa, McArthur River, Century, Lady Loretta, George Fisher, Hilton, Dugald River), Canada (Sullivan, Howard's Pass, Anvil, Tom, Jason), Germany (Meggen, Rammelsberg), Ireland (Tynagh, Silvermines, Navan), South Africa (Gamsberg, Aggeneys, Big Syn), USA (Red Dog), and India (Zawar, Rajpura-Dariba). The Balmat-Edwards Zn-Pb district in northwestern New York (USA), earlier considered to be of high-temperature magmatic and/or metamorphic origin (Lea & Dill 1968) and now generally accepted as premetamorphic, may represent a highly metamorphosed variant of the SMS class (Lydon 1983, Whelan et al. 1984).

Host rocks of SMS deposits fall into two main age intervals, Early to Middle Proterozoic (≈ 1700 -1400 Ma) and Lower to Middle Paleozoic (≈ 500 -320 Ma). Most of

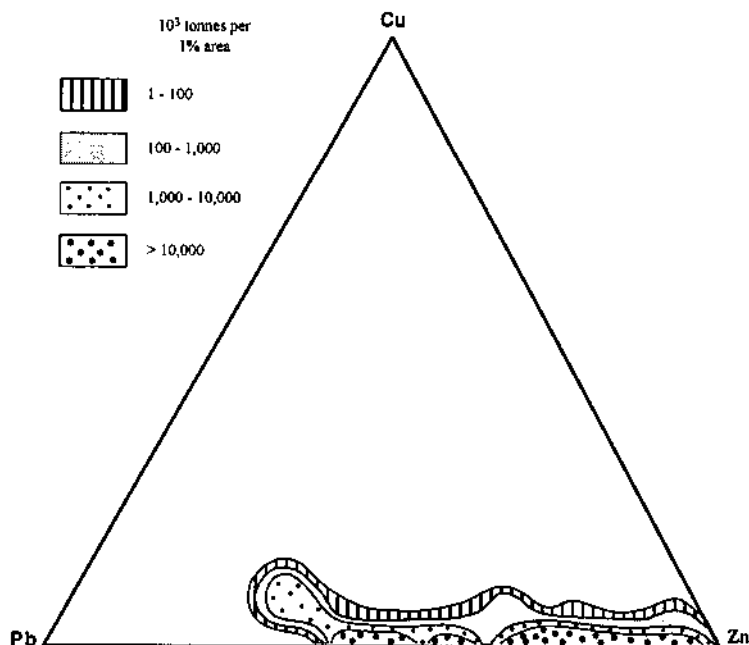


Figure 11.2. Cu:Pb:Zn proportions (wt%) of selected sediment-hosted massive Pb-Zn sulfide (SMS) deposits (after Lydon 1983). Note the lack of Cu compared with VMS deposits (Fig. 10.2).

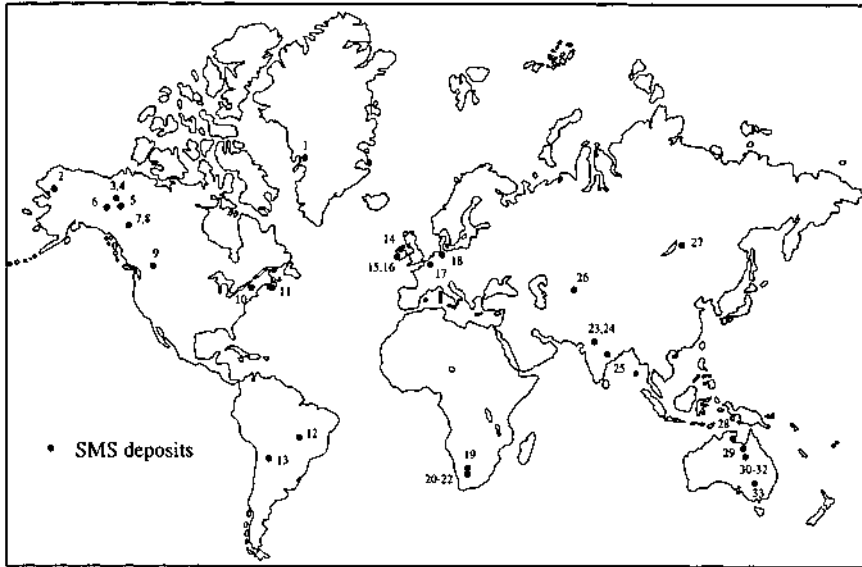


Figure 11.3. World distribution of major sediment-hosted massive sulfide (SMS) deposits: 1. Black Angel; 2. Red Dog; 3. Tom; 4. Jason; 5. Howard's Pass; 6. Anvil district (Faro, Grum, Dy); 7. Cirque; 8. Driftpile; 9. Sullivan; 10. Balmat-Edwards; 11. Walton; 12. Morro Agudo; 13. El Aguilar; 14. Navan; 15. Tynagh; 16. Silvermines; 17. Meggen; 18. Rammelsberg; 19. Aggeneys; 20. Gamsberg; 21. Big Syn; 22. Black Mountain; 23. Rajpura-Dariba; 24. Zawar; 25. Sargipali; 26. Mirgalimsai; 27. Kholodnina; 28. McArthur River (HYC); 29. Lady Loretta; 30. Mt. Isa; 31. Hilton; 32. Dugald River; 33. Broken Hill.

the giant deposits (e.g., Broken Hill, Mount Isa, McArthur River, Sullivan, Aggeneys, and Gamsberg, are hosted by Early to Middle Proterozoic rocks. Important examples of Paleozoic deposits are those of Ireland (e.g., Silvermines, Tynagh, Navan), Germany (Rammelsberg, Meggen), Kazakhstan (Tekeli, Mirgalimsai), Alaska (Red Dog), the Selwyn Basin in Canada (Howard's Pass, Tom, Jason, Anvil district), and South America (Aguiliar). The known younger deposits are small and very few in number; they are mostly restricted to the Jurassic strata of Pakistan, Cuba, and Azerbaijan.

The Broken Hill deposit is hosted by a package of clastic and chemical sediments of Early Proterozoic age, and its original features remain a contentious issue because of the overprint of amphibolite to granulite facies and intense tectonic deformation. It has been classified as: (a) a VMS deposit (e.g., Stanton 1976, Plimer 1979, Laing et al. 1984), mainly on the ground that the Potosi gneiss, which occurs both stratigraphically and spatially close to the orebody, has chemical composition consistent with a felsic volcanic precursor; (b) a SMS deposit (Lambert 1983, Sawkins 1984, Wright et al. 1987); and (c) a distinct type of deposit with features that are common to both SMS and VMS deposits (Beeson 1990, Parr & Plimer 1993). It is excluded from further consideration in this chapter.

TABLE 11.1. Selected sediment-hosted massive sulfide deposits/districts

	Reserves (million tonnes)	Average grade				Dominant lithology	Host rocks		Metamorphic facies
		Pb (%)	Zn (%)	Cu (%)	Ag (g/t)		Age		
Argentina	50	6.5	8.5	0.1	150	?	~ 450 Ma	?	
Australia	180	11.3	9.8	0.2	175	Sillimanite-garnet gneiss #	Early to Middle Proterozoic (~ 1800 Ma)	Granulite	
McArthur River (HYC)	104	6.4	14.1	-	64	Dolomitic siltstones and shales #	Middle Proterozoic (1640 ± 3 Ma)	Zeolite	
Century	118	1.5	10.2	-	36	Sideritic shale	1595 ± 6 Ma	Low grade	
Lady Loretta*	8.3	6.5	18.4	-	125	Calcareous siltstones and shales #	>1625 Ma	Low grade	
George Fisher	107	5.4	11.1	-	93	Calcareous siltstone	1654 ± 5 Ma	Low grade	
Hilton	49	6.5	9.3	-	151	Dolomitic siltstones and shales #	1654 ± 5 Ma	Lower greenschist	
Mt. Isa Cu Pb-Zn	255 89	- 7.1	- 6.1	3.3 0.06	7 160	'Silica Dolomite' Dolomitic and siliceous siltstones and shales #	1652 ± 7 Ma	Lower greenschist	
Dugald River	38	2.1	13.0	-	42	Dolomitic siltstones and shales	Middle Proterozoic	?	
Sullivan	155	6.6	5.7	-	68	Siltstones, quartzites, turbidites	Middle Proterozoic (~ 1430 Ma)	Lower amphibolite	
Canada									
Rammelsberg *	30	9.0	10.0	1.0	103	Black shale (slate) #	Middle Devonian	Greenschist	
Germany	60	1.3	10.0	0.2	3	Black shale (slate), pelagic limestone #	Middle Devonian	Greenschist	

TABLE 11.1 (continued)

	Reserves (million tonnes)	Average grade			Dominant lithology	Host rocks		Metamorphic facies
		Pb (%)	Zn (%)	Cu (%)		Age		
India								
Zawar	75	Pb + Zn = 5.5 - 6.7	-	-	Dolostone, phyllite, quartzite	Early Proterozoic (~ 1700 Ma)		Greenschist
Rajpura- Dariba	152	Pb + Zn + Cu = 2.6 - 7.4	122		Dolomitic marble, chert, schists	Early Proterozoic (~ 1800 Ma)		Max. meta. T = 555°C, P = 5.4 kbar
Ireland								
Tynagh*	9	6.2	5.0	-	Shallow marine carbonates #	Early Carboniferous		Not meta- morphosed
Silvermines*	18	2.5	6.4	-	Shallow marine carbonates	Early Carboniferous		Not meta- morphosed
Navan*	70	2.6	10.1	-	Mixed shallow-water carbonate facies -- micritic, sandy, oolitic and argillaceous	Early Carboniferous		Not meta- morphosed
South Africa								
Gamsberg*	143	0.6	7.4	0.03	Pelitic schist interbanded with quartzite and calc- silicate rock (Gams Iron Formation) #	Middle Proterozoic? (~1300 Ma)		Upper amphibolite
Aggenneys	>200	6.2	2.6	0.43	Pelitic schist interbanded with quartzite and calc- silicate rock (Aggenneys Ore Formation) #	Middle Proterozoic? (~1300 Ma)		Upper amphibolite
USA								
Red Dog	77	5.0	17.1	-	Black shale	Mississippian to Permian		?

*Deposit with significant amount of barite.

Volcanic rock present in the host rock sequence.

Sources of data: Rozendaal (1980), Gustafson & Williams (1981), Carne & Cathro (1982), Sawkins (1983), Lydon (1983), Ryan et al. (1986), Hitzman & Large (1986), Shanks et al. (1987), Deb and Sarkar (1990), Krat (1992), Goodfellow et al. (1993), Hitzman & Beatty (1996), Williams (1998).

11.4. Types of Deposits

Based on the lithology of host rocks, SMS deposits are divisible into two types: (a) clastic-hosted, and (b) carbonate-hosted (Lydon 1983). Except for two possible Proterozoic examples — Balmat-Edwards (USA) and Black Angel (Greenland) — the carbonate-hosted deposits, including the important deposits of Ireland, are Phanerozoic in age. Clastic-hosted deposits occur in both Proterozoic and Phanerozoic sequences, but all the giant deposits are Proterozoic. Carbonate rocks are an important component of the host sequences of Proterozoic SMS deposits in Australia (e.g., McArthur River, Mount Isa, Lady Loretta), but these are carbonaceous and argillaceous dolostones compared with the poorly argillaceous limestones of the Irish deposits.

A comparison of SMS deposits by dominant host lithology and age (Table 11.2) permits some generalizations (Lydon 1983): (a) for Phanerozoic deposits, there is virtually no difference in metal grades or ratios between the clastic and carbonate groups, suggesting little influence of the depositional environment on the chemistry of the deposit and derivation of ore fluids from similar geologic reservoirs in both cases; (b) the clastic-hosted Proterozoic deposits are the most enriched in Pb; and (c) the clastic-hosted deposits contain much larger tonnages of metals compared with the carbonate-hosted deposits, a difference attributable to greater abundance of argillaceous sediments (source of metals?) in the geological environments of the former.

TABLE 11.2. Weighted average grades and tonnages of sediment-hosted Zn-Pb deposits according to age and host rock lithology (after Lydon 1983)

	Number of deposits	Tonnage (million tonnes)	Grade				Zn:(Zn+Pb)
			Pb %	Zn %	Cu %	Ag g/t	
Phanerozoic							
Clastic-hosted	14	67.0	2.86	7.24	0.05	26	0.72
Carbonate-hosted	9	14.5	2.46	8.12	0.02	8	0.77
Proterozoic							
Clastic-hosted	13	90.0	5.09	7.14	0.13	71	0.58
Carbonate-hosted	2	12.2	1.78	11.51	-	9	0.87

11.5. Examples

11.5.1. McARTHUR RIVER (HYC), NORTHERN TERRITORY, AUSTRALIA

The McArthur River (also known as the HYC, a contraction of the expression "Here's Your Chance") deposit is one of many important SMS deposits located in Proterozoic sedimentary basins in northern Australia (Fig. 11.4). Particularly important are the

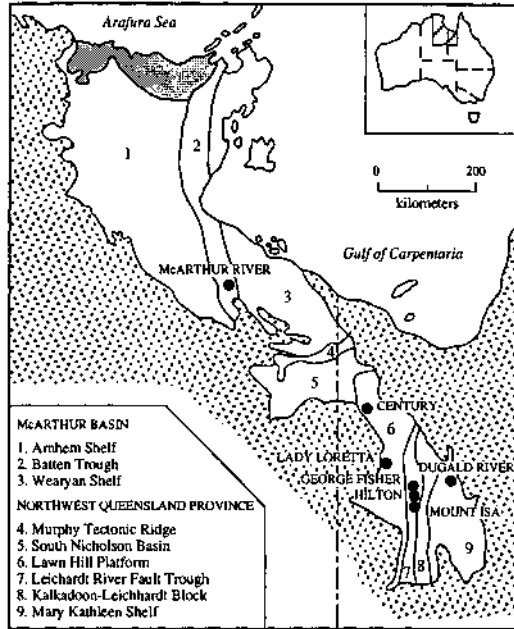


Figure 11.4. Geologic sketch map of the Precambrian rocks of the McArthur-Mt. Isa region, Northern Territory and Queensland, Australia, showing geologic domains and SMS deposits (after Williams 1980).

Batten Trough, the central structural element of the McArthur Basin, and the Leichardt River Fault Trough, both of which have been interpreted as intracratonic rifts that contain basinal facies sediments and are flanked by shallower-water sediments, predominantly shelf carbonates (Oehler & Logan 1977). The McArthur deposit, with resources of 237 million tonnes grading 9.2% Zn, 4.1% Pb, 0.2% Cu, and 41 g/t Ag (Gustafson and Williams 1981), is also one of the largest and least metamorphosed SMS deposits in the world. In the absence of metamorphic recrystallization, the sulfides are extremely fine-grained, diameters of sulfide grains seldom exceeding 10 microns compared with hundreds of microns in the more intensely metamorphosed Mount Isa deposit, and thus are not well suited for beneficiation. This has hindered commercial exploitation of the deposit, but the preservation of many original features of mineralization has rendered it an attractive target for investigating the genesis of SMS deposits (Croxford et al. 1975, Murray 1975, Walker et al. 1977, Oehler & Logan 1977, Lambert 1976, 1983, Williams 1978a, 1978b, 1979a, Eldridge et al. 1993, Perkins and Bell 1998, Large et al. 1998).

Zinc-lead-silver mineralization at McArthur occurs more than 3 km above the base of a thick (>5 km), Proterozoic sedimentary sequence that accumulated in the slowly

subsiding Batten Trough of the McArthur Basin (Fig. 11.4). The basinal sequence unconformably overlies an Early Proterozoic basement containing a thick pile of mixed mafic and felsic volcanic rocks, and is subdivided into three units (Williams 1979a): the Tawallah Group (Middle Proterozoic), consisting mostly of fluviatile and marginal marine sandstones in the upper part and volcanic rocks (dominantly mafic) in the lower part; the McArthur Group (Middle Proterozoic) dominated by evaporite-bearing dolomitic strata; and the Roper Group (Upper Proterozoic), composed of quartz-rich sandstone, micaceous siltstone, and carbonaceous shale.

Zn-Pb mineralization, restricted to the McArthur Group, is of two types: (a) a concordant (stratiform) type (HYC deposit) hosted by the carbonaceous and dolomitic HYC Pyritic Shale Member of the Barney Creek Formation (Fig. 11.5) dated by the U/Pb zircon method at 1640 ± 3 Ma; and (b) a relatively minor discordant type (Cooley and Ridge deposits), similar to carbonate-hosted Mississippi Valley-type deposits, hosted by brecciated dolostones. Williams and Logan (1981) interpreted the Barney Creek Formation to represent a mixture of shallow-water/ephemeral marginal marine or lacustrine sabkha deposition and turbiditic deposition at "intermediate" depths. On the other hand, Large et al. (1998) argued that water depth varied during deposition of the Pyritic Shale Member and that the HYC ore lenses were emplaced in the basal deep-water facies. Distant igneous activity during accumulation of the mineralized sequence is indicated by the presence of tuffaceous siltstones and many thin (8 to 30 cm thick), fine-grained, K-rich (up to 13% K_2O) tuffite beds. The tuffite has pseudomorphs of glass shards, now altered largely to K-feldspar (adularia) and, in some cases, replaced by sulfide minerals, probably during diagenesis. The deposit occurs close to the Emu fault (zone) that marks the eastern edge of the Batten Trough. The fault, interpreted as a growth fault that was active during mineralization, is believed to have provided the main conduit for mineralizing fluids (Williams 1978a).

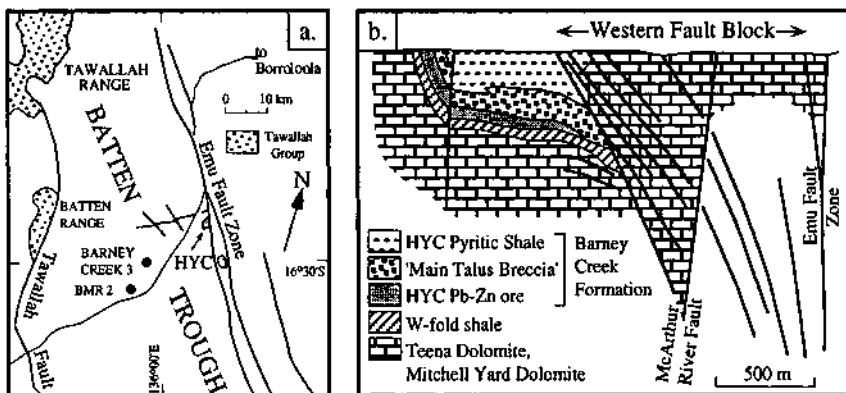


Figure 11.5. a. Sketch map showing the location of HYC deposit in relation to major faults; b. Cross section of HYC deposit, 182900N. (After Hinman 1995.)

The shallow-dipping HYC deposit is conformable with its host sediments and is tabular in shape with an average thickness of 55 m. The deposit contains seven highly mineralized groups of beds or potential orebodies separated from each other by relatively metal-poor, dolomite-rich, and commonly brecciated inter-ore beds (Murray 1975). The main sulfide minerals are pyrite, low-Fe sphalerite, and galena, and essentially monomineralic sulfide bands without any systematic ordering are common. Textural evidence points to at least two stages of pyrite formation: an earlier stage pyrite (Py_1) that occurs as euhedral crystals and spherical clusters (*framboids*); and a later stage pyrite (Py_2) that occurs as overgrowths on the earlier stage pyrite. Pyrite is also abundant at several levels in the hanging-wall strata and moderately abundant laterally away from the Pb-Zn mineralization. The deposit is not strongly zoned with respect to base metals, but there appears to be two cycles of decreasing Zn:Pb ratio upward from the bottom to the top of the ore horizon (Murray 1975). At the northern end of the deposit, a partly brecciated zone of mineralization that contains only minor sphalerite, but is relatively rich in chalcopyrite, galena, and freibergite, probably formed close to a major point of ore-fluid influx (Lambert 1983).

The origin of the HYC deposit is quite controversial. The stratiform nature of sulfide mineralization and the common occurrence of soft-sediment deformation structures (such as slumps, slides, and scours) in the ore horizon, are compatible with a *sedimentary-exhalative* model (Croxford & Jephcott 1972, Lambert 1976, 1983, Large 1983) as conceptualized in Figure 11.6a. Some authors, however, have advocated a syndiagenetic replacement origin for the Zn-Pb sulfides (Williams, 1978a, 1978b, 1979a, 1979b, Williams & Logan 1986, Eldridge et al. 1993, Hinman 1995). This interpretation (Fig. 11.6b) is based mainly on (a) textural relationships between the base metal sulfides and pyrite — the occurrence of galena and sphalerite as overgrowths on framboidal pyrite and within dolomite nodules, and (b) a discontinuity in the sulfur isotopic composition of the pyrites. According to Eldridge et al. (1993), the growth of Py_1 ($\delta^{34}S = -13$ to $+15\%$) and Py_2 ($\delta^{34}S = -5$ to $+45\%$) likely involved H_2S generation by biogenic reduction of sulfate in a system closed to sulfate. The relatively restricted sulfur-isotopic variability ($\delta^{34}S = -5$ to $+14\%$) of the base metal sulfides (sphalerite, galena, and chalcopyrite) was interpreted by these authors as evidence that the precipitation of the base metal sulfides did not involve biogenic H_2S , either directly through the use of residual microbially generated $H_2S(aq)$ or by replacement of Py_1 or Py_2 . They attributed the base metal sulfide emplacement to H_2S -bearing basinal brines that migrated along bedding planes. Recently, Large et al. (1998) have proposed a synsedimentary origin, a refinement of the exhalative model, to account for the sulfide sedimentary structures and the presence of Mn halos up to 20 km from HYC at the same stratigraphic position. Their interpretation of the sulfur isotope data may be summarized as follows: Py_1 was synsedimentary, formed with sulfur derived from dissolved H_2S in the anoxic bottom water; the galena-sphalerite layers were also synsedimentary, formed with sulfur derived from the anoxic bottom waters and from thermochemical reduction of SO_4^{2-} introduced in the metalliferous brine; and Py_2 was

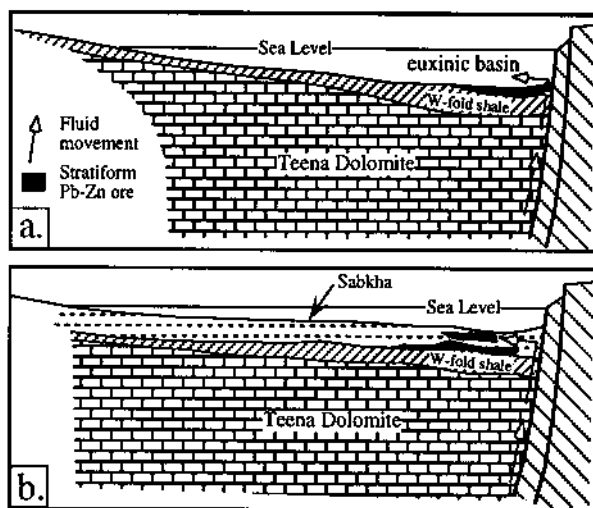


Figure 11.6. Digrammatic representation of genetic models for the HYC deposit: a. "Deep-water" sedimentary exhalative model (e.g., Croxford & Jephcott 1972, Lambert 1976); b. Shallow-water lagoonal syndiagenetic model (e.g., Williams & Logan 1986). (After Large et al. 1998.)

diagenetic, formed with sulfur derived by biogenic reduction of SO_4^{2-} introduced with the oxidized sedimentary and brine turbidites, which became trapped in the sediment-base metal sulfide layers. A further controversy has been introduced into the debate by the suggestion of Perkins and Bell (1998) that the HYC deposit formed by syntectonic replacement, an origin they favor for the Mount Isa and Hilton deposits.

11.5.2. MOUNT ISA, QUEENSLAND, AUSTRALIA

The sedimentary sequence in the Mount Isa region, the Mount Isa Group, is metamorphosed (lower greenschist facies) and deformed, but is broadly similar in character and age to that at McArthur. The Mount Isa Group, a ≈ 5 -km-thick package of mainly dolomitic and siliceous shales and siltstones, is part of the younger (1680-1600 Ma) of the two cover sequences in the Leichhardt River Fault Trough (Page & Sweet 1998). It unconformably overlies the Eastern Creek Volcanics, a pile of continental tholeiitic basalts with intercalated clastic sediments metamorphosed to amphibolite facies. This volcanic pile is believed to be the main source of copper for the Mount Isa copper sulfide mineralization (Smith & Walker 1971, Scott & Taylor 1982, Wilson et al. 1985, Wyborn 1987). In the mine area, the Mount Isa Group is truncated by a complex tectonic contact, the Paroo fault, which is underlain by altered Eastern Creek Volcanics (Bell et al. 1988). A minimum of three phases of deformation have been recognized regionally as well as in the mine area (Perkins 1984, Bell et al. 1988).

There are no talus or intraformational breccias in the mine, but thickness and facies changes provide evidence for syndepositional faulting and graben subsidence in the Mount Isa region (Smith 1969).

Disseminated framboidal pyrite is found throughout the sedimentary sequence in the carbonaceous horizons, but the massive sulfide mineralization (Mount Isa, Hilton, and George Fisher deposits) occurs more than 3 km above the base of the sequence, within the 1,500-m-thick Urquhart Shale (Fig. 11.7), which is composed mainly of tuffaceous, carbonaceous, dolomitic shale, and siltstone. Fine-grained tuffite bands, readily identifiable by their high potassium and chert contents, are common in the sedimentary sequence, and some are distinctive enough to be used as marker horizons. Recent SHRIMP geochronology of tuff bands at the Mount Isa and Hilton mines gave ages of 1652 ± 7 Ma and 1654 ± 5 Ma, respectively (Page & Sweet 1998). The presence of flat pebble conglomerates, pseudomorphs after evaporite minerals, stromatolites, oncooids, and tepee structures indicates that the upper Mount Isa Group, including the

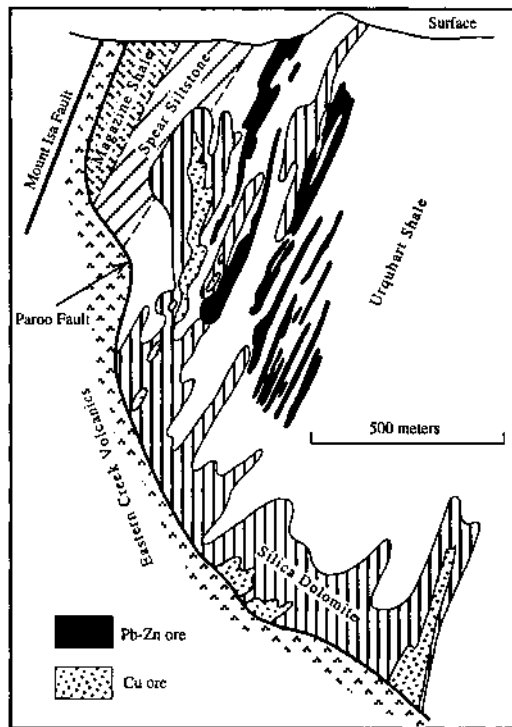


Figure 11.7. Generalized cross section of the Mount Isa deposit, located in the Batten Trough (Northern Territory, Australia), showing the *en echelon* configuration of stratiform Pb-Zn orebodies within the Urquhart Shale and the distribution of copper orebodies within the "silica dolomite". Structural details have been omitted for simplicity. (Simplified from Bell et al. 1988.)

Urquhart Shale, was deposited in shallow-water under hypersaline conditions (Neudert 1986).

The Mount Isa deposit, a major producer of base metals since the 1930's, comprises two physically distinct types of sulfide mineralization: stratiform Pb-Zn(-Ag) mineralization, and non-stratiform Cu mineralization. The stratiform mineralization occurs as conformable bodies that closely follow the sedimentary stratification and consist of individual laminae (0.5-10 cm thick) of fine-grained pyrite, galena, and sphalerite. Chalcopyrite, a very minor phase in the Pb-Zn ores, occurs as inclusions in Pb-Zn sulfide minerals. Where beds of economic sulfides are closely grouped together, they constitute an orebody. There are at least 14 distinct Pb-Zn orebodies in the deposit that stretch over a continuous strike length of more than 4 km. The inter-ore beds, composed mainly of dolomitic siltstone and shale, generally contain very little sulfide.

The stratiform Pb-Zn mineralization at Mount Isa is considered by most workers to be symsedimentary or syndiagenetic in origin (Stanton 1963, Mathias & Clark 1975, McClay 1983, Finlow-Bates & Stumpf 1979, Russell et al. 1981, Neudert 1984, Valenta 1994). Perkins (1997, 1998), on the other hand, has argued for a syntectonic origin. His main arguments are: (a) in gross terms, fine-grained pyrite distribution in the Mount Isa mine is discordant with the stratigraphy (including time markers provided by tuff bands), indicating a large-scale, post-sedimentation replacement process; (b) the fine-grained pyrite appears to have overprinted the main tectonic cleavage (nearly bedding-parallel, S_2); and (c) where there is an overprinting relationship between the fine-grained pyrite and the base metal sulfides, the pyrite is paragenetically earlier and either overgrown, or replaced, by the base metal sulfides, implying that the Pb-Zn mineralization was a late tectonic phenomenon. However, Valenta (1994) has reported that at the nearby Hilton mine, the fine-grained pyrite is overprinted by the tectonic cleavage and was deformed along with the Pb-Zn sulfides.

A special feature of the Mount Isa deposit (as well as of the Hilton deposit; Valenta 1994), compared with other giant Proterozoic Zn-Pb deposits, is the presence of major copper mineralization as irregular veinlets and patches. The copper orebodies, composed mainly of chalcopyrite, pyrrhotite, and cobaltite, are strata-bound within the Urquhart Shale and are hosted by the so-called "silica dolomite", an altered facies of the Urquhart Shale. The silica dolomite, as used in mine mapping, includes several related rock types characterized by brecciation and/or recrystallization, and either coarsely crystalline dolomite or high silica content (Mathias & Clark 1975, Perkins 1984). It truncates bedding, but lobes of alteration follow selected beds over distances of hundreds of meters and locally overprint Pb-Zn mineralization. The silica dolomite and the copper mineralization are most prominently developed in the southern part of the mine over the shallow-dipping contact with the Eastern Creek Volcanics, whereas toward the north the silica dolomite is split into a number of lobes (Fig. 11.7). Although the locus of the copper mineralization is south and downdip of the bulk of the Zn-Pb mineralization, individual Zn-Pb and Cu orebodies interfinger and both types of ores may be recovered from the same shaft.

The proposed models for the origin of the Cu ores and their relationship to the Zn-

Pb ores fall into five categories:

- (a) Both Zn-Pb and Cu ores are submarine exhalative in origin, but formed in different sedimentary environments; later tectonic processes produced brecciation of the silica dolomite and selective redistribution of the copper mineralization (Stanton 1963, Mathias & Clark 1975).
- (b) Both Zn-Pb and Cu ores are products of the same hydrothermal system; the Zn-Pb ores represent exhalative mineralization on the sea-floor, whereas the silica dolomite and Cu ore represent alteration and mineralization along conduits for hydrothermal solutions (Finlow-Bates & Stumpfl 1979), a model similar to that discussed earlier for VMS deposits, or replacement of the Zn-Pb mineralization (Goodfellow et al. 1993).
- (c) The Zn-Pb and Cu ores are cognetic, formed during or soon after sediment deposition. Neither formed on the sea-floor and their physical separation simply reflects differences in the relative solubilities of these metals. Subsequent tectonic and hydrothermal activity resulted in textural modification and redistribution of the primary Cu mineralization, but the Zn-Pb orebodies, farther removed from the basement contact, were not affected (McGoldrick & Keays 1990).
- (d) The Zn-Pb mineralization is syngenic to syndiagenetic, but the Cu mineralization is epigenetic and unrelated to the Zn-Pb ores (Murray 1975, Smith & Walker 1971, Smith et al. 1978, Muir 1981, Gulson et al. 1983, Swager 1985, Andrew et al. 1989, Heinrich et al. 1989, 1995).
- (e) Both the Zn-Pb mineralization and Cu mineralization were produced by epigenetic replacement during tectonic deformation (Perkins, 1997, 1998, Perkins and Bell 1998).

Textural and structural studies (Perkins 1984, Swager 1985) provide convincing evidence that the silica dolomite is a syntectonic hydrothermal alteration product of the Urquhart Shale hosting the Pb-Zn orebodies and that the copper mineralization resulted mainly through replacement, with or without attendant silicification, of previous coarsely crystalline dolomite. That the copper mineralization was a later event than the Zn-Pb mineralization is also indicated by the localized sulfur isotopic equilibrium among the major sulfides of the Zn-Pb orebodies, presumably due to metamorphism, and a lack of such equilibrium between pyrrhotite and chalcopyrite in the copper orebodies (Smith et al. 1978). Fluid inclusion and stable isotope studies (Heinrich et al. 1989) suggest that the dolomitic alteration was produced by chemical interaction between the Urquhart Shale and moderate amounts of two fluids — a CO₂-rich, local metamorphic fluid of the Urquhart Shale, and a CaCl₂-rich fluid introduced from the underlying greenstones. This was followed by silicification and copper mineralization by a NaCl-rich fluid under conditions of high fluid:rock ratios and near-lithostatic fluid pressures. Thus, the Mount Isa copper mineralization appears to be epigenetic and unrelated to the Zn-Pb ores. In fact, a study of many copper prospects in the Mount Isa

Block led Van Dijk (1991) to conclude that syndeformational dolomitization and copper mineralization, as recognized at Mount Isa, was a regional event.

11.5.3. ZAWAR, RAJASTHAN, INDIA

The productive massive sulfide belt of Rajasthan (Deb & Sarkar 1990) is located in the Aravalli-Delhi orogenic belt that extends some 700 km in a southwesterly direction from Delhi (Fig. 11.8). Supracrustal rocks of the region comprise an early to middle Proterozoic (1.8 to 1.1 Ga) sequence of metamorphosed sedimentary and volcanic rocks that is divisible into six lithostratigraphic domains: Bhilwara, Aravalli, Jharol, North Delhi, South Delhi, and Vindhyan. The orogen is divided into two distinct terranes by the Rakhadev lineament, a possible suture. The eastern terrane is underlain by an Archean basement composed of Banded Gneissic Complex (BCG), containing rocks as old as 3.5 Ga, and the large body of Berach Granite (2.6 Ga). The tectonic evolution of the Proterozoic sequence began with rifting of the Archean basement around 2.2 Ga and culminated with the development of an island-arc complex, represented by the South

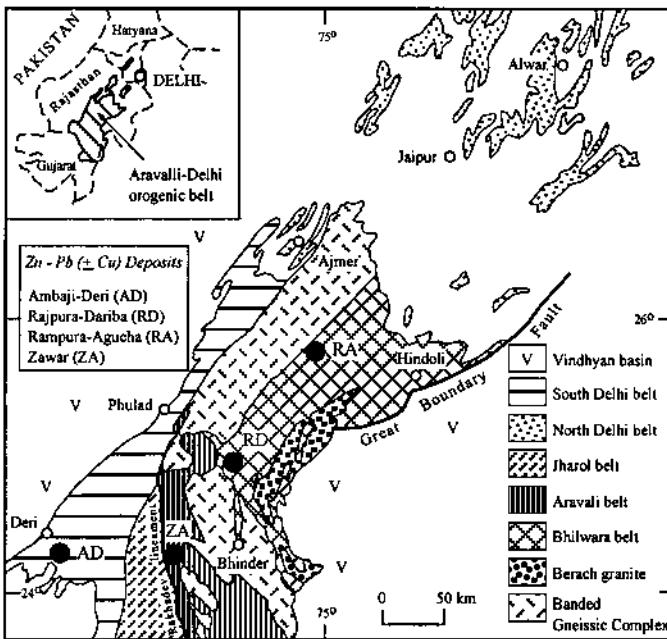


Figure 11.8. Simplified geologic map of a portion of the Aravalli-Delhi orogenic belt, Rajasthan, India, showing the location of major sediment-hosted Pb-Zn (\pm Cu) deposits: Ambaji-Deri (AD), Rajpura-Dariba (RD), Rampura-Agucha (RA), and Zawar (ZA). BCG = Banded Gneissic Complex, RL = Rakhadev lineament. (Simplified from Deb & Sarkar 1990.)

Delhi belt, around 1.1 Ga.. The Aravalli and Jharol belts (≈ 1700 Ma) represent two segments of a single basin. The Aravalli belt comprises a sequence of carbonate-bearing shelf sediments that were deposited on a passive continental margin at the rifted western edge of the Archean basement complex and subsequently folded and metamorphosed to greenschist facies. The carbonate-free deep-sea facies of this basin represents the Jharol belt (Roy et al. 1984). Mafic rocks occurring in the basal part of the Aravalli sequence have been interpreted as ocean-floor basalts (Deb & Sarkar 1990). Granitic intrusives are rare in the Aravalli and Jharol belts, which host all the massive Zn-Pb sulfide deposits of the region. The deposits have undergone appreciable deformation and metamorphism, but are believed to be exhalative in origin, formed in extensional tectonic settings, such as intracratonic and back-arc basins.

The Zawar district, located in the Aravalli belt, is the most important Zn-Pb mining district in India. The district includes several deposits (Mochia, Balaria, Zawar Mala, and Baroi), with pre-mining reserves estimated at about 75 million tonnes of ore with a combined (Pb+Zn) content of 5-6%. The main rock types of the district are quartzite, metagreywacke, phyllite, carbonaceous phyllite, and dolostone. The ore mineralization is restricted to the dolostone and the mineralized lenses terminate at the contact with phyllites. The principal ore minerals are sphalerite, galena, and pyrite, with minor amounts of pyrrhotite, arsenopyrite, argentite and native silver. The ores contain only trace amounts of copper as chalcopyrite and native copper. The pyrite occurs as both framboidal and non-framboidal forms, exhibiting various generations of diagenetic recrystallization, and is closely associated with sphalerite and galena suggesting a syngenetic origin of the sulfides (Chauhan 1984).

The Zn-Pb-Fe sulfide mineralization is of two types (Poddar 1965): (a) replacement bodies in dolostone along shear planes and later tensional fractures in zones of intense shearing, where primary stratification has been obliterated by deformation and recrystallization; and (b) stratiform mineralization, with well-preserved sedimentary structures, in dolostone free from considerable shearing and recrystallization. In the Mochia and Balaria mines, the mineralization is dominantly structurally controlled and was ascribed earlier to ascending hydrothermal solutions (Mookherjee 1964). The present consensus is in favor of syngenic-syndiagenetic sulfide mineralization with remobilization into structural planes during later deformation (Poddar 1965, Mukherjee & Sen 1980, Chauhan 1984).

11.5.4. SULLIVAN, BRITISH COLUMBIA, CANADA

The Sullivan deposit (Fig. 11.9), located near Kimberly, southeastern British Columbia, is the largest of several conformable Pb-Zn deposits (e.g., Kootenay King, North Star, and Vulcan) hosted by the Aldridge Formation of the Middle Proterozoic Purcell Supergroup. The Purcell Supergroup and its laterally equivalent Belt Supergroup in USA constitute a thick (>10,000 m) prism of dominantly clastic sediments that was probably deposited in an intracratonic basin (Hamilton et al. 1982). The Aldridge Formation, the lowest unit of the Purcell Supergroup exposed in the

Sullivan area, has been divided into three mappable units: the Lower, Middle, and Upper Aldridge. The Lower Aldridge is composed of a rhythmic succession of thin- to medium-bedded, very fine-grained quartz wacke that are commonly graded and interlayered with argillite and laminated sequences of dark mudstone. The Middle Aldridge is typically more arenaceous and coarse-grained, and has been interpreted as a turbidite sequence (Bishop et al. 1970). Thin-bedded to laminated carbonaceous mudstone is the dominant lithology of the Upper Aldridge. Pyrrhotite occurring as laminations and blebs is particularly abundant in the Lower Aldridge. The pyrrhotite is believed to be sedimentary, rather than metamorphic, in origin as its distribution throughout the Aldridge Formation is independent of metamorphic grade.

The Purcell sediments are associated with three igneous suites (Ethier et al. 1976, Hamilton et al. 1983). These are: (a) the Moyie (or Purcell) Sills (1433 ± 10 Ma, Zartman et al. 1982), a group of tabular gabbroic bodies that is most abundant in the Lower Aldridge Formation (the sill-like body of hornblende diorite in the Sullivan area belongs to this group); (b) the Nicol Creek Formation (or Purcell Lavas), dated at 1075 Ma (Hunt 1962), which occurs about 7,000 m above the Sullivan ore horizon (no flows have been found in the Aldridge Formation); and (c) the Hellroaring Creek Stock and related pegmatitic bodies (1300 Ma; Ryan & Blenkinsop 1971) that intrude metamorphosed and deformed Aldridge rocks and Moyie Sills in an area about 15 km southwest of the Sullivan mine. Based on the Pb-isotope data (Le Couteur 1979), the age of the Sullivan deposit is estimated to be ≈ 1500 Ma (Campbell & Ethier 1983).

The Sullivan deposit, about 2,000 m (N-S) \times 1,600 m (E-W) in lateral extent, is located near the top of the Lower Aldridge Formation, on the folded and faulted eastern limb of a broad north-trending anticline, and has the shape of an inverted and tilted saucer (Hamilton et al. 1983). It consists of a western proximal zone and an eastern distal zone, which differ significantly with respect to footwall rocks, style of mineralization, and associated hydrothermal alteration (Fig. 11.9). Pb:Zn ratios decrease from the western to the eastern zone.

The western zone, commonly greater than 60 m in thickness, is composed of a lower subzone of massive pyrrhotite and an upper subzone of massive to laminated pyrrhotite - sphalerite - galena (Fig. 11.9). In the latter, layering is defined by contorted wispy concentrations of galena and sphalerite in a pyrrhotite matrix and, toward the top part, by layers of fine-grained clastic sedimentary rock (Hamilton et al. 1983). According to Shaw and Hodgson (1980), the lower massive pyrrhotite subzone was originally composed of Pb-Zn-Fe sulfides, and the Pb and Zn leached from this zone by later, ore-stage fluids were redeposited at the sediment-seawater interface forming the overlying Pb-Zn-Fe ores. The eastern zone (maximum thickness 36 m) is conspicuously stratiform. It is characterized by sharply defined contacts between sulfide layers that differ strikingly in mineralogy and are conformable with the bedding of the intercalated and enclosing sedimentary rocks. Sedimentary features, such as soft-sediment slumps, graded beds, and sedimentary boudins, are observed in the eastern laminated ores. The ores in this zone are composed principally of pyrrhotite, sphalerite, and galena, but there is a gradual increase of pyrite relative to pyrrhotite

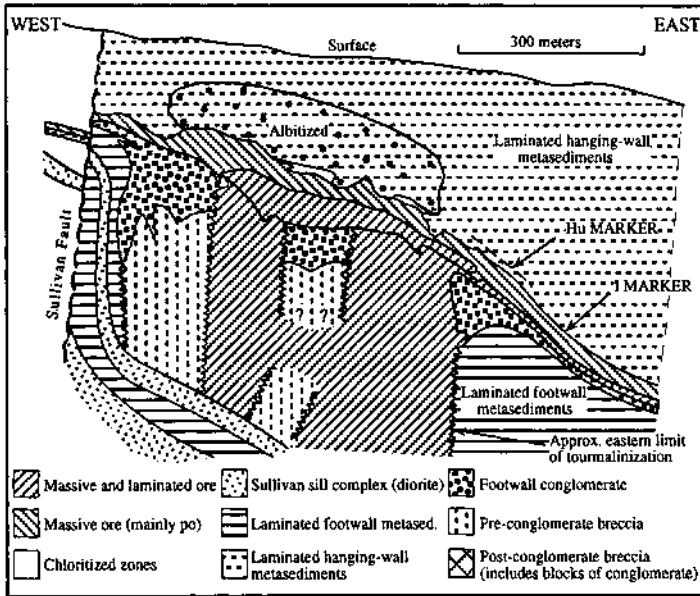


Figure 11.9. Schematic east-west cross section of the Sullivan deposit, British Columbia, Canada, showing the typical distribution of lithologic units and hydrothermal alteration (after Ethier et al. 1976). po = pyrrhotite.

toward the southeastern perimeter of the deposit. The Sullivan ores have been metamorphosed to greenschist facies, which is the typical metamorphic grade of the Aldridge Formation (Ethier et al. 1976).

Rocks typical of the upper part of the Lower Aldridge Formation occur within 200 m of the sulfide footwall. Immediately underlying the northern two-thirds of the orebody is an intraformational conglomerate (Fig. 11.9) that contains clasts and matrix of the same composition as the enclosing sedimentary rocks and appears to have been formed in a steep-sided depression as a result of syndepositional faulting. Zones of pre-conglomerate and post-conglomerate breccia have been recognized in the footwall of the western ore zone, the latter containing blocks of conglomerate (Jardine 1966). The breccia zones appear to be the result of local fracturing along northerly trending zones and associated collapse features (Ransom 1977, Campbell & Ethier 1983). The same fracture system probably served as channelways for hydrothermal fluids. Disseminated, concordant, and stockwork sulfide mineralization is widespread in the footwall rocks, especially below the western orebody. The principal sulfide minerals are pyrrhotite, pyrite, sphalerite, and galena; chalcopyrite and arsenopyrite are subordinate. The dominant non-sulfide minerals are quartz and calcite; cassiterite and scheelite occur locally. Unlike other major Proterozoic Zn-Pb deposits, Sullivan contains recoverable

quantities of tin, mainly as cassiterite, which occurs in the footwall fracture systems.

Also present in the footwall of the western ore zone is an extensive zone of tourmalinite, an extremely hard rock containing 30% or more tourmaline as felted masses of acicular to stubby crystals in a matrix of quartz, chlorite, K-feldspar, plagioclase, garnet, and minor muscovite (Hamilton et al. 1983). The tourmalinite zone is roughly funnel shaped with an elliptical top of approximately 1,400 m x 900 m, steep sides, and a vertical extent of at least 400 m. Within this zone, textures of breccia, footwall conglomerate, and normal bedding are well preserved, and crosscutting sulfide veins and discordant zones (1 to 30 cm wide) of albite - chlorite - pyrite - carbonate are common. In some places, the ore zone rests directly on top of the tourmalinite zone; elsewhere up to 5 m of tourmaline-poor sedimentary rocks separate the two. In the ore zone, tourmalinite occurs as tectonically rafted blocks, but more commonly disseminated tourmaline and rare patches of tourmalinite are erratically distributed in the hanging-wall overlying the western zone (Hamilton et al. 1983). Campbell and Ethier (1983) argued that the tourmaline formed from boron-rich fluids that invaded the Lower Aldridge Formation prior to the ore-forming event and attributed the source of boron to either leaching from the sedimentary pile or degassing of a granitic magma at great depth (probably the magma that ultimately produced the Hellroaring Creek stock and satellites). Hamilton et al. (1982, 1983), on the other hand, considered the footwall tourmalinitization as a product of hydrothermal alteration by the ore-forming fluids.

The hanging-wall of the Sullivan deposit, comprising Middle Aldridge sedimentary units with interbedded Fe or Fe-Pb-Zn sulfide layers, is intensely altered in the western zone to a coarse-grained rock composed of albite, chlorite, carbonate and pyrite (Fig. 11.9). This alteration zone extends for as much as 100 m above the ore zone and has a gradational contact with unaltered Middle Aldridge rocks. The alteration also extends into the top part of the ore zone, where the normal pyrrhotite-rich Zn-Pb ore is altered to a pyrite - chlorite - carbonate assemblage containing only minor amounts of pyrrhotite, sphalerite, and galena. The hanging-wall alteration clearly represents a continuation of the hydrothermal activity beyond the sulfide deposition event.

The Sullivan deposit formed from hydrothermal exhalations on the sea-floor (Cominco staff 1972, Ransom 1977, Campbell et al. 1978, LeCouteur 1979, Hamilton et al. 1982, Campbell & Ethier 1983, Nesbitt et al. 1984). This model is consistent with the sulfur isotope data for the ore sulfides suggesting a marine sulfate origin for the sulfur (Campbell et al. 1978, 1980), lead isotope data suggesting a crustal source for the lead and, by analogy, of the other metals (LeCouteur 1979), and the footwall alteration associated with the deposit (Hamilton et al. 1982, 1983).

11.5.5. RAMMELSBERG, HARZ MOUNTAINS, GERMANY

The Rammelsberg deposit is the largest sediment-hosted, "stratiform" Zn-Pb-Ag-barite deposit in Central Europe. It had been worked to shallow levels for silver over many centuries before its real extent and potential was recognized in late 19th century. A

detailed account of this highly deformed deposit is provided by Hannak (1981), which is the main source of the summary presented below.

The Lower Devonian (Emsian) sequence in the Harz Mountain, deposited in a littoral-neritic environment, contains minor syngenetic and epigenetic sulfide mineralization. During Middle Devonian (Eifelian), differential subsidence of the Variscan Trough led to two facies of sedimentation: a shallow-water facies of sandy and calcareous shales in the West Harz Rise; and a deeper-water, basinal shale facies (Wissenbach Shales) in the Goslar Trough. The Rammelsberg deposit, hosted by the Lower Wissenbach Shales, is believed to have formed in a local depression on the sea-floor close to the hinge zone between the Goslar Trough and the West Harz Rise. The shales that are contemporaneous with the ore horizon contain completely pyritized, dwarfed forms of brachiopods, goniatites, and tentaculites. Such dwarfed forms are typical of a biologically hostile environment, which was the consequence of metal-bearing sulfide solutions contaminating the seawater. More than 20 horizons of tuff, felsic to intermediate in composition, have been identified in the Lower and Middle Devonian strata below the ore horizon, but none above. A second period of regional volcanism, represented by diabasic greenstones, occurred during the late Middle Devonian to late Devonian time.

The Rammelsberg deposit consists of two sulfide orebodies which are designated, according to the relative dates of discovery, as the Old Orebody and the New Orebody. The Old Orebody has a strike length of 600 m, extends to a depth of over 3,000 m, and is approximately 15 m thick. The New Orebody extends to a depth of 500 m and has a true stratigraphic thickness of 10 m, but the thickness increases to about 50 m in the lower part of the orebody due to isoclinal folding. It is not certain whether the two orebodies are tectonically separated parts of an originally single orebody or they formed as separate entities. A further complication is the occurrence of a barite orebody ("gray ore") that overlies the Old Orebody and is physically separated from the sulfide orebodies. At present, the host rocks as well as the orebodies are part of a complicated isoclinal fold zone (the Orebody Syncline) overturned to the northwest, and the contacts between the orebodies and the host rocks are mostly marked by faults. The tectonic deformation, which occurred during the Variscan orogeny (late Carboniferous), has produced very complicated exposure patterns and fabrics within the orebodies as well as at their contacts with the host rocks.

Both orebodies are composed of two types of sulfide ores (Fig. 11.10): (a) massive ore, comprising layers with different proportions of pyrite, chalcopyrite, sphalerite, galena, and barite; and (b) banded ore, consisting of interlaminated stratiform sulfides (pyrite, sphalerite, galena, chalcopyrite) and black shale. The massive ore is characterized by colloform texture, including recrystallized framboidal pyrite, and an overall Fe (bottom) \Rightarrow Cu \Rightarrow Zn \Rightarrow Pb \Rightarrow Ba (top) zoning. Sedimentary structures such as graded bedding, cross-bedding, current-erosion channels, load casts, and slump folds are preserved in the banded ores. Gray ore in the New Orebody consists of massive barite with sphalerite, galena, and pyrite; the Gray Orebody above the Old Orebody is characterized by barite-shale alternation with scattered pyrite.

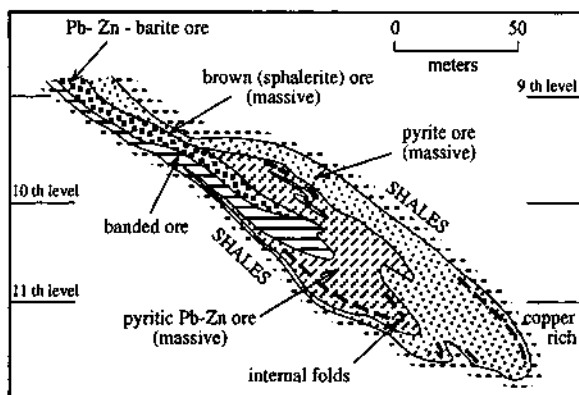


Figure 11.10. Cross section of the Rammelsberg New Orebody below the 9th level showing ore types and internal folds (after Kraume 1960).

The Rammelsberg orebodies are underlain by a discordant zone of "Kneist", a hard, partly brecciated and irregularly mineralized siliceous rock in which sulfides (sphalerite, galena, chalcopyrite, and pyrite) occur as veins and fracture-fillings. The Kneist has been interpreted by some as the discordant mineralization along the feeder zone to the overlying stratiform ore (Ramdohr 1953, Gunzert 1969), an interpretation consistent with the presence of a pronounced cone-shaped alteration zone in the footwall rocks with Fe-chlorites in the core and Mg-chlorites at its margin. Others have argued that the tectonic fabric and the lack of hydrothermal alteration in the Kneist indicate mineralization or remobilization subsequent to the formation of stratiform sulfides during a later tectonic event (Kraume 1960, Hannak 1981). A reconstruction of the

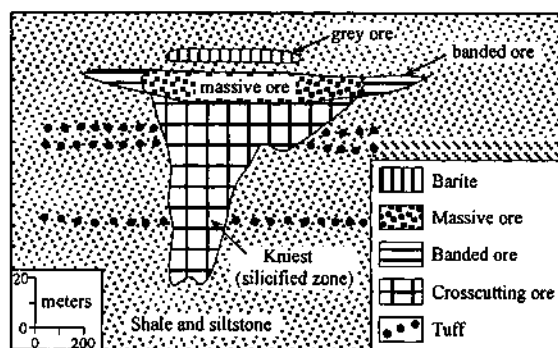


Figure 11.11. Reconstruction of the pre-deformation disposition of the Rammelsberg deposit, assuming that the deposit originally comprised a single orebody (after Ramdohr 1953). Vertical zoning in the massive ore (from bottom to top): Cu-rich ore \Rightarrow Zn-Pb ore \Rightarrow Pb-Zn-barite ore.

Rammelsberg deposit prior to deformation, assuming a single original orebody, is presented in Fig. 11.11.

11.5.6. NAVAN, IRELAND

A number of sediment-hosted Zn-Pb±Ba±Ag deposits (e.g., Navan, Lisheen, Tynagh, Silvermines, Galmoy) occur in the Lower Carboniferous, dominantly carbonate rocks, of the Irish Midlands. The deposits are generally restricted to three stratigraphic levels of a marine shelf succession: the Navan Group and equivalents; the Waulsortian facies; and the Supra-Waulsortian facies (Hitzman & Large 1986). The Navan Group in central Ireland is a mixed sequence of peritidal carbonate, clastic, and locally evaporitic sediments. The Waulsortian facies is a distinctive lithologic package composed mainly of poorly fossiliferous, micritic limestone derived from a mudbank complex. Rocks of the Supra-Waulsortian facies are shallow-water shelf limestones and deeper-water carbonate and argillites. Upper Carboniferous rocks in the Irish Midlands are generally terrigenous and record the transition from marine to non-marine sedimentation.

Massive Zn-Pb mineralization in the Navan Group and Waulsortian facies is broadly strata-bound (truly stratiform mineralization is present only in a few Irish deposits such as Silvermines and Navan), and is commonly associated with crosscutting, stockwork, and vein-type mineralization that extend from the base of the carbonate sequence (e.g., Ballinalack deposit). Most of the Irish deposits are located adjacent to faults that were active during mineralization and served as fluid conduits. Mineralization in the Supra-Waulsortian rocks generally occurs as crosscutting zones, commonly in breccia bodies.

The Navan deposit (Andrew & Ashton 1985, Ashton et al. 1986) in east-central Ireland, with initial ore reserves of 70 million tonnes averaging 12.7% (Zn+Pb), is the largest Zn-Pb deposit in Ireland. It was discovered in 1970 as a result of regional, shallow soil geochemical sampling and has been in production since 1977. About 97% of the ore at Navan is hosted by the Pale Beds (Navan Group), which comprise a 200 m-thick suite of pelletal, oolitic and bioclastic calcarenites, locally containing significant quantities of quartz sand and darker argillaceous layers. The Pale Beds-hosted ore is subdivided vertically into 5 lenses. The rest of the ore occurs within the Boulder Conglomerate, which has been interpreted as submarine debris-flow material deposited on a pre-Arundian erosion surface. No mineralization has been found in the Upper Dark Limestones overlying the Boulder Conglomerate. The Navan orebody occurs on the northwestern flank of a complex anticlinal structure that has been severely dislocated by a major NE-trending fault system, termed the A-C Fault Complex (Fig. 11.12). Although this fault system has post-ore movement of presumed Hercynian age, it was active during pre-Carboniferous time and during the mineralization event in the early Carboniferous time (Ashton et al. 1986).

Sphalerite with lesser amounts of galena comprise the main ore minerals of the Navan orebody; Fe-sulfides (pyrite and/or marcasite) are locally dominant in the ores of Conglomerate Group and in some parts of the Pale Beds. Barite and carbonates are the main gangue minerals.

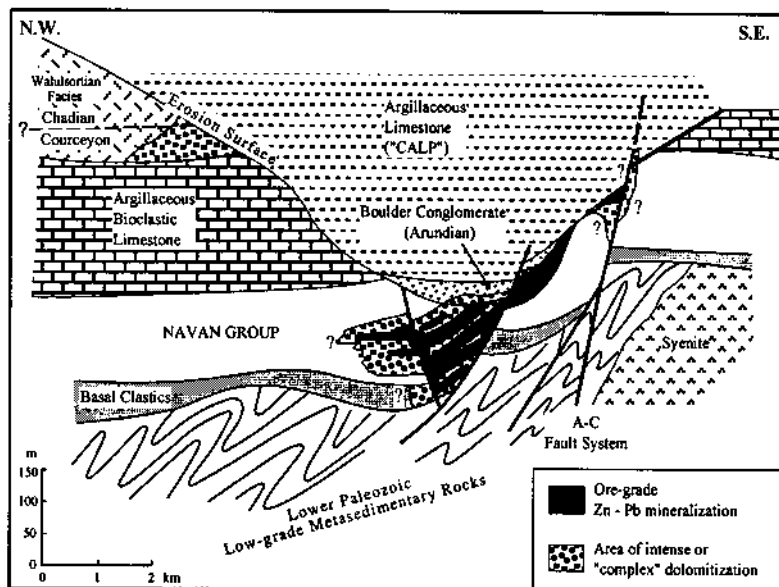


Figure 11.12. Schematic regional cross section through the Navan area based on data from Andrew and Ashton (1985) (after Hitzman & Large 1986).

Ores hosted by the Pale Beds show both bedding-parallel (stratiform) and crosscutting styles of mineralization. In its simplest form, the bedding-parallel mineralization consists of locally well-laminated sphalerite interlayered with smaller quantities of galena and, occasionally, thin bands of barite. The layering, however, is frequently disrupted by contortions and pull-apart structures with dislocation and rotation of broken fragments. In the absence of evidence for the presence of precursor material, such as evaporite, amenable to selective replacement by sulfide, the combination of well-developed laminated sulfide and soft-sediment deformation has been interpreted as evidence for the deformation of syngedimentary sulfide layers (Ashton et al. 1986). Crosscutting mineralization occurs in discrete veins and breccia zones, which predominantly strike NE to ENE and cut across the sedimentary stratification. The larger veins locally show crustification banding of galena and sphalerite, suggesting fracture filling-type, rather than replacement-type, mineralization. Some veins, particularly those containing pyrite or marcasite, postdate bedding-parallel sulfides, but many merge into bedding-parallel sulfide layers. The increase in thickness of the bedding-parallel sulfide layers near the zone of intersection suggests that the veins, formed by filling of hydraulic fractures (Phillips 1972), acted as feeders for the bed-parallel sulfide layers (Ashton et al. 1986).

The conglomerate-hosted mineralization is patchy and dominated by pyrite and/or marcasite of variable textures, ranging from fine-grained framboidal laminae of presumed syngenetic/early diagenetic origin to complex intergrowths with carbonate minerals. The highest grade mineralization takes the form of massive sulfides with irregular patches and locally laminated sphalerite and subordinate amounts of galena. This mineralization is also considered to be synsedimentary to early diagenetic (Ashton et al. 1986), and its feeders probably are represented by the pyrite-rich veins that pass through the stratiform sulfides hosted by the Pale Beds.

11.6. Ore Composition

11.6.1. MINERALOGY AND TEXTURES

SMS deposits typically contain one (e.g., Meggen) or more (e.g., Navan, Mount Isa) tabular bodies of stratiform sulfides up to a few tens of meters in thickness and hundreds to thousands of meters in lateral dimensions. In strongly deformed deposits (e.g., Rammelsberg), it is difficult to determine if the observed orebodies were originally separate bodies emplaced at the same or different stratigraphic levels, or they represent dismembered fragments of an originally continuous orebody. Some deposits (e.g., Sullivan) contain more than one orebody at the same stratigraphic level and may represent proximal and distal accumulations from the same mineralization event. Stockwork and vein-type sulfide mineralization is commonly found underlying or adjacent to the stratiform ore and the contact between the two styles of mineralization is usually quite distinct (Large 1983). As discussed earlier, the crosscutting mineralization in some deposits (e.g., Sullivan, Tynagh, Silvermines, Navan) is believed to represent epigenetic mineralization in the feeder system to the overlying stratiform ores; in others (e.g., Mount Isa, Rammelsberg), its relationship to the stratiform ores is controversial.

The dominant sulfide minerals of the bedded ore facies of stratiform mineralization are pyrite and/or pyrrhotite, sphalerite, galena, and minor chalcopyrite, arsenopyrite, and marcasite. The ratio of iron sulfides to base-metal sulfides varies from <1:1 to >5:1 (Goodfellow et al. 1993). The pyrrhotite is probably a primary phase rather than a product of metamorphism (Finlow-Bates & Large 1978, Hamilton et al. 1983). The most common non-sulfide gangue minerals are barite and chert, but carbonate minerals (siderite, ankerite, calcite, dolomite, witherite and other barium carbonate minerals) are quantitatively important in some deposits. Chert is spatially restricted to the ore deposits and probably represents an exhalative-hydrothermal silica phase (Large 1983). Layering defined by monomineralic layers of hydrothermal minerals, millimeters to tens of centimeters in thickness, is a conspicuous feature of the bedded ore facies. The distal sedimentary facies, which commonly has a gradational and assay-defined contact with the bedded ore facies, is simply a chemical sedimentary rock dominated by the more mobile or more stable and/or more oxidized, non-ore components of the bedded

ore facies. The vent complex (see Fig. 11.1), where present (e.g., Tom and Jason deposits, Canada), appears to be the product of partial replacement of previously deposited bedded ores by upward-flowing hydrothermal fluids. Commonly, the complex is a heterogeneous mixture of massive sulfide, replacement patches, and irregular veins and/or disseminations of sulfides, carbonates, and silicates (mostly quartz). The mineral assemblage is dominated by pyrite, pyrrhotite, galena, sphalerite, ferroan carbonate, dolomite, quartz, and tourmaline, and lesser amounts of muscovite, chlorite, chalcopyrite, arsenopyrite, and sulfosalt minerals (Goodfellow et al. 1993).

Many SMS deposits, especially those of Phanerozoic age, are associated with significant amounts of barite (see Table 11.1). The barite may occur stratigraphically above the sulfides (e.g., Rammelsberg), peripheral to the sulfide horizon (e.g., Meggen), as thin interbeds within stratiform sulfides (e.g., Tom, Navan), or as massive bodies within the sulfide zone (e.g., Silvermines). Some SMS deposits have no associated barite (e.g., HYC, Mount Isa, Sullivan). There is no apparent correlation between the Zn:(Zn+Pb) ratios and barite content in SMS deposits (Lydon 1983). The uneven distribution of barite, even among deposits of approximately the same age and tectonic setting (e.g., Mount Isa and Lady Loretta), is an unresolved issue.

Metal zoning is common in stratiform ores, but generally less systematic than in VMS deposits. The general sequence of zoning suggested by Large (1983), $(\text{Cu}) \Rightarrow \text{Pb} \Rightarrow \text{Zn} \Rightarrow (\text{Ba})$ in laterally zoned deposits and $(\text{Cu}) \Rightarrow \text{Zn} \Rightarrow \text{Pb} \Rightarrow (\text{Ba})$ in vertically zoned deposits, is an oversimplification. Lateral zoning, with Zn:Pb ratios increasing away from faults and/or breccia zones that have been interpreted as "feeder zones", is characteristic of both clastic-hosted and carbonate-hosted SMS deposits (Hamilton et al. 1983, Mathias & Clark 1975, Hitzman & Large 1986). The vertical zoning is much more variable. For example, upward in the stratigraphic sequence, Zn:Pb ratios tend to decrease at Rammelsberg, increase at Tom, Sullivan, and Navan, but show no systematic trend in HYC and Howard deposits (Lydon 1983, Ashton et al. 1986). With the exception of parts of the Rammelsberg deposit, chalcopyrite is usually not a significant component of the stratiform ores, but quite commonly an important phase in the stockwork part of the deposits. SMS deposits show no consistent trend in Cu:Zn or Cu:(Zn+Pb) ratios comparable to that in VMS deposits.

In addition to layering, the zone of stratiform mineralization commonly exhibits an array of sedimentary structures, such as graded bedding, cross-bedding, scours, slump folds, and intraformational breccia. Detailed structural analysis of Mount Isa and Sullivan deposits (McClay 1983) has shown that the major and minor structures in these deposits are overwhelmingly tectonic in origin, but synsedimentary folds produced by slumping can still be recognized. The latter are characterized by random structures with no particular geometric relationship to large-scale folds and a lack of axial planar sulfide fabrics or mobilization of sulfides to fold hinges. Evidence in favor of syngenetic emplacement of the stratiform sulfides is provided by the presence of intervals, at scales of a few centimeters or more, of irregularly folded, conformable sulfide laminae that are succeeded by undisturbed sulfide laminae (Lambert 1983).

11.6.2. BULK COMPOSITION

Almost all SMS deposits are bimetallic in Zn and Pb, but statistical correlation between the two metals is weak. Average Zn grades range between 2 and 10 wt%, with a maximum of about 19 wt%; Pb grades cluster between 1 and 4 wt%, with a maximum of just over 11 wt% (Sangster 1990). An analysis of bulk compositions of SMS deposits by Lydon (1983) has revealed several interesting features. The average grades and tonnages of SMS deposits (see Table 11.2) are much higher than those of VMS deposits. For example, the weighted average of 144 VMS deposits is 7.78 million tonnes of ore grading 1.25% Cu, 0.73% Pb, and 3.76% Zn, giving 0.45 million tonnes of combined metal; the weighted average of 38 SMS deposits is 59.57 million tonnes of ore grading 0.07% Cu, 2.98% Pb, and 7.29% Zn, which works out to 6.75 million tonnes of combined metal. Both VMS and SMS deposits have a bimodal distribution of Zn:(Zn+Pb) ratios. For VMS deposits, the two populations, with modes at 0.70-0.85 and >0.90, correspond to felsic volcanic and/or sedimentary rock association and mafic volcanic rock association, respectively. Metal ratios of SMS deposits also have a bimodal distribution, with mean Zn:(Zn+Pb) ratios of approximately 0.50 and 0.75 for the two populations (Sangster 1990). According to Lydon (1983), SMS deposits with the lower ratios tend to be hosted by clastic-dominated sedimentary sequences, whereas those with higher ratios occur in carbonate-dominated sequences.

There is no systematic difference in the distribution of Ag between the SMS and VMS deposits (Gustafson & Williams 1981). The Ag contents of SMS deposits are highly variable. For example, of the 38 SMS deposits listed by Lydon (1983), Ag grades are not reported for 10 deposits, probably because they are too low (<10 g/t) to be of economic significance, and 6 deposits have >100 g/t of Ag, the highest being ≈150 g/t in the Hilton deposit (Australia). An overall positive correlation between Ag and Pb in SMS deposits indicates galena to be an important carrier of Ag, but a significant amount of Ag is also contained in other sulfide and sulfosalt minerals in some deposits, such as Mount Isa, Broken Hill, and Sullivan. The most important of these are tetrahedrite, pyrrargyrite, and argentite (Riley 1974, Both & Stumpfl 1987).

11.7. Hydrothermal Alteration

Compared with VMS deposits, mineralization-related hydrothermal alteration associated with SMS deposits, generally, is quite subtle. This is so perhaps because of the less reactive nature and lower permeability of the fine-grained siliciclastic sediments that underlie most SMS deposits (Goodfellow et al. 1993). Examples of subtle hydrothermal alteration include the development of muscovite at the expense of chlorite and biotite in the immediately adjacent wallrocks of the Anvil district (Shanks et al. 1987), and an increase in dolomite:calcite ratio and in Mn and Fe contents of dolomite toward the deposits such as HYC, Mount Isa, Silvermines, and Navan (Lambert 1983,

Hitzman & Large 1986).

As discussed earlier, the "silica dolomite" of the Mount Isa deposit and the Kneist of the Rammelsberg deposit may represent zones of discordant, Cu-enriched mineralization and hydrothermal alteration comparable to those found in VMS deposits. In fact, the Rammelsberg deposit is associated with a cone-like, chlorite-rich footwall alteration zone (Renner & Brockamp 1985). The most pronounced hydrothermal alteration occurs in the footwall of the Sullivan deposit (Hamilton et al. 1983). Although tourmaline is a minor mineral in the alteration assemblages associated with many massive sulfide deposits (Taylor & Slack 1984, Slack & Coad 1989), the extent of tourmalinization at Sullivan is atypical of VMS and SMS deposits.

Hydrothermal alteration of the hanging-wall sequence (e.g., the albite - chlorite alteration at Sullivan) and the occurrence of low-temperature hydrothermal sediments (such as barite, phosphate, silica, and pyrite) in some deposits indicate that hydrothermal systems responsible for the formation of SMS deposits continued to operate, albeit at a lower intensity, for some time after ore deposition.

11.8. Origin

11.8.1. GENETIC MODEL

SMS deposits are believed by most workers (e.g., Hutchinson 1980, Large 1980, 1983, Lambert 1983, Sangster 1990, Goodfellow et al. 1993) to be dominantly syngenetic in origin, formed in an exhalative environment (Fig. 11.13). Such a model is compatible with the following characteristic features of SMS deposits:

- (a) the stratiform nature of sphalerite - galena - pyrite - barite mineralization (i.e., compositional layering parallel to bedding in the enclosing sediments), especially at the peripheral parts of orebodies;
- (b) the great lateral extent of the finely laminated sulfides at a single stratigraphic level;
- (c) the sharp contacts between the sulfide layers composed entirely of hydrothermal minerals and interbeds containing only trace amounts of the same hydrothermal minerals;
- (d) the associated sedimentary structures such as graded bedding, cross-bedding, scours, and sulfide clasts;
- (e) intervals of disharmonic folding of sulfide layers that are overlain by undisturbed layering; and
- (f) lateral and vertical metal zoning that is not consistent with a replacement origin, and discordant footwall mineralization and alteration in some deposits that may be reasonably interpreted as conduits of fluid discharge.

The majority of SMS deposits are not underlain by a discordant feeder/alteration zone

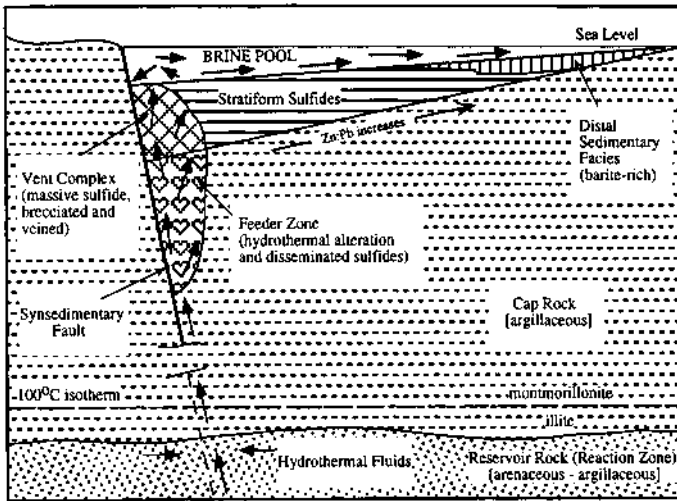


Figure 11.13. A conceptual exhalative model for the origin of a typical undeformed SMS deposits (after Large 1983, Lydon 1983, Goodfellow et al. 1993).

and, accordingly, may be regarded as distal-exhalative (Sangster 1990).

Some features of SMS deposits, especially those associated with carbonate rocks, appear to be syndiagenetic rather than synsedimentary or synmetamorphic. These include: contortion of crosscutting sulfide veins during sediment compaction at Navan (Ashton et al. 1986); association of stratiform sphalerite and galena with diagenetically recrystallized pyrite at Zawar (Chauhan 1984); replacement of stratiform pyrite, barite, and carbonate by Zn-Pb sulfide minerals at Silvermines (Andrew 1986); the occurrence of Zn-Pb sulfides as internal sediments in dissolution cavities at Tynagh (Boast et al. 1981); and the development of coarse-grained patches and large crystals of sulfides within fine-grained ores at Mount Isa (Lambert 1973). Perhaps the best case for predominantly syndiagenetic mineralization in a SMS deposit is provided by the HYC deposit in the McArthur basin of Australia.

The Irish deposits contain a variable combination of synsedimentary, syndiagenetic, and epigenetic mineralization, all related to the same mineralization event, and this may be a logical consequence of the ore-forming environment. Whether the mineralization was synsedimentary or syndiagenetic at a given locality was probably controlled by the relative rates of sedimentation and sulfide accumulation. For example, at Navan synsedimentary mineralization of an exhalative nature appears to have stayed abreast of rapid sedimentation, but mineralization also occurred at the same time in a range of diagenetic environments in the shallow-water carbonate sediments undergoing lithification (Andrew & Ashton 1985). The minor, vein-type Zn-Pb±Cu mineralization present in the older footwall sequence of many deposits (e.g.,

Silvermines, Navan) is clearly epigenetic.

Finlow-Bates and Large (1978) proposed that exhalative mineralization in shallow marine environments would tend to have a large proportion of epigenetic crosscutting mineralization with correspondingly less stratiform mineralization (e.g., Silvermines); the opposite would be the case in deep marine environments (e.g., Rammelsberg). This is because boiling of the hydrothermal fluids within the feeder zone would cause a rapid drop in temperature and, possibly, hydraulic fracturing, thus promoting crosscutting mineralization. However, fluid inclusion data do not support boiling as a major cause of mineralization at Silvermines (Samson & Russell 1987, Hitzman & Beaty 1996). The lack of evidence for boiling of the ore fluids, combined with the fluid inclusion data on temperature and salinity, were used by Sangster (1990) to constrain the minimum water depth of sulfide precipitation in selected SMS deposits to about 50 to 1,500 meters. The common occurrence of epigenetic mineralization in many Irish deposits, compared with typical SMS deposits, appears to be related to the presence of permeable and reactive carbonate host rocks (Lower Carboniferous) that consumed the mineralizing fluids before they could reach the sea-floor (Hitzman & Beaty 1996).

Most SMS deposits are associated with synsedimentary faults (Large 1983, Goodfellow et al. 1993). Evidence for contemporaneous fault movements at or close to the site of stratiform mineralization includes facies and thickness variation of host sediments across the fault, slump breccias and conglomerates, soft-sediment deformation indicated by local zones of folding and faulting of greater intensity relative to regional deformation, and the presence of sulfide ore fragments, sometimes with contorted sulfide laminae, within the breccias (Large 1983). The synsedimentary faults are believed to have controlled the generation of morphological traps (third-order basins) for accumulation of sulfides and provided near-surface, high-permeability channelways for ore fluids from deeper regions, probably through faults or fracture zones associated with local rifting or rapid differential subsidence of underlying sedimentary strata (Carne & Cathro 1982, Lydon 1983). They may also have initiated or accelerated convective circulation of overlying seawater to deeper levels of the crust (Russell et al. 1981).

11.8.2. ORE-FORMING FLUIDS

Very little fluid inclusion data, the main source of direct information on ore fluids, have been reported from the clastic-hosted SMS deposits because of the fine-grained nature of the primary sulfide minerals, the lack of associated coarse-grained gangue minerals, and the recrystallization of hydrothermal minerals by diagenesis and burial metamorphism. Estimates of temperature for these deposits, based on sulfur and/or oxygen isotopic ratios of coexisting mineral pairs, range from a low of $<100^{\circ}\text{C}$ for the Meggen deposit (Nielsen 1985) and $\approx 150^{\circ}\text{C}$ for the Sullivan deposit (Nesbitt et al. 1984) to a high of $\approx 300^{\circ}\text{C}$ for the Mount Isa and HYC deposits (Smith & Croxford 1973, Smith et al. 1978, Rye & Williams 1981). The lack of significant amounts of copper in most SMS deposits suggests that the temperature of the ore-forming fluid was generally below 300°C . [The solubility of chalcopyrite is <1 ppm Cu below 300°C at seawater

chloride concentrations and an oxygen partial pressure within the stability fields of sulfides (Lydon 1986).] This is consistent with the average homogenization temperatures of $\approx 260^{\circ}\text{C}$ and salinities of ≈ 9 wt% NaCl equivalent reported for Tom (Ansdell et al. 1989) and Jason (Gardner & Hutcheon 1985) deposits in Canada.

Fluid inclusion studies on the carbonate-hosted Irish deposits, generally limited to coarse-grained sphalerite and hydrothermal gangue minerals (dolomite, quartz, barite), indicate wide ranges of fluid temperature ($<100^{\circ}$ to $\approx 250^{\circ}\text{C}$) and salinity (<10 to ≈ 30 wt% NaCl equivalent). From an examination of all available fluid inclusion and stable isotopic thermometric data, Hitzman and Beaty (1996) concluded that the temperatures and salinities of fluids responsible for the mineralization in the Irish deposits were ≈ 100 - 190°C and ≈ 10 - 23 wt% NaCl equivalent, respectively. An overall negative correlation between homogenization temperature and salinity for quartz-hosted fluid inclusions from the Silvermines deposit has been interpreted as evidence of fluid mixing during the mineralizing process, both within and below the ore zone (Samson & Russell 1987). The fluids involved were Ca-depleted, one a high-temperature fluid of lower salinity (8-13 wt% NaCl equivalent) and the other a low-temperature fluid of high salinity (18-22 wt% NaCl equivalent). The presence of two fluids differing in temperature and salinity has also been inferred for mineralization at Lisheen (Thompson et al. 1992) and Tynagh (Banks & Russell 1992).

11.8.3. HYDROTHERMAL SYSTEMS

Many SMS deposits are associated with thin tuffite horizons (see Table 11.1) indicative of minor, penecontemporaneous volcanism. The eruptive centers of the tuffites have generally not been identified, but the fine-grained nature of the tuffites and the lack of lapilli in them suggest that the volcanic source must have been distant from the site of mineralization. In some areas, such as Ireland and the Rhenish Basin (Meggen deposit), there is evidence of an increase in volcanic activity during the mineralization event, but the two are not spatially related. A genetic connection between SMS deposits and magmas appears unlikely in view of a lack of coeval plutons either of sufficient size to have sustained hydrothermal convection for sufficient duration or of appropriate composition to have exsolved large quantities of Zn-Pb-rich fluids. Nevertheless, the time-frame of igneous activity in many areas containing SMS deposits does indicate higher than normal geothermal gradients during the mineralization event.

Considering the large tonnages of metals contained in individual SMS deposits and the low solubility of metals in saline hydrothermal fluids, the formation of a typical SMS deposit must have involved sustained flow of a large volume of ore-forming fluids. Moreover, the large ranges of fluid inclusion homogenization temperature and salinity for SMS deposits, often in the scale of an individual deposit (e.g. Silvermines), emphasize the complexity of the associated hydrothermal systems. Proposed models of fluid circulation can be grouped into three end-members: (a) one-pass flow along pressure gradients of basinal fluids expelled by sediment compaction (Walker et al. 1977, Williams 1978b, Badham 1981, Carne-Cathro 1982, Lydon 1983, Sawkins

1984); (b) thermally driven convection of seawater within an extensional basin to progressively deeper parts of the crust (Russell et al. 1981, Russell 1983); and (c) gravity-driven flow in a foreland basin (Hitzman & Beaty 1996), the model favored by many for Mississippi Valley-type deposits (see Ch. 13). The compaction driven fluid flow (stratal aquifer model) appears to be the more popular one at present. Modeling by Person and Garven (1994) suggests that compaction-driven groundwater flow dominates in the onlap facies during the thermal cooling (flexural) stage of the evolution of a continental-rift basin (when laterally extensive onlap facies are developed), as well as in the lacustrine facies deposited in the initial (stretching) phase of rifting.

The temperature and composition of the fluids derived by basin dewatering depends on the geothermal gradient and the minerals with which the fluid is in equilibrium. Dissolution of evaporites or the evaporation of marine or continental waters is the most direct way for achieving high salinities in basinal waters. The likely importance of this process is underscored by the observation that most SMS deposits lie within about 30° of the equator in paleogeographic reconstructions of land masses (Turner 1992). A possible alternative for producing high-salinity fluids is the reaction of connate fluids with the enclosing sediments. Computations by Lydon (1983) showed that under reasonable geothermal gradients connate fluids in a reservoir of arenaceous and argillaceous rocks would be buffered to a pH of about 4.5, attain temperatures of 100-200°C and salinity up to ≈25 wt% NaCl equivalent, and be capable of carrying high concentrations of Zn, Pb, Ba, Fe, and Ag as chloride complexes, but not much Cu at temperatures below 200°C. The metal ratios in the fluids and in the resulting SMS deposit would depend mainly on the fO_2 of the reservoir (reaction) zone.

Conditions favorable for the stratal aquifer model are (Lydon 1983, 1986): (a) a syn-rift clastic sequence containing adequate connate water; (b) an impermeable cap of argillaceous sediments that helps to maintain elevated temperatures in the underlying reaction zone by minimizing conductive and convective heat loss and to promote geopressuring of the hydrothermal reservoir; and (c) extensional faulting that provides a conduit for cross-stratal upward flow of the hydrothermal fluids to the sea-floor. As the basin dewatering is likely to be episodic (Cathless & Smith 1981), the stratal aquifer model offers a mechanism for the formation of stratigraphically stacked ore lenses separated by barren layers of host rock, each ore lens representing a separate influx of ore fluids (Sawkins 1984), although alternative mechanisms such as intermittent precipitation from a virtually stagnant brine pool or periodic influxes of sediments are possible (Lydon 1983). The model is also compatible with the close spatial association of SMS deposits with synsedimentary faults, because upward movement of high-salinity, hence high-density, brines by release of an over-pressured reservoir system or by seismic pumping (Sibson et al. 1975) would be facilitated by faulting. A criticism of the brine expulsion model is that the temperatures of ore fluids for SMS deposits range up to about 300°C, significantly higher than would be predicted by the model (Russell 1983). Lydon (1986) has pointed out that hydrothermal fluids for the Silvermines deposit in Ireland record an evolutionary path characterized by decreasing salinity with increasing temperature. This is the trend expected from progressive

tapping of a geopressed stratal aquifer, as saline pore waters of the reservoir are progressively diluted by water released from clay minerals with increasing temperature.

Both models envisage extensional structures as paths of fluid discharge, but they predict different spatial relationship among deposits in a given region. A cluster of deposits would reflect the distribution of favorable structural or stratigraphic traps according to the basin-expulsion model, but would require the operation of a number of convection cells, each with its own area of influence, for the convection model. A large mineralization trend, such as the 5 km-long trend in the Navan area, is difficult to reconcile with the convection model, but is compatible with the basin-expulsion model as representing suitable traps along an aquifer (Hitzman & Large 1986).

An attractive feature of the convection model (see Fig. 2.27e) is that it allows for variable temperature and composition of the hydrothermal fluids depending on the depth of penetration of the convection cell. For example, the later copper mineralization at Mount Isa may simply reflect significant (≥ 1 ppm) copper solubility in fluids that had attained higher temperatures because of penetration into basement rocks at greater depths. Using a thermal balance model of hydrothermal circulation, assuming a maximum temperatures of 200-500°C for the fluids and a porous medium, Sterns et al. (1987) computed that such a system would be capable of forming very large Zn-Pb deposits, provided that the metals were available to the system. But the question is whether rocks in a sedimentary basin are permeable enough for downward penetration of convection cells to depths of 6 to 10 km as envisaged in this model. The downward propagation of microfracturing necessary for this process requires the presence of extensively jointed rock (Pine & Batchelor 1984), but the sediments underlying SMS deposits were probably not lithified enough to be jointed. On the other hand, Mills et al. (1987) have argued that a progression to less radiogenic lead with time, as shown in their study of the Navan deposit, is best explained by the convection cell model that envisages extraction of metals from progressively deeper levels of the crust. The convection cell model is also consistent with the lead isotopic data for the Irish deposits suggesting a dominantly basement source for the lead (Caufield et al. 1986, LeHuray et al. 1987). A convection-cell model has also been proposed for the sea-floor sulfide accumulations in Middle Valley and the Guaymas Basin, although in these cases the convection cells appear to be driven by the heat of high-level magma bodies.

The foreland basin model proposed by Hitzman and Beaty (1996) for the Irish deposits envisages that the hydraulic head for gravity-driven flow was provided by the Lower Carboniferous uplift of the Hercynian mountains south of Ireland. The Old Red Sandstone (Upper Devonian to Lower Carboniferous) served as the principal aquifer for fluid migration. The migrating formation waters were heated either by relatively deep flow paths, or by the extension-related high heat flow along the flow path. Gravity-driven models, however, do not explain the correlation between SMS deposits and continental rifting and the localized submarine discharge of hydrothermal fluids at cratonic margins (Goodfellow et al. 1993).

A notable aspect of the giant SMS deposits (e.g. HYC, Mount Isa, Sullivan) is the considerable stratigraphic interval over which conformable mineralization occurs. In

addition, the hanging-wall in many SMS deposits shows hydrothermal alteration and precipitation (see Fig. 11.1). Thus, irrespective of the model, the hydrothermal system for these deposits must have remained active intermittently for millions of years. This is in sharp contrast to VMS deposits which probably formed over time periods of only hundreds of years (Sawkins 1983).

11.8.4. ORE ACCUMULATION

The mechanism of ore accumulation in SMS deposits is less clear than for VMS deposits, because modern analogs of SMS deposits are rather limited. That the process for proximal SMS deposits might have been initiated by a VMS-style build-up of sulfide mounds where feeders debouched on to the basin floor derives some support from the recent discovery of fossil hydrothermal chimneys at Silvermines (Boyce et al. 1983) and Tynagh (Banks 1986). These are tabular, concentrically zoned growth forms of pyrite-marcasite up to 5 cm long and 2 cm in diameter, resembling miniature versions of 'black smoker' chimneys of the East Pacific Rise at 21°N. Alternatively, the bedded ores may represent either a shower of sulfides onto the sea-floor from buoyant hydrothermal plumes or an apron of clastic sulfides shed from sulfide mounds (Goodfellow et al. 1993). The tabular morphology of the stratiform mineralization as well as the great lateral continuity of individual beds and laminae, however, are more in accord with sulfide accumulation of in brine pools formed at topographic lows on sea-floor, similar to the accumulation of metalliferous sediments in the Atlantis II Deep, Red Sea (see Ch. 2). Changes in the geochemical parameters (P , pH, fO_2 , sulfide concentration, salinity) required for precipitation of the observed sulfide assemblages in SMS deposits have been modeled assuming appropriate boundary conditions (e.g., Russell et al. 1981, Russell 1983, Lydon 1983, Large et al. 1998), but these models do not uniquely define the mechanism(s) of sulfide precipitation.

11.9. Metallogenesis

11.9.1. HOST ROCKS

Large (1981, 1983) characterized the geologic settings of SMS (SEDEX) deposits in terms of first-order, second-order, and third-order basins, a hierarchy of sedimentary basins of decreasing size. The first-order basins may be either epicratonic embayments into continental margins, usually initiated during extension of a passive continental margin, or intracratonic basins. They are commonly fault-bounded, half-graben features of lateral dimensions in excess of 100 km, containing thick sequences of clastic and/or carbonate sediments that were deposited during a prolonged period of crustal stability. The sedimentary facies vary from shallow-marine evaporite-bearing carbonates and sandstones (e.g., Batten Trough, Leichardt River Fault Trough), to delta-front sandstones and siltstones (e.g. Belt-Purcell Basin), to deeper marine turbidities, pelagic

carbonates, and shales (e.g., Selwyn Basin). Syndimentary differential subsidence within first-order basins gives rise to second-order basins of tens of kilometers in lateral dimensions flanked by rises (e.g., the Goslar Trough and the West Harz rise within the Variscan Trough). The presence of second-order basins can be identified by variation in sedimentary facies and thickness revealed through detailed geologic mapping. Third-order basins are relatively small depressions, several hundred meters to a few kilometers in lateral dimensions, and they represent actual depocenters of massive sulfide formation. Sediments that host SMS deposits in third-order basins may be viewed as a combination of "autochthonous" lithologies (fine-grained clastics and carbonates) and "allochthonous" lithologies (conglomerates, intraformational breccias, and coarse clastic sediments that are commonly interbedded with fine-grained sediments). The recognition of locally derived allochthonous lithologies helps in the identification of third-order basins, an important step in the exploration of SMS deposits. Sulfide deposits often occur close to the fault-controlled margins of the first- or second-order basins. As mentioned earlier, these faults were active during sedimentation and are believed to have provided the main conduit for the ore-forming fluids. Reactivation of these faulted margins may produce distinctive lineaments, such as the Emu fault (Fig. 11.5), the Mount Isa fault (Fig. 11.7), and the Balve-Overscheld fault zone at the western end of the Meggen basin (Werner 1989).

It is apparent from an examination of the host rocks that SMS deposits have formed both in the deep-water ('black shale') environment as well as in shallow basins dominated by carbonates and evaporites (Sangster 1990). Also, there is no simple relationship between host lithology and other features of SMS deposits. For example, the host lithology and tectonostratigraphic setting of Rammelsberg and Mount Isa deposits are quite different, but they are very similar in many other respects. The control of host lithology on SMS mineralization appears to be indirect, reflecting factors such as the distribution of organic matter and/or fortuitous proximity to plumbing systems (Gustafson & Williams 1981).

11.9.2. SOURCE OF SULFUR

From a comparison of $\delta^{34}\text{S}$ values of sulfides and barite with coeval seawater sulfate (see Fig. 4.4), Sangster (1990) concluded that the ultimate source of sulfur for SMS deposits was seawater sulfate. The interpretation of the sulfur isotopic data for individual deposits/districts (Fig. 11.14), however, is more complicated.

The close agreement between $\delta^{34}\text{S}$ values of coeval seawater and barite at Tynagh, Silvermines, Rammelsberg, Meggen, and in the deposits of Selwyn Basin suggests that the sulfate in these deposits was derived from marine sulfate in formation waters. The unusually high $\delta^{34}\text{S}$ of barite at Lady Loretta is probably a reflection of the restricted nature of the depositional basin in which the $\delta^{34}\text{S}$ of the residual seawater became higher after the precipitation of diagenetic pyrite.

In contrast to barite, $\delta^{34}\text{S}$ values of sulfide phases show considerable variation among deposits and even within a single deposit. The generally large variation in $\delta^{34}\text{S}$

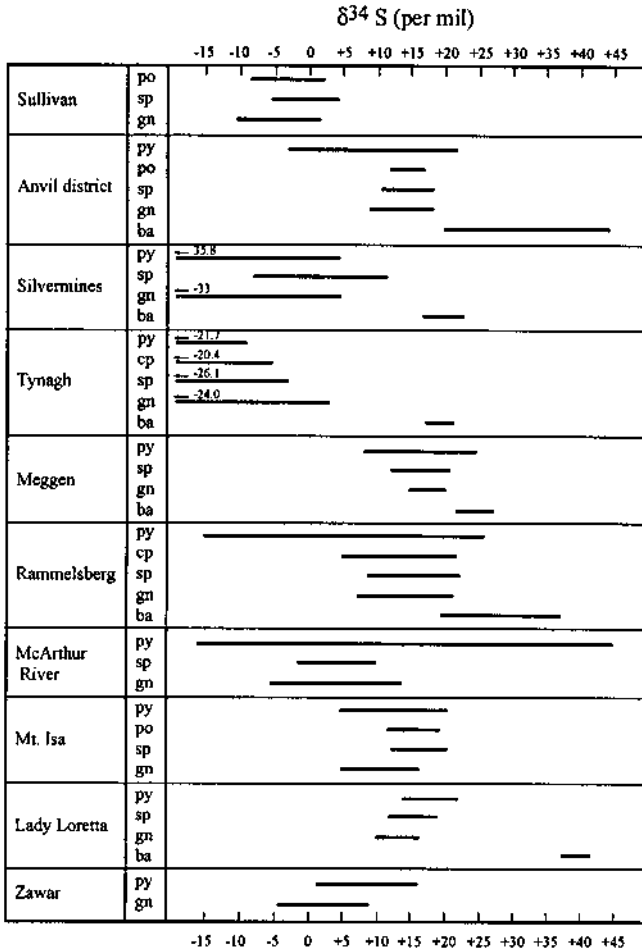


Figure 11.14. The range of $\delta^{34}\text{S}$ values in sulfides and barites of selected SMS deposits. Sources of data: compilation by Large (1981), Boast et al. (1981), Deb & Sarkar (1990), Eldridge et al. (1993), and Goodfellow et al. (1993).

of pyrite and an increase in $\delta^{34}\text{S}$ of pyrite stratigraphically upward suggest the precipitation of pyrite by biogenic reduction of seawater sulfate in a restricted basin (see Ch. 4). This interpretation is consistent with the observed $\delta^{34}\text{S}$ variation in the Selwyn Basin deposits (Anvil, early Cambrian; Howrad's Pass, early Silurian; Tom, Jason, Cirque, and Driftpile, late Devonian) that indicates the precipitation of pyrite with highly positive $\delta^{34}\text{S}$ values (about +30‰ or higher) under periodic anoxic

bottom-water conditions on a global scale in the Phanerozoic oceans (Goodfellow 1987). The highly variable isotopic composition of pyrite in the Rammelsberg deposit, which is not systematically correlated with the stratigraphy, is probably related to varied microenvironments at the site of biogenic pyrite precipitation (Large 1983) or, as argued by Goodfellow et al (1993), to a prolonged episode of bacterial sulfate reduction in the ambient water column.

The isotopic compositions of sphalerite and galena show no consistent pattern. For example, $\delta^{34}\text{S}$ values of galena and sphalerite systematically decrease upward in the Sullivan deposit (Campbell et al. 1978), increase upward in the Rammelsberg main ore bodies (Anger et al. 1966), and show no obvious stratigraphic relationship in the HYC and Lady Loretta deposits (Smith & Croxford 1973, Carr & Smith 1977). The frequency distribution of $\delta^{34}\text{S}$ values of galena and sphalerite are also highly variable, from modes centered around 0‰ (e.g., Sullivan, Broken Hill, Silvermines 'Lower G' orebody) to strongly positive values (e.g., Mount Isa, Rammelsberg, Meggen) and to strongly negative values (e.g., Silvermines 'B' and Tynagh 'Upper G' ore bodies).

In some SMS deposits, $\delta^{34}\text{S}$ values of sphalerite are higher than those for coexisting galena, as would be expected for a sphalerite-galena pair precipitated in equilibrium from the same solution (see Ch. 4). In contrast, there is commonly no evidence for isotopic equilibrium in the pyrite - galena and pyrite - sphalerite pairs, implying that the pyrite-sulfur had a different origin or that the pyrite precipitated under different physico-chemical conditions. Some interpretations of the sulfur isotope data for SMS deposits favor a dual sulfur-source model (Anger et al 1966, Smith & Crawford 1973, Large 1980,1983): (a) seawater sulfate at the site of accumulation for the barite and biologically reduced seawater sulfate for most of the pyrite; and (b) a "deep-seated" source for the sulfur in galena, sphalerite, pyrrhotite, and some of the pyrite, sulfur that was introduced into the site of mineralization in the same hydrothermal fluids that transported the metals. The coexistence of biogenic and hydrothermal sulfide may be explained by one or both of the following situations: (a) the discharge of hot hydrothermal fluids on the seafloor was episodic, allowing the bacteria to be active during the intermittent periods, and (b) the sphalerite and galena formed later than the bulk of the pyrite, as suggested by the textural relationships in many SMS deposits. The ultimate origin of the 'deep-seated' sulfur might be magmatic, but more likely, considering the paucity of contemporaneous volcanism, it was seawater sulfate that was inorganically reduced at high temperature (<200°C), perhaps during circulation of seawater through the underlying sedimentary prism. Other suggested sources of sulfur in sphalerite and galena include seawater sulfate at the site of mineralization (Campbell et al. 1978, Campbell & Either 1983, Shanks et al. 1987) and diagenetic pyrite and/or evaporite in the sediments within the reaction zone of a seafloor hydrothermal system (Hitzman & Large 1986).

A hydrothermal sulfur source may have been important in some SMS deposits, such as the Rammelsberg deposit, which have sulfide-rich feeder zones, but most deposits appear to have obtained their reduced sulfur (H_2S) from the sulfate of the ambient seawater column (Turner 1992, Goodfellow et al. 1993). This conclusion is

supported by the low H_2S content of modern metal-rich basinal and geothermal waters, and the evidence for anoxic ambient environments during the formation of SMS deposits at least during the lower Paleozoic. The evidence includes non-bioturbated laminated host rocks, high S:C ratios in coeval sediments, preservation of graded pyrite framboid beds, and the highly positive $\delta^{34}S$ values of the pyrite. This anoxic condition was also the likely reason why SMS-type sulfide accumulations on the seafloor were protected from destruction by oxidation.

11.9.3. SOURCE OF ORE METALS

There is little direct evidence for the metal source for SMS deposits, because the hydrothermal reservoir (or reaction) zone of the hydrothermal system responsible for a SMS deposit has not been positively identified in any specific case (Goodfellow et al. 1993). Lydon (1983) presented arguments, based on the geochemistry of the leaching process and the composition of oil field brines, that the source of metals for SMS deposits was primarily the underlying sedimentary pile. The lead isotope data (Fig. 11.15), however, are inconsistent with such a conclusion in some cases and equivocal in others. For example, the best fit line for the Irish deposits corresponds to a source 'age' of about 2350 Ma; Caulfield et al. (1986) interpreted this distribution to indicate mainly a lower crustal origin for the lead in Irish deposits. The isotopic ratios for the Australian deposits suggest either a common, homogeneous source of lead or, more likely, a smoothing of the isotopic variation in different source materials by a regionally extensive and long-lived hydrothermal system (Gulson 1985). Lambert (1983) has reported that the present-day lead isotopic ratios in the sedimentary strata underlying the HYC deposit define a linear array which extrapolates to pass through the ore lead. This relationship is compatible with derivation of the ore metals from such strata, but could be explained as well by addition of ore lead to the strata.

With minor exceptions, the lead isotope ratios of SMS deposits fall between the mantle and upper crust growth curves (Fig. 11.15). According to Doe and Zartman (1979), the lead isotopic characteristics of SMS deposits are more likely the result of a complex process involving the mixing and homogenization of lead from several isotopically heterogeneous sources during the orogenic melting of crustal rocks, the reworking of sediments, the leaching of sediments by circulating hydrothermal fluids, and the transportation of lead to the site of mineralization in these fluids. A major limitation in the use of lead isotopic ratios for deciphering the source of ore metals in SMS deposits is the uncertainty regarding the initial lead isotopic compositions of the associated sediments.

Metal leaching by hydrothermal reactions, which require high water:rock ratio, is unlikely to result in a hydrothermal fluid with more than a few ppm of (Pb+Zn), (see Ch. 2) — not enough to form a significant SMS deposit. Therefore, sialic crystalline crust is not a good candidate for the reaction zones of SMS-forming hydrothermal systems. On the other hand, pore fluids of a sedimentary sequence, undergoing the first cycle of burial and metamorphism, may achieve high enough concentrations of

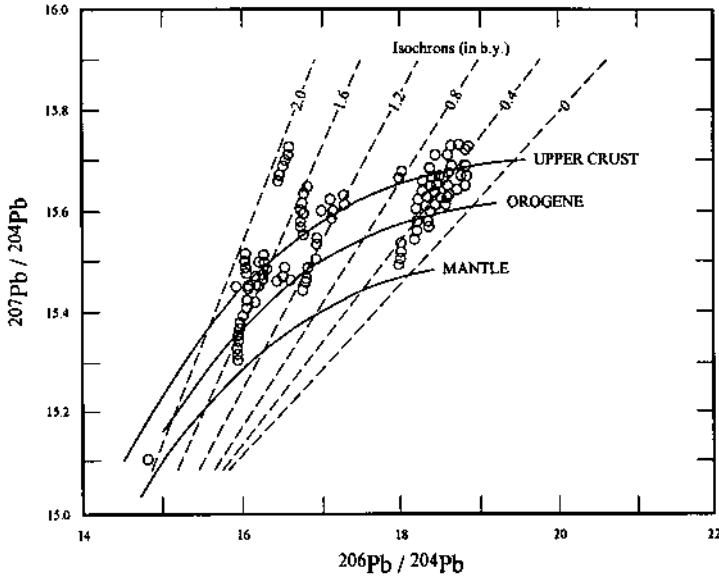


Figure 11.15. Lead isotopic ratios of SMS deposits in relation to the mantle, orogene, and upper crust growth curves of Zartman and Doe (1981). Source of data: compilation by Sangster (1990).

(Pb+Zn) to qualify as ore-forming fluids. Goodfellow et al. (1993) have outlined three favorable scenarios for the generation of viable ore-forming fluids for SMS deposits: (a) the burial and compaction of argillaceous sediments containing evaporites, in which thermal metamorphic reactions are driven by an increase in temperature due to burial; (b) a sedimentary sequence containing highly saline formation waters in which local prograde reactions are driven by the heat from a high-level magma body; and (c) the subsidence of an intracontinental rift to the point of allowing a marine transgression. The last one, they conclude, provides the best opportunity for forming SMS deposits.

A related question is whether the Proterozoic sediments contained enough lead to account for the vast quantities of lead in giant SMS deposits. The question is less critical to the generation of major SMS deposits in Phanerozoic time, because by then the concentration of lead in the upper crust was probably much higher. Sawkins (1989) argued that a critical factor in the formation of giant SMS deposits during the Proterozoic was a major outbreak of pre-mineralization, anorogenic felsic magmatism that brought significant amounts of lead (>30 ppm) to the surface of the Proterozoic cratons. Detritus derived from these volcanics transferred large amounts of the lead into sedimentary basins, rendering the basin-fill sediments a potential source of lead.

11.9.4. PALEOTECTONIC SETTINGS

Inferred tectonic settings proposed for SMS deposits include: (a) intracontinental rifts (e.g., Mount Isa, Lambert 1983; McArthur River, Williams 1978a, b; Sullivan, Kanasewich 1968b, Stewart 1972); (b) continental margin side of back-arc basins (e.g. Howard's pass, Badham 1981); (c) passive continental margins transected by incipient rifts or grabens (e.g., Meggen, Werner 1989); and (d) reactivated wrench fault systems in the basement of intracontinental basins (e.g., Navan and Silvermines, Andrew & Ashton 1985). Intracratonic grabens, characterized by elongate sediment-filled depressions bounded by normal faults that trend parallel to the axis of extension, appear to be the most frequent setting for the SMS deposits, especially the giant Proterozoic deposits (Gustafson & Williams 1981, Sawkins 1983). A particularly suitable environment for the formation of SMS deposits may have been aulcogens (failed arms of successful spreading systems) as these are sites of rapid clastic sedimentation, block faulting, and high heat flow (Sawkins 1976b).

Within the framework of a rift setting, the formation of SMS deposits appears to be related to tensional tectonism during the 'post-rift' thermal subsidence (Large 1992). This may be marked by: (a) the development of local basins and rises along sedimentary faults, as recognized by local facies changes, lateral variations in sedimentary thickness, and locally derived sedimentary conglomerates and breccias, (b) onset of rapid subsidence as evidenced by anomalously thick sedimentary sequences and sudden changes in sedimentary environment; and (c) development of a thermal anomaly along deeply penetrating structures, as indicated by volcanic rocks or tuffs.

11.9.5. AGE DISTRIBUTION

SMS deposits first appear at about 2000 Ma, attain their maximum development during early to middle Proterozoic, and become rare after the Mississippian. A conspicuous feature of this age distribution pattern (Fig. 11.16) is an antipathetic relationship between the temporal distribution of VMS and SMS deposits (Hutchinson 1980). There is a marked paucity of major VMS deposits (the "volcanogenic gap" of some authors) in the middle Proterozoic during which all the giant SMS deposits formed. Also, the younger Archean belts that contain abundant Noranda-type VMS deposits appear to be practically devoid of SMS deposits. A possible explanation may be that the dominant style of tectonism in the middle Proterozoic consisted of rifting and the formation of sedimentary basins, which contrasts with the compressional tectonism and associated prolific volcanism in the younger Archean greenstone belts and the Phanerozoic island arc environments that host most of the VMS deposits (Sawkins 1983). This, however, does not explain the lack of SMS deposits during post-Mississippian time despite the development of submarine rift environments in many parts of the Earth.

An alternative explanation may be that SMS deposits formed during intervals of anoxic bottom water condition in a stratified ocean that provided an adequate supply of

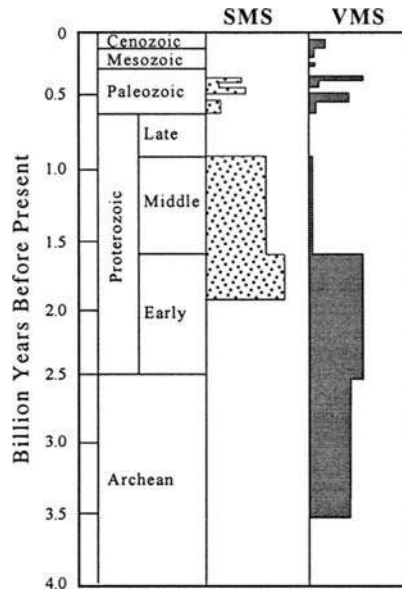


Figure 11.16. Age distribution of SMS and VMS deposits. SMS deposits first appeared around 1900 Ma (Goodfellow et al. 1993) and the oldest known VMS deposits are those of the Pilbara craton hosted by 3.46-Ga volcanics (Barley 1992). (Modified from Goodfellow et al. 1993).

reduced sulfur. As mentioned earlier, there is good evidence for four world-wide anoxic events (early Cambrian, middle Ordovician to early Silurian, early Devonian, and late Devonian), which correlate well with times when SMS and sediment-hosted barite deposits formed, whereas intervening periods correspond with the formation of barite deposits (Goodfellow 1987). The abundance of Proterozoic SMS deposits may be related to similar anoxic events, but there are no data to make such a case. The absence of Archean SMS deposits has been ascribed by Goodfellow (1992) to “the limiting effect of high reduced iron contents on the activity of reduced sulfur in anoxic oceans,” presumably because of Fe-sulfide precipitation. Under these conditions, metals in hydrothermal fluids vented into the water column were dispersed because of a lack of reduced sulfur to precipitate them. With the oxidation and deposition of iron as banded iron formations, the buildup of sulfate in the oceans during the early Proterozoic (Cameron & Hattori 1987b) and bacterial reduction of sulfate, anoxic oceans became H₂S-rich, and SMS-type sulfide deposition occurred when metalliferous fluids were discharged into euxinic basins (i.e., where H₂S was present in the water column).

11.10. Summary

SMS deposits include some of the largest Zn-Pb deposits of the world, and several contain significant amounts of barite and recoverable Ag. The host rocks are shallow to deep-water, marine clastics and carbonates, often with thin bands of K-rich tuffites as the manifestation of contemporaneous, albeit distant, volcanism. Contemporaneous igneous activity in the form of dikes and sills are present in a few districts, raising the possibility of a magmatic heat source for driving ore-fluid circulation, but there is no evidence of the involvement of magmatic fluids in the formation of SMS deposits.

The deposits typically consist of stacked lenses of massive, laterally zoned, Zn-Pb±Ba ore, characterized by stratiform mineralization of syngenetic, probably exhalative, origin. The massive ore zone may be underlain by a zone of discordant, epigenetic mineralization and hydrothermal alteration related to the same mineralization event. The ore-forming fluids were moderately hot ($\approx 80^\circ$ to $\approx 300^\circ\text{C}$) and saline (≈ 10 to 30 wt% NaCl equivalent). The H_2S for sulfide precipitation was derived mainly through bacterial reduction of seawater sulfate (although evaporite minerals of host rock sequences and dissolution of pyrite may have been important in some cases) and the ore accumulation occurred in localized brine pools within third-order basins. Synsedimentary faults played a key role in providing conduits for hydrothermal fluids to sites of mineralization. The deposits were emplaced in an extensional, intracontinental rift or continental margin wrench-fault setting.

Many aspects of SMS deposits are not well understood. These include the mechanism of stratiform mineralization, the source of metals, the irregular distribution of barite, and the relatively subdued footwall alteration in many large deposits that must have involved hydrothermal systems of considerable size and duration. The relatively restricted spatial and temporal distribution of SMS deposits is a puzzle, because compaction-driven and/or convective circulation of metalliferous brines should be a normal consequence of sedimentary basin development. Perhaps, the critical combination of large-scale metalliferous brine generation, efficient plumbing system, and favorable depositional environments did not occur too frequently (Sawkins 1984). The presence of euxinic ocean basins appears to have been a first-order control on the spatial and temporal distribution of SMS deposits, as well as for their preservation.

The SMS deposits, compared with VMS Deposits, are characterized by stratiform mineralization, much higher (Zn+Pb):Cu ratios, a lack of volcanic association, less pronounced footwall alteration, synsedimentary faulting, more saline hydrothermal fluids, a hydrothermal system of much longer duration, and bacterial reduction of seawater sulfate as the source of reduced sulfur (see Table 13.4).

11.11. Recommended Reading

Williams (1979a), Large (1983), Lambert (1983), Russell (1983), Sangster (1990), Goodfellow et al. (1993), Hitzman and Beaty (1996), Large et al (1998).

CHAPTER 12

SEDIMENT-HOSTED STRATIFORM COPPER (SSC) DEPOSITS

12.1. Introduction

Nomenclature for this class of sediment-hosted, Cu-dominated sulfide deposits is problematic. It has been variously described as, to name a few, sediment-hosted copper deposits (Edwards & Atkinson 1986), stratiform copper deposits (Brown 1978), strata-bound copper deposits (Maiden et al. 1984), sediment-hosted stratiform copper deposits (Kirkham 1989), a subclass of stratiform sulfides of marine and marine-volcanic association (Stanton 1972), and examples of sedimentary-type stratiform ore deposits formed in intracratonic basins (Morganti 1981). None of these names is entirely appropriate. The term *sediment-hosted stratiform copper (SSC) deposits* is considered to be the best compromise as it emphasizes, in addition to the sedimentary host rocks, two other characteristics — the stratiform nature of mineralization and the dominance of copper — that separate this class of deposits from other classes of sediment-hosted deposits. The descriptor 'stratiform' is not entirely accurate, because mineralized zones are not always conformable with bedding, but quite adequate if it is allowed to include slightly transgressive morphologies of such zones (Brown 1989). To describe such mineralization as strata-bound would be a greater distortion of the overall picture. The native copper (-native silver) deposits of the Keweenaw district, Michigan (USA), are not considered to be members of this class, because those are volcanic-hosted, flow-top deposits and their configurations are generally too irregular to qualify as stratiform, although the genesis of the two types of deposits have many features in common.

The SSC deposits account for about 20-25% of the world's copper production and reserves, and are second only to porphyry copper deposits in economic importance. They also constitute the world's most important source of cobalt (the Central African Copperbelt); some deposits have produced small amounts of silver, PGE, gold, rhenium, lead, and uranium as byproducts (Kirkham 1989). A recent publication of the *Geological Association of Canada (Special Paper 36)* edited by Boyle et al. (1989) contains an excellent collection of articles on the geology and genetic concepts pertaining to a number of SSC deposits around the world.

12.2. Distinguishing Features

Sediment-hosted stratiform copper deposits vary considerably in size, grade, and metal association (Table 12.1). There are, however, many features that provide a common link among deposits of this class and set them apart from other classes of copper deposits (Renfro 1974, Rose 1976, Jowett et al. 1987, Brown 1989, Kirkham 1989). The distinguishing features of SSC deposits are listed below.

- (a) The ore is localized in reduced horizons ('gray beds'), often at the boundary between oxidized and reduced facies, within carbonaceous and pyritic fine-grained clastic rocks (black shales and arenites), and carbonates. Associated sedimentary rocks include continental redbeds and, in many cases, evaporites (or at least evidence of hypersaline conditions during sedimentation).
- (b) The mineralization is predominantly stratiform in the sense that ore zones are typically confined to specific beds, which are commonly interbedded with subore-grade cupriferous beds (adjacent mineralized zones are normally uneconomic and peneconformable). This results in blanket-type ore zones of small thickness (less than a meter to several meters) and great lateral continuity (measured in kilometers).
- (c) The ores are composed of fine-grained, disseminated Cu-sulfides (mainly chalcocite, bornite, and chalcopyrite, with varying amounts of digenite, djurleite, and anilite); Pb-Zn, Ag, and Co are important constituents in some deposits.
- (d) The deposits are characterized by conspicuous lateral and vertical sulfide (and metal) zoning, with the general sequence: barren (no sulfide, often with hematite) \Rightarrow chalcocite \Rightarrow bornite \Rightarrow chalcopyrite \Rightarrow (galena \Rightarrow sphalerite) \Rightarrow pyrite.
- (e) There is little direct evidence of volcanic activity contemporaneous with the deposition of immediate host sediments or the base metal mineralization. (However, volcanic detritus in the clastic sequence or igneous bodies buried at deeper levels are possible sources of metals.)

It should be pointed out that the stratiform mineralization in SSC deposits is often associated with minor crosscutting, Cu-bearing, vein-type mineralization. Where investigated in detail, the vein-type mineralization has been interpreted to be later than and unrelated to the stratiform mineralization. Therefore, not much attention will be paid to the vein-type mineralization in this chapter.

Similarities between the SSC and SMS classes of deposits include carbonaceous clastic host rocks, a general lack of direct volcanic association, the association of ore sulfides with framboidal pyrite, and a general sequence of $\text{Cu} \Rightarrow (\text{Pb} + \text{Zn}) \Rightarrow$ pyrite zoning. Compared with SMS deposits, SSC deposits are characterized by: much higher $\text{Cu}:(\text{Zn}+\text{Pb})$ ratios (Fig. 11.2); lower-grade, disseminated, stratiform mineralization instead of high-grade, massive, strata-bound sulfide horizons (although the sulfides in

SMS deposits may be stratiform internally); a lack of pronounced hydrothermal alteration (except perhaps hematitization) zone below or around orebodies; a lack of association with synsedimentary faults; and fairly strong evidence for a diagenetic, rather than a syngenetic, origin in most cases.

12.3. Distribution

SSC deposits are widely distributed in space and time (Kirkham 1989); the most important of these are shown in Figure 12.1 and listed in Table 12.1. Most of the world's production, however, can be attributed to a few very large districts and deposits, such as the Central African Copperbelt in Zambia and Congo, the Dzhezkazgan region of former USSR, White Pine in Michigan (USA), Spar Lake in Montana (USA), Lubin-Sieroszowic district in Poland, and the Dongchuan district in China.

Compilation of available data for more than 820 SSC deposits and occurrences by Kirkham (1989) reveals that the host rocks range in age from Early Proterozoic to Cenozoic, but more than one-half of the deposits belong to two geologic age intervals, the Proterozoic and the Permo-Carboniferous. These two intervals also account for the most important SSC deposits — the Central African Copperbelt and Dongchuan

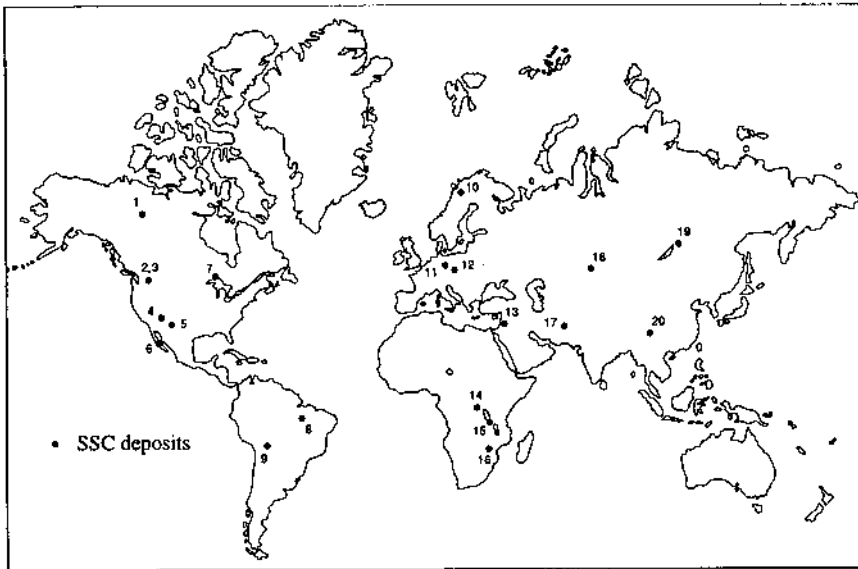


Figure 12.1. World distribution of important sediment-hosted stratiform copper deposits, districts, and belts: 1. Redstone; 2. Rock Lake; 3. Spar Lake; 4. Nacimientto; 5. Creta; 6. Boleo; 7. White Pine; 8. Bahia; 9. Corocoro; 10. Aitik; 11. Mansfeld-Sangerhausen; 12. Lubin-Sieroszowic district (Lubin, Połkowice, Rudna, Sieroszowic); 13. Fenan; 14. Congo belt; 15. Zambian belt; 16. Mangula; 17. Aynak; 18. Dzhezkazgan; 19. Udokan; 20. Dongchuan district (Ynmin, Laoxue, Tandan).

TABLE 12.1. Selected sediment-hosted stratiform copper deposits

Deposit/ District	Reserves (million tonnes)	Grade Cu %	Other Metals	Host Rocks	Age	Metamorphism
Bolivia Corocoro	7?	5.0	Ag 2 g/t	Arkostic red sandstone	Tertiary	None
Canada Redstone	37	3.9	Ag 11.3 g/t	Algal carbonates, associated with siltstones, mudstones, and evaporites	Late Proterozoic	None
China Dongchuan	10?	3.5	?	Stromatolitic dolostones	Proterozoic	Greenschist
Germany Mansfeld- Sangerhausen (Kupferschiefer)	75	2.9	Ag 150 g/t ± Zn 1.8 %	Bituminous marl, with localized carbonate- and clastic-rich facies	Upper Permian	Negligible
Mexico Boleo	14	4.8	Ag 9 g/t Zn 0.8 % Mn 3-4 %	Tuff above conglomerate	Early Pliocene	None
Poland Lubin- Sieroszowic (Kupferschiefer) (total metal)			Cu - 68 million tonnes Ag - 170,000 tonnes Pb - 5.2 million tonnes Zn - similar to Cu	Bituminous marl, arenite, and shale	Upper Permian	Negligible
USA Creta	2	2.3	Ag 5.5 g/t	Gray shale	Middle Permian	None
Nacimiento	9	0.7	?	Fluvial quartzose sandstone	Lower Triassic	None
Spar Lake	58	0.8	Ag 54 g/t	Feldspathic quartzite	Lower Proterozoic	Greenschist
White Pine	184	1.1	Ag 6.8 g/t	Siltstone, shale, and arenite	Lower Proterozoic	Negligible
USSR (Former) Dzhezkagan	400?	1.5	?	Arenite, with minor siltstone	Carboniferous	Zeolite
Udokan	1200	2.0	?	Arenite, with minor siltstone	Early Proterozoic	Greenschist

TABLE 12.1 (continued)

Deposit/ District	Reserves (million tonnes)	Grade Cu %	Other Metals	Host Rocks	Age	Metamorphism
Congo Tenke- Fungurume	>235	4.5	Co 0.4 %	Shale and arenite, minor dolostone	Middle-Late Proterozoic	None
Kotwezi Klippe	880	4.5	Co 0.4 %	Shale and arenite, minor dolostone	Middle-Late Proterozoic	None
Zambia Nchanga	112 197 203 P	3.96 2.2 5.03	Ag -2.7 g/t Au -0.03 g/t	Black shale and arkosic arenite	Proterozoic	Greenschist
Nkana	82 304 178 P	2.4 2.2 3.4	Co 0.14 % Co 0.05 % Co 0.17 % Ag 2.7 g/t	Argillite, sandstone, minor dolostone	Late-Middle Proterozoic	Greenschist
Mufulira	87 40 208	3.0 2.9 3.5	Ag 2.7 g/t	Arenite, minor argillite	Late-Middle Proterozoic	Greenschist
Chambishi	23 42 34P	2.8 2.3 2.9	Ag 15 g/t	Quartzose argillite, minor dolostone	Late-Middle Proterozoic	Greenschist
Konkola	52 421 53P	3.8 3.1 4.1	Ag 2.7 g/t	Dark gray siltstone, carbonaceous shale	Late-Middle Proterozoic	Greenschist
Baluba	50 20 21P	2.6 2.4 2.4	Co 0.16 % Co 0.15 % Ag 2.7 g/t	Argillite, minor dolostone	Late-Middle Proterozoic	Greenschist

Production (P) figures quoted here for Zambia were the amount of ore reserves depleted as of April 1, 1985. This amount was less than the "ore" produced by a factor of about 90 % and was about 1 % Cu higher in grade because of additional low-grade or barren material added by dilution during mining. Sources of data: compilations by Gustafson and Williams (1981) and Kirkham (1989); Kucha and Piestrzynski (1995).

(Proterozoic), Dzhezkazgan (Carboniferous), and Lubin- Sieroszowic (Permian). So far, no typical SSC deposit has been discovered in the Archean rocks.

12.4. Types of Deposits

The SSC deposits may be divided into two types (Kirkham 1984): (a) *Kupferschiefer-type*; and (b) *redbed-type* (Fig. 12.2). The Kupferschiefer-type deposits are found in anoxic fine-grained sediments that are rich in organic matter (from a few per cent to >20%) and range in composition from black shales to oil shales. The inorganic component of black shales is largely siliciclastic detrital matter (quartz, feldspars, and

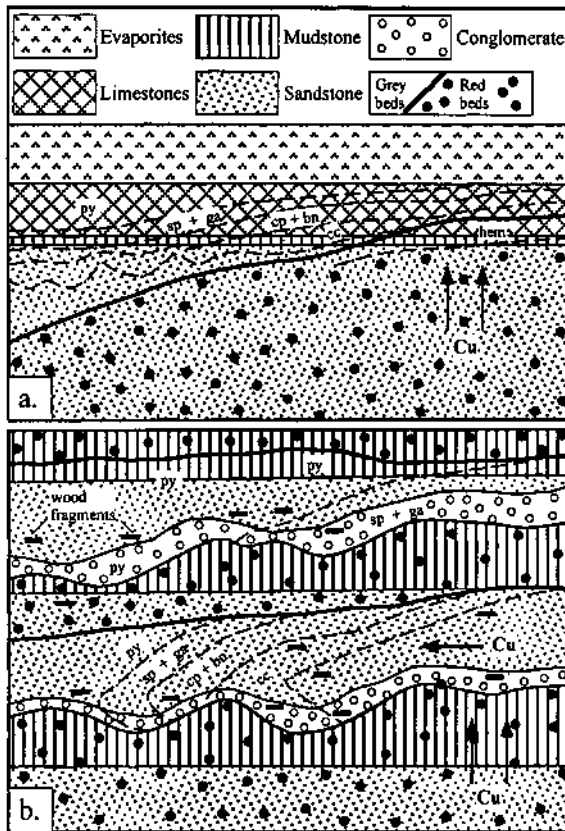


Figure 12.2. Schematic cross sections illustrating the difference in geologic settings of the sediment-hosted stratiform copper deposits: a. Kupferschiefer-type; and b. redbed-type. Arrows indicate the generalized patterns of ore fluid movement. Note that all Kupferschiefer-type deposits do not have an evaporite unit on the hanging-wall. (After Kirkham 1989.)

clay minerals), whereas oil shales consist dominantly of inorganic calcite and dolomite (Eugster 1989). The host rocks of the Kupferschiefer-type were deposited in paralic environments (coastal marine environments, including large-scale saline lacustrine environments resulting from marine transgressions) following continental redbed deposition. The zonal pattern of minerals in these deposits is usually upward and outward in an overlapping sequence from an oxidation-reduction front located near the redbed-graybed contact (Fig. 12.2a). Examples of this deposit type include, in addition to the Kupferschiefer (Germany-Poland), those of the Central African Copperbelt, White Pine and Creta (USA), and Dongchuan (China).

Redbed-type copper deposits are hosted by rocks deposited in continental environments. The mineralization, with a zonal pattern similar to that of the Kupferschiefer-type deposits, is also localized in organic-rich sediments, but these anoxic sediments occur within a redbed sequence (Fig. 12.2b), representing temporary and local interruption in redbed accumulation. The redbed-type deposits, to the extent known, are only of modest size and grade. Important examples are Corocoro (Bolivia), Nacimiento (New Mexico, USA), Dzhezkazgan (Kazakhstan), and Redstone (NWT, Canada).

12.5. Examples

12.5.1. KUPFERSCHIEFER, GERMANY-POLAND

Kupferschiefer ("copper shale") is a stratigraphic term for a thin bed (thickness ranging from 0.2 to 4.0 m, but generally <1m) of finely laminated, marine, pyritic, bituminous (up to 6% carbon) marl that persists over a very large area (>600,000 sq. km) in central Europe and is Upper Permian (Zechstein) in age. It stretches from Poland, through Germany and North Sea, to northeastern England where it is known as the Marl Slate (Fig. 12.3). Despite its name, the overall combined Zn and Pb content of the Kupferschiefer bed significantly exceeds its Cu content (Wedepohl 1971), but orebodies invariably contain much more Cu than Pb+Zn.

Large tracts of the Kupferschiefer contain only average, or even less than average, concentrations of base metals compared with other black shales and marls. Regions with >0.3% Cu approach only about 1% of the total area covered by the Kupferschiefer and are mainly restricted to the margins of the early Zechstein basin in Germany and Poland (Wedepohl 1980). Historically, the most important of these is the Mansfeld-Sangerhausen district at the southeastern margin of the Harz Mountains, where mining of Cu-Ag ores dates back to the Medieval times. Mining in this district was discontinued in 1970, after a total production of about 1.5 million tons of copper metal spanning a period of approximately 770 years, out of which about 0.5 million tons are estimated to have been produced between the years 1200 and 1687 (Jung & Knitzschke 1976). The currently active mines are located in the Spremberg-Weisswasser region, Germany (Wedepohl 1971, Jung & Knitzschke 1976, Schmidt & Friedrich 1988) and

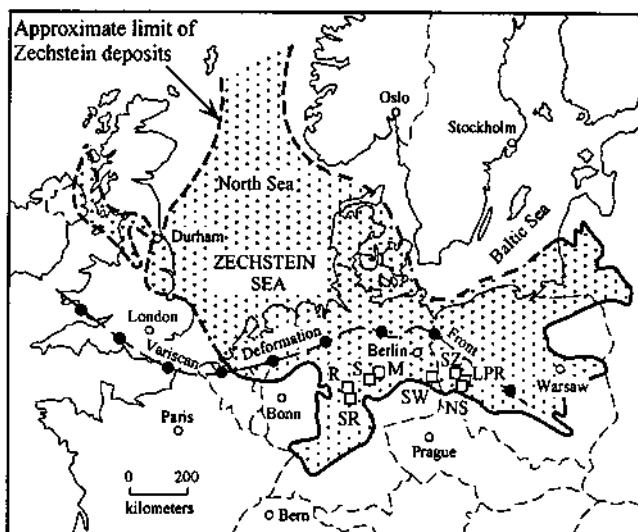


Figure 12.3. Approximate extent of the Zechstein basin in central Europe and locations of the principal Kupferschiefer ore deposits (after Rentzsch 1974, Oszczepalski 1989, Vaughan et al. 1989). Deposits: SR, Spessart-Rhön; R, Richelsdorf; S, Sangerhausen; M, Mansfeld; SW, Spremberg-Weisswasser; NS, North Sudetic (Konrad, Lena, Nowy Kosciol); LPR, Lubin-Polkowice-Rudna; SZ, Sieroszowice.

the Lubin-Sieroszowice district, Poland (Jowett 1986, Jowett et al. 1987, Oszczepalski 1989, Kucha & Piestrzynski 1995). The Lubin district, discovered in 1957, is one of the largest in the world and has made Poland the largest copper producer in Europe. The district carries an average of about 2% Cu, 40 ppm Ag, 0.2% Pb, and 0.1% Zn, and is estimated to contain about 68 million tonnes of Cu, 170,000 tonnes of Ag, 5.2 million tonnes of Pb and similar amounts of Zn (Kucha & Piestrzynski 1995). An excellent summary of the important mineralized districts in Germany, Poland, and England is given by Vaughan et al. (1989).

Figure 12.4 shows part of a typical stratigraphic section associated with Kupferschiefer mineralization. The Kupferschiefer is underlain by the Lower Permian Rotliegendes (red sandstone), which is composed of continental redbeds containing intercalated bimodal volcanics in the lower part and lenses of halite in the upper part. The Rotliegendes was deposited under arid to semi-arid conditions in fault-controlled, closed basins within a zone of intracontinental rifting that developed at the end of the Variscan orogeny (Carboniferous). In the Fore-Sudetic Monocline (southwest Poland), up to 1,500 m of alkaline volcanic rocks, with intercalated sediments, occupy the floor of the rift basins (Autunian). In the late Permian, transgression of the Zechstein sea deposited marine shales, dolostones, and evaporites across the former rift basins and their intervening highs, and some redbeds were reworked to form shallow-water marine

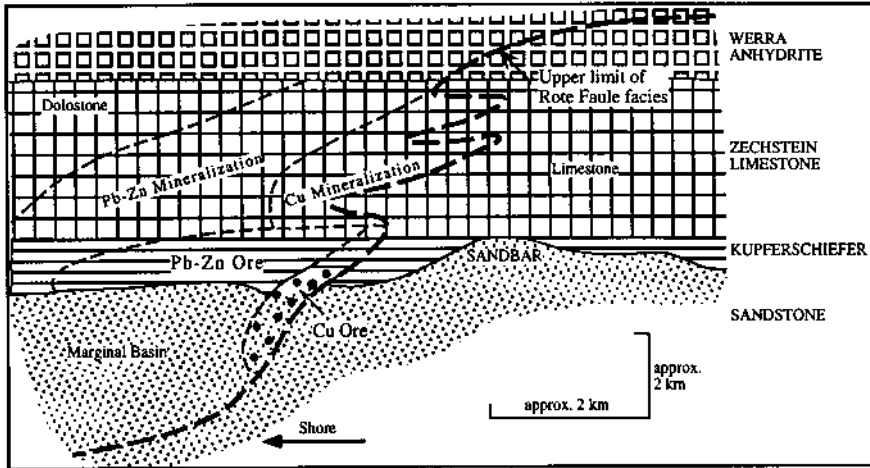


Figure 12.4. Typical stratigraphic sequence of the basal Zechstein (lower part of cycle PZ1) and the pattern of sulfide mineralization relative to the stratigraphy and the Rote Faule facies (after Rentzsch 1974).

clastics. Consequently, the Zechstein sediments rest on a variety of footwall rocks, such as Zechstein conglomerate, Grauliegende (gray sandstone), or Weissliegende (white sandstone). The tectonically quiet Zechstein sedimentation was followed by a further period of extension and rifting (this time with little igneous activity) during the Triassic and early Jurassic, perhaps related to the opening of the Tethys ocean to the south. This resulted in the deposition of up to 2,500 m of continental and shallow marine sediments in long, linear basins: continental Buntsandstein sandstone during synextensional subsidence, and Muschelkalk and Keuper marine carbonates and shales during the tectonically quieter, thermal subsidence phase.

The Upper Permian Zechstein marine succession consists of four depositional cycles, (PZ1 to PZ4; see Jowett et al. 1987, Table 1, p. 2,020), each cycle beginning with the deposition of a thin argillaceous member (marine transgression) and ending with the deposition of evaporites. The Kupferschiefer represents the basal portion of the first cycle of marine sediments (PZ1) after a long period of desert condition in the region. Lithologic variations within the Kupferschiefer are related to the paleotopography of the basin floor. In deeper parts of the basin, it comprises a black, laminated, sapropelic shale with carbonate-rich laminae, but in basin-margin and paleohigh locations it is much more dolomitic and silty. The overall pattern of Kupferschiefer deposition reflects decreasing oxygenation and increasing bottom energy as a function of increasing water depth and distance from the coast (Oszczepalski 1989). Everywhere the Kupferschiefer grades upward into limestone or dolomitic limestone (Zechsteinkalk or Zechstein Limestone), which in turn is overlain by anhydrite (Werra

Anhydrite). Although halite did not become an important precipitate until the second Zechstein cycle (PZ2), it occurs locally within the PZ1 sequence. The marine sequence is devoid of volcanic rocks, but the richest mineralization in the Kupferschiefer occurs in areas lying above the main centers of Lower Rotliegendes volcanism, as in southwestern Poland (Glennie 1989, Oszczepalski 1989). Locally, the ore zones are coincident with basement highs between Rotliegendes basins (Jowett 1989).

Depending on the thickness of the Kupferschiefer and its composition, the associated sulfide mineralization may occur in the Zechstein Conglomerate, Weissliegende, Kupferschiefer, or Zechsteinkalk. The bulk of the mineralization, however, is confined to the Kupferschiefer as fine-grained ($<50 \mu\text{m}$) disseminations concentrated in organic-rich bands parallel to the lamination. Some mineralization also occurs in coarser-grained ($>100 \mu\text{m}$) aggregates and lenses, and as veinlets that are both concordant (or peneconcordant) and discordant relative to lamination (Jowett et al. 1987, Oszczepalski 1989).

An observation of considerable exploration and genetic significance is the association of Kupferschiefer sulfide mineralization with, and its metal zoning relative to, the so called Rote Fäule facies (Fig. 12.5). The term *Rote Fäule* ("red fooling") was first used by miners in the Mansfeld area to describe barren (i.e., devoid of Cu-Pb-Zn sulfides), red-colored rocks found in the vicinity of the ore. The term is now applied to parts of the Weissliegende, Kupferschiefer, and Zechsteinkalk units that exhibit red coloration caused by the oxidation of original pyrite and other sulfides to hematite. The typical metal zonation sequence relative to the Rote Fäule front, both in the vertical and horizontal directions, is: Cu (chalcocite - bornite - chalcopyrite) \Rightarrow Pb + Zn (galena - sphalerite) \Rightarrow Fe (pyrite) (Fig. 12.5). Actually, the concentration of Fe remains at about the same level throughout, but changes from oxide in the Rote Fäule to sulfide in the ore zone and in the barren host rock beyond the mineralized area.

Based on the interpretation that the Rote Fäule was restricted to sediments likely to have been deposited on paleotopographic highs in the Kupferschiefer-stage of the Zechstein basin, Jung and Knitzschke (1976) concluded that adjacent sulfides hosted by the Kupferschiefer were syndepositional or very early diagenetic. Reversals in the sulfide zonation pattern were interpreted to have resulted from cyclic transgression and regression of the restricted sea, and the sulfide mineralization hosted by the arenite beneath the Kupferschiefer as post-sedimentary. A syndepositional origin of the Kupferschiefer sulfide ores, however, is incompatible with the observation (Rentzsch 1974) that the sulfide zones transgress lithologic layering at low angles ($<1^\circ$) to reach their highest stratigraphic levels around the Rote Fäule (Fig. 12.5). Moreover, iron oxide pseudomorphs after framboidal pyrite, relics of sulfides with a halo of hematite pigment, the irregular crosscutting configuration of the hematite zone relative to both bedding and lithostratigraphic units, and the very irregular top surface of this zone indicate that the Rote Fäule hematitization was the result of an influx of oxidizing solutions during diagenesis (Rentzsch 1974, Jowett et al. 1987, Oszczepalski 1989).

Disseminated framboidal pyrite, believed to have formed during the earliest stage of diagenesis, occurs throughout the Kupferschiefer and there is evidence (discussed later)

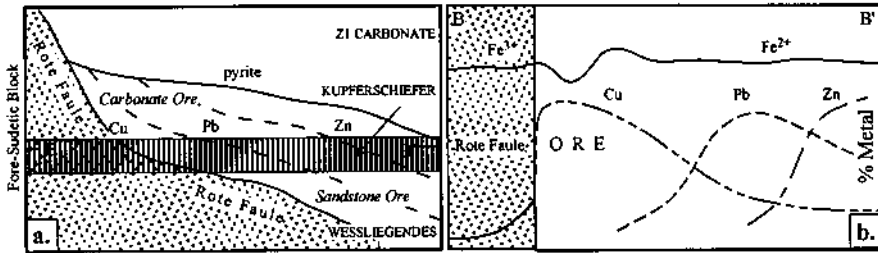


Figure 12.5. a. Schematic section of the ore zone in the Lubin deposit showing the vertical and lateral metal zoning with respect to the enclosing sediments and the Rote Fäule; and b. Section along the Kupferschiefer lunit [B-B' in (a)] showing lateral metal variations (after Jowett et al. 1987).

that this was later replaced by base metal sulfides. Noting that $\delta^{34}\text{S}$ values of the base metal sulfides (from -2‰ to -44‰ , with a mode of -25‰ to -43‰) are only slightly higher than those of pyrite (-3‰ to -44‰ , but mostly -30‰ to -40‰), Oszczepalski (1989) proposed that the stratiform base metal sulfides also formed near the sediment-water interface as a result of reaction with biogenic H_2S . The vein sulfides are isotopically heavier, implying a different origin. He proposed an early diagenetic (prior to complete lithification of the host sediments) emplacement of the stratiform ore sulfides and later diagenetic remobilization to account for the sulfide veinlets.

Relying on an alternative interpretation of the sulfur isotope data — that the sulfur for the base metal sulfides was introduced during ore formation (discussed later) — and the textural evidence for replacement of quartz grains, lithic fragments, diagenetic pyrite, and calcite cement by ore sulfides, Jowett (1986) and Jowett et al. (1987) favored a late diagenetic model for mineralization. This model involves convective circulation of chloride-rich fluids within the Rotliegendes, driven by elevated heat flow from the Triassic rifting event and overpressuring of the pore fluids by the Triassic sediments, and containment of the upwelling fluids by the barrier provided by the Zechstein shales, limestones, and evaporites (Fig. 12.6). Mass balance calculations by Cathles et al. (1993) for a single-compaction model indicate that, if the total dissolved copper content of the Rotliegendes brine was within a factor of two of ≈ 127 ppm (compared with ≈ 1 ppm observed in present-day Rotliegendes pore waters), the volume of brines required to mineralize the margins of the Fore-Sudetic block could have been derived locally from a 70 km x 190 km portion of the Lubin basin. To account for the mineralization from Rotliegendes pore waters containing significantly less dissolved copper would require, according to Cathles et al. (1993), extraction of additional copper from the representative source volume area through convective recirculation of the brine, derivation of the brines from a larger source area, or contribution of syngenetic or early diagenetic metal precipitation to the copper grade. The late diagenetic timing of mineralization in this model is constrained by a mid-Triassic paleomagnetic age of the Rote Fäule hematite, because the Rote Fäule is an integral part of the metal zoning

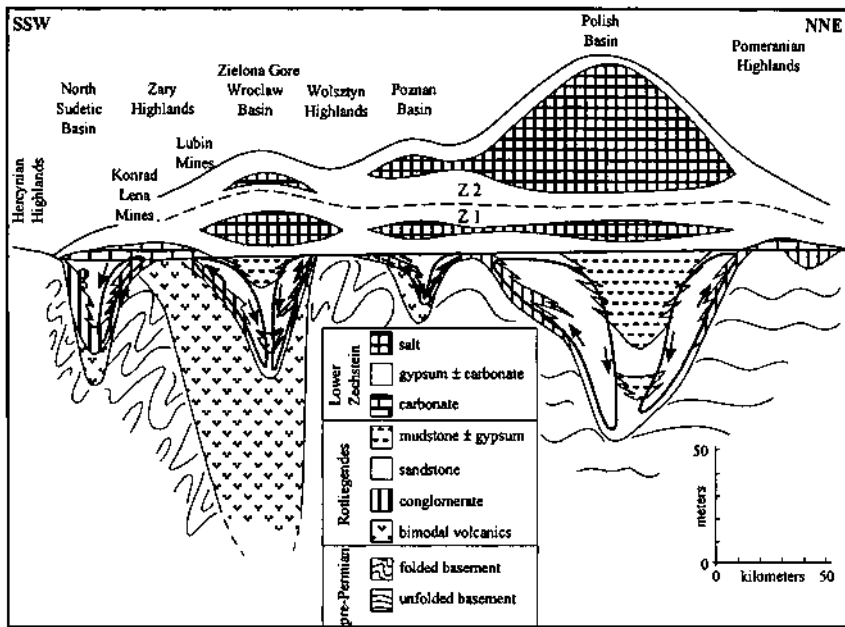


Figure 12.6. A conceptual genetic model for the SSC deposits of western Poland. The ore deposits occur near the flanks of basement highs. To the north, where there was little Rotliegendes igneous activity, the Kupferschiefer contains only background values of metals. According to this model, Rotliegendes brines, leaching metals from the volcanic detritus, migrated up the basement highs during late diagenesis to mineralize the pyritic Kupferschiefer above, apparently in a convective pattern as depicted. (After Jowett et al. 1987.)

and, therefore, was contemporaneous with the emplacement of base metal sulfides. Wodzicki and Piestrzynski (1994) have also attributed the main-stage mineralization to late diagenesis, although their elaborate scheme consists of four stages of mineralization spanning the spectrum from syngedimentary to epigenetic.

12.5.2. ZAMBIAN COPPERBELT

The Zambian Copperbelt (previously known as the Northern Rhodesian Copperbelt) refers to a remarkable concentration of SSC deposits in the Zambian sector of the Lufilian arcuate fold belt that stretches from Angola, through southeastern Congo (Shaba Province), into northern Zambia. About 60% of world's cobalt production comes from the SSC deposits of Congo and Zambia, which are estimated to contain more than 150 million tonnes of copper (Raybould 1978) and 8 million tonnes of cobalt (Annels & Simmonds 1984). Except for minor variations, the stratigraphy of the ore-bearing formations is remarkably consistent along the Lufilian arc, but detailed

correlation between the sectors in Zambia and Congo is not well established (Mendelsohn 1989). The focus here is on the Zambian Copperbelt, which carries a wealth of published literature (Mendelsohn 1961, Garlick 1961, Fleischer et al. 1976, Annels 1974, 1989, Sweeney & Binda 1989a, Sweeney et al. 1991).

Supracrustal rocks of the Lufilian fold belt belong to the Katanga Supergroup that is separated from the dominantly clastic sedimentary rocks of the basement (the Kibara Supergroup) by an unconformity commonly marked by a transgressive conglomerate horizon (Fig. 12.7). The Katangan sequence is believed to have accumulated in a fault-bounded intracratonic rift zone (Raybould 1978, Annels 1984), probably an aulacogen (Annels 1984, Unrug 1988), which closed during a protracted period of folding and thrusting (the Lufilian Orogeny) near the end of the Precambrian. The Katangan sequence, metamorphosed to greenschist facies over most of the mine areas and to amphibolite facies west of the Copperbelt, is now preserved in a series of structural basins separated by domal structures (Fig. 12.8). The age of these sediments is poorly constrained between the 1310 ± 25 Ma age of metamorphosed Kibaran basement and the 602 ± 20 Ma U-Pb age of post-Lufilian uraninite veins at Shinkolobwe in the Shaba Province of Congo (Cahen et al. 1984). Field and petrographic evidence, such as folding and faulting of mineralized horizons, uniformity of copper grade throughout the folded horizons, and metal zoning patterns, indicate that mineralization in the Copperbelt predated the Lufilian deformational event (Fleischer et al. 1976).

Copper deposits of the Zambian belt are essentially restricted to the Proterozoic Lower Rowan Group, which was deposited in an intracratonic rift basin. The Upper Rowan Group sediments, consisting of open marine dolostones and clastics, represent a thermal subsidence phase of basin development that produced a widespread marine transgression. Most of the copper deposits occur in the Ore Shale unit ("ore-shale orebodies"), which is bounded by an arkosic footwall and an arkosic-dolomitic hanging-

	Group	Lithology	
KATANGA SUPERGROUP	UPPER KUNDELUNGU	Shales, quartzites	
	MIDDLE KUNDELUNGU	Shales, tillite (?)	
	LOWER KUNDELUNGU	Shales, dolostones, tillite (?)	
	MWASHIA	Carbonaceous shales, siltstones, dolostones, quartzites, siltstones	
	UPPER ROAN	Dolostones, shales, quartzites	
	LOWER ROAN	HANGING-WALL	Quartzites, arkoses, siltstones, dolomitic sandstones
		ORE SHALE (Cu)	Laminated argillaceous siltstones with sandy interbeds and local dolostone
		FOOTWALL	Granitic conglomerates, coarse arkoses, argillaceous sandstones, dune-bedded quartzites, conglomerates
	Unconformity		
	BASEMENT		

Figure 12.7. Generalized stratigraphic column of the Zambian Copperbelt (after Richards et al. 1988b).

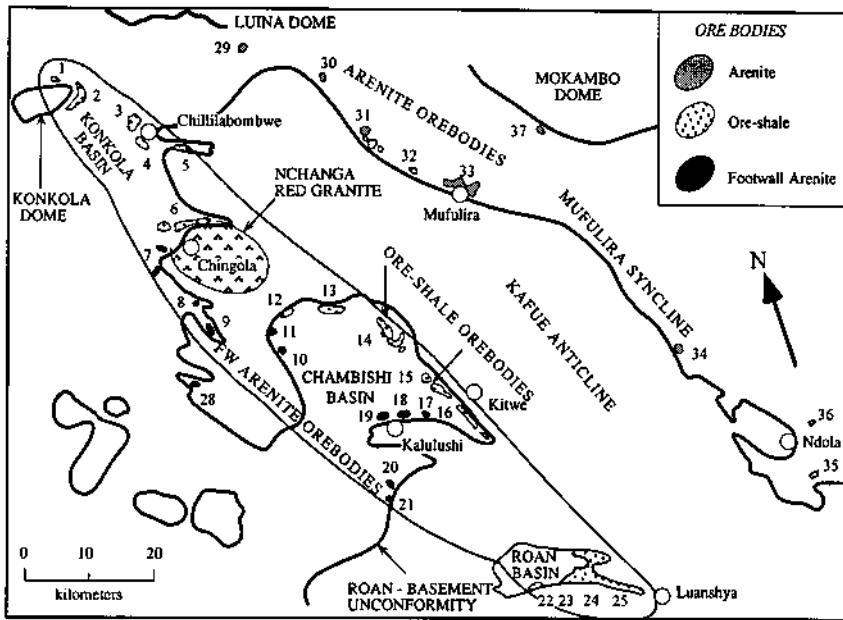


Figure 12.8. The Zambian Copperbelt showing the distribution of the ore-shale, footwall arenite, and arenite orebodies of the Zambian Copperbelt (compiled from Annels 1984, 1989, and Fleischer 1984). Important deposits: 1. Mushoshi; 2. Konkola; 3. Kirilabombwe North; 4. Kirilabombwe South; 5. Fitwaola; 6. Nchanga; 7. Chingola; 8. Mimbula I and II; 9. Fitula; 10. Mwambashi B; 11. Pitanda South; 12. Pitanda; 13. Chambishi; 14. Chambishi SE (formerly Nkana North Limb); 15. Mindola; 16. Nkana (Rhokana); 17. Nkana South Limb Prospect; 18. Chibuluma; 19. Chibuluma West; 20. Kalulushi East; 21. Chifupu; 22. Lufubu South; 23. Muliashi South; 24. Roan Extension; 25. Roan; 26. Baluba; 27. Baluba East; 28. Samba; 29. Tshinenda; 30. Lubembe; 31. Kasaria; 32. Luansobe; 33. Mufulira; 34. Mwekera; 35. Bwana Mkubwa; 36. Itawa; 37. Mokambo.

wall (Fig. 12.7). The shale layer in a similar sequence of rocks occurring at the top of the Lower Rowan Group contains a number of low-grade ($\approx 1\%$ Cu) deposits. At Nchanga, the major Upper Orebody probably represents the same or a similar layer (Mendelsohn 1989). The stratigraphically controlled ore-shale orebodies define a curvilinear trend that was interpreted by Garlick (1961) as the northeastern edge of the Ore Shale lagoon. The richest ore occurs near this edge and the copper content decreases seaward, although not regularly, to form a cupriferous zone about 2 km wide. Beyond this, the ore grades into pyritic carbonaceous shale, with very little or no copper, that forms a parallel zone about 10 km wide. Barren gaps occur throughout the Zambian Copperbelt and they are of three types: algal stromatolitic bioherms, arenaceous facies, and bedded dolomite. The barren gaps are generally flanked by high-grade ore containing Cu-rich sulfides (Mendelsohn 1989). To the northeast, at Mufulira, the Ore Shale is absent and mineralization occurs in three horizons of carbon-bearing sandstone.

The Ore Shale, typically about 5-20 m thick (maximum thickness about 55 m),

commonly is a silt-sized micaceous and calcareous argillite containing quartz, feldspar, organic carbon (<0.5%; Sweeney et al. 1986), and Cu-Fe sulfides, but locally becomes more siliceous (a siltstone) and highly carbonaceous (up to 2% carbon; Mendelsohn 1989). The depositional environment has been interpreted as intertidal to shallow subtidal (Sweeney et al. 1986). A siliceous dolostone, representing an intertidal deposit of algal mats, is generally present at the base of the Ore Shale, but it may also be interlayered with shale (e.g., at Nkana) representing a series of transgressions-regressions that led to carbonate accumulation in tidal flats (Clemmey 1974). Unlike the Kupferschiefer, the Lower Roan succession does not contain bedded evaporite, but the presence of nodular anhydrite, presumably of tidal flat origin, in the mineralized horizons suggests that hypersaline conditions existed at times during the Lower Roan sedimentation (Annels 1974).

Ore minerals are disseminated throughout the argillite in grain sizes similar to those of the host rocks, with higher concentrations in some laminae than in others. In the siliceous dolostone, the ore minerals tend to be coarser and more abundant locally (Mendelsohn 1989). Ore-grade concentration of disseminated copper mineralization generally occurs in the basal one-third of the Ore Shale as tabular orebodies of great strike length. Variations include mineralization at more than one level within the Ore Shale (e.g., the Roan Basin), in the hanging-wall quartzites (e.g., Chambishi SE deposits and Chingola orebodies), and in the footwall arenites (e.g., Chibuluma, and Chibuluma West deposits) referred to as "footwall arenite orebodies". A few arenite-hosted deposits, called "arenite orebodies", such as the Mufulira, also occur to the east of the Kafue anticline (Fig. 12.7). Correlation of orebodies across the Kafue anticline is uncertain, but it is possible that the mineralized horizons in the zone of arenite orebodies represent the lateral and more arenaceous equivalents of the Ore Shale and hanging-wall strata (Annels 1984).

The most abundant sulfide minerals of the Zambian Copperbelt are bornite followed by chalcocite (partly supergene near the surface) and chalcopyrite. Carrollite [Co_2CuS_4] occurs as an accessory phase of economic significance (up to 0.5% Co) in the ore-shale and arenite orebodies located west of the Kafue anticline (Fig. 12.7). The ore-shale deposits show pronounced lateral and vertical zoning from Cu-rich sulfides to Fe-rich sulfides. The generalized sequence according to Garlick (1961) is: barren argillite (no sulfide, often with hematite) \Rightarrow disseminated chalcocite \Rightarrow mixed chalcocite - bornite \Rightarrow bornite \Rightarrow mixed bornite - chalcopyrite with or without carrollite \Rightarrow chalcopyrite \Rightarrow mixed chalcopyrite - pyrite \Rightarrow pyrite with minor chalcopyrite and possibly sphalerite \Rightarrow pyritic shale. A similar zoning pattern (chalcocite \Rightarrow bornite \Rightarrow chalcopyrite \Rightarrow pyrite) is also discernible in arenite-hosted deposits (Fleischer et al. 1976). The lateral sulfide zoning was attributed by Garlick (1961, 1989) to synchronous sulfide precipitation down the paleoslope of the Ore Shale lagoon under increasing water depth and the vertical zoning to transgression-regression of the shoreline. This explanation is too simplistic to account for the variations, including reversals (e.g., in parts of the Mufulira deposit), in the zoning pattern observed in the Zambian copperbelt (Van Eden 1974, Clemmey 1978, Annels 1979).

During the early years of exploration, the sulfide mineralization in the Northern Rhodesian Copperbelt was attributed to replacement of the Ore Shale by hydrothermal solutions emanating from granites that intruded the Lower Rowan Group (Gray 1929, quoted in Garlick 1989). Schneiderhöhn (1932) was the first to contend that the granitic intrusions were pre-Katanga in age and that the mineralization was syngenetic, a hypothesis that was championed later by Garlick (1961, 1989). The main lines of evidence cited in favor of syngenetic incorporation of disseminated sulfides include: (a) the extreme continuity of conformable mineralization and the remarkably consistent copper tenor, especially in the ore-shale deposits; (b) sharp assay cut-offs at hanging-wall and footwall of the ore bodies; (c) barren bioherms (because they projected above the anoxic water, where the precipitation of syngenetic sulfide occurred) in contrast to high-grade ores at their flanks; (d) layers (from 2 cm to as much as 1 m thick) of massive sulfide (e.g., at Chibuluma); (e) sulfide concentration in small-scale sedimentary structures, such as cross-beds, ripple marks, and scours; and (f) metal zoning related to inferred paleogeography. The syngenetic model envisaged precipitation of sulfides in anoxic bottom waters by the mixing of metal-bearing solutions, surface water of the streams that brought the detritus into the depositional basin, and H_2S generated by anaerobic bacteria. Combinations and crystallization of the initial copper, iron, and cobalt sulfide precipitates to form the present sulfide phases probably occurred during early diagenesis. Metamorphism and deformation produced large pyrite cubes in metamorphosed shales (e.g., Roan Antelope West) and very minor mobilization of sulfides into joints and bedding planes. The persistence of adjacent sulfide-rich, sulfide-poor, and even barren laminae and beds for hundreds of meters in both ore-shale and arenite-hosted deposits argue against significant migration of sulfides during diagenesis and metamorphism.

The syngenetic hypothesis has fallen out of favor, mainly because of the realization that the variations in sulfide zoning probably reflect postdepositional gradients rather than paleogeography. If the sulfide zones were to reflect a change in water depth or distance from the paleo-shoreline, one would expect to find a concomitant change in sedimentary facies. This, however, is not the case. A diagenetic origin is now favored by many authors (van Eden 1974, Bartholomé 1974, Brown 1978, Annels 1979, 1984, 1989, Brown & Chartrand 1983, Brown 1984, Unrug 1988, Sweeney & Binda 1989a, Sweeney et al. 1991). This interpretation is supported by replacement of anhydrite by sulfide minerals (as well as an inverse correlation between anhydrite and sulfide mineralization in some deposits), replacement of early diagenetic pyrite by Cu-sulfides, and the association of diagenetic feldspar with and partial replacement by sulfides. Post-sedimentation addition of copper to pyritic host rocks in the Congo Copperbelt is indicated by the presence of pyrite, not Cu-sulfide, inclusions in early authigenic quartz, diagenetic magnesite nodules, and carrollite porphyroblasts, even though Cu-sulfide disseminations are abundant in the surrounding carbonate matrix (Bartholomé 1974). A later addition of Co, perhaps during the introduction of ore-stage Cu, is indicated by the recognition of Co-enriched growth zones on Co-free pyrite. The distribution of diagenetic sulfides was controlled to a large extent by primary porosity and permeability

of the host rocks. Thus, mineralization observed along sedimentary structures may simply reflect pathways for fluid movement and sites of organic material accumulation for fixation of sulfides.

Whether the main mineralization occurred during early diagenesis or late diagenesis is still a matter of debate. For example, Sweeney et al. (1986) and Sweeney and Binda (1989a) favored an early diagenetic origin for the mineralization in the Konkola Basin. Evidence cited for this inference includes: euhedral overgrowths of feldspar containing up to 0.25% Cu, indicating the presence of a Cu-rich pore fluid during early diagenesis; an early diagenetic origin of dolomites and calcites in the Ore Shale by replacement of gypsum or anhydrite in a sabkha setting; the common occurrence of carbonate-sulfide nodules in the ore horizon; $\delta^{34}\text{S}$ values of Ore Shale chalcopryrite and carrollite (-7.0 to +1.2‰, with an average value of -2.8‰) compatible with bacterial reduction of seawater sulfate; and the correlation of $\delta^{34}\text{S}$ variations with transgressive and regressive events demonstrated from sedimentological studies.

Annels and Simmonds (1984) and Annels (1989), on the other hand, proposed a late diagenetic model for mineralization in the Chambishi Basin (Fig. 12.9). They pointed out that the fairly large $\delta^{34}\text{S}$ range for stratiform sulfides in the Ore Shale (-11 to +11‰) could also be explained by abiotic high-temperature sulfate reduction. Moreover, a discernible upward decrease in ^{32}S in individual deposits, according to their interpretation, reflects a major infusion of metalliferous fluids from the base of the Ore Shale and the progressive depletion of ^{32}S in this limited reservoir through sulfide crystallization. The essential components of their model are the percolation of saline connate waters down crustal fractures, expulsion of high-temperature (>250°C) mineralizing fluids through rift-related faults into the Katangan sediments, and precipitation of sulfides in the pore spaces utilizing sulfur derived by the inorganic reduction of pore-water sulfate or early diagenetic anhydrite. An important observation in this context is the occurrence in the ore zones of subconcordant quartz - calcite - sulfide veinlets, which have the same sulfide mineralogy as veins in the adjacent argillites and are believed to be contemporaneous with the stratiform mineralization. Fluid inclusions in quartz and associated sulfide phases from these veins (Chambishi and Chambishi Southeast deposits) have yielded homogenization temperatures of about 110-170°C. The increased geothermal gradient necessary to account for the relatively high temperatures of the mineralizing fluids, according to Annels (1989), was caused by "deep magmatic activity, reflected in later high-level intrusions of gabbro (now amphibolite) bodies in basement faults and shear zones and in the Upper Roan Group." It has been argued, however, that this high temperature is related to later events, not the SSC mineralization (Sweeney et al. 1991). Similar hydrothermal veinlets associated with the Musoshi deposit (an extension of Zambian-type mineralization into Congo) are believed to represent a later overprint, unrelated to stratiform copper mineralization but perhaps related to a pulse of hydrothermal activity at the close of the Lufilian Orogeny (Richards et al. 1988a, b). Moreover, gravity and magnetic surveys of Zambia have failed to indicate the presence of any deep-seated plutonic body underlying the Copperbelt, nor is there any evidence of spatial association between richly mineralized

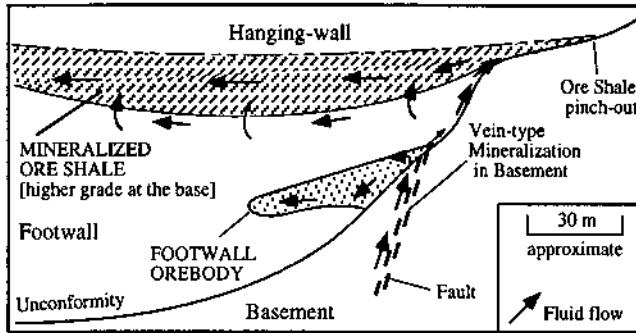


Figure 12.9. A generalized model for the genesis of SSC deposits of the Zambian Copperbelt as proposed by Anells (1984, 1989).

areas and faults as would be expected from the above model (Sweeney et al. 1991). A late diagenetic model proposed by Unrug (1988) relates the mineralization to an inferred second phase of rifting that produced the overlying Kundelungu Group. Volcaniclastics in the Lower Kundelungu Group provided copper to fluids that moved upward along high-angle faults in Roan Group sediments in upthrown blocks. The model is similar to the brine convection model of Jowett et al. (1987) for the Kupferschiefer mineralization (see Fig. 12.6), but has been questioned on grounds of insufficient evidence (Sweeney & Binda 1989b).

12.5.3. WHITE PINE, MICHIGAN, USA

The White Pine deposit (White & Wright 1954, Ensign et al. 1968, Brown 1971, Seasor & Brown 1989), the largest SSC deposit in USA, lies within a belt of copper mineralization that extends from northwestern Wisconsin to the tip of the Keweenaw Peninsula in Michigan (Fig. 12.10). The district lies in a Proterozoic basin in the exposed portion of the U.S. Mid-Continent Rift. Copper mineralization at White Pine, which is similar to the Kupferschiefer and Zambian Copperbelt deposits in many respects, is localized in the basal beds of the Upper Keweenaw (Upper Precambrian) Nonesuch Shale. The Nonesuch Shale is a distinctive gray, pyritic and carbonaceous siltstone unit (with organic carbon contents as high as 2.5%; Burnie et al. 1972), about 200 m in thickness, that was deposited under anoxic water conditions. Elmore et al. (1989) have argued that the unit is of lacustrine fresh water origin. It is overlain and underlain by redbeds (Freda Sandstone and Copper Harbor Conglomerate, respectively), without any marine evaporite in the hanging-wall or footwall sequence. The uppermost 5-6 m of the Copper Harbor Conglomerate may also be mineralized, typically with native copper. Deposits of the famous Michigan native copper district (White 1968), containing mineralization in amygdaloidal flows and conglomerate beds of the Middle

Keweenaw Portage Lake Volcanics (1086-1098 Ma; Bornhorst et al. 1988) are concentrated in the northern part of the Keweenaw Peninsula. The Portage Lake Volcanics is the upper part of a 5-10 km thick pile of subaerial tholeiitic flood basalts that represents volcanism associated with the failed Mid-Continent Rift system (Chase & Gilmer 1973, Green 1982).

The "cupriferous zone" of the mine sections comprises four informally named units of local usage (Fig. 12.11): Lower Sandstone, Parting Shale, Upper Sandstone, and Upper Shale. Although disseminated copper mineralization occurs over the entire thickness of these units, ore-grade disseminations are confined to a few lithologically favorable beds. Orebodies comprising one or more of these basal beds that are thick enough to be mineable have the form of thin blankets, square kilometers in lateral extent and generally 1 to 7 m in thickness. Chalcocite with subordinate amounts of native copper are the main copper minerals of the cupriferous zone, the native copper typically being concentrated in the Lower Sandstone where no sulfides are found.

The Cu-rich beds (up to 1-4% Cu) are of well-laminated, dark gray to black, organic-rich shale; other beds, particularly those with a reddish cast, may have average copper contents as low as 0.05%. In contrast to the cupriferous zone, the copper contents of all beds in the "pyrite zone", comprising the rest of the Nonesuch Shale with diagenetic pyrite as the characteristic sulfide mineral, are generally between 0.01

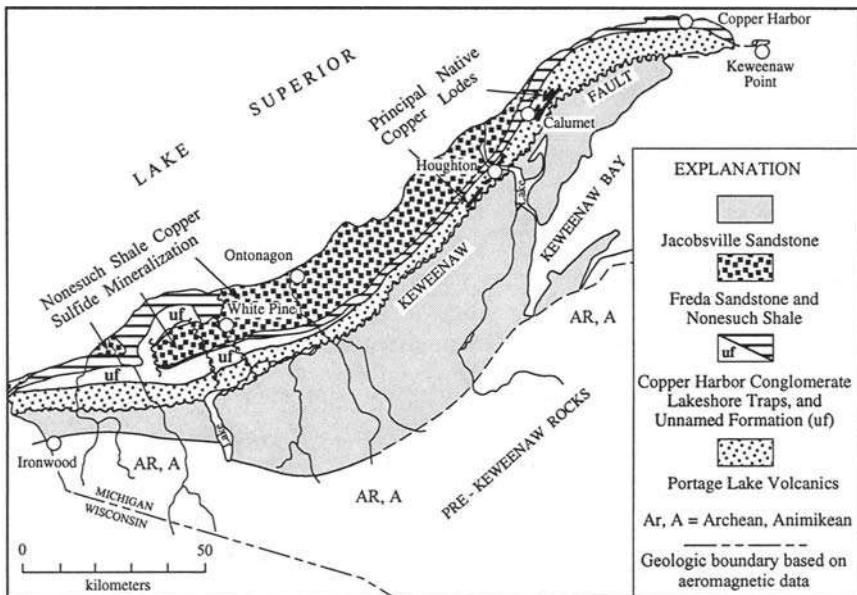


Figure 12.10. Geologic setting of the White Pine copper deposit, Michigan (simplified from Seasor & Brown 1989).

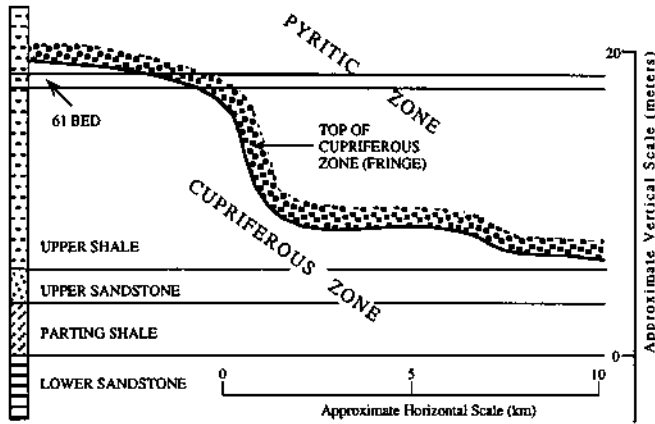


Figure 12.11. The transgressive nature of the "fringe" surface (the top of the cupriferous zone) in the lower Nonesuch Shale (after Brown 1971, Seasor & Brown 1989). According to diagenetic models of mineralization, the "fringe" represents the upper limit of copper mineralization from ascending ore fluids. The "fringe" is stratigraphically lower where greater amounts of introduced copper were precipitated in the basal Nonesuch beds.

and 0.02%. The top of the cupriferous zone is independent of lateral facies changes and transgresses bedding on a regional scale (Fig. 12.11). Thus, the same bed may be Cu-rich within the cupriferous zone but markedly Cu-poor in the pyrite zone. Textural relations suggest that the transition ("fringe") between the cupriferous and pyrite zones is characterized by a systematic step-by-step replacement of fine-grained diagenetic pyrite by chalcopyrite, bornite, digenite, and, finally, chalcocite (White 1960, Brown 1971).

Calcite-dominated veins containing pyrite, Cu-sulfides, and native copper cut the White Pine deposit at many places and are abundant in the vicinity of the White Pine fault that lies close to the deposit. This observation led Sales (1959) to propose an epigenetic, magmatic-hydrothermal origin for the White Pine mineralization. There is, however, little evidence that these veins were feeders to the stratiform mineralization. Ruiz et al. (1984) have reported a Rb-Sr age of 1047 ± 35 Ma for calcite veins that postdate the main-stage copper sulfide mineralization at White Pine, and Rb-Sr dating of amygdule-filling gangue minerals in the Portage Lake Volcanics suggests an age of 1060-1047 Ma for the native copper mineralization in the Keweenaw Peninsula (Bornhorst et al. 1988). Thus, the copper in the calcite veins probably represents a second-stage mineralization that was broadly contemporaneous with the epigenetic native copper mineralization in the footwall rocks, but the age of the main-stage mineralization in Nonesuch Shale remains poorly constrained.

A key element in the genesis of the White Pine copper mineralization is the

transgressive nature of the "fringe" surface. As discussed by Season and Brown (1989), a syngenetic origin proposed by some workers is based mainly on the interpretation that the "fringe" follows a time-equivalent surface, which was the sediment-water interface at a given moment during lower Nonesuch Shale sedimentation. Others (White & Wright 1955, Ensign et al. 1968, Brown 1971) have considered the ore emplacement to be a post-sedimentary, most likely an early diagenetic, phenomenon. The essence of this hypothesis is that the copper minerals precipitated from ascending ore fluids in the reducing environment of the Nonesuch Shale, largely by reaction with disseminated pyrite already present in the host rock, and that the "fringe" surface represents the upper limit of the copper mineralization front. This interpretation is in accord with a strong inverse correlation between the amount of copper in the lowermost beds of a mine section and the height of the "fringe" in the section, textural evidence of copper minerals replacing earlier-formed pyrite, and vertical zoning with the least soluble sulfide minerals (galena, sphalerite, greenockite) farthest along the path of the upward circulating ore fluids (Brown 1978, Season & Brown 1989).

12.6. Ore Composition

12.6.1. MINERALOGY AND TEXTURES

The mineralogy of SSC deposits is relatively simple. The major sulfide minerals are pyrite, chalcopyrite, bornite, and chalcocite (or similar Cu-S phases such as djurleite, diagenite, covellite, or anilite); native copper is found in some sulfide-poor deposits, and sphalerite and less commonly galena are important constituents in restricted portions of some deposits or districts. Detailed microscopic and X-ray studies, however, have identified more than 50 ore minerals (sulfides, arsenides, sulfosalts, native phases, natural alloys, and oxides) of Cu, Ag, Pb, Zn, Co, Ni, Mo, As, Sb, Bi, and U in these deposits (Rentzsch 1974, Banas 1980).

The average grain size of the sulfide minerals is very small (mostly <20 to 200 μm) and most are xenomorphic. Ni- and Co-minerals and Cu-sulfosalts commonly reveal idiomorphic textures, whereas pyrite commonly forms idiomorphic and framboidal grains. Bornite, chalcocite, galena, sphalerite, and chalcopyrite typically show recrystallization textures. Sawlowicz (1990) reported that small spherules and framboids (5 to 10 μm in size) and framboidal clusters of Cu-sulfide phases, especially abundant in the organic-rich laminae, are dispersed throughout the Kupferschiefer in Poland, and interpreted this as evidence for primary precipitation of Cu-sulfides ores during the sedimentation and/or early diagenesis of the Kupferschiefer. Several petrologic studies, however, have revealed clear textural evidence for the replacement of initial fine-grained, disseminated, syngenetic to early diagenetic pyrite by copper sulfides (Barthlomé 1974, Hagni & Gann 1976, Brown 1984, Jowett et al. 1987). Typical textures confirming such replacement are (Brown 1984): complete to partial pseudomorphs of chalcopyrite, bornite, and chalcocite after pyrite; halos of dusty

hematite around chalcocite nodules, most likely representing the redeposition of Fe liberated from the replacement of pyrite; and partial to complete replacement of pyrite nodules along specific stratigraphic horizons transgressed by the upper limit of the cupriferous zone. At places, as in some German Kupferschiefer deposits, Cu-Fe-As minerals (tennantite, enargite, löellingite, arsenopyrite) replace earlier Cu-sulfide minerals (chalcocite, chalcopyrite), but the timing of this replacement process is uncertain (Vaughan et al. 1989).

Sulfide zoning, both vertical and lateral, is a characteristic feature of SSC deposits, and generally shows the sequence: barren (no sulfide, often with hematite) \Rightarrow chalcocite, bornite \Rightarrow chalcopyrite \Rightarrow pyrite. Native copper overlaps and is adjacent to the chalcocite zone at White Pine, but is absent in most SSC deposits. A second common sulfide assemblage is chalcocite + pyrite, as in the Creta, Nacimientos, and Corocoro deposits. The actual zoning pattern in individual deposits or districts may show considerable departure from the generalized picture just described.

12.6.2. BULK COMPOSITION

SSC deposits, in general, are characterized by very high Cu:(Zn+Pb) ratios compared with SMS deposits. The average grade of copper in SSC deposits range from <1% to about 5 % Cu, but lies mostly in the 2-4% range (Table 12.1). Many deposits (e.g., White Pine, Redstone belt, Boleo, Dzhezkazkan) contain minor amounts of Zn±Pb, but in the Kupferschiefer deposits Zn contents may approach those of Cu and Pb contents are about half those of Cu (Jung & Knitzschke 1976). The lead-zinc facies succeeds the Cu-sulfide facies in both lateral and vertical directions (Fig. 12.4).

Cobalt contents are typically low, but discrete cobalt-rich zones occur within and toward the distal margins of copper-rich zones in several Central African Copperbelt deposits. Some of the cobalt-rich zones contain recoverable grades of cobalt. In the Zambian Copperbelt, the cobalt zone is composed of members of the linnaeite-carrollite series, with cobaltian pyrite, cattierite, and other cobalt sulfides, and it straddles the contact between bornite-bearing and chalcopyrite-bearing zones (Annels & Simmonds 1984). In the Congo Copperbelt, the cobalt zone, composed predominantly of linnaeite-carrollite, occurs within the chalcocite and bornite zones, with a concentration of Co in the contact region between chalcocite and bornite zones (Haynes & Bloom 1987b). For the Zambian Copperbelt as a whole, Cu:Co ratios lie between 30 and 40, whereas individual Co-bearing deposits contain 0.1-0.48% Co and have Cu:Co ratios ranging from 30 to 40. Cu:Co ratios in the Shaba Province of the Congo Copperbelt are much lower (10-17), because Co grades of the main deposits in this belt are considerably higher, averaging in excess of 0.3% (Annels & Simmonds 1974).

Many SSC deposits contain significant amounts of Ag (Table 12.1), reaching a peak value of 150 ppm Ag in some Kupferschiefer deposits. Ag occurs as native metal and in sulfides (mainly in chalcocite and bornite, but also in galena to a smaller extent) and a good linear correlation between Cu and Ag exists in several Kupferschiefer areas (Rentzsch 1974). Other minor constituents associated with SSC deposits include Ni,

V, Mo, and U, elements that are commonly enriched in black shales. The uranium mineralization in the Zambian copper belt occurs as disseminations or as veins of thorium-free pitchblende, and as secondary uranium minerals. The present uranium concentrations appear to be the result of remobilization of original mineralization that was co-genetic with the stratiform sulfides (Meneghel 1981).

12.7. Origin

12.7.1. GENETIC MODELS

There is little evidence for the control of folds, faults, or other crosscutting structures on localization of SSC deposits. The uniformity of copper grade through the crests, troughs, and limbs of drag folds in several Zambian Copperbelt deposits indicates that the stratiform ore sulfides predated folding and deformation of the host rocks (Garlick 1989). However, as mentioned earlier, many SSC deposits include minor vein-type mineralization, which is structurally controlled. In some cases (e.g., White Pine, Spar Lake, Kupferschiefer in Germany, Zambian Copperbelt), the vein-type mineralization clearly postdates the stratiform sulfides and, therefore, represents local redistribution of metals or a later mineralizing event; in other cases (e.g., Kupferschiefer in Poland), faulting and vein formation may have been contemporaneous with the stratiform mineralization (Jowett et al. 1987, Vaughan et al. 1989, Kirkham 1989). The following discussion pertains only to the stratiform mineralization.

Most models proposed for the origin of SSC deposits fall under two main groups — syngenetic (syngenetic) and diagenetic (syndiagenetic). In the syngenetic model, sulfides precipitated in an anoxic water column containing H_2S from bacterial sulfate reduction as in the present Black Sea. Normally, the most abundant metal available is iron, derived mainly from iron-bearing detrital minerals, which precipitates initially as a metastable phase that transforms rather rapidly to fine-grained pyrite (Bernier 1979). Precipitation of base metal sulfides in the quantities contained in SSC deposits is rather unlikely from normal seawater. Even in the Black Sea sediments, Zn and Cu concentrations exceeding 300 ppm and 120 ppm, respectively, are restricted to small areas. Moreover, the order of metals to be concentrated from normal seawater ($Zn > Cu > Ag > Pb$) does not correlate with the actual metal abundances, for example, in the Kupferschiefer bed ($Zn > Pb > Cu > Ag$). It is possible that metal concentrations in the Zechstein seawater were abnormally high, which might also account for the high Mn (6,000 ppm) in the carbonates and high V, Mo, Ni, Cr, U, and Co values in the organic fraction of the Kupferschiefer (Wedepohl 1980). However, past deposition of carbonates and evaporites similar to recent deposits indicates that the composition of seawater has not markedly changed over the last billion years (Holland 1984).

The evidence commonly cited for a syngenetic origin of SSC deposits (e.g., Fleischer et al. 1976) — such as the strong stratigraphic and lithologic control on mineralization, concentration of Cu-sulfides along sedimentary structures, the lateral

continuity of the ore horizon(s), the relation of mineralization to the paleotopography of the sedimentary basin — do not exclude the possibility of diagenetic emplacement of ore sulfides in favorable strata at hydrologically accessible sites. In addition, as discussed earlier, SSC deposits commonly show many features that are in accord with a syndiagenetic, rather than a syngenetic, origin. The most important of these are (Barthlomé 1974, Annels 1974, Renfro 1974, Brown 1978, 1984, Jowett et al. 1987):

- (a) the general extension of the metal-bearing zones into the oxidized strata below the principal hosts and into the overlying evaporites;
- (b) a moderately undulating upper surface of the cupriferous zone that transgresses bedding;
- (c) transgressive metal (and sulfide mineral) zoning related to diagenetically produced hematite-bearing rocks; and
- (d) textures interpreted as replacement of earlier formed iron sulfides and evaporite minerals by ore sulfides, and textural features indicative of the post-sedimentary addition of Cu and Co to previously pyritic host rocks.

Thus, although a small proportion of the stratiform mineralization may be symsedimentary (Wodzicki & Piestrzynski 1994), the main mineralization event appears to have been syndiagenetic.

Whether the ore emplacement occurred during early diagenesis or late diagenesis of the host sediments is a difficult question to answer, especially for deposits that have been subjected to metamorphism and deformation. In many SSC deposits, the ore sulfides tend to be disseminated and to occupy original pore spaces, suggesting sulfide introduction prior to complete lithification of the host rocks. However, some sedimentary rocks, such as sandstones, can maintain their porosity and permeability for tens, or perhaps hundreds, of million years even with deep burial. A well-documented example of early diagenetic mineralization may be the Redstone belt copper deposits in Canada (Chartrand & Brown 1985, Chartrand et al. 1989). This interpretation is based largely on textures suggestive of ore sulfide formation in original pore spaces of the host sediments and replacement of evaporitic sulfate minerals, early diagenetic calcite, and pre-existing pyrite by ore sulfides. On the other hand, as discussed earlier, the Kupferschiefer and Zambian Copperbelt deposits appear to be late diagenetic, although arguments have also been presented for early diagenetic mineralization. Perhaps, as proposed by Vaughan et al. (1989) and Wodzicki and Piestrzynski (1994), SSC-type mineralization spans a spectrum of ore deposition ranging from early to late diagenetic.

12.7.2. ORE-FORMING FLUIDS

The extremely fine-grained sulfide and gangue minerals of SSC deposits are not readily amenable to fluid inclusion microthermometry, but other lines of evidence point to temperatures of less than about 100°C for the formation of a majority of the deposits (Rose 1976). Perhaps the best evidence is that some bornite in these deposits is S-rich

and exsolves chalcopyrite when heated above 75°C, suggesting that this bornite had not formed at or been exposed to temperatures greater than about 75°C. A low temperature sulfide deposition is also corroborated by the presence of orthorhombic chalcocite that is stable only up to 103°C, replacement of plant material with preservation of cell structure, a lack of high-temperature hydrothermal alteration assemblage in or around orebodies, sulfur-isotope geothermometry yielding temperatures of <100°C (Jowett et al. 1991), and sulfur isotope data suggestive of bacterial reduction of sulfate.

The common association of SSC deposits with redbeds suggests that the ore-forming fluids either originated in or passed through the redbeds. In either case, the fluids must have been approximately in chemical equilibrium with these sediments, with their oxidation state defined by hematite stability and their pH constrained by carbonate equilibria, silicate equilibria (illite - K-feldspar or illite - kaolinite), or more complex reactions. In general, groundwaters and pore fluids at low temperatures rarely have pH values less than 6 (Rose 1989). With elevated salinities from several possible sources of chloride — dissociation of associated evaporites, the influx of marine pore fluids from underlying overlying sediments, or evaporative concentration during redbed deposition — these fluids could transport significant amounts of Cu (defined as ≥ 1 ppm or $10^{-4.8}$ *m* Cu) as Cu^+ -Cl complexes to the sites of ore deposition (Rose 1976, 1989). Thermodynamic modeling by Haynes (1986b) and Haynes and Bloom (1987a) predicts that pore waters in closed continental basin sediments would evolve very early in their burial history to a 3-molal NaCl brine (pH = 7 to 8, $f\text{O}_2 = 10^{-30}$ to 10^{-45} bars, temperature = 25°C) capable of transporting at least 100 ppm Cu. Also, calculations by Sverjensky (1987) indicate how relatively reducing oil-field brines (that transport zinc, lead, and reduced sulfur but hardly any copper) migrating through evaporitic and redbed aquifers may become oxidized and capable of transporting, when saturated with respect to hematite and chalcocite, at least 35 ppm each of Cu and SO_4^{2-} at 125°C and a pH of 6. Thus, ore-forming fluids for SSC deposits appear to be near-neutral (pH = 6 to 8), oxidized (in the stability field of hematite/ SO_4^{2-}), low-temperature ($\approx 100^\circ\text{C}$ or less) basinal fluids of moderate salinity.

The presence of significant amounts of Ag, Pb, Zn, and Co in some stratiform Cu ores, but not in others, places additional constraints on the chemistry of ore fluids (Rose 1989). All of these metals are relatively soluble at a pH near 7 in chloride-rich, oxidizing solutions that can transport Cu as Cu^+ -Cl complexes (and Ag as Ag-Cl complexes), but Pb, Zn, and Co may not be transported in the fluid because of their stronger adsorption, compared with Cu, on iron oxides and possibly other materials. Studies (e.g., Rose et al. 1986) have shown that redbeds associated with SSC deposits are relatively depleted in Cu, but not in Zn, Pb, or Co. Low Pb and Co solubility at pH = 8.5 may also separate the metals. The amounts of other metals that can be carried in a fluid capable of transporting significant amounts of Cu at low temperatures would depend on several factors, such as temperature, pH, $f\text{O}_2$, source rocks, and salinity of the fluid, and variations in these parameters may account for the range of Ag, Pb, Zn, and Co found in SSC deposits. In the case of some large SSC deposits (e.g.,

Dzhezkazgan and Kupferschiefer), there is ample evidence that large quantities of lead and zinc were mobilized with copper, but simply did not precipitate with or adjacent to the copper ore. Perhaps, the residual brines, after copper precipitation, either discharged to the surface, dispersing the zinc and lead, or passed through laterally beyond the zone of reduction before enough reduced sulfur could be produced for the precipitation of Zn- and Pb-sulfides (Gustafson & Williams 1981).

12.7.3. HYDROTHERMAL SYSTEMS

In well-documented deposits, the distribution of base metal sulfides and pyrite suggests upward and lateral movement of ore fluids from underlying sedimentary pile, rather than downward percolation from overlying sediments.

Renfro (1974) proposed that coastal sabkhas — evaporite flats that form along the subaerial landward margins of regressive seas — provided ideal settings for the formation of evaporite-associated SSC deposits (Fig. 12.12). Commonly, the coastal sabkhas are bordered on the seaward side by intertidal mudflats and lagoons that are carpeted by mats of sediment-binding, blue-green algae, and upon burial the algal-mat facies becomes saturated with H_2S generated by anaerobic bacteria. Metal-bearing terrestrial water, driven toward the sabkha by a subsurface hydraulic gradient set up by evaporative discharge of water through the sabkha, would pass through the H_2S -charged algal mat and precipitate sulfides. The metal zoning in this diagenetic setting is considered to be a function of the relative solubilities of the metals in the presence of H_2S . But, in addition to the fact that modern sabkhas lack high concentrations of ore metals, the Sabkha model does not explain the transgression of sulfide zones over several meters of section, including several sabkha-redbed cycles, in many Kupferschiefer-type deposits (Kirkham 1989).

Compaction-driven migration of basinal brines is an attractive possibility, especially for early diagenetic mineralization, because water-escape structures have been identified in some deposits (Lustwerk & Wasserman 1989). The migration of fluids

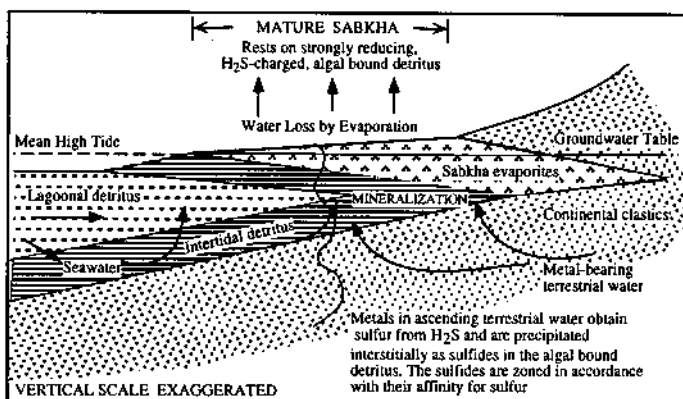


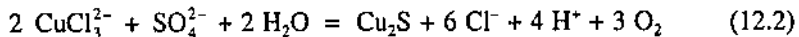
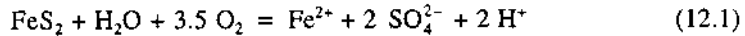
Figure 12.12. The sabkha model for evaporite-associated SSC deposits (after Renfro 1974).

could have also taken place along pre-existing faults and shear zones (Brown 1984, Annels & Simmonds 1984, Annels 1989). Brown (1984) termed this as the "pene-exhalative model" to emphasize its similarity to the model envisaged for SMS deposits (Fig. 11.16), but the term is inappropriate for SSC deposits as they show no evidence of exhalative-type mineralization.

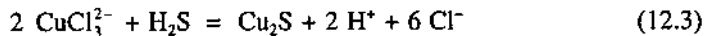
As mentioned earlier, Jowett et al. (1987) proposed a thermally-driven, late diagenetic, convective flow model for the Kupferschiefer of Poland (Fig. 12.6). Rift-faulting followed by compressive reverse movements on the faults may have triggered brine movement out of the Keweenaw rift to form deposits such as White Pine, but early tectonic movements have not been recognized in most SSC deposits (Kirkham 1989). It is likely that no single flow system is applicable to all SSC deposits or even to all deposits in a single large belt, such as the Kupferschiefer or the Central African Copperbelt.

12.7.4. ORE ACCUMULATION

Copper mineralization in both Kupferschiefer and redbed types of SSC deposits is restricted to reduced horizons, suggesting that sulfide precipitation occurred when oxidized metal-bearing fluids encountered a reduced horizon (i.e., with pyrite, H_2S , or organic matter). Within this framework, the generalized zoning pattern in SSC deposits, chalcocite \Rightarrow bornite \Rightarrow chalcopyrite \Rightarrow (galena - sphalerite) \Rightarrow pyrite, could be produced by two mechanisms (Ripley et al. 1985, Rose 1989) : (a) progressive reaction of the fluid with pyrite in host sediments, of the type



and (b) progressive addition of H_2S to the fluid at the deposition site, represented by reactions such as



Precipitation of Pb, Zn, and Co sulfides by similar reactions, after the fluid has precipitated all the Cu, would depend on the activities of the metals in the fluid and the availability of S^{2-} at the depositional site. The presence of major amounts of galena replacing pyrite in the Kupferschiefer indicates that this reaction is not kinetically inhibited. The paucity of Pb, Zn, or Co sulfides in deposits containing unreplaced pyrite probably reflects low activities of these metals in the fluid (Rose 1989).

Replacement of fossil spores has been an important process of ore genesis in some deposits, such as Creta and Nacimiento (Hagni & Gann 1976, Ripley et al. 1980), but the pyrite reaction model is the most popular one. This is so because partial to

complete replacement of pyrite, believed to be early diagenetic, by Cu-bearing minerals is recognized in most SSC deposits and unreplaced pyrite is preserved outside the copper ore area. The reaction path is determined by a number of variables (temperature, pH, fO_2 , aCu^+ , aCl^-), but a generalized picture may be presented in terms of the two end-member situations discussed by Ripley et al. (1985): (a) an ore fluid, initially lying within the chalcocite stability field, whose Cu content decreases with time due to continued Cu-sulfide precipitation (Fig. 12.13a); and (b) an ore fluid with only enough initial Cu to be in the chalcopyrite stability field, but whose input Cu content gradually increases with time (Fig. 12.13b). The zoning sequence in both cases (assuming nearly constant pH and fO_2) may be the same, chalcocite \Rightarrow bornite \Rightarrow chalcopyrite \Rightarrow unreplaced pyrite, but the reaction paths would be different. Case (a) involves successive replacement of pyrite by chalcocite, bornite, and chalcopyrite, the replacement process ending when the copper content of the fluid drops to a level in

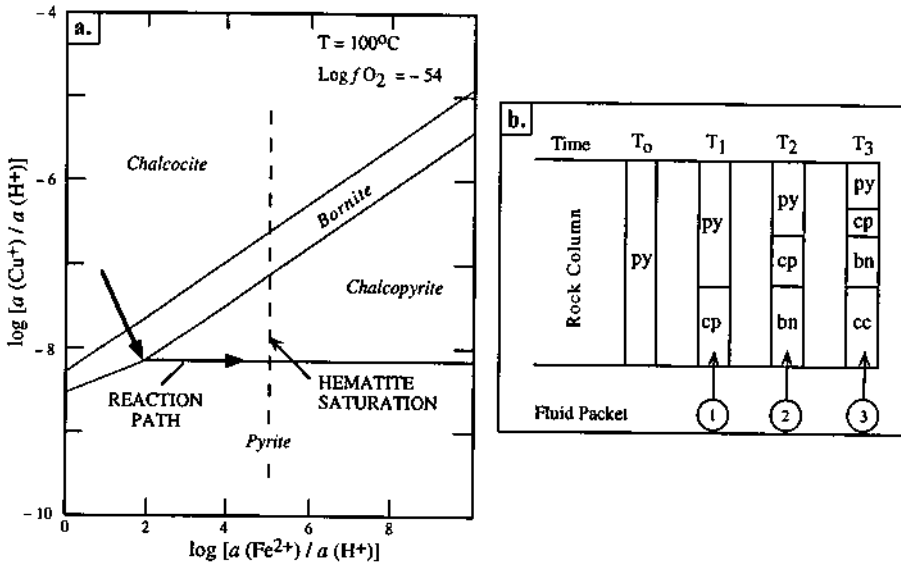
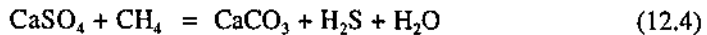


Figure 12.13. End-member situations to explain the zoning sequence chalcocite (cc) \Rightarrow bornite (bn) \Rightarrow chalcopyrite (cp) \Rightarrow pyrite (py) in SSC deposits by reaction of a Cu-bearing fluid with pyritic shale. a. Typical reaction path of an ore fluid initially in the chalcocite stability field, but whose copper content decreases with time because of Cu-sulfide precipitation. Activity or molality of Cl^- must be fixed to produce a mineral stability diagram of this type. The topology of the diagram remains the same whether the copper occurs as Cu^+ or as Cu^+ -chloride complex. b. Possible zoning sequence from an ore fluid initially in the chalcopyrite stability field, but whose input copper content (that at the redox boundary) gradually increases with time. Fluid packet 1 contains sufficient copper to convert pyrite in the rock (T_0) to chalcopyrite (T_1); packet 2 converts chalcopyrite to bornite (T_2) and unreplaced pyrite near the top of the sequence to chalcopyrite; packet 3 (T_3 , highest Cu content) causes chalcocite replacement of bornite, bornite replacement of chalcopyrite, and additional chalcopyrite replacement of initial pyrite near the top of the strata. Note that the final zoning sequence is the same in both cases, but the reaction paths are different. (After Ripley et al. 1985.)

equilibrium with chalcopyrite. In case (b), reaction proceeds by sequential replacement of pyrite by chalcopyrite, chalcopyrite by bornite, and bornite by chalcocite.

Whether the host rocks contain pyrite or not, a similar zoning sequence may result from progressive addition of H_2S to the metal-bearing fluid, until pyrite becomes a stable phase under relatively high fH_2S , because the stability of Cu-Fe sulfide phases is sensitive to fH_2S (Haynes & Bloom 1987b). The H_2S may be generated by biogenic or abiogenic reduction of SO_4^{2-} contained either in the pore fluids of the host sediments, or in the ore fluid itself, or both. Noting the conspicuous absence of anhydrite from high-grade ore zones, which are characterized instead by nodules of carbonate and quartz, Annels (1974) proposed anhydrite as the main source of H_2S in the Zambian Copperbelt. Bacterial reduction, he suggested, was probably the dominant processes in the near-surface diagenetic environment, but reactions such as



involving reduction by hydrocarbons may have become more important with increasing depth of burial.

The models discussed above account for the idealized zoning sequence in SSC deposits. Significant departures may arise because of initial or time-dependent variations in the fluid characteristics (T, pH, fO_2 , metal contents, salinity) and depositional environment (porosity, permeability, fH_2S) as well as the kinetics of sulfide precipitation.

12.8. Metallogenesis

12.8.1. HOST ROCKS

The immediate host rocks of the SSC deposits are mainly organic-rich sediments (shale, sandstone, conglomerate, marl, and carbonate), and continental redbeds constitute a characteristic component of the host rock sequence (Table 12.1). In the case of Kupferschiefer-type deposits, the gray beds (reduced facies) represent shallow-marine to lagoonal or lacustrine sedimentation. In the case of redbed-type deposits, the gray beds are part of a continental fluvial sequence. The host rock sequence of many SSC deposits also contain evaporite beds. A detailed analysis of the spatial distribution of SSC deposits and occurrences by Kirkham (1989) has shown that "most are hosted by sediments that were deposited within 20° - 30° of the paleoequator in close proximity to evaporites."

Although the mineralized horizons of SSC deposits seldom contain direct evidence of contemporaneous volcanic activity, many contain volcanic rocks in the footwall section. A thick footwall volcanic section, such as that at White Pine, is the exception, but significant amounts of continental bimodal volcanic rocks occur within

the footwall sediments at a number of deposits (e.g., the Congo Copperbelt, Kupferschiefer, Creta, Redstone).

12.8.2. SOURCE OF ORE METALS

Marine sediments are unlikely sources of metals for SSC deposits (Rose 1989). These sediments usually contain some organic matter and sulfate from seawater, resulting in the generation of at least small amounts of H_2S by bacterial sulfate reduction. Mobility of base metals under such reducing conditions is extremely limited.

Thick sections of mafic volcanic rocks underlying some SSC deposits should be considered as a potentially important source of metals for these deposits, because basalts formed in intracontinental rifts generally are enriched in Cu (≈ 100 ppm or more) and other base metals. The release of metals from basalts can be tied to dehydration reactions that accompany burial metamorphism to sub-greenschist facies (Jolly 1974) or the action of geopressured basinal brines. The relatively low temperature of mineralization from such fluids may be the result of cooling of the fluids by host rocks. For example, according to calculations by Brown (1984), a sufficient volume of solution at $120^\circ C$ and containing 10 ppm Cu (or at $150^\circ C$ and containing 25 ppm Cu) could be cooled to $<100^\circ C$ by some 250 km^3 of redbeds having an initial temperature of $30^\circ C$. Cooling of the ascending, hot, metal-bearing solutions (and precipitation of sulfides) could also be accomplished by mixing with downward percolating connate waters (Kucha & Pawlikowski 1986).

Zielinski et al. (1983) have shown that early diagenetic oxidation (reddening) of sediments result in redistribution of contained heavy metals from detrital minerals onto secondary iron oxides, but no significant open-system migration. Thus, a preferred source of metals is the redbeds that commonly accompany SSC deposits (Rose 1976), especially if the redbed sequence also contains abundant detritus of mafic volcanic rocks (Brown 1984, Haynes 1986b). Mafic detritus is a common feature of fault-bounded redbed sequences because basaltic flows generally constitute an important provenance for the rift-basin clastics. Metallogenic models based on a redbed source of metals have been proposed for the Kupferschiefer (Rentzsch 1974, Jowett et al. 1987), the White Pine (Brown 1984), and the Redstone copper belt (Chartrand & Brown 1985). For the Zambian Copperbelt deposits, an ultimate source of the metals from the pre-Katangan basement rocks is compatible with minor but widespread Cu and Co mineralization in these rocks as well as with the Pb-isotope composition of Lower Roan copper and cobalt sulfides relative to those of the basement rocks and gabbros (amphibolites) (Sweeney et al. 1991). The limited Pb isotopic data available for the Kupferschiefer provide no conclusive evidence for the metal source (Jowett et al. 1987).

12.8.3. SOURCE OF SULFUR

For diagenetic models of SSC mineralization, the two most obvious sources of sulfur are evaporitic sulfate minerals and diagenetic pyrite in the host sediments. In both

cases, the generation of reduced sulfur is believed to have involved bacterial sulfate reduction during early diagenesis of host sediments. The bacterial reduction model is largely based on the observation (Fig. 12.14) that the $\delta^{34}\text{S}$ values of ore-zone pyrites typically show a wide range of $\delta^{34}\text{S}$ values ($>30\text{‰}$) as is the case with recent normal marine sediments (e.g., Schwarcz & Burnie 1973).

Several lines of evidence, however, indicate that the bacterial reduction model alone cannot account for all the reduced sulfur in SSC deposits (Hoy & Ohmoto 1989). The $\delta^{34}\text{S}$ frequency distribution varies considerably among the different districts (Fig. 12.14) — from strongly negative (e.g., Kupferschiefer), typical of recent marine sediments, to close to 0‰ (e.g., Mufulira) and strongly positive (e.g., White Pine) that are not typical of marine sediments. Most SSC deposits are characterized by higher sulfide contents (often >2 wt%, as high as 10 wt%) and S:C (organic) mass ratios (often ≥ 1), whereas the sulfide contents of marine sediments rarely exceed 2 wt% and

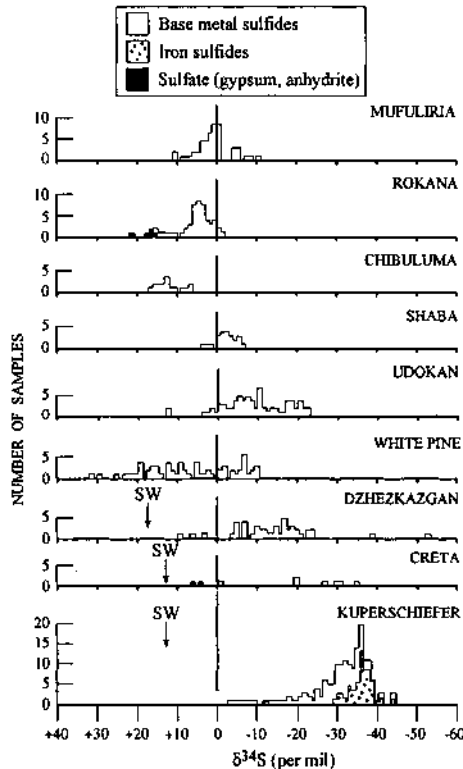


Figure 12.14. Sulfur isotope data for SSC deposits. SW arrows mark compositions of coeval seawater sulfate. Source of data: compilation by Gustafson and Williams (1981).

their S:C (organic) ratios are about 0.37 on the average. Many SSC deposits show a distinct sulfur isotopic compositional difference between the Cu-rich and Cu-poor pyritic zones and between pyrite-sulfur and sulfur from Cu-Zn-Pb sulfides, requiring more than one source of sulfur. Stratigraphically controlled vertical trends in the sulfur isotope composition of the sediments observed in some SSC deposits (e.g., White Pine, Kupferschiefer, Central African Copperbelt) have been attributed to basin isolation related to marine transgression-regression cyclicality. But, those sediments with higher $\delta^{34}\text{S}$ values often exhibit higher sulfide (and Cu) contents as well, whereas closed basin behavior should produce a decrease in sulfide content with increasing $\delta^{34}\text{S}$ values.

From a detailed study of three SSC deposits (White Pine; and Kamato Principal and Musoshi, Congo), Hoy and Ohmoto (1989) have proposed that the relationships among sulfur isotopic composition, sulfide contents, and organic carbon contents of sediments are best explained by the mixing of sulfide-sulfur having two distinct isotopic compositions, one derived by early diagenetic bacterial sulfate reduction, and the other introduced later during ore formation. For example, mass balance calculations indicate that the $\delta^{34}\text{S}$ distribution pattern in the Kamato Principal deposit can be accounted for by the addition of about 50% of the total sulfide-sulfur as non-diagenetic sulfur with $\delta^{34}\text{S}$ values around +9‰. A likely mechanism for the "secondary" sulfide is abiogenic reduction of SO_4^{2-} at the depositional site, either by interaction of organic matter in the sediments with SO_4^{2-} brought in by ore fluids or by interaction of organic matter in the ore fluids with SO_4^{2-} (as gypsum or anhydrite) in the sediments. Secondary sulfide addition has been suggested for other SSC deposits also (e.g., Branam & Ripley 1990, Jowett et al. 1991), and it may turn out to have been more important in the generation of SSC deposits than previously recognized.

12.8.4. PALEOTECTONIC SETTINGS

There appears to be a strong consensus that most, if not all, SSC deposits formed within continental rift basins (Sawkins 1976b, 1983, Raybould 1978, Annels 1984, Jowett 1986, 1989, Kirkham 1989), which are characterized by elongated sediment-filled depressions bounded by normal faults that trend parallel to the axis of extension. A convincing example is the White Pine deposit, because a rift setting for the Nonesuch Shale sedimentation is well documented by the bimodal Portage Lake volcanic suite and the Mid-continent Gravity High. Bimodal volcanics also occur in the footwall rocks of Kupferschiefer, Congo Copperbelt, and Creta deposits. Other lines of evidence that have been used for the interpretation of a rift setting include sedimentation in linear zones of fault-controlled basins with basin-and-range basement topography, evaporite deposits indicative of closed basins, immature clastic rocks with rapid facies changes, and positive gravity and magnetic anomalies (Jowett 1989, Kirkham 1989).

Jowett (1989) argued that a continental rift environment was the primary control in determining the location of SSC deposits, because this environment provided an

optimum combination of favorable conditions for ore formation during diagenesis. These conditions are: a Cu-enriched provenance provided by the rift-related basalts and the volcanic detritus in the overlying sediments; high sedimentation rates leading to early compaction and generation of chloride-rich brines in the hydrologically closed rift basins for transport of metals; and fluid migration along rift-related faults into overlying reduced-facies sediments. The conditions would be even more favorable if the fluid migration was facilitated by a later thermal or tectonic event (e.g., a late-diagenetic rifting event), as proposed by Jowett (1986) for the Kupferschiefer deposits in Poland.

The absence of SSC deposits in Archean terranes and their first appearance in early Proterozoic parallels the situation with SMS deposits and probably is related to the difference between Archean and Proterozoic tectonics discussed in the last chapter. It may also be related to the first appearance of redbeds, which seem to have played a major role in the genesis of SSC deposits, in the Early Proterozoic. There is an apparent correlation between a relatively high abundance of SSC occurrences in the geologic column (Proterozoic and Permo-Carboniferous) and low $\delta^{34}\text{S}$ values in marine evaporite sulfate (Kirkham 1989), but the validity of this correlation and its significance are yet to be evaluated by appropriate modeling.

12.9. Summary

SSC deposits, characterized by high Cu:(Zn+Pb) ratios, are only second in importance to porphyry copper deposits in terms of reserves and production of copper, and constitute the most important primary resource of Co. These deposits are localized in reduced sediments (gray beds) that either overlie or are interbedded with continental redbeds, and are commonly associated with evaporites. The combination of continental redbeds (oxidized), reduced (carbonaceous and pyritic) sediments, and evaporites is believed to have played a crucial role in the genesis of SSC deposits.

The mineralization, consisting of disseminated sulfides, is stratiform in the sense that it occurs in specific beds, resulting in a blanket-type configuration of the orebody. Sulfide (and metal) zoning is a characteristic feature of these deposits, the generalized sequence being barren (no sulfides, possibly hematite) \Rightarrow chalcocite \Rightarrow bornite \Rightarrow chalcopyrite \Rightarrow (galena \Rightarrow sphalerite) \Rightarrow pyrite. The stratiform mineralization is devoid of structural control and there is little evidence of volcanism contemporaneous with mineralization or with the immediate host rocks.

The main event of Cu (-Pb-Zn-Co) mineralization is considered to be syndiagenetic. Diagnostic evidence for this conclusion includes: the undulating nature of the upper surface of the cupriferous zone; the transgressive boundaries of the sulfide zones; and textural evidence for replacement of diagenetic pyrite and evaporitic sulfate minerals in the host rocks by Cu-sulfide minerals. The ore fluids and the metals are believed to have been derived from the underlying sedimentary pile, probably with a significant contribution of metals from volcanic detritus and older igneous bodies. Sulfide precipitation from metal-bearing oxidized fluids is attributed to either progressive

reaction with pre-existing pyrite or progressive addition of H_2S . The ultimate source of sulfide-sulfur is tied to both biogenic and abiogenic reduction of sulfate. The host sediments suggest a continental rift environment for the deposits, but their paleohydrologic systems are not well constrained.

Host rocks of SSC deposits range in age from early Proterozoic to Tertiary, but there is a marked concentration of large deposits in Proterozoic (e.g., Central African Copperbelt, White Pine) and Permo-Carboniferous (e.g., Kupferschiefer, Dzhezkazgan) rocks. This temporal distribution, as well as the apparent lack of SSC deposits in Archean rocks, are probably broadly related to the development of large-scale continental rifts.

12.10. Recommended Reading

Renfro (1974), Brown (1984), Jowett et al. (1987), Seasor and Brown (1989), Kirkham (1989), Annels (1989), Vaughan et al. (1989), Sweeney et al. (1991), Maynard (1991).

CHAPTER 13

MISSISSIPPI VALLEY-TYPE (MVT) ZINC-LEAD DEPOSITS

13.1. Introduction

Low-temperature, carbonated-hosted, strata-bound, Zn-Pb±fluorite±barite deposits are generally referred to as *Mississippi Valley-type (MVT) deposits* in recognition of the occurrence of many such deposits within the drainage basin of the Mississippi River in the central United States, where they were first studied in detail. MVT deposits contain a substantial proportion of the world's reserves of zinc and lead. They are the main source of these metals in the United States and contribute significantly to the production of lead and zinc in Canada and Europe.

Studies over the years have demonstrated a great diversity in features, and possibly in origin, among the deposits which have been included in this class (Heyl 1967, Ohle 1980, Sangster 1983), and some authors have even questioned the wisdom of lumping deposits of such varied character into one class. However, as has been pointed out by many others (e.g. Ohle 1959, Large 1983, Lydon 1986, Klau & Mostler 1986, Leach & Sangster 1993), MVT deposits, or at least the typical examples, share many common characteristics that set them apart as a class from SMS and SSC deposits (Ch. 11 and Ch. 12). The common link among these three classes of deposits is that they form as a consequence of the evolution of sedimentary basins.

The diversity in features and interpretation of these deposits is well documented in the proceedings of three symposia (Brown 1967, Kisvarsanyi et al. 1983, Sangster 1997), two special issues of *Economic Geology* (v. 66, No. 5, 1971; v. 72, No. 3, 1977), and the *Special publication* No. 4 of the Society of Economic Geologists (1996). Important review articles on the subject, particularly on North American deposits, include those by Ohle (1959, 1980), Snyder (1968), Anderson and Macqueen (1982), Anderson (1983), Heyl (1983), Sangster (1983, 1986, 1990), Sverjensky (1986), and Leach and Sangster (1993).

13.2. Distinguishing Features

The distinguishing features of typical MVT deposits, especially in comparison with other classes of sediment-hosted deposits, have been discussed by many authors (Ohle

1959, Snyder 1968, Brown 1970, Anderson & Macqueen 1982, Sangster 1983, Leach & Sangster 1993). The most important of these are summarized below.

- (a) The host rocks are overwhelmingly unmetamorphosed platformal carbonates — limestones and dolostones — with a strong bias toward dolostones. The limestone-dolostone interface is a particularly favorable locus of ore concentration.
- (b) The mineralization is strata-bound, localized in certain stratigraphic horizons or favorable strata; some are concordant bodies, resembling stratiform mineralization, but discordant bodies controlled by fractures, faults, and brecciation are more typical.
- (c) The features (excluding fractures and faults) responsible for localization of ores are related to paleogeography (Callahan 1967). These include (Fig. 13.1):
 - (i) sedimentary environments such as reefs and facies changes above an unconformity (A-1), compaction or drape structures (A-2), and in stratigraphic pinch-outs (A-3), talus or landslide breccias (A-4), all of which are distributed relative to the topographic relief on the unconformity;
 - (ii) below an unconformity in solution collapse breccias related to karstification on the surface of unconformity (B-1), or resulting from the thinning of underlying limestone beds by subsurface drainage system related to the unconformity (B-2); and
 - (iii) at a facies change in a formation or between basins of deposition, not clearly related to an unconformity (C-1).
- (d) The mineralogy is relatively simple, characterized by varying combination of low-Fe sphalerite, low-Ag galena, fluorite, barite, dolomite, and calcite. Cu- and Fe-sulfide minerals are of significance only in a few deposits.
- (e) The mineralization is predominantly of the cavity-filling type and in most cases clearly epigenetic, precipitated from low-temperature brines, but the paragenesis may be complex due to repeated dissolution and precipitation of ore and gangue minerals. Replacement-type mineralization is generally of minor importance, although there are exceptions (e.g., Polaris, Randell & Anderson 1997; Silesia-Cracow district, Leach et al. 1997).
- (f) The deposits are not associated with or genetically related to igneous rocks (except in the case of the Kentucky-Illinois fluorite district, USA).

Somewhat similar Zn-Pb deposits in the Alpine Mesozoic geosyncline of central Europe, particularly those in the eastern Alps (see Fig. 13.3), have been called 'Alpine-type' deposits. The Alpine-type deposits are also hosted by carbonate rocks and they show epigenetic features such as vein-fillings, breccia cementation, and replacement-type mineralization (Sangster 1976b). Klau and Mostler (1983,1986) interpreted the Alpine-type Zn-Pb deposits in the Eastern Alps as mineralization in a karst system that

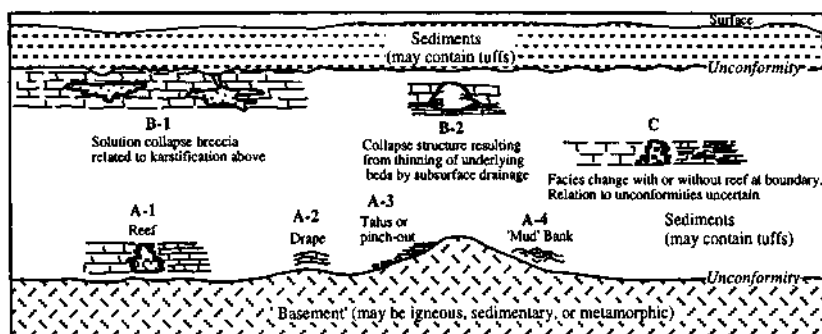


Figure 13.1. Idealized vertical section illustrating paleogeography related features responsible for the localization of MVT deposits (after Callahan 1967).

developed in a Triassic platform carbonate sequence during intra-Triassic uplift, a genetic model similar to that proposed for some unconformity-related MVT deposits. The Alpine-type deposits will not be considered in this chapter.

The Laisvall-type, sandstone-hosted, Pb-Zn(-calcite-fluorite-barite) deposits (Rickard 1983), so named after its famous occurrence at Laisvall (Sweden), has been variously classified as SSC and MVT deposits. The Laisvall-type deposits are similar to MVT deposits in terms of mineralogy, (Pb+Zn):Cu ratio, and fluid inclusion characteristics (Lindblom 1986), and the genetic model proposed for them by Rickard (1983) has many elements in common with the 'mixing' models proposed for MVT deposits (discussed later). However, Bjørlykke and Sangster (1981) have considered the Laisvall-type deposits constituting a distinct deposit type — "sandstone lead deposits" — that differs from MVT deposits not only in host rock characteristics but also in having much higher Pb:Zn ratios (Fig. 13.2). By world standards, this deposit type is of relatively minor economic significance, but it probably provides a link between the SSC and MVT deposits (Sverjensky 1986).

13.3. Distribution

MVT deposits usually occur in clusters (districts) which may extend over hundreds of square kilometers and contain up to ≈500 million tonnes of ore (Table 13.1). Most deposits are located at the edges of sedimentary basins, but some are associated with faults in the central parts of the basins. Individual deposits mostly contain <1 million tonne of Zn+Pb, but some districts exceed 10 million tonnes of metal. Average grades in the larger districts range between 3% and 10% Pb+Zn, but individual orebodies or zones may run up to 50% Pb+Zn (Sangster, 1990). With 22 million tonnes of ore grading 14% Zn and 4% Pb, the late Devonian Polaris deposit (Fig. 13.3), is an

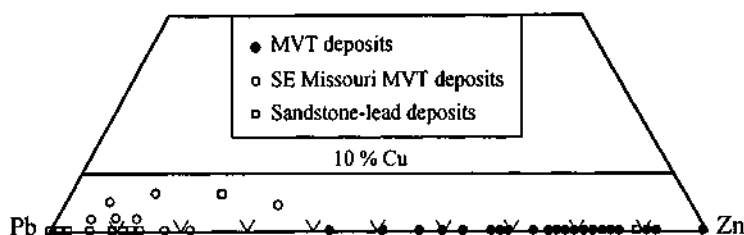


Figure 13.2. Cu-Zn-Pb proportions of MVT and sandstone-lead deposits. (Sources of data: Bjørlykke and Sangster 1981, Sangster 1983.)

TABLE 13.1. Approximate grade and tonnage of selected Mississippi Valley-type Pb-Zn districts (after Gibbins 1983)

District	Tonnage (10 ⁶ tonnes)	Zn (%)	Pb (%)
Pine Point, Canada	94.5	6.2	2.5
Cornwallis, Canada	24.1	13.8	4.2
Nanisivik, Canada *	6.4	11.5	1.2
Austinville, USA	25	3.7	0.7
Eastern Tennessee, USA	50	4.0	-
Illinois - Wisconsin, USA	100	5.0	0.5
Tri-State, USA	500	2.3	0.6
Old Lead Belt, Missouri, USA	340	-	3.0
Viburnum Trend, Missouri, USA @	420	1.0	6.0

* Single deposit

@ Estimated

unusually large and high-grade MVT deposit (Randell & Anderson 1997).

The geographic distribution of MVT deposits is rather limited, but they are particularly abundant in the United States (Heyl 1967). The most important districts within the United States are (Fig. 13.3): Upper Mississippi Valley (Wisconsin-Iowa-Illinois); Tri-State (Oklahoma-Kansas-Missouri); Southeast Missouri (Old Lead Belt, Viburnum Trend), Central Tennessee (Elmwood-Gordonsville); East Tennessee (Mascot-Jefferson City, Copper Ridge, Sweetwater); Austinville-Ivanhoe, Virginia; and Friedensville, Pennsylvania. Other important MVT districts are located in Canada (Pine Point, Polaris, Nanisivik, Gays River), Poland (Silesia-Cracow), and Australia (Sorby Hills, Coxco). The fracture-controlled, fluorite-dominant deposits of the Illinois-Kentucky district (USA) and the English Penines, although considered to be a

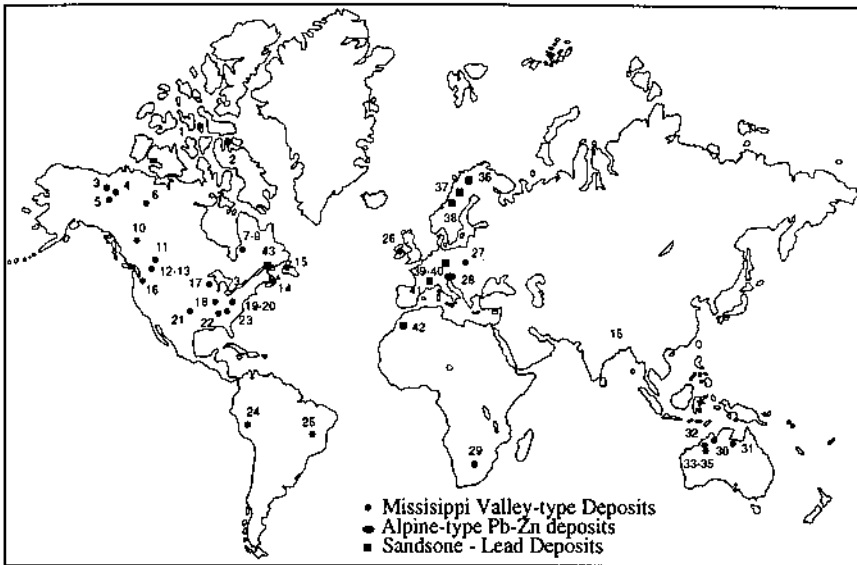


Figure 13.3. World distribution of Mississippi Valley-type Zn ± Pb districts and deposits. Also shown are the eastern Alps district of Alpine-type Pb-Zn deposits, and the major sandstone-lead deposits as defined by Bjørlykke and Sangster (1981). 1. Polaris; 2. Nanisivik; 3. Gayna; 4. Bear-Twit; 5. Godlin; 6. Pine Point district; 7. Lake Monte; 8. Nancy Island; 9. Ruby Lake; 10. Robb Lake; 11. Monarch-Kicking Horse; 12. Giant; 13. Silver Basin; 14. Newfoundland Zinc; 15. Gays River; 16. Metaline district; 17. Upper Mississippi Valley district; 18. Southeast Missouri district; 19. Austinville-Ivanhoe district; 20. Friedensville; 21. Tri-State district; 22. Central Tennessee district; 23. East Tennessee district; 24. San Vicente; 25. Vazante; 26. Harberton Bridge; 27. Silesia district; 29. Budd; 30. Sorby Hills; 31. Coxo; 32. Pillara; 33-35 Lennard Shelf district (Cadjebut, Blendevale, Twelve Mile Bore); 36. Laisvall; 37. Dorotea; 38. Vassbo; 39. Mechernich; 40. Maubach; 41. Largentiere; 42. Zeida; 43. Yava.

genetic variant of MVT deposits (e.g., Brown 1967, Leach & Sangster 1993), are not included in the present discussion.

Important MVT deposits occur in rocks of every age from the Proterozoic to the Cretaceous (Fig. 13.4). No MVT deposits have been reported from the Archean. In spite of the abundance of appropriate carbonate rocks, the Proterozoic contains only a few MVT deposits — e.g., Black Angel Mine, Greenland (Fish 1974); Nanisivik deposit, Canada (Clayton & Thorp 1982); and Coxco deposit, Australia (Walker et al. 1983). Paleozoic rocks, especially of Cambrian-Ordovician and Devonian-Carboniferous age, are the most important hosts to MVT deposits. Examples are: Cambrian — Viburnum Trend, Old Lead Belt, Austinville-Ivanhoe; Ordovician — East Tennessee, Central Tennessee, Friedensville; Devonian — Pine Point, Polaris; Carboniferous — Tri-State. The Silesian (Poland) and Alpine (Austria, Yugoslavia, Italy) districts are mainly in Triassic rocks, and small deposits in Algeria and Tunisia are hosted by Cretaceous rocks. Very few MVT deposits occur in rocks of Silurian or Permian age (Sangster 1990).

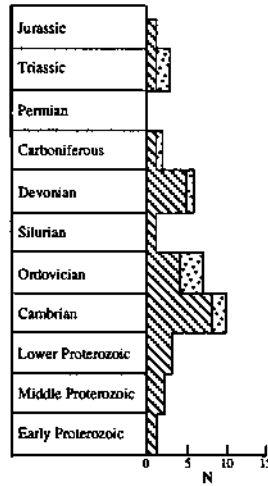


Figure 13.4. Age distribution of host rocks to individual MVT deposits (diagonal pattern) and districts comprising many deposits (stippled pattern). (After Sangster 1990.)

13.4. Examples

13.4.1. VIBURNUM TREND, SOUTHEAST MISSOURI, USA

In southeast Missouri, Mississippi Valley-type Pb-Zn±barite mineralization occurs in every formation from the Upper Cambrian Lamotte Sandstone to the Lower Ordovician Jefferson City Formation, over a stratigraphic interval of about 800 m in thickness. The Southeast Missouri Pb-Zn district (Fig. 13.5) located on the northeastern margin of the Ozark Dome, is arbitrarily defined as the area in which strata-bound deposits of Pb-Zn(-Cu) occur in the Upper Cambrian Bonneterre Formation (Fig. 13.6) and, to a minor extent, in the upper Lamotte Sandstone around the exposed Precambrian rocks of the St. Francois Mountains (Snyder & Gerdemann 1968). These deposits contain no barite. Mineralization in the stratigraphically higher formations contains, in addition to Pb-Zn, barite as a major constituent and is very similar, and probably genetically related, to the MVT Pb-Zn mineralization in the Bonneterre Formation (Kaiser et al. 1987). The Southeast Missouri barite district has been a major source of barite, nearly all of the barite being mined from extensive, low-grade, residual deposits derived chiefly from the weathering of the Potosi Dolomite and Eminence Dolomite.

The Southeast Missouri Pb-Zn district is comprised of four major subdistricts — Lamotte-Fredericktown, Old Lead Belt, Indian Creek, and Viburnum Trend (New Lead Belt) — and several inactive minor subdistricts (Fig. 13.5). Together, the Old Lead Belt, which was productive from about 1720 to 1972, and the Viburnum Trend, which

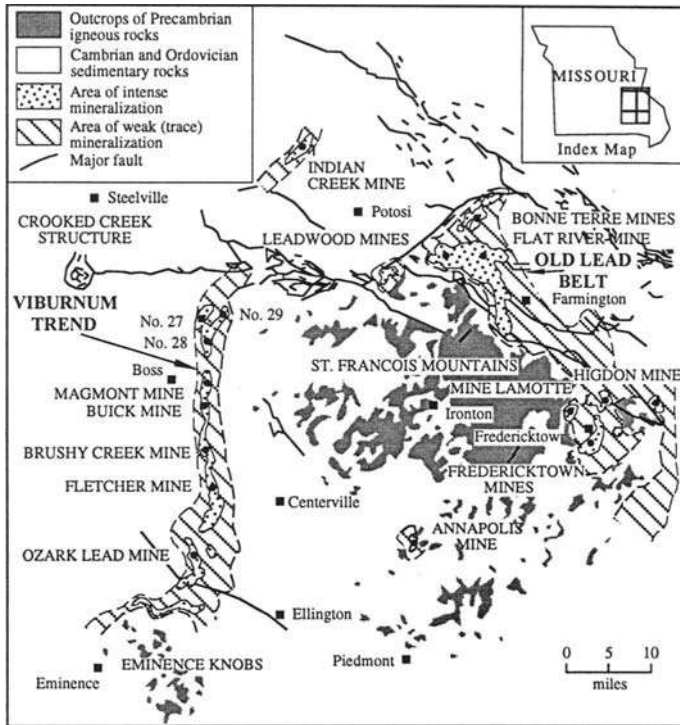


Figure 13.5. The southeast Missouri Pb-Zn district (compiled from Thacker & Anderson 1977, Kisvarsanyi 1977, Snyder & Gerdemann 1968, and Heyl 1983). The important MVT subdistricts, in order of discovery, are Mine LaMotte-Fredericktown, the Old Lead Belt, Indian Creek, and the Viburnum Trend. Also shown are areas of related Pb-Zn barite mineralization in younger formations (Kaiser et al. 1987).

was discovered in 1955 and has been in production since 1960, represent the greatest concentration of lead yet found in the Earth's crust. Total production from the Viburnum Trend from 1960 through 1984 was over 123 million tons of ore, yielding about 7.7 million tons of lead, over 1 million tons of zinc, about 181,000 tons of copper, and nearly 33 million troy ounces of silver (Wharton 1986, as quoted in Hagni 1995). Despite some significant differences in metal ratios and controls of ore localization, the overall close similarities between the two belts strongly suggest that they were parts of the same ore-forming system (Ohle 1990). The distinctive features of the Southeast Missouri district are (Kisvarsanyi 1983): (a) spatial relationship of the orebodies to Precambrian highs and local depositional basins; (b) dominance of Pb over Zn (Pb: Zn ratios range from >5 in the Viburnum Trend to >16 in the Old Lead Belt); and (c) high abundance of Cu, Ni, Co, and Cr compared with other MVT deposits. A

good summary of the Southeast Missouri district is provided by Hagni (1995).

The Viburnum Trend, currently the world's most productive lead-mining district, lies to the west of the St. Francois Mountains and approximately 160 to 190 km northwest of the New Madrid fault system and Reelfoot rift zone in the Mississippi Embayment area. It forms a narrow, north-south-trending belt of mineralization extending about 65 km and is known to consist of several discontinuous ore deposits ranging up to 30 m in thickness and from less than 100 m to more than 3 km in width. The core of the St. Francois Mountains is occupied by 1400-1270 Ma igneous rocks, primarily alkali rhyolite flows and pyroclastics intruded by granites and diabases. Similar rocks form the basement in the Viburnum Trend. The uplifted Precambrian basement areas were deeply eroded, resulting in a rugged topography upon which Upper Cambrian to Lower Ordovician formations were deposited in time-transgressive, epicontinental seas. Unconformably overlying the uneven Precambrian basement is the quartzose to arkosic Lamotte Sandstone (Upper Cambrian) of highly variable thickness that locally pinches out against Precambrian knobs. Only a very minor proportion of the ore in the Southeast Missouri district is hosted by the Lamotte Sandstone, but it is the most likely ore-fluid aquifer for the district. The localization of the orebodies was strongly controlled by the Precambrian knobs where pinch-out developed in the Lamotte Sandstone, with orebodies lying above the pinch-outs or above the apices of the knobs in the overlying draping sediments (Kisvarsanyi 1977). Minor lead-zinc mineralization is locally present in the Precambrian rocks, but it never reaches ore grade, except at Silver Mine, Missouri (Hagni 1995).

Almost all commercial ore in the district is contained in the Bonneterre Formation, a carbonate unit dominated by dolostones. It is overlain by the very sparsely mineralized Davis Formation comprised of interbedded shales and carbonates, which is believed to have acted as an impermeable barrier to the migration of ore fluids. The Bonneterre Formation in the Viburnum Trend area has been divided into four facies (Fig. 13.6) — fore reef, algal reef complex, back reef, and shelf facies. A limestone-dolostone interface is superimposed on the facies pattern. The crosscutting relationship of this interface indicates that the dolomitization was neither synsedimentary nor early diagenetic; the dolomitizing fluids probably came from an outside source. Another crosscutting, secondary alteration feature is a rock coloration boundary, termed the "brown rock-white rock interface". The carbonates on the shoreward side of this boundary are lighter in color than the carbonates to the seaward side. MVT deposits may occur anywhere in the Bonneterre Formation, but they are more abundant in the upper parts. The algal reef facies is commonly too impermeable for ore deposition and accounts for only 20% of the ore in the Viburnum Trend (Ohle 1983). Breccia bodies, 5-20 m in height and up to 30-100 m in width, extend at intervals for the entire length of the Viburnum Trend and are the main loci of ore deposition, although parts of the Trend are barren or too lean to be mineable. Most of the breccia bodies are solution-collapse features resulting from solution thinning of certain beds in the Bonneterre. Some of the breccias are partly or entirely pre-ore, but the cementation of older ore-breccia by later ore-breccia indicates that dissolution by ore fluids and brecciation

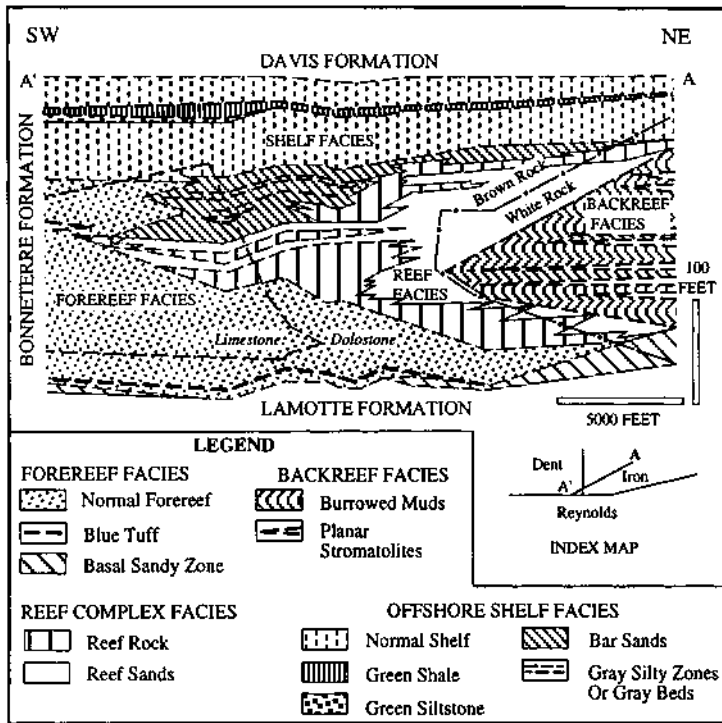


Figure 13.6. Facies relationships in the Bonneterre Formation of Viburnum Trend area. Also shown are the crosscutting limestone-dolostone interface and the "brown rock-white rock interface" (after Lyle 1977).

continued during ore deposition, perhaps enlarging pre-existing breccia bodies formed by total dissolution of local evaporites, gravity slides off local highs, or tectonic squeezing (Ohle 1983, 1985). Mineralization also occurs in sedimentary structures and as "marginal break" ores in fractures and faults bounding the breccia bodies. The major faults in the district, believed to be reactivated Precambrian faults, rarely contain commercial-grade ore, but they appear to have played an important role as fluid conduits and in ground preparation. Cavity-filling is the dominant style of mineralization, but replacement is important locally. The mineralogy and paragenesis of the Viburnum Trend has been discussed in great detail by Hagni and Trancyger (1977), Hagni (1983), Horrall et al. (1983), and Fennel et al. (1997). Generally, the paragenesis is very complex because of several stages of sulfide deposition (see Fig. 3.3).

Davis (1977) proposed an early diagenetic model of mineralization for the Southeast Missouri lead-zinc district and Stein (1980) argued for syngenetic replacement mineralization in intertidal to supratidal carbonates in the lower part of the Bonneterre Formation, beneath the epigenetic breccia mineralization. Most workers, however,

consider the Pb-Zn ores to be epigenetic; if syngenetic-diagenetic protores existed, they were completely remobilized during epigenesis. An epigenetic origin is in agreement with a Pennsylvanian-Permian age of mineralization inferred from paleomagnetic data (Wu & Beales 1981, Wisniowiecki et al. 1983). Rb-Sr systematics of galena from the Viburnum 27 mine was interpreted to indicate an early Devonian age of mineralization (Lange et al. 1983), but the interpretation has been questioned by Ruiz et al. (1985) (see Ch. 4).

The possible source(s) of the hydrothermal fluids, the migration of the fluids, and the mechanisms of sulfide precipitation for the MVT deposits in the Ozark region, including those of the Viburnum Trend, have been discussed by Leach and Rowan (1986), Rowan and Leach (1989), and Viets and Leach (1990), and summarized by Leach and Sangster (1993). The similarities of fluid inclusion temperatures and salinities from the Viburnum Trend mines and from unmineralized drill cores beyond the district suggest that the fluid flow occurred on a regional scale through not only the Lamotte Sandstone but also the Bonneterre Formation. The elevated fluid inclusion homogenization temperatures (90-160°C) are consistent with gravity-driven flow, rather than with compaction-driven fluid flow. The fluids appear to have been expelled from the Arkoma and/or Black Warrior basins of the Ouachita foreland trough in response to late Pennsylvanian-early Permian orogenesis. Other lines of evidence — minor and trace element distribution in the Bonneterre Dolomite (Gregg & Shelton 1989), oxygen and carbon isotopic compositions of dolomite (Gregg & Shelton 1989), sulfur isotopic composition of sulfides (Goldhaber & Mosier 1989, Shelton et al. 1995), stratigraphic relations in the Reelfoot rift zone to the southeast (Houseneck 1989), regional distribution of faults (Clendenin et al. 1994) — also indicate two or more fluid (and metal) sources that include Arkoma and/or Black Warrior basins, Illinois basin, Reelfoot rift, and Precambrian basement. Kisvarsanyi (1983) and Horrall et al. (1983) emphasized the multiple sources of metals for these deposits, including the distant and surrounding sedimentary basins, the Precambrian basement (especially for Pb), and the alkalic mafic-ultramafic plutons of the New Madrid Rift Complex (especially for Cu, Ni, and Co).

13.4.2. PINE POINT, NWT, CANADA

The Pine Point mining district, located on the southern shore of the Great Slave Lake (Fig. 13.7), was a major producer of MVT Zn-Pb ores. The district contains 87 known lead-zinc deposits, of which 36 have been mined. Pine Point Mines Ltd. (controlled and operated by Cominco Ltd.) started production in the district in late 1964 and, as the sole producer, had mined 70.8 million short tons of ore averaging 3.0% Pb and 6.6% Zn until the suspension of mining in 1987 (Rhodes 1991). Despite its short history, the district has been explored and studied intensively. The description presented below has been summarized mainly from Campbell (1967), Skall (1975), Kyle (1981), and Rhodes et al. (1984).

In the Pine Point area, 350 to 600 m of very gently west-dipping sedimentary strata



Figure 13.7. Regional geologic setting of the Pine Point Zn-Pb district (after Campbell 1967, and Rhodes et al. 1984).

of Ordovician to Devonian age overlie a basement of Archean crystalline rocks and Proterozoic sediments. Of particular interest are the strata of middle Devonian (Givetian) age, because they host all of the known ore deposits of the Pine Point district. Regionally, the Givetian strata consist of a narrow (10-km-wide) linear buildup of carbonate facies, the Pine Point barrier complex, which separates two depositional basins (Fig. 13.7). To the north and west of the barrier complex lies the Mackenzie Basin in which predominantly shales and argillaceous limestones were deposited in deep-water environments; to the south lies the Elk Point Basin in which evaporites and lesser amount of carbonates were deposited in a shallow-water back-reef environment. This geologic setting is a critical component of some models of ore genesis proposed for the Pine Point (Beales & Jackson 1966, Jackson & Beales 1967).

The Pine Point barrier complex is composed of a complex assemblage of diachronous carbonate lithofacies, all of which were deposited as limestones but extensively dolomitized later. These facies (and subfacies) are distinguished by composition, fabric, and paleoenvironments of sedimentation, although the contacts are generally gradational and interdigitated (Skall 1975, Rhodes et al. 1984). Karstification of the barrier complex, involving dissolution of carbonates, subsidence, and collapse, was the major control of ore deposition at Pine Point. Most orebodies were deposited in interconnected paleokarst networks that developed at the lower limits of the Presqu'île dolomite (facies K). Rock dissolution at this horizon produced cavities

ranging from narrow, small interconnected openings to wide and laterally continuous channelways. The channelways formed tabular karst structures which constitute the most common, widespread, and typical karstic phenomenon at Pine Point. There are two pronounced trends of tabular karst and associated mineralization — the 2-km-wide North Trend and the 3.3-km-wide Main Trend. Each occurs in a crudely strata-bound horizon coincident with the base of the Presqu'île dolomite and is known to extend for more than 50 km along the strike of the barrier.

At intervals along the tabular solution channels, chimney-like karst structures, referred to as "prismatic structures", extend upward from the tabular system. Kyle (1980) interpreted the prismatic structures as detritus-filled sinkholes that developed largely by dissolution in the limestone facies due to subaerial exposure. According to Rhodes et al. (1984), however, both the tabular and prismatic structures were parts of a single paleoaquifer system, the prismatic karst structures resulting from localized extreme karstification in the tabular karst horizon, commonly in structurally elevated areas where enhanced fracturing and jointing increased porosity and permeability.

The karstic networks at Pine Point contain pervasive Zn-Pb mineralization, but not necessarily of ore grade. Mineralization occurs as open-space filling, replacement of karst-filling internal sediments (i.e., solution opening filled by locally derived clastic carbonate sediments, presumably by subterranean streams; Rhodes et al. 1984) and breccias, and as peripheral mineralization in vuggy wallrocks. The sulfide bodies are composed almost exclusively of sphalerite, galena, pyrite, marcasite, dolomite, and calcite. Minor amounts of pyrrhotite, celestite, barite, gypsum, anhydrite, fluorite, sulfur, and bitumen are present in the host rocks.

The Pine Point district is probably best known for having provided the basis for the formulation of a popular model for the genesis of MVT deposits — the 'mixing' model of Beales and Jackson (1966) and Jackson and Beales (1967). In essence, this model envisages the sulfide precipitation to have occurred as a consequence of the mixing of two different fluids at the site of deposition: a metal-enriched fluid derived from the Mackenzie Basin as a result of compaction of argillaceous sediments, and a sulfur-enriched fluid derived from the Elk Point Basin evaporites. The $\delta^{34}\text{S}$ values of the Pine Point sulfides (averages of the different sulfide minerals ranging from +18.4 to +21.6‰) are very similar to those of the middle Devonian evaporites (Sasaki & Krouse 1969). The sulfur isotope data and stratigraphic considerations suggest that the most reasonable source for the sulfide sulfur was middle Devonian seawater sulfate, perhaps supplied through connate brines from Elk Point evaporites (Thide & Cameron 1978). Evidence for the Mackenzie Basin as the source of metals is less convincing. However, shales generally contain more Pb and Zn than do carbonate rocks, and Smith et al. (1983) have shown from an evaluation of geophysical logs for the middle Devonian shale sequence of the Mackenzie Basin that a substantial volume of water could have been expelled by late-stage shale compaction. Fluid inclusion studies of Pine Point minerals (Roedder 1968) indicate that the ore fluids were moderately hot (50°-100°C) and highly saline (15-23 wt% NaCl equivalent). If the mineralization at Pine Point occurred during the Permian, as is suggested by the Pb-isotope data (Sangster 1990),

then the burial of middle Devonian shales at normal geothermal gradients could account for the temperature of ore-forming fluids.

13.4.3. MASCOT-JEFFERSON CITY DISTRICT, EASTERN TENNESSEE, USA

The currently productive Mascot-Jefferson City (M-J) district in eastern Tennessee (Misra & Fulweiler 1992, Misra et al. 1997), one of the many MVT districts hosted by the Cambrian-Ordovician carbonate rocks of the Southern Appalachian Valley and Ridge province (Hoagland 1976), is a typical example of the Zn-rich type. The Valley and Ridge province comprises a thick sequence of Paleozoic (Cambrian to Pennsylvanian) carbonate and clastic sediments, which was disrupted by a series of NE-SW-trending thrust faults related to the middle Pennsylvanian-Permian Alleghenian orogeny (Hatcher & Odom 1980). The generally uniform pattern of parallel thrust sheets is modified in a few places by cross structures of secondary magnitude, which apparently have played no role in the localization of zinc mineralization.

Significant zinc mineralization in the M-J district is restricted to brecciated zones within the Lower Ordovician Kingsport Formation and Mascot Dolomite of the Knox Group, and almost all of the commercial ore occurs in a restricted interval that straddles the conformable Kingsport-Mascot boundary (Fig. 13.8). These formations are composed predominantly of carbonate rocks: limestone; medium- and coarse-grained dolostone, which represent dolomitized limestone (locally called "recrystalline"); and fine-grained ("primary"), dolostone formed by penecontemporaneous dolomitization of calcareous sediments in upper intertidal to supratidal depositional environments

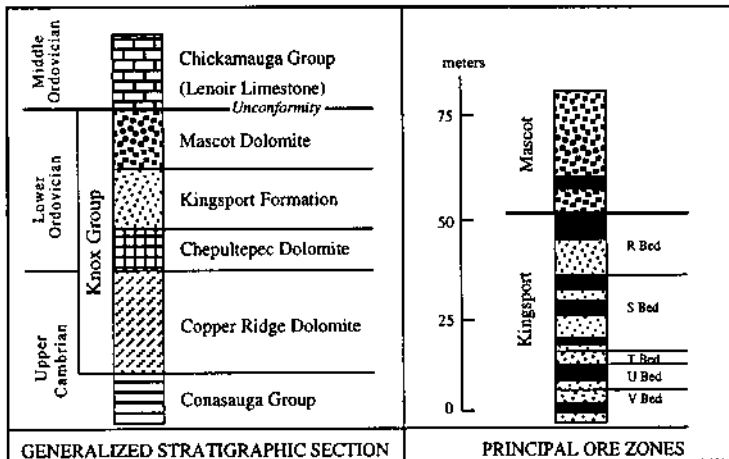


Figure 13.8. Generalized stratigraphic column, Mascot-Jefferson City zinc district, East Tennessee, showing major ore-bearing horizons in solid black (after Crawford et al. 1969). The upper part of the Kingsport Formation is divided into six beds — R, S, T, U, V, and W — which are separated by conspicuous marker horizons.

(Churnet & Misra 1981, Churnet et al. 1982). A regionally extensive unconformity, commonly referred to as the post-Knox unconformity, separates the Mascot Dolomite from the overlying, unmineralized middle Ordovician carbonate-clastic sequence.

The ore-bearing structures in the district are complex bodies of crackle and rubble breccias of two related types (Fig. 13.9): (a) breakthrough structures, which may cut through one or more stratigraphic horizons; and (b) bedded structures, which are confined to certain limestone horizons in the Kingsport Formation. The breakthrough breccia bodies are oriented, relatively narrow (a few meters to a maximum of few hundred meters in width), tabular bodies with linear dimensions up to several thousand meters and vertical thickness ranging from a few meters to more than 150 meters. These breccia bodies probably developed along pre-mineralization faults and joints, but the picture is obscured by post-mineralization movement along these zones. The bedded ore structures are of much smaller dimensions. A common type of bedded ore structure consists of fingerlike lateral extensions of brecciation and mineralization into limestone units cut by breakthrough breccia bodies (Fig. 13.9).

The mineralization occurs predominantly as open-space fillings in breccias. The breccias range from rock-matrix breccias to ore-matrix breccias in which the open spaces seem to have been enlarged by dissolution of the carbonate rock-matrix during the ore deposition process. The characteristic features of the ore-gangue mineralogy of the district include: a preponderance of honey-yellow to light brown, low-Fe (typically <1% Fe) sphalerite; sparry dolomite (locally referred to as "white gangue dolomite") as

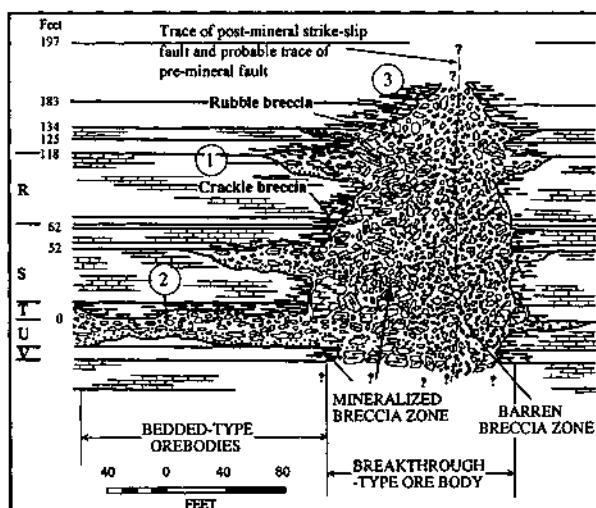


Figure 13.9. Schematic cross section of a major breccia system showing R-bed ore-shoot of the bedded-type (1), U-bed ore shoot of the bedded-type (2), and mineralized breccia in the breakthrough orebody (3) (after Crawford et al. 1969). The host rock sequence is composed of limestone (brick pattern) and dolostone (unpatterned).

the dominant gangue mineral; a virtual lack of galena; an absence of Cu- or Co-bearing minerals; minor amounts of pyrite/marcasite and bitumen; and only trace amounts of fluorite and calcite as late vug-filling minerals. Sphalerite commonly shows growth zoning marked by the alternation of light and dark colored bands, but there is no systematic correlation between the color of sphalerite and its Fe or Cd concentration (Churnet & Misra 1983, Craig et al. 1983).

The major breccia bodies, both mineralized and unmineralized, have been interpreted as solution-collapse features — partial dissolution of limestone by meteoric water, resulting in the collapse of overlying strata — related to the post-Knox uplift and erosion (Harris 1969, 1971). The strongest evidence cited in favor of the so-called “paleoaquifer hypothesis” is a systematic relationship between the thinning of Kingsport limestone, presumably from dissolution, and the location of breccia bodies (Wedow 1971). The occurrence of ore-matrix breccia clasts in sphalerite-bearing “sand” bodies (pockets of well-laminated internal sediments of sand-size material filling former cavities) in breccia zones indicates that some brecciation accompanied mineralization (Matlock & Misra 1993). The ore fluids probably enlarged the pre-existing breccia zones and enhanced the porosity within breccias through dissolution of the carbonate rock-matrix (Churnet & Misra 1983).

Pockets of internal sediments (also referred to as “sand” bodies) in breccias contain detrital sphalerite derived from mineralized wallrocks. Lamination in the internal sediments is parallel to the dip and strike of the country rock, indicating that the main-stage sphalerite mineralization occurred prior to the regional deformation event (Kendall 1960, Matlock & Misra 1993). The absence of any systematic structural control on mineralization, the offsetting of mineralized bodies by Alleghenian structures, and the widespread deformation of ore-stage sphalerites (Taylor et al. 1983) are consistent with this interpretation. Based on Rb-Sr isochron ages of 377 ± 29 Ma and 347 ± 20 Ma for sphalerites from the M-J district, Nakai et al. (1990, 1993) have proposed that the mineralization was emplaced prior to the Alleghenian orogeny (330-250 Ma), probably from fluids expelled during the older Acadian orogeny (380-350 Ma).

Fluid inclusion studies (see Misra & Fulweiler 1992 for references) indicate that the ore fluids were moderately hot (100-180°C) and highly saline (17-22 equivalent wt% NaCl). Taylor et al. (1983) found a general correlation between homogenization temperature and salinity of fluid inclusions and interpreted this as evidence for the mixing of two basinal brines for sulfide precipitation. Noting that the greater abundance of CH₄ in the inclusion fluids (0.3 to 2.9 mole%) than could be accommodated by the inclusions at the likely *P-T* of trapping is suggestive of the presence of a separate gas phase during mineralization, Jones and Kesler (1992) attributed the sphalerite precipitation in these deposits to the interception of Zn-rich brines by a pre-existing sour gas cap.

The breccia-fill deposits of the Central Tennessee zinc district, which is located on the Nashville Dome, is similar to the Mascot-Jefferson City deposits in terms of host rocks, nature of mineralization, very high Zn:Pb ratios, and the temperature and salinity of mineralizing fluids, but there are significant differences that argue against a genetic

connection (Misra et al. 1997). Compared with the eastern Tennessee district, the Central Tennessee district (a) has a more typical MVT mineralogy (sphalerite + minor galena + fluorite + barite), with sparry calcite, not sparry dolomite, as the principal gangue mineral; (b) is characterized by isotopically lighter sulfur ($\delta^{34}\text{S} = -8.4$ to -0.4%) derived from crude oil or other organic matter (in contrast to isotopically heavy sulfur, $\delta^{34}\text{S} = +27.4$ to $+33.4\%$, in East Tennessee derived by thermochemical reduction of seawater sulfate) (Kesler et al. 1994b, Misra and Torssander 1995); (c) has more uniform and more radiogenic ore lead, suggesting a well-mixed, older lead source for Central Tennessee (Kesler et al. 1994a, Misra et al. 1997); and (d) a younger age of sphalerite mineralization (see Table 13.2). Preliminary Na-Cl-Br systematics of mineralizing brines suggest that the two districts belong to separate brine provinces. The generation of brines appear to be related to evaporation of seawater in eastern Tennessee, but to evaporite dissolution in Central Tennessee (Kesler et al. 1995).

13.5. Ore Composition

13.5.1. MINERALOGY AND TEXTURES

The mineralogy of MVT deposits is rather simple, although considerable variation exists among districts in terms of the total ore-gangue assemblage. The main sulfide minerals are sphalerite and galena; the characteristic gangue minerals are fluorite, barite, dolomite, and calcite. Minor amounts of silicea minerals (quartz, chert, jasperoid) are commonly present. Some districts are dominated by either fluorite (e.g., Southern Illinois-Kentucky fluorite-Zn-Pb district), or barite (e.g., Central Missouri barite district), or both (e.g., Sweetwater barite-fluorite-Zn district, eastern Tennessee). Disseminated Fe-sulfides (pyrite and marcasite) of diagenetic origin are common in the host rocks; minor amounts of these may also occur in the ore zone as open-space filling. Most districts contain very little or no copper minerals. An exceptions is the Southeast Missouri district which contains significant amounts of chalcopyrite (sufficiently abundant to generate a byproduct copper concentrate at most mills) with lesser amounts of bornite and covellite. Southeast Missouri is also unique in that the ore fluids contained high enough concentrations of Ni and Co to cause the precipitation of thiospinel minerals such as siegenite $[(\text{Co},\text{Ni})_3\text{S}_4]$, nickelian carrollite $[\text{Cu}(\text{Co},\text{Ni})_2\text{S}_4]$, and polydymite $[\text{Ni}_3\text{S}_4]$. Trace amounts of enargite have also been reported (e.g., Central Tennessee district; Kopp & Misra 1982).

The style of MVT mineralization varies from being massive to disseminated. It is predominantly of the cavity-filling type, filling dissolution cavities, tensional fractures, and interfragmental open spaces in breccias. A texture characteristic of many deposits is a mosaic of sphalerite and hydrothermal dolomite completely cementing breccia clasts (ore-matrix breccia). The tops of some of the breccia clasts are preferentially coated with coarse sphalerite crystals (relative to the underside of the clasts), producing the characteristic 'snow-on-roof' texture (Oder & Hook 1950) of MVT deposits.

Replacement of host carbonate rocks, especially along faults, fractures and bedding planes, is quite pronounced in some deposits — e.g., the “pitches” and “flats” in the Upper Mississippi Valley district (Heyl 1983), the massive sulfide zones at Nanisivik and Polaris (Leach and Sangster 1993) — and very selective in others. Vein-type mineralization is rare. Ore-gangue assemblages are typically coarse-grained, a texture suggestive of a slow rate of precipitation and crystal growth. Some deposits (e.g. Pine Point, Silesia, Polaris) contain extremely fine-grained, laminated aggregates of botryoidal sphalerite, commonly intergrown with skeletal or dendritic crystallites of galena. This combination of textures is usually interpreted as recording extremely rapid precipitation of sulfides in gel-like or colloidal masses (Sangster 1990).

Growth banding of sphalerite is a characteristic feature of MVT deposits. In some deposits (e.g., the Upper Mississippi Valley MVT district; McLimans et al. 1980) correlation of individual bands over long distances has been referred to as *sphalerite microstratigraphy*. Similar cathodoluminescent microstratigraphy has also been observed in the sparry dolomite gangue (Ebers and Kopp 1979, Voss & Hagni 1985). The sphalerite is typically light-colored (honey-yellow, brownish, light orange), but darker colored (dark brown to blackish) sphalerite is present in many deposits (e.g., East Tennessee district) as rosettes of alternating light- and dark-colored bands. The Fe content of sphalerites ranges from <0.01% to >4%, but mostly are <1%; the Cd content is generally <0.5%, but occasionally may be as high as about 3% (Churnet & Misra 1983, Craig et al. 1983). McLimans et al. (1980) and Arne et al. (1991) found a tendency of the sphalerite to be darker in color with increasing Fe content, but other studies have shown a lack of such correlation (Roedder & Dwornik 1968, Churnet & Misra 1983, Craig et al. 1983, Gratz & Misra 1987). Often, the dark-colored sphalerite growth bands contain finely disseminated hydrocarbons and are also enriched in Cd.

The cavity-filing type of mineralization has enabled a detailed reconstruction of the paragenesis in many MVT deposits. Despite the simple mineralogy, the paragenesis is often quite complex (see Fig. 3.3), involving several stages of precipitation and dissolution (e.g., Hagni & Trancynger 1977, Horrall et al. 1983). Thus, the mineralizing event commonly appears to be a composite of several ore-fluid pulses of somewhat different characteristics.

13.5.2. BULK COMPOSITION

MVT deposits show a wide range of Zn:(Zn+Pb) ratios (Fig. 13.14), but the distribution is bimodal (Sangster 1983, 1990). For the Zn-rich group, which includes most of the districts, the ratios range from about 0.5 to 1.0 with a modal value of 0.8. For the Pb-rich group, represented by the entire southeast Missouri district (Viburnum Trend, Old Lead Belt) and a few smaller deposits elsewhere, the ratios are less than 0.2 with a modal value of 0.05. Such low ratios, similar to those of sandstone-lead deposits (e.g., Laisvall, Sweden), have been ascribed to “linkage” with cratonic basement (Sangster 1983) or migration of ore fluids through sandstone aquifers (Sverjensky 1986).

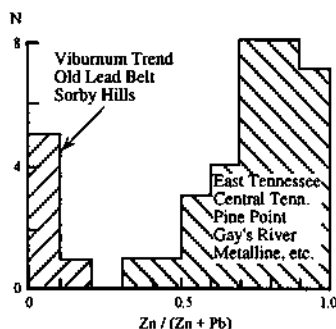


Figure 13.10. The bimodal distribution of Zn:(Zn+Pb) ratios (wt%) in MVT deposits and districts, with typical examples for each mode (after Leach & Sangster 1993).

Silver, cadmium, germanium, barite, and fluorite are being, or have been, recovered ranges from less than 1 ppm to about 1,000 ppm (commonly 30-40 ppm); the Cd content of sphalerite typically lies in the 0.1-1% range (Leach & Viets 1992). From 1960 through 1993, the Viburnum Trend mines produced 44.8 million troy ounces of silver (Hagni 1995).

Liquid and solid organic matter is ubiquitous in the MVT ores and associated horizons, and several authors have emphasized the reducing role of hydrocarbons and bitumens in the precipitation of ore sulfides (Barton 1967, Skinner 1967, Connan 1989, Powell & Macqueen 1984, Ravenhurst et al. 1987, Anderson 1991, Niewendorf & Clendenin 1993). The organic matter may be indigenous to the host carbonate rocks (Gize and Barnes (1987) or introduced by the ore fluids (Etminan & Hoffmann 1989).

13.6. Alteration

Wallrock alteration features, which have been attributed to the ore-forming fluids, include: (a) dissolution of carbonate host rocks, especially limestone; (b) dolomitization of limestone precursors; (c) silicification represented by drusy coarse quartz, jasperoid, and other forms of silica; (d) pyritization; and (e) formation of clay minerals.

The formation of clay minerals is particularly important because of its potential for providing constraints on the pH of the ore-forming fluid. The most widely quoted study in this context is that of Hosterman et al. (1964) on the Upper Mississippi Valley district, which used X-ray powder diffraction patterns of the acid-insoluble residue of a series of samples to identify well-defined alteration aureoles around ore zones. They documented that the clay minerals in a thin carbonaceous bed at the base of the Qumibys Mill Member of the Platville Formation changed progressively from

the *Md* polymorph of illite in the unaltered rock to *1M*- and *2M*-illite in the alteration aureoles, and that the amount of *2M*-illite increased markedly within the ore zones. These results were interpreted as being consistent with $a_{K^+}:a_{H^+}$ ratios of ore fluids appropriate for the assemblage K-feldspar - muscovite - quartz. Alteration of clay minerals, however, may indicate only the $a_{K^+}:a_{H^+}$ ratio of reacted fluid rather than of the ore-forming fluid (Sverjensky 1986). More recently, Panno and Moore (1994) have reported that the alteration in the basal Davis shale produced by hydrothermal activities associated with ore mineralization of the Viburnum Trend includes: (a) lowering of the illite crystalline index (decrease in the width of the (001) peak of illite plus illite-smectite); (b) a decrease in the concentration of K in the shale; and (c) the presence of gypsum in the $<2 \mu\text{m}$ fraction.

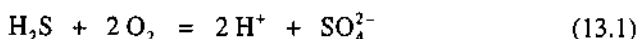
Dolomitization of precursor limestone host rock is a consistent feature of MVT deposits, but there are not many detailed studies on the origin of dolostones associated with MVT deposits. In some districts (e.g., Southeast Missouri; Shelton et al. 1992), dolomitization has been attributed to ore fluids (not to be confused with the precipitation of gangue sparry dolomite from ore fluids). In most MVT districts, however, dolomitization is generally much more extensive than sulfide mineralization, and in many districts (e.g., Pine Point, Silesia-Cracow, East Tennessee) the evidence is quite clear that dolomitization was predominantly diagenetic and unrelated to ore fluids. In the Tri-State district, the spatial association between sulfide mineralization and elongated zones of coarse-grained dolostone has been attributed to dolomitization of limestone by ore fluids, but Brockie et al. (1968) have argued for a pre-mineralization formation of the dolostone by selective replacement along some original sedimentary feature.

13.7. Brecciation

Mineralization in breccias is one of the most characteristic features of MVT deposits. The fact that much of the mineralization is found as a cement to the breccia fragments indicates that the brecciation occurred prior to or, at the latest, contemporaneously with mineralization. The breccia bodies are commonly interpreted as collapse features caused by partial dissolution of underlying limestone beds after lithification, or as features produced by hydraulic fracturing (Macqueen & Thompson 1978). In some districts (East Tennessee, Pine Point, Tri-State, Arkansas), the distribution of the breccia bodies appear to have been controlled by older fractures and faults.

As discussed earlier, in East Tennessee, a district with convincing evidence of a solution-collapse origin of breccia bodies, the selective dissolution of limestone of the ore-bearing Lower Ordovician sequence (the upper Knox Group) appears to have taken place due to recharge of meteoric water during the post-Knox erosion interval and the brecciation prior to deposition of the lowermost middle Ordovician rocks (Harris 1971). Surfaces of erosion are associated with all major MVT districts (Callahan 1967) and in most cases they lie no more than a few hundred meters above the ore-bearing unit. A

major exception is the Southeast Missouri district where the major erosional surface, represented by the unconformity separating Upper Cambrian sedimentary rocks from middle Proterozoic basement, lies below the ore-bearing unit. The karstic brecciation model, however, cannot be applied to all MVT districts. The time interval represented by the overlying erosion surface varies markedly (Sangster 1983) and its linkage with brecciation in the ore-bearing unit is not apparent in some districts. Another possible cause of pre-mineralization brecciation is the reduction of evaporitic sulfate to H_2S in the host rock sequence, because oxidation of this H_2S by groundwater



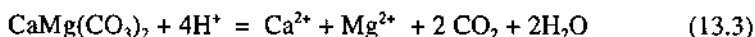
is an acid-producing reaction (Anderson 1983).

Some authors have attributed the host rock brecciation to the action of ore-forming fluids (Ohle 1990, Heyl 1983, Sass-Gustkiewica 1982), and it is likely that the hydrothermal fluids at least caused enlargement of pre-existing breccia bodies. This may be the reason, for example, why in the Central Tennessee district (Gaylord & Brisky 1983) some of the breakthrough breccia bodies rooted in the Mascot Dolomite extend into the overlying formation through the post-Knox unconformity. Convincing evidence of some dissolution of the host carbonate by ore fluids is the presence of "trash zones" (Hill et al. 1971), which represent the accumulation of insoluble material (dolomite, clay, chert, quartz, sulfides, and black carbonaceous material) at the bottom of the breccia bodies.

The chemistry of the hydrothermal brecciation process has been discussed by Anderson (1983). If the H_2S for sulfide precipitation is supplied from wallrocks (e.g., when sulfate reduction occurs away from the site of sulfide deposition), the acid generated by the sulfide precipitation reaction such as

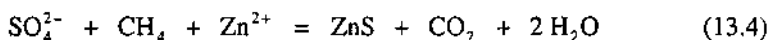


may cause carbonate dissolution by reactions of the type

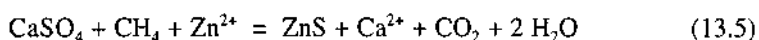


Paradoxically, the increased concentration of Ca^{2+} , Mg^{2+} , and CO_2 in the hydrothermal fluid due to carbonate dissolution at one place may induce the precipitation of secondary carbonate minerals at some other place in the system. Thus, a change in the site of sulfide deposition from time to time would provide a mechanism for the association of gangue carbonate minerals with previously precipitated ore sulfides.

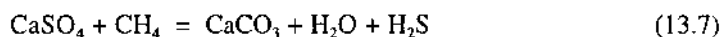
If the H_2S is produced in the ore zone (e.g., when sulfate contained in the ore fluid is reduced by organic matter encountered in its flow path), the overall reaction such as



provides a weak acid, such as H_2CO_3 , preventing the precipitation of a carbonate mineral without causing extensive carbonate dissolution. This may explain the lack of evidence for coprecipitation of sulfide and sparry dolomite/calcite in most MVT deposits. The alternation of sulfides and sparry dolomite observed in some deposits (Beales 1975) may be related to the fluctuations in metal supply at any instant during sulfate reduction (Anderson 1983). Sulfide precipitation may occur by reactions such as



and sparry dolomite/calcite precipitation by reaction such as



13.8. Origin

MVT deposits have been recognized as a distinct class of deposits for about a hundred years, but a unifying genetic model for them is yet to emerge. In fact, the targets for exploration of MVT deposits are commonly chosen by empirical criteria, such as lithostratigraphic and structural relationships, rather than by a genetic model.

An inherent limitation for the formulation of a common genetic model is the variation in geological parameters among MVT districts (Sangster 1983). The host rocks range from limestone containing minor dolostone (e.g., Tri-State) to dolostone with minor limestone (e.g., East Tennessee, Central Tennessee) to entirely dolostone (e.g., Pine Point, upper Silesia). The form of ore bodies range from highly concordant (e.g., blanket-type deposit in Tri-State) to highly discordant (e.g., breccia domes in East Tennessee and upper Silesia). The Zn:(Zn+Pb) ratios vary from more than 0.7 (most districts) to less than 0.2 (Southeast Missouri). Evidently, there were significant differences in the local conditions of mineralization.

Another limitation has been the uncertainty regarding the age of mineralization for most MVT deposits (Sangster 1983, 1986). Lead isotope ratios of galenas from MVT deposits (Fig. 13.11) typically either give model ages which are older than the host rock (B-type anomalous lead) or plot significantly beyond the geochron (J-type anomalous lead). For the latter, the age of mineralization cannot be calculated as the age of the source lead is not known. A few districts/deposits have now been dated using paleomagnetic and radiometric methods (Symons et al. 1997, Christensen et al. 1997), and the available data are summarized in Table 13.2.

The general framework of genetic models for typical MVT deposits is constrained by two important common factors: the ore fluids were moderately hot, highly saline brines, as is indicated by fluid inclusion data; and the mineralization was epigenetic, as is evidenced by the fact that ore minerals dominantly fill cavities in post-lithification

TABLE 13.2. Paleomagnetic and radiometric dates of mineralization (main-stage) in MVT districts and deposits

District / Deposit	Age of Host Rock	Age of Mineralization	
		Paleomagnetic	Radiometric
Southeast Missouri	Upper Cambrian	Pennsylvanian - Permian (1,2) Alleghenian/Ouachita orogeny	Devonian (392 ± 21 Ma) (3) * Taconic orogeny ??
Northern Arkansas	Ordovician - Mississippian	Permian (4) Alleghenian/Ouachita orogeny	
Upper Mississippi Valley	Ordovician		Permian (270 ± 4 Ma) (5) * Alleghenian/Ouachita orogeny
Tri-State	Mississippian	Permian (4) Alleghenian/Ouachita orogeny	Permian (~265 Ma) (6)
East Tennessee	Lower Ordovician	Pennsylvanian - Permian (7) Alleghenian orogeny	Devonian (377 ± 29 Ma) (8) * Devonian (347 ± 20 Ma) (9) * Acadian orogeny
Central Tennessee	Lower Ordovician	Late Permian (10) Alleghenian orogeny	Permian (260 ± 42 Ma) (6) # Alleghenian/Ouachita orogeny
Illinois-Kentucky (Fluorite)	Upper Mississippian		Permian (277 ± 16 Ma) (11) & Alleghenian/Ouachita orogeny
Pine Point	Middle Devonian	Cretaceous - Paleocene (12) Laramide orogeny	Permian (285 Ma) (13) @ Devonian (361 ± 13 Ma) (9) *
Polaris	Ordovician	Devonian (14) Ellesmerian orogeny	Devonian (366 ± 15 Ma) (15) *
Gays River	Mississippian	Pennsylvanian (16) Alleghenian orogeny	
Upper Silesia	Middle Triassic	Tertiary (17) Alpine orogeny	
Coxco	Proterozoic (1680 Ma)		Proterozoic (1580 Ma) (18) @

*Rb-Sr method, # Th-Pb method, & Sm-Nd method, @ Pb-Pb method.

Sources of data: (1) Wu and Beales (1981); (2) Wisniowiecki et al. (1983); (3) Lange et al. (1983); (4) Pan et al. (1990); (5) Brannon et al. (1992); (6) Brannon et al. (1995); (7) Bachtadse et al. (1987); (8) Nakai et al. (1990); (9) Nakai et al. (1993); (10) Lewchuk and Symons (1995); (11) Chesley et al. (1994); (12) Symons et al. (1993); (13) Sangster (1990); (14) Symons and Sangster (1992); (15) Christensen et al. (1995); (16) Pan et al. (1993); (17) Symons et al. (1995); (18) Walker et al. (1983).

structures, such as breccia bodies. The controversies lie in the details, such as the source and migration of ore fluids, the source(s) of the ore constituents, and the mechanisms of ore-gangue precipitation.

13.8.1. ORE-FORMING FLUIDS

The composition of ore fluids for MVT deposits is well constrained by numerous

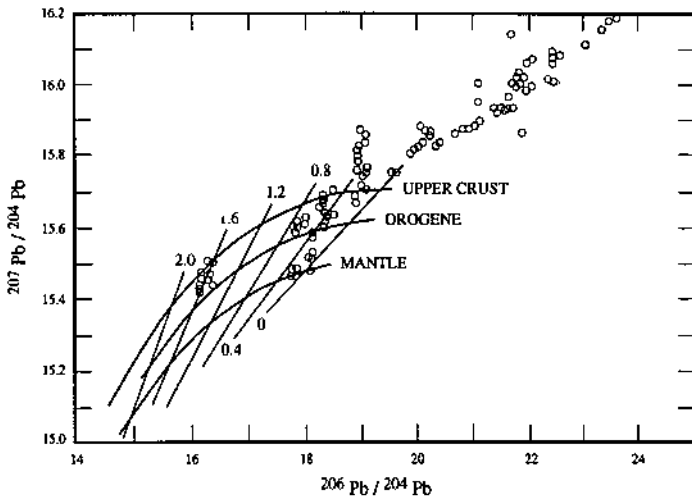


Figure 13.11. Lead isotopic composition of galena samples from 17 MVT deposits or districts. The lead growth curves are from Zartman and Doe (1981); isochrons are in million years. (After Sangster 1990.)

studies of primary fluid inclusions in the ore minerals (mainly sphalerite) and gangue minerals (mainly calcite and fluorite). The characteristics of inclusion fluids, believed to be representative of fluids responsible for the main-stage sphalerite±galena mineralization, may be summarized as follows (Roedder 1976, 1984):

- (a) The density is always $>1.0 \text{ g/cm}^3$ and frequently $>1.5 \text{ g/cm}^3$ at the time of trapping, i.e., they are invariably more dense than surface water.
- (b) The salinity is usually $>15 \text{ wt\% NaCl}$ equivalent and frequently $>20 \text{ wt\%}$ (up to $\approx 30 \text{ wt\%}$), compared with about 3.5 wt\% for normal seawater, but daughter crystals of NaCl are almost never found, implying appreciable amounts of cations other than Na.
- (c) Homogenization temperatures (T_h) vary from $\approx 80^\circ\text{C}$ to 220°C , but are commonly in the range of 100°C to 150°C .
- (d) The total pressure was presumably low but, as indicated by the lack of evidence of boiling, always greater than the vapor pressure of the brines. In most cases fluid inclusion microthermometry does not provide any upper limit of pressure.
- (e) The solutes consist mainly of Na and Ca chlorides, with minor amounts of K, Mg, and Br. The relative abundance (in wt%) of the major ions is $\text{Cl} > \text{Na} > \text{Ca} > \text{K} > \text{Mg} > \text{Br}$ for most MVT deposits. K:Na ratios of inclusion fluids are generally higher than modern oil-field brines, probably due to

extensive fluid-rock reactions during brine migration. HCO_3^- is probably low and total sulfur, expressed as SO_4^{2-} , seldom exceeds a few thousand ppm. There is not much data on the concentrations of heavy metals in the fluids. Values as high as 1% each of Cu and Zn, obtained by neutron activation analysis of a single inclusion in fluorite from southern Illinois, were reported by Czamanske et al. (1963), but atomic absorption analysis of other samples from the same locality by Pinckney and Hafty (1970) yielded much lower concentrations (350 ppm Cu and 1,040 ppm Zn).

- (f) Studies using crushing stage, Raman laser probe, and other techniques have revealed an appreciable amount of dissolved gases, mainly CH_4 and CO_2 , in the inclusion fluids. The CH_4 content of the fluids is perhaps in the order of 800 ppm, much higher than that of magmatic hydrothermal fluids. Immiscible oil-like droplets and a wide variety of dissolved organic compounds, probably derived from the sediments traversed by the fluids, are common (Gize & Hoering 1980).

The fluid inclusion data do not uniquely define the source of MVT ore fluids, but they provide useful constraints. The temperature ($>100^\circ\text{C}$) and salinity (>15 wt% NaCl equivalent) of the fluids, as well as their oxygen and hydrogen isotopic composition (Taylor 1974, White 1974), clearly eliminate normal seawater or meteoric water as likely candidates for the main-stage mineralization, but there is good fluid inclusion and isotopic evidence for dilution by meteoric water during the precipitation of late-stage gangue minerals, such as calcite and barite (Hall & Friedman 1969, Hannah & Stein 1984, Richardson et al. 1988, Misra & Lu 1992). High-salinity brines are typical of porphyry copper and other deposits with clear igneous associations, but magmatic hydrothermal fluids are characterized by lower Na:K, Na:Ca, and Na:Ca ratios (Roedder 1984). Moreover, except for the Illinois-Kentucky fluorite district (Plumlee & Goldhaber 1992, Taylor et al. 1992), there is little evidence of a magmatic contribution to MVT ore fluids. Compositional similarities between MVT fluid inclusions and oil-field brines (Carpenter et al. 1974) indicate that MVT fluids were derived from sedimentary basins (White 1974, Taylor 1979, Anderson & Macqueen 1982).

The exact cause of the high salinity of MVT fluids is not known. Of the potential mechanisms (see Ch. 2), evaporite dissolution, perhaps by meteoric water, offers an attractive possibility. Many basins associated with MVT deposits, however, lack extensive evaporites (e.g., the Illinois basin; Walter et al. 1992), although the host rock sequence of some deposits contain indirect evidence of the former presence of evaporites (Beales & Hardy 1977, Hersch & Misra 1979, Jones et al. 1996). A consideration of Cl:Br, cation:Cl (e.g., Na:Cl), and cation:Br (e.g., Na:Br) ratios of fluid inclusions in the sphalerite from a number of North American and European deposits has led Viets et al. (1997) to conclude that the MVT brines were primarily evaporated, halite-saturated seawater mixed with variable but small amounts of normal seawater and halite-dissolution water.

13.8.2. HYDROTHERMAL SYSTEMS

A viable hydrothermal system for MVT deposits must satisfy two basic constraints. First, a large volume of fluids must be generated during the evolution of the sedimentary basin. For example, it has been estimated that the Viburnum Trend contains about 3×10^{12} g of Pb (Gustafson & Williams 1981) and, at an assumed precipitation rate of 10 ppm Pb, this would require about 3,000 km³ of saline fluids (Anderson & Macqueen 1982). Second, the fluids should be able to reach the sites of ore deposition at temperatures (100°-150°C) consistent with those established by fluid inclusion studies. For MVT deposits located in relatively undisturbed platformal settings, stratigraphic evidence indicates that mineralization occurred at relatively shallow depths, perhaps a few hundred to about 1,000 m (Anderson & Macqueen 1982). Average host rock temperatures at such shallow depths, with geothermal gradients typically in the range of 25 to 30°C/km, are significantly less than 100°-150°C. Thus, the temperature constraint requires either a local heat source at shallow depths or the migration of heated fluids from a deeper source. The characteristic absence of shallow-level igneous intrusions in close proximity suggests that fluid temperatures for most, probably all, MVT deposits reflect derivation from, or circulation to, deep levels in sedimentary basins. Thermal perturbation of the basins was probably necessary for the migration of fluids from deeper portions to basin edges (Hanor 1979, Ohle 1980).

Two general models have been proposed for fluid migration in sedimentary basins (see Ch. 2): (a) compaction-driven flow; and (b) gravity-driven flow. Compaction-driven flow envisages fluid migration from depth, along shallow-dipping permeable aquifers over large horizontal distances, to the basin margin. As sediment porosity decreases from 70-80% at the sediment-water interface to 20% or less at a depth of about 3,000 m, a large volume of fluids is likely to be released by sediment compaction. The fluids would tend to migrate upward if the increase in their density due to increasing salt content was counterbalanced by the decrease in density due to increasing temperature (Hanor 1979). Calculations by Cathles and Smith (1983) and Bethke (1986), however, have shown that, for most migration paths and at average steady compaction ratios of sediments containing fluids under essentially hydrostatic pressures, the flow rates are far too low to carry ≈100°C temperatures to a near-surface environment.

To account for large volumes of ore fluids and the temperatures of mineralization, Cathles and Smith (1983) proposed an episodic dewatering model involving rapid release of geopressed fluids at pressures approaching lithostatic pressure by episodic rupturing of the compacting sediments. According to their calculations, if dewatering occurs in a cycle as fluid pressure builds to lithostatic pressure and is then released, subsidence of strata from 3 to 5 km depth will result in 50 dewatering pulses, approximately one every million years, with each pulse lasting only about 10,000 years. They suggested that the rupturing of sediments and the sudden draining of the fluids into basinal aquifers would take place during faulting and that the fluids would migrate updip along this aquifer. The upward migration of fluids could also be through

hydrofractures propagated due to the buoyancy forces exerted by the fluids (Deloule & Turcotte 1989). According to Cathles and Smith (1983), their model would produce high-salinity fluids by membrane filtration, the color banding of sphalerite observed in many districts (each color band corresponding to a dewatering pulse), and the distinctive local tectonic features associated with MVT deposits, as well as prove useful for identifying basins with potential for MVT deposits. A complicating factor would be the involvement of fluids from multiple basins as might have been the case in the Southeast Missouri district (Gregg & Shelton 1989, Shelton et al. 1992).

Gravity-driven fluid migration as a consequence of differences in hydrostatic head across a sedimentary basin has been modeled by Garven and Freeze (1984a, b) and applied to MVT deposits of Pine Point district (Garven 1985, 1986) and the Ozark region of Missouri, Arkansas, Kansas and Oklahoma (Leach & Rowan 1986). The model requires the uplift of a distal portion of the basin to produce a regional potential gradient for cross-formational fluid flow and a lower, permeable aquifer for focused fluid flow to thin edge of the basin (see Fig. 2.27c, d). Under these conditions, significant perturbations of the geothermal gradient elevate temperatures at the thin edge of the basin to values recorded for MVT ores. Also, such a system should be capable of sustaining a large volume of flow over geologically significant lengths of time, provided the hydraulic gradient is not disturbed by tectonism. A similar model has also been applied to the Upper Mississippi Valley district located at the edge of the Illinois basin, which did not develop significant overpressures during subsidence (Bethke 1986). The gravity-driven fluid flow model is consistent with the thermal equilibrium between main-stage ore minerals (fluid inclusion homogenization temperatures) and host rocks (temperatures estimated from conodont color indices) for a majority of the North American MVT districts (Pine Point, Newfoundland Zinc, Mascot-Jefferson City, Copper Ridge, Sweetwater, Central Missouri, Northern Arkansas, and Tri-State) investigated by Sangster et al. (1994).

Garven and Freeze (1984a, b) emphasized that compaction-driven, probably episodic, dewatering might be most important in the relatively early stages of basin development, whereas gravity-driven fluid migration might predominate in more mature sedimentary basins that have experienced tectonic uplift and erosion. The broad correlation between the age of main-stage mineralization and an orogenic event for almost all MVT deposits for which radiometric dates are available (Table 13.2) is evidence for gravity-driven hydrothermal systems for most North American MVT districts. The hydrothermal system in some districts, however, was more complex. In the Viburnum Trend, for example, sulfur isotope data indicate two different sources of fluid, one of which migrated through the underlying Precambrian granite basement (Shelton et al. 1995), which is assumed to be an impermeable (no flow) boundary in most gravity-flow models. In some cases, such as the Southeast Missouri district (Clendenin et al. 1994), the Nanisivik mine, Canada (Arne et al. 1991), and the Blendevale deposit, Western Australia (Vernacombe et al. 1995), the fluid migration appears to have been facilitated by regional-scale faults. The positive thermal anomaly (ore fluids significantly hotter than the host rocks) observed in a few districts (Upper

Mississippi Valley, Polaris, and Central Tennessee) has also been attributed to fluid movement through structurally controlled conduits (Sangster et al. 1994).

Fowler and Anderson (1991) argued that the large permeabilities required for rapid fluid migration to conserve heat would render long-distance migration models, whether compaction-driven or gravity-driven, inappropriate for basins that contain large amounts of shale. For such deposits a more appropriate fluid source for MVT deposits might have been proximal geopressured zones. More recently, Eisenlohr et al. (1994) proposed that the Lennard Shelf MVT deposits (northwestern Australia), which lie below a major mid-Carboniferous unconformity that is linked to a major eustatic sea-level drop, formed from overpressured hydrocarbon-rich brines. They presented calculations to show that the temperature increase in the basin due to the sea-level fall was sufficient to cause hydrocarbon gas maturation and the expulsion of a large quantity of hydrocarbon-rich brines. They suggested that such a scenario might explain the common occurrence of MVT deposits below major unconformities and the high content of hydrocarbon inclusions in their ore and gangue minerals. The Rb-Sr age of mineralization (357 ± 3 Ma) for the Lennard Shelf, however, is consistent with models of episodic basin-dewatering from overpressured zones (Christensen et al. 1997).

13.8.3. ORE ACCUMULATION

It is generally agreed that ore fluids for MVT deposits carry metals as soluble chloride complexes (see Ch. 2). The precipitation of metal sulfides to form an MVT deposit, therefore, requires the reaction of dissolved metal-chloride complexes with reduced sulfur at the site of deposition. The controversy about the precipitation mechanism centers mainly around the source of reduced sulfur. It should be evident from the following discussion that no single mechanism can account for the significant differences among the various MVT districts.

Proposed models for the deposition of metal sulfides from MVT ores fluids may be grouped into three broad categories (Table 13.3): (a) mixing models, which envisage addition of reduced sulfur to sulfur-deficient ore fluids at or near the site of ore deposition; (b) sulfate reduction models, which involve the transport of sulfur as sulfate (SO_4^{2-}) or thiosulfate ($\text{S}_2\text{O}_3^{2-}$) in the ore fluids; and (b) non-mixing (or reduced sulfur) models, which attribute sulfide deposition from sulfide-enriched ore fluids to change(s) in conditions that decrease the metal-sulfide solubilities at the site of deposition.

Mixing Models

Based on the geologic setting at Pine Point, Beales and Jackson (1966) proposed a model involving the mixing of two separate fluids at the site of deposition — a basinal, metal-bearing fluid derived from distant sources and a locally derived, H_2S -bearing fluid with bacterial reduction of evaporitic sulfate minerals (gypsum or anhydrite) accounting for the H_2S . Sulfate reduction at temperatures above $\approx 85^\circ\text{C}$ is likely to occur by reaction with organic matter (thermochemical reduction) rather than

TABLE 13.3. Models for the deposition of ore sulfides in Mississippi Valley-type deposit (modified from Anderson & Macqueen 1982, Sverjensky 1986)

Transport of ore-forming constituents	Precipitation mechanism
A. Mixing models	
Base metals transported by fluids without significant sulfur contents	(i) Mixing with fluids containing H ₂ S derived by bacterial or thermochemical reduction of evaporite sulfate
	(ii) Mixing with sulfur released by thermal degradation of sulfur-rich organic compounds
	(iii) Replacement of diagenetic or hydrothermal pyrite
B. Sulfate reduction models	
Base metals carried with sulfate (SO ₄ ²⁻) or thiosulfate (S ₂ O ₃ ²⁻) in the same fluids	Reduction of SO ₄ ²⁻ or S ₂ O ₃ ²⁻ to H ₂ S at the site of deposition by reaction with CH ₄ or other organic matter
C. Non-mixing (reduced sulfur) models	
Base metals transported together with reduced sulfur in the same solution	Decrease in temperature, decrease in pressure, increase in pH, dilution by meteoric water, or some combination of these

by bacterial mediation (Trudinger et al. 1985), and addition of H₂S to metal-bearing brines at the site of sulfide deposition is much more attractive hydrodynamically than the mixing of two separate fluids, but an evaporitic host rock environment makes a great deal of sense in a genetic model for MVT deposits (Anderson & Garven 1987). It provides an explanation for the occurrence of MVT deposits in carbonates rather than sandstones (this does not seem to be a question of permeability as petroleum deposits are as abundant in sandstones as in carbonates) and for the fact that in most cases the host is dolostone rather than limestone (as dolostones are more commonly associated with evaporitic settings than limestones). Also, because the H₂S is generated outside of the ore zone, the sulfide precipitation is an acid-generating process (Equation 13.2) which, as discussed earlier, can produce several of the characteristic features of MVT deposits, such as brecciation, replacement of carbonate by sulfide, and the precipitation of carbonate minerals (Anderson 1983). A Beales and Jackson-type model works well for the Pine Point district (Garven 1985), and it is supported by the abundance of fine-grained sulfides (because of rapid precipitation due to supersaturation caused by mixing), a lack of evidence of repetitive precipitation and dissolution of sulfides, and the uniformity of lead and sulfur isotopic compositions (Sverjensky 1986). Its applicability as a general genetic model, however, has been questioned on the basis that many MVT deposits were not emplaced in an evaporitic setting.

A mixing model proposed by Skinner (1967) does not involve sulfate reduction, but ascribes the addition of sulfur at the depositional site to thermal degradation of sulfur-containing organic compounds, particularly in petroliferous materials (commonly

containing 0.25-2 wt% S), by the rising hot brines.

Sulfate Reduction Models

Most subsurface brines contain a small amount of sulfur, in the range of few tens to a few thousands of ppm, which is almost always present as sulfate rather than as reduced sulfur. This has led some authors to propose models that rely on the introduction of sulfate with the metal-bearing fluids. Such models do not necessarily require an evaporitic host-rock setting, but they do require an organic reducing agent (CH_4 or other organic compounds), either in the host rock or in the ore fluids, for reducing the sulfate to H_2S (the sulfate reduction model).

Barton (1967) proposed that both organic carbon and sulfate were carried with the metals in the hydrothermal fluids. Hydrocarbons ranging from methane to oil to complex bitumens have actually been detected in fluid inclusions in sphalerite and dolomite of MVT deposits (Roedder 1976, Gize & Hoering 1980, Etminan & Hoffman 1989), but with sufficient organic carbon in the brines, the sulfides should have precipitated out all along the brine migration route as sulfate was reduced in the brine. It is, however, possible that only sulfides of lower solubilities, such as those of iron and copper, dribbled out along the brine migration route, leaving the lead and zinc in solution (Anderson & Garven 1987). The host rock acting as the reservoir of organic carbon is a more attractive proposal (Rickard 1983, Macqueen & Powell 1983), because bitumen is quite abundant in many MVT deposits, and in some cases — e.g., Upper Mississippi Valley and Nova Scotia (Gize & Barnes 1987) and Nanisivik (Arne et al. 1991) — appears to have been derived mostly from material indigenous to the host rock. Thermal maturation of the organic matter in the host carbonate rocks caused by the heat from the ore-forming solutions can generate enough reducing gases (mostly methane) for the reduction of aqueous sulfate to H_2S . Anderson (1991) has shown that the brown-rock facies of the Bonneterre Formation, which hosts most of the ore, could have produced the amount of methane needed to precipitate all the ore. Sulfide precipitation in the Gays River deposits has also been attributed to the transport of sulfate (evaporitic) in the ore fluids and complete reduction of the sulfate by methane at the depositional site (Ravenhurst et al. 1987). Spirakis & Heyl (1993, 1995) argued that the sulfur was carried not as sulfate but as partly oxidized, metastable thiosulfate. This model presumably removes the problem of sluggish kinetics of sulfate reduction and provides S^{2-} for pyrite precipitation. In addition, reactions involving intermediate-valency sulfur can account for extreme sulfur isotopic variations, the presence of botryoidal pyrite and marcasite, and extreme enrichments of elements such as As and Tl (Plumlee & Rye 1992). Note that when H_2S is generated at the site of ore deposition, sulfide precipitation (Equation 13.4) is not an acid-producing reaction and does not lead to carbonate dissolution.

Non-mixing Models

Many features of MVT districts are not easily reconciled with the premises of mixing models. These include: the district-wide sphalerite or gangue dolomite

microstratigraphy recognized in Upper Mississippi Valley (McLimans et al. 1980), East Tennessee (Ebers & Kopp 1979), and Southeast Missouri (Voss & Hagni 1985), which is inconsistent with local sources of sulfur; evidence of extensive dissolution of previously deposited sulfides (McLimans et al. 1980, Sverjensky 1981); the varied lead and sulfur isotopic compositions of the fluids (Sverjensky 1981); and the prevalence of large, well-formed sulfide crystals indicating a slow rate of precipitation.

The non-mixing (reduced sulfur) models are particularly attractive for deposits that lack evidence of sulfate reduction at or near the site of ore deposition. The Viburnum Trend deposits, for example, are believed to have formed from hydrothermal fluids that transported both metals and at least a part of the reduced sulfur (Ohmoto & Rye 1979, Sverjensky 1981, Goldhaber & Viets 1985), although more recent studies favor a fluid mixing model (Burstein et al. 1993). The main problem with the single-solution model is one of metal transport, because oil-field brines which contain even a small amount of H_2S are invariably very low in metal content, at least at temperatures ($<200^\circ C$) characteristic of MVT ore fluids. In order to carry adequate concentrations of both H_2S and metals as chloride complexes, the pH of such brines must be significantly less than neutral. For example, calculations by Sverjensky (1986), using the data of Barrett and Anderson (1982), show that in 3 molal NaCl solutions at $100^\circ C$ and with pH's of 4.5, the solubilities of ZnS and PbS are $10^{-5.0} m$ (0.5 ppm Zn) and $10^{-5.7} m$ (0.4 ppm Pb), respectively, with equivalent concentrations of H_2S . The solubilities would increase with increasing temperature and salinity of the fluid. Acidic pH values for MVT ore-forming fluids have been considered inconsistent with equilibrium between the fluids and host carbonate units because this would require partial pressures of CO_2 greater than 1 atm (Anderson 1975, 1983, Barrett & Anderson 1982). The pH values of MVT ore fluids are not well established, but at least in two well studied districts — Upper Mississippi Valley (McLimans et al. 1980) and Mascot-Jefferson City (Jones & Kesler 1992) — the CO_2 contents of fluid inclusions are consistent with partial pressures of CO_2 much higher than 1 atm and with pH values significantly lower than neutral. Anderson (1975) showed that from brines carrying both metals and H_2S , precipitation of sulfides could occur as a result of cooling, dilution by groundwater, or pH change (e.g., by reaction of the brine with host rocks).

13.9. Metallogenesis

13.9.1. HOST ROCKS

MVT deposits are hosted by platformal carbonate rocks, which are either undisturbed or lie within foreland fold and thrust belts. The principal role played by the carbonate host rocks appears to have been in providing open spaces through brecciation (e.g. East Tennessee, Central Tennessee, Silesia) and permeability barriers through facies changes (e.g. Pine Point, Southeast Missouri) for ore localization. Another possible connection is the shallow-water depositional environment that was conducive to

evaporite precipitation. Evaporite beds are potential contributors to both collapse brecciation and the supply of H_2S (and, possible, metals), but many MVT deposits lack clear evidence of evaporite involvement.

Host-rock sequences of MVT deposits contain varying proportions of dolostone relative to limestone, but no major MVT district is found in host rocks completely devoid of dolostone. The nature and extent of dolostones vary greatly from one district to another. In general, the dolostones are of two types: (a) fine-grained dolostone, composed almost entirely of finely crystalline dolomite, that is regionally extensive and believed to have formed by very early diagenesis of limestone, or even by penecontemporaneous dolomitization of lime mud in a supratidal environment; and (b) coarser-grained dolostone that represents diagenetic or epigenetic dolomitization of limestone. The mineralization is typically, but not necessarily, concentrated in horizons dominated by coarse-grained dolostone, which may be more or less restricted to ore zones and possibly related to ore fluids (e.g., Tri-State), or much more extensive and unrelated to ore fluids (e.g., East Tennessee, Central Tennessee). In the latter case, the preferential association is probably because of the higher permeability of the coarse-grained dolostone, as evidenced by the frequent occurrence of high-grade ores at the interface between coarse-grained dolostone and the less permeable limestone.

13.9.2. SOURCES OF ORE CONSTITUENTS

From the $\delta^{34}S$ data on MVT deposits (Fig. 13.12) it appears unlikely that the sulfur was derived from igneous sources. For the class as a whole, the $\delta^{34}S$ values of sulfides have a very wide range, from about -10 to $+30\%$, consistent with a spectrum of crustal sulfur sources, such as seawater sulfate or marine evaporites (positive $\delta^{34}S$ values), sulfur-rich organic material (slightly positive to negative $\delta^{34}S$ values), diagenetic pyrite in sedimentary rocks (very positive to very negative $\delta^{34}S$ values), and deep crustal sulfur ($\delta^{34}S$ values near 0%). A comprehensive interpretation of the sulfur isotopic data is unrealistic in view of the large variations in the $\delta^{34}S$ values and in the geologic settings of MVT deposits. A better approach is to consider the data and interpretation for a few individual districts for which detailed data are available.

Because of the similarity in $\delta^{34}S$ values of the sulfides and those of the anhydrite from Devonian evaporites in the adjacent Elk Point Basin ($+19\%$), the source of reduced sulfur for the Pine Point deposit has been attributed to almost complete reduction of evaporitic sulfate at the depositional site (Sasaki & Krouse 1969). The narrow range of sulfide $\delta^{34}S$ values suggests an abiologic reduction process, but it is not clear why most of the sulfide values are heavier than the evaporitic value and why the calculated $\delta^{34}S_{H_2S}$ values of the fluids in equilibrium with sphalerite or galena appear to be about $+22$ to $+23\%$ (Sverjensky 1986). In any case, the uniformity of the calculated $\delta^{34}S_{H_2S}$ values for the ore fluids as well as the uniform and nonradiogenic lead isotopic compositions of galena are consistent with the derivation of Pine Point ore fluids from either a single source or well-homogenized multiple sources.

Much of the sphalerite and galena in the Upper Mississippi Valley district appear to

have precipitated in isotopic equilibrium at temperatures above 100°C from fluids with a constant $\delta^{34}\text{S}_{\text{H}_2\text{S}}$ value of +14‰ (Sverjensky 1986). These features, as well as the sphalerite microstratigraphy in the district, suggest that ore-forming fluids derived both metals and reduced sulfur from deep sedimentary basins and migrated through homogeneous aquifers. The Gays River district, which is hosted in a Carboniferous carbonate bank, formed from ore fluids of similar $\delta^{34}\text{S}_{\text{H}_2\text{S}}$, and the source of sulfur in this case has been attributed to Mississippian evaporites ($\delta^{34}\text{S} = +14\text{‰}$) (Ravenhurst et al. 1987). Most of the sphalerite $\delta^{34}\text{S}$ values for MVT deposits hosted by the Lower Ordovician paleoaquifer (Mascot-Jefferson City, Copper Ridge, and Sweetwater districts) fall within a relatively narrow range of +26 to +36‰ (Jones et al. 1996). The sulfur is interpreted to have been derived by thermochemical reduction of Cambrian and Ordovician seawater sulfate with little or no fractionation and accumulated as a H_2S -bearing natural gas cap before sulfide deposition. In contrast, $\delta^{34}\text{S}$ values of sphalerite and galena (-8.4 to -0.4‰) in the Central Tennessee district are among the most ^{34}S -depleted recorded for MVT deposits and point to thermal degradation of oil or other

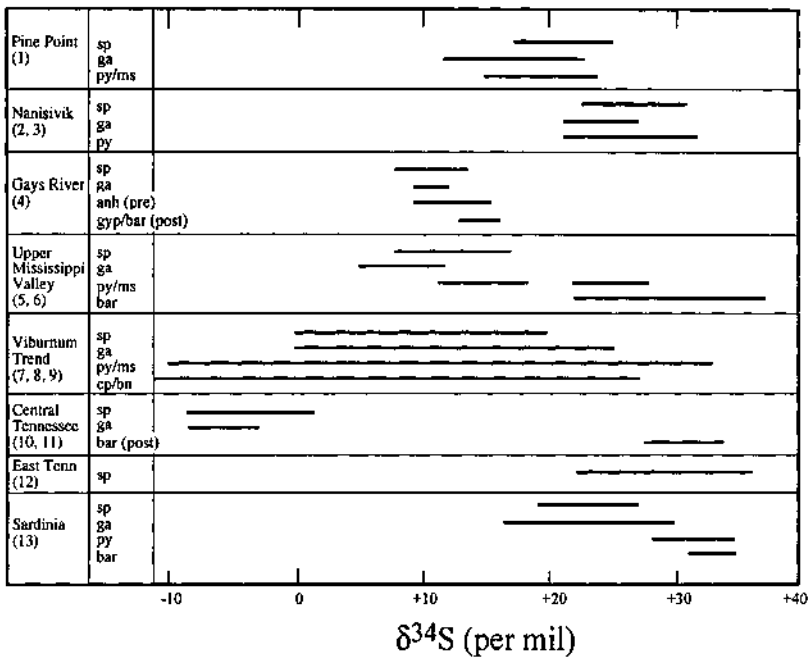


Figure 13.12. Selected sulfur isotopic data for MVT deposits. Abbreviations: sp = sphalerite, ga = galena, py = pyrite, ms = marcasite, cp = chalcopyrite, gyp = gypsum, anh = anhydrite, pre = pre-ore, post = post-ore. Sources of data: (1) Sasaki and Krouse (1969), (2) Ghazban et al. (1990), (3) Arne et al. (1991), (4) Akande and Zentilli (1984), (5) Pinckney and Rafter (1972), (6) McLimans (1977), (7) Sverjensky (1981), (8) Shelton et al. (1995), (9) McKibben and Eldridge (1995), (10) Kesler et al. (1994), (11) Misra and Torssander (1995), (12) Jones et al. (1996), (13) Boni et al. (1988).

organic matter as the most likely mechanism of sulfur derivation at the depositional site (Kesler et al. 1994b; Misra & Torssander 1995).

The Viburnum Trend, characterized by large ranges of $\delta^{34}\text{S}$ values for sulfide minerals, is an example of a complex hydrothermal system with multiple sources of sulfur. Sverjensky (1981) suggested that the metals and reduced sulfur derived from two different sources were transported together in the hydrothermal fluids. This interpretation was based on a broad correlation between the lead and sulfur isotopic compositions in galenas from the Viburnum district — higher $\delta^{34}\text{S}$ values (around +25‰) with less radiogenic lead and lower $\delta^{34}\text{S}$ values (around -1‰) with more radiogenic lead — that could be explained if two major types of rocks, each with distinct lead and sulfur isotopic characteristics, were the sources of both metals and reduced sulfur. However, using the sulfur isotopic data of Sverjensky (1981) for the Viburnum Trend, Ohmoto (1986) argued that not all of the reduced sulfur was transported with metal-bearing fluids; some sulfur was derived locally. The $\delta^{34}\text{S}$ values of coexisting (and coprecipitated) sphalerite and galena in the minor, late-stage mineralization may be interpreted as close to equilibrium values at temperatures around 100°C, suggesting the transport of $10^{-5} m$ of both H_2S and metals in the late-stage fluids and $m_{\text{H}_2\text{S}} > m_{\Sigma\text{metals}}$. In contrast, $\delta^{34}\text{S}$ values of coexisting (but probably not coprecipitated) sphalerite-galena pairs in the early and main stages of mineralization are essentially 0‰, suggesting that during these stages of mineralization the fluids had $m_{\Sigma\text{metals}} > 10^{-5} m > m_{\text{H}_2\text{S}}$. Other sulfur isotopic studies also indicate multiple sources of sulfur, but with significant differences in interpretation. A regional study led Goldhaber and Viets (1985) to suggest that most of the isotopically heavy (around +25‰) sulfur was derived locally from diagenetic pyrite in the host rock (the Bonneterre Formation), whereas the isotopically light (around -2‰) sulfur was introduced by the hydrothermal fluids. On the other hand, the sulfur isotopic data on Cu-Fe sulfides have been interpreted by Shelton et al. et al. (1995) to indicate a basinal source of sulfur for the ^{34}S -enriched sulfides ($\delta^{34}\text{S}$ approaching +25‰) and a granitic basement and/or pyritic sulfur contribution for the relatively ^{32}S -enriched sulfides ($\delta^{34}\text{S} < +5‰$).

Lead isotope data from MVT deposits around the world consistently point to an upper crustal source of the lead and, by implication, of the associated metals. This conclusion is consistent with the higher $^{87}\text{Sr}/^{86}\text{Sr}$ ratios of the gangue carbonate minerals compared with those of the host carbonate rocks (e.g., Ravenhurst et al. 1987, Kesler et al. 1988). The ore leads, however, show a wide range of isotopic composition among districts as well as within some districts (Heyl et al. 1974, Sangster 1986); even single crystals of galena may exhibit marked variation in lead (and sulfur) isotope ratios (Sverjensky et al. 1979, Hart et al. 1981, Deloule et al. 1986).

The lead isotopic data for MVT deposits (Fig. 13.11) fall into three main groups (Vaasjoki & Gulson 1986, Sangster 1990). A few deposits (e.g., Gays River, Silesia, Alpine) contain relatively homogeneous B-type lead (i.e., lead that gives model ages older than the host rock, according to the Zartman-Doe model), which probably represents more or less direct derivation of the lead from the basement. A second group is characterized by isotopic compositions that are homogeneous within each deposit and

are either 'normal' (e.g., Pine Point, Coxco, Nanisivik) or slightly radiogenic (e.g. Sorby Hills, Pillara) — i.e., they give model ages equal to or slightly younger than the age of the host rock. A third group (e.g., Viburnum Trend, Tri-State, Upper Mississippi Valley) contains J-type lead (i.e., highly radiogenic lead that plots significantly beyond the geochron) displaying linear arrays. The radiogenic leads have been interpreted as mixtures of lead from more than one source. The isotopic composition of lead in galenas of the Viburnum Trend, for example, has been attributed to the mixing of an oil-field brine component (normal lead) and a radiogenic lead component derived from Grenville-age (1.0-1.2 Ga) basement (Crocetti et al. 1988). According to Vaasjoki and Gulson (1986), the radiogeneity of the leads in MVT deposits increases with an increase in age difference between the crystalline basement and the time of ore deposition, presumably because of the availability of progressively greater amount of lead for incorporation into the ore fluids, whereas the homogeneity of the leads reflects the homogenization of source material due to the combined effects of sedimentation, diagenesis, and prolonged brine circulation.

13.9.3. PALEOTECTONIC SETTINGS

It is clear from field relations that MVT deposits formed in platformal carbonates deposited at or near the edges of intracratonic sedimentary basins or on shelf areas (passive continental margins). Sawkins (1976b) classified them as deposits related to early stages of continental rifting. A rift environment is an important aspect of the regional setting of some MVT deposits (e.g., Gays River, Nanisivik, Alpine district of central Europe, Viburnum Trend; Viets & Leach 1988, Clendenin & Duane 1990, Sangster 1990), but no systematic relationship between MVT deposits and rifting has yet been established. The Upper Mississippi Valley district, located at the western flank of the Michigan Basin and along the northern edge of the Illinois Basin, is the only major MVT district spatially associated with an intracratonic basin (Leach & Sangster 1993).

The vast majority of MVT deposits occur in platform-carbonate sequences of orogenic forelands, either in relatively flat-lying undeformed rocks of an orogenic forebulge (e.g., Southeast Missouri, Pine Point, Silesia) or in faulted rocks of a foreland thrust belt (e.g., East Tennessee).

In some districts (e.g., East Tennessee), ore horizons are offset by post-mineralization faults. But in many other districts (e.g., Viburnum Trend, Northern Arkansas, Tri-State, Upper Mississippi Valley, Silesia-Cracow), faults and fractures appear to have provided important local ore controls, mainly by facilitating the ascent of ore fluids through increased permeability (Leach & Viets 1992) and even providing open space for ore accumulation. However, because of poorly constrained mineralization age, the precise temporal relationship between tectonics and ore deposition is not known in most cases.

In general, tectonic processes have not been considered an important factor in the genesis of MVT deposits (e.g., Sangster 1979), but some recent studies have correlated

the migration of MVT ore fluids with compressional tectonics (Leach & Rowan 1986, Duane & de Wit 1988; Nakai et al. 1990). For example, Leach and Rowan (1986) have argued that the systematic variation in fluid inclusion homogenization temperatures and Na:K ratios, as well as available constraints on the age of mineralization, in MVT deposits of the Ozark region are consistent with fluid migration from the Arkoma foreland basin as a consequence of the Ouachita orogeny (late Pennsylvanian-early Permian). In fact, they have suggested that "in general, the single most important and unifying factor for MVT deposits in diverse geologic provinces may be proximity to a basin that has undergone some form of uplift or deformation." Another example is the Kicking Horse sphalerite-galena deposit (British Columbia, Canada) hosted by Middle Cambrian dolostones for which paleomagnetic dating indicates that the main fluid flow event in the basin occurred during the late Cretaceous-Paleocene Laramide orogeny (Symons et al. 1998). His hypothesis is supported by the correlation between the age of mineralization in several other MVT deposits/districts and regional orogenic activity (Table 13.2), but a proper evaluation requires reliable age data on many more MVT districts.

Christensen et al. (1997) have drawn attention to the fact that recent Rb-Sr dating of sphalerites from widely distributed MVT deposits (East Tennessee, Upper Mississippi Valley, Pine Point, Polaris, Lennard Shelf) show a striking concentration of ages (weighted average 358 ± 3 Ma) around the estimated Devonian-Carboniferous boundary (363 ± 5 Ma), implying a common global factor in the generation of these deposits. The end of the Devonian coincides with several important global geologic events that could have controlled MVT-forming processes. These include: widespread orogenic activity, major global extinction events, rapid spread of land plants, a major decrease in atmospheric CO_2 , widespread oceanic anoxic events, and an excursion in $\delta^{34}\text{S}$ of marine sulfate indicating increased bacterial activity associated with enhanced organic carbon burial. According to Christensen et al. (1997), the most likely common link was the oceanic anoxic events (Turner 1992), as has been proposed for the Devonian peak in the age distribution of SMS deposits (Goodfellow et al. 1993).

13.10. Summary

MVT deposits are distinguished by strata-bound, epigenetic, $\text{Zn}(\text{sphalerite}) \pm \text{Pb}(\text{galena}) \pm \text{fluorite} \pm \text{barite}$ mineralization in platform carbonate rocks, predominantly dolostones (dolomitized limestones), and a lack of igneous association. Mineralization occurs typically as interfragmental fillings in breccia bodies, which are commonly of dissolution-collapse origin related to an overlying unconformity and perhaps enlarged later by the action of ore-forming fluids. The ore-gangue assemblages reflect multiple events of dissolution and precipitation in many cases, and contain an abundance of sparry dolomite and/or calcite, but very little pyrite/marcasite, and no Cu-minerals. An exception is the Southeast Missouri district, which contains significant amounts of chalcopyrite and lesser amounts of bornite and covellite. Associated elements,

recoverable in some cases as byproducts, are cadmium, germanium, and silver. Liquid and solid organic matter is ubiquitous in the ores and immediate host rocks.

Host rocks of MVT deposits range in age from the Proterozoic to the Cretaceous, but Paleozoic rocks, especially of Cambrian-Ordovician and Devonian-Carboniferous age, are the most important. Most of the deposits are located at the edges of sedimentary basins in orogenic foreland belts, although some may be related to intracontinental rifts. Individual deposits are small in size but they tend to occur in clusters, and the aggregate ore potential of a district may be comparable to that of giant SMS deposits. The other important variables among MVT districts include: the host rock package (distribution of dolostone relative to limestone), Zn:(Zn+Pb) ratio (although Zn dominates over Pb in most), average grade (from $\approx 2.5\%$ to $>10\%$ Zn+Pb), relationship of ore horizon to erosion surface and facies changes in the host rock sequence, nature of mineralization (open-space filling versus replacement), and sulfur and lead isotope ratios.

Fluid inclusion data indicate that the ore fluids for the main-stage mineralization were mildly hot ($\approx 100^\circ\text{C}$), highly saline (>15 wt% NaCl equivalent), NaCl-dominated, basinal brines. The metals were transported as chloride complexes and Zn:Pb ratios of the ore fluids were probably controlled by the lithology of the aquifers they traveled through. The driving force for fluid migration was either the episodic compaction of basinal sediments or topographic gradients created by uplift. The latter is compatible with a broad correlation between the age of mineralization for many North American deposits and orogenic activity in the region. A marked concentration of MVT-forming processes around the Devonian-Carboniferous boundary is probably related to oceanic anoxic events on a global scale.

Sulfur isotope ratios are highly variable from one district to another, and even within individual districts, indicating multiple sources of sulfur such as seawater sulfate (the most important source for most deposits), sulfur-rich organic compounds, diagenetic pyrite, and granitic basement. It is not certain whether the reduced sulfur was transported in the same fluids as metals or became available only at the site of sulfide deposition. Ore leads are invariably anomalous and appear to have been derived from a single homogeneous source in some cases and from multiple sources in others. Because of the diversity among the MVT districts and a lack of knowledge regarding the absolute age of mineralization in most, it has not been possible to formulate a comprehensive genetic model for this class of deposits.

13.11. Comparison of VMS, SMS, SSC, and MVT Deposits

Table 13.4 presents a comparison of the three major classes of sediment-hosted hydrothermal sulfide deposits — SMS, SSC, and MVT — which are generally viewed having formed from fluids derived from sedimentary basins in the course of their normal evolution. The VMS class, characterized by host rock sequences dominated by volcanic rocks and mineralizing fluids dominated by marine water, is included in Table 13.4

TABLE 13.4. Comparison of VMS, SMS, SSC, and MVT deposits

Characteristic	VMS	SMS	SSC	MVT
<i>Size and grade of individual deposits</i>	Mostly 1 to 10 Mt ore; Cu + Zn + Pb < 10%, Cu 1 to 3%	Mostly > 30 Mt, many contain > 100 Mt ore Commonly Cu + Zn + Pb > 10%, Cu < 1%	< 1 to > 1,000 Mt. ore; Cu 1-5%, commonly no significant Zn or Pb	Mostly < 1 Mt. ore Zn + Pb 3 to 10%, typically no Cu
<i>Metals recovered or concentrated</i>	Bimodal Zn: (Zn + Pb) distribution Major: Cu, Zn, Pb Minor: Ag, Au	Bimodal Zn: (Zn + Pb) distribution Major: Zn, Pb (+ Cu in some deposits) Minor: Cu, Ag	Bimodal Zn: (Zn + Pb) distribution Major: Cu (+ Zn, Pb, Co in some deposits) Minor: Ag, Re	Bimodal Zn: (Zn + Pb) distribution Major: Zn, Pb Minor: Cd, Ag, Ge
<i>Characteristic ore-gangue assemblage</i>	py/po + cp + sp ± ga ± barite ± gypsum	py/po + sp + ga ± cp ± barite	py + cc + bn + cp ± ga ± sp	sp ± ga ± fluorite ± barite ± py/mns ± calcite/dolomite ± chert
<i>Typical host rock sequence</i>	Tholeiitic to calc-alkaline volcanic sequences, with volcanoclastics, clastics (graywacke), and chemical sediments	Shallow- to deep-water, marine clastics and carbonates, with thin bands of tuffite; evaporite and redbed association not typical	Carbonaceous shales, marls, arenites, minor carbonates; commonly associated with continental redbeds and evaporites	Shallow-water, platform carbonate rocks (limestones) and dolomitized limestones; ores localized in dolostone rather than in limestone
<i>Age of host rocks</i>	Archean to Tertiary; dominantly Archean to early Proterozoic	Early Proterozoic to late Paleozoic; dominantly early to middle Proterozoic	Early Proterozoic to Tertiary; dominantly Proterozoic and Permian-Carboniferous	Early Proterozoic to Jurassic, dominantly Paleozoic
<i>Nature of mineralization</i>	Conformable, massive sulfide lens (syngenetic) underlain by a zone of discordant, stockwork mineralization (epigenetic)	Conformable, stacked lenses of stratiform massive sulfide (syngenetic) underlain by a zone of discordant mineralization (epigenetic)	Stratiform mineralization of disseminated sulfides restricted to specific units; localized in reduced (gray) beds, especially at oxidation-reduction interfaces	Strata-bound, massive to disseminated, cavity-filling mineralization, most commonly cementing breccia fragments; minor replacement mineralization

TABLE 13.4 (continued)

Characteristic	VMS	SMS	SSC	MVT
<i>Hydrothermal alteration</i>	Pronounced chloritic and sericitic alteration and brecciation in the footwall rocks	Footwall alteration varies from pronounced to subtle to absent	No characteristic alteration pattern	Dolomitization (not necessarily by ore fluids), silicification, increased illite crystallinity
<i>Metal zoning</i>	Cu \Rightarrow Zn \Rightarrow Pb or Cu \Rightarrow (Zn + Pb), especially toward the stratigraphic top	Cu \Rightarrow Zn + Pb \Rightarrow barite	Pronounced lateral and vertical zoning: cc \Rightarrow bn \Rightarrow cp \Rightarrow (ga, sp) \Rightarrow py	No characteristic zoning pattern
<i>Ore-forming fluids</i>	Moderate salinity (4 - 8 wt % NaCl equiv.), moderate temperature (150° - 300°C)	High salinity (10 - 30 wt % NaCl equiv.), moderate temperature (100° - 300°C)	Moderate salinity, low temperature (~ 100°C), pH 6 to 8, oxidizing, sulfate-rich (?)	High salinity (> 15 wt % NaCl equiv.), low temperature (commonly 100° - 150°C)
<i>Controls of mineralization</i>	Volcanic stratigraphy, explosive volcanism, subsurface plutons	Rift-basins, synsedimentary faulting, anoxic basins, suitable source rocks for metals	Distribution of organic matter, redbeds, and evaporites; permeability for fluid migration	Platformal carbonates, breccia bodies, facies changes, basement highs and pinch-outs, faults, limestone-dolostone interfaces
<i>Genetic model</i>	Exhalative system (volcanic)	Synsedimentary - sedimentary exhalative to syndiagenetic from basinal brines	Syndiagenetic mineralization from basinal brines	Epigenetic mineralization from basinal brines
<i>Tectonic setting</i>	Extensional settings at convergent margins; divergent plate boundaries	Mostly intracontinental rifts	Intracontinental rifts	Foreland thrust belts, intracratonic sedimentary basins (edges)
<i>Typical examples</i>	Noranda district (Canada) Cyprus Kuroko district (Japan)	Mount Isa (Australia) Sullivan (Canada) Irish deposits (Navan)	Kupferschiefer (Poland) Zambian copperbelt White Pine (USA)	Pine Point (Canada) Vitburnum Trend (USA) Silesia (Poland)

Abbreviations: py = pyrite, ms = marcasite, po = pyrrhotite, sp = sphalerite, ga = galena, cp = chalcopyrite, cc = chalcocite, bn = bornite, Mt = million tonnes

merely to emphasize its contrasting features. Distal VMS deposits, however, are not easily distinguished from SMS deposits.

Of the three classes of sediment-hosted sulfide deposits, the SSC group is the most distinct in terms of observable features. Most SSC deposits are associated with redbeds, sulfate-rich evaporites, and redox fronts, and represent diagenetic mineralization. Whether the sulfate reduction was bacterial and occurred just below the sediment-water interface, or inorganic and occurred later and at higher temperatures, the ore fluids appear to have been of moderate salinity and near-neutral pH and Eh values within the hematite stability field. (i.e., above the field of Fe^{2+} solubility).

Sediment-hosted Zn-Pb deposits, on the other hand, formed from fluids of higher salinity. They range from stratiform, syngenetic-diagenetic mineralization hosted by dominantly clastic sequences (SMS deposits) to strata-bound, open-space filling type of epigenetic mineralization hosted almost exclusively by carbonate sequences (MVT deposits). There are many similarities between these two classes of deposits (Sangster 1990). These include: similar Zn:(Zn+Pb) ratios, skewed toward Zn-rich deposits in both cases; a preference for Cambrian-Ordovician and Devonian-Carboniferous host rocks; comparable sulfur-isotope composition of sulfides relative to those of sulfate coeval with the host rock; ore fluids of similar temperature and salinity; and an intracontinental rift setting for some deposits of both the classes. The occurrence of SMS and MVT deposits in the same sedimentary basin — e.g., in the Batten Trough, Australia (Walker et al. 1983) and in the Selwyn Basin area, northern Canada (Macqueen & Thompson 1978, MacIntyre 1982) — suggests the same clastic sedimentary fluid source for both classes of deposits. A marked concentration of both SMS and MVT mineralization around the Devonian-Carboniferous boundary may be related to a common set of global-scale geologic events, perhaps oceanic anoxic conditions, at the end of Devonian (Goodfellow et al. 1993, Christensen et al. 1997). However, considering the large overlap in the characteristics of MVT and SMS deposits (see Sangster 1990 for a more detailed discussion), the relative paucity of MVT deposits in Proterozoic rocks is intriguing.

In a series of papers, Sverjensky (1984, 1986, 1987, 1989) has attempted to show that, depending on the rock type of the aquifer unit encountered during migration, a single basinal brine may evolve chemically to become the ore-forming fluid for any one of a wide range of sediment-hosted base-metal sulfide deposits (Fig. 13.13). For this exercise, the input parameters estimated for the initial fluid were as follows: 50°-150°C; 2-6 molal chloride; maximum oxygen fugacities near hematite/magnetite; pH values from 4 to 6; initial saturation with respect to galena, chalcopyrite, pyrite, muscovite, kaolinite, and quartz, but undersaturation with respect to sphalerite. According to his calculations, such a fluid could contain about 1 ppm Pb, 0.1 ppm Cu, and up to 5 ppm Zn (Sverjensky 1989).

The major aquifers associated with the formation of SSC deposits appear to be the redbeds themselves (Rose 1976, Bjørlykke & Sangster 1981). Interaction of a basinal brine with hematite + anhydrite of the redbed aquifer and simultaneous scavenging of Cu, Zn, and Pb from the redbed would result in the fluid being saturated with respect to

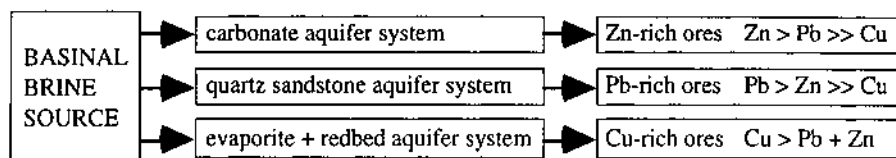


Figure 13.13. Digrammatic representation of a single source of basinal brine with three different aquifer systems, resulting in Zn-rich, Pb-rich, and Cu-rich deposits (after Sverjensky 1989).

pyrite, chalcocite, and chalcopyrite but undersaturated with respect to sphalerite and galena. Such a fluid, upon encountering a reducing environment, would precipitate only minor amounts of sphalerite and galena compared with Fe Cu sulfides. Lead and zinc, being more soluble than copper and not as influenced by redox conditions, would probably be dispersed at the surface rather than further along the plumbing system (Gustafson & Williams 1981).

Fluids migrating through a carbonate aquifer, as in the case of MVT deposits, are likely to be maintained near saturation with respect to sphalerite, galena, chalcopyrite, and pyrite, because the availability of small quantities of metal and sulfide from such an aquifer and the possibility of fluid reacting with trace quantities of detrital silicates would be enhanced by the retrograde solubility of carbonates. The Cu content of the fluids would remain low because of the H_2S dissolved in the fluid saturated with respect to chalcopyrite. The relative abundance of base metals in such a fluid would be $Zn > Pb > Cu$. In contrast, basinal fluids passing through a quartz-rich sandstone, believed to be the aquifer rock for sandstone-lead deposits (Bjørlykke & Sangster 1981), may evolve somewhat differently. Trace amounts of pyrite, without significant hematite, in an aquifer may enable the fluid to maintain its saturation in galena and chalcopyrite and undersaturation in sphalerite. Such fluids would precipitate sulfide ores with high Pb:Zn and high (Pb+Zn):Cu ratios. Fluids for SMS deposits were probably maintained at higher temperatures, as indicated by the large amounts of iron and barium they carried, and were involved in more complex fluid-rock interactions because of cross-stratal migration of fluids (compared with migration along stratal aquifers in the case of MVT deposits). Lead-zinc deposits without accompanying copper raise the interesting possibility of undiscovered copper deposits along the plumbing system (Gustafson & Williams 1981).

13.12. Recommended Reading

Anderson and Macqueen (1982), Anderson (1983), Heyl (1983), Sverjensky (1986, 1989), Rowan and Leach (1989), Sangster (1990), Misra and Fulweiler (1992), Leach and Sangster (1993), Spirakis and Heyl (1995), Symons et al. (1997), Leach et al. (1997), Misra et al. (1997).

CHAPTER 14

URANIUM DEPOSITS

14.1. Introduction

The earliest mining of uranium ore, in 1727, was for recovery of radium from pitchblende (a poorly crystalline variety of uraninite) in a vein deposit at Joachimstal, Bohemia (Joachimsthal, former Czechoslovakia). The first important sources of radium outside Czechoslovakia were the sandstone-hosted uranium-vanadium deposits of Colorado and Utah (USA) from which about 275,000 tons of ore were produced during 1898-1923. This ore yielded about 200 g of radium, 2,000 tons of vanadium, and a small but undetermined amount of uranium most of which went into the mine tailings. The increased demand for uranium since the early 1960's is almost entirely due to the development of nuclear reactors using uranium as the raw material. The Western world uranium production ranged between 55 to 61 million pounds of U_3O_8 during 1992-1995 (*The Mining Record*, March 1, 1995). Several intertwined factors — reactor safety, disposal of nuclear wastes, capital costs, political considerations — are responsible for the current stagnation and future uncertainty of the nuclear power industry and, along with it, of the uranium mining industry. Nevertheless, the uranium deposits offer a fascinating story because of their spatial, temporal, and genetic diversity.

The geologic literature is no longer being flooded with articles on uranium deposits as was the case only a few years ago. Perhaps the most comprehensive review article on uranium deposits is by Nash et al. (1981). Rich et al. (1977) and Ruzicka (1993a, 1993b) present valuable compilations and discussions of hydrothermal uranium deposits. Noteworthy publications devoted to specific deposits include special issues of *Economic Geology* (v. 73, No. 8, 1978), *Mineralogical Association of Canada Short Course Handbook* (v. 3, 1978), and *Philosophical Transactions of the Royal Society of London* (Series A, v. 291, 1978-1979).

14.2. Types of Deposits and Distribution

Uranium deposits are quite diverse in terms of host rocks, geologic setting, controls of mineralization, and genesis. A classification scheme of uranium deposits, based mainly on geological characteristics, is presented in Table 14.1. More than 90% of the 'reasonably assured resources' of uranium mineable at forward costs up to \$50 per pound of U_3O_8 (without allowance for profit, taxes, interest on capital, or previously

TABLE 14.1. Important uranium deposit types and their characteristics (McMillan 1978, Nash et al. 1981)

Deposit type	Host rocks (Age)	Mineralogy (Typical grade, % U ₃ O ₈)	Associated elements	Form	Important examples*
Conglomerate	Quartz-pebble conglomerate (late Archean - early Proterozoic)	Uraninite, uraniothorite, brannerite, pyrite, monazite, gold (<0.01 to 0.2)	Th, Ti, Au, REE, Zr, C, PGE	Tabular	South Africa (Fig. 14.8): Witwatersrand Basin (30) Canada: Blind-River-Elliott Lake (5) Brazil: Jacobina (18)
Sandstone	Fluvial, arkosic and quartzose sandstone (Upper Paleozoic to Tertiary)	Pitchblende, coffinite, carnotite, pyrite/marcasite (0.1 to 0.4)	Cu, V, Se, Mo, C	Tabular, 'rolls'	USA (Fig. 14.2): Colorado Plateau (14-15), Wyoming - South Dakota (10), Texas Coastal Plain (16) Niger: Arlit and Akouta (25)
Unconformity	Basement and overlying metasediments (Proterozoic)	Pitchblende, coffinite, pyrite, chalcopyrite, Ni-Co arsenides, chlorite, hematite (0.4 to >2)	Ni, Co, Ag, Mo, Cu, Pb, Zn, Bi, Se, As, Au	Vein	Canada (Fig. 14.5): Athabasca Basin (3) Australia (Fig. 14.7): Alligator Rivers (32), Rum Jungle (33)
(Classical) Vein	Granites, gneiss, tuffs, metasediments (Proterozoic to Tertiary)	Pitchblende, coffinite, base metal sulfides and arsenides, hematite, carbonates (0.1 to 1.0)	Cu, Co, Ni, Bi, As, Ag, Au, Se, Mo	Vein	Canada: Beaverlodge (2) USA: Schwartzwalder (11), Marysvale (12) France: Massif Central (20) Czechoslovakia: Jachymov (22), Příbram (21) Portugal: Urgeirica (24)
Ultrameta- morphic	Alaskite, pegmatite, aplite, metasediments (Proterozoic)	Uraninite, uraniothorite, molybdenite, zircon (< 0.1)	Th, Mo, Nb, Ti, REE	Dissem- inated, vein	Namibia (Fig. 2): Rössing (28) Canada: Bancroft (6)
Alkalic plutons	Alkalic plutons and stocks, carbonates (Proterozoic to Cretaceous)	Uraninite, uraniothorite, pyrochlore, apatite, zircon (0.01 to 0.2)	Th, Nb, REE, Zr, Be, REE, Ti, P	Dissem- inated, vein	Greenland: Ilímaussaq (1) Brazil: Pocos de Caldas (17) USA: Bokon Mtn. (8)

Table 14.1 (continued)

Deposit type	Host rocks (Age)	Mineralogy (Typical grade, % U ₃ O ₈)	Associated elements	Form	Important examples*
Alkalic plutons	Alkalic plutons and stocks, carbonatites (Proterozoic to Cretaceous)	Uraninite, uranothorite, pyrochlore, apatite, zircon (0.01 to 0.2)	Th, Nb, REE, Zr, Be, REE, Ti, P	Disseminated, vein	Greenland: Himaussaq (1) Brazil: Pocos de Caldas (17) USA: Bogan Mtn. (8)
Contact	Skarns	Pitchblende, coffinite, pyrite/marcasite (0.1 to 0.2)	Th, REE, B, P	Disseminated, stockwork	USA: Midnite (9) Australia: Mary Kathleen (35) Spain: La Fe (23)
Volcanogenic	Hypabyssal, volcanic, and volcanoclastic complexes	Uraninite, pitchblende, uranothorite, pyrite, base metal sulfides, fluorite, celestite	Th, Cu, REE, Mo, F, Sr	Disseminated, vein	USA: McDermitt (13) Canada: Rexspar (7)
Calcrete	Nonpedogenic calcrete in Tertiary drainage systems	Carnotite, gypsum (0.3)	V	Tabular	Australia: Yeelirrie (36) Namibia: Langer (28)
Phosphorite	Marine phosphorite, reworked pebble phosphorite	Uraniferous carbonate and apatite (0.01 to 0.02)		Bedded	USA: Boone Valley Formation (Florida), Phosphoria Formation (Western USA) Morocco - Algeria - Tunisia - Egypt - Israel belt
Black Shale	Marine carbonaceous shale (Paleozoic)	? (<0.01 to 0.02)	V, Cu, Co, Mo, Ni, Zn, Pb, C	Disseminated, bedded	USA: Chattanooga Shale (Tennessee - Kentucky - Alabama) Sweden: Alum Shale (Raunstad)

*Numbers in parentheses are indexed to Figure 14.1

incurred expenses) are accounted for by five major deposit types (Nash et al. 1981): sandstone (45%), conglomerate (20%), unconformity (16%), (classical) veins (5%), and ultrametamorphic (6%). Vein deposits dominated uranium production before significant production commenced during the 1950's from sandstone deposits in USA and conglomerate deposits in South Africa and Canada. Contributions of deposit types to the total production in 1988, as estimated by Ruzicka (1993), were as follows: sandstone (17.4%), conglomerate (22.6%), unconformity (33.0%), veins (9.2%), ultrametamorphic (8.4%), and others (9.4%). Ultrametamorphic deposits occur in or adjacent to granitoids formed by very high grade metamorphism, including partial to complete melting of the protoliths (ultrametamorphism) that concentrated uranium in the anatectic silicate melts. The best known example is the Rössing deposit (Namibia) described earlier (Ch. 2). This deposit type is not discussed in this chapter.

The world distribution of important uranium deposits and districts, excluding the former USSR and China for which reliable information is not available, is shown in Figure 14.1. Almost all the major uranium deposits as well as more than 70% of 'reasonably assured resources' of uranium occur in six countries. In decreasing order of resources, these are USA, South Africa, Australia, Canada, Niger, and Namibia. These

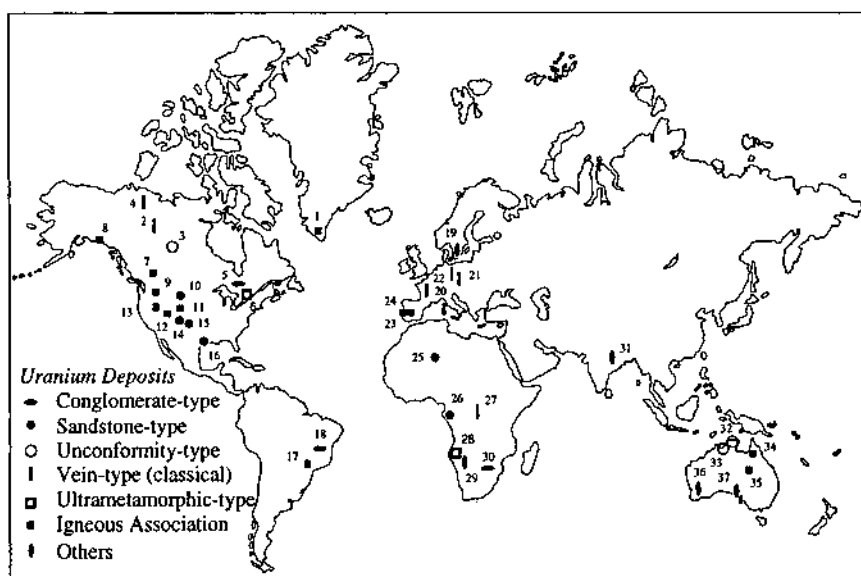


Figure 14.1. World distribution of important uranium deposits, districts, and belts: 1. Ilimaussaq; 2. Beaverlodge; 3. Athabasca Basin; 4. Great Bear Lake; 5. Blind River-Elliott Lake; 6. Bancroft; 7. Rexspar; 8. Bokan Mountain; 9. Midnite; 10. Wyoming-South Dakota; 11. Schwartzwalder; 12. Marysvale; 13. McDermitt; 14. Uruvan and Monument Valley-White Canyon belt; 15. Grants belt; 16. Texas Coastal Plain; 17. Pocos de Caldas; 18. Jacobina; 19. Ranstad; 20. Massif Central; 21. Pribram; 22. Jáchymov; 23. La Fe; 24. Urgeirica; 25. Arlit and Akouta; 26. Oklo; 27. Shinkolobwe; 28. Rössing; 29. Langer; 30. Witwatersrand Basin; 31. Singhbhum; 32. Alligator Rivers; 33. Rum Jungle; 34. Maureen; 35. Mary Kathleen; 36. Yeelirrie; 37. Olympic Dam.

six countries along with France accounted for more than 95% of the Western world uranium production in 1994 (57.1 million pounds of U_3O_8), with Canada contributing about 45% of the production (*The Mining Record*, March 1, 1995). Other major producers were Kazakhstan (5.9 million pounds), Uzbekistan (5.5 million pounds), and China (2.5 million pounds).

Excluded from present consideration is the enigmatic Olympic Dam copper-uranium-gold-silver-REE deposit in southern Australia, which was discovered in 1976, and its possible analogs such as the southeast Missouri iron province (USA) and the Kiruna iron deposits (Sweden). Hosted in a breccia complex, now recognized as a huge Proterozoic volcanic feature (Reeve et al. 1991), the Olympic Dam deposit contains 2,000 million tonnes of ore with an average grade of 1.6% Cu, 0.06% U_3O_8 , 0.6 g/t Au, and 3.5 g/t Ag. Considered the most exciting discovery in Australia since the Kambalda nickel sulfide deposits in 1966, it is one of the largest copper deposits ever discovered and the world's largest uranium deposit, and may ultimately rank with the Kalgoorlie district (Western Australia) in gold production. Olympic Dam may be an example of a class of shallow-level hydrothermal deposits (*Olympic Dam-type deposits*) characterized by iron oxides (hematite or magnetite) as the principal ore-forming minerals, extensive wallrock iron metasomatism, distinctive hydrothermal alteration (sodic at deep levels, potassic at intermediate to shallow levels, and sericitic in the near-surface environment), extensional tectonic environment, and mid-Proterozoic age (Oreskes & Hitzman 1993).

14.2.1. CONGLOMERATE-TYPE DEPOSITS

Auriferous and/or uraniferous conglomerates are not that common in the geologic record and most of the known occurrences are not economically exploitable. With the exception of the Tarkwa deposit in Ghana (Tarkwain Supergroup; 1900-1600 Ma), all economic conglomerate-type uranium deposits, with or without gold, are hosted by quartz-pebble conglomerates older than 2200 Ma in age. Almost all of the uranium production from *conglomerate-type deposits* has come from the Witwatersrand Basin (Witwatersrand Supergroup and Dominion Group; >2700 Ma) in South Africa (Kaalvaal craton) and the Elliot Lake-Blind River district in Canada (Matinenda Formation, Huronian Supergroup; 2500-2200 Ma). Estimated past gold productions from other pre-2200 Ma deposits — Tarkwa (250 tonnes), Jacobina (25 tonnes) and Moeda (10 tonnes) in Brazil, and Pongola (0.8 tonnes) in South Africa — were paltry compared with the recent production from deposits in the Kaalvaal craton (about 43,000 tonnes of gold from about 4.5 billion tonnes of conglomeratic ore between 1886 and 1990; Roscoe & Minter 1993). Gold production from some of the deposits in the Witwatersrand Basin, such as the Steyn/Basal placer in the Welkom goldfield and the Val placer in the Klerksdorp goldfield, exceeds 25 tonnes of gold per square kilometer (Minter 1991)! Informative reviews of the conglomerate-type uranium and gold deposits have been presented by Pretorius (1981) and Roscoe and Minter (1993).

U:Au ratio of mineralized conglomerates varies widely, most likely reflecting the

control of source rock composition. Witwatersrand deposits produce uranium (average grade 0.03% U_3O_8) as a byproduct of gold mining (average grade 10 ppm Au), whereas uranium is the primary product in the Elliot Lake-Blind River district. The Quirke Zone in the latter district, which is estimated to contain more than 224,000 tonnes U_3O_8 (average grade 0.1% U_3O_8), is the second largest economically exploitable uranium deposit in the world (Bray et al. 1987). Many Proterozoic auriferous conglomerates, such as those occurring in the Jacobina Group (Bahia, Brazil) and Bantek Group (Tarkwa, Ghana), are practically devoid of uranium. Compared with other types of sediment-hosted uranium deposits, the conglomerate-type deposits have a high U:Th ratio. The $UO_2:ThO_2$ ratio in the uranium minerals range from 5 to 12 in Elliot Lake deposits and from 6 to 18 in Witwatersrand deposits (Kimberly 1978).

The typical auriferous-uraniferous conglomerate is oligomictic (mostly vein-quartz, generally consisting >90% of the clasts, with minor amounts of chert, quartzite, and schist clasts) and was deposited in fluvial braided streams either as channel fills or as bars. The conglomerate is clast supported, with pebbles generally well rounded and well packed but not necessarily well sorted. Ore conglomerates commonly contain pebbles of both clear (or milky) quartz and smoky quartz, the smokiness being generally attributed to the formation of free silicon through exposure to radioactive minerals. At least part of the smoky quartz was inherited from a source lithology (Robinson & Spooner 1982). The conglomerate matrix is composed essentially of quartz, sericite, pyrite, chlorite, and chloritoid, and accessory amounts of heavy minerals, such as zircon, chromite, and leucoxene (an alteration product of primary titanium minerals). Gold in the native form and uranium, mostly as uraninite or brannerite, also occur as components of the matrix. The matrix of the conglomerate is cleaner than that of the enveloping arenites and shows the effects of reworking and winnowing of light and fine material.

14.2.2. SANDSTONE-TYPE DEPOSITS

Sandstone-type is the general term used for uranium deposits hosted by sandstones, arkoses, conglomerates and related clastic rocks, excluding deposits of quartz-pebble conglomerate association. The overwhelming majority of *sandstone-type deposits* occurs in USA, accounting for more than 95% of its uranium resources. The deposits are concentrated in three regions, each comprising several major mining districts and mineral belts. These are (Fig. 14.2): (a) Colorado Plateau region (Fischer 1968) — Monument Valley-White Canyon, Lisbon Valley (Big Indian), Uravan, and Grants (San Juan Basin); (b) Wyoming-South Dakota region (Harshman 1968a) — Powder River Basin, Shirley Basin, Gas Hills, Crooks Gap, Northern Black Hills, and Southern Black Hills; and (c) Texas Coastal Plain (Eargle et al. 1975) — Karnes and Live Oak.

Generalized characteristics of the sandstone-type deposits, based primarily on numerous studies of deposits in USA (Fischer, 1970, 1974, Nash et al. 1981, Sanford 1992), are summarized below:



Figure 14.2. Major mining districts and belts of sandstone-type uranium deposits in the United States: 1. Powder River Basin; 2. Shirley Basin; 3. Gas Hills; 4. Crooks Gap; 5. Uravan; 6. Big Indian (Lisbon Valley); 7. Monument Valley-White Canyon; 8. Grants; 9. Karnes; 10. Live Oak. (Modified from Fischer 1974.)

- (a) The host rock packages comprise fluvio-lacustrine sequences that are interpreted to have accumulated within intermontane basins and across broad intracratonic piedmonts and marginal marine plains. The immediate host rocks commonly are fluvial, arkosic to quartzose sandstones and conglomerates, which were deposited in alluvial fan, braided river, and meander belt environments. The original high permeability of the channel-fills was a significant factor in ore localization. Ore-bearing fluvial sandstones are often overlain by lacustrine mudstones and underlain by marine rocks including evaporites.
- (b) The age of the host sediments range from Upper Paleozoic to Tertiary, but is quite restricted in a given district. The most important host rocks in USA are Triassic (Chinle Formation) and Jurassic (Morrison Formation) in the Colorado Plateau region, Lower Cretaceous (Inyan Kara Group) and younger in the Black Hills area, Eocene (Wind River and Wasatch Formations) in Wyoming, and Tertiary (Whitsett Formation - Eocene, Catahoula Formation - Oligocene, Oakville Sandstone - Miocene, Goliad Sand - Pliocene) in the Texas Coastal Plain.
- (c) The host rocks of most deposits contain abundant organic matter of two types: detrital organic debris in the form of coalified fossil plant fragments

(including entire logs), which are often partly replaced by uranium minerals; and diagenetic, structureless (i.e., without any observable cellular structure), carbonaceous material that coats sand grains and authigenic minerals and fills intergranular pores and secondary voids in the host sandstone. Some deposits (e.g., in the Texas Coastal Plain) lack carbonaceous material.

- (d) The host rock sequence typically contains both oxidized and reduced facies (similar to the host rock sequence of typical SSC deposits). The oxidized (or redbed) facies is distinguished by its reddish to light-buff or tan color because of the contained hematite and its hydrated products. The reduced facies, in contrast, is characterized by a light-gray to greenish-gray color and an abundance of carbonaceous material and pyrite. Uranium deposits occur either in the reduced facies or at the interface between oxidized and reduced facies. The oxidized facies may be relatively insignificant or even missing in the vicinity of uranium orebodies, but the reduced facies is almost always closely associated with uranium mineralization.
- (e) There is no evidence of a direct genetic link between uranium mineralization and regional igneous activity. For some deposits volcanic ash found within the host-rock sequence (e.g., Texas Coastal Plain) or in the overlying sequence (e.g., Black Hills region) may have served as a source of uranium.
- (f) In unoxidized ores, the main uranium minerals are uraninite (or pitchblende) and coffinite. Accessory minerals include vanadium oxides and silicates, copper sulfides, and pyrite/marcasite. These minerals mainly impregnate the host sandstone, coating sand grains and filling pore spaces, but they also replace sand grains to a small extent and locally they replace coalified fossil plants. The deposits are relatively shallow, generally extending from the surface to a depth of 200 m and grades are generally greater than 0.1% U_3O_8 .
- (g) The deposits are strata-bound. The orebodies are of two geometric forms (Fig. 14.3): some are grossly *tabular* (or lenticular); others are pod-shaped, called *rolls* (or *roll-front* deposits). Both forms may occur in a district and even show gradational relationship, but generally one predominates over the other. Tabular bodies have yielded most of the ore only in the Colorado Plateau region.

The tabular orebodies, commonly hundreds of meters across but only a few meters thick, are peneconcordant — i.e., their long dimensions are nearly parallel to the gross stratification of the sedimentary host rocks but do not follow beds in detail (Fig. 14.3). They occur as discrete masses in lenses of sandstone, “like raisins in a loaf of raisin bread”, and represent fossil stream-channel deposits (Fischer 1974). Localization of ore within the paleochannels is controlled by local sedimentary features, such as thickness of permeable coarse-grained units, contacts of such units with relatively impermeable fine-grained units (e.g., mudstone), pinch-outs, and abundance of organic debris.

The roll-front orebodies are also elongate in plan and their long axes lie subparallel to the bedding of the host sandstone, but they are typically crescent-shaped in cross

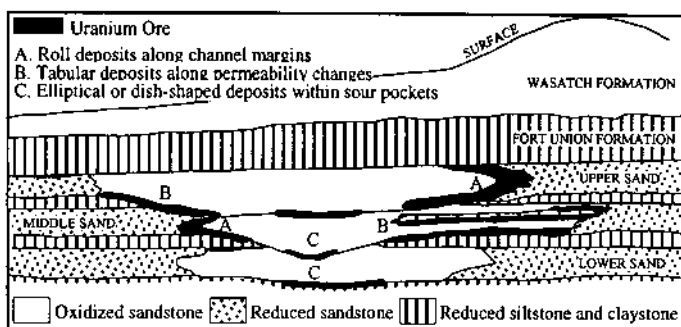


Figure 14.3. Generalized cross section (normal to sand channels) showing sandstone-type tabular and roll-front deposits, Highland deposit, Wyoming (after Langen & Kidwell 1974).

sections and discordant to the stratification of the host unit. The shapes of the rolls in cross sections are quite variable depending on the local pattern of permeability; 'C' and 'S' shapes are the most common. The roll is located at the interface between the reduced (also referred to as *unaltered*) and the oxidized (also referred to as *altered*) facies in a paleoaquifer. The oxidized sandstone on the concave side is generally reddish to drab-yellow (in contrast to the grayish color of the reduced sandstone) due to oxidation of iron disulfides to ferric oxide and hydroxide minerals and, compared with the reduced sandstone on the convex side, contains very little or no uranium minerals, carbonized fossil wood, calcite, or pyrite. The richest ore, associated with abundant pyrite or marcasite, is concentrated at the concave margin of the roll and the uranium concentration gradually diminishes to a trace within a few meters (Fig. 14.4). The interface between the oxidized and reduced rocks (the *redox front*) may extend laterally for kilometers within a sandstone unit, consisting of a string of roll orebodies of variable size and cross-sectional shape. A large roll orebody may be a few tens of meters high, as wide or wider, and extend hundreds of meters along the roll axis. Some roll-front deposits, such as those of the Ray Point district (Texas Coastal Plain), occur entirely enclosed within reduced rocks because of post-ore pyrite formation in the formerly oxidized tongue (Goldhaber et al. 1983).

14.2.3. UNCONFORMITY-TYPE DEPOSITS

The *unconformity-type deposits* are so named because of their spatial association with unconformities. Major concentrations of this deposit type occur in the Athabasca Basin (Saskatchewan, Canada) (Bray et al. 1988) and in the Alligator Rivers district within the Pine Creek geosyncline (Northern Territory, Australia) (Hegge & Rowntree 1978). Similar deposits in Lower Proterozoic rocks have also been reported from the Keewatin district of Canada (Curtis & Miller 1980) and the Oklo area in Gabon (Gauthier-Lafaye

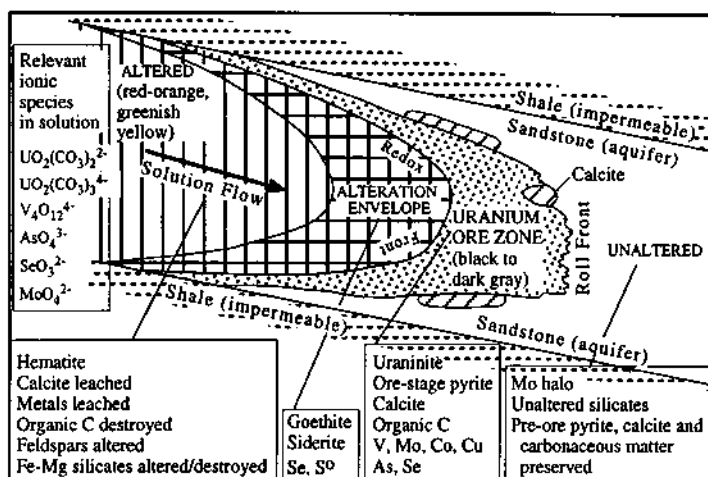


Figure 14.4. Schematic cross section of a roll-front uranium deposit showing the distribution of alteration and mineralization, and important characteristics of the various zones (modified from DeVoto 1978).

& Weber 1989). The Oklo area is better known for naturally occurring ^{235}U -depleted uranium (compared with the $^{235}\text{U}/^{238}\text{U}$ ratio of natural terrestrial uranium). The depletion of ^{235}U has been attributed to the fission of ^{235}U in self-sustaining chain reactions — that is, the Oklo uranium orebodies operated as natural fission reactors.

Characteristic features of unconformity-type deposits include the following (Hoeve & Sibbald 1978, Marmont 1987, Maas 1989, Ruzicka 1993a):

- (a) The deposits are hosted by a variety of rock types (carbonaceous metasediments, calc-silicates, carbonates, quartzite, amphibolite, anatectic gneisses, crystalline basement, etc.) but are always located immediately below, at, or immediately above an unconformity. In the Athabasca Basin, (Canada), the unconformity of interest lies between unmetamorphosed middle Proterozoic (Helikian) sediments of the Athabasca Group and metamorphosed Archean-Lower Proterozoic (Aphebian) (Fig. 14.5). In the Alligator Rivers district (Northern Territory, Australia), the unconformity is between Lower to Middle Proterozoic metasediments-metavolcanics and late Archean to Lower Proterozoic metamorphosed basement (the Nanambu Complex). In some deposits (e.g., Northern Territory, Australia), no mineralization occurs above the unconformity.
- (b) Commonly the ores are of relatively high grade and many deposits contain large tonnages, thus making this deposit type a preferred exploration target. Of the world's largest economically exploitable uranium deposits, three are

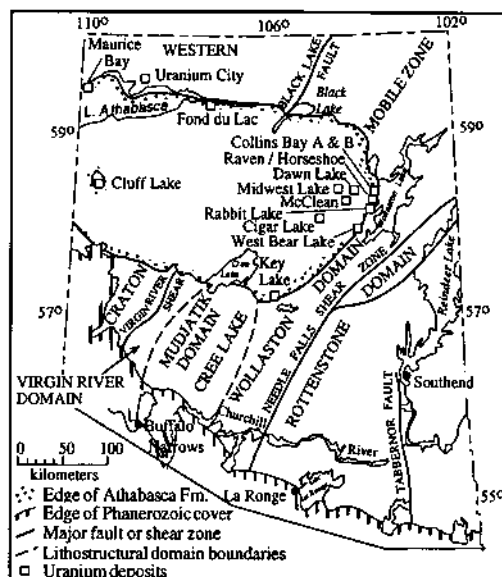


Figure 14.5. Major unconformity-type uranium deposits in the Athabasca Basin, Northern Saskatchewan, Canada (modified from Hoeve & Sibbald 1978).

- of the unconformity-type (Bray et al. 1987): Jabiluka Two deposit, East Alligator region, Australia (200,000 tonnes U_3O_8 , average grade 0.39% U_3O_8); Cigar Lake deposit, Athabasca Basin, Canada (177,000 tonnes U_3O_8 , average grade 4.7-14.2% U_3O_8); and Key Lake deposit, Athabasca Basin, Canada (89,000 tonnes U_3O_8 , average grade 0.70-2.88% U_3O_8).
- The deposits exhibit a strong structural control and occur as veins, breccias, and open-space fillings commonly associated with reverse and normal faulting. The faults are often best developed at contacts of lithological units with differing competencies. The breccia zones have been variously ascribed to collapse, hydraulic fracturing, and reverse faulting.
 - The mineralogy consists of uraninite and pitchblende as primary (hypogene) minerals and a number of secondary (supergene) minerals. Associated minerals include oxides of V and Mo, sulfides and arsenides of Ni, Co, Cu, Zn, and Pb (and in some cases of Ag), and native Au. No statistical correlation between U and Au has been discerned.
 - Hydrothermal alteration related to uranium mineralization is common and usually much more extensive than the mineralization. Chloritization is most characteristic. Argillization, dolomitization, silicification, sulfidization, hematization, and tourmalinization have also been reported.
 - Fluid inclusion microthermometry (Pagel et al. 1980, Poty & Pagel 1988,

Ypma & Fuzikawa 1980) indicates that ore-forming fluids were fairly hot (about 160°-220°C) and highly saline (up to 30 wt% NaCl equivalent). Mixing with meteoric water, especially during the later stages of mineralization, is suggested by variations in the fluid salinity.

- (g) Radiometric dating and field relations indicate that uranium mineralization in this deposit type is epigenetic. In northern Saskatchewan, the age of initial uranium mineralization (1350-1250 Ma) is about 100-150 m.y. younger than the depositional age of Athabasca sediments (Bray et al. 1987). This age is consistent with fluid inclusion (Pagel et al. 1980, Poty & Pagel 1988) and oxygen isotope (Wilson & Kyser 1987) data, which indicate that the uranium mineralization took place at 160-230°C and beneath 3,000 m of sediment cover, at a relatively advanced stage in the evolution of the Athabasca basin. In the Alligator Rivers area, the primary mineralization seems to have taken place soon after the deposition of the 1650 Ma-old Kombolgie Formation.

14.2.4. VEIN-TYPE DEPOSITS

Included in this category are deposits that occur as structurally controlled veins, but excluding those related to unconformities with which they share some common features. *Vein-type deposits* are hosted by a wide variety of rocks ranging in age from late Archean-early Proterozoic (<2.0 Ga) to late Tertiary. In terms of geologic setting, uranium vein deposits may be classified as (Ruzicka 1993b): intragranitic veins, hosted by granitic or syenitic rocks; perigranitic (or peribatholithic) veins, hosted typically by metasedimentary and metavolcanic rocks surrounding granitic plutons; and structurally controlled veins in shear and fault zones unrelated to granitic plutons. The most well-known intragranitic deposits are in France (Massif Central), Spain, and Portugal, typically associated with Hercynian granites (Carboniferous-Permian). A major part of China's uranium resources occur as intragranitic vein deposits; the most important is the Xiazhuang district, Guandong Province, southern China. Important perigranitic vein deposits occur in the Příbram and Jáchymov districts (Czech Republic), in the Ciudad Rodrigo district (Spain), and in the Great Bear Lake district (Northwest Territories, Canada). Typical examples of vein deposits in shear and fault zones include: the Fay-Ace-Verna zone (Eldorado mine), Beaverlodge district (Saskatchewan, Canada); Schwartzwalder deposit (Colorado, USA), and Shinkolobwe deposit (Shaba Province, Congo). Comprehensive accounts of the vein-type uranium deposits have been published by Rich et al. (1977) and Ruzicka (1993b); the characteristics of a few selected deposits are summarized in Table 14.2.

The common characteristics of vein-type uranium deposits may be summarized as follows (Rich et al. 1977, Nash et al. 1981, Ruzicka 1993b):

- (a) Uranium veins commonly occupy faults, joints, or fracture zones. Most deposits are quite shallow, rarely extending to depths greater than 300 m,

TABLE 14.2. Generalized characteristics of some important examples of vein-type uranium deposits (after Rich et al. 1977 and others as noted)

District/Deposit	Host rocks	Ore-gangue mineralogy	Wall-rock alteration	Age of uranium mineralization	Ore-forming fluids
Beaverlodge district, Saskatchewan, Canada	Mainly Archean-early Proterozoic Tazin Group metasediments and granites of metasomatic origin (basement complex)	Pitchblende, hematite, carbonates, chlorite ± sulfides and arsenides of Fe, Ni, Co, Cu, Bi ± gold, silver	Hematization, accompanied by calcite, chlorite, and red feldspar (adularia?)	Mineralization at 1.8 Ga, following granitization; uranium redistribution at about 1.1 Ga	Metamorphic-hydrothermal fluid (up to 440°C and 28 wt % NaCl equiv.); possible late-stage influx of meteoric water (Tremblay 1978)
Great Bear Lake district, NWT, Canada	Predominantly banded andesitic tuffs of the Proterozoic Echo Bay Group intruded by coeval and later granites	Pitchblende, hematite, Fe-Ni-Co-Bi sulfides and arsenides, quartz, acanthite, native silver, carbonates	Hematization, argillization, sulfidization, chloritization, carbonization	1450 Ma	100°-200°C, ≈30 wt % NaCl equiv. ore fluids, probably connate seawater that circulated through volcanics and felsic intrusives (Robinson & Badham 1974)
Front Range district (Schwarzwalder deposit), Colorado, USA	Proterozoic metasediments	Pitchblende (with minor coffinite), calcite, ankerite, hematite, adularia, base metal sulfides	Hematization, carbonatization, chloritization, feldspathization	69 Ma, related to the Laramide orogeny	Metamorphic-hydrothermal fluids derived from the Proterozoic basement (Wallace & Whelan 1986)
Marysvale district, Utah, USA	Quartz monzonite and granite bodies (23-26 Ma) that intrude the Bullion Canyon Volcanic Series (28-31 Ma) and also rhyolite nearby	Pitchblende, purple to black fluorite (radioactive), pyrite, quartz, sericite	Pervasive, pre-ore alunite alteration; syn-ore argillic alteration	10-13 Ma	Moderately hot (200°-250°C) ore fluids of unknown source (Walker & Osterwald 1963)
Jachymov district, Karlovy Vary Massif, northwest Czechoslovakia	Proterozoic to early Paleozoic metasediments (especially, pyritic and graphitic mica schists) peripheral to autometamorphic granite bodies (260-280 Ma)	Pitchblende (lower zone), arsenides and bismuth (middle zone), arsenides and silver; (upper zone); pre-ore quartz, arsenopyrite, base metal sulfides	Extensive pre-ore, syn-ore (silicification, carbonization, hematization) and post-ore alteration	Main-stage pitchblende deposition 220-230 Ma; minor pitchblende stages 5-160 Ma	Pitchblende deposition from high-temperature (370-470°C) fluids; uranium derived from both granites and metasediments (Ruzicka 1971)

TABLE 14.2 (continued)

District/Deposit	Host rocks	Ore-gangue mineralogy	Wall-rock alteration	Age of uranium mineralization	Ore-forming fluids
Příbram district, Bohemian Massif, Western Czechoslovakia	Upper Proterozoic graphitic metasediments that have been intruded by granites (Lower Carboniferous)	Pitchblende, carbonates, base metal sulfides, Ni-Co minerals, quartz	Hematization; also chloritization, sericitization, pyritization	270 Ma	?
Limousin region, Northwest Massif Central, France	Hercynian, anatectic two-mica granites (350-360 Ma), and 'episyenites' (altered granites)	Pitchblende, with minor coffinite and base metal sulfides, barite, carbonates, quartz	Hematization	Minimum 275 Ma, following the emplacement of lamprophyres and eptisyenitization	Pitchblende precipitation at about 345°C from ascending CO ₂ -rich fluids due to CO ₂ loss by boiling (LeRoy 1978)
Forez region, Eastern Massif Central, France	Hercynian, anatectic Bois Noirs granite (335 ± 8 Ma)	Pitchblende (with minor secondary coffinite), pyrite, marcasite, base metal sulfides and arsenides, quartz	Hematization	Magmatic-hydrothermal uraninite mineralization in altered Bois Noir granite (≈335 Ma); mobilization of uranium by deep-circulating meteoric water and deposition of pitchblende in veins (≈270 Ma); minor uranium remobilization during the Oligocene uplift (Cuney 1978)	
Urgesica deposit, northern Portugal	Hercynian granites	Pitchblende, jasper, sulfides	Sericitization, chloritization, tourmalinization, silicification, hematization, kaolinitization	80-100 Ma	
Shinkolobwe deposit, Shaba province, Congo	Mostly in the Schist-Dolomite Formation of the Precambrian Se'nne Mines, similar to the host rocks of the stratiform copper deposits	Uraninite, Ni-Co-S-Se minerals, pyrite, chalcopyrite, molybdenite; Ni:Co ratio from 3:1 near the uranium zone to 1:3 away from the zone	Chloritization	620-670 Ma (post-tectonic)	Remobilization of syngenetic uranium which had accumulated in sandy beds adjacent to Archean granite hills (Nash et al. 1981)

and contain only a few tonnes to a few million tonnes of ore, but deposits extending to more than 1,500 m depth and containing more than 10,000 tonnes of uranium are known (e.g., Beaverlodge district, Canada). The average grade of mined ore ranges from 0.10 to 1.0 wt% U_3O_8 .

- (b) In virtually all vein deposits, low-Th pitchblende is the predominant, if not the only, primary uranium mineral. The common gangue minerals are pyrite/marcasite, base metal sulfides, quartz, hematite, and carbonates. In terms of mineralogy, the vein deposits are classified as (a) monometallic, where uranium is the principal ore constituent (examples: Beaverlodge, Schwartzwald, Pribram); and (b) polymetallic, where uranium is accompanied by other metals, such as Ni, Co, As, Bi, Cu, Se, V, Ag, and Au, chiefly in the form of sulfides, selenides, and sulfarsenides (examples: Great Bear Lake, Jáchymov, Shinkolobwe).
- (c) Hematization of wallrocks is characteristic of most, but not all, vein-type deposits. Other types of wallrock alteration of varying importance include argillization, carbonization, silicification, chloritization, sericitization, albitization, and pyritization.

14.3. Examples

14.3.1. WITWATERSRAND BASIN, SOUTH AFRICA

The Witwatersrand Basin (Fig. 14.6), located in the former Transvaal and Orange Free State provinces of South Africa, ranks as one of the richest mining fields the world has ever known, primarily for its gold mineralization in quartz-pebble conglomerate horizons. Auriferous conglomerates had been discovered earlier — at Jacobina, Brazil, in 1745, and at Tarkwa, Gold Coast of West Africa (now in Ghana), in 1878 — but it was the Witwatersrand discovery in 1886 that established quartz-pebble conglomerates as a major potential resource of gold. Six major goldfields and several smaller mineralized areas have been discovered since 1886 (Fig. 14.6) and some 150 mines have been in operation at one time or another in this Basin. Recovery of the associated uranium as a byproduct started much later, only in 1953, and reached an annual rate of 4,958 tonnes U_3O_8 in 1959 (the same year the Elliot Lake district in Canada reached a production rate of 9,400 tonnes U_3O_8). South African uranium production from conglomeratic ores between 1952 and 1987 totaled approximately 125,600 tonnes U_3O_8 , about 14% of the uranium production in the Western World during that period (Roscoe & Minter 1993). It has been estimated (Pretorius, 1976b) that the Basin contains the world's largest reserves of Au-bearing ore (average grade of treated ore = 10 ppm Au) and ranks among the world's largest reserves of low-grade uranium ore (average recovery grade = 280 ppm U). Other byproducts recovered from the Witwatersrand conglomeratic ores are pyrite, which is used to produce sulfuric acid required by uranium extraction plants, and small amounts of osmium and iridium. The

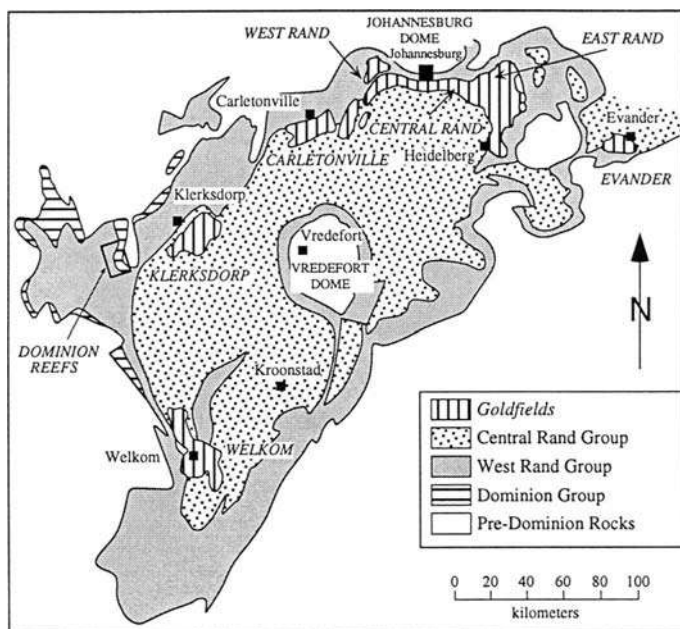


Figure 14.6. Location of major goldfields hosted by the Witwatersrand Supergroup (West Rand Group and Central Rand Group) and the Dominion Group, Kaapvaal craton, South Africa. Formations younger than the Witwatersrand Supergroup, which cover much of the area, are excluded. (After Pretorius 1976b, Roscoe & Minter 1993.)

discussion presented below has been extracted mainly from the review articles by Pretorius (1976a, 1976b, 1981), Minter (1991), and Roscoe and Minter (1993).

The Witwatersrand Basin is one of five "Proterozoic" sedimentary-volcanic basins that developed on the Kaapvaal craton of the African Shield (see Fig. 2.10). (The transition from Archean to Proterozoic style of crustal evolution on the Kaapvaal craton appears to have taken place at ≈ 3100 Ma (Pretorius 1981), significantly earlier than the 2500 Ma normally assigned to this boundary). The corresponding sedimentary-volcanic belts are: the Pongola Sequence, the Witwatersrand Sequence, the Ventersdorp Sequence, the Transvaal Sequence, and the Waterberg Sequence. Each basin lies on Archean granite-greenstone basement (3120 ± 5 Ma; Armstrong et al. 1991), which is now partially exposed within the Johannesburg and Vredefort domes, and has a somewhat similar stratigraphic sequence — volcanics at the base and top, and fine and coarse clastics in the middle. All formed under continental conditions and only in the Transvaal Sequence is there evidence (substantial dolostone development) of a major marine transgression. Minor amounts of gold have been recovered also from paleoplacers in the Pongola and Transvaal sequences, but the Witwatersrand sequence

contains the bulk of the gold and is the only one with uranium values.

The age of the Witwatersrand Supergroup (consisting of West Rand Group and Central Rand Group) is bracketed by a well-constrained U-Pb zircon age (3074 ± 6 Ma) for felsic porphyries of the underlying Dominion Group and a precise age (2714 ± 8 Ma) for the Klipriviersberg mafic volcanics at the base of the overlying Ventersdorp Supergroup (Armstrong et al. 1991). These age limits indicate that a period of 360 million years was available for the accumulation of the West Rand Group and then the Central Rand Group in the Witwatersrand Basin.

Mineralized conglomerate horizons occur throughout the Witwatersrand succession, but by far the greater proportion of well-mineralized conglomerates occur in the Central Rand Group. Only 10% of the periphery of the Central Rand Group is exposed, the rest is buried under younger Proterozoic and Phanerozoic rocks. The economically viable ore-bearing horizons, or "reefs" according to the local mining terminology, are almost entirely contained within the Central Rand Group. Several conglomeratic horizons occur within the West Rand Group, but they have contributed <1% of the gold mined from the Witwatersrand Basin (Robb & Meyer 1990). Conglomerate ores have also been mined from a basal unit (Renosterspruit Formation) of the underlying Dominion Group at the west side of the Witwatersrand Basin, in the Pongola Supergroup 400 km to the southeast, and in the Pietersburg greenstone belt 280 km northeast of the Witwatersrand goldfields. The ages of Pongola and Pietersburg host strata, bracketed between 2950 and 2700 Ma (Armstrong et al. 1991), are comparable to those of Witwatersrand rocks. At certain localities, where the younger Transvaal Supergroup overlaps on Witwatersrand mineralized strata, the basal conglomerate of the former contains reworked auriferous material from the underlying Witwatersrand rocks.

A Witwatersrand goldfield represents a fluvial fan, or a fan delta, composed of many cycles of sedimentation, with unconformities of varying magnitude separating the cycles. Gold and uranium mineralization predominantly occurs in, or immediately adjacent to, bands of quartz-pebble conglomerate which are preferentially developed at, or near, the base of each cycle of sedimentation. The conglomerate horizons constitute less than about 8-10% of the stratigraphic thickness of the Witwatersrand Supergroup and only a small proportion of them are economic.

The number of reefs that have been mined in a particular fan vary from a minimum of one (Evander goldfield) to a maximum of 10 (Klerksdorp and West Rand goldfields). Much of the gold recovered from the Witwatersrand mines have come from reefs less than 1 m thick, and a large fraction of it from reefs less than 0.1 m thick. In many reefs, there is a marked concentration of gold on the bottom contact where it is frequently associated with carbon of biogenic origin (Hallbauer 1975) occurring as a continuous mat over a few meters. Generally, the maximum gold concentration occurs at a different stratigraphic position than does the richest uranium mineralization.

Except for occasional veinlets and dust-like inclusions of sulfides, gold, and hydrocarbon (generally believed to be products of post-depositional mobilization), quartz pebbles of the conglomerate are barren. The matrix of the conglomerate, composed mainly of recrystallized quartz and phyllosilicate minerals, contains abundant

pyrite (and minor amounts of other sulfide and sulfarsenide minerals) and is enriched in heavy minerals, such as chromite, zircon, rutile, leucoxene, and uraninite. Generally, there is good correlation between uranium and gold, gold and zircon, and zircon and uranium in a given placer, and it appears that each placer has a characteristic uranium-gold correlation coefficient (Robb & Meyer 1995). Both gold-only reefs (e.g., Kimberly Reef, Evander goldfield) and uranium-only reefs (e.g., Beisa Reef, Welkom goldfield) are known. A high degree of correlation also exists between gold and silver, which is accounted for by the high Ag content of the gold. Compositional variations among individual gold particles at the centimeter-scale are small in some localities but large at others, and the average composition of gold particles in a given reef can change dramatically along strike on a kilometer scale. For example, gold particles from the Ventersdorp Contact Reef in the Klerksdorp and Carletonville goldfields show a wide range in composition (wt%): Au - 80.9 to 92.9; Ag - 6.0 to 17.6; and Hg - 0.6 to 5.8. Individual gold particles, however, tend to be homogeneous in composition, except in the late hydrothermal quartz veins (Frimmel & Gartz 1997).

The bulk of the gold and uranium is concentrated in the sandy matrix of the conglomerates, but a small proportion is also found on surfaces (e.g., cross-beds, scour surfaces, unconformities between successive cycles of sedimentation, etc.) within the sediment pile where sorting by water took place. Only locally has some gold been remobilized by post-depositional processes. The gold occurs in the matrix in native state, the bulk of it as free particles of small size (average size about 120 μm) that appear to have preserved their original detrital morphology (Utter 1979, Hallbauer & Barton 1987, Minter et al. 1993) and some are attached to large pyrite crystals. Only a few pyrite grains contain inclusions of gold; gold inclusions are more common within grains of pyrrhotite, chalcopyrite, galena, pentlandite, sphalerite, arsenopyrite, and cobaltite. Rich concentrations of gold, uraninite, and other detrital heavy minerals are associated with kerogen, particularly on major scour surfaces. The kerogen is believed to be syngenetic and derived from prokaryotic microbial mats. The high gold values of the fossil algal/bacterial mats (e.g. Carbon Leader Reef) is ascribed to trapping of the gold by microorganisms from Au-bearing colloids or solutions (Mossman & Dyer 1985).

The only primary uranium mineral is uraninite, and it is found as discrete, isolated grains, but more often in groups of five to ten, and less commonly in clusters or stringers of a hundred or more particles. The grain size varies between 30 and 350 μm , the average being about 75 μm . The mineral is extremely well sorted, even if the sorting of the associated heavy minerals is poor. It occurs as rounded grains and is generally interpreted as detrital (Smits 1984). Some uraninite grains contain inclusions of gold, pyrrhotite, pyrite, radiogenic galena, chalcopyrite, quartz, or phyllosilicates. Other uranium minerals include coffinite, which is relatively common in the West Rand goldfield and is thought to be an alteration product of uraninite, and minor amounts of authigenic brannerite.

The most conspicuous mineral in the conglomerate matrix is pyrite, which constitutes 2 to 20% of the matrix, and in many cases there is a strong positive

correlation between the pyrite and gold contents of a reef. Four types of pyrite have been recognized in the Witwatersrand conglomerates (Utter 1978, Hallbauer 1986, Hallbauer & Barton 1987): (a) detrital (allogenic) pyrite, derived from a source external to the Basin or from erosion of pre-existing reefs; (b) authigenic pyrite, formed *in situ* after deposition of the conglomerate by sulfidation of Fe-bearing minerals; (c) synsedimentary pyrite, which often contains significant concentrations of gold; and (d) framboidal pyrite, believed to have been formed by the action of reducing bacteria. Texturally, the detrital pyrite is characterized by compact rounded grains, the authigenic pyrite by idiomorphic crystals, and the synsedimentary pyrite by concretionary forms (oölitic, radial, "mudball"). The detrital origin of the compact rounded pyrite is supported by the truncation of growth zones (identified by the variation in As content) at grain boundaries (MacLean & Fleet 1989).

14.3.2. GRANTS MINERAL BELT, NEW MEXICO, USA

The Grants mineral belt, which is located along the southern edge of the San Juan Basin in northwestern New Mexico, contains slightly more than 50% of the USA uranium resources. Five mining districts — Laguna, Ambrosia Lake, Smith Lake, Crownpoint, and Church Rock — and several subeconomic deposits attest to uranium mineralization along the entire belt that stretches for about 130 km with a width of less than 15 km. Extensive sandstone-type deposits occur in the upper part of the Jurassic Morrison Formation, a sequence of continental fluvial and lacustrine sediments that locally exceeds 150 m in thickness. Some ore has also been mined from the middle Jurassic portion of the Morrison Formation, especially the Todilto Limestone Member, and the Cretaceous Dakota Sandstone (Kelly et al. 1968).

The upper part of the Morrison Formation consists of three members (Granger 1968): (a) the Recapture Member, sandstones and siltstones deposited as a broad alluvial fan; (b) the Westwater Canyon Member (including the Poison Canyon tongue), sandstones and intercalated mudstones deposited in a fluivial-lacustrine environment; and (c) the Brushy Basin Member, predominantly montmorillonitic mudstone derived from volcanic ash, with scattered, discontinuous, lenticular channel sandstones. Up to 30 individual air-fall ash beds have been recognized locally within the Brushy Basin Member (Bell 1986), but the bulk of the mudstone was deposited either by streams that were overloaded with fine volcanic debris or in lakes fed by these streams (Nash et al. 1981). Included in the Brushy Basin Member is a large continuous unit of channel sand, the Jackpile Sandstone, which is directly overlain by the Dakota Sandstone. Uranium orebodies occur within the Westwater Canyon Member and in sandstone lenses within the Brushy Basin Member, particularly the Jackpile Sandstone.

The major deposits in the Grants belt comprise two distinctive types of orebodies (Fig. 14.7): (a) *trend* (also called "run" or "prefault") orebodies, with radiometric ages (>100 Ma.) indicating a late Jurassic to early Cretaceous age of formation; and (b) *stacked* (also called "redistributed" or "postfault") orebodies, which have yielded radiometric ages of 10 Ma or less. The trend orebodies are tabular and peneconcordant,

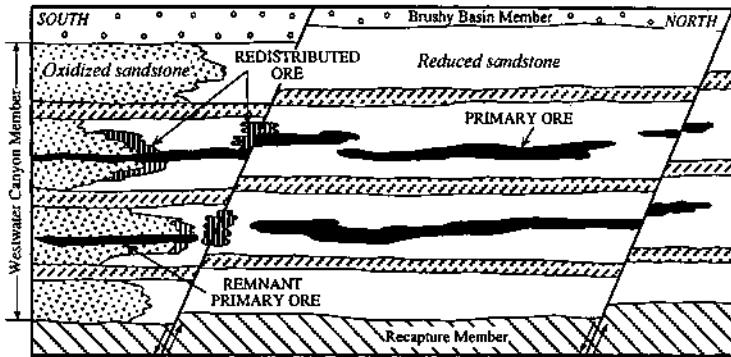


Figure 14.7. Schematic diagram showing the distribution of primary ore, redistributed ore, and remnant ore in the Morrison Formation, San Juan Basin, New Mexico (after Turner-Peterson 1985).

and they “float” in light-gray, reduced sandstone that contains scattered fragments of carbonized plant fossils and some finely disseminated pyrite. The main identified uranium mineral in unoxidized ores is fine-grained coffinite, but very fine-grained uraninite is probably present, and part of the uranium is thought to be in the form of urano-organic compounds (Haji-Vassiliou & Kerr 1973).

The tabular orebodies are coextensive with structureless diagenetic or epigenetic organic matter, which is believed to be the main control of uranium localization (Granger et al. 1961, Moench & Schlee 1967). This is consistent with a positive correlation between the organic carbon and uranium contents of the ore horizons (Fishman & Reynolds, 1986). The organic matter is humate, precipitate formed from humic acids (a general term for aqueous soluble extracts of humus), rather than of hydrocarbon origin (Turner-Peterson 1985). The source of the humic acids and the mechanism of humate precipitation are controversial (see Granger & Santos 1986, Turner-Peterson & Fishman 1986). Granger (1968) suggested that the humate was precipitated at an interface between a brine and meteoric water carrying soluble humic acids that were derived from decaying terrestrial plant material in the Morrison Formation or in Lower Cretaceous units that have been eroded away. Based on regional paleohydrological modeling, Sanford (1992, 1994) proposed a similar model in which the humate was precipitated at a density-stabilized interface between uranium- and humic acid-bearing shallow groundwater and regional groundwater carrying dissolved salts from underlying evaporites. In contrast, Squyres (1980) and Turner-Peterson (1985) argued against two-solution models and in favor of the precipitation of humate from a single solution. According to these models, humic acids were derived from decaying plant material in the Morrison Formation and transported by compaction-driven formation waters; humate precipitation occurred when the solutions became overloaded with cations scavenged from the sediments. The tabular disposition of the

humate-uranium orebodies, however, is better explained by models involving a two-solution interface and the vertical migration of the interface with time. Irrespective of the model, some uranium (and vanadium) transported as soluble organic complexes might have been retained by the humate (Fishman & Reynolds 1986), but uranium enrichment through chelation and adsorption probably continued over a period of time (Hansley 1986).

The stacked orebodies, mostly associated with fracture zones, are younger (Shawe & Granger 1965) and have been interpreted as secondary, formed by the destruction of the earlier-formed tabular (primary) ore by oxidizing groundwater and reprecipitation of the uranium downdip in a reducing environment. They resemble roll-front orebodies in their vertical extension through a sandstone unit, localization along a regional redox boundary that cuts across bedding, and low carbon content (Granger et al. 1961, Rackley 1976). That they do not have the crescent shape, so typical of roll-front orebodies, is perhaps because of the influence of fracture zones on ore localization (Fischer 1974).

14.3.3. ATHABASCA BASIN, SASKATCHEWAN, CANADA

The following summary is based on the articles by Hoeve and Sibbald (1978), Tremblay (1982), and Hoeve and Quirt (1989). The Athabasca Basin is a 100,000 km² fault-controlled, pull-apart, intracratonic depression in northern Saskatchewan filled with unmetamorphosed sediments of the middle Proterozoic Athabasca Group. The floor of the basin is composed of a Lower Proterozoic supracrustal rock suite that overlies a granitoid Archean basement. Both the basement and the supracrustal suite were metamorphosed during the Hudsonian orogeny (≈ 1800 Ma).

The Athabasca Group has a preserved thickness of about 2,200 m. It is composed of a sequence of mature, fluvialite, quartzose sandstones and conglomerates deposited in a shallow-water, braided-stream environment, which is interrupted by two marine intercalations. The sub-Athabasca unconformity is underlain by a kaolinite-rich, locally diaspore-bearing, regolith of deeply weathered hematite-stained basement, which is similar to Recent laterites. Unconformity-type of deposits are located at or in the immediate vicinity of the sub-Athabasca unconformity (see Fig. 14.5) and in the paleoweathering profile. Some vein-type uranium deposits (e.g., Beaverlodge), occur in the northwestern corner of the area, in the Western Craton. These vein-type deposits (also referred to as *Beaverlodge-type deposits*) represent epigenetic mineralization along major faults in the Archean basement, before the deposition of the Athabasca Group, and are not related to the sub-Athabasca unconformity (Tremblay 1978).

The Athabasca unconformity-type of mineralization is localized in steeply dipping faults that run for several kilometers and offset the unconformity. A typical deposit may be up to 2,000 m long, 200 m wide, and a few tens of meters thick, consisting of several ore pods along the strike of the ore-bearing structure. The ore pods consist of a high-grade core at or just below the unconformity. The ore is usually surrounded by a shell of secondary hematite (Fig. 14.8) interpreted as being a redox front. The high-

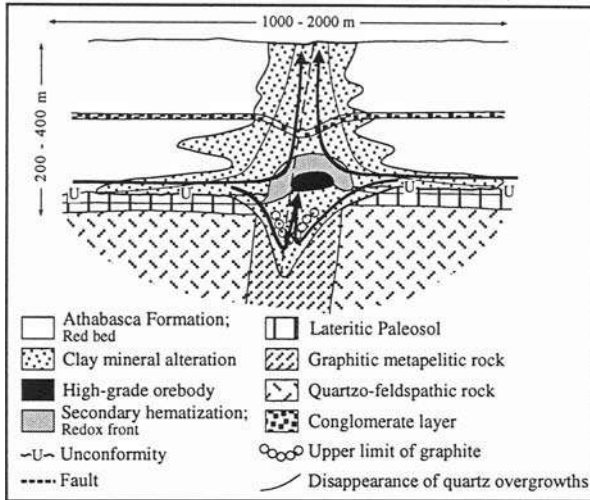


Figure 14.8. Generalized cross section through an idealized unconformity-type uranium deposit of the Athabasca Basin. Arrows indicate inferred dual fluid flow regime. (After Hovee & Quirt 1989.)

grade ore is typically enveloped by a halo of alteration and lower grade ore. The alteration envelope is much smaller and funnel-shaped below the unconformity, except in deposits associated with basement carbonates (e.g., Rabbit Lake deposit).

The mineralization clearly occurred after the deposition of Athabasca sandstone, because the sandstone itself is mineralized. Fluid inclusion studies of quartz and dolomite from the Rabbit Lake deposit and of overgrowths on clastic quartz grains in the Athabasca sequence indicate that the mineralizing fluids were medium temperature (about 160°-220°C), high-salinity (about 30 wt% NaCl equivalent), Na-Ca-Cl brines (Pagel et al. 1980). In almost all unconformity-type deposits of the Athabasca basin, three distinct stages of mineralization, each accompanied by its own alteration of the host rocks, can be recognized and correlated with the evolution of the Athabasca basin. The evidence includes radiometric dates on pitchblende and crosscutting relationships, the abundance of graphitic metasediments in the basement complex, the close spatial relationship of the uranium deposits to faults and the unconformity, and the oxygen-hydrogen isotope ratios of the mineralized zones and alteration haloes indicating the involvement of Athabasca formation waters (Bray et al. 1988). The magmatic activity in the basin appears to have provided only a heat source for fluid circulation, because there is no fluid inclusion or isotopic evidence of direct involvement of magmatic fluids in the mineralization process.

14.4. Mineralogy and Textures

About 135 mineral species are known in which uranium is an essential constituent and another 25 contain uranium as a major though not essential constituent (Stacey and Kaiman 1978). Many accessory minerals — apatite, sphene, zircon, and Nb-Ta minerals — carry U and Th as minor constituents. Some of the uranium in rocks and ores is also held by sorption, especially by organic matter. A uranium-enriched organic material encountered in many uranium deposits has been referred to as *thucholite* after the five main elements (Th, U, C, H, O) it contains. It is generally believed to have formed either by polymerization of fluid hydrocarbons exposed to radioactive emanations or by precipitation of urano-organic complexes.

The majority of uranium minerals are of secondary (supergene) origin. They occur mostly as stains and thus are of limited economic significance, but these hydrated minerals, easily identified by their bright colors, serve as field indicators of primary uranium mineralization. The more common secondary minerals are uranophane [$\text{Ca}(\text{UO}_2)_2 \text{Si}_2\text{O}_7 \cdot 6\text{H}_2\text{O}$, white to deep-yellow], autunite [$\text{Ca}(\text{UO}_2)_4(\text{PO}_4)_2 \cdot 10-12\text{H}_2\text{O}$, lemon-yellow to greenish-yellow], carnotite [$\text{K}_2(\text{UO}_2)_2(\text{VO}_4)_2 \cdot 3\text{H}_2\text{O}$, lemon-yellow], and tyuyamunite [$\text{Ca}(\text{UO}_2)_2(\text{VO}_4)_2 \cdot 5-8 \text{H}_2\text{O}$, bright-yellow].

Unoxidized uranium ores in known economic deposits around the world are characterized by one or more of a handful of uranium minerals (see Table 14.1): uraninite [UO_2], pitchblende [UO_2], brannerite $\{(\text{U}, \text{Ca}, \text{Ce})(\text{Ti}, \text{Fe})_2\text{O}_6\}$, coffinite [$\text{U}(\text{SiO}_4)_{1-x}(\text{OH})_{4x}$], and uranothorite $\{(\text{Th}, \text{U})\text{SiO}_4\}$. Uraninite normally contains some Th and REE in the crystal structure and thorium contents as high as 4-8% ThO_2 have been found in Elliot Lake (Canada) uraninite grains. Pitchblende is the poorly crystalline variety of uraninite and is normally free of Th and REE. It often occurs with a botryoidal or colloform texture and intergrowth with gangue minerals, such as quartz or calcite, gives it a somewhat pitchy luster (Stacey & Kaiman 1978). Pitchblende is typical of low-temperature hydrothermal deposits.

Brannerite is the main uranium mineral in the Elliot Lake district, where it is closely associated with rutile. The "rutile-brannerite aggregates" are believed to have formed through reactions between a uranium-bearing pore fluid and the rutile remnants of intrastatically altered detrital titaniferous minerals, mostly ilmeno-magnetite (Robinson & Spooner 1984a). Uranous titanates of varying composition in the Witwatersrand deposits have been attributed to the reaction of uraninite and leucoxene with post-depositional intrastatal solutions (Smits 1984). Coffinite is common in sandstone-type deposits, although subordinate to uraninite/pitchblende. Uranothorite (uranian thorite) is most common in siliceous granite and syenite bodies and pegmatites, but also occurs in conglomerate-type deposits.

Pyrite of diverse texture and of both allochthonous and authigenic origin (Utter 1978, Dimroth 1979) is the most conspicuous gangue mineral of conglomerate-type deposits, constituting up to 15-25% of the conglomerate matrix and 90% of the sulfides present. The rest of the matrix is composed of silicate minerals (quartz, pyrophyllite, sericite, chlorite, chloritoid, etc.) formed during diagenesis and metamorphism, and a subordinate

suite of heavy minerals (Ti-oxides, chromite, zircon, uranium minerals, gold, base metal sulfides, sulfarsenides, PGE minerals, etc.). The average PGE content of all the Witwatersrand goldfields is less than 12 ppb and the silver content of the gold ranges from about 5% to 16% (Pretorius 1976b).

The sandstone-type deposits lack the heavy mineral suite characteristic of conglomerate-type deposits, but contain variable amounts of pyrite/marcasite. The iron sulfide may be of multiple generations (pre-, syn-, and post-ore) and the pre-ore pyrite, as will be discussed later, may have played an important role in uranium precipitation. Other important constituents are detrital woody and epigenetic amorphous organic matter (humate), authigenic smectite and smectite-illite, chalcopyrite, and vanadium minerals such as roscoelite (vanadium mica) and montroseite [VO(OH)]. On the basis of chemistry, the sandstone-type deposits are divisible into three subtypes (Sanford 1992): (a) vanadium-rich subtype (e.g., UraVan mineral belt, Colorado Plateau) with V:U ratio by weight reaching as high as 20 at places; (b) copper-rich subtype (e.g., White Canyon-Monument Valley area of Utah) with Cu:U ratios ranging from 1 to 18 by weight; and (c) humate-rich subtype (e.g. Grants mineral belt, Colorado Plateau) with moderate amounts of both V and Cu. Ores high in vanadium are generally low in copper and vice versa. Some of the copper-rich ores are relatively enriched in silver. Copper-rich deposits occur in first-generation arkosic sandstones derived from granitic terrains, whereas vanadium-rich deposits occur in multi-cycle sandstones, which may have contained, compared with first-cycle sandstones, a higher concentration of vanadium-bearing ilmenite and magnetite (Fischer and Stewart 1961).

As mentioned earlier, the unconformity- and vein-type deposits are characterized by pronounced hydrothermal alteration and a wide spectrum of sulfides, arsenides, sulfarsenides, Fe-Ti oxides, and organic matter.

14.5. Origin

14.5.1. GEOCHEMISTRY OF URANIUM

In nature, uranium occurs mainly in two valence states: uranous (U^{4+}) and uranyl (U^{6+}). Because of a combination of high charge and large ionic radius (0.93 Å), U^{4+} (the dominant uranium ionic species in magmas) is not easily accommodated in the lattice of common rock-forming minerals, but it readily substitutes for Th^{4+} , Zr^{4+} , REE (especially Ce), and to a limited extent for Ca^{2+} . Thus, as a magma crystallizes, U^{4+} tends to be concentrated in the residual melt until it can enter one of the accessory minerals (such as thorite, zircon, monazite, apatite, sphene) or form minerals of its own (e.g., uraninite). This is the reason why higher concentrations of uranium (up to about 15 ppm) are usually associated with late magmatic differentiates, such as granitic rocks, which are also believed to be the ultimate source of the metal in sediment-hosted uranium deposits. If the granite weathers in an oxidizing environment, the uranium may be oxidized and removed in solution, but thorium having no oxidized state would

remain behind as an insoluble resistate. Thus, uranium deposits involving solution transport of uranium should have a relatively high U:Th ratio.

The behavior of uranium in aqueous environments is governed by the stability of various uranous and uranyl complexes as a function of temperature, Eh-pH, P_{CO_2} , and concentration of the ligands. Low-temperature stability relations of these complexes, based on available thermodynamic data, have been discussed in detail by Langmuir (1978). A few of the salient points relevant to the transport and deposition of uranium in sedimentary environments are summarized below.

Because of the extremely low solubility of uraninite in aqueous solutions of normal pH's (Parks & Pohl 1988), the concentrations of uranous hydroxyl complexes are usually below 0.05 ppb and so undetectable in natural waters. Thus, in normal sedimentary environments not much uranium is transported as uranous complexes. In aqueous solutions, U^{4+} is readily oxidized to $(\text{U}^{6+}\text{O}_2)^{2+}$ which forms stable complexes with hydroxyl, carbonate, fluoride, chloride, sulfate, and phosphate ions. At typical ligand concentrations in groundwater, the most important uranyl complexes at 25°C are formed with fluoride under acidic conditions (pH <4), with phosphate under near-neutral conditions (pH = 5 to 7.5), and with carbonate under alkaline conditions (pH >8). The stability relationships of the various uranous and uranyl minerals found in sediments, relative to the aqueous complexes, are conveniently depicted in Eh-pH diagrams constructed for appropriate aqueous systems. An example is presented in Figure 14.9, which illustrates the stability of uraninite, one of the most important ore minerals of uranium in sedimentary environments, in the system $\text{U-O}_2\text{-CO}_2\text{-H}_2\text{O}$ at 25°C and $P_{\text{CO}_2} = 10^{-2}$ atm. It can be seen from this Eh-pH diagram that, under the natural pH conditions of near-surface environments (pH = 4 to 9), uranium would be transported in an aqueous solution mainly as uranyl carbonate complexes and precipitated as uraninite if the Eh was lowered to some appropriate level. Similar Eh-pH diagrams may be constructed for other pertinent systems (subject to the availability of thermodynamic data), assuming reasonable concentrations of the relevant ligands, to depict the stability relationships between aqueous complexes and other uranium minerals such as carnotite (Langmuir 1978) and coffinite (Galloway & Kaiser 1980).

The behavior of uranyl complexes at elevated temperatures is not well known. Using published thermodynamic data, Kojima et al. (1994) calculated the relative abundances of various dissolved uranium complexes in saline solutions at 100°C ($m_{\text{NaCl}} = 5 m$), 150°C ($m_{\text{NaCl}} = 5 m$), and 200°C ($m_{\text{NaCl}} = 7 m$), with the a_{O_2} defined by hematite stability. Their calculations show that (a) at the three temperatures considered, UO_2Cl^+ , $\text{U}(\text{OH})_4^0$, and $\text{UO}_2(\text{CO}_3)_3^{4-}$ dominate under acidic (pH <4), slightly acidic (pH = 4 to 6), and neutral to alkaline (pH >6) conditions, respectively, and (b) the relative abundances of UO_2Cl^+ and $\text{UO}_2(\text{CO}_3)_3^{4-}$ increase with increasing temperature. Thus, uranium can be transported as UO_2Cl^+ in acidic solutions (e.g., Alligator Rivers' ore fluids; Wilde et al. 1989), or as $\text{UO}_2(\text{CO}_3)_3^{4-}$ in near-neutral range of pH (e.g., Athabasca ore fluids). Uranium may be transported also as soluble organometallic

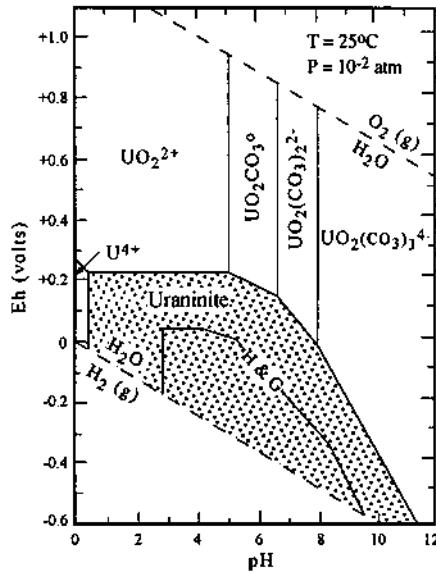
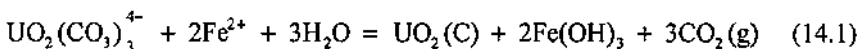


Figure 14.9. Eh-pH diagram for the U-O₂-CO₂-H₂O system at 25°C and $P_{\text{CO}_2} = 10^{-2}$ atm. Uraninite, UO₂ (c), solution boundaries are drawn at 10^{-6} m (0.24 ppm) dissolved uranium species. "H & G" denotes the boundary of the uraninite stability field according to Hostetler and Garrels (1962). (After Langmuir 1978.)

complexes. An informative summary of the organic geochemistry related to the transportation and precipitation of uranium has been presented by Nash et al. (1981).

14.5.2. ORE ACCUMULATION

The primary uranium minerals in economically important deposit types occur in the lower oxidation state, i.e., as uranous minerals, such as uraninite and coffinite. As uranous complexes are much less soluble than uranyl complexes, the accumulation of uranous minerals is attributed either to transport as detrital particles or to reduction of uranyl complexes at the site of deposition. The bulk composition of the ore environments suggest three likely reductants: organic material, reduced sulfur species (H₂S or HS⁻), and Fe²⁺. Reduction by Fe²⁺ involves oxidation of Fe²⁺ to Fe³⁺ by reactions such as (Langmuir 1978):

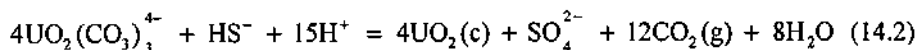


Uranous minerals are seldom found in paragenetic association with ferric oxides or hydroxides in low-temperature deposits, but such an association is common in high-

temperature vein deposits, suggesting that Fe^{2+} may be an effective reductant only at higher temperatures (Rich et al. 1977).

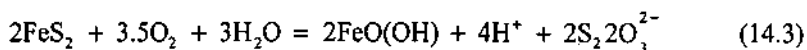
In sandstone-type deposits, the frequent association of uranium mineralization with organic matter, especially the partial to complete replacement of coalified plant fragments by uranium minerals, attests to the ability of organic matter to reduce soluble uranyl complexes to insoluble uranous minerals. The mechanism of this reduction is not entirely clear. From thermodynamic reasoning and experiments, Andreyev and Chumachenko (1964) concluded that the process was one of direct reduction, its efficiency varying with pH and the kind of organic matter. They proposed a two-step process: adsorption of U^{6+} on the solid organic matter forming complexes and salts with its functional groups (carboxyl, carbonyl, hydroxyl, etc.); and reduction of U^{6+} in the uranium-organic complexes to U^{4+} , with simultaneous oxidation of the organic matter resulting in the regeneration of the functional groups. The process continues until either all the organic matter is consumed or there is no further replenishment of U^{6+} -bearing solution. The other proposed mechanism of organics-induced reduction is through bacterially mediated generation of H_2S (Adler 1974, Rackley 1976).

Reduction of uranyl complexes by aqueous sulfide species (H_2S or HS^-) may be represented by reactions such as (Langmuir 1978):



Possible mechanisms for the availability of sulfide species include bacterial action or thermal decomposition of sulfur-bearing compounds in sour gas or fluids introduced into the host rocks through faults (Eargle & Weeks 1961, Cathey 1980), decomposition of pre-ore pyrite in the host rocks (Granger & Warren 1969, Rackley 1976), and influx of magmatic hydrothermal fluids that commonly contain H_2S and other reduced sulfur species (Burnham 1979).

Both biogenic and inorganic processes have been invoked to explain the involvement of pre-ore pyrite in the reduction process. The proposed biogenic model is quite complex (see Rackley 1976, Fig. 16), but in essence it relies on the action of two different types of bacteria: one type (e.g., *Thiobactillus ferroxidans*) to oxidize pyrite to soluble SO_4^{2-} ; and the other type (e.g., *Desulfovibrio desulfuricans*) to reduce the SO_4^{2-} to aqueous H_2S (or HS^-) by a process that is coupled to the oxidation of organic matter. The aqueous sulfide species acts as a reductant for the precipitation of uranous minerals and its reaction with available non- FeS_2 iron in the host rock provides a mechanism for the generation of ore-stage FeS_2 minerals. The abiogenic model proposed by Granger and Warren (1969) is also a two-step oxidation-reduction process, but without the involvement of bacteria or organic matter. Under hydrous conditions and oxidation potentials in which sulfide minerals are unstable, but with limited amounts of available oxygen, FeS_2 oxidizes mainly to metastable species — sulfite (SO_3^{2-}), bisulfite (HSO_3^-), and thiosulfate ($\text{S}_2\text{O}_3^{2-}$) — by reactions such as:



The metastable species eventually disproportionate to H_2S and SO_4^{2-} . Because SO_4^{2-} is kinetically inert to low-temperature abiogenic oxidation-reduction reactions, whereas H_2S remains an active reducing agent, the net result of limited oxidation is to produce a strongly reducing environment conducive to uranium localization. Some of the intermediate sulfur species or H_2S may recombine with Fe^{2+} to form the FeS_2 minerals associated with uranium ores. Spirakis (1981) suggested that a similar change to a more reducing environment could be accomplished by the mere cooling of a mineralizing solution containing both H_2S and SO_4^{2-} , because oxidation by SO_4^{2-} is kinetically impeded at lower temperatures.

Uranium may also be trapped by adsorption on colloidal matters such as ferric oxyhydroxides, Mn- and Ti-oxyhydroxides, zeolites, and clays, but this was not a major concentrating process in most uranium deposits (Nash et al. 1981).

14.5.3. CONGLOMERATE-TYPE DEPOSITS

The origin of conglomerate-type uranium deposits has been controversial for almost as long as these deposits have been mined. The persisting controversy is mainly between two very different genetic models: the *paleoplacer model* (or, more appropriately, the *modified paleoplacer model*), which has a large following (e.g., Pretorius 1976b, 1981, Grandstaff 1980, Schidlowski 1981, Hallbauer 1986, Minter 1990, Smits 1984, Smith 1989, Reimer & Mossman 1990b, Roscoe & Minter 1993, Frimmel et al. 1993, Robb & Meyer 1995, Frimmel & Gartz 1997); and the less popular epigenetic *hydrothermal-replacement model* (e.g., Clemmey 1981, Phillips & Myers 1989, Phillips et al. 1987, 1989; Phillips & Law 1997, Barnicoat et al. 1997).

The paleoplacer model, the current basis of exploration strategy within existing goldfields, considers the initial U-Au gold mineralization to be of placer (detrital) origin, but recognizes that the mineralogy and textures have been modified by later diagenesis and metamorphism, including small-scale mobilization of certain components. Evidence for a synsedimentary origin of most of the Witwatersrand gold and uranium, particularly in the conglomerate reefs, are: (a) close association of U-Au mineralization with paleosurfaces of erosion that separate unconformity-bounded formations in the Witwatersrand stratigraphic sequence (Pretorius 1976b, Minter et al. 1988, Minter 1990); (b) frequent occurrence of U-Au mineralization in sedimentary structures, such as fluvial channelways, cross-bed foreset laminae, and minor deflation surfaces (Smith & Minter 1980, Pretorius 1981); (c) presence of detrital uraninite, gold, and pyrite in the matrix of reef conglomerates (Utter 1978, Schidlowski 1981, Smits 1984, MacLean & Fleet 1989, Minter et al. 1993); (d) highly variable U:Th ratios in the uraninite with high Th contents (Grandstaff 1981), suggesting that the uraninite originated from granitic and pegmatitic source rocks, and not within the basin by low-temperature hydrothermal fluids; (e) a REE spectrum for the uraninites similar to that

for uraninites in likely source rocks for detrital particles such as granites, but quite distinct from the spectrum for hydrothermal uraninites such as in Athabasca deposits (Fryer & Taylor 1987); (f) a lack of hydrothermal alteration and structural control on mineralization, features which are typically associated with epigenetic hydrothermal deposits; and (g) radiometric ages of round pyrite, sphalerite, and osmiridium indicating an older age than the maximum age of the Witwatersrand basin (e.g., Hart & Kinloch 1989). Responses to the criticisms raised against the paleoplacer model are summarized in Table 14.3. Mineralogical and textural modifications produced by post-depositional metamorphic and alteration processes include: authigenic growth of gold and sulfides (which coexist with allogenic gold and sulfides); preferential association of remobilized gold with paragenetically-late phases, such as authigenic sulfides, kerogen, and secondary chlorite; occurrence of gold as fracture-fillings in, and as overgrowths on, allogenic pyrite, which only occasionally contains primary gold inclusions; partial replacement of compact pyrite by secondary gold; and homogenization of gold particles on a hand specimen scale with respect to Ag and Hg by intercrystalline diffusion (Smits 1984, Robb & Meyer 1995; Frimmel et al. 1993, Frimmel & Gartz 1997). A small proportion of the gold was formed by the recrystallization of detrital gold (Utter 1979) and uraninite was extensively altered to secondary minerals such as brannerite.

A strong case for a modified placer origin has also been presented for the Elliot Lake-Blind Lake (Canada) conglomerate-type uranium deposits (e.g., Roscoe 1969, Theis 1979, Robinson & Spooner 1984a). The reader is referred particularly to the paper by Robinson and Spooner (1984a) which discusses many post-depositional features which might be mistaken as evidence of hydrothermal uranium mineralization.

14.5.4. SANDSTONE-TYPE DEPOSITS

The sandstone-type uranium deposits are clearly not syngenetic. There is a general lack of concordance between the orebodies and the stratification of the host sandstone. Also, the uranium minerals fill interstices between detrital fragments and replace them. There is little doubt that uranium was introduced by aqueous solutions into the host sandstone after its deposition.

As the primary uranium-bearing phases (pitchblende, coffinite, urano-organic mixtures) in these deposits are typically fine grained, poorly crystalline, and fractured on a micro-scale, their high specific surface areas are conducive to outward diffusion of Pb (radioactive daughter of ^{238}U), and even of uranium itself, in an oxidizing environment (Ludwig et al. 1984). Consequently, U-Pb isotopic ratios of the primary uranium-bearing phases show a lot of scatter and yield mostly discordant ages. Minimum ages obtained from some studies on tabular orebodies in the Colorado Plateau region, however, suggest that these formed shortly after the deposition of the host sediment, perhaps during, or even before, the sedimentation of the overlying strata. For example, Ludwig et al. (1984) obtained a minimum age of 130 Ma for the tabular ores of the Ambrosia Lake district (Grants mineral belt) located in the upper part of the Jurassic Morrison Formation. This age is much older than that of the overlying

TABLE 14.3. Summary of argument against, and response in support of, the *modified* placer hypothesis for the origin of Witwatersrand conglomerate-type uranium deposits

Argument against	Response
1. Disproportionately large amount of pyrite relative to Fe-Ti-oxides (ilmenite, magnetite, hematite) in Witwatersrand conglomerate horizons, although magnetite is stable in anoxic conditions and it is abundant in underlying and overlying strata (Clemmey 1981, Phillips et al. 1987, Phillips & Myers 1989).	There is no evidence for widespread sulfidization of Fe-Ti oxide minerals, as envisaged by Phillips et al. (1987). The generally low amounts of Fe-Ti oxide minerals (1-6 % of the total heavy minerals) is best explained by a combination of two factors (Reimer & Mossman 1990a): (a) a large component of recycled older sedimentary material in the source area, in which the Fe-Ti mineral grains had been altered to rutile-leucoxene prior to erosion; and (b) in situ alteration of Fe-Ti mineral grains to rutile-leucoxene, with authigenic brannerite providing an important sink for titanium. Moreover, predominance of detrital pyrite over Fe-Ti oxide minerals is characteristic of virtually all South African Archean conglomerates, irrespective of Au-U mineralization.
2. The rounded shape of pyrite grains, the commonly used evidence for a detrital origin of pyrite, is not diagnostic, whereas observed replacement textures are consistent with pervasive sulfidation of Upper Witwatersrand rocks (Phillips et al. 1989).	There is evidence of extensive post-depositional redistribution of pyrite, and even of complete replacement of compact rounded pyrite grains by gangue minerals. But the truncation of growth zones (marked by variation in the As content) at the grain boundaries of this textural variety of pyrite is "highly suggestive of mechanically abraded pre-existing growth-zoned pyrite grains", as would be expected for detrital pyrite (MacLean & Fleet 1989).
3. The reported hydraulic equivalence between uranium, gold, quartz pebbles, and pyrite in the reefs, perhaps the strongest evidence for the placer origin of the gold, is based on a fallacious premise, because virtually all gold has secondary shapes and the present size cannot be used to estimate hydraulic equivalence (Phillips et al. 1987).	A large portion of the gold particles appears to have retained the original shape (Utter 1979, Halbauer & Barton 1987), and the <i>modified</i> placer model allows for recrystallized morphologies of detrital grains. Keon (1961) had suggested hydraulic (settling) equivalence between uraninite, chromite, and zircon, but hydraulic equivalence between gold and associated quartz pebbles has never been demonstrated or claimed, nor is it expected because of the complex sorting processes during the transport and deposition of detrital particles (Smith 1989).
4. A detrital origin of the vast amount of gold in the Witwatersrand would require an unrealistic scenario for the source area — the equivalent of one giant deposit (~1,000 tonne Au) for each of the 40 large Witwatersrand mines.	Gold transported from the source area involved some particulate gold (under oxygen-deficient conditions) but most of it was in solution or in colloidal form (Reimer 1984, Hutchinson & Viljoen 1988). Gold was deposited in braided alluvial fans from which it was, at least in part, reworked and concentrated mechanically in the conglomerate horizons (Mossman & Dyer 1985). [See text for a discussion of the source problem.]
5. The placer hypothesis fails to predict that otherwise subeconomic reefs may carry economic grades of gold downdip from unconformities below the major reefs (Phillips et al. 1987).	There is no indication of an increase in grade in subeconomic reefs close to intraformational unconformities (Minter 1989), although some high-grade ores may be related to remobilization by post-depositional hydrothermal activity.

TABLE 14.3 (continued)

Argument against t	Response
6. Numerous examples from Witwatersrand mines suggest that a structural control may exist in the gold distribution pattern (Phillips et al. 1989).	The examples cited have been misinterpreted (Minter 1989, Reimer & Mossman 1990b).
7. There is no diagnostic evidence for an early atmosphere with less oxygen than today, a requirement for transport of uraninite as detrital particles (Phillips et al. 1987).	Studies of paleosols indicate that the late Archean atmosphere had a much lower oxygen partial pressure compared with the present (Pinto & Holland 1988). Moreover, an oxygen-free atmosphere may not be a prerequisite for the transport of uraninite as detrital particles (Grandstaff 1980, Simpson & Bowles 1981, Robinson & Spooner 1984b). [See text for a discussion pertaining to the evolution of atmospheric oxygen.]

Dakota Sandstone (Rb-Sr isochron age 92-96 Ma, Brookins 1981), but quite close to the age of the Morrison Formation (142 ± 33 Ma, Brookins 1980). In view of the uncertainties involved, Ludwig et al. (1984) concluded that the time of uranium mineralization "might have overlapped the early part of the long erosional interval represented by the Jurassic-Cretaceous unconformity." Such an age would be consistent with the introduction of a large volume of oxygenated, possibly metal-bearing, meteoric water into the formation below the unconformity. Stacked orebodies in the Ambrosia Lake district, interpreted as redistributed tabular ore, gave concordant to nearly concordant ages of 3.5 to 12.5 Ma and, thus, are distinctly epigenetic. Similar slightly younger ages of mineralization have also been reported for the roll ores of the Wyoming districts hosted by sediments of Eocene age (Fischer 1974) and those of the Texas Coastal Plain hosted by the Miocene Oakville Sandstone (Ludwig et al. 1982).

The temperature of formation of sandstone-type uranium deposits is not well constrained. Indirect estimates based on the upper stability limits of ore minerals (Coleman 1957) and the temperature dependence of extraction of residual humic acids in coalified logs sampled from mineralized horizons (Berger & Chandler 1960) suggest a temperature of about 100°C for uranium mineralization. Fluid inclusion measurements on associated calcite and barite, rather limited because of small size and paucity of inclusions, also suggest a similar temperature and a low salinity of the mineralizing fluids (Poty & Pagel 1988). Thus, the sandstone-type uranium deposits are believed to have formed from low-temperature, fairly dilute aqueous solutions that transported uranium as soluble uranyl complexes, most likely as uranyl carbonate complexes, in slightly alkaline solutions.

Almost all genetic models for tabular uranium deposits in the Colorado Plateau region visualize groundwater moving along the host beds as the mineralizing solution and organic matter in the host rocks as the reductant for ore precipitation, although this scenario does not explain either the tabular nature of the orebodies or their localization

relative to the distribution of carbonaceous detritus. As discussed earlier, the humate-uranium tabular orebodies in the Grants mineral belt, hosted by the Upper Jurassic Morrison Formation, is best explained by a two-step process: precipitation of humate layers from a single solution or at the interface of two solutions; and continued enrichment of these layers in uranium. However, tabular deposits hosted by the Morrison Formation in other Colorado Plateau districts lack such humate-uranium ores, requiring the formulation of different genetic models. For example, the origin of the tabular orebodies in the Henry Basin of Utah, which occur only in rocks containing abundant organic material, has been attributed to uranium precipitation at the interface of U-bearing meteoric water and SO_4^{2-} -bearing basinal brine, with the reducing environment provided by the bacterial reduction of SO_4^{2-} to H_2S (Wanty et al. 1990, Northrop & Goldhaber 1990). Hansley and Spirakis (1992) argued that humate was crucial to the formation of all Morrison-hosted tabular deposits, but many became impoverished in humate because it was destroyed during various stages of post-ore diagenesis. It is tempting to speculate a similar history as well for tabular deposits hosted by the Chinle Formation.

It is widely accepted that roll-front deposits represent uranium precipitation at a reduction front encountered by oxygenated, uranium-bearing groundwater moving downdip by gravity along gently dipping sandstone beds. It was a dynamic system in the sense that continued supply of oxygenated groundwater caused dissolution behind (up-dip from) and reprecipitation of ore constituents ahead of (downdip from) the concave roll margin, resulting in a progressive downdip migration of the roll-front and the development of a tongue of oxidized rock. The oxidized zone may contain small pockets of uranium ore (e.g., in Wyoming districts), remnants that were somewhat protected from oxidation.

Two genetic models have been proposed for the concentration of uranium in roll-front deposits. Both involve oxidation of FeS_2 in the oxidized tongue and generation of H_2S downdip for the precipitation of uranous minerals and ore-stage FeS_2 , but one emphasizes biogenic processes requiring organic matter to provide bacterial nutrients, whereas the other emphasizes inorganic processes, which are independent of organic matter. The biogenic model is clearly inapplicable to deposits lacking organic material in the reduced host rocks, such as those of the Texas Coastal Plain hosted by the Catahoula Tuff and Oakville Sandstone. It is also difficult to imagine how the sparsely scattered coalified plant debris, typical of reduced rocks associated with other roll-front deposits (e.g. Shirley Basin), could provide bacterial nutrients along the entire roll-front (Granger & Warren 1969).

The fundamental similarity between the tabular and roll deposits lies in the localization of both at oxidation-reduction interfaces. The differences are probably related to different hydrodynamic conditions of the respective paleoaquifer system, which resulted in a down-dip migrating redox front in the case of roll deposits, but a static or vertically upward migrating redox front in the case of tabular deposits. Shawe (1956) postulated that the formation of roll orebodies was linked to the presence of

mudstone interbeds in the sandstone that funneled a moving sheet of oxygenated water into smaller channels. The significance, if any, of the age difference between the tabular deposits (dominantly Mesozoic) and the roll deposits (dominantly Tertiary) in USA is not known.

14.5.5. UNCONFORMITY-TYPE DEPOSITS

To accommodate the critical features of the unconformity-type deposits — the consistent spatial association of the deposits with unconformity, mineralization both below and above the unconformity, and the strong structural control on ore localization — Nash et al. (1981) proposed what Marmont (1987) has termed a “polygenetic, multiphase model”. The emplacement of uranium deposits, according to this model, involved four evolutionary stages: (1) synsedimentary or diagenetic enrichment of uranium in the sedimentary rocks within which the deposits occur or with which they are associated; (2) upgrading of uranium concentration during metamorphism (probably similar to the process of ore formation in ultrametamorphic deposits such as Rössing); (3) supergene enrichment at the unconformity; and (4) remobilization under the cover of younger sediments. There is no evidence of a sedimentary preconcentration of uranium (stage 1), but the lack of such evidence may well be due to redistribution of uranium during metamorphism and recent near-surface leaching. The most problematic aspect of the model is the timing of events. Radiometric dates, where available, indicate that uranium mineralization postdated the deposition of rocks above the unconformity.

A model that seems to account for most of the features of the Athabasca deposits is the *diagenetic-hydrothermal model* proposed by Hovee and Sibbald (1978) and elaborated in a series of later papers (e.g., Hovee et al. 1980, Hovee & Quart 1989). The model, involving a coupling of diagenesis and ore formation to basin evolution, envisages a dual flow regime on a deposit scale: a large-scale free convection in the Athabasca sandstone (redbeds) aquifer above the unconformity, driven by the overall heat flow through the basin floor; and a small-scale forced convection in the basement, driven by channeled heat through graphite-rich metapelitic rocks below the unconformity (Fig. 14.8). Uranium mineralization occurred where the descending metal-bearing, oxidizing Athabasca formation waters intersected a reducing environment in the form of either carbonaceous metasediments in the basement or methane-bearing fluids ascending through faults and fractures in the basement. The site of primary mineralization relative to the unconformity in a given deposit was determined by the position of the reduction front during an advanced stage of basin evolution under conditions of deep burial and intense diagenesis. In broad terms, the model is similar to the diagenetic model for SSC deposits discussed earlier (Ch. 12). According to Hovee and Quirt (1989), the deposit type would, to a large degree, depend on the mineralogical and chemical composition of the redbed source rocks and their diagenetic history. Mineralogically mature redbeds, such as those of the Athabasca Basin, would tend to generate U-Ni-Co-As deposits and mineralogically immature redbeds, such as those of Kupferschiefer or Central Africa, might produce SSC deposits.

The diagenetic-hydrothermal genetic model is consistent with the three stages of mineralization and alteration in the Athabasca Basin (discussed earlier). A broadly similar origin also appears to be applicable to the Nabarlek, Jabiluka II, and Koongarra unconformity-type deposits in the Alligator Rivers uranium field, Australia. The narrow range of Sm-Nd ages for these deposits (1600-1650 Ma) indicates that the initial uranium mineralization took place soon after the deposition of the unconformably overlying Kombolgie Formation (1600 Ma). The age data are consistent with models of ore deposition involving reaction of hot, oxidized, U-bearing, formation-meteoric waters derived from the sandstones and volcanics of the Kombolgie Formation with reducing metasediments of the Lower Proterozoic basement (Maas 1989).

14.5.6. VEIN-TYPE DEPOSITS

Vein-type deposits are too variable in character (see Table 14.2) to fit a single genetic model. An important constraint is that the deposits represent epigenetic mineralization in open spaces, requiring the derivation of uranium from some uranium-enriched sources by hydrothermal fluids. Another is the common association of pitchblende and hematite in these deposits, suggesting oxidizing ore fluids. Available fluid inclusion data, as summarized by Rich et al. (1977) and Poty and Pagel (1988), indicate that ore fluids for most vein-type deposits were moderately hot (about 200°C or less) and of low to moderate salinities (<15 wt% NaCl equivalent). Notable exceptions are the high temperatures for the Beaverlodge district and the Limousin region (>300°C), and the high salinities reported for the Beaverlodge and Great Bear Lake districts (up to 35 wt% NaCl equivalent). The calculated $\delta^{18}\text{O}$ values for the ore fluids for the Great Bear Lake district approximate the value of present-day seawater, which led Robinson and Ohmoto (1973) to suggest deep-circulating seawater as the ore fluids for this district. Oxygen and carbon isotope studies on many other deposits, however, indicate a component of meteoric water in the mineralizing fluid (Ruzicka 1993b).

The majority of vein-type deposits appear to be spatially related to granitic intrusives, but there is no compelling evidence for magmatic-hydrothermal ore fluids, even for the intragranitic vein deposits hosted by Hercynian granites in the Massif Central, France. As uranium tends to be concentrated, along with Th, in late magmatic differentiates such as granites, the source of uranium for these uranium vein deposits has been ascribed mostly to remobilization of uranium in the granites and surrounding metamorphic rocks by circulating hydrothermal fluids. Perhaps, a necessary condition for producing uranium deposits in such a setting is a later heat source that would force circulation of formational and meteoric waters (LeRoy 1978).

Rich et al. (1977) proposed three generalized models for the origin of vein-type uranium deposits: (a) very shallow uranium leaching by oxidizing surface waters, followed by pitchblende deposition at depth (supergene model); (b) uranium leaching by deeply circulating oxidizing waters of surface origin, followed by pitchblende precipitation (deep meteoric water model); and (c) uranium leaching by deeply circulating oxidizing waters which are not of direct surface origin (e.g., magmatic,

metamorphic, or connate waters), followed by equilibration with a hematitic aquifer and subsequent deposition of pitchblende (non-meteoritic water model).

Fluid inclusions in vein-type uranium deposits commonly contain more than one mole% CO_2 , suggesting transport of uranium as uranyl carbonate complexes. Also, a correlation between uranium ore grade and the CO_2 concentration in associated inclusion fluids and the lower CO_2 contents of fluid inclusions in post-pitchblende minerals, compared with those in pre-pitchblende minerals, in some vein deposits are compatible with pitchblende precipitation from highly carbonated solutions due to loss of CO_2 . However, loss of CO_2 should also result in the precipitation of carbonates and probably increase the oxidation state of the residual solution. The lack of coprecipitation of carbonates with pitchblende in vein deposits as well as the evidence of reducing conditions (precipitation of sulfides) following the precipitation of pitchblende argue against CO_2 loss as the main mechanism of pitchblende precipitation (Rich et al. 1977). Reduction of U^{6+} complexes to pitchblende by Fe^{2+} is an attractive mechanism in view of the close paragenetic association between pitchblende and hematite (reflecting concurrent oxidation of Fe^{2+} to Fe^{3+}) in the vein deposits. Other likely reductants include reduced sulfur species and organic carbon, either transported with the ore fluids or derived from the wallrocks.

14.6. Metallogenesis

14.6.1. SOURCES OF URANIUM

Except for disseminated uranium mineralization in silicic and alkalic plutons, and possibly volcanogenic and contact metamorphic-type uranium deposits, there is little evidence for a direct magmatic source of the uranium. Sources of uranium for major types of uranium deposits appear to be pre-existing rocks enriched in uranium by some earlier process. From a consideration of spatial association, uranium tenor, leachability, and composition of the ore material, the most likely uranium sources are Precambrian basement gneisses and metasediments, anatectic granites, silicic tuffs, and oxidized sediments (redbeds) linked to a provenance of uranium-enriched rocks.

Granitic plutonic and volcanic rocks are considered to be particularly favorable sources of leachable uranium, because they are often enriched in uranium (>5 ppm U) and because of experimental studies (e.g., Rosholt et al. 1971, Zielinski 1979) suggesting significant leachability of uranium in such rocks by alkaline, oxygenated groundwater. Intragranitic vein-type deposits, such as those in the Massif Central (France) associated with uraniferous leucocratic granites, present the best setting for a granitic source. For unconformity-type deposits and many vein-type deposits, the basement metasediments appear to have provided much of the uranium.

Clear identification of the source of the uranium (and other metals) in sandstone-type deposits remains elusive. A granitic source for the deposits in Wyoming Tertiary basins is compatible with anomalously high uranium contents of the upland granites

(Rosholt & Bartel 1969). The deposits throughout the Colorado Plateau province also occur adjacent to areas of exposed Precambrian rocks which contain anomalous concentrations of uranium. A possible alternative source for these deposits as well as those of the Black Hills region is tuffaceous material that occurs in the host rocks and surrounding horizons (Fischer 1970). Volcanic ash is the most likely source of the uranium deposits in the Texas Coastal Plain, and many authors have placed particular emphasis on the volcanic debris in the Catahoula Formation (Eargle et al. 1975, Galloway 1978, Cathey 1980). Glassy volcanic ash or ash-rich sediments are considered viable sources of uranium because of their high, or potentially high, trace uranium contents and the relative ease with which uranium is released from such material during diagenesis or weathering (Rosholt et al. 1971, Walton et al. 1981, Zielinski 1983).

The source of detrital uraninite in the conglomerate-type deposits is believed to be the granitic rocks of the Archean granite-greenstone terrane, the basement to the sedimentary basins. Based on the suite of detrital minerals (smoky quartz, uraninite, microcline, pyrite, monazite, zircon, chromite) and the types of fluid inclusions in detrital quartz (aqueous inclusions with $\text{CO}_2 \pm$ solid minerals), Robinson and Spooner (1982) concluded that the source rock for the Elliot Lake uraniferous conglomerate was a uraninite-bearing, pegmatitic, alaskitic granite, similar to the host rock of the Rössing deposit in Namibia. A granitic source of uranium is also compatible with the $\delta^{18}\text{O}$ values of quartz pebbles from the Huronian district — a strong mode at about 10‰, which is identical to the mode for Archean granites (Vannemann et al. 1992).

Most authors agree on a granitic source for the detrital uranium and other clastic components in the Witwatersrand conglomerate-type deposits, but the source of the large amount of associated gold (as well as of Witwatersrand sediments dominantly composed of quartz, sericite, and pyrite) is controversial and unresolved. Pretorius (1976b) proposed that the detrital uraninite (dated at 3040 ± 100 Ma in the basal members of the Witwatersrand Sequence) and gold were derived from two different populations of mineralized rocks in the Archean granite-greenstone terrane of the Kaapvaal craton: the gold (as well as pyrite, Co-Ni sulfides, chromite, and platinoids) from greenstones similar to those of the Barberton Mountain Land (older than 3250 Ma) or from younger greenstones such as those of the Murchison greenstone belt (3070-2970 Ma; Poujol et al. 1996); and the uraninite (as well as quartz, zircon, cassiterite, and garnet) from younger granites (2900-3250) that enveloped the belt. However, the evidence for a greenstone source of gold is equivocal. Some studies have reported similar U-Pb isotopic composition (Koppel & Saager 1974) and trace element trends (Saager 1981) between allogenic pyrites in the Witwatersrand reefs and pyrites from gold deposits in the greenstone belts. Other studies have pointed out the lack of similarity in the trace element compositions of pyrites (Utter 1978) and gold (Hallbauer & Barton 1987) from these two populations. The $\delta^{18}\text{O}$ distribution of quartz pebbles from the conglomeratic ores of the Witwatersrand district is more complicated than that of the Huronian district. Vannemann et al. (1992) interpreted the broad $\delta^{18}\text{O}$ distribution (about 9 to 15‰) skewed toward high $\delta^{18}\text{O}$ values as compatible with a

dual source as proposed by Pretorius (1976b). Large quartzite and chert clasts from various gold-bearing reefs analyzed by Barton et al. (1992) gave a similar range (8.7 to 13.1‰), but a distinct clustering at 10-12‰. From a comparison with $\delta^{18}\text{O}$ values of potential source materials in the region, they concluded that the source for the quartz clasts was no longer exposed. In any case, a granitoid-greenstone provenance of gold does not explain the unique richness of the Witwatersrand Basin. There is clear evidence that Archean granite-greenstone terranes formed the hinterlands to other Proterozoic intercratonic basins, both older and younger than the Witwatersrand, in which apparently similar processes and environments of sedimentation had prevailed. Why, then, is the Witwatersrand Basin virtually unique in the extent and degree of gold mineralization? Also, why are there no placer gold accumulation even remotely comparable to that in the Witwatersrand in the Canadian and Yilgarn cratons, which contain a much greater abundance of gold deposits compared with the Kaapvaal craton?

A viable source for the Witwatersrand gold must satisfy the mass balance requirement, estimated by Phillips et al. (1987) as the equivalent of one giant deposit (1,000 tonnes of contained Au) for each of the 40 large Witwatersrand mines, if the gold was detrital in origin. This constraint has led to several alternative proposals. Reimer (1984) proposed that some detrital gold was derived from the greenstone belts and older arenaceous sediments, but much of the gold was leached from a variety of sources (gold deposits, mafic and ultramafic volcanic rocks, and auriferous banded iron-formations) and transported in solution to the basin. Hutchinson and Viljoen (1988) argued that, if hydrothermal leaching of the mafic and ultramafic rocks could provide the gold for the Archean greenstone-hosted gold deposits (probably not a correct assumption, see Ch. 16), the large volume of tholeiitic basalts at the base of the Witwatersrand Supergroup (Dominion Group) could have also provided the gold for the Witwatersrand deposits. Their speculative model visualizes the leaching of the basalts by hydrothermal fluids moving upward along basin-margin faults, discharging of the fluids into the Witwatersrand Basin and forming siliceous and auriferous pyritic exhalites near the basin edge, and reworking of the exhalites and redeposition as gold-enriched pyritic conglomeratic reefs. This model, they claimed, could explain the unique situation at Witwatersrand, because of all the paleoplacer successions, only the Witwatersrand contains thick tholeiitic basalts that are petrochemically similar to those associated with the Archean lode gold deposits. A problem with this model is that the association of putative auriferous discharge vents with tholeiitic volcanics and chemical sediments appears to be restricted to the gold-poor West Rand Group and that such associations are apparently absent in the gold-bearing upper sequences of the Witwatersrand Basin (Robb & Meyer 1995). Moreover, $\delta^{18}\text{O}$ values of chert pebbles from both Huronian and Witwatersrand conglomerates (9 to 11.5‰) are much lower than those expected for Archean and Proterozoic marine cherts (commonly >16‰; Knauth & Epstein 1976) and effectively exclude auriferous iron-formations and exhalites as likely sources of gold in these deposits (Vennemann et al. 1992).

Robb and Meyer (1990) suggested that the gold and uranium could have been stripped by erosion from the roof zones of hydrothermally altered granitoids adjacent to

the basin. Detrital quartz particles from the Basal Reef contain two generations of fluid inclusions — one set comprising moderately saline (7-16 wt% NaCl equivalent), predominantly NaCl solutions with homogenization temperatures of 200° to 220°C; and the other set comprising low-salinity (<5 wt% NaCl equivalent), NaCl-bearing aqueous inclusions with homogenization temperatures of 160° to 190°C. The latter values compare well with fluid inclusions which have been described from hydrothermally altered Archean granites around the Witwatersrand Basin (Frimmel et al. 1993), but the hydrothermal event has not yet been dated. On the other hand, the so-called mass balance problem may have been overemphasized. A mass balance calculation by Loen (1992), modeled after Cenozoic gold placers, suggests that a gold concentration of about 0.43 to 6.8 ppb Au in the source rock would be adequate to account for the gold contained in the Witwatersrand deposits. This is close to the weighted average gold content of about 4 ppb Au for the Witwatersrand Archean basement of the Kaapvaal craton and well below the gold contents (arithmetic average 109 ppb Au, maximum value 5.9 ppm Au) of hydrothermally altered granites in the terrane (Robb & Meyer 1990). The hydrothermally altered granites are also enriched in uranium, to a maximum value of 34 ppm U compared with 1-10 ppm U in the unaltered granites. Recently, Blenkinsop and Eriksson (1995) proposed that the gold in the Witwatersrand placers could largely or entirely be concentrated by cannibalization of gold from the placer footwall degradation. The proposal lacks direct proof, but is supported by mass balance calculations, the observation that the highest grade placers mostly overlie low-angle unconformities, and the interpretation of Button and Adams (1981) that the unconformities and overlying placers are product of degradation related to a lowering of the base level of erosion.

14.6.2. TIME-BOUND DISTRIBUTION OF URANIUM DEPOSITS

The time-bound character of the various types of uranium deposits has been noted by many authors (Robertson et al. 1978, Derry 1980, Nash et al. 1981, Pretorius 1981, Toens 1981). The data for the concept is illustrated in Figure 14.10, which is a plot of reserves of uranium in economically viable deposits against time. For the purpose of this plot, an economically viable deposit is defined as one which is estimated to have a reasonable profit potential at a forward price of \$40 (U.S.) per pound of U_3O_8 (1976 dollars). The exception is the Cambrian-Devonian peak for low-grade (up to about 100 ppm U_3O_8), black (organic-rich) shale, which is included because of its large resource potential. The time-axis in this plot represents the age of the host rocks. The age of mineralization would not significantly alter the character of the diagram, because the mineralization in the diagenetic or epigenetic unconformity-type and sandstone-type deposits is only slightly younger than the host rocks.

Despite the uncertainties regarding the precise positioning of the time boundaries, there appears to have been three major time intervals of uranium mineralization during crustal evolution. The first peak (2800-2200 Ma) represents the conglomerate-type deposits (accepting that they are modified paleoplacers); the second peak (2000-1500

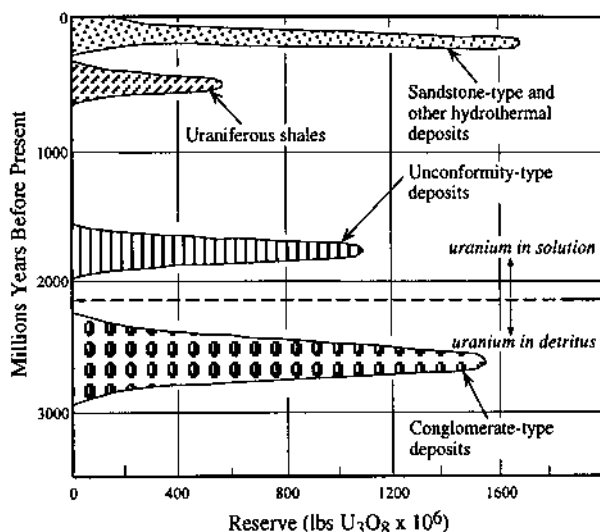


Figure 14.10. Time-bound character of uranium deposits (after Robertson et al. 1978). The time-axis refers to the position of the deposit in the geological section. Reserves are based on forward price of \$40 per pound of U₃O₈ (1976 dollars), except for the peak for shales.

Ma) corresponds to the paleosurface-related unconformity-type deposits; and the third peak (<400 Ma) comprises predominantly sandstone-type deposits. Vein-type deposits (not included in Fig. 14.10) are younger than 2000 Ma, and most of them would fall into one of the other two peaks (see Table 14.2). Note that no uranium deposit of any type is known in rocks older than 2800 Ma, but conglomerate-type gold deposits occur in rocks as old as 3100 Ma in South Africa (Uitkyk Formation, Pietersburg Supergroup, Transvaal). Conglomerates with either gold or uranium virtually disappear at 2200 Ma, coincidental with the worldwide development of banded iron-formation (see Ch. 15). The exception is the Tarkwaian-type auriferous conglomerates (1900 Ma) in which the characteristic heavy mineral is hematite, not pyrite. Thus, gold mineralization does occur in conglomerates younger than 2200 Ma in age, but auriferous and/or uraniferous conglomerates of an age between 1600 and 700 Ma are not known. Minor gold and uranium (predominantly gold) mineralization in conglomerates reappear in the Phanerozoic, but the source of the metals is believed to be immediately underlying and adjacent strata mineralized during the Precambrian (Pretorius 1981).

The time-related distribution of uranium deposits may be ascribed to an interplay of two factors: (a) evolution of the crust, resulting in the development of uranium-enriched source rocks, such as granites, and intracratonic sedimentary basins to accommodate the accumulation of uranium-enriched sediments; and (b) evolution of the atmospheric oxygen with geologic time.

Basalts of all ages today contain less than 0.6 ppm uranium and the concentration was probably in the order of 1 ppm uranium in the early Archean crustal basaltic rocks. Thus, the crust was a poor source of uranium as long as it remained dominantly basaltic. There is good radiometric evidence that at least some continental crust had appeared by 4.2 Ga (Holland and Kasting 1992), but the continental nuclei probably became a viable source of uranium only during the late stages of cratonization when uranium was fractionated into regionally extensive anatectic granites and transferred to the upper levels of the crust. Suitable source granites may have developed as early as 3100 Ma (Allsopp 1964) and much more were added in the late Archean and early Proterozoic. It is perhaps no mere coincidence that the two Precambrian peaks in Figure 14.10 roughly correspond to two periods of abundant development of continental crust — 2750-2450 Ma and 1900-1600 Ma (Gastil 1960). The tectonic activity during late Archean and early Proterozoic times produced substantial topographic relief for rapid weathering of the granites and extensional sedimentary basins for the deposition of conglomeratic sediments. The uraninite in the granites remained insoluble because of an essentially anoxic atmosphere and accumulated as detrital particles in the conglomerates. This scenario is compatible with the development of earliest uranium deposits, in the form of conglomerate-type deposits, during the 2800-2200 Ma interval.

The evolution of atmospheric oxygen has been discussed extensively since the early 1950's (e.g., Rubey 1951, Holland 1962, 1984, Cloud 1973, Schidlowski 1976, Walker et al. 1983, Kasting 1987, 1993, Kasting et al. 1992, Krupp et al. 1994), but the details are still uncertain. The model discussed below is a three-box framework of the atmosphere-ocean system originally proposed by Walker et al. (1983) and subsequently refined by Kasting (1987) and Kasting et al. (1992). The three 'boxes' in the model represent the atmosphere, the surface ocean (the uppermost 75 m or so of water that is stirred rapidly by the action of the winds), and the deep ocean. The evolution of atmospheric oxygen is conceptualized to have progressed in three stages (Fig. 14.11). Stage I, called "reducing", corresponds to a situation in which both the atmosphere and the ocean were essentially devoid of free O_2 . Stage II, termed "oxidizing", represents a period in which small amounts of O_2 were present in the atmosphere and surface ocean, but during which the deep ocean remained anoxic. Stage III, termed "aerobic", represents a situation, similar to the present one, in which free O_2 pervaded the entire system and the P_{O_2} was high enough to support aerobic respiration.

It needs to be emphasized that, although the existence of three distinct stages is well supported by geologic and biologic evidence, the quantitative aspects of the model, in terms of both the duration and P_{O_2} (and P_{CO_2}) levels of the three stages, are far from certain. Figure 14.12 shows what Kasting (1993) has called his "best guess" of how the concentrations of various gases in the Earth's atmosphere changed with time.

Stage I.

The marked depletion of the terrestrial atmosphere in noble gases, by factors of 10^{-7} to 10^{-11} compared with their cosmic abundances, suggests that either the Earth did not

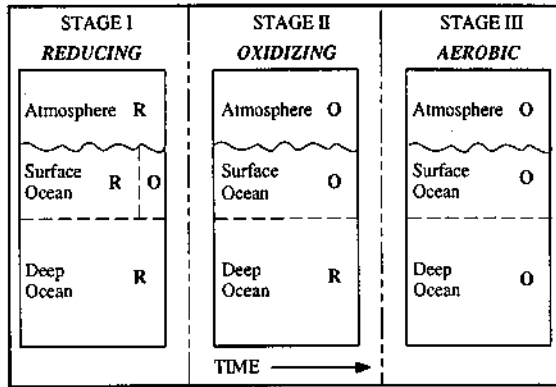


Figure 14.11. The three-box model of the ocean-atmosphere system pertaining to the rise of atmospheric oxygen with geologic time (after Kasting 1987). O = oxidizing, R = reducing. Note that during Stage I, the surface ocean was oxidizing locally.

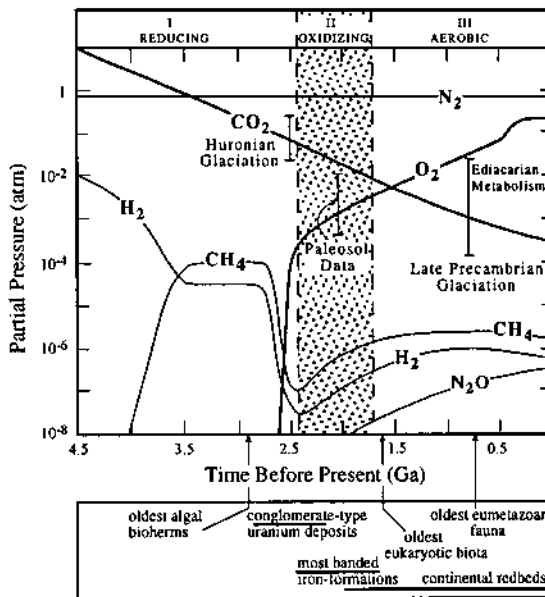
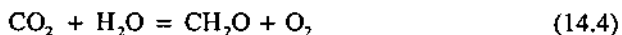


Figure 14.12. "Best guess" changes in the atmospheric composition consistent with the predictions of the three-box model shown in Fig. 14.11 (after Kasting 1993). The two error bars on the CO₂ curve show upper and lower limits on P_{CO_2} during glacial periods as calculated by Kasting et al. (1992). The error bar on the O₂ curve shows upper and lower limits P_{O_2} between 1.5 Ga and 2.5 Ga, based on a combination of paleosol data and the theoretically derived P_{CO_2} curve. The curves for H₂, CH₄, and NO₂ are based entirely on theoretical estimations. Also shown for reference are some important markers in the geologic record related to the evolution of the atmosphere-ocean system.

inherit a primordial atmosphere (a remnant of the solar nebula) or, more likely, such an atmosphere was dissipated, probably completely, in a thermal episode before the accumulation of the present, secondary atmosphere (Cloud 1968, Walker 1977). The current opinion leans toward a primitive steam atmosphere generated by the degassing of in-falling planetesimals and vaporization of any water that was present at the surface of the proto-Earth (Walker 1977, Kasting 1993), but this atmosphere was perhaps largely removed by a giant moon-forming impact toward the end of the main accretion period (Hartman et al. 1986). If so, much of the Earth's early atmosphere was probably the result of heavy bombardment by asteroids or comets during the 4.5-3.8 Ga period (Chyba 1987). In any case, toward the end of the accretion period, much of the water vapor in the atmosphere would have condensed to form an ocean, leaving the atmosphere dominated by carbon compounds (mostly CO₂ and CO) and N₂, and essentially devoid of free O₂.

The supply of molecular oxygen to the atmosphere-ocean system must have been caused by photochemical reactions utilizing solar radiation as the energy source. The two likely processes were: (a) photolysis (or photodissociation) of water vapor in the upper atmosphere by the short wavelength radiation (≈300 to 450 nm) of the solar spectrum, accompanied by the escape of the very light hydrogen atoms (thus preventing recombination) and atmospheric reactions involving OH, and by photolysis of CO₂; and (b) photosynthesis of primitive organisms, particularly the blue-green algae (cyanophytes), by the low-energy (visible) solar radiation, producing oxygen by reactions such as



Canuto et al. (1983) suggested that photolysis was particularly important in the very early Earth's atmosphere because the sun was emitting much more ultraviolet (UV) radiation and there was no ozone screen. The present escape rate of hydrogen atoms released by photolysis, however, does not provide an important oxygen source and probably never did so in the geologic past (Schidlowski 1976, 1984). It is, therefore, reasonable to assume that photosynthesis has been the dominant contributor of molecular oxygen to the terrestrial atmosphere. The impact of photosynthesis on the oxygen budget of the atmosphere progressively increased with time, especially after the proliferation of phytoplankton beginning around 2.0 Ga. The proliferation was probably related to an increase in the atmospheric ozone that provided a protective screen to the phytoplanktons from the solar UV radiation. It is estimated that the UV screen should have started to be effective at an O₂ level of 10⁻³ PAL (*Present Atmospheric Level*) and firmly established at a level of 10⁻² PAL (Kasting et al. 1992).

During Stage I, prior to the development of oxygenic photosynthesis, the supply rate of reduced substances (H₂, CO, and H₂S from volcanoes, and Fe²⁺ from seawater-basalt interaction) would almost certainly have exceeded the production of O₂ from

photolysis. It is not clear as to when exactly photosynthesis became a viable process. Stromatolites, resulting possibly from the matting behavior of benthonic prokaryotes (organisms with cells which lacked a membrane around the nucleus and which were incapable of cell division, notably cyanobacteria or green algae) occur in 3400-3500 Ma sediments (Walter et al. 1980, Orpen & Wilson 1981), but they lack fossil bacteria and may have been abiotic in origin (Lowe 1994). However, the presence of bacterial communities on the Earth before 3.2 Ga is indicated by the continuous record of organic carbon as CH_2O in sediments dating back to the 3.8 Ga Issua succession in Greenland and by the carbon isotopic data suggesting that some of the organisms were autotrophs. However, even after photosynthesis became operative, atmospheric P_{O_2} remained at low levels until the net production rate of oxygen exceeded the supply of reduced gases to the atmosphere. Typical ground level P_{O_2} during Stage I, calculated from atmospheric photochemical models, was in the order of 10^{-14} PAL. The formation of oxidized chemical precipitates such as banded iron-formations in the Archean (see Ch. 15) is not necessarily an evidence of O_2 -rich atmosphere. It may simply indicate that localized areas of the surface ocean were highly oxidizing, with O_2 concentration approaching possibly as high as 0.1 PAL, even though the atmosphere was essentially anoxic (Kasting et al. 1992).

The Stage I atmosphere is believed to have been CO_2 -rich, with P_{CO_2} possibly as high as 20 bars to 10 bars at the close of the accretion. The likely sources of CO_2 were volcanic eruptions, assuming a similar oxidation state of the upper mantle in the past, and the oxidation of CO and CH_4 by the byproducts of water vapor photolysis. An important clue to the likely higher CO_2 concentration in the early atmosphere is provided by the lower luminosity of the Sun, perhaps about 30% lower at 4.6 Ga than today. Modeling by Kasting (1987) suggests that CO_2 concentration in the Archean atmosphere was at least 100-1,000 times the present level to keep the Earth's surface temperature above freezing in the face of lower solar luminosity. A chemical equilibrium model by Krupp et al (1994), involving minerals, seawater, and atmospheric gases, has yielded a broadly similar picture. According to their calculations, before approximately 2350 Ma, the atmosphere was practically oxygen-free ($P_{\text{O}_2} \ll 10^{-10}$ bars), and consisted mainly of CO_2 ($P_{\text{CO}_2} \leq 1$ bar) and nitrogen, with minor amounts of H_2 and H_2S .

The essentially anoxic atmosphere is considered to have been the critical factor in the restricted age of conglomerate-type deposits containing detrital uraninite. This conclusion appears contradictory to the presence of detrital uraninite in modern sediments of the Indus River fluival system (Simpson & Bowles 1977), but the Indus system is not a proper analog for the Precambrian uraniferous conglomerates. Petrographic analysis indicates that the detrital uraninite in the Indus sediments can be explained by the virtual absence of chemical weathering in its source region, whereas the source region for the Witwatersrand sediments was subjected to strong chemical alteration (Maynard 1991a). Holland (1962) calculated that uraninite would be

thermodynamically stable at P_{O_2} values of less than 10^{-21} atm, but the detrital uraninite may not have been in equilibrium with surface water (Robinson & Spooner 1984b). From calculations based on dissolution kinetics, Grandstaff (1980) showed that uraninite in the Witwatersrand Sequence could have survived as a detrital mineral at oxygen pressures as high 0.01 PAL. He concluded that the deposition of mid-Precambrian uraniferous conglomerates may have occurred under an atmosphere containing small amounts of oxygen, less than 10^{-2} to 10^{-6} PAL (rather than an essentially anoxic atmosphere, as previously proposed), consistent with photodissociation of water vapor and limited photosynthesis.

Stage II

The transition from a weakly reducing, essentially anoxic atmosphere to an oxidizing atmosphere marked the beginning of Stage II sometime around 2.4-2.0 b.y. ago (Kasting 1987, Kasting et al. 1992, Kasting 1993). An increase in the atmospheric oxygen level during this period is supported by the lack of detrital uraninite deposits after 2.2 Ga and the widespread occurrence of redbeds (sandstone with a hematite-pigmenting agent commonly forming a coating around the sand grains) after approximately 2.0 Ga. (Red iron oxides exist in Archean marine rocks, but they are probably indicative of locally available biogenic oxygen rather than of atmospheric oxygenation, Mason & von Brunn 1977.) Such a date for the appearance of free oxygen is also consistent with the sulfur isotopic data (Schidlowski et al. 1983, Hayes et al. 1992). Measured $\delta^{34}S$ values for Archean sulfides generally fall within the range of -4 to $+4\%$ (exceptions such as sulfides of the Michipicoten iron-formation are probably of hydrothermal origin, see Ch. 15). The first good evidence of bacterial sulfate reduction — a large spread of $\delta^{34}S$ values — is found in the sulfides of early Proterozoic age (2.2-2.3 Ga). This difference in $\delta^{34}S$ values between Archean and early Proterozoic sulfides is particularly pronounced for sulfides in continental sedimentary rocks (Hattori et al. 1986). A possible explanation is that oceanic sulfate levels increased around 2.2 Ga as a consequence of an increase in oxidative weathering of pyrite on the continents, implying an increase in atmospheric P_{O_2} . Alternative explanations include a much smaller degree of isotopic fractionation in the Archean oceans because of higher temperatures (Ohmoto & Felder 1987) or the absence of bacterial sulfate reduction during the Archean time (Schidlowski 1979), except perhaps in localized areas of the oceans. Re-evaluation of the redbed and BIF data indicates that the duration of Stage II was probably much shorter (2.0-1.8 Ga) than indicated in Figure 14.12 (Kasting 1993).

The near-surface ocean during this stage would have been oxygenated globally, not just locally as in Stage I, but the deep ocean generally remained anoxic and carried ppm quantities of Fe^{2+} in solution, presumably due to a large influx of iron from mid-oceanic ridge volcanism (Vizer 1983). The abundance of iron-formations in the mid-Proterozoic time may be ascribed to a combination of the upwelling of Fe^{2+} -enriched deep ocean waters and oxygenated surface waters (see Ch. 15). Kasting (1987)

estimated an upper limit of 0.03 PAL for the P_{O_2} of Stage II, assuming that the rate of organic carbon burial and the rate of deep ocean mixing were the same as today. This is consistent with the range of P_{O_2} (4×10^{-4} to 10^{-2} atm) calculated by combining the $P_{O_2} : P_{CO_2}$ ratio of 0.03 ± 0.01 indicated by paleosols ranging in age from 1.5 Ga to 2.5 Ga (Holland 1992) with 0.02-0.25 atm as the upper limit on P_{CO_2} (Kasting et al. 1992). The significant increase in atmospheric P_{O_2} changed the process of uranium mineralization to one controlled by solution transport of uranium as uranyl complexes.

Stage III

The termination of major iron-formation deposition worldwide at about 1.8-1.7 b.y. ago is taken as the onset of the Stage III atmosphere. In the absence of Fe^{2+} to serve as an immediate sink for photosynthetic oxygen, atmospheric P_{O_2} must have begun to climb toward its present value, but the rate of this rise is unclear. It may have risen rapidly (within a few hundred million years) to near its present level, the increase eventually being arrested as aerobic respiration by organisms living within marine sediments reduced the percentage of buried organic carbon, the feedback mechanism that is believed to control P_{O_2} today. But the burial rate of organic carbon could have been affected by a number of factors — such as sea-floor spreading rates, area of continental shelves, climate, and the availability of phosphorous — causing appreciable fluctuation in P_{O_2} even during the Phanerozoic. As was pointed out by Kasting (1987), a lower bound of 0.01 PAL at 1.5 Ga is required to fulfill the oxygen requirements of eukaryotic organisms which had proliferated by this time, and at the beginning of Cambrian the P_{O_2} must have been at least an order of magnitude higher to permit the evolution of shell-forming creatures. According to the model discussed by Berner and Canfield (1989), atmospheric oxygen probably has fluctuated appreciably over the Phanerozoic time, largely controlled by sedimentation. For example, their model suggests a much higher level of oxygen (compared with PAL) during the late Carboniferous and Permian periods, because of the rise of vascular land plants and widespread burial of organic matter in vast coal swamps, and a lower level of oxygen during the late Permian and Triassic periods, partly due to the drying-up of coal swamps and deposition of a large proportion of total sediments as continental redbeds free of carbon and sulfur.

It is reasonable to conclude that the Earth's atmosphere was sufficiently oxidizing soon after 2200 Ma for the onset of solution transport of uranium, a condition that has continued to the present time. The 2000-1500 Ma peak in Figure 14.10 probably reflects the relatively sudden release of unusually large amounts of uranium from uraniferous granites and uranium-enriched sediments. Much of the leached uranium was probably lost to the oceans. The youngest peak in Figure 14.10, representing mainly sandstone-type deposits, cannot be correlated with any especially prolific generation of uranium-enriched source material or continental arkosic sandstone. A linkage with the

appearance of land plants in the Devonian is a possibility (Nash et al. 1981), as the host sandstones commonly contain an abundance of plant debris. However, as discussed earlier, the organic matter was not the common thread for the formation of these deposits. Robertson et al. (1978) have proposed that the relatively young age and the apparently time-bound character of most, if not all, sandstone-type deposits is an artifact of preservation, the older deposits formed in similar environments having been thoroughly flushed away through time.

14.7. Summary

Uranium deposits were formed in diverse geologic settings and are hosted by a variety of rocks ranging in age from the Archean to the Tertiary. Producing deposits are of five types (Table 14.1): unconformity-type, conglomerate-type, sandstone-type, vein-type, and ultrametamorphic-type. Almost all the major uranium deposits as well as more than 70% of 'reasonably assured resources' of uranium occur in six countries. In decreasing order of resources, these are USA, South Africa, Australia, Canada, Niger, and Namibia.

Economic conglomerate-type deposits are hosted by quartz-pebble conglomerates older than 2200 Ma. in age. Almost all current production from this deposit type is accounted for by the Witwatersrand Basin (South Africa), where uranium is recovered as a byproduct of gold, and the Elliot Lake-Blind River district (Canada), which is practically devoid of gold. Uranium, mostly as uraninite or brannerite, and gold in the native form occur as components of the conglomerate matrix, which is composed essentially of quartz, sericite, pyrite, chlorite, and chloritoid, and accessory amounts of heavy minerals such as zircon, chromite, and leucoxene.

The overwhelming majority of the important deposits of the sandstone-type occur in USA and account for more than 95% of its uranium resources. The USA deposits are concentrated in three regions — Colorado Plateau (Triassic to Jurassic), Wyoming-South Dakota (Cretaceous to Eocene), and Texas Coastal Plain (Eocene to Pliocene) — each of which comprises several major mining districts and mineral belts. The immediate host rocks commonly are fluvialite, arkosic to quartzose sandstones and conglomerates, which were deposited in alluvial-fan, braided-river and meander-belt environments. Uranium deposits occur either in the reduced facies or at the interface between oxidized and reduced facies. The deposits are strata-bound and peneconcordant, and the geometric form of the orebodies is either grossly tabular (or lenticular) or podiform with crescent-shaped cross sections ("rolls"). In unoxidized ore, the main uranium minerals are uraninite (or pitchblende) and coffinite; accessory minerals include vanadium oxides and silicates, copper sulfides, and pyrite/marcasite. The host rocks of most, but not all, sandstone-type deposits contain abundant organic material.

Unconformity-type deposits are particularly abundant in the Athabasca Basin (Canada) and the Pine Creek geosyncline (Australia). The deposits occur at or in the immediate vicinity of unconformities that separate Archean-Proterozoic basement from

younger metasediments-metavolcanics and exhibit a strong structural control. Uraninite and pitchblende are the typical primary uranium minerals, and the grade of the ores tends to be relatively high. Hydrothermal alteration, especially chloritization, related to uranium mineralization is a characteristic feature.

Vein-type deposits, which commonly occur within or adjacent to granitic (-syntetic) plutons, are also structurally controlled, but most are relatively small in size. Low-Th pitchblende is the predominant primary uranium mineral and some vein deposits are polymetallic (Ni, Co, Bi, Cu, Se, V, Ag, Au) with a large suite of sulfide, selenide, and sulfarsenide minerals. Hematization of wallrocks is a common characteristic of vein-type deposits. Ultrametamorphic deposits are not that common. The best known example is the Rössing deposit (Namibia), which consists of disseminated uranium mineralization (uraninite, betafite, and secondary uranium minerals) associated with concordant and discordant alaskitic granite/pegmatite bodies that were emplaced preferentially in migmatized calcareous rocks.

Conglomerate-type deposits are interpreted as paleoplacers, which have been modified by later hydrothermal alteration and metamorphism, whereas ultrametamorphic deposits owe their origin to very high grade metamorphism, including partial to complete melting of the protoliths (ultrametamorphism) that concentrated uranium in the anatectic silicate melts. The other deposit types are hydrothermal, involving the transport of uranium as soluble U^{6+} -complexes under relatively oxidizing conditions and deposition as U^{4+} -minerals in reducing environments. The most likely reductants are organic material, reduced sulfur species (H_2S or HS^-), and Fe^{2+} , but exact mechanisms of the reduction processes are not well understood. Potential sources of uranium, depending on the geologic setting, include granites, rhyolites, glassy volcanic ash or ash-rich sediments, redbeds, and Precambrian basement gneisses and metasediments, but the precise source for any particular deposit type or deposit remains elusive.

A fascinating aspect of uranium deposits is the time-bound character of their distribution, which appears to be broadly correlated with the evolution of atmospheric oxygen through geologic time. The 2800-2200 Ma restricted age interval for conglomerate-type deposits (accepting that they are paleoplacers) is compatible with an essentially anoxic atmosphere in the Archean and early Proterozoic that permitted the transport and accumulation of detrital uraninite. The appearance of hydrothermal uranium deposits, involving solution transport of uranium as oxidized U^{6+} -complexes, reflects a relatively oxic atmosphere after about 2200 Ma.

14.8. Recommended Reading

Fischer (1974), Nash et al. (1981), Pretorius (1981), Hoeve & Quirt (1989), Turner-Peterson & Fishman (1986), Marmont (1987), Kasting (1993), Ruzicka (1993a, 1993b), Roscoe and Minter (1993).

CHAPTER 15

PRECAMBRIAN IRON-FORMATIONS

15.1. Introduction

Sedimentary rocks, including chemical precipitates formed by exhalative processes, often contain high enough iron to be considered ferruginous, or even iron deposits. Two major groups of iron-rich sedimentary rocks are recognized (James 1966): (a) ironstones, which are non-cherty, oölitic, poorly banded, and largely of Phanerozoic age; and (b) iron-formations, which are typically laminated with chert, generally non-oölitic, and largely (but not exclusively) of Precambrian age. Other groups of iron-rich rocks of lesser economic importance not considered here (but discussed, for example, by Borchert 1960, Stanton 1972) include: (a) the blackband and clayband ores, most of which are diagenetic and post-diagenetic deposits of siderite found in coal measures and in some clays; (b) the bog iron ores found in many bogs and small lakes in higher latitudes; and (c) laterites derived by weathering of Fe-rich rocks (see Ch. 2). In this chapter we restrict our attention to the so called iron-formations, which constitute by far the most abundant and economically the most important iron-rich sediments.

15.2. Iron-formation

Contracting the old term 'iron-bearing formation' used in early reports on the Lake Superior iron ore range, James (1954) formally defined an *iron-formation* as "a chemical sediment, typically thin-bedded or laminated, containing 15% or more iron of sedimentary origin, commonly but not necessarily containing layers of chert." The 15% Fe lower limit has been criticized as arbitrary and restrictive by Trendall (1983a). The iron content of Precambrian sedimentary rocks, however, has a bimodal distribution, and a 15% value approximates the low-frequency trough that separates the common rock average (about 4% Fe) from the iron-formation average (about 29% Fe) (Lepp 1987). Some have argued that chert-banding should be a necessary component of the definition of iron-formation, but this would arbitrarily exclude, despite a common depositional history, equally iron-rich but non-cherty strata intercalated with an iron-formation.

Adopting the past and currently predominant usage, we use the term *iron-formation* in this book essentially as defined by James (1954) but incorporating a minor

modification suggested by Trendall (1983a). Thus, iron-formation is redefined as "a chemical sediment, typically thin-bedded or laminated, whose principal characteristic is an anomalously high content of iron, commonly but not necessarily containing layers of chert" (Klein & Beukes 1992). The term is commonly used interchangeably with *banded iron-formation* (BIF), to emphasize its typically cherty-banded character, or with 'cherty iron-formation', to emphasize its distinction from oölitic ironstone. The hyphenation is retained, following James (1992), to remind us that iron-formation is a rock name, not a stratigraphic designation (e.g., Brockman Iron Formation). Equivalent terms used around the world include itabirite (Brazil), banded ironstone (South Africa), quartz-banded ores (Sweden), banded hematite quartzite or banded magnetite quartzite (India), jaspilite (USA and Australia), and taconite (USA).

Ironstones may be subdivided into two broad types (Stanton 1972): (a) the Minette-type, which appears to have been deposited in near-shore marine sedimentary sequences (Borchert 1960, Van Houten & Bhattacharyya 1982); and (b) Lahn-Dill-type, which is generally underlain by spilitic tuff and overlain by pelagic limestones or shales with intercalations of clastic material (Quade 1976). The Lahn-Dill-type deposits are principally confined to "eugeosynclinal" furrows of the Variscan system in Central Europe. Minette-type deposits are quite abundant. The best known examples are those of Alsace-Lorraine in France (Jurassic), the Clinton ironstone beds in eastern USA (Silurian), and Frodingham and Cleveland in England (Lower Jurassic beds). A comparison of the Minette-type ironstone with the iron-formations of the Superior-type is presented in Table 15.1.

15.3. Distribution

Except for a few minor occurrences, some of which are of uncertain age, (banded) iron-formations are virtually confined to Precambrian shield areas (Fig. 15.1), often forming prominent iron ranges. In fact, there is no major cratonic area that lacks iron-formations as prominent members of its stratigraphic column.

Major districts and belts of (banded) iron-formation deposits are truly gigantic in size, with estimates of original ore material containing about 30% Fe and 45% SiO₂, in the range of 10⁹-10¹⁴ tonnes (James 1983). The most important of these in terms of initial tonnage are: Hamersley Basin, Western Australia (≈2.5 Ga); the Transvaal Supergroup (Kuruman and Griguetown iron-formations), South Africa (≈2.5-2.3 Ga); Labrador Trough, Quebec-Newfoundland, Canada (≈2.1 Ga); Lake Superior region, USA-Canada (≈2.7-1.9 Ga); Quadrilatero Ferrifero, Minas Gerais (≈2.3 Ga), and Serra dos Carajas district, Brazil; Krivoy-KMA (Kursk Magnetic Anomalies), Ukrainian Shield (≈2.2 Ga); Singhbhum-Bonai-Keonjhar-Mayurbhanj region, Orissa-Bihar, India (≈3.0 Ga); Imataca Complex, Venezuela (≈3.4 Ga); Liberia-Sierra Leone, Liberian Shield (≈3.0 Ga); and Nabberu Basin, Australia (≈2.1 Ga). The economically mineable, higher grade material in any region is much more limited and, in many cases, is restricted to protoliths upgraded by supergene enrichment processes.

TABLE 15.1. Comparison of Minette-type ironstone and Superior-type iron-formation (James 1966, Eichler 1976)

	Minette-type ironstone	Superior-type iron-formation
Age	Phanerozoic (most important deposits are of lower Paleozoic and Jurassic age)	Precambrian (dominantly older than 1800 Ma)
Dimensions	Lateral extent of individual bodies measured in kilometers and thickness in meters	Lateral extent of individual bodies measured in hundreds of kilometers and thickness in tens to a few hundred meters
Sedimentary Structures	Massive to poorly banded; commonly oolitic; no chert	Commonly banded with alternating iron-rich and chert-rich bands; oolitic texture rare, except in hematitic and silicate facies in some areas
Mineralogy	Dominant oxide is goethite; hematite is fairly common, magnetite relatively rare; chamosite is the primary silicate mineral, glauconite (chlorite and stilpnomelane in metamorphosed ironstones) is minor; calcite and dolomite are common constituents; pelletal collophane may be abundant	Dominant oxides are magnetite and hematite, no goethite; primary silicate mineral is greenalite, with minnesotaite, stilpnomelane, and chlorite in rocks of slightly higher metamorphic grade; no pelletal phosphate, chamosite, or glauconite; dolomite is present in some units, but calcite is rare or absent
Chemistry	Al ₂ O ₃ : typically >4% Alkalis: up to 10% or more P ₂ O ₅ : typically >1%	Al ₂ O ₃ : 0.1 - 1.5% Alkalis: usually < 2% P ₂ O ₅ : typically < 0.2%

15.4. Iron-formation Facies

Most iron-formations are chemical precipitates and, therefore, their mineralogy is strongly controlled by the Eh-pH of the aqueous medium (Fig. 15.2). Applying this principle, James (1954) divided the iron-formations in the Lake Superior region (USA) into four major sedimentary facies — oxide, silicate, carbonate, and sulfide — that apparently formed in environmental conditions defined by the stability fields of their dominant iron minerals. Characteristics of the facies are summarized in Table 15.2. Average bulk chemical compositions of the different facies, as estimated by Gross (1986), are presented in Table 15.3.

Based on the dominance of the iron-oxide species (magnetite or hematite), the *oxide facies* iron-formations may be subdivided into magnetitic and hematitic subfacies, which represent different Eh-pH environments of deposition. Hematitic iron-formations are the most distinctive, although not necessarily the most abundant in a given district. Most contain appreciable amounts of magnetite, often demonstrably of diagenetic origin, and minor amounts of carbonate minerals (ankerite, dolomite, and calcite, but rarely siderite). The magnetite subfacies is the most abundant type of iron-formation and is often regarded as the type example of BIF. Iron silicates and siderite are

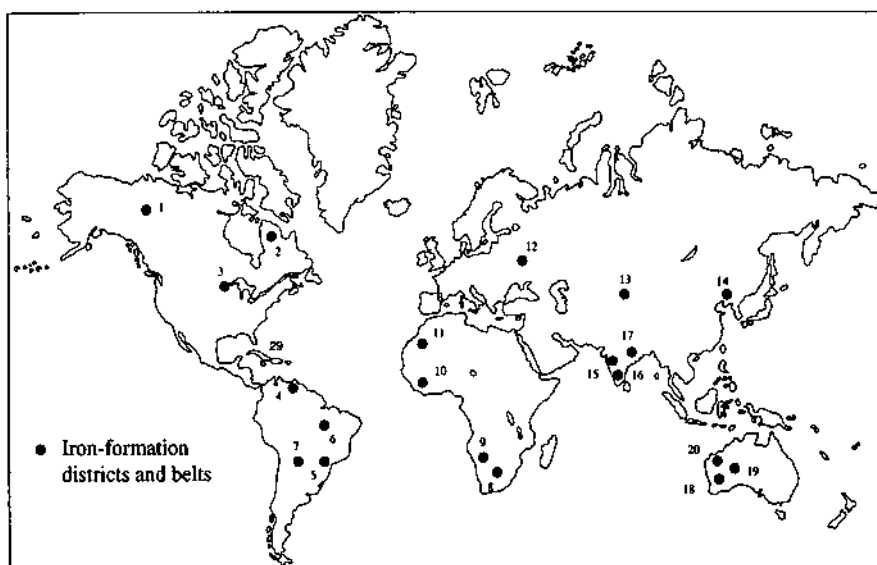


Figure 15.1. World distribution of major iron-formation belts and districts. Canada: Rapitan (1), Labrador Trough (2); USA-Canada: Lake Superior region (3); Venezuela: Imataca Complex (4); Brazil: Quadrilatero Ferrifero (5), Serra dos Carajas (6), Urucum (7); South Africa: Transvaal-Griquatown belt (8); Namibia: Damara belt (9); West Africa: Liberian Shield (10); Mauritania: Ijil Group (11); USSR (former): Krivoy Rog and Kursk Magnetic Anomaly (12), Baykal region (13), Anshan (14); India: Goa (15), Karnataka (16), Bihar-Orissa belt (17); Australia: Yilgarn Block greenstone belts (18), Nabberu Basin (19), Hamersley Basin (20).

common constituents of magnetitic subfacies and ankerite, presumably of diagenetic origin, may be present. In some districts, both the subfacies may be recognizable and, in fact, may be interbedded on a scale of meters (James 1992).

Silicate facies iron-formations are easily recognized by the distinct green or olive-green to khaki color imparted by the iron-silicate minerals. Minnesotaite and stilpnomelane are the typical silicate minerals and appear to replace earlier greenalite; chlorite is common and chamosite may be present. Magnetite and siderite may be quite abundant and occur as discrete layers.

The ubiquitous mineral of the *carbonate facies* is siderite, and monomineralic siderite beds, often alternating with chert beds, are quite common. In many districts, siderite beds are composed of tiny spherules, generally 10-40 μm in diameter, that are believed to be primary sedimentary features. Transitions from carbonate facies into silicate or silicate-magnetite facies on the one hand, and into sulfide facies on the other, are recognized in a number of districts, but coexistence of carbonate and hematitic facies has not been observed (James 1992).

The *sulfide facies*, the least abundant of all facies, is essentially a black shale with disseminated pyrite (\pm pyrrhotite). Although present in all types of iron-formations regardless of age, it is not easily recognized because of the extremely fine grain size of

TABLE 15.2. Principal features of iron-formation facies (James 1954, 1992, Gross 1965)

Facies	Iron minerals*	wt % Fe	Lithology	Depositional environment	Distinctive features
Oxide					
Hematitic	Hematite (magnetite)	30-40	Thin-bedded to wavy-bedded; alternate layers of bluish black hematite and gray or reddish chert	strongly oxidizing	Abundant specularite; oölitic in many districts
Magnetitic	Magnetite (minnesotaite, stilpnomelane, greenalite, siderite)	25-35	Evenly bedded to irregularly bedded; layers of magnetite alternate with dark chert and mixtures of silicates and siderite	Weakly oxidizing to weakly reducing	Strongly magnetic
Silicate	Minnesotaite, stilpnomelane (magnetite, siderite, greenalite, chamosite, chlorite)	20-30	Light to dark green rock of Fe-silicate minerals; generally laminated or even-bedded, but may be wavy to irregularly bedded; commonly interlayered with magnetite oxide facies or carbonate facies, much of the chert is interstitial rather than in discrete layers	Weakly reducing	Commonly magnetic, may be granule-bearing
Carbonate	Siderite (stilpnomelane, minnesotaite, magnetite, pyrite)	20-30	Evenly bedded or laminated alternation of siderite and chert	Reducing	Generally non-magnetic; stylolites common
Sulfide	Pyrite (siderite, greenalite)	15-25	Laminated to thinly layered carbonaceous argillite; rare chert	Strongly reducing	Commonly graphitic

* In rocks of low metamorphic grade; common but non-essential minerals in parenthesis.

pyrite (often about 0.005 mm) and its susceptibility to chemical weathering.

Examples of stability-field diagrams (Fig. 15.2) show that at given anion concentrations almost any combination of oxides, silicates, carbonates and sulfides of iron can coexist in equilibrium at some geologically reasonable values of Eh and pH. Note that a decrease in Eh would result in sequential intersection of the stability fields of oxide, carbonate, and sulfide. In an idealized restricted basin in which iron-rich sediments are being deposited, this corresponds to a progressive decrease in available oxygen in the bottom environment.

The idealized distribution of iron-formation facies in a depositional basin with restricted circulation, as conceptualized by James (1954), is illustrated in Figure 15.3, although nowhere has a complete transition of the facies actually been observed. The

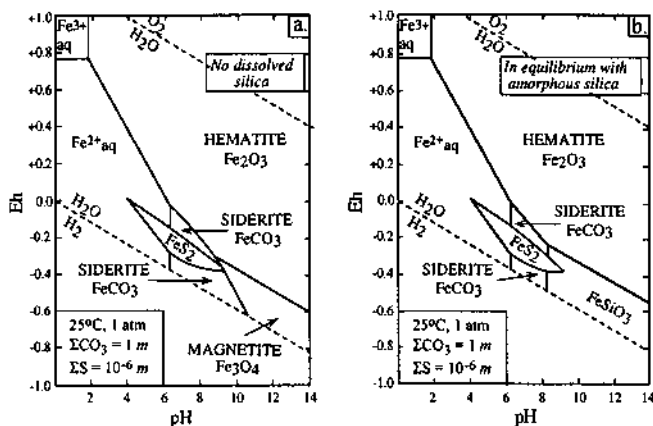


Figure 15.2. Eh-pH stability relations of common iron minerals and ionic species in aqueous solutions at 25°C and 1 atm total pressure: a. with no dissolved silica; b. in equilibrium with amorphous silica. Other boundary conditions for the diagrams are as follows: total concentration of dissolved carbonate ($\Sigma\text{CO}_3 = 1\text{ m}$); total dissolved sulfur ($\Sigma\text{S} = 10^{-6}\text{ m}$). Note that pyrite is a stable phase at nearly neutral pH values if the aqueous system contains even very minute quantities of divalent sulfur, and the field of magnetite is replaced by a field for iron silicate in the presence of silica. It can be shown that the pyrite field would expand to the lower pH side with increasing concentration of dissolved sulfur, where as the siderite field would shrink with decreasing concentration of dissolved carbonate (and would disappear altogether when ΣCO_3 is less than 10^{-2} m). (After Garrels & Christ 1965.)

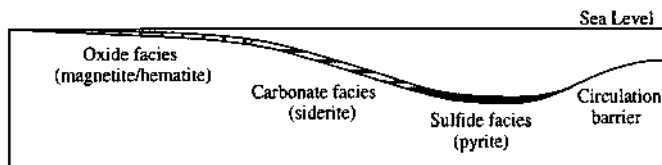


Figure 15.3. Schematic distribution of iron-formation sedimentary facies in a hypothetical, restricted basin (after James 1954). The silicate facies would partly overlap both the oxide and carbonate facies.

oxide (especially hematitic) facies is on the wave- and current-swept shelf, where the environment is oxidizing. At the deeper end of the basin, behind the circulation barrier, anoxic conditions lead to the generation of H_2S by bacterial decomposition of organic matter and promote the precipitation of iron as a sulfide. In the intervening region, characterized by milder reducing or oxidizing conditions, iron is precipitated in the ferrous state, as a carbonate (siderite), or in the ferrous-ferric state, as magnetite. A similar shore-to-basinward ideal transition of hematite, siderite, and 'pyrite' zones in a BIF has been attributed by Drever (1974) to an increasing amount of organic carbon incorporated into the sediment.

TABLE 15.3. Average composition (in wt %) of Algoma-type (A) and Superior-type (S) iron-formations by dominant sedimentary facies (source of data: Gross 1986)

Facies	Oxide		Silicate		Carbonate		Sulfide
	A	S	A	S	A	S	A
# samples*	965	176	18	25	32	33	77
SiO ₂	47.83	47.70	64.20	58.83	44.50	36.91	40.94
Al ₂ O ₃	2.65	1.27	2.52	2.18	6.67	1.31	6.64
Fe ₂ O ₃	30.33	35.60	10.91	8.98	2.70	6.89	13.15
FeO	12.70	7.80	10.67	16.73	13.39	21.53	15.96
MgO	1.58	1.24	3.57	2.84	6.18	4.45	2.29
CaO	1.66	1.60	4.94	2.26	4.66	4.93	2.45
Na ₂ O	0.33	0.11	0.22	0.18	1.23	0.14	0.86
K ₂ O	0.71	0.14	0.24	0.55	0.89	0.14	0.94
P ₂ O ₅	0.21	0.05	0.07	0.10	0.14	0.14	0.11
H ₂ O (total)	0.77	1.13	1.25	2.48	1.65	1.37	3.25
CO ₂	0.88	2.72	2.19	4.29	15.54	20.92	2.05
S	0.176	0.025	0.164	0.079	1.431	1.064	12.045
As	0.012	0.299	--	--	1.072	0.277	0.253
Mn	0.112	0.513	0.219	0.40	0.172	0.739	0.233
Ti	0.075	0.017	0.191	0.16	0.309	0.034	0.262
V	0.006	0.003	0.011	0.01	0.017	0.006	0.009
Cr	0.008	0.011	0.014	0.01	0.039	0.008	0.016
Co	0.004	0.003	0.004	0.003	0.003	0.003	0.008
Ni	0.008	0.003	0.034	0.005	0.022	0.004	0.013
Cu	0.005	0.001	0.002	0.004	0.003	0.001	0.063
Zn	0.006	0.003	0.005	0.004	0.009	0.010	0.343
Sr	0.007	0.003	0.009	0.002	0.021	0.003	0.010
Ba	0.021	0.017	0.013	0.015	0.024	0.004	0.015
Au (ppm) [@]	0.038	0.019	0.006	0.003	0.007	0.018	
	(52)	(16)	(2)	(5)	(1)	(6)	(5)
Fe (total)	31.08	30.96	15.92	19.28	12.30	21.55	21.61
Fe ³⁺ :Fe ²⁺	2.15	4.11	0.92	0.48	0.18	0.29	0.74
SiO ₂ :Al ₂ O ₃	18.05	37.56	25.48	26.99	6.67	28.18	6.17

* Minor elements were not analyzed for all the samples.

@ Number of samples analyzed for each category is shown in parenthesis.

The facies concept is based on primary (depositional) mineral assemblages, whereas the present assemblages are at least diagenetic and, for most Precambrian iron-formations, metamorphic. The primary precipitates are more likely to have been in the form of metastable iron compounds (e.g., Fe³⁺-hydroxides) whose Eh-pH stability fields cannot be defined with much confidence due to inadequate thermodynamic data (Ewers & Morris 1981). Thus, the facies classification of James (1954) may be applicable, at best, to conditions of diagenesis rather than of deposition.

Goodwin (1973) used the distribution pattern of Archean iron-formations by facies, along with other paleoenvironmental indicators, to identify a number of primitive depositional basins in the Archean crust of the Canadian Shield. However, the validity of the iron-formation facies as a paleodepth indicator is open to question. Observed facies patterns in Recent sediments do not conform to the pattern inferred by James (1954) (see Dimroth 1975), and Archean oxide iron-formations occur in deep-water

turbidite sequences in Canada (Walker 1978, Shegelski 1987). The rapid cyclic change from oxide facies to silicate-carbonate facies to oxide facies in the Hamersley Group BIF (Western Australia) appears to be related to volcanic activity, not depth control (Morris 1993). In the transgressive-regressive depositional model for the Transvaal Supergroup of southern Africa proposed by Klein and Beukes (1989), hematitic sequences were deposited in deeper water, away from a shallow water carbon supply, whereas pyritic shales formed in shallower waters with high carbon supply.

15.5. Types of Iron-formations

On the scale of entire stratigraphic units, iron-formations may be classified into three types (Gross 1965, 1973): (a) *Algoma-type*; (b) *(Lake) Superior-type*; and (c) *Rapitan-type*. A comparison of the three types is presented in Table 15.4.

Iron-formations associated with Precambrian greenstone belts constitute typical examples of the Algoma-type, although the Algoma-type is not strictly restricted to the Precambrian. The associated rocks — shale, graywacke, volcanics — indicate an “eugeosynclinal” environment of deposition with close spatial and temporal relationship to volcanism. Individual iron-formations seldom exceed 50 m in thickness and a few kilometers in lateral extent, but they are marked by rapid changes in thickness, sedimentary facies, and lithologic association. Thin-banding or lamination is characteristic, and oölitic or granular textures are absent or inconspicuous, except in post-Precambrian rocks.

The Superior-type iron-formations, so named because of their abundance in the Lake Superior region of USA and Canada (Fig. 15.4), are mostly Proterozoic in age. Closely associated rocks typically are quartzite and carbonaceous black shale, but the iron-formation itself is practically devoid of clastic material. Volcanic rocks, either as flows or more commonly as tuffs, are always present in the succession, but may not occur in direct contact with the iron-formation. Other characteristic features include alternate or rhythmic banding of iron-rich and iron-poor cherty layers, and granular and oölitic textures of both chert and iron minerals in some iron-formations (e.g., in the Lake Superior area and Labrador Trough). The depositional environment of Superior-type iron-formation is interpreted to be shallow-water continental shelves or “miogeosynclinal” basins close to continental margins.

The Rapitan-type, the least abundant of the three types of iron-formation, derives its name from the type occurrence (Snake River Iron Formation) in the late Proterozoic (about 700 Ma) Rapitan Group in the Mackenzie Mountain, NWT-Yukon, Canada (Yeo 1986, Young 1988). The Rapitan Group, the lowest unit of a passive margin sequence which passes up into the lower Cambrian, is an extensive, thick glacial-marine sequence. The iron-formation, up to 150 m in thickness, occurs in the lower part of the Rapitan Group, and is characterized by irregular banding between hematite and jasper. Iron-formations of similar age, character, and glaciogenic association include those of the Jacadigo Group, Urucum, Brazil (Hoppe et al. 1987) and Damara

TABLE 15.4. Comparison of Algoma-type, Superior-type, and Rapitan-type iron-formations (Eichler 1976, Gross 1980, James 1992)

	Algoma-type	Superior-type	Rapitan-type
Dimensions	Lenticular bodies, meters to tens of meters in thickness and a few kilometers in lateral extent	Large bodies, 100 m or more in thickness and tens to hundreds of kilometers in lateral extent	Large bodies, tens to hundreds of meters in thickness and up to hundreds of kilometers in lateral extent
Associated strata	Volcanic rocks and pyroclastics, graywacke; iron-formation irregularly distributed; volcanic components characteristic	Quartzite, dolostone, conglomerate, black shale; iron-formation generally in lower part of the sedimentary sequence; volcanic components relatively minor, but almost always present in the succession	Mudstone, shale, conglomerate, diamictite; stratigraphic position of iron-formation uncertain; some of associated rocks are of glaciogenic origin
Depositional environment	Orogenic, "eugeosynclinal" — submarine volcanic greenstone belts	Epeiorogenic, "miogeosynclinal" — stable shelf, marginal basins, generally nonvolcanic	Non-volcanic rift zones at continental margins
Sedimentary facies	All facies represented; oxide-facies predominant, but hematitic oxide facies rare	All facies represented; order of abundance of facies: oxide, carbonate, silicate, sulfide; sulfide facies may be insignificant or absent	Hematitic oxide facies only
Age	Predominantly Archean (> 2600 Ma), particularly late Archean, but some are as young as Paleozoic	Predominantly early Proterozoic (1900-2500 Ma)	Known deposits are late Proterozoic (800-700 Ma)
Examples			
USA	Vermilion district (Soudan IF), Lake Superior region	Marquette district (Negaunee IF), Menominee district (Vulcan IF), and Mesabi district (Biwabik IF), Lake Superior region	
Canada	Michipicoten district (e.g., Helen IF), Ontario; Abitibi greenstone belt, Ontario (Adams and Sherman mines)	Labrador Trough (Sokoman IF), Thunder Bay district (Gunflint IF), Ontario	McKenzie Mountains (Rapitan Group)
Southern Africa	?	Transvaal Supergroup (Kuruman and Penge IF) Transvaal and Northern Cape Province	Damara Supergroup
Australia	Greenstone belts of Yilgarn and Pilbara Blocks	Hammersley Basin (Hammersley Group), Pilbara Block	
USSR (former)	Urals	Krivoy Rog Basin and Kursk Magnetic Anomaly (KMA), Ukrainian Shield	
Brazil	Rio das Velhas Series	Quadrilatero Ferrifero (Minas Series), Serra dos Carajas (Grao Para Group)?	Urucum (Jacadigo Group)
India	Greenstone belts of the Indian Shield, Karnataka	Bihar and Orissa (Iron Ore Group) (Algoma-type?)	

Supergroup, southern Africa (Breitkopf 1988), both about 0.8 Ga in age.

The above classification scheme has served well to separate deposits of distinctly different associations (and perhaps genesis), but many iron-formations do not fit neatly into this scheme. For example, the iron-formations of the very extensive Orissa-Bihar belt in India (older than the Singhbhum Granite which is dated at 3.12 ± 0.01 Ga) have been classified as Superior-type by Chakraborty and Majumder (1986), but as Algoma-type by Radhakrishnan et al. (1986). Also, Radhakrishnan et al. (1986) have argued that iron-formations in the Archean granulite terrains of southern India are not merely high-grade metamorphic equivalents of Algoma- or Superior-type, but represent a distinct type, the "Tamil Nadu-type" of Prasad et al. (1982).

15.6. Examples

15.6.1. MICHIPICOTEN DISTRICT, LAKE SUPERIOR REGION, CANADA

The Michipicoten area, located in the northeastern Lake Superior region (Fig. 15.4), lies on the western part of the Algoma Basin, which is one of the 10 Archean volcano-tectonic basins in the Canadian Shield (Goodwin 1973). Each of the basins is characterized by a typical greenstone assemblage of mafic volcanics, related piles of felsic pyroclastics (tuff, breccia, agglomerate), clastic sediments (conglomerate, graywacke, arkose, shale), and chemical sediments (iron-formation).

The rocks of the complexly folded and faulted Michipicoten area (Michipicoten Group) are dominantly of submarine volcanic origin and, as is the case with most Archean greenstone belts, of mixed tholeiitic and calc-alkaline affinity. The mafic volcanic rocks are mainly flows of basalt with some andesite; the felsic volcanic rocks are dacitic to rhyolitic in composition and clearly of pyroclastic origin. The clastic rocks (the Dore sediments) range from thick, conglomeratic units in the western part to thin, fine-grained, graywacke-mudstone in the central and eastern parts. Banded iron-formation is widespread and displays systematic facies variation. In the western part, iron-formation units are enclosed in clastic sedimentary rocks and are typically composed of interbanded chert, magnetite, and jasper (oxide facies); sulfide and carbonate members are absent. In the central and eastern parts they occur at a prominent contact between felsic and mafic volcanic rocks and represent, respectively, chert-rich carbonate facies (containing minor sulfide members) and chert-poor sulfide facies (containing substantial carbonate members). A reconstruction of the pre-deformation stratigraphic section of the area by Goodwin and Shklanka (1967) is shown in Figure 15.5. The main paleoslope indicator used in this reconstruction is the triple lithofacies association of (a) oxide-carbonate-sulfide facies transition, (b) arc-type felsic pyroclastic piles, and (c) coarse-grained clastics including thick conglomeratic beds. The lensoid pattern of the stratigraphic units, with rapid facies changes, indicates that the Michipicoten Group was deposited in an "eugeosynclinal" environment.

The most important iron-formation in Michipicoten area is the 2.7 Ga-old Helen

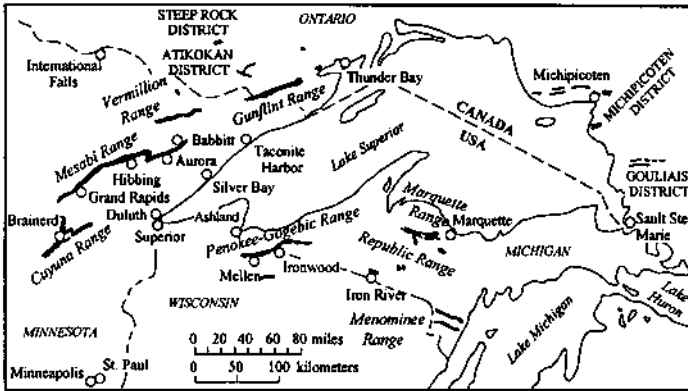


Figure 15.4. Sketch map of the Lake Superior region, USA-Canada, showing the location of major iron ore districts (modified from Marsden 1968).

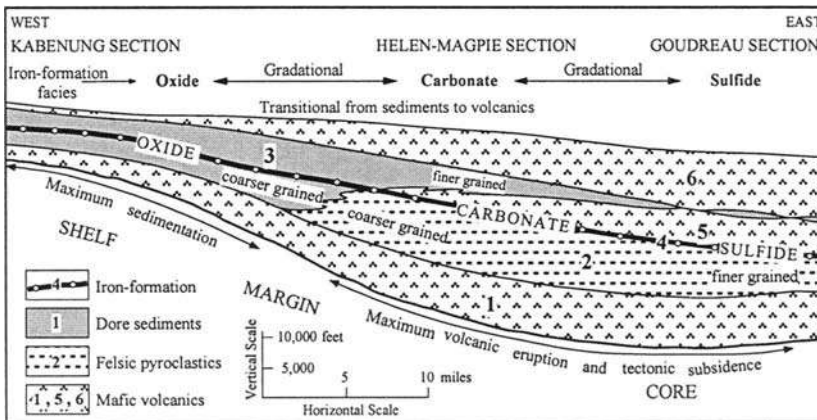


Figure 15.5. Reconstructed stratigraphic section of the Michipicoten area. Note the transition of iron-formation facies from oxide facies at the edge of the basin to sulfide facies in deeper parts. (After Goodwin 1973.)

Iron Formation (HIF), which is exposed in the 3.5 km-long Helen iron range and has been mined continuously since 1937. The mildly metamorphosed (greenschist facies) HIF overlies chemically altered rhyolite-dacite pyroclastics and is conformably overlain by pillowed mafic lava flows (Fig. 15.6). The HIF is divisible into a basal siderite-pyrite member, the 'ore' horizon, and an overlying banded chert member. Goodwin et al. (1985) proposed that the HIF was deposited in a transient cauldron subsidence basin undergoing intense exhalative activity. The deposition of different iron-formation

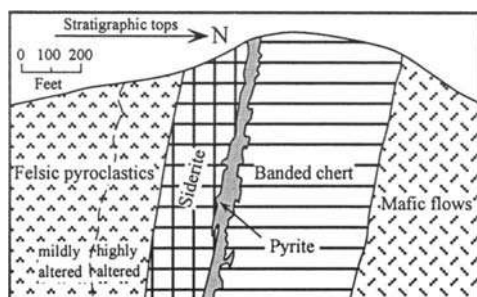


Figure 15.6. Cross section of the Helen Iron Formation, Michipicoten district, Ontario, Canada (after Goodwin 1964).

facies, according to this model, resulted from variations in Eh-pH and bacterial activity caused by three cycles of massive seawater-bearing volcanic exhalations. A *volcanic-exhalative model* is supported by the stratigraphic position of the iron-formation facies relative to the mafic and felsic volcanic units. Further evidence is provided by the presence of an ottrelite (Mn-chloritoid)-bearing footwall alteration pipe beneath the thickest and purest part of the siderite-pyrite member of HIF (Goodwin et al. 1985). The sulfur and carbon isotope data, according to Thode and Goodwin (1983), suggest a marine sulfate and marine carbonate origin for the sulfides and carbonates, respectively, and a vital role of organic activity as a catalyst in the carbonate-sulfide precipitation.

15.6.2. HAMERSLEY BASIN, PILBARA BLOCK, WESTERN AUSTRALIA

The present outcrop area of the Hamersley Basin in the western part of the Pilbara Block extends in excess of 1,00,000 km². All the iron-formations in the basin are hosted by the Hamersley Group (≈ 2.5 Ga), which is exposed discontinuously over an area of about 60,000 km² and attains a thickness of nearly 2,600 m. The following description has been extracted mostly from the review articles by Trendall (1983b), Morris and Horwitz (1983), McConchie (1987), and Morris (1993), which adequately summarize the information in earlier publications.

The Hamersley Group has been divided into eight formations (Fig. 15.7), which show remarkable lateral continuity and are separated by conformable contacts. Approximate modal values of lithotypes in the Hamersley Group are: 40% BIF, including six major, lithologically distinctive BIF units (Boolgeeda Iron Formation; Weeli Wollli Formation, excluding dolerite (diabase) sills; Joffre Member and Dales George Member of Brockman Iron Formation; Mount Sylvia Iron Formation; and Marra Mamba Iron Formation); 26% felsic volcanics; 15% dolerite sills, mostly within the Weeli Wollli Formation; 12% shale; 5% dolostone (mainly in the lower part of the Wittenoorn Dolomite Formation); and 2% tuff. The Woongarra Volcanics includes

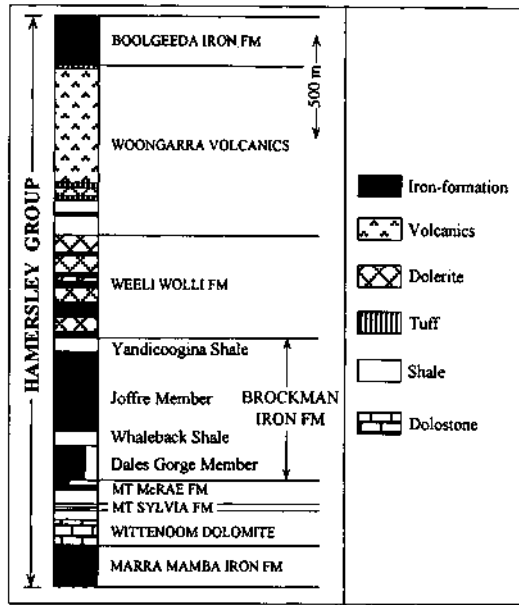


Figure 15.7. Generalized stratigraphic column for the Hamersley Group (after Morris 1993).

discrete bands of rhyolite and dacite as well as stratified tuff horizons, at least one major intercalation of BIF, and a dolerite sill. The felsic igneous rocks of Woongarra may actually be intrusives, rather than extrusives. The iron-formations show no evidence of lateral facies changes of the type described by James (1954). Fine-grained and commonly finely laminated shale, ranging in color from shades of green or gray to black (with an increase in carbon or sulfur content), is the main or an important constituent of Mount McRae Formation, Mt. Sylvia Formation, and Whaleback and Yandicooguna members of the Brockman Iron Formation. The shale contains intermixed chert and carbonate, and sometimes a minor proportion of iron-formation. The upper part of Mount McRae Formation contains thin bands of shard-bearing volcanic ash (now composed dominantly of stilpnomelane), but there is no direct evidence of a volcanic contribution (Trendall 1983b).

The Brockman Iron Formation comprises about 25% of the Hamersley Group succession and has experienced only low grade regional metamorphism, with maximum metamorphic temperatures between 270° and 310°C. The Dales George Member (approximately 160 m in thick) is of special significance as it is the major source of high-grade, low-phosphorous, hematite ore (>64% Fe, 0.5% P) in the Hamersley Range and, consequently, has been the subject of many detailed studies (e.g., Trendall & Blockley 1970, Morris 1980, Ewers & Morris 1981). The most conspicuous feature

of the Dales George Member is the banding on all scales, from several meters in thickness (macrobands) to very fine bands discernible only under a microscope (microlaminae). The terminology used for describing the hierarchy of banding is not uniform and tends to be confusing. The scheme adopted here, after Morris (1993), is summarized in Table 15.5 and schematically illustrated in Figure 15.8.

TABLE 15.5. Descriptive terminology for banding in banded iron-formation (BIF) in the Hamersley Basin, Australia (summarized from Morris 1993)

Terminology	Explanation
Macrobanding	Banding on a scale of decimeters to tens of meters between oxide-defined BIF and neighboring units which may or may not be BIF.
Mesobanding	Millimeter to decimeter scale (but typically in the centimeter range) banding (bedding) that is characteristic of BIF, each mesoband differing from its immediate neighbors by some significant variation in composition and texture (although, in practice, the demarcation may not be sharp).
Microbanding (Aftbanding)	Generally sub-millimeter scale (but ranging up to 5 mm or so) banding within a mesoband. The term was originally introduced by Trendall and Blockley (1970) to describe iron-rich and iron-poor couplets in a mesoband and equated with varves (in the usual sense of contrasting laminae representing seasonal deposition within one year), but is now often misused to describe individual laminae. The preferred term is "aftbands" (named so after A.F. Trendall) or "aftvarves" to emphasize its similarity to varves.
Microlaminae	Laminations measured in micrometers to tens of micrometers. A microlamina is generally monomineralic and rarely contains more than two components, forming a single, clearly defined microscopic layer.

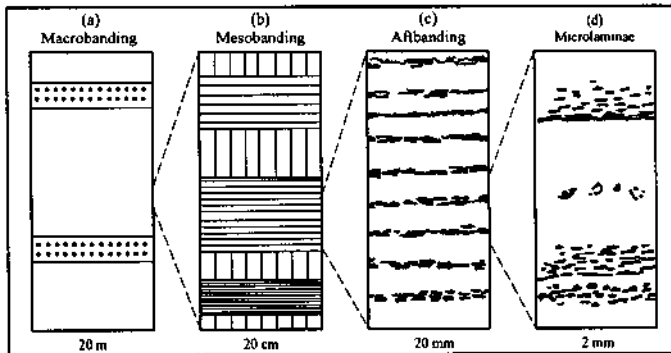


Figure 15.8. Schematic illustration of the hierarchy of banding (see Table 15.5) in Dales George Member of the Brockman Iron Formation, Hamersley Basin, Western Australia (modified from Trendall 1983b): a. macrobands of BIF (unpatterned) and S (stippled) units; b. mesobands of aftbanded chert (horizontal stripes) and chert-matrix (vertical stripes); c. aftbands within a chert mesoband; and d. microlaminae of hematite in iron-rich components of two successive aftbands. See text for explanation.

The Dales George Member, as defined by Trendall and Blockley (1970), comprises 33 macrobands — 17 chert-iron oxide 'BIF-macrobands' (2 to 15 m thick) alternating with 16 'S-macrobands' (<1 to 5 m thick). In unaltered material, the BIF-macrobands are characterized by the presence of magnetite + hematite and are analogous to typical Precambrian oxide-facies BIF of other continents. The magnetite ranges from overgrowths on primary hematite, through magnetite with hematite nuclei (Morris 1980), to magnetite that has been rendered essentially homogeneous by metamorphism. The S-macrobands, which typically contain no iron oxides, are composed mainly of dark-green to black, iron-rich, stilpnomelane-bearing and often finely laminated shale, and of interbanded chert and green siderite, which may be very finely laminated, more or less structureless, or thinly bedded. Thus, the S-macrobands also conform to James' (1954) definition of BIF (chert-carbonate and silicate facies).

From a careful analysis of continuous drill-core samples, Ewers and Morris (1981) have shown that, despite considerable variability within each macroband, the overall compositional difference between BIF- and S-macrobands is quite pronounced. However, most elements present in higher concentrations in S-macrobands are also relatively more abundant in the parts of BIF-macrobands immediately above and below the S-macrobands than in the central zones of the BIF-macrobands. These gradational zones are relatively depleted in iron oxides and enriched in siderite, ankerite, and silicates, which are more typical of S-macrobands. The relative enrichment of the "shale" component of S-macrobands in Al_2O_3 , TiO_2 , and K_2O , as well as the presence of occasional silicate (now dominantly stilpnomelane)-pseudomorphed shard bands (LaBerge 1966), suggest a pyroclastic origin of the "shale". However, the composition of the "shale", including its anomalous iron content, is not attributable directly to any known igneous rock type. Thus, it is likely that the "shale" contains at least a significant hemipelagic component, a product of reactions between iron-rich Hamersley waters and aluminous material of volcanogenic source (Ewers & Morris 1981).

Based on distinctive mineralogy (and lamination), a large variety of mesobands can be recognized in the BIF units. The most important of these are mesobands of relatively iron-poor (3-30% Fe) chert and iron-rich (average about 40% Fe) cherty material (designated as "cherty matrix" by Trendall & Blockley 1970) that commonly range from 5 to 15 mm in thickness and comprise about 60% and 20%, respectively, of the total BIF volume. Thus, the distribution of the chert and iron oxides forms the framework of the BIF; the remainder is made up of more random distribution of carbonates, apatite, riebeckite, and minor amounts of other silicates.

Regular to irregular internal laminations are a common feature of the Hamersley Group BIF. In many chert mesobands, the lamination is defined by layers of some iron-bearing mineral within the general mosaic of chert, and is known as "aftbanding" (Fig. 15.8). The defining mineral of the main iron-rich component of each aftband is normally hematite, siderite, or ankerite, but may also be magnetite, stilpnomelane, or riebeckite. An aftband was originally defined to consist of a simple iron-rich/iron-poor couplet (Trendall 1983a); in reality it may be much more complex, some containing as many as 20 subzones (Ewers & Morris 1981). Chert-matrix mesobands, in contrast,

have no regular aftbanding, although there is often a vaguely defined and irregular streakiness, or sometimes even a very regular, fine lamination. As illustrated by Ewers and Morris (1981), there is a significant level of repetitive fine lamination which appears to represent some episodic feature, but it is too complex to be attributed entirely to annual cycles of deposition (Morris 1993).

A remarkable feature of the Dales George Member is the lateral continuity of various scales of banding. The macrobands are unbroken over virtually the entire outcrop area; only at a few southern marginal localities do some S-macrobands appear to be absent. The lateral continuity of smaller scale banding, especially of aftbands, is not so clearly demonstrable. Using drill-core samples, Ewers and Morris (1981) correlated mesobands in a BIF macroband of the Dales George Member over a strike distance of 130 km. [McConchie (1987) mentioned tentative correlation of mesobands in the Joffre and Whaleback members between localities over 400 km apart!] Lateral continuity on such a scale may be the exception rather than the rule, but the overall style of banding can be matched on a basin-wide scale, suggesting relatively uniform depositional conditions for each mesoband. The lateral variations in the composition and internal structure of mesobands probably reflect local fluctuations in the depositional setting as well as the effects of later diagenesis and metamorphism.

15.7. Ore Composition

15.7.1. MINERALOGY AND TEXTURES

The mineralogy of iron-formations varies with facies and is the result of a combination of depositional, diagenetic, and metamorphic processes. The most important minerals, depending on the facies, are hematite [α - Fe_2O_3], magnetite, siderite, pyrite, and chamosite [$(\text{Mg,Fe,Al})_6(\text{Si,Al})_4\text{O}_{14}(\text{OH})_4$]. Other important associated minerals include quartz (chert, jasper), carbonates (ankerite, dolomite, calcite), and silicates (riebeckite, greenalite [$\text{Fe}_9^{2+}\text{Fe}_2^{3+}\text{Si}_8\text{O}_{22}(\text{OH})_{12}\cdot 2\text{H}_2\text{O}$], minnesotaite [$\text{Fe}_3(\text{OH})_2\text{Si}_4\text{O}_{10}$], members of the cummingtonite-grunerite series, and iron-chlorite). The physical and chemical characteristics of the common minerals in iron-formations have been described in detail by Gross (1965) and James (1966).

Primary sedimentary features in iron-formations described in the literature include banding, cross-stratification, flat-bed conglomerates, scour-and-fill structures, oölitic textures, soft-sediment deformation structures, and stromatolites (Simonson 1985). A distinctive and common feature of iron-formations is the banding on all scales (see Fig. 15.8 and Table 15.5) and its lateral continuity, especially in relatively undeformed sequences such as those of the Hamersley Range (Western Australia) and the Kuruman Iron Formation Sequence (South Africa). Most typical is the centimeter- to millimeter-scale mesobanding comprised of alternating silica-rich and iron-rich layers. Typically, the mineral constituents of a given layer are uniform laterally (except where there is

independent evidence of diagenetic alteration), but abrupt changes from one layer to the next are not uncommon. The alternation of iron-rich and silica-rich mesobands is attributed to controls that permitted the accumulation of one to dominate over the other (Ewers & Morris 1981). The alternative model involving diagenetic differentiation of a relatively uniform, gel-like, primary precipitate due to vertical escape of silica, as was proposed by Trendall and Blockley (1970), is not compatible with the highly variable total REE to total Fe ratio in each matching set of high- and low-iron mesoband (Morris 1993). This ratio should be quite uniform if the relatively high concentration of iron in a mesoband was the consequence of silica loss. Where the lutitic and arenitic iron-formations are interbedded on a scale of centimeters to tens of centimeters, the arenites are segregated into lenses and wavy layers, whereas the lutitic layers tend to be more even and continuous (Simonson 1985). Such structures, which have been termed "wavy banding" if the sands form continuous layers, or "lenticular bedding" if the sands form trains of discontinuous lenses, probably resulted from differential compaction rather than depositional processes.

Transitions between mesobanded iron-formations and granular iron-formations are not common in the stratigraphic record. A well-studied occurrence of such transition is between the banded Kuruman iron-formation and the granular Griquatown iron-formation in the early Proterozoic Transvaal Supergroup (Beukes & Klein 1990). The non-banded iron-formations containing granules, ooids, and cross-bedding are generally considered the shallow water equivalents of the BIF of deeper water origin (Simonson 1985). The Kuruman-Griquatown transition zone, however, lacks the oolitic textures, cross-bedding, and hematite typical of other granular iron-formations, and its deposition appears to have taken place in relatively deep water, probably by storm-reworking of what originally may have been a typical mesobanded iron-formation sequence.

15.7.2. BULK COMPOSITION

The chemical composition of iron-formations vary according to facies, reflecting the differences in mineralogy. Table 15.3 gives the average compositions of Algoma-type and Superior-type iron-formations as estimated by Gross and McLeod (1980) using the data base compiled at the Geological Survey of Canada. It should be noted that the average values in this table offer no insight into the wide range and prominent skewness in many of the data sets. Compositional data compiled by Davy (1983) clearly show that considerable variations exist among mesobands of the same facies, and even within the same mesoband, in a given iron-formation. On the other hand, Klein and Beukes (1992) have argued that the averages for the major oxide components as well as of sulfur and carbon contents (recalculated on H₂O- and CO₂-free basis to make the analyses of unmetamorphosed and metamorphosed samples comparable) for a range of Precambrian iron-formations (Isua, Transvaal, Hamersley, Labrador Trough, Lake Superior region) are remarkably similar. The only iron-formation which is radically different from any of the others is the Rapitan iron-formation, which is composed almost entirely of chert and hematite. The averages for this comparison are

based on relatively small number of samples and are not weighted against the relative abundances of the iron-formation facies, but the overall similarity in bulk composition across space and time, excluding the Rapitan-type, does suggest a broadly common genesis for iron-formations.

As expected, silica and iron are the predominant constituents of all iron-formations. $\text{Fe}^{3+}:(\text{Fe}^{2+}+\text{Fe}^{3+})$ ratios are relatively low (0.3-0.6), reflecting the abundance of magnetite as well as Fe^{2+} -minerals, such as iron-carbonates and iron-silicates (Gole & Klein 1981). This means that the oxygen partial pressure required for the deposition of iron-formations was significantly less than what would have been required if hematite were the predominant iron mineral. Al_2O_3 , Na_2O , K_2O , and P_2O_5 are typically very low, as are base metals (Cu, Pb, Zn, Co, Ni). Manganese commonly occurs only in trace amounts, but many Algoma- and Superior-type iron-formations contain interbedded manganese-rich horizons ("banded cherty manganese iron facies"), some of which are rich enough to qualify as manganese ore. The majority of these manganese occurrences are associated with tuff or other volcanic rocks and are believed to have been deposited in environments similar to Algoma-type iron-formations (Gross 1986).

Small but significant concentrations of gold occur in the different facies of iron-formations (Table 15.3), the background values ranging up to 120 ppb in Algoma-type and 75 ppb in Superior-type (Gross 1986). Gold deposits hosted by iron-formations are quite common in the Archean greenstone belts of Canada (Colvine et al. 1984) and southern Africa (Fripp 1976, Foster & Gilligan 1987). These deposits are of two types: strata-bound, disseminated deposits in which the gold usually occurs in free state or in a finely divided state in sulfate or arsenide minerals; and lode deposits consisting of zones of quartz veins or stockworks in which gold is generally present in the native state. The latter type is clearly epigenetic and is believed to be related to tectonic deformation. Gold enrichment of the former type has been ascribed to chemical sedimentation (e.g., Fripp 1976) or hydrothermal replacement (Phillips et al. 1984).

15.7.3. ORGANIC MATTER

Morphological fossils have been reported from about 30 Precambrian iron-formations around the world, but only half a dozen of these have remains that can be unequivocally called biogenic (Walter & Hofmann 1983). Neither stromatolites nor convincing microfossils are known from Archean iron-formations, although both are known from other kinds of Archean sediments. The oldest definite microbial fossils yet described are from carbonaceous cherts of the Warawoona Group (3.5 to 3.3 Ga) in Western Australia (Schopf & Packer 1987). Archean iron-formations, however, contain organic matter in the form of kerogen (degraded chemical remnants of macromolecular organic matter), and the highly metamorphosed, 3.8 Ga-old iron-formation of the Isua belt (Greenland) contains graphite of possible biogenic precursor.

Although microfossils are not widespread in Proterozoic iron-formations, several (e.g., Gunflint, Biwabik, Sokoman) contain structurally preserved remains of organisms in stromatolitic microbial mats as well as in non-stromatolitic beds. These

organisms are all microscopic, generally between 1 to 10 mm in cell diameter; the most common types are spheroidal and filamentous.

Indirect evidence of microbial activity during the Precambrian is provided by carbon isotope ratios of kerogen in sediments. Compilation of isotopic composition as a function of time (Schidlowski et al. 1983) shows that $\delta^{13}\text{C}$ (PDB) values of late Archean (2.5-2.8 Ga) kerogens range from about -10‰ to less than -40‰ , similar to those for Precambrian iron-formations (-15 to -38‰ ; Walter & Hofmann 1983). Considering that highly negative $\delta^{13}\text{C}$ values have so far been reported only in connection with reprocessing of organic material involving biogenic methane, it is logical to suggest that the ^{13}C -depleted kerogens are linked in some way to the production and utilization (i.e., to make cellular material which is incorporated in kerogen) of biogenic methane. This conclusion implies that methanogens (bacteria capable of producing methane as a metabolic byproduct of the reduction of CO_2) and methyltrophs (bacteria capable of metabolically oxidizing methane) had developed at least by the late Archean, perhaps even earlier. The required oxidant is believed to have been oxygen, rather than sulfate, as is the case in some modern anaerobic sedimentary environments (Hayes 1983). The widespread development of iron-formations in the Archean, requiring oxidizing conditions at least locally in sedimentary basins, also points to the availability of some free oxygen at this time.

15.8. Metamorphism

All exposed iron-formations are metamorphosed to some degree. A comparison of bulk compositions of major iron-formations around the world suggests that metamorphism was essentially isochemical except for the loss of H_2O and CO_2 (Gole & Klein 1981, Klein 1983). The mineralogic evolution of iron-formations as a result of metamorphism, reviewed in considerable detail by Klein (1983), is summarized in Figure 15.9. For this figure, low-grade corresponds to chlorite-biotite zones of regional metamorphism (greenschist facies), medium-grade to garnet-staurolite zones (epidote-amphibolite and lower amphibolite facies), and high-grade to sillimanite zone (upper amphibolite and granulite facies) and contact metamorphic hornfels facies.

The transition from diagenesis to low-grade metamorphism is probably marked by the formation of minnesotaite at the expense of greenalite. For this reaction, Miyano (1987) estimated a minimum temperature of 130°C at 1 kb in the presence of magnetite (hematite absent). Medium-grade assemblages are characterized by the common development of amphiboles, mainly members of the cummingtonite-grunerite series. The upper stability limit of minnesotaite in a minnesotaite - grunerite - quartz assemblage of pure phases was calculated by Miyano (1987) as $330^\circ\text{--}360^\circ\text{C}$ at pressures below 3 kb. Anhydrous assemblages dominated by variable amounts of orthopyroxene and clinopyroxene are typical of high-grade metamorphism. *P-T* estimates indicate granulite facies conditions for many regionally metamorphosed iron-formations: for example, $700^\circ\text{--}750^\circ\text{C}$ and 10-11 kb in Labrador Trough (Klein 1978); $745^\circ \pm 50^\circ\text{C}$ and

		GRADE OF METAMORPHISM			
		LOW	MEDIUM		HIGH
DIAGENETIC		BIOTITE ZONE	GARNET ZONE	STAUROLITE-KYANITE AND KYANITE ZONE	SILLIMANITE ZONE
Early	Late				
chert	→	quartz			
"Fe ₃ O ₄ ·H ₂ O"	→	magnetite			
"Fe(OH) ₃ "	→	hematite			
greenalite					
stilpnomelane					
		ferri-annite			
		talc - minnesotaite			
		Fe-chlorite (ripidolite)			
		dolorite - ankerite			
		calcite			
		siderite - magnesite			
		riebeckite			
		cummingtonite - grunerite (anthophyllite)			
		tremolite - ferroactinolite (hornblende)			
		almandine			
		orthopyroxene			
		clinopyroxene			
					fayalite

Figure 15.9. Stability ranges of principal constituents of iron-formations, from sedimentary-diagenetic stage to high-grade metamorphic stage (after Klein 1983).

6-8 kb in Tobacco Root Mountains of southwestern Montana (Dahl 1979); and 720°-820°C and 7-11 kb in southern Karnataka, India (Devraju & Laajoki 1986). Fayalite-bearing assemblages occur mainly in iron-formations of hornfels facies within the contact metamorphic aureoles of major mafic intrusions. Maximum *P-T* estimates are in the order of 800°C and 2 kb for Biwabik and Gunflint Iron Formations in the contact zone of the Duluth Gabbro Complex (French 1968, Floran & Papike 1978).

Magnetite and hematite are diagenetic products of ferrous and ferric hydrate precipitates. Once formed, both persist as stable phases through metamorphism, although the degree of metamorphism has a definite effect on the internal microstructure of magnetite. An increase in the magnetite:hematite ratio with increasing metamorphic grade has also been reported in some cases (Floran & Papike 1978, Ewers & Morris 1981). The oxide-facies iron-formations, which consist mainly of a mixture of quartz, magnetite, and hematite, show no reactions among the constituent minerals even at the highest grades of metamorphism, but tend to become coarser grained and equigranular due to recrystallization (Klein 1983). The consistency of mineralogy is the reason why oxide facies iron-formation is readily recognized irrespective of the metamorphic grade.

Metamorphic recrystallization may accentuate the primary banding, or obscure it if

individual minerals grow to grain sizes which exceed the thickness of primary banding, especially if reactions involving initial silicate and carbonate minerals result in the formation of new minerals. The metamorphic banding is commonly parallel to the primary bedding planes, but it may also follow the schistosity of the rock, thus obliterating the original bedding (Eichler 1976). In general, much of the characteristic thin bedding of iron-formations survives metamorphism.

15.9. Secondary Enrichment

Much of the BIF-hosted iron ores actually mined today around the world are from hematite (martite)- or goethite-rich deposits, with grades ranging from about 50-55% Fe to more than 68% Fe, produced by secondary enrichment. Details of the enrichment process vary from one iron-formation to another, depending on the starting material and subsequent geologic history. A generalized conceptual model incorporating alternate pathways to iron enrichment has been described by Morris (1985).

The most important component of the iron enrichment process is one or more stages of supergene enrichment (see Ch. 2). Morris (1985) argued that exposed iron-formations throughout the world experienced significant supergene iron enrichment at about 2000 ± 200 Ma because of an increase in the atmospheric oxygen, and that the major, *in situ* BIF-derived iron ores of the world formed either entirely or at least initially by supergene enrichment. In essence, the process involved conversion of magnetite to martite and goethite, metasomatic replacement of gangue minerals by goethite, and leaching of soluble constituents. The hematite of BIF was not affected, although much of the 'hematite' in the ores may actually be martite. Leaching of silica is a prerequisite for the development of high-grade ores and, because of its low solubility, is likely to have been the rate-controlling process.

15.10. Origin

Iron-formations exhibit significant differences in thickness, lateral continuity, sedimentary structures, lithologic association, and stratigraphic framework, indicating a spectrum of depositional environments. However, their similarities in terms of bulk composition, mineralogy, and banding point to deposition under broadly similar chemical conditions.

A variety of models have been proposed for the origin of iron-formations (see Gross 1965 for a review of earlier literature). A major limitation is the absence of convincing modern analogs. The critical features which must be accounted for by a viable genetic model are: (a) source(s) of the vast amounts of iron and silica, and transport of the ore-forming constituents to the sites of deposition; (b) mechanisms of iron and silica precipitation and facies variations; (c) rhythmic banding and the lateral continuity of mesobanding; and (d) a virtual lack of iron-formations younger than 1.7 Ga.

15.10.1. TRANSPORT OF IRON AND SILICA

Iron-formations are believed to be chemical sediments deposited in an aqueous medium into which iron and silica were introduced as dissolved constituents. It is unlikely that these constituents were introduced as solid particles, because terrigenous sediments would inevitably have contained more aluminum relative to iron and cosmic dust would have contained more nickel.

In aqueous solutions, iron can occur in two valence states, ferrous (Fe^{2+}) and ferric (Fe^{3+}), and form various complexes in the presence of anions. Sulfate and chloride complexes are stable only in very acidic environments; carbonate and bicarbonate complexes are unstable; and phosphate complexes are of no practical importance because of the extremely low concentration of phosphoric acids in natural waters. Iron is virtually insoluble in the ferric state (as Fe^{3+} , FeOH^{2+} , $\text{Fe}(\text{OH})_2^+$ aqueous species) in the pH range of most natural waters (pH = 4 to 9). Colloidal solutions of Fe^{3+} prepared in the laboratory can remain stable to high concentrations in dilute electrolyte solutions, but they are readily destabilized by salts and are unlikely to have transported large quantities of iron (Mel'nik 1982). Thus, there is general agreement that iron was transported in solution in the Fe^{2+} state, as $\text{Fe}^{2+}(\text{aq})$ or $\text{FeOH}^+(\text{aq})$ species, and precipitated as various Fe^{3+} -bearing compounds depending on the geochemical parameters of the depositional environment.

The solubility of various ionic species and compounds of iron in an aqueous medium is controlled by both pH and Eh of the medium, as well as by the interdependent activities of other species of which the most important, in the present context, are those that govern oxide, carbonate, sulfide, and silicate equilibria. Examples of stability relations at standard temperature and pressure conditions and geologically reasonable values of Eh, pH, and ionic concentrations are shown in Figures 15.2 and 15.10; similar diagrams for other specified boundary conditions can easily be constructed from available thermodynamic data. Eh-pH diagrams constructed for manganese species under similar constraints (Garrels & Christ 1965) provide a likely explanation for the separation of Fe from Mn in the aqueous environment. Soluble Mn has a considerably larger stability field than soluble Fe under moderately reducing conditions and, because many sediments become reducing a few centimeters below the sediment-water interface, there should be mobilization of Mn^{2+} into the pore water, while iron remains fixed as an oxide or hydroxide (Maynard 1983). A limitation to the application of these theoretical diagrams is that in nature iron compounds (especially carbonate, silicate, and sulfide minerals) seldom form as pure phases as is assumed for constructing these diagrams. Also, reactions of $\text{Fe}^{2+}(\text{aq})$ to form stable phases, such as crystalline Fe_2O_3 , may be inhibited by kinetic barriers and metastable phases, such as amorphous $\text{Fe}(\text{OH})_3$, may form instead (Ewers & Morris 1981).

In aqueous solutions, silicon exists in only one valence state, as Si^{4+} , and in natural surface environments the initial precipitation of silica normally occurs as amorphous silica or magadiite [$\text{NaSi}_7\text{O}_{13}(\text{OH})_3$], rather than as crystalline α -quartz. The solubility

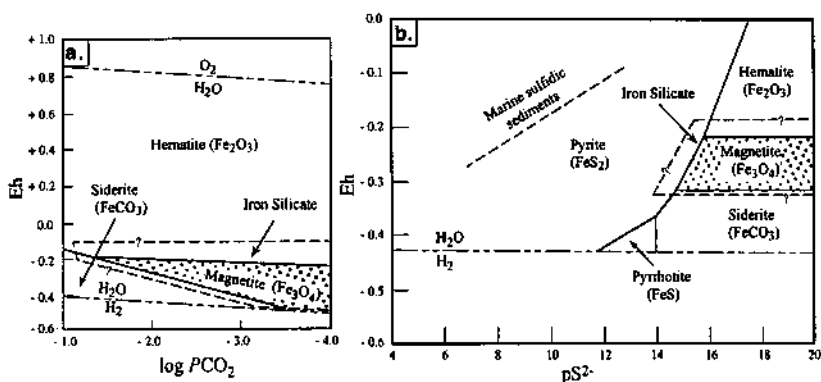


Figure 15.10. Stability fields of common iron minerals at $T = 25^\circ\text{C}$ and $P_{\text{total}} = 1$ atm, calculated from thermodynamic data (after Berner 1971): a. Eh- $\log P_{\text{CO}_2}$ diagram, assuming $a_{\text{Ca}^{2+}} = 10^{-2.58}$, equilibrium with calcite, and a $p\text{S}^{2-}$ value high enough to exclude pyrite and pyrrhotite as stable phases; b. Eh- $p\text{S}^{2-}$ diagram, assuming $\log P_{\text{CO}_2} = -2.40$ corresponding to $\text{pH} = 7.37$. $p\text{S}^{2-} = -\log a\text{S}^{2-}$ and, unlike pH , is independent of Eh. Measurements of natural sulfidic marine sediments fall closely along the dashed line. The stability fields of iron silicate minerals, taken from Dimroth (1977b), are not well constrained.

of amorphous silica, as $\text{Si}(\text{OH})_4^0$ or H_4SiO_4^0 , is in the order of ≈ 120 mg/l (compared to only ≈ 6 mg/l for α -quartz), and the solubility is affected very little by pH over the range encountered in natural waters or by salinity up to the composition of modern seawater (Fig. 15.11). Crystalline magadiite in contact with seawater is less soluble than amorphous silica at pH values above 5.2. The kinetics of magadiite precipitation are not known, so that the solubility of either magadiite or amorphous silica may have limited the dissolved silica content of seawater at intermediate pH values ($\text{pH} = 6$ to 8). The low concentration of dissolved silica in the modern oceans, increasing from $\ll 1$ mg/l at the surface to < 10 mg/l at depth, is attributed to the uptake of silica by marine organisms (MacKenzie 1975). It is likely that the Precambrian oceans, in the absence of silica-secreting organisms, were saturated with respect to amorphous silica (Siever 1957) and/or magadiite. Using reasonable estimates for the pertinent fluxes and reaction rates, Siever (1992) arrived at a silica concentration of about 60 ppm for late Precambrian seawater, and it is reasonable to assume this as a minimum concentration of silica in seawater earlier in the Earth's history (Simonson & Hassler 1996).

15.10.2. SOURCES OF IRON AND SILICA

In the absence of terrigenous clastics in iron-formations, the chemically precipitated components must have been derived mainly from the oceans. Three major sources of iron and silica in the oceans have been proposed: (a) chemical weathering of continents

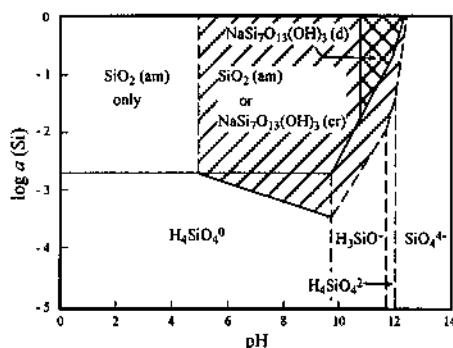


Figure 15.11. Calculated stability fields of aqueous ionic species and amorphous silica precipitate [$\text{SiO}_2(\text{am})$] and the fields (diagonally hatched) of possible formation of crystalline magadiite [$\text{NaSi}_7\text{O}_{13}(\text{OH})_3(\text{cr})$] and freshly precipitated amorphous (dispersed) magadiite [$\text{NaSi}_7\text{O}_{13}(\text{OH})_3(\text{cr})$] at 25°C and for a sodium concentration of about 1 g.ion/l, which approximately corresponds to the salt content of the present ocean. Note that the solubility of amorphous silica is independent of pH up to about pH = 10, and that crystalline magadiite is significantly less soluble than amorphous silica at pH >5.2; both are considerably more soluble than α -quartz. (After Mel'nik 1982.)

under anoxic atmospheric conditions (James 1954, Lepp & Goldich 1964, Garrels et al. 1973, Schidlowski 1976, Reimer 1987); (b) continental sediments in the ocean (Strakhov 1959, Borchert 1960, Holland 1973, Drever 1974); and (c) submarine reactions of 'hot spot' or MOR-type lavas and concomitant hydrothermal emanations (Goodwin 1973, Goodwin et al. 1985, Gross 1965, 1980, Dymek & Klein 1988, Beukes et al. 1990). Most genetic models emphasize one of these sources, none of which is entirely satisfactory. The variations in mesobanding in iron-formations suggest the irregular dominance of one or other of the sources, with pyroclastic and hemipelagic components adding further complexities (Morris 1993). Manikyamba et al. (1993) showed that the trace element composition of BIF of the Archean Sandur greenstone belt (India) requires the mixing of minor volcanoclastic and terrigenous components with a dominantly MOR-type hydrothermal source.

Accepting that the Precambrian atmosphere had a much higher P_{CO_2} (see Ch. 14), the surface water in equilibrium must have been more acidic, promoting faster chemical weathering of continental rocks. However, an entirely continental source of iron by chemical weathering, even under a presumably Precambrian anoxic atmosphere that would facilitate the transport of iron as soluble $\text{Fe}^{2+}(\text{aq})$ or $\text{Fe}(\text{OH})^+$ aqueous complex, is untenable because of mass balance constraint (Holland 1973). For example, Trendall and Blockley (1970) estimated a total of 10^{20} g of Fe in the Hamersley Basin BIF and a depositional duration of about 6 million years, implying a depositional rate of some 2×10^{13} g Fe/year and an equal or greater rate of iron flow into the basin. It is difficult to reconcile how such a high rate of flow, about five times that of the Mississippi

River, would deliver sediments devoid of terrigenous detritus. Even an order of magnitude higher content of dissolved Fe because of likely higher CO₂ content of the Precambrian atmosphere, or a significantly longer duration of iron deposition, would not resolve the problem. Another objection to a landward source of iron is the shallow-water deposition of the oxide-facies of many iron-formations indicating mildly oxidizing condition of surface waters, which would have prevented the transport of significant quantities of dissolved Fe²⁺ to deeper parts of the basin (Simonson 1985).

The idea of an oceanic source of iron, chiefly from sea-bottom clastic sediments, was suggested by Strakhov (1959) and Borchert (1960), and later by Holland (1973). The concentration of iron in the modern ocean is about 0.01 mg/l, so that the total iron content of the oceans, which contains about 1.286×10^{21} liters of water, is less than the iron contained only in the Hamersley Basin BIF. However, under an oxygen-deficient atmosphere, it is likely that the bottom waters of the Archean and early Proterozoic oceans were reducing (see Fig. 14.18) and could contain about 3 ppm Fe²⁺ at pH = 7.0 and 30 ppm Fe²⁺ at pH = 8.0, if the water was saturated with calcite and siderite (Holland 1973). Upwelling of such bottom waters to continental margin basins and shelves could lead to oxidation and precipitation of Fe(OH)₃ in shallow waters. The process of transfer of dissolved Fe²⁺ to sites of deposition was probably analogous to the upwelling mechanism that brings phosphorous-rich waters from deeper parts to shallow shelves of the present oceans and is invoked to explain the occurrence of major phosphorite deposits in the stratigraphic record (Button et al. 1982). If the Precambrian oceans were saturated with respect to amorphous silica and/or magadiite, the upwelling could also cause supersaturation and precipitation of silica because of decreased solubility with decreasing pressure. Silica saturation in the shallow waters could also be attained through evaporation (Eugster & Chou 1973). The quantitative aspects of the model are quite satisfactory. For example, deposition of the 2×10^{13} g Fe/year in the Hamersley Basin from waters with 3 ppm Fe would require passage of seawater through the basin at a rate of 0.7×10^{16} l/year (Holland 1973), which is comparable to the present-day annual circulation in the Mediterranean Sea (Schink 1967).

For Algoma-type iron-formations, which are closely associated with volcanic complexes, submarine volcanic exhalations appear to be a reasonable source of the iron, and even some silica, through a combination of direct magmatic differentiation and leaching of volcanic rocks by saline waters. If the iron for Superior-type iron-formations, which are not typically associated with volcanic rocks, was also derived from contemporaneous volcanism, the source had to be distal, as was proposed by Trendall and Blockley (1970) for the Hamersley Basin. Using the rate of iron discharge (30 to 50 tons/year) from Ebeko volcano in the Kurile Islands, the most productive volcanic source of iron yet known, Holland (1973) estimated that, to supply in six million years the quantity of iron present in the Hamersley Basin, the basin had to be rimmed with active, iron-producing volcanoes at one-mile intervals. Such a setting would be inconsistent with the structural stability indicated by the great lateral continuity of banding and the general absence of recognizable volcanic debris in the BIF. Morris (1993), on the other hand, discussed the possibility of MOR-type volcanic

activity not far away from the present outcrop limits of the Hamersley Group, along a divergent plate margin that led to the breakup of the Pilbara continent.

As discussed by several authors (Dymek & Klein 1988, Derry & Jacobsen 1990, Beukes et al. 1990, Danielson et al. 1992, Klein & Beukes 1992), involvement of MOR-type hydrothermal fluids in the deposition of Archean and early Proterozoic iron-formations is supported by their REE patterns normalized to the North American Shale Composite (NASC) of Gromet et al. (1984). The REE patterns, characterized by pronounced positive Eu anomalies, negative Ce anomalies, and relatively depleted light REE (Fig. 15.12), are similar to those of some modern deep-sea MOR vent fluids and hydrothermal sediments. The size of the Eu anomaly decreases progressively from older to younger iron-formations and disappears in iron-formations younger than middle Proterozoic, suggesting a gradual decrease in the hydrothermal input. This is illustrated in Figure 15.12 by the pattern for a typical Rapitan-type iron-formation sample (nodular, laminated hematite-chert), which lacks an Eu anomaly and is actually similar to the REE pattern of modern seawater at 100 m depth. The pattern for the granular Rapitan sample, which has a volcanoclastic component, does show an Eu anomaly similar to that in rift areas of modern oceans, probably reflecting the proximity of this sample to hydrothermal source terranes.

A contribution of mantle-derived hydrothermal fluids in the deposition of pre-middle Proterozoic BIF is also supported by the available Nd isotopic data (Derry & Jacobsen 1990). Precambrian BIFs show a consistent pattern of mantle-like positive initial ϵ_{Nd} values ($0 < \epsilon_{Nd} < +4$) prior to about 2.0 Ga, which contrasts strongly with the negative, continental-like values of Phanerozoic seawater (Jacobsen & Pimentel-Klose 1988). The relatively large range of ϵ_{Nd} may be explained by the precipitation of BIF due to

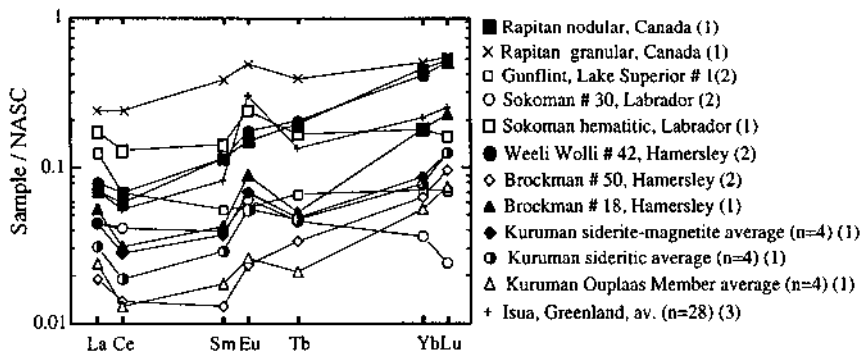


Figure 15.12. REE patterns of selected Archean and Proterozoic iron-formations. The REE values are normalized to the North American Shale Composite (NASC) given by Gromet et al. (1984). Note the positive europium anomaly and negative cerium anomaly for most of the samples. Sources of data: (1) Klein & Beukes 1992, (2) Danielson et al. 1992, (3) Dymek & Klein 1988.

mixing of Fe-poor surface waters with $\epsilon_{\text{Nd}} < 0$ and Fe-enriched deep waters with $\epsilon_{\text{Nd}} \approx +4$. The depositional model proposed by Morris (1993) for the Hamersley BIF postulated the mixing of surface waters containing 1-3 ppm Fe^{2+} with upwelling bottom waters containing 4-20 ppm Fe^{2+} . According to Derry and Jacobsen (1990), the transition from Archean mantle-dominated systematics to modern seawater behavior was established by approximately 0.7-0.8 Ga.

15.10.3. SOURCE OF SULFUR

The source of sulfur in iron-formations is believed to be the sulfate in contemporary seawater, but the sulfur isotopic data do not provide a clear picture regarding the mechanism of sulfate reduction. Thode and Goodwin (1983) found highly variable sulfide $\delta^{34}\text{S}$ values from the sulfide and pyrite-siderite facies of five Archean (≈ 2.7 Ga) iron-formations distributed across the Canadian Shield. For example, the Helen Iron Formation, excluding the oxide facies, showed a $\delta^{34}\text{S}$ range of 30.2‰, a mean value of 2.5‰, and a standard deviation of 7.3‰. They concluded that only bacterial reduction of seawater sulfate at low temperatures could produce such wide ranging, highly variable $\delta^{34}\text{S}$ values. A compilation of $\delta^{34}\text{S}$ values for Precambrian sulfides, predominantly from BIF and stratiform to strata-bound sulfide deposits and their associated sediments, also suggests that a bacterial origin of sulfur (i.e., characterized by wide spreads and preponderance of negative values) can be traced to about 2.7 Ga, although good evidence of bacterial sulfate reduction is found in the sulfides of somewhat younger age (2.2-2.3 Ga) (Schidlowski et al. 1983). In contrast, $\delta^{34}\text{S}$ values of all known older sulfide occurrences cluster closely around 0‰. Such a pattern is particularly pronounced for the sulfide samples from the BIF of the 3.8 Ga-old Isua supracrustal belt (West Greenland), whose mean $\delta^{34}\text{S}$ value of $+0.5 \pm 0.9\%$ (Monster et al. 1979) represents the oldest data point in the sulfur isotope record. Considering that sulfate may have been quite abundant in the oceans as early as 3.5 billion years ago (Lowe & Knauth 1977), the modest variations in $\delta^{34}\text{S}$ values of sulfides in Archean sediments older than 3.2 Ga (Perry et al. 1971) may be interpreted as constraining the advent of sulfate reducers. Others have appealed to abiogenic mechanisms to explain the Precambrian sulfur isotope data. For example, the $\delta^{34}\text{S}$ values of seven units of Proterozoic sulfide-facies iron-formation — -4.9 to $+6.6\%$, with low sample variance within each unit — were interpreted by Cameron (1983) to indicate sulfide of hydrothermal origin, from high-temperature reduction of seawater sulfate and from magmatic sulfide. Skyring and Donnelly (1982) suggested that the late Archean patterns might be indicative of a combination of magmatic sulfide and sulfide derived from either hydrothermal or biogenic sulfate reduction.

15.10.4. PRECIPITATION MECHANISMS

Noting the similarity in sedimentary textures and structures between iron-formations and limestones, Dimroth (1977a) proposed that iron-formations were precipitated

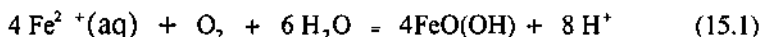
inorganically or organically as CaCO_3 , probably as aragonite, which was then replaced by silica and iron compounds during diagenesis. This interpretation is not compatible with the scale of BIF deposits and the completeness of the presumed replacement (James 1992). The suggestion that the chert layers represent replaced non-iron carbonate material (Lepp & Goldich 1964, Lougheed 1983, Lepp 1987) should also be rejected on the same grounds. It is generally agreed now that the components of iron-formations were deposited as chemical precipitates, probably as gels and other colloids (Ewers & Morris 1981, Ewers 1983), which were reorganized into stable mineral assemblages during diagenesis (Fig. 15.13), but without significant change in bulk composition.

<i>Seabottom accumulates</i>	<i>Diagenetic Products</i>	
	<i>Early</i>	<i>Late</i>
Ferric hydrate		Hematite
Ferrous hydrate "Hydromagnetite"		Magnetite 1 (layered) Magnetite 2 (replacement)
Siderite		
Non-iron carbonate		Dolomite Calcite Ankerite
Fe-rich silicate gel		Greenalite Chamosite Chlorite
Silica gel		
Magadiite		Chert Riebeckite
Organic mud		Carbonaceous shale Pyrite

Figure 15.13. Paragenesis of initial precipitates and diagenetic products in the formation of iron-formations (after James 1992).

Possible mechanisms for the precipitation of iron and silica have been discussed by several authors (e.g., Ewers & Morris 1981, Ewers 1983, Morris 1983, McConchie 1987, Beukes & Klein 1992, Castro 1994). The dominant process in the deposition of the iron oxide component was the near-surface oxidation of Fe^{2+} to Fe^{3+} and subsequent hydrolysis to ferric hydroxide, which is generally symbolized as $\text{Fe}(\text{OH})_3$. The oxidation might have been caused by one or more of the following:

- (a) atmospheric molecular oxygen at relatively low partial pressures (Holland 1973, Drever 1974, Button et al. 1982, Klein & Beukes 1989) by reactions of the type

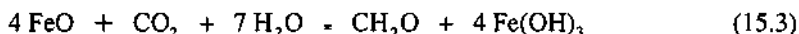


- (b) oxygen released by photosynthesis of marine organisms (Lepp & Goldich 1964, Cloud 1973, 1983, Manikyamba et al. 1993) by reactions such as 14.5; and
 (c) photons of ultraviolet and blue light (<450 nm) (Cairns-Smith 1978, Braterman et al. 1983, Braterman & Cairns-Smith 1987, Anbar & Holland 1992, Castro 1994) producing photo-oxidation reactions such as



near the surface of Precambrian oceans, prior to the development of the ozone layer that filters ultraviolet radiation.

The equilibrium $f\text{O}_2$ value for the reaction (15.1) is very small ($\approx 10^{-68}$ at pH = 7), but continued precipitation of $\text{Fe}(\text{OH})_3$ would require a continuous supply of oxygen and an atmospheric P_{O_2} somewhat higher than 10^{-68} atm to provide a sufficiently rapid flux of oxygen into the Fe^{2+} -bearing upwelled water. An unsolved problem with the biotic oxidation for iron precipitation is the mass balance with respect to carbon (Beukes & Klein 1992). An iron precipitating reaction such as



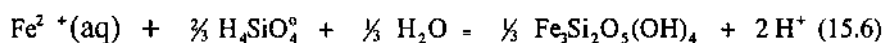
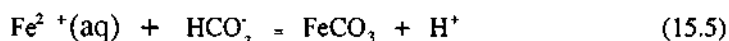
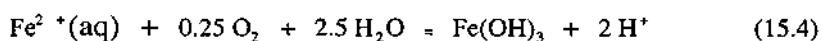
produces about 5 wt% carbon relative to the precipitated $\text{Fe}(\text{OH})_3$, whereas the organic carbon content of BIF, where it can be extracted as kerogen, is generally much less than 1 wt%, even in siderite-rich iron-formations that must have been deposited under reducing conditions and thus preserved the organic carbon. Mass balance is not a problem with direct photo-oxidation. The pH of the oceans during the peak period of BIF deposition was probably ≈ 7.0 (Holland 1984). In dilute, near-neutral solutions, the rate of photo-oxidation is enhanced by the presence of the $\text{FeOH}^+(\text{aq})$ complex, which is sensitive to wavelengths of >300 nm. Braterman et al. (1983) estimated that, in areas of vigorous upwelling of waters containing 10-100 mM total dissolved iron, photo-oxidation of Fe^{2+} by solar UV (300 nm < λ < 450 nm) could have precipitated more than 22.5 mg/cm² of iron per year. This quantity happens to be the average rate of precipitation estimated by Trendall and Blockley (1970) for 22 mesobands of the Hamersley BIF, based on their annual varve hypothesis. Support for the photo-oxidation model also comes from the recent experiments of Anbar and Holland (1992)

in which γ -FeOOH or amorphous ferric hydroxide precipitated at a reasonable rate when UV light was passed through a solution of NaCl + MnCl₂ + FeCl₂ buffered at pH = 7, and the Mn:Fe ratio of the precipitates (about 1:50) was similar to the ratios observed in BIFs. Thus, the photo-oxidation model for the origin of oxide facies BIFs under an anoxic atmosphere is consistent with field observations, although this does not necessarily preclude oxidation of Fe²⁺ by molecular O₂ under an oxygenated atmosphere. An interesting corollary of the photo-oxidation model is that the absorption of ultraviolet radiation by Fe²⁺ may have promoted biological evolution by providing a protective screen for microorganisms.

The role of microorganisms in mediating the deposition of BIF is inconclusive. According to some authors (e.g., Walter & Hofmann 1983, James 1992) there is no convincing evidence that microorganisms played major role in the precipitation of iron minerals, except perhaps indirectly through photosynthetic production of oxygen. Others (e.g., Brown et al. 1995) have argued that microbial mediation "was essential for the deposition of narrow interbedded layers of minerals rich in iron and silica found in the typical oxide, silicate, and carbonate BIF lithofacies."

Primary magnetite, requiring coprecipitation of Fe²⁺ and Fe³⁺, probably formed initially as hydromagnetite (Fe₃O₄·H₂O) by neutralization of an acidic solution of mixed Fe²⁺ and Fe³⁺ salts (Mel'nik 1982), or as 'green rusts' — complexes of anions such as chloride, carbonate, or sulfate with Fe²⁺-Fe³⁺-hydroxides — from solutions above pH 6.5. The possibility of an active role by iron-stripping bacteria in producing iron oxides and carbonates has also been suggested (La Berge 1973, La Berge et al. 1987, Robbins et al. 1987).

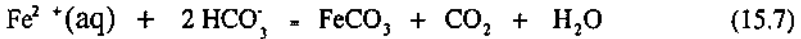
The precipitation of iron, whether by oxidation of Fe²⁺ to Fe³⁺ and subsequent hydrolysis to Fe(OH)₃, or in the form of carbonates and silicates, involves release of acid to the system through the following types of reactions (Ewers 1983):



The progress of these acid-producing reactions would require neutralization by alkali, presumably introduced into the water buffered by reactions with silicates. In the absence of terrigenous clastics, the source of silicates is believed to have been volcanic material generated within or outside the depositional area. The constraint is less critical for Fe(OH)₃ (Eqns. 15.2 and 15.4) which can be precipitated over a wide range of pH.

Eugster and Chou (1973) and Garrels (1987) considered evaporation in a restricted basin environment as a major process in the precipitation of iron and silica. As discussed by Ewers (1983), evaporation would not be a significant factor in the

precipitation of $\text{Fe}(\text{OH})_3$ without the addition of oxygen from an external source, but may have been important for carbonate and silicate components. The loss of water alone from a solution saturated in siderite or greenalite could precipitate these phases, although the reverse of reactions 15.5 and 15.6 would be favored by the resulting lowering of pH. If CO_2 was also lost to the atmosphere during evaporation, siderite could be precipitated by the reaction



The precipitation of silica is as problematic as that of iron. Most Phanerozoic cherts are considered to have been biologically precipitated by siliceous algae (e.g., diatoms and chrysophytes) and siliceous protozoans (e.g., radiolaria). A biogenic origin has also been advocated for the silica in iron-formations (e.g., La Berge et al. 1987, Robbins et al. 1987), based mainly on the occurrence of spheroidal structures (5 mm to 40 mm in diameter) which have been interpreted as fossils. Such forms, however, can be produced abiotically by crystallization of silica gel (Oehler 1976). Besides, no silica-secreting organisms have been recognized in Precambrian age rocks (Cloud 1973, Walter & Hofmann 1983). Thus, an inorganic precipitation of silica for iron-formations appears more likely. Eugster and Chou (1973) suggested that textural evidence and the presence of riebeckite indicate a magadiite precursor for the chert in some BIFs. They postulated an "evaporative playa lake complex" in which silica was precipitated as magadiite, which then converted to chert, as has been observed at Lake Magadi, Kenya. Drever (1974) presented calculations showing that only a small amount of evaporation of the silica-saturated seawater was required to produce the $\text{SiO}_2:\text{Fe}_2\text{O}_3$ ratios commonly observed in BIFs, not enough to precipitate minerals such as gypsum and calcite. In the absence of unequivocal evidence for biogenic precipitation, evaporative concentration appears to be a reasonable alternative for silica precipitation (James 1992, Morris 1993).

15.10.5. BANDING

Perhaps the least understood feature of iron-formations is the persistent banding on different scales and the associated variations in mineralogy. The subject has been discussed by several authors (e.g., Trendall & Blockley 1970, Cloud 1973, Ewers & Morris 1981, McConchie 1987, Klein & Beukes 1989, James 1992, Morris 1993), but with no conclusive answers. In general, the banding is attributed to variations in precipitation rates related to the supply of iron by upwelling and, possibly, the supply of oxygen determined by the level of biological activity, but the details are not clear.

Trendall and Blockley (1970) considered the periodicity of BIF as annual, each cycle of an iron-rich layer and a silica-rich layer representing an annual varve. Recently, Castro (1994) has proposed that each cycle represents a "daily varve" during one diurnal period of solar illumination. This is based on the premise that photo-oxidation by

sunlight was the main mechanism of iron precipitation (and its absence at night the cause for silica precipitation). However, it is difficult to envisage a depositional environment in which iron and silica saturation could be maintained on an annual or daily basis despite massive precipitation.

The Precambrian ocean was probably saturated in silica. A possible scenario for the generation of mesobanding would involve a fairly steady rain of dominantly silica precipitates due to supersaturation of surface ocean waters by evaporation (or by some other mechanism), interrupted at intervals by heavy iron precipitation due to cyclic upwelling and/or seasonally induced, explosive growth of photosynthetic organisms.

Accepting that the BIF precipitation involved the formation of gels and other colloids, a possible explanation for the separation of iron and silica at the sub-mesoband level may lie in the very different *isoelectric points* of their hydrated precipitates (McConchie 1987). Colloidal particles are very fine and have a high charge to mass ratio in water, and the sign and magnitude of the charge is a function of pH and gel composition. The pH at which the particle surfaces are neutral, in the absence of contaminant charged species, is the isoelectric point; at or near this point, forces of mutual attraction promote particle coagulation and hence gravitative settling. The isoelectric point for colloidal $\text{Si}(\text{OH})_4$ is about $\text{pH} = 1-3$ (Iler 1979), whereas for colloidal $\text{Fe}(\text{OH})_3$ it is about $\text{pH} = 7.8$ (McConchie 1987). The mean pH of modern oceans is between 8.1 and 8.3. If the pH of the surface ocean water was about 8 during BIF deposition, a slight lowering of the pH to about 7.8, for example by H^+ -producing reactions such as 15.3 and 15.4, would cause coagulation of the iron hydroxide particles and lead to segregation of the iron from the dispersed silica by relatively rapid settling. The banding may have been accentuated by differentiation during diagenesis. The coexistence of iron and silica in an iron-formation band may be explained by the entrainment of some silica by the settling iron gel.

From an experimental investigation McConchie (1987) concluded that, below $\text{pH} = 7.8$, $\text{Fe}(\text{OH})_3$ gel is unlikely to react with available cationic species and hence is likely to crystallize as oxide, whereas above $\text{pH} = 7.8$, an iron-hydroxide precipitate is likely to bind with some cationic species (presumably derived from volcanic ash) and react with them during later diagenesis. With the ubiquitous presence of silica all around, this mechanism should produce silicate minerals from iron-rich colloidal sediments. Thus, minor pH variations due local conditions could produce differing mineral assemblages without necessarily changing the basic structure or the gross chemical composition of the fine banding (Morris 1993).

15.10.6. DEPOSITIONAL MODELS

Iron-formations are marine deposits that accumulated in a variety of subtidal environments (Dimroth 1977a, Simonson 1985, James 1992, Morris 1993). This is supported by the marine origin of sediments that conformably overlie and underlie many iron-formations, extensive thick beds of dolostone in Superior-type sequences, and the association of oceanic-type basalts with Algoma-type iron-formations. Detailed

interpretation of the depositional environment of iron-formations in individual basins is a difficult task, especially for metamorphosed sequences, as there is a paucity of sedimentologic studies necessary for such interpretation.

Goodwin (1973) proposed that Algoma-type iron-formations of the Canadian Shield formed as a result of hot spring-fumarolic (exhalative) activities in Archean volcano-tectonic basins. Development of the basins was controlled by thermal plumes or 'hot spots', each basin representing a center of crustal spreading that was accompanied by oceanic-type volcanics in the interior part and arc-type volcanics at the margin. As mentioned earlier, a refined version of the volcanic-exhalative model, with supporting evidence, has been discussed by Goodwin et al. (1985) for the Helen Iron Formation. Their model is similar to that illustrated in Figure 2.27a in the sense that both involve convective circulation of seawater through a volcanic pile before discharge onto the seafloor. A major difference lies in the limited leaching of metals due to the lower temperature of hydrothermal fluids (<200°C) in the case of iron-formations, a possible explanation for the impoverishment of metals (other than Fe) in iron-formations.

The lack of any consistent relationship to volcanism requires different settings for the Rapitan-type and Superior-type iron-formations, although at least the Superior-type appears to have involved MOR-type hydrothermal fluids. Superior-type iron-formations were deposited in shelves and continental margins. Essential requirements of their formation were: (a) an anoxic deep ocean (see Figure 14.18) for increased solubility of Fe^{2+} , in the order of 3 ppm (Holland 1973) to 10 ppm (Drever 1974), or even 20 ppm (Morris 1993); (b) an abundant supply of iron to the deep ocean, presumably from spatially and temporally associated MOR-type volcanic sources; (c) upwelling of the Fe^{2+} -rich bottom waters and mixing with Fe-poor surface waters; and (d) an oxidizing surface ocean for the precipitation of Fe^{3+} -compounds. The spectrum of possible physical configurations of the depositional system is considerable, ranging from simple broad shelves open to the sea, to discrete marginal basins of varying size, depth, and degree of restriction. Two generalized models, after James (1992), are shown schematically in Figure 15.14. More specific models have been described in the literature, for example, by Klein and Beukes (1989), Beukes and Klein (1992), and Morris (1993). Castro (1994) has proposed a subduction model (Fig. 15.15) for the deposition of BIF, including the Cauê Itabirite hosted by the Minas Supergroup in the Quadrilátero Ferrífero area of Brazil. The model envisages the fractured oceanic plate as the source of iron and silica, which were carried to the seafloor by hydrothermal convection in the oceanic lithosphere. BIF was deposited both on the oceanic plate and on the margins of the continental plate, with the grade of iron decreasing away from the oceanic trench, but the BIF on the oceanic plate was lost due to subduction.

The uniformly oxide facies in Rapitan-type deposits suggests deposition in relatively shallow, rift-bound basins at continental margins. The glaciogenic association of Rapitan-type deposits may simply be fortuitous (James 1983), or the glaciation may have provided the opportunity for the accumulation of undiluted chemical sediments by cutting off the supply of clastic sediments (Young 1988). The transport and deposition of the iron-formation components have been attributed by Yeo

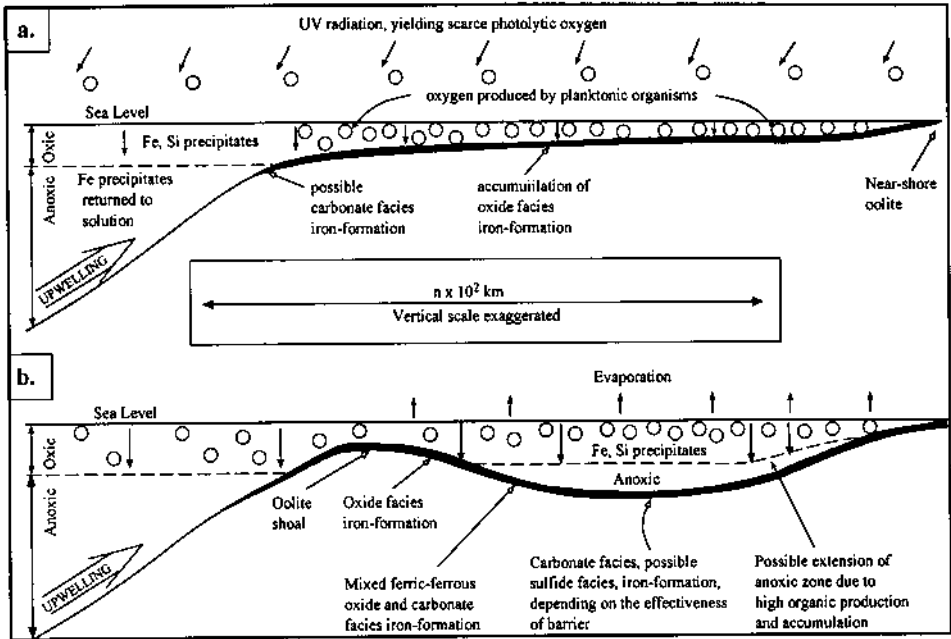


Figure 15.14. Examples (conceptual) of possible configurations for upwelling-related, shelf and marginal marine basin deposition of iron-formation: a. simple broad shelf, no restriction; b. marginal basin, partly to wholly restricted depending upon height of barrier at any particular time (after James 1992).

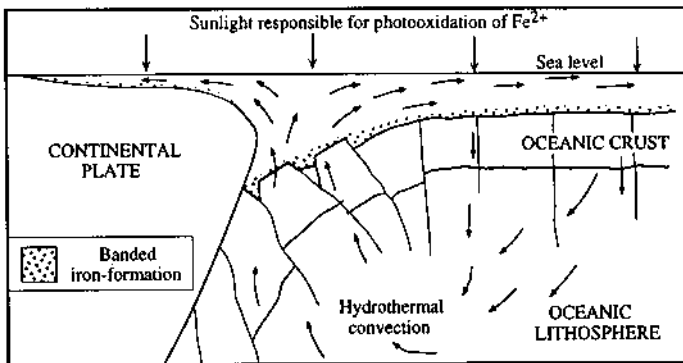


Figure 15.15. Conceptual model of iron-formation deposition in a Precambrian active continental margin. Iron and silica are leached from the oceanic crust by hydrothermal convection, and iron-formation is deposited on both oceanic and continental plates, but only the fraction deposited on the continental margin survives subduction. The grades are the richest above the trench and decrease away from it. (After Castro 1994.)

(1986) and Young (1988) to hydrothermal fluids that ascended along rift breaks and mixed with normal seawater of the rift trough but, as discussed earlier, the REE data do not support a MOR-type hydrothermal component in the Rapitan-type iron-formations.

15.11. Time-bound Distribution of Iron-formations

Due to a lack of minerals in iron-formations suitable for radiometric age determinations, a precise dating of these sediments has been possible only in rare cases — e.g., a lead whole-rock isochron age of 3760 ± 70 Ma for the Isua BIF, Greenland (Moorbath et al. 1973), the oldest iron-formation yet identified. K-Ar and Rb-Sr ages are useful, but they generally represent the time of metamorphism, not of deposition. The limits placed on the ages of iron-formations, as compiled by various authors (e.g., Lepp & Goldich 1964, Goldich 1973, James 1983, Gross 1986, James 1992), are based predominantly on age determinations of the underlying basement rocks, interlayered volcanic rocks, or post-depositional metamorphism or igneous intrusion, with an uncertainty range commonly in the order of several hundred million years. Nevertheless, it is clear from the available data that iron-formations are overwhelmingly concentrated in the Precambrian, especially in the early Proterozoic.

Figure 15.16 is an approximate time versus abundance curve based on age and tonnage estimates for iron-formations deposited through geologic time. The curve is meant to be illustrative rather than quantitative. The four peaks in this curve, representing time intervals of pronounced iron-formation deposition, correspond to middle Archean (3500-3000 Ma), late Archean (2900-2600 Ma), early Proterozoic (2500-1900 Ma), and late Proterozoic-early Phanerozoic (750-450 Ma). Goldich (1973) had proposed a very similar four-fold subdivision of iron-formations.

Some relatively minor, middle Archean deposits (e.g., those of the Swaziland Supergroup, southern Africa) are associated with greenstone belts and may be regarded as Algoma-type. But most iron-formations belonging to the middle Archean group occur in highly deformed, high-grade metamorphic terrains and are not readily classified. Some important examples are the BIFs of the Guyana Shield of Venezuela and Guyana (South America), the probable correlatives in the Liberian Shield of Liberia, Sierra Leone, Guinea, and Ivory Coast (West Africa), and the highly productive deposits of the Orissa-Bihar belt in the Indian Shield. The late Archean peak is accounted for predominantly by thousands of relatively small, Algoma-type deposits widely distributed in greenstone belts, although all iron-formations of probable late Archean age are not of Algoma-type (e.g., the iron-formations in the Witwatersrand Supergroup of South Africa and the northern Rocky Mountains of Montana, USA). The early Proterozoic peak, which represents about 90% of the estimated total tonnage of iron-formations, includes most of the giant deposits of the Superior-type.

Iron-formations of the late Proterozoic-early Paleozoic interval are not well understood. Part of the problem is the uncertainty in the age of some deposits. For example, the Himalayan deposits considered as Paleozoic by O'Rourke (1961) are now

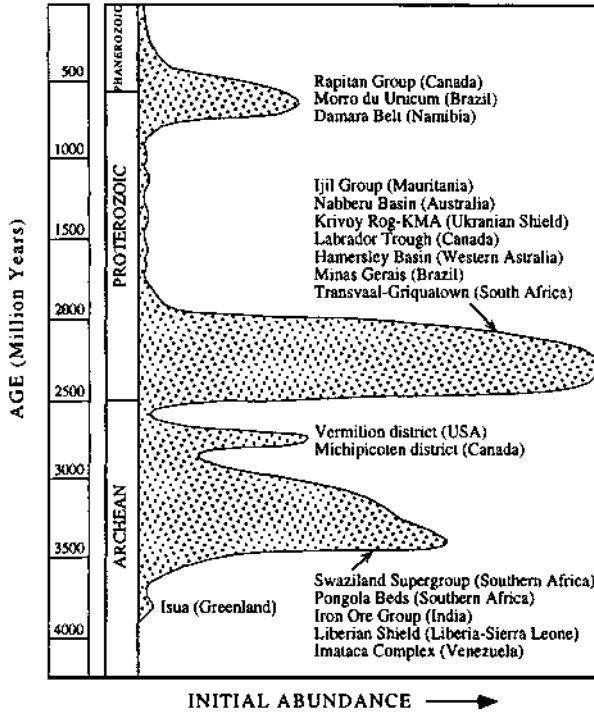


Figure 15.16. Estimated abundance of iron-formations deposited through geologic time, with some important examples for the various peaks. The horizontal (initial abundance) scale is nonlinear, approximately logarithmic; range 0-10¹⁵ tonnes. The curve, especially the shape of the peaks, is meant to be illustrative rather than quantitative. (Modified from James 1983.)

believed to be Precambrian in age (Radhakrishnan et al. 1986). The other problem is that the assigned deposits may include several genetically unrelated types. Some appear to be of the Algoma-type, associated with contemporaneous volcanism (e.g., Mayikhinghan district of the so called 'Far East Region' of the former USSR); some are of the Rapitan-type, possibly related to late Proterozoic glaciation; and some may not even be iron-formations as defined here.

Despite the uncertainty involved in the estimated age and tonnage of most deposits included in Figure 15.16, there is no doubt that the deposition of iron-formations was more prolific in certain geologic intervals compared to others. The late Archean peak is apparently linked to the development of greenstone belts as part of the worldwide cratonization process. The cratonization was not synchronous on a global scale, or even within a single shield (see Ch. 6), but it appears to have attained a maximum in many parts of the world about 2700 million years ago. The strong early Proterozoic peak probably reflects the development of regionally extensive, stable continental

shelves that followed the late Archean cratonization and served as repositories of sediments including iron-formations. As discussed earlier (Ch. 14), a necessary condition for prolific deposition of iron-formations was a stratified ocean system characterized by a reducing deep ocean to hold a relatively high level of dissolved Fe^{2+} and an oxidizing surface ocean for the precipitation of Fe^{3+} -compounds. The termination of the phenomenal period of iron-formation deposition around 1.9-1.8 Ga marks the transition to an oxidizing deep ocean owing to an increase in the atmospheric oxygen (see Figs. 14.18, 14.19). The termination may have been caused by a lack of abundant Fe^{2+} in the ocean water and/or the development of the ozone layer that drastically diminished the ultraviolet radiation necessary for photo-oxidation. The brief reappearance of iron-formations of the Rapitan-type in late Proterozoic does not coincide with any particular stage of atmosphere-ocean evolution, but it may be related in some way to the rifting and breakup of Proterozoic supercontinents in late Precambrian time (Yeo 1986).

15.12. Summary

Iron-formations, as defined here, are iron-rich, chemically precipitated sedimentary rocks characterized by rhythmic banding between iron-rich and silica-rich layers on all scales (macrobands, mesobands, microbands). They occur in all shield areas of the world, are overwhelmingly Precambrian in age, and constitute the most important source of iron ore. Some major iron-formations are very large, containing in the order of 10^{12} - 10^{14} tonnes of iron, although mineable higher-grade ores are commonly restricted to portions upgraded by secondary enrichment.

Depending on the mineralogy, iron-formations may be assigned to one of four sedimentary facies — oxide, silicate, carbonate, and sulfide. The oxide facies is characterized by magnetite (magnetitic subfacies, the most abundant type of BIF) or hematite (hematitic subfacies), the silicate facies by various iron-silicate minerals (minnesotaite, stilpnomelane, greenalite, Fe-chlorite, etc.), the carbonate facies by siderite, and the sulfide facies by pyrite. The idealized distribution of the facies in a depositional basin with restricted circulation, as conceptualized by James (1954), is from oxide facies in the oxygenated, shallow waters of the shelf to sulfide facies in the anoxic, deeper parts of the basin, although nowhere has a complete transition of the facies been actually observed.

Based on lithologic association, iron-formations are classified into three types: Algoma-type, Superior-type, and Rapitan-type. The Algoma-type is closely associated with volcanism, indicating an 'eugeosynclinal' environment of deposition. Typical examples (such as the Helen Iron Formation, Canada) are those of the Precambrian (especially late Archean) greenstone belts. The Superior-type, predominantly early Proterozoic in age, is associated with clastic-carbonate sequences suggestive of a "miogeosynclinal" depositional environment. Most of the giant iron-formations — such as those of the Lake Superior region (USA-Canada), Labrador Trough (Canada),

Krivoy Rog Basin (Ukraine), Hamersley Basin (Australia) — belong to this category. Only a few examples of the Rapitan-type are known; these are late Proterozoic in age, are associated with coarse clastic deposits, including some of glaciogenic origin, and appear to have been deposited in rift-bounded basins at continental margins.

Beyond the well established conclusion that iron must have been transported as soluble Fe^{2+} -complexes and precipitated as insoluble Fe^{3+} -compounds, almost all aspects of iron-formation genesis are quite speculative and controversial. The essential requirements for the deposition of Algoma- and Superior-type iron-formations are: source(s) of abundant iron and silica; very little or no input of clastic or volcanoclastic material to the basins of deposition; and suitable depositional sites. The most likely source of the vast amounts of iron appears to have been MOR-type hydrothermal fluids discharged into an anoxic deep ocean. The iron was transported to the oxidizing surface ocean by periodic upwelling and precipitated as ' $\text{Fe}(\text{OH})_3$ ' gels. In the absence of biogenic precipitation of silica, the Precambrian ocean was probably saturated with silica, and the precipitation of silica, perhaps as a steady rain of colloidal particles, may have been caused by evaporative concentration. The separation of iron from silica at the mesoband level may be attributed to cyclic supply of iron through upwelling, whereas differential settling rate of iron and silica gels may be a plausible explanation at the sub-mesoband level. There is no convincing evidence for biogenic precipitation of iron and silica, but the evolution of photosynthetic organisms is believed to be the prime reason for the prolific deposition of iron-formations in late Proterozoic.

Iron-formations constitute a relatively minor proportion of the Precambrian sedimentary record, but they are significant indicators of certain large-scale aspects of the earth's evolution. Iron-formations range in age from 3.8 Ga (Isua belt, Greenland) to early Paleozoic (Rapitan-type BIF), but in terms of tonnage of iron they are virtually restricted to the 3.5-1.8 Ga time interval. This restricted time distribution is related to the evolution of atmospheric oxygen as discussed in the previous chapter. The widespread development of Superior-type iron-formations in the early Proterozoic strongly suggests that the earth's atmosphere at this time must have contained some oxygen, resulting in a stratified ocean which was still anoxic at deeper levels but became oxic at the surface. The lack of Algoma- and Superior-type iron-formations younger than 1.8-1.7 Ga is the evidence that, because of an increase in the level of atmospheric oxygen, the deep ocean became oxic and, therefore, no longer a storehouse for dissolved ferrous iron. The Rapitan-type iron-formations, although still not well understood, do provide support for the concept of a (possibly) worldwide epoch of continental rifting in late Proterozoic time.

15.13. Recommended Reading

Ewers & Morris (1981), Cloud (1983), Goodwin et al. (1985), Beukes & Klein (1992), Klein & Beukes (1992), James (1992), Morris (1993), Castro (1994).

CHAPTER 16

GOLD DEPOSITS

16.1. Introduction

Gold was among the first metals to be mined because it commonly occurs in the easily extractable native form, is beautiful and imperishable (a noble metal), and because exquisite objects can be crafted from this highly malleable and ductile metal. The earliest gold miners were the Sumerians, who were working deposits in the present-day Iran by 3800 B.C., and the Egyptians, who had organized gold mining on a significant scale by at least 3000 B.C.. In ancient civilizations, gold was mostly used for lavish decoration of temples and kings' tombs. Gold coinage appeared much later, around 700 B.C., and practically disappeared as a legal tender with the demise of the Roman Empire. Gold production slowed down in the Middle Ages but increased again with the great economic expansion of the 16th century. The 'gold fever' of the middle and late 19th century, which led to the discovery of many rich placer deposits in Siberia, Alaska, California, Australia, and South Africa, was probably triggered by the adoption of gold as the monetary standard by the British Empire in 1821.

In 1944, the U.S. dollar became the world's monetary standard at gold parity of \$35 per troy ounce (1 troy ounce = 31.1035 g), a situation that continued until 1968 when the U.S. government declared a *de facto* abandonment of the gold standard. The gold price rose slightly at first to about \$40 per troy ounce, but very rapidly after 1971 when the United States officially came off the gold standard and its citizens were again allowed to own gold. The price peaked at \$843 in January, 1980, and then fell, somewhat erratically, to an average price of around \$300-\$400 per troy ounce; this price has been fairly stable since 1981. Major reasons for the relatively lower gold prices have been the periodic heavy bullion sales by the central banks of several nations and the reluctance of investors to rely on gold as a significant part of their investment portfolio. However, the rise in demand for gold, particularly for jewelry fabrication, resulted in a steady increase in the world gold production, from 1,873 tonnes in 1988 to about 2,248 tonnes in 1992 (Lucas 1992); the production in 1994 was \approx 2,300 tonnes. Of the total amount of about 4 billion troy ounces of gold that has been produced through human history about one-third is held in Central Banks, another one-third is held privately as a store of wealth, and the rest has been used in jewelry (also a store of wealth), production of coins and medallions, electronics, and dentistry (Shawe 1988).

A significant part of the available information on gold deposits gathered by the

exploration and mining companies is not accessible to the public, but the published literature is vast. Excellent sources of information, to name a few, are Boyle (1979, 1982), Foster (1984, 1991), Berger and Bethke (1985), Keppie et al. (1986), Roberts (1987), Colvine et al. (1988), Keays et al. (1989), Groves & Foster (1991), Sillitoe (1991), Foster and Piper (1993), Kerrich and Cassidy (1994), and Arehart (1996).

16.2 Distribution

There are hundreds of thousands of reported gold occurrences around the world. Most of these are small and relatively unimportant at the world production level; the bulk of the mined gold has been produced by a small number of giant deposits in a few countries. For example, about 85% of the 1992 world gold production came from only 9 countries: South Africa (27%), USA (15%), Australia (11%), Canada (7%), Russia (6.5%), China (6%), Papua New Guinea (4%), Uzbekistan (4%), and Brazil (3%); 70 countries, with contributions ranging from less than 1 tonne to about 40 tonnes, accounted for the balance (Lucas 1992). Known world resources of gold are estimated to be about 193,000 tonnes (6 billion troy ounces) (Singer 1995).

Gold deposits range in age from Archean to late Tertiary and are found in all parts of the world (Fig. 16.1) in a variety of host rocks and geologic settings, but there are some noticeable clusters in the distribution pattern. The most conspicuous of these are the greenstone belts in Archean cratons and the circum-Pacific belt. Other important districts or deposits are located in South Africa (Witwatersrand), former USSR (Muruntau, Sovetskoe, Zod), China (Zhao Ye, Jia Pi Gou, eastern Hebei, Little Qin Hill), Australia (Kidston, Telfer), Ghana (Ashanti), and India (Kolar Schist Belt). The Witwatersrand Basin is by far the largest contributor to the world's gold production and the Muruntau mine, with an annual production capacity of 700,000 ounces, is believed to be the world's largest single gold producer despite its low grade (≈ 0.06 oz/t Au and 3-8 oz/t Ag; Boyle 1986). A fairly comprehensive catalog of significant gold deposits and mines around the world is given by Elevatorski (1988a, b) and Woodall (1988).

16.3. Types of Gold Deposits

Trace amounts of gold are present in a wide variety of mineral deposits, ranging from <0.01 ppm Au in SSC and MVT deposits to concentrations in some sulfide deposits high enough to be recoverable as a byproduct. Byproduct gold probably accounts for about 5 to 10% of the total world gold production and about 40% of U.S. gold output (Simons & Prinz 1973). Three types of ores that routinely produce byproduct gold are: Ni-Cu sulfide ores associated with mafic and ultramafic rocks; VMS ores; and Cu ores of porphyry copper deposits, especially those of dioritic association. The Sudbury Ni-Cu deposits are estimated to contain, on the average, 0.08 ppm Au and 2.3 ppm Ag, and they produce annually some 50,000 ounces of gold and 2,000,000 ounces of silver

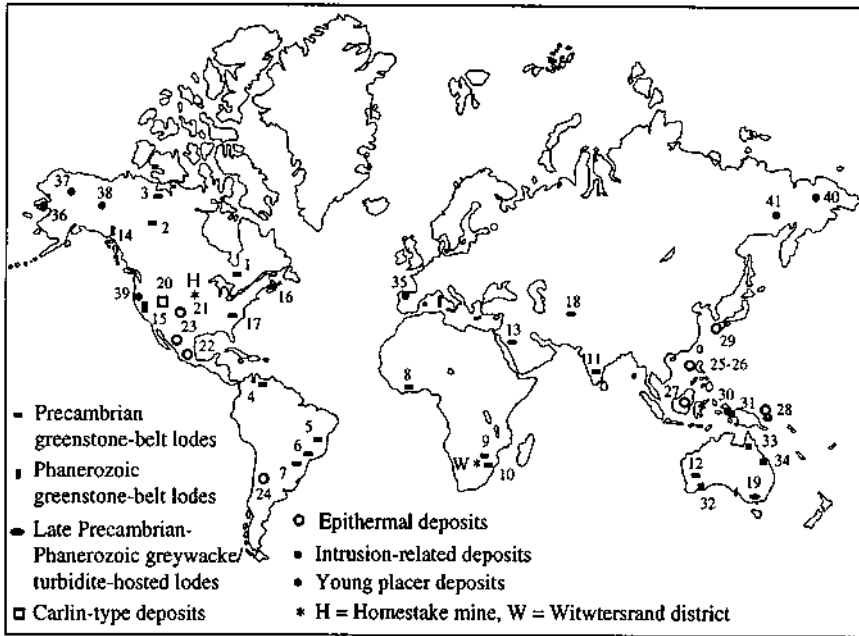


Figure 16.1. World distribution of important gold deposits, districts, and belts. Precambrian greenstone-belt lodes (all Archean, except 13 which is Proterozoic): 1. Superior Province (see Fig. 16.6); 2. Slave Province (Yellowknife district); 3. Lupin; 4. El Callao, Venezuela; 5. Bahia district; 6. Minas Gerais (Morro Velho); 7. Goiás district; 8. Ashanti, Ghana; 9. Zimbabwe (Kodoma, Kwekwe, Shamva); 10. Barberton (Consort, Sheba, Fairview, Agnes); 11. Kolar (Kolar, Hutti); 12. Yilgarn Craton (see Fig. 6.5); 13. Mahd-el-Dahab, Saudi Arabia. Phanerozoic greenstone-belt lodes: 14. Juneau, Alaska; 15. Mother Lode, California. Late Precambrian-Phanerozoic greywacke/turbidite-hosted lodes: 16. Meguma, Nova Scotia; 17. Carolina State Belt, southern Appalachians; 18. Muruntau, Uzbekistan; 19. Ballarat-Bendigo, Australia. Carlin-type deposits: 20. western United States (see Fig. 16.2). Epithermal deposits: 21. western United States (see Fig. 16.2); 22. Pachuca and Guanajuato, Mexico; 23. Durango, Mexico; 24. El Indio, Chile; 25. Lepanto, Philippines; 26. Baguio, Philippines; 27. Keilan, Indonesia; 28. Ladolam, Papua New Guinea; 29. Hishikari, Japan. Intrusion-related deposits: 30. Ok Tedi, Papua New Guinea; 31. Porgera, Papua New Guinea; 32. Boddington, Australia; 33. Kidston, Australia; 34. Mount Morgan, Australia; 35. Salave, Spain. Young placer deposits: 36. Nome, Alaska; 37. Yukon River, Alaska; 38. Klondike, Yukon Territory; 39. Sierra Nevada, California; 40-41. Siberia.

(Boyle 1979). Published gold grades of VMS deposits are typically between 0.2 and 2 ppm, but some higher grade deposits average between 2 and 20 ppm Au. The highest gold tenor found in deposits of this type occur in the Kuroko ores of Japan (up to 51.3 ppm Au). Most of the gold in VMS deposits is generally present as the native metal or as tellurides; some gold probably occupies lattice sites in various sulfosalts, particularly tetrahedrite-tennantite, and in sulfides such as chalcopyrite, bornite, pyrite, and arsenopyrite. The total past production and current reserves of gold in VMS deposits worldwide is estimated at about 2,900 tonnes (Hannington et al. 1991). A significant amount of gold is produced also from Mesozoic-Cenozoic porphyry copper deposits (see Ch. 8). The gold tenor of porphyry copper deposits ranges from <0.05

ppm to >1 ppm and the average is around 0.05 ppm. Porphyry systems in which gold ranks as the principal contained metal, or in which gold and copper share coproduct status or have the potential to do so, may be referred to as *porphyry gold deposits* (see Ch. 8). For porphyry deposits of the western Pacific region, Sillitoe (1989) considered 10 million tonnes of ore averaging >1.5 ppm Au as the lower limit. Some porphyry copper deposits, such as the Ok Tedi (Papua New Guinea), owed their development to the presence of a gold-rich secondary cap.

Auriferous deposits have been classified in a number of ways (see discussion in Bache 1987). Noteworthy among these are the detailed classification schemes proposed by Boyle (1979), which was based on lithologic associations as well as the ore localization structures, and by Bache (1987) and Bache and Sunarya (1987), which emphasized the tectonic setting of host rocks and metal association. The classification scheme followed here is more pragmatic because of its closer correspondence to the terminology used in recent literature on gold deposits.

Most of the important gold deposits, which are considered so primarily for their gold content, belong to one of the following seven types:

- (a) Young placer deposits
- (b) Deposits hosted by quartz-pebble conglomerates (Witwatersrand-type)
- (c) Volcanic-associated epithermal deposits
- (d) Sediment-hosted, disseminated deposits (Carlin-type)
- (e) Deposits hosted by banded iron-formations
- (f) Intrusion-related deposits
- (g) Lode deposits

The conglomerate-type gold (-uranium) deposits of the Witwatersrand Basin, which practically contains all currently productive deposits of this type, have been discussed earlier (Ch. 14). The general characteristics of the other deposit types are summarized below and a few typical examples described in a later section.

16.3.1. YOUNG PLACER GOLD DEPOSITS

Alluvial placers have been the prime producers of placer gold, although eluvial gold placers were mined in many parts of the world in the later part of the 19th century. Tertiary alluvial placers have contributed about 25% of all the gold ever produced, and the total contribution of placers may be close to two-thirds of the world's gold production if the conglomerate-hosted Witwatersrand deposits are accepted as paleoplacers (Boyle 1979). Some of the 'giant' alluvial gold placer districts (placers from which gold production has exceeded 4 million ounces; Henley & Adams 1979), now largely or almost completely exhausted, include those of Klondike (Yukon, Canada), Cariboo (British Columbia, Canada), Sierra Nevada (California, USA), Nome (Alaska, USA), Choco (Columbia), Victoria (NSW, Australia), Westland and Otago (New Zealand), and the Lena, Aldan, Yenisy, and Amur drainage systems in Siberia

(Russia). Even today, a large proportion of the gold production in the former USSR, China, Columbia, and Brazil comes from alluvial placers, accounting for about 5-10% of the world gold production. The only reported production of gold from a marine placer is a small amount of gold recovered as a byproduct of tin dredging in Malaysia.

Alluvial placers are composed of loose, unconsolidated to semiconsolidated gravels and sands that are commonly relatively clean. The distribution of gold values is very irregular, with average grades of pay streaks generally in the range of 0.1 to 3 ppm Au. The gold is much coarser grained compared with the Witwatersrand deposits and occurs in the native state but in varied forms. The most common habit is as moderately fine particles known as 'dust'; extremely fine particles of gold, called 'flour' or 'skim' gold, are common in some placer districts. The *fineness* or purity of placer gold (the proportion of gold present in the naturally occurring mineral and commonly expressed as $[1,000 \text{ Au}:(\text{Au}+\text{Ag})]$) is mostly greater than 850 and the Au:Ag ratio generally exceeds 1 (Boyle 1979). Placers, especially of the eluvial type, have produced some of the largest gold nuggets. The most famous of these are the Welcome Stranger (2,516 troy oz) and Blanch Barkley (1,743 troy oz) recovered in Victoria (Australia) and the Crown Hill nugget (1,296 troy oz) recovered in California (USA).

Gold does not oxidize at the temperature and oxygen fugacity conditions of the Earth's surface. It also has a very high specific gravity, 19.3 for pure gold compared to less than about 3.0 for most crustal minerals and rocks. Thus native gold can easily be transported as detrital particles and concentrated as placer deposits. However, several aspects of placer gold formation are yet to be resolved. In some districts, intrusions of felsic to intermediate composition, veinlets of auriferous quartz and base metal sulfides, or an abundance of pyrite or arsenopyrite containing trace amounts of gold may be reasonably construed to have supplied the gold concentrated in placers, but other districts lack such apparent source of gold. Another problem is the detrital versus chemical origin of the rare gold nuggets recovered from the placers. Do they represent lode gold which has been liberated from its original host rock by mechanical weathering or gold that has been mobilized in solution and reprecipitated? Another issue is the variations in Au:Ag ratios in placer gold — have the ratios been inherited from their supergene environment or have they changed because of preferential leaching of silver during the placer-forming process?

The bulk of the world's young gold placer deposits is of Tertiary and Quaternary age, perhaps because of accelerated erosion that followed the rapid uplift of mountainous terrains during the Alpine orogeny. Removal of older placers by erosion is also a factor in this age distribution.

16.3.2. EPITHERMAL GOLD DEPOSITS

Because of its genetic connotation, *epithermal* is not an ideal term in the classification scheme of gold deposits. Moreover, most of the deposits normally included in this group appear to have formed from fluids hotter than the 200°C upper limit set by Lindgren (1933) for epithermal deposits (see Ch. 2). However, the term is well

entrenched in the literature since the 1940's to emphasize the distinctiveness of this group of deposits from mesothermal gold deposits that share some common characteristics. In current practice, the recognition of epithermal gold deposits relies more on the geological and hydrothermal environment of mineralization and less on set temperature-pressure limits. Following the current usage, we restrict our discussion to high-level mineralization broadly coeval with volcanism and epizonal plutonism (e.g., Berger & Bethke 1985). Sediment-hosted, Carlin-type gold deposits also appear to have formed in epithermal environments, but are believed to be genetically distinct (Berger & Henley 1989). Some Archean lode gold deposits were also emplaced at shallow levels, but long after volcanism.

Almost all epithermal precious metal deposits are located in the circum-Pacific volcanic belt, and they are particularly well developed in the Basin and Range province of the western USA (Fig. 16.2) and in the western Pacific island arcs. Because of their relatively higher grades and amenability to cheaper open-pit mining and heap-leach extraction of gold, epithermal deposits have been a favored target of exploration since the early 1970's. Major recent discoveries include the deposits at Kelian in Indonesia, Ladolam in Papua New Guinea, Hishikari in Japan, and Sleeper in Nevada (USA).

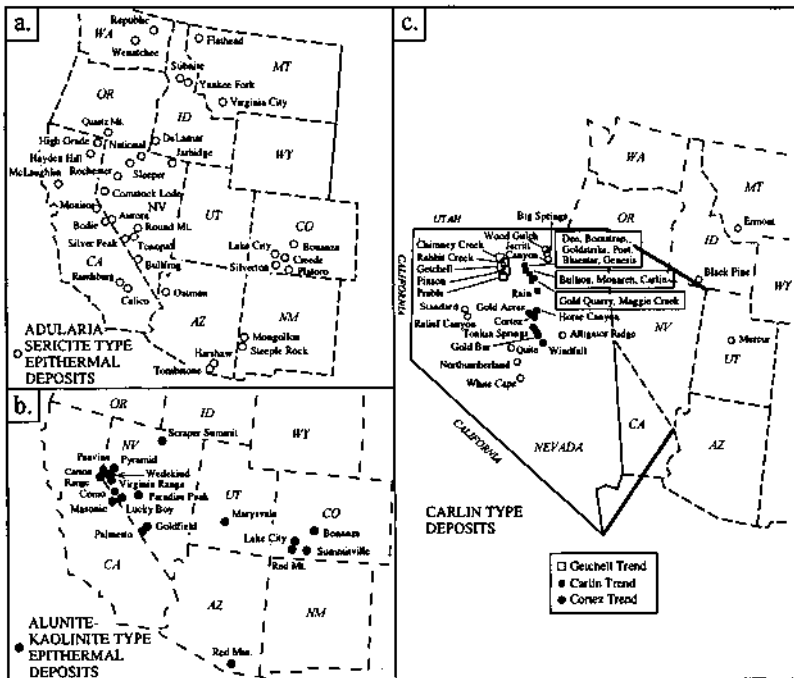


Figure 16.2. Location of selected gold deposits in the western United States: a. Adularia-sericite type epithermal deposits (after Berger & Henley 1989); b. Alunite-kaolinite type epithermal deposits (after Berger & Henley 1989); and c. Carlin-type deposits. (After Berger & Bagby 1991.)

Listed below is a summary of the distinguishing characteristics of epithermal gold deposits as discussed by a number of authors (Buchanan 1981, Hayba et al. 1985, Silberman & Berger 1985, Panteleyev 1986, Heald et al. 1987, Berger & Henley 1989, White & Hedenquist 1995):

- (a) The host is typically an early to late Tertiary calc-alkaline volcanic pile composed of well-differentiated, subaerial, pyroclastic rocks, but in some cases shows a close association with alkalic volcanics (e.g., the Cripple Creek district, Colorado, USA). Andesitic volcanic and pyroclastic rocks are the more common host to ore; basalts seldom carry significant amount of ore. Most districts have some felsic units, and some deposits in the western Pacific rim are associated with porphyry-type intrusions.
- (b) The deposits formed in extensional tectonic settings, in areas with well-developed tension fracture systems and normal faults that could channel hydrothermal fluids and localize mineralization. Caldera or resurgent caldera settings are favorable, but not a requisite.
- (c) The mineralization is epigenetic and occurs commonly in the form of quartz veins, which flare upward into complicated wedge-like or cone-like features, but also as silicified breccia zones and stockworks. The ore zone may have a considerable strike length, but the vertical extent is restricted to intervals varying from about 100 to 1,000 m and rarely exceeds 600 m. Above this interval, precious metal values drop sharply, but the quartz vein filling may extend well above the top of the ore zone. The downward limit of the ore zone is marked by anomalous but very subgrade material with or without a concomitant increase in base metal sulfides. Within the ore interval, ore shoots rarely fill the entire vein structure, but rather tend to be related to structural features such as dilatant zones and areas of vein intersection.
- (d) Some of the deposits contain, or have produced, large tonnages of high-grade ore (Table 16.1), but this is not always the case. The reference to these deposits as *bonanzas* is somewhat misleading. Actually, gold grades are highly variable even within deposits containing bonanza orebodies. For example, some pockets at Goldfield, Nevada, contained 20 troy ounces of gold per tonne, but most of the ore probably contained only 0.5-1 oz/t. The bonanza orebodies simply reflect the result of a larger volume of fluid flow through a favorable structural zone and/or more efficient precipitation of gold along steeper physiochemical gradients (Romberger 1992).
- (e) Ore and associated minerals occur dominantly as open-space fillings, producing characteristic banded and crustiform textures. Repeated cycles of hydrofracturing, brecciation, and mineral deposition, as well as replacement textures (e.g., pseudomorphs of quartz after calcite), are commonly evident.
- (f) Gold and silver are the principal economic metals. Main ore minerals in the veins are native gold and silver, electrum, acanthite (argentite), Ag-bearing As-Sb sulfosalts, and Au-bearing pyrite. Associated base metal sulfides,

TABLE 16.1. Characteristics of selected epithermal gold deposits

Deposit/ District	Production (P) or Reserves(R)	Host Rocks	Nature of Mineralization	Fluid Inclusion Data		Sources of data
				T _h	Salinity	
<i>USA</i>						
Comstock Lode, Nevada	(P) 8.3x10 ⁶ oz Au and 200x10 ⁶ oz Ag from 19x10 ⁶ tons of ore	Andesite (Miocene)	Ag-rich quartz vein and hanging-wall stockwork	250-300	2-6	1, 2
Tonopah, Nevada	(P) 1.86x10 ⁶ oz Au and 174x10 ⁶ oz Ag from 8.8x10 ⁶ tons of ore	Andesite flows, rhyolite tuffs (Miocene)	Quartz-adularia-sericite- pyrite veins	240-290	1-3	1, 3
Goldfield, Nevada	(P) 4.2x10 ⁶ oz Au and 1.65x10 ⁶ oz Ag from 5.5x10 ⁶ tons of ore	Dacite and andesite (Miocene)	Quartz-alumite-kaolinite-pyrite veins	100-290	0.2-7.9	1, 4
Sleeper, Nevada	(R) 79 tonnes of Au, average grade 7.5 g/t	Rhyolite dikes, domes, and flows (Miocene)	High-grade, banded quartz- Au-Ag veins and low-grade stockworks and breccia zones	n.d.	n.d.	5
Round Mountain, Nevada	(P) 0.84x10 ⁶ oz Au, 85.2x10 ⁶ oz Ag from 12.7x10 ⁶ tons of ore	Rhyolitic ash-flows tuff (Miocene)	Sheeted, quartz-adularia- pyrite veins	150-290	<1	1, 6
Creede, Colorado	(P) 0.15x10 ⁶ oz Au, 85.2x10 ⁶ oz Ag, and approximately 7.5% Pb+Zn+Cu from 5x10 ⁶ tons of ore	Andesite and rhyolite tuff (Oligocene)	Ag-bearing base-metal vein system in southern part of the district	120-280	4-12	1, 7, 8
Summitville, Colorado	(P) 0.24x10 ⁶ oz Au, 0.34x10 ⁶ oz Ag, and 0.427x10 ⁶ pounds Cu	Quartz latite plug (Miocene)	Quartz-alumite pods	230-320	4-6	7, 8
<i>Mexico</i>						
Pachuca, Hidalgo	(P) 6.2x10 ⁶ oz Au, and 1500x10 ⁶ oz Ag from 100x10 ⁶ tons of ore	Andesite, dacite, and rhyolite dikes (Miocene-Pliocene)	Base metal-rich quartz vein system	200-250	n.d.	1

TABLE 16.1 (continued)

Deposit/ District	Production (P) or Reserves(R)	Host Rocks	Nature of Mineralization	Fluid Inclusion Data		Sources of data
				T _h	Salinity	
Tayoltita, Durango	(P) 6.24x10 ⁶ oz Au and 3.18x10 ⁶ oz Ag from >12x10 ⁶ tons of ore	Andesitic stock and flows (Eocene)	Quartz veins	250-265	0-13 (mostly 0.3-1.5)	1, 9, 10
<i>Chile</i>						
El Indio	(R) 108 tonnes Au, average grade 12 g/t Au	Rhyolitic to dacitic pyroclastics (Miocene)	Enargite-pyrite and quartz veins	n.d.	n.d.	11
<i>Indonesia</i>						
Kelian, Kalimantan	(R) 40x10 ⁶ tonnes ore with average grade of 2 g/t Au	Andesite, tuff (Oligocene- Miocene)	Intrusion and hydrothermal breccias	270-310	0.5-4.2	12
<i>Papua New Guinea</i>						
Ladolam, Lihir Island	(R) 167x10 ⁶ tonnes ore with average grade of 3.43 g/t Au	Volcanics and monzonitic intrusives	Breccia related to volcanic, intrusive and hydrothermal events	140-220	3.8 (av.)	12
<i>Japan</i>						
Hishikari, Kyushu	(R) 1.4x10 ⁶ tonnes ore with average grade of 70 g/t Au	Andesite, shale (Quaternary)	Quartz-adularia veins	150-300	n.d.	12, 13, 14

T_h = Homogenization temperature (°C); Salinity is expressed as wt% NaCl equivalent.
 Sources of data: (1) Buchanan 1981; (2) Virke 1989a; (3) Fahley 1981, quoted in Romberger 1992; (4) Virke 1989b; (5) Nash et al. 1991; (6) Sander and Einaudi, 1990; (7) Silberman and Berger 1985; (8) Hayba et al. 1985; (9) Smith et al. 1982; (10) Courad et al. 1992; (11) Siddley and Araneida 1986; (12) Henley 1991; (13) Ishihara et al. 1986; (14) Izawa & Urashima 1989.
 1 troy oz = 31.1035 g; 1 g/t = 0.032 oz/t

which are generally concentrated below the precious metal horizon, include sphalerite, galena, and chalcopyrite or enargite (\pm covellite). Quartz and calcite are the most abundant gangue minerals in the veins. Where high precious metal values exist within a vein, the quartz gangue is typically fine-grained and contains significant amounts of adularia+sericite or alunite + kaolinite intimately mixed with the precious metals. Deposits associated with alkaline volcanic rocks (e.g., Cripple Creek, Colorado, USA; Emperor, Fiji) may contain significant amounts of telluride minerals, such as calaverite $[\text{AuTe}_2]$, krennerite $[\text{AuTe}_2]$, montbrayite $[\text{Au}_2\text{Te}_3]$ and sylvanite $[(\text{Ag,Au})\text{Te}_4]$. Au:Ag ratios vary widely, but are typically <1 . The districts higher in base metal contents usually have lower Au:Ag ratios, which would be consistent with the transport of gold as bisulfide complexes and of silver and base metals as chloride complexes (Heald et al. 1987).

- (g) Hydrothermal alteration of wallrock is a characteristic feature of all epithermal precious metal deposits. Based on the dominant hydrothermal alteration and sulfide assemblages, the volcanic-hosted epithermal precious metal deposits have been divided into two main subtypes (Table 16.2): (a) *adularia-sericite* (or *low-sulfidation*) type (Fig. 16.3); and (b) *alunite-kaolinite* (or *high-sulfidation*) type, also referred to as *acid-sulfate* type (Fig. 16.4). The alunite-kaolinite subtype is characterized by the assemblage enargite-luzonite + pyrite \pm covellite, advanced argillic alteration as indicated by major amounts of hypogene alunite $[\text{KAl}_3(\text{SO}_4)_2(\text{OH})_6]$ representing sulfate fixation and kaolinite representing extreme base leaching, and the absence of adularia. The adularia-sericite subtype, the predominant source of epithermal gold in western North America, is distinguished by the presence of adularia and sericitic alteration (white mica or mica-type minerals such as illite or illite-smectite + quartz + pyrite) in or near the veins, very little or no enargite-luzonite, and a lack of hypogene alunite and kaolinite (although both of these minerals are common in areas affected by overprinting caused by downward percolation of steam-heated acid-sulfate water). Propylitic alteration (an assemblage of chlorite, albite, epidote, carbonate, minor sericite \pm pyrite) commonly forms halos that extend hundreds of meters from the fluid conduit zones (i.e., in areas of low water:rock ratios) in both subtypes, but this alteration is believed to be pre-ore and unrelated to the ore-forming hydrothermal system. The distinction between the two subtypes is important because, although the two styles show broadly similar alteration mineralogy, the distribution of the alteration zones is different, and the economic mineralization is localized in different parts of the system. In high-sulfidation deposits, the ore is typically closely associated with, or lies within, the zone of most acidic alteration, and is surrounded by mineral assemblages indicating less acidic conditions. In contrast, in low-sulfidation deposits, the ore is associated with the least acidic alteration (recognized by the presence of adularia and calcite or illite).

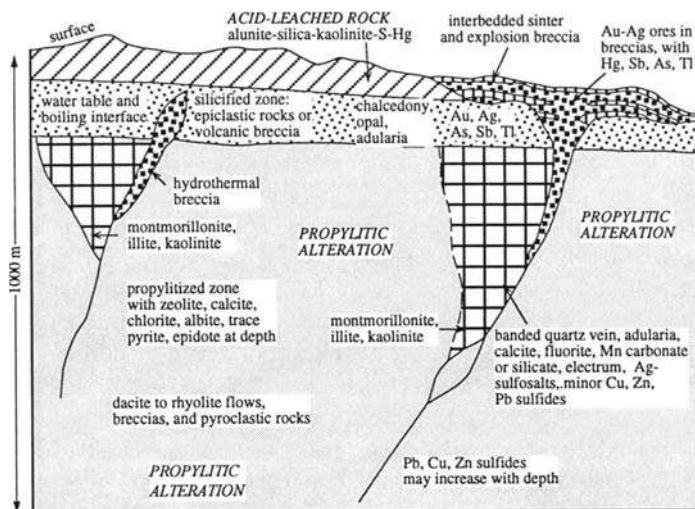


Figure 16.3. Schematic cross section of idealized adularia-sericite (low-sulfidation) type epithermal gold deposit (modified from Bonham 1989).

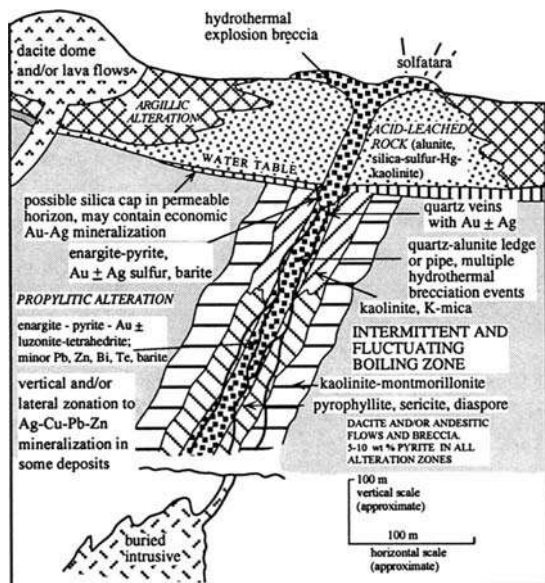


Figure 16.4. Schematic cross section of idealized alunite-kaolinite (high-sulfidation or acid-sulfate) type epithermal gold deposit (modified from Bonham 1989).

TABLE 16.2. Characteristics of alunite-kaolinite type and adularia-sericite type epithermal gold deposits

Characteristic	Alunite-kaolinite type (high-sulfidation)	Adularia-sericite type (low-sulfidation)
Geologic setting	Intrusive centers; most deposits are related to the margins of calderas.	Structurally complex volcanic environments, commonly located within calderas; regional extensional faulting.
Host rocks	Typically calc-alkalic andesite, dacite, and especially rhyodacite; commonly porphyritic. Ore deposition soon (<0.5 m.y.) after emplacement of the host rocks.	Typically calc-alkalic or alkalic-calcic andesite, dacite, rhyodacite, or rhyolite; commonly varies in the same district. Ore deposition almost always later (>1 m.y.) than the host rocks.
Location and size of deposits	Relatively small and equidimensional; vertical extent, usually <500 m, much smaller than horizontal extent.	Variable, some very large; length-to-width ratio usually $\geq 3:1$; vertical extent 400-700 m compared to strike length of several kilometers.
Nature of mineralization	Mostly disseminated ores that replace or impregnate leached country rock; open-space filling of hydrofractures and hydrothermal breccias are locally hosts to higher grade ore; minor stockwork mineralization.	Open-space filling (crustiform and comb structures) typical; stockwork ore common; disseminations and replacement minor; chalcedony veins and druse-lined cavities; hydrothermal brecciation common, but not pervasive.
Ore mineralogy	Characteristic: vein mineral assemblage enargite (-luzonite) + pyrite \pm covellite; 10-90 volume per cent sulfides. Common: native gold; minor sphalerite, galena, chalcopryrite, tetrahedrite-tennantite, bismuthinite; pyrite (abundant). Uncommon: electrum, tellurides, selenides, arsenopyrite.	Characteristic: enargite-luzonite, tetrahedrite-tennantite, and covellite very minor to absent; 1-20 volume per cent sulfides. Common: very minor sphalerite, galena, chalcopryrite; electrum, arsenopyrite, tellurides-selenides, pyrite (abundant). Uncommon: cinnabar
Metal production and association	Both gold-rich and silver-rich deposits. Noteworthy copper production, but lead is more important in silver-rich districts (Cu:Pb = 1:2). Anomalously high As, Cu, Sb, Bi, Hg, Te, Sn, Pb, Mo, Te:Se; anomalously low K, Zn, Ag:Au ratio.	Both gold-rich and silver-rich deposits. Variable base metal production. Anomalously high As, Sb, Hg, Zn, Pb, Se, K, Ag:Au; anomalously low Cu, Te:Se.
Hydrothermal alteration and zoning	Massive bodies of vuggy quartz (due to acid leaching) in the ore host to advanced argillic to argillic alteration outward; an outermost zone of propylitic alteration (Fig. 16.3B); alteration zone areally extensive (several km ²) and visually prominent. Common: hypogene alunite and kaolinite; barite (above ore); quartz (abundant). Rare or absent: adularia, calcite, chalcedony, selenides, chlorite.	Sericitic \pm argillic alteration adjacent to veins and mineralized fractures; an outer envelope of propylitic alteration (Fig. 16.3A); no hypogene alunite; alteration zone restricted and visually subtle. Common: adularia (characteristic), illite, Mn-calcite, chlorite, quartz (abundant), silica sinter, barite, supergene alunite. Rare or absent: kaolinite, pyrophyllite, hypogene alunite.
Hydrothermal fluids	Acidic, H ₂ S-rich; 200-300°C; salinities range from 1 to 24 wt% NaCl equivalent, but higher salinities (5-24 wt% NaCl equivalent) probably relate to pre-ore acid sulfate alteration. Dominantly meteoric water with likely significant magmatic components (SO ₂ , HCl).	Alkaline to near-neutral pH; 100-200°C; low salinity (0-5 wt% NaCl equivalent, up to 13 wt% NaCl equivalent for base metal sulfides), low total S, variable CO ₂ and CH ₄ contents. Dominantly meteoric water, essentially identical to fluids in modern low-S geothermal systems.

TABLE 16.2 (continued)

Characteristic	Alunite-kaolinite type (high-sulfidation)	Adularia-sericite type (low-sulfidation)
Sources of constituents	Deep-seated, probably magmatic S; Pb from volcanic rocks or magmatic fluids.	S from wallrocks deep in the system or from a deep seated magmatic source; Pb from Precambrian or Phanerozoic rocks beneath volcanic pile.
Environment of ore formation	Near-surface parts of plutonic-volcanic complexes such as porphyry copper systems.	Complex zones of mixing and boiling in the upper few hundred meters of large geothermal systems.
Examples	USA: Summitville (Colorado); Goldfield (Nevada). Chile: El Indio Philippines: Lepanto Peru: Julcani Japan: Keshi, Iwato, Kasuga	USA: Creede (Colorado); Tonopah, Comstock, Round Mountain (Nevada); Silver City (Idaho) Indonesia: Kelian Mexico: Tayoltita, Pachuca Japan: Hishikari

Sources of data: Hayba et al. (1985), Heald et al. (1987), Bonham (1988), Berger & Henley (1989), Henley (1991), Sillitoe (1993b), White & Hedenquist (1995).

16.3.3. CARLIN-TYPE GOLD DEPOSITS

The Carlin gold deposit in Nevada was discovered by Newmont Mining Corporation in 1962. The discovery was the result of an exploration program based on the concept advocated by Roberts (1960) that the search for a large, near-surface gold deposit in north-central Nevada should be concentrated near the tectonic windows through the Paleozoic Roberts Mountains thrust fault. Sediment-hosted, very finely disseminated Au-Ag deposits with mineralogy, host rocks, and trace elements similar to the Carlin deposit have become known as *Carlin-type deposits*. Carbonate-replacement gold deposits associated with alkaline igneous intrusions (e.g., Black Hills, South Dakota, USA) have some similarities with the Carlin-type and have been termed as "Carlin-like deposits" (Berger & Bagby 1991); these will not be discussed here.

The greatest concentration of known Carlin-type deposits occurs in the Cordillera of western USA, especially in the state of Nevada (Fig. 16.2). Several Carlin-type deposits have also been recognized in south-eastern China within the past decade. These deposits are hosted by Cambrian to Triassic sediments and are located near the southern edge of the Yangtze craton adjoining an accretionary fold belt (Cunningham et al. 1988, Ashley et al. 1991). Similar deposits also occur in southeast Asia (Sillitoe & Bonham 1990) and Peru (Alvarez & Noble 1988).

Characteristics of the Carlin-type deposits, based almost entirely on the occurrences in western USA, have been reviewed in several recent articles (Radtke & Dickson 1976, Radtke 1985, Bagby & Berger 1985, Romberger 1986, Berger & Bagby 1991, Arehart 1996). The distinguishing features are summarized below:

- (a) The host rocks are predominantly marine sedimentary rocks ranging from sandstones to siltstones to carbonates. The most favorable are the more

- permeable, very finely laminated silty carbonates and carbonate-bearing siltstones and shales (Table 16.3). Apparently, permeability of the host rock, not its chemistry, played a controlling role in gold deposition.
- (b) Host-rock ages range from Cambrian to Triassic; the most favorable hosts in western USA are Cambrian to Mississippian in age. The ages of gold mineralization, as determined by radiometric dating of hydrothermal sericites, are poorly constrained. Reported ages range from 152 Ma (Mercur deposit; Wilson & Parry 1995) to 8 Ma (Alligator Ridge deposit; Ilchik 1990), but most appear to be late Cretaceous to Tertiary, perhaps no younger than Miocene (Berger & Bagby 1991). Seedorff (1991) suggested that the regional gold mineralization event was related to the onset of the Basin and Range extension during late Eocene to early Oligocene (42-34 Ma).
 - (c) The deposits occur within or adjacent to overthrust terranes related to continental margin tectonics. High-angled, normal faults, believed to be the main conduits of hydrothermal fluids, and fault-generated breccias are important controls of ore localization. On a more local scale, the mineralization is controlled by fractures which provided not only the permeability for solution migration but also open spaces for mineral precipitation. Replacement mineralization seldom extends far from mappable fractures.
 - (d) The deposits vary considerably in size and grade (Table 16.3) and in many the gold ore persists to depths exceeding 1 km down-dip without apparent mineralogic zoning.
 - (e) Dissolution of carbonate minerals (decarbonatization) followed by the precipitation of silica (silicification) constitute the most characteristic hydrothermal alteration associated with Carlin-type deposits. Other alteration styles such as argillic alteration (especially at the cores of the hydrothermal systems), introduction and/or mobilization of carbonaceous material, and veining (veins typically of quartz and calcite, with variable amounts of fluorite, barite, and dolomite) are also common. Gold mineralization generally occurs in zones of silicification, but may be associated with some or all of these alteration styles, attesting to its hydrothermal origin. The existence of fault-controlled, intensely silicified tabular zones, referred to as "jasperoids" and interpreted by most workers as a pre-ore alteration product (Berger & Henley 1989), is commonly a good indicator of the presence of gold mineralization, but the zones vary in gold content from being barren to containing several ounces of gold per tonne. Gold is closely associated with hydrothermal pyrite and locally arsenopyrite.
 - (f) The gold occurs in the native state and is extremely fine-grained (<1 to ≈30 μm in diameter, but mostly 1-5 μm) and irregularly disseminated. Native silver and electrum have also been reported. The Au:Ag ratio varies from very high in most deposits (Table 16.3) to very low in a few deposits (e.g.,

TABLE 16.3. Characteristics of selected Carlin-type gold deposits in the western United States

Deposit	Tonnage (million tonnes)	Au grade (g/t)	Major mineralized horizons	Form of orebodies	Hypogene alteration
Alligator Ridge (Nevada)	5.4	3.39	Calcareous, carbonaceous siltstones and claystones (Devonian- Mississippian)	Pods near high- angle faults, extending into sediments	Decarbonization decalcification, silicification, carbon remobilization
Carlin (Nevada)	10	10.97	Silty to sandy, carbonaceous, dolomitic limestone (Silurian to early Devonian)	Pods along high- angle faults, extending into sediments	Decarbonization calcification, silicification, argillization, carbon mobilization
Cortez (Nevada)	3.3	9.57	Silty, argillaceous, carbonaceous limestone with dolostone (Silurian to early Devonian)	Elongated zones parallel to faults, breccia zones associated with folds	Decalcification, dedolomitization silicification
Getchell (Nevada)	13.97	6.65	Phyllitic shale with interbedded limestone (Cambrian- Ordovician)	Sheet-like zones along Getchell fault and pods in fold hinges	Decarbonization argillization, silicification, early skarn formation
Gold Quarry (Nevada)	166	1.47	Silty, carbonaceous limestone and dolostone (Ordovician)	Stockwork system of ore zones along faults	Decarbonization argillization, silicification
Horse Canyon (Nevada)	4.5	3.43	Siltstone and chert; silty carbonaceous limestone (Ordovician- Devonian)	Zones along fractures, extending into sediments	Decalcification, silicification, carbon mobilization
Jerritt Canyon (Nevada)	12.76	8.33	Carbonaceous, shaly limestone with chert; bioclastic limestone (Ordovician)	Pods conformable to bedding near faults	Decalcification, silicification, remobilization of organic matter
Mercur (Utah)	12.98	3.50	Limestone; local bioclastic micrites and wackestones with siltstones (Mississippian)	Strongly conformable to bedding	Decalcification, silicification
Northumb- erland (Nevada)	15.42	1.54	Silty limestones, shales, and siltstone (Silurian)	Tabular zones along sediment- sill contact, diffuse in breccia zones, stratiform in sediments	Early skarn formation, argillization (intense), silicification
Rain (Nevada)	7.53	2.85	Siltstone, shales, and fine-grained sandstone (Mississippian)	Localized within a high-angle fault zone extending into sediments	Silicification, argillization, baritization

Sources of data: Bagby & Berger (1985), Rota & Ekberg (1988), Berger & Bagby (1991).

Taylor deposit). The gold mineralization is commonly accompanied by anomalous concentrations of As, Sb, Hg, and, especially, Tl. This is reflected by the presence of tetrahedrite-tennantite, cinnabar, and Tl-minerals, such as lorandite [TlAsS₂], weissbergite [TlSbS₂], christite [TlHgAsS₃], ellisite [Tl₃AsS₃], and carlinite [Tl₂S]. Pyrite is the most abundant ore-stage sulfide mineral and much of the gold occurs either within the pyrite or as coatings on the pyrite. Cu-Zn-Pb sulfides, often accompanied by barite, occur only in very small quantities as late-stage vein constituents. An exception is the Mercur district, Utah (USA), which contains a paragenetically early silver-base metal mineralized area referred to as Silver Chert.

- (g) Direct observation of gold in unweathered hypogene ore in Carlin-type deposits is extremely limited. As discussed by Bakken et al. (1989), gold particles ranging from 0.05 to 0.10 μm in diameter in contact with pyrite, illitic clay, quartz, dolomite, barite, and carbonaceous matter have been reported in a few studies. Other studies employing X-ray mapping techniques have indicated an association of gold with fine-grained pyrite and in the rims of coarse-grained pyrite and/or clay minerals. Using high-resolution transmission and auger electron microscopy, Bakken et al. (1989) have shown that, in unoxidized ores of the Carlin deposit, gold is present in two habits: (a) as discrete particles, 50 to 200 \AA in diameter, that are encapsulated mostly in pyrite, but also in quartz and cinnabar; and (b) as free gold particles, up to 1,000 \AA in diameter, that are associated with illite.
- (h) Carbonaceous matter in some form is present in the unoxidized ore of all Carlin-type deposits. This includes amorphous carbonaceous matter, pyrobitumen, kerogen, and graphite. Hydrocarbons have been identified only at Mercur. In some deposits, the mineralized rock contains much more carbonaceous matter than the unmineralized counterpart (for example, <0.1% in unmineralized rock compared to 0.3-5% in the mineralized rock in the Jerritt Canyon deposit), but the correlation is not systematic. The organic matter does not seem to have played an active role in gold deposition (Radtke 1985, Arehart 1996).
- (i) Fluid inclusion studies indicate that the ore fluids were of moderate temperature (200^o-300^oC), very low salinity (commonly <5 wt% NaCl equivalent), and CO₂-bearing.
- (j) Felsic (granodioritic to granitic) intrusive rocks, commonly in the form of dikes and sills, occur within, or in the vicinity of, nearly all Carlin-type deposits. Some deposits (e.g., Getchell, Northumberland, Gold Acres) are contemporaneous with adjacent Cretaceous plutonic activity. It has been argued that epizonal intrusions served as the source of heat, and possibly of hydrothermal fluids, for most Carlin-type gold deposits (Sillitoe 1989, 1991, Sillitoe & Bonham 1990, Berger & Bagby 1991).

16.3.4. IRON-FORMATION-RELATED GOLD DEPOSITS

According to the review presented by Kerswill (1993), from which the brief summary presented here is extracted, combined total gold production and reserves for BIF-hosted deposits exceed 100 million ounces. The Homestake gold mine in South Dakota (USA) probably belongs to this type. It is the largest producing gold mine in North America and has produced more than 32 million ounces of gold bullion since its discovery in 1876. Important common features of BIF-hosted gold deposits are: (a) a strong association between native gold and iron sulfide minerals; (b) the presence of gold-bearing quartz veins and/or shear zones; (c) the occurrence of deposits in structurally complex terranes; and (d) a lack of lead and zinc enrichment in the ores. Gold concentration in the ores commonly average between 6 and 10 g/t.

Based on the dominant style of gold distribution, BIF-hosted deposits may be classified into two subtypes: (a) stratiform, in which much of the gold is uniformly disseminated in thin, laterally continuous, sulfide-rich layers of the BIF; and (b) non-stratiform (but commonly strata-bound), in which gold is restricted to late structures (quartz veins and/or shear zones) and/or to sulfide-rich BIF adjacent to such structures. Both subtypes occur within Algoma-type BIF, but not necessarily of sulfide facies. Oxide BIF is the principal lithology of the stratiform deposits; non-stratiform deposits lack oxide BIF irrespective of metamorphic grade. Non-stratiform deposits are more common but generally small. They tend to be less deformed than the host rocks, have alteration products generally similar to those associated with 'mesothermal vein' gold deposits, and are relatively silver-poor (Au:Ag ratios of gold grains are generally >8.0). In fact, the non-stratiform deposits may be considered as a variant of the Archean lode gold deposits. Stratiform deposits, on the other hand, can be very large, as deformed as the host rocks, and relatively silver-enriched (Au:Ag ratios of gold grains range from about 3 to 7). Some of the most productive BIF-hosted deposits — for example, Morro Velho (Minas Gerais district, Brazil), and Lupin (NWT, Canada) — are of the stratiform variety. Even the Homestake deposit, which contains ore as nearly conformable replacement bodies in dilatant zones in highly deformed Precambrian metasediments (Homestake Formation), has been considered as stratiform by some authors. The age and origin of Homestake gold mineralization is controversial, the main hypotheses being Tertiary-hydrothermal (Noble 1950), Precambrian-hydrothermal (Gustafson 1933), and Precambrian-(exhalative) syngenetic (Sawkins & Rye 1974, Rye & Rye 1974, Rye et al. 1974).

16.3.5. INTRUSION-RELATED GOLD DEPOSITS

Included in intrusion-related deposits are those which exhibit a clear spatial and genetic relationship with igneous intrusions, although a magmatic contribution is most likely not restricted to this deposit type. Sillitoe (1991) subdivided the intrusion-related gold deposits, excluding those in which gold is of byproduct status only, into seven categories:

- (a) Porphyry gold and gold-copper deposits (characterized, as in the case of porphyry Cu-Mo deposits, by multidirectional stockwork mineralization and associated K-silicate alteration);
- (b) Non-porphyry-type gold deposits with stockwork and disseminated gold mineralization;
- (c) Vein gold deposits (not to be confused with Archean lode gold deposits);
- (d) Skarn gold deposits;
- (e) Carbonate-replacement gold deposits;
- (f) Stockwork, disseminated, and replacement gold deposits in non-carbonate rocks; and
- (g) Breccia-hosted gold deposits.

Characteristics of a few large and producing gold deposits belonging to the various categories are summarized in Table 16.4. The grade of intrusion-related gold deposits lies mostly between 1 to 10 g/t Au and the total gold content between 10 and 100 tonnes. The different subtypes listed above commonly occur in juxtaposition and locally exhibit transitions between one another, both on the scale of a gold province as well as within individual deposits. Although the spatial association of most of these deposits with igneous intrusions is quite apparent, the source of ore constituents and ore-forming hydrothermal fluids were not necessarily all magmatic (discussed later).

16.3.6. LODE GOLD DEPOSITS

Epigenetic vein deposits of gold in metamorphic terranes have variously been called 'Archean gold', 'mesothermal gold', 'gold only', or 'lode gold'. Following Kerrich (1993), we use the term *lode gold deposits* to include all Au (-Ag) vein deposits in metamorphic rocks, irrespective of age and metamorphic grade. Depending on the *P-T* environment of emplacement, the deposits may be classified further as epizonal (150°-300°C, 0.5-1.5 kb), mesozonal (300°-475°C, 1.5-3 kb), or hypozonal (475°-700°C, 3-6 kb) (Gebre-Mariam et al. 1995).

The most widespread occurrence of lode gold deposits is in the greenstone belts of Archean cratons (Fig. 16.1). The vast majority of these are relatively small deposits with production + reserves of less than 1 tonne Au, but most cratonic areas are endowed with one or more giant (containing >500 tonnes Au) gold districts or camps (Table 16.5). The truly impressive examples appear to be concentrated in the late Archean (2.7 Ga) greenstone belts: the Timmins (Porcupine) district (Abitibi belt, Superior Province, Canada), which has produced more than 1,800 tonnes of gold (Duff 1991); the Golden Mile (Kalgoorlie, Yilgarn Block, Western Australia), which has produced about 1,150 tonnes of gold (Groves & Foster 1991); and the Kolar gold field (Kolar Schist Belt, Dharwar Craton, India), which has produced approximately 790 tonnes of gold (Hamilton & Hodgson 1986). Localized high degree of gold mineralization and large gold fields do occur in older (3.0-2.9 Ga) greenstone belts of the Superior Province (e.g., Red Lake), Yilgarn Block (e.g., Mount Magnet- Meekatharra), and

TABLE 16.4. Characteristics of selected intrusion-related gold deposits (modified from compilation by Sillitoe 1991)

Deposit	Contained Au (tonnes)	Ore-related intrusion	Age (Ma)	Associated mineralization	Host rocks	Metal association	Key hypogene alteration
<i>(a) Porphyry gold and copper-gold deposits</i>							
Oak Tedi, Papua New Guinea	368	Monzonite porphyry stock	1.2	Cu-Au skarn deposits	Late Cretaceous siltstone; Eocene-Miocene limestone	Cu-Mo-Au	Biotite, K-feldspar
Boddington, Western Australia	120	Quartz microdiorite bodies	2650-2670	None	Archean andesitic flows	Au-Cu-Mo-W	Biotite, K-feldspar, actinolite, epidote
<i>(b) Non-porphyry-type stockwork and disseminated gold deposits hosted by intrusions</i>							
Gilt Edge, South Dakota, USA	87	Trachyte porphyry stocks	50-60	Porphyry-Mo protore (in breccia clasts)	Y-Proterozoic metasediments and amphibolite; Cambrian sandstone	Au-Cu-As-Mo-(Pb-An-Te)	Sericite, clay minerals, K-feldspar
Salave, Spain	30	Granodiorite stock cut by granodiorite dikes	285	None	Cambro-Ordovician quartzite and slate	Au-As-Mo-Sb-(Zn)	Sericite, albite, calcite
<i>(c) Vein gold deposits related to intrusions</i>							
Zhao-Ye (Jiaojia), Shandong, China	~500	Granite and granodiorite pluton	~150	None	Granite and granodiorite	Au-Cu-Pb-Zn-Ag-Bi	Sericite, K-feldspar, chlorite, carbonate
Segovia, Columbia	>200	Quartz diorite pluton	Jurassic	None	Jurassic granite and granodiorite	Au-Ag-Pb-Zn-(Cu-As-W)	Sericite
<i>(d) Skarn gold deposits</i>							
Suan district, North Korea	>100	Granite pluton	Jurassic	Au veins	Late Proterozoic-Cambrian limestone and dolostone	Cu-Au-(Ag-Pb-As-Bi)	Garnet, diopside, actinolite, tremolite, phlogopite, chlorite, wollastonite

TABLE 16.4 (continued)

Deposit	Contained Au (tonnes)	Ore-related intrusion	Age (Ma)	Associated mineralization	Host rocks	Metal association	Key hypogene alteration
Nickel Plate, British Columbia, Canada	83.5	Diorite and quartz diorite porphyry sills and dikes	Early Jurassic	None	Triassic calcareous and tuffaceous siltstone	Au-Cu-As-Zn-(Co-Ni-Bi-Mo-Te)	Clinopyroxene, garnet, epidote, chlorite
<i>(e) Carbonate-replacement gold deposits</i>							
Cove, Nevada, USA	149	Granodiorite or quartz monzonite porphyry stock, dikes, and sills	39.5	Au-skarn (McCoy deposit)	Triassic limestone and clastic rocks	Au-Ag-Zn-Pb-Cu-Sn-As	Jasperoid, sericite, clay minerals
<i>(f) Stockwork, disseminated, and replacement gold deposits in non-carbonate rocks</i>							
Muntau, Uzbekistan	1,000-2,500	Peraluminous syenite and granite dikes (buried pluton inferred)	Late Paleozoic	None	Late Proterozoic (?) shale and siltstone	Au-As-W-Cu-Pb-Zn-Sb-Bi-Ag	Silica, alkali feldspar, chlorite, tourmaline, biotite
Porgera, Papua New Guinea	420	Diorite stocks, sills and dikes	7-10	Au-bearing stockwork and breccia in some stocks	Late Cretaceous silty shale	Au-Ag-An-Pb-As-Te (Hg)	Sericite, dolomite, quartz, anhydrite
Mount Morgan, Queensland, Australia	280	Tonalite pluton	362	Small breccia pipes with minor Cu-Au	Middle Devonian felsic volcanics	Au-Cu-(Zn-Bi-Te)	Quartz, pyrite, sericite, chlorite
<i>(g) Breccia-hosted gold deposits</i>							
Kidston, Queensland, Australia	101	Rhyolite plugs and dikes	321	Porphyry-molybdenum protore	Proterozoic metamorphics and Proterozoic or Paleozoic granodiorite	Au-Zn-Cu-Mo-Pb-(As-Bi-Te)	K-feldspar, biotite, sericite, carbonates

Zimbabwe craton (e.g., Kadoma, Limpopo, Harara, Gwanda, Umtali), but the gold mineralization in these cases probably postdated greenstone belt volcanism by more than 200 m.y. Older (3.3-3.5 Ga) greenstone belts in the Pilbara Block of Western Australia is poorly mineralized, but part of the similar age greenstone terrane of the Barberton Mountain Land carries anomalous gold concentrations where there is a high density of fault/shear zones. No significant Archean gold mineralization has been found in the cratons of Finland and the former USSR (Groves & Foster 1991).

Lode gold deposits in Proterozoic greenstone belts are relatively small and unimportant on a global scale; the most important example is the Mahd-el-Dahab deposit in Saudi Arabia (Fig. 16.1). Most of the Paleozoic lode deposits are hosted by greywacke-pelite assemblages formed in continental margin turbidite settings. Best examples of this type occur in rocks of lower Paleozoic age: Meguma Group of Nova Scotia (e.g., the Goldenville deposit) and the Carolina slate belt, both in the Appalachian orogen of eastern North America; the Ballarat and Bendigo districts of the Victoria gold belt, eastern Australia; and the deposits at Muruntau in Uzbekistan. Such deposits have been described in the literature as *turbidite-hosted deposits* (Keppie et al. 1986). However, they share the same characteristics of regional structural control, brittle-ductile deformation, vein paragenesis, and ore fluid properties with the older greenstone-hosted lode deposits, suggesting a common genetic process (Hutchinson 1987, Nesbitt 1991, Kerrich & Wyman 1990, Kerrich & Cassidy 1994).

Significant lode gold mineralization is also found in Mesozoic-Cenozoic volcano-sedimentary settings. The best examples of these are the so-called mesothermal vein gold deposits (Nesbitt et al. 1986, Nesbitt & Muehlenbachs 1989a) of the Mother Lode belt of California, the Juneau belt of southern Alaska, and the Canadian Cordillera (Coquihalla, Bralorne-Pioneer, Cariboo, Cassiar districts). These deposits are hosted by lithologically diverse units, including mafic to felsic volcanic rocks, serpentinites, carbonates, and clastic sedimentary rocks, collectively at greenschist facies metamorphism. The essentially 'greenstone' environment of the main host rocks (Hutchinson 1987), the structural control, and the accretionary tectonic setting of the younger mesothermal deposits suggest an origin similar to that of the Archean lode gold deposits.

In this chapter we will focus on lode gold deposits of the Archean greenstone terranes. Their general characteristics may be summarized as follows (Roberts 1987, Colvine et al. 1988, Groves & Foster 1991, Groves 1993, Kerrich & Cassidy 1994):

- (a) The host rocks are highly variable and range from metamorphosed ultramafic, mafic, and felsic metavolcanic rocks, to felsic and mafic intrusions, to clastic and chemical sediments. (Fig. 16.5). Many large to giant deposits occur in rocks with high Fe:(Fe+Mg) ratios, such as tholeiitic and komatiitic volcanic rocks, dolerite, and BIF. A particular host lithology may predominate in a given deposit, but the host rock is highly variable from one deposit to another, even in the same camp. Granitoid batholiths, the dominant component of most greenstone-granitoid terranes,

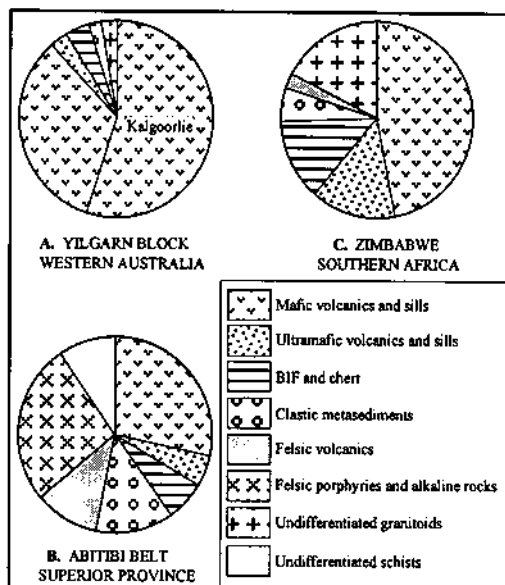


Figure 16.5. Host rocks to Archean lode gold deposits in: A. the Yilgarn Block, Western Australia; B. the Abitibi belt, Superior Province, Canada; and C. Zimbabwe craton, southern Africa (after Groves & Foster 1991).

are relatively poorly mineralized. Overall, banded iron-formations do not constitute a major ore host, but they do host some important gold deposits (e.g., the Lupin deposit, NWT, Canada; the Mallappakonda deposit, Kolar Schist belt, India; the Gwanda greenstone belt, Zimbabwe).

- (b) The spatial association between igneous intrusions and gold mineralization varies from craton to craton. The association is quite pronounced in the Superior Province and about 25% of the gold production in the Abitibi belt comes from deposits hosted by post-volcanic felsic intrusions (Colvine et al. 1988). A broad spatial association between gold deposits and felsic intrusions is apparent in the Yilgarn Block and Zimbabwe craton, but the intrusions themselves do not host any major deposits. There is no evidence that felsic intrusions directly contributed to the gold metallogenic event.
- (c) Most gold deposits, including giant gold camps such as Timmins and Kalgoorlie, occur in middle- to upper-greenschist facies metamorphic domains (mesozonal deposits), which corresponds broadly to the transition between the domains of ductile and brittle deformation. Some major deposits (e.g., Hemlo, Big Bell, Kolar) do occur in middle- to upper- amphibolite facies rocks and a few small deposits have also been identified

- in granulite facies domains (e.g., Norseman, Western Australia).
- (d) Structure is the single most important control in the distribution of Archean lode gold deposits. The first order, regional control appears to be crustal-scale deformation (shear) zones of anomalously high strain (in otherwise generally low-strain greenstone successions) that may transect lithologic boundaries and generally contain highly altered rocks. In the Superior Province, the deformation zones resulted either from large-scale crustal shortening or in response to the ascent and emplacement of major batholiths that are external to greenstone belts and smaller plutons within greenstone belts (Colvine et al. 1988). In general, deformation zones resulting from crustal shortening have greater strike lengths and host most of the gold deposits. In the Norseman-Wiluna belt of the Yilgarn Block, gold deposits occur adjacent to crustal-scale, strike- to oblique-slip shear zones, which might in part be reactivated synvolcanic faults that also apparently controlled the emplacement of suites of lamprophyric to felsic porphyry intrusions (Groves & Foster 1991). Syn- to late-tectonic stocks and dikes of various compositions, including lamprophyre dike swarms, have commonly intruded deformation zones also in the Superior Province.
- (e) Individual gold deposits are composed of one or more ore zones whose shapes, orientations, and distribution are controlled by small-scale, second order structures geometrically related to crustal-scale shear zones (Table 16.5). Ore zones are lenticular, tabular, or irregularly shaped bodies, typically comprising a complex assemblage of gold-bearing quartz 'veins'. Colvine et al. (1988) described three types of gold-bearing veins: extension veins; breccia and fracture veins; and replacement veins. A more detailed review is given by Hodgson (1989). Most structures that control gold mineralization show features typical of brittle-to-ductile transition, but the spectrum extends from brittle faults and fracture zones in greenschist facies domains, through brittle-ductile structures in greenschist facies domains, to ductile shear zones in amphibolite to lower granulite facies domains. This is evidenced by a general change in the style of mineralization from breccias and crosscutting quartz-vein sets to more foliation-parallel quartz veins and shear-zone replacements with increasing metamorphic grade. Many examples of the occurrence of both brittle and ductile structures in the same district (e.g., Golden Mile, Kalgoorlie) at the same metamorphic grade suggest that the brittle to ductile transition is probably not a simple function of depth, as was visualized by Colvine et al. (1988), but is also affected by factors such as strain rate, fluid pressure, and the competency of the rock. The influence of competency contrast in host rocks on the mineralized structures is evidenced by abundant mineralization in shear zones along lithologic contacts and the restriction of discordant, vein-style mineralization to competent lithologies.
- (f) The most distinctive occurrence of gold is in discordant quartz veins, but it

TABLE 16.5. Characteristics of selected large to giant Archean lode gold deposits (modified from compilation by Groves & Foster 1991)

Region/ Deposit	Gold production (tonnes)	Host rock	Metamorphic domain	Lode type	Alteration in ore zone	Ore minerals
<i>Yilgarn Craton, Australia</i>						
Golden Mile, Kalgoorlie	~1,200	Tholeiitic dolerite sill	Greenschist	Steeply dipping brittle-ductile shear zones and brittle fracture sets; some breccias	Muscovite + ankerite + pyrite; some silicification and quartz veining	Gold + pyrite + minor scheelite, arsenopyrite, and anhydrite; late tellurides
Sons of Gwalia, Leonora	> 90	Tholeiitic to high-Mg basalts	Greenschist	Steeply dipping major shear zone with local boudinaged quartz veins	Muscovite + biotite + ankerite + pyrite; quartz veins	Gold + pyrite + arsenopyrite ± pyrrhotite; minor chalcopyrite
Big Bell, Murchison	> 90	Tholeiitic basalt or dolerite	Amphibolite	Steeply dipping shear zones	Pyrite + quartz + muscovite or K- feldspar; minor sillimanite and rutile	Gold + pyrite ± arsenopyrite ± pyrrhotite ± stibnite ± galena ± sphalerite ± magnetite
<i>Canadian Shield</i>						
Hollinger, Timmins district, Abitibi belt, Superior Province	> 600	Mafic flows, minor felsic flows and pyroclastics, quartz-feldspar porphyries	Greenschist	Quartz veins and stockworks; steeply dipping shear zones	Sericite + ankerite ± chlorite ± calcite; quartz and albite	Gold + pyrite + pyrrhotite ± galena ± sphalerite
Kerr-Addison, Larder Lake district, Abitibi belt, Superior Province	> 320	High-Mg and tholeiitic basalts; felsic to syenite dikes; clastic sediments	Greenschist	Stockworks and ladder veins	Ankerite-albite- muscovite	Gold + pyrite + scheelite + arsenopyrite

TABLE 16.5 (continued)

Region/ Deposit	Gold production (tonnes)	Host rock	Metamorphic domain	Lode type	Alteration in ore zone	Ore minerals
Sigma, Val d'Or, Abitibi belt, Superior Province	> 110	Intrusive dolerite plug with andesite flows; minor porphyry dikes	Amphibolite	Subvertical veins and breccias in brittle-ductile shear zones; flat veins	Calcite + white mica	Gold + pyrite + pyrrhotite; minor chalcocopyrite, sphalerite, galena, scheelite, tellurides
Hemlo, Hemlo-Heron Bay belt, Superior Province	> 300	Andesitic to rhyolitic volcanics or pyroclastics; some clastic sediments	Amphibolite	Steeply dipping ductile to brittle-ductile shear zones	Quartz + muscovite ± biotite ± phlogopite ± microcline ± barite ± titanite	Gold + pyrite + molybdenite ± sphalerite ± arsenopyrite ± stibnite; various minor Pb-, Cu-, Sb-, Hg-, Tl- and Te- bearing minerals
Giant Yellowknife, NWT	> 177	Pillowed and massive basalt	Amphibolite	Steeply dipping brittle-ductile shear zone	Sericite ± ankerite ± chlorite ± albite	Gold ± pyrite ± stibnite + sulfosalts + sphalerite + galena
<i>Zimbabwe Craton</i>						
Cam and Motor, Kadoma	> 145	Tholeiitic basalt/andesite; high-Mg basalts; dolerite intrusions; minor clastic sediments	Greenschist	Steeply dipping veins, shear zone vein arrays and stockworks	Quartz + ankerite; serpentine in high- Mg rocks	Gold + pyrite + arsenopyrite + stibnite ± sphalerite ± galena
Phoenix, Kwekwe	> 105	Dunite-peridotite intrusive complex	Greenschist	Quartz-veins; minor stockworks	Magnesite ± fuchsite ± talc	Gold + pyrite + stibnite + arsenopyrite
<i>Dharwar Craton, India</i>						
Kolar schist belt	> 790	Mainly basaltic rocks; some ultramafic rocks and minor chemical sediments	Amphibolite	Quartz veins and sheeted veinlets related to brittle- ductile shear zones; minor replacements of BIF	Quartz + diopside ± hornblende ± biotite; minor sericite and chlorite near veins; calcite and tourmaline	Gold in quartz ± pyrite ± pyrrhotite ± arsenopyrite ± sphalerite ± galena

is common for some or most of the gold of an ore zone to be contained in wallrocks adjacent to veins (e.g., Hollinger mine, Superior Province), usually associated with iron sulfides. Mineralization in layer-parallel shear zones (e.g., in the Kalgoorlie district, Yilgarn Block) have a grossly strata-bound appearance (in the sense that each individual deposit is more or less restricted to a sedimentary unit or facies) and deposits hosted by banded iron-formations may even appear grossly stratiform in places. Such deposits in a district, however, are not restricted to a particular stratigraphic interval the way VMS deposits are.

- (g) Gold occurs in the native state, generally in small fractures in quartz but also in pyrite \pm pyrrhotite \pm arsenopyrite. Electrum (fineness <800) may be present locally in place of gold of high fineness. Opaque minerals rarely constitute more than 5% of a vein. Pyrite is invariably present and is the most abundant sulfide. Pyrrhotite and arsenopyrite are common. Other opaque minerals may include galena, sphalerite, chalcopyrite, löellingite, molybdenite, stibnite, tellurides, scheelite, magnetite, hematite, and anhydrite. More complex assemblages of sulfides, sulfarsenides, and sulfosalts, as described from the Hemlo deposit in the Superior Province (Harris 1986), are unusual. Multiple phases of mineralization are common, although these probably represent a fluid continuum within an evolving brittle-ductile shear zone rather than temporally discrete phases of hydrothermal activity (Groves & Foster 1991). Gold mineralization is commonly an integral part of wallrock alteration, and in greenschist facies rocks minerals characteristic of the alteration (carbonates, quartz, sericite, albite) may also be present in the veins. The deposits are typically enriched in As, W, Ag, Sb, Te, Mo, and B, and have low base metal contents. Au:Ag ratios are commonly around 10:1.
- (h) The grade of the deposits, as mined, varies widely, even from a single deposit or within a single camp, and generally has been on the decline because of exhaustion of higher grade ores and advancing technology. Ores currently being produced by underground mining have grades in the range 4 to 8 g/t Au, but many small and a few large deposits (e.g., Teck-Corona, Hemlo district) have grades as high as 10-15 g/t. In the Yilgarn Block, it has been possible to exploit weathered ore zones with grades typically below 5 g/t by open-pit mining (Groves & Foster 1991). The vertical extent of mineralization may be up to 2 km, but vertical zoning is weak to absent within individual deposits, although some zoning of metal contents may be discernible at the scale of an entire mining district.
- (i) All Archean lode gold deposits are accompanied by intense and extensive wallrock alteration, which tends to decrease in intensity with increasing distance from areas of gold concentration. The hydrothermal alteration commonly involves massive introduction of CO_2 , K, S, and H_2O , along with either introduction or redistribution of silica. In some deposits there is

evidence of addition of other elements such as As, Sb, W, Mo, B, Ag, Li, Ba, Rb, and Cr, but this is not a consistent feature. Carbonatization (replacement by carbonate minerals such as magnesite, ankerite-dolomite, and calcite) is the most prominent and common alteration on both regional and mine scales. Mineral assemblages indicative of sulfidation, oxidation, and potassic metasomatism are also characteristic, but tend to be more locally associated with gold. As discussed by Roberts (1987), Colvine et al. (1988), and Witt et al. (1997), the variations in alteration assemblages have been controlled by three variables: host rock composition, rock permeability, and the timing and *P-T* conditions of metamorphism.

- (j) The ubiquitous spatial association of gold mineralization with hydrothermal alteration is a strong evidence of their broad contemporaneity. This is consistent with the typically identical range of $\delta^{18}\text{O}$ values (+8 to +16‰) of vein quartz and the quartz of the altered host rock. In greenschist facies settings, alteration minerals often overprint peak-metamorphic assemblages, indicating that wallrock hydrothermal alteration (and, hence, gold mineralization) closely postdated peak metamorphism (Phillips 1985, Kerrich & Wyman 1990, Witt et al. 1997). The temporal relationship between gold-related alteration and peak metamorphism in amphibolite facies domains is controversial. In the Superior Province, such alteration has been interpreted as pre-metamorphic (Burk et al. 1986, Kuhns 1986, Kuhns et al. 1994) and syn- to post-metamorphic (Pan & Fleet 1995) in the Hemlo district. However, there is convincing petrographic, geothermometric, and isotopic evidence that the alteration was syn-metamorphic for amphibolite facies-hosted deposits in the Yilgarn Block (Barnicoat et al. 1991, Mueller et al. 1991, Knight et al. 1993, Witt et al. 1997). Considering that lode gold mineralization in greenstone belts is believed to have been a craton-scale event, its different timing relative to peak metamorphism at different crustal levels is a problem for any hydrothermal genetic model.
- (k) In any one terrane, gold mineralization appears to broadly represent a single event related to late-deformation accompanying or outlasting peak metamorphism and postdating most of the felsic intrusions. The absolute age of lode gold mineralization in the Superior Province, the Yilgarn Block, and the Zimbabwe craton, constrained by limited data on either the ages of older and younger intrusions or the ages of gold-associated hydrothermal minerals, is estimated to be 2.6-2.7 Ga (see, for example, discussions in Kerrich & Kyser 1994, Anglin et al. 1996, and Witt et al. 1997). Probably the closest to the timing of gold mineralization in the Superior Province are the lamprophyre dikes, dated at 2674 ± 2 Ma in the Kirkland area and at 2675 ± 5 Ma in the Hemlo area, as they both cut and are cut by mineralized structures (Wyman & Kerrich 1988). Lamprophyres with similar relationship to gold mineralization in the Yilgarn Block have been dated at

2.6-2.7 Ga (Rock & Groves 1988), and pegmatite dikes that crosscut gold-bearing structures indicate a regionally extensive gold mineralization event in the craton at about 2630 ± 10 Ma (Kent et al. 1996).

16.4. Examples

16.4.1. CARLIN DEPOSIT, NEVADA, USA

Most of the Carlin-type deposits in Nevada are located along one of three recognized mineral belts (Fig. 16.2): the Carlin Trend (previously called the Lynn-Pinson mineral belt), the Getchell Trend, and the Cortez Trend. The 60 km-long Carlin Trend is identified by an alignment of about 10 major Carlin-type deposits and many more centers of gold mineralization, with total gold resources exceeding 80 million ounces. By the end of 1996, more than 25 million ounces of gold had been mined from 26 separate operating or past-producing mines on the Carlin Trend (Teal & Jackson 1997). The Trend is not a manifestation of any singular fault zone, but rather a combination of structural features in a zone of crustal weakness and sustained high heat flow caused by intrusive activity that began in the late Triassic and continued through the late Tertiary. A prominent feature of the Trend is the Roberts Mountains thrust, which marks the eastward thrusting of an western "eugeosynclinal" assemblage of predominantly siliciclastic rocks over the eastern autochthonous "miogeosynclinal" assemblage of silty carbonate rocks during the Devonian to early Mississippian Antler orogenic event (Stewart 1980). Effects of the Antler orogeny or later Mesozoic deformation and intrusive activity resulted in the formation of broad amplitude, N25-35°W trending, northerly plunging antiforms within the autochthonous sequence now preserved in several uplifted tectonic windows along the Carlin Trend (Roberts 1960). The tectonic windows were the sites of early discoveries of Carlin-type gold mineralization, but many deposits have since been discovered outside of, but proximal to, these windows (e.g., the Rain deposit). The autochthonous sequence (the Silurian-Devonian Roberts Mountains Formation and the Devonian Popovich Formation) is the host to majority of gold deposits on the Carlin Trend, with most occurring in the upper 400-500 m of the sequence. The allochthonous sequence (the Silurian Vinini Formation) is host to smaller, high-angle fault-controlled deposits and a few vein deposits.

The Carlin deposit is the most important gold deposit of the Carlin Trend and has been the subject of many investigations (e.g., Radtke & Dickson 1976, Radtke et al. 1980, Radtke 1985, Burton et al. 1985, Bakken & Einaudi 1986, Kuehn & Rose 1992, 1995, Christensen 1993). It was discovered in 1961 by Newmont Mining Company geologists and brought into production in 1965. The total amount of recoverable gold in this deposit, including the amount already produced, is estimated to be in excess of 107 million ounces (Teal & Jackson 1997).

The Carlin deposit is located in the northern portion of the Lynn window along the eastern flank of the Tuscorora anticline. The Roberts Mountains thrust fault is exposed

in the Carlin mine (Fig. 16.6). The allochthonous western assemblage (Vinini Formation) is composed of chert, shale, quartzite, and minor carbonate rock and greenstone. The autochthonous eastern assemblage (Roberts Mountains Formation and Popovich Formation), is a shelf to outer-shelf carbonate and clastic sequence. The upper part of the Roberts Mountains Formation is divisible into two mappable units (Bakken & Einaudi 1986): an upper unit of silty to muddy limestone; and an underlying unit (≈ 150 m thick) of fossiliferous limestone beds (MFL) intercalated with centimeters-to-meter thick sections of thinly laminated, silty dolomitic limestone beds (LSL). Gold mineralization at Carlin occurs mainly in the lower unit and extends semiconformably over a strike length of about 2 km.

A series of near-vertical, ENE- and NNW-trending normal faults crosscut the autochthonous sequence and offset the Roberts Mountains thrust, and a few of the NNW-trending structures are filled with hydrothermally altered, felsic dikes. These normal faults may have formed in response to the middle Tertiary pre-Basin and Range extension, which began in this portion of the Great Basin at about 37 Ma (Zoback et al. 1981). The localization of jasperoid veins (silicification) and the zoning of alteration and mineralization relative to these faults suggest that the crosscutting structures served as major conduits for hydrothermal fluids (Bakken & Einaudi 1986, Kuehn & Rose 1992).

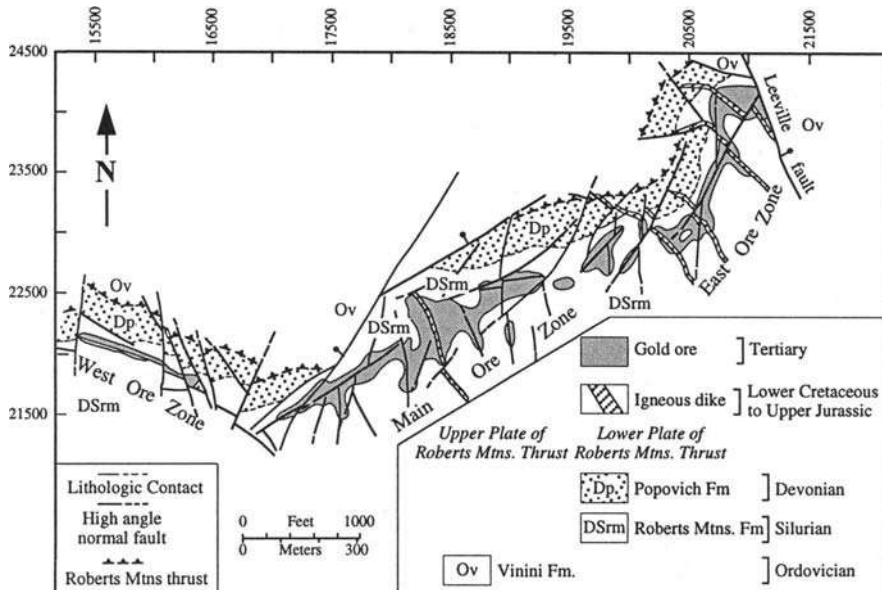


Figure 16.6. Generalized geologic map of the Carlin deposit (simplified from Bakken & Einaudi 1986). Some of the minor faults have been omitted for clarity.

$^{40}\text{Ar}/^{39}\text{Ar}$ dating led Groff et al. (1997) to conclude that Carlin type deposits at Getchell and Twin Creeks (Getchell Trend) consists of a late Cretaceous (83 Ma) quartz - pyrite - gold mineralization overprinted by an Eocene (42 Ma) orpiment - stibnite - pyrite - gold mineralization. The age of mineralization at Carlin has not yet been determined directly. A maximum age of 120-130 Ma is suggested by the ages of an igneous dike within the deposit and of the Gold Strike pluton north of Carlin, both of which are hydrothermally altered and mineralized. A minimum age is provided by the mid-Miocene (14 Ma) unaltered rhyolitic lavas that unconformably overlie Au-bearing rocks. Bakken and Einaudi (1986) preferred an early to middle Tertiary age of mineralization on the basis of the likely ages of crosscutting faults that appear to have served as hydrothermal conduits.

The rocks around the deposit have been subjected to both hypogene and supergene alteration. Supergene alteration includes oxidation of sulfide minerals and acid-leaching of rocks; it is not spatially related to gold distribution at the mine or on a district-wide scale, and is interpreted as post-ore (Kuehn & Rose 1992). The main types of hypogene alteration are decarbonatization (carbonate dissolution), argillization, silicification, and calcification. The removal of carbonate minerals from silty dolostones and limestones was early and resulted in increased porosity and permeability. Argillization accompanied decarbonatization and resulted in the formation of illite from detrital feldspar with minor amounts of montmorillonite and kaolinite. Silicification was pervasive and produced jasperoid. Late-stage calcification is represented by calcite veinlets.

Major through-going veins are rare at Carlin, but small, discontinuous veins ("veinlets") of barite, calcite, quartz, and quartz-pyrobitumen, typically 0.5 to 5 mm in thickness, are common at many locations. The paragenesis of the veinlets has been discussed by many authors (e.g., Radtke 1985, Bakken & Einaudi 1986, Kuehn & Rose 1992), but with substantially different interpretations. Bakken and Einaudi (1986) described ten types of veinlets in terms of mineralogy and, based on observed crosscutting relations, suggested four distinct periods of veining: (a) veinlets that predate hydrothermal activity and are not related to gold mineralization; (b) veinlets that are associated with hydrothermal alteration; (c) veinlets and vug fillings that developed after the rocks were altered; and (d) veinlets that may be related to weathering. Veinlets tend to be concentrated in intensely silicified rocks of decreased permeability, but there is no spatial correlation between the density of quartz veins and the grade of gold mineralization. An important step in the mineralization process was the removal of up to 50% of the original calcite in the carbonate rocks. It appears that the carbonate host rocks were sufficiently permeable, or became sufficiently permeable, during carbonate dissolution to have permitted the flow of hydrothermal fluids along beds.

Detectable gold is present in subeconomic quantities throughout most of the altered MFL and LSL beds of the Roberts Mountains Formation. In general, ore-grade gold values (>0.5 oz/t) occur in incipiently to moderately silicified, weakly calcareous rocks and higher grade ore zones are localized around crosscutting faults. Owing to the extremely fine-grained and relatively low-grade, disseminated style of mineralization, it

is usually difficult, if not impossible, to separate visually the ore from the waste, and the delineation of ore zones is based entirely on gold assay values.

16.4.2. MCINTYRE-HOLLINGER DEPOSIT, SUPERIOR PROVINCE, CANADA

The Superior Province of the Canadian Shield has produced in excess of 4,500 tonnes of gold, more than any other Archean craton (Colvine 1989), predominantly from lode gold deposits located within greenstone terranes or at their margins (Fig. 16.7). Byproduct gold from base metal deposits accounts for <5% of the total production. Of the hundreds of gold deposits in the province, 120 deposits exceed 1 million ounces of past production + reserves, and more than 80% of the gold has been recovered from about 30 lode gold deposits, each with a past production of more than 30 tonnes.

The Superior Province contains two different categories of gold deposits, although many individual deposits (e.g., Dome mine) have characteristics of both types (Card et al. 1989). One category consists of sulfide schist deposits, such as those of Hemlo and Bousquet, which are characterized by a dominance of sulfide mineralization over quartz veins, a paraconcordant position within their host volcanic-sedimentary sequences, and localization in ductile shear zones. This is the style of gold mineralization for which an exhalative origin has been proposed (Kerrick & Fryer 1979, Proudlove et al. 1989). The other category is the more abundant, unquestionably epigenetic, lode gold deposits that are typical of Archean greenstone belts. The lode deposits are closely associated with major shear systems (deformation zones), tens to hundreds of kilometers long and up to 10 km wide, within or along the edges of greenstone belts. On a local scale, the sites of gold concentration generally correspond to zones of dilation during shearing. The overall morphology of gold deposits tend to be tabular to rodlike, with the minimum dimension parallel to the shear plane, which commonly has a steep plunge (Hodgson 1989). Most deposits occur in greenschist facies rocks, but some also occur in amphibolite facies rocks. The style of mineralization varies with the metamorphic grade of wallrocks (Colvine et al. 1988). Mineralization in brittle structures, such as veins and breccias, predominate in areas of lowest greenschist facies. Systematic veining in brittle-ductile structures is typical in areas of middle to upper greenschist facies, and foliation-parallel mineralization in ductile shears, with minimal veining, is characteristic of amphibolite facies domains.

The Abitibi greenstone belt accounts for approximately 80% of total production, reserves, and number of significant deposits in the Superior Province, and the Timmins (Porcupine) gold camp is the largest in this belt. So far 51 gold deposits have been discovered in the Timmins area, 21 of which have become major gold mines. Since the commencement of gold mining operations in the early 1900's to the end of 1988, the Timmins area had produced some 217 million tonnes of ore with an average grade of 9.17 g/t Au, representing about 27% of the Canadian gold output. Approximately 70% of the Timmins production has come from the McIntyre-Hollinger and Dome mines (Duff 1991). To date, the McIntyre mine is the only primary gold mining operation to have produced copper. A pipe-like zone of Cu-Au-Ag-Mo mineralization within the

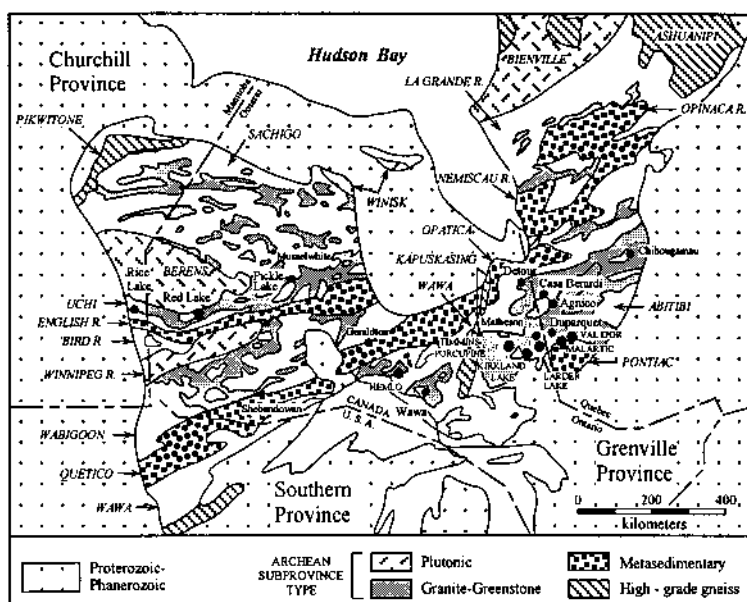


Figure 16.7. Major gold camps (solid circles) in the Superior Province of the Canadian Shield (modified from Colvine 1989).

Pearl Lake porphyry was discovered in 1959 and was mined from 1963 to 1982, resulting in the production of 66.8 million kg of Cu, 5,874 kg of Au, and 29,368 kg of Ag from 10 million tonnes of ore (Burrows & Spooner 1986).

The rocks in the Timmins area is subdivided into an upper sedimentary sequence and a lower volcanic sequence (Fig. 16.8). The entire package is 2,500-3,000 m thick and 2454-2727 Ma in age (Duff 1991). Calc-alkaline, quartz-feldspar porphyry plutons (e.g., Pearl Lake, Paymaster, Preston) intrude the stratigraphic succession and crosscut all other rock units. All the gold deposits of the camp are spatially related either to the Porcupine-Destor fault ("break") or to the Dome fault and the Ancestral Hollinger main fault, which formed as splays off the Porcupine-Destor fault late in the folding episode (Hodgson 1986).

The characteristics of gold mineralization in the McIntyre-Hollinger deposits have been described by Wood et al. (1986). The ore zone cuts across a series of strained and metamorphosed tholeiitic flows and carbonaceous interflow sediments of the Tisdale Group. Some amount of mineralization is also hosted by strained quartz-feldspar porphyry intrusions. Thus, the gold mineralization is interpreted to be syn- to late-tectonic, and later than and unrelated to the porphyry intrusions. Gold-associated scheelite samples have given a Nd-Sm age of 2403 ± 47 Ma (Bell et al. 1989), but the

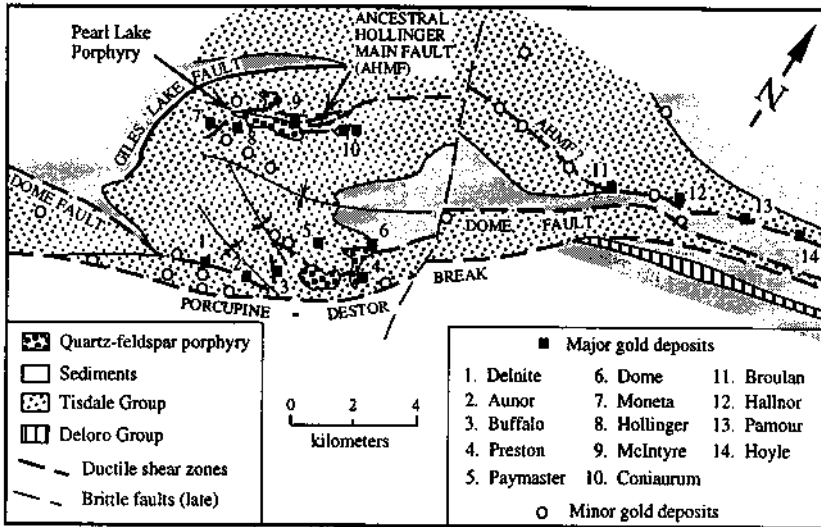


Figure 16.8. Generalized geologic map of the Timmins (Porcupine) gold camp showing relationship between locations of lode gold deposits and smaller-scale structures in the vicinity of a transcraton deformation (Porcupine-Destor "break") (after Hodgson 1986).

relatively young age appears to reflect a resetting by the Matchewan diabase dike swarm event (≈ 2400 Ma). A much older age (2.68-2.58 Ga) obtained by Hanes et al. (1992) from $^{40}\text{Ar}/^{39}\text{Ar}$ ratios of muscovite in gold-quartz veins is almost identical to that of the lamprophyre dikes mentioned earlier.

The principal type of gold mineralization consists of quartz-carbonate veins and stringers, filling dilational zones and hydrofractures as well as their well-developed pyrite - ankeritic carbonate - sericite alteration envelopes. The veins consist of about 95% white quartz, the remainder being comprised of ankeritic carbonate, albite, scheelite, chlorite, tourmaline, minor sulfides (pyrite, sphalerite, chalcopyrite, pyrrhotite, and galena), tellurides, native bismuth, and gold. Coarse, visible gold occurs intergrown with carbonate and quartz, mostly at the fringes of the veins. The bulk of the gold (about 95%) is localized in the alteration envelopes, typically as discrete particles of various shapes in pyrite. A very small proportion of the wallrock gold occurs in fractures in pyrite and is also associated with arsenopyrite, carbonate, and silicate gangue minerals. The gold and pyrite are cogenetic. This is corroborated by back-scattered electron imagery suggestive of submicron-size pyrite inclusions in tiny (3-15 μm) gold flakes.

The vein and wallrock alteration assemblages were formed by the same hydrothermal fluids. This is evidenced by the fact that isotope ratios of vein minerals — $\delta^{13}\text{C}$ (carbonate) = $-2.8 \pm 1.8\text{‰}$; $\delta^{18}\text{O}$ (carbonate) = $11.8 \pm 0.4\text{‰}$; $\delta^{34}\text{S}$ (pyrite) = $3.0 \pm 1.9\text{‰}$ — are statistically indistinguishable from those of wallrock alteration minerals

— $\delta^{13}\text{C}$ (carbonate) = $-3.2 \pm 1.3\text{‰}$, $\delta^{18}\text{O}$ (carbonate) = $11.7 \pm 0.5\text{‰}$, $\delta^{34}\text{S}$ (pyrite) = $3.7 \pm 1.2\text{‰}$. Fluid inclusion data indicate gold deposition at $277^\circ \pm 48^\circ\text{C}$ from a fluid of low salinity (5.6 ± 1.2 wt% NaCl equivalent) and high CO_2 (6 equivalent mole%), and do not allow discrimination between a magmatic source and a metamorphic source for the fluids. Based mainly on the carbon isotope data, Burrows et al (1986) and Wood et al. (1986) argued that the mineralizing fluids were magmatically derived and that components of domal tonalite gneiss-granodiorite-quartz monzonite-type material, which intrudes the lower parts of greenstone belts in the Superior Province, could constitute a direct or indirect source region. However, as will be discussed later, the carbon isotope data are equivocal.

16.5. Origin of Hydrothermal Gold Deposits

16.5.1. TRANSPORT OF GOLD

In aqueous systems, gold exists essentially in two valence states, Au^+ (aurous) and Au^{3+} (auric); higher oxidation states, although possible, are rare in nature. At moderate temperatures and pressures, it is the coordination chemistry of Au^+ in aqueous solutions that controls the transport and deposition of gold in hydrothermal ore depositing systems (Seward 1973, 1984, 1991; Romberger 1988).

Au^+ is potentially capable of forming aqueous complexes with a variety of ligands, but the most important for gold transport is believed to be the complexes with Cl^- [mainly AuCl_2^- , and possibly also AuClOH^-] and HS^- [mainly $\text{Au}(\text{HS})_2^-$ and $\text{HAu}(\text{HS})_2^0$, and possibly also $\text{Au}(\text{HS})_2^0$]. The hydroxo-gold complex, $\text{Au}(\text{OH})_2^-$, is the most stable inorganic Au species over a wide range of Eh, pH, and ligand activities and is probably the dominant dissolved gold species at ligand activities typical of both fresh water and seawater. Complexing with ligands such as HS^- and Cl^- , $\text{S}_2\text{O}_3^{2-}$, NH_3 , and SCN^- become more important in hydrothermal fluids containing high concentrations of these ligands (Vlassopoulos & Wood 1990).

The relative importance of chloride versus bisulfide complexes in the hydrothermal transport of gold is a function of several parameters: temperature, pH, salinity (Cl^- concentration), pH, $f\text{O}_2$ (related to $f\text{H}_2$), and sulfur concentration. Experimental studies (Seward 1973, Hayashi & Ohmoto 1991) indicate that, in general, gold is most soluble as chloride complexes in acidic, oxidizing solutions, where sulfur would exist as HSO_4^- or SO_4^{2-} , but as bisulfide complexes in alkaline, reducing solutions, where sulfur would occur as either H_2S or HS^- (Fig. 16.9). From experiments with aqueous solutions containing both NaCl and H_2S at $250\text{--}350^\circ\text{C}$, Hayashi and Ohmoto (1991) concluded that: (a) the solubility of gold in ore-forming fluids in equilibrium with pyrite \pm pyrrhotite in this temperature range is typically between 0.1 ppb to 1 ppm Au, mostly as bisulfide complexes; (b) the dominant bisulfide complex is $\text{HAu}(\text{HS})_2^0$ at $\text{pH} \leq 5.5$ opposite to that of S concentration. From thermodynamic extrapolation of

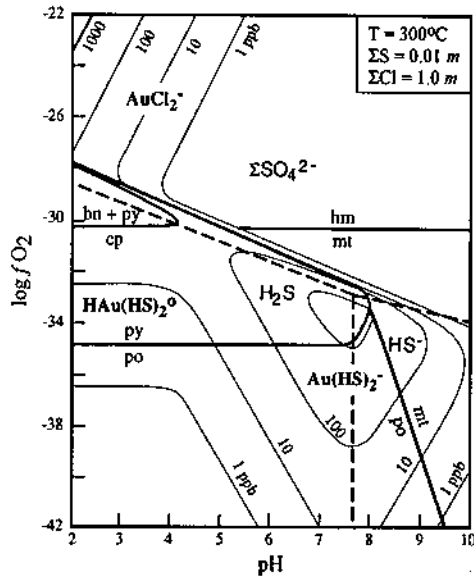


Figure 16.9. Solubility contours of gold, as a function of fO_2 and pH at $T = 300^\circ\text{C}$, in an aqueous solution containing $\Sigma S = 0.01\text{ m}$ and $\Sigma Cl = 1.0\text{ m}$ (after Hayashi & Ohmoto 1991). Note that chloride complexes of gold are important only in the region of high fO_2 and very low pH, and that gold can be transported as bisulfide complexes over a wide range of pH and fO_2 conditions.

Helgeson and Garrels (1986) and unpublished experimental data, Henley (1991) estimated that, at lower temperatures, the solubility of gold due to $AuCl_2^-$ would be important only under extreme salinity (near halite saturation) (Fig. 16.10a) but might become more important at higher temperatures ($\approx 400^\circ\text{C}$), for example, in porphyry-type mineralization. In chloride-sulfide solutions, the solubility of base metals is controlled primarily by chloride complexes and it decreases rapidly with decreasing salinity. This is the reason why gold deposits commonly are relatively impoverished in base metals. Gold solubility decreases with increasing CO_2 concentration in the fluid (Fig. 16.10b), which is inversely related to the concentration of H_2S through fluid-mineral equilibria.

16.5.2. MECHANISMS OF GOLD PRECIPITATION

As the solubility of both chloride and bisulfide complexes increases with increasing temperature (Henley 1973, Seward 1973, Wood et al. 1994), a decrease in temperature should lead to the precipitation of gold from a gold-saturated solution. The temperature effects on natural systems, however, are difficult to evaluate, because temperature affects other parameters, such as fO_2 , which may have a greater influence on gold solubility. Generally, an increase in pressure increases the solubility of minerals, but

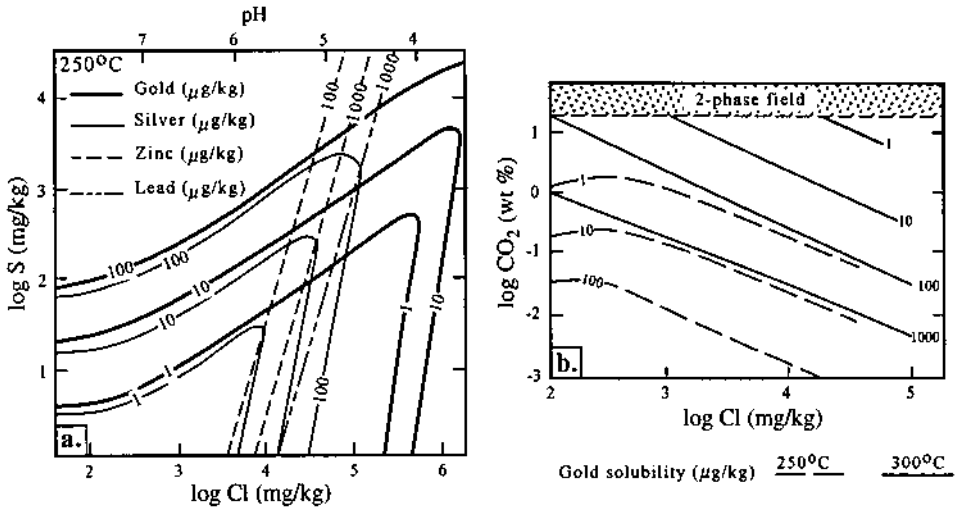
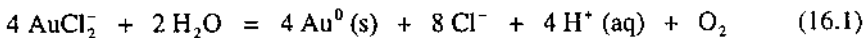


Figure 16.10. Solubilities of gold, silver, zinc, and lead as a function of sulfur, chloride, and CO₂ concentrations in hydrothermal solutions. a. Relative solubilities of precious and base metals at 250°C in chloride-sulfide solutions, the pH and redox state of which are controlled by common wallrock alteration mineral assemblages (after Henley 1991). H₂S is the dominant sulfide species across much of the S-Cl space included in the diagram, but sulfate occurs in the region at the bottom left corner of the S-Cl space marked by low salinity and low sulfur conditions. Halite saturation is at about Cl = 10^{5.54} mg/kg. b. Solubility of gold at 250° and 300°C in chloride-sulfide-CO₂ solutions buffered by common mineral equilibria. (After Berger & Henley 1989.)

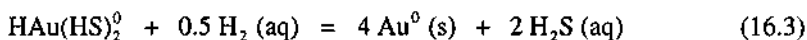
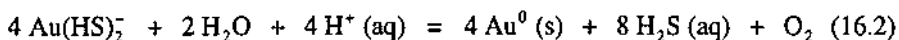
Seward (1973) argued that the solubility of Au(HS)₂⁻ above 250°C would increase with a decrease in pressure. As will be discussed later, the relationship between pressure and gold precipitation by boiling is an indirect one.

Conditions favorable for gold precipitation from a hydrothermal fluid depends on its dominant Au-complexes. This may be illustrated by considering a few likely reactions for the precipitation of native gold, the most common form of gold in ore deposits. For chloride complexes, a likely reaction is



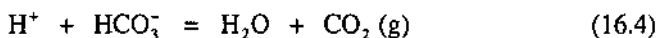
This reaction indicates that gold precipitation will be caused by an increase in pH or a decrease in either a_{Cl^-} or a_{O_2} . Using thermodynamic data, Huston and Large (1989) argued that, in a system of fairly constant a_{Cl^-} , gold precipitation would be caused by a decrease in temperature, followed in importance by an increase in pH and a decrease in a_{O_2} . Mechanisms commonly invoked for gold deposition involving AuCl₂⁻ are fluid mixing (dilution) and boiling. Fluid mixing may decrease not only the temperature but also the chloride activity by dilution. Boiling of the fluid would increase its pH.

Temperature decrease alone is not an effective mechanism for precipitating gold from bisulfide complexes, because the stability constants for gold bisulfide complexes change very little with temperature over the 150-350°C range (Seward 1973; Hayashi & Ohmoto 1991). Gold precipitation from bisulfide complexes may be represented by reactions such as (Huston and Large 1989, Hannington et al. 1991, Hayashi & Ohmoto 1991)



It follows that gold precipitation can be caused by a decrease in $a\text{H}_2\text{S}$ in either case and by either a decrease in $a\text{O}_2$ or an increase in $a\text{H}_2$ depending on the bisulfide complex. If $\text{HAu}(\text{HS})_2^0$ is the dominant gold-bearing species, a change in pH will not cause precipitation of gold, but a decrease in pH may cause gold precipitation if $\text{Au}(\text{HS})_2^-$ is the dominant gold-bearing species. Such changes may be brought about by interaction of the gold-bearing fluid with wallrocks (see, for example, Fyfe & Kerrich 1984). Thermodynamic calculations predict that the most efficient method of precipitating gold is to decrease the activity of reduced sulfur, because the solubility of gold decreases by two orders of magnitude for each order of magnitude decrease in the activity of reduced sulfur, but only by one order of magnitude for each unit decrease in pH (Huston & Large 1989). Suggested mechanisms for decreasing the activity of reduced sulfur in a hydrothermal fluid include: mixing with S^{2-} -impoverished fluids (dilution); oxidation of H_2S and HS^- to sulfate and sulfur, perhaps due to mixing with oxygenated meteoric water; boiling; and deposition of sulfide minerals, for example, by interaction of the fluid with Fe-rich wallrock (Phillips & Groves 1984) or by precipitation from the residual fluids after boiling (Drummond & Ohmoto 1985). Note that the increase in gold solubility caused by an increase in $a\text{O}_2$ is relatively small compared to the decrease in gold solubility caused by a decline in $a\text{H}_2\text{S}$ due to oxidation.

Based on fluid inclusion evidence, many authors have suggested that boiling of the hydrothermal fluids might have a major role in the precipitation of gold, especially in epithermal systems (Lyakhov & Popivnyak 1978, Buchanan 1981, Cole & Drummond 1986, Spooner et al. 1987, Naden & Shepherd 1989, Seward 1991). Boiling results in the loss of volatiles, particularly CO_2 and H_2S , to the vapor phase by reactions such as



and



resulting in an increase in the pH of the residual fluid. The increase in pH leads to immediate deposition of gold if it is present as AuCl_2^- (reaction 16.1), but enhances the

solubility of gold if it is present as $\text{Au}(\text{HS})_2^-$ (reaction 16.2). However, with continued boiling, the effect of the loss of reduced sulfur to the vapor phase may overtake the effect of increased pH on the solubility of sulfide complexes, causing the gold to precipitate. The actual reaction paths are much more complicated because of fluid-rock interaction, including dissolution and precipitation of various mineral phases occurring simultaneously with fluid phase separation (Bowers 1991).

16.5.3. GENETIC MODELS

Intrusion-related Deposits

Based primarily on gold mineralization in the western Pacific island arcs, which ranges from gold-enriched porphyry copper deposits to various intrusion-related and epithermal gold deposits, Sillitoe (1989, 1991) proposed a conceptual genetic model linking all of these deposit types to the evolution of porphyry systems (Fig. 16.11). The framework of this model lies in the partly interdependent fluid regimes in an intrusion-centered system of porphyry type (Henley & McNabb 1978, Eastoe 1982). These are: (a) relatively dense, high-salinity (30 to >75 wt% NaCl equivalent), high-temperature (400° to >700°C) magmatic hydrothermal brines that tend to reflux within the cooling intrusion; (b) ascendant plumes of lower-density, sulfur-rich, magmatic volatiles that condense upwards and mix with meteoric fluids; and (c) convectingly circulating meteoric water cells marginal to the intrusion that tend to collapse progressively onto the intrusion as magmatic fluid generation wanes. These fluid regimes, with magma and/or country rocks serving as the source of gold, are capable of producing a variety of gold deposits from fluids of varying temperature and salinity and at variable distances relative to the intrusion (Fig. 16.11). In the oxidized, saline, high-temperature magmatic hydrothermal fluids responsible for porphyry-type $\text{Au} \pm \text{Cu}$ mineralization, gold — like copper — must have been introduced as chloride complexes and precipitated with K-silicate assemblage as a consequence of cooling and/or pH increase. The intrusion-related, non-porphyry-type gold mineralization probably represents the involvement of a smaller volume of magmatic hydrothermal brine that behaved less violently or of a concealed porphyry-type deposit at a deeper level. Intrusion-related gold deposits beyond the limits of the intrusion are formed from relatively less oxidized, more dilute, cooler fluids, resulting from the mixing of magmatic hydrothermal fluids and variable amounts of convectively circulating meteoric water that are likely to transport gold as bisulfide complexes. The alteration characteristics of these deposits — decarbonatization and/or silicification of carbonate host rocks and feldspar-destructive alteration of silicate host rocks — and their distribution are compatible with movement of such fluids through stratigraphic and/or structural conduits. The possible source of gold for these deposits include magmatic fluids, country rocks scavenged by meteoric fluids, and gold remobilized from the porphyry-type mineralization.

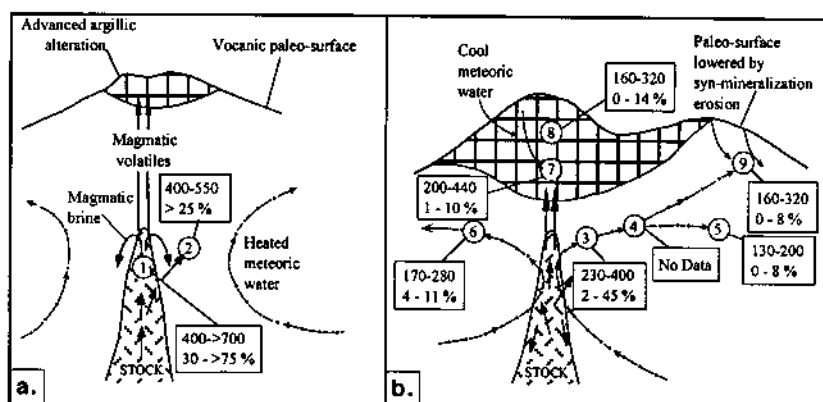


Figure 16.11. Conceptual genetic model for intrusion-related and epithermal gold deposits in a porphyry environment: a. Early-stage dominated by magmatic hydrothermal fluids; and b. Late-stage with 'collapse' of meteoric system (after Sillitoe 1991). Numbers denote the approximate locations of different deposit types relative to the porphyry stock and paleosurface: 1. porphyry-type; 2. prograde skarn; 3. retrograde skarn; 4. carbonate-replacement Au-base metals; 5. carbonate-replacement Au-As-Sb (Carlin-type); 6. non-carbonate disseminated, stockwork, and replacement; 7. deep acid-sulfate; 8. epithermal acid-sulfate; and 9. epithermal adularia-sericite. Arrows represent inferred flow-lines for different types of fluids. Boxes corresponding to the various deposit types show the homogenization temperatures ($^{\circ}\text{C}$) and salinities (wt% NaCl equivalent) of representative ore fluids as compiled by Sillitoe (1991).

Epithermal Deposits

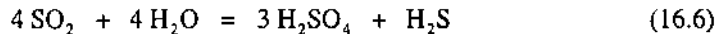
Alunite-kaolinite (acid-sulfate or high-sulfidation) type of epithermal deposits are interpreted to be located at shallow depths in the core of a volcanic dome, above porphyry-type mineralization associated with intermediate to felsic intrusions (Sillitoe 1989, Heald et al. 1987, Stoffregen 1987, Berger & Henley 1989, Rye et al. 1992, Hedenquist & Lowenstern 1994), although the epithermal mineralization may be displaced laterally because of structural control on mineralization. The evidence for this genetic link includes the significant copper contents of the alunite-kaolinite type gold deposits, their association with porphyritic rocks, and, most importantly, the characteristic advanced argillic alteration that also commonly occurs in volcanic rocks overlying porphyry gold-copper-bearing stocks (Fig. 16.11). More direct evidence of a genetic link has also been documented in a few cases. One good example is the Tavua caldera in Fiji, where drill hole data indicate a continuum of mineralization and alteration, from porphyry-style copper-gold at depth to acid-sulfate style epithermal gold near the surface (Eaton & Setterfield 1993). Even more convincing of contemporaneous formation is the example from northern Luzon, Philippines, described by Arribas et al. (1995). There the Lepanto epithermal Cu-Au deposit overlies the Far Southeast (FSE) porphyry Cu-Au deposit, and the alunite from Lepanto has the same range of ages as the hydrothermal biotite and illite from the FSE deposit.

Even if there was no direct link between ore-forming processes in the porphyry and

epithermal regimes, an intrusive event could facilitate the formation of epithermal gold deposits by introducing a large quantity of low-grade gold that would be available for later remobilization and concentration by circulating fluids of nonmagmatic origin. Moreover, an early porphyry event might cause widespread sulfidation of surrounding rocks. Later fluids of meteoric origin circulating through this pyrite-rich wallrock would have H_2S concentrations that remain elevated during cooling and ascent, increasing the chances of forming a large, high-grade epithermal gold deposit (Gammons & William-Jones 1997).

Acid-sulfate alteration is a subset of advanced argillic alteration and is distinguished by the presence of hypogene alunite in the assemblage alunite + kaolinite + quartz \pm pyrite. This alteration can develop by different mechanisms, all requiring extreme base leaching by very low-pH fluids relatively concentrated in H_2SO_4 at temperatures approximately below 400°C (Rye et al. 1992). In the supergene environment, H_2SO_4 is produced by the oxidation of sulfide minerals, especially pyrite, whereas in the steam-heated environment at or above the water table, as is the case in active hydrothermal systems, H_2SO_4 is produced by the oxidation of H_2S separated from deep, near-neutral brines during boiling. Common attributes of fossil steam-heated environments include the presence of excessive sinter (often at a distance from the acid-sulfate alteration), a vertical zonation downward from alunite through kaolinite to argillic or propylitic alteration assemblage, and an age coincident with underlying mineralization (Rye et al. 1992).

The hypogene acid-sulfate alteration associated with epithermal gold deposits develops in a magmatic hydrothermal environment below the water table. In this environment, H_2SO_4 is produced by the disproportionation of magmatic SO_2 with decreasing temperature



which is followed by dissociation of H_2SO_4 . The disproportionation probably begins in the magmatic vapor plume consisting mostly of water vapor, and acid-sulfate wallrock alteration commences at shallow depth when the vapor begins to condense producing a H_2SO_4 -bearing, highly acidic (pH \approx 2), oxidized, hot (200-300°C) fluid. Boiling of such a fluid at higher levels in the system may lead to a further decrease in pH. Very little meteoric water is entrained in the magmatic vapor plume as it effectively displaces meteoric water in the country rock, but when the vapor condenses, it eventually mixes with meteoric water to form kaolinite (Rye 1993). This scenario of acid-sulfate alteration is supported by stable isotope ratios of hydrothermal (hypogene) alunite from several alunite-kaolinite type deposits (Rye et al 1992). δD values of alunites are close to those of magmatic water and $\delta^{34}S$ values are +16 to +28‰ larger than those for associated pyrite, reflecting equilibrium between aqueous H_2S and SO_4 formed by the disproportionation of SO_2 . $\delta^{18}O$ (SO_4) values of alunites are generally +8 to +18‰ and vary systematically with $\delta^{34}S$ values, reflecting variations in

temperature and/or $\text{H}_2\text{S}:\text{SO}_4$ ratios in the fluid; larger variations in $\delta^{18}\text{O}(\text{SO}_4)$ may result if SO_2 condenses in mixed magmatic-meteoric water fluids. Rye et al. (1992) also showed that alunite formed in the magmatic steam environment (a subset of magmatic hydrothermal environment, dominated by a vapor phase of magmatic origin) could usually be distinguished by $\delta^{34}\text{S}$ near $\delta^{34}\text{S}_{\text{ES}}$ values and δD and $\delta^{18}\text{O}(\text{SO}_4)$ values close to magmatic values. The deposition of gold and sulfides occurs later when the magmatic vapor-dominated system collapses and is replaced by a liquid-dominated system with a significant meteoric water component, accompanied by changes in pH and $\text{H}_2\text{S}:\text{H}_2\text{SO}_4$ ratio because of interaction with the wallrocks. The involvement of meteoric water during the gold precipitation stage is consistent with the lower salinity and temperature of ore-forming fluids in alunite-kaolinite type deposits compared with porphyry copper deposits dominated by magmatic hydrothermal systems. Such a two-stage model — an early stage of extreme base leaching and alunite formation under the influence of magmatic volatiles, followed by gold precipitation in high-sulfidation assemblages — has been proposed by Stoffregen (1987) for the Summitville deposit and it may be generally applicable to other acid-sulfate type epithermal gold deposits.

Adularia-sericite (low-sulfidation) type epithermal deposits are interpreted to have formed in the upper few hundred meters of large hydrothermal systems driven by volcanic heat energy but dominated by meteoric water, analogous to such low-sulfur modern geothermal systems as Steamboat Springs (Nevada, USA) and Broadlands (New Zealand) (Hedenquist & Henley 1985a, b). The temperatures and salinities of fluids for adularia-sericite deposits are broadly similar to those for alunite-kaolinite deposits, and gold-rich systems form at shallow depths in both types. As in the case of kaolinite-alunite type deposits, a local intrusion is also likely to have been the heat source in each district of adularia-sericite deposits. No heat source has yet been observed for any of these deposits, but geophysical studies at Creede and Tonopah suggest an intrusion beneath the ore zones. Also, oxygen and hydrogen isotopic data on several epithermal deposits, including the Hishikari deposit (Japan), indicate that the mineralizing fluids involved the mixing of meteoric water with magmatic water (Giggenbach 1992, Matsuhisa & Aoki 1994). The vertical and lateral dimensions of the adularia-sericite deposits are substantially more extensive than those of the kaolinite-alunite type. The large areal dimensions require an extensive lateral fluid flow regime and may result in ore localization being displaced from the proposed heat source at depth.

The differences between the adularia-sericite and alunite-kaolinite types arise primarily because of significant differences in the two hydrothermal systems, including fluid chemistry (Fig. 16.12). The absence of high-sulfidation minerals enargite \pm covellite and the presence of adularia + sericite as the characteristic alteration assemblage indicate higher (near-neutral) pH, more reducing, and lower sulfur activity conditions for the adularia-sericite deposits (Heald et al. 1987). This difference in fluid chemistry may be attributed to a dominance of meteoric water and greater degree of equilibration with host rocks below the depth of ore deposition (Giggenbach 1992, Rye 1993). The equilibration results in CO_2 , H_2S , and NaCl being the principal species in the fluid, although some systems contain water and reactive gases (CO_2 , SO_2 , HCl)

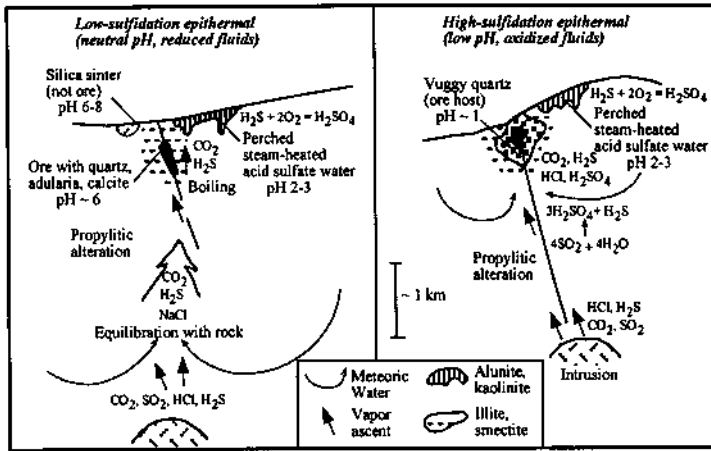


Figure 16.12. Generalized sketches illustrating the difference in the geochemical environments of alunite-kaolinite (high-sulfidation) and adularia-sericite (low-sulfidation) types of epithermal deposits. In low-sulfidation systems, the inferred magmatic input at great depth includes acid gases (CO_2 , SO_2 , HCl), NaCl , and possibly ore metals. Following wallrock interaction and dilution, the fluid at depths of 1-2 km is reduced and of near-neutral pH, and in equilibrium with the host rocks at depth. The boiling fluid rises along permeable zones, depositing gangue and possibly ore minerals, and may discharge from near-neutral pH hot springs. The separated vapor with CO_2 and H_2S condenses in the vadose zone to form steam-heated water, which becomes acidic from oxidation of H_2S . In high-sulfidation systems, magmatic volatiles ascend with little or no modification until they reach the epithermal environment where they become absorbed by meteoric water and form highly acidic solution that leaches the rock outward from the fluid conduit. Ore metals may be introduced into this leached rock by later magmatic-meteoric fluid mixtures. (After White & Hedenquist 1995.)

of magmatic origin (Hedenquist & Lowenstern 1994). Alunite may occur in the adularia-sericite deposits and it is the result of overprinting caused by downward percolation of steam-heated acid-sulfate water. This acid-sulfate water is produced by the atmospheric oxidation of H_2S at or above the water table. The supergene alunite is much younger than the mineralizing event.

In both adularia-sericite and alunite-kaolinite environments, gold is believed to be transported as, and precipitated from, bisulfide complexes. The broad range of lead and zinc contents in both deposit types is consistent with similar solubilities of the chloride complexes of these metals in both environments. The districts higher in base metal contents usually have higher $\text{Ag}:\text{Au}$ ratios and this is compatible with similar mechanisms of transport and deposition of silver and base metals. The relative copper enrichment in alunite-kaolinite deposits is probably due to the stability of $\text{Cu}(\text{HS})_2^-$ complex at high H_2S concentrations in the mineralizing fluids (Barton et al. 1977).

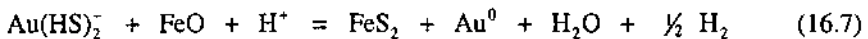
Carlin-type Deposits

Detailed fluid inclusion and stable isotope data are available only for a few Carlin-type

deposits, and the data in all cases clearly indicate the involvement of several fluids in the process of hydrothermal alteration and gold mineralization. The complexity of fluid evolution is best illustrated in the well-studied Jerritt Canyon district where three distinct fluids have been identified (Hofstra et al. 1987, Northrop et al. 1987, Hofstra et al. 1991). The earliest fluid to invade the district was an isotopically heavy ($\delta^{18}\text{O} = +17$ to $+28\text{‰}$), gas-enriched ($\text{CO}_2 + \text{CH}_4$) brine (≈ 10 wt% NaCl equivalent) at 250° - 300°C and 1-5 kb. This fluid, considered to be a product of regional metamorphism during the Antler orogeny, precipitated silica along and adjacent to fractures, forming tabular, often stratiform jasperoid bodies in the incipient ore host. The early silicification event can be traced in most Carlin-type deposits throughout the length of the thrust belts in western United States irrespective of the host rock or age of mineralization.

Data on ore-stage jasperoid, barite, and calcite indicate that two distinctly different fluids were present during ore deposition. One was a gold-bearing, highly evolved meteoric water ($\delta\text{D} \approx -111\text{‰}$, $\delta^{18}\text{O} \approx +5\text{‰}$) containing about 2-4 mole% CO_2 and about 0.1 mole% H_2S . The salinity and temperature of this fluid was on the order of 3-10 wt% NaCl equivalent and 200° - 300°C , respectively. The gold was scavenged from the host sedimentary sequence, an inference consistent with the $\delta^{34}\text{S}$ values of ore-stage sulfides ($+5$ to $+10\text{‰}$), which lie within the range of $\delta^{34}\text{S}$ values for Paleozoic sedimentary sulfides in the region. Speciation calculations show that the gold was transported dominantly as bisulfide complexes and that the solubility of silver and base metals was suppressed by the high H_2S concentration in the fluid. The fluid was probably undersaturated with gold, but became saturated through sulfidation of wallrock iron during migration to the sites of mineralization.

The other fluid was dilute (<1 wt% NaCl equivalent), unexchanged meteoric water ($\delta\text{D} \approx -118\text{‰}$, $\delta^{18}\text{O} \approx -16\text{‰}$) with <0.5 mole% CO_2 and <0.01 mole% H_2S . There is no fluid inclusion evidence of boiling, but strong evidence for mixing of the two fluids during gold deposition is provided by a log-linear correlation between the Au contents (0.03-300 ppm) and $\delta^{18}\text{O}$ values ($+1$ to $+15\text{‰}$) of gold-stage jasperoid. Fluid inclusion data indicate a pressure of 0.5-1.0 kb during gold deposition, corresponding to a depth of about 2.4 km. Chemical reaction-path modeling by Hofstra et al. (1991) suggests that the gold mineralization and associated alteration features of the Jerritt Canyon district may be explained by a "combination of fluid mixing, including simultaneous cooling, dilution, and oxidation of the ore fluid, and wallrock reaction, with sulfidation of reactive iron in the host rock" by reactions such as



Hydrothermal activity continued beyond the main gold mineralization event and was dominated by dilute meteoric water (<0.5 wt% NaCl equivalent, 0.5-1.5 mole% gas consisting mostly of CO_2). Late-stage calcite veins and a widespread halo of ppb-level gold plus As, Sb, and Hg were deposited during the time this meteoric water flooded the

system. It follows from reaction (16.7) that the iron content of the wallrock (e.g., as ferroan dolostone) and decarbonatization processes that liberate this iron are important factors controlling the formation of Carlin-type gold deposits.

According to the genetic model proposed by Radtke (1985) for the Carlin deposit, gold was precipitated by wallrock reaction from a fluid that was weakly acidic and had a salinity of 2-4 wt% NaCl equivalent at temperatures of 175°-200°C. Calculated $\delta^{18}\text{O}$ values of this fluid (-0.2 to +6.5‰) are compatible with a meteoric water origin and considerable exchange with carbonate-rich host rocks. The main episode of ore deposition was terminated by a rise in temperature of the ore fluids to 275°-300°C that resulted in widespread boiling of the fluids and coincided with the formation of barite veins. A similar interpretation, involving the interaction of gold-bearing fluids from an overpressured zone at depth with meteoric water, has been offered recently by Kuehn and Rose (1995). Their fluid inclusion and isotopic data indicate the presence of two fluids during the episode of gold deposition. The main gold ore (MGO)-stage fluid was gas-rich (containing 5-10 mole% CO_2 and appreciable H_2S), had higher salinity (2-4 wt% NaCl equivalent), and was ^{18}O -enriched ($\delta^{18}\text{O} = +6.5$ to $+10\text{‰}$ at 225°C) as a result of considerable exchange with surrounding country rocks, but dominantly of meteoric origin as evidenced by its δD values (-87 to -165‰). At least portions of MGO-stage mineralization were characterized by two-phase boiling (CO_2 exsolution) at $215 \pm 30^\circ\text{C}$ and 800 ± 400 bars. In contrast, the late gold ore (LGO)-stage fluid was gas-poor (containing only minor CO_2 and trace H_2S), relatively cooler (175-250°C?), unevolved meteoric water ($\delta^{18}\text{O} < -4$ to -3‰ , and $\delta\text{D} = -139$ to -149‰) of lower salinity (≤ 1.5 wt% NaCl equivalent). The gas-rich fluid, because of its high H_2S content, was capable of carrying significant amount of dissolved gold, derived from magma or sediments. The CO_2 in the fluid might have come from deep metamorphic fluids, contact metamorphosed carbonates lower in the Paleozoic section, or yet unidentified magmatic sources. Ore deposition appears to have occurred in a zone of throttling at a pressure seal between normally pressured and overpressured regimes, where fluids experienced a transition from near-lithostatic to hydrostatic conditions (Fig. 16.13). Mixing of the two fluids and interaction with host rocks along thin permeable bioclastic horizons are believed to have been the major factors for ore deposition. Fluid inclusion studies show that three fluids of similar salinity (5-8 wt% NaCl equivalent) were involved in the Mercur deposit (Utah, USA) — a 220°-270°C fluid for the early jasperoid-facies rocks, a 150°-190°C fluid for ore-stage mineralization, and a 180°-380°C fluid for the deposition of late-stage hydrothermal barite, but the precise mechanism of gold precipitation is not known (Jewell & Parry 1988).

The large volumes of fluids necessary for the formation of Carlin-type deposits would require a sustained heat source for fluid circulation. An increase in geothermal gradient, either regionally or on a local scale is a possibility (Romberger 1986), but the close spatial and temporal association between Carlin-type deposits and igneous intrusions has led to the speculation that such intrusions created the necessary thermal gradient and may even have contributed magmatic fluid and metals to the mineralizing

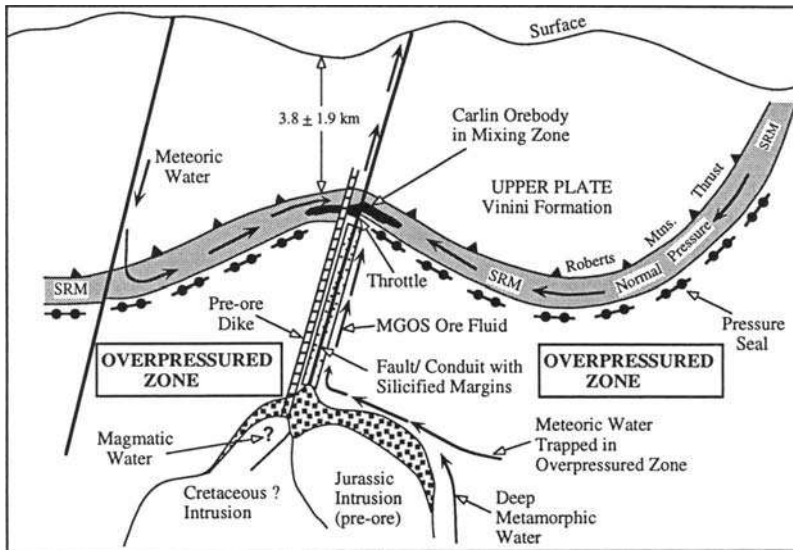


Figure 16.13. Schematic illustration of the genetic model for the formation of the Carlin deposit proposed by Kuehn and Rose (1995). The ore deposition is interpreted to have occurred in a zone of throttling at a pressure seal between normally pressured and overpressured regimes, where fluids experienced a transition from near-lithostatic to hydrostatic conditions, leading to mixing of fluids. Mixing of two fluids and interaction with host rocks along thin permeable bioclastic horizons are believed to have been the main controls of ore deposition. SRM = Silurian Roberts Mountains Formation.

process (Alvarez & Noble 1988, Berger & Henley 1989, Sillitoe & Bonham 1990, Berger & Bagby 1991). A generalized genetic model proposed by Berger and Bagby (1991) envisages the involvement of three distinct fluid types in the formation of Carlin-type ore and wallrock alteration assemblages: magmatic, metalliferous fluids from granodioritic or alkalic magmas that may also form tungsten-bearing skarn deposits and/or molybdenum-bearing stockwork deposits; connate brines entrapped in the marine sedimentary sequences of the imbricate thrust sheets; and deeply circulating meteoric waters. Calculated δD - $\delta^{18}O$ values for fluids, based on fluid inclusions and measurements on associated hydrothermal minerals, indicate that evolved meteoric water was the dominant component in most Carlin-type deposits (Arehart 1996).

Thus, Carlin-type deposits may actually be distal replacement-type deposits related to porphyry-type or skarn-forming magmatic hydrothermal systems (Fig. 16.11) and represent yet another variant of intrusion-related gold deposits. The more distal position of the Carlin-type deposit relative to the base metal sulfide replacement deposit in Fig. 16.11 may be ascribed to progressively increasing dilution of the fluids by meteoric water. In fluids dominated by meteoric water, the salinity becomes too low to permit appreciable base metal complexing, and only Sb, As, and any remaining gold

are capable of further transport as, and eventual deposition from, bisulfide complexes (Sillitoe & Bonham 1990).

Archean Lode Gold Deposits

Following the recognition of a syngenetic exhalative origin for VMS deposits in the late 1960's, which proved to be a highly successful exploration strategy, a similar genetic concept was also proposed for the Archean lode gold deposits. The best candidate for such an analogy was the peneconcordant to stratiform gold mineralization associated with sulfide-rich chemical sedimentary units in greenstone belt sequences (Fripp 1976, Fryer et al. 1979, Fehlberg & Giles 1984, Viljoen 1984, Saager et al. 1987, Siddaiah et al. 1994); structurally controlled vein systems were interpreted as metamorphic remobilization of the exhalative gold (Rye & Rye 1974, Hutchinson & Burlington 1984). Gold enrichment in a variety of rock types by sea-floor hydrothermal activity is well documented (Hannington et al. 1991), but several lines of evidence suggest that this is not a viable genetic model for most Archean lode gold deposits.

Gold-enriched lithologies that have been interpreted as evidence for syngenetic gold precipitation generally fall into two categories: gold-bearing laminated units in volcanic rocks; and gold-bearing iron sulfide-rich units in banded iron-formations. The problem with the gold-bearing laminated units, such as the ankeritic units at the Dome mine (Timmins district, Superior Province, Canada), is that more likely they represent vein systems in shear zones rather than sedimentary units (see discussion in Roberts 1987). For gold-bearing banded iron-formations, there is no dispute regarding the sedimentary character of the host rock and the stratiform deposits may indeed be syngenetic, but a high degree of systematic structural control on gold localization in the non-stratiform deposits suggests epigenetic, not syngenetic, mineralization (Macdonald 1984, Phillips et al. 1984, Bullis et al. 1994). Moreover, Phillips et al. (1984) have documented that gold-bearing sulfides in some BIF are not of sedimentary origin, but represent selective replacement of magnetite. A separate origin of chemical sediments and the associated gold is also indicated by stable isotope ratios and REE data (Wyman et al. 1986). Moreover, the syngenetic model does not account for the timing of lode gold mineralization in Precambrian greenstone belts.

The strong structural control and the consistent correlation with hydrothermal alteration leave little doubt regarding the epigenetic nature of most lode gold deposits. Although the mineralization process is not understood in every detail, the broad picture is fairly clear (Colvine et al. 1988, Groves et al. 1988, Groves & Foster 1991). The flow of Au-bearing fluids was focused along transcrustal faults and shear zones during the late stages of greenstone belt deformation and metamorphism. The channelization of the fluid into shear and fault zones was most likely via mass-transfer processes, such as seismic pumping, which resulted in high fluid:rock ratios along the fluid channels. The gold was transported as bisulfide complexes in low-salinity, relatively high-CO₂, near-neutral to slightly alkaline (due to interaction with dominantly mafic and ultramafic rocks), aqueous fluids and deposited in brittle-ductile and brittle structures in

greenstone belt rocks as concordant and discordant veins, generally under greenschist to amphibolite facies conditions ($\approx 250^{\circ}$ - 500° C, 1-4.5 kb). Local temperature decreases alone were probably not the determining factor for gold precipitation, because vertical mineral zonation and temperature gradients are not a feature of Archean lode gold deposits. Gold deposition occurred primarily through the interaction between ore-forming fluids and wallrocks, either due to destabilization of bisulfide complexes by sulfidation reactions (the favored mechanism in the case of relatively Fe-rich host rocks, such as tholeiitic basalts and BIF) or due to changes in fO_2 , pH, and concentration of reduced sulfur species (particularly applicable to carbonaceous wallrocks). The former is supposed to explain the common association of gold values with Fe-sulfides, but gold is normally paragenetically later than the sulfides. Perhaps the gold was precipitated with arsenopyrite (Cathelineau et al. 1989) and pyrite (Fleet et al. 1989) and redistributed later. An alternative explanation may be the adsorption of aqueous gold-bearing complexes on earlier-formed sulfides followed by autocatalytic reduction of the complex to native gold, a process that might occur even if the fluid was undersaturated with respect to gold (Starling et al. 1989, Knipe et al. 1992). Gold precipitation could have also been caused due to phase separation into H_2O -rich and CO_2 -rich fluids, thus changing the concentration of H^+ , CH_4 , and H_2S in the fluid (Spooner et al. 1987, Sibson et al. 1988).

One of the main, and yet unresolved, controversies pertaining to the origin of lode gold deposits centers on the source of mineralizing fluids (which, in turn, constrains the source of gold). Proposed models are: (a) magmatic hydrothermal fluids derived from syn- to late-tectonic felsic magmas (Hodgson & MacGeehan 1982, Burrows et al. 1986, Cameron & Hattori 1987a) or from late-tectonic lamprophyric magmas (Rock & Groves 1988, Rock et al. 1989, Wyman & Kerrich 1989); (b) metamorphic fluids derived by devolatilization of dominantly volcanic sequences at the base of the greenstone pile (Kerrich & Fryer 1979, Phillips & Groves 1984, Fyfe & Kerrich 1984, Phillips et al. 1986a); and (c) juvenile fluids formed by granulitization of the lower crust and/or degassing of the upper mantle during late Archean cratonization (Colvine et al. 1988, Cameron 1988, Colvine 1989, Fyon et al. 1989, Groves 1993). The relative merits of these models are briefly discussed below; a more comprehensive discussion of the various genetic models has been presented by Kerrich and Cassidy (1994).

Archean lode gold deposits are predominantly mesozonal, emplaced at depths of about 6 to 12 km. Fluid inclusion studies indicate that the mineralizing fluids are characterized by a combination of moderately high temperature (200° - 450° C, generally 250° - 350° C), low salinity (<6 wt% NaCl equivalent, generally <2), moderate density (0.8 - 1.0 g/cm³, generally 0.9), near-neutral to alkaline pH, and relatively high CO_2 content (3-25 mole%, generally 10-15 mole%). The low content of base metal sulfides in the lode gold deposits may be attributed to the limited potential of chloride complexing of base metals in the typically low-salinity fluids. Salinities up to 35 wt% NaCl equivalent, comparable to porphyry Cu-Mo type of mineralization, has been documented (e.g., Sigma mine, Superior Province; Robert & Kelly 1987), but these are from H_2O -rich inclusions produced by phase separation. Schmidt Mumm et al. (1997)

reported very CO₂-rich (CO₂ » H₂O) fluid inclusions in quartz from gold deposits in the Ashanti belt (Ghana) and proposed that such CO₂-rich fluids might represent a distinct category of ore-forming fluids for lode gold deposits, but Klemd (1998) argued that most of the CO₂-rich inclusions were the result of post-trapping deformation-recrystallization processes during retrograde conditions.

The small variation in stable isotope ratios among the many deposits in Superior Province and Yilgarn Block for which data are available suggest that a compositionally uniform fluid was involved in the gold mineralization events regardless of deposit location. The isotope data, however, do not converge to a particular fluid source. Calculated $\delta^{18}\text{O}$ (SMOW) and δD (SMOW) values for the H₂O component of ore fluids are from +2.5 to +10‰ (generally +5 to +8‰) and from 0 to -70‰ (generally -70 to -30‰), respectively. These values exclude a typical seawater or meteoric fluid source, but do not discriminate between magmatic and metamorphic fluid sources. Calculated $\delta^{13}\text{C}$ (PDB) values for CO₂ in the ore fluids (-8 to -3‰, generally -4 to -2‰), which approximate the $\delta^{13}\text{C}$ values of carbonate minerals deposited from the fluids, have been variously interpreted as being compatible with a magmatic source (Burrows et al. 1986, Colvine et al. 1988), with a juvenile source (Cameron 1988), or with metamorphic dissolution of carbonation zones that had formed earlier along regional shear zones by mantle-derived CO₂ (Groves et al. 1988). However, $\delta^{13}\text{C}$ values of this range are difficult to interpret in terms of the carbon source, because mantle CO₂ and average igneous, metamorphic, and sedimentary carbon reservoirs all possess $\delta^{13}\text{C}$ values in this range (Ohmoto & Rye 1979). Kerrich et al. (1987) attributed the $\delta^{13}\text{C}$ range to mixtures of crustal and juvenile carbon, and the geographic variation (isotopic "provinciality") to heterogeneous crustal source rocks. Gold-associated pyrite has a large range of $\delta^{34}\text{S}$ values (-17 to +10‰), but most cluster around 0‰ (-1 to +5‰). Sulfur of this isotopic composition could have been derived from a magmatic source, a juvenile source, or via metamorphic devolatilization or dissolution of sulfur in volcanic terranes such as greenstone belts. The large range of $\delta^{34}\text{S}$ values may be attributed to isotopic partitioning between oxidized and reduced sulfur species in the hydrothermal fluid (Cameron & Hattori 1987b) or extensive fluid-rock interaction (Phillips et al. 1986b, Thode et al. 1991).

A purely magmatic fluid source is not supported by: (a) a lack of systematic relationship between the distribution of felsic plutons of appropriate ages and lode gold deposits in Archean greenstone terranes (Groves et al. 1988; Anglin et al. 1996); and (b) the high CO₂ content and low salinity of the fluids in contrast to typically much lower CO₂ content and higher salinity of magmatic hydrothermal fluids. However, there exists the possibility of a genetic link between gold mineralization and the broadly contemporaneous, late-tectonic alkaline intrusions in greenstone terranes. The youngest recognized Archean intrusions may represent either a high-level expression of more extensive magmatism at depth, which could have exsolved large volumes of fluids, or an expression of magmatism produced before or during the processes that also generated hydrothermal fluids (Rock & Groves 1988, Colvine 1989).

Several aspects of the ore-forming fluids, including compatible $\delta^{18}\text{O}$, δD , and

$\delta^{13}\text{C}$ values, are in accord with their derivation by dehydration reactions during prograde metamorphism of greenstone volcanic sequences. According to computations by Fyfe and Kerrich (1984), enough fluids — on the order of 0.5 km^3 of fluids per 10 km^3 of rock — would be generated across major metamorphic facies boundaries to account for the volumes of quartz gangue and gold transport if precipitation was efficient. The fluids would be CO_2 -bearing and of low salinity ($\text{H}_2\text{O} > \text{CO}_2 \gg \text{Cl}$). One problem with this model is that in many cases the mineralization apparently postdates the peak metamorphism (e.g., Val d'Or, Canada; Anglin et al. 1996); another is that it does not predict the potassic nature of the alteration assemblages (Witt et al. 1997). Moreover, the occurrence of gold deposits in granulite-facies rocks cogenetic with greenschist-facies gold mineralization cannot be reconciled with high-level sources, such as greenschist-amphibolite devolatilization, as the sole origin of mineralizing fluids (Barnicoat et al. 1991). In fact, a lower crustal component in the ore fluids is mandated by strontium, lead, and neodymium isotopic data. Gold-associated scheelite from the Val d'Or area has a depleted mantle-like ϵ_{Nd} (2.5) (Anglin et al. 1996). As documented by Kerrich et al. (1987), $^{87}\text{Sr}/^{86}\text{Sr}$ initial ratios (0.7010-0.7041) of altered rocks in fault zones related to gold mineralization in the Abitibi belt point to a sialic basement fluid source that was isotopically heterogeneous and more radiogenic than both the upper mantle at 2690 Ma (0.700 ± 0.001) and contemporaneous volcanic rocks of mafic to ultramafic composition (0.700-0.7012). Similar high strontium initial ratios (0.7014-0.7043) in the Yilgarn Block has also been interpreted to imply a lower crustal felsic source region for the ore fluid (Ho et al. 1992). Lead isotopic ratios of galenas from some deposits in greenstone terranes (Franklin et al. 1983, Browning et al. 1987) are also more radiogenic than those of the contemporary mantle and confirm the isotopic provinciality of the ore fluid. Fyfe and Kerrich (1985) and Kerrich (1989) proposed a tectonic-controlled metamorphic devolatilization model to account for the timing of gold mineralization as well as the isotopic ratios. The essence of this model is that the dehydration was induced by slowly rising isotherms through the cool, tectonically thickened crust in a collisional plate-tectonic regime during stalled subduction or during the transition to oblique subduction.

Figure 16.14 is a diagrammatic representation of the *cratonization model* for the genesis of Archean lode gold deposits as conceptualized by Colvine et al. (1988) and further elaborated by Fyon et al. (1989). The gold mineralization is considered to be an integral part of the cratonization of the Archean crust that involved crustal thickening by diapiric rise of magma from the upper mantle and the granulitization of the lower crust as a result of the introduction of magma, heat, and volatiles (principally CO_2). CO_2 -enriched, auriferous fluids were generated in the upper mantle and lower crust and channeled to the upper crust through craton-scale faults and shear zones. The CO_2 streaming was not only responsible for the dehydration of amphibolite facies rocks to granulite (Newton et al. 1980) but also for the transport of gold (Fyon et al. 1983). Streaming of CO_2 vapor at the P - T conditions of the lower crust would require an $f\text{O}_2$ above that of the faylite-magnetite-quartz buffer (Lamb & Valley 1984), and a high $f\text{O}_2$ would favor the solubility of gold. Two principal lines of evidence have been cited in

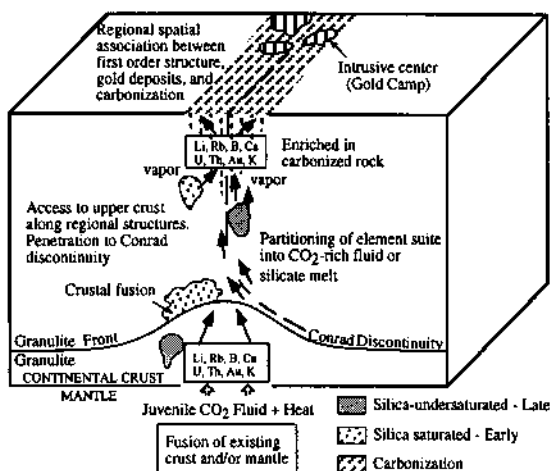


Figure 16.14. Schematic representation of the granulitization model for the genesis of Archean lode gold deposits (modified from Colvine et al. 1988). The top surface represents an erosional level, as observed presently. Crustal cratonization culminates with the addition of mafic magma to the base of and into existing lower crust. Crustal thickening is accomplished in part by the addition of diapiric mass to the base of the crust, which grows downward to form a sub-continental keel. Granulitization of the lower crust results from the introduction of magma, heat and volatiles, principally CO_2 . Silicate magmas, ranging in composition from silica-saturated to silica-undersaturated, are generated by partial melting of upper mantle and lower crust, in the presence of fluids of varying CO_2 : H_2O ratios. Fluids may originate by exsolution from silicate magmas anywhere between the upper mantle and upper crust and evolve compositionally as a result of reaction with rock (granulitization) and immiscible separation. Chemical mass transfer from the mantle, lower and middle crust to the upper crust is effected by silicate magma and fluids, which migrate along zones of crustal weakness (deep regional structures). Gold concentration in the upper crust is a consequence of this late crustal magmatic, tectonic, and thermal history.

favor of the linkage of granulitization with gold mineralization: (a) the deposits are characteristically enriched in large-ion lithophile (LIL) elements (such as K, Rb, etc.), with complementary depletion of these elements in granulites (Cameron 1989); and (b) calculated $\delta^{13}\text{C}$ values of hydrothermal fluids carrying Au and LIL elements, which average -4% , are believed to be the signature of mantle-derived juvenile CO_2 (-6 to $+2\%$) that caused the granulitization and concomitant LIL depletion in the lower crust (see discussion by Cameron 1988).

The validity of the model has been challenged by Kerrich (1989) on several grounds: (a) the $\delta^{13}\text{C}$ data are compatible with a mantle origin of the CO_2 , but do not prove such an origin; (b) the LIL element ratios of the gold-related silicate alteration zones are not complementary to real or apparent LIL element depletion pattern in granulites; and (c) the CO_2 : H_2O ratios of the mineralizing fluids, as evidenced by fluid inclusion data, are lower than ratios typical of granulite facies (see Ch. 3). However, as the late Archean (3.0-2.5 Ga) is believed to be the major period of crustal growth and stabilization and granulite formation, the model does offer a reasonable explanation for

the timing of Archean gold mineralization (Cameron 1988). More specifically, the model is consistent with the time-frame (2710-2670 Ma) of north to south diachronous accretionary assembly of the Superior Province and with the late kinematic timing of lode gold deposits in the Yilgarn Block (\approx 2600 Ma). Evidence that granulitic crust may underlie much of the Superior Province raises the question as to why gold deposits are restricted to volcanic-plutonic subprovinces if the granulitization was so widespread. According to Card et al. (1989), the answer probably lies in the depth of emplacement of the gold mineralization versus the subsequent differential uplift. A consideration of the metamorphic record indicates metamorphic depths of 15-20 km for the central parts of metasedimentary subprovinces, whereas the burial depths in the volcano-plutonic terranes probably never exceeded 10 km. Present-day juxtaposition of such different crustal levels attests to substantial differences in syn- or post-metamorphic uplift that may also account for the difference in the occurrence of lode gold deposits between adjacent terranes.

Considering that the Archean lode gold deposits formed under a range of crustal regimes (sub-greenschist to lower granulite facies) and that the isotopic data are compatible with multiple fluid sources, a more realistic genetic model may be the *crustal continuum model* proposed by Groves and his coworkers and summarized in Groves (1993) and Gebre-Mariam et al. (1995). This model, partly based on those of Colvine et al. (1988), Foster (1989), and Barnicoat et al. (1991), envisages the existence of giant, late Archean hydrothermal systems with various potential sources of fluids and solutes at different crustal levels (Fig. 16.15). The potential sources include basal portions of greenstone belt sequences (metamorphic devolatilization), deep-level intrusive granitoids (magmatic hydrothermal fluid), lower crust and upper mantle (degassing), and even subducted lithosphere. The model is consistent with the ages of gold mineralization linked to accretionary tectonics in the Superior Province and the Yilgarn Block. It even allows for the mixing of meteoric water or seawater in lower- or sub-greenschist facies settings at upper crustal levels, as has been found to be the case with shallow-level lode deposits in the Yilgarn Block (Hagemann et al. 1994) and has also been emphasized by Nesbitt and Muehlenbachs (1989b) for mesothermal lode gold deposits in the North American cordillera. A problem with the crustal continuum model is the timing of peak metamorphic event at different levels of the crust, for example, a 2600 Ma age for peak metamorphism in high-grade domains and a 2630 Ma age for greenschist lode gold mineralization in southern Kalgoorlie and Norseman terranes (Witt et al. 1997). The earlier timing of peak metamorphic event at upper crustal levels (greenschist facies domains) relative to deeper crustal levels (amphibolite and granulite facies domains) may have resulted from crustal thickening due to thrusting, but medium- to high-pressure metamorphic assemblages that might be expected in an overthrust terrane have not been observed (Groves 1993).

A *synmetamorphic lateral flow model* proposed by Witt et al. (1997) attempts to address this shortcoming, at least for the deposits in the Kalgoorlie and Norseman terranes (Yilgarn Block, Western Australia). Their model envisages a two-step process, the first driven by dominantly vertical temperature gradients, as is postulated for the

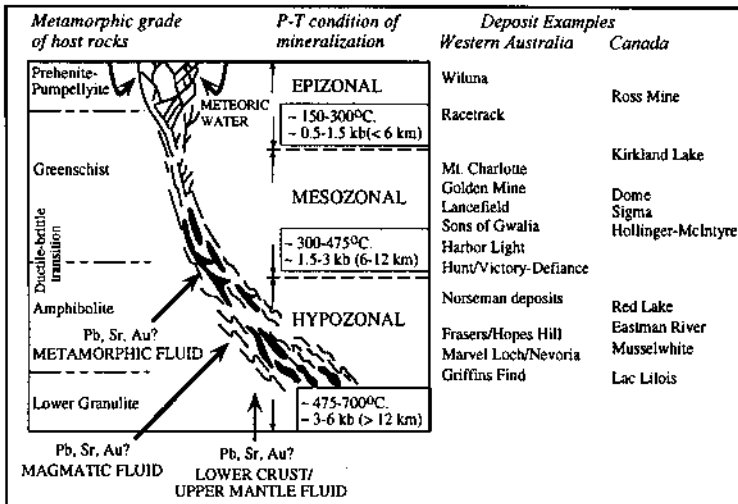


Figure 16.15. Schematic illustration of the crustal continuum of Archean lode gold deposits (after Groves 1993, Hagemann et al. 1994, and Gere-Mariam et al. 1995). The continuous section is a composite of deposits in a number of discrete areas that represent specific sections of vertical profile; continuous mineralization from granulite facies terrains to prehnite-pumpellyite facies terrains has not been observed in any single greenstone belt. Note the various potential sources for fluids and radiogenic isotopes.

cratonization and crustal continuum models discussed above, and the second by dominantly lateral temperature gradients induced by differential uplift at the margins of the greenstone terranes accompanied by granitic intrusions. The first step involved the ascent of CO_2 -bearing, low-K fluids from the lower part of the greenstone pile, the deep crust, or mantle regions via regional shear zones during the early stages of regional metamorphism and the dispersion of these fluids through the greenstone sequence via smaller scale structures. The gold mineralization occurred from a small number of large hydrothermal systems during the later stages of regional metamorphism due to lateral flow of fluids derived by devolatilization reactions at or near the transition from greenschist to amphibolite facies conditions. However, the model, like other synmetamorphic models, does not account for lode gold deposits such as those of the Val d'Or camp (Canada), if the gold mineralization in this area was indeed emplaced 60 m.y. later than peak regional metamorphism as claimed by Anglin et al. (1996).

16.6. Metallogensis

16.6.1. HOST ROCKS

Host rocks and lithologic successions of gold deposits, except for the Witwatersrand-

type and young placer deposits, are quite varied. For example, the host rocks for lode gold deposits include tholeiitic and komatiitic basalts, fragmental pyroclastics, felsic plutons, turbiditic greywackes, carbonaceous and sulfidic sediments, and iron formations. A genetic link between the host rock and hydrothermal gold mineralization is extremely likely in the case of intrusion-related deposits, but in all other types of hydrothermal gold deposits ore localization appears to have been controlled primarily by a favorable combination of factors, such as a large fluid and solute source, focused fluid flow, fracture permeability for fluid circulation, and the availability of dilational zones for ore deposition. The relative competency of the host rocks were important in the orientation and distribution of ore-gangue veins and their composition determined the hydrothermal alteration and metamorphic assemblages, and may even have played a role in the gold precipitation, but the host rock was not the determining factor in ore localization in most cases.

16.6.2. SOURCES OF GOLD

As discussed earlier (Ch. 14), there is considerable uncertainty regarding the precise source of the gold for placer deposits. The problem is worse for the hydrothermal gold deposits because of diverse geologic settings and indications of multiple fluid sources.

Crustal sources are not intrinsically enriched in gold. The average gold contents of crustal rocks vary from a low of about 1 ppb in slates and argillites to a high of 6-8 ppb in ultramafic rocks and hornfels (Romberger 1988). It is, of course, possible that rocks richer in gold were encountered in the flow path of mineralizing solutions. For example, Viljoen et al. (1970) suggested that mafic and ultramafic rocks in Archean greenstone belts were anomalously high in gold, but there appears to be no detectable difference between the gold content of mineralized and unmineralized rocks (Anhaeusser et al. 1975). The potential of Archean volcanic sequences as source rocks was more likely linked to some process of enhanced concentration, such as the preferential partitioning of gold into immiscible sulfide phases or trapping of the gold released from sea-floor alteration of komatiitic basalts in sulfidic interflow sediments and exhalites, and later mobilization of the gold by hydrothermal fluids (Saager et al. 1982, Viljoen 1984, Keays 1987, Hutchinson 1993). Rocks with high gold content would certainly be a more favorable source, and the non-availability of such source rocks might explain in part the spatial and temporal distribution of gold deposits. However, given the constraint of gold solubility, which requires the involvement of a very large volume of fluid for any significant gold mineralization, and enough permeability for fluid circulation, even rocks with average gold concentration could have served as a viable source of gold, but this is difficult to document. For example, a deposit containing 10^6 ounces of gold could be formed by removing only 1 ppb of gold from 10 km^3 of rock, and such a depletion would be very difficult to detect using present analytical methods, even if the original gold content was known precisely enough to consider a difference of 1 ppb gold as significant. Factors such as leachability of gold and permeability created by shearing were probably more important than the gold contents of source rocks.

As discussed earlier, the formation of most types of hydrothermal gold deposits appears to have involved some contribution of fluids from felsic magmas, especially I-type granitoids and felsic porphyries (Sillitoe 1991), but their role as source of gold is neither apparent nor proven in any instance. Initial gold contents of silicic volcanic rocks, irrespective of geographic location, are generally in the range of 0.1 to 1.0 ppb, but these values should be considered only as minimum limits on magmatic gold concentration (Connors et al. 1993). Gold is removed from magma by the separation of vapor, crystalline, and immiscible melt phases, as is evidenced by gold in volcanic emissions during noneruptive magmatic degassing (Meeker et al. 1991) and by the concentration of gold, along with many other metals, in fumarolic incrustations (Papike et al. 1991). The existence of felsic magmas with elevated gold contents is also suggested by the fact that many gold-rich porphyry copper deposits, which are associated with high-level stocks of silicic and intermediate composition, contain from 0.3 to >1 ppm gold (Cox & Singer 1992). Solomon (1990) suggested that the porphyry copper-gold mineralization in the island arcs of the Pacific rim was not only broadly restricted to subduction but was also dependent on arc reversal. This is because in arc-reversal systems melting must commonly involve a modified, previously partially-melted mantle, which according to Hamlyn et al. (1985) should contain immiscible sulfide moderately enriched in gold (and PGE). Lode gold deposits in Archean greenstone belts are not genetically related to felsic intrusions. For this type of gold mineralization, much of the gold may have been scoured from the lower crust as a consequence of granulite facies metamorphism (Colvine et al. 1988, Cameron 1988, 1989) or from the mantle through lamprophyric magmatism with which the gold mineralization is commonly coeval as well as cospatial (Rock & Groves 1988). Rock and Groves (1988) hypothesized that the lamprophyres, which they claimed to be particularly gold-enriched, were the transporting agents for gold from gold-rich sources in the deep mantle (or even the core), which then underwent extensive crustal interactions, generating Au-enriched felsic magmas or releasing their gold into metamorphic-hydrothermal systems. However, Wyman and Kerrich (1989) did not find the lamprophyres to be particularly gold-enriched and considered the association between lamprophyres and gold deposits to reflect merely emplacement of both in a similar tectonic environment.

Titley (1991) has cautioned against ignoring sediments as the possible source of gold for Phanerozoic sediment-hosted ores. His argument is that ages of marine sediments hosting such gold deposits correlate well with time intervals when the oceans were reducing. Thus, these sediments could have been relatively enriched in gold, either by accumulation of detrital gold particles or by precipitation from ocean water, and become viable metallotects of gold.

In summary, the source of gold for any particular deposit or class of deposits is largely an unresolved question. Possible sources in any given case can be somewhat constrained by viable genetic models, but only within broad limits. The task becomes immensely more complicated when the consideration is expanded to encompass the abundances and ratios of other characteristic elements associated with gold mineralization and hydrothermal alteration.

16.6.3. AGE DISTRIBUTION AND PALEOTECTONIC SETTINGS

Gold mineralization on some scale has occurred over the entire span of geologic time, but with varying intensity and noticeable gaps (Fig. 16.16). Two distinct metallogenic intervals are apparent. The first is the Precambrian, which contains two very different types of gold deposits: lode deposits in Archean greenstone belts, and paleoplacer deposits of the Witwatersrand type. The Archean was a major interval of gold metallogeny, unparalleled, if not unique, in geologic time. The second interval, consisting of a variety of volcanic- and sediment-hosted deposits, started in late Mesozoic and is continuing to the present. The cause of this 2000 million years gap between the two peaks is not known.

Our understanding of the Archean lode gold deposits is limited by the uncertainties in the interpretation of the tectonic setting(s) of the Archean greenstone terranes (see Ch. 6). The geologic settings of the Archean lode gold deposits best fit an accretionary convergent plate-tectonic regime, although the details vary from one craton to another. The common occurrence of gold mineralization postdating peak metamorphism probably reflects a lag in thermal relaxation during collisional processes, with peak metamorphism at depths of 60 km postdating peak metamorphism at shallow (≈ 10 km) depths by as much as 40 million years (Kerrick 1993). Lode gold deposits are much better developed in the younger, late Archean (< 2.9 Ga) greenstone belts than in the older, early Archean greenstone belts. The reason for this difference is not entirely clear. It is well established that the gold mineralization in the Canadian and West

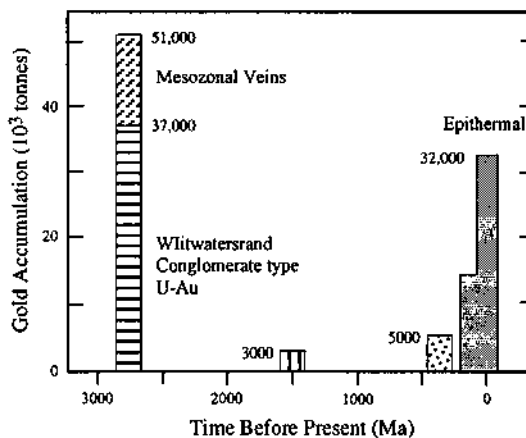


Figure 16.16. Age distribution of gold deposits (after Woodall 1988). The overall pattern is real, but considerable uncertainties exist in the data for both tonnage and age of mineralization.

Australian shields was broadly contemporaneous with the latest regional tectonometamorphic event. Based on the present data base, the best explanation for the preferential concentration of gold deposits in the late Archean greenstone belts is the temporal linkage between structurally controlled gold mineralization in the upper crust and tectonic activity in the lower crust, manifested as granulitization and magma generation, that led to the generation of gold-bearing hydrothermal fluids (Colvine 1989). Although some early orogenic events occurred at ≈ 3.0 Ga and 2.8 Ga, the major deformation and metamorphism in the Superior Province accompanied subduction-related accretion of crustal fragments during the late Archean Kenoran orogeny at ≈ 2.7 Ga (see Ch. 6). The deformation resulting from the compressional tectonics was characteristically ductile and extensive in early stages, but became more brittle and localized with time, culminating in late shearing and faulting. Most gold districts in the Superior Province have experienced a progressive transpressional deformation, probably resulting from oblique subduction or collision, from early coaxial shortening to late dextral transcurrent shearing, and individual deposits typically contain gold-quartz veins that can be related to both of these stages. The late stages of deformation were accompanied by the deposition of Timiskaming-type sequences in pull-apart basins formed by strike-slip movements on major faults (Poulsen et al. 1992). The major shear zones ("breaks") produced by transpressive deformation provided conduits for gold-bearing hydrothermal fluids from deeper sources and the Timiskaming-type sequences became the hosts for structurally-controlled gold mineralization.

Gold mineralization in the Norseman-Wiluna Belt (Yilgarn Block) was related to oblique closure of a volcanic arc and marginal basin in a convergent margin orogen (Groves & Foster 1991). This interpretation is consistent with the structural style in the arc-facies rocks of the belt — such as a regional network of oblique-slip shear zones, and faults and folds with a dominant oblique- or strike-slip movement — indicative of oblique crustal shortening. Mineralization in older greenstone sequences in adjacent provinces of the Yilgarn Block is of similar age and the host structures developed probably in response to the oblique closure (see Ch. 6). The late Archean gold mineralization in Zimbabwe has been linked temporally to the major tectonothermal events that immediately preceded and accompanied the onset of cratonization (Foster 1989). However, it is difficult to formulate a precise and widely applicable tectonothermal framework for the gold mineralization in Africa because of the apparently diachronous nature of cratonization, ranging from about 3.0 Ga in the southern Kaapvaal craton to about 2.6-2.5 Ga in Zimbabwe and 2.0 Ga in West Africa. Moreover, unlike the major cratons of Canada and Western Australia, where the gold mineralization is exclusively related to the late Archean cratonization events, some gold-related hydrothermal events in Africa appear to have continued in areas marginal to the stabilized cratons beyond the cratonization events. Nevertheless, in a general sense, the Archean-Proterozoic boundary (ca. 2.7-2.0) provided an important, global-scale, thermal and tectonic window in the Earth's evolution during which tectonism, fluid mobilization, and mantle heat flow provided optimum conditions for the formation of lode gold deposits, possibly in accretionary tectonic settings. The general Archean-

Proterozoic boundary in Africa remains a major focus of gold metallogenesis and exploration, as in other Precambrian shields (Foster & Piper 1993).

Next to appear in the geologic record are the paleoplacer deposits of the Witwatersrand basin, which is late Archean in absolute age but early Proterozoic in tectonic style. It is noteworthy that paleoplacers older and younger than those of the Witwatersrand are known around the world, but they do not carry any significant gold mineralization (Hutchinson 1987). The uniqueness of the Witwatersrand deposits, all hosted by conglomerates of approximately the same age (2.8-2.5 Ga), is an unresolved question (see Ch. 14). The abundance of young placer deposits rules out the essentially anoxic atmosphere during the Archean as the determining factor. Hutchinson (1987) proposed that a possible explanation might lie in the fact that, of the paleoplacer successions, only the Witwatersrand contains thick tholeiitic basalts (a large part of the 8,000-ft thick Dominion Group) that are petrochemically similar to those associated with Archean lode gold deposits. Basaltic rocks are a viable potential source of hydrothermal gold (although they were perhaps not a major contributor to the Archean lode gold deposits), but there is no documented evidence that the Dominion Group basalts were the source of the Witwatersrand gold.

The "eugeosynclinal" turbidite-hosted gold deposits of upper Proterozoic and Paleozoic age have many similarities with Archean lode gold deposits, but lack the association with thick tholeiitic and high-Mg basalts and felsic igneous rocks so distinctive of the latter. This deposit type may represent a younger, evolutionary metallogenic variant of the older greenstone-hosted type, related to continental-margin plate tectonic mechanisms initiated in late Precambrian time (Hutchinson 1987).

The Carlin-type and mesothermal lode deposits (as well as gold-bearing porphyry copper deposits) of the North American Cordillera range in age from ≈ 90 to ≈ 17 Ma and can be linked to particular stages of the complex plate-tectonic evolution of the Cordillera (Berger & Henley 1989, Berger & Bonham 1990). Mesozoic and Cenozoic igneous activity along the western margin of North America comprised subduction-related magmatic arcs of calc-alkaline affinity. The majority of the epithermal deposits were emplaced in the back-arc region, where more potassic and silicic magmatic activity occurred within areas of extensional faulting. By mid-Jurassic time, the western margin of North America had become an Andean-type plate margin and a volcanic arc of typical basaltic to andesitic-dacitic composition extended continuously from Canada through the western United States to northern Mexico. Some epithermal mining districts in British Columbia, Nevada, and Arizona resulted from this magmatic activity. The magmatic arc is represented today by the calc-alkaline batholiths of British Columbia, Idaho, the Sierra Nevada, and Southern California-Sonora. After continued accretion of the arc until the end of the Cretaceous, a change in the direction of plate motion caused changes in the convergence rate, and the arc became discontinuous. Two segments of the arc, one in northwestern Mexico and the other in the Pacific northwest of USA, remained active and their migration during the period from Paleocene to early Miocene resulted in their convergence. Except for an apparent gap in southeastern California, a continuous volcanic arc was established once again at the western margin of North

America. The continuity of the arc system was maintained from 21 to 17 Ma. Around 17 Ma, the Tertiary subduction ceased along a portion of the North American plate and the arc separated into two segments due to the development of the Pacific plate-North American plate transform margin (San Andreas fault), and this configuration has been maintained to the present. From about 17 Ma onward, the extensional faulting to the east of the transform margin and the contemporaneous inception of the Basin and Range physiographic province was accompanied largely by bimodal basalt-rhyolite volcanism.

The numerous post-Laramide epithermal deposits in the Cordillera are related to back-arc volcanism (primarily continental andesite-rhyolite suites) during this sweep of volcanic activity from the north and from the south. Cenozoic epithermal systems were also operative in accreted terranes east of the San Andreas transform fault. Of particular importance during these intervals of back-arc volcanism were deep-seated extensional fault zones and rifts, some reactivated from earlier periods of tectonism, that provided access to deep sources of magma, gases, and metals. The productive districts, such as those in Nevada and Colorado, were the sites where extensional faulting, volcanic activity, and magmatic underplating of the crust prevailed for much of the Tertiary. Adularia-sericite type systems, which seem to occur in association with both calc-alkaline andesite-rhyodacite and basalt-rhyolite sequences, are common throughout the western Cordillera. In contrast, alunite-kaolinite type systems appear to be associated with dacitic to rhyodacitic magmas and more restricted in time and space. Both types of hydrothermal systems involved large quantities of meteoric water and active tectonism during ore deposition.

The sediment-hosted Carlin-type deposits of the western Cordillera were emplaced also along deep-seated extensional fault zones, but in the regional overthrust belts and at deeper levels. Although not located at magmatic centers, these deposits appear to be linked to some type of igneous activity. The repeated continental-margin orogenic events of the Paleozoic and Mesozoic resulted in crustal thickening through imbricated thrust sheets and the gold mineralization was emplaced in the sediments of thrust slices from a hydrothermal system fed by meteoric water, connate water entrapped within the marine sedimentary rock sequences, and magmatic fluids from shallow plutons and magma underplating the crust (Berger & Bonham 1990).

On a regional scale, the emplacement of mesothermal lode gold deposits of the Cordillera, such as those of Juneau (Alaska) and Mother Lode (California), was controlled by regional-scale, deep-seated right-lateral strike-slip faults (Nesbitt 1991). Although the main strike-slip fault itself may be mineralized, the mineralization generally is localized in subsidiary faults related to the main structures and is believed to have been dominated by meteoric hydrothermal system.

The intrusion-related and epithermal gold deposits of the western Pacific gold province, extending from Japan to New Zealand, are integral parts of at least 10 volcanic-plutonic arcs, which were constructed by I-type, magnetite-series magmas during or immediately following episodes of subduction of the Pacific and marginal basin lithosphere (Sillitoe 1989). Extension affected all or parts of several arcs at the time of gold mineralization and led to the generation of weakly bimodal magmatic

suites or, in the case of more advanced extension in back-arc settings, alkalic suites. The deposits were emplaced during the last 25 million years at depths of about 3 km.

The formation and preservation of large numbers of productive gold placers along the Pacific margins during Cenozoic time, particularly in the Tertiary period, is indeed remarkable. The Cenozoic was marked by extensive regional uplift and generally hot and humid climate over much of the world, conditions that were favorable for rapid weathering. According to Boyle (1979), a possible explanation for their preservation may lie in the fact that nearly all Tertiary and younger placers are hosted by first, or locally second, generation sediments, so that the gold has not been cominuted and dispersed by repeated cycling of the sediments.

16.7. Summary

A small amount of the present world gold production is a byproduct of porphyry copper and VMS ores; the rest comes from deposits mined primarily for their gold (and silver) contents. Such deposits belong to one of the following seven broad categories: (a) young placer deposits; (b) deposits hosted by quartz-pebble conglomerates (Witwatersrand-type); (c) volcanic-hosted epithermal deposits; (d) sediment-hosted, disseminated deposits (Carlin-type); (e) iron-formation-hosted stratiform and non-stratiform deposits; (f) intrusion-related deposits; and (g) lode deposits.

Deposits hosted by quartz-pebble conglomerates have been the leading producer of gold since a long time and virtually all of it is accounted for by the late Archean quartz-pebble conglomerates of the Witwatersrand Basin (South Africa). Gold mineralization occurs in the native state in the conglomerate matrix and, along with the associated uraninite, is believed to be dominantly detrital, although the paleoplacer model allows for solution transport and chemical precipitation of gold on a local scale. The provenance of the gold (and uranium) remains an unresolved question. Young (mostly Tertiary) placer deposits, the main target of the 'gold rushes' in the middle and late 19th Century, have contributed about one-fourth of the world's gold production, but are not major contributors at present.

The other types of gold deposits are epigenetic and hydrothermal in origin, ranging from mesothermal to epithermal in terms of P - T conditions of emplacement. They are hosted by a variety of rock types (volcanics, dolerite dikes, felsic plutons, sediments) and typically exhibit distinctive coeval hydrothermal alteration. All appear to have been emplaced at convergent plate boundaries and in some way linked to igneous intrusions, although the magmatic connection varies from obvious spatial association to inference based on characteristics of mineralizing fluids. Other differences among the different types of hydrothermal gold deposits lie in their age distribution, regional and local structural setting, structural control on mineralization, abundance of base metal sulfides, hydrothermal alteration assemblages, element association, and the relative importance of magmatic versus meteoric fluids (Table 16.6).

Intrusion-related deposits mostly contain less than 100 tonnes of gold and are

TABLE 16.6. Comparison of general characteristics of principal types of hydrothermal gold deposits

Characteristic	Archean Lode	Mesothermal Lode	Epithermal	Carlin-type
<i>Age of mineralization</i>	Archean (> 2500 Ma)	Mainly late Jurassic to Tertiary	Late Jurassic to Tertiary	Tertiary (perhaps no younger than Miocene)
<i>Host rocks</i>	Mafic to felsic volcanics, komatiites, dolerites, felsic intrusions (minor), clastic and chemical sedimentary units	Mafic to felsic volcanics and plutons, serpentinites, clastic to carbonate sedimentary units	Mafic to felsic volcanics, especially andesitic volcanic and pyroclastic rocks	Marine sedimentary rocks of varied lithology; most favorable are carbonate-bearing siltstones and shales
<i>Metamorphism</i>	Subgreenschist to granulite facies, mostly greenschist to lower amphibolite	Typically subgreenschist to upper greenschist facies	Unmetamorphosed to zeolite facies	Unmetamorphosed
<i>Structural setting</i>				
<i>Regional</i>	Major, crustal-scale, oblique-slip fault systems and shear zones	Major transcurrent fault systems	Calderas, volcanic centers, high-level plutons	Regional extensional zones
<i>Deposit scale</i>	Subsidiary normal to reverse faults; brittle, brittle-ductile, and ductile shear zones	Normal to reverse faults	Faults, tensional fractures, hydrothermal breccias	Normal faults, fault-generated breccias, and fractures
<i>Ores</i>				
<i>Style of mineralization</i>	Disseminations in shear zones, massive to laminated veins, quartz-vein sets, stockworks, strata-bound lenses (replacements)	Massive to laminated veins, strata-bound lenses (replacements), occasional stockworks and disseminations	Vein fillings with crustification banding, stockworks, replacements	Disseminations, veinlets
<i>Mineralogy</i>	Native gold \pm electrum, Fe-sulfide \pm arsenopyrite \pm stibnite \pm scheelite; minor base metal sulfides	Native gold, Fe-sulfides \pm scheelite \pm arsenopyrite; minor base metal sulfides and tellurides	Native gold, electrum, native silver, acanthite, Fe-sulfides, arsenopyrite, stibnite, cinnabar, sulfosals, significant base metal sulfides \pm tellurides	Native gold (very fine grained), Fe-sulfides, stibnite arsenopyrite, bante cinnabar, fluorite; sulfosals, Ti-minerals; very minor base metal sulfides
<i>Au:Ag ratio</i>	Au > Ag; ratio varies from 3:1 to 20:1, average ~ 9:1	1 to 10, typically > 1	Highly variable (20:1 to 1:100), typically < 1	Typically Au > Ag, ratio varies from 9:1 to 30:1, a few have Au < Ag

TABLE 16.6 (continued)

Characteristic	Archean Lode	Mesothermal Lode	Epithermal	Carlin-type
Au grade	Highly variable, mostly 0.1-0.2 oz/t	Typically 0.1-0.8 oz/t	Highly variable, bonanza orebodies containing up to about 6 oz/t Au have been reported	Typically 0.1-0.35 oz/t
Hydrothermal alteration	Fe-sulfide-K-mica-albite-carbonate minerals, silicification, chloritization, biotitization; lateral zonation	Fe-sulfide-K-mica-albite, carbonate minerals, silicification, chloritization	Argillic to advanced argillic, silicification, sericitization, propylitic; vertical \pm lateral zonation	Silicification, decarbonatization, sericitization, argillic
<i>Mineralizing fluids</i>				
Fluid Salinity (wt % NaCl equivalent)	Low; < 6 (generally < 2)	Low; < 5	Low; 0-4	Low; 0-8
CO ₂ content (mol %)	High; 3-25 (generally 10-15)	High; generally > 4	Low; < 4	Variable; 2-10
pH	Near neutral (to slightly alkaline)	Near neutral	Acidic to alkaline	Slightly to highly acidic
Fluid type	Metamorphic \pm magmatic (\pm meteoric)	Metamorphic \pm meteoric	Meteoric + magmatic	Magmatic + connate + meteoric
<i>Depositional conditions</i>				
Temperature (°C)	200-450 (generally 250-350)	200-350	100-350	200-300
Fluid pressure (kb)	1-2	> 0.2	< 0.2	0.7-1.6
Emplacement depth (km)	< 5 to 10	> 2	0.1 - 0.3	2-4
Plate tectonic setting	Convergent margins	Convergent margins	Back-arc and island-arc	Overthrust belts related to continental margin tectonics

Sources of data: Hutchinson (1987), Barley et al. (1989), Nesbitt (1991), Henley (1991), Groves and Foster (1991), Hagemann et al. (1994).

particularly abundant in the island-arc belt of the western Pacific. These are essentially extensions of porphyry copper systems and encompass a variety of mineralization styles, ranging from porphyry- and non-porphyry-type stockwork and disseminated mineralization to replacement and skarn-type mineralization. Magmas were a major source of fluids and solutes for the intrusion-related deposits, with convecting meteoric water and gold from country rocks becoming generally more important at increasing distances from the intrusion.

Epithermal deposits, including the so-called bonanza ore shoots, are typically hosted by early to late Tertiary, subaerial calc-alkaline volcanic piles and particularly well developed in the Basin and Range province of western United States and in the western Pacific island arcs. They are characterized by either adularia-sericite (low-sulfur) or alunite-kaolinite-energite (high-sulfur) hydrothermal assemblages. Deposits of the alunite-kaolinite (acid-sulfate) subtype are interpreted to have formed in the upper levels of porphyry-type mineralization systems, involving both buoyant magmatic fluids and convecting groundwater. The adularia-sericite subtype, which has yielded most of the epithermal gold production, represent ancient analogs of gold concentration in modern geothermal systems driven by volcanic heat energy but dominated by meteoric water.

Carlin-type, sediment-hosted gold deposits in overthrust terranes are best developed in the Cordillera of western USA, especially in the state of Nevada. They are characterized by extremely fine-grained native gold, anomalous concentration of As, Sb, Hg, and especially Tl, and very low contents of base metal sulfides. Associated hydrothermal alteration consists mainly of dissolution of carbonates and precipitation of silica. Carlin-type deposits involved fluids from multiple sources and may represent distal replacement-type deposits related to porphyry-type or skarn-forming magmatic hydrothermal systems.

Lode gold deposits are particularly abundant in the Archean greenstone belts, although gold mineralization of similar style occurs also in Phanerozoic volcanosedimentary settings (e.g., the Mother Lode of California, USA) and turbidites (e.g., the Ballarat and Bendigo districts, Victoria, Australia). Typical features of Archean lode deposits include spatial association with crustal-scale deformation zones, strong local structural control, intense and extensive wallrock alteration, and greenschist to amphibolite facies metamorphism. The source of gold and mineralizing fluids are highly controversial. Of the various genetic models proposed so far, the crustal continuum model, which provides the derivation of fluids and solutes from sources at different crustal levels, appears to best satisfy the constraints imposed by field relations of lode gold deposits and their geochemical characteristics.

16.8. Recommended Reading

Berger and Bagby (1991), Roberts (1987), Hutchinson (1987), Colvine et al. (1988), Groves (1993), Groves & Foster (1991), Henley (1991), Hofstra et al. (1991), Sillitoe (1991), Hayashi and Ohmoto (1991), Poulsen et al. (1992).

REFERENCES

- Adler, H.H. 1974. Concepts of uranium ore formation in reducing environments in sandstones and other sediments. In *Formation of uranium ore deposits*, 141-168. Vienna: International Atomic Energy Agency.
- Aggarwal, P.K., and B.E. Nesbitt 1984. Geology and geochemistry of the Chu Chua massive sulfide deposit, British Columbia. *Econ. Geol.*, 79, 815-825.
- Ahmad, S.N., and A.W. Rose 1980. Fluid inclusions in porphyry and skarn ore at Santa Rita, New Mexico. *Econ. Geol.*, 75, 229-250.
- Akande, S.O., and M. Zentilli 1984. Geologic, fluid inclusion and stable isotope studies of the Gays River lead-zinc deposit, Nova Scotia, Canada. *Econ. Geol.*, 79, 1187-1211.
- Alabaster, T., and J.A. Pearce 1985. The interrelationships between magmatic and ore-forming hydrothermal processes in the Oman ophiolite. *Econ. Geol.*, 80, 1-16.
- Alapieti, T.T., J. Kujanpää, J.J. Lahtinen, and H. Papunen 1989. The Kemi stratiform chromite deposit, northern Finland. *Econ. Geol.*, 84, 1057-1077.
- Albers, J.P., and J.H.C. Bain 1985. Regional setting and some new information on some critical geologic features of the West Shasta district, California. *Econ. Geol.*, 80, 2072-2091.
- Allègre, C.J., 1982. Genesis of Archean Komatiites in a wet ultramafic subducted plate. In *Komatiites*, N.T. Arndt and E.G. Nisbet (eds.), 495-500. London: Allen & Unwin.
- Allison, M.C., and K.C. Misra 1984. Trace element distribution in pyrite and pyrrhotite, Ducktown mining district [abs.]. *Geol. Soc. Am. Abstracts with Programs*, 16, 428.
- Ailsopp, H.L. 1964. Rubidium/strontium ages from the western Transvaal: *Nature*, 204, No. 4956, 361-363.
- Alt, J.C. 1988. The chemistry and sulfur isotope composition of massive sulfide and associated deposits on Green seamount, East Pacific. *Econ. Geol.*, 83, 1026-1033.
- Alvarez, A.A., and D.C. Noble 1988. Sedimentary rock-hosted disseminated precious metal mineralization at Purísima Concepción, Yauricocha district, central Peru. *Econ. Geol.*, 83, 1368-1378.
- Amossé, J., M. Allibert, W. Fischer, and M. Piboule 1990. Experimental study of the solubility of platinum and iridium in basic silicate melts — implications for the differentiation of platinum-group elements during magmatic processes. *Chem. Geol.*, 81, 45-53.
- Anbar, A.D., and H.D. Holland 1992. The photochemistry of manganese and the origin of banded iron formations. *Geochim. Cosmochim. Acta*, 56, 2595-2603.
- Anderson, A.R., Jr., and M. Morin 1968. Two types of massif anorthosites and their implications regarding the thermal history of the crust. In *Origin of anorthosite and related rocks*, Y.W. Isachsen (ed.), N.Y. State Mus. Sci. Serv. Mem 18, 57-69.
- Anderson, A.T. 1974. Chlorine, sulfur, and water in magmas and oceans. *Geol. Soc. Am. Bull.*, 85, 1485-1492.
- Anderson, A.T., Jr. 1966. Mineralogy of the Labrieville anorthosite, Quebec. *Am. Mineral.*, 33, 491-501.
- Anderson, C.A., and J.T. Nash 1972. Geology of the massive sulfide deposits at Jerome, Arizona: a reinterpretation. *Econ. Geol.*, 67, 845-863.
- Anderson, G.M. 1975. Precipitation of Mississippi Valley-type ores. *Econ. Geol.*, 70, 937-942.
- Anderson, G.M. 1983. Some geochemical aspects of sulfide precipitation. In *International Conference on Mississippi Valley-type lead-zinc deposits — Proc. Vol.*, G. Kisvarsanyi, S.K. Grant, W.P. Pratt, and J.W. Koenig (eds.), 61-76. Rolla, Missouri: Univ. Missouri-Rolla Press.
- Anderson, G.M. 1991. Organic maturation and ore precipitation in southeast Missouri. *Econ. Geol.*, 86, 909-926.
- Anderson, G.M., and G. Garven 1987. Sulfate-sulfide-carbonate associations in Mississippi Valley-type lead-zinc deposits. *Econ. Geol.*, 82, 482-485.
- Anderson, G.M., and R.W. Macqueen 1982. Ore deposit models — 6. Mississippi Valley-type lead-zinc deposits. *Geoscience Canada*, 9, 108-117.
- Anderson, J.A. 1982. Characteristics of leached capping and technique of appraisal. In *Advances in Geology of the porphyry copper deposits, southwestern North America*, S.R. Titley (ed.), 275-295. Tucson, Arizona: Univ. Arizona Press.
- Andrew, A.S., C.A. Heinrich, R.W.T. Wilkins, and D.J. Patterson 1989. Sulfur isotope systematics of copper ore formation at Mount Isa, Australia. *Econ. Geol.*, 84, 1614-1626.

- Andrew, C.J., and J.H. Ashton 1985. Regional setting, geology and metal distribution patterns of Navan ore body, Ireland. *Inst. Mining Metall. Trans.*, 94, B66-B93.
- Andrew, R.L. 1980. Supergene alteration and gossan textures of base-metal ores in Southern Africa. *Minerals Sci. Eng.*, 12, 193-215.
- Andrews, A.J., L. Owsjiacki, R. Kerrich, and D.F. Strong 1986. The silver deposits at Cobalt and Gowganda, Ontario. I: Geology, petrography, and whole rock geochemistry. *Can. J. Earth Sci.*, 23, 1480-1506.
- Andreyev, P.F., and A.P. Chumachenko 1964. Reduction of uranium by natural organic substances. *Geochem. International*, 1, 3-7.
- Anger, G., H. Neilsen, H. Puchelt, and W. Ricke 1966. Sulfur isotopes in the Rammelsberg ore deposit (Germany). *Econ. Geol.*, 61, 511-536.
- Anglin, C.D., I.R. Jonasson, and J.M. Franklin 1996. Sm-Nd dating of scheelite and tourmaline: implications for the genesis of Archean gold deposits, Val d'Or, Canada. *Econ. Geol.*, 91, 1372-1382.
- Anhaeusser, C.R., K. Fritze, W.S. Fyfe, and R.C.O. Güll 1975. Gold in "primitive" Archean volcanics. *Chem. Geol.*, 26, 129-135.
- Annels, A.E. 1974. Some aspects of the stratiform ore deposits of the Zambian Copperbelt and their genetic significance. In *Gisements stratiformes et provinces cuprifères*, P. Bartholomé (ed.), 235-254. Liege: Soc. Géol. Belgique.
- Annels, A.E. 1979. Mufulira greywackes and their associated sulfides. *Inst. Mining Metall. Trans.*, 88, B15-B23.
- Annels, A.E. 1984. The geotectonic environment of Zambian copper-cobalt mineralization. *J. Geol. Soc. London*, 141, 279-289.
- Annels, A.E. 1989. Ore genesis in the Zambian Copperbelt with particular reference to the northern sector of the Chambeshi Basin. *Geol. Assoc. Canada Spec. Paper* 36, 427-452.
- Annels, A.E. and J.R. Simmonds 1984. Cobalt in the Zambian Copperbelt. *Precamb. Res.*, 25, 75-98.
- Anthony, E.Y., and S.R. Titley 1988a. Progressive mixing of isotopic reservoirs during magma genesis at the Sierrita porphyry copper deposits, Arizona: inverse solutions. *Geochim. Cosmochim. Acta*, 52, 2235-2249.
- Anthony, E.Y., and S.R. Titley 1988b. Pre-mineralization igneous processes at the Sierrita porphyry copper deposit, Arizona, USA. *Proc. 7th Quad. IAGOD Symp.*, 535-546.
- Arai, S. 1992. Chemistry of chromium spinel in volcanic rocks as a potential guide to magma chemistry. *Mineral. Mag.*, 56, 173-184.
- Arai, S., and H. Yurimoto 1994. Podiform chromites of the Tari-Masaka ultramafic complex, southwestern Japan, as mantle-melt interaction products. *Econ. Geol.*, 89, 1279-1288.
- Arehart, G.B. 1996. Characteristics and origin of sediment-hosted gold deposits: a review. *Ore Geol. Rev.*, 11, 383-403.
- Armstrong, R.A., W. Compston, E.A. Retief, I.S. Williams, and H.J. Welke 1991. Zircon ion microprobe studies bearing on the age and evolution of the Witwatersrand triad. *Precamb. Res.*, 53, 243-266.
- Arndt, N.T. 1977. Ultrabasic magmas and high degree of melting of the mantle. *Contrib. Mineral. Petrol.*, 64, 205-221.
- Arndt, N.T. 1983. Role of a thin, komatiite-rich oceanic crust in the Archean plate-tectonic process. *Geology*, 11, 372-375.
- Arndt, N.T., and G.A. Jenner 1986. Crustally contaminated komatiites from Kambalda, Western Australia. *Chem. Geol.*, 56, 229-256.
- Arndt, N.T., and C.M. Lesher 1992. Fractionation of REEs by olivine and the origin of Kambalda komatiites, Western Australia. *Geochim. Cosmochim. Acta*, 56, 4191-4204.
- Arndt, N.T., and E.G. Nisbet 1982. What is a komatiite? In *Komatiites*, N. T. Arndt and E. G. Nisbet (eds.), 19-27. London: Allen & Unwin.
- Arndt, N.T., and D.R. Hunter 1997. Ore deposits associated with mafic magmas in the Kapvaal craton. *Mineral. Deposita*, 32, 323-334.
- Arndt, N., G. Ginibre, C. Chauvel, F. Albarède, M. Cheadle, C. Herzberg, G. Jenner, and Y. Lahaye 1998. Were komatiites wet? *Geology*, 26, 739-742.
- Arne, D.C., L.W. Curtis, and S.A. Kissin 1991. Internal zonation in a carbonate-hosted Zn-Pb-Ag deposit, Nanisivik, Baffin Island, Canada. *Econ. Geol.*, 86, 699-717.
- Arne, D.C., I.R. Ruddy, and P.F. Green 1989. Thermal histories of Mississippi Valley-type ore districts from apatite fission track analysis [abs.]. *Abstracts International Geol. Congress, 28th, Washington, D.C.*, 1, 54.
- Arnold, R.G., and L.E. Reichen 1962. Measurement of the metal content of naturally occurring metal deficient hexagonal pyrrhotite by an x-ray spacing method. *Am. Mineral.*, 47, 105-111.
- Arora, M., P.K. Govil, S.N. Charan, B. Uday Raj, V. Balaram, C. Manikyamba, A.K. Chatterjee, and S.M. Naqvi 1995. Geochemistry and origin of Archean banded iron-formation from the Bababudan scist belt, India. *Econ. Geol.*, 90, 2040-2057.

- Arribas, A., Jr., J.W. Hedenquist, T. Itaya, T. Okada, R.A. Concepción, and J.S. Garcia, Jr. 1995. Contemporaneous formation of adjacent porphyry and epithermal Cu-Au deposits over 300 Ka in northern Luzon, Philippines. *Geology*, 23, 337-340.
- Arth, J.G., and N.T. Arndt, and A.J. Naldrett 1977. Genesis of Archean komatiites from Munro Township, Ontario: trace element evidence. *Geology*, 5, 590-594.
- Ashley, P.M., and I.R. Palmer 1989. "Stratiform skarns" — a re-evaluation of three eastern Australian deposits. *Mineral. Deposita*, 24, 289-298.
- Ashley R.P., C.G. Cunningham, N.H. Bostick, W.E. Dean, and I.-M. Chou 1991. Geology and geochemistry of three sedimentary-rock hosted disseminated gold deposits in Guizhou Province, People's Republic of China. *Ore Geol. Rev.*, 6, 133-151.
- Ashton, J.H., D.T. Downing, and S. Finlay 1986. The geology of the Navan Zn-Pb orebody. In *Geology and genesis of mineral deposits in Ireland*, C.J. Andrew, R.W.A. Crowe, S. Finlay, W.M. Pennall, and J.F. Payne (eds.), 243-280. Dublin: Irish Assoc. Econ. Geol.
- Atkinson, B.K. 1974. Experimental deformation of polycrystalline galena, chalcopyrite and pyrrhotite. *Inst. Mining Metall. Trans.*, 83, B19-B28.
- Atkinson, B.K. 1975. Experimental deformation of polycrystalline pyrite: effects of temperature, confining pressure, strain rate and porosity. *Econ. Geol.*, 70, 473-483.
- Atkinson, W.W., Jr., and M.T. Einaudi 1978. Skarn formation and mineralization in the contact aureole at Carr Fork, Bingham, Utah. *Econ. Geol.* 73, 1326-1365.
- Bache, J. J. 1987. *World gold deposits: a geological classification*. New York: Elsevier, 178p.
- Bache, J. J., and Y. Sunarya 1987. World gold deposits: a metallogenic quantitative classification. *AGID News*, No. 53, 26-34.
- Bachinski, D.J. 1969. Bond strength and sulfur isotopic fractionation in coexisting sulfides. *Econ. Geol.*, 64, 56-65.
- Bachinski, D.J. 1976. Metamorphism of supereiferous iron sulfide deposits. *Econ. Geol.*, 71, 443-452.
- Bachinski, D.J. 1977. Sulfur isotope composition of ophiolitic cupriferous iron sulfide deposits, Notre Dame Bay, Newfoundland. *Econ. Geol.*, 72, 243-257.
- Badham, J.P.N. 1976. Orogenesis and metallogenesis with reference to the silver-nickel, cobalt arsenide ore association. In *Metallogeny and plate tectonics*. *Geol. Assoc. Canada Spec. Paper* 14, 559-571.
- Badham, J.P.N. 1981. Shale-hosted Pb-Zn deposits: products of exhalation of formation waters? *Inst. Mining Metall. Trans.* 90, B70-B76.
- Badham, J.P.N. 1982. A comparison of tin and copper mineralization in felsic igneous rocks — where are the tin exhalites? In *Metallization associated with acid magmatism*, A.M. Evans (ed.), 29-35. New York: Wiley.
- Bagby, W.C., and B.R. Berger 1985. Geological characteristics of sediment-hosted, disseminated precious-metal deposits in the western United States. *Rev. Econ. Geol.*, 2, 169-202.
- Bajwah, Z.U., P.K. Secombe, and R. Offler 1987. Trace element distribution, Co:Ni ratios and genesis of the Big Cadia iron-copper deposit, New South Wales, Australia. *Mineral. Deposita*, 22, 292-300.
- Bakken, B.M., and M.T. Einaudi 1986. Spatial and temporal relations between wall rock alteration and gold mineralization, Main Pit, Carlin Gold Mine, Nevada, U.S.A. In *Proc. Gold '86 Symposium*, Toronto, A.J. Macdonald (ed.), 388-403. Willowdale, Ontario: Konsult International.
- Bakken, B.M., M.F. Hochella, Jr., A.F. Marshall, and A.M. Turner 1989. High-resolution microscopy of gold in unoxidized ore from the Carlin mine, Nevada. *Econ. Geol.*, 84, 171-179.
- Baldwin, J.A., and J.A. Pearce 1982. Discrimination of productive and nonproductive porphyritic intrusions in the Chilean Andes. *Econ. Geol.*, 77, 664-674.
- Baldwin, J.T., H.D. Swain, and G.H. Clark 1978. Geology and grade distribution of the Panguna porphyry copper deposit, Bougainville, Papua New Guinea. *Econ. Geol.*, 73, 690-702.
- Ballhaus, C.G. 1988. Potholes of the Merensky Reef at Brakspruit Shaft, Rustenburg Platinum Mines: primary disturbances in the magmatic stratigraphy. *Econ. Geol.* 83, 1140-1158.
- Ballhaus, C.G. 1998a. Origin of podiform chromite deposits by magma mingling. *Earth Planet. Sci. Lett.*, 156, 185-193.
- Ballhaus, C.G. 1998b. PGE enrichment process in the Merensky Reef [abs.]. *8th International Platinum Symposium Abstracts*, June 28-July 3, 1998, Rustenburg, South Africa, 25-28.
- Ballhaus, C.G., and E.F. Stumpfl 1985. Occurrence and petrological significance of graphite in the Upper Critical Zone, Western Bushveld Complex, South Africa. *Earth Planet. Sci. Lett.*, 74, 58-68.
- Ballhaus, C.G., and E.F. Stumpfl 1986. Sulfide and platinum mineralization in the Merensky Reef: evidence from hydrous silicates and fluid inclusions. *Contrib. Mineral. Petrol.*, 94, 193-204.
- Ballhaus, C.G., M. Cornelius, and E.F. Stumpfl 1988. The upper Critical Zone of the Bushveld Complex and the origin of Merensky-type ores — a discussion. *Econ. Geol.*, 83, 1081-1085.
- Bamford, R.W. 1972. The Mount Fubilan (Ok Tedi) porphyry copper deposit, Territory of Papua and New Guinea. *Econ. Geol.*, 67, 1019-1033.
- Banas, M. 1980. Zechstein copper deposits in Poland. In *European copper deposits*, S. Jankovic and R.H. Sillitoe (eds.), 136-145. Djusina, Yugoslavia: Dept. Econ. Geol., Fac. Mining Geol.

- Banks, D.A., and M.J. Russell 1992. Fluid mixing during ore deposition at the Tynagh base-metal deposit, Ireland. *European J. Mineral.*, 4, 921-931.
- Banks, N.G. 1973. Biotite as a source of some of the sulfur in porphyry copper deposits. *Econ. Geol.*, 68, 697-703.
- Banks, N.G. 1974. Distribution of copper in diorite and biotite alteration products in intrusive rocks near two Arizona porphyry copper deposits. *U.S. Geol. Survey J. Res.*, 2, 195-211.
- Banno, S., and R. Kanehira 1961. Sulfide and oxide minerals in schists of the Sambagawa and Central Abukuma metamorphic terranes. *Japan J. Geol. Geogr. Trans.*, 32, 331-348.
- Baragar, W.R.A. 1968. Major-element geochemistry of the Noranda volcanic belt, Quebec-Ontario. *Can. J. Earth Sci.*, 5, 773-790.
- Baragar, W.R.A., and I.C. McGlynn 1976. Early Archean basement in the Canadian Shield: a review of the evidence. *Geol. Survey Canada Paper* 76-14, 21 p.
- Barbieri, M., U. Masi, and L. Tolomeo 1984. Strontium geochemical evidence for the origin of the barite deposits from Sardinia, Italy. *Econ. Geol.*, 79, 1360-1365.
- Bardossy, G. 1982. *Karst bauxites*. Amsterdam: Elsevier, 441 p.
- Barker, C., and M. P. Smith 1986. Mass spectrometric determination of gases in individual fluid inclusions in natural minerals. *Anal. Chem.*, 58, 1330-1333.
- Barker, W. W. 1983. The Fe-Ni-S system + (Co, Cu). *CSIRO (Australia) Rept.* FP-26.
- Barley, M.E. 1986. Incompatible-element enrichment in Archean basalts: a consequence of contamination by older sialic crust rather than mantle heterogeneity. *Geology*, 14, 947-950.
- Barley, M.E. 1992. A review of Archean volcanic-hosted massive sulfide and sulfate mineralization in Western Australia. *Econ. Geol.*, 87, 855-872.
- Barley, M.E., and D.I. Groves 1990. Deciphering the tectonic evolution of Archean greenstone belts: the importance of contrasting histories to the distribution of mineralization in the Yilgarn Craton, Western Australia. *Precamb. Res.*, 46, 3-20.
- Barley, M.E., B.N. Eisenlohr, D.I. Groves, C.S. Perring, and J.R. Vearncombe 1989. Late Archean convergent margin tectonics and gold mineralization: a new look at the Norseman-Wiluna belt, Western Australia. *Geology*, 17, 826-829.
- Barnes, H.L. 1962. Mechanisms of mineral zoning. *Econ. Geol.*, 57, 30-37.
- Barnes, H.L. 1975. Zoning of ore deposits: types and causes. *Trans. Royal Soc. Edinburgh*, 69, 295-311.
- Barnes, H.L. 1979. Solubilities of ore minerals. In *Geochemistry of hydrothermal ore deposits*, 2nd. edn., H.L. Barnes (ed.), 404-460. New York: Wiley.
- Barnes, H.L. 1983. Ore depositing reactions in Mississippi Valley-type deposits. In *International Conference on Mississippi Valley-type lead-zinc deposits — Proc. Vol.*, G. Kisvarsany, S.K. Grant, W.P. Pratt, and J.W. Koenig (eds.), 61-76. Rolla, Missouri: Univ. Missouri-Rolla Press.
- Barnes, H.L., and T.M. Seward 1997. Geothermal systems and mercury deposits. In *Geochemistry of hydrothermal ore deposits*, 3rd. ed., H.L. Barnes (ed.), 699-736. New York: Wiley.
- Barnes, R.G. 1983. Stratiform and stratabound tungsten mineralization in the Broken Hill Block, N.S.W. *J. Geol. Soc. Australia*, 30, 225-239.
- Barnes, R.G. 1987. Multi-stage mobilization and remobilization of mineralization in the Broken Hill Block, Australia. *Ore Geol. Rev.*, 2, 247-267.
- Barnes, S.J. 1985. The petrology and geochemistry of komatiite flows from the Abitibi greenstone belt, Canada: a model for their formation. *Lithos*, 18, 241-270.
- Barnes, S.J. 1986. The distribution of chromium among orthopyroxene, spinel and silicate liquid at atmospheric pressure. *Geochim. Cosmochim. Acta*, 50, 1889-1909.
- Barnes, S.J., and Sarah-Jane Barnes 1990. A new interpretation of the Katiniq nickel deposit, Ungava, northern Quebec. *Econ. Geol.*, 85, 1269-1272.
- Barnes, S.J., and I.H. Campbell 1988. Role of magmatic fluids in Merensky-type platinum deposits: a discussion. *Geology*, 16, 488-491.
- Barnes, S.J., and A.J. Naldrett 1985. Geochemistry of the J-M (Howland) Reef of the Stillwater Complex, Minneapolis Adit area. I. Sulfide chemistry and sulfide-olivine equilibrium. *Econ. Geol.*, 80, 627-645.
- Barnes, S.J., and A.J. Naldrett 1986a. Geochemistry of the J-M (Howland) Reef of the Stillwater Complex, Minneapolis Adit area. I. Sulfide chemistry and sulfide-olivine equilibrium — a reply. *Econ. Geol.*, 81, 203-206.
- Barnes, S.J., and A.J. Naldrett 1986b. Geochemistry of the J-M Reef of the Stillwater Complex, Minneapolis Adit area. II. Silicate mineral chemistry and petrogenesis. *J. Petrol.*, 27, 791-825.
- Barnes, S.J., C.J.A. Coates, and A.J. Naldrett 1982. Petrogenesis of a Proterozoic nickel sulfide-komatiite association: the Katiniq sill, Ungava, Québec. *Econ. Geol.*, 77, 413-429.
- Barnes, S.J., M.J. Gole, and R.E.T. Hill 1988a. The Agnew nickel deposit, Western Australia: Part I. Structure and stratigraphy. *Econ. Geol.*, 83, 524-536.
- Barnes, S.J., M.J. Gole, and R.E.T. Hill 1988b. The Agnew nickel deposit, Western Australia: Part II. Sulfide geochemistry, with emphasis on platinum-group elements. *Econ. Geol.*, 83, 537-550.
- Barnes, Sarah-Jane, and A.J. Naldrett 1987. Fractionation of platinum group elements and gold in some komatiites of the Abitibi greenstone belt, northern Ontario. *Econ. Geol.*, 82, 165-183.

- Barnes, Sarah-Jane, A.J. Naldrett, and M.P. Gorton 1985. The origin of fractionation of platinum-group elements in terrestrial magmas. *Chem. Geol.*, 53, 303-323.
- Barnicoat, A.C., R.J. Fare, D.I. Groves, and N.J. McNaughton 1991. Synmetamorphic lode-gold deposits in high-grade Archean settings. *Geology*, 19, 921-924.
- Barrett, F.M., D.I. Groves, and R.A. Binns 1976. Importance of metamorphic processes at the Nepean nickel deposit, Western Australia. *Inst. Mining. Metall. Trans.*, 85B, 252-273.
- Barrett, F.M., R.A. Binns, D.I. Groves, R.J. Marston, and K.G. McQueen 1977. Structural history and metamorphic modification of Archean volcanic-type nickel deposits, Yilgarn Block, Western Australia. *Econ. Geol.*, 72, 1195-1223.
- Barrett, T.J., and G.M. Anderson 1982. The solubility of sphalerite and galena in NaCl brines. *Econ. Geol.*, 77, 1923-1933.
- Barrett, T.J., and G.M. Anderson 1988. The solubility of sphalerite and galena in 1-5 m NaCl solutions to 300°C. *Geochim. Cosmochim. Acta*, 52, 813-820.
- Barrett, T.J., G.M. Anderson, and J. Lugowski 1988. The solubility of hydrogen sulfide in 0-5 m NaCl solutions at 25°-95°C and one atmosphere. *Geochim. Cosmochim. Acta*, 52, 807-811.
- Barrie, C.T., and A.J. Naldrett 1990. Geochemical constraints on the genesis of Montcalm gabbroic complex and Ni-Cu deposit, western Abitibi Subprovince, Ontario. *Can. Mineral.*, 28, 451-474.
- Bartholomé, P. 1974. On the diagenetic formation of ores in sedimentary beds, with special reference to the Kamoto copper deposit, Shaba, Zaire. In *Gisements stratiformes et provinces cuprifères*, P. Bartholomé (ed.), 203-214. Liege: Soc. Geol. Belgique.
- Bartholomé, P., P. Evrand, F. Katekesha, J. Lopez-Ruiz and M. Ngongo 1972. Diagenetic ore-forming processes at Komoto Katanga, Republic of the Congo. In *Ores in sediments*, G.C. Amstutz and A.J. Bernard (eds.), 21-41. Berlin: Springer-Verlag.
- Barton, J.M., R.G. Cawthorn, and J. White 1986. The role of contamination in the evolution of the Platreef of the Bushveld Complex. *Econ. Geol.*, 81, 1096-1104.
- Barton, J.M., Jr., D.B. Wenner, and D.K. Hallbauer 1992. Oxygen isotopic study of the nature and provenance of large quartz and chert clasts in gold-bearing conglomerates of South Africa. *Geology*, 20, 1123-1126.
- Barton, P.B., Jr. 1967. Possible role of organic matter in the precipitation of the Mississippi Valley ores. *Econ. Geol. Mono.* 3, 371-378.
- Barton, P.B., Jr. 1970. Sulfide petrology. *Mineral. Soc. Am. Spec. Paper* 3, 187-198.
- Barton, P.B., Jr. 1978. Some ore textures involving sphalerite from the Furutobe Mine, Akita Prefecture. *Japan. Mining Geol.*, 28, 293-300.
- Barton, P.B., Jr., and P.M. Bethke 1987. Chalcopyrite disease in sphalerite: pathology and epidemiology. *Am. Mineral.*, 72, 451-467.
- Barton, P.B., Jr., and B.J. Skinner 1979. Sulfide mineral stabilities. In *Geochemistry of hydrothermal ore deposits*, 2nd edn., H.L. Barnes (ed.), 278-403. New York: Wiley.
- Barton, P.B., Jr., and P. Toulmin, III. 1966. Phase relations involving sphalerite in the Fe-Zn-S system. *Econ. Geol.*, 61, 815-849.
- Barton, P.B., Jr., P.M. Bethke, and E. Roedder 1977. Environment of ore deposition in the Creede mining district, San Juan Mountains, Colorado: Part III. Progress toward interpretation of the chemistry of the ore-forming fluid for the OH vein. *Econ. Geol.*, 72, 1-24.
- Basaltic Volcanism Study Project 1981. *Basalt volcanism on the terrestrial planets*. New York: Pergamon.
- Bastin, E.S. 1950. Interpretations of ore textures. *Geol. Soc. Am. Mem.* 45.
- Bastin, E.S., L.C. Graton, W. Lindgren, W.H. Newhouse, G.M. Schwartz, and M.N. Short 1931. Criteria of age relations of minerals with special reference to polished sections of ores. *Econ. Geol.*, 26, 561-610.
- Bateman, A.M. 1951. The formation of late magmatic oxide ores. *Econ. Geol.* 46, 404-426.
- Baur, M.E., J.M. Hayes, S.A. Studley, and M.R. Walter 1985. Millimeter-scale variations of stable isotope abundances in carbonates from banded iron-formations in the Hamersley Group of Western Australia. *Econ. Geol.*, 80, 270-282.
- Bavinton, O.A. 1981. The nature of sulfidic metasediments at Kambalda and their broad relationships with associated ultramafic rocks and nickel ores. *Econ. Geol.*, 76, 1606-1628.
- Beales, F.W. 1975. Precipitation mechanisms for Mississippi Valley-type deposits. *Econ. Geol.* 70, 943-948.
- Beales, F.W., and J. L. Hardy 1977. The problem of recognition of occult evaporites with special reference to southeast Missouri. *Econ. Geol.*, 72, 487-490.
- Beales, F.W., and S.A. Jackson 1966. Precipitation of lead-zinc ores in carbonate reservoirs as illustrated by Pine Point ore field, Canada. *Inst. Mining. Metall. Trans.*, 75, Sec. B, 278-285.
- Beane, R.E. 1974. Biotite stability in the porphyry copper environment. *Econ. Geol.*, 69, 241-256.
- Beane, R.E. 1982. Hydrothermal alteration in silicate rocks, southwestern North America. In *Advances in Geology of the porphyry copper deposits, southwestern North America*, S.R. Titley (ed.), 117-138. Tucson, Arizona: Univ. Arizona Press.
- Beane, R.E. and S.R. Titley 1981. Porphyry copper deposits: Part II. Hydrothermal alteration and mineralization. *Econ. Geol. 75th Anniv. Vol.*, 235-269.

- Beaty, D.W., and H.P. Taylor, Jr. 1982. Some petrologic and oxygen isotopic relationships in the Amulet mine, Noranda, Quebec, and their bearing on the origin of Archean massive sulfide deposits. *Econ. Geol.*, 77, 95-108.
- Beaty, D.W., H.P. Taylor, Jr., and P.R. Coad 1988. An oxygen isotope study of the Kid Creek, Ontario, volcanogenic massive sulfide deposit: evidence for a high ^{18}O ore fluid. *Econ. Geol.*, 83, 1-17.
- Beeson, R. 1990. Broken Hill-type lead-zinc deposits — an overview of their occurrence and geologic setting. *Inst. Mining Metall. Trans.*, 99, B163-B175.
- Bell, K., and J. Blenkinsop 1989. Neodymium and strontium isotope geochemistry of carbonatites. In *Carbonatites*, K. Bell (ed.), 278-300. London: Unwin Hyman.
- Bell, K., C.D. Anglin, and J.M. Franklin 1989. Sm-Nd and Rb-Sr isotope systematics of scheelites: possible implications for the age and genesis of vein-hosted gold deposits. *Geology*, 17, 500-504.
- Bell, T.E. 1986. Deposition and diagenesis of the Brushy Basin Member and upper part of the Westwater Canyon Member of the Morrison Formation, San Juan Basin, New Mexico. *Am. Assoc. Petroleum Geologists Studies in Geology*, 22, 77-91.
- Bell, T.H., W.G. Perkins, and C.P. Swager 1988. Structural controls on development and localization of syntectonic copper mineralization at Mount Isa, Queensland. *Econ. Geol.*, 83, 69-85.
- Berger, B.R., and W.C. Bagby 1991. The geology and origin of Carlin-type gold deposits. In *Gold metallogeny and exploration*, R.P. Foster (ed.), 210-248. Glasgow: Blackie.
- Berger, B.R., and P.M. Bethke (eds.) 1985. Geology and geochemistry of epithermal systems. *Rev. Econ. Geol.*, 2, 298 p.
- Berger, B.R., and Henley, R.W. 1989. Advances in the understanding of epithermal gold-silver deposits, with special reference to western United States. *Econ. Geol. Mono.* 6, 405-419.
- Berger, I.A., and J.C. Chandler 1960. Extractability of humic acid from coalified logs as a guide to temperature in Colorado Plateau sediments. *Econ. Geol.*, 55, 1039-1047.
- Bergeron, M. 1972. Quebec Iron and Titanium Corporation ore deposit at Lac Tio, Quebec. *International Geol. Congress*, 24th, Montreal, 1972, Guidebook excursion B-09, 8p.
- Berman, R. 1965. Thermal properties. In *Physical properties of diamond*, R. Berman (ed.), 371-393. Oxford: Oxford Univ. Press.
- Berner, R. A. 1964. Iron sulfides formed from aqueous solution at low temperatures and atmospheric pressures. *J. Geol.*, 72, 293-306.
- Berner, R.A. 1971. *Principles of chemical sedimentology*. New York: McGraw Hill, 240p.
- Berner, R.A. 1979. Sedimentary pyrite formation. *Am. J. Sci.*, 268, 1-23.
- Berner, R.A. 1985. Sulfate reduction, organic matter decomposition, and pyrite formation. *Phil. Trans. Royal Soc. London*, A315, 25-38.
- Berner, R.A. 1995. Chemical weathering and its effect on atmospheric CO_2 and climate. *Rev. in Mineralogy*, 31, 565-583.
- Berner, R.A., and D.E. Canfield 1989. A new model for atmospheric oxygen over Phanerozoic time. *Am. J. Sci.*, 289, 333-361.
- Berning, J., R. Cooke, S.A. Heimstra, and U. Hoffman 1976. The Rössing uranium deposit, South-West Africa. *Econ. Geol.*, 71, 351-368.
- Berry, F.A.F. 1969. Relative factors influencing membrane filtration. *Chem. Geol.*, 4, 295-301.
- Berry, L.G. (ed.) 1971. The silver-arsenide deposits of the Cobalt-Gowganda region, Ontario. *Can. Mineral.*, 11, Pt. 1, 429p.
- Bethke, C.M. 1986. Hydrologic constraints on the genesis of the Upper Mississippi Valley mineral district from Illinois Basin brines. *Econ. Geol.*, 81, 233-249.
- Bethke, P.M., and P.B. Barton, Jr. 1971. Distribution of some minor elements between coexisting sulfide minerals. *Econ. Geol.*, 66, 140-61.
- Bethke, P.M., and R. O. Rye 1979. Environment of ore deposition in the Creede mining district, San Juan Mountains, Colorado. Pt. IV: sources of fluids from oxygen, hydrogen and carbon isotope studies. *Econ. Geol.* 74, 1832-1851.
- Beukes, N.J., and C. Klein 1990. Geochemistry and sedimentology of a facies transition — from microbanded to granular iron-formation — in the early Proterozoic Transvaal Supergroup, South Africa. *Precamb. Res.*, 47, 99-139.
- Beukes, N.J., and C. Klein 1992. Models for iron-formation deposition. In *Proterozoic biosphere*, J. W. Schopf and C. Klein (eds.), 147-151. New York: Cambridge Univ. Press.
- Beukes, N.J., C. Klein, A.J. Kaufman, and J.M. Hayes 1990. Carbonate petrography, kerogen distribution, and carbon and oxygen isotope variations in an early Proterozoic transition from limestone to iron-formation deposition, Transvaal Supergroup, South Africa. *Econ. Geol.*, 85, 663-690.
- Bezmen, N.I., V.I. Tikhomirova 1975. The effect of temperature on distribution of cobalt and nickel between iron sulfides and solutions of different composition. *Geochem. International*, 12, 60-65.
- Bezmen, N.I., V.I. Tikhomirova, and V.P. Kosogova 1975. Pyrite-pyrrhotite geothermometer: partition of nickel and cobalt. *Geochem. International*, 12, 45-59.
- Bezmen, N.I., M. Asif, G.E. Brugman, I.M. Romanenko, and A.J. Naldrett 1994. Distribution of Pd, Rh, Ir, Os, and Au between sulfide and silicate melts. *Geochim. Cosmochim. Acta*, 58, 1251-1260.

- Bichan, R. 1969. Origin of chromite seams in the Hartley Complex of the Great Dyke, Rhodesia. *Econ. Geol. Mono.* 4, 95-113.
- Bickle, M.J. 1982. The magnesium contents of komatiitic liquids. In *Komatiites*, N.T. Arndt, and E.G. Nisbet (eds.), 479-494. London: Allen and Unwin.
- Bickle, M.J., C.E. Ford, and E.G. Nisbet 1977. The petrogenesis of peridotitic komatiites: evidence from high-pressure melting experiments. *Earth Planet. Sci. Lett.*, 37, 97-106.
- Billings, G.K., S.E. Kesler, and S.A. Jackson 1969. Relation of zinc-rich formation waters, northern Alberta, to the Pine Point ore deposit. *Econ. Geol.*, 64, 385-391.
- Binns, R.A. 1964. Zones of progressive regional metamorphism in the Willyama Complex, Broken Hill district, N.S.W.. *J. Geol. Soc. Australia*, 11, 283-330.
- Binns, R.A., and D. I. Groves 1976. Iron-nickel partition in metamorphosed olivine-sulfide assemblages from Preservance, Western Australia. *Am. Mineral.*, 61, 782-787.
- Binns, R.A., D.I. Groves, and R.J. Gunthorpe 1977. Nickel sulphides in Archean ultramafic rocks of Western Australia. In *Correlation of the Precambrian*, A.V. Sidorenko (ed.), Nauka, 2, 349-380.
- Bischoff, J.L. 1969. Red Sea geothermal brine deposits: their mineralogy, chemistry, and genesis. In *Hot brines and recent heavy metal deposits in the Red Sea*, E.T. Degens and D.A. Ross (eds.), 368-401. New York: Springer-Verlag.
- Bischoff, J.L., and F.W. Dickson 1975. Basalt-seawater interaction at 200°C and 500 bars: implications for origin of seawater chemistry. *Earth Planet. Sci. Lett.*, 25, 285-397.
- Bischoff, J.L., and K.S. Pitzer 1985. Phase relations and adiabats in boiling seafloor geothermal systems. *Earth Planet. Sci. Lett.*, 75, 327-338.
- Bischoff, J.L., A.S. Radtke, and R.J. Rosenbauer 1981. Hydrothermal alteration of greywacke by brine and seawater: roles of alteration and chloride complexing on metal solubilization at 200° and 350°C. *Econ. Geol.*, 76, 659-676.
- Bishop, D.T., H.C. Morris, and F.R. Edmunds 1970. Turbidites and depositional features in the Lower Belt-Purecell Supergroup [abstr.]. *Geol. Soc. Am. Abstracts with Programs*, 2, 497.
- Bjørlykke, H. and S. Jarp 1950. The content of cobalt in some Norwegian sulphide deposits. *Norsk Geol. Tidsskrift*, 28, 151-156.
- Bjørlykke, A., and D.F. Sangster 1981. An overview of sandstone lead deposits and their relation to red-bed copper and carbonate-hosted lead-zinc deposits. *Econ. Geol. 75th Anniv. Vol.*, 179-213.
- Blain, C.F., and R.L. Andrew 1977. Sulfide weathering and evaluation of gossans in mineral exploration. *Minerals Sci. Eng.*, 9, 119-150.
- Blake, M.C., Jr. and B.A. Morgan 1976. Rutile and sphene in blueschist and related high-pressure facies rocks. *U.S. Geol. Survey Prof. Paper* 959-C, C1-C6.
- Blanchard, R. 1947. Detailed studies of zoning in ore districts. *Econ. Geol.* 42, 543-545.
- Blenkinsop, T.G., and K.A. Eriksson 1995. Gold concentration in the Witwatersrand reefs by footwall cannibalization. *Econ. Geol.*, 90, 200-202.
- Bloom, M.S. 1981. Chemistry of inclusion fluids: stockwork molybdenum deposits from Questa, New Mexico, Hudson Bay Mountain, and Endako, British Columbia. *Econ. Geol.*, 76, 1906-1920.
- Boast, A.M., M.L. Coleman, and C. Halls 1981. Textural and stable isotopic evidence for the genesis of the Tynagh base metal deposit, Ireland. *Econ. Geol.*, 76, 27-55.
- Bochert, H. 1960. Genesis of marine sedimentary iron ores. *Inst. Mining Metall. Trans.*, 69, 261-279.
- Boctor, N. J. 1981. Partitioning of nickel between olivine and iron monosulfide melts. *Carnegie Inst. Washington Year Book*, 80, 356-359.
- Boctor, N. J. 1982. The effect of the fO_2 , fS_2 , and temperature on Ni partitioning between olivine and iron sulfide melts. *Carnegie Inst. Washington Year Book*, 81, 366-369.
- Bodnar, R.J. 1981. Use of fluid inclusions in mineral exploration: comparison of features with theoretical and experimental data on ore genesis [abs.]. *Geol. Soc. Am. Abstracts with Programs*, 13, 412.
- Bodnar, R.J. 1983. A method of calculating fluid inclusion volumes based on vapor bubble diameters and P-V-T-X properties of inclusion fluids. *Econ. Geol.*, 78, 535-542.
- Bodnar, R.J. 1993. Revised equation and table for determining the freezing point depression of H₂O-NaCl solutions. *Geochim. Cosmochim. Acta*, 57, 683-684.
- Bogashova, L.G. 1987. The role of evaporite basins in producing stratiform mineralization. *International Geol. Review*, 29, 481-490.
- Bonham, H.F., Jr. 1988. Models for volcanic-hosted epithermal precious metal deposits: a review. In *Bulk mineable precious metal deposits of the western United States*, R. W. Schafer, J. J. Cooper, and P.G. Virke (eds.), 259-272. Reno, Nevada: Geol. Soc. Nevada.
- Bonham, H.F., Jr. 1989. Bulk mineable gold deposits of the western United States. *Econ. Geol. Mono.* 6, 193-207.
- Boni, M., A. Lannace, and C. Pierre 1988. Stable-isotope compositions of Lower Cambrian Pb-Zn-Ba deposits and their host carbonates, southwestern Sardinia, Italy. *Chem. Geol. (Isotope Geoscience Section)*, 72, 267-282.
- Bookstrom, A.A. 1981. Tectonic setting and generation of Rocky Mountain porphyry molybdenum deposits. *Arizona Geol. Soc. Digest*, 14, 215-226.

- Bookstrom, A.A., R.B. Carten, J.R. Shannon, and R.P. Smith 1988. Origins of bimodal leucogranite-lamprophyre suites, Climax and Red Mountain porphyry molybdenum system, Colorado, petrologic and strontium isotopic evidence. *Colorado School of Mines Quarterly*, 83, 1-24.
- Boorman, R.S. 1967. Subsolidus studies in the ZnS-FeS-FeS₂ system. *Econ. Geol.*, 62, 614-631.
- Boorman, R.S., J.K. Sutherland, and L.V. Chernyshev 1971. New data on sphalerite-pyrrothite-pyrite solvus. *Econ. Geol.*, 66, 670-675.
- Bornhorst, T.J., J.B. Paces, N.K. Grant, J.D. Obradovich, and N. King Huber 1988. Age of native copper mineralization, Keweenaw Peninsula, Michigan. *Econ. Geol.*, 83, 619-625.
- Bortnikov, N.S., A.D. Genkin, M.G. Dobrovol'skaya, G.N. Muravitskaya, and A.A. Filimonova 1991. The nature of chalcopyrite inclusions in sphalerite: exsolution, coprecipitation, or "disease"? *Econ. Geol.*, 86, 1070-1082.
- Bortnikov, N.S., M.G. Dobrovol'skaya, A.D. Genkin, V.B. Naumov, and V.V. Shapenko 1995. Sphalerite-galena geothermometers: distribution of cadmium, manganese, and the fractionation of sulfur isotopes. *Econ. Geol.*, 90, 155-180.
- Both, R.A. 1973. Minor element geochemistry of sulfide minerals in the Broken Hill lode (N. S. W.) in relation of the origin of the ore. *Mineral. Deposita*, 8, 349-369.
- Both, R.A. 1978. Remobilization of mineralization during retrograde metamorphism, Broken Hill, New South Wales, Australia. *S. African Geol. Soc. Publ.*, 4, 481-489.
- Both R.A., and J.W. Smith 1975. A sulfur isotopic study of base metal mineralization in the Wellyama Complex, Western New South Wales, Australia. *Econ. Geol.*, 70, 308-318.
- Both R.A., and E.F. Stumpf 1987. Distribution of silver in the Broken Hill orebody. *Econ. Geol.*, 82, 1037-1043.
- Boudreau, A.E. 1988. Investigations of the Stillwater Complex. IV. The role of volatiles in the petrogenesis of the J-M Reef, Minneapolis Adit section. *Can. Mineral.*, 26, 193-208.
- Boudreau, A.E., and I.S. McCallum 1986. Investigations of the Stillwater Complex, Part III: The Picket Pin Pt/Pd deposit. *Econ. Geol.*, 81, 1953-1975.
- Boudreau, A.E., and I.S. McCallum 1989. Investigations of the Stillwater Complex: Part V. Apatites as indicators of evolving fluid composition. *Contrib. Mineral. Petrol.*, 102, 138-153.
- Boudreau, A.E., and I.S. McCallum 1992. Concentration of platinum-group elements by magmatic fluids in layered intrusions. *Econ. Geol.*, 87, 1830-1848.
- Boudreau, A.E., E.A. Mathez, and I.S. McCallum 1986. Halogen geochemistry of the Stillwater and Bushveld complexes: evidence for transport of platinum-group elements by Cl-rich fluids. *J. Petrol.*, 27, 967-986.
- Bourcier, W.L., and H. L. Barnes 1987. Ore-solution chemistry - VII. Stabilities of chloride and bisulfide complexes of zinc to 350°C. *Econ. Geol.*, 82, 1839-1863.
- Bow, C., D. Wolfgram, A. Turner, S. Barnes, J. Evans, M. Zdepski, and A. Boudreau 1982. Investigations of the Howland Reef of the Stillwater Complex, Minneapolis Adit area: Stratigraphy, structure, and mineralization. *Econ. Geol.*, 77, 1481-1492.
- Bowen, N.L. 1928. *The evolution of the igneous rocks*. Princeton, New Jersey: Princeton Univ. Press.
- Bowers, T.S. 1989. Stable isotope signatures of water-rock interaction in Mid-ocean Ridge hydrothermal systems: sulfur, oxygen, and hydrogen. *J. Geophys. Res.*, 94, B5, 5775-5786.
- Bowers, T.S. 1991. The deposition of gold and other metals: pressure-induced fluid immiscibility and associated stable isotope signatures. *Geochim. Cosmochim. Acta*, 55, 2417-2434.
- Bowers, T.S., and H.C. Helgeson 1983. Calculation of the thermodynamic and geochemical consequences of nonideal mixing in the system H₂O-CO₂-NaCl on phase relations in geologic systems: equation of state for the H₂O-CO₂-NaCl fluids at high pressures and temperatures. *Geochim. Cosmochim. Acta*, 47, 1247-1275.
- Bowles, J.F.W. 1986. The development of platinum-group minerals in laterites. *Econ. Geol.*, 81, 1278-1285.
- Bowman, J.R., J.J. Covert, A.H. Clark, and G.A. Mathieson 1985. The CanTung E Zone scheelite skarn orebody, Tungsten, Northwest Territories: oxygen, hydrogen, and carbon isotope studies. *Econ. Geol.*, 80, 1872-1895.
- Bowman, J.R., W.T. Parry, W.P. Kropp, and S.A. Krueger 1987. Chemical and isotopic evolution of hydrothermal solutions at Bingham, Utah. *Econ. Geol.*, 82, 395-428.
- Boyce, A.J., M.L. Coleman, and M.J. Russell 1983. Formation of fossil hydrothermal chimneys and mounds from Silvermines, Ireland. *Nature*, 306, 545-550.
- Boyd, F.R. 1982. Predicting the occurrence of diamondiferous kimberlites. *Ind. Diamond Q.*, 33, 31-34.
- Boyle, R.W. 1979. The geochemistry of gold and its deposits. *Geol. Survey Canada Bull.*, 280, 584 p.
- Boyle, R. W. 1982. Gold deposits: a review of their geological and geochemical setting. *Can. Inst. Mining Metall. Spec. Vol.* 24, 1-5.
- Boyle, R.W. 1986. Gold deposits in turbidite sequences: their geology, geochemistry, and history of the theories of their origin. In *Turbidite-hosted gold deposits*, J.D. Keppie, R.W. Boyle, and S.J. Haynes (eds.), *Geol. Assoc. Canada Spec. Paper* 32, 1-14.

- Boyle, R.W., A.C. Brown, C.W. Jefferson, E.C. Jowett, and R.V. Kirkham 1989 (eds.). Sediment-hosted stratiform copper deposits. *Geol. Assoc. Canada Spec Paper* 36.
- Bradbury, J.W. 1983. *Pyrrhotite solubility in hydrous albite melts*. Unpubl. Ph.D. dissertation, Penn. State Univ.
- Bralia, G.S., G. Sabiti, and F. Troja 1979. The reevaluation of the Co:Ni ratio in pyrite as a geochemical tool in ore genesis problems. *Mineral. Deposita*, 14, 353-374.
- Branam, T.D., and E.M. Ripley 1990. Genesis of sediment-hosted copper mineralization of south-central Kansas: sulfur/carbon and sulfur isotope systematics. *Econ. Geol.*, 85, 601-621.
- Brand, U., and J. Veizer 1980. Chemical diagenesis of a multicomponent carbonate system — I. Trace elements. *J. Sed. Petrol.*, 50, 1219-1236.
- Brannon, J.C., F.A. Podosek, and R.K. McLimans 1992. Alleghenian age of the Upper Mississippi Valley zinc-lead deposit determined by Rb-Sr dating of sphalerite. *Nature*, 356, 509-511.
- Brannon, J.C., F.A. Podosek, and R.K. McLimans 1993. Age and isotopic composition of gangue versus ore minerals in the Upper Mississippi Valley Zn-Pb district. In *Geology and geochemistry of Mississippi Valley-type ore deposits*, K. Shelton and R. Hagni (eds.), Proc. Vol., 95-103. Rolla, Missouri: Univ. Missouri-Rolla Press.
- Brannon, J.C., S.C. Cole, F.A. Podosek, and K.C. Misra 1995. Radiometric dating of ancient calcite: Th-Pb and U-Pb isochrons for ore-stage and late-stage calcite from the Central Tennessee zinc district, an Appalachian-Ouachita age MVT deposit [abs.]. *Geol. Soc. Am. Abstracts with Programs*, 27, A-118.
- Brateman, P.S., A.G. Cairns-Smith, and R.W. Sloper 1983. Photo-oxidation of hydrated Fe^{2+} — significance for banded iron formations. *Nature*, 303, 163-164.
- Brateman, P.S., and A.G. Cairns-Smith 1987. Iron photoprecipitation and the genesis of banded iron formations. In *Precambrian iron-formations*, P. W. U. Appel and G. L. LaBerge (eds.), 215-245.
- Brathwaite, R.L. 1974. The geology and origin of the Rosebery ore deposit, Tasmania. *Econ. Geol.*, 69, 1086-1101.
- Bray, C.J., E.T.C. Spooner, and F.J. Longstaffe 1988. Unconformity-related uranium mineralization, McClean deposits, North Saskatchewan, Canada: hydrogen and oxygen isotope geochemistry. *Can. Mineral.* 26, 249-268.
- Bray, C.J., E.T.C. Spooner, C.M. Hall, D. York, T.M. Bills, and H.W. Krueger 1987. Laser probe $^{40}Ar/^{39}Ar$ and conventional K/Ar dating of illites associated with McClean unconformity-related uranium deposits, north Saskatchewan, Canada. *Can. J. Earth Sci.*, 24, 10-23.
- Breitkopf, J.H. 1988. Iron-formations related to mafic volcanism and ensiatic rifting in the southern margin zone of the Damara Orogen, Namibia. *Precamb. Res.*, 38, 111-130.
- Breitkopf, J.H., and K.J. Maiden 1988. Tectonic setting of the Matchless Belt pyritic copper deposits, Namibia. *Econ. Geol.*, 83, 710-723.
- Brenner, T.L., N.A. Teixeira, J.A.L. Oliveira, N.D. Franke, and J.F.H. Thompson 1990. The O'Toole nickel deposit, Morro de Ferro greenstone belt, Brazil. *Econ. Geol.*, 85, 904-920.
- Brett, R., and G. Kullerud 1966. Melting relations of galena-pyrite-pyrrhotite assemblages: a homogeneous sulfide melt at 718°C [abs.]. *Econ. Geol.*, 61, 1302.
- Bristol, C.C. 1979. Application of sphalerite geobarometry to ores from the Ruttan mine. *Econ. Geol.*, 74, 1496-1503.
- Brockie, D.C., E.H. Hare, Jr., and P.R. Dingess 1968. The geology and ore deposits of the Tri-state district of Missouri, Kansas, and Oklahoma. In *Ore Deposits of the United States, 1933-1967 (Graton-Sales Volume)*, J.D. Ridge (ed.), 400-430. New York: Am. Inst. Mining Metall. and Petroleum Engineers.
- Brookins, D. G. 1981. Primary uranophane from the Ambrosia Lake uranium district, Grants mineral belt, U.S.A. *Mineral. Deposita*, 16, 3-5.
- Brooks, C.K., and T.F.D. Nielsen 1982. The eastern Greenland continental margin: a transition between oceanic and continental magmatism. *Geol. Soc. London J.*, 139, 265-275.
- Brown, A.C. 1971. Zoning in the White Pine copper deposit, Ontonagon County, Michigan. *Econ. Geol.*, 66, 543-573.
- Brown, A.C. 1978. Stratiform copper deposits — evidence from their post-sedimentary origin. *Minerals Sci. Eng.*, 10, 172-181.
- Brown, A.C. 1984. Alternative sources of metals for stratiform copper deposits. *Precamb. Res.*, 25, 61-74.
- Brown, A.C. 1989. Sediment-hosted stratiform copper deposits: deposit-type name and related terminology. *Geol. Assoc. Canada Spec. Paper*, 36, 39-52.
- Brown, A.C. and F.M. Chartrand 1983. Stratiform copper deposits and interactions with co-existing atmospheres, hydrospheres, biospheres and lithospheres. *Precamb. Res.*, 20, 533-542.
- Brown, A.C. and F.M. Chartrand 1986. Sequence of mineralization in sediment-hosted copper deposits. Part I. Diagenetic features at White Pine (Michigan), Redstone (N.W. Territories, Canada) and Kamoto (Zaire). *Soc. For Geology Applied to Ore Deposits Spec. Publ.* 4, 390-397.
- Brown, D.A., G.A. Gross, and J.A. Sawicki 1995. A review of the microbial geochemistry of banded iron formations. *Can. Mineral.*, 33, 1321-1334.

- Brown, J.S. (ed.) 1967. Genesis of stratiform lead-zinc-barite-fluorite deposits. *Econ. Geol. Mono.* 3, 443p.
- Brown, M. 1980. Textural and geochemical evidence for the origin of some chromite deposits in the Oman ophiolite. In *International Ophiolite Symposium Proc.*, A. Panayiotou (ed.), 715-721. Nicosia: Cyprus Geol. Survey.
- Brown, P.E., E. Essene, and W. C. Kelly 1978. Sphalerite geobarometry in the Balmat-Edwards district, New York. *Am. Mineral.*, 63, 250-257.
- Browning, P., D.I. Groves, J.R. Blockley, and K.J.R. Rosman 1987. Lead isotopic constraints on the age and source of gold mineralization in the Archean Yilgarn Block, Western Australia. *Econ. Geol.*, 82, 971-986.
- Brynard, H.J., de Villiers, J.P.R., and Viljoen, E.A. 1976. A mineralogical investigation of the Merensky Reef at the Western Platinum mine, near Marikana, South Africa. *Econ. Geol.*, 71, 1299-1307.
- Bryndzia, L.T., S.D. Scott, and J.E. Farr 1983. Mineralogy, geochemistry, and mineral chemistry of siliceous ore and altered footwall rocks in the Uwamuki 2 and 4 deposits, Kosaka mine, Hokuroku district, Japan. *Econ. Geol. Mono.* 5, 507-522.
- Bryndzia, L.T., S.D. Scott, and P.G. Spry 1988. Sphalerite and hexagonal pyrrhotite geobarometer: experimental calibration and application to the metamorphosed sulfide ores of Broken Hill, Australia. *Econ. Geol.*, 83, 1193-1204.
- Bryndzia, L.T., S.D. Scott, and P.G. Spry 1990. Sphalerite and hexagonal pyrrhotite geobarometer: correction in calibration and application. *Econ. Geol.*, v. 85, p. 405-411.
- Bubela, B. 1981. Banded sulfide ores: the experimental formation of sulfide bands in sediments from flowing liquids. *Econ. Geol.*, 76, 171-172.
- Buchanan, D.L. 1979. Chromite production from the Bushveld Complex. *World Mining*, 32, 97-101.
- Buchanan, D.L., and J. Nolan 1979. Solubility of sulfur and sulfide immiscibility in synthetic tholeiitic melts and their relevance to Bushveld Complex rocks. *Can. Mineral.*, 17, 483-494.
- Buchanan, D.L. and J.E. Rouse 1984. Role of contamination in the precipitation of sulfides in the Platreef of the Bushveld Complex. In *Sulfide deposits in mafic and ultramafic rocks*, D. L. Buchanan and M. J. Jones (eds.), 141-146. London: Inst. Mining Metall.
- Buchanan, D.L., J. Nolan, N. Wilkinson, and J.P.R. de Villiers 1983. An experimental investigation of sulfur solubility as a function of temperature in synthetic silicate melts. *Geol. Soc. South Africa Spec. Pub.* 7, 383-391.
- Buchanan, L.J. 1979. *The Las Torres mine, Guanajuato, Mexico: ore controls of a fossil geothermal system*. Unpublished Ph.D. dissertation, Colorado School of Mines, Boulder, Colorado.
- Buchanan, L.J. 1981. Precious-metal deposits associated with volcanic environments in the southwest. In *Relations of tectonics to ore deposits in the southern Cordillera*, W. R. Dickinson and W. D. Payne (eds.), *Geol. Soc. Arizona Digest*, 14, 237-261.
- Buddington, A.F. 1931. The Adirondack magmatic stem. *J. Geol.*, 39, 240-263.
- Buddington, A.F. 1935. High-temperature mineral associations at shallow to moderate depths. *Econ. Geol.*, 30, 205-222.
- Buddington, A.F. and D.H. Lindsley 1964. Iron-titanium oxide minerals and synthetic equivalents. *J. Petrol.*, 5, 310-357.
- Bullis, H.R., R.A. Hureau, and B.D. Penner 1994. Distribution of gold and sulfides at Lupin, Northwest Territories. *Econ. Geol.*, 89, 1217-1227.
- Buntin, T.J., D.E. Grandstaff, G.C. Ulmer, and D.P. Gold 1985. A pilot study of geochemical and redox relationships between potholes and adjacent normal Merensky Reef of the Bushveld Complex. *Econ. Geol.*, 80, 975-987.
- Burke, W.H., R.E. Denison, E.A. Hetherington, R.B. Koepnick, H.F. Nelson, and J.B. Otto 1982. Variation of seawater $^{87}\text{Sr}/^{86}\text{Sr}$ throughout Phanerozoic time. *Geology*, 10, 516-519.
- Burnham, C.W. 1959. Metallogenic provinces of the south-western United States and northern Mexico. *New Mexico Bureau of Mines Bull.*, 65, 76p.
- Burnham, C.W. 1979. Magmas and hydrothermal fluids. In *Geochemistry of hydrothermal ore deposits*, 2nd edn., H.L. Barnes (ed.), 71-136. New York: Wiley.
- Burnham, C.W. 1981. Physicochemical constraints on porphyry mineralization. In *Relations of tectonics to ore deposits in the southern Cordillera*, R.W. Dickinson and W.D. Payne (eds.), *Arizona Geol. Soc. Digest*, 14, 71-77.
- Burnham, C.W. 1997. Magmas and hydrothermal fluids. In *Geochemistry of hydrothermal ore deposits*, 3rd edn., H.L. Barnes (ed.), 63-123. New York: Wiley.
- Burnham, C.W. and H. Ohmoto 1980. Late-stage processes of felsic magmatism. In *Granitic magmatism and related mineralization*, S. Ishihara and S. Takenouchi (eds.), *Mining Geol. Spec. Issue* 8, 1-11.
- Burnie, S.W., H.P. Schwarcz, and J.H. Crocket 1972. Sulfur isotopic study of the White Pine Mine, Michigan. *Econ. Geol.*, 67, 895-914.
- Burrows, D.R., and E.T.C. Spooner 1986. The McIntyre Cu-Au deposit, Timmins, Ontario, Canada. *Proc. Gold '86 Symposium*, Toronto, A.J. Macdonald (ed.), 23-39. Toronto: Konsult International Inc.

- Burrows, D.R., P.C. Wood, and E.T.C. Spooner 1986. Carbon isotope evidence for a magmatic origin for Archean gold-quartz vein ore deposits. *Nature*, 321, 851-854.
- Burst, J.F. 1969. Diagenesis of Gulf Coast clayey sediments and possible relation to petroleum migration. *Bull. Am. Assoc. Petroleum Geol.*, 53, 73-93.
- Burstein, I.B., K.L. Shelton, J.M. Gregg, and R.D. Hagni 1993. Complex, multiple ore fluids in the world class southeast Missouri Pb-Zn-Cu MVT deposits: sulfur isotope evidence. In *Geology and geochemistry of Mississippi Valley-type ore deposits, Proceedings Volume*, K.L. Shelton and R.D. Hagni (eds.), 1-15. Rolla: Univ. Missouri-Rolla Press.
- Burt, D.M. 1974. Metasomatic zoning in Ca-Fe-Si exoskarns. In *Geochemical transport and kinetics*, A. W. Hoffman (eds.), 287-293. Washington, D. C.: Carnegie Instn. Washington.
- Burt, D.M. 1977. Mineralogy and petrology of skarn deposits. *Soc. Italiana Mineralogia Petrologia Rendiconti*, 33, 859-873.
- Burt, D.M. 1978. Tin silicate-borate-oxide equilibria in skarns and greisens — the system $\text{CaO-SnO}_2\text{-SiO}_2\text{-H}_2\text{O-B}_2\text{O}_3\text{-CO}_2\text{-F}_2\text{O}$. *Econ. Geol.*, 73, 269-282.
- Burton, J.C., J.P. Lawler, and D.E. Ayres 1985. Genesis of Carlin-type gold deposits [abs.]. *Geol. Soc. Am. Abstracts with Programs*, 17, 536.
- Burton, J.C., L.A. Taylor, and I-Ming Chou, 1982. The $f\text{O}_2\text{-T}$ and $f\text{S}_2\text{-T}$ stability relations of hedenbergite and hedenbergite-johannesenite solid solutions. *Econ. Geol.*, 77, 764-783.
- Butler, B.S. and W.S. Burbank 1929. Relation of electrode potential of some elements to formation of hypogene mineral deposits. *Am. Inst. Mining Engineers Trans. Yearbook*, 341-356.
- Button, A., and S.S. Adams 1981. Geology and recognition criteria for uranium deposits of the quartz-pebble conglomerate type. *U.S. Dept. Energy National Uranium Resource Evaluation Report GJBX-3(81)*, 390 p.
- Button, A., T. D. Brock, P. J. Cook, H. P. Eugster, A. M. Goodwin, H. L. James, L. Margulis, K. H. Nealson, J. O. Nriagu, A. F. Trendall, and M. R. Walter 1982. Sedimentary iron deposits evaporites, and phosphorites: state of the art report. In *Mineral deposits and the evolution of the biosphere*, H. D. Holland and M. Schidlowski (eds.), 259-273. New York: Springer-Verlag.
- Byers, A. R., S. S. T. Kirkland, and W. J. Pearson 1965. Geology and mineral deposits of the Flin Flom area, Saskatchewan. *Saskatchewan Dept. Mineral Resources Rept.* 62, 95 p.
- Cabri, L.J. 1976. Glossary of platinum-group minerals. *Econ. Geol.*, 71, 1476-1480.
- Cabri, L.J. 1981. Analyses of minerals containing platinum-group elements. *Can. Inst. Mining Metall. Spec. Publ.* 23, 151-174.
- Cabri, L.J., and J.H.G. Laflamme 1976. The mineralogy of the platinum-group elements from the Deep Ore Zone, strathcona mine, Sudbury, Ontario. *Econ. Geol.*, 71, 1131-1158.
- Cahen, L., N.J. Snelling, J. Delhal, and J.R. Vail 1984. *The geochronology and evolution of Africa*. Cambridge: Oxford University Press.
- Cahn, R.W. 1971. Recovery and recrystallization. In *Physical metallurgy*, R.W. Cahn (ed.), 1129-1198. Amsterdam: North-Holland.
- Cairns-Smith, A.G. 1978. Precambrian solution photochemistry, inverse segregation, and banded iron-formation. *Nature*, 276, 807-808.
- Callahan, W.H. 1967. Some spatial and temporal aspects of the localization of Mississippi Valley-Appalachian type ore deposits. *Econ. Geol. Mono.* 3, 14-19.
- Cambel, B., and J. Jarkovsky 1968. Geochemistry of nickel and cobalt in pyrrhotites of different genetic types. *International Geol. Congress, 23rd.* (Prague), 6, 169-183.
- Cameron, E.M. 1983. Genesis of Proterozoic iron-formation: sulphur isotope evidence. *Geochim. Cosmochim. Acta*, 47, 1069-1074.
- Cameron, E.M. 1988. Archean gold: relation to granulite formation and redox zoning in the crust. *Geology*, 16, 109-112.
- Cameron, E.M. 1989. Scouring of gold from the lower crust. *Geology*, 17, 26-29.
- Cameron, E.M., and K. Hattori 1987a. Archean gold mineralization and oxidized hydrothermal fluids. *Econ. Geol.*, 82, 1177-1199.
- Cameron, E.M., and K. Hattori 1987b. Archean sulfur cycle: evidence from sulphate minerals and isotopically fractionated sulphides in Superior Province. *Isotope Geoscience*, 65, 341-358.
- Cameron, E.N. 1961. *Ore microscopy*. New York: Wiley.
- Cameron, E.N. 1980. Evolution of the Lower Critical Zone, Central Sector, Eastern Bushveld Complex, and its chromite deposits. *Econ. Geol.*, 75, 845-871.
- Cameron, E.N. and G.A. Desborough 1969. Occurrence and characteristics of chromite deposits — Eastern Bushveld Complex. *Econ. Geol. Mono.* 4, 23-40.
- Campbell, A., D. Rye, and U. Petersen 1984. A hydrogen and oxygen isotope study of the San Cristobal mine, Peru: implications of the role of water to rock ratio for the genesis of wolframite deposits. *Econ. Geol.*, 79, 1818-1832.
- Campbell, F.A., and V.G. Ethier 1983. Environment of deposition of the Sullivan orebody. *Mineral. Deposita*, 18, 39-55.

- Campbell, F.A., and V.G. Ethier 1984. Nickel and cobalt in pyrrhotite and pyrite from the Faro and Sullivan orebodies. *Can. Mineral.*, 22, 503-506.
- Campbell, F.A., V.G. Ethier, and H.R. Krouse 1980. The massive sulfide zone: Sullivan orebody. *Econ. Geol.*, 75, 916-926.
- Campbell, F.A., V.G. Ethier, H.F. Krouse, and R.A. Both 1978. Isotopic composition of sulfur in the Sullivan orebody, British Columbia. *Econ. Geol.*, 73, 246-268.
- Campbell, I.H. 1977. A study of micro-rhythmic layering and cumulate process in the Timberlana intrusion, Western Australia: I. The Upper Layered Series. *J. Petrol.*, 18, 183-215.
- Campbell, I.H. 1978. Some problems with cumulus theory. *Lithos*, 11, 311-323.
- Campbell, I.H. 1986. A fluid dynamic model for the potholes of the Merensky Reef. *Econ. Geol.*, 81, 1118-1125.
- Campbell, I.H., and S.J. Barnes 1984. A model for the geochemistry of platinum group elements in magmatic sulfide deposits. *Can. Mineral.*, 22, 151-160.
- Campbell, I.H., and A.J. Naldrett 1979. The influence of silicate:sulfide ratios on the geochemistry of magmatic sulfide deposits. *Econ. Geol.*, 74, 1503-1506.
- Campbell, I.H., A.J. Naldrett, and S.J. Barnes 1983. A model for the origin of the platinum-rich sulfide horizons in the Bushveld and Stillwater complexes. *J. Petrol.*, 24, 133-165.
- Campbell, I. H., J.M. Franklin, M.P. Gorton, T.R. Hart, and S.D. Scott 1981. The role of subvolcanic sills in the generation of massive sulfide deposits. *Econ. Geol.*, 76, 2248-2253.
- Campbell, N. 1967. Tectonics, reefs, and stratiform lead-zinc deposits of the Pine Point area, Canada. *Econ. Geol. Mono.* 3, 59-70.
- Campbell, W.R. 1993. Research drilling into the "fluid reservoir" of the Creede epithermal vein system, San Juan Mountains, Colorado. *Soc. Econ. Geol. Newsletter*, 13, 1 and 12-16.
- Candela, P.A. 1989. Felsic magmas, volatiles, and metallogenesis. *Rev. Econ. Geol.* 4, 223-233.
- Candela, P.A., and H.D. Holland 1984. The partitioning of copper and molybdenum between silicate melts and aqueous fluids. *Geochim. Cosmochim. Acta*, 48, 373-380.
- Candela, P.A., and H.D. Holland 1986. A mass-transfer model for copper and molybdenum in magmatic hydrothermal systems: the origin of porphyry-type ore deposits. *Econ. Geol.*, 81, 1-19.
- Cann, J.R., M.R. Sterns, and A. Rice 1985. A simple magma-driven thermal balance model for the formation of volcanogenic massive sulfides. *Earth Planet. Sci. Lett.*, 75, 123-134.
- Cannon, R.S., A.P. Pierce, T.C. Antweiler, and K.L. Buck 1961. The data of lead isotope geology related to problems of ore genesis. *Econ. Geol.*, 56, 1-38.
- Canuto, V.M., J.S. Levine, T.R. Augustsson, and C.L. Imhoff 1983. Oxygen and ozone in the early Earth's atmosphere. *Precamb. Res.*, 20, 109-120.
- Capobianco, C.J., and M.J. Drake 1990. Partitioning of ruthenium, rhodium, and palladium between spinel and silicate melt and implications for platinum group element fractionation trends. *Geochim. Cosmochim. Acta*, 54, 869-874.
- Card, K.D. 1990. A review of the Superior Province of the Canada Shield, a product of Archean accretion. *Precamb. Res.*, 48, 99-156.
- Card, K. D., K. H. Poulsen, and F. Robert 1989. The Archean Superior Province of the Canadian Shield and its lode gold deposits. *Econ. Geol. Mono.* 6, 19-36.
- Carlson, S.R., and F.J. Sawkins 1980. Mineralogic and fluid inclusion studies of the Turmalina Cu-Mo bearing breccia pipe, northern Peru. *Econ. Geol.*, 75, 1233-1238.
- Carmichael, I.S.E., F.J. Turner, and J. Verhoogen 1975. *Igneous petrology*. New York: McGraw Hill.
- Carne, R.C., and R.J. Cathro 1982. Sedimentary exhalative (sedex) zinc-lead-silver deposits, northern Canadian Cordillera. *Can. Inst. Mining Bull.*, 76, 66-78.
- Carpenter, A.B., M.L. Trout, and E. Pickett 1974. Preliminary report on the origin and chemical evolution of lead-and-zinc-rich oil field brines in Central Mississippi. *Econ. Geol.*, 69, 1191-1206.
- Carpenter, R.H. 1974. Pyrrhotite isograd in southeastern Tennessee and southwestern North Carolina. *Geol. Soc. Am. Bull.*, 85, 451-456.
- Carr, G.R., and J.W. Smith 1977. A comparative isotopic study of the Lady Loretta zinc-lead-silver deposit. *Mineral. Deposita*, 12, 105-110.
- Carr, H.W., D.I. Groves, and R.G. Cawthorn 1994. The importance of synmagmatic deformation in the formation of Merensky Reef potholes in the Bushveld Complex. *Econ. Geol.*, 89, 1398-1410.
- Carr, H.W., F.J. Kruger, D.I. Groves, and R.G. Cawthorn 1999. The petrogenesis of Merensky Reef potholes at the Western Platinum mine, Bushveld Complex: Sr-isotopic evidence for synmagmatic deformation. *Mineral. Deposita*, 34, 335-347.
- Carroll, M.R., and M.J. Rutherford 1985. Sulfide and silicate saturation in hydrous silicate melts. *J. Geophys. Res.*, 90, C601-C612.
- Carten, R.B., W.H. White, and H.J. Stein 1993. High-grade granite-related molybdenum systems: classification and origin. *Geol. Assoc. Canada Spec. Paper* 40, 521-554.
- Carten, R.B., E.P. Geraghty, B.M. Walker, and J.R. Shannon 1988. Cyclic generation of weakly and strongly mineralizing intrusions in the Henderson porphyry molybdenum deposit, Colorado: correlation of igneous features with high-temperature hydrothermal alteration. *Econ. Geol.*, 83, 266-296.

- Cassard, D., M. Rabinovitch, A. Nicholas, J. Moutte, M. Leblanc, and A. Prinzhofer 1981. Structural classification of chromite pods in southern New Caledonia. *Econ. Geol.*, 76, 805-831.
- Castro, L.O. 1994. Genesis of banded iron-formations. *Econ. Geol.*, 89, 1384-1397.
- Cathelineau, M., M-C Boiron, P. Holliger, P. Marion, and M. Denis 1989. Gold in arsenopyrites: crystal chemistry, location and state, physical and chemical conditions of deposition. *Econ. Geol. Mono.* 6, 328-341.
- Cathey, W. B. 1980. *Implications of the geology and geochemistry of the MacLean Five uranium deposit, Three Rivers, Texas.* Unpublished M.S. Thesis, Univ. of Tennessee, Knoxville, 125p.
- Cathles, L.M. 1977. An analysis of the cooling of intrusives by groundwater convection which includes boiling. *Econ. Geol.*, 72, 804-826.
- Cathles, L.M. 1981. Fluid flow and hydrothermal ore deposit genesis. *Econ. Geol. 75th Anniv. Vol.*, 424-457.
- Cathles, L.M. 1993. A capless 350°C flow zone model to explain megaplumes, salinity variations, and high temperature veins in ridge axis hydrothermal systems. *Econ. Geol.*, 88, 1977-1988.
- Cathles, L.M., and A.T. Smith 1983. Thermal constraints on the formation of Mississippi Valley-type lead-zinc deposits and their implications for episodic basin dewatering and deposit genesis. *Econ. Geol.*, 78, 983-1002.
- Cathles, L.M., III, S. Oszczepalski, and E.C. Jowett 1993. Mass balance evaluation of late diagenetic hypothesis for Kupferschiefer Cu mineralization in the Lubin Basin of southwestern Poland. *Econ. Geol.*, 88, 948-956.
- Cathles, L.M., A.L. Guber, T.C. Lenagh, and F.O. Dudás 1983. Kuroko-type massive sulfide deposits of Japan: products of an aborted island-arc rift. *Econ. Geol. Mono.* 5, 96-114.
- Caulfield, J.B.D., A.P. LetHuray, and D.M. Rye 1986. A review of lead and sulphur isotope investigations of Irish sediment-hosted base metal deposits with new data from the Keel, Ballinalack, Moyvoughly, and Tatestown deposits. In *Geology and genesis of mineral deposits in Ireland.* C.J. Andrew et al. (ed.), 591-616. Dublin: Irish Assoc. Econ. Geol.
- Cawthorn, R.G. 1975. Degrees of melting in mantle diapirs and the origin of ultrabasic liquids. *Earth Planet. Sci. Lett.*, 27, 113-120.
- Cawthorn, R.G. and C. Lee 1998 (eds.). *Bushveld Complex excursion field guide*, 8th International Platinum Symposium, June 28-July 3, 1998. Johannesburg: Geol. Soc. S. Africa.
- Cawthorn, R.G. and T.S. McCarthy 1985. Incompatible trace element behavior in the Bushveld Complex. *Econ. Geol.*, 80, 1016-1026.
- Cawthorn, R.G., G. Davies, A.R. Clublely-Armstrong, and T.S. McCarthy 1981. Sills associated with the Bushveld Complex, South Africa: an estimate of the parental magma compositions. *Lithos*, 14, 1-15.
- Chai, G., and A.J. Naldrett 1992. Characteristics of Ni-Cu-PGE mineralization and genesis of the Jinchuan deposit, northwest China. *Econ. Geol.*, 87, 1475-1495.
- Chakraborty, K.L. and T.L. Chakraborty 1984. Geological features and origin of the chromite deposits of Sukinda Valley, Orissa, India. *Mineral. Deposita*, 19, 256-265.
- Chakraborty, K. L., and T. Majumder 1986. Geological aspects of the banded iron-formation of Bihar and Orissa. *J. Geol. Soc. India*, 28, 109-133.
- Changkakoti, A., J. Gray, D. Krstic, G.L. Cumming, and R.D. Morton 1988. Determination of radiogenic isotopes (Rb/Sr, Sm/Nd and Pb/Pb) in fluid inclusion waters: an example from the Blue Bell Pb-Zn deposit, British Columbia, Canada. *Geochim. Cosmochim. Acta*, 52, 961-967.
- Chartrand, F.M., and A.C. Brown 1985. The diagenetic origin of stratiform copper mineralization, Coates Lake, Redstone Copper Belt, N.W.T., Canada. *Econ. Geol.*, 80, 325-343.
- Chartrand, F.M., A.C. Brown, and R.V. Kirkham 1989. Diagenesis, sulphides, and metal zoning in the Redstone copper deposit, Northwest Territories. *Geol. Assoc. Canada Spec. Paper* 36, 189-206.
- Chase, C.G., and T.H. Gilmer 1973. Precambrian plate tectonics: the Midcontinent Gravity High. *Earth Planet. Sci. Lett.*, 21, 70-78.
- Chase, M.W., J.L. Curnutt, H. Prophet, R.A. McDonald, and A.N. Syverud 1975a. JANAF thermochemical tables, 1975 supplement. *J. Phys. Chem. Ref. Data*, 4, 1-176.
- Chase, M.W., J.L. Curnutt, R.A. McDonald, A.N. Syverud, and E.A. Valenzuela 1975b. JANAF thermochemical tables, 1978 supplement. *J. Phys. Chem. Ref. Data*, 7, 793-940.
- Chase, M.W., J.L. Curnutt, J.R. Downey, Jr., R.A. McDonald, and A.N. Syverud 1975c. JANAF thermochemical tables, 1982 supplement. *J. Phys. Chem. Ref. Data*, 11, 695-940.
- Chase M.W., J.L. Curnutt, A.T. Hu, H. Prophet, A.N. Syverud, and L.C. Walker 1974. JANAF thermochemical tables, 1974 supplement. *J. Phys. Chem. Ref. Data*, 3, 311-480.
- Chauhan, D.S. 1984. Sedimentary pyrite from Pb-Zn deposits of the Zawar and Rajpura-Dariba regions and its bearing on the genesis of base metal sulfides. In *Syngeneses and epigenesis in the formation of mineral deposits*, A. Wauschkuhn, C. Luth, and R.A. Zimmermann (eds.), 36-42. Berlin: Springer-Verlag.
- Chauvel, C., B. Dupre, and G.A. Jenner 1985. The Sm-Nd age of Kambalda volcanics is 500 Ma too old! *Earth Planet. Sci. Lett.*, 74, 315-324.

- Chen, J.H., G.J. Wasserburg, K.L. von Damm, and J.M. Edmond 1986. The U-Th-Pb systematics in hot springs on the East Pacific Rise at 21°N and Guaymas Basin. *Geochim. Cosmochim. Acta*, 50, 2467-2479.
- Chesley, J.T., A.N. Halliday, T.K. Kyser, and P.G. Spry 1994. Direct dating of Mississippi Valley-type mineralization: use of Sm-Nd in fluorite. *Econ. Geol.*, 89, 1192-1199.
- Chi, G., J. Guha, and H-Z. Lu 1993. Separation mechanism in the formation of proximaland distal tin polymetallic deposits, Xinlu ore field, southern China — evidence from fluid inclusion data. *Econ. Geol.*, 88, 916-933.
- Christensen, J.N., A.N. Halliday, S.E. Kesler, and D.F. Sangster 1993. Further evaluation of the Rb-Sr dating of sphalerite: the Nanisivik Precambrian MVT deposit, Baffin Island, Canada [abs.]. *Geol. Soc. Am. Abstracts with Programs*, 25, 471.
- Christensen, J.N., A.N. Halliday, and S.E. Kesler 1995. Rb-Sr dating of sphalerite and the ages of MVT's. *Extended Abstracts, International Field Conference on Carbonate Hosted Lead-Zinc Deposits*, Soc. Econ. Geol., St. Louis, Missouri, June 3-7, 1995, 41-44.
- Christensen, J.N., A.N. Halliday, and S.E. Kesler 1997. Rb-Sr dating of sphalerite and the ages of Mississippi-Valley-type Pb-Zn deposits. *Soc. Econ. Geol. Spec. Publ.* 4, 527-535.
- Christensen, J.N., A.N. Halliday, S.E. Kesler, and J.R. Vernacombe 1994. Age of mineralization in the Canning Basin, Australia: Rb-Sr analysis of sphalerite from the Blendevale deposit [abs.]. *Geol. Soc. Am. Abstracts with Programs*, 26, 381.
- Christensen, O.D. 1993. Carlin Trend geologic overview. In *Gold deposits of the Carlin Trend, Nevada*, O.D. Christensen (ed.), *Econ. Geol. Guidebook Series*, 18, 12-26.
- Churnet, H.G. 1985. Fluid inclusion evidence for fluid mixing, Mascot-Jefferson City zinc district, Tennessee — a discussion. *Econ. Geol.*, 80, 1440-1443.
- Churnet, H.G., and K.C. Misra 1981. Genetic implications of the trace element distribution pattern in the Upper Knox carbonate rocks, Copper Ridge district, East Tennessee. *Sed. Geol.*, 30, 173-194.
- Churnet, H.G., and K.C. Misra 1983. Sphalerite mineralization and its relationship to carbonate facies boundaries, Copper Ridge district, East Tennessee. In *International Conference on Mississippi Valley-type lead-zinc deposits — Proc. Vol.*, G. Kisvarsanyi et al. (eds.), 360-372. Rolla, Missouri: Univ. Missouri-Rolla Press.
- Churnet, H.G., K.C. Misra, and K.R. Walker 1982. Deposition and dolomitization of Upper Knox carbonate sediments, Copper Ridge district, East Tennessee. *Geol. Soc. Am. Bull.*, 93, 76-86.
- Chyba, C.F. 1987. The cometary contribution to the oceans of primitive Earth. *Nature*, 330, 632-635.
- Clark, A.H., and E. Farrar 1973. The Bolivian tin province; notes on the available geochronological data. *Econ. Geol.*, 68, 102-106.
- Clark, B.R., and W.C. Kelly 1973. Sulfide deformation studies: I. Experimental deformation of pyrrhotite and sphalerite to 2,000 bars and 500°C. *Econ. Geol.*, 68, 332-352.
- Clark, B.R., F.R. Price, and W.C. Kelly 1977. Effects of annealing on deformation textures in galena. *Contrib. Mineral. Petrol.*, 64, 149-165.
- Clark, L.A. 1960a. The Fe-As-S system: phase relations and applications. *Econ. Geol.*, 55, 1345-1381 and 1631-1652.
- Clark, L. A. 1960b. The Fe-As-S system. Variations of arsenopyrite composition as a function of T and P. *Carnegie Inst. Washington Year Book* 59, 127-130.
- Clark, T., and A. J. Naldreit 1972. The distribution of Fe and Ni between synthetic olivine and sulfide at 900°C. *Econ. Geol.*, 67, 939-952.
- Claypool, G.E., W.T. Holser, J.R. Kaplan, H. Sakai, and I. Zak 1980. The age curves of sulfur and oxygen isotopes in marine sulfate and their mutual interpretations. *Chem. Geol.*, 28, 199-260.
- Clayton, R.H., and L. Thorpe 1982. Geology of the Nanisivik zinc-lead deposit. *Geol. Assoc. Canada Spec. Pap.* 25, 739-760.
- Clayton, R.N., L.J.P. Muffler, and D.E. White 1968. Oxygen isotopic study of calcite and silicates of the River Ranch No. 1 well, Salton Sea geothermal field, California. *Am. J. Sci.*, 266, 968-979.
- Clement, C.R., E.M.W. Skinner, and B.H. Scott Smith 1984. Kimberlite redefined. *J. Geol.*, 32, 223-228.
- Clemmey, H 1974. Sedimentary geology of a Late Precambrian copper deposit at Kitwe, Zambia. In *Gisements stratiformes et provinces cuprifères*, P. Bartholomé (ed.), 255-266. Liege: Soc. Géol Belgique.
- Clemmey, H. 1981. Some aspects of the genesis of heavy mineral assemblages in Lower Proterozoic uranium-gold conglomerates. *Mineral. Mag.* 44, 399-403.
- Cledenin, C.W., and M.J. Duane 1990. Focused fluid flow and Ozark Mississippi Valley-type deposits. *Geology*, 18, 116-119.
- Cledenin, C.W., C.A. Niwendorp, M.J. Dunne, and G.R. Lowell 1994. The paleohydrology of southeast Missouri Mississippi Valley-type deposits: interplay of faults, fluids, and adjoining lithologies. *Econ. Geol.*, 89, 322-331.
- Cline, J.S., and R.W. Bodnar 1991. Can economic porphyry copper mineralization be generated by a typical calc-alkaline melt? *J. Geophys. Res.*, 96, 8113-8126.

- Cline, J.S., and R.J. Bodnar 1994. Direct evolution of brine from a crystallizing silicate melt at the Questa, New Mexico, molybdenum deposit. *Econ. Geol.*, 89, 1780-1802.
- Coetzee, J., and D. Twist 1989. Disseminated tin mineralization in the roof of the Bushveld Granite pluton at the Zaaiploots mine, with implications for the genesis of magmatic hydrothermal tin systems. *Econ. Geol.*, 84, 1817-1834.
- Cole, D. R., and S. E. Drummond 1986. The effect of transport and boiling on Ag/Au ratios in hydrothermal solutions: a preliminary assessment and possible implications for the formation of epithermal precious-metal ore deposits. *J. Geochem. Exploration*, 25, 45-79.
- Coleman, R.C., and M. Delevaux 1957. Occurrence of selenium in sulfides from some sedimentary rocks of the Western United States. *Econ. Geol.*, 52, 499-527.
- Coleman, R. G. 1957. Mineralogical evidence on the temperature of formation of the Colorado Plateau uranium deposits. *Econ. Geol.*, 52, 1-4.
- Coleman, R.G. 1977. *Ophiolites: ancient oceanic lithosphere?* New York: Springer-Verlag.
- Coleman, R.G. 1984. The diversity of ophiolites. *Geol. Mijnbouw*, 63, 141-150.
- Collins, P. L. F. 1979. Gas hydrates in CO₂-bearing fluid inclusions and the use of freezing for estimation of salinity. *Econ. Geol.*, 74, 1435-1444.
- Colvine, A.C. 1989. An empirical model for the formation of Archean gold deposits: products of final cratonization of the Superior Province, Canada. *Econ. Geol. Mono.* 6, 37-53.
- Colvine, A.C., A.J. Andrews, M.E. Cherry, M.E. Durocher, A.J. Fyon, M.J. Lavigne, A.J. Macdonald, S. Marmont, K.H. Poulson, J.S. Springer, and D.G. Troop 1984. An integrated model for the origin of Archean gold deposits. *Ontario Geol. Survey Open File Report* 5524, 98p.
- Colvine, A. C., J. A. Fyon, K. B. Heather, S. Marmont, P. M. Smith, and D. G. Troop 1988. Archean lode gold deposits in Ontario. *Ontario Geol. Survey Misc. Paper* 139, 136p.
- Cominco Staff 1972. An outline of the geology of the Sullivan mine, Kimberley, British Columbia. In *Major lead-zinc deposits of Western Canada, 24th International Geol. Congress Guidebook for Field Excursion A*, 24-C, 26-36.
- Compton, W.S., I.S. Williams, I.H. Campbell, and J.J. Gresham 1986. Zircon xenocrysts from the Kambalda volcanics: age constraints and direct evidence for older continental crust below the Kambalda-Norseman greenstones. *Earth Planet. Sci. Lett.*, 76, 299-311.
- Coney, P.J. 1976. Plate tectonics and the Laramide orogeny. *New Mexico Geol. Soc. Spec. Publ.* 6, 5-10.
- Coney, P.J. and S.J. Reynolds 1977. Cordilleran Benioff zones. *Nature*, 270, 403-406.
- Connan, J. 1989. Genetic relation between oil and ore in some Pb-Zn-Ba ore deposits. *Geol. Soc. S. Africa Spec. Publ.* 5, 263-274.
- Connors, K.A., D.C. Noble, S.D. Bussey, and S.I. Weiss 1993. Initial gold contents of silicic volcanic rocks: bearing on the behavior of gold in magmatic systems. *Geology*, 21, 937-940.
- Conrad, M.E., U. Petersen, and J.R. O'Neil 1992. Evolution of an Au-Ag-producing hydrothermal system: the Tayollita mine, Durango, Mexico. *Econ. Geol.*, 87, 1451-1474.
- Constantinou, G. 1980. Metallogenesis associated with Troodos ophiolite. In *International Ophiolite Symp. Proc.*, A. Panayiotou (ed.), 663-673. Nicosia: Cyprus Geol. Survey.
- Constantinou, G. and G.J.S. Govett 1973. Geology, geochemistry, and genesis of Cyprus sulfide deposits. *Econ. Geol.*, 68, 843-858.
- Constantopoulos, J., and P.B. Larson 1991. Oxygen and hydrogen isotope geochemistry of the Star-Morning mine, Coeur d'Alene mining district, Idaho. *Geology*, 19, 131-134.
- Cook, N.J., C. Halls, and P.O. Kaspersen 1990. The geology of the Sulitjelma ore field, northern Norway — some new interpretations. *Econ. Geol.*, 85, 1720-1737.
- Cook, P.J., and M.W. McElhinny 1979. A reevaluation of the spatial and temporal distribution of sedimentary phosphate deposits in the light of plate tectonics. *Econ. Geol.*, 74, 315-330.
- Cooke, D.R., S.W. Bull, S.D. Donovan, and J.R. Rogers 1998. K-metasomatism and base metal depletion in volcanic rocks from the McArthur Basin, Northern Territory — implications for base metal mineralization. *Econ. Geol.*, 93, 1237-1263.
- Cooper, J.A., and J.R. Richards 1969. Lead isotope measurements on volcanics and associated galenas from the Coromandel-Te-Aroha region, New Zealand. *Geochem. J.*, 3, 1-14.
- Costa, U. R., R. L. Barnett, and R. Kerrich 1983. The Mattagami Lake mine Archean Zn-Cu sulfide deposit, Quebec: hydrothermal coprecipitation of talc and sulfides in a sea-floor brine pool — evidence from geochemistry, ¹⁸O/¹⁶O, and mineral chemistry. *Econ. Geol.*, 78, 1144-1203.
- Cotterill, P. 1969. The chromite deposits of Selukwe, Rhodesia. *Econ. Geol. Mono.* 4, 154-186.
- Cowden, A. 1988. Emplacement of komatiite lava flows and associated nickel sulfides at Kambalda, Western Australia. *Econ. Geol.*, 83, 430-442.
- Cowden, A., and N. T. Archibald 1987. Massive-sulfide fabrics at Kambalda and their relevance to the inferred stability of monosulfide solid-solution. *Can. Mineral.*, 25, 37-50.
- Cowden, A., and P. Woolrich 1987. Geochemistry of the Kambalda iron-nickel sulfides: implications for models of sulfide-silicate partitioning. *Can. Mineral.*, 25, 21-36.

- Cowden, A., M.J. Donaldson, A.J. Naldrett, and I.H. Campbell 1986. Platinum-group elements and gold in the komatiite-hosted Fe-Ni-Cu sulfide deposits at Kambalda, Western Australia. *Econ. Geol.*, 81, 1226-1235.
- Cox, D.P., and D.A. Singer 1992. Gold — Distribution of gold in porphyry copper deposits. *U.S. Geol. Survey Bull.* 1877, C1-C14.
- Cox, S.F. 1987. Flow mechanisms in sulfide minerals. *Ore Geol. Rev.*, 2, 133-171.
- Cox, S.F., M.A. Etheridge, V.J. Wall 1987. The role of fluids in syntectonic mass transport, and the localization of metamorphic vein-type ore deposits. *Ore Geol. Rev.*, 2, 65-86.
- Craig, H. 1961. Isotopic variations in meteoric waters. *Science*, 133, 1702-1703.
- Craig, H. 1966. Isotopic composition and origin of the Red Sea and Salton Sea geothermal brines. *Science*, 154, 1544-1548.
- Craig, H. 1969. Geochemistry and origin of Red Sea brines. In *Hot brines and recent heavy metal deposits in the Red Sea*, E.T. Degens and D.A. Ross (eds.), 208-242. Berlin: Springer-Verlag.
- Craig, J.R. 1973. Pyrite-pentlandite and other low-temperature relations in the Fe-Ni-S system. *Am. J. Sci.*, 273-A, 496-510.
- Craig, J.R. 1983. Metamorphic features in Appalachian massive sulfides. *Min. Mag.*, 47, 515-525.
- Craig, J.R., and G. Kullerud 1969. Phase relations in the Cu-Fe-Ni-S system and their application to magmatic ore deposits. *Econ. Geol. Mono.* 4, 344-358.
- Craig, J.R. and D. J. Vaughan 1994. *Ore microscopy and ore petrography*, 2nd. edn. New York: Wiley.
- Craig, J.R., T.N. Solberg, and D.J. Vaughan 1983. Growth characteristics of sphalerites in Appalachian zinc deposits. In *International Conference on Mississippi Valley-type lead-zinc deposits — Proc. Vol.*, G. Kisvarsanyi et al. (eds.), 317-327. Rolla, Missouri: Univ. Missouri-Rolla Press.
- Cranstone, D. A. and A. Turek 1976. Geological and geochronological relationships of the Thompson nickel belt, Manitoba. *Can. J. Earth Sci.*, 5, 439-453.
- Crawford, J., R.E. Fulweiler, and H.W. Miller 1969. Mine geology of the New Jersey Zinc Company's Jefferson City mine. *Tenn. Div. Geol. Rept. Inv.* 23, 64-75.
- Crawford, M.L. 1981. Phase equilibria in aqueous fluid inclusions. In *Short course in fluid inclusions: applications to petrology*, L. S. Hollister and M. L. Crawford (eds.), 75-100. Calgary: Mineral. Assoc. Canada.
- Creasey, S.C. 1959. Some phase relations in hydrothermally altered rocks of porphyry copper deposits. *Econ. Geol.*, 54, 351-373.
- Crerar, D.A., and H.L. Barnes 1976. Ore solution chemistry V. Solubilities of chalcopyrite and chalcocite assemblages in hydrothermal solution at 200° to 350°C. *Econ. Geol.*, 71, 772-794.
- Criss, R.E., and H.P. Taylor, Jr. 1986. Meteoric-hydrothermal systems. *Reviews in Mineralogy*, 16, 373-424.
- Crocket, J.H. 1981. Geochemistry of platinum-group elements. In *Platinum group elements: mineralogy, geology, and recovery*, L. Cabri (ed.). *Can. Inst. Min. Metall. Spec. Vol.* 23, 47-64.
- Crocket, J.H., M.E. Fleet, and W. Stone 1992. Experimental partitioning of osmium, iridium and gold between basalt melt and sulfide liquid at 1300°C. *Australian J. Earth Sci.*, 39, 427-432.
- Crowe, D.E. 1994. Preservation of original hydrothermal $\delta^{34}\text{S}$ values in greenschist to upper amphibolite volcanogenic massive sulfide deposits. *Geology*, 22, 873-876.
- Croxford, N.J.W., and S. Jephcott 1972. The McArthur lead-zinc-silver deposit, Northern Territory, Australia. *Proc. Australian Inst. Mining Metall.*, 243, 1-26.
- Croxford, N.J.W., B.L. Gulson, and J.W. Smith 1975. The McArthur River deposit: a review of the current situation. *Mineral. Deposita*, 10, 302-304.
- Cumming, J.L., and J.R. Richards 1975. Ore lead isotope ratios in a continuously changing earth. *Earth Planet. Sci. Lett.*, 28, 155-171.
- Cunningham, C.G. 1978. Pressure gradients and boiling as mechanisms for localizing ore in porphyry systems. *U.S. Geol. Survey J. Res.*, 6, 745-754.
- Cunningham, C.G., R.P. Ashley, I.M. Chou, Z. Huang, C. Wan, and W. Li 1988. Newly discovered sedimentary-rock hosted disseminated gold deposits in the People's Republic of China. *Econ. Geol.*, 83, 1462-1467.
- Curtis, L., and A. R. Miller 1980. Uranium geology in the Amer-Dubawnt-Yathkyed-Baker Lake region, Keewatin district, N. W.T., Canada. In *Uranium in the Pine Creek geosyncline*, J. Ferguson, and A. B. Goley (eds.), 595-616. Vienna: International Atomic Energy Agency.
- Czamanske, G.K., and P. Mihalik 1972. Oxidation during magmatic differentiation, Finnmarka Complex, Oslo area, Norway: Part I, The opaque oxides. *J. Petrol.*, 13, 493-509.
- Czamanske, G.K., and J.G. Moore 1977. Composition and phase chemistry of sulfide globules in basalt from the Mid-Atlantic Ridge rift valley near 37°N lat. *Geol. Soc. Am. Bull.*, 88, 587-599.
- Czamanske, G.K., and R.O. Rye 1974. Experimentally determined sulfur isotopic fractionations between sphalerite and galena in the temperature range 600°C to 275°C. *Econ. Geol.*, 69, 17-25.
- Czamanske, G.K., G.R. Himmelberg, and F.E. Goff 1976. Zoned Cr, Fe-spinel from the La Perouse layered gabbro, Fairweather Range, Alaska. *Earth Planet. Sci. Lett.*, 33, 111-118.

- Czamanske, G.K., E. Roedder and F.C. Burns 1963. Neutron activation analysis of fluid inclusions for copper, manganese, and zinc. *Science*, 140, 401-403.
- Dahl, P.S. 1979. Comparative geothermometry based on major-element and oxygen isotope distributions in Precambrian metamorphic rocks from southwestern Montana. *Am. Mineral.*, 64, 1280-1293.
- Dahlkamp, F.J. 1978a. Classification of uranium deposits. *Mineral. Deposita*, 13, 83-104.
- Dahlkamp, F.J. 1978b. Geological appraisal of the Key Lake U-Ni deposits, northern Saskatchewan. *Econ. Geol.*, 73, 1430-1449.
- Dallmeyer, R.D. 1979. $^{40}\text{Ar}/^{39}\text{Ar}$ dating: principles, techniques, and applications in orogenic terranes. In *Lectures in isotope Geology*, E.J. Nger and J.C. Hunziker (eds.), 77-104. Berlin: Springer-Verlag.
- Dairymple, G.B., and M.A. Lanphere 1974. $^{40}\text{Ar}/^{39}\text{Ar}$ technique of K/Ar dating: a comparison with the conventional technique. *Earth Planet. Sci. Lett.*, 12, 300-308.
- Daly, R.A. 1933. *Igneous rocks and the depths of the earth*. New York: McGraw Hill.
- Damon, P.E., M. Shafiqullah, and K.F. Clark 1981. Age trends of igneous activity in relation to metallogenesis in the southern Cordillera. In *Relations of tectonics to ore deposits in the southern Cordillera*, W. R. Dickinson and W. D. Payne (eds.), *Arizona Geol. Soc. Digest* 14, 173-154.
- Danielson, M.J. 1975. King Island scheelite deposits. In *Economic geology of Australia and Papua, New Guinea, I. Metals*, C.L. Knight (ed.), *Austral. Inst. Mining Metall. Mono.* 5, 592-598.
- Danielson, A., P. Moller, and P. Dulski 1992. The europium anomalies in banded iron formations and the thermal history of the oceanic crust. *Chem. Geol.*, 97, 89-100.
- Dasgupta, H.C. 1970. Influence of temperature and oxygen fugacity on the fractionation of manganese between coexisting titaniferous magnetite and ilmenite. *J. Geol.*, 78, 243-249.
- Davidson, C.F. 1962. On the cobalt:nickel ratio in ore deposits. *Mining Mag.*, 106, 78-85.
- Davidson, C.F. 1966. Some genetic relationships between ore deposits and evaporites. *Inst. Mining Metall. Trans.*, 75, B216-B225.
- Davies, G., and M. Tredoux 1985. The platinum group element and gold contents of the marginal rocks and sills of the Bushveld Complex. *Econ. Geol.*, 80, 838-848.
- Davies, J.L., and A.L. McAllister 1980. Geology and massive sulphides of the Bathurst area, New Brunswick. *Geol. Assoc. Canada Annual Mtg.*, 1980, Halifax, *Field Trip Guidebook* 16, 1-16.
- Davis, B. 1986. *Carbonate-replacement mechanism and structure of the Renison-Bell deposit, Tasmania, Australia*. Unpublished Ph.D. thesis, James Cook Univ, Australia.
- Davis, J.H. 1977. Genesis of the Southeast Missouri lead deposits. *Econ. Geol.*, 72, 443-450.
- Dawson, J.B. 1962. as from Oldinyo Lengai, Tanganyika. *Nature*, 195, 1075-1076.
- Dawson, J.B. 1980. *Kimberlites and their xenoliths*. Berlin: Springer-Verlag.
- Dawson, J.B., H. Pinkerton, D.M. Pyle, and C. Nyamweru 1994. June 1993 eruption of Oldoinyo Lengai, Tanzania: exceptionally viscous and large carbonatite lava flows and evidence for coexisting silicate and carbonate magmas. *Geology*, 22, 799-802.
- De Geoffroy, J., and T.K. Wignall 1972. A statistical study of geological characteristics of porphyry copper-molybdenum deposits in the Cordilleran belt — application to the rating of porphyry prospects. *Econ. Geol.*, 67, 656-668.
- Deans, T. 1966. Economic mineralogy of African carbonatites. In *Carbonatites*, O.F. Tuttle and J. Gittins (eds.), 385-413. New York: Interscience.
- Deb, M. and S.C. Sarkar 1990. Proterozoic tectonic evolution and metallogenesis in the Aravalli-Delhi orogenic complex, northwestern India. *Precamb. Res.*, 46, 115-137.
- Deines, P. 1989. Stable isotope variations in carbonatites. In *Carbonatites*, K. Bell (ed.), 301-359. London: Unwin Hyman.
- Deloule, E., and D.L. Turcotte 1989. The flow of hot brines in cracks and the formation of ore deposits. *Econ. Geol.*, 84, 2217-2225.
- Deloule, E., C. Allegre, and B. Doe 1986. Lead and sulfur isotope microstratigraphy in galena crystals from Mississippi Valley-type deposits. *Econ. Geol.*, 81, 1307-1321.
- Delvevaux, M.H., B.R. Doe, and G.F. Brown 1967. Preliminary lead-isotope investigations of brine from the Red Sea, galena from the Kingdom of Saudi Arabia, and galena from United Arab Republic (Egypt). *Earth Planet. Sci. Lett.*, 3, 139-144.
- DePaolo, D.J., and G.J. Wasserburg 1979. Neodymium isotopes in flood basalts from the Siberian platform and inferences about their mantle sources. *Proc. National Acad. Sci. USA* 76, 3056-3060.
- Derbikov, L.V., and Y.A. Nuravyeva 1967. Paravolcanic zoning in volcanic-sedimentary ore deposits. *Akad. Nauk SSSR Doklady Earth Sci.*, Sec. 176, 103-105.
- Derry, D.R. 1980. Uranium deposits through time. *Geol. Assoc. Canada Spec. Paper* 20, 625-632.
- Derry, L.A., and S.B. Jacobson 1990. The chemical evolution of seawater: evidence from REEs in banded iron formations. *Geochim. Cosmochim. Acta*, 54, 2965-2977.
- Descarreaux, J. 1973. A petrochemical study of the Abitibi volcanic belt and its bearing on the occurrence of massive sulphide ores. *Can. Inst. Mining Bull.*, 66, No. 730, 61-69.
- DeSitter, L.U. 1947. Diagenesis of oil field brines. *Am. Assoc. Petroleum Geol. Bull.*, 31, 2030-2040.

- Devaraju, T. C., and K. Laajoki 1986. Mineralogy and mineral chemistry of the manganese-poor and manganese-rich iron-formations from the high grade metamorphic terrain of southern Karnataka, India. *J. Geol. Soc. India*, 28, 134-164.
- DeVoto, R.H. 1978a. *Uranium Geology and exploration*. Golden, Colorado: Colorado School of Mines.
- DeVoto, R.H. 1978b. Uranium in Phanerozoic sandstone and volcanic rocks. *Mineral. Assoc. Canada Short Course Handbook*, 3, 293-306.
- Dewey, J.F. 1976. Ophiolite subduction. *Tectonophysics*, 31, 93-120.
- Dexter-Dyer, B., M. Kretzschmar, and W.E. Krumbein 1984. Possible microbial pathways in the formations of Precambrian ore deposits. *J. Geol. Soc. London*, 141, 251-262.
- Dick, H.J.B., and T. Bullen 1984. Chromium spinel as a petrogenetic indicator in abyssal and alpine-type peridotites and spatially associated lavas. *Contrib. Mineral. Petrol.*, 86, 54-76.
- Dick, L.A., and C.J. Hodgson 1982. The MacTung W-Cu (Zn) contact metasomatic and related deposits of the northeastern Canadian Cordillera. *Econ. Geol.*, 77, 845-867.
- Dickey, J.S., Jr. 1975. An hypothesis of origin for podiform chromite deposits. *Geochim. Cosmochim. Acta*, 39, 1061-1074.
- Dickinson, W.R., and W.S. Snyder 1978. Plate tectonics of the Laramide orogeny. *Geol. Soc. Am. Mem.* 151, 355-366.
- Dietz, R.S. 1984. Sudbury Structure as an astrobleme. *J. Geol.*, 72, 412-434.
- Dillon-Leitch, H.C.H., D.H. Watkinson, and C.J.A. Coats 1986. Distribution of platinum-group elements in the Donaldson West deposit, Cape Smith Belt, Quebec. *Econ. Geol.*, 81, 1147-1158.
- Dimroth, E. 1975. Paleo-Environment of iron-rich sedimentary rocks. *Geol. Rundschau*, 64, 751-767.
- Dimroth, E. 1977a. Facies models. 5. Models of physical sedimentation of iron-formations. *GeoScience Canada*, 4, 23-30.
- Dimroth, E. 1977b. Facies models. 6. Diagenetic facies of iron-formation. *GeoScience Canada*, 4, 83-88.
- Dimroth, E. 1979. Significance of diagenesis for the origin of Witwatersrand-type uraniferous conglomerates. *Phil. Trans. Royal Soc. London. Ser. A*, 291, 277-287.
- Dinur, D., B. Spiro, and Z. Aizenshtat 1980. The distribution and isotopic composition of sulfur in organic-rich sedimentary rocks. *Chem. Geol.*, 31, 37-51.
- Dobson, D.C. 1982. Geology and alteration of the Lost River tin-tungsten-fluorine deposit, Alaska. *Econ. Geol.*, 77, 1033-1052.
- Doe, B.R., and M.H. Delavaux 1972. Sources of lead in southeast Missouri galena ores. *Econ. Geol.*, 67, 409-425.
- Doe, B.R., and J.S. Stacey 1974. The application of lead isotopes to problems of ore genesis and ore prospect evaluation. *Econ. Geol.*, 69, 757-776.
- Doe, B.R., and R.E. Zartman 1979. Plumbotectonics, the Phanerozoic. In *Geochemistry of hydrothermal ore deposits*, 2nd edn., H.L. Barnes (ed.), 22-70. New York: Wiley.
- Doe, B.R., C.E. Hedge, and D.E. White 1966. Preliminary investigation of the source of lead and strontium in deep geothermal brines underlying the Salton Sea geothermal area. *Econ. Geol.*, 61, 462-483.
- Doe, B.R., H. Kurasawa, and T.A. Steven 1968. Lead-isotope studies of igneous rocks and ores in the San Juan Volcanic Area, Colorado [abs.]. *Geol. Soc. Am. Spec. Pap.* 101, 54.
- Donaldson, M.J. 1981. Redistribution of ore elements during serpentinization and talc-carbonate alteration of some Archean dunites, Western Australia. *Econ. Geol.*, 76, 1698-1713.
- Donaldson, M.J., C.M. Lesher, D.I. Groves, and J.J. Gresham 1986. Comparison of Archean dunites and komatiites associated with nickel mineralization in Western Australia: implications for dunite genesis. *Mineral. Deposita*, 21, 296-305.
- Donnelly, T.H., I.B. Lambert, D.Z. Oehler, J.A. Hallberg, D.R. Hudson, J.W. Smith, O.A. Bavinton, and L. Golding 1977. A reconnaissance study of stable isotope ratios in Archean rocks from the Yilgarn Block, Western Australia. *J. Geol. Soc. Australia*, 24, 409-420.
- Dorr, J.V., I. Soares, and A. Horsen 1956. The manganese deposits of Minas Gerais, Brazil. *International Geol. Congress, 20th*, Mexico, Manganese Symposium 3, 279-346.
- Doyle, C.D., and A.J. Naldrett 1987. The oxygen content of "sulfide" magma and its effect on the partitioning of nickel between coexisting olivine and molten ores. *Econ. Geol.*, 82, 208-211.
- Drever, J.I. 1974. Geochemical model for the origin of Precambrian banded iron formations. *Geol. Soc. Am. Bull.*, 35, 1099-1106.
- Drummond, S.E., and H. Ohmoto 1985. Chemical evolution and mineral deposition in boiling hydrothermal systems. *Econ. Geol.*, 80, 126-147.
- Duane, M.J., and M.J. de Wit 1988. Pb-Zn ore deposits of the northern Caledonides: products of continental-scale fluid mixing and tectonic expulsion during continental collision. *Geology*, 16, 999-1002.
- Duchesne, J.C., and D. Demaiffe 1978. Trace elements and anorthosite gneiss. *Earth Planet. Sci. Lett.*, 38, 249-272.
- Duckworth, R.C., W.C. Shanks III, D.A.H. Teagle, and R.A. Zierenberg 1998. High grade sediment-hosted sulfide deposits on the seafloor: preliminary results from ODP Leg 169 drilling, Middle Valley, Juan de Fuca Ridge. *Soc. Econ. Geol. Newsletter*, no. 32, 20-21.

- Dudás, F.O., I.H. Campbell, and M.P. Gorton 1983. Geochemistry of igneous rocks in the Hokuroku district, northern Japan. *Econ. Geol. Mono.* 5, 115-133.
- Duff, D.J. 1991. A review of the geology of gold deposits in the Porcupine mining camp, Timmins, Ontario, Canada. *Irish Assoc. for Econ. Geol. Annual Review 1990*, 31-38.
- Duke, J.M. 1983. Ore deposit models 7. Magmatic segregation deposits of chromite. *Geoscience Canada*, 10, 15-24.
- Duke, J.M. 1990. Mineral deposit models: nickel sulfide deposits of the Kambalda type. *Can. Mineral.*, 28, 379-388.
- Du Plessis, A. and R.J. Kleywecht 1987. A dipping sheet model for the mafic bodies of the Bushveld Complex. *S. African J. Geol.*, 90, 1-6.
- Dymek, R.F., and C. Klein 1988. Chemistry, petrology and origin of banded iron-formation lithologies from the 3800 MA Isua Supracrustal Belt, West Greenland. *Precamb. Res.*, 39, 247-302.
- Eales, H.V., W.J. de Klerk, and B. Teigler 1990. Evidence for magma mixing processes within the Critical and Lower zones of the northwestern Bushveld Complex. *Chem. Geol.*, 88, 261-278.
- Eagle, D.H., and A.M.D. Weeks 1961. Possible relation between hydrogen sulfide-bearing hydrocarbons in fault line oil fields and uranium deposits in the southeast Texas coastal plain. *U.S. Geol. Survey Prof. Paper* 424-D, 7-9.
- Eagle, D.H., K.A. Dickinson, and B.O. Davis 1975. South Texas uranium deposits. *Am. Assoc. Petroleum Geol. Bull.*, 59, 766-779.
- Eastlick, J.T. 1968. Geology of the Christmas mine and vicinity, Banner mining district, Arizona. In *Ore deposits of the United States, 1933-1967 (Graton-Sales Volume)*, J.D. Ridge (ed.), 2, 1191-1210. New York: Am. Inst. Mining Metall. and Petroleum Engineers.
- Eastoe, C.J. 1978. A fluid inclusion study of the Panguna porphyry copper deposit, Bougainville, Papua New Guinea. *Econ. Geol.*, 73, 721-748.
- Eastoe, C.J. 1982. Physics and chemistry of the hydrothermal system at the Panguna porphyry copper deposit, Bougainville, Papua New Guinea. *Econ. Geol.*, 77, 127-153.
- Eastoe, C.J. 1983. Sulfur isotope data and the nature of the hydrothermal systems at the Panguna and Frieda porphyry copper deposits, Papua New Guinea. *Econ. Geol.*, 78, 201-213.
- Eastoe, C.J., and P.J. Eadington 1986. High-temperature inclusions and the role of biotite granodiorite in mineralization at the Panguna porphyry copper deposit, Bougainville, Papua New Guinea. *Econ. Geol.*, 81, 478-483.
- Eastoe, C.J., M. Solomon, and F.G. Palomero 1986. Sulphur isotope study of massive and stockwork pyrite deposits at Rio Tinto, Spain. *Inst. Mining Metall. Trans.*, 95, B201-207.
- Ebers, M.L., and O.C. Kopp 1979. Cathodoluminescent microstratigraphy in gangue dolomite, the Mascot-Jefferson City district, Tennessee. *Econ. Geol.*, 74, 908-918.
- Eckstrand, O.R. 1975. The Dumont serpentinite: a model for control of nickeleriferous opaque mineral assemblages by alteration reactions in ultramafic rocks. *Econ. Geol.*, 70, 183-201.
- Economou-Eliopoulos, M. 1996. Platinum-group element distribution in chromite ores from ophiolite complexes: implications for exploration. *Ore Geol. Rev.*, 11, 363-381.
- Edmond, J.M., C. Measures, B. Mongum, B. Grant, F.R. Sclater, R. Collar, and A. Hudson 1979. On the formation of metal-rich deposits at ridge crests. *Earth Planet. Sci. Lett.*, 46, 19-30.
- Edwards, A.B. 1947. *Textures of ore minerals*. Austral. Inst. Mining Metall., Melbourne.
- Edwards, A.B., and G.C. Carlos 1954. The selenium content of some Australian sulfide deposits. *Proc. Austral. Inst. Mining Metall.* 172, 32-63.
- Edwards, A.B., G. Baker, and K.J. Callow 1956. Metamorphism and metasomatism at King Island scheelite mine. *J. Geol. Soc. Australia* 3, 55-100.
- Edwards, R., and K. Atkinson 1986. *Ore deposit Geology and its influence on mineral exploration*. London: Chapman & Hall.
- Eichler, J. 1976. Origin of the Precambrian banded iron-formations. In *Handbook of strata-bound and stratiform ore deposits*, K.H. Wolf (ed.), 7, 157-201. Amsterdam: Elsevier.
- Eidel, J.J., J.E. Frost, and D.M. Clippinger 1968. Copper-molybdenum mineralization at Mineral Park, Mohave County, Arizona. In *Ore deposits of the United States, 1933-1967 (Graton-Sales Volume)*, J.D. Ridge (ed.), 2, 1258-1281. New York: Am. Inst. Mining Metall. and Petroleum Engineers.
- Einaudi, M.T. 1982a. Description of skarns associated with porphyry copper plutons, southwestern North America. In *Advances in Geology of the porphyry copper deposits, southwestern North America*, S.R. Titley (ed.), 139-183. Tucson, Arizona: Univ. Arizona Press.
- Einaudi, M.T. 1982b. General features and origin of skarns associated with porphyry copper plutons, southwestern North America. In *Advances in Geology of the porphyry copper deposits, southwestern North America*, S.R. Titley (ed.), 185-209. Tucson, Arizona: Univ. Arizona Press.
- Einaudi, M.T. and D.M. Burt 1982. Terminology, classification and composition of skarn deposits. *Econ. Geol.*, 77, 745-754.
- Einaudi, M.T., L.D. Meinert, and R.J. Newberry 1981. Skarn deposits. *Econ. Geol. 75th Anniv. Vol.*, 317-391.

- Eisenlohr, B.N., L.A. Tompkins, L.M. Cathles, M.E. Barley, and D.I. Groves 1994. Mississippi Valley-type deposits: products of brine expulsion by eustatically induced hydrocarbon generation? An example from northwestern Australia. *Geology*, 22, 315-318.
- Elderfeld, H., I.G. Gass, A. Hammond, and L.M. Bear 1972. The origin of ferromanganese sediments associated with the Troodos Massif of Cyprus. *Sedimentology*, 19, 1-19.
- Eldridge, C.S., P.B. Barton, Jr., and H. Ohmoto 1983. Mineral textures and their bearing on formation of the Kuroko orebodies. *Econ. Geol. Mono.* 5, 241-281.
- Eldridge, C.S., N. Williams, and J.L. Walshe 1993. Sulfur isotope variability in sediment-hosted massive sulfide deposits as determined by using the ion microprobe SHRIMP: II. A study of the H.Y.C. deposit at McArthur River, Northern Territory, Australia. *Econ. Geol.*, 88, 1-26.
- Eldridge, C.S., W.L. Bourcier, H. Ohmoto, and H.L. Barnes 1988. Hydrothermal inoculation and incubation of the chalcopyrite disease in sphalerite. *Econ. Geol.*, 83, 972-989.
- Elevatroski, E.A. 1988a. *World gold: mines-deposits-discoveries; Vol. I: North Central and South America*. Fallbrook, California: Minobras Mining Services.
- Elevatroski, E.A. 1988b. *World gold: mines-deposits-discoveries; Vol. II: Europe, Africa, Asia, Oceania, Australia*. Fallbrook, California: Minobras Mining Services.
- Elliot, W.C., D.E. Grandstaff, G.C. Ulmer, T. Buntin, and D.P. Gold 1982. An intrinsic oxygen fugacity study of platinum-carbon associations in layered intrusions. *Econ. Geol.*, 77, 1493-1510.
- Ellis, A.J. 1969. Present-day hydrothermal systems and mineral deposition. *Proc. 9th Commonwealth Mining and Metallurgical Congress (Mining and Petroleum Section)*, 1-30. London: Inst. Mining and Metall.
- Elmore, R.D., G.J. Milavec, S.W. Imbus, and M.H. Engel 1989. The Precambrian Nonesuch Formation of the North American Mid-Continent Rift, sedimentology and organic geochemical aspects of lacustrine deposition. *Precamb. Res.*, 43, 191-213.
- Elsdon, R. 1975. Iron-titanium oxide minerals in igneous and metamorphic rocks. *Minerals Sci. Eng.*, 7, 48-70.
- Emmett, D.T.G. 1998. AMPLATS. *Paper presented at the 8th International Platinum Symposium, Rustenburg, S. Africa, June 29-July 3, 1998*.
- Emmons, W.H. 1936. Hypogene zoning in metalliferous lodes. *International Geol. Congress, 16th, Washington, 1933, Rept 1*, 417-432.
- Emslie, R.F. 1975. Nature and origin of anorthositic suites. *Geoscience Canada*, 2, 99-116.
- Emslie, R.F. 1978. Anorthosite massifs, Rapakivi granites, and late Proterozoic rifting of North America. *Precamb. Res.*, 7, 61-98.
- Engelder, T., and S. Marshak 1985. Disjunctive cleavage formed at shallow depths in sedimentary rocks. *J. Struc. Geol.*, 7, 327-343.
- Ensign, C.O., Jr., W.S. White, J.C. Wright, J.L. Patrick, R.J. Leone, D.J. Hathway, J.W. Trammell, J.J. Fritts, and T.L. Wright 1968. Copper deposits in the Nonesuch Shale, White Pine, Michigan. In *Ore deposits of the United States, 1933-1967 (Graton-Sales Volume)*, J.D. Ridge (ed.), 1, 460-488. New York: Am. Inst. Mining, Metall. and Petroleum Engineers.
- Erdosh, G. 1970. Geology of the Bogala mine, Ceylon and the origin of vein type graphite. *Mineral. Deposita*, 5, 375-382.
- Ethier, V.G., F.A. Campbell, R.A. Both, and H.R. Krouse 1976. Geological setting of the Sullivan orebody and estimates of temperatures and pressure of metamorphism. *Econ. Geol.*, 71, 1570-1588.
- Etmann, H., and C.F. Hoffmann 1989. Biomarkers in fluid inclusions: a new tool in constraining source regimes and its implications for the genesis of Mississippi Valley-type deposits. *Geology*, 17, 19-22.
- Eugster, H.P. 1985. Oil Shales, evaporites and ore deposits. *Geochim. Cosmochim. Acta*, 49, 619-635.
- Eugster, H. P., and I-Ming Chou 1973. The depositional environments of Precambrian banded iron-formations. *Econ. Geol.*, 68, 1144-1168.
- Evans, B.W. and B.R. Frost 1975. Chrome-spinel in progressive metamorphism — a preliminary analysis. *Geochim. Cosmochim. Acta*, 39, 959-972.
- Ewers, G.R., and S. -S. Sun 1988. Genesis of the Red Dome deposit, northeast Queensland. *Bicentennial Gold 88, Melbourne, May 1988, Proceedings*, 2, 110-115.
- Ewers, W.E. 1983. Chemical factors in the deposition and diagenesis of banded iron-formation. In *Iron-formation: facts and problems*, A. F. Trendall and R. C. Morris (eds.), 491-512. Amsterdam: Elsevier.
- Ewers, W.E., and D.R. Hudson 1972. An interpretative study of a nickel-iron sulfide ore intersection, Lunnon Shoot, Kambalda, Western Australia. *Econ. Geol.*, 67, 1075-1092.
- Ewers, W.E., and R.C. Morris 1981. Studies of the Dales George Member of the Brockman Iron Formation, Western Australia. *Econ. Geol.*, 76, 1929-1953.
- Ewers, W. E., J. Graham, D. R. Hudson, and J. M. Rolls 1976. Crystallization of chromite from nickel-iron sulfide melts. *Contrib. Mineral. Petrol.*, 54, 61-64.
- Faggart, B.E., Jr., A.R. Basu, and M. Tatsumoto 1985. Origin of the Sudbury Complex by meteoritic impact: neodymium isotopic evidence. *Science*, 230, 436-439.

- Farmer, G.L., and D.J. DePaolo 1987. A Nd and Sr isotopic study of hydrothermally altered granite at San Manuel, Arizona: implications for element migration paths during the formation of porphyry copper deposits. *Econ. Geol.*, 82, 1142-1151.
- Farquhar, R.M., and I.R. Fletcher 1980. Ore-lead isotopes and Grenville plate tectonics. In *The continental crust and its mineral deposits*, D.W. Strangway (ed.). *Geol. Assoc. Canada Spec. Paper* 20, 771-788.
- Farrell, C.W., and H.D. Holland 1983. Strontium isotope geochemistry of the Kuroko deposits. *Econ. Geol. Mono.* 5, 302-319.
- Farrow, C.E.G., D.H. Watkinson, and P.C. Jones 1994. Fluid inclusions in sulfides from North and South Range Cu-Ni-PGE deposits, Sudbury structure, Ontario. *Econ. Geol.*, 89, 647-655.
- Faure, G. 1986. *Principles of isotope geology*, 2nd. edn. New York: Wiley.
- Faure, G.P., P.M. Hurley, and H.W. Fairbairn 1963. An estimate of the isotopic composition of strontium in rocks of the Precambrian Shield of North America. *J. Geophys. Res.*, 68, 2323-2329.
- Fehlberg, B., and C.W. Giles 1984. Archean volcanic exhalative gold mineralization at Spargoville, Western Australia. In *Gold'82: the geology, geochemistry and genesis of gold deposits*, R.P. Foster (ed.), 285-304. Rotterdam: Balkema.
- Feiss, P.G. 1978. Magmatic sources of copper in porphyry copper deposits. *Econ. Geol.*, 73, 397-404.
- Ferry, J.M. 1981. Petrology of graphitic sulfide-rich schists from south-central Maine: an example of desulfidation during prograde regional metamorphism. *Am. Mineral.*, 66, 908-930.
- Ferry, J.M. 1986. Reaction progress: a monitor of fluid-rock interaction during metamorphic and hydrothermal events. In *Fluid-rock interactions during metamorphism*, J.V. Walther and B.J. Wood (eds.), 60-88. New York: Springer-Verlag.
- Ferry, J.M., and D.M. Burt 1982. Characterization of metamorphic fluid composition through mineral equilibria. *Rev. in Mineralogy*, 10, 207-262.
- Field, C.W., and L.B. Gustafson 1976. Sulfur isotopes in the porphyry copper deposit at El Salvador, Chile. *Econ. Geol.*, 71, 1553-1548.
- Finlow-Bates, T., and D.L. Large 1978. Water depth as a major control on the formation of submarine exhalative ore deposits. *Geol. Jahrb.*, D 30, 27-39.
- Finlow-Bates, T., and E.F. Stumpfl 1979. The copper and lead-zinc-silver orebodies of Mount Isa mine, Queensland: products of one hydrothermal system. *Annales Soc. Geol. Belgique*, 102, 497-517.
- Fischer, R.P. 1968. The uranium and vanadium deposits of the Colorado Plateau region. In *Ore deposits of the United States, 1933-1967 (Graton-Sales Volume)*, J.D. Ridge (ed.), 2, 735-746. New York: Am. Inst. Mining Metall. and Petroleum Engineers.
- Fischer, R.P. 1970. Similarities, differences, and some genetic problems of the Wyoming and Colorado Plateau types of uranium deposits in sandstone. *Econ. Geol.*, 65, 778-784.
- Fischer, R.P. 1974. Exploration guides to new uranium districts and belts. *Econ. Geol.*, 69, 362-376.
- Fischer, R.P., and J.H. Stewart 1961. Copper, vanadium, and uranium deposits in sandstone — their distribution and geochemical cycles. *Econ. Geol.*, 56, 509-520.
- Fish, R. 1974. Mining in Arctic lands: the Black Angel experience. *Can. Mining J.*, 8, 24-36.
- Fishman, N.S., and R.L. Reynolds 1986. Origin of the Mariano Lake uranium deposit, McKinley County, New Mexico. *Am. Assoc. Petroleum Geologists Studies in Geology* 22, 211-226.
- Fleet, M.E. 1977. Origin of disseminated copper-nickel sulfide ore at Frood, Sudbury, Ontario. *Econ. Geol.*, 72, 1449-1456.
- Fleet, M.E. 1979. Partitioning of Fe, Co, Ni, and Cu between sulfide liquid and basaltic melts and the composition of Ni-Cu sulfide deposits. *Econ. Geol.*, 74, 1517-1519.
- Fleet, M.E. 1986. Geochemistry of the J-M (Howland) Reef of the Stillwater Complex, Minneapolis adit area. I. Sulfide chemistry and sulfide-olivine equilibrium — a discussion. *Econ. Geol.*, 81, 199-203.
- Fleet, M.E., and R.L. Barnett 1978. Al^{IV}/Al^{VI} partitioning in calciferous amphiboles from the Frood mine, Sudbury, Ontario. *Can. Mineral.*, 16, 527-532.
- Fleet, M.E., and N.D. MacRae 1983. Partition of Ni between olivine and sulfide and its application to Ni-Cu sulfide deposits. *Contrib. Mineral. Petrol.*, 83, 75-81.
- Fleet, M.E., and N.D. MacRae 1987. Partition of Ni between olivine and sulfide: the effect of temperature, fO₂, and fS₂. *Contrib. Mineral. Petrol.*, 95, 336-342.
- Fleet, M.E., P.J. MacLean, and J. Barbier 1989. Oscillatory-zoned As-bearing pyrite from strata-bound and stratiform gold deposits: an indicator of ore fluid evolution. *Econ. Geol. Mono* 6, 356-362.
- Fleet, M.E., N.D. MacRae, and C.T. Herzberg 1977. Partition of nickel between olivine and sulfide: a test for immiscible sulfide liquids. *Contrib. Mineral. Petrol.*, 65, 191-197.
- Fleet, M.E., N.D. MacRae, and M.D. Osborne 1981. The partition of nickel between olivine, magma and immiscible sulfide liquid. *Chem. Geol.*, 32, 119-127.
- Fleet, M.E., W.E. Stone, and J.H. Crockett 1991. Partitioning of palladium, iridium, and platinum between sulfide liquid and basalt melt: effects of melt composition, concentration, and oxygen fugacity. *Geochim. Cosmochim. Acta*, 55, 2545-2554.
- Fleischer, M. 1955. Minor elements in some sulfide minerals. *Econ. Geol. 50th Anniv. Vol.*, 970-1024.
- Fleischer, R.L., P.B. Price, and R.M. Walker 1975. *Nuclear tracks in solids*. Univ. California Press.

- Fleischer, V.D. 1984. Discovery, geology and genesis of copper-cobalt mineralization at Chambishi Southeast prospect, Zambia. *Precamb. Res.*, 25, 119-133.
- Fleischer, V.D., W.G. Garlick and R. Haldane 1976. Geology of the Zambian copper belt. In *Handbook of strata-bound and stratiform ore deposits*, K.H. Wolf (ed.), 6, 223-352. Amsterdam. Elsevier.
- Fletcher, C.J.N. 1977. The geology, mineralization, and alteration of Ilkwang mine, Republic of Korea: a Cu-W-bearing tourmaline breccia pipe. *Econ. Geol.*, 72, 753-768.
- Fletcher, I.R., and R.M. Farquhar 1982. Lead isotopic compositions of Balmat ores and their genetic implications. *Econ. Geol.*, 77, 464-473.
- Floyd, P.A., and J.A. Winchester 1975. Magma type and tectonic setting discrimination using immobile elements. *Earth Planet. Sci. Lett.*, 27, 211-218.
- Foley, N.K., and R.A. Ayuso 1994. Lead isotope compositions as guides to early gold mineralization: the North Amethyst vein system, Creede district, Colorado. *Econ. Geol.*, 89, 1842-1859.
- Foley, N.K., P.M. Bethke, and R.O. Rye 1989. A reinterpretation of the δD_{H_2O} of inclusion fluids in contemporaneous quartz and sphalerite, Creede mining district, Colorado: a genetic problem from shallow orebodies? *Econ. Geol.*, 84, 1966-1977.
- Foose, M.P., W.D. Menzie, D.A. Singer, and J.T. Hanley 1980. The distribution and relationships of grade and tonnage among some nickel deposits. *U.S. Geol. Survey Prof Paper* 1160.
- Force, E.R. 1991. Placer deposits. *Rev. Econ. Geol.*, 5, 131-140.
- Ford, J.H. 1978. A chemical study of alteration at the Panguna porphyry copper deposit, Bougainville, Papua New Guinea. *Econ. Geol.*, 73, 703-720.
- Ford, J.H., and D.C. Green 1977. An oxygen- and hydrogen-isotope study of the Panguna porphyry-copper deposit, Bougainville. *J. Geol. Soc. Austral.*, 24, 63-80.
- Foster, R.P. 1984 (ed.). *Gold '82: the geology, geochemistry, and genesis of gold deposits*. Rotterdam: Balkema, 432p.
- Foster, R.P. 1989. Archean gold mineralization in Zimbabwe: implications for metallogenesis and exploration. *Econ. Geol. Mono.* 6, 54-70.
- Foster, R.P. 1991 (ed.). *Gold metallogeny and exploration*. Glasgow: Blackie, 432p.
- Foster, R.P., and J. M. Gilligan 1987. Archean iron-formation and gold mineralization in Zimbabwe. In *Precambrian iron-formations*, P.W.U. Appel and G.L. LaBarge (eds.), 635-674. Athens: Theophrastus Publ. S.A.
- Foster, R.P., and D.P. Piper 1993. Archean gold deposits in Africa: crustal setting, metallogenesis and cratonization. *Ore Geol. Rev.*, 8, 303-347.
- Fountain, R.J. 1972. Geochronology of the Panguna copper deposit, Bougainville Island, New Guinea. *Econ. Geol.*, 67, 1065-1074.
- Fouquet, Y., U. von Stackelberg, J.L. Charlou, J. Erzinger, P.M. Herzig, R. Mühle, and M. Wiedicke 1993. Metallogenesis in back-arc environments: the Lau Basin example. *Econ. Geol.*, 88, 2154-2181.
- Fowler, A., and M.T. Anderson 1991. Geopressure zones as proximal sources of hydrothermal fluids in sedimentary basins and the origin of Mississippi Valley-type deposits in shale-rich sequences. *Inst. Mining Metall. Trans., Sec. B*, 100, B14-B18.
- Fox, J.S. 1984. Besshi-type volcanogenic sulphide deposits - a review. *Can. Inst. Mining Metall. Bull.*, 77 (864), 57-68.
- Frakes, L., and B. Bolton 1984. Origin of manganese giants: sea-level change and anoxic-oxic history. *Geology*, 12, 83-86.
- Frakes, L., and B. Bolton 1992. Effects of ocean chemistry, sea level, and climate on the formation of primary sedimentary manganese ore deposits. *Econ. Geol.*, 87, 1207-1217.
- Francis, C.A., M.E. Fleet, K.C. Misra, and J.R. Craig 1976. Orientation of exsolved pentlandite in natural and synthetic nickeliferous pyrrhotite. *Am. Mineral.*, 61, 913-920.
- Franklin, J.M. 1986. Volcanic-associated massive sulphide deposits - an update. *Irish Assoc. Econ. Geol. Spec. Publ.* 4, 49-69.
- Franklin, J.M. 1993. Volcanic-associated massive sulfide deposits. *Geol. Assoc. Canada Spec. Paper* 40, 315-334.
- Franklin, J.M., and R.I. Thorpe 1982. Comparative metallogeny of the Superior, Slave and Churchill Provinces. *Geol. Assoc. Canada Spec. Paper* 25, 3-90.
- Franklin, J.M., J. Kasarda, and K.H. Poulson 1975. Petrology and chemistry of the alteration zone of the Mattabi massive sulfide deposit. *Econ. Geol.*, 70, 63-79.
- Franklin, J.M., J.W. Lydon, and D.F. Sangster. 1981. Volcanic-associated massive sulfide deposits. *Econ. Geol. 75th Anniv. Vol.*, 485-627.
- Franklin, J.M., S.M. Roscoe, W.D. Loveridge, and D.F. Sangster 1983. Lead isotope studies in Superior and Southern province. *Geol. Survey Can. Bull.* 351, 60p.
- Frater, K.M. 1985a. Mineralization at the Golden Grove Cu-Zn deposit, Western Australia. I. Premetamorphic textures of the opaque minerals. *Can. J. Earth Sci.*, 22, 1-14.
- Frater, K.M. 1985b. Mineralization at the Golden Grove Cu-Zn deposit, Western Australia. II. Deformation textures of the opaque minerals. *Can. J. Earth Sci.* 22, 15-26.

- French, B.M. 1968. Progressive contact metamorphism of the Biwabik Iron Formation, Mesabi Range, Minnesota. *Minn. Geol. Survey Bull.*, 45, 103 p.
- Frimmel, H.E., A.P. LeRoex, J. Knight, and W.E.L. Minter 1993. A case study of the postdepositional alteration of the Witwatersrand Basal Reef gold placer. *Econ. Geol.*, 88, 249-265.
- Fripp, R.E.P. 1976. Stratabound gold deposits in Archean banded iron-formation, Rhodesia. *Econ. Geol.*, 71, 58-75.
- Fritz, P. 1976. Oxygen and carbon isotopes in ore deposits in sedimentary rocks. In *Handbook of strata-bound and stratiform ore deposits*, K. H. Wolf (ed.), 2, 191-217. Amsterdam: Elsevier.
- FrondeL, C., and J.L. Baum 1974. Structure and mineralogy of the Franklin Zn-Fe-Mn deposit, N.J.. *Econ. Geol.*, 69, 157-160.
- Fryer, B.J., and R.P. Taylor 1987. Rare-earth element distribution in uraninites: implications for ore genesis. *Chem. Geol.*, 63, 101-108.
- Fryer, B.J., R. Kerrich, R.W. Hutchinson, M.G. Pierce, and D.S. Rogers 1979. Archean precious metal hydrothermal systems, Dome Minee, Abitibi greenstone belt. I. Patterns of alteration and metal distribution. *Can. J. Earth Sci.*, 16, 421-439.
- Fu, M.A. Changkakoti, H.R. Krouse, J. Gray, and T.A.P. Kwak 1991. An oxygen, hydrogen, sulfur, and carbon isotope study of carbonate-replacement (skarn) tin deposits of the Dachang tin field, China. *Econ. Geol.*, 86, 1683-1703.
- Fuchs, W.A., and A.W. Rose, Jr. 1974. The geochemical behavior of platinum and palladium in the weathering cycle in the Stillwater Complex, Montana. *Econ. Geol.*, 69, 332-346.
- Fyfe, W.S., and R. Kerrich 1984. Gold: natural concentration processes. In *Gold '82: the geology, geochemistry and genesis of gold deposits*, R.P. Foster (ed.), 99-127. Amsterdam: A. A. Balkema.
- Fyfe, W.S., and R. Kerrich 1985. Fluids and thrusting. *Chem. Geol.*, 49, 353-362.
- Fyfe, W.S., N.J. Price, and A.B. Thompson 1978. *Fluids in the earth's crust*. Amsterdam: Elsevier.
- Fyon, J.A., J.H. Crockett, and H.P. Schwartz 1983. Application of stable isotope studies to gold metallogeny in the Timmins-Porcupine Camp. *Ontario Geol. Survey Open File Rept.* 5464, 182 p.
- Fyon, J.A., D.G. Troop, S. Marmont, and A.J. Macdonald 1989. Introduction of gold into Archean crust, Superior Province, Ontario — coupling between mantle-initiated magmatism and lower crustal thermal maturation. *Econ. Geol. Mono.* 6, 479-490.
- Gaál, G., and J. Parkkinen 1993. Early Proterozoic ophiolite-hosted copper-zinc-cobalt deposits of the Outokumpu type. *Geol. Assoc. Canada Spec. Paper* 40, 335-342.
- Gain, S.B. 1985. The geologic setting of the platiniferous UG-2 chromitite layer on the farm Maandagshoek, Eastern Bushveld Complex. *Econ. Geol.*, 80, 925-943.
- Gain, S.B., and A.B. Mostert 1982. The geochemical setting of the platinoid and base metal sulfide mineralization in the Platreef of the Bushveld Complex in Drenthe, north of Potgietersrus. *Econ. Geol.*, 77, 1395-1404.
- Gale, G.H. 1977. Proterozoic massive sulphide deposits. *Geol. Soc. Am. Mem.* 161, 191-207.
- Galloway, W.E. 1978. Uranium mineralization in a coastal-plain fluvial aquifer system: Catahoula Formation, Texas. *Econ. Geol.*, 73, 1655-1676.
- Galloway, W.E., and W.R. Kaiser 1980. Catahoula Formation of the Texas Coast Plain: origin, geochemical evolution, and characteristics of uranium deposits. *Univ. Texas Austin Bur. Econ. Geol. Rept. Inv.* 100, 81p.
- Gamble, R.P. 1982. An experimental study of sulfidation reactions involving andradite and hedenbergite. *Econ. Geol.*, 77, 784-797.
- Gammons, C.H., and M.S. Bloom 1993. Experimental investigations of the hydrothermal geochemistry of Pt and Pd. II. The solubility of PtS and PdS in aqueous sulfide solutions at 300°C. *Geochim. Cosmochim. Acta*, 57, 2451-2467.
- Gammons, C.H., A.E. Williams-Jones 1997. Chemical mobility of gold in the porphyry epithermal environment. *Econ. Geol.*, 92, 45-59.
- Gammons, C.H., M.S. Bloom, and Y. Yu 1992. Experimental investigations of the hydrothermal geochemistry of Pt and Pd. I. Solubility of Pt and Pd sulfide minerals in NaCl/HCl solutions at 300°C. *Geochim. Cosmochim. Acta*, 56, 3881-3894.
- García, M.O. 1978. Criteria for identification of ancient volcanic arcs. *Earth Sci. Rev.*, 14, 147-165.
- Gardner, H.D., and I. Hutcheon 1985. Geochemistry, mineralogy and geology of the Jason Pb-Zn deposits, Macmillan Pass, Yukon, Canada. *Econ. Geol.*, 80, 1257-1276.
- Garlick, W.G. 1961. The syngenetic theory. In *The Geology of the Northern Rhodesian Copperbelt*, F. Mendelsohn (ed.), 146-165. London: Macdonald.
- Garlick, W.G. 1989. Genetic interpretation from ore relations to algal reefs in Zambia and Zaire. *Geol. Assoc. Canada Spec. Paper* 36, 471-498.
- Garrels, R.M. 1941. The Mississippi Valley-type lead-zinc deposits and the problem of mineral zoning. *Econ. Geol.*, 36, 729-744.
- Garrels, R.M. 1954. Mineral species as functions of pH and oxidation-reduction potentials, with special reference to the zone of oxidation and secondary enrichment of sulfide ore deposits. *Geochim. Cosmochim. Acta*, 5, 153-168.

- Garrels, R.M. 1987. A model for the deposition of microbanded Precambrian iron-formations. *Am. J. Sci.*, 287, 81-106.
- Garrels, R.M., and C.L. Christ 1965. *Solutions, minerals and equilibria*. New York: Harper and Row.
- Garrels, R.M., E.A. Perry, Jr., and F.T. McKenzie 1973. Genesis of Precambrian iron-formations and the development of atmospheric oxygen. *Econ. Geol.*, 68, 1173-1179.
- Garson, M.S. 1984. Relationship of carbonatites to plate tectonics. *Indian Mineral.*, Sukheswala Volume, 163-188.
- Garson, M.S., and A.H.G. Mitchell 1973. Mineralization at destructive plate boundaries — a brief review. *Geol. Soc. London Spec. Publ.* 7, 81-97.
- Garven, G. 1985. The role of regional fluid flow in the genesis of Pine Point deposit, Western Canada sedimentary basin. *Econ. Geol.*, 80, 307-324.
- Garven, G. 1986. The role of regional fluid flow in the genesis of the Pine Point deposit, western Canada sedimentary basin — a reply. *Econ. Geol.*, 81, 1015-1020.
- Garven, G. and R.A. Freeze 1984a. Theoretical analysis of the role of groundwater flow in the genesis of stratabound ore deposits 1. Mathematical and numerical model. *Am. J. Sci.*, 284, 1085-1124.
- Garven, G. and R.A. Freeze 1984b. Theoretical analysis of the role of groundwater flow in the genesis of stratabound ore deposits 2. Quantitative results. *Am. J. Sci.*, 284, 1125-1174.
- Garven, G., and J. P. Raffensperger 1997. Hydrogeology and geochemistry of ore genesis in sedimentary basins. In *Geochemistry of hydrothermal ore deposits, 3rd edn.*, H.L. Barnes (ed.), 125-190. New York: Wiley.
- Gass, I.G. 1980. The Troodos Massif: its role in unravelling of the ophiolite problem and its significance in the understanding of constructive plate margin processes. In *International Ophiolite Symp. Proc.*, A. Panayiotou (ed.), 23-35. Nicosia: Cyprus Geol. Survey.
- Gastil, G. 1960. Continents and mobile belts in the light of mineral dating. *Am. J. Sci.*, 258, 162-169.
- Gauthier-Lafaye, F., and F. Weber 1989. The Francevillian (Lower Proterozoic) uranium ore deposits of Gabon. *Econ. Geol.*, 84, 2267-2285.
- Gaylord, W.B., and J.A. Briskey 1983. Geology of the Elmwood and Gordonsville mines, Central Tennessee zinc district. In *Tennessee zinc deposits fieldtrip guidebook*, J.R. Craig (ed.), Virginia Tech. Dept. Geol. Sciences Guide Book 9, 116-151. Blacksburg, Virginia: Virginia Polytec. Inst. and State Univ.
- Gebre-Mariam, S.G. Hagemann, and D.I. Groves 1995. A classification scheme for epigenetic Archean Iode-gold deposits. *Mineral. Deposita*, 30, 408-410.
- Gee, R.D., J.L. Baxter, S.A. Wilde, and I.R. Williams 1981. Crustal development in the Archean Yilgarn block, Western Australia. *Geol. Soc. Australia Spec. Pub.* 7, 43-56.
- Geijer, P. and N.H. Magnusson 1952. The iron ores of Sweden. *International Geol. Congress, 19th, Algeris, 1952*, 2, 477-499.
- Genkin, A.D., and T.L. Evstigneeva 1986. Associations of platinum-group minerals of the Noril'sk copper-nickel sulfide ores. *Econ. Geol.*, 81, 1203-1212.
- Gerstner, M.R., J.R. Bowman, and J.D. Pasteris 1989. Skarn formation at the MacMillan Pass tungsten deposit (MacTung), Yukon and Northwest Territories. I. P-T-X-V characterization of the methane-bearing, skarn-forming fluids. *Can. Mineral.*, 27, 545-564.
- Gervilla, F., E. Makovicky, M. Mackovicky, and J. Rose-Hansen 1994. The system Pd-Ni-As at 790° and 450°C. *Econ. Geol.*, 89, 1630-1639.
- Ghazban, F., H.P. Schwarz, and C.D. Ford 1990. Carbon and sulfur isotope evidence for in situ reduction of sulfate, Nanisivik lead-zinc deposits, Northwest Territories, Baffin Island, Canada. *Econ. Geol.*, 85, 360-375.
- Ghosh-Dastidar, P., G.E. Pajari, Jr., and L.T. Trembath 1970. Factors affecting the trace element partition coefficients between coexisting sulfides. *Econ. Geol.*, 65, 815-837.
- Gibbins, W.A. and R.H. McNutt 1975. The age of the Sudbury Nickel Intrusive and Murray Granite. *Can. J. Earth Sci.*, 12, 1970-1989.
- Gibson, H.L., D.H. Watkinson, and C. D.A. Comba 1983. Silicification: hydrothermal alteration in an Archean geothermal system within the Amulet Rhyolite Formation, Noranda, Quebec. *Econ. Geol.*, 78, 954-971.
- Giggenbach, W.F. 1992a. Isotopic shifts in waters from geothermal and volcanic systems along convergent plate boundaries and their origin. *Earth Planet. Sci. Lett.*, 113, 495-510.
- Giggenbach, W.F. 1992. Magma degassing and mineral deposition in hydrothermal systems along convergent plate boundaries. *Econ. Geol.*, 87, 1927-1944.
- Gijbels, R., H.T. Millard, G.A. Desborough, and A.J. Bartel 1974. Osmium, ruthenium, iridium and chromium from the eastern Bushveld Complex, South Africa. *Geochim. Cosmochim. Acta*, 38, 319-337.
- Gilligan, L.B., and B. Marshall 1987. Textural evidence for remobilization in metamorphic environments. *Ore Geol. Rev.*, 2, 205-229.
- Gilmour, P. 1977. Mineralized intrusive breccias as guides to concealed porphyry copper systems. *Econ. Geol.*, 72, 290-297.

- Gilmour, P. 1982. Grades and tonnages of porphyry copper deposits. In *Advances in Geology of the porphyry copper deposits, southwestern North America*, S.R. Titley (ed.), 7-35. Tucson, Arizona: Univ. Arizona Press.
- Giordano, T.H. 1985. A preliminary evaluation of organic ligands and metal-organic complexing in Mississippi Valley-type ore solutions. *Econ. Geol.*, 80, 96-106.
- Giordano, T.H. 1990. Organic ligands and metal-organic complexing in ore fluids of sedimentary origin. *U.S. Geol. Survey Cir.* 1058, 31-41.
- Giordano, T.H., and H.L. Barnes 1981. Lead transport in Mississippi Valley-type ore solutions. *Econ. Geol.*, 76, 2200-2211.
- Gitlin, E. 1985. Sulfide remobilization during low temperature alteration of seafloor basalt. *Geochim. Cosmochim. Acta*, 49, p. 1567-.
- Gize, A.P. and H.L. Barnes 1987. The organic geochemistry of two Mississippi Valley-type lead-zinc deposits. *Econ. Geol.*, 82, 457-470.
- Gize, A.P., and T.C. Hoering 1980. The organic matter in Mississippi Valley-type deposits. *Carnegie Inst. Washington Year Book* 79, 384-388.
- Glasson, M.J., and R.R. Keays 1978. Gold mobilization during cleavage development in sedimentary rocks from the auriferous slate belt of central Victoria, Australia: some important boundary conditions. *Econ. Geol.*, 73, 496-511.
- Glennie, K.W. 1989. Some effects of the Late Permian Zechstein transgression in northwestern Europe. *Geol. Assoc. Canada Spec. Paper* 36, 557-566.
- Goble, R.J., S.D. Scott, and R.G.V. Hancock 1979. Diffusion rates for Zn and Fe in sphalerite [abs.]. *Geol. Assoc. Canada - Mineral Assoc. Canada Abstracts with Programs* 4, 53.
- Godlevsky, M.N., and L.N. Grinenko 1963. Some data on the isotopic composition of sulfur in the sulfides of the Noril'sk deposit. *Geochemistry*, 1, 35-41.
- Godlevsky, M.N., and A.P. Likhachev 1986. Types and distinctive features of ore-bearing formations of copper-nickel deposits. In *Geology and metallogeny of copper deposits*, G. H. Friedrich, A. D. Genkin, A. J. Naldrett, J. D. Ridge, R. H. Sillitoe, and F. M. Vokes (eds.), 124-134. Berlin: Springer-Verlag.
- Goldfarb, M.S., D.R. Converse, H.D. Holland, and J.M. Edmond 1983. The genesis of hot spring deposits on the East Pacific Rise, 21°N. *Econ. Geol. Mono.* 5, 507-522.
- Goldhaber, M.B., and J.R. Kaplan 1975. Controls and consequences of sulfate reduction rates in recent marine sediments. *Soil Sci.* 119, 42-55.
- Goldhaber, M.B., and J.G. Vietz 1985. Isotope evidence for sulfur sources for the Viburnum Trend of lead-zinc mineralization, southeast Missouri [abs.]. *Geol. Soc. Am. Abstracts with Programs*, 17, 495.
- Goldhaber, M.B., R.L. Reynolds, and R.O. Rye 1978. Origin of a South Texas roll-type uranium deposit: II. Sulfide petrology and sulfur isotope studies. *Econ. Geol.*, 73, 1690-1705.
- Goldich, S.S. 1973. Ages of Precambrian banded iron-formation. *Econ. Geol.*, 68, 1126-1134.
- Goldschmidt, V.M. 1954. *Geochemistry*. London: Oxford Univ. Press.
- Gole, M. J., and C. Klein 1981. Banded iron-formations through much of Precambrian time. *J. Geol.*, 89, 169-183.
- Golightly, J.P. 1981. Nickeliferous laterite deposits. *Econ. Geol. 75th Anniv. Vol.*, 710-735.
- Goodfellow, W.D. 1987. Anoxic stratified oceans as a source of sulphur in sediment-hosted stratiform Zn-Pb deposits (Selwyn basin, Yukon, Canada). *Chem. Geol.*, 65, 359-382.
- Goodfellow, W.D. 1992. Chemical evolution of the oceans as discerned from the temporal distribution of sedimentary exhalative (SEDEX) Zn-Pb-Ag deposits [abs.]. *International Geol. Congress. Kyoto, Japan, Programs with Abstracts*, 1, 185.
- Goodfellow, W.D., J.W. Lydon, and R.J.W. Turner 1993. Geology and genesis of stratiform sediment-hosted (SEDEX) zinc-lead-silver sulfide deposits. *Geol. Assoc. Canada Spec. Paper* 40, 201-252.
- Goodwin, A. M. 1964. Geochemical studies at the Helen iron range. *Econ. Geol.*, 59, 684-718.
- Goodwin, A. M. 1973. Archean iron-formations and tectonic basins of the Canadian Shield. *Econ. Geol.*, 68, 915-933.
- Goodwin, A.M. 1977. Archean volcanism in Superior Province, Canadian Shield. *Geol. Assoc. Canada Spec. Paper* 16, 205-241.
- Goodwin, A.M., and R.H. Ridler 1970. The Abitibi orogenic belt. *Geol. Survey Canada Paper* 70-40, 1-28.
- Goodwin, A. M., and R. Shklanka 1967. Archean volcanic-tectonic basins: form and pattern. *Can. J. Earth Sci.*, 4, 777-795.
- Goodwin, A.M., H.G. Thode, G.L. Chou, and S.H. Karkhanis 1985. Chemostratigraphy and origin of the late Archean siderite-pyrite rich Helen Iron Formation, Michipicoten belt, Canada. *Can. J. Earth Sci.*, 22, 72-84.
- Govett, G.J.S. and R.E.S. Whitehead 1974. Origin of metal zoning in stratiform sulfides: a hypothesis. *Econ. Geol.*, 66, 940-946.
- Graf, D.L., Jr. 1977. Rare earth elements as hydrothermal tracers during the formation of massive sulfide deposits in volcanic rocks. *Econ. Geol.*, 72, 527-548.

- Graf, D.L. 1982. Chemical osmosis, reverse chemical osmosis, and the origin of subsurface brines. *Geochim. Cosmochim. Acta*, 46, 1431-1448.
- Grandstaff, D. E. 1980. Origin of uraniferous conglomerates at Elliot Lake, Canada and Witwatersrand, South Africa: implications for oxygen in the Precambrian atmosphere. *Precamb. Res.*, 13, 1-26.
- Grandstaff, D. E. 1981. Microprobe analyses of uranium and thorium in uraninite from the Witwatersrand, South Africa, and Blind River, Ontario, Canada. *U.S. Geol. Survey Prof. Paper* 1161, J1-J5.
- Granger, H.C. 1968. Localization and control of uranium deposits in the southern San Juan Basin mineral belt, New Mexico — an hypothesis. *U.S. Geol. Survey Prof. Paper* 600-B, B60-B70.
- Granger, H.C., and E.S. Santos, 1986. Geology and ore deposits of the Section 23 mine, Ambrosia Lake district, New Mexico. *Am. Assoc. Petroleum Geologists Studies in Geology* 22, 185-210.
- Granger, H.C., and C.G. Warren 1969. Unstable sulfur compounds and the origin of roll-type uranium deposits. *Econ. Geol.*, 64, 160-171.
- Granger, H.C., E.S. Santos, B.G. Dean, and F.B. Moroe 1961. Sandstone-type uranium deposits at Ambrosia Lake, New Mexico — an interim report. *Econ. Geol.*, 56, 1179-1210.
- Grant, J.N., C. Halls, W. Avila, and G. Avila 1977. Igneous geology and the evolution of hydrothermal systems in some volcanic tin deposits of Bolivia. *Inst. Mining Metall. Spec. Paper* 7, 117-126.
- Grant, J.N., S.M.F. Sheppard, and W. Avila 1980. Evolution of the porphyry tin deposits of Bolivia. *Soc. Min. Geol. Japan, Spec. Issue* 8, 151-174.
- Grant, N.K., and M.C. Bliss 1983. Strontium isotope and rare earth element variations in non-sulfide minerals from the Elmwood-Gordonsville mines, central Tennessee. In *Proc. International Conf. Mississippi Valley-type Pb-Zn deposits, Rolla, Missouri, 1982* — Proc. Vol. G. Kisvarsanyi, S. K. Grant, W. P. Pratt, and J. W. Koenig (eds.), 206-210. Rolla, Missouri: Univ. Missouri Press.
- Graton, L.C. 1933. The depth-zones in ore deposition. *Econ. Geol.*, 28, 513-555.
- Gratz, J.F. and K.C. Misra 1987. Fluid inclusion study of the Gordonsville zinc deposit, central Tennessee. *Econ. Geol.*, 82, 1790-1804.
- Gray, G.J., and M.J. Russell 1984. Regional Mn-Fe lithochemistry of Lower Carboniferous Waulsortian Reef limestone in Ireland. In *Prospecting in areas of glaciated terrain*, 57-67. London: Inst. Mining Metallurgy.
- Gray, J., A. Changkakoti, and R.D. Morton 1987. Simultaneous extraction of hydrogen and oxygen from fluid inclusion waters for isotopic analysis. *Am. Current Res. Fluid Inclusions meeting*, Jan 5-7, 1987, Socorro, New Mexico.
- Green, A.H., and A.J. Naldrett 1981. The Langmuir volcanic peridotite-associated nickel deposits: Canadian equivalents of the Western Australian occurrences. *Econ. Geol.*, 76, 1503-1523.
- Green, D.H. 1975. Genesis of Archean peridotitic magmas and constraints on Archean geothermal gradients and tectonics. *Geology*, 3, 15-18.
- Green, D.H., I.A. Nicholls, M.J. Viljoen, and R.P. Viljoen 1975. Experimental demonstration of the existence of peridotitic liquids in earliest Archean magmatism. *Geology*, 3, 11-14.
- Green, G.R., H. Ohmoto, J. Date, and T. Takahashi 1983. Whole-rock oxygen isotope distribution in the Fakazawa-Kosaka area, Hokuroku district, Japan. *Econ. Geol. Mono.* 5, 395-411.
- Green, J.C. 1982. Geology of Keweenawan extrusive rocks. *Geol. Soc. Am. Mem.*, 156, 47-55.
- Green, J.R., H. Ohmoto, J. Date, and T. Takahashi 1983. Whole-rock oxygen isotope distribution in the Fukazawa-Kosaka area, Hokuroku district, Japan. *Econ. Geol. Mono.* 5, 395-411.
- Greenbaum, D. 1977. The chromitiferous rocks of the Troodos ophiolite complex, Cyprus. *Econ. Geol.*, 72, 1175-1194.
- Gregg, J.M., and K.L. Shelton 1989. Minor- and trace-element distributions in the Bonnetterre Dolomite (Cambrian), southeast Missouri: evidence for possible multiple-basin fluid sources and pathways during lead-zinc mineralization. *Geol. Soc. Am. Bull.*, 101, 221-230.
- Gregory, R.T., and R.E. Criss 1986. Isotope exchange in open and closed systems. *Rev. in Mineralogy* 16, 91-127.
- Grenne, T. 1986. Ophiolite-hosted Cu-Zn deposits at Løkken and Høydal, Trondheim nappe complex, upper allochthon. *Sveriges Geol. Undersökning*, 60, 55-65.
- Grenne, T. 1989. The feeder zone to the Løkken ophiolite-hosted massive sulfide deposit and related mineralizations in the central Norwegian Caledonides. *Econ. Geol.*, 84, 2173-2195.
- Grenne, T., and F.M. Vokes 1990. Sea-floor sulfides at the Høydal volcanogenic deposit, central Norwegian Caledonides. *Econ. Geol.*, 85, 344-359.
- Grenne, T., G. Grammelvedt, and F.M. Vokes 1980. Cyprus-type sulfide deposits in the western Trondheim district, central Norwegian Caledonides. In *Proc. International Ophiolite Symp., 1979*, Cyprus, 727-743. Nicosia: Cyprus Ministry Agriculture Nat. Resources, Geol. Surv. Dept.
- Gresens, R.L. 1967. Composition-volume relationships of metasomatism. *Chem. Geol.*, 2, 47-65.
- Gresham, J.J. 1986. Depositional environments of peridotite-associated nickel sulfide deposits with special reference to the Kambalda dome. In *Geology and metallogeny of copper deposits*, G. H. Friedrich, G. H. Genkin, A. J. Naldrett, J. D. Ridge, R. H. Sillitoe, and F. M. Vokes (eds.), 63-90. Berlin: Springer-Verlag.

- Gresham, J.J., and G.D. Loftus-Hills 1981. The geology of the Kambalda nickel field, Western Australia. *Econ. Geol.*, 76, 1373-1416.
- Griffiths, J.R., and C.I. Godwin 1983. Metallogeny and tectonics of porphyry copper-molybdenum deposits in British Columbia. *Can. J. Earth Sci.*, 20, 1000-1018.
- Griffiths, W. R., J. P. Albers, and O. Oner 1972. Massive sulfide copper deposits of the Ergani-Maden area, southeastern Turkey. *Econ. Geol.*, 67, 701-716.
- Grinenko, L.N. 1985. Sources of sulfur of the nickeliferous and barren gabbro-dolerite intrusions of the northwest Siberian platform. *International Geol. Rev.*, 27, 695-708.
- Groff, J.A., M.T. Heizler, W.C. McIntosh, and D.L. Norman 1997. $^{40}\text{Ar}/^{39}\text{Ar}$ dating and mineral paragenesis for Carlin-type gold deposits along the Getchell Trend, Nevada: evidence for Cretaceous and Tertiary gold mineralization. *Econ. Geol.*, 92, 601-622.
- Gromet, L.P., R.F. Dymek, L.A. Haskin, and R.L. Korotev 1984. The "North American Shale Composite": its compilation, major and trace element characteristics. *Geochim. Cosmochim. Acta*, 47, 925-939.
- Gross, G.A. 1965. Geology of iron deposits in Canada. *Geol. Survey Canada Econ. Geol. Rept.* 22, 1, 111p.
- Gross, G.A. 1973. The depositional environment of principal types of Precambrian iron-formations. In *Genesis of Precambrian iron and manganese deposits*, M.P. Semenenko (ed.), *Proc. Kiev Symposium, 1970*, UNESCO Earth Sci., 9, 15-21.
- Gross, G.A., 1980. A classification of iron formations based on depositional environments. *Can. Mineral.*, 18, 215-222.
- Gross, G.A. 1986. The metallogenetic significance of iron-formation and related stratafer rocks. *J. Geol. Soc. India*, 28, 92-108.
- Gross, G.A., and C.R. McLeod 1980. A preliminary assessment of the chemical composition of iron formations in Canada. *Can. Mineral.*, 18, 223-229.
- Gross, S.O. 1968. Titaniferous ores of the Sanford Lake district, New York. In *Ore deposits of the United States, 1933-1967 (Graton-Sales Vol.)*, J.D. Ridge (ed.), 1, 140-153. New York: Am. Inst. Mining Metall. and Petroleum Engineers.
- Grove, T.L., M.J. de Wit, and J. Dan 1997. Komatiites from the Komati Type Section, Barberton, South Africa. In *Greenstone belts*, M.J. de Wit and L. D. Ashwal (eds.), 422-437. Oxford: Oxford Science Publications.
- Groves, D.I. 1993. The crustal continuum model for late-Archean lode-gold deposits of the Yilgarn Block, Western Australia. *Mineral. Deposita*, 28, 366-374.
- Groves, D.I., and W.D. Blatt 1984. Spatial and temporal variations of Archean metallogenic associations in terms of evolution of granitoid-greenstone terrains with particular emphasis on the Western Australian Shield. In *Archean geochemistry*, A Kroner, G. N. Hanson, and A. M. Goodwin (eds.), 73-98. Berlin: Springer-Verlag.
- Groves, D.I. and D.R. Hudson 1981. The nature and origin of Archean strata-bound volcanic-associated nickel-iron-copper sulphide deposits. In *Handbook of strata-bound and stratiform ore deposits*, K.H. Wolf (ed.), 9, 306-410. Amsterdam: Elsevier.
- Groves, D.I., and R.P. Foster 1991. Archean lode gold deposits. In *Gold metallogeny and exploration*, R.P. Foster (ed.), 63-103. Glasgow: Blackie.
- Groves, D.I. and T.S. McCarthy 1978. Fractional crystallization and the origin of tin deposits in granitoids. *Mineral. Deposita*, 13, 11-26.
- Groves, D. I., F. M. Barrett, and K. G. McQueen 1978. Geochemistry and origin of cherty metasediments within ultramafic flow sequences and their relationship to nickel mineralization. Univ. Western Australia, *Geol. Dept. Ext. Survey Publ.* 2, 57-69.
- Groves, D.I., F.M. Barrett, and K.G. McQueen 1979. The relative roles of magmatic segregation, volcanic exhalation and regional metamorphism in the generation of volcanic-associated nickel ores of Western Australia. *Can. Mineral.*, 17, 319-336.
- Groves, D.I., C.M. Lesher, and R.D. Gee 1984. Tectonic setting of the sulphide nickel deposits of the Western Australian shield. In *Sulphide deposits in mafic and ultramafic rocks*, D. L. Buchanan and M. J. Jones (eds.), 1-13. London: Inst. Mining & Metall.
- Groves, D.I., F.M. Barrett, R.A. Binns, and K.G. McQueen 1977. Spinel phases associated with metamorphosed volcanic-type iron-nickel sulfide ores from Western Australia. *Econ. Geol.*, 72, 1224-1244.
- Groves, D.I., R.A. Binns, F.M. Barrett, and K.G. McQueen 1975. Sphalerite compositions from western Australia nickel deposits, a guide to equilibria below 300°C. *Econ. Geol.*, 71, 1570-1588.
- Groves, D.I., E.A. Korhonen, N.J. McNaughton, C. M. Lesher, and A. Cowden 1986. Thermal erosion by komatiites at Kambalda and genesis of nickel ores. *Nature*, 319, 136-139.
- Groves, D.I., S.E. Ho, N.J. McNaughton, A.G. Mueller, C.S. Perring, N.M.S. Rock, and M.S. Skwarnecki 1988. Genetic models for Archean lode-gold deposits in Western Australia. *Geol. Dept. Univ. Extension, Univ. Western Australia Publ.* 12, 1-22.
- Guilbert, J.M., and C.F. Park, Jr. 1986. *The Geology of ore deposits*. New York: Freeman.

- Guilbert, J.M., and J.D. Lowell 1974. Variations in zoning patterns in porphyry copper deposits. *Can. Inst. Mining Metall. Bull.*, 67, 99-109.
- Guild, P.W. 1972. Metallogeny and the new global tectonics. *24th Int. Geol. Congr. Rept.*, sec. 4, Mineral Deposits, 17-24.
- Gulson, B.L. 1986. Lead isotopes in mineral exploration. Amsterdam: Elsevier.
- Gulson, B.L., W.G. Perkins, and K.J. Mizon 1983. Lead isotope studies bearing on the genesis of copper orebodies at Mount Isa, Queensland. *Econ. Geol.*, 78, 1466-1504.
- Gurr, T.M. 1979. Geology of US phosphate deposits. *Mining Eng.*, 31, 682-691.
- Gustafson, J.K. 1933. Metamorphism and hydrothermal alteration of the Homestake gold-bearing formation. *Econ. Geol.*, 28, 123-162.
- Gustafson, L.B., and J.P. Hunt 1975. The porphyry copper deposit at El Salvador, Chile. *Econ. Geol.*, 70, 857-912.
- Gustafson, L.B. and N. Williams 1981. Sediment-hosted stratiform deposits of copper, lead, and zinc. *Econ. Geol. 75th Anniv. Vol.*, 139-178.
- Gwosdz, W., and W. Krebs 1977. Manganese halo surrounding Meggen ore deposit, Germany. *Inst. Mining Metall. Trans.*, 86, 873-877.
- Haack, U., H. Heinrichs, M. Boness, and A. Schneider 1984. Loss of metals from pelites during regional metamorphism. *Contrib. Mineral. Petrol.*, 85, 116-132.
- Haas, J.L., Jr. 1971. The effect of salinity on the maximum thermal gradient of a hydrothermal system at hydrostatic pressure. *Econ. Geol.*, 66, 940-946.
- Hackett, J.P., Jr. and J.L. Bischoff 1973. New data on the stratigraphy, extent and geologic history of the Red Sea geothermal deposits. *Econ. Geol.*, 68, 553-564.
- Hagemann, S.G., M. Gebro-Mariam, and D.I. Groves 1994. Surface-water influx in shallow-level Archean lode-gold deposits in Western Australia. *Geology*, 22, 1067-1070.
- Haggerty, S.E. 1991. Oxide mineralogy of the upper mantle. *Reviews in Mineralogy*, 25, 355-407.
- Hagni, R.D. 1978. Ore microscopy applied to beneficiation. *Mining Eng.*, 30, 1137-1147.
- Hagni, R.D. 1983. Ore microscopy, paragenetic sequence, trace element content, and fluid inclusion studies of the copper-lead-zinc deposits of the Southeast Missouri lead district. In *International Conference on Mississippi Valley-type lead-zinc deposits — Proc. Vol.*, G. Kisvarsanyi, S.K. Grant, W.P. Pratt, and J.W. Koenig (eds.), 243-256. Rolla: Univ. Missouri-Rolla Press.
- Hagni, R.D. 1995. The Southeast Missouri lead district. *Soc. Econ. Geol. Field Guidebook Series*, 22, 44-78.
- Hagni, R.D., and D.E. Gann 1976. Microscopy of copper ore at the Creta mine, southwestern Oklahoma. *Oklahoma Geol. Survey Circular* 77, 40-50.
- Hagni, R.D. and T.C. Trancynger 1977. Sequence of deposition of the ore minerals at the Magmont mine, Viburnum Trend, Southeast Missouri. *Econ. Geol.*, 72, 451-464.
- Hajash, A. 1975. Hydrothermal processes along mid-ocean ridges: an experimental investigation. *Contrib. Mineral. Petrol.*, 53, 205-226.
- Haji-Vassiliou, A., and P.F. Kerr 1973. Analytical data on nature of urano-organic deposits. *Am. Assoc. Petroleum Geologists Bull.*, 57, 1291-1296.
- Hall, W.E., and I. Friedman 1969. Oxygen and carbon isotopic composition of ore and host rock of selected Mississippi Valley deposits. *U.S. Geol. Survey Prof. Paper* 650-C, C140-C148.
- Hall, W.E., I. Friedman, and J.T. Nash 1974. Fluid inclusion and light stable isotope study of the Climax molybdenum deposits, Colorado. *Econ. Geol.*, 69, 884-901.
- Hall, W.E., H.J. Rose, Jr., and F. Simon 1971. Fractionation of minor elements between galena and sphalerite, Darwin lead-silver-zinc mine, Inyo County, California, and its significance in geothermometry. *Econ. Geol.*, 66, 602-606.
- Hallbauer, D.K. 1975. The plant origin of the Witwatersrand carbon. *Minerals Sci. Eng.*, 7, 111-131.
- Hallbauer, D.K. 1986. The mineralogy and geochemistry of Witwatersrand pyrite, gold, uranium and carbonaceous matter. In *Mineral deposits of southern Africa*, C. R. Anhaeusser and S. Maske (eds.), 1, 731-752. Johannesburg: Geol. Soc. S. Africa.
- Hallbauer, D.K., and J.M. Barton, Jr. 1987. The fossil gold placers of the Witwatersrand. *Gold Bull.*, 20, 68-79.
- Hallberg, J.A., and J.F.H. Thompson 1985. Geologic setting of the Teutonic Bore massive sulfide deposit, Archean Yilgarn Block, Western Australia. *Econ. Geol.*, 80, 1953-1964.
- Hamelin, B., B. Dupré, O. Brévert, and C.J. Allègre 1988. Metallogenesis at paleo-spreading centers: lead isotopes in sulfides, rocks and sediments from the Troodos ophiolite (Cyprus). *Chem. Geol.*, 68, 229-238.
- Hamilton, J. 1977. Sr isotope and trace element studies of the Great Dike and Bushveld mafic phase and their relation to early Proterozoic magma genesis in Southern Africa. *J. Petrol.*, 18, 24-52.
- Hamilton, J.M., D.T. Bishop, H.C. Morris, and O.E. Owens 1982. Geology of the Sullivan orebody, Kimberley, B.C. Canada. *Geol. Assoc. Canada Spec. Paper*, 25, 597-666.
- Hamilton, J.M., G.D. Delany, R.L. Hauser, and P.W. Ransom 1983. Geology of the Sullivan deposit, Kimberley, B.C., Canada. *Mineral. Assoc. Canada Short Course Handbook*, 8, 31-84.

- Hamilton, J.V., and C.J. Hodgson 1986. Mineralization and structure of the Kolar gold field, India. *Proc. Gold '86 Symposium*, Toronto, 270-283. Toronto: Konsult International Inc.
- Hamilton, W. 1969. The volcanic central Andes — a modern model for the Cretaceous batholiths and tectonics of western North America. *Oregon Dept. Geol. Mineral Resources Bull.*, 65, 175-184.
- Hamilton, W. 1970. Bushveld Complex — product of impacts? *Geol. Soc. S. Africa Spec. Publ.* 1, 367-374.
- Hamlyn, P.R., and R.R. Keays 1986. Sulfur saturation and second-stage melts: application to the Bushveld platinum metal deposits. *Econ. Geol.*, 81, 1431-1445.
- Hamlyn, P.R., R.R. Keays, W.E. Cameron, A.J. Crawford, and H.M. Waldron 1985. Precious metals in magnesian low-Ti lavas: implications for metallogenesis and sulfur saturation in primary magmas. *Geochim. Cosmochim. Acta*, 49, 1797-1811.
- Hammerbeck, E.C.I. 1984. Aspects of nickel metallogeny in Southern Africa. In *Sulphide deposits in mafic and ultramafic rocks*, D. L. Buchanan and M. J. Jones (eds.), 135-140. London: Inst. Mining & Metall.
- Hammond, P. 1952. Allard Lake ilmenite deposits. *Econ. Geol.*, 47, 634-649.
- Hammond, P., and L.A. Taylor 1982. The ilmenite/titano-magnetite assemblage: kinetics of re-equilibration. *Earth Planet. Sci. Lett.*, 61, 143-150.
- Hanes, J.A., D.A. Archibald, C.J. Hodgson, and F. Robert 1992. Dating of Archean auriferous quartz vein deposits in the Abitibi greenstone belt, Canada: $^{40}\text{Ar}/^{39}\text{Ar}$ evidence for a 70- to 100-m.y. time gap between plutonism-metamorphism and mineralization. *Econ. Geol.*, 87, 1849-1861.
- Hannah, J.L. and H.J. Stein 1984. Evidence of changing ore composition: stable isotope analyses of secondary sedimentary carbonates, Bonnetterre Formation, Missouri. *Econ. Geol.*, 79, 1930-1935.
- Hannak, W.W. 1981. Genesis of the Rammelsberg ore deposit near Goslar/Upper Harz, Federal Republic of Germany. In *Handbook of strata-bound and stratiform ore deposits*, K.H. Wolf (ed.), 9, 551-642. Amsterdam: Elsevier.
- Hannington, M.D., P.M. Herzig, and S.D. Scott 1991. Auriferous hydrothermal precipitates on the modern seafloor. In *Gold metallogeny and exploration*, R.P. Foster (ed.), 249-282. Glasgow: Blackie.
- Hannington, M.D., M.K. Tivey, A.C. Larcque, S. Petersen, and P.A. Rona 1995. The occurrence of gold in sulfide deposits of the TAG hydrothermal field, Mid-Atlantic Ridge. *Can. Mineral.*, 33, 1285-1310.
- Hanor, J.S. 1979. The sedimentary genesis of hydrothermal fluids. In *Geochemistry of hydrothermal ore deposits*, 2nd edn., H.L. Barnes (ed.), 137-172. New York: Wiley.
- Hanor, J.S. 1983. Fifty years of development of thought on the origin and evolution of subsurface sedimentary brines. In *Revolutions in the earth sciences*, S.J. Boardman (ed.), 99-111. Dubuque, Iowa: Kendall/Hunt.
- Hanor, J.S. 1995. Controls on the solubility of lead and zinc in basinal brines: field evidence. *Extended Abstracts, International Field Conference on carbonate-hosted lead-zinc deposits*, St. Louis, Missouri, June 1995, 121-123.
- Hansley, P. L. 1986. Regional diagenetic trends and uranium mineralization in the Morrison Formation across the Grants uranium region. *Am. Assoc. Petroleum Geologists Studies in Geology* 22, 277-301.
- Hansley, P.L., and C.S. Spirakis 1992. Organic matter diagnosis as the key to a unifying theory for the genesis of tabular uranium-vanadium deposits in the Morrison Formation, Colorado Plateau. *Econ. Geol.*, 87, 352-365.
- Hanson, G.N. 1980. Rare earth elements in petrogenetic studies of igneous systems. *Annual Rev. Earth Planet. Sci.* 8, 371-406.
- Harder, V.M. 1986. Fluorite: a fission track age dating material [abs.]. *Geol. Soc. Am. Abstracts with Programs* 18, 628.
- Harmer, R.E. and M.R. Sharpe 1985. Field relations and strontium isotope systematics of the marginal rocks of the eastern Bushveld Complex. *Econ. Geol.*, 80, 813-837.
- Harrar, J.E., and E. Raber 1984. Chemical analysis of geothermal waters and strategic petroleum reservoir brines for metals of economic importance. *Geothermics*, 13, 349-360.
- Harris, D.C. 1986. Mineralogy and geochemistry of the Main Hemlogold deposit, Hemlo, Ontario, Canada. In *Proc. Gold '86 Symposium*, A.J. Macdonald (ed.), 297-310. Toronto: Konsult International Inc.
- Harris, L.D. 1969. Kingsport Formation and Mascot Dolomite (Lower Ordovician) of East Tennessee. *Tenn. Div. Geol. Rept. Inv.* 23, 1-29.
- Harris, L.D. 1971. A Lower Paleozoic paleoaquifer — the Kingsport Formation and Mascot Dolomite of Tennessee and southwest Virginia. *Econ. Geol.*, 66, 735-743.
- Harris, N.B., and M.T. Einaudi 1982. Skarn deposits in the Yerrington district, Nevada: Metasomatic skarn evolution near Ludwig. *Econ. Geol.*, 77, 877-898.
- Harrison, A.G., and H.G. Thode 1957. The kinetic isotope effect in the chemical reduction of sulphate. *Trans. Faraday Soc.*, 53, 1648-1651.
- Harshman, E.N. 1968a. Uranium deposits of Wyoming and South Dakota. In *Ore deposits of the United States 1933-1967 (The Graton-Sales Volume)*, J. D. Ridge (ed.), 2, 815-821. New York: Am. Inst. Mining Metall. and Petroleum Engineers.

- Harshman, E.N. 1986b. Uranium deposits of the Shirley Basin, Wyoming. In *Ore deposits of the United States, 1933-1967 (Graton-Sales Volume)*, J.D. Ridge (ed.), 2, 849-856. New York: Am. Inst. Mining Metall. and Petroleum Engineers.
- Hart, S.R., and E.D. Kinloch 1989. Osmium isotope systematics in Witwatersrand and Bushveld ore deposits. *Econ. Geol.*, 84, 1651-1655.
- Hart, S.R., N. Shimizu, and D. A. Sverjensky 1981. Lead isotope zoning in galena: an ion microprobe study of a galena from the Buick mine. *Econ. Geol.*, 76, 1873-1878.
- Harte, B. 1978. Kimberlite nodules, upper mantle petrology, and geotherms. *Phil. Trans. Royal Soc. London, A*, 288, 487-500.
- Hartman, W.K., R.J. Phillips, and G.J. Taylor 1986. *Origin of the Moon*. Huston: Lunar and Planetary Institute.
- Hatcher, R.D., Jr., and A.L. Odom 1980. Timing of thrusting in the southern Appalachians, USA: model for orogeny? *J. Geol. Soc. London*, 137, 321-327.
- Hatton, C.J. 1989. Continental configuration during the formation of the Bushveld Complex [abs.]. *International Geol. Congress, 28th, Washington, 1989, Abstracts*, 2, 40.
- Hatton, C.J., and G. von Gruenewaldt, 1987. The geological setting and petrogenesis of the Bushveld chromitite layers. In *Evolution of chrome ore fields*, C.W. Stowe (ed.), 109-143. New York: Van Nostrand-Reinhold.
- Hattori, K., and K. Muehlenbachs 1980. Marine hydrothermal alteration at a Kuroko ore deposit, Kosaka, Japan. *Contrib. Mineral. Petrol.*, 74, 285-292.
- Hattori, K., F.A. Campbell, and H.R. Krouse 1986. Sulfur isotope abundances in sedimentary rocks, relevance to the evolution of the Precambrian atmosphere. *Geochem. International*, 22, 97-115.
- Houghton, D.R., P.L. Roeder, and B.J. Skinner 1974. Solubility of sulfur in mafic magmas. *Econ. Geol.*, 69, 451-467.
- Hawkesworth, C.J. 1982. Isotopic characteristics of magmas erupted along destructive plate margins. In *Andesites: orogenic andesites and related rocks*, R.S. Thorpe (ed.), 549-571. New York: Wiley.
- Hawley, J.E. 1962. The Sudbury ores: their mineralogy and origin. *Can. Mineral.*, 7, 1-207.
- Hawley, J.E., and I. Nichol 1961. Trace elements in pyrite, pyrrhotite and chalcopyrite of different ores. *Econ. Geol.*, 56, 467-487.
- Hayashi, K., and H. Ohmoto 1991. Solubility of gold in NaCl- and H₂S-bearing aqueous solutions at 250-350°C. *Geochim. Cosmochim. Acta*, 55, 2111-2126.
- Hayba, D.O. 1997. Environment of ore deposition in the Creede mining district, San Juan Mountains, Colorado: Part V. Epithermal mineralization from fluidmixing in the OH vein. *Econ. Geol.*, 92, 29-44.
- Hayba, D.O., P.M. Bethke, P. Heald, and N.K. Foley 1985. Geologic, mineralogic, and geochemical characteristics of volcanic-hosted epithermal precious-metal deposits. *Rev. Econ. Geol.*, 2, 129-167.
- Hayes, J. M. 1983. Geochemical evidence bearing on the origin of aerobiosis, a speculative hypothesis. In *The Earth's earliest biosphere: its origin and evolution*, J.W. Schopf (ed.), 291-301. Princeton, New Jersey: Princeton Univ. Press.
- Hayes, T.S., and M.T. Einaudi 1986. Genesis of the Spar Lake strata-bound copper-silver deposit, Montana. Part I. diagenesis. *Econ. Geol.*, 87, 1899-1931.
- Haymon, R.M. 1983. Growth history of hydrothermal black smoker chimneys. *Nature* 301, 695-698.
- Haymon, R.M., and M. Kastner 1981. Hot spring deposits on the East Pacific Rise at 21°N, preliminary description of mineralogy and genesis. *Earth Planet. Sci. Lett.*, 53, 363-381.
- Haymon, R.M., and K.C. Macdonald 1985. The geology of deep sea hot springs. *Am. Scientist*, 73, 441-450.
- Haymon, R.M., R.A. Koski, and C. Sinclair 1984. Fossils of hydrothermal vent worms discovered in Cretaceous sulfide ores of the Samail ophiolite, Oman. *Science*, 223, 1407-1409.
- Haynes, D.W. 1986a. Stratiform copper deposits hosted by low-energy sediments: I. Timing of sulfide precipitation- an hypothesis. *Econ. Geol.*, 81, 250-265.
- Haynes, D.W. 1986b. Stratiform copper deposits hosted by low-energy sediments. II. Nature of source rocks and composition of metal-transporting water. *Econ. Geol.*, 81, 266-280.
- Haynes, D.W., and M.S. Bloom 1987a. Stratiform copper deposits hosted by low-energy sediments: III. Aspects of metal transport. *Econ. Geol.*, 82, 635-648.
- Haynes, D.W., and M.S. Bloom 1987b. Stratiform copper deposits hosted by low-energy sediments: IV. Aspects of sulfide precipitation. *Econ. Geol.*, 82, 875-893.
- Haynes, F.M., and S.E. Kesler 1987. Chemical evolution of brines during Mississippi Valley-type of mineralization: evidence from East Tennessee and Pine Point. *Econ. Geol.*, 82, 482-488.
- Haynes, F.M., S.E. Kesler, and R.E. Beane 1987. Chemical analysis of fluid inclusions by SEM/EDA: an application to Mississippi Valley-type mineralization. *Am. Current Res. Fluid Inclusions meeting, Jan. 5-7, 1987, Socorro, New Mexico*.
- Heald, P., N.K. Foley, and D.O. Hayba 1987. Comparative anatomy of volcanic-hosted epithermal deposits: acid-sulfate and adularia-sericite types. *Econ. Geol.*, 82, 1-26.

- Hedenquist, J.W., and R.W. Henley 1985a. The importance of CO₂ on freezing point measurements of fluid inclusions: evidence from active geothermal systems and implications for epithermal ore deposition. *Econ. Geol.*, 80, 1379-1406.
- Hedenquist, J.W., and R.W. Henley 1985b. Hydrothermal eruptions in the Waiotapu geothermal system, New Zealand: their origin, associated breccias, and relation to precious metal mineralization. *Econ. Geol.*, 80, 1640-1668.
- Hedenquist, J.W., and J.B. Lowenstern 1994. The role of magmas in the formation of hydrothermal ore deposits. *Nature*, 370, 519-527.
- Hedge, C.E. 1974. Strontium isotopes in economic geology. *Econ. Geol.*, 69, 823-825.
- Hegge, M. R., and J. C. Rowntree 1978. Geologic setting and concepts of the origin of main deposits in the East Alligator River region, N. T., Australia. *Econ. Geol.*, 73, 1420-1429.
- Heidrick, T.L., and S.R. Titley 1982. Fracture and dike patterns in Laramide plutons and their structural and tectonic implications, American Southwest. In *Advances in Geology of the porphyry copper deposits of the American southwest*, S.R. Titley (ed.), 73-91. Tucson: Univ. Arizona Press.
- Heinrich, C.A., A.S. Andrew, R.W.T. Wilkins, and D.J. Patterson 1989. A fluid inclusion and stable isotope study of synmetamorphic copper ore formation at Mount Isa, Australia. *Econ. Geol.*, 84, 529-550.
- Heinrich, C.A., J.H.C. Bain, T.P. Mernagh, L.A. Wyborn, A.S. Andrew, and C.L. Waring 1995. Fluid and mass transfer during metabasalt alteration and copper mineralization at Mount Isa, Australia. *Econ. Geol.*, 90, 705-730.
- Heinrich, E.W. 1966. *The Geology of carbonatites*. Chicago: Rand McNally.
- Hekinian, H., and D. Bideau 1986. Volcanism and mineralization of the oceanic crust on the East Pacific Rise. In *Metallogeny of basic and ultrabasic rocks*, M. J. Gallagher, R. A., Ixer, C. R. Neary, and H. M. Prichard (eds.), 3-20. London: Inst. Mining Metall.
- Hekinian, H., and Y. Fouquet 1985. Volcanism and metallogenesis of axial and off-axial structures on the East Pacific Rise near 13°N. *Econ. Geol.*, 80, 221-249.
- Hekinian, R., M. Fevrier, J.L. Bischoff, P. Picot, and W.C. Shanks 1980. Sulfide deposits from the East Pacific Rise near 21°N. *Science*, 207, 1433-1444.
- Helgeson, H.C. 1964. *Complexing and hydrothermal ore deposition*. New York: Pergamon Press.
- Helgeson, H.C. 1970. A chemical and thermodynamic model of ore deposition in hydrothermal systems. *Mineral. Soc. Am. Spec. Paper* 3, 155-186.
- Helgeson, H. C. 1974. Chemical interactions of feldspars and aqueous solutions. In *The feldspars*, W. S. MacKenzie and J. Zussman (eds.), 184-215. Manchester: Manchester University Press.
- Helgeson, H.C., and R.M. Garrels 1986. Hydrothermal transport and deposition of gold. *Econ. Geol.*, 63, 622-635.
- Hellingwerf, R. 1986. Regional and localized hydrothermal alterations during sub-seafloor metamorphism in western Bergslagen, Sweden: implications for metal prospecting [abs.]. *Terra Cognita*, 6, 545.
- Hemley, J.J., and W.R. Jones 1964. Chemical aspects of hydrothermal alteration with emphasis on hydrogen metasomatism. *Econ. Geol.*, 59, 538-569.
- Hemley, J.J., G.L. Cygan, and W.M. d'Angelo 1986. Effect of pressure on ore mineral solubilities under hydrothermal conditions. *Geology*, 14, 377-379.
- Hemley, J.J., P.B. Hosteller, A.J. Gude, and W.T. Mountjoy 1969. Some stability relations of alunite. *Econ. Geol.*, 64, 599-612.
- Hemley, J.J., J.W. Montoya, J.W. Marinenko, and R.W. Luce 1980. General equilibrium in the system Al₂O₃-SiO₂-H₂O and some implications for alteration/mineralization processes. *Econ. Geol.*, 75, 210-228.
- Hemley, J.J., J.W. Montoya, A. Nigrini, and H.A. Vincent 1971. Some alteration reactions in the system CaO-Al₂O₃-SiO₂-H₂O. *Soc. Mining Geol. Japan Spec. Issue* 2, 58-63.
- Hemley, J.J., G.L. Cygan, J.B. Fein, G.R. Robinson, and W.M. D'Angelo 1992. Hydrothermal ore-forming processes in the light of studies in rock-buffered systems: I. Iron-copper-zinc-lead sulfide solubility relations. *Econ. Geol.*, 87, 1-22.
- Henley, R.W. 1973. Solubility of gold in hydrothermal chloride solutions. *Chem. Geol.*, 11, 73-87.
- Henley, R.W. 1991. Epithermal gold deposits in volcanic terranes. In *Gold metallogeny and exploration*, R.P. Foster (ed.), 133-164. Glasgow: Blackie.
- Henley, R.W., and J. Adams 1979. On the evolution of giant gold placers. *Inst. Mining Metall. Trans.*, 88, B41-B50.
- Henley, R.W., and A.J. Ellis 1983. Geothermal systems ancient and modern: a geochemical review. *Earth Sci. Rev.*, 19, 1-50.
- Henley, R.W., and A. McNabb 1978. Magmatic vapor plumes and ground-water interaction in porphyry copper emplacement. *Econ. Geol.*, 73, 1-20.
- Henley, R.W., and P. Thornley 1979. Some geothermal aspects of polymetallic massive sulfide formation. *Econ. Geol.*, 74, 1600-1612.
- Hennet, R.J.C., D.A. Crerar, and J. Schwartz 1988. Organic complexes in hydrothermal systems. *Econ. Geol.*, 83, 742-764.

- Henry, D.J. and L.G. Medaris, Jr. 1980. Application of pyroxene and olivine-spinel geothermometers to spinel peridotites in southwestern Oregon. *Am. J. Sci.*, 280-A, 211-231.
- Hersch, J.B., and K.C. Misra 1979. Role of evaporites in the formation of Mississippi Valley-type deposits [abs.]. *Program and Abstracts, 108th AIME Mtg., New Orleans, 1979*, 55.
- Herz, N. 1976a. Titanium deposits in alkaline igneous rocks. *U.S. Geol. Survey Prof. Paper* 959-E, E1-E6.
- Herz, N. 1976b. Titanium deposits in anorthositic massifs. *U.S. Geol. Survey Prof. Paper* 959-D, D1-D6.
- Herzig, P.M., and M.D. Hannington 1995. Polymetallic massive sulfides at the modern seafloor: a review. *Ore Geol. Rev.*, 10, 95-115.
- Hewlett, R.L., and P.J. Solomon 1964. The role of mobilization in silver-lead-zinc sulphide assemblages, with particular reference to Mt. Isa, Australia. *International Geol. Congress, 22nd, New Delhi, India* (unpublished report).
- Heyl, A.V. 1967. Some aspects of genesis of stratiform zinc-lead-barite-fluorite deposits in the United States. *Econ. Geol. Mono* 3, 20-32.
- Heyl, A.V. 1983. Geologic characteristics of three major Mississippi Valley districts. In *International Conference on Mississippi Valley type lead-zinc deposits — Proc. Vol.*, G. Kisvarsanyi, S.K. Grant, W.P. Pratt, and J.W. Koenig (eds.), 27-60. Rolla: Univ. of Missouri-Rolla Press.
- Hiemstra, S.A. 1985. The distribution of some platinum group elements in the UG2 chromitite layer of the Bushveld Complex. *Econ. Geol.*, 80, 944-957.
- Higgins, N.C. 1985. Wolframite deposition in a hydrothermal vein system: the Grey River tungsten prospect, Newfoundland, Canada. *Econ. Geol.*, 80, 1297-1327.
- Hill, R. and P. Roeder 1974. The crystallization of spinel from basaltic liquid as a function of oxygen fugacity. *J. Geol.*, 82, 709-729.
- Hill, R.E.T. 1984. Experimental study of phase relations at 600°C in a portion of the Fe-Ni-Cu-S system and its application to natural sulfide assemblages. In *Sulfide deposits in mafic and ultramafic rocks*, D. Buchanan and M.J. Jones (ed.), 14-21. London: Inst. Mining Metall.
- Hill, W.T., R.G. Morris, and C.G. Hagegeorge 1971. Ore controls and related sedimentary features at the Flat Gap mine, Treadway, Tennessee. , 66, 748-756.
- Hilpert, L. S. 1969. Uranium resources of northwestern New Mexico. *U.S. Geol. Survey Prof. Paper* 603, 166p.
- Hinman, M.C. 1995. Base-metal mineralization at McArthur River: structure and kinematics of the HYC-Cooly zone at McArthur River. *Austral. Geol. Survey Organization Record* 1995/5, 29 p.
- Hitzman, M.W., and D.W. Beaty 1996. The Irish Zn-Pb-(Ba) orefield. *Soc. Econ. Geol. Spec. Pub.* 4, 112-143.
- Hitzman, M.W., and D. Large 1986. A review and classification of the Irish carbonate-hosted base metal deposits. In *Geology and genesis of mineral deposits in Ireland*, C.J. Andrew, R.W.A. Crowe, S. Finlay, W.M. Pennell, and J.F. Payne (eds.), 217-238. Dublin: Irish Assoc. Econ. Geol.
- Hobbs, B.E. 1987. Principles involved in mobilization and remobilization. *Ore Geol. Rev.*, 2, 37-45.
- Hodgson, C.J. 1986. Place of gold ore formation in the geological development of Abitibi greenstone belt, Ontario, Canada. *Inst. Mining Metall. Trans.*, 95B, 183-194.
- Hodgson, C.J. 1989. The structure of shear-related, vein-type gold deposits: a review. *Ore Geol. Rev.*, 4, 231-273.
- Hodgson, C. J., and J. W. Lydon 1977. Geological setting of volcanogenic massive sulfide deposits and active hydrothermal systems: some implications for exploration. *Can. Inst. Mining Metall. Bull.*, 70, 95-106.
- Hodgson, C.J. and P.J. MacGeehan 1982. A review of the geological characteristics of 'gold only' deposits in the Superior Province of the Canadian Shield. *Can. Inst. Mining Metall. Spec. Vol.* 24, 211-228.
- Hoefs, J. 1987. *Stable isotope geochemistry*, 3rd. edn.. New York: Springer.
- Hoeve, J., and D. Quirt 1989. A common diagenetic-hydrothermal origin for unconformity-type uranium and stratiform copper deposits? *Geol. Assoc. Canada Spec. Paper*, 36, 151-172.
- Hoeve, J., and T.I.I. Sibbald 1978. On the origin of Rabbit Lake and other unconformity-type uranium deposits in northern Saskatchewan, Canada. *Econ. Geol.*, 73, 1450-1473.
- Hoeve, J., T.I.I. Sibbald, P. Ramaekers, and J.F. Lewry 1980. Athabasca Basin unconformity-type uranium deposits: a special-class of sandstone-type deposits? In *Uranium in the Pine Creek geosyncline*, J. Ferguson and A. B. Goleby (eds.), 575-594. Vienna: International Atomic Energy Agency.
- Hoffman, E.L., A. J. Naldrett, R.A. Alcock, and R.G.V. Hancock 1979. The noble metal content of ore in the Levack West and Little Stobie mines. *Can. Mineral.*, 17, 437-452.
- Hofstra, A.H., G.P. Landis, and W.A. Rowe 1987. Sediment-hosted disseminated gold mineralization at Jerritt Canyon, Nevada. II- Fluid geochemistry [abs.]. *Geol. Soc. Am. Abstracts with Programs*, 19, 704.
- Hofstra, A.H., J.S. Leventhal, H.R. Northrop, G.P. Landis, R.O. Rye, D.J. Birak, and A.R. Dahl 1991. Genesis of sediment-hosted disseminated-gold deposits: chemical-reaction-path modeling of ore-depositional processes documented in the Jerritt Canyon district, Nevada. *Geology*, 19, 36-40.

- Holdaway, M.J. 1971. Stability of andalusite and the aluminum silicate phase diagram. *Am. J. Sci.*, 271, 97-131.
- Holland, H.D. 1959. Some applications of thermodynamic data to problems of ore deposits. I. Stability relations among the oxides, sulfides, sulfates and carbonate of ore and gangue minerals. *Econ. Geol.*, 54, 184-233.
- Holland, H.D. 1962. Model for the evolution of the earth's atmosphere. In *Petrologic studies: a volume to honor A. F. Buddington*, A. E.J. Engel, H.L. James, and B.F. Leonard (eds.), 447-477. Boulder, Colorado: Geol. Soc. Am.
- Holland, H.D. 1965. Some applications of thermodynamical data to problems of ore deposits. II. Mineral assemblages and the compositions of ore-forming fluids. *Econ. Geol.*, 60, 1101-1166.
- Holland, H.D. 1972. Granites, solutions and base metal deposits. *Econ. Geol.*, 67, 281-301.
- Holland, H.D. 1973. The oceans: a possible source of iron in iron-formations. *Econ. Geol.*, 68, 1169-1172.
- Holland, H.D. 1984. *The Chemical Evolution of the Atmosphere and the Oceans*. Princeton: Princeton Univ. Press.
- Holland, H.D. 1992. Distribution and paleoenvironmental interpretation of Proterozoic paleosols. In *The Proterozoic biosphere: a multidisciplinary study*, J.W. Schopf and C. Klein (eds.), 153-155. New York: Cambridge Univ. Press.
- Holland, H.D., and J.F. Kasting 1992. The environment of the Archean earth. In *The Proterozoic biosphere: a multidisciplinary study*, J.W. Schopf and C. Klein (eds.), 21-24. New York: Cambridge Univ. Press.
- Holland, H.D., and S.D. Malinin 1979. The solubility and occurrence of non-ore minerals. In *Geochemistry of hydrothermal ore deposits, 2nd. edn.*, H.L. Barnes (ed.), 461-508. New York: Wiley.
- Hollister, L.S., and M.L. Crawford (eds.). *Short course in fluid inclusions: applications to petrology*. Calgary: Mineral. Assoc. Canada.
- Hollister, V.F. 1973. Regional characteristics of porphyry copper deposits of South America. *Mining Eng.*, 51-56.
- Hollister, V.F. 1975. An appraisal of the nature and source of porphyry copper deposits. *Minerals Sci. Eng.*, 7, 225-233.
- Hollister, V.F. 1978. *Geology of the porphyry copper deposits of the Western Hemisphere*. New York: Soc. Mining Engineers.
- Hollister, V.F., R.R. Potter, and A.L. Barker 1974. Porphyry-type deposits of the Appalachian orogen. *Econ. Geol.*, 69, 618-630.
- Holloway, J.R. 1981. Compositions and volumes of supercritical fluids in the earth's crust. In *Short course in fluid inclusions: applications to petrology*, L.S. Hollister and M.J. Crawford (eds.), 13-38. Calgary: Mineral. Assoc. Canada.
- Holmden, C.E., and K. Muehlenbachs 1993. The $^{18}\text{O}/^{16}\text{O}$ ratio of 2-billion-year-old seawater inferred from ancient oceanic crust. *Science*, 259, 1733-1736.
- Hoppe, A., C. Schobbenhaus, and D.H. G. Walde 1987. Precambrian iron-formation in Brazil. In *Precambrian iron-formations*, P.W.U. Appel and G.L. LaBerge (eds.), 347-392. Athens: Theophrastus Publ.
- Horikoshi, E. 1990. Opening of the Sea of Japan and Kuroko deposit formation. *Mineral. Deposita*, 25, 140-145.
- Horrall, K.B., R.D. Hagni, and G. Kisvarsanyi 1983. Mineralogical, textural, and paragenetic studies of selected ore deposits of the Southeast Missouri lead-zinc-copper district and their genetic implications. In *International Conference on Mississippi Valley type lead-zinc deposits — Proc. Vol.*, G. Kisvarsanyi, S.K. Grant, W.P. Pratt, and J.W. Koenig (eds.), 289-316. Rolla, Missouri: Univ. Missouri - Rolla Press.
- Horton, D.J. 1978. Porphyry-type copper-molybdenum mineralization belts in eastern Queensland, Australia. *Econ. Geol.*, 73, 904-921.
- Hosking, K.F.G. 1979. Tin distribution patterns. *Geol. Soc. Malaysia Bull.*, 11, 1-70.
- Hosterman, J.W., A.V. Heyl, and J.L. Jolly 1964. Qualitative x-ray emission analysis studies of enrichment of common elements in wall-rock alteration in the Upper Mississippi Valley zinc-lead district. *U.S. Geol. Survey Prof. Paper* 501-D, 50-54.
- Housenack, D.W. 1989. Earliest Paleozoic stratigraphy and facies, Reelfoot basin and adjacent craton. In *Field guide to the Upper Cambrian of Southeastern Missouri: stratigraphy, sedimentology, and economic geology*, J.M. Gregg (ed.), 25-42. Rolla, Missouri: Univ. Missouri-Rolla.
- Hoy, L.D., and H. Ohmoto 1989. Constraints for the genesis of red bed-associated stratiform Cu deposits from sulphur and carbon mass-balance relations. *Geol. Assoc. Canada Spec. Paper* 36, 135-150.
- Hsu, L.C., P.J. Lechler, and J.H. Nelson 1991. Hydrothermal solubility of palladium in chloride solutions from 300° to 700°C: preliminary experimental results. *Econ. Geol.*, 86, 422-427.
- Hunt, G. 1962. Time of Purcell eruption in southeastern British Columbia and southwestern Alberta. *Alberta Soc. Petroleum Geol. J.*, 10, 438-442.
- Huppert, H.E. and R.S.J. Sparks 1985. Komatiites I: Eruption and flow. *J. Petrol.*, 26, 694-725.
- Huston, D.L., and R.R. Large 1989. A chemical model for the concentration of gold in volcanogenic massive sulfide deposits. *Ore Geol. Rev.*, 4, 174-200.

- Hutchinson, C.S. 1983. *Economic deposits and their tectonic setting*. New York: Wiley.
- Hutchinson, C.S. 1996. *South-east Asian oil, gas, coal and mineral deposits*. Oxford: Clarendon Press.
- Hutchinson, C.S., and K.R. Chakraborty 1979. Tin: a mantle or crustal source? *Geol. Soc. Malaysia Bull.*, 2, 71-79.
- Hutchinson, M.N. and S.D. Scott 1980. Sphalerite geobarometry applied to metamorphosed sulfide ores of the Swedish Caledonides and U. S. Appalachians. *Norges geologiske undersokelse*, 360, 59-71.
- Hutchinson, M.N., and S.D. Scott 1981. Sphalerite geobarometry in the Cu-Fe-Zn-S system. *Econ. Geol.*, 76, 143-158.
- Hutchinson, M.N., and S.D. Scott 1983. Experimental calibration of the sphalerite cosmobarometer. *Geochim. Cosmochim. Acta*, 47, 101-108.
- Hutchinson, R. W. 1973. Volcanogenic sulfide deposits and their metallogenic significance. *Econ. Geol.*, 68, 1223-1246.
- Hutchinson, R.W. 1979. Evidence for exhalative origin for Tasmanian tin deposits. *Can. Inst. Mining Metall. Bull.*, 72, 808, 90-104.
- Hutchinson, R.W. 1980. Massive base metal sulphide as guides to tectonic evolution. *Geol. Assoc. Canada Spec. Paper* 20, 659-684.
- Hutchinson, R.W. 1987. Metallogeny of Precambrian gold deposits: space and time relationships. *Econ. Geol.*, 82, 1993-2007.
- Hutchinson, R.W. 1993. A multi-stage, multi-process genetic hypothesis for greenstone-hosted gold lodes. *Ore Geol. Rev.*, 8, 349-382.
- Hutchinson, R.W., and J.L. Burlington 1984. Some broad characteristics of greenstone belt gold lodes. In *Gold '82*, R.P. Foster (ed.), *Geol. Soc. Zimbabwe Spec. Publ.* 1, 339-372. Rotterdam: A. A. Balkema Publ.
- Hutchinson, R.W., and D.L. Searle 1971. Stratabound pyrite deposits in Cyprus and relation to other sulphide ores. *Soc. Mining Geol. Japan Spec. Issue* 3, 198-205.
- Hutchinson, R.W. and R.P. Viljoen 1988. Re-evaluation of gold sources in Witwatersrand ores. *S. African J. Geol.*, 91, 157-173.
- Hutchinson, R.W., W.S. Fyfe, and R. Kerrich 1980. Deep fluid penetration and ore deposition. *Minerals. Sci. Eng.*, 12, 107-120.
- Iijima, A. 1974. Clay and zeolitic alteration zones surrounding Kuroko deposits in the Hokuroku district, Northern Akita, as submarine hydrothermal-diagenetic alteration products. *Soc. Mining Geol. Japan Spec. Issue* 6, 267-290.
- Ilchik, A. 1990. Geology and geochemistry of the Vantage gold deposits, Alligator Ridge-Bald Mountain mining district, Nevada. *Econ. Geol.*, 85, 50-75.
- Iler, R. K. 1979. *The chemistry of silica*. New York: Wiley.
- Innes, D.G., and A.C. Colvine 1984. The regional metallogenic setting of Sudbury. In *The Geology and ore deposits of the Sudbury Structure*, E. G. Pye, A. J. Naldrett, and P. E. Giblin (eds.), *Ont. Geol. Survey Spec. Vol.* 1, 45-56. Toronto: Ontario Geol. Survey.
- Irvine, T.N. 1965. Chromian spinel as a petrogenetic indicator, Part 1, Theory. *Can. J. Earth Sci.*, 2, 648-672.
- Irvine, T.N. 1967. Chromian spinel as a petrogenetic indicator, Part 2, Petrologic applications. *Can. J. Earth Sci.*, 4, 71-103.
- Irvine, T.N. 1975. Crystallization sequence in the Muskox intrusion and other layered intrusions-II. Origin of chromitite layers and similar deposits of other magmatic ores. *Geochim. Cosmochim. Acta*, 39, 991-1020.
- Irvine, T.N. 1977. Origin of chromitite layers in the Muskox intrusion and other stratiform intrusions: a new interpretation. *Geology*, 5, 273-277.
- Irvine, T.N. 1980. Infiltration metasomatism, accumulate growth and double-diffusive fractional crystallization in the Muskox intrusion and other layered intrusions. In *Physics of magmatic processes*, R.B. Hargraves (ed.), 325-383. Princeton, New Jersey: Princeton Univ. Press.
- Irvine, T.N. and M.R. Sharpe 1982. Source-rock compositions and depths of origin of Bushveld and Stillwater magmas. *Carnegie Inst. Washington Year Book* 81, 294-303.
- Irvine, T.N., and M.R. Sharpe 1986. Magma mixing and the origin of stratiform oxide ore zones in the Bushveld and Stillwater Complexes. In *Metallogeny of basic and ultrabasic rocks*, M. J. Gallagher, R. A. Ixer, C. R. Neary, and H. M. Pritchard (eds.), 183-198. London: Inst. Mining and Metall.
- Irvine, T.N., D.W. Keith, and S.G. Todd 1983. The J-M platinum-palladium Reef of the Stillwater Complex, Montana: II. Origin by double-diffusive convective magma mixing and implications for the Bushveld Complex. *Econ. Geol.*, 78, 1287-1334.
- Ishihara, S. 1977. The magnetite-series and ilmenite-series granitic rocks. *Mining Geol.*, 26, 293-305.
- Ishihara, S. 1981. The granitoid series and mineralization. *Econ. Geol. 75th Anniv. Vol.*, 458-484.
- Ishihara, S., Y. Sakamaki, A. Sasaki, Y. Teraoka, and S. Treashima 1986. Role of the basement in the genesis of the Hishikari gold-quartz vein deposit, southern Kyushu, Japan. *Mining Geol.*, 36, 233-266.
- Isuk, E.E., and J.H. Carman 1981. The system $\text{Na}_2\text{Si}_2\text{O}_7\text{-K}_2\text{Si}_2\text{O}_7\text{-MoS}_2\text{-H}_2\text{O}$ with implications for molybdenum transport in silicate melts. *Econ. Geol.*, 76, 2222-2235.

- Itoh, S. 1971a. Chemical composition of country rocks and minor elements in sulphide minerals from bedded cuprififerous pyrite deposits of Tenryu River basin. *Bull. Geol. Survey Japan*, 22, 117-132.
- Itoh, S. 1971b. Minor elements in sulphide minerals from Shirataki mine, Kochi Prefecture, Japan. *Bull. Geol. Survey Japan*, 22, 367-384.
- Izawa, E., and Y. Urashima 1989. Quaternary gold mineralization and its geologic environments in Kyushu, Japan. *Econ. Geol. Mono.* 6, 233-241.
- Jackson, E.D. 1961. Primary textures and mineral associations in the Ultramafic Zone of the Stillwater Complex, Montana. *U.S. Geol. Survey Prof. Paper* 358, 106p.
- Jackson, E.D. 1968. The chromite deposits of the Stillwater Complex, Montana. In *Ore deposits of the United States (Graton-Sales Volume)*, J.D. Ridge (ed.), 2, 1495-1510. New York: Am. Inst. Mining Metall. and Petroleum Engineers.
- Jackson, E.D. 1969. Chemical variation in coexisting chromite and olivine in chromite zones of the Stillwater Complex. *Econ. Geol. Mono.* 4, 41-71.
- Jackson, E.D. and T.P. Thayer 1972. Some criteria for distinguishing between stratiform, concentric, and Alpine peridotite-gabbro complexes. *Proc. International Geol. Congress*, 24th, 2, 289-296.
- Jackson, N.J. 1979. Geology of the Cambrian tin field: a review. In *Geology of tin deposits*, C.H. Yeap (ed.), *Geol. Soc. Malaysia Bull.*, 11, 209-238.
- Jackson, S.A. and F.W. Beales 1967. An aspect of sedimentary basin evolution: the concentration of Mississippi Valley-type ores during late stages of diagenesis. *Can. Petroleum Geol. Bull.*, 15, 383-433.
- Jacobson, S.B., and M.R. Pimentel-Klose 1988. A Nd isotopic study of the Hamersley and Michipicoten banded iron formations: the source of REE and Fe in Archean oceans. *Earth Planet. Sci. Lett.*, 87, 29-44.
- Jahns, R.H. 1946. Mica deposits of the Petaca district, Rio Arriba County, New Mexico. *New Mexico Bur. Mines Mineral Res. Bull.*, 25.
- Jambor, J.L. 1971a. Gangue mineralogy. In *The silver-arsenide deposits of the Cobalt-Gowganda region, Ontario*, L.G. Berry (ed.), *Can. Mineral.*, 11, Pt. 1, 232-262.
- Jambor, J.L. 1971b. Origin of the silver veins. In *The silver-arsenide deposits of the Cobalt-Gowganda region, Ontario*, L.G. Berry (ed.), *Can. Mineral.*, 11, Pt. 1, 402-423.
- Jambor, J.L. 1979. Mineralogical evaluation of proximal-distal features in New Brunswick massive-sulfide deposits. *Can. Mineral.*, 17, 649-664.
- James, D.E. 1971. Plate tectonic model for the evolution of the Central Andes. *Geol. Soc. Am. Bull.*, 82, 3325-3346.
- James, H.L. 1954. Sedimentary facies of iron-formation. *Econ. Geol.*, 49, 235-293.
- James, H.L. 1966. Chemistry of the iron-rich sedimentary rocks. *U.S. Geol. Survey Prof. Paper* 440W, 60p.
- James, H.L. 1983. Distribution of banded iron-formation in space and time. In *Iron-formation: facts and problems*, A. F. Trendall and R. C. Morris (eds.), 471-490. Amsterdam: Elsevier.
- James, H.L. 1992. Precambrian iron-formations: nature, origin, and mineralogic evolution from sedimentation to metamorphism. In *Diagenesis, III. Developments in Sedimentology*, K. H. Wolf and G.V. Chilingarian (eds.), 543-589. Amsterdam: Elsevier.
- James, L.P. 1976. Zoned alteration in limestone at porphyry copper deposits, Ely, Nevada. *Econ. Geol.*, 71, 488-512.
- Janecky, D.R., and W.E. Seyfried, Jr. 1984. Formation of massive sulfide deposits on oceanic ridge crest: incremental reaction models for mixing between hydrothermal solutions and seawater. *Geochim. Cosmochim. Acta*, 48, 2723-2738.
- Jardine, D.E. 1966. *An investigation of brecciation associated with the Sullivan mine orebody at Kimberley, B.C.* Unpublished M.S. thesis, Univ. Manitoba, Canada.
- Jewell, P. W., and W.T. Parry 1988. Geochemistry of the Mercur gold deposit (Utah, U.S.A.). *Chem. Geol.*, 69, 245-265.
- Jolly, W.T. 1974. Behavior of Cu, Zn, and Ni during prehnite-pumpellyite rank metamorphism of the Keweenaw basalts, northern Michigan. *Econ. Geol.*, 69, 1118-1125.
- Jolly, W.T., and J.A. Hallberg 1990. Role of crustal contamination in heterogeneous Archean volcanics from the Leonora region, Western Australia. *Precamb. Res.*, 48, 75-90.
- Jones, H.D., S.E. Kesler, F.C. Furman, and J.R. Kyle 1996. Sulfur isotope geochemistry of southern Appalachian Mississippi Valley-type deposits. *Econ. Geol.*, 91, 355-367.
- Jowett, E.C. 1986. Genesis of Kupferschiefer Cu-Ag deposits by convective flow of Rotligendes Brines during Triassic rifting. *Econ. Geol.*, 81, 1823-1837.
- Jowett, E.C., A. Rydzewski, and R.J. Jowett 1987. The Kupferschiefer Cu-Ag ore deposits in Poland: a re-appraisal of the evidence of their origin and presentation of a new genetic model. *Can. J. Earth Sci.*, 24, 2016-2037.
- Jowett, E.C., T. Roth, A. Rydzewski, and S. Oszczepalski 1991. Background $\delta^{34}\text{S}$ values of Kupferschiefer sulphides in Poland: pyrite-marcasite nodules. *Mineral. Deposita*, 26, 89-98.

- Jung, W., and G. Knitzschke 1976. Kupferschiefer in German Democratic Republic (GDR) with special reference to the Kupferschiefer deposits of the southeast Harz Foreland. In *Handbook of strata-bound and stratiform ore deposits*, K.H. Wolf (ed.), 6, 353-406. Amsterdam: Elsevier.
- Juve, G. 1967. Zinc and lead deposits in the Håfjell syncline, Ofoten, northern Norway. *Norg. Geol. Unders.*, 244, 1-54.
- Kaiser, C.J., W.C. Kelly, R.J. Wagner, and W.C. Shanks III 1987. Geologic and geochemical controls of mineralization in the Southeast Missouri barite district. *Econ. Geol.*, 82, 719-734.
- Kajiwaru, Y. 1970. Syngenetic features of the Kuroko ore from the Shakanai mine. In *Volcanism and ore genesis*, T. Tatsumi (ed.), 197-213. Tokyo: Univ. Tokyo Press.
- Kajiwaru, Y. 1971. Sulfur isotope study of the Kuroko-ores of Shakanai No. 1 deposits, Akita Prefecture, Japan. *Geochem. J.*, 4, 157-181.
- Kalliokoski, J. 1965. Metamorphic features in North America massive sulfide deposits. *Econ. Geol.*, 60, 485-505.
- Kamilli, R.J. 1978. The genesis of stockwork molybdenite deposits: implications from fluid inclusion studies at the Henderson mine [abs.]. *Geol. Soc. Am. Abstracts with Programs*, 10, 431.
- Kanasewich, E.R. 1968a. The interpretation of lead isotopes and their geological significance. In *Radiometric dating for geologists*, E. I. Hamilton and R. M. Farquhar (eds.), 147-223. New York: Interscience.
- Kanasewich, E.R. 1968b. Precambrian rift: genesis of strata-bound ore deposits. *Science*, 161, 1002-1005.
- Kanasewich, E.R., and R.M. Farquhar 1965. Lead isotope ratios from the Cobalt-Noranda area, Canada. *Can. J. Earth Sci.*, 2, 361-384.
- Kanehira, K. 1959. Geology and ore deposits of Chihara mine, Ehime Prefecture, Japan. *J. Faculty Sci., Tokyo*, Sec II, 11, 309-388.
- Kanehira, K., and T. Tatsumi 1970. Bedded cupriferous iron sulfide deposits in Japan, a review. In *Volcanism and ore genesis*, T. Tatsumi (ed.), 55-76. Tokyo: Univ. Tokyo Press.
- Kanehira, K., S. Banno, and K. Nishida 1964. Sulfide and oxide minerals in some metamorphic terranes in Japan. *Jap. J. Geol. Geogr. (Tokyo)*, 35, 175-191.
- Kasting, J.F. 1987. Theoretical constraints on oxygen and carbon dioxide concentrations in the Precambrian atmosphere. *Precamb. Res.*, 34, 205-229.
- Kasting, J.F. 1993. Evolution of the earth's atmosphere and hydrosphere — Hadean to Recent. In *Organic geochemistry*, M.H. Engel and S.A. Macko (eds.), 611-623. New York: Plenum Press.
- Kasting, J.F., H.D. Holland, and L.E. Kump 1992. Atmospheric evolution: the rise of oxygen. In *The Proterozoic biosphere: a multidisciplinary study*, J.W. Schopf and C. Klein (eds.), 159-163. New York: Cambridge Univ. Press.
- Katz, M.B. 1987. Graphite deposits of Sri Lanka: a consequence of granulite facies metamorphism. *Mineral. Deposita*, 22, 18-25.
- Kaufman, A.J., J.M. Hayes, and C. Klein 1990. Primary and diagenetic controls of isotopic compositions of iron-formation carbonates. *Geochim. Cosmochim. Acta*, 54, 3461-3473.
- Keays, R.R. 1982. Palladium and iridium in komatiites and associated rocks: application to petrogenetic problems. In *Komatiites*, N.T. Arndt and E.G. Nisbet (eds.), 435-457. London: Allen & Unwin.
- Keays, R.R. 1987. Principles of mobilization (dissolution) of metals in mafic and ultramafic rocks — the role of immiscible magmatic sulfides in the generation of hydrothermal gold and volcanogenic massive sulfide deposits. *Ore Geol. Rev.*, 2, 47-63.
- Keays, R.R., and R.M. Davison 1976. Palladium, iridium, and gold in the ores and host rocks of nickel sulfide deposits in Western Australia. *Econ. Geol.*, 71, 1214-1228.
- Keays, R.R., W.R.H. Ramsay, and D.I. Groves (eds.) 1989. The geology of gold deposits: the perspective in 1988. *Econ. Geol. Mono.* 6, 667 p.
- Keays, R.R., E.H. Nickel, D.I. Groves, and P.J. McGoldrick 1982. Iridium and palladium as discriminants of volcanic-exhalative, hydrothermal, and magmatic nickel sulfide mineralization. *Econ. Geol.*, 77, 1535-1547.
- Keith, M.L., and E.T. Degens 1959. Geochemical indicators of marine and fresh-water sediments. In *Researches in geochemistry*, P.H. Abelson (ed.), 38-61. New York: Wiley.
- Kelemen, P.B., H.J.B. Dick, and J.E. Quick 1992. Formation of harzburgite by pervasive melt/rock reaction in the upper mantle. *Nature*, 358, 635-641.
- Kelly, V.C., D.F. Kittel, and P.E. Melancon 1968. Uranium deposits of the Grants region. In *Ore deposits of the United States, 1933-1967 (Graton-Sales Volume)*, J.D. Ridge (ed.), 2, 747-769. New York: Am. Inst. Mining Metall. Petroleum Engineers.
- Kelly, W.C., and B.R. Clark 1975. Sulfide deformation studies: III. Experimental deformation of chalcopyrite to 2,000 bars and 500°C. *Econ. Geol.*, 70, 431-453.
- Kelly, W.C., and R.O. Rye 1979. Geologic, fluid inclusion and stable isotope studies of the tin-tungsten deposits of Panasqueira, Portugal. *Econ. Geol.*, 74, 1721-1822.
- Kendall, D.L. 1960. Ore deposits and sedimentary features, Jefferson City mine, Tennessee. *Econ. Geol.*, 55, 985-1003.

- Kent, A.J.R., and I. McDougall 1995. $^{40}\text{Ar}/^{39}\text{Ar}$ and U-Pb age constraints on the timing of gold mineralization in the Kalgoorlie gold field, Western Australia. *Econ. Geol.*, 90, 845-859.
- Kent, A.J.R., K.F. Cassidy, and C.M. Fanning 1996. Archean gold mineralization synchronous with final stages of cratonization, Yilgarn Craton, Western Australia. *Geology*, 24, 879-882.
- Keppie, J.D., R.W. Boyle, and S.J. Haynes (eds.) 1986. Turbidite-hosted gold deposits. *Geol. Assoc. Canada Spec. Paper* 32, 186p.
- Kerrick, R. 1989. Archean gold: relation to granulite formation or felsic intrusions? *Geology*, 17, 1011-1015.
- Kerrick, R. 1993. Perspectives on genetic models for lode gold deposits. *Mineral. Deposita*, 28, 362-365.
- Kerrick, R. and K.F. Cassidy 1994. Temporal relationships of lode gold mineralization to accretion, magmatism, metamorphism and deformation — Archean to present: a review. *Ore Geol. Rev.*, 9, 263-310.
- Kerrick, R., and B.J. Fryer 1979. Archean precious metal hydrothermal systems, Dome Mine, Abitibi greenstone belt. II. REE and oxygen isotope relations. *Can. J. Earth Sci.*, 16, 440-458.
- Kerrick, R., and T.K. Kyser 1994. 100 Ma timing paradox of Archean gold, Abitibi greenstone belt (Canada): new evidence from U-Pb and Pb-Pb evaporation ages of hydrothermal zircons. *Geology*, 22, 1131-1134.
- Kerrick, R., and D. Wyman 1990. Geodynamic setting of mesothermal gold deposits: an association with accretionary tectonic regimes. *Geology*, 18, 882-885.
- Kerrick, R., T.E. LaTour, and L. Willmore 1984. Fluid precipitation in deep fault zones: evidence from geological, geochemical, and $^{18}\text{O}/^{16}\text{O}$ relations. *J. Geophys. Res.*, 89, 4331-4343.
- Kerrick, R., D.F. Strong, A.J. Andrews, and L. Owsicki 1986. The silver deposits at Cobalt and Gowganda, Ontario. III. Hydrothermal regimes and source reservoirs — evidence from H, O, C, and Sr isotopes and fluid inclusions. *Can. J. Earth Sci.*, 23, 1519-1550.
- Kerrick, R., B.J. Fryer, R.W. King, L.M. Willmore, and E. Van Hees 1987. Crustal outgassing and LILE enrichment in major lithospheric structures, Archean Abitibi greenstone belt: evidence on the source reservoir from strontium and carbon isotope tracers. *Contrib. Mineral. Petrol.*, 97, 156-168.
- Kerswill, J.A. 1993. Models for iron-formation-hosted gold deposits. *Geol. Assoc. Canada Spec. Paper* 40, 171-199.
- Kesler, S.E. 1973. Copper, molybdenum, and gold abundances in porphyry copper deposits. *Econ. Geol.*, 68, 106-112.
- Kesler, S.E., L.M. Jones, and J. Ruiz 1988. Strontium isotopic geochemistry of Mississippi Valley-type deposits, East Tennessee: implications for age and source of mineralizing brines. *Geol. Soc. Am. Bull.*, 100, 1300-1307.
- Kesler, S.E., L.M. Jones, and R.L. Walker 1975a. Intrusive rocks associated with porphyry copper mineralization in islands arc areas. *Econ. Geol.*, 70, 515-526.
- Kesler, S.E., J. Ruiz, and L.M. Jones 1983. Strontium-isotopic geochemistry of fluorite mineralization (Coahuila, Mexico). *Isotope Geoscience*, 1, 65-75.
- Kesler, S.E., P.S. Haynes, M.Z. Creech, and J.A. Morgan 1986. Application of fluid inclusion gas analysis in mineral exploration. *J. Geochem. Exploration*, 25, 201-215.
- Kesler, S.E., M.J. Issigonis, A.H. Brownlow, P.E. Damon, W.J. Moore, K.E. Northcote, and V.A. Petro 1975b. Geochemistry of biotites from mineralized and barren intrusive systems. *Econ. Geol.*, 70, 559-567.
- Kesler, S.E., M.S. Appold, A.M. Martini, L.M. Walter, T.J. Huston, and J.R. Kyle 1995. Na-Cl-Br systematics of mineralizing brines in Mississippi Valley-type deposits. *Geology*, 23, 641-644.
- Kesler, S.E., H.D. Jones, F.C. Furman, R. Sassen, W.H. Anderson, and J.R. Kyle 1994. Role of crude oil in the genesis of Mississippi Valley-type deposits; evidence from the Cincinnati arch. *Geology*, 22, 609-612.
- Kilburn, L.C., H.D. B. Wilson, A.R. Graham, Y. Ogura, C.J.A. Coats, and R.F.J. Scoates 1969. *Econ. Geol. Mono.* 4, 276-293.
- Kimberly, M.M. 1978. Origin of stratiform uranium deposits in sandstone, conglomerate and pyroclastic rock. *Mineral. Assoc. Canada Short Course Handbook* 3, 339-382.
- Kinkel, A.R., Jr. 1967. The Ore Knob copper deposits, North Carolina, and other massive sulfide deposits of the Appalachians. *Geol. Survey Prof. Paper* 558, 1-58.
- Kinloch, E.D. 1982. Regional trends in the platinum-group mineralogy of the Critical Zone of the Bushveld Complex, South Africa. *Econ. Geol.*, 77, 1328-1347.
- Kinloch, E.D., and W. Peyerl 1990. Platinum-group minerals in various rock types of the Merensky Reef: genetic implications. *Econ. Geol.*, 85, 537-555.
- Kirkham, R.V. 1989. Distribution, settings, and genesis of sediment-hosted stratiform copper deposits. *Geol. Assoc. Canada Spec. Paper* 36, 3-38.
- Kirkham, R.V., and A.E. Soregaroli 1975. Preliminary assessment of porphyry deposits in the Canadian Appalachians. *Geol. Survey Canada Paper* 75-1A.
- Kissin, S.A. 1992. Five-element (Ni-Co-As-Ag-Bi) veins. *Geoscience Canada*, 19, 113-124.

- Kissin, S.A., S.D. Scott. 1982. Phase relations involving pyrrhotite below 350° C. *Econ. Geol.*, 77, 1739-1754.
- Kissin, S.A., H.P. Schwarcz, and S.D. Scott 1986. Application of the sphalerite cosmobarometer to group IAB iron meteorites. *Geochim. Cosmochim. Acta*, 50, 371-378.
- Kisvarsanyi, G. 1977. The role of the Precambrian igneous basement in the formation of stratabound lead-zinc-copper deposits in southeast Missouri. *Econ. Geol.*, 72, 435-442.
- Kisvarsanyi, G. 1983. Multiple source and multiple stage theory of ore genesis in the Southeast Missouri district. In *International Conference on Mississippi Valley type lead-zinc deposits — Proc. Vol.*, Kisvarsanyi, G., S.K. Grant, W.P. Pratt, and J.W. Koenig (eds.), 486-496. Rolla, Missouri: Univ. of Missouri-Rolla Press.
- Kisvarsanyi, G., S.K. Grant, W.P. Pratt, and J.W. Koenig (eds.) 1983. *International Conference on Mississippi Valley type lead-zinc deposits — Proc. Vol.* Rolla, Missouri: Univ. Missouri-Rolla Press, 603p.
- Kjarsgaard, B.A., and D.L. Hamilton 1989. The genesis of carbonatites by immiscibility. In *Carbonatites: genesis and evolution*, K. Bell (ed.), 388-404. London: Allen & Unwin.
- Klau, W., and D.E. Large 1980. Submarine exhalative Cu-Pb-Zn deposits, a discussion of their classification and metallogenesis. *Geol. Jahrb.*, D 40, 13-58.
- Klau, W., and H. Mostler, 1983. Alpine Middle and Upper Triassic Pb-Zn deposits. In *International Conference on Mississippi Valley-type lead-zinc deposits — Proc. Vol.*, G. Kisvarsanyi, S.K. Grant, W.P. Pratt, and J.W. Koenig (eds.), p. 113-128. Rolla, Missouri: Univ. Missouri-Rolla Press.
- Klau, W., and H. Mostler 1986. On the formation of Alpine Middle and Upper Triassic Pb-Zn deposits, with some remarks on Irish carbonate-hosted base metal deposit. In *Geology and genesis of mineral deposits in Ireland*, C.J. Andrew et al. (eds.), 663-675. Dublin: Irish Assoc. for Econ. Geol.
- Klein, C., Jr. 1973. Changes in mineral assemblages with metamorphism of some banded Precambrian iron formation. *Econ. Geol.*, 68, 1075-1088.
- Klein, C. 1978. Regional metamorphism of Proterozoic iron-formation, Labrador Trough, Canada. *Am. Mineral.*, 63, 898-912.
- Klein, C. 1983. Diagenesis and metamorphism of Precambrian banded iron-formations. In *Iron-formation: facts and problems*, A.F. Trendall and R. C. Morris (eds.), 417-469. Amsterdam: Elsevier.
- Klein, C., and N.J. Beukes 1989. Geochemistry and sedimentology of a facies transition from limestone to iron-formation deposition in the early Proterozoic Transvaal Supergroup, South Africa. *Econ. Geol.*, 84, 1733-1774.
- Klein, C., and N.J. Beukes 1992. Time distribution, stratigraphy, and sedimentologic setting, and geochemistry of Precambrian iron-formations. In *The Proterozoic biosphere*, J. W. Schopf and C. Klein (eds.), 139-146. New York: Cambridge Univ. Press.
- Klemm, R. 1998. Comment on the paper by Schmidt Mumm et al., High CO₂ content of fluid inclusions in gold mineralizations in the Ashanti Belt, Ghana: a new category of ore-forming fluids? *Mineral. Deposita*, 33, 317-319.
- Klemm, R., K. J. Maiden, M. Okrusch, and P. Richter 1989. Geochemistry of the Matchless metamorphosed massive sulfide deposit, South West Africa/Namibia: wall-rock alteration during submarine ore-forming processes. *Econ. Geol.*, 84, 603-617.
- Klemm, D.D., S. Ketterer, F. Reichhardt, J. Steindl, and K. Weber-Diefenbach 1985. Implications of vertical and lateral compositional variations across the Pyroxenite Marker and its associated rocks in the upper part of the Main Zone in the eastern Bushveld Complex. *Econ. Geol.*, 80, 1007-1015.
- Klemm, D.D., J. Henckel, R. Dehm, and G. von Gruenewaldt 1985. The geochemistry of titanomagnetite in magnetite layers and their host rock of the eastern Bushveld Complex. *Econ. Geol.*, 80, 1075-1088.
- Knauth, L.P., and M.A. Beeunas 1986. Isotope geochemistry of fluid inclusions in Permian halite with implications for the isotopic history of ocean water and the origin of saline formation waters. *Geochim. Cosmochim. Acta*, 50, 419-433.
- Knauth, L.P., and S. Epstein 1971. Oxygen and hydrogen isotope relationships in cherts and implications regarding the isotopic history of the hydrosphere [abs.]. *Geol. Soc. Am. Abstracts with Programs*, 3, 624.
- Knauth, L.P., and S.K. Roberts 1991. The hydrogen and oxygen isotope history of the Silurian-Permian hydrosphere as determined by direct measurement of fossil water. In *Stable isotope geochemistry: a tribute to Samuel Epstein*, H.P. Taylor, Jr., J. R. O'Neil, and I.R. Kaplan (eds.), *Geochem. Soc. Spec. Publ.* 3, 91-103.
- Knight, J.T., D.I. Groves, and J.R. Ridley 1993. The Coolgardie goldfield, western Australia; district-scale controls on an Archean gold camp in an amphibolite facies terrane. *Mineral. Deposita*, 28, 436-456.
- Knipe, S.W., R.P. Foster, and C.J. Stanley 1992. Role of sulfide surfaces in sorption of precious metals from hydrothermal fluids. *Inst. Mining. Metall. Trans.*, 101, B83-B88.
- Knuckey, M.J., and J.J. Watkins 1982. The geology of the Corbet massive sulphide deposit, Noranda district, Quebec, Canada. *Geol. Assoc. Canada Spec. Paper* 25, 297-317.
- Knutson, J., J. Ferguson, W.M.B. Roberts, T.H. Donnelly, and I.B. Lambert 1979. Petrogenesis of the copper-bearing breccia pipes, Redbank, Northern Territory, Australia. *Econ. Geol.*, 74, 814-826.

- Koen, G.M. 1961. The genetic significance of the size distribution of uraninite in Witwatersrand bankets. *Geol. Soc. S. Africa Trans.*, 64, 23-54.
- Kojima, S. 1990. A coprecipitation experiment on intimate association of sphalerite and chalcopyrite and its bearing on the genesis of Kuroko ores. *Mining Geol.*, 40, 147-158.
- Kojima, S., and A. Sugaki 1985. Phase relations in the Cu-Fe-Zn-S system between 500° and 300°C under hydrothermal conditions. *Econ. Geol.*, 80, 158-171.
- Kojima, S., S. Takeda, and S. Kogita 1994. Chemical factors controlling the solubility of uraninite and their significance in the genesis of unconformity-related uranium deposits. *Mineral. Deposita*, 29, 353-360.
- Kolodny, Y., and B. Luz 1991. Oxygen isotopes in phosphates of fossil fish — Devonian to Recent. In *Stable isotope geochemistry: a tribute to Samuel Epstein*, H.P. Taylor, Jr., J. R. O'Neil, and I.R. Kaplan (eds.), *Geochem. Soc. Spec. Publ.* 3, 105-119.
- Koo, J., and D.J. Mossman 1975. origin and Metamorphism of the Flin Flon stratabound Cu-Zn sulfide deposit, Saskatchewan and Manitoba. *Econ. Geol.*, 70, 48-62.
- Kopp, O.C. 1981. Cathodoluminescence petrography: a valuable tool for teaching and research. *J. Geol. Education*, 29, 108-113.
- Kopp, O.C., and K.C. Misra 1982. An occurrence of enargite in central Tennessee. *Econ. Geol.*, 77, 474-476.
- Koppel, V.H., and R. Saager 1974. Lead isotope evidence on the detrital origin of Witwatersrand pyrite and its bearing on the provenance of the Witwatersrand gold. *Econ. Geol.*, 69, 318-331.
- Koppel, V., and R. Saager 1976. Uranium-, thorium- and lead - isotope studies of strata-bound ores. In *Handbook of strata-bound and stratiform ore deposits*, K.H. Wolf (ed.), 2, 267-316. Amsterdam: Elsevier.
- Korzhinskii, D. 1959. *Physicochemical basis of the analysis of the paragenesis of minerals*. New York: Consultants Bureau.
- Koski, R.A., and D.S. Cook 1982. Geology of the Christmas porphyry copper deposit, Gila County, Arizona. In *Advances in Geology of the porphyry copper deposits, southwestern North America*, S.R. Titley (ed.), 353-374. Tucson, Arizona: Univ. Arizona Press.
- Kozłowski, A., L. Karwowski, and E. Roedder 1980. Parent fluids of the zinc and lead ores from the Silesia-Cracow region. *Acta Geol. Polonica*, 30, 147-152.
- Kral, S. 1992. Red Dog: Cominco's Arctic experience pays off again. *Mining Eng.*, 44, 43-49.
- Kramers, J.B. 1979. Pb, U, Sr, K, and Rb in inclusion-bearing diamonds and mantle-derived xenoliths from southern Africa. *Earth Planet. Sci. Lett.*, 42, 58-70.
- Kraume, E. 1960. Stratigraphie und tektonik der Rammelsberger Erzlager unter besonderer Berücksichtigung des Neuen Lagers unter der 10. Sohle. *Erzmetall*, 13, 7-12.
- Krauskopf, K.B. 1964. The possible role of volatite metal compounds in ore genesis. *Econ. Geol.*, 59, 22-45.
- Krauskopf, K.B. 1967a. Source rocks for metal-bearing solutions. In *Geochemistry of hydrothermal ore deposits*, H.L. Barnes (ed.), 1-33. New York: Holt, Rinehart and Winston.
- Krauskopf, K.B. 1967b. *Introduction to geochemistry*. New York: McGraw Hill.
- Krauskopf, K.B. 1971. The source of ore metals. *Geochim. Cosmochim. Acta*, 35, 643-659.
- Krauskopf, K.B., and D.K. Bird 1995. *Introduction to geochemistry*, 3rd. edn. New York: McGraw Hill.
- Kretschmar, U., and S.D. Scott 1976. Phase relations involving arsenopyrite in the system Fe-As-S and their application. *Can. Mineral.*, 23, 364-386.
- Kretz, R. 1966. Interpretation of the shape of mineral grains in metamorphic rocks. *J. Petrol.*, 7, 68-94.
- Krogh, T.E., and G.L. Davis 197. Zircon U-Pb ages of Archean metavolcanic rocks in the Canadian Shield. *Carnegie Inst. Washington Year Book* 1970, 241-242.
- Krogstad, E.J., S. Balakrishnan, D.K. Mukhopadhyay, V. Rajamani, and G.N. Hanson 1989. Plate tectonics 2.5 billion years ago: evidence at Kolar, South India. *Science*, 243, 1337-1340.
- Kruger, F.J. 1994. The Sr-isotopic stratigraphy of the western Bushveld Complex. *S. African J. Geol.*, 97, 393-398.
- Kruger, F.J., and J.S. Marsh 1985. The mineralogy, petrology, and origin of the Merensky cyclic unit in the Western Bushveld Complex. *Econ. Geol.*, 80, 958-974.
- Krumbein, W.C., and R.M. Garrels 1952. Origin and classification of chemical sediments in terms of pH and oxidation-reduction potentials. *J. Geol.*, 60, 1-33.
- Krupp, R.E. and T.M. Seward 1987. The Rotokawa geothermal system, New Zealand: an active epithermal gold-depositing environment. *Econ. Geol.*, 82, 1109-1129.
- Krupp, R., T. Oberthür, and W. Hirdes 1994. The early Precambrian atmosphere and hydrosphere: thermodynamic constraints from mineral deposits. *Econ. Geol.*, 89, 1581-1598.
- Kubaschewski, O., E.L. Evans, and C.B. Alcock 1967. *Metallurgical thermochemistry*, 4th edn. Oxford: Pergamon Press.
- Kucha, H. 1982. Platinum-group metals in the Zechstein copper deposits, Poland. *Econ. Geol.*, 77, 1578-1594.
- Kucha, H. and M. Pawlikowski 1986. Two-brine model of the genesis of strata-bound Zechstein deposits (Kupferschiefer type), Poland. *Mineral. Deposita*, 21, 70-80.

- Kucha, H., and A. Piestrzynski 1995. *Excursion Guide: Polish Kupferschiefer deposits*. Third Biennial SGA meeting, Prague, Czech Republic, Aug 28-31, 1995.
- Kuehn, C.A., and A.W. Rose 1992. Geology and geochemistry of wall-rock alteration at the Carlin gold deposit, Nevada. *Econ. Geol.*, 87, 1697-1721.
- Kuehn, C.A., and A.W. Rose 1995. Carlin gold deposits, Nevada: origin in a deep zone of mixing between normally pressured and overpressured fluids. *Econ. Geol.*, 90, 17-36.
- Kuhns, R.J. 1986. Alteration styles and trace element dispersion associated with the Golden Giant deposit, Hemlo, Ontario, Canada. In *Proc. Gold '86 Symposium*, A.J. Macdonald (ed.), 340-354. Toronto: Konsult International Inc.
- Kuhns, R.J., F.J. Sawkins, and E. Ito 1994. Magmatism, metamorphism, and deformation at Hemlo, Ontario, and the timing of Au-Mo mineralization in the Golden Giant mine. *Econ. Geol.*, 89, 720-756.
- Kullerud, G. 1953. The FeS-ZnS system, a geological thermometer. *Norsk. Geologisk Tidsskrift*, 32, 61-147.
- Kullerud, G. 1963. Thermal stability of pentlandite. *Can. Mineral.*, 7, 353-366.
- Kullerud, G. 1964. Review and evaluation of recent research on geologically significant sulfide-type systems. *Fortschr. Mineral.*, 41, 221-270.
- Kullerud, G. 1971. Experimental techniques in dry sulfide research. In *Research techniques for high pressure and high temperature*, G. C. Ulmer (ed.), 288-315. New York: Springer-Verlag.
- Kwak, T.A.P. 1987. *W-Sn skarn deposits and related metamorphic skarns and granitoids*. Amsterdam: Elsevier.
- Kyle, J.R. 1981. Geology of the Pine Point lead-zinc district. In *Handbook of strata-bound and stratiform ore deposits*, K.H. Wolf (ed.), 9, 643-741. Amsterdam: Elsevier.
- La Berge, G.L. 1966. Altered pyroclastic rocks in the Hamersley Range, Western Australia. *Econ. Geol.*, 61, 147-161.
- La Berge, G.L. 1973. Possible biological origin of Precambrian iron-formations. *Econ. Geol.*, 68, 1098-1109.
- La Berge, G.L., E.I. Robbins, and T.M. Han 1987. A model for the biological precipitation of Precambrian iron-formations. In *Precambrian iron-formations*, P.W.U. Appel and G.L. LaBerge (eds.), 69-96. Athens: Theophrastus Publ. S.A.
- Labotka, T.C., C.E. White, and J.J. Papike 1984. The evolution of water in the contact-metamorphic aureole of the Duluth Complex, northeastern Minnesota. *Geol. Soc. Am. Bull.*, 95, 788-804.
- Lago, B.L., M. Rabinowicz, and A. Nicolas 1982. Podiform chromite ore bodies: a genetic model. *J. Petrol.*, 23, 103-125.
- Laing, W.P., S.S. Sun, and R.W. Neebitt 1984. Acid volcanic precursor to Potosi genesis at Broken Hill and its implication for ore genesis [abs.]. *Geol. Soc. Australia, 7th Austral. Geol. Congress Abstracts*, 318-321.
- Lamb, W.M., and J.W. Valley 1984. Metamorphism of reduced granulites in low-CO₂ vapor-free environments. *Nature*, 312, 56-68.
- Lambe, R.N. and R.G. Rowe 1987. Volcanic history, mineralization, and alteration of the Crandon massive sulfide deposit, Wisconsin. *Econ. Geol.*, 82, 1204-1238.
- Lambert, D.D., and E.C. Simmons 1988. Magma evolution in the Stillwater Complex, Montana: II. Rare-earth element evidence for the formation of the J-M Reef. *Econ. Geol.*, 83, 1109-1126.
- Lambert, D.D., J.W. Morgan, R.J. Walker, S.B. Shirey, R.W. Carlson, M.L. Zientek, and M.S. Koski 1989. Rhenium-osmium and samarium-neodymium isotopic systematics of the Stillwater Complex. *Science*, 244, 1169-1174.
- Lambert, D.D., J.G. Foster, L.R. Frick, E.M. Ripley, and M.L. Zientek 1998. Geodynamics of magmatic Cu-Ni-PGE sulfide deposits: new insights from the Re-Os isotope system. *Econ. Geol.*, 93, 121-137.
- Lambert, I.B. 1973. Post-depositional availability of sulphur and metals and formation of secondary textures and structures in stratiform sedimentary sulphide deposits. *J. Geol. Soc. Australia*, 20, 205-215.
- Lambert, I.B. 1976. The McArthur zinc-lead-silver deposit: features, metallogenesis and comparisons with some other stratiform ores. In *Handbook of strata-bound and Stratiform ore deposits*, K.H. Wolf (ed.), 6, 535-585. Amsterdam: Elsevier.
- Lambert, I.B. 1979. Massive copper-lead-zinc deposits in felsic volcanic sequences of Japan and Australia; comparative notes. *Mining Geol.*, 29, 11-20.
- Lambert, I.B. 1983. The major stratiform lead-zinc deposits of the Proterozoic. *Geol. Soc. Am. Mem.* 161, 209-226.
- Lambert, I. B., and T. Sato 1976. The Kuroko and associated ore deposits of Japan: A review of their features and metallogenesis. *Econ. Geol.*, 69, 1215-1236.
- Landis, G.P., and R.O. Rye 1974. Geologic, fluid inclusion, and stable isotope studies of the Pasto Bueno tungsten-base metal deposit, Northern Peru. *Econ. Geol.*, 69, 1025-1059.
- Lang, J.R., and C.J. Eastoe 1988. Relationships between a porphyry Cu-Mo deposit, base and precious metal veins, and Laramide intrusions, Mineral Park, Arizona. *Econ. Geol.*, 83, 551-567.

- Lange, S., S. Chaudhuri, and N. Clauer 1983. Strontium isotopic evidence for the origin of barites and sulfides from the Mississippi Valley-type ore deposits in southeast Missouri. *Econ. Geol.*, 78, 1255-1261.
- Langen, R. E., and A. L. Kidwell 1974. Geology and geochemistry of the Highland uranium deposit. *Earth Sci. Bull.*, 6, 41-48.
- Langmuir, D. 1978. Uranium solution-mineral equilibria at low temperatures with applications to sedimentary ore deposits. In *Uranium deposits, their mineralogy and origin*, M.M. Kimberley (ed.), *Mineral. Assoc. Canada Short Course Handbook* 3, 17-55.
- Langmuir, C.H., J.F. Bender, A.E. Bence, G.N. Hanson, and S.R. Taylor 1977. Petrogenesis of basalts from the FAMOUS area, mid-Atlantic ridge. *Earth Planet. Sci. Lett.*, 36, 133-156.
- Lanphere, M.A. 1988. High-resolution $^{40}\text{Ar}/^{39}\text{Ar}$ chronology of Oligocene volcanic rocks, San Juan Mountains, Colorado. *Geochim. Cosmochim. Acta*, 52, 1425-1434.
- Large, D.E. 1981. Sediment-hosted submarine exhalative lead-zinc deposits — a review of their geological characteristics and genesis. In *Handbook of strata-bound and stratiform ore deposits*, K.H. Wolf (ed.), 9, 469-507. Amsterdam: Elsevier.
- Large, D.E. 1983. Sediment-hosted massive sulfide lead-zinc deposits: an empirical model. In *Short course in sediment-hosted stratiform lead-zinc deposits*, D.F. Sangster (ed.), *Mineral. Assoc. Canada Short Course Handbook* 8, 1-29.
- Large, D.E. 1992. Problems encountered in the application of geological models to the exploration of sediment-hosted massive sulphide deposits. *Irish Assoc. Econ. Geol. Annual Rev. 1991*, 128-131.
- Large, P.R. 1972. Metasomatism and scheelite mineralization at Bold Head, King Island. *Austral. Inst. Mining Metall. Proc.*, 238, 31-45.
- Large, R.R. 1977. Chemical evolution and zonation of massive sulfide deposits in volcanic terrains. *Econ. Geol.*, 72, 549-572.
- Large, R.R., S.W. Bull, D.R. Cooke, and P.J. McGoldrick 1998. A genetic model for the HYC deposit, Australia: based on regional sedimentology, geochemistry, and sulfide-sediment relationships. *Econ. Geol.*, 93, 1345-1368.
- Lawrence, L.J. 1973. Polymetamorphism of the sulfides of Broken Hill, N.S.W., Australia. *Mineral. Deposita*, 8, 211-236.
- Layne, G.D., F.J. Longstaffe, and E.T.C. Spooner 1991. The JC tin skarn deposit, southern Yukon Territory: II. A carbon, oxygen, hydrogen, and sulfur stable isotope study. *Econ. Geol.*, 86, 48-65.
- Laznicka, P. 1976. Porphyry copper and molybdenum deposits of the U.S.S.R. and their plate tectonic setting. *Inst. Mining Metall. Trans.*, 85, B13-B32.
- Lea, E.R., and D.B. Dill, Jr. 1968. Zinc deposits of the Balmat-Edwards district, N.Y. In *Ore deposits of the United States, 1933-1967 (Graton-Sales Volume)*, J.D. Ridge (ed.), 1, 20-48. New York: Am. Inst. Mining Metall. and Petroleum Engineers.
- Leach, D.L., and E.L. Rowan 1986. Genetic link between Ouchita foldbelt tectonism and the Mississippi Valley-type lead-zinc deposits of the Ozarks. *Geology*, 14, 931-935.
- Leach, D.L., and D.F. Sangster 1993. Mississippi Valley-type lead-zinc deposits. *Geol. Assoc. Canada Spec. Paper* 40, 289-314.
- Leach, D.L., G.P. Landis, and A.H. Hofstra 1987. Gas contents of Mississippi Valley-type ore fluids. *Am. Current Res. Fluid Inclusions meeting*, Jan 5-7, 1987, Socorro, New Mexico.
- Leach, D.L., G.P. Landis, and A.H. Hofstra 1988. Metamorphic origin of the Coeur d'Alene base- and precious-metal veins in the Belt basin, Idaho and Montana. *Geology*, 16, 122-125.
- Le Bas, M.J. 1989. Diversification of carbonatite magmas. In *Carbonatites*, K. Bell (ed.), 428-447. London: Unwin Hyman.
- Lebedev, L.M. 1973. Minerals of contemporary hydrotherms of Cheleken. *Geochem. International*, 9, 485-504.
- Leblanc, M. 1987. Chromite in oceanic arc environments: New Caledonia. In *Evolution of chromium ore fields*, C.W. Stowe (ed.), 265-296. New York: Van Nostrand.
- Leblanc, M., and G. Ceulener 1992. Chromite crystallization in a multicellular magma flow: evidence from a chromite dike in the Oman ophiolite. *Lithos*, 27, 231-257.
- Leblanc, M., and J.F. Violette 1983. Distribution of Al-rich and Cr-rich pods in ophiolites. *Econ. Geol.*, 78, 293-301.
- Leblanc, M., C. Dupuy, D. Cassard, J. Moutte, A. Nicolas, A. Prinzhofer, and M. Rabinovitch 1980. Essai sur la genèse des corps podiformes de chromite dans les péridotites ophiolitiques de Nouvelle-Calédonie et de Méditerranée orientale. In *International Ophiolite Symp. Proc.*, A. Panayiotou (ed.), 691-701. Nicosia: Cyprus Geol. Survey.
- Lechler, P.J. 1998. Global hydrothermal PGE mineralization [abs.]. *8th International Platinum Symposium Abstracts, June 28-July 3, 1998, Rustenburg, South Africa*, 193-196.
- Le Couteur, P.C. 1979. Age of the Sullivan lead-zinc deposit [abs.]. *Geol. Assoc. Canada Cordilleran Sec., Abstracts*, 19.
- Lee, C.A. 1983. Trace and platinum group element geochemistry and the development of the Merensky Reef of the western Bushveld Complex. *Mineral. Deposita*, 18, 173-190.

- Lee, C.A., and H.W. Fesq 1986. Au, Ir, Ni and Co in some chromitites of the eastern Bushveld Complex, South Africa. *Chem. Geol.*, 62, 227-237.
- Lee, C.A., and S.J. Parry 1988. Platinum-group element geochemistry of the lower and middle group chromitites of the eastern Bushveld Complex. *Econ. Geol.*, 83, 1127-1139.
- Lee, C.A., and M. Tredoux 1986. Platinum-group element abundances in the Lower and Critical Zones of the eastern Bushveld Complex. *Econ. Geol.*, 81, 1087-1095.
- Lee, I., and E.M. Ripley 1995. Genesis of Cu-Ni sulfide mineralization in the South Kawishiwi intrusion, Spruce Reed area, Duluth Complex, Minnesota. *Can. Mineral.*, 33, 723-744.
- Lee, T., and Chi-Lung Yao 1970. Abundance of chemical elements in the earth's crust and its major tectonic units. *International Geol. Rev.*, 12, 778-786.
- Lehmann, B. 1982. Metallogeny of tin: magmatic differentiation versus geochemical heritage. *Econ. Geol.*, 77, 50-59.
- LeHuray, A.P. 1984. Lead and sulfur isotopes and a model for the origin of the Ducktown deposit, Tennessee. *Econ. Geol.*, 79, 1561-1573.
- LeHuray, A.P., J.B.D. Caulfield, D.M. Rye, and O.R. Dixon 1987. Basement controls on sediment-hosted Zn-Pb deposits: a Pb isotope study of Carboniferous mineralization in central Ireland. *Econ. Geol.*, 82, 1695-1709.
- LeHuray, A.P., S.E. Church, R.A. Koski, and R.M. Bouse 1988. Pb isotopes in sulfides from mid-ocean ridge hydrothermal sites. *Geology*, 16, 362-365.
- Leistel, J.M., E. Marcoux, D. Thiéblemont, C. Quesada, A. Sánchez, G.R. Almodóvar, E. Pascual, and R. Sáez 1998. The volcanic-hosted massive sulfide deposits of the Iberian Pyrite Belt: review and preface to the thematic issue. *Mineral. Deposita*, 33, 2-30.
- Lelong, F., Y. Tardy, G. Grandin, J.J. Trescases, and B. Boulange 1976. Pedogenesis, chemical weathering and processes of formation of supergene ore deposits. In *Handbook of strata-bound and stratiform ore deposits*, K.H. Wolf (ed.), 3, 93-173. Amsterdam: Elsevier.
- Lentini, M.R., and W.C. Shanks, III 1983. Experimental study of brine-arkose interaction at 200°C and 500 bars: origin of metalliferous oil field brines and Mississippi Valley-type deposits at Fredericktown, Missouri. In *International Conference on Mississippi Valley-type zinc-lead deposits — Proc. Vol.*, G. Kisvarsanyi, S.K. Grant, W.P. Pratt, and J.W. Koenig (eds.), 195-205. Rolla, Missouri: Univ. Missouri-Rolla Press.
- Lepp, H. 1987. Chemistry and origin of Precambrian iron-formations. In *Precambrian iron-formations*, P. W. U. Appel and G. L. LaBerge (eds.), 3-30. Athens: Theophrastus Publ. S.A.
- LeRoy, J. 1978. The Margnac and Fanay uranium deposits of the LaCrouzille district (Western Massif Central, France): geologic and fluid inclusion studies. *Econ. Geol.*, 73, 1611-1634.
- Leshner, C.M. 1989. Komatiite-associated nickel sulfide deposits. *Rev. Econ. Geol.*, 4, 45-101
- Leshner, C.M., and I.H. Campbell 1993. Geochemical and fluid dynamic modeling of compositional variations in Archean komatiite-hosted nickel sulfide ores in Western Australia. *Econ. Geol.*, 88, 804-816.
- Leshner, C.M., and D.I. Groves 1986. Controls on the formation of Komatiite-associated nickel-copper sulfide deposits. In *Geology and metallogeny of copper deposits*, G.H. Friedrich, A.D. Genkin, A.J. Naldrett, J.D. Ridge, R.H. Sillitoe, and F.M. Vokes (eds.), 43-62. Berlin: Springer-Verlag.
- Leshner, C.M., and R.R. Keays 1984. Metamorphically and hydrothermally mobilized Fe-Ni-Cu sulphides at Kambalda, Western Australia. In *Sulphide deposits in mafic and ultramafic rocks*, D.L. Buchanan and M. J. Jones (eds.), 62-69. London: Inst. Mining & Metall.
- Leshner, C.M., N.T. Arndt, and D.I. Groves 1984. Genesis of komatiite-associated nickel sulphide deposits at Kambalda, Western Australia: a distal volcanic model. In *Sulphide deposits in mafic and ultramafic rocks*, D. L. Buchanan and M. J. Jones (eds.), 70-80. London: Inst. Mining & Metall.
- Leshner, C.M., A.M. Goodwin, I.H. Campbell, and M.P. Gorton 1985. Trace-element geochemistry of ore-associated and barren, felsic metavolcanic rocks in the Superior Province, Canada. *Can. J. Earth Sci.*, 23, 222-237.
- Leshner, C.M., R.F. Lee, D. I. Groves, M.J. Bickle, and M.J. Donaldson 1981. Geochemistry of komatiites at Kambalda: I. Chalcophile element depletion — a consequence of sulfide liquid separation from Komatiitic magmas. *Econ. Geol.*, 76, 1714-1728.
- Lewchuk, M.T., and D.T.A. Symons 1995. Age and distribution of Mississippi Valley-type ore-mineralizing events. *Geology*, 23, 233-236.
- Li, C., and A.J. Naldrett 1993. Sulfide capacity of magma: a quantitative model and its application to the formation of sulfide ores at Sudbury, Ontario. *Econ. Geol.*, 88, 1253-1260.
- Li, C., and A.J. Naldrett 1994. A numerical model for the compositional variations of Sudbury sulfide ores and its application to exploration. *Econ. Geol.*, 89, 1599-1607.
- Lightfoot, P.C., R.R. Keays, G.G. Morrison, A. Bite, and K.P. Farrell 1997. Geochemical relationships in the Sudbury igneous complex: origin of the main mass and offset dikes. *Econ. Geol.*, 92, 289-307.
- Likhachev, A.P. 1975. Redoxposition of ore-producing and petrogenetic components by aqueous solutions. *Geochem. International*, 12, 101-113.

- Lindberg, P.A. 1985. A volcanogenic interpretation for massive sulfide origin, West Shasta district, California. *Econ. Geol.*, 80, 2240-2254.
- Lindblom, S. 1986. Textural and fluid inclusion evidence for ore deposition in the Pb-Zn deposit at Lisvall, Sweden. *Econ. Geol.*, 81, 46-64.
- Lindgren, W. 1933. *Mineral deposits, 4th Ed.* New York: McGraw Hill.
- Lindsley, D.H. Fe-Ti oxides in rocks as thermometers and oxygen barometers. *Carnegie Inst. Washington Year Book* 62, 60-65.
- Lindsley, D.H. 1976. Experimental studies of oxide minerals. In *Mineral. Soc. Am. Short Course Notes 3: Oxide minerals*, 61-88. Washington: Geol. Soc. Am.
- Lipin, B.R. 1993. Pressure increases, the formation of chromite seams, and the development of the Ultramafic Series in the Stillwater Complex, Montana. *J. Petrol.*, 34, 955-976.
- Lister, G.F. 1966. The composition and origin of selected iron-titanium deposits. *Econ. Geol.*, 61, 275-310.
- Geol.*, 87, 1624-1634.
- Loftus-Hills, G., and M. Solomon 1967. Cobalt, nickel and selenium in sulfides as indicators of ore genesis. *Mineral. Deposita*, 2, 228-242.
- Long, D.T. and E.E. Angino 1982. The mobilization of selected trace metals from shales by aqueous solutions: effects of temperature and ionic strength. *Econ. Geol.*, 77, 646-652.
- Lougheed, M. S. 1983. Origin of Precambrian iron-formations in the Lake Superior region. *Geol. Soc. Am. Bull.*, 94, 325-340.
- Lovering, T.S. 1949. Rock alteration as a guide to ore-East Tintic district, Utah. *Econ. Geol. Mono.* 1.
- Lovering, T.S. 1961. Sulfide ores formed from sulfide-deficient solutions. *Econ. Geol.*, 56, 68-99.
- Lowe, D. R. 1985. Sedimentary environment as a control on the formation and preservation of Archean volcanogenic massive sulphide deposits. *Geol. Assoc. Canada Spec. Paper* 28, 193-201.
- Lowe, D.R. 1994. Abiological origin of described stromatolites older than 3.2 Ga. *Geology*, 22, 387-390.
- Lowe, D.R., and W.G. Ernst 1992. The Archean geological record. In *The Proterozoic biosphere: a multidisciplinary study*, J.W. Schopf and C. Klein (eds.), 13-19. New York: Cambridge Univ. Press.
- Lowe, D.R., and L.P. Knauth 1977. Sedimentology of the Onverwacht Group (3.4 billion years), Transvaal, South Africa, and its bearing on the characteristics and evolution of the early Earth. *J. Geol.*, 85, 699-723.
- Lowell, J.D. 1989. Gold mineralization in porphyry copper deposits discussed. *Mining Eng.*, 41, 227-231.
- Lowell, J.D. 1974. Regional characteristics of porphyry copper deposits of the southwest. *Econ. Geol.*, 69, 601-617.
- Lowell, J.D., and J.M. Guilbert 1970. Lateral and vertical alteration-mineralization zoning in porphyry ore deposits. *Econ. Geol.*, 65, 373-408.
- Lowell, R.P. and P.A. Rona 1985. Hydrothermal models for generation of massive sulfide ore deposits. *J. Geophys. Res.*, 90, 8769-8783.
- Lucas, J. M. 1992. *Gold*. U.S. Bureau of Mines Annual Report, 40p.
- Ludden, J., C. Hubert, and C. Garièpy 1986. The tectonic evolution of the Abitibi greenstone belt of Canada. *Geol. Mag.*, 123, 153-166.
- Ludington, S.D. 1986. Descriptive model of Climax Mo deposits. *U.S. Geol. Survey Bull.* 1693, 73-74.
- Ludwig, K.R., M.B. Goldhaber, R.L. Reynolds, and K.R. Simmons 1982. Uranium-lead isochron age and preliminary sulfur isotopic systematics of the Felder uranium deposit, South Texas. *Econ. Geol.*, 77, 557-563.
- Ludwig, K.R., K.R. Simmons, and J.D. Webster 1984. U-Pb isotope systematics and apparent ages of uranium ores, Ambrosia Lake and Smith Lake districts, Grants mineral belt, New Mexico. *Econ. Geol.*, 79, 322-337.
- Lusk, J. 1972. Examination of volcanic-oxhalative and biogenic origins for sulfur in the stratiform massive sulfide deposits of New Brunswick. *Econ. Geol.*, 67, 169-183.
- Lusk, J. 1976. A possible volcanic-exhalative origin for lenticular nickel sulfide deposits of volcanic association with special reference to these in Western Australia. *Can. J. Earth Sci.*, 13, 451-469.
- Lusk, J., and C.E. Ford 1978. Experimental investigation of sphalerite geobarometer to 10 kbar. *Am. Mineral.*, 63, 516-519.
- Lusk, J., F.A. Campbell, and H.R. Krouse 1975. Application of sphalerite geobarometry to ores of the Queumont mine, Normanda, Quebec. *Econ. Geol.*, 70, 1070-1083.
- Lusk, J., S.D. Scott, and C.E. Ford 1993. Phase relations in the Fe-Zn-S system to 5 kbars and temperatures between 325° and 150°C. *Econ. Geol.*, 88, 1880-1903.
- Lyakhov, Y.V., and I.V. Popivnyak 1978. Physiochemical conditions of development of gold mineralization in northern Buryatia. *International Geol. Rev.*, 20, 955-967.
- Lydon, J.W. 1983. Chemical parameters controlling the origin and deposition of sediment-hosted stratiform lead-zinc deposits. In *Short course in sediment-hosted stratiform lead-zinc deposits*, D.F. Sangster (ed.), 175-250. Victoria: Min. Assoc. of Canada.
- Lydon, J.W. 1984a. Volcanogenic sulphide deposits. Part 1: A descriptive model. *Geoscience Canada*, 11, 195-202.

- Lydon, J.W. 1984b. Some observations on the morphology and ore textures of volcanogenic sulphide deposits of Cyprus. *Geol. Survey Canada Paper* 84-1A, 601-610.
- Lydon, J.W. 1986. Models for the generation of metalliferous hydrothermal systems within sedimentary rocks and their applicability to the Irish Carboniferous Zn-Pb deposits. In *Geology and genesis of mineral deposits in Ireland*, C.J. Andrews, R.W.A. Crowe, S.Finlay, W.M. Pennell, and J.F. Pyne (eds.), 555-577. Dublin: Irish Assoc. Econ. Geol.
- Lydon, J.W. 1988. Volcanogenic massive sulphide deposits. Part 2: Genetic models. *Geoscience Canada*, 15, 43-65.
- Lydon, J.W., and A. Galley 1986. Chemical and mineralogical zonation of the Mathiati alteration pipe, Cyprus, and its genetic significance. In *Metallogeny of basic and ultrabasic rocks*, M. J. Gallagher, R. A. Ixer, C. R. Neary, and H. M. Prichard (eds.), 49-68. London: Inst. Mining and Metall.
- Lyle, J.R. 1977. Petrography and carbonate diagenesis of the Bonnetterre Formation in the Viburnum Trend area, southeast Missouri. *Econ. Geol.*, 72, 420-434.
- Maas, R. 1989. Nd-Sr isotopes constraints on the age and origin of unconformity-type uranium deposits in the Alligator Rivers uranium field, Northern Territory, Australia. *Econ. Geol.*, 84, 64-90.
- Macdonald, A.J. 1984. Gold mineralization in Ontario, I: The role of banded iron formation. In *Chibougamau — stratigraphy and mineralization*, J. Guha and E. H. Chown (eds.), *Can. Inst. Mining and Metall. Spec. Vol.* 34, 412-430.
- Macdonald, A.J. 1987. Ore deposit models #12. The platinum group element deposits: classification and genesis. *Geoscience Canada*, 14, 155-166.
- MacDonald, K.C., K. Becker, F.N. Speiss, and R.D. Ballard 1980. Exhalations of metalliferous solutions from the seafloor of the East Pacific Rise at 21° N. *Earth Planet. Sci. Lett.*, 48, 1-7.
- MacGeehan, P.J. 1978. The geochemistry of altered volcanic rocks at Matagami, Quebec: a geothermal model for massive sulphide genesis. *Can. J. Earth Sci.*, 15, 551-570.
- MacGeehan, P.J., and W.H. MacLean 1980a. Tholeiitic basalt-rhyolite magmatism and massive sulphide deposits at Matagami, Quebec. *Nature*, 283, 153-157.
- MacGeehan, P.J., and W. H. MacLean 1980b. An Archean sub-seafloor geothermal system, "calc-alkali" trends, and massive sulphide genesis. *Nature*, 286, 767-771.
- MacIntyre, D.G. 1982. Geologic setting of recently discovered stratiform-barite-sulfide deposits in northeastern British Columbia. *Can. Inst. Mining Metall. Bull.*, 75, 99-113.
- MacKenzie, F.T. 1975. Sedimentary cycling and the evolution of sea water. In *Chemical oceanography*, J. P. Riley and G. Skirrow (eds.), 1, 309-364. London: Academic Press.
- MacLean, P.J., and M.E. Fleet 1989. Detrital pyrite in the Witwatersrand gold fields of South Africa: evidence from truncated growth banding. *Econ. Geol.*, 84, 2008-2011.
- MacLean, W.H. 1969. Liquidus phase relations in the FeS-FeO-Fe₂O₄-SiO₂ system, and their application in geology. *Econ. Geol.*, 64, 865-884.
- Macqueen, R.W., and T.G. Powell 1983. Organic geochemistry of the Pine Point lead-zinc ore field and region, Northwest Territories, Canada. *Econ. Geol.*, 78, 1-25.
- Macqueen, R.W., and R.I. Thompson 1978. Carbonate-hosted lead-zinc occurrences in northeastern British Columbia with emphasis on the Robb Lake deposit. *Can. J. Earth Sci.*, 15, 1737-1762.
- Maiden, K.J., A.H. Innes, M.J. King, S. Master, and I. Pettitt 1984. Regional controls on the localization of stratabound copper deposits: Proterozoic examples from southern Africa and South Australia. *Precamb. Res.*, 25, 99-118.
- Mainwaring, P.R., and A.J. Naldrett 1977. Country rock assimilation and the genesis of Cu-Ni sulfides in the Water Hen intrusion, Duluth Complex, Minnesota. *Econ. Geol.*, 72, 1269-1284.
- Malpas, J. and P.T. Robinson 1987. Chromite mineralization in the Troodos ophiolite, Cyprus. In *Evolution of chromium ore fields*, C.W. Stowe (ed.), 220-237. New York: Van Nostrand.
- Manikyamba, C., V. Balram, and S.M. Naqvi 1993. Geochemical signatures of polygenetic origin of a banded iron formation (BIF) of the Archean Sandur greenstone belt (schist belt) Karnataka nucleus, India. *Precamb. Res.*, 61, 137-164.
- Marmont, S. 1987. Ore deposit models #13. Unconformity-type uranium deposits. *Geoscience Canada*, 14, 219-229.
- Marsden, R.W. 1968. Geology of the iron ores of the Lake Superior region in the United States. In *Ore deposits of the United States, 1933-1967, (Graton-Sales Volume)*, J.D. Ridge (ed.), 1, 489-506. New York: Am. Inst. Mining, Metall. and Petroleum Engineers.
- Marshall, B., and L.B. Gilligan 1993. Remobilization, syn-tectonic processes and massive sulphide deposits. *Ore Geol. Rev.*, 8, 39-64.
- Marshall, D.D., L.W. Diamond, and G.B. Skippen 1993. Silver transport and deposition at Cobalt, Ontario, Canada: fluid inclusion evidence. *Econ. Geol.*, 88, 837-854.
- Marston, R.J., D.J. Groves, D.R. Hudson, and J.R. Ross 1981. Nickel sulfide deposits in Western Australia: a review. *Econ. Geol.*, 76, 1330-1363.
- Mason, D.R. 1978. Compositional variations in ferromagnesian minerals from porphyry copper-generating and barren intrusions of the Western Highlands, Papua New Guinea. *Econ. Geol.*, 73, 878-890.

- Mason, D.R., and P.G. Feiss 1979. On the relationship between whole rock chemistry and porphyry copper mineralization. *Econ. Geol.*, 74, 1506-1510.
- Mason, D.R., and J.A. McDonald 1978. Intrusive rocks and porphyry copper occurrences of the Papua New Guinea-Solomon Islands region: a reconnaissance study. *Econ. Geol.*, 73, 857-877.
- Mason, T.R. and V. von Brunn 1977. 3 G yr-old stromatolite from South Africa. *Nature*, 266, 47-49.
- Mathez, E.A. 1995. Magmatic metasomatism and formation of the Merensky Reef, Bushveld Complex. *Contrib. Mineral. Petrol.*, 119, 277-286.
- Mathez, E.A., P. Agriner, and R. Hutchinson 1994. Hydrogen isotope composition of the Merensky Reef and related rocks, Atok section, Bushveld Complex. *Econ. Geol.*, 89, 791-802.
- Mathias, B.V., and G.J. Clark 1975. Mount Isa copper and silver-lead-zinc orebodies — Isa and Hilton mines. In *Economic geology of Australia*, 1, C.L. Knight (ed.), 351-376. Melbourne: Austral. Inst. Mining and Metall.
- Mathison, C.I., and A.E. Marshall 1981. Ni-Cu sulfides and their host mafic-ultramafic rocks in the Mt. Sholl intrusion, Pilbara region, Western Australia. *Econ. Geol.*, 76, 1581-1596.
- Matlock, J.F., and K.C. Misra 1993. Sphalerite-bearing detrital "sand" bodies in Mississippi Valley-type zinc deposits, Mascot-Jefferson City district, Tennessee: implications for the age of mineralization. *Mineral. Deposita*, 28, 344-353.
- Matsuhisa, Y., and M. Aoki 1994. Temperature and oxygen isotope variations during formation of the Hishikari epithermal gold-silver veins, southern Kyushu, Japan. *Econ. Geol.*, 89, 1608-1613.
- Matsukuma, T., and E. Horikoshi 1970. Kuroko deposits in Japan, a review. In *Volcanism and ore genesis*, T. Tatsumi (ed.), 153-179. Tokyo: Univ. Tokyo Press.
- Mauger, R.L. 1972. A sulfur isotope study of the Ducktown, Tennessee, district, U.S.A. *Econ. Geol.*, 67, 497-510.
- May, E.R., and P.G. Schmidt 1982. The discovery, geology and mineralogy of the Crandon Precambrian massive sulphide deposit, Wisconsin. *Geol. Assoc. Canada Spec. Paper* 25, 447-480.
- Maynard, J.B. 1983. *Geochemistry of sedimentary ore deposits*. New York: Springer Verlag.
- Maynard, J. B. 1991. Uranium: syngenetic to diagenetic deposits in foreland basins. *Rev. Econ. Geol.* 5, 187-197.
- McBirney, A.R., and R.M. Noyes 1979. Crystallization and layering of the Skaergaard intrusion. *J. Petrol.*, 20, 487-554.
- McCallum, I.S., L.D. Raedeke, and E.A. Mathez 1980. Investigation of the Stillwater Complex: Part 1. Stratigraphy and structure of the banded zone. *Am. J. Sci.*, 280-A, 59-87.
- McCallum, M.E., R.R. Loucks, R.R. Carlson, E.F. Cooley, and T.A. Doerge 1976. Platinum metals associated with hydrothermal copper ores at the New Rambler mine, Medicine Bow Mountain, Wyoming. *Econ. Geol.*, 71, 1429-1450.
- McClay, K.R. 1983. Deformation of Stratiform lead-zinc deposits. *Min. Assoc. Canada Short Course Handbook*, D.F. Sangster (ed.), 8, 283-309.
- McClay, K.R. and D.G. Carlisle 1978. Mid-Proterozoic sulphate evaporites at Mount Isa mine, Queensland, Australia. *Nature*, 274, 240-241.
- McConchie, D. 1987. The geology and geochemistry of the Joffre and Whaleback Shale Members of the Brockman Iron Formation, Western Australia. In *Precambrian iron-formations*, P.W.U. Appel and G.L. LaBerge (eds.), 541-597. Athens: Theophrastus Publ.
- McCulloch, M.T. and W.E. Cameron 1983. Nd-Sr isotopic study of primitive lavas from the Troodos ophiolite, Cyprus: evidence for a subduction-related setting. *Geology*, 11, 727-731.
- McDonald, J.A. 1967. Metamorphism and its effects in sulfide assemblages. *Mineral. Deposita*, 2, 200-220.
- McDonald, J.A. 1970. Some effects of deformation on sulfide-rich layers in lead-zinc orebodies, Mount Isa, Queensland. *Econ. Geol.*, 65, 273-298.
- McDougall, T.J. 1984. Convective processes caused by a dense, hot saline source flowing into a submarine depression from above. *Deep-Sea Res.*, 31, 1287-1309.
- McGoldrick, P.J. and R.R. Keays 1990. Mount Isa copper and lead-zinc-silver ores: coincidence of cogenesis? *Econ. Geol.*, 85, 641-650.
- McGoldrick, P.J., R.R. Keays, and B.B. Scott 1979. Thallium: a sensitive indicator of rock/seawater interaction and sulfur saturation of silicate melts. *Geochim. Cosmochim. Acta*, 43, 1303-1311.
- McKelvey, V.E. 1973. Abundance and distribution of phosphorous in the lithosphere. In *Environmental phosphorous handbook*, E.J. Griffith, A. Beeton, J.M. Spencer, and D.T. Mitchell (eds.), 13-31. New York: Wiley.
- McKibben, M.A., and W.A. Elders 1985. Fe-Zn-Cu-Pb mineralization in the Salton Sea geothermal system, Imperial Valley, California. *Econ. Geol.*, 80, 539-559.
- McKibben, M.A., and C.S. Eldridge 1995. Microscopic sulfur isotopic variations in ore minerals from the Viburnum Trend, SE Missouri, U.S.A.: a SHRIMP study. *Econ. Geol.*, 90, 228-245.
- McKibben, M.A., and A.E. Williams 1989. Metal speciation and solubility in saline hydrothermal fluids: an empirical approach based on geothermal brine data. *Econ. Geol.*, 84, 1996-2007.

- McKibben, M.A., A.E. Williams, and C.S. Eldridge 1989. Ore genesis in saline sediment-hosted hydrothermal systems: constraints from active geothermal systems [abs.]. *Abstracts 28th International Geol. Congress*, 2, 2-400 - 2-401.
- McKibben, M.A., A.E. Williams, and G.E.M. Hall 1990. Solubility and transport of platinum-group elements and Au in saline hydrothermal fluids: constraints from geothermal brine data. *Econ. Geol.*, 85, 1926-1934.
- McKibben, M.A., A.E. Williams, and S. Okubo 1988. Metamorphosed Plio-Pleistocene evaporites and the origins of hypersaline brines in the Salton Sea geothermal system, California: Fluid inclusion evidence. *Geochim. Cosmochim. Acta*, 52, 1047-1056.
- McKibben, M.A., A.E. Williams, W.A. Elders, and C.S. Eldridge 1987. Saline brines and metallogenesis in a modern sediment-filled rift: the Salton Sea geothermal system, California, U.S.A. *Appl. Geochem.*, 2, 563-578.
- McLaren, C.H., and J.P.R. de Villiers 1982. The platinum-group chemistry and mineralogy of the UG-2 chromite layers of the Bushveld Complex. *Econ. Geol.*, 77, 1348-1386.
- McLimans, R.K., H.L. Barnes, and H. Ohmoto 1980. Sphalerite stratigraphy of the Upper Mississippi Valley zinc-lead district, southwest Wisconsin. *Econ. Geol.*, 75, 351-361.
- McMillan, R.H. 1978. Genetic aspects and classification of important Canadian uranium deposits. *Mineral. Assoc. Canada Short Course Handbook* 3, 187-204.
- McMillan, W.J., and A. Panteleyev 1980. Ore deposit models - 1. Porphyry copper deposits. *Geoscience Canada*, 7, 52-63.
- Medford, R.R. J. Maxwell, and R.L. Armstrong 1983. $^{87}\text{Sr}/^{86}\text{Sr}$ ratio measurements on sulfides, carbonates and fluid inclusions from Pine Point, Northwest Territories, Canada: an $^{87}\text{Sr}/^{86}\text{Sr}$ ratio increase accompanying the mineralizing process. *Econ. Geol.*, 78, 1375-1378.
- Meeker, K.A., R.L. Chuan, P.R. Kyle, and J.M. Palais 1991. Emission of elemental gold particles from Mount Erebus, Ross Island, Antarctica. *Geophys. Res. Lett.*, 18, 167-172.
- Meillon, J.J. 1978. Economic geology and tropical weathering. *Can. Inst. Mining Metall. Bull.*, 71, 61-70.
- Meinert, L.D. 1983. Variability in skarn deposits: guides to exploration. In *Revolution in earth sciences*, S.J. Boardman (ed.), 301-317. Dubuque, Iowa: Kendall/Hunt.
- Meinert, L.D. 1984. Mineralogy and petrology of iron skarns in western British Columbia, Canada. *Econ. Geol.*, 79, 869-882.
- Meinert, L.D. 1992. Skarns and skarn deposits. *Geoscience Canada*, 19, 145-162.
- Meinert, L.D. 1993. Igneous petrogenesis and skarn deposits. *Geol. Assoc. Canada Spec. Paper* 40, 569-583.
- Mel'nik, Yu. P. 1982. *Precambrian banded iron-formations: physicochemical conditions of formation*. Amsterdam: Elsevier, 310 p.
- Mendelsohn, F. 1961. *The Geology of the Northern Rhodesian Copperbelt*. London: Macdonald.
- Mendelsohn, F. 1989. Central/southern African Ore Shale deposits. *Geol. Assoc. Canada Spec. Paper*, 36, 453-470.
- Meneghel, L. 1981. The occurrence of uranium in the Katanga System of northwestern Zambia. *Econ. Geol.*, 76, 56-68.
- Mercer, W. 1976. Minor elements in metal deposits in sedimentary rocks — a review of the recent literature. In *Handbook of strata-bound and stratiform ore deposits*, K.H. Wolf (ed.), 2, 1-27. Amsterdam: Elsevier.
- Meyer, C., and J.J. Hemley 1967. Wall rock alteration. In *Geochemistry of hydrothermal ore deposits*, H.L. Barnes (ed.), 166-235. New York: Holt, Rinehart and Winston.
- Meyer, C., E.P. Shea, C.C. Goddard, Jr., and Staff 1968. Ore deposits at Butte, Montana. In *Ore deposits of the United States, 1933-1967 (Graton-Sales Volume)*, J.D. Ridge (ed.), 2, 1373-1416. New York: Am. Inst. Mining Metall. Petroleum Engineers.
- Meyer, H.O.A. 1985. Genesis of diamond: a mantle saga. *Am. Mineral.*, 70, 344-355.
- Mihalik, P., J.B.E. Jacobsen, and S.A. Hiemstra 1974. Platinum-group minerals from a hydrothermal environment. *Econ. Geol.*, 69, 257-262.
- Mills, H., A.M. Halliday, J.H. Aston, I.K. Anderson, and M.H. Russell 1987. Origin of a giant orebody at Navan, Ireland. *Nature*, 327, 223-226.
- Mills, K.C. 1974. *Thermodynamic data for inorganic sulfides, selenides and tellurides*. London: Butterworths.
- Minter, W.E.L. 1989. Comment on "Problems with the placer model for Witwatersrand gold". *Geology*, 16, 1153-1154.
- Minter, W. E. L. 1990. Paleoplacers of the Witwatersrand basin. *Mining Eng.*, 42, 195-199.
- Minter, W.E.L., C.E. Feather, and C.W. Glatthaar 1988. Sedimentological and mineralogical aspects of the newly discovered Witwatersrand placer deposit that reflect Proterozoic weathering, Welkom Gold Field, South Africa. *Econ. Geol.*, 83, 481-491.
- Minter, W.E.L., M. Goedhart, J. Knight, and H.E. Frimmel 1993. Morphology of Witwatersrand gold grains from the Basal Reef: evidence from their detrital origin. *Econ. Geol.*, 88, 237-248.

- Mishra, B., and A. Mookherjee 1988. Geothermometry based on fractionation of Mn and Cd between coexisting sphalerite and galena from some carbonate-hosted sulfide deposits in India. *Mineral. Deposita*, 23, 179-185.
- Misra, K. C. 1992. Characteristics and tectonic settings of massive sulfide deposits, southern Appalachian Blue Ridge belt, USA. In *Metallogeny related to tectonics of the Proterozoic mobile belts*, S.C. Sarkar (ed.), 103-132. New Delhi: Oxford & IBH Publ. Co.
- Misra, K.C. and M.E. Fleet 1973. The chemical composition of synthetic and natural pentlandite assemblages. *Econ. Geol.*, 68, 518-539.
- Misra, K.C. and M.E. Fleet 1974. Chemical composition and stability of violartite. *Econ. Geol.*, 69, 391-403.
- Misra, K.C. and R.E. Fulweiler 1992. Zinc deposits of the Mascot-Jefferson City district, East Tennessee. *Soc. Econ. Geol. Guidebook Series*, 14, 9-24.
- Misra, K.C., and C. Lu 1992. Hydrothermal calcites from the Mississippi Valley-type Elmwood-Gordonsville zinc deposits, Central Tennessee, U.S.A.: Fluid inclusion and stable isotope data. *Eur. J. Mineral.*, 4, 977-988.
- Misra, K.C., and F.B. Keller 1978. Ultramafic bodies in the southern Appalachians. *Am. Mineral.*, 278, 389-418.
- Misra, K.C., and P. Torssander 1995. Sulfur and carbon isotopic data for the Central Tennessee zinc district: constraints on mechanism of sulfide precipitation [abs.]. *Geol. Soc. Am. Abstracts with Programs*, 27, 76.
- Misra, K.C., J.F. Gratz, and C. Lu 1997. Carbonate-hosted Mississippi Valley-type mineralization in the Elmwood-Gordonsville deposits, Central Tennessee zinc district: a synthesis. *Soc. Econ. Geol. Spec. Publ.* 4, 58-73.
- Mitchell, A.H.G., and M.S. Garson 1972. Relationship of porphyry copper and circum-Pacific tin deposits to paleo-Benioff zones. *Inst. Mining Metall. Trans.*, 81, B10-B35.
- Mitchell, A.H.G., and M.S. Garson 1976. Mineralization at plate boundaries. *Minerals Sci. Eng.*, 8, 129-169.
- Mitchell, R.H. 1973. Composition of olivine, silica activity and oxygen fugacity in kimberlite. *Lithos*, 6, 65-81.
- Mitchell, R.H. 1986. *Kimberlites: mineralogy, geochemistry, and petrology*. New York: Plenum Press.
- Mitchell, R.H., and R.R. Keays 1981. Abundance and distribution of gold, palladium and iridium in some spinel and garnet lherzolites: implications for the nature and origin of precious metal-rich intergranular components in the upper mantle. *Geochim. Cosmochim. Acta*, 45, 2452-2442.
- Miyanao, T. 1987. Diagenetic to low-grade metamorphic conditions of Precambrian iron-formations. In *Precambrian iron-formations*, P.W.U. Appel and G.L. LaBerge (eds.), 155-186. Athens: Theophrastus Publ.
- Moench, R. H., and J. S. Schlee 1967. Geology and uranium deposits of the Laguna ditrict, New Mexico. *U.S. Geol. Survey Prof. Paper* 519, 117p.
- Mogessie, A., E.F. Stumpfl, and P.W. Weiblen 1991. The role of fluids in the formation of platinum-group minerals, Duluth Complex, Minnesota: mineralogic, textural, and chemical evidence. *Econ. Geol.*, 86, 1506-1518.
- Moh, G.H. 1975. Ore mineral systems. *N. Jb. Miner. Abh.*, 126, 126-145.
- Molnár, F., D.H. Watkinson, P.C. Jones, and I. Gatter 1997. Fluid inclusion evidence for hydrothermal enrichment of magmatic ore at the contact zone of the Ni-Cu platinum-group element 4b deposit, Lindsley mine, Sudbury, Canada. *Econ. Geol.*, 92, 674-685.
- Molyneux, T.G. 1970. The geology of the area in the vicinity of Magnet Heights, eastern Transvaal, with special reference to magnetic iron ore. *Geol. Soc. S. Africa Spec. Publ.* 1, 228-241.
- Monster, J., P.W.U. Appel, H.G. Thode, M. Schidlowski, and C.M. Carmichael 1979. Sulfur isotope studies in early Archean sediments from Isna, West Greenland: implications for the antiquity of bacterial sulfide reduction. *Geochim. Cosmochim. Acta*, 43, 405-413.
- Monster, J., P.W.U. Appel, H.G. Thode, M. Schidlowski, C.M. Carmichael, and D. Bridgewater 1979. Sulfur isotope ratios in later and early Precambrian sediments and their implications regarding early environments and early life. *Origins of Life*, 10, 127-136.
- Montoya, J.W., and J.J. Hemley 1975. Activity relations and stabilities in alkali feldspar and mica alteration reactions. *Econ. Geol.*, 70, 577-594.
- Mookherjee, A. 1964. The geology of the Zawar lead-zinc mine. *Econ. Geol.*, 59, 656-677.
- Mookherjee, A. 1970. Dykes, sulphide deposits, and regional metamorphism: criteria for determining their time relationship. *Mineral. Deposita*, 5, 120-144.
- Mookherjee, A. 1976. Ores and metamorphism: temporal and genetic relationships. In *Handbook of strata-bound and stratiform ore deposits*, K.H. Wolf (ed.), 4, 203-260. Amsterdam: Elsevier.
- Mookherjee, A., and G. Suffel 1968. Massive sulphide-late diabase relationships, Horne mine, Quebec: genetic and chronological implications. *Can. J. Earth Sci.*, 5, 421-432.
- Mookherjee, A., and N. K. Dutta 1970. Evidence of incipient melting of sulphides along a dike contact, Geco mine, Manitouwadge, Ontario. *Econ. Geol.*, 65, 706-713.

- Moorbath, S., R. K. O'Nions, and R. V. Pankhurst 1973. Early Archean age for the Isua iron formation, West Greenland. *Nature*, 245, 138-139.
- Moore, J.G. and B.P. Fabbi 1971. An estimate of the juvenile sulfur content of basalt. *Contrib. Mineral. Petrol.*, 33, 118-127.
- Moore, W.J., and J.T. Nash 1974. Alteration and fluid inclusion studies of the porphyry copper ore body at Bingham, Utah. *Econ. Geol.*, 69, 631-645.
- Moores, E.M. 1982. Origin and emplacement of ophiolites. *Rev. Geophys. Space Phys.*, 20, 735-760.
- Moores, E.M. 1986. The Proterozoic ophiolite problem, continental emergence, and the Venus connection. *Science* 234, 65-68.
- Moores, E.M., P.T. Robinson, J. Malpas, and C. Xenophontos 1984. A model for the origin of the Troodos massif, Cyprus, and other Mideast ophiolites. *Geology*, 12, 500-503.
- Morganti, J.M. 1981. Ore deposit models-4. Sedimentary-type stratiform ore deposits: some models and a new classification. *Geoscience Canada*, 8, 65-75.
- Morris, R.C. 1980. A textural and mineralogical study of the relationship of iron ore to banded iron-formation in the Hamersley iron province of Western Australia. *Econ. Geol.*, 75, 184-209.
- Morris, R.C. 1985. Genesis of iron ore in banded iron formation by supergene and supergene-metamorphic process — a conceptual model. In *Handbook of strata-bound and stratiform ore deposits*, K.H. Wolf (ed.), 13, 33-235. Amsterdam: Elsevier.
- Morris, R.C. 1986. The cycling redox state of iron in the genesis of banded iron-formations and their associated enrichment iron ores. *J. Geol. Soc. India*, 28, 227-286.
- Morris, R.C. 1993. Genetic modelling for banded iron-formation of the Hamersley Group, Pilbara craton, Western Australia. *Precamb. Res.*, 60, 243-286.
- Morris, R.C. and R.C. Horwitz 1983. The origin of the iron-formation-rich Hamersley Group of Western Australia — deposition on a platform. *Precamb. Res.* 21, 273-297.
- Morrison, G.G. 1984. Morphological features of the Sudbury structure in relation to an impact origin. *Ontario Geol. Survey Spec. Vol. 1*, 513-520.
- Morton, R.L., and J.M. Franklin 1987. Two-fold classification of Archean volcanic-associated massive sulfide deposits. *Econ. Geol.*, 82, 1057-1063.
- Mossman, D.J. and B.D. Dyer 1985. The geochemistry of Witwatersrand-type gold deposits and the possible influence of ancient prokaryotic communities on gold dissolution and precipitation. *Precamb. Res.*, 30, 303-319.
- Mottl, M.J., and H.D. Holland 1978. Chemical exchange during hydrothermal alteration of basalt by seawater. I. Experimental results for major and minor components of seawater. *Geochim. Cosmochim. Acta*, 42, 1103-1115.
- Mottl, M.J., H.D. Holland, and R.F. Carr 1979. Chemical exchange during hydrothermal alteration of basalt by seawater. II. Experimental results for Fe-, Mn and sulfur species. *Geochim. Cosmochim. Acta*, 43, 869-884.
- Mountain, B.W., and S.A. Wood 1988. Chemical controls on the solubility, transport, and deposition of platinum and palladium in hydrothermal solutions: a thermodynamic approach. *Econ. Geol.*, 83, 492-510.
- Mueller, A.G., J.R. de Laeter, and D.I. Groves 1991. Strontium isotope systematics of hydrothermal minerals from epigenetic Archean gold deposits in the Yilgarn Block, Western Australia. *Econ. Geol.*, 86, 780-809.
- Muir, M.D. 1981. The microfossils from the Proterozoic Urquhart Shale, Mount Isa, Queensland, and their significance in relation to the depositional environment, diagenesis, and mineralization. *Mineral. Deposita*, 16, 51-58.
- Muir, M.D. 1983. Depositional environments of host rocks to northern Australian lead-zinc deposits, with special reference to McArthur River. In *Short course in sediment-hosted stratiform lead-zinc deposits*, D.F. Sangster (ed.), 141-174. Victoria: Min Assoc. Canada.
- Mukherjee, A.D., and R.N. Sen 1980. Geochemical implications in the genesis of Zawar lead-zinc deposit, Rajasthan. *Proc. 5th Quad. IAGOD Symp.*, 709-718. Stuttgart: E. Schweizerbartsche Verlagsbuchhandlung.
- Munha, J. 1979. Blue amphiboles, metamorphic regime and plate tectonic modelling in the Iberian pyrite belt. *Contrib. Mineral. Petrol.*, 69, 279-289.
- Munha, J., F.J.A.S. Barriga, and R. Kerrich 1986. High ^{18}O ore-forming fluids in volcanic-hosted base metal massive sulfide deposits: Geologic, $^{18}\text{O}/^{16}\text{O}$, and D/H evidence from the Iberian pyrite belt; Crandon, Wisconsin; and Blue Hill, Maine. *Econ. Geol.*, 81, 530-552.
- Murck, B.W., and I.H. Campbell 1986. The effects of temperature, oxygen fugacity and melt composition on the behavior of chromium in basic and ultrabasic melts. *Geochim. Cosmochim. Acta*, 50, 1871-1887.
- Murray, W.J. 1975. McArthur River H.Y.C. lead-zinc and related deposits. In *Economic Geology of Australia and Papua New Guinea*, 1, C.L. Knight (ed.) 329-339. Melbourne: Austral. Inst. Mining Metall.

- Mutschler, F.E., E.G. Wright, S. Ludington, and J.T. Abbott 1981. Granite molybdenite systems. *Econ. Geol.*, 76, 874-897.
- Myers, G.L., and L.D. Meinert 1991. Alteration, mineralization, and gold distribution in the Fortitude gold skarn. In *Geology and ore deposits of the Great Basin*, G.L. Raines, R.E. Lisle, R.W. Schafer, and W.H. Wilkinson (eds.), 1, 407-418. Reno, Nevada: Geol. Soc. Nevada.
- Nabelek, P.I., T.C. Labotka, J.R. O'Neil, and J.J. Papike 1984. Contrasting fluid/rock interaction between the Notch Peak granitic intrusion and argillites and limestones in western Utah: evidence from stable isotopes and phase assemblages. *Contrib. Mineral. Petrol.*, 86, 25-34.
- Naeser, C.W. 1977. Fission-track dating and geologic annealing of fission. In *Lectures in isotope Geology*, E. Jager and J. C. Hunziker (eds.), 154-168. New York: Springer-Verlag.
- Nakai, S., A.N. Halliday, S.E. Kesler, and H.D. Jones 1990. Rb-Sr dating of sphalerites from Tennessee and the genesis of Mississippi Valley-type ore deposits. *Nature*, 346, 354-357.
- Nakai, S., A. N. Halliday, S.E. Kesler, H.D. Jones, J.R. Kyle, and T.E. Lane 1993. Rb-Sr dating of sphalerites from Mississippi Valley-type (MVT) ore deposits. *Geochim. Cosmochim. Acta*, 57, 417-427.
- Nakamura, Y. and H. Shima 1982. Fe and Zn partitioning between sphalerite and stannite [abst.]. *Joint Mtg. of Soc. Mining Geol. Japan. Assoc. Mineral. Petrol. Econ. Geol. and Mineral. Soc. Japan A-8*. (Japanese)
- Naldrett, A.J. 1966. The role of sulphurization in the genesis of iron-nickel sulphide deposits of the Porcupine district, Ontario. *Can. Inst. Mining. Metall. Trans.*, 69, 147-155.
- Naldrett, A.J. 1969. A portion of the system Fe-S-O between 900 and 1080°C and its application to sulfide ore magmas. *J. Petrol.*, 10, 171-201.
- Naldrett, A.J. 1973. Nickel sulfide deposits—their classification and genesis, with special emphasis on deposits of volcanic association. *Can. Inst. Mining. Metall. Trans.*, 76, 183-201.
- Naldrett, A.J. 1979. Partitioning of Fe, Co, Ni, and Cu between sulfide liquid and basaltic melts and the composition of Ni-Cu sulfide deposits — a reply and further discussion. *Econ. Geol.*, 74, 1520-1529.
- Naldrett, A.J. 1981a. Nickel sulfide deposits: classification, composition, and genesis. *Econ. Geol. 75th Anniv. Vol.*, 628-685.
- Naldrett, A.J. 1981b. Pt group element deposits. *Can. Inst. Mining. Metall. Spec. Vol. 23*, 197-232.
- Naldrett, A.J. 1984a. Summary, discussion, and synthesis. In *The Geology and ore deposits of the Sudbury Structure*, E.G. Pye, A.J. Naldrett, and P.E. Giblin (eds.), *Ont. Geol. Surv. Spec. Vol. 1*, 533-569. Toronto: Ontario Geol. Survey.
- Naldrett, A.J. 1984b. Mineralogy and composition of the Sudbury ores. In *The Geology and ore deposits of the Sudbury Structure*, E.G. Pye, A.J. Naldrett, and P.E. Giblin (eds.), *Ontario Geol. Surv. Spec. Vol. 1*, 309-325. Toronto: Ontario Geol. Survey.
- Naldrett, A.J. 1989. *Magmatic sulfide deposits*. New York: Oxford Univ. Press.
- Naldrett, A.J. 1998. The use of PGE in understanding accumulations of magmatic sulfides [abs.]. *8th International Platinum Symposium Abstracts*, June 28-July 3, 1998, Rustenburg, South Africa, 281-284.
- Naldrett, A.J. 1999. World-class Ni-Cu-PGE deposits: key factors in their genesis. *Mineral. Deposita*, 34, 227-240.
- Naldrett, A.J., and S.-J. Barnes 1986. The behavior of platinum group elements during fractional crystallization and partial melting with special reference to the composition of magmatic sulfide ores. *Fortschritte der Mineralogie*, 64, 113-133.
- Naldrett, A.J., and L.J. Cabri 1976. Ultramafic and related mafic rocks: Their classification, and genesis with special reference to the concentration of nickel sulfides and platinum-group elements. *Econ. Geol.*, 71, 1131-1158.
- Naldrett, A.J., and I.H. Campbell 1982. Physical and chemical constraints on genetic models for komatiite-related Ni-sulphide deposits. In *Komatiites*, N.T. Arndt and E.G. Nisbet (eds.), 423-434. London: Allen & Unwin.
- Naldrett, A. J., and J. M. Duke 1980. Platinum metals in magnetic sulfide ores. *Science*, 208, 1417-1428.
- Naldrett, A.J. and R.H. Hewins 1984. The main mass of the Sudbury igneous complex. In *The geology and ore deposits of the Sudbury Structure*, E.G. Pye, A.J. Naldrett, and P.E. Giblin (eds.), *Ontario Geol. Survey Spec. Vol. 1*, p. 235-251.
- Naldrett, A.J. and G. Kullerud 1967. A study of the Stratheona mine and its bearing on the origin of the nickel-copper sulfide ores of the Sudbury district, Ontario. *J. Petrol.*, 8, 453-531.
- Naldrett, A.J., and J. Lehmann 1987. Spinell non-stoichiometry as the explanation for Ni-, Cu-, and PGE-enriched sulfides in chromitites [abs.]. *Geo-Platinum 87 Symposium*, The Open Univ., Milton Keynes, Paper T10.
- Naldrett, A.J., and A.J. Macdonald 1980. Tectonic setting of some Ni-Cu sulfide ores: their importance in genesis and exploration. *Geol. Assoc. Canada Spec. Paper 20*, 633-657.
- Naldrett, A.J., and A.R. Turner 1977. The geology and petrogenesis of a greenstone belt and related nickel sulfide mineralization at Yakabindie, Western Australia. *Precamb. Res.*, 5, 43-103.
- Naldrett, A.J., and G. von Gruenewaldt 1988. The upper Critical Zone of the Bushveld Complex and the origin of Merensky-type ores — a reply. *Econ. Geol.*, 83, 1085-1091.

- Naldrett, A.J., and G. von Gruenewaldt. 1989. Association of platinum-group elements with chromitite in layered intrusions and ophiolitic complexes. *Econ. Geol.*, 84, 180-187.
- Naldrett, A.J., G.E. Brügmann, and A.H. Wilson 1990. Models for the concentration of PGE in layered intrusions. *Can. Mineral.*, 28, 389-408.
- Naldrett, A.J., J.R. Craig, and G. Kullerud 1967. The central portion of the Fe-Ni-S system and its bearing on pentlandite exsolution in iron-nickel sulfide ores. *Econ. Geol.*, 62, 826-847.
- Naldrett, A.J., G. Cameron, G. von Gruenewaldt, and M.R. Sharpe 1987. The formation of stratiform PGE deposits in layered intrusions. In *Origins of igneous layering*, I. Parsons (ed.), NATO Adv. Sci. Inst. Series, Ser. C., 196, 313-397. Dordrecht: Reidel.
- Naldrett, A.J., J.M. Duke, P.C. Lightfoot, and J.F.H. Thompson 1984. Quantitative modelling of the segregation of magmatic sulphides: an exploration guide. *Can. Inst. Mining Metall. Bull.*, 77, 46-56.
- Naldrett, A.J., E.C. Gasparrini, S.J. Barnes, G. von Gruenewaldt, and M.R. Sharpe 1986. The upper Critical Zone of the Bushveld Complex and the origin of Merensky-type ores. *Econ. Geol.*, 81, 1105-1117.
- Naldrett, A.J., P.C. Lightfoot, V. Fedorenko, W. Doherty, and N.S. Gorbachev 1992. Geology and geochemistry of the Noril'sk region, USSR, with implications for the origin of the Ni-Cu ores. *Econ. Geol.*, 87, 975-1004.
- Nash, J.T. 1976. Fluid inclusion petrology — data from porphyry copper deposits and application to exploration. *U. S. Geol. Survey Prof. Paper* 907-D, D1-D16.
- Nash, J.T., H.C. Granger, and S.S. Adams 1981. Geology and concepts of genesis of important types of uranium deposits. *Econ. Geol. 75th Anniv. Vol.*, 63-116.
- Nash, J.T., W.C. Utterback, and J.A. Saunders 1991. Geology and geochemistry of the Sleeper gold-silver deposit, Humboldt County, Nevada — an interim report. In *Geology and ore deposits of the Great Basin*, G.L. Raines et al. (eds.), 1063-1064. Reno: Geol. Soc. Nevada.
- Nesbitt, B.E. 1982. Metamorphic sulfide-silicate equilibria in the massive sulfide deposits at Ducktown, Tennessee. *Econ. Geol.*, 77, 364-378.
- Nesbitt, B.E. 1986a. Oxide-sulfide-silicate equilibria associated with metamorphosed ore deposits. Part I: Theoretical considerations. *Econ. Geol.*, 81, 831-840.
- Nesbitt, B.E. 1986b. Oxide-sulfide-silicate equilibria associated with metamorphosed ore deposits. Part II: Pelitic and felsic volcanic terrains. *Econ. Geol.*, 81, 841-856.
- Nesbitt, B.E. 1988. Gold deposit continuum: a genetic model for lode mineralization in the continental crust. *Geology*, 16, 1044-1048.
- Nesbitt, B.E. 1991. Phanerozoic gold deposits in tectonically active continental margins. In *Gold metallogeny and exploration*, R. P. Foster (ed.), 104-132. Glasgow: Blackie.
- Nesbitt, B.E., and E.J. Essene 1982. Metamorphic thermometry and barometry of a portion of the southern Blue Ridge province. *Am. J. Sci.*, 282, 701-729.
- Nesbitt, B.E., and W.C. Kelly 1980. Metamorphic zonation of sulfides, oxides and graphite in and around the orebodies at Ducktown, Tennessee. *Econ. Geol.*, 75, 1010-1021.
- Nesbitt, B.E., and K. Muehlenbachs 1989a. Geology, geochemistry, and genesis of mesothermal lode gold deposits of the Canadian Cordillera: evidence of ore formation from evolved meteoric water. *Econ. Geol. Mono.* 6, 552-563.
- Nesbitt, B.E., and K. Muehlenbachs 1989b. Origins and movement of fluids during deformation and metamorphism in the Cordillera. *Science*, 245, 733-735.
- Nesbitt, B.E., J.B. Murowchick, and K. Muehlenbachs 1986. Dual origins of lode gold deposits in the Canadian Cordillera. *Geology*, 14, 506-509.
- Nesbitt, B.E., F.J. Longstaffe, D.R. Shaw, and K. Muehlenbachs 1984. Oxygen isotope geochemistry of the Sullivan massive sulfide deposit, Kimberley, British Columbia. *Econ. Geol.*, 79, 933-946.
- Nesbitt, R. W., Shen-Su Sun, and A. C. Purvis 1979. Komatiites: geochemistry and genesis. *Can. Mineral.*, 17, 165-186.
- Neudert, M. 1984. Are the Mount Isa ores really syngenetic? [abs.]. *Geol. Soc. Austral. Abstracts*, 12, 402-403.
- Neudert, M. 1986. Sedimentology of the Middle Proterozoic Mount Isa Group, Queensland, Australia [abs.]. *International Sedimentology Congress*, 12th, Abstracts, 229.
- Newberry, R.J. 1982. Tungsten-bearing skarns of Sierra Nevada, I: The Pine Creek mine, California. *Econ. Geol.*, 77, 823-844.
- Newberry, R.J., and M.T. Einaudi 1981. Tectonic and geochemical setting of tungsten skarn mineralization in the Cordillera. *Arizona Geol. Soc. Digest*, 14, 99-112.
- Newberry, R.J., and S.E. Swanson 1986. Scheelite skarn granitoids: an evaluation of the roles of magmatic source and process. *Ore Geol. Rev.*, 1, 57-81.
- Newnham, L.A. 1975. Renison Bell Tinfield. In *Economic Geology of Australia and Papua New Guinea*, I, Metals. *Austral. Inst. Mining Metall. Mono.* 5, 581-583.
- Newton, R.C. 1989. Metamorphic fluids in the deep crust. *Ann. Rev. Earth Planet Sci.*, 17, 385-412.
- Newton, R.C., J.V. Smith, and B.F. Windley 1980. Carbonic metamorphism, granulites and crustal growth. *Nature*, 288, 130-149.

- Nickel, E.H., and M.R. Thornber 1977. Chemical constraints on the weathering of serpentinites containing nickel-iron sulphides. *J. Geochem. Exploration*, 8, 235-245.
- Nickel, E.H., J.A. Hallberg, R. Halligan 1979. Unusual nickel mineralization of Nullagine, Western Australia. *Geol. Soc. Austral. J.*, 26, 61-71.
- Nickel, E.H., J.R. Ross, and M.R. Thornber 1974. The supergene alteration of pentlandite-pyrrhotite ore at Kambalda, Western Australia. *Econ. Geol.*, 69, 93-107.
- Nicolas, A. 1989. *Structures of ophiolites and dynamics of oceanic lithosphere*. Dordrecht, The Netherlands: Kluwer.
- Nielsen, H. 1985. Sulfur isotope ratios in strata-bound mineralizations in Central Europe. *Geol. Jahrb.*, D 70, 225-262.
- Nielsen, R.L. 1976. Recent developments in the study of porphyry copper geology: a review. In *Porphyry deposits of the Canadian Cordillera*, A.S. Brown (ed.), *Can. Inst. Mining Metall. Spec. Vol. 15*, 487-500.
- Niewendorp, C.A., and C.W. Clendenin 1993. Paragenetic link between organic matter and late-stage ore deposition in the Sweetwater mine, Viburnum Trend, Southeast Missouri. *Econ. Geol.*, 88, 957-960.
- Nisbet, E.G. 1982. The tectonic setting and petrogenesis of komatiites. In *Komatiites*, N.T. Arndt and E.G. Nisbet (eds.), 501-520. London: Allen & Unwin.
- Nisbet, E.G., and D. Walker 1982. Komatiites and the structure of the Archean mantle. *Earth Planet. Sci. Lett.*, 60, 105-113.
- Nixon, P.H., and F.R. Boyd 1973. Petrogenesis of the granular and sheared ultrabasic nodule suite in kimberlites. In *Lesotho kimberlites*, P.H. Nixon (ed.), 48-56. Maseru: Lesotho National Development Corporation.
- Noble, E.A. 1963. Formation of ore deposits by waters of compaction. *Econ. Geol.*, 58, 1145-1156.
- Noble, J.A. 1950. Ore mineralization in the Homestake gold mine, Lead, South Dakota. *Geol. Soc. Am. Bull.*, 61, 221-252.
- Norman, D.I. 1978. Analysis of Rb, Sr and Sr isotopes in fluid inclusion waters. *Inst. Mining Metall. Trans.*, Sec. B, 87, 34-35.
- Norman, D.I., and G.P. Landis 1983. Source of mineralizing components in hydrothermal ore fluids as evidenced by $^{87}\text{Sr}/^{86}\text{Sr}$ and stable isotope data from the Pasto Bueno deposit, Peru. *Econ. Geol.*, 78, 451-465.
- Northrop, H.R., and M.B. Goldhaber (eds.) 1990. Genesis of the tabular-type uranium deposits of the Henry Basin. *Econ. Geol.*, 85, 215-269.
- Northrop, H.R., R.O. Rye, G. P. Landis, R. Lustwerk, M.B. Jones, and W.E. Daly 1987. Sediment-hosted gold mineralization at Jerritt Canyon, Nevada. V - Stable isotope geochemistry and a model of ore deposition [abs.]. *Geol. Soc. Am. Abstracts with Programs*, 19, 791.
- Norton, D. 1978. Source-lines, source regions, and pathlines for fluids in hydrothermal systems related to cooling plutons. *Econ. Geol.*, 73, 21-28.
- Norton, D., 1982. Fluid and heat transport phenomena typical of copper-bearing pluton environments. In *Advances in Geology of the porphyry copper deposits, southwestern North America*, S.R. Titley (ed.), 59-72. Tucson, Arizona: Univ. Arizona Press.
- Norton, D., and J. Knight 1977. Transport phenomena in hydrothermal systems: cooling plutons. *Am. J. Sci.*, 277, 937-981.
- Norton, S.A. 1973. Laterite and bauxite formation. *Econ. Geol.*, 68, 353-361.
- O'Driscoll, E.S.T. 1989. The tectonic setting of sulphide nickel deposits in the Western Australian shield as shown by major gravity lineaments. *Global Tectonics & Metallogeny*, 3, 177-185.
- O'Hara, M.J., M.J. Saunders, and E.L.P. Mercy 1975. Garnet-peridotite, primary ultrabasic magma and eclogite: interpretation of upper mantle processes in kimberlite. *Phys. Chem. Earth*, 9, 571-604.
- O'Neil, J.R., and M.L. Silberman 1974. Stable isotope relations in epithermal Au-Ag deposits. *Econ. Geol.*, 69, 902-909.
- O'Rourke, J. E. 1961. Paleozoic banded iron-formations. *Econ. Geol.*, 56, 331-361.
- Oder, C.R.L., and J.W. Hook 1950. Zinc deposits in the southeastern states. In *Symposium on mineral resources of the southeastern United States*, F.G. Snyder (ed.), 72-87. Knoxville, Tennessee: Univ. Tenn. Press.
- Oehler, J. H. 1976. Hydrothermal crystallization of silica gel. *Geol. Soc. Am. Bull.*, 87, 1143-1152.
- Oehler, J.H., and R.G. Logan 1977. Microfossils, cherts, and associated mineralization in the Proterozoic McArthur (H.Y.C.) lead-zinc-silver deposit. *Econ. Geol.*, 72, 1393-1409.
- Ohle, E.L. 1959. Some considerations in determining the origin of ore deposits of the Mississippi Valley type. *Econ. Geol.*, 54, 769-789.
- Ohle, E.L. 1972. Evolution of iron ore deposits. *Econ. Geol.*, 67, 953-964.
- Ohle, E.L. 1980. Some considerations in determining the origin of ore deposits of the Mississippi Valley-type — Part II. *Econ. Geol.*, 75, 161-172.
- Ohle, E.L. 1990. A comparison of the Old Land Belt and the New Lead Belt in southeast Missouri. *Econ. Geol.*, 85, 1894-1895.

- Ohmoto, H. 1972. Systematics of sulfur and carbon isotopes in hydrothermal ore deposits. *Econ. Geol.*, 67, 551-578.
- Ohmoto, H. 1978. Submarine calderas: a key to the formation of volcanogenic massive sulfide deposits? *Mining Geol.*, 18, 219-231.
- Ohmoto, H. 1983. Geologic setting of the Kuroko deposits, Japan; Part I. Geologic history of the Green Tuff region. *Econ. Geol. Mono.* 5, 9-24.
- Ohmoto, H. 1986. Stable isotope geochemistry of ore deposits. In *Reviews in Mineralogy* 16 (Stable Isotopes), 491-559. Blacksburg, Virginia: Min. Soc. Am.
- Ohmoto, H. 1989. Archean volcanogenic massive sulfide deposits: products of warmer sulfate-bearing oceans and warmer crusts [abs.]. *Abstracts, 28th International Geol. Congress*, 1989, Washington, D. C., 2-541.
- Ohmoto, H., and R.P. Felder 1987. Bacterial activity in the warmer sulphate-bearing, Archean oceans. *Nature*, 328, 244-246.
- Ohmoto, H., and M.B. Goldhaber 1997. Sulfur and carbon isotopes. In *Geochemistry of hydrothermal ore deposits*, 3rd. edn., H.L. Barnes (ed.), 517-612. New York: Wiley.
- Ohmoto, H., and R.O. Rye 1974. Hydrogen and oxygen isotopic compositions of fluid inclusions in the Kuroko deposits, Japan. *Econ. Geol.*, 69, 947-953.
- Ohmoto, H., and R.O. Rye 1979. Isotopes of sulfur and carbon. In *Geochemistry of hydrothermal ore deposits*, 2nd edn., H.L. Barnes (ed.), 509-567. New York: Wiley.
- Ohmoto, H., and B. J. Skinner 1983. The Kuroko and related volcanogenic massive sulfide deposits: Introduction and summary of new findings. *Econ. Geol. Mono.* 5, 1-8.
- Ohmoto, H., and T. Takahashi 1983. Geologic setting of the Kuroko deposits, Japan; Part III. Submarine calderas and Kuroko genesis. *Econ. Geol. Mono.* 5, 39-54.
- Ohmoto, H., S.R. Hart, and H.D. Holland 1966. Studies of the Providencia area, Mexico, II. K-Ar and Rb-Sr ages of intrusive rocks and hydrothermal minerals. *Econ. Geol.*, 61, 1205-1213.
- Ohmoto, H., M. Mizukami, S.E. Drummond, C.E. Eldridge, V. Pisutha-Arnond, and T. C. Lenagh 1983. Chemical processes of ore formation. *Econ. Geol. Mono.* 5, 570-604.
- Oliver, J. 1986. Fluids expelled tectonically from orogenic belts: their role in hydrocarbon migration and other geologic phenomena. *Geology*, 14, 99-102.
- Olsen, J.C., D.R. Shawe, L.C. Pray, W.N. Sharp, and D.F. Hewitt 1954. Rare earth mineral deposits of the Mountain Pass district, San Bernardino County, California. *U.S. Geol. Survey Prof. Paper* 261.
- Oreskes, N., and M.W. Hitzman 1993. A model for the origin of Olympic Dam-type deposits. *Geol. Assoc. Canada Spec. Paper* 40, 615-633.
- Orpen, J.Z., and J.F. Wilson 1981. Stromatolites at 3500 Myr and a greenstone-granite unconformity in the Zimbabwean Archean. *Nature*, 291, 218-220.
- Osborn, E.F. 1959. Role of oxygen pressure in the crystallization and differentiation of basaltic magma. *Am. J. Sci.*, 257, 609-647.
- Osborn, E.F. 1978. Change in phase relations in response to change in pressure from 1 atm to 10 kbar for the system Mg_2SiO_4 -iron oxide-CaAl₂Si₂O₇-SiO₂. *Carnegie Inst. Washington Year Book*, 77, 784-790.
- Oshima, T., T. Hashimoto, H. Komono, S. Kawabe, K. Suga, S. Tanimura, and Y. Ishikawa 1974. Geology of the Kosaka mine. *Soc. Mining Geol. Japan Spec. Issue* 6, 183-189.
- Oshin, I.O., and J.H. Crockett 1982. Noble metals in the Thetford mines ophiolite, Quebec, Canada. Part I. Distribution of gold, iridium, platinum and palladium in the ultramafic and gabbroic rocks. *Econ. Geol.*, 77, 1556-1570.
- Oszczepalski, S. 1989. Kupferschiefer in southwestern Poland: sedimentary environments, metal zoning, and ore controls. *Geol. Assoc. Canada Spec. Paper* 36, 571-600.
- Oudin, E., and G. Constantinou 1984. Black smoker chimney fragments in Cyprus sulphide deposits. *Nature*, 308, 349-352.
- Page, N.J., and R.W. Talkington 1984. Palladium, platinum, rhodium, ruthenium, and iridium in peridotites and chromites from ophiolite complexes in Newfoundland. *Can. Mineral.*, 22, 137-149.
- Page, N. J., and Zientek, M.L. 1985. Geologic and structural setting of the Stillwater Complex. *Montana Bur Mines and Geology Spec. Publ.* 92, 1-8.
- Page, N.J., P.K. Banerjee, and J. Haffty 1985. Characterization of the Sukinda and Nausahi ultramafic complexes, Orissa, India by platinum-group element geochemistry. *Precamb. Res.*, 30, 27-41.
- Page, N.J., J.J. Rowe, and J. Haffty 1976. Platinum metals in the Stillwater Complex, Montana. *Econ. Geol.*, 71, 1352-1363.
- Page, N.J., J.S. Pallister, M.A. Brown, J.D. Smewing, and J. Haffty 1982. Palladium, platinum, rhodium, iridium and ruthenium in chromite-rich rocks from the Samail ophiolite, Oman. *Can. Mineral.*, 20, 537-548.
- Page, R.W., and I. McDougall 1972. Geochronology of the Panguna porphyry copper deposit, Bougainville Island, New Guinea. *Econ. Geol.*, 67, 1049-1064.
- Pagel, M. 1977. Microthermometry and chemical analysis of fluid inclusions from the Rabbit Lake uranium deposit, Saskatchewan, Canada [abs.]. *J. Geol. Soc. London*, 134, 392.

- Pagel, M., B. Poty, and S. M. F. Sheppard 1980. Contribution to some Saskatchewan uranium deposits mainly from fluid inclusion and isotopic data. In *Uranium in the Pine Creek geosyncline*, 639-654. Vienna: International Atomic Energy Agency.
- Page, R.W., and I.P. Sweet 1998. Geochronology of basin phases in the western Mt. Isa Inlier, and correlation with the McArthur basin. *Austral. J. Earth Sci.*, 45, 219-232.
- Paktunc, A.D. 1984. Petrogenesis of ultramafic and mafic rocks of the Thompson nickel belt, Manitoba. *Contrib. Mineral. Petrol.*, 88, 348-353.
- Palabora Geological and Mineralogical Staff 1976. The geology and economic deposits of copper, iron, and vermiculite in the Palabora Complex: a brief review. *Econ. Geol.*, 71, 177-192.
- Pan, H., D.T.A. Symons, and D.F. Sangster 1990. Paleomagnetism of the Mississippi Valley-type ores and host rocks in northern Arkansas and Tri-State districts. *Can. J. Earth Sci.*, 27, 923-931.
- Pan, H., D.T.A. Symons, and D.F. Sangster 1993. Paleomagnetism of the Gays River zinc-lead deposit, Nova Scotia: Pennsylvanian ore genesis. *Geophys. Res. Lett.*, 20, 1159-1162.
- Pan, P. and S.A. Wood 1994. Solubility of Pt and Pd sulfides and Au metal in aqueous bisulfide solutions. II. Results at 200° to 350°C and saturated vapor pressure. *Mineral. Deposita*, 29, 373-390.
- Pan, Y., and M.E. Fleet 1995. The late Archean Hemlo gold deposit, Ontario, Canada: a review and synthesis. *Ore Geol. Rev.*, 9, 455-488.
- Panigrahi, M.K., and A. Mookherjee 1997. The Malanjikhand copper (+molybdenum) deposit: mineralization from a low-temperature ore fluid of granitoid affiliation. *Mineral. Deposita*, 32, 133-148.
- Panno, S.V., and D.M. Moore 1994. Mineralogy of the clay-sized fraction of the Davis Shale, Southeast Missouri: alteration associated with a Mississippi Valley-type ore deposit. *Econ. Geol.*, 89, 333-340.
- Panno, S.V., G. Harbottle, and E.V. Sayre 1983. Genetic implications of halide enrichment near a Mississippi Valley-type ore deposit. *Econ. Geol.*, 78, 150-156.
- Panteleyev, A. 1986. Ore deposits #10. A Canadian Cordilleran model for epithermal gold-silver deposits. *Geoscience Canada*, 13, 101-111.
- Papike, J.J., T.E.C. Keith, M.N. Spilde, K.C. Galbroth, C.K. Shearer, and J.C. Laul 1991. Geochemistry and mineralogy of furarolic deposits, Valley of Ten Thousand Smokes, Alaska: bulk chemical and mineralogical evolution of dacite-rich protolith. *Am. Mineral.*, 76, 1662-1673.
- Pardee, J.T., and C.F. Park, Jr. 1948. Gold deposits of the southern Piedmont. *U.S. Geol. Survey Prof. Paper* 213.
- Park, C.F., Jr. 1955. The zonal theory of ore deposits. *Econ. Geol. 50th Anniv. Vol.*, 226-248.
- Park, J.F. 1983. Paleomagnetism for geologists. *Geoscience Canada*, 10, 180-187.
- Parks, G.A., and D.C. Pohl 1988. Hydrothermal solubility of uraninite. *Geochim. Cosmochim. Acta*, 52, 863-875.
- Parmentier, M. and E.T.C. Spooner 1978. A theoretical study of hydrothermal convection and the origin of the ophiolite sulfide ore deposits of Cyprus. *Earth Planet. Sci. Lett.*, 40, 33-44.
- Parr, J.M., and I.R. Plimer 1993. Models of Broken Hill-type lead-zinc-silver deposits. *Geol. Assoc. Canada Spec. Paper* 40, 253-288.
- Parry, W.T. 1986. Estimation of X_{CO_2} , P, and fluid inclusion volume from fluid inclusion temperature measurements in the system NaCl-CO₂-H₂O. *Econ. Geol.*, 81, 1009-1013.
- Parry, W.T., and D.C. Jacobs 1975. Fluorine and chlorine in biotite from Basin and Range plutons. *Econ. Geol.*, 70, 554-558.
- Parry, W.T., and M.P. Nackowski 1963. Copper, lead, and zinc in biotites from Basin and Range plutons. *Econ. Geol.*, 58, 1126-1144.
- Pasteris, J.D. 1983. Spinel zonation in the De Beers kimberlite, South Africa: possible role of phlogopite. *Can. Mineral.*, 21, 41-58.
- Pasteris, J.D., C.A. Kuehn, and R.J. Bodnar 1986. Applications of the Laser Raman microprobe RAMAROM U-1000 to hydrothermal ore deposits: Carlin as an example. *Econ. Geol.*, 81, 915 - 930.
- Paterson, H.L., M.J. Donaldson, R.N. Smith, M.F. Lenard, J.J. Gresham, D.J. Boyack, and R.R. Keays 1984. Nickeliferous sediments and sediment-associated nickel ores at Kambalda, Western Australia. In *Sulfide deposits in mafic and ultramafic rocks*, D.L. Buchanan and M.J. Jones (eds.), 81-94. London: Inst. Mining & Metall.
- Patterson, D.J., H. Ohmoto, and M. Solomon 1981. Geological setting and genesis of casiterite-sulfide ore deposits at Renison Bell, western Tasmania. *Econ. Geol.*, 76, 393-438.
- Patwardhan, A.M., and S.S. Oka 1984. Syngensis and epigenesis in strata-bound metamorphosed Precambrian sulfide deposits of India. In *Syngensis and epigenesis in the formation of mineral deposits*, A. Wauschkuhn, C. Luth, and R.A. Zimmermann (eds.), 102-119. Berlin: Springer-Verlag.
- Peach, C.L., and E.A. Mathez 1993. Sulfide melt-silicate melt distribution coefficients for nickel and iron and implications for the fractionation of other chalcophile elements. *Geochim. Cosmochim. Acta*, 57, 3013-3021.
- Peach, C.L., and E.A. Mathez 1996. Constraints on the formation of platinum-group element deposits in igneous rocks. *Econ. Geol.*, 91, 439-450.

- Peach, C.L., E.A. Mathez, and R.R. Keays 1990. Sulfide melt-silicate melt distribution coefficients for noble metals and other chalcophile elements as deduced from MORB: implications for partial melting. *Geochim. Cosmochim. Acta*, 54, 3379-3389.
- Peach, C.L., E.A. Mathez, R.R. Keays, and S.J. Reeves 1994. Experimentally determined sulfide melt-silicate melt partition coefficients for iridium and palladium. *Chem. Geol.*, 117, 361-377.
- Pearce, J.A. 1975. Basalt geochemistry used to investigate past tectonic environments on Cyprus. *Tectonophysics*, 25, 41-67.
- Pearce, J.R. 1980. Geochemical evidence for the genesis and eruptive setting of lavas from Tethyan ophiolites. In *International Ophiolite Symp. Proc.*, A. Panayiotou (ed.), 261-272. Nicosia: Cyprus Geol. Survey.
- Pearce, J.A., and J.R. Cann 1973. Tectonic setting of basic volcanic rocks determined using trace element analysis. *Earth Planet. Sci. Lett.*, 19, 290-300.
- Pearce, J.A., and G.H. Gale 1977. Identification of ore deposition environment from trace-element geochemistry of associated igneous rocks. In *Volcanic Processes in ore genesis*, *Geol. Soc. London Spec. Publ.* 7, 14-24. London: Inst. Mining Metall. and Geol. Soc. London.
- Pearce, J.A., S.J. Lippard, and S. Roberts 1984. Characteristics and tectonic significance of supra-subduction zone ophiolites. In *Marginal basin geology*, B. P. Kokelaar and M. F. Howells (eds.), *Geol. Soc. London Spec. Publ.* 16, 77-16.
- Peck, D.C., and R.R. Keays 1990. Insights into the behavior of precious metals in primitive, S-undersaturated magmas: evidence from the Hazlewood River Complex, Tasmania. *Can. Mineral.*, 28, 553-577.
- Pedersen, A. K. 1979. Basaltic glass with high-temperature equilibrated immiscible sulphide bodies with native iron from Disko, central west Greenland. *Contrib. Mineral. Petrol.*, 69, 397-407.
- Pedersen, F.D. 1980. Remobilization of the massive sulphide ore of the Black Angel mine, Central West Greenland. *Econ. Geol.*, 75, 1022-1041.
- Pedersen, R., G.M. Johannesen, and R. Boyd 1993. Stratiform platinum-group element mineralizations in the ultramafic cumulates of the Leka ophiolite complex, central Norway. *Econ. Geol.*, 88, 782-803.
- Peredery, W.V. 1979. Relationship of ultramafic amphibolites to metavolcanic rocks and serpentinites in the Thompson Belt, Manitoba. *Can. Mineral.*, 17, 187-200.
- Peredery, W.V. 1984. Geology and nickel sulfide deposits of the Thompson belt, Manitoba. *Geol. Assoc. Canada Spec. Paper* 25, 761-791.
- Peredery, W.V., and Geological Staff 1982. Geology and nickel sulfide deposits of the Thompson Belt, Manitoba. *Geol. Assoc. Canada Spec. Paper* 25, 165-209.
- Perkins, W.G. 1984. Mount Isa silica dolomite and copper orebodies: the result of a syntectonic hydrothermal alteration system. *Econ. Geol.*, 79, 601-637.
- Perkins, W.G. 1997. Mount Isa lead-zinc orebodies: replacement lodes in a zoned syndeformational copper-lead-zinc system? *Ore Geol. Rev.*, 12, 61-110.
- Perkins, W.G. 1998. Timing of Proterozoic stratiform fine-grained pyrite: post-diagenetic cleavage replacement at Mount Isa? *Econ. Geol.*, 93, 1153-1164.
- Perkins, W.G., and T.H. Bell 1998. Stratiform replacement lead-zinc deposits: a comparison between Mount Isa, Hilton, and McArthur River. *Econ. Geol.*, 93, 1190-1212.
- Perry, D.V. 1969. Skarn genesis at the Christmas mine, Gila County, Arizona. *Econ. Geol.*, 64, 255-270.
- Perry, E.C., Jr., J. Monster, and T. Reimer 1971. Sulfur isotopes in Swaziland system barites and the evolution of the Earth's atmosphere. *Science*, 171, 1015-1016.
- Perry, E.G. 1967. The oxygen isotope chemistry of ancient cherts. *Earth Planet. Sci. Lett.*, 3, 62-66.
- Person, M., and G. Garven 1994. A sensitivity study of the driving forces on fluid flow during continental-rift basin evolution. *Geol. Soc. Am. Bull.*, 106, 461-475.
- Petruk, W. 1971. Mineralogical characteristics of the deposits and textures of the ore minerals. In *The silver-arsenide deposits of the Cobalt-Gowganda region, Ontario*, L.G. Berry (ed.), *Can. Mineral.*, 11, Pt. 1, 108-189.
- Peyerl, W. 1982. The influence of the Dreikop dunite pipe on the platinum-group mineralogy of the UG-2 chromitite in its vicinity. *Econ. Geol.*, 77, 1432-1438.
- Phillips, G.N. 1985. Geology and alteration in the Golden Mile, Kalgoorlie. *Econ. Geol.*, 89, 779-808.
- Phillips, G.N. 1987. Metamorphism of the Witwatersrand gold fields: conditions during peak metamorphism. *J. Meta. Geol.*, 5, 307-322.
- Phillips, G.N. 1988. Widespread fluid infiltration during metamorphism of the Witwatersrand goldfields: generation of chloritoid and pyrophyllite. *J. Meta. Geol.*, 6, 311-332.
- Phillips, G.N., and D.I. Groves. 1984. Fluid access and fluid-wall rock interaction in the genesis of the Archean gold-quartz vein deposit at Hunt mine, Kambalda, Western Australia. In *Gold '82: the Geology, geochemistry, and genesis of gold deposits*, R.P. Foster (ed.), 389-416. Rotterdam: Balkema.
- Phillips, G.N., and J.D.M. Law 1997. Hydrothermal origin for Witwatersrand gold. *Soc. Econ. Geol. Newsletter*, no. 31, 26-33.
- Phillips, G.N., and R.E. Myers 1989. The Witwatersrand gold fields: Part II. An origin for Witwatersrand gold during metamorphism and associated alteration. *Econ. Geol. Mono.* 6, 598-608.

- Phillips, G.N., D.I. Groves, and J.E. Martyn 1984. An epigenetic origin for Archean banded iron formation-hosted gold deposits. *Econ. Geol.*, 79, 162-171.
- Phillips, G.N., R.E. Myers, and J.A. Palmer 1987. Problems with the placer model for Witwatersrand gold. *Geology*, 15, 1027-1030.
- Phillips, G.N., D.I. Groves, S.E. Ho, and F.B. Neal 1986a. A metamorphic-replacement model for genesis of Archean gold deposits. *International Conference on the Metallogeny of the Precambrian (IGCP Project 91)*, 125-132. Prague: Geological Survey (UUG).
- Phillips, G.N., D.I. Groves, F.B. Neall, T.H. Donnelly, and I.B. Lambert 1986b. Anomalous sulfur isotopic compositions in the Golden Mile, Kalgoorlie. *Econ. Geol.*, 81, 2008-2015.
- Phillips, G.N., R.E. Myers, J.D.M. Law, A.C. Bailey, A.B. Cadle, S.D. Bencke, and L. Giusti 1989. The Witwatersrand gold fields: Part I. Post depositional history, synsedimentary processes, and gold distribution. *Econ. Geol. Mono.* 6, 585-597.
- Phillips, W.J. 1973. Mechanical effects of retrograde boiling and its probable importance in the formation of some porphyry ore deposits. *Inst. Mining. Metall. Trans.*, Sec. B, 82, B90-B98.
- Pinckney, D.M., and J. Haffty 1970. Content of zinc and copper in some fluid inclusions from the Cave-in-Rock district, southern Illinois. *Econ. Geol.*, 65, 451-458.
- Pinckney, D.M., and R.O. Rye 1972. Variation of O^{18}/O^{16} , C^{13}/C^{12} , textures, and mineralogy in altered limestones in the Hill mine, Cave-in-Rock district, Illinois. *Econ. Geol.*, 67, 1-18.
- Pine, R.J., and A.S. Batchelor 1984. Downward migration of shearing in jointed rock during hydraulic injections. *International J. Rock Mech. Min. Sci.*, 21, 249-263.
- Pingitore, N.E., Jr., 1978. The behavior of Zn^{2+} and Mn^{2+} during carbonate diagenesis: theory and application. *J. Sed. Petrol.*, 48, 799 - 814.
- Pisutha-Armond, V., and H. Ohmoto 1983. Thermal history, and chemical and isotopic compositions of ore-forming fluids responsible for the Kuroko massive sulfide deposits in the Hokuroku district of Japan. *Econ. Geol. Mono.* 5, 523-558.
- Plant, J.A. 1986. Models for granites and their mineralizing systems in British and Irish Caledonides. In *Geology and genesis of mineral deposits in Ireland*, C.J. Andrew, R.W.A. Crowe, S. Finlay, W.M. Pennell, and J.F. Pyne (eds.), 121-156. Dublin: Irish Assoc. Econ. Geol.
- Plimer, I.R. 1977. The mineralogy of the high grade metamorphic rocks enclosing the Broken Hill orebodies, Australia. *N. Jb Miner. Abh.*, 131, 115-139.
- Plimer, I.R. 1978. Proximal and distal stratabound ore deposits. *Mineral. Deposita*, 13, 345-353.
- Plimer, I.R. 1979. Sulphide rock zonation and hydrothermal alteration at Broken Hill, Australia. *Inst. Mining. Metall. Trans.*, 88, B161-B176.
- Plimer, I.R. 1987. Remobilization in high-grade metamorphic environments. *Ore Geol. Rev.*, 2, 231-245.
- Plimer, I.R., and T. Finlow-Bates 1978. Relationship between primary iron sulphide species, sulphur source, depth of formation and age of submarine exhalative deposits. *Mineral. Deposita*, 13, 399-410.
- Plumlee, G.S. 1994. Fluid chemistry evolution and mineral deposition in the main-stage Creede epithermal system. *Econ. Geol.*, 89, 1860-1882.
- Plumlee, G.S., and M.B. Goldhaber 1992. The possible role of magmatic gases in the genesis of Illinois-Kentucky fluorspar deposits: implications from chemical reaction path modeling. *U.S. Geol. Survey Open-File Rept.* 92-1, 47-49.
- Plumlee, G.S., and R.O. Rye 1992. Mineralogic, isotopic, and other characteristics of the fringes of diverse hydrothermal systems: the perithermal environment [abs.]. *Programs and Abstracts, V.M. Goldschmidt Conference, Reston, Virginia*, A84-A85.
- Plumlee, G.S., P. Heald, and P.H. Whitehouse-Veaux 1994. Mineralogy, paragenesis, and mineral zoning of the Bulldog Mountain Vein system, Creede district, Colorado. *Econ. Geol.*, 89, 1883-1905.
- Poddar, B.C. 1965. Lead-zinc mineralization in the Zawar belt, India. *Econ. Geol.*, 65, 636-638.
- Pottorf, R.J. and H.L. Barnes 1983. Mineralogy, geochemistry, and ore genesis of hydrothermal sediments from the Atlantis II Deep, Red Sea. *Econ. Geol. Mono.* 5, 198-223.
- Poty, B., and M. Pagel 1988. Fluid inclusions related to uranium deposits: a review. *J. Geol. Soc. London*, 145, 157-162.
- Poujol, M., L.J. Robb, J-P. Respaut, and C.R. Anhaeusser 1996. 3.07-2.97 Ga greenstone belt formation in the northeastern Kaapvaal craton: implications for the origin of the Witwatersrand Basin. *Econ. Geol.*, 91, 1455-1461.
- Poulsen, K.H., K.D. Card, and J.M. Franklin 1992. Archean tectonic and metallogenic evolution of the Superior Province of the Canadian Shield. *Precamb. Res.*, 58, 25-54.
- Powell, T.G., and R.W. Macqueen 1984. Precipitation of sulfide ores and organic matter: sulfate reaction at Pine Point, Canada. *Science*, 224, 63-66.
- Poyla, A. 1989. Chemistry of the main-stage ore-forming fluids of the Panasqueira W-Cu (Ag)-Sn deposit, Portugal: implications of ore genesis. *Econ. Geol.*, 84, 1134-1152.
- Prasad, C.V.R.K., N. Subba Reddy, and B.F. Wendley 1982. Iron-formations in Archean granulite gneiss belts with special reference to Southern India. *J. Geol. Soc. India*, 15, 112-122.

- Preece, R.K., III and R.E. Beane 1982. Contrasting evolution of hydrothermal alteration in quartz monzonite and quartz diorite wallrocks at the Serrita porphyry copper deposit, Arizona. *Econ. Geol.*, 77, 1621-1641.
- Prendergast, M.D. 1984. Chromium deposits of Zimbabwe. *Chromium Rev.*, 2, 5-9.
- Prendergast, M.D. 1987. The chromite ore field of the Great Dyke, Zimbabwe. In *Evolution of chromium ore fields*, C.W. Stowe (ed.), 89-108. New York: Van Nostrand.
- Prendergast, M.D. 1998 (ed.) *Guidebook for pre-symposium excursion to the Great Dyke of Zimbabwe, June 23-28, 1998*, 8th International Platinum Symposium, June 29-July 3, Rustenburg, South Africa. Harare: Geological Soc. Zimbabwe.
- Pretorius, D.A. 1976a. Gold in the proterozoic sediments of South Africa: systems, paradigms, and models. In *Handbook of strata-bound and stratiform ore deposits*, K.H. Wolf (ed.), 7, 1-27. Amsterdam: Elsevier.
- Pretorius, D.A. 1976b. The nature of the Witwatersrand gold-uranium deposits. In *Handbook of strata-bound and stratiform ore deposits*, K.H. Wolf (ed.), 7, 29-88. Amsterdam: Elsevier.
- Pretorius, D.A. 1981. Gold and uranium in quartz-pebble conglomerates. *Econ. Geol. 75th Anniv. Volume*, 117-138.
- Pretorius, D.A., and S. Maske 1976. An issue devoted to mineral deposits in southern Africa: Preface. *Econ. Geol.*, 71, 1-4.
- Price, B.J. 1972. *Minor elements in pyrites from the Sixthers Map area, B.C. and exploration application of minor element studies*. Unpublished M.S. thesis, Univ. of British Columbia, Vancouver, Canada.
- Proudlove, D.C., R.W. Hutchinson, and D.S. Rogers 1989. Multiphase mineralization in concordant and discordant gold veins, Dome mine, South Porcupine, Ontario, Canada. *Econ. Geol. Mono.* 6, 112-123.
- Putman, G.W., and C.W. Burnham 1963. Trace elements in igneous rocks, northwestern and central Arizona. *Geochim. Cosmochim. Acta*, 27, p. 53-106.
- Pye, E.G., A.J. Naldrett, and P.E. Giblin (eds.) 1984. *The Geology and ore deposits of the Sudbury Structure, Ont. Geol. Surv. Spec. Vol. 1*, 533-569. Toronto: Ontario Geol. Survey. Toronto: Ontario Geol. Survey.
- Quade, H. 1976. Genetic problems and environmental features of volcano-sedimentary iron-ore deposits of the Lahn-Dill type. In *Handbook of strata-bound and stratiform ore deposits*, K.H. Wolf (ed.), 7, 255-294. Amsterdam: Elsevier.
- Rackley, R.I. 1972. Environment of Wyoming Tertiary uranium deposits. *Am. Assoc. Petroleum Geol. Bull.*, 56, 755-774.
- Radhakrishnan, B.P., T.C. Devaraju, and B. Mahabaleswar 1986. Banded iron-formation of India. *J. Geol. Soc. India*, 28, 71-91.
- Radtke, A.S. 1985. Geology of the Carlin gold deposit. *U.S. Geol. Survey Prof. Paper* 1267, 124p.
- Radtke, A.S., and F.W. Dickson 1976. Genesis and vertical position of fine-grained disseminated replacement-type gold deposits in Nevada and Utah, U.S.A. In *Problems of Ore Deposition, Proc. 4th Quad. IAGOD Symp., Varna, Bulgaria, 1974*, 1, 71-78. Sofia: Bulgarian Acad. Sciences.
- Radtke, A.S., R.O. Rye, and F.W. Dickson 1980. Geology and stable isotope studies of the Carlin gold deposit, Nevada. *Econ. Geol.*, 75, 641-662.
- Raedeke, L.D. 1981. Mineralogy and petrology of layered intrusions: a review. In *Magmatic processes of early planetary crusts: magma oceans and stratiform layered intrusions*, LPI Tech. Rept. 82-01, 128-134.
- Raedeke, L.D., and R.W. Vian 1986. A three-dimensional view of mineralization in the Stillwater J-M Reef. *Econ. Geol.*, 81, 1186-1195.
- Rajamani, V. and A.J. Naldrett 1978. Partitioning of Fe, Co, Ni, and Cu between sulfide liquid and basaltic melts and the composition of Ni-Cu sulfide deposits. *Econ. Geol.*, 73, 82-93.
- Ramdohr, P. 1953. Mineralbestand, Strukturen und Genese der Rammelsberg lagerstätte. *Geol. Jahrb.*, 67, 367-494.
- Ramdohr, P. 1967. A widespread mineral association connected with serpentinization. *N. Jahrb. Mineral. Abh.*, 107, 241-265.
- Ramdohr, P. 1980. *The ore minerals and their intergrowths*, 2nd. edn. (two volumes). Oxford: Pergamon Press.
- Randell, R.N., and G.M. Anderson 1997. Geology of the Polaris Zn-Pb deposit and surrounding area, Canadian Arctic Archipelago. *Soc. Econ. Geol. Spec. Publ.* 4, 307-319.
- Ransom, P.W. 1977. Geology of the Sullivan orebody. In *Lead-zinc deposits of southeastern British Columbia, Field Trip no. #1*, Geol. Assoc. Canada, Vancouver Annual Meeting, 7-21.
- Ravenhurst, C.E., P.H. Reynolds, and M. Zentilli 1987. Isotopic constraints on the genesis of Zn-Pb mineralization at Gays River, Nova Scotia, Canada. *Econ. Geol.*, 82, 1294-1308.
- Ray, G.E., and I.C.L. Webster 1991. An overview of skarn deposits. *British Columbia Ministry of Mines and Petroleum Resources Paper* 1991-4, 213-252.
- Reed, M.H. 1982. Calculation of multicomponent equilibria and reaction processes involving minerals, gases, and an aqueous phase. *Geochim. Cosmochim. Acta*, 46, 513-528.

- Reed, M.H. 1983. Seawater-basalt reaction and the origin of greenstones and related ore deposits. *Econ. Geol.*, 78, 466-485.
- Reed, M.H. 1997. Hydrothermal alteration and its relationship to ore fluid composition. In *Geochemistry of hydrothermal ore deposits*, 3rd edn., H.L. Barnes (ed.), 303-366. New York: Wiley.
- Reed, M.H. and N. Spycher 1984. Calculation of pH and mineral equilibria in hydrothermal waters with application to geothermometry and studies of boiling and dilution. *Geochim. Cosmochim. Acta*, 48, 1479-1492.
- Rees, C.E. 1973. A steady-state model for sulfur isotope fractionation in bacterial reduction process. *Geochim. Cosmochim. Acta*, 37, 1141-1162.
- Reesman, R.H. 1968. Strontium isotopic compositions of gangue minerals from hydrothermal vein deposits. *Econ. Geol.*, 63, 731-736.
- Reeve, J.S., K.C. Cross, R.N. Smith, and N. Oreskes 1991. Olympic Dam copper-uranium-gold-silver deposit. In *The Geology of the mineral deposits of Australia and Papua New Guinea*, 2, 1009-1035. Melbourne: Australia Inst. Mining Metall.
- Reimer, T.O. 1979. Platinoids in auriferous Proterozoic conglomerates of South Africa: evaluation of existing data. *N. Jahrb. Mineral. Abh.*, 135, 287-314.
- Reimer, T.O. 1984. Alternative model for the derivation of gold in the Witwatersrand Supergroup. *J. Geol. Soc. London*, 141, 263-272.
- Reimer, T.O. 1987. Weathering as a source of iron in iron-formations: the significance of alumina-enriched paleosols from the Proterozoic of southern Africa. In *Precambrian iron-formations*, P.W.U. Appel and G.L. LaBerge (eds.), 601-619. Athens: Theophrastus Publ.
- Reimer, T.O., and D.J. Mossman 1990a. Sulfidization of Witwatersrand black sands: from enigma to myth. *Geology*, 18, 426-429.
- Reimer, T.O., and D. J. Mossman 1990b. The Witwatersrand controversy revisited. *Econ. Geol.*, 85, 337-343.
- Renfro, A.R. 1974. Genesis of evaporite-associated stratiform metalliferous deposits — a sabkha process. *Econ. Geol.*, 69, 33-45.
- Rentzsch, J. 1974. The 'Kupferschiefer' in comparison with the deposits of the Zambian copper belt. In *Gisements stratiformes et province cuprifères*, P. Bartholemé (ed.), 403-426. Lige, Belgium: Societ Geologique de Belgique.
- Reynolds, I.M. 1985. The nature and origin of titaniferous magnetite-rich layers in the Upper Zone of the Bushveld Complex: a review and synthesis. *Econ. Geol.*, 80, 1089-1108.
- Reynolds, T.J., and R.E. Beane 1985. Evolution of hydrothermal fluid characteristics at the Santa Rita, New Mexico, porphyry copper deposit. *Econ. Geol.*, 80, 1328-1347.
- Rhodes, D. 1991. Pine Point North Trend tabular orebodies. *Irish Assoc. for Econ. Geol. Annual Rev.* 1990, 26-27.
- Rhodes, D., E.A. Lantos, J.A. Lantos, R.J. Webb, and D.C. Owens 1984. Pine Point orebodies and their relationship to the stratigraphy, structure, dolomitization, and karstification of the Middle Devonian barrier complex. *Econ. Geol.*, 79, 991-1055.
- Rhodes, R.C. 1975. New evidence for impact origin of the Bushveld Complex. *Geology*, 3, 549-554.
- Ribbe, P.H. (ed.) 1974. *Mineral. Soc. Am. short course notes: sulfide mineralogy*. Washington: Mineral. Soc. Am.
- Rich, R.A., H.D. Holland, and U. Petersen 1977. *Hydrothermal uranium deposits*. New York: Elsevier.
- Richards, J.P., T.E. Krogh, and E.T.C. Spooner 1988a. Fluid inclusion characteristics and U-Pb rutile age of late hydrothermal alteration and veining at the Musoshi stratiform copper deposit, Central African Copper Belt, Zaire. *Econ. Geol.*, 83, 118-139.
- Richards, J.P., G.L. Cumming, D. Krstic, P.A. Wagner, and E.T.C. Spooner 1988b. Pb isotope constraints on the age of sulfide ore deposition and U-Pb age of late uraninite veining at Musoshi stratiform copper deposit, Central African Copper Belt, Zaire. *Econ. Geol.*, 83, 724-741.
- Richards, J.R. 1971. Major lead orebodies — mantle origin? *Econ. Geol.*, 66, 425-434.
- Richards, S.M. 1966. Mineralogy of fault-zone sulfides, Broken Hill, N.S.W. *C. S. I. R. O. Mineral. Invest. Tech. Paper* 5, 24p.
- Richardson, C.K., and D.M. Pinckney 1984. The chemical and thermal evolution of the fluids in the Cave-in-Rock fluorospar district, Illinois: mineralogy, paragenesis, and fluid inclusions. *Econ. Geol.*, 79, 1833-1856.
- Richardson, C.K., R.O. Rye, and M.D. Wasserman 1988. The chemical and thermal evolution of the fluids in the Cave-in-Rock fluorospar district, Illinois: stable isotope systematics at the Deardorff mine. *Econ. Geol.*, 83, 765-783.
- Richardson, S.H., J.J. Gurney, A.J. Erlank, and J.W. Harris 1984. Origin of diamonds in old enriched mantle. *Nature*, 310, 198-202.
- Rickard, D.T. 1983. Precipitation and mixing mechanisms in Laisvall-type sandstone lead-zinc deposits. In *International Conference on Mississippi Valley-type lead-zinc deposits — Proc. Vol.*, G. Kisvarsanyi, S.K. Grant, W.P. Pratt, and J.W. Koenig (eds.), 449-458. Rolla, Missouri: Univ. Missouri-Rolla Press.
- Riggs, S.R. 1979a. Petrology of the Tertiary phosphorite system of Florida. *Econ. Geol.*, 74, 195-220.

- Riggs, S.R. 1979b. Phosphorite sedimentation in Florida — a model phosphogenic system. *Econ. Geol.*, 74, 285-314.
- Riley, J.F. 1974. The tetrahedrite-freibergite series, with reference to the Mount Isa Pb-Zn-Ag orebody. *Mineral. Deposita*, 9, 117-124.
- Ringler, R.W. 1979. Sphalerite geobarometry at the Calloway mine, Ducktown, Tennessee. *Econ. Geol.*, 74, 937-942.
- Ringwood, A.E., and T. Irifune 1988. Nature of the 650-km seismic discontinuity: implications for mantle dynamics and differentiation. *Nature*, 331, 131-136.
- Ripley, E.M. 1986a. Application of stable isotopic studies to problems of magmatic sulfide ore genesis with special reference to the Duluth Complex, Minnesota. In *Geology and metallogeny of copper deposits*, G.H. Friedrich, A.D. Genkin, A.J. Naldrett, J.D. Ridge, R.H. Sillitoe, and F.M. Vokes (eds.), 25-42. Berlin: Springer-Verlag.
- Ripley, E.M. 1986b. Origin and concentration mechanisms of copper and nickel in the Duluth Complex — a dilemma. *Econ. Geol.*, 81, 974-978.
- Ripley, E.M., and J.A. Alawi 1988. Petrogenesis of pelitic xenoliths at the Babbitt Cu-Ni deposit, Duluth Complex, Minnesota, U.S.A.. *Lithos*, 21, 143-159.
- Ripley, E.M., and T.J. Al-Jassar 1987. Sulfur and oxygen isotope studies of melt-country rock interaction, Babbitt Cu-Ni deposit, Duluth Complex, Minnesota, U.S.A.. *Econ. Geol.*, 82, 87-107.
- Ripley, E.M., and H. Ohmoto 1977. Mineralogic, sulfur isotope, and fluid inclusion studies of the stratabound copper deposits at the Raul mine, Peru. *Econ. Geol.*, 72, 1017-1041.
- Ripley, E.M., M.W. Lambert, and P. Berendsen 1980. Mineralogy and paragenesis of red-bed copper mineralization in the Lower Permian of South Central Texas. *Econ. Geol.*, 75, 722-729.
- Ripley, E., E. Merino, C. Moore, and P. Ortoleva 1985. Mineral zoning in sediment-hosted copper deposits. In *Handbook of strata-bound and stratiform ore deposits*, K.H. Wolf (ed.), 6, 237-260. Amsterdam: Elsevier.
- Rittenhouse, G. 1967. Bromine in oil field waters and its use in determining possibilities of origin of these waters. *Am. Assoc. Petrol. Geol. Bull.*, 51, 2430-2440.
- Riverin, G., and C. J. Hodgson 1980. Wall-rock alteration at the Millenbach Cu-Zn mine, Noranda, Quebec. *Econ. Geol.*, 75, 424-444.
- Robb, L.J., and F.M. Meyer 1990. The nature of the Witwatersrand hinterland: conjectures on the source area problem. *Econ. Geol.*, 85, 511-536.
- Robb, L.J., and F.M. Meyer 1995. The Witwatersrand Basin, South Africa: geological framework and mineralization process. *Ore Geol. Rev.*, 10, 67-94.
- Robbins, E.I., G.L. La Berge, and R.G. Schmidt 1987. A model for the biological precipitation of Precambrian iron formations — B. Morphological evidence and modern analogs. In *Precambrian iron-formations*, P.W.U. Appel and G.L. LaBerge (eds.), 97-139. Athens: Theophrastus Publ.
- Robert, F., and W.C. Kelly 1987. Ore-forming fluids in Archean gold-bearing quartz veins at the Sigma Mine, Abitibi greenstone belt, Quebec, Canada. *Econ. Geol.*, 82, 1464-1482.
- Roberts, D., T. Grenne, and P.D. Ryan 1984. Ordovician marginal basin development in the central Norwegian Caledonides. *Geol. Soc. London Spec. Pub.* 16, 232-244.
- Roberts, R.G. 1975. The geological salting of the Mattagami Lake Mine, Quebec: a volcanogenic massive sulfide deposit. *Econ. Geol.*, 70, 115-129.
- Roberts, R.G. 1987. Ore deposit models #11. Archean lode gold deposits. *Geoscience Canada*, 14, 37-52.
- Roberts, R.G., and E.J. Reardon 1978. Alteration and ore-forming processes at Mattagami Lake mine, Quebec. *Can. J. Earth Sci.*, 15, 1-21.
- Roberts, R.J. 1960. Alignment of mining districts in north-central Nevada. *U.S. Geol. Survey Prof. Paper* 400-B, B17-B19.
- Robertson, D.S. 1974. Basal Proterozoic units as fossil time markers, and their use in uranium prospecting. In *Formation of uranium ore deposits*, 495-512. Vienna: International Atomic Energy Agency.
- Robertson, D.S., J.E. Tilsley, and G.M. Hogg 1978. The time-bound character of uranium deposits. *Econ. Geol.*, 73, 1409-1419.
- Robie, R.A. and D.R. Waldbaum 1968. Thermodynamic properties of minerals and related substances at 298.15°K (25°C) and one atmosphere (1.013 bars) and at higher temperatures. *U.S. Geol. Survey Bull.* 1259.
- Robie, R.A., B.S. Hemingway and J.R. Fisher 1978. Thermodynamic properties of minerals and related substances at 298.15 K and 1 bar (10⁵ Pascals) pressure and at high temperatures. *U.S. Geol. Survey Bull.* 1452.
- Robinson, B.W., and H. Ohmoto 1973. Mineralogy, fluid inclusions, and stable isotopes of the Echo Bay U-Ni-Ag-Cu deposits, Northwest Territories, Canada. *Econ. Geol.*, 68, 635-656.
- Robinson, A., and E.T.C. Spooner 1982. The source of the detrital components of uraniferous conglomerates, Quirke Ore Zone, Elliot Lake, Ontario. *Nature*, 299, 622-624.
- Robinson, A., and E.T.C. Spooner 1984a. Postdepositional modification of uraninite-bearing quartz-pebble conglomerates from the Quirke ore zone, Elliot Lake, Ontario. *Econ. Geol.*, 79, 297-321.

- Robinson, A., and E.T.C. Spooner 1984b. Can the Elliot Lake uraninite-bearing quartz pebble conglomerates be used to place limits on the oxygen content of the early Proterozoic atmosphere? *J. Geol. Soc. London*, 141, 221-228.
- Robinson, D.J., and R.W. Hutchinson 1982. Evidence for a volcanogenic-exhalative origin of a massive nickel sulphide deposit at Redstone, Timmins, Ontario. *Geol. Assoc. Canada Spec. Paper* 25, 212-254.
- Robinson, D.N. 1978. The characteristics of natural diamond and their interpretation. *Minerals Sci. Eng.*, 10, 55-72.
- Robinson, D.S., J.E. Tilsley, and G.M. Hogg 1978. The time-bound character of uranium deposits. *Econ. Geol.*, 73, 1409-1419.
- Rock, N.M.S. and D.I. Groves 1988. Can lamprophyres resolve the genetic controversy over mesothermal gold deposits? *Geology*, 16, 538-541.
- Rock, N.M.S., D.I. Groves, C.S. Perring, and S.D. Golding 1989. Gold, lamprophyres, and porphyries: what does their association mean? *Econ. Geol. Mono.* 6, 609-625.
- Roedder, E. 1960. Fluid inclusions as samples of the ore-forming fluids. *International Geol. Congress, 21st, Copenhagen, 1960*, pt. 16, 218-229.
- Roedder, E. 1968. Temperature, salinity, and origin of the ore-forming fluids at Pine Point, Northwest Territories, Canada, from fluid inclusion studies. *Econ. Geol.*, 63, 439-450.
- Roedder, E. 1976. Fluid inclusion evidence on the genesis of ores in sedimentary and volcanic rocks. In *Handbook of strata-bound and stratiform ore deposits*, K.H. Wolf (ed.), 4, 67-110. Amsterdam: Elsevier.
- Roedder, E. 1979a. Fluid inclusion evidence on the environments of sedimentary diagenesis, a review. *Soc. Economic Paleontol. Mineral. Spec. Pub.* 26, 89-107.
- Roedder, E. 1979b. Fluid inclusions as samples of ore fluids. In *Geochemistry of hydrothermal ore deposits, 2nd edn.*, H. Barnes (ed.), p. 684-737. New York: Wiley.
- Roedder, E. 1984. Fluid inclusions. *Rev. in Mineralogy* 12. Washington: Mineral. Soc. Am.
- Roedder, E. and R.J. Bodnar 1980. Geologic pressure determinations from fluid inclusion studies. *Ann. Rev. Earth Planet. Sci.*, 8, 263-301.
- Roedder, E., and R.J. Bodnar 1997. Fluid inclusion studies of hydrothermal ore deposits. In *Geochemistry of hydrothermal ore deposits, 3rd edn.*, H.L. Barnes (ed.), 657-698. New York: Wiley.
- Roedder, E., and E.J. Dwornik 1968. Sphalerite color banding: lack of correlation with iron content, Pine Point, Northwest Territories, Canada. *Am. Mineral.* 53, 1523-1529.
- Roedder, P.L., and I. Reynolds 1991. Crystallization of chromite and chromium stability in basaltic melts. *J. Petrol.*, 32, 909-934.
- Rogerson, R., and C. McKee 1990. Geology, volcanism and mineral deposits of Papua New Guinea. *Australasian Inst. Mining Metall. Mono.* 14, 1747-1754.
- Rollinson, H. 1995. Composition and tectonic settings of chromite deposits through time — a discussion. *Econ. Geol.*, 90, 2091-2098.
- Rollison, H. 1997. The Archean komatiite-related Inyala chromitite, southern Zimbabwe. *Econ. Geol.*, 92, 98-107.
- Romberger, S.B. 1986. Ore deposits #9. Disseminated gold deposits. *Geoscience Canada*, 13, 23-31.
- Romberger, S.B. 1988. Geochemistry of gold in hydrothermal deposits. *U.S. Geol. Survey Bull.* 1957-A, A9-A25.
- Romberger, S.B. 1992. A model for bonanza gold deposits. *Geoscience Canada*, 19, 63-72.
- Rona, P. 1984. Hydrothermal mineralization at seafloor spreading centers. *Earth Sci. Rev.*, 20, 1-104.
- Rona, P.A., 1988. Hydrothermal mineralization at oceanic ridges. *Can. Mineral.*, 26, 431-465.
- Rona, P.A., G. Klinkhammer, T.A. Nelsen, J.H. Trefry, and H. Elderfield 1986. Black smokers, massive sulphides and vent biota at the Mid-Atlantic Ridge. *Nature*, 321, 33-37.
- Roscoe, S.M. 1969. Huronian rocks and uraniumiferous conglomerates in the Canadian Shield. *Can. Geol. Survey Paper* 68-40.
- Roscoe, S.M. 1965. Geochemical and isotopic studies, Noranda and Matagami areas. *Can. Mining Metall. Bull.*, 58, 965-971.
- Roscoe, S.M., and W.E.L. Minter 1993. Pyritic paleoplacer gold and uranium deposits. *Geol. Assoc. Canada Spec. Paper* 40, 103-124.
- Roscoe, W.E. 1975. Experimental deformation of natural chalcopyrite at temperatures up to 300°C over the strain rate range 10^{-2} to 10^{-6} sec⁻¹. *Econ. Geol.*, 70, 454-472.
- Rose, A.W. 1970a. Origin of trace element distribution patterns in sulfides of the Central and Bingham districts, western U.S.A. *Mineral. Deposita*, 5, 157-163.
- Rose, A.W. 1970b. Zonal relations of wallrock alteration and sulfide distribution at porphyry copper deposits. *Econ. Geol.*, 65, 920-936.
- Rose, A.W. 1976. The effect of cuprous chloride complexes in the origin of red-bed copper and related deposits. *Econ. Geol.*, 71, 1036-1048.
- Rose, A.W. 1989. Mobility of copper and other heavy metals in sedimentary environments. *Geol. Assoc. Canada Spec. Paper* 36, 97-110.

- Rose, A.W. and D. M. Burt 1979. Hydrothermal alteration. In *Geochemistry of hydrothermal ore deposits*, 2nd edn., H.L. Barnes (ed.), 173-235. New York: Wiley.
- Rose, A.W., D.C. Herrick, and P. Deines 1985. An oxygen and sulfur isotope study of skarn-type magnetite deposits of the Cornwall type, southeastern Pennsylvania. *Econ. Geol.*, 80, 418-443.
- Rose, A.W., A.T. Smith, R.L. Lustwerk, H. Ohmoto, and L.D. Hoy 1986. Geochemical aspects of stratiform and redbed copper deposits in the Catskill Formation (Pennsylvania, USA) and Redstone area (Canada). In *Geology and metallogeny of copper deposits*, G.H. Friedrich, A.D. Genkin, A.J. Naldrett, J.D. Ridge, R.H. Sillitoe, and F.M. Vokes (eds.), 412-421. Berlin: Springer-Verlag.
- Rosenbauer, R.J., J.L. Bischoff, and A.S. Radtke 1983. Hydrothermal Alteration of greywacke and basalt by 4 molal NaCl. *Econ. Geol.*, 78, 1701-1710.
- Rosholt, J.N., and A.J. Bartel 1969. Uranium, thorium and lead systematics in Granite Mountains, Wyoming. *Earth Planet. Sci. Lett.*, 7, 141-147.
- Rosholt, J.N., Prijana, and D.C. Noble 1971. Mobility of uranium and thorium in glassy and crystallized silicic volcanic rocks. *Econ. Geol.*, 66, 1061-1069.
- Ross, J.R. and G.M.F. Hopkins 1975. Kambalda nickel sulfide deposits. In *Economic Geology of Australia and Papua New Guinea*, C.L. Knight (ed.), 1, 100-121. Melbourne: Austral. Inst. Mining Metall.
- Ross, J.R. and R.R. Keays 1979. Precious metals in volcanic-type nickel sulfide deposits in Western Australia. Part I: Relationship with composition of the ores and their host rocks. *Can. Mineral.*, 17, 417-436.
- Ross, J.R. and G.A. Travis 1981. The nickel sulfide deposits of Western Australia in global perspective. *Econ. Geol.*, 76, 1291-1329.
- Ross, V. 1957. Geochemistry, crystal structure and mineralogy of the sulfides. *Econ. Geol.*, 52, 755 - 774.
- Rowan, E.L. 1986. Cathodoluminescent zonation in hydrothermal dolomite cements: relationship to Mississippi Valley-type Pb-Zn mineralization in southern Missouri and northern Arkansas. In *Process mineralogy VI: Including applications to precious metals and cathodoluminescence*, R.D. Hagni (ed.), 69-87. Warrendale, Pennsylvania: Metall. Soc. Am. Inst. Mining Metall. and Petroleum Engineers.
- Rowan, E.L., and D.L. Leach 1989. Constraints on fluid inclusions on sulfide precipitation mechanisms and ore fluid migration in the Viburnum Trend lead district, Missouri. *Econ. Geol.*, 84, 1948-1965.
- Rowell, W.F., and A.D. Edgar 1986. Platinum-group element mineralization in a hydrothermal Cu-Ni sulfide occurrence, Rathbun Lake, northeastern Ontario. *Econ. Geol.*, 81, 1272-1277.
- Roy, A.B., B.S. Paliwal, and B.R. Bejarnia 1984. The Aravalli rocks: an evolutionary model and metallogenic trends. *Indian J. Earth Sci.*, CEISM Seminar vol., 73-83.
- Roy, S. 1966. *Syngenetic manganese formations of India*. Calcutta: Jadavpur Univ. Press.
- Roy, S. 1976. Ancient manganese deposits. In *Handbook of strata-bound and stratiform ore deposits*, K.H. Wolf (ed.), 7, 395-476. Amsterdam: Elsevier.
- Roy, S. 1992. Environments and processes of manganese deposition. *Econ. Geol.*, 87, 1218-1236.
- Rozendaal, A. 1980. The Gamsberg zinc deposit, South Africa: a banded stratiform base-metal sulfide ore deposit. *Proc. 5th Quad. IAGOD Symposium*, 619-633. Stuttgart: E. Schweizerbartsche Verlagsbuchhandlung.
- Ruaya, J.R. 1988. Estimation of instability constants of metal chloride complexes in hydrothermal solutions up to 300°C. *Geochim. Cosmochim. Acta*, 52, 1983-1996.
- Ruaya, J.R., and T.M. Seward 1986. The stability of chlorozinc (II) complexes in hydrothermal solutions up to 350°C. *Geochim. Cosmochim. Acta*, 50, 651-661.
- Rubey, W.W. 1951. Geologic history of seawater. *Geol. Soc. Am. Bull.*, 62, 1111-1148.
- Rubey, W.W., and M.K. Hubert 1959. Role of fluid pressure in mechanics of overthrust faulting I. Mechanics of fluid-filled porous solids and its applications to overthrust faulting. *Geol. Soc. Am. Bull.*, 70, 115-166.
- Rubright, R.D., and O.J. Hart 1968. Non-porphyry ores of the Bingham district, Utah. In *Ore deposits of the United States, 1933-67 (Graton-Sales Volume)*, J.D. Ridge (ed.), 1, 886-907. New York: Am. Inst. Mining, Metall. and Petroleum Engineers.
- Ruiz, J., W.C. Kelly, and C.J. Kaiser 1985. Strontium isotopic evidence for the origin of barites and sulfides from the Mississippi Valley-type ore deposits in southeast Missouri — a discussion. *Econ. Geol.*, 80, 773-778.
- Rumble, D., III (ed.) 1976. Oxide minerals. *Reviews in Mineralogy* 3. Washington: Mineral. Soc. Am.
- Rumble, D., III, and F.S. Spear 1983. Oxygen-isotope equilibration and permeability enhancement during regional metamorphism. *J. Geol. Soc. London*, 140, 619-628.
- Rumble, D., III, J.M. Ferry, T.C. Hoering, and A.J. Boucot 1982. Fluid flow during metamorphism at the Beaver Brook fossil locality, New Hampshire. *Am. J. Sci.*, 282, 886-919.
- Runyon, G.A., and K.C. Misra 1985. metamorphic mobilization of sulfur in the Ducktown district, Tennessee, U. S. A.. *Geologicky Zbornik - Geologica Carpathica*, 36, 555-574.
- Russell, M.J. 1974. Manganese halo surrounding the Tynagh ore deposit, Ireland: a preliminary note. *Inst. Mining, Metall. Trans.*, 83, B65-B66.

- Russell, M.J. 1983. Major sediment-hosted exhalative zinc+lead deposits: formation from hydrothermal convection cells that deepen during crustal extension. In *Short course in sediment-hosted stratiform lead-zinc deposits*, D.F. Sangster (ed.), 251-282. Victoria: Mineral. Assoc. of Canada.
- Russell, M.J. 1986. Extension and convection: a genetic model for the Irish Carboniferous base metal and barite deposits. In *Geology and genesis of mineral deposits in Ireland*, C.J. Andrew, R.W.A. Crowe, S. Finlay, W.M. Pennell, and J.F. Pyne (eds.), p. 545-554. Dublin: Irish Assoc. Econ. Geol.
- Russell, M.J., M. Solomon, and J.L. Walshe 1981. The genesis of sediment-hosted exhalative zinc+lead deposits. *Mineral. Deposita*, 16, 113-127.
- Russell, R.D., and R.M. Farquhar 1960. *Lead isotopes in Geology*. New York: Interscience.
- Russell, R.D., and W.F. Slawson 1967. Constraints imposed by lead isotope abundances on the origin of ores. *Econ. Geol. Mono.* 3, 383-391.
- Ruzicka, V. 1971. Geological comparison between East European and Canadian uranium deposits. *Geol. Survey Canada Paper* 70-48, 196p.
- Ruzicka, V. 1993a. Unconformity-type uranium deposits. *Geol. Assoc. Canada Spec. Paper* 40, 125-149.
- Ruzicka, V. 1993b. Vein uranium deposits. *Ore Geol. Rev.*, 8, 247-276.
- Ryan, B.D., and J. Blenkinsop 1971. Geology and geochronology of the Hellroaring Creek stock, British Columbia. *Can. J. Earth Sci.*, 8, 85-95.
- Ryan, P.J., A.L. Lawrence, R.D. Lipson, J.M. More, A. Paterson, D.P. Stedman, and D. Van Zyl 1986. The Aggenys base metal sulphide deposits, Namaqualand district. In *Mineral deposits of Southern Africa*, C.R. Anhaeusser and S. Maske (eds.), 2, 1447-1473. Johannesburg: Geol. Soc. S. Africa.
- Rye, D.M., and R.O. Rye 1974. Homestake gold mine, South Dakota: I. Stable isotope studies. *Econ. Geol.*, 69, 293-317.
- Rye, D.M. and N. Williams 1981. Studies of base metal sulfide deposits at McArthur River Northern Territory, Australia III. The stable isotope geochemistry of the H.Y.C. Ridge, and Cooley deposits. *Econ. Geol.*, 76, 1-26.
- Rye, D.M., B.R. Doe, and M.H. Delevaux 1974. Homestake gold mine, South Dakota: II. Lead isotopes, mineralization ages, and source of lead in ores of the Northern Black Hills. *Econ. Geol.*, 69, 814-822.
- Rye, R.O. 1966. The carbon, hydrogen, and oxygen isotopic compositions of the hydrothermal fluids responsible for the lead-zinc deposits at Providencia, Zacatecas, Mexico. *Econ. Geol.*, 61, 1399-1427.
- Rye, R.O. 1993. The evolution of magmatic fluids in epithermal environment: the stable isotope perspective. *Econ. Geol.*, 88, 733-753.
- Rye, R.O., and J. Haffty 1969. Chemical composition of the hydrothermal fluids responsible for the lead-zinc deposits at Providencia, Zacatecas, Mexico. *Econ. Geol.*, 64, 629-643.
- Rye, R.O. and H. Ohmoto 1974. Sulfur and carbon isotopes and ore genesis: a review. *Econ. Geol.*, 69, 826-842.
- Rye, R.O. and J.R. O'Neil 1968. The ^{18}O content of water in primary fluid inclusions from Providencia, north central Mexico. *Econ. Geol.*, 63, 232-238.
- Rye, R.O., and F.J. Sawkins 1974. Fluid inclusion and stable isotope studies on the Casapalca Ag-Pb-Zn-Cu deposit, central Andes, Peru. *Econ. Geol.*, 69, 181-205.
- Rye, R.O., P. M. Bethke, and M.D. Wasserman 1992. The stable isotope geochemistry of acid sulfate alteration. *Econ. Geol.*, 87, 225-262.
- Saager, R. 1981. Geochemical studies on the origin of the detrital pyrites in the conglomerates of the Witwatersrand goldfields, South Africa. *U.S. Geol. Survey Prof. Paper* 1161, 11-117.
- Saager, R., R.M. Meyer, and R. Muff 1982. Gold distribution in supracrustal rocks from Archean greenstone belts of southern Africa and from Paleozoic ultramafic complexes of the European Alps — metallogenic and geochemical implications. *Econ. Geol.*, 77, 1-24.
- Saager, R., T. Oberthür, and H.P. Tomschi 1987. Geochemistry and mineralogy of banded iron-formation-hosted gold mineralization in the Gwanda greenstone belt, Zimbabwe. *Econ. Geol.*, 82, 2017-2032.
- Sakai, H. 1968. Isotopic properties of sulfur compounds in hydrothermal processes. *Geochem. J.*, 2, 29-49.
- Sakai, H., T. Gamo, E.-S. Kim, M. Tsutsumi, T. Tanaka, J. Ishbashi, H. Wakita, M. Yamano, and T. Oomori 1990. Venting of carbon dioxide-rich fluid and hydrate formation in mid-Okinawa Trough back-arc basin. *Science*, 248, 1093-1096.
- Sales, R.H. 1959. The White Pine copper deposit. *Econ. Geol.*, 54, 947-950.
- Sales, R.H. and C. Meyer 1948. Wall-rock alteration at Butte, Montana. *Am. Inst. Mining Eng. Trans.*, 178, 9-35.
- Sales, R.H., and C. Meyer 1951. Effect of post-ore dyke intrusions on Butte ore minerals. *Econ. Geol.*, 46, 813-820.
- Salmon, B.C., B.R. Clark, and W.C. Kelly 1974. Sulfide deformation studies: II. Experimental deformation of galena to 2,000 bars and 400°C. *Econ. Geol.*, 69, 1-16.
- Samson, I.M. and M.J. Russell 1987. Genesis of the Silvermines zinc-lead-barite deposit, Ireland: fluid inclusion and stable isotope evidence. *Econ. Geol.*, 82, 371-394.
- Sander, M.V., and M.T. Einaudi 1990. Epithermal deposition of gold during transition from propylitic to potassic alteration at Round Mountain, Nevada. *Econ. Geol.*, 85, 285-311.

- Sanford, R.F. 1992. A new model for tabular-type uranium deposits. *Econ. Geol.*, 87, 2041-2055.
- Sanford, R.F. 1994. A quantitative model of ground-water flow during formation of tabular sandstone uranium deposits. *Econ. Geol.*, 89, 341-360.
- Sangster, D.F. 1976a. Sulfur and lead isotopes in strata-bound deposits. In *Handbook of strata-bound and stratiform ore deposits*, K.H. Wolf (ed.), 2, 219-266. Amsterdam: Elsevier.
- Sangster, D.F. 1976b. Carbonate-hosted lead-zinc deposits. In *Handbook of strata-bound and stratiform ore deposits*, K.H. Wolf (ed.), 6, 447-456. Amsterdam: Elsevier.
- Sangster, D.F. 1979. Plate tectonics and mineral deposits. A view from two perspectives. *Geoscience Canada*, 6, 185-188.
- Sangster, D.F. 1980a. Quantitative characteristics of volcanogenic massive sulphide deposits. *Can. Inst. Mining Bull.*, 73, (814), 74-81.
- Sangster, D.F. 1980b. Distribution and origin of Precambrian massive sulfide deposits of North America. *Geol. Assoc. Canada Spec. Paper* 20, 723-739.
- Sangster, D.F. 1983. Mississippi Valley-type deposits: a geological melange. In *International Conference on Mississippi Valley-type lead-zinc deposits — Proc. Vol.*, G. Kisvarsanyi, S.K. Grant, W.P. Pratt, and J.W. Koenig (eds.), 7-19, Rolla: Univ. Missouri-Rolla Press.
- Sangster, D.F. 1986. Age of mineralization in Mississippi Valley-type (MVT) deposits: a critical requirement for genetic modelling. In *Geology and genesis of mineral deposits in Ireland*, C.J. Andrew, R.W.A. Crowe, S. Finlay, W.M. Pennell, and J.F. Pyne (eds.), 625-634. Dublin: Irish Assoc. Econ. Geol.
- Sangster, D.F. 1990. Mississippi Valley-type and SEDEX lead-zinc deposits: a comparative examination. *Inst. Mining Metall. Trans.*, 99, B21-B42.
- Sangster, D.F. (ed.) 1997. Carbonate-hosted lead-zinc deposits. *Soc. Econ. Geol. Spec. Publ* 4, 75th Anniv. Vol., 664 p.
- Sangster, D.R., and S.D. Scott 1976. Precambrian strata-bound massive Cu-Zn-Pb sulphide ore of North America. In *Handbook of strata-bound and stratiform ore deposits*, K.H. Wolf (ed.), 6, 129-222. Amsterdam: Elsevier.
- Sangster, D.F., G.S. Nowlan, and A.D. McCracken 1994. Thermal comparison of Mississippi Valley-type lead-zinc deposits and their host rocks using fluid inclusion and conodont color alteration index data. *Econ. Geol.*, 89, 493-514.
- Sarkar, S.C., S. Kabiraj, and A.B. Paul 1996. Nature, origin and evolution of the granitoid-hosted early Proterozoic copper-molybdenum mineralization at Malanjhand, central India. *Mineral. Deposita*, 31, 419-431.
- Sasaki, A. and H.R. Krouse 1969. Sulfur isotopes and the Pine Point lead-zinc mineralization. *Econ. Geol.*, 64, 718-730.
- Sasaki, A. and Y. Kajiwaru 1971. Evidence of isotopic exchange between seawater sulfate and some syngenetic sulfide ores. *Soc. Mining Geol. Japan Spec. Issue* 3, 289-294.
- Sassani, D.C., and E.L. Shock 1990. Speciation and solubility of palladium in aqueous magmatic-hydrothermal solutions. *Geology*, 18, 925-928.
- Sato, T. 1972. Behaviour of ore-forming solutions in seawater. *Mining Geol.*, 22, 31-42.
- Sato, T. 1973. A chloride complex model for Kuroko mineralization. *Geochem. J.*, 7, 245-270.
- Sato, T. 1974. Distribution and geological salting of the Kurocodeposits. *Soc. Mining Geol. Japan Spec. Issue* 6, 1-9.
- Sato, T., T. Shojiro, and T. Ohtagaki 1974. Geology and ore deposits of the Hokoroku district, Akita Prefecture. *Soc. Mining Geol. Japan Spec. Issue* 6, 11-18.
- Saunders, A.D., J. Tarney, and S.D. Weaver 1980. Transverse geochemical variations across the Antarctic Peninsula: implications for the genesis of calc-alkaline magmas. *Earth Planet. Sci. Lett.*, 46, 344-360.
- Savin, S.M. and S. Epstein 1970. The oxygen and hydrogen isotope geochemistry of clay minerals. *Geochim. Cosmochim. Acta*, 34, 43-64.
- Sawkins, F.J. 1964. Lead-zinc ore deposition in the light of fluid inclusion studies, Providencia Mine, Zacatecas, Mexico. *Econ. Geol.*, 59, 883-919.
- Sawkins, F.J. 1972. Sulfide ore deposits in relation to plate tectonics. *J. Geol.*, 80, 377-397.
- Sawkins, F.J. 1976a. Massive sulfide deposits in relation to geotectonics. *Geol. Assoc. Canada Spec. Paper* 14, 221-242.
- Sawkins, F.J. 1976b. Metal deposits related to intracontinental hot-spot and rifting environments. *J. Geol.*, 80, 1028-1041.
- Sawkins, F.J. 1983. Tectonic controls of the time-space distribution of some Proterozoic metal deposits. *Geol. Soc. Am. Mem.*, 161, 179-189.
- Sawkins, F.J. 1984. Ore genesis by episodic dewatering of sedimentary basins: application to giant Proterozoic lead-zinc deposits. *Geology*, 12, 451-454.
- Sawkins, F.J. 1989. Anorogenic felsic magmatism, rift sedimentation, and giant Proterozoic Pb-Zn deposits. *Geology*, 17, 657-660.
- Sawkins, F.J. 1990a. Integrated tectonic-genetic model for volcanic-hosted massive sulfide deposits. *Geology*, 18, 1061-1064.

- Sawkins, F.J. 1990b. *Metal deposits in relation to plate tectonics*, 2nd. edn. Berlin: Springer-Verlag.
- Sawkins, F.J., and J. Kowalik 1981. The source of ore metals at Buchans: magmatic versus leaching models. *Geol. Assoc. Canada Spec. Paper* 22, 255-267.
- Sawkins, F.J., and D.M. Rye 1974. Relationship of Homestake-type gold deposits to iron-rich Precambrian sedimentary rocks. *Inst. Mining. Metall. Trans.*, 83, B56-B60.
- Sawlowicz, Z. 1990. Primary copper sulphides from the Kupferschiefer, Poland. *Mineral. Deposita*, 25, 262-271.
- Scherkenbach, D.A., F.J. Sawkins, and W.E. Seyfried, Jr. 1985. Geologic, fluid inclusion and geochemical studies of the mineralized breccias at Cumobabi, Sonora, Mexico. *Econ. Geol.*, 80, 1566-1592.
- Schidlowski, M. 1976. Archean atmosphere and evolution of the terrestrial oxygen budget. In *The early history of the earth*, B.F. Windley (ed.), 525-534. New York: Wiley.
- Schidlowski, M. 1979. Antiquity and evolutionary status of bacterial sulfate reduction: sulfur isotope evidence. *Origins of Life*, 9, 299-311.
- Schidlowski, M. 1981. Uraniferous constituents of the Witwatersrand conglomerates: ore microscopic observations for the Witwatersrand metallogeny. In *Genesis of uranium- and gold-bearing Precambrian quartz-pebble conglomerates: U.S. Geol. Survey Prof. Paper* 1161, N1-N29.
- Schidlowski, M. 1984. Early atmospheric oxygen levels: constraints from Archean photoautotrophy. *J. Geol. Soc. London*, 141, 243-250.
- Schidlowski, M., J.M. Hayes, and I.R. Kaplan 1983. Isotopic inferences of ancient biochemistries: Carbon, sulfur, hydrogen, and nitrogen. In *Earth's earliest biosphere: its origin and evolution*, J.W. Schopf (ed.), 149-186. Princeton, New Jersey: Princeton Univ. Press.
- Schiffries, C.M. 1982. The petrogenesis of a platiniferous dunite pipe in the Bushveld Complex: infiltration metasomatism by a chloride solution. *Econ. Geol.*, 77, 1439-1453.
- Schiffries, C.M., and D.M. Rye 1990. Stable isotope systematics of the Bushveld Complex: II. Constraints on hydrothermal processes in layered intrusions. *Am. J. Sci.*, 290, 209-245.
- Schilling, J.G. 1971. Sea-floor evolution: rare-earth evidence. *Phil. Trans. Royal Soc. London*, A268, 663-706.
- Schink, D.R. 1967. Budget for dissolved silica in the Mediterranean Sea. *Geochim. Cosmochim. Acta*, 31, 987-999.
- Schmidt, F.P., and G. Friedrich 1988. Geologic setting and genesis of Kupferschiefer mineralization in West Germany. *Soc. Geology Appl. Mineral Deposits Spec. Publ.* 5, 25-29.
- Schmidt Mumm, A., T. Oberthür, U. Vetter, and T.G. Blenkinsop 1997. High CO₂ content of fluid inclusions in gold mineralizations in the Ashanti Belt, Ghana: a new category of ore-forming fluids? *Mineral. Deposita*, 32, 107-118.
- Schmitt, H.A. 1966. The porphyry copper deposits in their regional setting. In *The Geology of the porphyry copper deposits: southwestern North America*, S.R. Titley and L. Hicks (eds.), 17-34. Tucson, Arizona: Univ. Arizona Press.
- Schneiderhöhn, H. 1932. Mineralische Bodenschätze in Südlichen Afrika (the geology of the copperbelt, Northern Rhodesia, translation in abstract). *Mining Mag.*, 46, 241-245.
- Schoell, M.N. Backer, and Q. Baumann 1976. The Red Sea geothermal systems-new aspects on their brines and associated sediments. *International Assoc. Genesis of Ore Deposits, Symposium, 4th, Varne 1974*, 1, 303-373.
- Schopf, J.W., and B.M. Packer 1987. Early Archean (3.3-billion to 3.5-billion-year-old) microfossils from Warrawoona Group, Australia. *Science*, 237, 70-73.
- Schreyer, W., G. Kullerud, and P. Ramdohr 1964. Metamorphic conditions or ore and country rock of the Bodenmais, Bavaria, sulfide deposits. *N. Jahrb. Mineral. Abh.*, 101, 1-26.
- Schuiling, R.D. 1967. Tin belts on the continents around the Atlantic Ocean. *Econ. Geol.*, 62, 540-550.
- Schulz, O. 1976. Typical and nontypical sedimentary ore fabrics. In *Handbook of strata-bound and stratiform ore deposits*, K.H. Wolf (ed.), 3, 295-338. Amsterdam: Elsevier.
- Schwarcz, H.P. and S.W. Burnie 1973. Influence of sedimentary environments on sulfur isotope ratios in clastic rocks: a review. *Mineral. Deposita*, 8, 264-277.
- Schwarcz, H.P., S.D. Scott, and S.A. Kissin 1975. Pressures of formation of iron meteorites from sphalerite compositions. *Geochim. Cosmochim. Acta*, 39, 1457-1466.
- Schwartz, G.M. 1951. Classification and definitions of textures and mineral structures in ores. *Econ. Geol.*, 46, 578-591.
- Scoon, R.N., and A.A. Mitchell 1994. Discordant iron-rich pegmatites in the Bushveld Complex and their relationship to iron-rich intercumulus and residual liquids. *J. Petrol.*, 35, 881-917.
- Scott, K.M., J.W. Smith, S.-S. Sun, and G.F. Taylor 1985. Proterozoic copper deposits in NW Queensland, Australia: sulfur isotopic data. *Mineral. Deposita*, 20, 116-126.
- Scott, S.D. 1976. Application of sphalerite geobarometer to regionally metamorphosed terrains. *Am. Mineral.*, 61, 661-670.
- Scott, S.D. 1980. Geology and structural control of Kuroko-type massive sulfide deposits. *Geol. Assoc. Canada Spec. Paper* 70, 705-722.

- Scott, S.D. 1983. Chemical behavior of sphalerite and arsenopyrite in hydrothermal and metamorphic environments. *Mineral. Mag.*, 47, 427-435.
- Scott, S.D. 1985. Seafloor polymetallic sulfides: scientific curiosities or mines of the future? In *Marine Minerals*, P.G. Telesi et al. (eds.), 277-300. Dordrecht: Reidel.
- Scott, S.D. 1992. Polymetallic sulfide riches from the deep: fact or fallacy? In *Use and misuse of the seafloor*, K Hsu and J. Thiede (ds.), 87-115. New York: Wiley.
- Scott, S.D. 1997. Submarine hydrothermal systems and deposits. In *Geochemistry of hydrothermal ore deposits, 3rd. edn.*, H.L. Barnes (ed.), 97-875. New York: Wiley.
- Scott, S.D. and H.L. Barnes 1971. Sphalerite geothermometry and geobarometry. *Econ. Geol.*, 66, 653-669.
- Scott, S.D. and S.A. Kissin 1973. Sphalerite composition in the Zn-Fe-S system below 300°C. *Econ. Geol.*, 68, 475-479.
- Scott, S.D., R.A. Both, and S.A. Kissin 1977. Sulfide petrology of the Broken Hill region, New South Wales. *Econ. Geol.*, 72, 1410-1425.
- Seasor, R.W., and A.C. Brown 1989. Syngenetic and diagenetic concepts at the White Pine copper deposit, Michigan. *Geol. Assoc. Canada Spec. Paper* 36, 257-268.
- Secombe, P.K., D.I. Groves, R.A. Binns, and J.W. Smith 1977. A sulphur isotope study to test a genetic model for Fe-Ni sulphide mineralization at Mt. Windarra, Western Australia. In *Stable isotopes in the Earth sciences*, B.W. Robinson (ed.), *New Zealand Dept. Sci. Ind. Res. Bull.*, 220, 187-202.
- Seedorff, E. 1988. Cyclic development of hydrothermal mineral assemblages related to multiple intrusions at the Henderson porphyry molybdenum deposit, Colorado. *Can. Inst. Mining Metall. Spec. Vol.* 39, 367-393.
- Seedorff, E. 1991. Magmatism, extension, and ore deposits of Eocene to Holocene age in the Great Basin: mutual effects and preliminary proposed genetic relationships. In *Geology and ore deposits of the Great Basin*, G.L. Raines, R.E. Lisle, R.W. Schafer, and W.H. Wilkinson (eds.), Symposium Proceedings, 1, 133-178. Reno: Geol. Soc. Nevada.
- Sen, R., A.D. Mukherjee, and A. K. Banherji 1973. Metamorphism and deformation of sulphides: I. General remarks. *N. Jahrb. Miner. Abh.*, 119, 155-162.
- Seward, T. M. 1973. Thio complexes of gold in hydrothermal ore solutions. *Geochim. Cosmochim. Acta*, 37, 379-399.
- Seward, T. M. 1984. The transport and deposition of gold in hydrothermal systems. In *Gold '82: the Geology, geochemistry and genesis of gold deposits*, R.P. Foster (ed.), 165-181. Rotterdam: Balkema.
- Seward, T.M. 1991. The hydrothermal geochemistry of gold. In *Gold metallogeny and exploration*, R.P. Foster (ed.), 37-62. Glasgow: Blackie.
- Seward, T.M., and H.L. Barnes 1997. Metal transport by hydrothermal fluids. In *Geochemistry of hydrothermal ore deposits, 3rd. edn.*, H.L. Barnes (ed.), 435-486. New York: Wiley.
- Seyfried, W.E., Jr. and J.L. Bischoff 1979. Low temperature basalt alteration by seawater: an experimental study at 70°C and 150°C. *Geochim. Cosmochim. Acta*, 43, 1937-1947.
- Seyfried, W.E., Jr. and J.L. Bischoff 1981. Experimental seawater-basalt interaction at 300°C, 500 bars: chemical exchange, secondary mineral formation and implications for the transport of heavy metals. *Geochim. Cosmochim. Acta*, 45, 1325-147.
- Seyfried, W.E., Jr. and D.R. Janecky 1985. Heavy metal and sulfur transport during subcritical hydrothermal alteration of basalt: influence of fluid pressure and basalt composition and crystallinity. *Geochim. Cosmochim. Acta*, 49, 2545-2560.
- Seyfried, W.E., Jr. and M.J. Mottl 1982. Hydrothermal alteration of basalt by seawater under seawater-dominated conditions. *Geochim. Cosmochim. Acta*, 46, 985-1002.
- Shanks, W.C. III. and J.L. Bischoff 1980. Geochemistry, sulfur isotope composition, and accumulation rates of Red Sea geothermal deposits. *Econ. Geol.*, 75, 445-459.
- Shanks, W.C., III and W.E. Seyfried, Jr. 1987. Stable isotope studies of vent fluids and chimney minerals, southern Juan de Fuca Ridge: sodium metasomatism and seawater sulfate reduction. *J. Geophys. Res.*, 92, 11387-11399.
- Shanks, W.C., III, L.G. Woodruff, G.A. Jilson, D.S. Jennings, J.S. Modene, and B.D. Ryan 1987. Sulfur and lead isotope studies of stratiform Zn-Pb-Ag deposits, Anvil Range, Yukon: basinal brine and anoxic bottom-water mixing. *Econ. Geol.*, 82, 600-634.
- Sharp, Z.D., E.J. Essene, and W.C. Kelly 1985. A re-examination of the arsenopyrite geothermometer: pressure considerations and applications to natural assemblages. *Can. Mineral.*, 23, 517 - 534.
- Sharpe, M.R. 1981. The chronology of magma influxes to the eastern Bushveld compartment of the Bushveld Complex as exemplified by its marginal border groups. *Geol. Soc. London J.*, 138, 307-326.
- Sharpe, M.R. 1982. Noble metals in the marginal rocks of the Bushveld Complex. *Econ. Geol.*, 77, 1286-1295.
- Sharpe, M.R. 1985. Strontium isotopic evidence for preserved density stratification in the Main Zone of the Bushveld Complex, South Africa. *Nature*, 316, 119-126.

- Sharpe, M.R., and L.J. Hulbert 1985. Ultramafic sills beneath the eastern Bushveld Complex: mobilized suspensions of early Lower Zone cumulates in a parental magma with boninitic affinities. *Econ. Geol.*, 80, 813-837.
- Sharpe, M.R., and T.N. Irvine 1983. Melting relations of two Bushveld chilled margin rocks and implications for the origin of chromitite. *Carnegie Inst. Washington Year Book* 82, 295-300.
- Shaw, D.R. and C.J. Hodgson 1980. Wall-rock alteration at the Sullivan mine, Kimberley, British Columbia [abs.]. *Can. Mining Metall. Bull.*, 73, 821, 75.
- Shawe, D.R. 1956. Significance of roll ore bodies in genesis of uranium-banadium deposits on the Colorado Plateau. *U.S. Geol. Survey Prof. Paper* 800, 239-241.
- Shawe, D.R., and H.C. Granger 1965. Uranium rolls — an analysis. *Econ. Geol.*, 60, 240-250.
- Shegelski, R.J. 1987. The depositional environment of Archean iron formations, Sturgeon-Savart greenstone belt, Ontario, Canada. In *Precambrian iron-formations*, P.W.U. Appel and G.L. LaBerge (eds.), 329-344. Athens: Theophrastus Publ.
- Shelton, K.L. 1983. Composition and origin of ore-forming fluids in a carbonate-hosted porphyry copper and skarn deposit: a fluid inclusion and stable isotope study of Mines Gaspé, Quebec. *Econ. Geol.*, 78, 387-421.
- Shelton, K.L., I.B. Burstein, R.D. Hagni, C.B. Vierrether, S.K. Grant, Q.T. Hennigh, M.F. Bradley, and R.T. Brandon 1995. Sulfur isotope evidence for penetration of MVT fluids into igneous basement rocks, southeast Missouri, USA. *Mineral. Deposita*, 30, 339-350.
- Shepherd, T.J. and D. P.F. Darbyshire 1981. Fluid inclusion Rb-Sr isochrons for dating mineral deposits. *Nature*, 290, 578-579.
- Shepherd, T.J., and A.H. Rankin 1998. Fluid inclusion techniques of analysis. *Rev. in Econ. Geol.*, 10, 125-149.
- Shepherd, T.J., S.H. Bottrell, and M.F. Miller 1991. Fluid inclusion volatiles as an exploration guide to black shale-hosted gold deposits, Dolgellau gold belt, North Wales, UK. *J. Geochem. Exploration*, 42, 5-24.
- Sheppard, S.M.F. 1986. Characterization and isotopic variations in natural waters. *Reviews in Mineralogy*, 16, 163-183. Blacksburg, Virginia: Am. Mineral. Soc.
- Sheppard, S.M.F., and L.B. Gustafson 1976. Oxygen and hydrogen isotopes in the porphyry copper deposit at El Salvador, Chile. *Econ. Geol.*, 71, 1549-1559.
- Sheppard, S.M.F., and H.P. Taylor, Jr. 1974. Hydrogen and oxygen isotope evidence for the origin of water in the Boulder batholith and the Butte ore deposits, Montana. *Econ. Geol.*, 69, 926-946.
- Sheppard, S.M.F., R.L. Nielsen, and H.P. Taylor, Jr. 1971. Hydrogen and oxygen isotope relations in minerals from porphyry copper deposits. *Econ. Geol.*, 66, 515-542.
- Sheridan, D.M., and W.H. Raymond 1984. Precambrian deposits of zinc- copper- lead sulfides and zinc spinel (gahnite) in Colorado. *U. S. Geol. Survey Bull.* 1550.
- Shervais, J.W., L.A. Taylor, and J.C. Laul 1987. Magma mixing and kimberlite genesis; mineralogic, petrologic and trace element evidence from eastern U.S.A. kimberlites. *Geol. Soc. Am. Spec. Paper* 215, 101-114.
- Shikazono, N., H.D. Holland, and R.F. Quirk 1983. Anhydrite in Kuroko deposits; mode of occurrence and depositional mechanisms. *Econ. Geol. Mono.* 5, 329-344.
- Shinohara, H. 1994. Exsolution of immiscible vapor and liquid phases from a crystallizing silicate melt: implications for chlorine and metal transport. *Geochim. Cosmochim. Acta*, 58, 5215-5221.
- Shima, H. and A.J. Naldrett 1975. Solubility of sulfur in an ultramafic melt and the relevance of the system Fe-S-O. *Econ. Geol.*, 70, 960-967.
- Shimazaki, H. 1980. Characteristics of skarn deposits and related acid magmatism in Japan. *Econ. Geol.*, 75, 173-183.
- Shimazaki, H. 1982. The Sasano hastingsite-bearing copper skarn deposit formed in aluminous sediment at the Yoshioka mine, Japan. *Econ. Geol.*, 77, 868-876.
- Shimazaki, H., and L.A. Clark 1973. Liquidus relations in the FeS- FeO-SiO₂-Na₂O system and geological implications. *Econ. Geol.*, 68, 79-96.
- Shimazaki, Y. 1974. Ore minerals of the Kuroko-type deposits. *Soc. Mining Geol. Japan Spec. Issue* 6, 303-311.
- Shimizu, M., and N. Shikazono 1985. Iron and zinc partitioning between coexisting stannite and sphalerite: a possible indicator of temperature and sulfur fugacity. *Mineral. Deposita*, 20, 314-320.
- Shinohara, H., K. Kazahaya, and J.B. Lowenstern 1995. Volatile transport in a convecting magma column: implications for porphyry Mo mineralization. *Geology*, 23, 1091-1094.
- Shirozo, H. 1974. Clay minerals in altered wall rocks of the Kuroko type deposits. *Soc. Mining Geol. Japan Spec. Issue* 6, 303-311.
- Shock, E.L., and D.A. Sverjensky 1989. Hydrothermal organometallic complexes of base metals [abs.]. *Geol. Soc. Am. Abstracts with Programs*, 21, A8.
- Sibson, F.H., F. Robert, and K.H. Poulsen 1988. High-angle reverse faults, fluid-pressure cycling, and mesothermal gold-quartz deposits. *Geology*, 16, 551-555.

- Sibson, R.H., J.M. More, and A.J. Rankin 1975. Seismic pumping — a hydrothermal fluid transport mechanism. *Geol. Soc. London J.*, 131, 653-659.
- Siddaiah, N.S., G.N. Hanson, and V. Rajamani 1994. Rare earth element evidence for syngenetic origin of an Archean stratiform gold sulfide deposit, Kola Scist Belt, South India. *Econ. Geol.*, 89, 1152-1566.
- Siddeley, G., and R. Araneda 1986. The El Indio-Tambo deposits, Chile. In *Proc. Gold '86 Symposium*, A.J. Macdonald (ed.), 445-446. Willowdale, Ontario: Konsult International.
- Siever, R. 1957. The silica budget in the sedimentary cycle. *Am. Mineral.*, 42, 821-841.
- Siever, R. 1992. The silica cycle in the Precambrian. *Geochim. Cosmochim. Acta*, 56, 3265-3272.
- Sikka, D., and C.E. Nehru 1997. Review of Precambrian porphyry Cu \pm Mo \pm Au deposits with special reference to Malanjkhanda porphyry copper deposit, Madhya Pradesh, India. *J. Geol. Soc. India*, 49, 239-288.
- Silberman, M.L., and B.R. Berger 1985. Relationship of trace-element patterns to alteration and morphology in epithermal precious-metal deposits. *Rev. Econ. Geol.*, 2, 203-232.
- Sillitoe, R.H. 1972a. Relation of metal provinces in western America to subduction of oceanic lithosphere. *Geol. Soc. Am. Bull.*, 83, 813-818.
- Sillitoe, R.H. 1972b. A plate tectonic model for the origin of porphyry copper deposits. *Econ. Geol.*, 67, 184-197.
- Sillitoe, R.H. 1973. The tops and bottoms of porphyry copper deposits. *Econ. Geol.*, 68, 799-815.
- Sillitoe, R.H. 1975. Subduction and porphyry copper deposits in southwestern North America — a reply to recent objections. *Econ. Geol.*, 70, 1474-1477.
- Sillitoe, R.H. 1976. Andean mineralization: a model for the metallogeny of unconvergent plate margins. In *Metallogeny and plate tectonics*, D.F. Strong (ed.), *Geol. Assoc. Canada Spec. Paper* 14, 59-100.
- Sillitoe, R.H. 1977. Permo-Carboniferous, Upper Cretaceous and Miocene porphyry copper-type mineralization in the Argentinian Andes. *Econ. Geol.*, 72, 99-103.
- Sillitoe, R.H. 1979. Some thoughts on gold-rich porphyry copper deposits. *Mineral. Deposita*, 14, 161-174.
- Sillitoe, R.H. 1980. Types of porphyry molybdenum deposits. *Mining Mag.*, 142, 550-553.
- Sillitoe, R.H. 1985. Ore-related breccias in volcano-plutonic arcs. *Econ. Geol.*, 80, 1467-1514.
- Sillitoe, R.H. 1986. Space-time distribution, crustal setting and Cu/Mo ratios of Central Andean porphyry copper deposits: metallogenic implications. In *Geology and metallogeny of copper deposits*, G.H. Friedrich, A.D. Genkin, A.J. Naldrett, J.D. Ridge, R.H. Sillitoe, and F.M. Vokes (eds.), 235-50. Berlin: Springer-Verlag.
- Sillitoe, R.H. 1988. Epochs of intrusion-related copper mineralization in the Andes. *J. South Am. Earth Sci.*, 1, 89-108.
- Sillitoe, R.H. 1989. Gold deposits in western Pacific island arcs: the magmatic connection. *Econ. Geol. Mono.* 6, 274-291.
- Sillitoe, R. H. 1991. Intrusion-related gold deposits. In *Gold metallogeny and exploration*, R.P. Foster (ed.), 165-209. Glasgow: Blackie.
- Sillitoe, R.H. 1993a. Epithermal models: genetic types, geometrical controls and shallow features. *Geol. Assoc. Canada Spec. Paper* 40, 403-417.
- Sillitoe, R.H. 1993b. Gold-rich porphyry copper deposits: geological model and exploration implications. *Geol. Assoc. Canada Spec. Paper* 40, 465-478.
- Sillitoe, R.H., and H.F. Bonham, Jr. 1990. Sediment-hosted gold deposits: distal products of magmatic hydrothermal systems. *Geology*, 18, 157-161.
- Sillitoe, R.H., and F.J. Sawkins 1971. Geologic, mineralogic, and fluid inclusion studies relating to the origin of copper-bearing tourmaline breccia pipes, Chile. *Econ. Geol.*, 66, 1028-1041.
- Sillitoe, R.H., C. Halls, and J.N. Grant 1975. Porphyry tin deposits in Bolivia. *Econ. Geol.*, 70, 913-927.
- Simmons, B.D. 1973. Geology of the Millenbach massive sulfide deposit, Noranda, Quebec. *Can. Mining Metall. Bull.*, 166, No. 739, 67-78.
- Simons, F.S., and W.C. Prinz 1973. Gold. *U.S. Geol. Survey Prof. Paper* 820, 263-275.
- Simonson, B. M. 1985. Sedimentological constraints on the origins of Precambrian iron-formations. *Geol. Soc. Am. Bull.*, 96, 244-252.
- Simonson, B.M., and S.W. Hassler 1996. Was the deposition of large Precambrian iron formations linked to major marine transgressions? *J. Geol.*, 104, 665-676.
- Simpson, P.R., and J.F. Bowles 1977. Uranium mineralization of the Witwatersrand and Dominion Reef systems. *Phil. Trans. Royal Soc. London*, A 286, 527-548.
- Simpson, P.R., and J.F. Bowles 1981. Detrital uraninite and pyrite: are they evidence for a reducing atmosphere? *U.S. Geol. Survey Prof. Paper* 1161, S1-S12.
- Singer, D.A. 1995. World class base and precious metal deposits — a quantitative analysis. *Econ. Geol.*, 90, 85-104.
- Singerland, R.L., and N.D. Smith 1986. Occurrence and formation of water-laid placers. *Ann. Rev. Earth and Planet. Sci. Lett.*, B.F. Windley (ed.), 525-534. New York: Wiley.
- Skall, H. 1975. The paleoenvironment of the Pine Point lead-zinc district. *Econ. Geol.*, 70, 22-47.
- Skinner, B.J. 1967. Precipitation of Mississippi Valley-type ores: a possible mechanism. *Econ. Geol. Mono.* 3, 363-370.

- Skinner, B.J. 1979. The many origins of hydrothermal mineral deposits. In *Geochemistry of hydrothermal ore deposits*, 2nd. edn., H.L. Barnes (ed.), 1-21. New York: Wiley.
- Skinner, B.J., and C.A. Johnson 1987. Evidence for movement of ore materials during high-grade metamorphism. *Ore Geol. Rev.*, 2, 191-204.
- Skinner, B.J., and D.L. Peck 1969. An immiscible sulfide melt from Hawaii. *Econ. Geol. Mono.* 4, 310-322.
- Skinner, B.J., D.E. White, H.J. Rose, and R.E. Mays 1969. Sulfides associated with the Salton Sea geothermal brine. *Econ. Geol.*, 62, 316-330.
- Skinner, B.J., F.D. Luce, J.A. Dill, P.E. Ellis, H.A. Hagan, D.M. Lewis, D.A. Odell, D.A. Sverjensky, and N. Williams 1976. Phase relationships in ternary portions of the system Pt-Pd-Fe-As-S. *Econ. Geol.*, 71, 1469-1475.
- Skirrow, R.G., and J.M. Franklin 1994. Silicification and metal leaching in semiconformable alteration beneath the Chisel Lake massive sulfide deposit, Snow Lake, Manitoba. *Econ. Geol.*, 89, 31-50.
- Skyring, G.W., and T.H. Donnelly 1982. Precambrian sulfur isotopes and a possible role for sulfite in the evolution of biological sulfate reduction. *Precamb. Res.*, 17, 41-61.
- Slack, J.F. 1993. Descriptive and grade-tonnage models for Besshi-type massive sulphide deposits. *Geol. Assoc. Canada Spec. Paper* 40, 343-372.
- Slack, J.F. and P.R. Coad 1989. Multiple hydrothermal and metamorphic events in the Kid Creek volcanogenic massive sulphide deposit, Timmins, Ontario: evidence from tourmalines and chlorites. *Can. J. Earth Sci.*, 26, 694-715.
- Slack, J.F., and W.C. Shanks III 1989. Geologic and isotopic characteristics of modern and ancient Besshi-type massive sulfide deposits [abs.]. *Abstracts, International Geol. Congress, 28th, Washington, D.C. U.S.A.*, 3-132.
- Smimov, V.I. 1977. *Ore deposits of the U.S.S.R.*, 1 (English translation), 179-236. London: Pitman.
- Smith, C.S. 1964. Some elementary principles of polycrystalline microstructure. *Metallurgical Rev.*, 9, 1-48.
- Smith, D.M., T. Albinson, and F.J. Sawkins 1982. Geologic and fluid inclusion studies of the Tayoltita silver-gold vein deposit, Durango, Mexico. *Econ. Geol.*, 77, 1120-1145.
- Smith, H.S., and A.J. Erlank 1982. Geochemistry and petrogenesis of komatiites from the Barberton greenstone belt, South Africa. In *Komatiites*, N.T. Arndt and E.G. Nisbet (eds.), 348-393. London: Allen & Unwin.
- Smith, J.W. and N.J.W. Croxford 1973. Sulfur-isotope ratios in the McArthur lead-zinc-silver deposit. *Nature*, 245, 10-12.
- Smith, J.W., M.S. Burns, and N.J.W. Croxford 1978. Stable isotope studies of the origins of mineralization at Mount Isa. *Mineral. Deposita*, 13, 369-381.
- Smith, N. D. 1989. Comment on "Problems with the placer model for Witwatersrand and gold". *Geology*, 17, 91-92.
- Smith, N.D., and W.E.L. Minter 1980. Sedimentological controls of gold and uranium in two Witwatersrand paleoplacers. *Econ. Geol.*, 75, 1-14.
- Smith, N.G., J.R. Kyle, and K. Magara 1983. Geophysical log documentation of fluid migration from compacting shales: a mineralization model from the Devonian strata of the Pine Point area, Canada. *Econ. Geol.*, 78, 1364-1374.
- Smith, S.E. and K.R. Walker 1971. Primary element dispersion associated with mineralization at Mount Isa, Queensland. *Austral. Bur. Min. Res. Geol. and Geophys. Bull.*, 131, 80 p.
- Smith, T.J., and S.E. Kesler 1985. Relation of fluid inclusion geochemistry to wallrock alteration and lithogeochemical zonation at the Hollinger-McIntyre gold deposit, Timmins, Ontario, Canada. *Can. Inst. Mining Metall. Bull.*, 34, 35-94.
- Smith, W.D. 1969. Penecontemporaneous faulting and its likely significance in relation to Mount Isa ore deposition. *Geol. Soc. Austral. Spec. Publ.*, 2, 225-235.
- Smits, G. 1984. Some aspects of the uranium minerals in Witwatersrand sediments of the early Proterozoic. *Precamb. Res.*, 25, 37-59.
- Snyder, F.G. 1967. Criteria for origin of stratiform ore bodies with application to southeast Missouri. *Econ. Geol. Mono* 3, 1-13.
- Snyder, F.G. 1968. Geology and mineral deposits, midcontinent United States. In *Ore Deposits of the United States, 1933-1967 (Graton-Sales Volume)*, J.D. Ridge (ed.), 1, 257-286. New York: Am. Inst. Mining Metall. and Petroleum Engineers.
- Snyder, F.G., and P.E. Gerdemann 1968. The geology of the southeast Missouri lead district. In *Ore deposits of the United States, 1933-1967 (Graton-Sales Volume)*, J.D. Ridge (ed.), 1, 327-358. New York: Am. Inst. Mining Metall. and Petroleum Engineers.
- Solomon, M. 1976. 'Volcanic' massive sulphide deposits and their host rocks — a review and explanation. In *Handbook of strata-bound and stratiform ore deposits*, K.H. Wolf (ed.), 6, 21-50. Amsterdam: Elsevier.
- Solomon, M. 1980. Evidence of exhalative origin for Tasmanian tin deposits (Discussion). *Can. Inst. Mining Metall. Bull.*, 78, 166-167.

- Solomon, M. 1990. Subduction, arc reversal, and the origin of porphyry-copper gold deposits in island arcs. *Geology*, 18, 630-633.
- Solomon, M., and J.L. Walshe 1979a. The formation of massive sulfide deposits on the sea floor. *Econ. Geol.*, 74, 797-813.
- Solomon, M., and J.L. Walshe 1979b. The behaviour of massive-sulphide ore solutions entering seawater and the development of zoned deposits. *Bull. Mineralogique*, 102, 402-470.
- Soloman, M., D.I. Groves, and J. Klominsky 1972. Metallogenic provinces and districts in the Tasman orogenic zone of eastern Australia. *Australasia Inst. Mining Metall. Proc.*, 242, 9-24.
- Solomon, M., J.L. Walshe, and C.J. Eastoe 1987. Experiments on convection and their relevance to the genesis of massive sulphide deposits. *Austral. J. Earth Sci.*, 34, 311-328.
- Souch, B.E., T. Pololsky, and Geological Staff of the International Nickel Co. of Canada Ltd. 1969. The sulfide ores of Sudbury: their particular relationship to a distinctive inclusion-bearing facies of the nickel irruptive. *Econ. Geol. Mono.* 4, 252-261.
- Sparks, R.S., H.E. Huppert, and J.S. Turner 1984. The fluid dynamics of evolving magma chambers. *Phil. Trans. Royal. Soc. London*, A 310, 511-534.
- Speidel, D.H. 1970. Effect of magnesium on the iron-titanium oxides. *Am. J. Sci.*, 268, 341-353.
- Spence, C.D., and A.F. de Rosen-Spence 1975. The place of sulfide mineralization in the volcanic sequence at Noranda, Quebec. *Econ. Geol.*, 70, 90-101.
- Spencer, K.J., and D.H. Lindsley 1981. A solution model for the coexisting iron-titanium oxides. *Am. Mineral.*, 66, 1189-1201.
- Spirakis, C. S. 1981. The possible role of sulfate reduction kinetics in the formation of hydrothermal uranium deposits. *Econ. Geol.*, 76, 2236-2239.
- Spirakis, C.S., and A.V. Heyl 1993. Organic matter (bitumen and other forms) as the key to localization of Mississippi Valley-type ores. In *Bitumen in ore deposits*, J. Parnell, H. Kucha, and P. Landais (eds.), 381-398. Berlin: Springer-Verlag.
- Spirakis, C.S., and A.V. Heyl 1995. Evaluation of proposed precipitation mechanisms for Mississippi Valley-type deposits. *Ore Geol. Rev.*, 10, 1-17.
- Spooner, E.T.C. 1977. Hydrodynamic model for the origin of the ophiolitic cupriferous pyrite ore deposits of Cyprus. *Geol. Soc. London Spec. Pub.* 7, 58-71.
- Spooner, E. T. C. 1980. Cu-pyrite mineralization and seawater convection in oceanic crust — the ophiolitic ore deposits of Cyprus. *Geol. Assoc. Canada Spec. Paper* 20, 685-704.
- Spooner, E.T.C. 1981. Fluid inclusion studies of hydrothermal ore deposits. In *Short course in fluid inclusions: applications to petrology*, L.S. Hollister and M.L. Crawford (eds.), 209-240. Calgary: Mineral. Assoc. Canada.
- Spooner, E.T.C., and W.S. Fyfe 1973. Sub-sea-floor metamorphism, heat and mass transfer. *Contrib. Mineral. Petrol.*, 42, 287-304.
- Spooner, E.T.C. and N.H. Gale 1982. Pb isotopic composition of ophiolitic volcanogenic sulphide deposits, Troodos Complex, Cyprus. *Nature*, 296, 239-242.
- Spooner, E.T.C., C.J. Bray, P.C. Wood, D.R. Burrows, and N.J. Callan 1987. Au-quartz vein and Cu-Au-Ag-Mo-anhydrite mineralization, Hollinger-McIntyre mines, Timmins, Ontario: $\delta^{13}\text{C}$ values (McIntyre), fluid inclusion gas chemistry, pressure (depth) estimation, and $\text{H}_2\text{O}-\text{CO}_2$ phase separation as a precipitation and dilation mechanism. *Ontario Geol. Survey Misc. Paper* 136, 35-56.
- Spry, P.G. and S.D. Scott 1986. Zincian spinel and staurolite guides to ore in the Appalachians and Scandinavian Caledonides. *Can. Mineral.*, 24, 147-163.
- Spurr, J.E. 1907. A theory of ore deposition. *Econ. Geol.*, 2, 781-795.
- Spycher, N.F., and M.H. Reed 1989. Boiling of a Broadlands-type epithermal ore fluid along alternative P-T paths: implications for the transport and deposition of base, precious, and volatile metals. *Econ. Geol.*, 84, 328-359.
- Squyres, J.B. 1980. Origin and significance of organic matter in uranium deposits of Morrison Formation, San Juan Basin, New Mexico. *New Mexico Bureau Mines Mineral Resources Mem.* 38, 86-97.
- Stacey, J.S., and J.D. Kramers 1975. Approximation of terrestrial lead isotope evolution by a two-staged model. *Earth Planet. Sci. Lett.*, 26, 207-221.
- Stacey, J.S., R.D. Zartman, and I.T. Nkomo 1968. A lead isotope study of galenas and selected feldspars from mining districts in Utah. *Econ. Geol.*, 63, 796-814.
- Stanton, R.L. 1963. Constitutional features of the Mount Isa sulphide ores and their interpretation. *Austral. Inst. Mining Metall. Proc.*, 205, 131-153.
- Stanton, R.L. 1964. Mineral interfaces in stratiform ores. *Inst. Mining Metall. Trans.*, 74, 45-79.
- Stanton, R.L. 1972. *Ore petrology*. New York: McGraw-Hill, 771p.
- Stanton, R.L. 1976. Petrochemical studies of the ore environment at Broken Hill, New South Wales: 4 - Environmental synthesis. *Inst. Mining Metall. Trans.*, 85, B221-B233.
- Stanton, R.L. 1986. Stratiform ores and geological processes. *Inst. Mining Metall. Trans.* 95, B165-B178.
- Stanton, R.L. 1987. Constitutional features and some exploration implications of three zinc-bearing stratiform skarns of eastern Australia. *Inst. Mining Metall. Trans.*, Sec. B, 96, B37-B57.

- Stanton, R.L., and H. Gorman 1968. A phenomenological study of grains boundary migration in some common sulfides. *Econ. Geol.*, 63, 907-923.
- Stanton, R.L., and T.A. Rafter 1966. The isotopic constitution of sulfur in some stratiform lead-zinc sulfide ores. *Mineral. Deposita*, 1, 16-29.
- Stanton, R.L., and R.D. Russell 1959. Anomalous leads and the emplacement of lead sulfide ores. *Econ. Geol.*, 54, 588-607.
- Stanton, R. L., and H.G. Wiley 1970. Natural work-hardening in galena, and its experimental reduction. *Econ. Geol.*, 65, 182-194.
- Starling, A., J. M. Gilligan, A. H. C. Carter, R.P. Foster, and R.A. Saunders 1989. High-temperature hydrothermal precipitation of precious metals on the surface of pyrite. *Nature*, 340, 298-300.
- Stein, H. 1980. Evidence for intertidal-supratidal facies control of stratiform ore at Magmont mine, Viburnum Trend, Southeast Missouri. *Proc. 5th Quad. IAGOD Symp.*, 768-784. Stuttgart: E. Schweizerbartsche Verlagsbuchhandlung.
- Stein, H. 1988. Genetic traits of Climax-type granites and molybdenum mineralization, Colorado mineral belt. *Can. Inst. Mining Metall. Spec. Vol.* 39, 394-401.
- Stein, H., and J.L. Hannah 1985. Movement and origin of ore fluids in Climax-type tungsten. *Geology*, 13, 469-474.
- Stein, H., and M. Huebner 1984. A heavy isotope enriched sulfur source for Climax-type porphyry molybdenum deposits: molybdenite compositions [abs.]. *Geol. Soc. Am. Abstracts with Programs*, 16, 667.
- Stein, H.J., J.W. Morgan, R.J. Markey, and J.L. Hannah 1998. An introduction to Re-Os: what's in it for the mineral industry. *Soc. Econ. Geol. Newsletter*, no. 32, 1 and 8-15.
- Stephens, M.B., H.S. Swinden, and J.F. Slack 1984. Correlation of massive sulfide deposits in the Appalachian-Caledonian orogen on the basis of paleotectonic salting. *Econ. Geol.*, 79, 1442-1478.
- Sterner, S.M., D.L. Hall, and R.J. Bodnar 1988. Synthetic fluid inclusions: V. Solubility relations in the system NaCl-KCl-H₂O under vapor saturated conditions. *Geochim. Cosmochim. Acta*, 52, 989-1006.
- Sterns, M.R., D.L. Cann, and J.R. Cann 1987. A thermal balance model of the formation of sedimentary-exhalative lead-zinc deposits. *Econ. Geol.*, 82, 1192-1203.
- Stewart, J.H. 1972. Initial deposits of the Cordilleran Geosyncline: evidence of Late Precambrian (> 850 m.y.) continental separation. *Geol. Soc. Am. Bull.*, 83, 1345-1360.
- Stewart, J.H. 1980. Geology of Nevada. *Nevada Bur. Mines and Geol. Spec. Publ.* 4, 136 p.
- Stockman, H.W., and P.F. Hlava 1984. Platinum-group minerals in alpine chromitites from southwestern Oregon. *Econ. Geol.*, 79, 191-508.
- Stoffregen, R. 1987. Genesis of acid-sulfate alteration and Au-Cu-Ag mineralization at Summitville, Colorado. *Econ. Geol.*, 82, 1575-1591.
- Stone, W.E., J.H. Crockett, and M.E. Fleet 1990. Partitioning of palladium, iridium, platinum, and gold between sulfide liquid and basalt melt at 1200°C. *Geochim. Cosmochim. Acta*, 54, 2341-2344.
- Stone, W.E., J.H. Crockett, and M.E. Fleet 1993. Sulfide-poor platinum-group mineralization in komatiitic systems: Boston Creek Flow, layered basaltic komatiite, Abitibi belt, Ontario. *Econ. Geol.*, 88, 817-836.
- Stowe, C.W. 1987a. *Evolution of chrome ore fields*. New York: Van Nostrand.
- Stowe, C.W. 1987b. The chromite deposits of the Shurughi greenstone belt, Zimbabwe. In *Evolution of chrome ore fields*, C.W. Stowe (ed.), 71-88. New York: Van Nostrand.
- Stowe, C.W. 1989. Chromite deposits through time [abs.]. *International Geol. Congress., 28th, Washington, 1989, Abstracts*, 3, 189-190.
- Stowe, C.W., 1994. Composition and tectonic settings of chromite deposits through time. *Econ. Geol.*, 89, 528-546.
- Strauss, G.K., and K.G. Gray 1986. Base metal deposits in the Iberian pyrite belt. In *Geology and metallogeny of copper deposits*, G.H. Friedrich, A.D. Genkin, A.J. Naldrett, J.D. Ridge, R.H. Sillitoe, and F.M. Vokes (eds.) 304-423. Berlin: Springer-Verlag.
- Strong, D.F. 1981. Ore deposit models-5. A model for granophile mineral deposits. *Geoscience Canada*, 8, 155-161.
- Stull, D.R., and H. Prophet 1971. *JANAF Thermochemical Tables, 2nd. edn.*, National Standards Ref. Data Serv. U. S. National Bureau Standards, NSRDS-NBS 37. Washington, D.C.: U.S. Dept. of Commerce.
- Stumpfl, E.F. 1979. Manganese haloes surrounding metamorphic stratabound base metal deposits. *Mineral. Deposita*, 14, 207-217.
- Stumpfl, E.F., and C.G. Ballhaus 1986. Stratiform platinum deposits: new data and concepts. *Fortschritte der Mineralogie*, 64, 205-214.
- Stumpfl, E.F., and J.C. Rucklidge 1982. The platiniferous dunite pipes of the eastern Bushveld. *Econ. Geol.*, 77, 1419-1431.
- Styrt, M.M., Brackmann, A.J., and H.D. Holland 1981. The mineralogy and the isotopic composition of sulfur in hydrothermal sulfide/sulfate deposits on the East Pacific Rise, 21°N latitude. *Earth Planet. Sci. Lett.*, 53, 382-390.

- Sugaki, A., A. Kitakaze, and S. Kojima 1987. Bulk compositions of intimate intergrowths of chalcopyrite and sphalerite and their genetic implications. *Mineral. Deposita*, 22, 26-32.
- Sun, S. 1982. Chemical composition and origin of the earth's primitive mantle. *Geochim. Cosmochim. Acta*, 46, 179-192.
- Sunbald, K. 1982. Distribution of gahnite-bearing sulphidic deposits in the Scandinavian Caledonides. *Inst. Mining Metall. Trans.*, 91, B214-B218
- Susak, N.J., and D.A. Crerar 1982. Factors controlling mineral zoning in hydrothermal ore deposits. *Econ. Geol.*, 77, 476-482.
- Sverjensky, D.A. 1987. The role of migrating oil field brines in the formation of sediment-hosted Cu-rich Deposits. *Econ. Geol.*, 82, 1130-1141.
- Sverjensky, D.A. 1981. The origin of a Mississippi Valley-type deposit in the Viburnum Trend, southeast Missouri. *Econ. Geol.*, 76, 1848-1872.
- Sverjensky, D.A. 1984. Oil field brines as ore-forming solutions. *Econ. Geol.*, 79, 23-37.
- Sverjensky, D.A. 1986. Genesis of Mississippi Valley-type lead-zinc deposits. *Ann. Rev. Earth Planet. Sci.*, 14, 17-199.
- Sverjensky, D.A. 1989. Chemical evolution of basinal brines that form sediment-hosted Cu-Pb-Zn deposits. *Geol. Assoc. Canada Spec. Paper* 36, 127-134.
- Sverjensky, D.A., D.M. Rye, and B.R. Doe 1979. The lead and sulfur isotopic compositions of galena from a Mississippi Valley-type deposit in the New Lead Belt, southeast Missouri. *Econ. Geol.*, 74, 149-153.
- Swager, C.P. 1985. Syndeformational carbonate-replacement model for the copper mineralization at Mount Isa, Northwest Queensland: a microstructural study. *Econ. Geol.*, 80, 107-125.
- Sweeney, M.A., and P.L. Binda 1989a. The role of diagenesis in the formation of the Konkola Cu-Co ore body of the Zambian Copperbelt. *Geol. Assoc. Canada Spec. Paper* 36, 499-518.
- Sweeney, M.A., and P.L. Binda 1989b. Mineralization and source of metals in the Lufilian fold belt, Shaba (Zaire), Zambia, and Angola — a discussion. *Econ. Geol.*, 84, 963-964.
- Sweeney, M.A., P. Turner, and D.J. Vaughan 1986. Stable isotope and geochemical studies of the role of early diagenesis in ore formation, Konkola Basin, Zambian Copperbelt. *Econ. Geol.*, 81, 1838-1852.
- Sweeney, M.A., P.L. Binda, and D.J. Vaughan 1991. Genesis of the ores of the Zambian Copperbelt. *Ore Geol. Rev.*, 6, 51-76.
- Swinden, H.S. 1991. Paleotectonic settings of volcanogenic massive sulfide deposits in the Dunnage Zone, Newfoundland Appalachians. *Can. Inst. Mining Metall. Bull.*, 84, 59-69.
- Swinden, H.S., and D.F. Strong 1976. A comparison of plate tectonic models in metallogenesis in the Appalachians, the North American Cordillera, and the east Australian Paleozoic. In *Metallogeny and Plate Tectonics*, D.F. Strong (ed.). *Geol. Assoc. Canada Spec. Paper* 14, 443-471.
- Sylvester, P.I., K. Altou, and K.J. Schulz 1987. Tectonic setting of late Archean bimodal volcanism in the Michipicoten (Wawa) greenstone belt, Ontario. *Can. J. Earth Sci.*, 24, 1120-1134.
- Syme, E.C., and A.H. Bailes 1993. Stratigraphic and tectonic setting of early Proterozoic volcanogenic massive sulfide deposits, Flin Flon, Manitoba. *Econ. Geol.*, 88, 566-589.
- Symons, D.T.A. 1995. Summary of paleomagnetic dating studies of Mississippi Valley-type deposits. *International Field Conference on Carbonate-hosted Lead-Zinc Deposits, June 3-6, 1995, St. Louis, Missouri, Extended Abstracts*, 308-310.
- Symons, D.T.A., and D.F. Sangster 1992. Late Devonian paleomagnetic age for the Polaris Mississippi Valley-type Zn-Pb deposit, Canadian Arctic Archipelago. *Can. J. Earth Sci.*, 29, 15-25.
- Symons, D.T.A., M.T. Lewchuk, and D.F. Sangster 1998. Laramide orogenic fluid flow into the western Canada sedimentary basin: evidence from paleomagnetic dating of the Kicking Horse Mississippi Valley-type ore deposit. *Econ. Geol.*, 93, 68-83.
- Symons, D.T.A., D.F. Sangster, and D.L. Leach 1995. A Tertiary age from paleomagnetism for Mississippi Valley-type zinc-lead mineralization in upper Silesia, Poland. *Econ. Geol.*, 90, 782-794.
- Symons, D.T.A., H. Pan, D.F. Sangster, and E.C. Jowett 1993. Paleomagnetism of the Pine Point Zn-Pb deposits. *Can. J. Earth Sci.*, 30, 1028-1036.
- Takahashi, E., and C.M. Scarfe 1985. Melting of peridotite to 14 GPa and the genesis of komatiite. *Nature*, 315, 566-568.
- Takahashi, T., and K. Suga 1974. Geology and ore deposits of the Hanaoka Kuroko belt, Akita Prefecture. *Soc. Mining Geol. Japan Spec. Issue* 6, 101-113.
- Talkington, R.W., and B.R. Lipin 1986. Platinum-group minerals in chromite seams of the Stillwater Complex, Montana. *Econ. Geol.*, 81, 1179-1186.
- Talkington, R.W., and D.H. Watkinson 1986. Whole rock platinum-group element trends in chromite-rich rocks in ophiolitic and stratiform igneous complexes. In *Metallogeny of basic and ultrabasic rocks*, M.J. Gallaher, R.A. Ixer, C.R. Neary, and H.M. Prichard (eds.), 427-440. London: Inst. Mining Metall.
- Tarney, J., I.W.D. Dalziel, and M.J. DeWit 1976. Marginal basin 'Rocas Verdes' complex from S. Chile: a model for Archean greenstone belt formation. In *The early history of the earth*, B.F. Windley (ed.), 131-155. New York: Wiley.
- Taylor, B.E. and J.F. Slack 1984. Tourmaline from Appalachian-Caledonian massive sulfide deposits: textural, chemical, and isotopic relationships. *Econ. Geol.*, 79, 1703-1726.

- Taylor, B.E., J.L. Hannah, H.J. Stein, and M.W. Ganster 1984. The Mount Emmons porphyry molybdenum deposit, Colorado: magmatic degassing and meteoric water overprinting [abs.]. *Geol. Soc. Am. Abstracts with Programs*, 16, 674.
- Taylor, H.P., Jr. 1963. Importance of chalcophile element abundances in determining the sequence of sulfide mineral deposition from monoascendent ore-forming solutions. In *Problems of post-magmatic ore deposition symposium, Czechoslovakia Geol. Survey* 1, 267-272.
- Taylor, H.P., Jr. 1974. The application of oxygen and hydrogen isotope studies to problems of hydrothermal alteration and ore deposition. *Econ. Geol.*, 69, 843-883.
- Taylor, H.P., Jr. 1979. Oxygen and hydrogen isotope relationships in hydrothermal mineral deposits. In *Geochemistry of hydrothermal ore deposits*, 2nd. edn., H.L. Barnes (ed.), 236-277. New York: Wiley.
- Taylor, H.P., Jr. 1980. The effects of assimilation of country rocks by magmas on $^{18}\text{O}/^{16}\text{O}$ and $^{87}\text{Sr}/^{86}\text{Sr}$ systematics on igneous rocks. *Earth Planet. Sci. Lett.*, 47, 243-254.
- Taylor, H.P., Jr. 1997. Oxygen and hydrogen isotope relationships in hydrothermal mineral deposits. In *Geochemistry of hydrothermal ore deposits*, 3rd. edn., H.L. Barnes (ed.), 229-302. New York: Wiley.
- Taylor, M., S.E. Kesler, P.L. Cloke, and W.C. Kelly 1983a. Fluid inclusion evidence for fluid mixing, Mascot-Jefferson City zinc district, Tennessee. *Econ. Geol.*, 78, 1425-1439.
- Taylor, M., W.C. Kelly, S.E. Kesler, J.E. McCormick, F.D. Ransick, and W.V. Mellon 1983b. Relationships of zinc mineralization in East Tennessee to Appalachian orogenic events. In *International Conference on Mississippi Valley-type lead-zinc deposits — Proc. Vol.*, G.K. Kisvarsanyi, S.K. Grant, W.P. Grant, and J.H. Koenig (eds.), 27-278. Rolla, Missouri: Univ. Missouri-Rolla Press.
- Teal, L., and M. Jackson 1997. Geologic overview of the Carlin-trend gold deposits and descriptions of recent deep discoveries. *Soc. Econ. Geol. Newsletter*, no.31, 1 and 13-25.
- Teigler, B., and H.V. Eales 1993. Correlation between chromite composition and PGE mineralization in the Critical Zone of the western Bushveld Complex. *Mineral. Deposita*, 28, 291-302.
- Thacker, J.L., and K.H. Anderson 1977. The geologic setting of the Southeast Missouri lead district — Regional geologic history, structure and stratigraphy. *Econ. Geol.*, 72, 339-348.
- Thayer, T.P. 1960. Some critical differences between alpine-type and stratiform peridotite-gabbro complexes. In *International Geol. Congress Rept., 21st session, Copenhagen*, T. Sorgenfrei (ed.), 13, 247-259. Copenhagen: Det Berligrske Bogtrykkeri.
- Thayer, T.P. 1964. Principal features and origin of podiform chromite deposits, and some observations on the Suleman-Soridag district, Turkey. *Econ. Geol.*, 59, 1497-1524.
- Thayer, T.P. 1969. Gravity differentiation and magmatic re-emplacment of podiform chromite deposits. *Econ. Geol. Mono.* 4, 132-146.
- Thayer, T.P. 1980. Synchronizalation and subsolidus deformation in ophiolite peridotite and gabbro. *Am. J. Sci.*, 280-A, 269-283.
- Theis, N. J. 1979. Uranium-bearing and associated minerals in their geochemical and sedimentological context, Elliot Lake, Ontario. *Can. Geol. Survey Bull.*, 304, 50p.
- Theodore, T.G. 1986. Descriptive model of porphyry Mo, low F. *U.S. Geol. Survey Bull.* 1693, 120.
- Theodore, T.G., G.J. Oris, J.M. Hammarstrom, and J.D. Bliss 1991. Gold-bearing skarns. *U.S. Geol. Survey Bull.* 1930, 61 p.
- Thiede D.S. and E.N. Cameron 1978. Concentration of heavy metals in the Elk Point evaporite sequence, Saskatchewan. *Econ. Geol.*, 73, 405-415.
- Thode, H.G. 1970. Sulfur isotope geochemistry and fractionation between coexisting sulfide minerals. *Mineral. Soc. Am. Spec. Paper* 3, 133-144.
- Thode, H.G. and A.M. Goodwin 1983. Further sulphur and carbon isotope studies of late Archean iron-formations of the Canadian Shield and the rise of sulfate reducing bacteria. *Precamb. Res.*, 20, 337-356.
- Thode, H.G., and J. Monster 1965. Sulfur isotope geochemistry of petroleum, evaporites and ancient seas. *Am. Assoc. Petroleum Geol. Mem.* 4, 367-377.
- Thode, H.G., T. Ding, and J.H. Crockett 1991. Sulfur-isotope and elemental geochemistry studies of the Hemlo gold mineralization, Ontario: sources of sulphur and implications for the mineralization process. *Can. J. Earth Sci.*, 28, 13-25.
- Thompson, J.F.H., S.J. Barnes, and J.M. Duke 1984. The distribution of nickel and iron between olivine and magmatic sulfides in some natural assemblages. *Can. Mineral.*, 22, 55-66.
- Thompson, J.B., Jr. 1959. Local equilibrium in metasomatic processes. In *Researches in geochemistry*, P.H. Abelson (ed.), 427-457. New York: Wiley.
- Thompson, J.B., Jr., and S.A. Norton 1968. Paleozoic regional metamorphism in New England and adjacent areas. In *Studies of Appalachian geology, Northern and Maritime*, E-an Zen, W.S. White, and J.B. Hadley (eds.). New York: Wiley.
- Thompson, T.B., M.W. Hitzman, and D.W. Beaty 1992. Paragenesis and fluid inclusions of the Lisheen Zn-Pb deposit, Co. Tipperary, Ireland [abs.]. *Geol. Soc. Am. Abstracts with Programs*, 24, A354.
- Thorn, P.G. 1988. Fluid inclusion and stable isotope studies at the Chicote tungsten deposit, Bolivia. *Econ. Geol.*, 83, 62-68.

- Thorpe, R.S. 1974. Lead isotope evidence on the genesis of silver-arsenide vein deposits of the cobalt and Great Bear Lake areas, Canada. *Econ. Geol.*, 69, 777-91.
- Thorpe, R.S., P.W. Francis, and R.S. Harmon 1981. Andean andesites and crustal growth. *Phil. Trans. Royal Soc. London*, Ser. A, 301, 305-320.
- Thurlow, J.G., and E.A. Swanson 1981. Geology and ore deposits of the Buchans area, central Newfoundland. *Geol. Assoc. Canada Spec. Paper* 22, 113-142.
- Thurlow, J.F. and E.A. Swanson 1987. Stratigraphy and structure of the Buchans Group. *Geol. Survey Canada Paper* 86-24, 35-46.
- Thurlow, J.G., E.A. Swanson, and D.F. Strong 1975. Geology and litho geochemistry of the Buchans polymetallic sulfide deposits, Newfoundland. *Econ. Geol.*, 70, 130-144.
- Thurston, P.C., and K.M. Chivers 1990. Secular variation in greenstone sequence development emphasizing Superior Province, Canada. *Precamb. Res.*, 46, 21-58.
- Thurston, P.C. L.D. Ayres, G.R. Edwards, L. Gélinas, J.N. Ludden, P. Verpaelst 1985. Archean bimodal volcanism. *Geol. Assoc. Canada Spec. Paper* 28, 7-21.
- Thy, P., and E.M. Moores 1988. Crustal accretion and tectonic setting of the Troodos ophiolite, Cyprus. *Tectonophysics*, 147, 221-245.
- Tikkanen, G.D. 1986. World resources and supply of lead and zinc. In *Economics of internationally traded minerals*, W.R. Bush (ed.), 242-250. Littleton, Colorado: Soc. Mining Engineers.
- Titley, S.R. 1975. Geological characteristics and environments of some porphyry copper occurrences in the southwestern Pacific. *Econ. Geol.*, 70, 499-514.
- Titley, S.R. 1978. Copper, molybdenum and gold content of some porphyry copper systems of the southwestern and western Pacific. *Econ. Geol.*, 73, 977-981.
- Titley, S.R. 1982a. Geologic setting of porphyry copper deposits, southeastern Arizona. In *Advances in Geology of the porphyry copper deposits, southwestern North America*, S.R. Titley (ed.), 37-58. Tucson, Arizona: Univ. Arizona Press.
- Titley, S.R. 1982b. The style and progress of mineralization and alteration in porphyry copper systems. In *Advances in Geology of the porphyry copper deposits, southwestern North America*, S.R. Titley (ed.), 93-116. Tucson, Arizona: Univ. Arizona Press.
- Titley, S.R. 1982c. Some features of tectonic history and ore genesis in the Pima mining district, Pima County, Arizona. In *Advances in Geology of the porphyry copper deposits, southwestern North America*, S.R. Titley (ed.), 387-406. Tucson, Arizona: Univ. Arizona Press.
- Titley, S. R. 1991. Phanerozoic ocean cycles and sedimentary-rock-hosted gold ores. *Geology*, 19, 645-648.
- Titley, S.R. 1993. Characteristics of porphyry copper occurrence in the American southwest. *Geol. Assoc. Canada Spec. Paper* 40, 433-464.
- Titley, S.R., and R.E. Beane 1981. Porphyry copper deposits: Part I. Geologic settings, petrology, and tectogenesis. *Econ. Geol. 75th Anniv. Vol.*, 214-235.
- Titley, S.R., and T.L. Heidrick 1978. Intrusion and fracture styles of some mineralized porphyry systems of the southwestern Pacific and their relationship to plate interactions. *Econ. Geol.*, 73, 891-903.
- Todd, S.G., D.W. Keith, D.J. Schissel, L.L. Leroy, E.L. Mann, and T.N. Irvine 1982. The J-M platinum-palladium reef of the Stillwater Complex, Montana: I. Stratigraphy and petrology. *Econ. Geol.*, 77, 1454-1480.
- Toens, P. D. 1981. Uranium provinces and their time-bound characteristics. *Trans. Geol. Soc.*, 84, 293-312.
- Tooms, J.S. 1970. Review of knowledge of metalliferous brines and related deposits. *Inst. Mining Metall. Trans.*, 79, B116-B126.
- Toulmin, P. III., and P.B. Barton 1964. A thermodynamic study of pyrite and pyrrhotite. *Geochim. Cosmochim. Acta*, 28, 641-671.
- Toulmin, P., III, P.B. Barton, and L.B. Wiggins 1991. Commentary on sphalerite geobarometer. *Am. Mineral.*, 76, 1038-1051.
- Touret, J. 1981. Fluid inclusions in high-grade metamorphic rocks. In *Fluid inclusions: applications to petrology*, L.S. Hollister and M.L. Crawford (eds.), 182-208. Calgary: Mineral. Assoc. Canada.
- Tourtetot, E.B., and J.D. Vine 1976. Copper deposits in sedimentary and volcanogenic rocks. *U.S. Geol. Survey Prof. Paper* 907C, 1-34.
- Tremblay, L. P. 1978. Geologic setting of the Beaverlodge-type vein-uranium deposit and its comparison to that of the unconformity-type. *Mineral. Assoc. Canada Short Course Handbook*, 3, 431-456.
- Tremblay, L.P. 1982. Geology of the uranium deposits related to the sub-Athabasca unconformity, Saskatchewan. *Geol. Survey Canada Paper* 81-20, 56p.
- Trendall, A.F. 1968. Three great basins of Precambrian banded iron formation deposition: a systematic comparison. *Geol. Soc. Am. Bull.*, 79, 1527-1544.
- Trendall, A.F. 1983a. Introduction. In *Iron formation: facts and problems*, A.F. Trendall and R.C. Morris (eds.), 1-12. Amsterdam: Elsevier.
- Trendall, A.F. 1983b. The Hamersley Basin. In *Iron formation: facts and problems*, A.F. Trendall and R.C. Morris (eds.), 69-130. Amsterdam: Elsevier.

- Trendall, A.F., and J. G. Blockley 1970. *The iron formation of the Precambrian Hamersley Group, Western Australia, with special reference to the associated crocidolite*. Geol. Survey Western Australia, 336 p.
- Trudinger, P.A., L.A. Chambers, and J.W. Smith 1985. Low temperature sulphate reduction: biological vs. abiological. *Can. J. Earth Sci.*, 12, 1910-1918.
- Tsutsumi, M., and H. Ohmoto 1983. A preliminary oxygen isotope study of the tetsusekiei ores associated with Kuroko deposits in the Hokuroku district, Japan. *Econ. Geol. Mono.* 5, 433-438.
- Tudge, A.P. and H.G. Thode 1950. Thermodynamic properties of isotopic compounds of sulfur. *Can. J. Res.*, B28, 567-578.
- Turekian, K.K., and K.H. Wedepohl 1961. Distribution of the elements in some major units of the earth's crust. *Geol. Soc. Am. Bull.*, 72, 175-192.
- Turneaure, F.S. 1955. Metallogenic provinces and epochs. *Econ. Geol. 50th Anniv. Vol.*, 38-98.
- Turneaure, F.S. 1971. The Bolivian tin-silver province. *Econ. Geol.*, 66, 215-225.
- Turner, A.R., D. Wolfgram, and S.J. Barnes 1985. Geology of the Stillwater Country sector of the J-M Reef, including the Minneapolis Adit. *Montana Bur. Mines Geol. Spec. Publ.* 92, 210-230.
- Turner, J.S., and I.H. Campbell 1987. Temperature, density and buoyancy fluxes in "black smoker" plumes and the criterion for buoyancy reversal. *Earth Planet. Sci. Lett.* 86, 85-92.
- Turner, J.S. and L.B. Gustafson 1978. The flow of hot saline solutions from vents in the sea floor — some implications for exhalative massive sulfide and other ore deposits. *Econ. Geol.* 73, 1082-1100.
- Turner, R.J.W. 1992. Formation of Phanerozoic stratiform sediment-hosted zinc-lead deposits: evidence for the critical role of oceanic anoxic events. *Chem. Geol.*, 99, 165-188.
- Turner-Peterson, C.E. 1985. Lacustrine-humate model for primary uranium ore deposits, Grants uranium region, New Mexico. *Am. Assoc. Petroleum Geologists Bull.*, 69, 1999-2020.
- Tweto, O. 1979. The Rio Grande rift system in Colorado. In *Rio Grande rift: tectonics and magmatism*, R.E. Riecker (ed.), 33-56. Washington, D.C.: Am. Geophys. Union.
- Ulmer, G.C. 1969. Experimental investigation on chromite spinels. *Econ. Geol. Mono.* 4, 114-131.
- Unrug, R. 1988. Mineralization controls and source of metals in the Lufilian fold belt, Shaba (Zaire), Zambia, and Angola. *Econ. Geol.*, 83, 1247-1258.
- Upadhyay, H.D., and D.F. Strong 1973. Geological salting of the Belts Cove copper deposits, Newfoundland; and example of ophiolite sulfide mineralization. *Econ. Geol.*, 68, 161-167.
- Urabe, T., S.D. Scott, and K. Hattori 1983. A comparison of footwall-rock alteration and geothermal systems beneath some Japanese and Canadian volcanogenic massive sulfide deposits. *Econ. Geol. Mono.* 5, 345-364.
- Urabe, T. 1974. Mineralogical aspects of the Kuroko deposits in Japan and their implications. *Mineral. Deposita*, 9, 309-324.
- Urabe, T. 1985. Aluminous granite as a source magma of hydrothermal ore deposits. *Econ. Geol.*, 80, 148-157.
- Urabe, T. 1987. The effect of pressure on the partitioning ratios of lead and zinc between vapor and rhyolite melts. *Econ. Geol.*, 82, 1049-1052.
- Urabe, T., and K. Marumo 1991. A new model for Kuroko-type deposits of Japan. *Episodes*, 14, 246-251.
- Urabe, T., and T. Sato 1978. Kuroko deposits of the Kosaka mine, northeast Honshu, Japan — products of submarine hot springs on Miocene sea floor. *Econ. Geol.*, 73, 161-179.
- Urabe, T., S.D. Scott, and K. Hattori 1983. A comparison of footwall-rock alteration and geothermal systems beneath some Japanese and Canadian volcanogenic massive sulfide deposits. *Econ. Geol. Mono.* 5, 345-364.
- Usselman, T. M., D. S. Hodge, A. J. Naldrett, and I. H. Campbell 1979. Physical constraints on the localization of nickel sulfide ore in ultramafic lavas. *Can. Mineral.*, 17, 361-372.
- Utter, T. 1978. Morphology and geochemistry of pyrite types from the Upper Witwatersrand System of the Klerksdorp Goldfield, South Africa. *Geol. Rundschau*, 67, 774-804.
- Utter, T. 1979. The morphology and silver content of gold from the Upper Witwatersrand and Ventersdorp Systems of the Klerksdorp Gold Field, South Africa. *Econ. Geol.*, 74, 27-44.
- Uyeda, S., and C. Nishiwaki 1980. Stress field, metallogenesis, and mode of subduction. *Geol. Soc. Canada Spec. Paper* 20, 323-339.
- Uytenbogaardt, W. and E.A.J. Burke 1971. *Tables for microscopic identification of ore minerals*. Amsterdam: Elsevier.
- Vaasjoki, M. and B.L. Gulson 1986. Carbonate-hosted base metal deposits: lead isotope data bearing on their genesis and exploration. *Econ. Geol.*, 81, 156-172.
- Valenta, R. 1994. Deformation of host rocks and stratiform mineralization in the Hilton mine area, Mt. Isa. *Australian J. Earth Sci.*, 41, 429-444.
- Valeton, I. 1983. Paleoenvironment of lateritic bauxites with vertical and lateral differentiation. *Geol. Soc. London Spec. Publ.*, 11, 77-90.
- Valley, J.W. 1986. Stable isotope geochemistry of metamorphic rocks. *Rev. in Mineralogy*, 16, 445-489.
- Van der Merwe, M.J. 1976. The layered sequence of the Potgietersrus limb of the Bushveld Complex. *Econ. Geol.*, 71, 1337-1351.

- Van Dijk, P.M. 1991. Regional syndeformational copper mineralization in the western Mount Isa Block, Australia. *Econ. Geol.*, 86, 278-301.
- Van Eden, J.G. 1974. Depositional and diagenetic environment related to sulfide mineralization, Mufulira, Zambia. *Econ. Geol.*, 69, 59-79.
- Van Houten, F.B. 1991. Interpreting Silurian Clinton ironstones - 1850-1975. *J. Geol. Education*, 39, 19-22.
- Van Houten, F.B., and D.P. Bhattacharyya 1982. Phanerozoic oolitic ironstones — geologic record and facies model. *Ann. Rev. Earth Planet Sci.*, 10, 441-457.
- Vaughan, D.J. 1976. Sedimentary geochemistry and mineralogy of the sulfides of lead, zinc, copper and iron and their occurrence in sedimentary ore deposits. In *Handbook of strata-bound and stratiform ore deposits*, K.H. Wolf (ed.), 2, 317-363. Amsterdam: Elsevier.
- Vaughan, D.J., and J.R. Craig 1997. Sulfide ore mineral stabilities, morphologies, and intergrowth textures. In *Geochemistry of hydrothermal ore deposits*, 3rd. edn., H.L. Barnes (ed.), 367-434. New York: Wiley.
- Vaughan, D.J., M. Sweeney, G. Friedrich, R. Diedel, and C. Haranczyk 1989. The Kupferschiefer: an overview with an appraisal of the different types of mineralization. *Econ. Geol.*, 84, 1003-1027.
- Veizer, J. 1983. Geologic evolution of the Archean-early Proterozoic Earth. In *Earth's earliest biosphere: its origin and evolution*, J.W. Schopf (ed.), 240-259. Princeton, N.J.: Princeton Univ. Press.
- Veizer, J. 1989. Strontium isotopes in seawater through time. *Ann. Rev. Earth Planet Sci.*, 17, 141-167.
- Veizer J., J.Lemieux, B. Jones, M.R. Gibling and J. Savelev 1977. Sodium: paleosalinity indicator in ancient carbonate rocks. *Geology*, 5, 177-179.
- Vennemann, T.W., S. E. Kesler, and J. R. O'Neil 1992. Stable isotope compositions of quartz pebbles and their fluid inclusions as tracers of sediment provenance: implications for gold- and uranium-bearing quartz pebble conglomerates. *Geology*, 20, 837-840.
- Vermaak, G.F. 1976. The Merensky Reef — thoughts on its environment and genesis. *Econ. Geol.*, 71, 1270-1298.
- Vermaak, C.F. 1985. The UG2 layer — South Africa's slumbering chromite giant. *Chromium Rev.*, 5, 9-23.
- Vermaak, C.F., and L.P. Henriks 1976. A review of the mineralogy of the Merensky Reef, with specific reference to new data on the precious metal mineralogy. *Econ. Geol.*, 71, 1244-1269.
- Vernon, R.H. 1968. Microstructures of high-grade metamorphic rocks at Broken Hill, Australia. *J. Geol.*, 9, 1-22.
- Verwoerd, W.J. 1989. Genetic types of ore deposits associated with carbonatites [abs.]. *Abstracts International Geol. Congress*, 28th, 3, 295-296.
- Viets, J.G., and D.L. Leach 1988. Ore deposition in the Viburnum Trend of southeast Missouri by two geochemically distinct fluids [abs.]. *Geol. Soc. Am. Abstracts with Programs*, 20, A39.
- Viets, J.G., and D.L. Leach 1990. Genetic implications of regional and temporal trends in ore fluid geochemistry of Mississippi Valley-type deposits in the Ozark region. *Econ. Geol.*, 85, 842-861.
- Viets, J.G., A.F. Hofstra, and P. Emsbo 1997. Solute compositions of fluid inclusions in sphalerite from North American and European Mississippi Valley-type ore deposits: ore fluids derived from evaporated seawater. *Soc. Econ. Geol. Spec. Publ.* 4, 465-482.
- Viljoen, M.J. 1984. Archean gold mineralization and komatiites in southern Africa. In *Gold '82: the geology, geochemistry and genesis of gold deposits*, R.P. Foster (ed.), 595-627. Amsterdam: Balkema.
- Viljoen, M.J., and R.N. Scoon 1985. The distribution and main geologic features of discordant bodies of rion-rich ultramafic pegmatite in the Bushveld Complex. *Econ. Geol.*, 80, 1109-1128.
- Viljoen, M. J., and R. P. Viljoen 1969. Evidence for the existence of a mobile extrusive peridotite magma from the Komati Formation of the Onverwacht Group. *Geol. Soc. S. Africa Spec. Publ.* 2, 87-112.
- Viljoen, R.P., R. Saager, and M.J. Viljoen 1970. Some thoughts on the origin and processes responsible for the concentration of gold in the early Precambrian of southern Africa. *Mineral. Deposita*, 5, 164-180.
- Virke, P.G. 1989a. Fluid-mineral relations in the Comstock Lode. *Econ. Geol.*, 84, 1574-1613.
- Virke, P.G. 1989b. Ledge formation at the Sandstorm and Kendall gold mines, Goldfield, Nevada. *Econ. Geol.*, 84, 2115-2138.
- Vlassopoulos, D., and S.A. Wood 1990. Gold speciation in natural waters: I. Solubility and hydrolysis reactions of gold in aqueous solution. *Geochim. Cosmochim. Acta*, 54, 3-12.
- Vogt, J.H.L. 1926. Magmas and igneous ore deposits. *Econ. Geol.*, 21, 207-223.
- Vokes, F.M. 1969. A review of the metamorphism of sulfide deposits. *Earth Sci. Rev.*, 6, 99-143.
- Vokes, F.M. 1971. Some aspects of regional metamorphic mobilization of preexisting sulphide deposits. *Mineral. Deposita*, 6, 122-129.
- Vokes, F.M. 1976. Caledonian massive deposits in Scandinavia: a comparative review. In *Handbook of strata-bound and stratiform ore deposits*, K. H. Wolf (ed.), 6, 80-127. Amsterdam: Elsevier.
- Volborth, A., and R.M. Housley 1984. A preliminary description of complex graphite, sulfide, arsenide, and platinum-group element mineralization in a pegmatoidal pyroxenite of the Stillwater Complex, Montana, U.S.A. *Tschermaks Mineralog. Petrolog. Mitt.*, 33, 213-230.

- Volborth, A., M. Tarkian, E.F. Stumpff, and R.M. Housley 1986. A survey of the Pd-Pt mineralization along the 35-km strike of the J-M Reef, Stillwater Complex, Montana. *Can. Mineral.*, 24, 329-346.
- von Backstrom, J.W., and R.E. Jacob 1979. Uranium in South Africa and South West Africa (Namibia). *Phil. Trans. Royal Soc. London*, ser. A, 291, 307-319.
- von Damm, K.L. 1990. Seafloor hydrothermal activity: black smoker chemistry and chimneys. *Ann. Rev. Earth Planet. Sci.*, 18, 173-204.
- von Gruenewaldt, G. 1977. The mineral resources of the Bushveld Complex. *Minerals Sci. Eng.*, 9, 83-95.
- von Gruenewaldt, G. 1979. A review of some recent concepts of the Bushveld Complex with particular reference to the sulfide mineralization. *Can. Mineral.*, 17, 235-256.
- Von Gruenewaldt, G., and R.E. Harmer 1992. Tectonic setting of Proterozoic layered intrusions with special reference to the Bushveld Complex. In *Proterozoic crustal evolution*, K.C. Condie (ed.), 181-213. Amsterdam: Elsevier.
- von Gruenewaldt, G., M.R. Sharpe, and C.J. Hatton 1985. The Bushveld Complex: introduction and review. *Econ. Geol.*, 80, 803-812.
- von Gruenewaldt, G., C.J. Hatton, and R.K.W. Merkle, and S.B. Gain 1986. Platinum-group element-chromitite associations in the Bushveld Complex. *Econ. Geol.*, 81, 1067-1079.
- Voss, R.L., and R.D. Hagni 1985. The application of cathodoluminescence microscopy to the study of sparry dolomite from the Viburnum Trend, southeast Missouri. In *Mineralogy — Applications to the minerals industry*, D.M. Hausen and O.C. Kopp (eds.), 51-68. New Orleans: Am. Inst. Mining Engineers.
- Wager, L.R., E.A. Vincent, and A.A. Smales 1957. Sulfides in the Skaergaard intrusion. *Econ. Geol.*, 52, 855-903.
- Wagner, P.A. 1929. *The platinum deposits and mines of South Africa*. Edinburgh: Oliver & Boyd.
- Walker, G.W., and F.W. Osterwald 1963. Concepts of origin of uranium-bearing veins in the conterminous United States. *U.S. Geol. Survey Prof. Paper* 455-F, 104-120.
- Walker, J.C.G., and P. Brimblecombe 1985. Iron and sulfur in the pre-biological ocean. *Precamb. Res.*, 28, 205-222.
- Walker, J.C.G., C. Klein, M. Schidlowski, J.W. Schopf, C.J. Stevenson, and M.R. Walter 1983. Environmental evolution of the Archean-Early Proterozoic earth. In *Earth's earliest biosphere*, J.W. Schopf (ed.), 260-290. Princeton, New Jersey: Princeton Univ. Press.
- Walker, R.G. 1978. A critical appraisal of Archean basin-carbon complexes. *Can. J. Earth Sci.*, 15, 1213-1218.
- Walker, R.J., J.W. Morgan, A.J. Naldrett, C. Li, and J.D. Fassett 1991. Re-Os isotope systematics of Ni-Cu sulfide ores, Sudbury Igneous Complex: evidence for a major crustal component. *Earth Planet. Sci. Lett.*, 105, 416-429.
- Walker, R.N., R.G. Logan, and J.G. Binnekamp 1977. Recent geological advances concerning the H.Y.C. and associated deposits, McArthur River, N.W.T. *Geol. Soc. Austral. J.*, 24, 365-380.
- Walker, R.R., A. Matulich, A.C. Amos, J.J. Watkins and G.W. Mannard 1975. The geology of Kidd Creek mine. *Econ. Geol.* 70, 80-89.
- Wallace, S.R. 1995. The Climax-type molybdenite deposits: what they are, where they are, and why they are. *Econ. Geol.*, 90, 1359-1380.
- Wallace, S.R., MacKenzie, W.B., Blair, R.G., and Muncaster, J.E. 1978. Geology of the Urad and Henderson molybdenite deposits, Clear Creek County, Colorado, with a section on comparison of these deposits with those at Climax, Colorado. *Econ. Geol.*, 73, 325-368.
- Wallace, S.R., N.K. Munchaster, D.C. Johnson, W.B. Mackenzie, A.A. Bookstrom, and V.E. Surface 1968. Multiple intrusion and mineralization at Climax, Colorado. In *Ore deposits of the United States, 1933-1967 (Graton-Sales Volume)*, J.D. Ridge (ed.), 1, 605-640. New York: Am. Inst. Mining and Petroleum Engineers.
- Wallis, F.H., N. Saracoglu, J.J. Brummer, and J.P. Goightly 1984. The geology of the McClean uranium deposits, north Saskatchewan. *Can. Inst. Mining and Metall. Bull.*, 77, 69-96.
- Walraven, F., R.A. Armstrong, and F.J. Kruger 1990. A chronostratigraphic framework for the north-central Kaapvaal Craton, the Bushveld Complex and Vredefort structure. *Tectonophysics*, 171, 173-181.
- Walter, L.M., A. Stueber, T.J. Huston, A. Martini, V. Granath, and R.R. Blake 1992. Origin, evolution and migration of Illinois Basin brines. *U.S. Geol. Survey Open-File Rept.* 92-1, 67-68.
- Walter, M.R., R. Buick, and J.S.R. Dunlop 1980. Stromatolites 3400-3500 Myr old from the North Pole area, W. Australia. *Nature*, 284, 443-445.
- Walther, J.V., and P.M. Orville 1982. Volatile production and transport in regional metamorphism. *Contrib. Mineral. Petrol.*, 79, 252-257.
- Walther, J.V., and B.J. Wood 1986. *Fluid-rock interactions during metamorphism*. New York: Springer-Verlag.
- Walton, A.W., W.E. Galloway, and C.D. Henry 1981. Release of uranium from volcanic glass in sedimentary sequences: an analysis of two systems. *Econ. Geol.*, 76, 69-88.

- Wanty, R.B., M.B. Goldhaber, and H.R. Northrop 1990. Geochemistry of vanadium in an epigenetic, sandstone-hosted vanadium-uranium deposit, Henry Basin, Utah. *Econ. Geol.*, 85, 270-284.
- Warnaars, F.W., H.D. Carmen, and B.F. Sergio 1985. Porphyry copper and tourmaline breccias at Los Bronces-Rio Blanco, Chile. *Econ. Geol.*, 80, 1544-1565.
- Warren, H.V., and R.M. Thompson 1945. Sphalerites from western Canada. *Econ. Geol.*, 40, 309-335.
- Warren, P. H. 1984. Primordial degassing, lithosphere thickness and origin of komatiites. *Geology*, 12, 335-338.
- Watanabe, M., and H. Sakai 1983. Stable isotope geochemistry of sulfates from the Neogene ore deposits in the Green Tuff region, Japan. *Econ. Geol. Mono.* 5, 282-291.
- Watanabe, T. 1943. Geology and mineralization of the Suian district, Tyosen (Korea). *Hokkaido Imperial Univ., J. Geol. Min. Ser. IV*, VI, 285-286.
- Wedepohl, K.H. 1971. "Kupferschiefer" as a prototype of syngenetic sedimentary ore deposits. *Soc. Mining Geol. Japan Spec. Issue* 3, 268-273.
- Wedow, H. Jr. 1971. Models of mineralized solution-collapse structures from drilling statistics: an aid to exploration. *Econ. Geol.*, 66, 770-776.
- Weissberg, B.G., P.R.L. Browne, and T.M. Seward 1979. Ore metals in active geothermal systems. In *Geochemistry of hydrothermal ore deposits, 2nd ed.*, H.L. Barnes (ed.), 738-780. New York: Wiley.
- Wendlandt, R. F. 1982. Sulfide saturation of basalt and andesite melts at high pressures and temperatures. *Am. Mineral.*, 67, 877-885.
- Werner, W. 1989. Contribution to the genesis of the SEDEX-type mineralizations of the Rhenish Massif (Germany) — implications for future Pb-Zn exploration. *Geol. Rundschau*, 78, 571-598.
- Westowski, D. 1984. *Geochemistry of tungsten in scheelite deposits: The skarn ores at King Island, Tasmania*. Unpublished Ph.D. dissertation, Penn State Univ.
- Westra, G. and S.B. Keith 1981. Classification and genesis of stockwork molybdenum deposits. *Econ. Geol.*, 76, 844-873.
- Whelan, J.F., R.O. Rye, and W. DeLorraine 1984. The Balmat-Edwards zinc-lead deposits — synsedimentary ore from Mississippi Valley-type fluids. *Econ. Geol.*, 79, 239-265.
- White, A.J.R., and B.W. Chappell 1977. Ultrametamorphism and granitoid gneiss. *Tectonophysics*, 43, 7-22.
- White, C.H. 1945. The abyssal versus the magmatic theory of ore genesis. *Econ. Geol.*, 40, 342-343.
- White, D.E. 1974. Diverse origins of hydrothermal ore fluids. *Econ. Geol.*, 69, 954-973.
- White, D.E. 1981. Active geothermal systems and hydrothermal ore deposits. In *Economic Geology 75th Anniv. Vol.*, 392-423.
- White, N.C., and J.W. Hedenquist 1995. Epithermal gold deposits: styles, characteristics and exploration. *Soc. Econ. Geol. Newsletter*, no. 23, 1 and 9-13.
- White, W.H., A.A. Bookstrom, R.J. Kamilli, M.W. Ganster, R.P. Smith, D.E. Ranta, and R.C. Steininger, 1981. Character and origin of Climax-type molybdenum deposits. *Econ. Geol. 75th Anniv. Vol.*, 270-316.
- White, W.S. 1960. The White Pine copper deposit. *Econ. Geol.*, 55, 402-409.
- White, W.S. 1968. The native-copper deposits of northern Michigan. In *Ore deposits of the United States, 1933-1967 (Graton-Sales Volume)*, J.D. Ridge (ed.), 1, 303-325. New York: Am. Inst. Mining, Metall., and Petroleum Engineers.
- White, W.S. 1971. A paleohydrologic model for mineralization of the White Pine copper deposit, northern Michigan. *Econ. Geol.*, 66, 1-13.
- White, W.S., and J.C. Wright. 1954. The White Pine copper deposit, Ontonagon County, Michigan. *Econ. Geol.*, 49, 675-716.
- Whitney, J.A. 1975. Vapor generation in a quartz monzonite magma: a synthetic model with application to porphyry copper deposits. *Econ. Geol.*, 70, 346-358.
- Whitney, J.A. 1977. A synthetic model for vapor generation in tonalite magmas and its economic ramifications. *Econ. Geol.*, 72, 686-690.
- Wiggins, L.B., and J.R. Craig 1980. Reconnaissance of the Cu-Fe-Zn-S system: sphalerite phase relationships. *Econ. Geol.*, 75, 742-752.
- Wilde, A.R., M.S. Bloom, and V.J. Wall 1989. Transport and deposition of gold, uranium, platinum-group elements in unconformity-related uranium deposits. *Econ. Geol. Mono.* 6, 637-650.
- Wilkinson, W.H., L.A. Vega, and S.R. Titley 1982. Geology and ore deposits at Mineral Park, Mohave County, Arizona. In *Advances in Geology of the porphyry copper deposits, southwestern North America*, S.R. Titley (ed.), 523-542. Tucson: Univ. Arizona Press.
- Willan, R.C.R., and A. J. Hall 1980. Sphalerite geobarometry and trace-element studies on stratiform sulphide from McPhun's Cairn, Loch Fyne, Argyll, Scotland. *Inst. Mining. Metall. Trans.*, 89, B31-B40.
- Willemse, J. 1969a. The geology of the Bushveld igneous complex, the largest depository of magmatic ore deposits in the world. *Econ. Geol. Mono.* 4, 1-22.
- Willemse, J. 1969b. The vandiferous magnetite iron ore of the Bushveld igneous complex. *Econ. Geol. Mono.* 4, 187-208.

- Williams, D., R.L. Stanton, and F. Rambaud 1975. The Planes-San Antonio pyritic deposit of Rio Tinto, Spain: its nature, environment, and genesis. *Inst. Mining Metall. Trans.*, 84, B73-B84.
- Williams, H., M.J. Kennedy, and E.R.W. Neale 1974. The northeastward termination of the Appalachian Orogen. In *The ocean basins and margins*, 2, A. E.M. Nairn and F.G. Stehli (eds.), 79-123. New York: Plenum.
- Williams, N. 1978a. Studies of base metal sulfide deposits at McArthur River, Northern Territory, Australia: I. The Cooley and Ridge deposits. *Econ. Geol.*, 73, 1005-1035.
- Williams, N. 1978b. Studies of base metal sulfide deposits at McArthur River, Northern Territory, Australia: II. The Sulfide-S and organic-C relationships of the concordant deposits and their significance. *Econ. Geol.*, 73, 1036-1056.
- Williams, N. 1979a. The timing and mechanisms of formation of the Proterozoic stratiform Pb-Zn and related Mississippi Valley-type deposits at McArthur River, N.T., Australia: *Soc. Economic Geologists — Am. Inst. Mining Engineers, Joint Mtg., New Orleans, Preprint 79-51*, 15p.
- Williams, N. 1979b. Studies of the base metal sulfide deposits at McArthur River, Northern Territory, Australia: II. The sulfide-S and organic-C relationships of the concordant deposits and their significance — a reply. *Econ. Geol.*, 74, 1695-1697.
- Williams, N. 1980. Precambrian mineralization in the McArthur-cloncurry region, with special reference to stratiform lead-zinc deposits. In *Geology and geophysics of Northern Australia*, P.J. Stephenson and R.A. Henderson (eds.), 89-107. Geol. Soc. Australia, Queensland Division.
- Williams, N., and R.G. Logan 1986. Geology and evolution of the Hyc stratiform Pb-Zn orebodies, Australia [abs.]. *Stanford University Publication Geol. Sci.*, 20, 57-60.
- Wilson, A.H. 1982. The geology of the "Great Dyke", Zimbabwe: the ultramafic rocks. *J. Petrol.*, 23, 240-292.
- Wilson, A.H., A.J. Naldrett, and M. Tredoux 1989. Distribution and controls of platinum group element and base metal mineralization in the Darwendale subchamber of the Great Dyke, Zimbabwe. *Geology*, 17, 649-652.
- Wilson, I.H., G.M. Derrick, and D.J. Perkin 1985. Eastern Creek volcanics: their geochemistry and possible role in copper mineralisation at Mount Isa, Queensland. *BMR J. Austral. Geol. Geophys.*, 9, 317-328.
- Wilson, P.N., and W.T. Parry 1995. Characterization and dating of argillic alteration in the Mercur gold district, Utah. *Econ. Geol.*, 90, 1197-1216.
- Wilson, M.R., and T.K. Kyser 1987. Stable isotope geochemistry of alteration associated with the Key Lake uranium deposit, Canada. *Econ. Geol.*, 82, 1540-1557.
- Wisniowiecki, M.J., R. Van der Voo, C. McCabe, and W.C. Kelly 1983. A Pennsylvanian paleomagnetic pole from mineralized Late Cambrian Bonnetterre Formation, southeast Missouri. *J. Geophys. Res.*, 88, 6540-6548.
- Witt, W.K., J.T. Knight, and E.J. Mikucki 1997. A synmetamorphic lateral fluid flow model for gold mineralization in the Archean southern Kalgoorlie and Norseman terranes, Western Australia. *Econ. Geol.*, 92, 407-437.
- Wolfhard, M.R., and C.S. Ney 1976. Metallogeny and plate tectonics in the Canadian Cordillera. *Geol. Assoc. Canada Spec. Paper 14*, 361-392.
- Wood, P.C., A.V. Burrows, A.V. Thomas, and E.T.C. Spooner 1986. The Hollinger-McIntyre Au-quartz vein system, Timmins, Ontario, Canada: geologic characteristics, fluid properties and light stable isotope geochemistry. In *Proc. Gold '86 Symposium*, A.J. Macdonald (ed.), 56-80. Toronto: Konsult International Inc.
- Wood, S.A., and B.W. Mountain 1991. Hydrothermal solubility of palladium in chloride solutions from 300° to 700°C: preliminary experimental results — a discussion. *Econ. Geol.*, 86, 1562-1563.
- Wood, S.A., and I.M. Samson 1998. Solubility of ore minerals and complexation of ore metals in hydrothermal solutions. *Rev. in Econ. Geol.*, 10, 33-80.
- Wood, S.A., and D. Vlassopoulos 1990. The dispersion of Pt, Pd, and Au in surficial media about two PGE-Cu-Ni prospects in Quebec. *Can. Mineral.*, 28, 649-663.
- Wood, S.A., B.W. Mountain, and B.J. Fenlon 1989. Thermodynamic constraints on the solubility of platinum and palladium in hydrothermal solutions: reassessment of hydroxide, bisulfide, and ammonia complexing. *Econ. Geol.*, 84, 2020-2028.
- Wood, S.A., P. Pan, Y. Zhang, and A. Mucci 1994. Solubility of Pt and Pd sulfides and Au metal in aqueous bisulfide solutions. II. Results at 25°-90°C and 1 atm. *Mineral. Deposita*, 29, 373-390.
- Woodall, R. 1988. Gold in 1988 (Extended Abstracts, oral programme, Bicentennial Gold '88, Melbourne). *Geol. Soc. Austral. Abstracts*, 22, 1-12.
- Woolley, A.R. 1989. The spatial and temporal distribution of carbonatites. In *Carbonatites*, K. Bell (ed.), 15-37. London: Unwin Hyman.
- Woolrich, P., A. Cowden, and N.E. Giorgetta 1981. The chemical and mineralogical variation in the nickel mineralization associated with the Kambalda Dome, Western Australia. *Econ. Geol.*, 76, 1629-1644.
- Worthington, J.E., I.T. Kiff, E.M. Jones, and P.E. Chapman 1980. Applications of the hot springs or fumarolic model in prospecting for lode gold deposits. *Mining Eng.*, 32, 73-79.

- Wright, J.V., R.C. Haydon, and G.W. McConachy 1987. Sedimentary model for the giant Broken Hill Pb-Zn deposit, Australia. *Geology*, 15, 598-602.
- Wu, L., and U. Petersen 1977. Geochemistry of tetrahedrite and mineral zoning at Casapalca, Peru. *Econ. Geol.*, 72, 993-1016.
- Wu, Y., and F.W.S. Beales 1981. A reconnaissance study by paleomagnetic methods of the age of mineralization along the Viburnum Trend, southeast Missouri. *Econ. Geol.*, 76, 1879-1894.
- Wyborn, L.A.I. 1987. The petrology and geochemistry of alteration assemblages in the Eastern Creek Volcanics, as a guide to copper and uranium mobility associated in the regional metamorphism and deformation, Mount Isa, Queensland. *Geol. Soc. London Spec. Publ.* 33, 425-434.
- Wyllie, P.J. 1989. Origin of carbonatites: evidence from phase equilibrium studies. In *Carbonatites*, K. Bell (ed.), 500-545. London: Unwin Hyman.
- Wyman, D. and R. Kerrich 1988. Alkaline magmatism, major structures, and gold deposits: implications for greenstone belt gold metallogeny. *Econ. Geol.*, 83, 454-461.
- Wyman, D., and R. Kerrich 1989. Archean shoshonitic lamprophyres associated with Superior Province gold deposits: distribution, tectonic setting, noble metal abundances, and significance for gold mineralization. *Econ. Geol. Mono.* 6, 651-667.
- Yamamoto, M. 1976. Relationship between Se/S and sulfur isotope ratios of hydrothermal sulfide minerals. *Mineral. Deposita*, 11, 197-209.
- Yamamoto, M., M. Endo, and K. Ujihira 1984. Distribution of selenium between galena and sphalerite. *Chem. Geol.*, 42, 243-248.
- Yeo, G. M. 1986. Iron-formation in the late Proterozoic Rapitan Group, Yukon and Northwest Territories. *Can. Inst. Mining Metall. Spec. Vol.* 37, 143-153.
- York, D., A. Masliwec, P. Kuybida, J.A. Hanes, C.M. Hall, W.J. Kenyon, E.T.C. Spooner, and S.D. Scott 1982. $^{40}\text{Ar}/^{39}\text{Ar}$ dating of pyrite. *Nature*, 300, 52-53.
- Young, L.E. 1995. Empirical applications of common lead-isotope ratios to exploration. *Soc. Econ. Geol. Newsletter*, no. 22, 1 and 7-12.
- Young, T. P. 1989. Phanerozoic ironstones: an introduction and review. In *Phanerozoic ironstones*, T.P. Young and W.E.G. Taylor (eds.), ix-xxv. London: Geol. Soc.
- Yunker, L.W., P.W. Kasameyer, and J.D. Tewhey 1982. Geological, geophysical, and thermal characteristics of the Salton Sea geothermal field, California. *J. Volcanology Geother. Res.*, 12, 221-258.
- Yui, S. 1983. Textures of some Japanese Besshi-type ores and their implications for Kuroko deposits. *Econ. Geol. Mono.* 5, 231-240.
- Yund, R.A., and H.T. Hall 1969. Hexagonal and monoclinic pyrrhotites. *Econ. Geol.* 64, 420-424.
- Yund, R.A., and R.H. McCallister 1970. Kinetics and mechanism of exsolution. *Chem. Geol.*, 6, 5-30.
- Zang, W., and W.S. Fyfe 1993. A three-stage genetic model for the Igarape' Bahia lateritic gold deposit, Carajas, Brazil. *Econ. Geol.*, 88, 1768-1779.
- Zartman, R.E., and B.R. Doe 1981. Plumbotectonics — the model. *Tectonophysics*, 75, 135-162.
- Zartman, R.E., Z.E. Peterman, J.D. Obradovich, M.D. Gallego, and D.T. Bishop 1982. Age of Crossport sill near Eastport, Idaho. *Idaho Bur. Mineral. Geol. Bull.*, 24, 61-69.
- Zhou, Mei-Fu, and P.T. Robinson 1997. Origin and tectonic environment of podiform chromite deposits. *Econ. Geol.*, 92, 259-262.
- Zhou, Mei-Fei, P.T. Robinson, and W.-J. Bai 1994. Formation of podiform chromites by melt/rock interaction in the upper mantle. *Mineral. Deposita*, 29, 98-101.
- Zielinski, R.A. 1979. Uranium mobility during interaction of rhyolitic obsidian, perlite and felsite with alkaline carbonate solution: $T = 120^\circ\text{C}$, $P = 210 \text{ kg/cm}^2$. *Chem. Geol.*, 27, 47-63.
- Zielinski, R.A. 1983. Tuffaceous sediments as source rocks for uranium: a case study of the White River Formation, Wyoming. *J. Geochem. Exploration.*, 18, 285-306.
- Zielinski, R.A., S. Bloch, and T.R. Walker 1983. The mobility and distribution of heavy metals during the formation of first cycle red beds. *Econ. Geol.*, 78, 1574-1589.
- Zientek, M.L., and E.M. Ripley 1990. Sulfur isotope studies of the Stillwater Complex associated rocks, Montana. *Econ. Geol.*, 85, 376-391.
- Zientek, M.L., G.K. Czamanske, and T.N. Irvine 1985. Stratigraphy and nomenclature of the Stillwater Complex. *Montana Bur. Mines Geol. Spec. Publ.* 92, 21-32.
- Zimmerman, R.K., and S. E. Kesler 1981. Fluid inclusion evidence for solution mixing, Sweetwater (Mississippi Valley-type) district, Tennessee. *Econ. Geol.*, 76, 134-142.
- Zoback, M.L., R.E. Anderson, and G.A. Thompson 1981. Cainozoic evolution of the state of stress and style of tectonism of the basin and Range province of the western United States. *Phil. Trans. Royal Soc. London*, A300, 407-434.
- Zoltai, T. 1974. *Systematics of sulfide structures: simple sulfides*. Unpublished report, Dept. Geology & Geophysics, Univ. Minnesota, Minneapolis, U. S. A.
- Zurbrigg, H.F. 1963. Thompson mine geology. *Can. Inst. Min. Metall. Trans.*, 66, 227-236.

SUBJECT INDEX

- Absolite 38
- Adularia-sericite type epithermal gold deposits
703, 707, 708, 709, 736, 738, 739, 755,
759
- Age distribution of deposits or host rocks
anorthosite-Ti deposits 30
bauxite deposits 35
carbonatites 21
chromite deposits 269-270
gold deposits 704, 711, 718, 724, 727,
729, 752
iron-formations 694-696
kimberlites 24
MVT deposits 577, 593, 594, 607
Ni-sulfide deposits 308
porphyry copper deposits 354-355, 356,
372-376, 389-390
porphyry molybdenum deposits 398
sedimentary manganese deposits 47-48
skarn deposits 445-446
SMS deposits 509, 536-537
SSC deposits 541, 571
uranium deposits 617, 619, 629, 650
VMS deposits 452, 453, 454, 537
- Aggeneys deposit, South Africa 500, 501,
503
- Agnew (Preservance) nickel deposit ,
Western Australia 276, 279, 280, 297
- Algoma-type iron-formation 667, 668, 669,
677, 684, 692, 695
- Allard Lake, Canada 31
- Alligator Rivers uranium district, Australia
622, 623, 624
- Alpine-type Zn-Pb deposits 574-575
- Alpine-type ultramafic complexes 19, 239,
244-245, 321
- Alunite-kaolinite type epithermal gold deposits
703, 708, 709, 736, 737, 738, 739, 755,
759,
- Anomalous lead 180
- Anorthosites 28-31
- Anvil SMS deposit, Canada 500, 501, 532
- Aqueous metal complexes
chloride complexes 65-67, 488, 563, 565,
602
gold complexes 731-735
iron complexes 681, 689
molybdenum complexes 407
Pt- and Pd-complexes 343-344
organometallic complexes 65
silicon complexes 682, 689
sulfide complexes 65-69
uranyl complexes 635, 637, 638-639
- Athabasca Basin, Canada 622, 623, 624, 633-
634
- Austinville MVT district, USA 576, 577
- Balmat-Edwards district, USA 184-185, 500,
504
- Bathurst VMS district, Canada 463
- Battle Mountain skarn deposit, USA. 424
- Bauxite deposits 34, 35-37
- Beaverlodge uranium district, Canada 622,
624, 627, 633
- Besshi-type VMS deposits 184, 456, 458, 461,
486, 487, 496
- Bingham district, USA 126, 127, 139, 355,
362, 387, 415-420, 428-430
- Billiard ball model 306-307
- Bird River Sill, Canada 239, 240
- Bisbee porphyry copper deposit, USA 372
- Black Hills uranium deposits, USA 618, 620
- Black smokers 483, 485, 530
- Blue Bell Zn-Pb deposit, Canada 173, 428
- Boiling 10, 61, 68, 78, 89, 140-141, 216, 382,
526, 733, 734, 735, 737, 739, 740, 741
- Bolivia tin deposits 410, 411, 412
- Bonanza 704, 759
- Boxwork 42, 43
- Breccias 360-361, 574, 580, 581, 584, 586,
587, 588, 591-592, 600, 602, 603, 607, 717
- Brockman Iron Formation, Australia 661, 671,
672-675, 685
- Broken Hill deposit, Australia 227, 500, 501,
502, 523, 533
- Buchans VMS district, Canada 463
- Bushveld Complex, S.Africa 19-20, 71, 239-
240, 243, 248-253, 258, 263-265, 267,
269, 271, 274, 276, 301, 306, 321, 322,
323-331, 340, 345, 347
- Butte deposit, USA 384, 385, 387, 409
- Campo Formoso district, Brazil 239, 240, 243
- Canadian Shield 274, 721, 724, 729,
- Carbon isotopic composition
carbonatites 20-24
gold deposits 730, 745
hydrothermal deposits 167-169
Precambrian sulfides 678
- Carlin gold deposit, USA 725-728
- Carlin-type gold deposits, USA 710-714, 739-
743, 754, 757-758
- Carlin Trend, Nevada, USA 725
- Casapalca Ag-Pb-Zn-Cu vein deposit , Peru
83-84, 163, 167, 174

- Central African Copperbelt 539, 541, 560, 565, 572
 Central Tennessee zinc district, USA 576, 577, 587, 588, 592, 593, 599, 603, 604
 Chalcopyrite disease 106, 207
 Chemical/biochemical precipitation 33, 34, 44-49

 Chrome Mine, Cyprus 256
 Chrome ratio (chrome spinel) 257, 258
 Chromitite 242, 243, 251, 252, 261-265, 270, 324, 325, 336, 337, 342, 347, 349
 Chuquicamata porphyry copper deposit, Chile 354, 355, 375
 Churchill Province, Canada 285
 Climax-type deposits 399, 400, 401-404
 Climax porphyry molybdenum deposit, USA 399, 401, 403, 405, 406, 408
 Cobalt-Gowganda silver-arsenide vein deposits, Canada 87-89
 Coeur d'Alene vein deposit, USA 54, 184
 Colorado Plateau uranium deposits, USA 618, 619, 620, 647
 Common lead 178
 Compaction-driven fluid flow 72-73, 527, 564, 597, 598
 Concentration factor 5
 Condensed system 108
 Conglomerate-type gold deposits *see conglomerate-type uranium deposits*
 Conglomerate-type uranium deposits 614, 617-618, 635, 640-641, 651
 Congo Copperbelt 554, 560, 568, 570
 Convective fluid flow 73, 386-387, 528, 565
 Copper skarns 420, 422-423, 424, 425, 428, 430, 444, 445, 447, 449
 Cornwall district, England 126
 Cornwallis MVT deposit, Canada 576, 577
 Cortex Trend, Nevada, USA 725
 Cratonization model (Archean gold) 746-747
 Creede Pb-Zn-Cu-Ag-Au vein deposit, USA 163, 186, 231-235
 Creta SSC deposit, USA 541, 545, 560, 565, 568, 570
 Crustal continuum model (Archean gold) 748
 Cut-off grade 1, 31
 Cyclic units 241, 242, 323
 Cyprus-type VMS deposits 456-458, 460-461, 462, 472, 476, 486, 490, 491, 496

 Dalmatianite 468, 478
 Darwin Zn-Pb skarn deposit, USA 163, 174, 215, 427
 Dating of mineral deposits
 fission-track 230
 lead isotopes 177-180
 paleomagnetism 230
 strontium isotopes 186-187
 Dharwar craton, India 313, 722
 Diagenetic 228-229, 499, 510, 511, 513, 521, 523, 541, 548, 549, 554, 555, 556, 557, 558, 559, 561, 562, 564, 566, 567, 568, 570, 571, 632, 645, 646, 650, 660, 662, 663, 666, 675, 676, 679, 687
 Diamonds 24-28
 Diamond-graphite inversion 27
 Dihedral angle 98-99
 Diorite model (porphyry copper) 369
 Distal deposits 78, 307, 417, 451, 521
 Distribution coefficient 212-213
 Dongchuan SSC deposit, China 541, 545
 Ducktown sulfide deposit, USA 223-225, 461
 Duluth Complex, USA 274, 276, 296, 306, 311, 611
 Dumont nickel deposit, Canada 279, 280, 297
 Dynamic partial melting 350-351
 Dzhezkazgn SSC deposit, former USSR 541, 544, 545, 572

 East Tennessee zinc district, USA 576, 577, 591, 593, 602, 603, 606
 El Salvador porphyry copper deposit, Chile 374-378, 386
 Elliot Lake-Blind River uranium district, Canada 617, 618, 627, 635
 Elmwood zinc deposit, USA 192
 Endoskarn 418, 419, 420-421, 422, 423, 431, 440, 446
 Epigenetic 228-229, 353, 511, 517, 521, 526, 550, 558, 582, 624, 632, 633, 636, 640, 641, 643, 646, 650, 677, 704, 715, 728, 743, 756
 Epithermal 57, 74, 75-76, 83
 Epithermal gold deposits 702-710, 736-739, 755, 757-758
 Epithermal precious metal systems 74-76
 Evaporites 34, 61, 506, 509, 520, 528, 530, 531, 533, 535, 538, 539, 544, 546, 547, 549, 553, 556, 561, 562, 563, 564, 567, 570, 571, 573, 583, 584, 588, 596, 603, 604, 611
 Evolution of atmospheric oxygen 652-658
 Exhalative 5, 507, 511, 521, 525, 526, 539, 565, 671
 Exhalite 299
 Exoskarn 418, 423, 424, 440, 448

 Filter pressing 18
 Fiskenaeset Complex, Greenland 239, 240, 270, 321
 Fluid flow 51-52, 69-73
 Fluid inclusion data
 gold deposits 437-438, 758
 MVT deposits 587
 porphyry copper deposits 382-383
 porphyry molybdenum deposits 496
 porphyry tin deposits 411
 skarn deposits 437-438
 SMS deposits 527
 SSC deposits 555, 562
 uranium deposits 647, 650
 Froot Ni-sulfide deposit 276, 290

- Gamsberg SMS deposit, South Africa 500, 501, 503
- Gangue 1
- Gays River MVT district, Canada 576, 577, 603, 605, 606
- Geobarometry
 fluid inclusions 216-219
 geobarometer 193, 199
 phase equilibria 199-200
 sphalerite composition 205-207
- Geochron 180, 181
- Geothermometry
 arsenopyrite composition 207-209
 fluid inclusions 135, 216
 geothermometer 193, 199
 magnetite-ilmenite compositions 210-212
 oxygen isotopic fractionation 198
 phase equilibria 199-200
 pyrrhotite composition 200-202
 sphalerite composition 202-205
 sulfur isotopic fractionation 195-197
 trace element partitioning 212-216
- Getchell Trend, Nevada, USA 725, 727
- Gold minerals 707, 713, 716
- Gold skarns 415, 424-425, 443, 446
- Gossan 40, 281
- Grade 1, 31, 35, 38, 39, 84, 243, 275, 280, 284, 307, 317, 321, 322, 324, 327, 328, 329, 330, 331, 345, 353, 354, 356-357, 362, 363, 370, 375, 379, 380, 395, 398, 399, 400, 403, 420-421, 423, 424, 425, 426, 427, 428, 429, 450, 455, 458, 461, 467, 502-503, 504, 523, 542-543, 560, 575, 576, 608, 609, 613, 615-616, 618, 620, 623, 627, 650, 664, 699, 700, 702, 705-706, 712, 715, 723, 727, 728
- Grants Mineral belt (uranium), USA 618, 619, 631-633
- Grasvalley Chrome Mine, South Africa 251
- Gravitational settling 16, 18
- Gravity-driven fluid flow 72-73, 528, 597, 598
- Great Bear Lake district, Canada 624, 627
- Great Dyke, Zimbabwe 239-240, 243, 258, 263, 268, 274, 276, 321, 322
- Greenstone belts
 Abitibi, Canada 274, 279, 316, 311, 464-467, 474, 494, 715, 719, 728, 746
 Barberton, South Africa 277, 308, 310, 314, 494
 Belingwe, Zimbabwe 240, 313
 Norseman-Wiluna, Western Australia 274, 281, 282, 313, 315, 316, 317, 494
 Shurugwi, Zimbabwe 239, 240, 270
- Hammersley Basin, Australia 661, 663, 671, 673, 683, 684, 697
- Helen Iron Formation 670, 671, 686, 692, 696
- Hilton SMS deposit, Australia 500, 501, 502, 508, 510, 523
- Homestake goldmine, USA 227
- Homogenization temperature 133, 135, 141
- Hornfels 415, 416, 440
- Hydraulic equivalence 18, 44, 54
- Hydrofracturing 12, 53
- Hydrothermal alteration
 aluminosilicates 121-124
 gold deposits 707, 711, 712, 714, 723, 724, 726, 727, 730, 733, 735, 738, 740, 742, 743, 746, 747, 750, 756, 759,
 iron-formations 671
 MVT deposits 580, 590-591, 595-596
 Ni-sulfide deposits 298
 oxygen isotope ratios 176-177
 porphyry copper deposits 364-366, 368-370, 388-389
 porphyry molybdenum deposits
 reactions 117-119
 skarn deposits 414, 417, 422, 423, 425, 426, 427, 428, 430, 432, 437, 438, 439, 441, 445, 448
 SMS deposits 498, 510, 511, 514, 515, 516, 518523-524, 530, 538
 SSC deposits 541, 563
 uranium deposits 617, 622, 623, 627, 634, 636, 641, 646, 655, 659
- VMS deposits 451, 452, 455, 456, 459, 461, 462, 466, 468, 470, 473-477, 478, 479, 481, 482, 486, 488, 490, 493, 494, 495, 496
- Hydrothermal deposits 82-83
- Hydrothermal flow systems 69-73
- Hypothermal 57
- I-type magma 9, 10, 12, 392
- Iberian pyrite belt 463, 464
- Illinois-Kentucky MVT district, USA 576, 577, 588
- Industrial mineral deposits 1
- Interfacial free energy 97-98, 101
- Intermediate solid solution (iss) 114
- Internal sediments 584
- Intrusion-related gold deposits 714-715, 716, 735-736, 755
- Iron-formation 34, 48, 221, 660, 661
- Iron-formation facies 662-667
- Iron skarns 415, 418, 419, 420, 422, 442, 444, 446, 449
- Ironstone 661
- Isochron 179, 187, 230, 595
- Isotopic composition of seawater
 oxygen and hydrogen 171
 strontium 189-190
 sulfur 160-162
- Isoelectric Point 691
- Isotope standards 149, 140
- Isotopic exchange reactions 151
- Isotopic fractionation 149-151
 carbon 166
 geothermometry 194-198
 oxygen and hydrogen 170
 sulfur, equilibrium 155-157
 sulfur, bacterial 157-159
- Isotopic fractionation factor 150, 152-153
- J-M Reef, Stillwater Complex 322, 325, 332, 333, 334, 337, 345, 347

- Jinchuan nickel deposit, China 274, 275, 321
- Kaapvaal craton, southern Africa 25, 248, 274, 617, 628
- Kalgoorlie gold district, Western Australia 715, 719, 720, 723, 748
- Kambalda-type Ni-sulfide deposits 279, 299-307
- Kambalda nickel district 276, 279, 281-285, 311
- Kaolinite line 171, 172, 384, 385
- Katiniq sill, Canada 279
- Kemi Complex, Finland 239, 240, 243, 263
- Kid Creek deposit, Canada 177, 434, 465, 471
- Killingdal VMS deposit, Norway 461
- Kimberlites 24-28
- Kinetic isotopic effect 152, 159, 171
- King Island tin deposit, Tasmania 415, 421, 431-432, 438
- Kolar Schist Belt, India, 699, 700, 715, 719
- Komatiite 276, 277, 285, 293, 309-310
- Komatiite-dumite association 276, 279
- Komatiite-peridotite association 276, 279
- Komatiitic magma 309-310
- Krumen Iron Formation, South Africa 661, 675, 676, 685
- Kupferschiefer, Germany-Poland 343, 545-550, 559, 560, 561, 562, 565, 567, 568, 569, 570, 571
- Kuroko deposits, Japan 163, 184, 462, 463, 464, 470, 471, 472, 473, 476, 477, 480, 490, 493, 496
- Kuroko-type VMS deposits 456, 458, 462-464, 467, 469, 471, 472, 476, 478, 479, 480, 486, 493, 494, 495
- Lac Tio Ti deposit, Canada 31-32
- Lady Loretta SMS deposit, Australia 500, 501, 502, 504, 522, 531, 532
- Laisvall deposit, Sweden 575, 577
- Laterites 35
- Lateritic nickel deposits 37-40
- Layered intrusions 19, 20, 239, 241, 242, 259, 260, 267, 275, 276, 321
- Lead isotopic evolution
dynamic models 183
single-stage lead evolution 178, 179, 181
- Lead isotope ratios of mineral deposits 182, 184
MVT deposits 593, 594, 595, 605-606
porphyry molybdenum deposits 407, 408
SMS deposits 516, 529, 534, 535
VMS deposits 461, 489
- Levack Ni-sulfide deposit, Canada 276, 290
- Limonite 40-41
- Liquid immiscibility 13-17, 22
- Ltallagua tin deposit, Bolivia 409, 411
- Lode gold deposits 715-725, 743-749, 752, 757-758
- Lubin SSC district, Poland 541, 544, 546, 549
- Lunnon Shoot, Western Australia 284, 285
- Magadiite 682
- Magma 7
- Magmatic 300-307
- Magmatic differentiation 12
- Magmatic fluids 10-12
- Magmatic hydrothermal 385-386
- Magmont Pb-Zn mine, Missouri 108-109
- Magnesium ratio (chrome spinel) 257, 258
- Malanjkhand copper deposit, India 354, 355
- Malayaite 427
- Manganesite deposits 34
- Mantle diapirs 19, 244
- Mascot-Jefferson City zinc district, USA 585-585, 604
- Massif Central, France 624
- Matchless VMS deposit, Namibia 461
- Mattabi-type VMS deposits 456, 458, 459, 472, 475, 476, 494, 496
- McArthur River (HYC) SMS deposit, Australia 500, 501, 502, 504-508, 522, 523, 525, 526, 529, 532, 533, 534, 536
- McIntyre-Hollinger deposit, Canada 728-731
- Meggen SMS deposit, Germany 500, 501, 521, 522, 526, 527, 531, 532, 533, 536
- Melodezhnoe chromite mine 246
- Membrane filtration 61
- Mercury-depositing systems 74
- Merensky-type PGE deposits 337-347
- Merensky Reef, Bushveld Complex 251, 253, 322, 323, 325-327, 337, 338, 344, 345-347
- Mesothermal 57, 715, 757
- Mesothermal gold deposits 715, 757-758
- Metallic mineral deposits 1
- Metallogenic epoch 3
- Metallogenic province 3
- Metamorphic deposits 50, 54
- Metamorphic fluid composition 50-51
- Metamorphic fluid flow 51-53
- Metamorphic fluids 50-53
- Metamorphic remobilization 222-225
- Metamorphism
Archean gold deposits effects 219-216
gold deposits 718, 724, 740, 743, 746, 748, 749, 751, 752, 753, 757
iron-formations 672, 674, 678-680, 694
Ni-sulfide deposits 298, 299
SMS deposits 502-503, 511, 513, 521, 526, 534
SSC deposits 542-543
VMS deposits 462, 471, 477-478, 487
- Metamorphosed deposits 50, 218-222
- Meteoritic water line 171, 172
- Michigan Peninsula native copper 539, 557
- Millenbach VMS deposit, Canada 472, 474
- Mineral deposits 1
- Minette-type iron-formation 661, 662
- Mobilization 53-54
- Model lead age 180
- Modern sea-floor 77-80
- Molybdenum skarns 415, 424, 437
- Monosulfide solid solution (mss) 14, 292

- Mount Isa SMS deposit, Australia 227, 500, 501, 502, 504, 521, 522, 523, 525, 529, 532, 533, 536
- Murray Ni-sulfide deposit, Canada 276, 290
- Nanisivik deposit, Canada 576, 577, 598, 606
- Navan SMS deposit, Ireland 500, 501, 503, 519-521, 523, 525, 529, 536
- Newfoundland, Canada - tectonostratigraphic
- Nonmetallic mineral deposits 1
- Noranda-type VMS deposits 456-457, 458, 459, 467, 472, 474, 475, 476, 488, 489, 494, 496
- Noranda VMS district, Canada 458, 459, 465, 466, 467, 468, 482, 494
- Noril'sk-Talnakh deposits, Russia 274, 275, 276, 306, 311, 321, 322, 325
- Norseman-Wiluna belt *see greenstone belts*
- Oil-field brines 80-81
- Ok Tedi deposit, Papua New Guinea 396
- Oklo uranium deposit, Nigeria 622
- Old Lead Belt, USA 576, 577
- Oldoinyo Lengai, Tanzania 21
- Olympic Dam deposit, Australia 617
- Ophiolites 19, 20, 62, 69, 244, 245, 254, 258, 259, 260, 321, 335, 456, 460, 491, 493
- Ordinary lead 180
- Orebody 1
- Ore deposits 1
- Ore minerals 96-97
- Orthomagmatic process 6-7, 20
- Orthomagmatic deposits 18-33
- Outokumpo VMS district, Finland 461
- Oxygen-hydrogen isotopic composition of mineral deposits
- gold deposits 724, 730, 737, 740-741, 745
- hydrothermal deposits 173-174
- porphyry copper deposits 377, 384-385
- porphyry molybdenum deposits 385, 406-407
- VMS deposits 479-480
- uranium deposits 646, 648, 649
- Palabora copper deposit, South Africa 24
- Paleotectonic settings
- chromite deposits 267-269
- gold deposits 752-756
- MVT deposits 606-607
- Ni-sulfide deposits 312-316
- porphyry copper deposits 394-396
- skarn deposits 446-448
- SMS deposits 536
- SSC deposits 570-571
- VMS deposits 492-494
- Panasqueira vein deposit, Portugal 85-87, 163
- Panda Hill, Tanzania 23
- Panguna deposit, Papua New Guinea 372-374
- Paragenesis 103-106, 687
- Paramirim craton, Brazil 274
- Partial melting 7-8, 224
- Partition coefficient 294, 295, 296, 297, 303, 330, 340-342, 383
- Pasto Bueno tungsten vein deposit, Peru 87, 163, 174, 192-193
- Pechanga nickel deposit 274, 276, 301
- PGE profiles of chromite deposits 260
- Phase diagrams
- activity-activity diagrams 112, 113, 120-121
- activity-pH diagram 114, 115-116
- activity-temperature diagram 112, 113
- Eh-pH diagram 638, 665
- Eh-P_{CO2} diagram 682
- Cu-S system 109
- Fe-S system 200
- Fe-Ni-S system 110
- Fe-As-S system 208, 209
- Fe-Zn-S system 203
- Fe-Zn-As-S system 209
- fO₂-pH diagram 732
- molality-temperature diagram 119
- thermodynamic principles 108-109, 111-112, 114, 119-120
- Phosphorite deposits 34, 44-46
- Photo-oxidation 688, 689, 690, 696
- Photolysis 654, 655
- Photosynthesis 654, 655, 656
- Pilbara Block 274, 282, 309, 310, 671
- Pine Point MVT deposit, Canada 80, 163, 167, 576, 577, 582-585, 589, 591, 593, 598, 603, 606
- Placer deposits 33, 34, 42-44
- Placer gold 701-702, 754, 756
- Platinum-group minerals 320
- Platreef, Bushveld Complex 322, 323, 327-329
- Podiform chromite deposits 239, 244-247, 258-259, 266-272
- Polaris deposit, Canada 575, 577, 589, 599
- Porphyry-type deposits 353
- Porphyry copper-gold deposits 362-363, 716
- Porphyry gold deposits 353
- Porphyry tin deposits 409-412
- Porphyry uranium deposits 353, 701, 715, 716
- Potholes 326, 327, 329
- Providencia Pb-Zn deposit, Mexico 163, 167, 174, 415, 421, 435-437
- Proximal deposits 78, 307, 417, 451, 470, 521, 530
- R factor 15-17, 294, 302, 303, 307, 330, 340, 349
- Rabbit Lake uranium deposit 622, 624
- Rajpura-Dariba SMS deposit, India 500, 501, 503
- Rammelsberg SMS deposit, Germany 227, 500, 501, 502, 516-518, 521, 522, 526, 531, 532, 533
- Rapitan-type iron-formation 667, 668, 685, 692
- Recrystallization 103
- Redbed 540, 544, 545, 546, 556, 563, 564, 565, 567, 568, 571, 653
- Red Dog deposit, USA 500, 501, 503
- Red Sea 77, 173

- Redstone district, Canada 541, 545, 560, 562, 568
- Remobilization 53, 220, 222-224, 226, 286, 513
- Renison Bell tin deposit, Tasmania 427, 432-435
- Reserves 1, 2, 23, 47, 55, 239, 241, 274, 275, 322, 327, 328, 353, 354, 356-357, 378, 395, 398, 405, 420-421, 423, 424, 425, 428, 463, 467, 472, 502-503, 504, 513, 519, 542-543, 576, 609, 627, 651, 700, 705-706, 712, 714, 715, 728,
- Residual concentration 33-35
- Rhodesian craton, Zimbabwe 274
- Roll-front (roll) uranium deposits 620, 621, 643, 644, 645
- Rosebery deposit, Tasmania 126, 128
- Rössing uranium deposit 55-56, 616
- Rote Fäule 547, 548, 549
- Rustenburg Layered Suite 249-252
- S-type magma 9-12
- Sabkha 564
- Salinity (fluid inclusion) 136-138, 141
- Salton Sea 76-77, 173
- Sandstone-type uranium deposits 614, 618-621, 631, 636, 641, 643-645, 651
- Sandstone lead deposits 575
- Sanford Lake titanium deposit 31-32
- Schwartzwalder vein-type uranium deposit, USA 624, 627
- Second (retrograde) boiling 11, 360, 391
- Sedimentary deposits 34
- Seismic pumping 72
- Selwyn Basin, Canada 501, 531, 532
- Silesia-Cracow d MVT istrict, Poland 576, 577, 589, 591, 593, 605, 606
- Silvermines SMS deposit, Ireland 500, 501, 503, 521, 522, 523, 525, 526, 527, 528, 530, 531, 532, 533, 536
- Sitampundi anorthosite complex, India 239, 240
- Skaergaard Complex, Greenland 13, 19
- Skarn 414-417, 419, 420-421, 422, 424, 425, 426, 427, 440-444, 445
- Skarnoid 416
- Solubility of metals 63-68
- Southeast Missouri MVT district, USA 578-579, 588, 589, 591, 592, 593, 598, 602, 606
- Sphalerite microstratigraphy 589, 604
- Stillwater Complex, USA 239-240, 242-243, 252, 258, 263, 265, 268, 271, 274, 276, 297, 326, 332-335, 340, 344
- Strata-bound 498, 510, 514, 519-531, 574, 620
- Stratiform 497, 498, 506, 510, 513, 516, 517, 518, 519, 520, 521, 524, 526, 530, 574
- Stratiform chromite deposits 239, 258, 270-271
- Strontium isotope initial ratio 187, 290, 390, 394, 408, 435, 746
- Styles of mineralization 2
- Sudbury Complex, Canada 13, 19, 20, 114-115, 187, 274, 275, 288-291, 293, 306, 322, 325, 343
- Sukinda-Nausahi chromite district, India 239-240, 260
- Sulfide Queen deposit USA 23
- Sulfide segregation 13, 303-306
- Sulfur Bank mercury deposit 74
- Sulfur isotopic composition
 effects of metamorphism 226-227
 gold deposits 730, 745
 hydrothermal mineral deposits 163
 iron-formations 686
 MVT deposits 588, 603-605
 Ni-sulfide deposits 311
 porphyry copper deposits 378, 391, 393
 porphyry molybdenum deposits 407
 SMS deposits 507, 531-534
 SSC deposits 549, 555, 569-570
 VMS deposits 490-492
- Sulfur solubility 8-9
- Sullivan SMS deposit, Canada 434, 500, 501, 502, 513-516, 521, 522, 523, 524, 526, 533, 536
- Supergene alteration
 iron-formations, 371, 661, 680
 porphyry copper 370
 supergene enrichment 33, 40-43
- Superior-type iron-formation 661, 667, 668, 671, 684, 692, 695,
- Superior Province, Canada 285, 313, 314, 698, 700, 715, 719, 720, 723, 724, 728, 729, 731, 743, 744, 745, 748, 753
- Sweetwater MVT district, USA 588, 604
- Syngenic (see Diagenetic)
- Syngenetic 44, 228-229, 299, 517, 521, 522, 524, 541, 549, 554, 559, 561, 562, 581, 630, 641, 714, 743
- Synmetamorphic lateral flow model (Archean gold) 748-749
- Synsedimentary 499, 507, 510, 511, 513, 520, 521, 525, 525, 526, 548, 549, 631
- Syntectonic 508, 510, 511
- Telethermal 57
- Tenor 1
- Texas Coastal Plain uranium deposits 618, 619, 620, 621
- Textures
 annealing 102-103, 104
 deformation 102, 104, 105
 exsolution 101, 104
 foam 99
 fibroblastic 540, 548, 559, 631
 magmatic crystallization 104
 metamorphic 220
 myrmekitic 100
 net 244, 246, 301
 nodular 247, 267
 occluded silicate 244, 246
 open-space filling 101, 104
 orbicular 247
 replacement 102, 104
 schlieren 247
 sedimentation 104

- Thompson Ni-sulfide deposit, Canada 287
 Thompson nickel belt, Canada 276, 279, 285-287, 301
 Thucolite 635
 Timmins gold district, Canada 465, 715, 719, 728, 729, 730, 743
 Tin granite 426, 444
 Tin skarns 415, 418, 421, 426-427, 438, 442, 443, 444, 447, 449
 Titanium deposits 28-33
 Tom deposit, Canada 527, 532
 Trapping temperature 133, 135
 Trapping pressure 134, 135
 Tri-State MVT district, USA 576, 577, 591, 593, 603, 606
 Triple junction 99
 Troodos ophiolite complex 247, 254-256
 Tungsten skarns 415, 421, 423, 425-426, 431, 432, 437, 438, 442, 444, 445, 447, 449
 Tynagh deposit, Ireland 500, 501, 503, 521, 525, 527, 530, 531, 532, 533
- UG-2 chromitite, Bushveld Complex 322, 323, 325, 329-331
 Ultramafic-mafic complexes 19, 241
 Ultramafic pipes 323, 331, 344
 Ultrametamorphic uranium deposits 616
 Unconformity-type uranium deposits 614, 621-624, 645-646, 651
 Ungava nickel belt, Canada 279, 280
 Upper Mississippi Valley MVT district, USA 576, 577, 589, 598, 602, 603, 606
 Urad-Henderson molybdenum deposit, USA 401, 403, 404, 407, 408
- Vein deposits 83
 Vein-type uranium deposits 614, 624-627, 636, 646-647, 651
 Viburnum Trend (MVT), USA 191, 576, 577, 578-582, 598, 602, 605, 606
 Voisey's Bay nickel deposit, Canada 275
 Water-rock isotopic exchange 175-177
 White Pine SSC deposit, USA 541, 545, 556-559, 560, 561, 565, 567, 568, 569, 570, 572
 Wisconsin-Illinois MVT district, USA 576, 577
 Witwatersrand, South Africa 321, 617, 618, 627-631, 641-643, 648-650
- World distribution of mineral deposits
 bauxite deposits 36
 carbonatite complexes 21
 chromite deposits 240
 gold deposits 670, 703, 699
 iron-formations 661, 663
 kimberlite fields (southern Africa) 25
 lateritic nickel deposits 36
 MVT deposits 576, 577
 manganese deposits 47
 Ni-sulfide deposits 274
 phosphorite deposits (southern USA) 45
 porphyry copper deposits 355, 356
 porphyry molybdenum deposits 355, 397-398
 skarn deposits 415
 SMS deposits 501
 SSC deposits 541
 uranium deposits 616
 VMS deposits 452
- Xenothermal 57
- Yilgarn Block, Western Australia 274, 279, 282, 283, 700, 715, 719, 720, 721, 723, 724, 745, 746, 748, 753,
- Zambian Copperbelt 541, 550-556, 560, 561, 562, 567, 568
 Zawar SMS deposit, India 500, 501, 503, 512-513, 525, 532
 Zechstein 545, 546, 547, 548, 549
 Zinc-lead skarns 415, 421, 427-428, 445, 447
- Zoning
 district-scale 125, 126-127
 gold deposits 711
 hydrothermal deposits 130
 orebody-scale 125, 128
 porphyry copper 367-370
 regional-scale 124-125
 skarn deposits 416, 419, 422, 429, 430, 439, 448
 SMS deposits 498, 517, 518, 522, 524
 SSC deposits 540, 549, 551, 553, 554, 559, 560, 562, 564, 565, 566, 567, 571,
 VMS deposits 130, 131, 463, 470, 471-472, 475, 477, 479, 486, 487-489, 494, 496